De-Shuang Huang Kang-Hyun Jo
Hong-Hee Lee Hee-Jun Kang
Vitoantonio Bevilacqua (Eds.)

Emerging Intelligent Computing Technology and Applications

With Aspects of Artificial Intelligence

LNAI 5755

5th International Conference on Intelligent Computing, ICIC 2009
Ulsan, South Korea, September 2009
Proceedings

Springer

Lecture Notes in Artificial Intelligence 5755

Edited by R. Goebel, J. Siekmann, and W. Wahlster

Subseries of Lecture Notes in Computer Science

De-Shuang Huang Kang-Hyun Jo
Hong-Hee Lee Hee-Jun Kang
Vitoantonio Bevilacqua (Eds.)

Emerging Intelligent Computing Technology and Applications

With Aspects of Artificial Intelligence

5th International Conference
on Intelligent Computing, ICIC 2009
Ulsan, South Korea, September 16-19, 2009
Proceedings

Springer

Series Editors

Randy Goebel, University of Alberta, Edmonton, Canada
Jörg Siekmann, University of Saarland, Saarbrücken, Germany
Wolfgang Wahlster, DFKI and University of Saarland, Saarbrücken, Germany

Volume Editors

De-Shuang Huang
Institute of Intelligent Machines
Intelligent Computing Laboratory
Chinese Academy of Sciences
Hefei, Anhui, China
E-mail: dshuang@iim.ac.cn

Kang-Hyun Jo
Hong-Hee Lee
Hee-Jun Kang
University of Ulsan
School of Electrical Engineering
Ulsan, South Korea
E-mail: jokanghyun@gmail.com, {hhlee, hjkang}@ulsan.ac.kr

Vitoantonio Bevilacqua
Polytechnic of Bari
eBIS and DEE
Valenzano, Bari, Italy
E-mail: vitoantonio.bevilacqua@gmail.com

Library of Congress Control Number: 2009932883

CR Subject Classification (1998): I.2.3, I.5.1, I.4, I.5, F.1, F.2

LNCS Sublibrary: SL 7 – Artificial Intelligence

ISSN 0302-9743
ISBN-10 3-642-04019-5 Springer Berlin Heidelberg New York
ISBN-13 978-3-642-04019-1 Springer Berlin Heidelberg New York

Typesetting: Camera-ready by author, data conversion by Scientific Publishing Services, Chennai, India
Printed on acid-free paper SPIN: 12743049 06/3180 5 4 3 2 1 0

Preface

The International Conference on Intelligent Computing (ICIC) was formed to provide an annual forum dedicated to the emerging and challenging topics in artificial intelligence, machine learning, bioinformatics, and computational biology, etc. It aims to bring together researchers and practitioners from both academia and industry to share ideas, problems, and solutions related to the multifaceted aspects of intelligent computing.

ICIC 2009, held in Ulsan, Korea, September 16-19, 2009, constituted the 5th International Conference on Intelligent Computing. It built upon the success of ICIC 2008, ICIC 2007, ICIC 2006, and ICIC 2005 held in Shanghai, Qingdao, Kunming, and Hefei, China, 2008, 2007, 2006, and 2005, respectively.

This year, the conference concentrated mainly on the theories and methodologies as well as the emerging applications of intelligent computing. Its aim was to unify the picture of contemporary intelligent computing techniques as an integral concept that highlights the trends in advanced computational intelligence and bridges theoretical research with applications. Therefore, the theme for this conference was "Emerging Intelligent Computing Technology and Applications." Papers focusing on this theme were solicited, addressing theories, methodologies, and applications in science and technology.

ICIC 2009 received 1,082 submissions from 34 countries and regions. All papers went through a rigorous peer review procedure and each paper received at least three review reports. Based on the review reports, the Program Committee finally selected 257 high-quality papers for presentation at ICIC 2009, of which 214 papers have been included in two volumes of proceedings published by Springer: one volume of *Lecture Notes in Computer Science* (LNCS) and one volume of *Lecture Notes in Artificial Intelligence* (LNAI). The other 22 papers will be included in two international journals.

This volume of *Lecture Notes in Computer Science* (LNCS) includes 106 papers.

The organizers of ICIC 2009, including the University of Ulsan, Korea, Institute of Intelligent Machines of Chinese Academy of Sciences, made an enormous effort to ensure the success of ICIC 2009. We hereby would like to thank the members of the Program Committee and the referees for their collective effort in reviewing and soliciting the papers. We would like to thank Alfred Hofmann, executive editor at Springer, for his frank and helpful advice and guidance throughout and for his support in publishing the proceedings. In particular, we would like to thank all the authors for contributing their papers. Without the high-quality submissions from the authors, the success of the conference would not have been possible. Finally, we are especially grateful to the IEEE Computational Intelligence Society, the International Neural Network Society and the National Science Foundation of China for their sponsorship.

July 2009

De-Shuang Huang
Kang-Hyun Jo
Hong-Hee Lee
Hee-Jun Kang
Vitoantonio Bevilacqua

Organization

General Co-chairs	De-Shuang Huang, China
	Honghee Lee, Korea
	Frank L Lewis, USA
Program Committee Co-chairs	Kanghyun Jo, Korea
	Vitoantonio Bevilacqua, Italy
Organizing Committee Co-chairs	Kang-Hyun Jo, Korea
	In-Soo Koo, Korea
	Youngsoo Suh, Korea
	Naoyuki Tsuruta, Japan
	Chun-Hou Zheng, China
Award Committee Chair	Daniel S. Levine, USA
Publication Chair	Heejun Kang, Korea
Special Session Chair	Prashan Premaratne, Australia
	Tokuro Matsuo, Japan
	Vasily Gubarev, Russia
Tutorial Chair	Laurent Heutte, France
International Liaison Chair	Frank Neumann, Germany
Publicity Co-chairs	Kyungsook Han, Korea
	Vladimir Filaretov, Russia
	Zhongming Zhao, USA
	Maolin Tang, Australia
	Muhammad Khurram Khan, Saudi Arabia
	Valeriya Gribova, Russia
Exhibition Co-chairs	Young-Soo Suh, Korea
	In-Soo Koo, Korea
	Jin Hur, Korea

Organizing Committee Members

Myeong-Jae Yi, Korea	Sang-Bock Cho, Korea	Dong-Joong Kang, Korea
Myung-Kyun Kim, Korea	Munho Jeong, Korea	Jong-Bae Lee, Korea
Byeong-Ryong Lee, Korea	Jongeun Ha, Korea	Sang-Moo Lee, Korea
Won-Ho Choi, Korea		

Program Committee Members

Andrea Francesco Abate, Italy
Shafayat Abrar, UK
Peter Andras, UK
Sabri Arik, Turkey
Vasily Aristarkhov, Russian Federation
Costin Badica, Romania
Vitoantonio Bevilacqua, Italy
David B. Bracewell, USA
Uday K. Chakraborty, USA
Shih-Hsin Chen, Taiwan, China
Wen-Sheng Chen, China
Xiyuan Chen, China
Yang Chen, China
Yuehui Chen, China
Sang-Bock Cho, Korea
Won-Ho Choi, Korea
Michal Choras, Poland
Tommy Chow, Hong Kong, China
Jose Alfredo F. Costa, Brazil
Angelo Ciaramella, Italy
Kevin Curran, UK
Mingcong Deng, Japan
Eng. Salvatore Distefano, Italy
Karim Faez, Iran
Jianbo Fan, China
Minrui Fei, China
Wai-Keung Fung, Canada
Liang Gao, China
Qing-Wei Gao, China
Xiao-Zhi Gao, Finland
Chandan Giri, India
Dunwei Gong, China
Valeriya Gribova, Russia
Kayhan Gulez, Turkey
Ping Guo, China
Jongeun Ha, Korea
Aili Han, China
Fei Han, China
Kyungsook Han, Korea
Haibo He, USA
Laurent Heutte, France
Wei-Chiang Hong, Taiwan, China
Yuexian Hou, China
Peter Hung, Ireland
Chuleerat Jaruskulchai, Thailand
Munho Jeong, Korea
Li Jia, China
Zhenran Jiang, China
Jih-Gau Juang, Taiwan, China
Dah-Jing Jwo, Taiwan, China
Dong-Joong Kang, Korea
Sanggil Kang, Korea
Uzay Kaymak, The Netherlands
Muhammad Khurram Khan, Saudi Arabia
Myung-Kyun Kim, Korea
Sungshin Kim, Korea
In-Soo Koo, Korea
Donald H. Kraft, USA
Harshit Kumar, Ireland
Yoshinori Kuno, Japan
Takashi Kuremoto, Japan
Wen-Chung Kuo, Taiwan, China
Hak-Keung Lam, UK
Byeong-Ryong Lee, Korea
Jong-Bae Lee, Korea
Sang-Moo Lee, Korea
Vincent C.S. Lee, Australia
Guo-Zheng Li, China
Kang Li, UK
Li Li, China
Peihua Li, China
Hualou Liang, USA
Chunmei Liu, USA
Ju Liu, China
Van-Tsai Liu, Taiwan, China
Marco Loog, Denmark
Ahmad Lotfi, UK
Jinwen Ma, China
Shiwei Ma, China
Vishnu Vardhan Makkapati, India
Cheolhong Moon, Korea
Tarik Veli Mumcu, Germany
Roman Neruda, Czech Republic
Frank Neumann, Germany
Minh Nhut Nguyen, Singapore
Ben Niu, China
Sim-Heng Ong, Singapore
Francesco Pappalardo, Italy
Caroline Petitjean, France
Prashan Premaratne, Australia
Shaoqi Rao, China
Seeja K.R., India
Angel Sappa, Spain
Aamir Shahzad, China
Li Shang, China
Jiatao Song, China
Nuanwan Soonthornphisaj, Thailand
Joao Miguel Sousa, Portugal
Min Su, USA
Zhan-Li Sun, Singapore
Maolin Tang, Australia

Antonios Tsourdos, UK
Naoyuki Tsuruta, Japan
Sergio Vitulano, Italy
Anhua Wan, China
Chao-Xue Wang, China
Hong-Qiang Wang, USA
Jinlian Wang, China
Ling Wang, China
Xueqin Wang, China
Yong Wang, China
Xuesong Wang, China
Ling-Yun Wu, China
Shunren Xia, China
Yu Xue, China
Ching-Nung Yang, Taiwan, China
Jun-Heng Yeh, Taiwan, China
Myeong-Jae Yi, Korea
Zhi-Gang Zeng, China
Jun Zhang, China
Yong Zhang, China
Xing-Ming Zhao, China
Zhongming Zhao, USA
Bo-Jin Zheng, China
Fengfeng Zhou, USA
Huiyu Zhou, Italy

Reviewers

Li Ding, Alessandro Ibba, Al Savvaris, Antonio Celesti, Adam Ghandar, Adriao Duarte, Asit Das, Andreas Konstantinidis, Alaa Sagheer, Alan Ritz, Aldayr Araujo, Alessia D'Introno, Alessia Albanese, Alessio Ferone, Alexander Hogenboom, Jose Alfredo F. Costa, Rui Jorge Almeida, Andrey Logvinov, Soon-Min Hwang, Saleh Aly, Amar Khoukhi, Amar Balla, Amelia Badica, Asunción Mochón, Aimin Zhou, Anbumani Subramanian, Andreas Schmidt, Wen-Yuan Liao, Andrey Larionov, Angelo Ciaramella, Angelo Riccio, Anne Canuto, Wei Yu, Antonino Staiano, Anvita Bajpai, Alexander Ponomarenko, Xinping Xie, Aravindan Chandrabose, Joongjae Lee, Ardelio Galletti, Irene Artemieva, Arun D. Mahindrakar, Asaduzzaman, Asharaf S, Atsushi Shimada, Wee Keong Ng, Banu Diri, Bao Vo-Nguyen, Bo-Chao Cheng, Beilu Shao, Beilu Shao, Ibrahim Beklan Kucukdemiral, Bo-Hyeun Wang, Bijaya Ketan Panigrahi, Bin Qian, Bin Li, Shuhui Bi, Xiangrong Zhang, Bekir Karlik, Jiguang Wang, Bogdan Raducanu, Barbara Pizzileo, Ni Bu, Cheon Seong-Pyo, B.V. Babu, Alessia D'Introno, Galip Cansever, Jianting Cao, Karina Shakhgendyan, Carme Julia, Caroline Petitjean, Chia-Mei Chen, Guisheng Chen, Gang Chen, Kuei-Hsiang Chao, Tariq Chattha, Chungho Cho, Jianhua Che, bo chen, Chun Chen, Chengjian Wei, Yuhu Cheng, chen hui, Chenkun Qi, Yang Chen, Chen Asia, Chee-Meng Chew, Ching-Hung Lee, Chuang Ma, Cuco Cuistana, C.-H. Yang, Alessandro Cincotti, Chenn-Jung Huang, Ching-kun Chen, Chunlin Chen, Jimmy Lin, Chi-Min Li, Quang Nguyen, Carmelo Ragusa, Wenjie Li, Min-Chih Chen, Ching-Ti Liu, Chingti Liu, Chi Zhou, Chin-Chun Chang, Chang Wook Ahn, Joo Seop Yun, Chieh-yao Chang, Changyin Sun, dong yang, Louis Wu, Yu-Chen Lin, Ping-Min Hsu, Danfeng Zhu, Vincenzo Daniele Cunsolo, Peng Zhang, David Bracewell, Dario Bruneo, Dajun Du, David Geronimo, Liya Ding, Dmitry Serkin, Jiayin Zhou, Dongsheng Che, Yan Dong, Yongsheng Dong, Denis Orel, Jun Qin, WeiWu Wang, Woosung Yang, Ben Niu, derchian tsaih, Dunwei Gong, Wenyong Dong, Lipo Wang, Hong Fu, Tolga Ensari, Shaoli Wang, Eylem Yucel, Erkan Zergeroglu, Filippo Castiglione, Li-Jen Kao, Chonglun Fang, Ingo Feldmann, Fei Ge, Fengfeng Zhou, LingFeng Liu, Frederik Hogenboom, Chien-Yuan Lai, Wei-Chiang Hong, Francesco Longo, Francesco Napolitano, Francesco Camastra, Nuanwan Soonthornphisaj, Fu-Shiung Hsieh, Shaojing Fan, Francesco Tusa, Fu Yonggui, Lina Lu, Yen Ming Chiu, Zhaohui Gan, Xiao-Zhi Gao, Dingfei Ge, Gerrit K. Janssens, Gwang-Hyun Kim, Ginny Wong, Giuseppe Agrillo, Yaroslava Katueva, Giuseppe Mangioni, Fahad Muhaya, Guang-Ming Wu, Xiujun Gong, Gouhei Tanaka, Muhammad Khurram

Khan, Ge Lei, Zhongsheng Wang, Guo Weidong, Jie Gui, Guilherme Barreto, Tiantai Guo, Gurumurthy Swaminathan, Guangwei Zhang, Gwo-Ruey Yu, Moussa Haddad, Haibing Gao, H.K. Lam, Hanif Ullah, Hanlin He, Haini Qu, Chiung-Hua Huang, Houshang Darabi, Tomohiro Henmi, Herbert Iu, Tiefang He, Han-min Chien, Honorius Galmeanu, Hassan Taheri, Huang Ping, Wei Huang, Weitong Huang, Huifang Li, Huiyu Zhou, Junhao Hu, Hameed Ullah Khan, Rong-xiang Hu, Shahid Hussain, Bo Chen, Jaehyung Park, Hsiang-Yi Lee, Hoang-Yang Lu, Hyun-Sik Kim, Zhongkun He, Ibrahim Aliskan, Irene Artemieva, Indrajit Banerjee, Ing-Chyuan Wu, Ikhyeon Jang, Jianli Li, Seong-Joe Lim, Francesco Iorio, yaou zhao, Jin Zhou, Insoo Koo, Jian Xun Peng, John Economou, Jackson Souza, Jose Alvarez, James Cai, James Walton, James Yeh, Hasan Jamil, Janset Dasdemir, Jawid Azizi, Jayasudha John Suseela, Jianbo Fan, Jiande Sun, Jih-Gau Juang, Javad Haddadnia, Hongjun Jia, Jiajun Yan, Peilin Jiang, Changan Jiang, Jiang jl, Kai Jiang, Lihua Jiang, Wei Jia, Jindong Liu, Guang Jin, Jinsoo Kim, Jungkyu Rho, Josep M. Mirats Tur, Jun Liu, John Klein, Jong Min Lee, Ji-Hun Bae, Joydeb Mukherjee, Jianping Qiao, Jinn-Shing Cheng, Joaquin Torres-Sospedra, Joaquin Torres-Sospedra, Jyh-Ching Juang, Juan Jose Gonzalez de la Rosa, Junaid Ahmed, Jun Du, Junlin Chang, Kang Li, Kanghee Kim, Wei Jing, Kaushik Roy, Iroshi Awasaki, Tsung-Yi Chen, Ke Tang, Hyun-Deok Kang, Alexander Kleschev, Kunikazu Kobayashi, Krishna Chandramouli, Krishnanand Kaipa Narasimha, Seeja K.R.H. K, Lance C. Fung, Laks Raghupathi, Lalit Gupta, Chin-Feng Lin, Le Dong, Sungon Lee, Hong-Bo Lei, Jie Lei, Yingke Lei, Kok-Leong Ong, Lin Gao, Sun Cheol Bae, Laurent Heutte, Hualiang Li, Lijuan Xiao, Lin Li, Guohui Zhang, Lin Wang, Yuxi Liu, Bo Liu, Huiran Liu, Lei Liu, Wenyun Li, Xinyu Li, Ling-po Li, Linlin Shen, Leh Luoh, Lingling Wang, Peixing Li, Milan Lovric, Li Qingfeng, Liqing Zhang, Tian-Yu Liu, Liangxu Liu, Yixiang Lu, Marco Cortellino, Maciej Hrebien, Yasushi Mae, Sakashi Maeda, Sakashi Maeda, Margaret Knyaseva, Margarita Knyazeva, Manish Srivastava, Maqsood Mahmud, M. Loog, JeongHyun Kim, Mario Marinelli, Mario Marinelli, Markus Koskela, Kazuyuki Matsumoto, Maqsood Mahmud, Max Power, Maysam Abbod, Zhongqiang Wu, Mark Halling-Brown, Aizhong Mi, Mika Sulkava, Min Jiang, Min Wu, Mine Tsunenori, hai min, Meiling Hou, Hamid Abrishami Moghaddam, Mohammad Narimani, Monalisa Mazumdar, Lucia Moreno, Santo Motta, Marzio Pennisi, Minh-Tri Pham, Mutsumi Watanabe, Mingyu You, Naeem Ramzan, Naiara Aginako, Nestor Arana, Beijing Chen, Nelson Mascarenhas, Seref Naci Engin, Neyir Ozcan, Mingxiao Li, Li Nie, Xiushan Nie, Nataliya Nikiforova, Nataliya Nikifirova, Nitthinun Suphasetthawit, Nikolay Mikhaylov, Qun Niu, Nhan Nguyen-Thanh, Evgeni Nurminski, Bunyarit Uyyanonvara, Masaru Okumura, Olesya Kazakova, Won-Kyu Kim, Kazunori Onoguchi, Ajiboye Osunleke, Ertan Ouml Znergiz, Ping Zhang, Pallavi Vajinepalli, Pandu Devarakota, Yehu Shen, Chen Peng, Alessandro Perfetto, Hyun-Ju Park, Ping Wang, Peilin Jia, Litt Teen Hiew, Elvira Popescu, Roy Power, Roy Power, Pradip Ghanty, Pramod NC, Pramuditha Suraweera, Prashan Premaratne, Prashan Premaratne, Qi Yu, Qiao Wang, Qi Liu, Qingwei Gao, Quande Qin, Jinpeng Qi, Peng Qiu, Quanke Pan, Thanh Tho Quan, Quang Nguyen, Hai-Tao Zheng, Qi Wang, Ruhul Sarker, Rafal Kozik, Raffaele Montella, M. Rafiq Swash, M.K.M. Rahman, Randeep Singh, Peng Ren, Xianwen Ren, Romina Oliva, Rong Jin, Rosa de Duonni, Lijun Xu, Nidhi Arora, Ryuzo Okada, Shaomin Zhang, Chin-yuan Fan, Saad Bedros, Xin Hao, Sarif Naik, Mihnea Scafes, Sheng Chen, Chen Shao, Jong

Hyun Park, Sanggil Kang, Changho Yun, Shafayat Abrar, Elena Shalfeeva, Li Shang, Shao jj, Xiaojian shao, Sherif Sherif, Chuan Shi, Shaohui Liu, Shripad Kondra, S. Jamal H Zaidi, Shi-Jay Chen, Jiping SHI, Seokjoo Shin, Shiuh-Jeng Wang, Sawomir Lasota, Zhijun Tan, Mingguang Shi, Vitaliy Snytyuk, Xiaojing Song, Shengping Zhang, Sriparna Saha, Sibel Senan, Seokjin Sung, Eung Nam Ko, Sungshin Kim, S Kim, Xueqiang Zeng, Lei Zhang, Steve Ling, Steven Guan, Shih-Ting Yang, Zhang Li, Cheng Sun, Jie Sun, Tingxu Yan, You Ouyang, Supriya Rao, Susana Vieira, Suwon Lee, Yang Shi, Syed Ismail Shah, Peixing Li, Tiong Goh, Shin-ya Takahashi, Shinya Takahashi, Toshihisa Tanaka, Atsushi Yamashita, Weidong Xu, Zhi Teng, Zhu Teng, Thomas Tawiah, Thuc Kieu Xuan, Timo Honkela, Toshiaki Kondo, Tsang-Long Pao, ThanhVu Nguyen, Thomas O'Daniel, Tomasz Andrysiak, Tomasz Rutkowski, Toni Zgaljic, Gyung-Jin Hong, Tomoaki Tsuruoka, Naoyuki Tsuruta, Mengru Tu, U. Kaymak, Uttam Roy, Youngbae Hwang, Mario Rossi, Vanta Dimitrova, Vasily Aristarkhov, Venugopal Chakravarthy, Vinod Pathangay, Bae-guen Kwon, Vito Santarcangelo, Victor Jin, Vladimir Brusic, Wan-Jui Lee, Chih-Hung Wang, Chao Wang, Furong Wang, Wang Haili, Ling Wang, Xiaojuan Wang, Yongcui Wang, Zhengyou Wang, Wen-Chung Chang, Woochang Shin, Wuchuan Yang, Wudai Liao, Wei-Chih Yang, Weidong Li, Weifeng Li, Wenkai Li, Wen Shengjun, Yu-Chen Lin, Wangheon Lee, Wing-Kuen Ling, Shanwen Zhang, Wai-keung Fung, Worasait Suwannik, Takashi Kuremoto, Chao Wu, Yu Wu, Zikai Wu, Jun Zhang, Wei Xiong, Xin Zou, Xiaochun Cao, Chungui Xu, XiaoFeng Wang, Junfeng Xia, Xian-xia Zhang, Xiaomin Liu, Xianjun Shen, Xuemei Ren, De Xu, Bing Xue, Yu Xue, Huan Xu, Lu Xu, Ye Xu, Yun Xu, Xiaolei Xia, Xiaoyan Sun, Xiaoying Wang, Yang Song, Yago Saez, Yan Li, Banghua Yang, Yan Yang, Zhixia Yang, Yanmin Liu, Akira Yanou, Yasuhiro Taniguchi, Yuan-Chang Chang, Yu-Chiun Chiou, Ye Bin, Yeonsik Kang, Y.F. Xu, Yifeng Zhang, Zhao Yinggang, Yinglei Song, Lei Yang, Yangmin Li, Mi-ran Yun, Yoshinori Kobayashi, Yu-Qing Qiu, Yoon-Seok Nam, Yuanling Hao, Ming Yu, Yong Wang, Yue Wang, Yen-Wen Wang, Zhigang Wang, Zanchao Zhang, Zhenbing Zeng, Guowei Zhang, Hehua Zhang, Jun Zhang, Liang Zhao, Zhaohui Sun, Chunhou Zheng, Min Zheng, Zhigang Yan, Zhijun Yang, Lin Zhu, Zhong Jin, Zujun Hou, Dao Zhou, Sulan Zhang, Xiangbin Zhu, Shuanghe Zhu, Xuefen Zhu, Yihai Zhu, Zhang Liangsheng, Liu Zhiping, Guoyu Zuo, Zhongming Zhao.

Table of Contents

Neural Networks

Evolutionary Learning and Genetic Algorithms

Granular Computing and Rough Sets

Fuzzy Theory and Models

Fuzzy Systems and Soft Computing

Swarm Intelligence and Optimization

Supervised and Semi-supervised Learning

Kernel Methods and Supporting Vector Machines

Combinatorial and Numerical Optimization

Systems Biology and Computational Biology

Neural Computing and Optimization

Knowledge Discovery and Data Mining

Artificial Life and Artificial Immune Systems

Ensemble Methods

Machine Learning Theory and Methods

Biological and Quantum Computing

Intelligent Computing in Pattern Recognition

On Dynamic Spectrum Sharing Systems

On New Particle Swarm Optimization and Its Applications

On Intelligent Signal Processing for Interactive Brain-Machine-Interfacing

On Advances in Intelligent Information Processing

On Computational Intelligence in Bioinformatics and Systems Biology

On Network-Based Intelligent Technologies

On 2D versus 3D Intelligent Biometric and Face Recognition Techniques

Erratum

An Ensemble of Neural Networks for Stock Trading Decision Making

Pei-Chann Chang[1,*], Chen-Hao Liu[2], Chin-Yuan Fan[3], Jun-Lin Lin[1], and Chih-Ming Lai[1]

[1] Department of Information Management,
Yuan Ze University, Taoyuan 32026, Taiwan
iepchang@saturn.yzu.edu.tw
[2] Department of Information Management,
Kainan University, Taoyuan 32026, Taiwan
[3] Department of Business Innovation and Development, Ming Dao University,
Changhua 52345, Taiwan

Abstract. Stock turning signals detection are very interesting subject arising in numerous financial and economic planning problems. In this paper, Ensemble Neural Network system with Intelligent Piecewise Linear Representation for stock turning points detection is presented. The Intelligent piecewise linear representation method is able to generate numerous stocks turning signals from the historic data base, then Ensemble Neural Network system will be applied to train the pattern and retrieve similar stock price patterns from historic data for training. These turning signals represent short-term and long-term trading signals for selling or buying stocks from the market which are applied to forecast the future turning points from the set of test data. Experimental results demonstrate that the hybrid system can make a significant and constant amount of profit when compared with other approaches using stock data available in the market.

Keywords: Stock turning signals; Ensemble neural network; PLR method; Financial time series data.

1 Introduction

Stock turning signal is a local peak or valley during a stock price variation. The turning signals are also represented as a short-term or long term investment decision. However, these turning signals are very difficult to be detected or even observed since the price variation is subject to the problems of high dimensionality and non-stationary.

Although some trading rules are clear, most of them are vague and fuzzy. Therefore, an investor cannot be the winner all the time with the same set of trading rules. In literature, researchers have spent a lot of efforts in forecasting the price variation and have tried to come up with numerous sophisticated techniques in predicting the stock price or the price movement. Technical analysis is the most widely used method in this area. However, the results are still quite limited .

* Corresponding author.

D.-S. Huang et al. (Eds.): ICIC 2009, LNAI 5755, pp. 1–10, 2009.

The major contribution of this research is to take a different approach by evolving a piecewise linear representation method with Ensemble neural networks system to predict the future turning signals of a stock price. Turning signals identified by PLR are represented using a nonlinear relationship among the stock closed price, i.e., y_i and various technical indexes, i.e., x_i and this nonlinear relationship will be studied intensively through Ensemble neural network. In other words, local stock turning signals can be detected using PLR preprocessing technique. Later on, these turning signals governing the relationship among the stock closed price with various technical indexes will be inputted into the Ensemble neural network system for training. Then, the trained model can be applied as a universal predicator for predicting the future turning points in the set of test data. Finally, an investor then can apply these future signals as trading signals and make profits no matter short-term or long term trading decisions.

The rest of the paper is divided into five sections. Section 2 reviews the literature in the areas of stock forecasting. Section 3 describes the development of an evolving PLR model and an ensemble neural network for stock trading point decision. Section 4 is the experimental tests conducted to test the effectiveness of trading points generated by using the evolving PLR approach. Finally, conclusions and future directions of the research are provided.

2 Literature Survey

Prediction of a financial market is rather challenging due to chaos and uncertainty of the system. In the past, many statistics and artificial intelligence tools were applied to financial time series analysis. Kovalerchuk et al.(2000) XXclassifies the current methods into three categories: numerical models (ARIMA models, Instance-based learning, neural networks, etc.), rule-based models (decision tree and DNF learning, naive Bayesian classifier, hidden Markov model etc.), and relational data mining (inductive logic programming) ,among these approaches, soft computing techniques (including fuzzy logic, neural networks, Genetic algorithms…..etc) becomes the most popular forecasting model in this area, because of their abilities to handle uncertainty and noise in a stock market. These soft computing techniques are used for quantitative inputs, like technical indices, qualitative factors, political effects…etc to automate stock market forecasting and trend analysis. Neural Network (NNS) have been applied to this area (refer to Aiken and Bsat(1994), Baba et al.(2000), Brownstone(1996), Chen(2003), Pendharkar(2001), Schapire(1990) X). However, these models have their limitations subjecting to the tremendous noise and complex dimensionality of stock price data. The quantity of data itself and the input variables also interfere with each other. Therefore, the result may not be as convincing.

Ensemble strategies have been used to solve Neural Network limitations in West et al. (2005)X inX. The basic concept of the ensemble method is that diverse perspective on different aspects of a problem can be combined to produce a high quality. The most important three strategies have been advanced for forming ensembles of predictors. That includes Cross-validation, Bagging ensembles and Boosting. Cross-validation is the simplest ensemble rule which used in ensemble all methods are trained with the same data.

Nearly ,AdaBoost becomes another popular ensemble strategy that uses perturbation in an attempt to improve the performance of the learning algorithm in Schapire(1990)X. AdaBoost technique has become an attractive ensemble method in machine learning since it is low in errorrate, performing well in the low noise data set inX Henley(1996), Jensen(1992). As a successor of the boosting algorithm, it is used to combine a set of weak classifiers to form a model with higher prediction outcomes in Henley(1996) XX. As a result, several research studies have successfully applied the AdaBoost algorithm to solve classification problems in object detection, including face recognition, video sequences and signal processing systems. For example, Zhou and Wei (2006) Xutilized the AdaBoost algorithm to extract the top 20 significant features. from the XM2VT face database. Their results showed that the AdaBoost algorithm reduces 54.23 % of the computation time. Additionally, Sun et al. (2006) applied the AdaBoost algorithm to extract high-order pattern and weight of evidence rule based classifiers from the UCI Machine Learning Repository.

In this work, Adaboost algorithm ensembles two different kinds of neural net works. Those two different kinds of work include traditional BPN neural networks and evolving neural networks. This techniques will combined with PLR(Piecewise Linear Representation) to forecast Stock Trading Decision. In previous research, just few researches have focused on developing trading signals for effective stock trading. A stock trading method based on dynamic Bayesian networks is applied to model the dynamics of the trend of stock prices inn Jangmin et al .(2004) and it is a three level hierarchical hidden Markov model. This research tries to find the best way to solve these problems.

3 Applying Ensemble Neural Network –PLR to Generate Historical Turning Signals

This research applies a Piecewise Linear Representation technique to effectively select turning points from the historic stock price database first. Ensemble Neural Network has been used to train trading signals and finally a new set of input data is processed to generate a signal for stock trading decision in the future. Flow chart of the Ensemble neural network system is described as follow: (Please see figure 1).

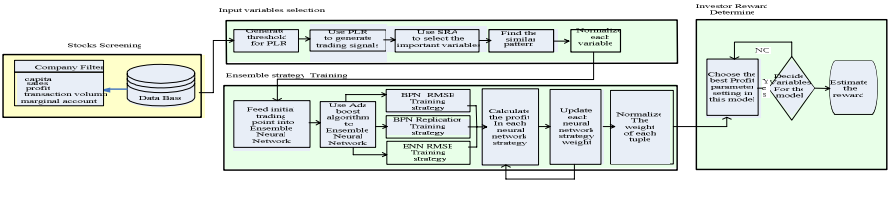

Fig. 1. The flow chart of Ensemble Neural Network model

The detail procedure describe as follows

3.1 Candidate Stocks Screening

A set of candidate stocks will be selected based on the following criteria: 1. Capital Size; 2. Monthly Sales; 3. EPS (Earnings per Share); 4. Transaction Volume per day

and 5. Marginal cost of capital (MCC). According to those indices, 7 stocks has been selected in this research.

3.2 Generating an Initial Threshold

An initial threshold is generated randomly for PLR in time series data segmentation.

3.3 Use PLR to Segment the Stock data

PLR is used to segment the selected stock data using the initial threshold generated in step 1. The stock data segmented will be transformed into trading signals. From the previous study in Abu-Mostafa(1996) and Baba et al (2000)X, trading points of stocks are observed from the variation of technical indexes. This study attempts to develop an intelligent trading point prediction system. Investors can make a good trading strategy by applying this intelligent model. This study takes a different approach by using PLR to decide the trough or peak of the historical data and based on these trading points.The main procedures of PLR in predicting the trading point has been shown in our previous workX0Xand pseudo code describe as follows:(show in Fig2).

```
Procedure BuildTree (S).
Input: A financial time series S.
Let S be represented as x[1..n], y[1..n].
If (Max (y[1..n] == y[1] OR Max (y[1..n] == y[n])
OR Min (y[1..n] == y[1] OR Min (y[1..n] == y[n]))
  Create a node in the hierarchy for this segment;
  Draw a line between (x[1],y[1]) and (x(n), y(n));
  Max d = maximum Euclidean distance of (x[i],y[i]) to the line;
  If (Max d < threshold ( δ ))
    This segment is good enough; no further work
  Else
Let (x[j],y[j]) be the point with maximum Euclidean distance to the line.
    Break the segment S into S1 and S2 at the point (x[j],y[j]);
    PARENT (S1) = S;
    PARENT (S2) = S;
    BuildTree (S1);
    BuildTree (S2);
  End If
Else
  Break the segment at the maximum and/or minimum point(s) into smaller ones S1,..., Sm;
  For i = 1 to m
    PARENT (Si) = PARENT (S);
  End For
  Delete (S);
  For i = 1 to m
    BuildTree (Si)
  End For
  End If
```

Fig. 2. The pseudo code of the PLR

3.4 Input Variables Selection Using Stepwise Regression Analysis (SRA)

As shown in TABLE 1, a set of technical indices affecting the stock price movement have been identified by Chang, et al. (2004)(2008). These input factors will be further selected using Stepwise Regression Analysis (SRA) model.

Table 1. Technical Indices used as input variables

Technical index	Technical Index (input in our system)	Explanation
Moving Average(MA)	5MA,6MA,10MA, 20MA	Moving averages are used to emphasize the direction of a trend and smooth out price and volume fluctuations that can confuse interpretation.
Bias (BIAS)	5BIAS, 10BIAS	The difference between the closing value and moving average line, which uses the stock price nature of returning back to average price to analyze the stock market.
relative strength index (RSI)	6RSI,12RSI	RSI compares the magnitude of recent gains to recent losses in an attempt to determine overbought and oversold conditions of an asset
nine days Stochastic line (K, D)	KD	The stochastic line K and line D are used to determine the signals of over-purchasing, over-selling, or deviation.
Moving Average Convergence and Divergence (MACD)	9 MACD	MACD shows the difference between a fast and slow exponential moving average (EMA) of closing prices. Fast means a short-period average, and slow means a long period one.
Williams %R (pronounced "percent R")	12W%R	Williams %R is usually plotted using negative values. For the purpose of analysis and discussion, simply ignore the negative symbols. it is best to wait for the security's price to change direction before placing your trades.
Transaction Volume	Transaction Volume	Transaction volume is a basic yet very important element of market timing strategy. Volume provides clues as to the intensity of a given price move.
Differences of technical index (•)	•5MA , •6MA, •10MA, •5BIAS , •10BIAS, •6RSI, •12RSI, •12W%R, •9K, •9D, •9 MACD	Differences of technical index between t day and t+1 day.

3.5 Normalized Variables Input to Ensemble Neural Network Strategy for Trading Point Prediction

The set of normalized variables and trading points will be inputted into BPN for training the connection weight. Once the model is trained, it can be applied for future trading point prediction.

3.6 Ensemble Neural- Networks Training Strategy

In this section, Adaboost has been used for our major ensemble strategy in this forecasting system. Adaboost is a popular boosting algorithm. In our research, we use adaboost methods to ensemble different kinds of learning Neural networks methods. These methods include BPN neural network models and Evolving Neural network models. Detail describe has been shown in our previous research Chang et al. (2004)(2006)(2008)

3.7 Ensemble Neural Network Strategy

In this section, the proposed hybrid model applied adaboost model to ensemble three different neural network models to derive the highest profit from the financial series data. AdaBoost maintains a set of training samples in weight distribution for these three models. Assume W_t is the training sample weight distribution and Adaboost uses Component Learn algorithm repeatedly in a series of cycles, i.e., k. In response, the Component Learn trains a classified h_t using the total profit earned. The weight distribution W_t is updated after each cycle according to the total profit derived from the training samples. ‘‘low- profit ’’ samples that are correctly classified h_t get lower weights, and ‘‘Higher-Profit’’ samples that get higher weights. Thus, AdaBoost focuses on the samples with higher weights and this process continues for T cycles, and

finally, AdaBoost linearly combines all the component methods into a single final hypothesis f. Greater weights are given to component methods with lower training errors. The pseduo code of Adaboost is described as follows:

```
    Input : D , a set of d class-labeled training tuples
            k , the number of rounds
            a classification
    Output : A composite model
    Method :
(1)     Initialize the weight of each tuple in D to 1/d
(2)     for i :=1 to k do
(3)       sample D with replacement according to the tuple weights to obtain DBiB ;
(4)     use training set DBiB to derive a model , MBiB ;
(5)     computer error(MBiB) , the error rate of MBiB ;
(6)       if error(MBiB) > 0.5 then
(7)         reinitialize the weights to 1/d
(8)         go back to step 3 and try again ;
(9)       endif
(10)      for each tuple in Di that was correctly classified do
(11)        multiply the weight of each by error(MBiB)/(1-error(MBiB)) ;
(12)      normalize the weight of each tuple ;
(13)    endfor
```

Fig. 3. The pseduo code of Adaboost

Through this process, we can keep the best models weight and earn most profit in our hybrid system. But how to generate profits using BPN & ENN After generate the sub-segments by using PLR, the trading signals need to be transformed into 0 or 1 before they are fed into ensemble models (includes BPN &ENN). By adopting PLR, the sub-segments will be divided and the trends of time series data are defined as follows:

$$\begin{aligned} &If\ C_i \geq C + \delta, \quad trend = upward, \\ &If\ C_i \leq C - \delta, \quad trend = downward, \\ &If\ C_i - \delta < C < C_i + \delta, \quad trend = steady, \end{aligned} \tag{1}$$

Where, C_i means the stock price of the *i*-th turning points; and *C* is the stock price of the current turning points; δ means the threshold for judging the trend of stock price. And the trend will be transferred as output value of our BPN. If the trend changes from up to down, the trading signal will be changed from 0 to 0.5; If the trend changes from down to up, the trading signal will be changed from 1 to 0.5; otherwise, the signal will not be changed.

However, the above definition of trading signal is not quite related to the price variation. A trading signal should be able to reflect the price variation and provide more inside information for investor to make a precise decision for stock trading. Therefore, we redefine the trading signals according to the tendency of the stock and it is shown in as follows:

If a stock is on up-trend

$$t_i = \left[\frac{C_i - \min\{C_i, C_{i+1}, C_{i+2}\}}{\max\{C_i, C_{i+1}, C_{i+2}\} - \min\{C_i, C_{i+1}, C_{i+2}\}} \right] \cdot 0.5. \tag{2}$$

If a stock is on down-trend

$$t_i = \left(\left[\frac{C_i - \min\{C_i, C_{i+1}, C_{i+2}\}}{\max\{C_i, C_{i+1}, C_{i+2}\} - \min\{C_i, C_{i+1}, C_{i+2}\}} \right] \cdot 0.5 \right) + 0.5, \quad (3)$$

Where C_i means the stock price of the i-th transaction day. This new definition of trading signals is more proper in representing the momentum of a stock price. The trading signals in Table 2 are recalculated and they are shown in Table 3. Instead of 0 or 1, this new trading signal is more informative and it is in the range of 0 to 1 which can provide more insightful information related to the movement of the stock price (Takes Google for example).

Table 2. The Trading Signals and t_i of Google

Time series	Stock price	Trend	Trading point	Trading signal	t_i
110	176.29	Down	Buy	1	0.5
111	171.43			1	0.7
112	169.98	Down	Buy	1	0.9
113	173.43	Down	Buy	1	0.9
114	171.65			1	0.7
115	170.45	Up	Sell	0	0.5
116	178.69			0	0
117	179.78	Down	Buy	1	0.5
118	176.47	UP	Sell	0	0.5
119	180.08			0	0
120	176.29	Down	Buy	1	0.5

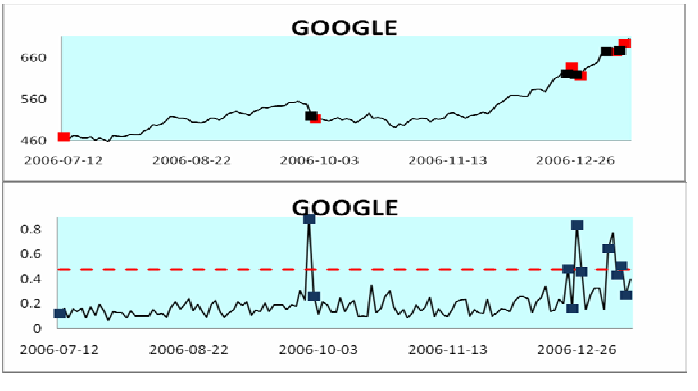

Fig. 4. The Forecasted Trading points by Ensemble neural network in Google.(red is buy, black is sell).

All t_i values will be fed into ensemble model for training the network to learn the best connection weights. After the training process, the outputs of ensemble models ([0.0, 1.0]) need to be transformed into trading decision in the testing period. In this study, the average of t_i in training stage will be regarded as the boundary when make a trading decision as shown in Table 2 . In the case example, 0.50 is the boundary.

4 Numerical Examples

Seven different stocks are selected for performance comparisons of the system in this study. All these stocks were chosen by Dow Jones Industrial Average (DJIA). These stocks span different industries and thus offer an opportunity to test our ensemble neural network on stock data. These companies include B.A. (Boeing, Aerospace & Defense), Google, C.A.T (Caterpillar, Commercial Vehicles &Trucks), D.D (DuPont Commodity, Chemicals), G.M (General Motors Automobiles), IBM (IBM, Computer Services), MSFT (Microsoft, Software) and the overall comparison of all instances will be presented in Table 3. In this research, we take IPLR in Chang et al (2008) and Genetic Program in Mallick et al .(2008) as our comparison benchmarks.

Table 3. The overall comparisons of ENNPLR, Genetic Program X0X, and IPLR X0X in Rate of Profit

Stocks	ENN-PLR	GP	IPLR
B.A	166.93%	-63.79%	95.52%
Google	39.74%	N/A	25.23%
CAT	51.49%	-33.96%	45.16%
D.D	12.69%	122.79%	10.12%
GM	149.12%	102.93%	4.13%
IBM	103.08%	522.36%	59.62%
MSFT	110.65%	-89.92%	62.16%

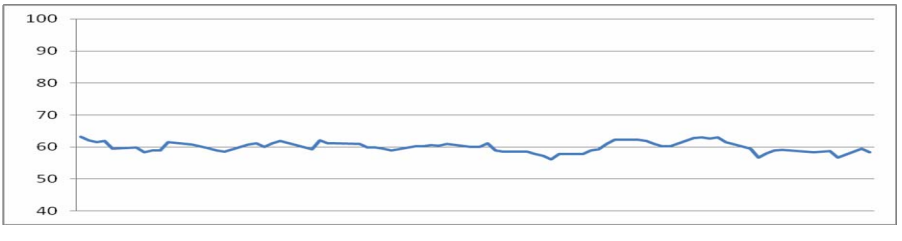

Fig. 5. The trends of CAT in steady-state

Through this table comparison, our system shows very exciting results in B.A., Google, MSFT. GM.The profit gains in other stocks do not perform very well and there are still rooms for our proposed model to improve. The reason for this partly is

because our model applies PLR to pre-define the trading points. Therefore, if the stocks are in steady-state as shown in Figure 5, PLR will not be able to detect the trading signals properly which will confuse our system thus not making the right decisions.

5 Conclusion

Considerable amount of researches have been conducted to study the behavior of a stock price movement. However, the investor is more interesting in making profit by providing simple trading decision such as Buy/Hold/Sell from the system rather than predicting the stock price itself. Therefore, we take a different approach by applying PLR to decompose the historical data into different segments. As a result, turning signals (trough or peak) of the historical stock data can be detected and then be input into the Ensemble strategy to train the connection weight of the model. Then, a new set of input data can trigger the model when a buy or sell point is detected by the Ensemble strategy. An intelligent piecewise linear representation model is further developed by integrating the Genetic Algorithm with the PLR to evolutionarily improve the threshold value of PLR to further increase the profitability of the model. The proposed system is tested on most popular stock IBM. The experimental results show that our approach can make significant and stability amount of your investment. In summary, the proposed system is very effective and encouraging in predicting the future trading points of a specific stock. However, there is one issue to be further discussed and that is the price variation of the stock. It is observed that if the price variation of the current stock to be forecasted either in a up-trend or a down-trend then it is better that we trained our model with the similar pattern, i.e., either in a similar up-trend or down-trend period in future.

References

1. Kovalerchuk, B., Vityaev, E.: Data Mining in Finance. Kluwer Academic Publisher, USA (2000)
2. Abu-Mostafa, Y.S., Atiya, A.F.: Introduction to financial forecasting. Applied Intelligence 6, 205–213 (1996)
3. Aiken, M., Bsat, M.: Forecasting Market Trends with Neural Networks. Information Systems Management 16(4), 42–48 (1994)
4. Baba, N., Inoue, N., Asakawa, H.: Utilization of Neural Networks & s for Constructing Reliable Decision Support Systems to Deal Stocks. In: IEEE-INNS-ENNS International Joint Conference on Neural Networks (IJCNN 2000), vol. 5, pp. 5111–5116 (2000)
5. Brownstone, D.: Using Percentage Accuracy to Measure Neural Network Predictions in Stock Market Movements. Neurocomputing 10, 237–250 (1996)
6. Chang, P.C., Liao, T.W.: Combing SOM and Fuzzy Rule Base for Flow Time Prediction in Semiconductor Manufacturing Factory. Applied Soft Computing 6(2), 198–206 (2006a)
7. Chang, P.C., Wang, Y.W.: Fuzzy Delphi and Back-Propagation Model for sales forecasting in PCB Industry. Expert Systems with Applications 30(4), 715–726 (2006b)
8. Chang, P.C., Fan, C.Y., Liu, C.H.: Integrating a Piecewise Linear Representation Method and a Neural Network Model for Stock Trading Points Prediction. IEEE Transactions on Systems, Man and Cybernetics Part C: Applications and Reviews (December 2008)

9. Chang, P.C., Wang, Y.W., Yang, W.N.: An Investigation of the Hybrid Forecasting Models for Stock Price Variation in Taiwan. Journal of the Chinese Institute of Industrial Engineering 21(4), 358–368 (2004)
10. Chen, A.S., Leung, M.T., Daouk, H.: Application of Neural Networks to an Emerging Financial Market: Forecasting and Trading the Taiwan Stock Index. Computers and Operations Research 30, 901–923 (2003)
11. West, D., Dellana, S., Qian, J.: Neural network ensemble strategies for financial decision applications. Computers and Operations Research 32(10), 2543–2559 (2005)
12. Hansen, L.K., Salamon, P.: Neural network ensembles. IEEE Transactions on Pattern Analysis and Machine Intelligence 12, 993–1001 (1990)
13. Pendharkar, P.C.: An empirical study of design and testing of hybrid evolutionary-neural approach for classiffcation. Omega-International Journal of Management Science 29, 361–374 (2001)
14. Schapire, R.E.: The strength of weak learnability. Machine Learning 1990.5, 197–227 (19905)
15. Henley, W.E., Hand, D.J.: A k-nearest neighbor classi&er for assessing consumer credit risk. Statistician 996.44, 77–95 (1990)
16. Jensen, H.L.: Using neural networks for credit scoring. Managerial Finance 18, 15–26 (1992)
17. Zhou, M., Wei, H.: Face Verification Using GaborWavelets and AdaBoost. In: The Eighteenth International Conference on Pattern Recognition, Hong Kong, pp. 404–407 (2006)
18. Sun, Y., Wang, Y., Wong, A.K.C.: Boosting an associative classifier. IEEE Trans. Knowledge and Data Engineering 18, 988–992 (2006)
19. Jangmin, O., Lee, J.W., Park, S.B., Zhang, B.T.: Stock Trading by Modelling Price Trend with Dynamic Bayesian Networks. In: Yang, Z.R., Yin, H., Everson, R.M. (eds.) IDEAL 2004. LNCS, vol. 3177, pp. 794–799. Springer, Heidelberg (2004)
20. Mallick, D., Lee, V.C.S., Ong, Y.S.: An empirical study of genetic programming generated trading rules in computerized stock trading service system. In: 5th International Conference Service Systems and Service Management - Exploring Service Dynamics with Science and Innovative Technology, ICSSSM 2008 (2008)

A SOM Based Stereo Pair Matching Algorithm for 3-D Particle Tracking Velocimetry

Kazuo Ohmi[1], Basanta Joshi[2], and Sanjeeb Prasad Panday[2]

[1] Dept. of Information Systems Engineering, Osaka Sangyo University, Daito-shi, Osaka 574-8530, Japan
[2] Dept. of Information Systems Engineering, Graduate Student of Faculty of Engineering, Osaka Sangyo University, Daito-shi, Osaka 574-8530, Japan
ohmi@ise.osaka-sandai.ac.jp

Abstract. A self-organizing map (SOM) based algorithm has been developed for 3-D particle tracking velocimetry (3-D PTV) in stereoscopic particle pairing process. In this process every particle image in the left-camera frame should be paired with the most probably correct partner in the right-camera frame or vice versa for evaluating the exact coordinate. In the present work, the performance of the stereoscopic particle pairing is improved by applying proposed SOM optimization technique in comparison to a conventional epipolar line analysis. The algorithm is tested with the 3-D PIV standard image of the Visualization Society of Japan (VSJ) and the matching results show that the new algorithm is capable of increasing the recovery rate of correct particle pairs by a factor of 9 to 23 % compared to the conventional epipolar-line nearest-neighbor method.

Keywords: Particle pairing problem; Particle tracking velocimetry; PIV; PTV; Stereoscopic PIV; Neural network; Self-organizing map; SOM.

1 Introduction

The basic algorithm of the 3-D particle tracking velocimetry is composed of two successive steps of particle pairing [1] (or identification of same particles) as depicted in Fig.1. The first one is the spatio-differential (parallactic) particle pairing, in which the particles viewed by two (or more) stereoscopic cameras with different viewing angles have to be correctly paired at every synchronized time stage. This is an indispensable procedure for computing the 3-D coordinates of individual particles. And the second one is the time-differential particle pairing, where the 3-D individual particles have to be correctly paired between two time stages in a short interval. Of these two steps of particle pairing, the second one is relatively rich in methodology because many of the known 2-D time-differential tracking algorithms can be extended into 3-D tracking without any additional complexity. However, the first step particle pairing is difficult when 3-D particle coordinates must be calculated with accuracy and with high recovery ratio. When the parallactic angle between the two camera axes is small (say 10 or less), some of the currently used temporal particle pairing algorithm can be applied to the spatial particle pairing, but in this

D.-S. Huang et al. (Eds.): ICIC 2009, LNAI 5755, pp. 11–20, 2009.

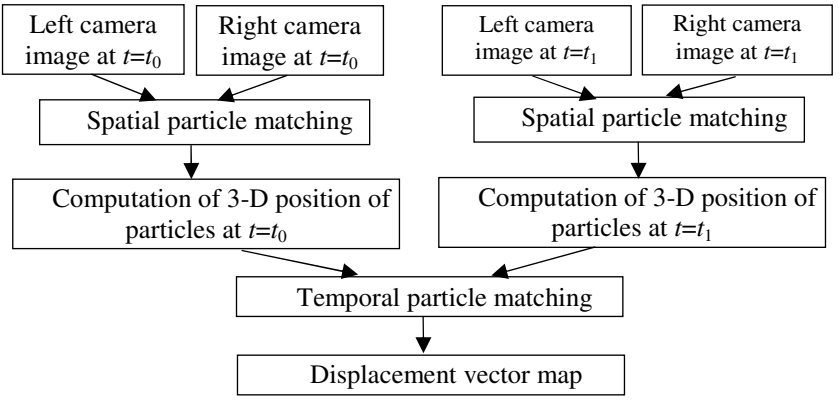

Fig. 1. Typical flow chart of 3-D particle tracking velocimetry

case, the resultant measures of particle coordinates are not so much resolved in depth direction as in the two planar directions. For more depth resolution, the parallactic angle has to be larger and the most commonly used method for the particle pairing is the epipolar line nearest neighbor analysis [2]. But with this method the recovery ratio of correct particle pairs is relatively low, especially with densely seeded particle images.

One of the present author and his coworkers have already tried to improve this low recovery ratio by using a genetic algorithm in the epipolar line nearest neighbor analysis [3] [4].The basic concept of this method is to find out a condition in which the sum of the normal distance between an epipolar line and its pairing particle image should be minimized. The accuracy of particle pairing was indeed increased to some extent but even with a new-concept high speed genetic algorithm, the computation time for particle pairing was increased exponentially with the number of particles. For this reason, realistic computation time is only met with less than 1000 particles. Another problem of the genetic algorithm is that the calculation is not reproducible because the results of genetic operations depend on random numbers. In most cases, this drawback can be cancelled by setting up a strict terminal condition for the iterative computation. But even with this the pairing results are not always reproducible if the number of pairing particles is much increased. So, In the present work,a self-organizing maps (SOM) neural network is applied to the epipolar line proximity analysis for more accuracy in the stereoscopic particle pairing with a large parallax.

2 SOM Neural Network

Neural networks are one of the most effective and attractive algorithms for the particle matching problem of the particle tacking velocimetry (PTV) because in many cases they work without preliminary knowledge of the flow field to be examined. Among others, the self-organising maps (SOM) model seems to have turned out particularly useful tool for this pupose. The principles of SOM neural network were originally proposed [5], basically aimed at clumped distribution of like terms. There was room for application of this principle to clumped distribution of correct particle

pairs between two time-differential or spatio-differential particle images. In this regard, the SOM neural network was used for 2-D time-differential particle tacking velocimetry by Labonté [6] and then improved by one of the authors [7] with successful results. In the present work SOM neural network is applied to spatio-differential particle images.

The SOM neural network consists of an input layer composed of a number of input vectors (multi-dimensional input signals) and an output (competitive) layer composed of network neurons as shown in Fig.2. All the neurons in the output layer are subject to learning from the input layer and the connection between inputs and neurons is represented by weight vectors defined for each of their combinations. According to the SOM implementation by Labonté [6] for particle pairing of the 2-D time-differential particle images, the input vectors are given by the 2-D coordinates of particle centroids in one of the two image frames and the network neurons are the relocation of particle centroids of the opposite image frame. In response to every input vector signal, the network neurons are subjected to the Kohonen learning (displacement of neurons in reality). And as a result of iteration of this Kohonen leaning, more probable particle pairs come in more proximity and less probable ones are kept away gradually.

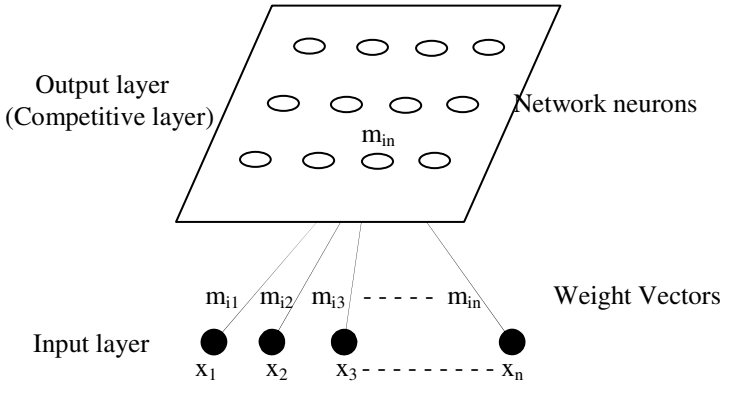

Fig. 2. SOM neural network architecture by Kohonen [5]

In spatio-differential particle matching, the SOM learning is based on the Epipolar line normal distance projected on one of the two stereoscopic camera screens. Theoretically, on either of these two camera screens, the particles viewed directly by one camera should be located exactly on their respective Epipolar lines derived from the particles viewed by the other camera. But in reality, the algebraic equation of the Epipolar line is determined through a camera calibration process, which is not free from experimental errors [1]. As a result, the particles viewed directly by each camera are not necessarily located on their respective Epipolar lines but slightly separated from them as shown Fig.3. So in order to match the particles on the two stereoscopic camera screens, minimization of the normal distance between direct-view particles and Epipolar lines is usually used as a particle match condition. But this condition is not always correctly applied as the number of particles in the image is increased. So

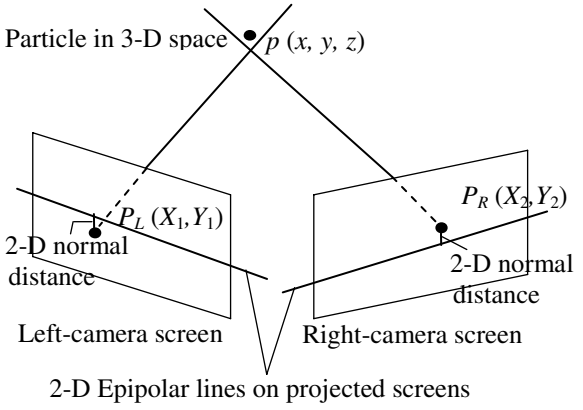

Fig. 3. Epipolar line normal distance for stereoscopic particle matching

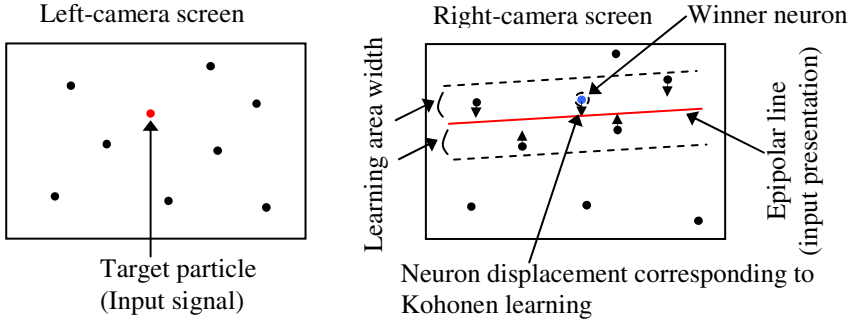

Fig. 4. Schematic illustration of one single step of Kohonen learning

the most probable coupling of the particles and their respective Epipolar lines must be found out by using some optimization method. And one of the best methods for this would be the use of the SOM neural network.

In the present case of spatio-differential particle images, the network neurons are represented by the centroid of every individual particle in one of the two image frames. But the input signal to this network is not given by the particle centroids of the opposite image frame but by the epipolar lines derived from the related particle centroids. And the Kohonen learning is realized by the displacement of neurons in the normal direction to the epipolar line presented as an input. This learning is iterated until the best possible combinations of a single particle and a single epipolar line are established as shown in Fig.4.

3 Particle Pairing and SOM Implementation

The mathematical form of the epipolar line in a stereoscopic camera arrangement can be formulated from the following perspective transform equations [8]:

$$\begin{cases} c_{11}x + c_{12}y + c_{13}z + c_{14} - c_{31}xX_1 - c_{32}yX_1 - c_{33}zX_1 = X_1 \\ c_{21}x + c_{22}y + c_{23}z + c_{24} - c_{31}xY_1 - c_{32}yY_1 - c_{33}zY_1 = Y_1 \\ d_{11}x + d_{12}y + d_{13}z + d_{14} - d_{31}xX_2 - d_{32}yX_2 - d_{33}zX_2 = X_2 \\ d_{21}x + d_{22}y + d_{23}z + d_{24} - d_{31}xY_2 - d_{32}yY_2 - d_{33}zY_2 = Y_2 \end{cases} \quad (1)$$

where x, y and z are the physical-space 3-D coordinates of a particle centroid, X_1 and Y_1 the 2-D particle coordinates on the left-camera projection screen, and X_2 and Y_2 those on the right-camera projection screen. The two sets of matrix coefficients c_{xx} and d_{xx} are the camera parameters for left and right cameras, which are determined by means of calibration using a given number of calibrated target points viewed by the same two cameras. In these equations, if either set of (X_1, Y_1) or (X_2, Y_2) is given, the other set of X and Y comes into a linear relation, providing an arithmetic equation of the relevant epipolar line. Once the camera parameters are known, for any particle image in one of the two camera frames, the corresponding epipolar line in the other camera frame is mathematically defined and, then, the normal distance between the epipolar line and any candidate pairing particle is calculated by a simple geometric algebra.

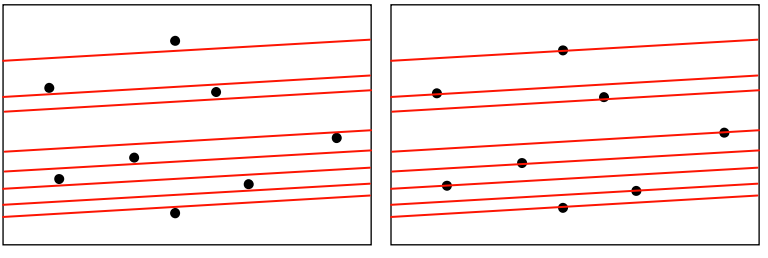

(a) Before learning (b) After learning

Fig. 5. SOM learning for stereoscopic particle pairing

The conventional stereoscopic particle pairing uses this normal distance as a definite index. For more assurance, the sum of the two normal distances for the same particle pair derived from different camera image frames is used but no more than that. By contrast, the SOM particle pairing is a kind of topological optimization process, in which more probable pairs of a particle centroid and an epipolar line come close together and others get away. The key factor of the Kohonen learning is assigning the neuron (particle centroid) with a minimum of this normal distance as winner but the learning itself applies to all the neighboring neurons. And this learning goes on with different input vector signals so that all the opposite-frame particle centroids are presented as epipolar lines as shown in Fig. 5 (a).This learning cycle is iterated until the fixed and unique combinations of a particle and an epipolar line are established as shown in Fig.5 (b).After the establishment of one to one relationship between the particle centroids, the 3D particle coordinates are computed by solving (1).

The SOM Neural network system is implemented by considering two similar networks covering the particles of the two camera frames. Let $\boldsymbol{x}_i$ (i=1,..,N) and $\boldsymbol{y}_j$ (j=1,..,M) be the 2-D coordinate vectors of the particles in the left-camera and right-camera frames respectively. The left network has N neurons situated at $\boldsymbol{x}_i$ and the right one has M neurons at $\boldsymbol{y}_j$. Each neuron has two weight vectors, corresponding to the two components of the coordinate vectors $\boldsymbol{x}_i$ and $\boldsymbol{y}_j$, and is denoted by $\boldsymbol{v}_i$ for the left network and by $\boldsymbol{w}_j$ for the right one. These weight vectors are assigned the following initial values:

$$\boldsymbol{v}_i = \boldsymbol{x}_i \quad (i = 1,..,N), \qquad \boldsymbol{w}_j = \boldsymbol{y}_j \quad (j = 1,..,M) \tag{2}$$

The weight vectors are so updated that the neurons of one network should work as stimuli for the other network. More concretely, the stimulus vector $\boldsymbol{v}_i$ from the left network is presented to the right network in the form of the corresponding epipolar line. Then, a winner neuron is selected from the latter network as the one with the weight vector closest to the epipolar line derived from $\boldsymbol{v}_i$. Let c be the index of this winner neuron and $\boldsymbol{w}_c$ its weight vector, $\boldsymbol{u}_i$ be the intersection of the epipolar line and the normal line dropped from $\boldsymbol{w}_c$, then each neuron of the right network is subjected to the following displacement of weight vectors:

$$\Delta \boldsymbol{w}_j(c) = \alpha_j(\boldsymbol{u}_i - \boldsymbol{w}_c) \qquad (j = 1,...,M), \alpha_j = \begin{cases} \alpha & \text{if neuron } j \in S_c(r) \\ 0 & \text{otherwise} \end{cases} \tag{3}$$

where α_j is a scalar variable between 0 and 1 and $S_c(r)$ the closed band region with a half width r centered by the epipolar line. The increment of weight vector in (3) is given an important modification from the original Kohonen (1982) network model, in which the right-hand term is expressed as $(\boldsymbol{u}_i - \boldsymbol{w}_c)$ instead of $(\boldsymbol{u}_i - \boldsymbol{w}_j)$. Each time the input vector, or the epipolar line derived from $\boldsymbol{v}_i$, is presented to the right network, the weight vectors of the latter network are updated according to:

$$\boldsymbol{w}_j \leftarrow \boldsymbol{w}_j + \sum_{i=1}^{N} \Delta \boldsymbol{w}_j(c_i) \qquad (j = 1,...,M) \tag{4}$$

In the next step, on the contrary, the stimulus vector $\boldsymbol{w}_j$ from the right network is presented to the left network in the form of the corresponding epipolar line. A winner neuron is selected as the closest one to the epipolar line. Each time the weight vector $\boldsymbol{w}_j$ is presented to the left network, the weight vectors of the latter network are updated according to:

$$\boldsymbol{v}_i \leftarrow \boldsymbol{v}_i + \sum_{j=1}^{M} \Delta \boldsymbol{v}_i(c_j) \qquad (i = 1,...,N) \tag{5}$$

Each time the weight vectors from either network are updated, the width r of the band region, within which the weight vectors of neurons are changed, is altered by $r \leftarrow \beta r$ $(0 < \beta < 1)$. At the same time, the amplitude α of the weight translation is altered by $\alpha \leftarrow \alpha / \beta$.

These alternate steps are iterated until the width r of the band reaches a given threshold value of r_f, which should be small enough to include only the winner neuron. Since the resultant correspondence between a left network neuron and its matching

right network neuron is not always reciprocally identical, a final nearest-neighbor check is done with a neighborhood criterion of small distance ε Out of the probable neurons in the neighborhood, a tolerance distance ε is set, within which two neuron weight vectors will be considered equal. The solution time can be shortened by taking εlarger.

4 Results and Discussion

The present new particle pairing algorithm is tested by using synthetic particle images, namely the PIV Standard Images by Okamoto[9], which are now available at the web site of the Visualization Society of Japan (http://vsj.or.jp/piv/). Out of 6 sets of 3-D particle images offered at this site, only 4 image sets (Series #351, #352, #371 and #377) are selected for the present work. Table 1 gives the technical details of all these Standard Images. All of these are synthetic particle images showing different portions of a 3-D transient flow induced by an impinging jet. The parallax angle between the view axes of the two cameras is also different from series to series. In order to simulate particle refraction effect in a real experimental environment, the use of cylindrical volume illumination and water refractive index of 1.33 are taken into account.

Fig.6 shows a sample pair of the 3-D PIV Standard Image tested in the present work and Fig.7 is the corresponding pair of marker particle images used for the

Table 1. Summary of the tested 3-D PIV Standard Images

Series # / Frame #		352 / 0000	351 / 0000	371 / 0000	377 / 0000
Number of existing particles		372	2092	366	939
Minimum /Mean particle diameter		1/5 pix	1/5 pix	1/5 pix	1/5 pix
Standard deviation of diameter		2 pix	2 pix	2 pix	2 pix
Volume of visualized flow (in situ)		2cm3	2cm3	1cm3	0.5cm3
Maximum flow rate (in situ)		12 cm/sec	12 cm/sec	12 cm/sec	12 cm/sec
Refraction index		1.33	1.33	1.33	1.33
Number of calibr. marker particles		27	27	125	27
Left camera	Distance to origin center	20 cm	20 cm	20 cm	11.5 cm
	Inclination from x-axis	-30 deg	-30 deg	-30 deg	-29.9 deg
	Inclination from y-axis	0 deg	0 deg	-10 deg	-45 deg
	Inclination from z-axis	0 deg	0 deg	0 deg	16.1 deg
Right camera	Distance to origin center	20 cm	20 cm	20 cm	11.5 cm
	Inclination from x-axis	30 deg	30 deg	30 deg	0 deg
	Inclination from y-axis	0 deg	0 deg	-10 deg	-90 deg
	Inclination from z-axis	0 deg	0 deg	0 deg	30 deg

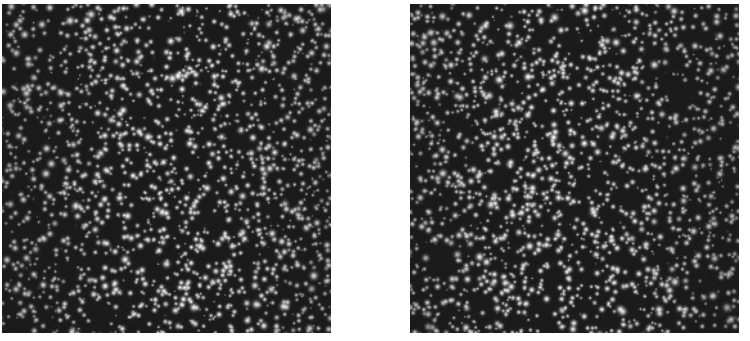

(a) Left frame (frame# 0000) (b) Right frame (frame# 2000)

Fig. 6. 3-D PIV Standard Images – Series #351

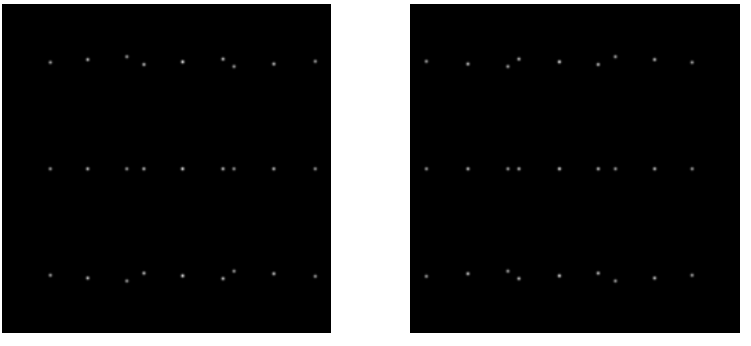

(a) Left frame (frame# 0999) (b) Right frame (frame# 2999)

Fig. 7. 3-D calibration marker images – Series #351

stereoscopic camera calibration In each calibration image, there are 27 calibration points in a cubic cell arrangement with known absolute coordinates in a real 3-D space and they are used for computing the 11 camera parameters of each camera which becomes input to (1).

The particle pairing results from these 3-D PIV Standard Images are shown in Table 2, in which the performance of the two algorithms (epipolar-line nearest-neighbor pairing with and without SOM) are compared in terms of the "correct pair rate". The SOM computation parameters for these four series of PIV images are kept within: r (initial radius) = 5, r_f (final radius) = 0.01 to 0.001, α(initial translation rate) = 0.05 to 0.005, β(attenuation rate) = 08 to 0.9 and ε(max distance for final pairing) = 0.01. It can be seen from these results that the performance of the particle pairing is improved with the introduction of the SOM neural network strategy and this improvement is more marked when the number of existing particles is increased up to 1000 or more. This is indicative of the practical-use effectiveness of the SOM neural

Table 2. Particle pairing results with or without SOM neural network

Series # / Frame #	Particle pairing with SOM			Particle pairing without SOM		
	Number of existing particle pairs	Number of correct pairs	Correct pair rate	Number of existing particle pairs	Number of correct pairs	Correct pair rate
#352/000	283	263	92.93 %	283	239	84.45 %
#351/000	1546	1129	73.03 %	1546	986	63.78 %
#371/000	157	145	92.36 %	157	134	85.35 %
#377/000	352	286	81.25 %	352	233	66.19 %

network particle pairing for 3-D particle tracking velocimetry. The computational cost variation for Image #352, #371, #377 is about 1 sec(s) and that of Image #351 is 20s. However, the computational cost variation for the proposed algorithm with reference to previous algorithms is insignificant.

Further, it was observed that correct pairing rate for the performance is even better than that of the genetic algorithm particle pairing proposed earlier by the one of the author and his coworkers [3] [4]. Another merit of the SOM neural network particle pairing is that the performance is considerably stable regardless of the optical conditions of particle imaging. Even with or without incidence, yaw and roll angles of the two stereoscopic cameras, the correct pair rate keeps a constantly high level. This is certainly important when the stereoscopic PTV has to be employed in many industrial applications, where the positions of cameras and of laser light units are more or less restricted.

5 Conclusions

A SOM neural network based algorithm was successfully implemented for the stereoscopic particle pairing step in 3D particle tracking velocimetry and tested with the PIV standard image data. With this scheme, the overall performance of particle pairing is improved and the correct pairing rate for two sets of the synthetic 3D particle images goes up to 93%. The increase factor is not dramatic but it should be noted here that the accuracy of the subsequent time series particle tracking is fairly sensitive to that of the parallactic particle pairing. A slight improvement of the parallactic particle pairing may cause considerable increase in the correct time series particle tracking in the 3D particle tracking velocimetry. Further, efforts should be made to apply the methodology to more densely seeded particle images with larger numbers of particles. Moreover, the particle matching process can be made more accurate in presence of loss-of-pair particles.

References

1. Mass, H.G., Gruen, A., Papantoniou, D.: Particle tracking velocimetry in three-dimensional flows. Experiments in Fluids 15, 133–146 (1993)
2. Nishino, K., Kasagi, N., Hirata, M.: Three-dimensional particle tracking velocimetry based on automated digital image processing. Trans. ASME, J. Fluids Eng. 111, 384–391 (1989)
3. Ohmi, K., Yoshida, N.: 3-D Particle tracking velocimetry using a genetic algorithm. In: Proc. 10th Int. Symposium Flow Visualization, Kyoto, Japan, F0323 (2002)
4. Ohmi, K.: 3-D particle tracking velocimetry with an improved genetic algorithm. In: Proc. 7th Symposium on Fluid Control, Measurement and Visualization, Sorrento, Italy (2003)
5. Kohonen, T.: A simple paradigm for the self-organized formation of structured feature maps. In: Competition and cooperation in neural nets. Lecture notes in biomathematics, vol. 45. Springer, Heidelberg (1982)
6. Labonté, G.: A new neural network for particle tracking velocimetry. Experiments in Fluids 26, 340–346 (1999)
7. Ohmi, K.: Neural network PIV using a self-organizing maps method. In: Proc. 4th Pacific Symp. Flow Visualization and Image Processing, Chamonix, France, F-4006 (2003)
8. Hall, E.L., Tio, J.B.K., McPherson, C.A., Sadjadi, F.A.: Measuring Curved Surfaces for Robot Vision. Computer 15(12), 42–54 (1982)
9. Okamoto, K., Nishio, S., Kobayashi, T., Saga, T., Takehara, K.: Evaluation of the 3D-PIV Standard Images (PIV-STD Project). J. of Visualization 3(2), 115–124 (2000)

Spiking Neural Network Performs Discrete Cosine Transform for Visual Images

Qingxiang Wu, T.M. McGinnity, Liam Maguire, Arfan Ghani, and Joan Condell

Intelligent Systems Research Centre, University of Ulster at Magee Campus
Derry, BT48 7JL, Northern Ireland, UK
{q.wu,tm.mcginnity,lp.maguire,a.ghani,j.condell}@ulster.ac.uk

Abstract. The human visual system demonstrates powerful image processing functionalities. Inspired by the principles from neuroscience, a spiking neural network is proposed to perform the discrete cosine transform for visual images. The structure and the properties of the network are detailed in this paper. Simulation results show that the network is able to perform the discrete cosine transform for visual images. Based on this mechanism, the key features can be extracted in ON/OFF neuron arrays. These key features can be used to reconstruct the visual images. The network can be used to explain how the spiking neuron-based system can perform key feature extraction. The differences between the discrete cosine transform and the spiking neural network transform are discussed.

Keywords: spiking neural networks; visual system; discrete cosine transform; visual image.

1 Introduction

The human visual system demonstrates powerful image processing functionalities. The retina contains complex circuits of neurons that extract salient information from visual inputs. Signals from photoreceptors are processed by retinal interneurons, integrated by retinal ganglion cells and sent to the brain by axons of retinal ganglion cells. Different cells respond to different visual features, such as light intensity, colour or moving objects [1–5]. Mammalian retinas contain approximately 55 distinct cell types, each with a different function [1]. The exact neuronal circuits for extraction of key features and identification of various visual images still need to be determined. Similarly, there is a need to simulate the neuronal circuits in electronic circuits as a precursor to their application in artificial intelligent systems. These are still open questions. The Discrete Cosine Transform (DCT) [6] is an efficient approach for key feature extraction in the image processing domain. Based on the spiking neuron model [7-12], a neuronal circuit is proposed to perform discrete cosine transform and explain how a spiking neural network can extract key features of a visual image. The neuronal circuit has been simulated using Matlab and the results show that the key features of a visual image can be extracted by the neural network and the visual image can be reconstructed using the key features.

D.-S. Huang et al. (Eds.): ICIC 2009, LNAI 5755, pp. 21–29, 2009.

The remainder of this paper is organized as follows. In Section 2, the architecture of the neural network is proposed to extract the key features and the network is shown to be able to reconstruct the visual image. The network model is based on simplified conductance-based integrate-and-fire neurons. The behaviors of the neural network are governed by a set of equations discussed in Section 3. Simulation results are presented in Section 4. The network performance is discussed in Section 5.

2 Spiking Neural Network Model for Discrete Cosine Transform

The human visual system performs feature extraction very efficiently. Neuroscientists have found that there are various receptive fields from simple cells in the striate cortex to those of the retina and lateral geniculate nucleus [13]. The different pathways, which are composed of different types of neurons, play different roles in the visual system. ON/OFF pathways [3] were found in the visual system. Inspired by the mechanism of ON/OFF pathways, a spiking neural network model is proposed to perform the discrete cosine transform as shown in Fig. 1.

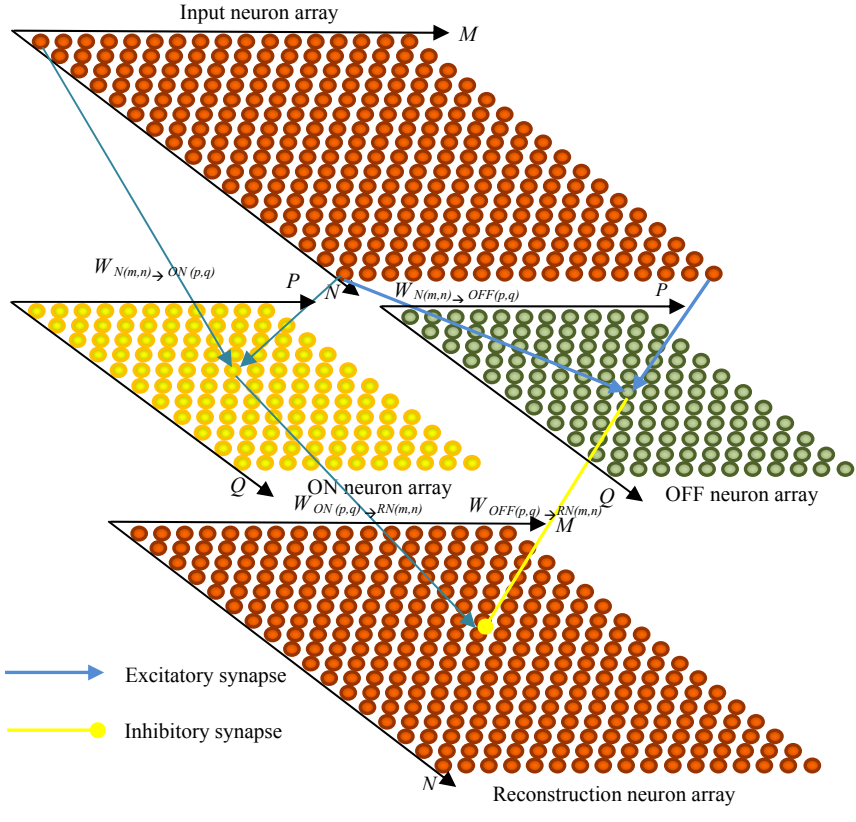

Fig. 1. Spiking neural network for feature extraction and image reconstruction

Suppose that each neuron in the input neuron array generates spikes induced by a synapse current of photonic receptor according to the corresponding pixel brightness in a visual image. The dimension of the input neuron array is $M \times N$. A neuron in the array is labeled with $N(m, n)$, where $m=0,\ldots,M-1$ and $n=0,\ldots,N-1$. Each pixel of the image corresponds to a receptor. The intermediate layer is composed of two neuron arrays; one is the ON neuron array and other is the OFF neuron array. The ON/OFF neuron arrays have the same dimension $P \times Q$, where $P \le M$ and $Q \le N$. Neurons in the ON/OFF neuron arrays are labeled with ON(p, q) and OFF(p, q), where $p=0,\ldots,P-1$ and $q=0,\ldots,Q-1$. Each neuron in the ON/OFF arrays receives spike trains from all neurons in the input array through excitatory synapses with specific strength distributions $W_{N(m,n)\to ON(p,q)}$ for ON neurons and $W_{N(m,n)\to OFF(p,q)}$ for the OFF neurons. Based on the principle of the Discrete Cosine Transform (DCT)[6], synapse strength distribution can be set as follows.

$$W_{N(m,n)\to \mathrm{ON}(p,q)} = \begin{cases} \alpha_p \alpha_q \cos\dfrac{\pi(2m+1)p}{2M}\cos\dfrac{\pi(2n+1)q}{2N}, & if \cos\dfrac{\pi(2m+1)p}{2M}\cos\dfrac{\pi(2n+1)q}{2N} > 0 \\ 0, & if \cos\dfrac{\pi(2m+1)p}{2M}\cos\dfrac{\pi(2n+1)q}{2N} \le 0 \end{cases} \tag{1}$$

$$W_{N(m,n)\to \mathrm{OFF}(p,q)} = \begin{cases} -\alpha_p \alpha_q \cos\dfrac{\pi(2m+1)p}{2M}\cos\dfrac{\pi(2n+1)q}{2N}, & if \cos\dfrac{\pi(2m+1)p}{2M}\cos\dfrac{\pi(2n+1)q}{2N} < 0 \\ 0, & if \cos\dfrac{\pi(2m+1)p}{2M}\cos\dfrac{\pi(2n+1)q}{2N} \ge 0 \end{cases} \tag{2}$$

where $0 \le p \le M-1$, and $0 \le q \le N-1$,

$$\alpha_p = \begin{cases} 1/\sqrt{M}, & p = 0 \\ \sqrt{2/M}, & 1 \le p \le M-1 \end{cases}, \alpha_q = \begin{cases} 1/\sqrt{N}, & q = 0 \\ \sqrt{2/N}, & 1 \le q \le M-1 \end{cases} \tag{3}$$

If less neurons are used in the ON/OFF neuron arrays, i.e. $P<<M$ and $Q<<N$, only key features remain. Using these key features the visual image can still be reconstructed. The reconstruction neuron layer is used to demonstrate reconstruction of the visual image using these key features. Suppose that all neurons in the ON array connect to a neuron in the reconstruction neuron array with excitatory synapses with specific strength distribution $W_{ON(m,n)\to RN(p,q)}$ and all neurons in the OFF array connect to the same neuron with inhibitory synapses with specific strength distribution $W_{OFF(m,n)\to RN(p,q)}$. Fig.1 demonstrates a neuron in the reconstruction array receiving spikes through excitatory synapse from an ON neuron and through inhibitory synapse from an OFF neuron. The strength distribution is set as follows.

$$W_{ON(p,q)\to RN(m,n)} = W_{N(m,n)\to ON(p,q)} \tag{4}$$

$$W_{OFF(p,q)\to RN(m,n)} = W_{N(m,n)\to OFF(p,q)} \tag{5}$$

If the key features appear in the ON/OFF neuron arrays, the image will be reconstructed in the reconstruction neuron array. A colour image can be dealt with similar networks, in three chanels corresponding to R, G, B colours.

3 Spiking Neuron Model and Simulation Algorithms

Considering computational cost, a simplified conductance-based integrate-and-fire neuron model is used to simulate the network. Let $G_{m,n}(t)$ represent the gray scale of an image pixel at a point (m, n) at time t. Suppose that each photonic receptor transfers the image pixel brightness to a synapse current $I_{m,n}(t)$. The synapse current can be represented as follows:

$$\frac{dI_{m,n}(t)}{dt} = -\frac{1}{\tau} I_{m,n}(t) + \alpha G_{x,y}(t). \tag{6}$$

where α is a constant for transformation from pixel value to current, and τ is a time constant for decay of the synapse current. According to the integrate-and-fire neuron model [6-11], the potential of a neuron $N(m, n)$ is governed by the following equation:

$$c\frac{dv_{m,n}(t)}{dt} = g_l(E_l - v_{m,n}(t)) + I_{m,n}(t) + I_0\,, \tag{7}$$

where g_l is the membrane conductance, E_l is the reverse potential, $v_{m,n}(t)$ is the membrane potential of the neuron $N(m, n)$, c represents a capacitance of the membrane, and I_0 is simulated by an average current produced by background noise. If the membrane potential passes threshold v_{th}, then the neuron generates a spike. Let $S_{m,n}(t)$ represent the spike train generated by the neuron such as that:

$$S_{m,n}(t) = \begin{cases} 1 & if\ neuron\ (m,n)\ fires\ at\ time\ t. \\ 0 & if\ neuron\ (m,n)\ does\ not\ fire\ at\ time\ t. \end{cases} \tag{8}$$

Through equations (6)-(8), gray scale $G_{m,n}(t)$ has been transferred to spike trains. These spike trains are transferred to the ON/OFF neuron arrays in the intermediate layer through excitatory synapses with strength distributions $W_{N(m,n)\to ON(p,q)}$ and $W_{N(m,n)\to OFF(p,q)}$. As each neuron in the ON/OFF arrays receives all spikes from the top neuron array, the total synapse currents $I_{ON(p,q)}(t)$ and $I_{OFF(p,q)}(t)$, which are caused by the spikes, can be represented as follows.

$$\frac{dI_{ON(p,q)}(t)}{dt} = -\frac{1}{\tau} I_{ON(p,q)}(t) + \sum_{m=0}^{M-1}\sum_{n=0}^{N-1} W_{N(m,n)\to ON(p,q)} \beta S_{m,n}(t)\,, \tag{9}$$

$$\frac{dI_{OFF(p,q)}(t)}{dt} = -\frac{1}{\tau} I_{OFF(p,q)}(t) + \sum_{m=0}^{M-1}\sum_{n=0}^{N-1} W_{N(m,n)\to OFF(p,q)} \beta S_{m,n}(t)\,, \tag{10}$$

where β is a constant. The neuron potential $v_{ON(p,q)}(t)$ in the ON array is governed by the following equation:

$$c\ \frac{dv_{ON(p,q)}(t)}{dt} = g_l(E_l - v_{ON(p,q)}(t)) + I_{ON(p,q)}(t) + I_0\,. \tag{11}$$

Potential $v_{OFF(p,q)}(t)$ in the OFF array is governed by following equation.

$$c\ \frac{dv_{OFF(p,q)}(t)}{dt} = g_l(E_l - v_{OFF(p,q)}(t)) + I_{OFF(p,q)}(t) + I_0 \cdot \tag{12}$$

Let $S_{ON(p,q)}(t)$ represent a spike train which is generated by the ON neurons and $S_{OFF(p,q)}(t)$ represent a spike train which is generated by the OFF neurons such that:

$$S_{ON(p,q)}(t) = \begin{cases} 1 & \text{if ON neuron } (p,q) \text{ fires at time } t. \\ 0 & \text{if ON neuron } (p,q) \text{ does not fire at time } t. \end{cases} \tag{13}$$

$$S_{OFF(p,q)}(t) = \begin{cases} 1 & \text{if OFF neuron } (p,q) \text{ fires at time } t. \\ 0 & \text{if OFF neuron } (p,q) \text{ does not fire at time } t. \end{cases} \tag{14}$$

For the reconstruction neuron array (bottom layer), each neuron $RN(m,n)$ receives spikes from all neurons in the ON array through excitatory synapses and receives spikes from all neurons in the OFF array through inhibitory synapses. The synapse current to neuron $RN(m, n)$ is as follows:

$$\begin{aligned} \frac{dI_{RN(m,n)}(t)}{dt} = & -\frac{1}{\tau} I_{RN(m,n)}(t) + \sum_{p=0}^{P-1}\sum_{q=0}^{Q-1} W_{ON(p,q)\to RN(m,n)} \gamma S_{ON(p,q)}(t) \\ & - \sum_{p=0}^{P-1}\sum_{q=0}^{Q-1} W_{OFF(p,q)\to RN(m,n)} \gamma S_{OFF(p,q)}(t), \end{aligned} \tag{15}$$

where γ is a constant. The membrane potential of the neuron $RN(m,n)$ is governed by the following equation:

$$c\ \frac{dv_{RN(m,n)}(t)}{dt} = g_l(E_l - v_{RN(m,n)}(t)) + I_{RN(m,n)}(t) + I_0 \cdot \tag{16}$$

Let $S_{RN(m,n)}(t)$ represent spike train generated by the neuron $RN_{(m,n)}$ in the bottom layer. The firing rate for the neuron $RN_{(m,n)}$ is calculated by the following expression:

$$r_{RN(m,n)}(t) = \frac{1}{T}\sum_{t}^{t+T} S_{RN(m,n)}(t)\,. \tag{17}$$

A firing rate map can be obtained by plotting $r_{RN(m,n)}(t)$. Let r_{max} represent the maximum firing rate in the neuron array. The reconstructed image $R_{m,n}(t)$ with 255 gray scale levels is obtained using the following equation:

$$R_{m,n}(t) = \frac{255}{r_{\max}} r_{RN(m,n)}(t)\,. \tag{18}$$

4 Simulation Results

This network is simulated in Matlab using the Euler method with a time step of 0.1 ms. Corresponding to biological neurons [9], the following parameters for the

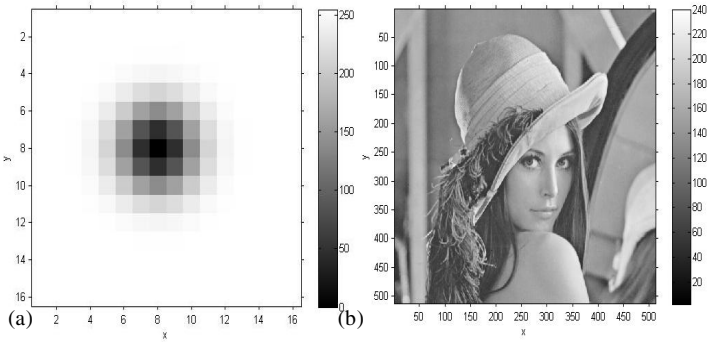

Fig. 2. Images to test network: (a)Gaussian grayscale distribution; (b)Lena image

network were used in the experiments. v_{th} = -60 mv. E_l= -70 mv. g_l=1.0 μs/mm^2. c=8 nF/mm^2. τ = 16ms. T=400ms. These parameters can be adjusted to get a good quality output image. α=0.02. β=0.13. γ=5.1. I_0=7μA. These parameters can be determined by trial/error method according to single neuron behaviours.

In order to demonstrate the behavior of the network, two images (as shown in Fig.2) are presented to the network. Fig.2(a) is a black point with a Gaussian gray scale distribution in a 16×16 area (shown with increased pixel size for clarity). Fig. 2(b) is the Lena image which is widely used as a benchmark image in the image processing domain. When the Gaussian black point presented to the network for a period 400ms, the firing rate maps of top-right 8×8 neurons in the ON/OFF neuron arrays are shown in Fig.3(a) and Fig.3(b). If these firing patterns go to the bottom neuron array through excitatory and inhibitory synapses shown in Fig.1, a firing rate map of the reconstruction array is obtained in Fig.3(c). Transformed the firing rate map to a gray scale image by Equation (18), the result is obtained in Fig.3(d). This means that the key feature of the Gaussian black point in dimension 16×16 can be preserved by the firing patterns of the ON/OFF neuron arrays in dimension 8×8. If the dimension of the ON/OFF array is the same as the N neuron array (top layer), almost the same black point can be obtained in the construction image shown in Fig.3(e). If less neurons are used to preserve the pattern in the ON/OFF arrays (e. g. only 4×4 neurons in the ON/OFF arrays are used), a black point will be obtained in the reconstruction image Fig.3(f). It is more vague than Fig.3(d), however the key features still remain. This example shows that the key features can be preserved by a small number of top-right neurons in the ON/OFF arrays.

In order to demonstrate this behaviour further the network was used to transfer the Lena image (see Fig. 2(b)). In our experiments, the Lena image (512×512) has been divided into 32×32 blocks. Each block contains 16×16 pixels. Each block is transferred to ON/OFF firing patterns with only 4×4 neurons, and then the firing pattern is transferred to the reconstructed image blocks. Reconstructed image blocks are put together to form a fully reconstructed image as shown in Fig. 4(a). This image is comparable with the DCT reconstructed image in Fig. 4(b) with a 4×4 mask filter. Comparing Fig. 4(a) to the original Lena image in Fig. 2(b) the deference errors can be computed as shown in Fig. 4(c) which is also comparable with the DCT errors shown in Fig. 4(d).

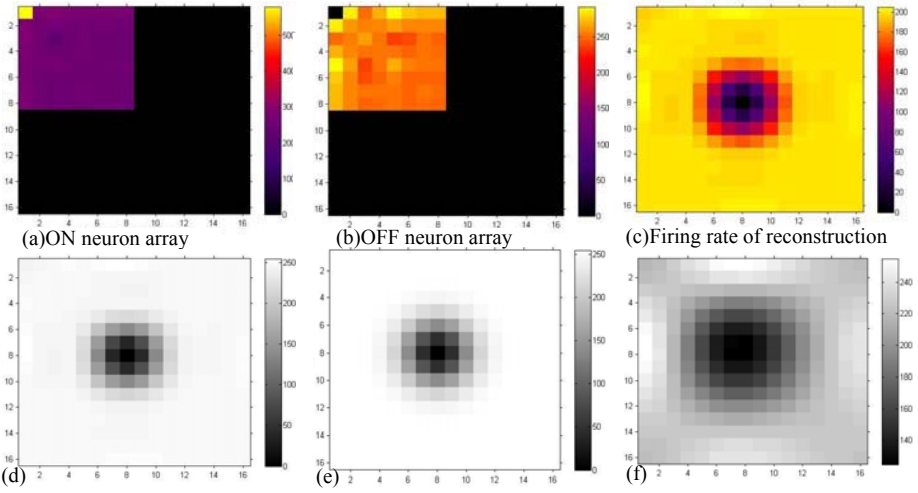

Fig. 3. Firing rate in neuron arrays (a-c) and reconstructed images (d-f)

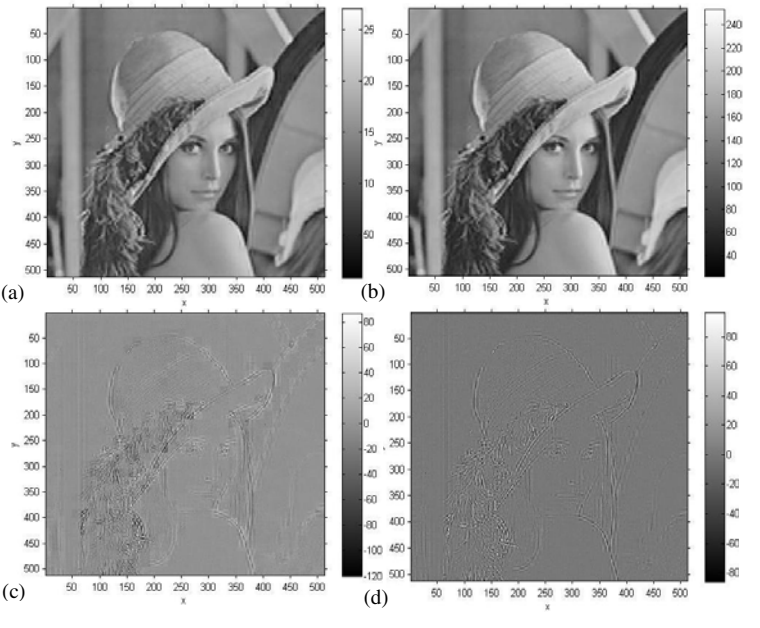

Fig. 4. Comparison between SNN network and DCT results

5 Discussion

Using ON/OFF neuron pathways, a spiking neural network is proposed to extract features from a visual image. An integrate-and-fire spiking neuron model and a synapse current mechanism are used to construct and simulate the network. The experimental results show that the network can perform the image transformation similar to the discrete cosine transform and can be used to extract key features in visual images. In the simulations the network is assumed to be implemented in a fully parallel network like biological system. The results can be achieved by presenting test images to the network for 400ms. If the hardware implementation of the network can reach the speed as same as biological neuron network, the key feature extraction can be completed in 400ms, and this network can be applied to spiking neuron-based artificial intelligent systems to extract key features from visual images. However, there are still some issues for discussion. (1) It is very efficient for the brain to extract key features from a visual image. This network can be used to explain how the spiking neuron-based network is capable of extracting key features in the manner of the proposed network. Further research is required to establish the actual mechanisms employed by the visual cortex. (2) In this network, the information is transferred based on spike trains. Using such a biological information transfer manner, the network is more robust to noise. For example, the average noise current has been considered in the simulation. However it is very difficult to exactly perform the inverse transform as in mathematical discrete cosine transforms. (3) In this paper, the synapse strength distributions are set based on principles taken from discrete cosine transform theory. If it is considered to use the spike timing dependent plasticity of synapses, it is possible to train the network to obtain the synapse strength using sample visual images. This is a topic for further study.

References

1. Masland, R.H.: The Fundamental Plan of the Retina. Nature Neurosci. 4, 877–886 (2001)
2. Wassle, H.: Parallel Processing in the Mammalian Retina. Nature Rev. Neurosci. 5, 747–757 (2004)
3. Nelson, R., Kolb, H.: On and Off Pathways in the Vertebrate Retina and Visual System. In: Chalupa, L.M., Werner, J.S. (eds.) The Visual Neurosciences, pp. 260–278. MIT Press, Cambridge (2003)
4. Demb, J.B.: Cellular Mechanisms for Direction Selectivity in the Retina. Neuron 55, 179–186 (2007)
5. Taylor, W.R., Vaney, D.I.: New Directions in Retinal Research. Trends Neurosci. 26, 379–385 (2003)
6. Ahmed, N., Natarajan, T., Rao, K.R.: Discrete Cosine Transform. IEEE Trans. Computers, 90–93 (1974)
7. Koch, C.: Biophysics of Computation: Information Processing in Single Neurons. Oxford University Press, Oxford (1999)
8. Dayan, P., Abbott, L.F.: Theoretical Neuroscience: Computational and Mathematical Modeling of Neural Systems. The MIT Press, Cambridge (2001)
9. Gerstner, W., Kistler, W.: Spiking Neuron Models: Single Neurons, Populations, Plasticity. Cambridge University Press, Cambridge (2002)

10. Müller, E.: Simulation of High-Conductance States in Cortical Neural Networks. Masters thesis, University of Heidelberg, HD-KIP-03-22 (2003)
11. Wu, Q.X., McGinnity, T.M., Maguire, L.P., Glackin, B., Belatreche, A.: Learning Mechanism in Networks of Spiking Neurons. In: Studies in Computational Intelligence, vol. 35, pp. 171–197. Springer, Heidelberg (2006)
12. Wu, Q., McGinnity, T.M., Maguire, L.P., Belatreche, A., Glackin, B.: Adaptive coordinate transformation based on a spike timing-dependent plasticity learning paradigm. In: Wang, L., Chen, K., S. Ong, Y. (eds.) ICNC 2005. LNCS, vol. 3610, pp. 420–428. Springer, Heidelberg (2005)
13. Kandel, E.R., Shwartz, J.H.: Principles of Neural Science. Edward Amold Publishers Ltd., London (1981)

Spam Detection Based on a Hierarchical Self-Organizing Map

Esteban José Palomo, Enrique Domínguez, Rafael Marcos Luque, and José Muñoz

Department of Computer Science
E.T.S.I. Informatica, University of Malaga
Campus Teatinos s/n, 29071 – Malaga, Spain
{ejpalomo,enriqued,rmluque,munozp}@lcc.uma.es

Abstract. The GHSOM is an artificial neural network that has been widely used for data clustering. The hierarchical architecture of the GHSOM is more flexible than a single SOM since it is adapted to input data, mirroring inherent hierarchical relations among them. The adaptation process of the GHSOM architecture is controlled by two parameters. However, these parameters have to be established in advance and this task is not always easy. In this paper, a new hierarchical self-organizing model that has just one parameter is proposed. The performance of this model has been evaluated by building a spam detector. Experimental results confirm the goodness of this approach.

Keywords: Data clustering, hierarchical self-organization, spam detection.

1 Introduction

Concern about the proliferation of unsolicited bulk email, commonly referred to as spam, has been steadily increasing. The spam concept is diverse: advertisements for products and web sites, make money fast schemes, chain letters, pornography, etc. As spam recipients become increasingly annoyed, Internet Service Providers (ISPs) have been deluged with complaints. Furthermore, some ISPs report that spam places a considerable burden on their systems. A variety of technical countermeasures to spam have been proposed: the simplest are already being implemented; some of the more extreme could require dramatic changes to the ways we communicate electronically [1]. Unlike traditional techniques, clustering methods analyze the message content and classify the e-mail consistently.

Data clustering is an unsupervised learning method to find a structure in a collection of unlabeled input data that are usually represented as feature vectors in a high-dimensional space. This structure represents most similar input data into a cluster according to a similarity measure, where data belonging to one cluster are most similar than data belonging to different clusters. These methods are especially useful when no information about input data is available.

D.-S. Huang et al. (Eds.): ICIC 2009, LNAI 5755, pp. 30–37, 2009.

Several clustering techniques have addressed the spam problem, including neural networks [2,3]. The self-organizing map (SOM) has been widely used for detecting inherent structures in high-dimensional data and mapping these data into a two-dimensional representation space [4]. This mapping retains the relationship among input data and preserves their topology. The main advantage of this method is visual understanding of data structure. However, SOMs have fixed network architecture in terms of size and arrangement of neurons, which has to be defined in advance. In addition, hierarchical relations among input data are not represented. The growing hierarchical SOM (GHSOM) was proposed in [5] to solve both limitations. This neural network model has a hierarchical architecture of layers, where each layer is composed of different single SOMs with an adaptative architecture that is determined during the unsupervised learning process according to input data.

Each map in the GHSOM is a growing SOM [6], which add rows or columns of neurons to adapt the map to input data. After growing, each neuron of the map is analyzed to see whether they represent their mapped data at a specific level of granularity. Those neurons that represent too heterogeneous input data are expanded to form a new map at a subsequent layer. Growing and expansion in a GHSOM are controlled by two parameters: τ_1 and τ_2, respectively. These parameters have to be defined prior to training. Although these parameters provide flexibility to choose the size of the neural network, it remains far from trivial to determine and combine the two parameters that provide satisfying results.

In this paper, a new GHSOM model that has just one parameter to control the growing and expansion of the architecture is proposed. This parameter keeps providing the flexibility to choose the size of the network and at the same time makes easy its election. The elimination of one parameter is consequence of analyzing the differences between growing and expansion in the GHSOM model.

The effectiveness of this approach has been evaluated by building a spam detection system. To this end, the new model has been trained and tested with the Spambase data set from UCI Machine Learning repository [7].

The remainder of this paper is organized as follows. Section 2 describes the new GHSOM model proposed. In Section 3, a spam detector based on the new approach is introduced. Then, some experimental results are presented by using the Spambase dataset. Section 4 concludes this paper.

2 New Hierarchical Self-Organizing Map

2.1 GHSOM Overview

The GHSOM has a hierarchical architecture, where SOM-like neural networks with adaptive architecture build the various layers of the hierarchy [5]. Initially, the GHSOM consists of a single SOM of 2x2 neurons. During the training, the SOM can grow by adding neurons until reach a certain level of detail in the representation of the data mapped onto the SOM. After growing, each neuron of the map has to be checked to see whether they represent a set of heterogeneous

or homogeneous input data. If a neuron has a bad representation of the data, it is expanded in a new map in the next layer of the hierarchy in order to provide a more detailed representation. Once training has finished, the GHSOM mirrors the inherent structure of the input patterns, improving the representation achieved with a single SOM. Therefore, each neuron represents a data cluster, where data belonging to one cluster are more similar than data belonging to different clusters. An example of a GHSOM architecture is shown in Fig.1.

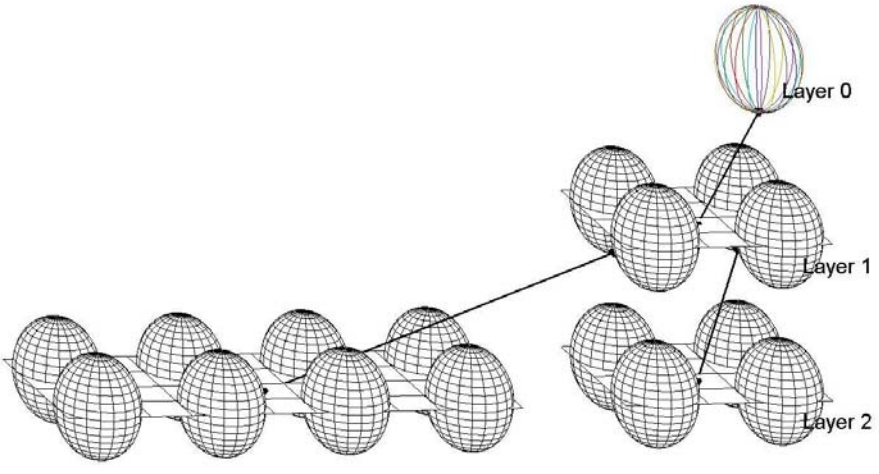

Fig. 1. An example of a GHSOM architecture

The adaptative growth process of a GHSOM is controlled by two parameters, $\tau 1$ and $\tau 2$, which are used to control the growth of a map and to control the hierarchical growth of the GHSOM, respectively. Although these parameters provide flexibility to choose the size of the neural network, it is usually difficult to determine and combine the two parameters to obtain successful results. In this paper, these parameters have been replaced by only one parameter τ to control both, growing and expansion of the network, so that the initial setup of the neural network is facilitated, keeping the possibility of choosing different network sizes.

$$qe_i = \sum_{x_j \in C_{ij}} \|w_i - x_j\| \tag{1}$$

In the GHSOM, the growing of a map is done by inserting a row or a column of neurons between two neurons, the neuron with the highest quantization error and its most dissimilar neighbor. The quantization error of a neuron is defined as [1]. The stopping criterion for the growth of a map is defined as $MQE_m < \tau_1 \cdot qe_u$, where MQE_m is the mean of the quantization error of the map m and qe_u is quantization error of the parent neuron u in the upper layer. Thus, the growth

process continues until the MQE_m of the map m reaches a certain fraction τ_1 of the quantization error of the corresponding parent neuron u in the upper layer. Also, the stopping criterion for the expansion of a neuron i is defined as $qe_i < \tau_2 \cdot qe_0$. Specifically, a neuron i is expanded into a new map at a subsequent layer unless its quantization error (qe_i) is smaller than a fraction τ_2 of the initial quantization error (qe_0).

2.2 New Hierarchical Self-Organizing Model

The starting point for our training process is to compute the quantization error at layer 0 as given in (2), where w_0 is the mean of the all input data I. The qe_0 measures the dissimilarity of all input data and it is used for the expansion process of the GHSOM neurons.

$$qe_0 = \sum_{x_j \in I} \|w_0 - x_j\| \tag{2}$$

The quality of the adaptation process to input data is measured by the quantization error of a neuron (qe). The qe is a measure of the similarity of data mapped onto each neuron, where the higher is the qe, the higher is the heterogeneity of the data cluster. Let (i, j) be the position of a neuron in a map of NxM neurons. The quantization error of a neuron (i, j) is defined as follows

$$qe_{ij} = \sum_{x_j \in C_{ij}} \|w_{ij} - x_j\| \tag{3}$$

where C_{ij} is the set of patterns mapped onto the neuron (i, j), x_j is the jth input pattern from C_{ij}, and w_{ij} is the weight vector of the neuron (i, j).

In order to consistently combine these two criteria, we have to distinguish in what situations are better to grow a map rather than expand their neurons. The difference lies in the use of the data mapped into the map, i.e. after growing the map is trained again with all its input data, whereas after expanding, new maps are just trained with data mapped into their respective parent neurons. Then, growing or expansion are decided depending on the proximity of the error neurons in the map, which are the neurons that no satisfy the condition given in (4). This way, the qe of a neuron (i, j) must be smaller than a fraction τ of the quantization error of its parent neuron u in the upper layer.

$$qe_{i,j} < \tau \cdot qe_u \tag{4}$$

In the GHSOM, the growing of a map is done by inserting a row or a column of neurons between two neurons, the neuron with the highest quantization error and its most dissimilar neighbor. Here, once the error neurons are computed, if in a row or column there are more error neurons than non-error neurons, a row or a column of neurons is inserted and the map grows. To decide what insert (a row or a column) and where, the row quantization error rqe and the column quantization error cqe must be computed for each of the N rows and the M columns of the map as given in 5. Then, the error row er, i.e. the row with

the highest sum of their quantization errors, and the error column ec, i.e. the column with the highest sum of their quantization errors are chosen following the expressions in 6. If the rqe of the er is bigger than the cqe of the ec, a row of neurons is inserted between the er and its neighbor row with the highest rqe. Likewise, if the cqe of the ec is bigger than the rqe of the er, a column of neurons is inserted between the ec and its neighbor column with the highest cqe (see Fig. 2). The weight vectors of the new neurons are initialized as the mean of their respective neighbors.

$$rqe_r = \sum_{j=1}^{M} qe_{rj} \qquad cqe_c = \sum_{i=1}^{N} qe_{ic} \tag{5}$$

$$er = \arg\max_i \{rqe_i\} \qquad ec = \arg\max_j \{cqe_j\} \tag{6}$$

On the other hand, if the error neurons of each row and column are less than the non-error neurons in their respective rows and columns, the error neurons will be expanded in a new map in the next level of the hierarchy. When a new map is created, a coherent initialization of the weight vectors of the neurons of the new map is used as proposed in [8]. This initialization provides a global orientation of the individual maps in the various layers of the hierarchy. Thus, the weight vectors of neurons mirror the orientation of the weight vectors of the neighbor neurons of its parent. The initialization proposed computes the mean of the parent and its neighbors in their respective directions.

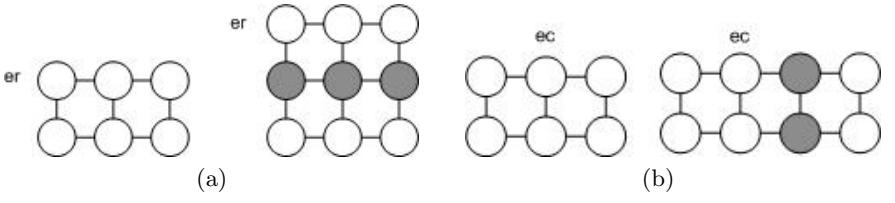

Fig. 2. An example of neurons insertion: (a) A row or (b) a column of neurons (shaded gray) is inserted between the error row er or the error column ec and its neighbor with the highest quantization error in the row or column

A new map created from an expanded neuron is trained as a single SOM. During the training, the set of input patterns are those that were mapped onto the upper expanded neuron u. In each iteration t, an input pattern is randomly selected from this data subset. The winning neuron of the map is the neuron with the smallest Euclidean distance to the input pattern, whose index r is defined in (7).

$$r(t) = \arg\min_i \{\|x(t) - w_i(t)\|\} \tag{7}$$

The winner's weight vector is updated guided by a learning rate α, decreasing in time (8). In addition to the winner, the neighbors of the winner are updated

depending on a Gaussian neighborhood function h_i and its distance to the winner. This neighborhood function reduces its neighborhood kernel in each iteration.

$$w_i(t+1) = w_i(t) + \alpha(t)h_i(t)[x(t) - w_i(t)] \tag{8}$$

3 Experimental Results

In order to evaluate the proposed hierarchical self-organizing map, a spam detector has been built. To this end, the neural network has been trained and tested with the Spambase data set from UCI Machine Learning Repository. This data set has 4,601 instances represented by 57 numerical features. In the data set, 1,813 instances are spam (39.4%) and 2,788 are non-spam (60.6%). Two data sets have been randomly selected from the 4,601 instances: the training and test data set, with 3,221 (60%) and 1,380 (40%) instances, respectively. For each data set, the class distribution of the initial data set (40% spam - 60% non-spam) has been preserved. Data distribution of each data set is shown in Table 1.

Table 1. Data distribution of different data sets

Class	Spambase	Training	Test
All	4,601	3,221	1,380
Spam	1,813	1,281	532
Non-spam	2,788	1,940	848

Table 2. Training results for different τ values

τ	Detection(%)	False Positive(%)	Neurons	Layers
0.05	77.28	4.43	1289	14
0.1	75.4	6.39	533	16
0.2	76.19	9.27	154	21
0.3	76.28	13.24	116	24
0.4	80.64	15.61	76	19

For our experiments, the hierarchical model has been trained using different values for the τ parameter (from 0.05 to 0.4). The training results together with the different obtained architectures are shown in Table 2. The detection rate is the percentage of spam that was detected as spam and the false positive rate is the percentage of good mail that was detected as spam. Note that the bigger the τ parameter the smaller the resulting network architecture will be in terms of number of neurons, but not in number of layers, which are adapted to reflect input data. After training, we achieved a detection rate of 81.57% and a 11.08% false positive rate by setting τ to 0.2. This parameter generated

Table 3. Test results for different trained neural networks

τ	**Detection(%)**	**False Positive(%)**
0.05	78.19	6.01
0.1	78	7.78
0.2	74.06	9.78
0.3	79.13	15.68
0.4	74.43	14.03

Table 4. Test results for different trained GHSOMs with different τ_1 and τ_2 values

τ_1	τ_2	**Detection(%)**	**False Positive(%)**	**Neurons**	**Layers**
0.05	0.1	51.5	7.07	52	3
0.1	0.1	65.03	8.25	53	4
0.2	0.1	72.74	12.02	54	6
0.3	0.1	75.37	12.26	44	8
0.4	0.1	71.99	12.14	48	9

a network architecture of just 167 neurons arranged in 23 layers. Since false positives (marking good mail as spam) are very undesirable, a better result could be the obtained with 0.1 as τ value, where the false positive rate fell a 4.18% and the detection rate just fell a 1.79%.

The trained neural networks have been tested with the randomly selected test data set, which has 1,380 instances. The test results are given in Table 3. We achieved higher detection rates although the false positive rates increased too. Only for the trained neural network with $\tau = 0.05$, the false positive rate decreased a 0.85%.

The test results have been compared with those achieved by the standard GHSOM model, as given in Table 4. The GHSOM neural networks have been trained and tested setting the parameter τ_1 to the same values as used for the parameter τ, and τ_2 to 0.1. Note that both detection and false positive rates are better than those achieved by the GHSOM for τ values under 0.3. For 0.3 and 0.4 τ values, we keep achieving higher detection rates, although false positive rates are also higher.

4 Conclusions

In this paper, a new hierarchical self-organizing model is proposed. This model is based on the GHSOM; however the GHSOM needs define two parameters prior to training, which control the growth of a map and the expansion of neurons in new maps at a subsequent layer in the hierarchy. Our approach uses just one parameter to control the whole growth process of the neural network by analyzing

the differences between growing and expansion. In fact, growing is needed when error neurons are near, whereas if they are isolated is better expand the neuron. Therefore, an only criterion for both, growth and expansion, can be utilized, obtaining a neural network determined during the training process according to input data.

In order to evaluate the new hierarchical self-organizing map, a spam detector has been implemented. It was trained and tested with the Spambase data set from the UCI Machine Learning Repository. After testing, we achieved a detection rate of 78.19% and a false positive rate of 6.01%, which confirm better results than those achieved by the GHSOM model.

Acknowledgements. This work is partially supported by the Spanish Ministry of Science and Innovation under contract TIN-07362.

References

1. Cranor, L., LaMacchia, B.: Spam! Commun. ACM 41(8), 74–83 (1998)
2. Clark, J., Koprinska, I., Poon, J.: A Neural Network Based Approach to Automated E-Mail Classification. In: Proceedings of IEEE/WIC International Conference on Web Intelligence, 2003. WI 2003, pp. 702–705 (2003)
3. Yang, Y., Elfayoumy, S.: Anti-Spam Filtering Using Neural Networks and Bayesian Classifiers. In: International Symposium on Computational Intelligence in Robotics and Automation, 2007. CIRA 2007, pp. 272–278 (2007)
4. Kohonen, T.: Self-Organized Formation of Topologically Correct Feature Maps. Biological cybernetics 43(1), 59–69 (1982)
5. Rauber, A., Merkl, D., Dittenbach, M.: The Growing Hierarchical Self-Organizing Map: Exploratory Analysis of High-Dimensional Data. IEEE Transactions on Neural Networks 13(6), 1331–1341 (2002)
6. Alahakoon, D., Halgamuge, S., Srinivasan, B.: Dynamic Self-Organizing Maps with Controlled Growth for Knowledge Discovery. IEEE Transactions on Neural Networks 11, 601–614 (2000)
7. Asuncion, A., Newman, D.: UCI machine learning repository (2007)
8. Dittenbach, M., Rauber, A., Merkl, D.: Recent Advances with the Growing Hierarchical Self-Organizing Map. In: 3rd Workshop on Self-Organising Maps (WSOM), pp. 140–145 (2001)

The Analysis of the Energy Function of Chaotic Neural Network with White Noise

Yaoqun Xu and Feng Qin

Institute of Computer and Information Engineering, Harbin University of Commerce, 150028, Harbin, China
Xuyq@hrbcu.edu.cn, woqf@tom.com

Abstract. In order to study the anti-noise capability of chaotic neural network in this paper, noise function is introduced into Chen's chaotic neural network model. The time evolution of the reverse bifurcation and the Lyapunov exponents is applied to study the neuron of chaotic neural network model with white noise. Based on the chaotic neuron model, we construct the chaotic neural network model with white noise, and study its energy function The simulation result illustrates the influence of white noises on the model. The simulation results show that the system still has good optimization ability under the white noises with suitable parameter.

Keywords: chaotic neural network, white noise, Lyapunov exponent, energy function.

1 Introduction

Since the Hopfield network model has solved the TSP (Traveling Salesman Problem) successfully, people realize the feasibility of large-scale collective computing power of artificial neural networks and remarkable achievements that engineering applications would achieve. Unfortunately, Hopfield network can be easily trapped in local minimum and even can not find solutions of optimization problems. Chaos theory was widely studied, and chaotic optimization approach provides a new optimization means method for the global optimization. Using the traversal property of the chaotic search, chaotic neural network can overcome the weaknesses of the Hopfield neural network [1~11] in resolving variety of combinatorial optimization problems. However, the realization of the hardware of the neural computer is the ultimate goal of the study on neural networks. Therefore, the construction of the hardware to observe the chaos phenomenon in the chaotic neurons or neural networks not only can make the dynamics of chaotic neural network easier to be observed, but also can lay the foundation for the manufacture of chaotic neural computers. During the practical applications and hardware realization of the chaotic neural network model, the system is inevitably subject to noise interference due to the instability of the components and the impact of the surrounding environment. As a result, these systems would be interfered with by the noisy and even deviate from the correct results. Therefore, people usually think that noise is harmful. In this paper, white noise is introduced into Chen's

D.-S. Huang et al. (Eds.): ICIC 2009, LNAI 5755, pp. 38–47, 2009.

chaotic neural network, and the influence of the noise on the optimization performance and the energy function of the chaotic neural network is studied by regulating the noise parameters. The results show that the proper regulation of noise and its related parameters would continue to enable the system to exhibit good performance and stability. Because white noise is the most common kind of noise in daily life, the application study of chaotic neural network in the real world is of great significance.

2 The Chaotic Neuron Model with White Noise

$$x(\mathrm{t}) = 1/(1+\exp(-y(t)/\varepsilon)) \tag{1}$$

$$y(\mathrm{t}+1) = ky(\mathrm{t}) + \eta Gn(x(t)) - z(\mathrm{t})(x(\mathrm{t}) - I_0) \tag{2}$$

$$z(\mathrm{t}+1) = (1-\beta)z(\mathrm{t}) \tag{3}$$

$$Gn(x(t)) = AWGN(x(t), SNR) \tag{4}$$

where $x(\mathrm{t})$ is output of neuron i; $y(\mathrm{t})$ is input of neuron i; k is damping factor of nerve membrane, $0 \le k \le 1$; ε is the steepness of the parameters in Sigmoid function; $z(\mathrm{t})$ is the feedback connection weight; I_0 is a parameter, and β is the annealing parameters; $Gn(x(t))$ is used to generate white noise, SNR is the ratio of the signal to noise, and η is the noise regulation parameters.

Select appropriate parameters, neurons can show transiently chaotic dynamics behavior. In the following, the time evolutional figures of reverse bifurcation and the largest Lyapunov exponents are applied to analyze the dynamics property of the proposed model.

The parameters in the single neuron are set as follows: $\varepsilon = 0.004$, $y(1) = 0.5$, $z(1) = 0.1$, $k = 1$, $I_0 = 0.15$, $\beta = 0.0002$, SNR=50, $\eta = 0.01$. The time evolutional figures of reverse bifurcation and the largest Lyapunov exponents are shown in Figure 1.

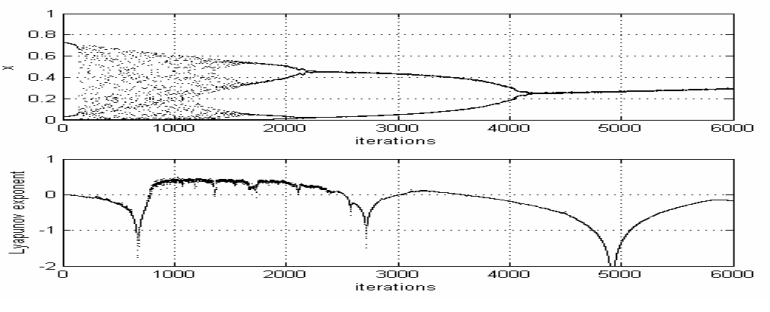

Fig. 1. The figure of the reverse bifurcation and the largest Lyapunov exponents in $\eta = 0.01$

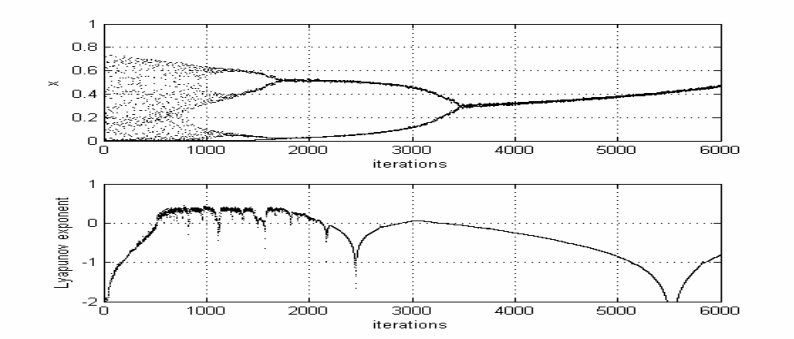

Fig. 2. The figure of the reverse bifurcation and the largest Lyapunov exponents in $\eta = 0.02$

By adjusting the white noise factor $\eta = 0.02$, the figure of the reverse bifurcation and the largest Lyapunov exponents are shown in Figure 2:

We also can put the practical application into the appropriate environment in order to reduce the noise caused by interference, making the system more stable. For example, take the following $\eta = -0.01$:

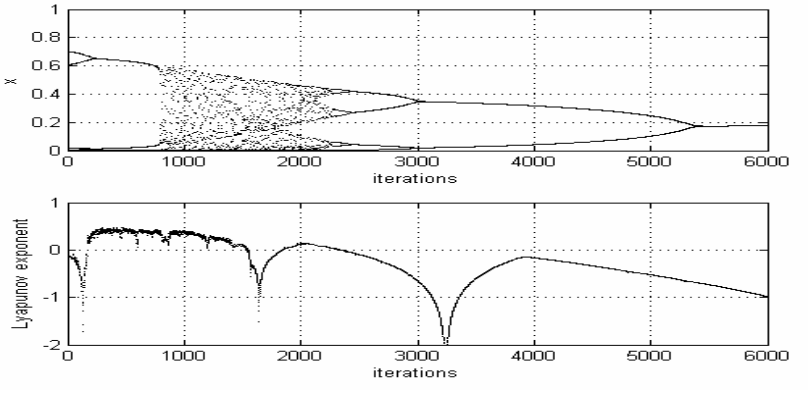

Fig. 3. The figure of the reverse bifurcation and the largest Lyapunov exponents in $\eta = -0.01$

The above time evolutions of the reverse bifurcation and the largest Lyapunov exponents show that the network has a transiently chaotic dynamics behavior, with the $z(t)$ in time of the attenuation constant, the network will gradually achieve a stable equilibrium point through a chaotic process of bifurcation.

Other than to maintain the same parameters, x-conditioning, we find that if the noise is controlled in a reasonable scope, the system is acceptable. But when the noise is too large, the system would be chaotic property or loss of interference and is very difficult to achieve stability. Therefore, in the practical application of our environment the system needs a good operating environment.

3 The Chaotic Neural Network with White Noise

Based on the above chaotic neuron model, the following structure with white noise of chaotic neural network can be described as follows:

$$x_i(\mathrm{t}) = \frac{1}{1+\exp(-y_i(t)/\varepsilon)} \tag{5}$$

$$y_i(\mathrm{t}+1) = ky_i(\mathrm{t}) + \alpha\left[\sum_{\substack{j=1 \\ j\neq i}}^{n} w_{ij}x_j(\mathrm{t}) + I_i\right] - z_i(\mathrm{t})(x_i(\mathrm{t}) - I_0) + \eta Gn(x_i(t)) \tag{6}$$

$$z_i(\mathrm{t}+1) = (1-\beta)z_i(\mathrm{t}) \tag{7}$$

$$Gn = AWGN(x(i), SNR) \tag{8}$$

In the network model, $i = 1,2,3,\cdots,\mathrm{n}$, $x_i(\mathrm{t})$, $y_i(\mathrm{t})$, $z_i(\mathrm{t})$ are respectively, the output neurons i, the internal state of connection and self-feedback; w_{ij} from neuron to neuron j connection i weight; I_i is the input neurons i deviation; ε is the steepness of the Sigmoid function parameters; k is the nerve of the diaphragm damping factor, $0 \le k \le 1$; α is not in response to measure parameters; I_0 is a parameter, β is the annealing parameters; $Gn(x(t))$ is used to generate white noise function, SNR is the signal to noise ratio, η is the noise regulation parameters. Gn is as follows: $Gn(x_i) = x_i \pm \psi$, ψ -noise ratio based on the value of the SNR, making $0 \le \psi \le 1$ produces small random noise.

4 The Analysis of Network Energy Function and Stability

Stability of nonlinear systems is an important consideration. Analysis of Lyapunov energy function is an important method for the stability of nonlinear systems. According to Chen-Aihara way, we propose the network energy function and stability of the analysis in this paper. For convenience, $x(t)$ will be written x.

$$E(X) = -\frac{\alpha}{2}\sum_{i,j}^{n} w_{ij}x_i x_j - \alpha\sum_{i}^{n} I_i x_i + \sum_{i}^{n}\int_0^{x_i} z_i(x - I_0)dx - \sum_{i}^{n}\int_0^{x_i} \eta Gn(x)dx - (k-1)\varepsilon\sum_{i}^{n}\int_0^{x_i} \ln\frac{x}{1-x}dx \tag{9}$$

The result of last part of the above formula can be described as follows:

$$\int_0^{x_i} \ln\frac{x}{1-x}dx = x_i \ln x_i + (1-x_i)\ln(1-x_i) \tag{10}$$

$$X=[x_1,x_2,\cdots,x_n]^T,\quad W=W^T,\quad w_{ii}=0,\quad k\geq 0.$$

$$\frac{dy_i}{dt}=-\frac{\partial E}{\partial x_i}=(k-1)y_i+\alpha\left[\sum_{j=1,j\neq i}^{n}w_{ij}x_j+I_i\right]-z_i(x_i-I_0)+\eta Gn(x_i) \tag{11}$$

Applying Euler discretization, (11) can be rewritten as follows:

$$y_i(t+1)=ky_i(t)+\alpha\left[\sum_{j=1,j\neq i}^{n}w_{ij}x_j(t)+I_i\right]-z_i(t)(x_i(t)-I_0)+\eta Gn(x_i(t)) \tag{12}$$

$$x_i(t+1)=\frac{1}{1+\exp\left\{-\frac{1}{\varepsilon}\left[k\varepsilon\ln\frac{x_i(t)}{1-x_i(t)}+\alpha\left[\sum_{j=1,j\neq i}^{n}w_{ij}x_j(t)+I_i\right]-z_i(t)(x_i(t)-I_0)+\eta Gn(x_i(t))\right]\right\}} \tag{13}$$

$$\alpha\left[\sum_{j=1,j\neq i}^{n}w_{ij}x_j(t)+I_i\right]-z_i(t)(x_i(t)-I_0)+\eta Gn(x_i(t))=\varepsilon\ln\frac{x_i(t+1)}{1-x_i(t+1)}-k\varepsilon\ln\frac{x_i(t)}{1-x_i(t)} \tag{14}$$

A detailed analysis of the stability is shown as follows:

$$\begin{aligned}&E(X(t+1))-E(X(t))\\&=-\frac{\alpha}{2}\sum_{i,j}^{n}w_{ij}\Delta x_i\Delta x_j-\alpha\sum_{i,j}^{n}w_{ij}x_j(t)\Delta x_i-\alpha\sum_{i}^{n}I_i\Delta x_i+\sum_{i}^{n}\int_{x_i(t)}^{x_i(t+1)}z_i(x-I_0)dx\\&-\sum_{i}^{n}\int_{x_i(t)}^{x_i(t+1)}\eta Gn(x)dx-(k-1)\varepsilon\sum_{i}^{n}\int_{x_i(t)}^{x_i(t+1)}\ln\frac{x}{1-x}dx\end{aligned} \tag{15}$$

The result of last part of the above formula is, $\Delta x_i=x_i(t+1)-x_i(t)$, $\Delta x_j=x_j(t+1)-x_j(t)$; According to the mean value theorem,

$$\int_{x_i(t)}^{x_i(t+1)}z_i(x-I_0)dx=[x_i(t+1)-x_i(t)]z_i(\bar{x}_i-I_0)=\Delta x_i z_i(\bar{x}_i-I_0) \tag{16}$$

The result of last part of the above formula is, $\bar{x}_i(t)=x_i(t)+\bar{\theta}_i\Delta x_i$, $0\leq\bar{\theta}_i\leq 1$;

By the same token:

$$\int_{x_i(t)}^{x_i(t+1)}Gn(x)dx=[x_i(t+1)-x_i(t)]Gn(\tilde{x}_i)=\Delta x_i z_i(\tilde{x}_i-I_0)$$

The last part of the above formula is,

$$\tilde{x}_i(t)=x_i(t)+\tilde{\theta}_i\Delta x_i,\quad 0\leq\tilde{\theta}_i\leq 1; \tag{17}$$

Substitute (16) and (17) into (15) :

$$\begin{aligned}
&E(X(t+1))-E(X(t))\\
&=-\frac{\alpha}{2}\sum_{i,j}^{n}w_{ij}\Delta x_i\Delta x_j-\alpha\sum_{i,j}^{n}w_{ij}x_j(t)\Delta x_i-\alpha\sum_{i}^{n}I_i\Delta x_i+\sum_{i}^{n}\Delta x_i z_i(x_i-I_0)-\sum_{i}^{n}\Delta x_i\eta Gn(x_i)\\
&-(k-1)\varepsilon\sum_{i}^{n}\int_{x_i(t)}^{x_i(t+1)}\ln\frac{x}{1-x}dx+\sum_{i}^{n}\Delta x_i z_i\left[(\bar{x}_i-I_0)-(x_i-I_0)\right]-\sum_{i}^{n}\Delta x_i\eta[Gn(\tilde{x}_i)-Gn(x_i)]\\
&=-\frac{\alpha}{2}\sum_{i,j}^{n}w_{ij}\Delta x_i\Delta x_j-\sum_{i}^{n}\Delta x_i\left\{\alpha\left[\sum_{i,j}^{n}w_{ij}x_j(t)+I_i\right]-z_i(x_i-I_0)+\eta Gn(x_i)\right\}\\
&-(k-1)\varepsilon\sum_{i}^{n}\int_{x_i(t)}^{x_i(t+1)}\ln\frac{x}{1-x}dx+\sum_{i}^{n}z_i\bar{\theta}_i[\Delta x_i]^2-\sum_{i}^{n}\Delta x_i\eta[Gn(\tilde{x}_i)-Gn(x_i)]
\end{aligned}\tag{18}$$

According to the nature of the Gn :

$$Gn(\tilde{x}_i)-Gn(x_i)=\tilde{x}_i-x_i\pm\psi=\tilde{\theta}_i\Delta x_i\pm\psi\tag{19}$$

According to the mean value theorem :

$$\int_{x_i(t)}^{x_i(t+1)}\ln\frac{x}{1-x}dx=[x_i(t+1)-x_i(t)]\ln\frac{\varphi_i}{1-\varphi_i}=\Delta x_i\ln\frac{\varphi_i}{1-\varphi_i}\tag{20}$$

where $\varphi_i=x_i(t)+\theta_i\Delta x_i$, $0\le\theta_i\le1$

Substitute (14) (19) (20) into (18), and take into account $w_{ii}=0$:

$$\begin{aligned}
&E(X(t+1))-E(X(t))\\
&=-\frac{\alpha}{2}\sum_{i,j}^{n}w_{ij}\Delta x_i\Delta x_j-\sum_{i}^{n}\Delta x_i\left\{\varepsilon\ln\frac{x_i(t+1)}{1-x_i(t+1)}-k\varepsilon\ln\frac{x_i(t)}{1-x_i(t)}\right\}\\
&-(k-1)\varepsilon\sum_{i}^{n}\Delta x_i\ln\frac{\varphi_i}{1-\varphi_i}+\sum_{i}^{n}[\Delta x_i]^2z_i\bar{\theta}_i-\sum_{i}^{n}\Delta x_i\eta(\tilde{\theta}_i\Delta x_i\pm\psi)
\end{aligned}\tag{21}$$

According to the differential intermediate value theorem:

$$\begin{aligned}
&\ln\frac{x_i(t+1)}{1-x_i(t+1)}-\ln\frac{\varphi_i}{1-\varphi_i}=(x_i(t+1)-\varphi_i)\left(\ln\frac{x}{1-x}\right)'\Big|_{x=\gamma_{i1}}\\
&=(1-\theta_i)\Delta x_i\frac{1}{-(\gamma_{i1}-1/2)^2+1/4}\ge4(1-\theta_i)\Delta x_i
\end{aligned}\tag{22}$$

The last part of the above formula is, $\gamma_{i1}=\varphi_i+\gamma_1[(1-\theta_i)\Delta x_i]$, $0<\gamma_1<1$;

$$\begin{aligned}
&\ln\frac{\varphi_i}{1-\varphi_i}-\ln\frac{x_i(t)}{1-x_i(t)}=(\varphi_i-x_i(t))\left(\ln\frac{x}{1-x}\right)'\Big|_{x=\gamma_{i2}}\\
&=\theta_i\Delta x_i\frac{1}{-(\gamma_{i2}-1/2)^2+1/4}\ge4\theta_i\Delta x_i
\end{aligned}\tag{23}$$

And the part is, $\gamma_{i2} = x_i(t) + \gamma_2[\theta_i \Delta x_i]$, $0 < \gamma_2 < 1$;

Substitute (22) and (23) into (21) :

$$\begin{aligned} & E(X(t+1)) - E(X(t)) \\ & \le -\frac{\alpha}{2}\sum_{i,j}^{n} w_{ij}\Delta x_i \Delta x_j - \varepsilon\sum_{i}^{n}\{4(1-\theta_i)+4k\theta_i\}[\Delta x_i]^2 + \sum_{i}^{n}\bar{\theta}_i z_i[\Delta x_i]^2 - \sum_{i}^{n}\Delta x_i \eta(\tilde{\theta}_i \Delta x_i \pm \psi) \\ & = -\frac{1}{2}\sum_{i,j}^{n}\left\{w_{ij}^{'} + 2\varepsilon[4(1-\theta_i)+4k\theta_i]\delta_{ij}\right\}\Delta x_i \Delta x_j \\ & = -\frac{1}{2}\Delta X(t)^T\left\{W^{'} + 2\varepsilon[4(1-\theta_i)+4k\theta_i]I_n\right\}\Delta X(t) \end{aligned} \tag{24}$$

where $\delta_{ij} = \begin{cases} 1, i = j \\ 0, i \ne j \end{cases}$, $\begin{cases} w_{i,j\ne i}^{'} = \alpha w_{i,j\ne i} \\ w_{ii}^{'} = \alpha w_{ii} - \bar{\theta}_i z_i + \eta(\tilde{\theta}_i \pm \tilde{\psi}) = \eta\tilde{\theta}_i - \bar{\theta}_i z_i \pm \eta\tilde{\psi} \end{cases}$, $\psi = \tilde{\psi}\Delta x_i$, I_n is a unit matrix, $\Delta X(t) = X(t+1) - X(t)$. Therefore, when the minimum $W^{'}$ matrix eigenvalue $\lambda^{'}$ meet:

$$-\lambda^{'} < 2\varepsilon[4(1-\theta_i)+4k\theta_i] = 8\varepsilon[1-(1-k)\theta_i] \tag{25}$$

That is :

$$-\lambda^{'} < \begin{cases} 8\varepsilon, & \theta_i = 0 \\ 8k\varepsilon, & \theta_i = 1 \end{cases} \tag{26}$$

$E(X(t+1)) - E(X(t)) \le 0$, the network can achieve stability.

According to a detailed analysis of the above, we conclude the following conclusions:

White noise with the gradual stability in the chaotic neural network is a sufficient condition: the existence of a minimum eigenvalue of the matrix is the $\lambda^{'}$ and $W^{'}$, as well as network-related $\bar{\theta}_i$, $\tilde{\theta}_i$, η , $\tilde{\psi}$ （$0 \le \bar{\theta}_i, \tilde{\theta}_i, \eta, \tilde{\psi} \le 1$, to meet

$$\begin{cases} w_{i,j\ne i}^{'} = \alpha w_{i,j\ne i} \\ w_{ii}^{'} = \alpha w_{ii} - \bar{\theta}_i z_i + \eta(\tilde{\theta}_i \pm \tilde{\psi}) = \eta\tilde{\theta}_i - \bar{\theta}_i z_i \pm \eta\tilde{\psi} \end{cases}, \quad -\lambda^{'} < \begin{cases} 8\varepsilon, & \theta_i = 0 \\ 8k\varepsilon, & \theta_i = 1 \end{cases} \tag{27}$$

The stability theorem of the chaotic neural network with white noise of shows that the network can be able to achieve stability in the gradual, with white noise of chaotic neural network to meet the connection gradual and stable right on the diagonal matrix elements have changed. As the network model to control noise figure and η-noise ratio SNR, therefore, η and $\tilde{\psi}$ can be controlled to a certain extent, the network has made a very good performance and stability, with more than the white noise of neurons in the chaotic dynamics of Analysis has also proved effective. The model is compared with other network model with better controllability, for the future of the neural computer is of great significance.

5 The Optimization Application of Chaotic Neural Network with the White Noise

Traveling Salesman Problem (TSP) is a classic combinatorial optimization problem including many local minimum. The proposed model is used in 10-city traveling salesman problem.

The shortest path to reach and satisfy all the conditions of an energy function can be described as (28). In (28), V_{xi} is the output neurons, it represents the first x cities in the first i was on the order of the visit, d_{xy} is the distance between the city x and y. The proposed network model (6) can be described as (29) .

$$E = \frac{A}{2}\sum_{x=1}^{n}(\sum_{i=1}^{n}V_{xi}-1)^2 + \frac{B}{2}\sum_{i=1}^{n}(\sum_{x=1}^{n}V_{xi}-1)^2 + \frac{D}{2}\sum_{x=1}^{n}\sum_{y=1}^{n}\sum_{i=1}^{n}d_{xy}V_{xi}V_{y,i+1} \tag{28}$$

$$\begin{aligned} y_i(\mathrm{t}+1) &= ky_i(\mathrm{t}) + \eta Gn(x_i(t)) \\ &+ \alpha[-A(\sum_{j=1}^{n}V_{xj}-1) - B(\sum_{y=1}^{n}V_{yi}-1) - D\sum_{y=1}^{n}d_{xy}V_{y,i+1}] - z_i(\mathrm{t})(x_i(\mathrm{t})-I_0) \end{aligned} \tag{29}$$

In this paper, the following classics normalized after the coordinates of the 10 cities: (0.4, 0.4439); (0.2439, 0.1463); (0.1707, 0.2293); (0.2293, 0.716); (0.5171,0.9414); (0.8732, 0.6536); (0.6878, 0.5219); (0.8488, 0.3609); (0.6683, 0.2536); (0.6195, 0.2634). The 10 cities in the shortest path to 2.6776.

First of all, the different parameters of the 10 cities in solving TSP are studied.

Take A=1 , D=1 , k =1 , I_0 =0.5 , β_1 =0.008 , $z(1)$ =0.3 , ε =1/250 , α =0.015, SNR=50

Table 1 in the noise parameters for different values of η randomly assigned to the initial 1000 value of the simulation test data.

Table 1. Simulation Results

η	α	Legal path	Optimal path	The proportion of legal	Optimal ratio
0	0.015	918	869	91.8%	86.9%
0.01	0.015	914	833	91.4%	83.3%
0.02	0.015	867	819	86.7%	81.9%
0.03	0.015	881	784	88.1%	78.4%
-0.01	0.015	937	921	93.7%	92.1%
-0.02	0.015	994	994	99.4%	99.4%
-0.025	0.015	1000	1000	100%	100%
-0.027	0.015	1000	1000	100%	100%
-0.03	0.015	0	0	0%	0%

Through the above analysis in Table 1, we can conclude that

1) The system has certain anti-interference capability. As long as a certain noise control within the framework of the system will not have much impact.
2) When the noise disturbance is too large, the ability to optimize the system would be affected. In the face of the adoption of single neurons in the analysis of the dynamics we know that the noise factor will have an impact on its chaotic characteristics, we adjust to changes in the network model of the characteristics of chaos, which can control the ability to optimize the system.
3) When there is noise in the environment, we can adjust the noise figure due to the negative, thereby eliminating noise interference and control the appropriate value we can be as shown in table 1 very good results of the optimization.

Through the analysis of the experiments that can be drawn the following conclusions: the noise of the system is running is a certain danger, when the system too much noise, the system may not work properly, but we can adjust the noise to a certain limit, so that it with a good performance.

6 Conclusions

Noise has an important role in the realization of the hardware of neural network, so the anti-noise capability of networks is also one aspect of the hardware. In this paper the proposed network is applied to the traveling salesman problem. Through the appropriate adjustment parameters, chaotic neural network with the noise is still capable of higher accuracy to solve problem, indicating chen's chaotic neural network has some anti-noise capability, and describing the appropriate Parameters selected. Meantime, through the noise of a negative factor, we can improve the ability to optimize the system in the practical application of the elimination of white noise in the environment. The appropriate noise value has a superior optimization capability to the original chaotic neural network model.

Acknowledgment

This work is supported by Program for New Century Excellent Talents In Heilongjiang Provincial University (1153-NCET-007).

References

1. Hopfield, J.J., Tank, D.W.: Neural Computation of Decision in Optimization Problems. Biol. Cybern. 52, 141–152 (1985)
2. Hopfield, J.: Neural Networks and Physical Systems with Emergent Collective Computational Abilities. Proc. Natl. Acad. Sci. 79, 2554–2558 (1982)
3. Hopfield, J.: Neural Networks and Physical Systems with Emergent Collective Computational Abilities. Proc. Natl. Acad. Sci. 81, 3088–3092 (1984)

4. Xu, Y.-q., Sun, M., Duan, G.-R.: Wavelet chaotic neural networks and their application to optimization problems. In: Wang, J., Yi, Z., Żurada, J.M., Lu, B.-L., Yin, H. (eds.) ISNN 2006. LNCS, vol. 3971, pp. 379–384. Springer, Heidelberg (2006)
5. Chen, L., Aihara, K.: Chaotic Simulated Annealing by a Neural Network Model with Transient Chaos. Neural Networks 8, 915–930 (1995)
6. Sun, S.Y., Zheng, J.L.: A Kind of Improved Algorithm and Theory Testify of Solving TSP in Hopfield Neural Network. Journal of electron 1, 73–78 (1995)
7. Xu, Y.-q., Sun, M., Shen, J.-h.: Gauss chaotic neural networks. In: Yang, Q., Webb, G. (eds.) PRICAI 2006. LNCS (LNAI), vol. 4099, pp. 319–328. Springer, Heidelberg (2006)
8. Aihara, K.: Chaos engineering and its application to parallel distributed processing with chaotic neural networks. Proceedings of the IEEE 90, 919–930 (2002)
9. Wang, L.P., Li, S., Tian, F.Y., Fu, X.J.: A noisy chaotic neural network for solving combinatorial optimization problems: Stochastic chaotic simulated annealing. IEEE Trans. System, Man, Cybern, Part B – Cybernetics 34, 2119–2125 (2004)
10. Wang, L., Shi, H.: A noisy chaotic neural network approach to topological optimization of a communication network with reliability constraints. In: Yin, F.-L., Wang, J., Guo, C. (eds.) ISNN 2004. LNCS, vol. 3174, pp. 230–235. Springer, Heidelberg (2004)
11. Wang, L.P., Smith, K.: On chaotic simulated annealing. IEEE Trans Neural Networks 9, 716–718 (1998)

The Classification of a Simulation Data of a Servo System via Evolutionary Artificial Neural Networks

Asil Alkaya and G. Miraç Bayhan

Dokuz Eylul University The Faculty of Engineering
Industrial Engineering Department
Tinaztepe Campus 35160 Buca Izmir, Turkey
asil.alkaya@deu.edu.tr, mirac.bayhan@deu.edu.tr

Abstract. Evolutionary neural networks (EANNs) are the combination of artificial neural networks and evolutionary algorithms. This merge enabled these two methods to complement the disadvantages of the other methods. Traditional artificial neural networks based on backpropagation algorithms have some limitations. Contribution by artificial neural networks was the flexibility of nonlinear function approximation, which cannot be easily implemented with prototype evolutionary algorithm. On the other hand, evolutionary algorithm has freed artificial neural networks from simple gradient descent approaches of optimization. Classification is an important task in many domains and though there are several methods that can be used to find the relationship between the input and output space , among the different works, EAs and NNs stands out as one of the most promising methods. In this study, the data gathered from a simulation of a servo system involving a servo amplifier, a motor, a lead screw/nut, and a sliding carriage of some sort is classified by the application coded in Qt programming environment to predict the rise time of a servomechanism in terms of two (continuous) gain settings and two (discrete) choices of mechanical linkages.

1 Introduction

Evolutionary neural networks (EANN) are the combination of artificial neural networks and evolutionary algorithms. This merge enabled these two methods to complement the disadvantages of the other methods. For example, a contribution by artificial neural networks was the flexibility of nonlinear function approximation, which cannot be easily implemented with prototype evolutionary algorithm. On the other hand, evolutionary algorithm has freed artificial neural networks from simple gradient descent approaches of optimization. Classification is an important task in many domains and though there are several methods that can be used to find the relationship between the input and output space, among the different works, EAs and NNs stands out as one of the most promising methods.

Indeed, traditional artificial neural networks based on backpropagation algorithms have some limitations. At first, the architecture of the artificial neural networks is fixed and a designer needs much knowledge to determine it. Also, error function of the learning algorithm must have a derivative.

D.-S. Huang et al. (Eds.): ICIC 2009, LNAI 5755, pp. 48–54, 2009.

EA and ANN were combined, and more sophisticated versions of these methods could produce better results. For example, the use of indirect representation encoding chromosomes, use of EANN for feature selection, etc. could bring different results.

The inclusion of backpropagation training in the EANN have consequences of longer computation times, so alternatives to backpropagation should be tested in order to reduce time costs.

2 Neural Network Architecture

The neural network architecture modeled by genetic programming based evolutionary technique consists of an input layer, a hidden layer and an output layer. As it is well known that a single hidden layer is sufficient for a multilayer perceptron to compute an uniform approximation to a given training set (universal approximation theorem), the number of hidden layer is fixed at 1. Using more hidden layers increases the network complexity; however, it does not guarantee better results. The combination of evolutionary algorithm and artificial neural networks can overcome these shortcomings and is particularly useful when the activation function of the neurons is non-differentiable and traditional gradient-based training algorithms cannot be used.

A lot of works have been made on EANN. Evolutionary algorithms have been used to help to obtain more accurate ANN with better generalization abilities. For example, searching the optimal weight set of a ANN, designing its architecture, finding it's most adequate parameter set (number of neurons in the hidden layer, learning rate, etc.) among others tasks.

3 Methodology

This method aims to search for the best ANN among evolving populations of potential solutions, regarding their ability to classification. To do so, we evaluate the strength of the correlation between each individual and samples.

Each sample is used to train each individual of the population (a set of individuals). A data separation procedure divides the data into three distinct sample sets without overlapping: training set, and test set.

The designed algorithm is specified in the following procedure:

1. Generate a random initial population of potential solutions with random initial weights and within certain ranges according to a uniform distribution.
2. Each individual in the population is trained partially by genetic algorithms for a certain number of epochs on the training set to help the evolution search.
3. Evaluate the individuals in the population based on their error.
4. Pick the best individuals in the population as elite individual and select individuals based on rank-based select mechanism. (for elitist strategy.) No pick up for revolutionary strategy. Convergence coefficient is important for revolution.
5. Pick the best individuals in the population as elite individual and select individuals based on rank-based select mechanism. (for elitist strategy.) No pick up for revolutionary strategy. Convergence coefficient is important for revolution.
6. Apply tailored genetic operations to selected individuals and obtain offspring.

7. Replace the worst individuals with the new ones only when the offspring is better than the current worst and form a new generation. (for elitist strategy)
8. Loop to Step 2 until an individual shows better performance than predefined accuracy or iteration number exceeds predefined maximum number of generations.
9. Use the best ANN on an unseen testing set and evaluate the testing error.

3.1 Overall Stopping Criteria

Neural networks that are under-trained will not be able to learn the problem well, on the other hand, overtraining might cause overfitting (a network with larger training error could be better than one with lower training error as the one with lower training error has concentrated on the peculiarities while losing the regularities needed for good generalization accuracy.

One of the well-known methods in addressing this issue is to use a validation set. The validation set is used as a pseudo-test set and is not used for training but for stopping criteria. Training stops when minimum validation error is reached and the current network state is used on the testing set.

However, as there are many local optima in the validation set, there are some issues when using it. First, during the initial phase of training, the error on validation set will be oscillatory and secondly, in order to recognize a minimum, training has to proceed until the error increases.

3.2 The Train/Test Strategy

Because of the ever-present danger that a neural network will memorize a set of patterns rather than generalize them, the dataset is split into two portions. The network is trained on the first, but tested on the second. 80% of data is used for training and 20% percent is used for testing purposes.

4 Application Coded for the Classification Problem

Application is built in Qt programming. Qt is a cross-platform application framework. Program is coded in the linux / X11 environment

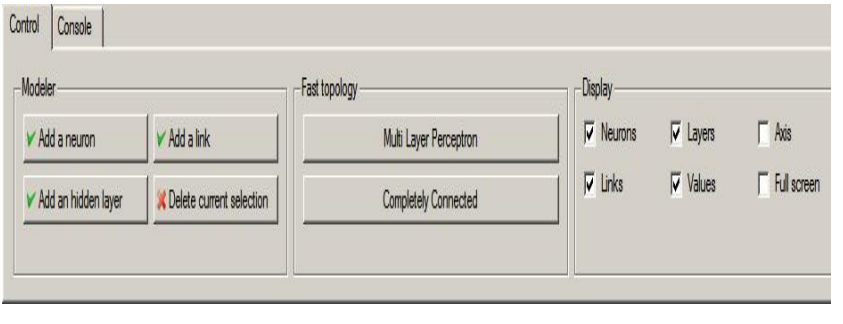

Fig. 1. Program main

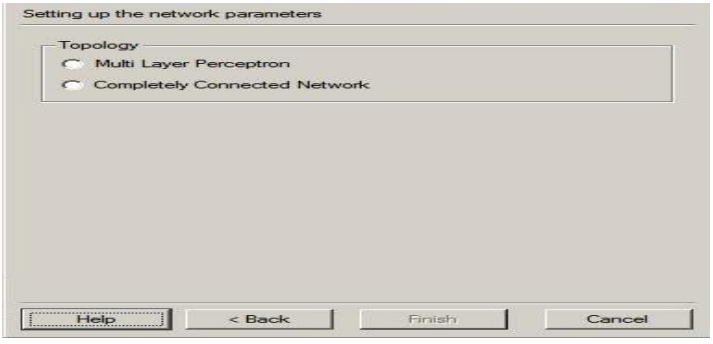

Fig. 2. New network wizard

In the program main, the parameters are selected to be structured. You can either add a neuron or a hidden layer with its connections in detail.

Automated network wizard is prepared by setting up the network parameters. According to the articles inspected, two main topologies are selected:

- Multi-layer perceptron
- Completely connected network

After selecting the topology, the neural network's design should be taken into consideration. For the classification problem; one input layer, one hidden layer and one output layer is selected.

The number of the attributes defined in the classification problem is declared as the number of neurons in the input layer. The number of neurons in the hidden layer plays an important role on training and testing purposes for the problem data. According to the literature, (2n+1) neurons should be chosen for the number of neurons in the hidden layer for best performance where n is the number of attributes of data considered.

4.1 Parameters Used for EANN

- Number of chromosomes: 50
- Maximum generations number (stoppping criteria): 1000
- Error threshold (stopping criteria): 0.005
- Mutation rate: 1.6 (experimentally optimized)
- Sigmoid coefficient:1.000

The parameters are fixed due to performance comparison.

4.2 Data for Application

The data gathered from a simulation of a servo system involving a servo amplifier, a motor, a lead screw/nut, and a sliding carriage of some sort.

In any case, the output value is almost certainly a rise time, or the time required for the system to respond to a step change in a position set point. It covers an extremely

non-linear phenomenon - predicting the rise time of a servomechanism in terms of two (continuous) gain settings and two (discrete) choices of mechanical linkages.

The data is obtained from the simulation studies of Quinlan and classified to predict the rise time of the servo system. Data have five different attributes. Four of them have the alphanumeric and one of them has a numeric attribute. *Motor* means the electric motor type of the servo mechanism; A, B, C, D, E. *Screw* used for the servo mechanism is defined as A, B, C, D, E. *pgain* is the power gain that the servo mechanism has according to the motor and the screw type. Also, *vgain* is the velocity gain that the servo mechanism has according to the motor and the screw type.

Table 1. Information about data

Number of Instances:		167
Number of Attributes:		4 + numeric class attribute
Attribute information:		
1.	motor:	A, B, C, D, E
2.	screw:	A, B, C, D, E
3.	pgain:	3, 4, 5, 6
4.	vgain:	1, 2, 3, 4, 5
5.	class:	0.13 to 7.10
Missing Attribute Values		None

4.3 Run Results for Optimal EANN Architecture

According to the experiment results, the best results are obtained by 5-11-1 multi layer perceptron EANN architecture.

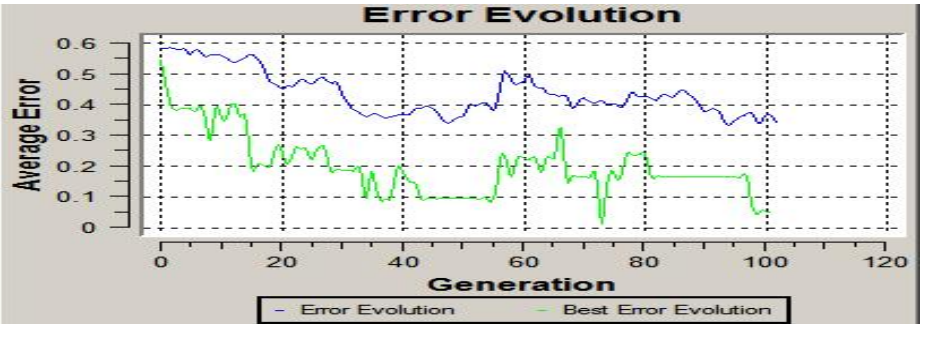

Fig. 3. One point crossover 5-11-1 EANN error

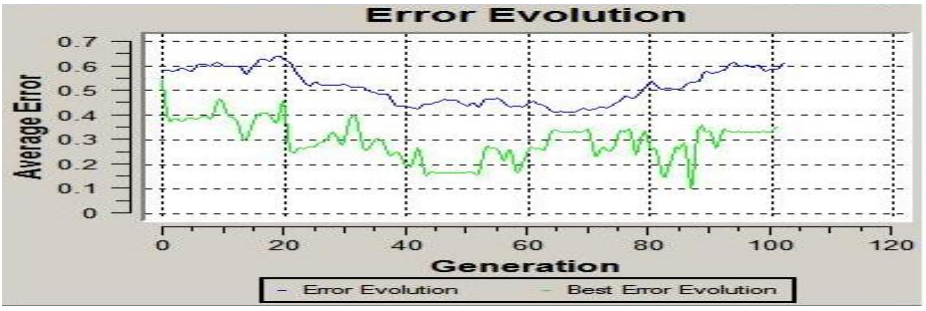

Fig. 4. Two points crossover 5-11-1 EANN error

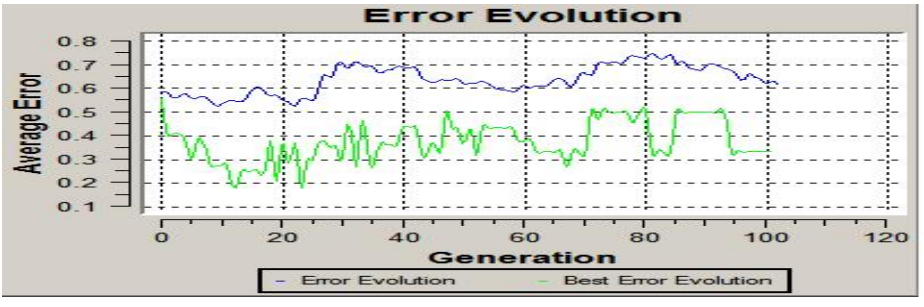

Fig. 5. Random crossover 5-11-1 EANN error

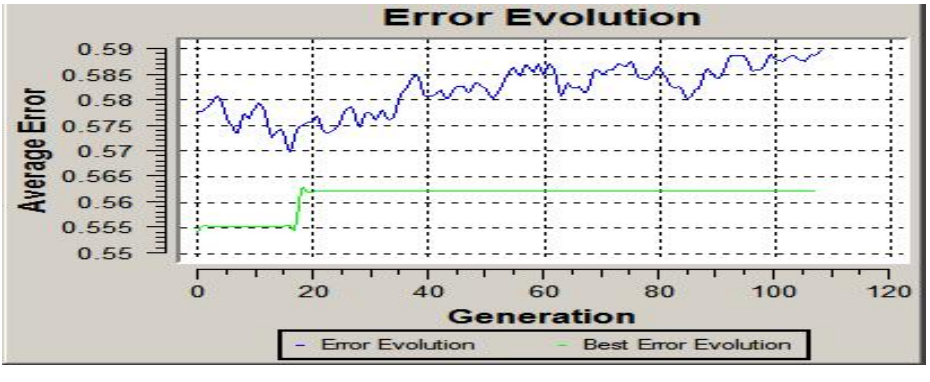

Fig. 6. Uniform crossover 5-11-1 EANN error

After training, 10% noise amount is added for testing purposes. As seen from Table 2, one point crossover and random crossover policies have nearly the same effect on the EANN algorithm.

Table 2. Test results

Crossover policy		Test deviation
One point crossover	10% noise amount	% 8 (%2 best)
Two point crossover	10% noise amount	% 16
Uniform	10% noise amount	% 9,6
Random	10% noise amount	% 8,38

5 Conclusion

The system designed and presented herein successfully produced networks with the maximum theoretical accuracy on previously unseen data. When training networks by hand, varying numbers of hidden units were employed with awide variety in training epochs.

The results were compared, and the best were selected.The performance measure used was the accuracy on the training and test data set. The system is by no means a finished product; many avenues are open for future exploration. It is felt, however, that the basis of the underlying theories is promising, and that future work will result in increasing flexible automated neural network design systems.

References

1. Haykin, S.: Neural Networks: A Comprehinsive Foundation. Macmillan College, New York (1994)
2. Rogers, J.: Object-oriented Neural Networks in C++. Academic Press, San Diego (1997)
3. Quinlan, J.R.: Learning with Continuous Classes. In: Adams, A., Sterling, L. (eds.) Proc. 5th Australian Joint Conference on AI. World Scientific, Singapore (1992)
4. Quinlan, J.R.: Combining Instance-based and Model-based Learning
5. Stevens, W.R.: Advanced Programming in the UNIX Environment. Addison-Wesley, Reading (1992)
6. Wasserman, P.D.: Advanced Methods in Neural Computing. Van Nos-trand Reinhold, New York (1993)
7. Weiss, S.M., Kulikowski, C.A.: Computer Systems that Learn. Morgan Kaufmann, San Francisco (1991)
8. Rocha, M., Cortez, P., Neves, J.: Neurocomputing 70 (2007)
9. Dietterich, T., Kittler, J., Roli, F.: Ensemble methods in machine learning. In: Kittler, J., Roli, F. (eds.) MCS 2000. LNCS, vol. 1857, pp. 1–15. Springer, Heidelberg (2000)

A New Source and Receiver Localization Method with Erroneous Receiver Positions

Yingke Lei[1,2] and Junfeng Xia[1]

[1] Intelligent Computing Lab, Institute of Intelligent Machines,
Chinese Academy of Sciences, P.O. Box 1130, Hefei Anhui 230031, China
[2] Electronic Engineering Institute, 230037 Hefei, China
leiyingke@163.com

Abstract. Receiver location uncertainty plays an important role in passive source localization since it can significantly deteriorate the accuracy of the source location. In this paper, we first derive a joint position estimation model for source location and receiver positions with erroneous receiver positions, and then, based on this model, an efficient algorithm for estimation the location of source and the positions of receivers using Time Difference of Arrival (TDOA) measurements is proposed. The proposed method employs modified Genetic Algorithm (MGA) and jointly estimates both source and receiver positions simultaneously. Simulation results show that when receiver position or TDOA measurement errors are large, the proposed method can achieve better performance than the modified Taylor method and the original Taylor method. It is more suitable for adverse measurement conditions.

Keywords: Erroneous receiver positions; TDOA; MGA.

1 Introduction

TDOA localization has been an active research area for more than decade. It is an important problem in many applications including radar, sonar, seismology, radio astronomy, and mobile communications [1]-[9]. Various Algorithms have been proposed to estimate the source location. Previous methods assumed that receiver positions are known exactly, which may not be true in practice [1]-[2]. Some study has indicated that even relatively small amount of receiver location uncertainty can seriously deteriorate the source localization accuracy [3]-[4]. Consequently, improving the source location estimate under receiver position errors is an important issue and has attracted much effort over the years [3]-[9]. Rockah and Schultheiss [3]-[4] utilized the CRLB to derive a Direction of Arrival (DOA) estimation method in the presence of receiver position uncertainty, which assumes that the knowledge of one receiver location and its direction to the second receiver is known exactly. Chen et al. [5] used the Toeplitz approximation to find the Angle of Arrival estimation in the presence of the sensor position errors. Ng et al. [6] applied the first order Taylor-series expansion to approximate the true array steering vector from the measurement, and applied the MUSIC to estimate the source DOA. Weiss and Friedlander [7] proposed an exact Maximum-Likelihood method which estimates the DOA and the

D.-S. Huang et al. (Eds.): ICIC 2009, LNAI 5755, pp. 55–63, 2009.

receiver locations alternately until convergence is achieved. However, these techniques focus on searching the bearing angle or angle of arrival of multiple sources.

There are very few literatures on the source localization using TDOA in the presence of receiver position errors. Ho et al. [8] proposed a closed-form solution that requires only 2 least squares (LS) minimization steps to estimate the source location in the presence of receiver position errors. However, this method provides the source location estimate only and the solution accuracy does not reach the CRLB. Kovavisaruch and Ho [9] proposed an iterative algorithm based on the Taylor-series for estimating the location of source and the positions of receivers using TDOA measurements, when the receivers have random position errors. However, the proposed method requires good initial solution guess close to the true solution to begin with in order to ensure convergence.

In this paper we consider estimating exactly the positions of source and receivers simultaneously using the modified Genetic Algorithm (MGA) [10] in the presence of random receiver position error. Our results demonstrate that the proposed method significantly improves the location accuracy of the source and receivers when receiver position errors are taken into account.

The rest of this paper is organized as follows. In section 2, we start the analysis by briefly reviewing source location model without erroneous receiver positions. Following that, the joint position estimation model with erroneous receiver positions is derived, and then, based on this model, an efficient optimization algorithm for source and receiver positions is proposed. In section 3, two sets of experiments are presented to demonstrate the effectiveness of the proposed algorithm. Conclusions are summarized in Section 4.

2 The Proposed Method

2.1 Source Location Model without Erroneous Receiver Positions

Consider a scenario where an array of M receivers, $\mathbf{s}_i^0 = [x_i^0, y_i^0]^T$, for $i = 1, 2, ..., M$, is used to determine the unknown emitter source position $\mathbf{u} = [x, y]^T$. The true distance between the source and the ith receiver is

$$r_i^0 = \left\| \mathbf{u} - \mathbf{s}_i^0 \right\| = \sqrt{\left(x - x_i^0\right)^2 + \left(y - y_i^0\right)^2} \,. \tag{1}$$

Let the TDOA of a signal received by the receiver pair i and 1 be d_{i1}, and c be the signal propagation speed. Then the set of TDOA measurement equations is

$$\begin{aligned} r_{i1} &= cd_{i1} = r_{i1}^0 + cn_{i1} = r_i^0 - r_1^0 + cn_{i1} \\ &= \sqrt{\left(x - x_i^0\right)^2 + \left(y - y_i^0\right)^2} - \sqrt{\left(x - x_1^0\right)^2 + \left(y - y_1^0\right)^2} + cn_{i1} \; i = 2, 3, ...M \end{aligned} \,, \tag{2}$$

where r_{i1} is the TDOA measurement and $n_{i1}, i = 2, \cdots, M$ is measurement noise with mean 0 and variance σ^2.

Let $\mathbf{r} = \left[r_2^0, r_3^0, \cdots, r_M^0\right]^T_{(M-1)\times 1}$, $\mathbf{r_1} = \left[r_1^0, r_1^0, \cdots, r_1^0\right]^T_{(M-1)\times 1}$ and $\mathbf{n} = \left[n_{21}, n_{31}, \cdots, n_{M1}\right]^T_{(M-1)\times 1}$.

Based on these, TDOA measurement vector $\Delta\mathbf{r} = \left[r_{21}, r_{31}, \cdots, r_{M1}\right]^T$ can be obtained as

$$\begin{aligned}\Delta\mathbf{r} &= \mathbf{r} - \mathbf{r_1} + c\mathbf{n} \\ &= \begin{bmatrix} \sqrt{\left(x-x_2^0\right)^2+\left(y-y_2^0\right)^2} - \sqrt{\left(x-x_1^0\right)^2+\left(y-y_1^0\right)^2} \\ \sqrt{\left(x-x_3^0\right)^2+\left(y-y_3^0\right)^2} - \sqrt{\left(x-x_1^0\right)^2+\left(y-y_1^0\right)^2} \\ \vdots \\ \sqrt{\left(x-x_M^0\right)^2+\left(y-y_M^0\right)^2} - \sqrt{\left(x-x_1^0\right)^2+\left(y-y_1^0\right)^2} \end{bmatrix} + c\mathbf{n}\end{aligned} \quad . \tag{3}$$

The ith entry of $\Delta\mathbf{r}$, Δr_i, is normal distribution with mean $\left(r_i^0 - r_1^0\right)$ and variance σ^2. We use Maximum-Likelihood estimation to solve the emitter source location (x, y). According to the assume that all entries of $\Delta\mathbf{r}$ are independent, the likelihood function $f(x, y)$ is derived as

$$\begin{aligned} f(x,y) &= \prod_{i=2}^{M} \frac{1}{\sqrt{2\pi}\sigma} \exp\left\{-\frac{\left(\Delta r_i - r_i^0 + r_1^0\right)^2}{2\sigma^2}\right\} \\ &= \left(\frac{1}{\sqrt{2\pi}\sigma}\right)^{M-1} \exp\left\{-\frac{\left(\Delta\mathbf{r}-\mathbf{r}+\mathbf{r}_1\right)^T\left(\Delta\mathbf{r}-\mathbf{r}+\mathbf{r}_1\right)}{2\sigma^2}\right\} \end{aligned} \quad . \tag{4}$$

Thus, the emitter source location (x, y) can be optimized as

$$(x,y)^* = \arg\left\{\min\left[\left(\Delta\mathbf{r}-\mathbf{r}+\mathbf{r}_1\right)^T\left(\Delta\mathbf{r}-\mathbf{r}+\mathbf{r}_1\right)\right]\right\}. \tag{5}$$

We can obtain the optimal solution to the source location without erroneous receiver positions by (5). However in practice the receiver positions have measurement errors at different levels. The receiver position errors have to be taken into account in order to more accurately estimate the source location.

2.2 Source Location Model with Erroneous Receiver Positions

Since the receiver positions have error so that only

$$\mathbf{s}_i = \mathbf{s}_i^0 + \boldsymbol{\varepsilon}_i \quad i = 1, \cdots M \tag{6}$$

are available, where $\mathbf{s}_i^0 = [x_i^0, y_i^0]^T$ is the ith receiver's true position, and $\boldsymbol{\varepsilon}_i = [\varepsilon_{xi}, \varepsilon_{yi}]^T$ is the error vector in the receiver position $\mathbf{s}_i$. The task is to find $\mathbf{u}$ and $\mathbf{s}_i^0$, for $i = 1, 2, ..., M$.

Let $\boldsymbol{\theta}=\left[\mathbf{u}^T,(\mathbf{s}_1^0)^T,(\mathbf{s}_2^0)^T,\cdots,(\mathbf{s}_M^0)^T\right]^T$ be the unknown parameter vector of true emitter source and receiver positions. The mathematical problem of estimating $\boldsymbol{\theta}$ can be expressed as the following algebraic relationship

$$f\left(\boldsymbol{\theta}\right)=\mathbf{T}=\mathbf{M}-\mathbf{E} \tag{7}$$

where $\mathbf{T}=\left[r_{21}^0,\cdots,r_{M1}^0,(\mathbf{s}_1^0)^T,\cdots,(\mathbf{s}_M^0)^T\right]^T=\left[\Delta\mathbf{r}^T,(\mathbf{s}^0)^T\right]^T$, $\Delta\mathbf{r}=\left[r_{21}^0,\cdots,r_{M1}^0\right]^T$, is the vector of true TDOA values, and $\mathbf{s}^0=\left[(\mathbf{s}_1^0)^T,\cdots,(\mathbf{s}_M^0)^T\right]^T$ is the vector of true receiver positions, $\mathbf{M}=\left[r_{21},\cdots,r_{M1},(\mathbf{s}_1)^T,\cdots,(\mathbf{s}_M)^T\right]^T$ is the vector of measurement data, and $\mathbf{E}=\left[cn_{21},\cdots,cn_{M1},(\boldsymbol{\varepsilon}_1)^T,\cdots,(\boldsymbol{\varepsilon}_M)^T\right]^T$ is the vector of error.

We assume that all entries of $\boldsymbol{\theta}$ are independent with each other and employ Maximum-Likelihood method to estimate $\boldsymbol{\theta}$. The likelihood function is obtained as

$$\begin{aligned} f(\boldsymbol{\theta})&=\prod_{i=2}^{M}\frac{1}{\sqrt{2\pi}\sigma_i}\exp\left\{-\frac{\left(\Delta r_i-r_i+r_1\right)^2}{2\sigma_i^2}\right\}\prod_{i=1}^{M}\frac{1}{\sqrt{2\pi}\sigma_{\varepsilon i}}\exp\left\{-\frac{\left(x_i-x_i^0\right)^2+\left(y_i-y_i^0\right)^2}{2\sigma_{\varepsilon i}^2}\right\}\cdot\\ &=\prod_{i=1}^{M}\frac{1}{(2\pi)^{M-1+\frac{1}{2}}\sigma_i\sigma_{\varepsilon i}}\exp\left\{-\sum_{i=1}^{M}\left[\frac{\left(\Delta r_i-r_i+r_1\right)^2}{2\sigma_i^2}+\frac{\left(x_i-x_i^0\right)^2+\left(y_i-y_i^0\right)^2}{2\sigma_{\varepsilon i}^2}\right]\right\}\end{aligned} \tag{8}$$

Define $J(\boldsymbol{\theta})$ as follows:

$$J(\boldsymbol{\theta})=\sum_{i=1}^{M}\left(\left(\Delta r_i-r_i+r_1\right)^2+\left(x_i-x_i^0\right)^2+\left(y_i-y_i^0\right)^2\right)\cdot \tag{9}$$

Thus, the parameter set $\boldsymbol{\theta}^*$ can be optimized as

$$\begin{aligned}\boldsymbol{\theta}^*&=\arg\left\{\min\left[\sum_{i=1}^{M}\left(\left(\Delta r_i-r_i+r_1\right)^2+\left(x_i-x_i^0\right)^2+\left(y_i-y_i^0\right)^2\right)\right]\right\},\\ &=\arg\left\{\min\left[\left(\Delta\tilde{\mathbf{r}}-\mathbf{r}+\mathbf{r}_1\right)^T\left(\Delta\tilde{\mathbf{r}}-\mathbf{r}+\mathbf{r}_1\right)+\left(\mathbf{s}-\mathbf{s}^0\right)^T\left(\mathbf{s}-\mathbf{s}^0\right)\right]\right\}\end{aligned} \tag{10}$$

where $\Delta\tilde{\mathbf{r}}=\left[\Delta r_1,\Delta r_2,\cdots,\Delta r_M\right]^T$ and $\mathbf{s}=[(\mathbf{s}_1)^T,...,(\mathbf{s}_M)^T]^T$.

2.3 Modified Genetic Algorithm

The function $f\left(\boldsymbol{\theta}\right)$ is not convex, and it is very difficult for analytical methods to solve this problem. In this paper, $f\left(\boldsymbol{\theta}\right)$ is optimized by the modified Genetic Algorithm. The algorithmic procedure is given as follows:

A. Encoding

Since the range of solution space and corresponding localization accuracy are unknown, we employ real code, instead of the commonly used binary code. The solved emitter location and receiver positions are aligned as a chromosome vector

$$\boldsymbol{\theta}^{(i)} = \left[x^{(i)}, y^{(i)}, x_1^{0(i)}, y_1^{0(i)}, \cdots, x_M^{0\,(i)}, y_M^{0\,(i)} \right]$$

where $\left(x^{(i)}, y^{(i)}\right)$ is the source location, and $\left(x_j^{0(i)}, y_j^{0(i)}\right), j = 1, \cdots, M$ is the receiver positions.

B. Deciding on a fitness function

According to the theory of the maximum likelihood estimation, each individual regards (9) as the objective function. Smaller value of $J(\boldsymbol{\theta}^{(i)})$ indicates better fitness. Thus, the fitness function can be defined as

$$g\left(\boldsymbol{\theta}^{(i)}\right) = \frac{1}{J(\boldsymbol{\theta}^{(i)})} = \frac{1}{\left(\Delta\mathbf{r} - \mathbf{r} + \mathbf{r}_1\right)^T \left(\Delta\mathbf{r} - \mathbf{r} + \mathbf{r}_1\right) + \left(\mathbf{bs} - \mathbf{bs}^0\right)^T \left(\mathbf{bs} - \mathbf{bs}^0\right)\Big|_{\boldsymbol{\theta}^{(i)}}}$$

the total fitness is obtained as

$$F = \sum_{i=1}^{N} g\left(\boldsymbol{\theta}^{(i)}\right)$$

where N is the population size.

C. Selection operator

In this paper, we employ the most common selection operator-roulette wheel. It is implemented as follows:

① Compute each individual's fitness value $g\left(\boldsymbol{\theta}^{(i)}\right)$ and total fitness value F.

② Compute each individual's selection probability $P_i = g\left(\boldsymbol{\theta}^{(i)}\right)/F$, and accumulated probability $q_i = \sum_{j=1}^{i} P_j$.

③ Divide the roulette wheel into different sector regions according to the selection probability P_i, and then rotate the roulette wheel to select N individuals.

D. Crossover operator

It is well known that a constant crossover probability may lead to poor efficiency. In order to improve the robustness and efficiency of the algorithm, the adaptive crossover probability is adopted

$$P_c = \begin{cases} k_1 \times \dfrac{f_{\max} - f'}{f_{\max} - f_{avg}} & f' \geq f_{avg} \\ k_2 & f' < f_{avg} \end{cases} \tag{11}$$

where $k_1\,(0 \leq k_2 < k_1 \leq 1)$ and $k_2\,(0 \leq k_2 \leq 1)$ are constants, $f_{\max}$ and f_{avg} denote the maximum and average fitness of the whole population, respectively. f' is larger one between the two parents' fitness values.

The crossover operation is shown below:

① Select the L individuals for crossover according to the crossover probability.
② Swap between pair parent organisms and render two child organisms. Let $parent_1$ and $parent_2$ denote the two parent organisms for crossover operation, $child_1$ and $child_2$ denote the new two child organisms.

$$child_1 = \alpha \bullet parent_1 + \beta \bullet parent_2$$
$$child_2 = \beta \bullet parent_1 + \alpha \bullet parent_2$$

where $\alpha (0 \le \alpha \le 1)$ and $\beta = 1 - \alpha$ are randomly generated weights.

E. Mutation operator

The mutation probability is defined as

$$P_c = \begin{cases} k_3 \times \dfrac{f_{\max} - f'}{f_{\max} - f_{avg}} & f' \ge f_{avg} \\ k_4 & f' < f_{avg} \end{cases} \tag{12}$$

where k_3 ($0.001 \le k_4 < k_3 \le 0.01$) and k_4 ($0.001 \le k_4 \le 0.01$) are constants. $f_{\max}$, f_{avg}, and f' are the same as (11).

The main steps of mutation operation are as follows:

① Select mutation component from the L individuals which have carried out the crossover operation according to the mutation probability.
② Add a perturbation which is normally distributed to the mutation component.

3 Experimental Results

In this section, we conduct two sets of experiments in order to compare our proposed method with the original Taylor-series method [1] and modified Taylor-series method [9] in terms of the improvements in the performance of estimating source location and receiver positions. In the first set of experiments, we study the performance of three algorithms when the TDOA noise power is fixed and the receiver noise power varies. The second set of experiments examines the effect on the performance when the receiver noise power is fixed and the TDOA noise power varies.

We only consider the typical 7 base-station cellular network that has cells with a three-kilometre radius. The TDOA measurement vector is obtained by adding zero mean Gaussian noise with variance 100 to the true values. The receiver position noise and TDOA noise are independent. All experimental results are averaged over 100 trials and reported in Fig. 1-4. The horizontal axes of Fig.1-2 are the standard deviation of the receiver noise. The horizontal axes of Fig.3-4 are the standard deviation of the TDOA measurement. All the vertical axes are the root-mean-square error (RMSE). In these figures, MGA, Taylor and MTaylor stand for our proposed method, the original Taylor method, and the modified Taylor method.

In the first set of experiments, the TDOA noise power is set to $100/c^2$. All results are shown in Fig. 1-2. Fig. 1 compares accuracy of source and receiver positions estimation when the noise power factors of 7 receivers are identical and are set to $\sigma^2[1,1,1,1,1,1,1]$. As shown in Fig. 1, MGA performs better than MTaylor not only for estimating source location but also for estimating receiver positions. Fig. 1(a) shows that the original Taylor method produces slightly better performance than the MTaylor method when the standard deviation of the receiver position is less than 1. This is not surprising because MTaylor considers the receiver position errors. Fig. 2 compares performance of source and receiver positions estimation when the noise power factors of 7 receivers are set to $\sigma^2[1,1,1,1,7.5,10,2.5]$. It can be seen that when σ is relatively small, MGA and MTaylor give similar performance. However, MTaylor achieves better performance than MGA when σ is more than 10.

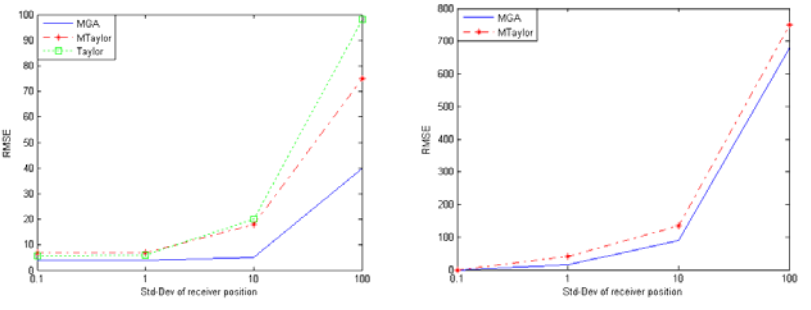

(a) (b)

Fig. 1. Comparison of the accuracy of source and receiver position estimation. Note that the noise power factors of 7 receivers are identical and are set to $\sigma^2[1,1,1,1,1,1,1]$. (a) The RMSE of source location estimation. (b) The RMSE of receiver position estimation.

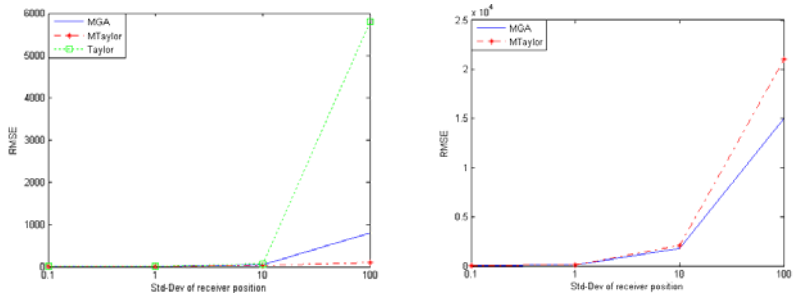

(a) (b)

Fig. 2. Comparison of the accuracy of source and receiver position estimation. Note that the noise power factors of 7 receivers are set to $\sigma^2[1,1,1,1,7.5,10,2.5]$. (a) The RMSE of source location estimation. (b) The RMSE of receiver position estimation.

In the second set of experiments, Fig. 3 compares accuracy of source and receiver position estimation using MGA, MTaylor and Taylor when each receiver position noise power is fixed at 100. Fig. 4 shows comparison result when the noise powers of 7 receivers are set to $[100,100,100,100,750,1000,250]$. As shown in Fig.3-4, MGA is worse than MTaylor when TDOA measurement noise is relatively small. However, MTaylor achieves significantly better performance when TDOA measurement noise is large. It shows that our proposed method provides more reasonable solution for adverse measurement circumvents.

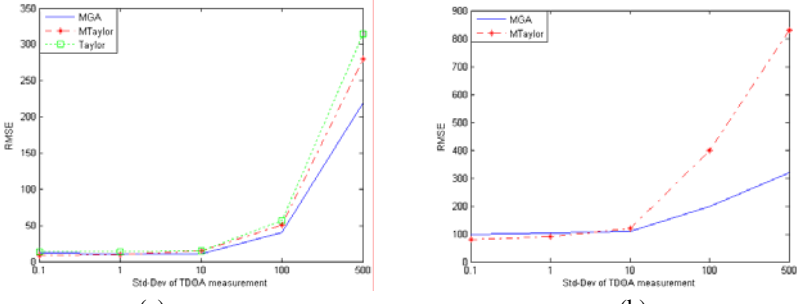

Fig. 3. Comparison of the accuracy of source and receiver position estimation. Note that each receiver noise power is fixed at 100. (a) The RMSE of source location estimation. (b) The RMSE of receiver position estimation.

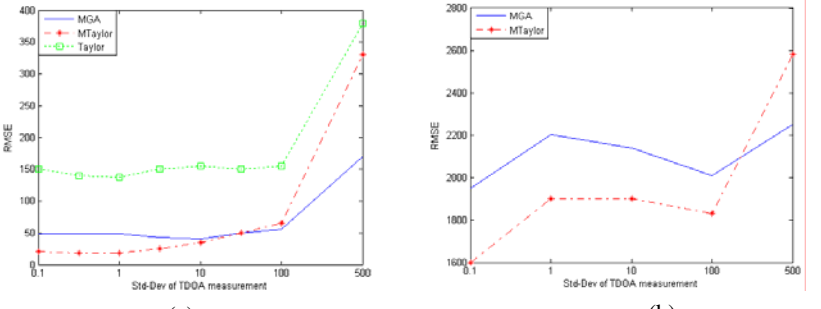

Fig. 4. Comparison of the accuracy of source and receiver position estimation. Note that the noise powers of 7 receivers are set to $[100,100,100,100,750,1000,250]$. (a) The RMSE of source location estimation. (b) The RMSE of receiver position estimation.

These two sets of experiments reveal a number of interesting points:

① When each receiver noise has identical normal distribution, MGA obtains better performance than other two methods as the receiver position error or TDOA measurement error becomes large.

② When each receiver noise has different normal distribution and the receiver position error or TDOA measurement error is small, MGA is worse than MTaylor. However, MGA can achieve significantly better performance than other two methods as the receiver position error or TDOA measurement error becomes large.
③ MGA is the best choice among the tree compared algorithms for adverse measurement circumvents.

4 Conclusions

In this paper, we proposed an efficient source and receiver position localization method. In our algorithm, joint estimation of the emitter location and the receiver positions based on TDOA measurement is considered. It combines Genetic Algorithm and TDOA to provide an efficient approach. Specifically, MGA demonstrates better performance for adverse measurement circumvents. Extensive experimental results show that our method consistently outperforms MTaylor and Taylor when the receiver position error or TDOA measurement error become large.

References

1. Foy, W.H.: Position-location Solution by Taylor-series Estimations. IEEE Trans. Aerosp. Electron. Syst. AES-12, 187–194 (1976)
2. Chan, Y.T., Ho, K.C.: An Efficient Closed-form Localization Solution from Time Difference of Arrival Measurements. In: Proc. IEEE ICASSP, Australia, pp. II/393–II/396 (1994)
3. Rockah, Y., Schultheiss, P.M.: Array Shape Calibration Using Sources in Unknown Location Part I: Far-field Source. IEEE Trans. Acoust., Speech, Signal Processing ASSP-35(3), 286–299 (1987)
4. Rockah, Y., Schultheiss, P.M.: Array Shape Calibration Using Sources in Unknown Location Part II:Near-field Source and Estimator Implementation. IEEE Trans. Acoust., Speech, Signal Processing ASSP-35(6), 724–735 (1987)
5. Chen, Y.M., Lee, J.H., Yeh, C.C.: Two-dimensional Angle-of-arrival Estimation for Uniform Planar Array with Sensor Position Errors. In: IEE Proc. Radar, Signal Processing, vol. 140(1), pp. 37–42 (1993)
6. Ng, B.P., Er, M.H., Kot, C.: Array Gain/Phase Calibration Techniques for Adaptive Beam Forming and Direction Finding. In: Proc. IEE Radar, Sonar Navig., vol. 141(1), pp. 25–29 (1994)
7. Weiss, A.J., Friedlander, B.: Array Shape Calibration Using Sources in Unknown Locations - a Maximum Likelihood Approach. In: Proc. IEEE ICASSP, New York, pp. 2670–2673 (1988)
8. Ho, K.C., Kovavisaruch, L., Parikh, H.: Source Localization Using TDOA with Erroneous Receiver Positions. In: Proc. IEEE ISCAS, Vancouver, pp. II/453–II/456 (2004)
9. Kovavisaruch, L., Ho, K.C.: Modified Taylor-series Method for Source and Receiver Localization Using TDOA Measurements with Erroneous Receiver Positions. In: Proceedings of the IEEE International Symposium on Circuits and Systems, Kobe, Japan, pp. 2295–2298 (2005)
10. Li, L.C., Ran, C.S., Wei, F.: An Enhanced Genetic Algorithm for the Nonlinear Optimization in TDOA-based Location. System Engineering and Electronics 25(8), 971–973 (2003)

Interactive Genetic Algorithms with Variational Population Size*

Jie Ren, Dun-wei Gong, Xiao-yan Sun, Jie Yuan, and Ming Li

School of Information and Electrical Engineering,
China University of Mining and Technology, 221008, Xuzhou, China
renjie19850210@sina.com

Abstract. Traditional interactive genetic algorithms often have small population size because of a limited human-computer interface and user fatigue, which restricts these algorithms' performances to some degree. In order to effectively improve these algorithms' performances and alleviate user fatigue, we propose an interactive genetic algorithm with variational population size in this paper. In the algorithm, the whole evolutionary process is divided into two phases, i.e. fluctuant phase and stable phase of the user's cognition. In fluctuant phase, a large population is adopted and divided into several coarse clusters according to the similarity of individuals. The user only evaluates these clusters' centers, and the other individuals' fitness is estimated based on the acquired information. In stable phase, the similarity threshold changes along with the evolution, leading to refined clustering of the population. In addition, elitist individuals are reserved to extract building blocks. The offspring is generated based on these building blocks, leading to a reduced population. The proposed algorithm is applied to a fashion evolutionary design system, and the results validate its efficiency.

Keywords: Interactive genetic algorithms, User fatigue, Variational population size, Clustering, Building blocks.

1 Introduction

Interactive genetic algorithms (IGAs), proposed in mid 1980s, are effective methods to solve an optimization problem with implicit or fuzzy indices [1]. These algorithms combine traditional evolution mechanism with a user's intelligent evaluation, and the user assigns an individual's fitness rather than a function that is difficult or even impossible to be explicitly expressed. Up to now, they have been successfully applied in design of simple emoticons [2], color design [3], hearing aid fitting [4] and so on.

The obvious characteristic of IGAs, compared with traditional genetic algorithms, is that the user assigns an individual's fitness. Frequent interactions result in user fatigue, therefore traditional IGAs often have small population

* This work was supported by NSFC with grant No.60775044 and Program for New Century Excellent Talents in University with grant No.NCET-07-0802.

D.-S. Huang et al. (Eds.): ICIC 2009, LNAI 5755, pp. 64–73, 2009.

size and few evolutionary generations, which restrict the performance of these algorithms in exploration and their applications in complicated optimization problems. Therefore user fatigue problem becomes the core problem of IGAs.

In general, if a large population size is adopted, more different individuals can be searched through evolving a generation, which increases the opportunity of looking for satisfactory individuals. However, if traditional approaches are still adopted to evaluate all these individuals, user fatigue will be unavoidably increased. In fact, many algorithms have adopted clustering methods to deal with a large population. Lee and Kim et al. proposed IGAs and GAs with a large population based on K-means clustering algorithm, respectively [5] [6]. The user only evaluates the center of a cluster, and the fitness of the other individuals in the same cluster is allocated with proportional to the distance from the center. But the value of K, a key parameter in these algorithms, needs to be determined in advance. Too large or too small value of K will result in bad performance of these algorithms. The clustering method proposed in [7] overcomes the above defect. The number of clusters is not set in advance but changes along with the evolution. Whether some individuals belong to the same cluster or not is determined by the similarity threshold which is set in advanced. However, the threshold is constant during the evolution. If it is too large, a cluster may include only few individuals; otherwise, if it is too small, this algorithm is hard to convergence in anaphase. Therefore a constant similarity threshold is unreasonable.

In order to improve the performance of IGAs in exploration and exploitation as well as not increasing user fatigue, we propose a novel clustering method in which the similarity threshold is variational along with the evolution. The whole evolutionary process is divided into two phases, i.e. fluctuant phase and stable phase of a user's cognition. In fluctuant phase, constant population size is adopted and the similarity threshold does not change. In stable phase, a population with variational population size is adopted, and the similarity threshold changes along with the evolution. The following section presents the proposed algorithm in detail.

2 Interactive Genetic Algorithms with Variational Population Size

2.1 Ideas of Algorithms

The following optimization problem is considered in this paper:

$$\begin{aligned} & \max f(x), \\ \texttt{s.t. } & x = (x_1, x_2, \ldots, x_I) \in S, \\ & S = g_1 \times g_2 \times \ldots \times g_I, \\ & x_i \in g_i, i = 1, 2, \ldots, I \ , \end{aligned} \tag{1}$$

where $f(x)$ is a performance index to be optimized, and cannot be expressed by an explicit function, x is an I-dimensional integer decision variable belonging to

the domain S. On condition of not causing confusion, we also denote x and S as the corresponding individual and the search space, respectively.

The idea of the proposed algorithm is as follows. The whole evolutionary process is divided into two phases. The first phase is evolutionary prophase and called fluctuant phase of the user's cognition. In this phase, a large population is adopted to evolve and divided into several coarse clusters according to the similarity of individuals. The user only evaluates these clusters' centers, and the other individuals' fitness is estimated based on the fitness of these centers. The population size and the similarity threshold are constant in this phase. The second phase is evolutionary anaphase and called stable phase of the user's cognition. In this phase, the similarity threshold changes along with the evolution, leading to refined clustering of the population. In addition, some elitist individuals are reserved to extract building blocks. The offspring is generated based on these building blocks, leading to a reduced population.

2.2 Division of Evolutionary Process

In this paper, the case that an individual's genotype is divided into $N_{\mathbf{g}}$ gene meaning units and expressed with several integers is considered. For details about gene meaning units, please refer to [8]. For the i-th individual x_i , its genotype can be expressed as $x_i = x_{i1}x_{i2}\ldots x_{iN_{\mathbf{g}}}$. The proportion of an individuals' allele gene meaning units changes along with the evolution, and a larger proportion of some allele gene meaning units indicates that the user's preference on them is clear. Therefore, the whole evolutionary process is divided into two phases according to the variation of the proportion, i.e. fluctuant phase and stable phase of the user's cognition.

The population in the t-th generation is denoted as $X(t) = \{x_1(t), x_2(t), \ldots, x_{N_{(t)}}(t)\}$, with $N(t)$ being the population size. The number of individuals with j-th gene meaning unit being k is denoted as $r_k(j)$. Then proportion of $r_k(j)$ in the current population $X(t)$ is expressed as $p_k(j) = \frac{r_k(j)}{N(t)}$. For the whole evolutionary process, the bigger $p_k(j)$ is, the more the user prefers the part corresponding to the j-th gene meaning unit being k, and the clearer the user's cognition on this gene meaning unit is. If the following formula is met:

$$p_k(j) > \mu_0 \ , \tag{2}$$

where μ_0 is a division threshold set in prior, we say that the user's cognition is clear, and the evolution goes into stable phase of the user's cognition.

In fluctuant phase, the user's preference is fluctuant, and the population size is set a large constant in order to ensure the diversity of the population. On condition of not increasing the number of individuals being evaluated by the user, it is necessary to divide the large population into several clusters. The user only evaluates one representative individual of a cluster, and the fitness of the other individuals is estimated based on that of the evaluated ones.

2.3 Clustering of Population

In this paper, the population is divided into several clusters according to the similarity of individuals. The user evaluates all clusters' centers, and the fitness of the other individuals is estimated based on the information.

For two individuals $x_i(t)$ and $x_j(t)$, the more they have the same allele gene meaning units, the higher the similarity degree of their phenotypes is. Therefore, the similarity degree of individuals can be defined as follows.

$$\alpha(x_i(t), x_j(t)) = \frac{1}{N_{\mathrm{g}}} \sum_{m=1}^{N_{\mathrm{g}}} \alpha_m(x_i(t), x_j(t)) \ , \tag{3}$$

where

$$\alpha_m(x_i(t), x_j(t)) = \begin{cases} 1 & x_{im} = x_{jm} \ , \\ 0 & x_{im} \neq x_{jm} \ . \end{cases}$$

Based on the above definition of the similarity degree, the principle of clustering the evolutionary population is given as follows. If there exists an $m \in \{1, 2, \ldots, N_g\}$ with $\alpha_m(x_i(t), x_j(t)) = 1$ and $\alpha(x_i(t), x_j(t)) \geq \alpha_0(t)$, then $x_i(t)$ and $x_j(t)$ belong to the same cluster, where $\alpha_0(t)$ is a similarity threshold and set in prior.

Supposing that $X(t)$ can be divided into $N_c(t)$ clusters, and $N_c(t) \leq N_{\mathtt{maxd}}$, where $N_{\mathtt{maxd}}$ is the maximum number of clusters and determined by the human-computer interface. In order to obtain those clusters of $X(t)$, first, an individual is randomly selected from $X(t)$, e.g. $x_i(t)$, to be the center of the first cluster, and then a gene meaning unit in $x_i(t)$ is randomly chosen, e.g. the m-th. Then we look for all individuals $x_j(t), j = 1, 2, \ldots, N(t), j \neq i$ from $X(t)$ satisfying $\alpha_m(x_i(t), x_j(t)) = 1$ and $\alpha(x_i(t), x_j(t)) \geq \alpha_0(t)$, and obtain the first cluster of $X(t)$, denoted as $\{c_1(t)\} = \{x_j(t) | \alpha_m(x_i(t), x_j(t)) = 1, \alpha(x_i(t), x_j(t)) \geq \alpha_0(t), x_j(t) \in X(t)\}$, and its center as $c_1(t)$, i.e. $c_1(t) = x_i(t)$. Let $X(t) \leftarrow X(t) \backslash \{c_1(t)\}$, and another individual is randomly selected from $X(t)$ to be the center of the second cluster, repeating the above process to obtain the second cluster $\{c_2(t)\}$,..., until $X(t)$ has no individual or $N_c(t) = N_{\mathtt{maxd}}$.During clustering $X(t)$, when $N_c(t) = N_{\mathtt{maxd}} - 1$ and $X(t)$ still has some individuals not being clustered, they will be put into the $N_{\mathtt{maxd}}$-th cluster regardless of their similarity degree.

In general, the population is much dispersive in fluctuant phase and often divided into $N_c(t) = N_{\mathtt{maxd}}$ clusters. Whereas the population is often convergent in stable phase. During the clustering, if $X(t)$ has no individual and $N_c(t) < N_{\mathtt{maxd}}$, it is necessary to increase the value of $\alpha_0(t)$ in order to guarantee $N_c(t) = N_{\mathtt{maxd}}$, which indicates refined clustering of the population.

Having obtained these $N_c(t)$ clusters of $X(t)$, i.e, $\{c_1(t)\}, \{c_2(t)\}, \ldots, \{c_{N_c}(t)\}$ with centers being $c_1(t), c_2(t), \ldots, c_{N_c}(t)$, respectively, all these centers are displayed to the user for evaluation. The fitness of the other individuals is estimated using the method proposed in [7].

Obviously, the value of $\alpha_0(t)$ determines the granularity of the population's clustering, which will greatly influence the estimation of an individual's fitness. Therefore the value of $\alpha_0(t)$ should be changed along with the evolution.

2.4 Variation of $\alpha_0(t)$

$\alpha_0(t)$ reflects the similarity degree of individuals in the same cluster. The bigger the value of $\alpha_0(t)$, the more similar the individuals in the same cluster are, and vice versa. Furthermore, the bigger the value of $\alpha_0(t)$, the more refined the clustering is. In fluctuant phase, a small constant of $\alpha_0(t)$ is adopted to roughly cluster the population. Whereas in stable phase, the diversity of the population decreases and the individuals are similar to each other. If the value of $\alpha_0(t)$ is still constant, the clustering is too rough and the maximum number of clusters is hard to reach. Therefore, the value of $\alpha_0(t)$ should increase to refine the clustering of the population so as to increase the accuracy of the estimated individual's fitness.

In fluctuant phase, $\alpha_0(t)$ is set $\frac{1}{N_g}$. When the population evolves into stable phase, if $N_c(t) < N_{\texttt{maxd}}$, which indicates that the current $\alpha_0(t)$ cannot guarantee the maximum number to be reached, the value of $\alpha_0(t)$ is increased to $\alpha_0(t) \leftarrow \alpha_0(t) + \frac{1}{N_g}$ to increase the number of clusters, hence improving the clustering precision.

2.5 Variations of Population Size

The user's cognition is clear in stable phase, the gene meaning units that the user prefers are more and more, and they are all reserved to the next generation, i.e. the number of individuals' uncertain gene meaning units are less and less, so the number of new individuals different from their parents decreases. In order to reduce the user's evaluation burden, duplicative individuals should be avoided, therefore the population size should be changed, i.e., the population size is different in different generations of stable phase.

First, individuals from k_s clusters with superior centers are reserved, and denoted as $X_s(t) = \{X_{s1}(t), X_{s2}(t), \ldots, X_{s\overline{N}_t}(t)\}$, where $\overline{N}(t)$ is the total number of selected individuals. Based on these individuals in $X_s(t)$, building blocks are extracted so as to generate non-duplicated new individuals.

Let $B = b_1 b_2 \ldots b_{N_g}$ be a building block. For all individuals in $X_s(t)$, the proportion of the individuals whose j-th allele meaning unit being the value of k is calculated, and denoted as $p_k^{'}(j) = \frac{r_k^{'}(j)}{\overline{N}(t)}$. A larger $p_k^{'}(j)$ means that the value of the j-th gene meaning unit of B has more opportunities to be k. Therefore, the building block can be as follows.

$$b_j = \begin{cases} k & p_k^{'}(j) \geq \alpha \ , \\ * & p_k^{'}(j) < 1 - \alpha \ , \end{cases} \tag{4}$$

where $\alpha \in (0.5, 1)$ and is set in prior.

In the subsequent evolution, new individuals are generated according to the extracted building blocks. The number of non-duplicated new individuals is determined by the number of $*$ in B, therefore the population size is related with the number of $*$. The determined bits of building blocks based on the superior individuals become more and more along with the evolution, hence the number of non-duplicated new individuals is smaller and smaller. It is necessary to change population size during the evolution. It is easy to understand that the number of $*$ is closely related with the similarity degree of those superior individuals in $X_s(t)$. Denoted the similarity degree of $X_s(t)$ as $A(X_s(t))$, then $A(X_s(t))$ can be expressed as follows.

$$A(X_s(t)) = \frac{2}{\overline{N}(t)(\overline{N}(t)-1)} \sum_{i=1}^{\overline{N}(t)-1} \sum_{j=i+1}^{\overline{N}(t)} \alpha(x_{si}(t), x_{sj}(t)) \ . \tag{5}$$

It is easy to observe that $A(X_s(t)) \in [0,1]$, and the more similar the individuals in $X_s(t)$, the closer $A(X_s(t))$ approaches to 1, and the less the number of $*$ in building blocks is, so the population size should be decrease, and vice versa. Therefore, the population size can be varied according to

$$N(t) = \lceil ((1 - N(t_1)) \cdot A(X_s(t)) + N(t_1)) \cdot e^{-\frac{t-t_1}{\beta - t_1}} \rceil, t_1 < t < \beta \ , \tag{6}$$

where t_1 is the generation when the user's cognition becomes stable, and obtained according to formula (2), $N(t_1)$ is the population size in that generation, β is a constant larger than t_1, and $\lceil \cdot \rceil$ is the upper integer function. In the evolutionary anaphase, if $N(t)$ is bigger than $N^{'}$, the number of non-duplicated new individuals generated by building blocks, then we let $N(t) = N^{'}$.

3 Analysis of Algorithm's Performances

In this section, the performance of the proposed algorithm (IGA-VPS, for short) is quantitatively analyzed and compared with a traditional IGA (TIGA, for short).

First, on condition of the same evolutionary generations, the algorithm's performance in having more opportunities to look for satisfactory solutions is investigated by considering the number of different individuals being searched. Denote $N_{\texttt{maxd}}$ as the number of individuals being evaluated by the user in each generation, and T as the terminative evolutionary generation. For convenience, that the searched individuals are non-duplicated is assumed. For TIGA, the total number of individuals being searched is $N_{\texttt{maxd}} \cdot T$; But for IGA-VPS, the population size of each generation is $N(t) = \sum_{i=1}^{N_{\texttt{maxd}}} L(c_i(t))$, where $L(c_i(t))$ is the number of individuals in $\{c_i(t)\}$, and the number of individuals being searched in IGA-VPS is $\sum_{t=1}^{T} \sum_{i=1}^{N_{\texttt{maxd}}} L(c_i(t))$. For $L(c_i(t)) \geq 1, i = 1, 2, \ldots, N_{\texttt{maxd}}$, and the equality is held only when $\alpha_0(t) = 1$, hence $\sum_{t=1}^{T} \sum_{i=1}^{N_{\texttt{maxd}}} L(c_i(t)) > N_{\texttt{maxd}} \cdot T$, i.e. IGA-VPS has more opportunities to look for satisfactory individuals compared with TIGA.

Second, also on the above condition, the number of individuals being evaluated by the user is considered so as to illustrate the user's evaluation burden. For TIGA, the user evaluates $N_{\texttt{maxd}} \cdot T$ individuals. For IGA-VPS, there are $t_1 - 1$ and $T - (t_1 - 1)$ generations in fluctuant phase and stable phase, respectively. Thus the number of individuals being evaluated by the user is $(t_1 - 1) \cdot N_c(t) + (T - t_1 + 1) \cdot N_{\texttt{maxd}}$. For $N_c(t) \leq N_{\texttt{maxd}}$, $(t_1 - 1) \cdot N_c(t) + (T - t_1 + 1) \cdot N_{\texttt{maxd}} \leq N_{\texttt{maxd}} \cdot T$ is held, which indicates that the number of individuals being evaluated by the user in IGA-VPS does not increase compared with that in TIGA.

It can be concluded from the above analysis that IGA-VPS has more opportunities to look for satisfactory individuals than TIGA on condition of not increasing user fatigue, which indicates that IGA-VPS is more advantageous in exploration than TIGA.

4 Application in Fashion Evolutionary Design System

Fashion evolutionary design system is a typical application platform for interactive genetic algorithms. Therefore, we develop a fashion evolutionary design system using Visual Basic 6.0 to validate the performance of our algorithm compared with TIGA.

4.1 Parameter Settings

In order to compare the performance of the two algorithms, the same genetic operators and parameters are adopted, including tournament selection with size being 2, one-point crossover and one-point mutation with their probabilities being 0.6 and 0.02, respectively, as well as the elitism strategy. The population size of TIGA is equal to the maximum number of clusters $N_{\texttt{maxd}} = 10$ of IGA-VPS, and the upper limit and lower limit of fitness are 1000 and 0, respectively. The initial population size of IGA-VPS is 200, other parameters are $\mu_0 = 0.25$, i.e., if proportion of one allele meaning unit is larger than one quarter, evolution goes into stable phase of the user's cognition, $\alpha = 0.8$, $k_s = 1$ and $\beta = 25$. The terminative criterion of these algorithms is that the optimal solution is found.

4.2 Evolutionary Interfaces and Individual's Evaluation

The interactive interface of IGA-CPS, shown as Fig. 1, includes 3 parts. The first one is individuals' phenotypes, their fitness and the common gene meaning unit of each cluster. The second one is some command buttons for a population evolving, e.g., "Initialize", "Next Generation", "End" and "Exit." And the third one is some statistical information of the evolution, including the current generation, time-consuming, and the best individual being searched so far.

By clicking the "Initialize" button, an initial large population is randomly generated, the population is then clustered, and those clusters' centers are displayed through the interface to the user for evaluation. The fitness of these centers is an accurate number and assigned by the user, as shown in Fig. 1. It can be observed from Fig. 1 that the number of individuals being evaluated in the first generation

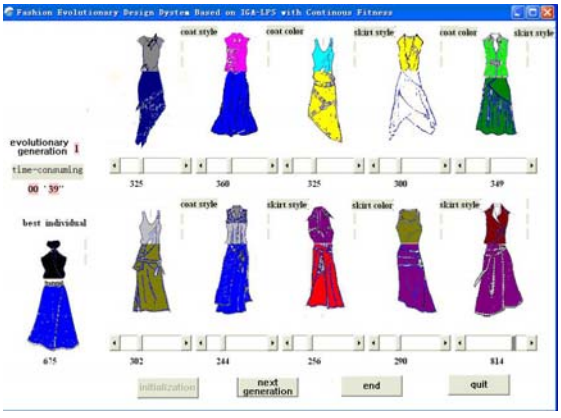

Fig. 1. Interface of human-computer interaction in IGA-VPS

is 10, $N_c(1) = N_{\texttt{maxd}} = 10$. Having evaluated $N_c(t)$ centers of the population in the t-th generation, if the user clicks "Next Generation" button, the system will generate offspring according to the evolutionary strategies set in subsection 4.1, cluster them, and display all clusters' centers to the user. The system will cycle the above process, until the user manually stops the evolution.

4.3 Results and Analysis

First, the variation of $\alpha_0(t)$ along with the evolution is investigated. We run the experimental system for 10 times and the average of $\alpha_0(t)$ is calculated. The result is shown as Fig. 2. It can be observed from Fig. 2 that in the prophase evolution, about 4 generations, the average of $\alpha_0(t)$ keeps constant, which indicates that the evolution is in fluctuant phase of the user's cognition. In the evolution of stable phase, the average of $\alpha_0(t)$ increases along with t, which indicates that the difference among individuals decreases and the clustering is more and more refined.

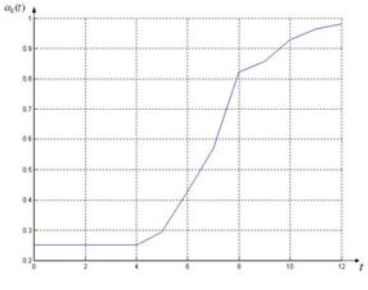

Fig. 2. Variation of $\alpha_0(t)$ along with t

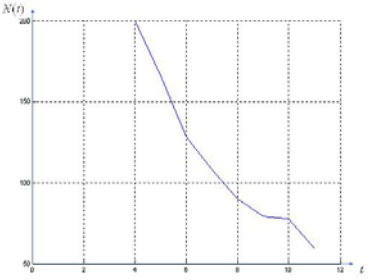

Fig. 3. Variation of population size along with t

Second, the variation of the population size along with the evolution is investigated, and the result is shown in Fig. 3. It can be concluded from Fig. 3 that the population size does not change in the first 4 generations, which implies that the evolution is in fluctuant phase, hence well according with the conclusion about $\alpha_0(t)$. Similarly, in the evolution of stable phase, the population size decreases along with t.

Finally, the performance of IGA-VPS and TIGA is compared. We perform 10 independent runs for each algorithm, and the statistical results are listed in Table 1.

Table 1. Statistical results

algorithm	generations	♯ of individuals evaluated by user	time-consuming
IGA-VPS	13.7	137	3'46"
TIGA	31.2	226.4	7'37"

It can be observed from Table 1 that the average evolutionary generations of TIGA is 31.2, which is over the double of that of IGA-VPS. The results illuminate that the proposed algorithm greatly reduces the evolutionary generations on condition of finding the expected optimal solution. The average number of individuals being evaluated by the user of IGA-VPS (137) is much less than that of TIGA (226.4). Combined with evolutionary generations of the two algorithms, the results are consequential. The main reason is that the diversity of the population is well maintained by adopting the individuals' generation method and more opportunities are guaranteed to find the optimal solution. It can be known that the more the number of individuals being evaluated by the user in the evolution, the more he/she feels tired. Therefore IGA-VPS greatly alleviates user fatigue. This conclusion is also validated by the average time-consuming of the user's evaluation. For TIGA, the time-consuming is 7'37", about the double of that of IGA-VPS with 3'46".

It can be concluded from above comparisons that the proposed algorithm greatly alleviates user fatigue and has more opportunities to find the optimal solutions.

5 Conclusions

In TIGAs, the population size is generally small due to the human-computer interface and user fatigue, which greatly influences the algorithms' performances. To overcome such disadvantage, we propose an IGA with variational population size based on our previous work on clustering methods of a large population. First, the whole evolutionary process is divided into two phases, and then different population size and clustering thresholds are adopted in different phases. The experimental results show that the proposed algorithm is advantageous in alleviating user fatigue and improving the ability in exploration.

An individual's fitness in our algorithm is an accurate number that cannot well reflect the user's fuzzy cognition, so how to express and estimate an individuals uncertain fitness in IGAs with large population size is a problem to be further researched.

References

1. Dawkins, R.: The Blind Watchmaker. Longman, Harlow (1986)
2. Dozier, G., Carnahan, B., Seals, C., et al.: An Interactive Distributed Evolutionary Algorithm (IDEA) for Design. In: The IEEE International Conference on Systems, Man and Cybernetics, pp. 418–422. IEEE Press, New York (2005)
3. Kagawa, T., Nishino, H., Utsumiya, K.: A Color Design Assistant Based on User's Sensitivity. In: The IEEE International Conference on Systems, Man and Cybernetics, pp. 974–979. IEEE Press, Los Alamitos (2003)
4. Takagi, H., Ohsaki, M.: Interactive Evolutionary Computation-based Hearing Aid Fitting. J. IEEE Transactions on Evolutionary Computation 11, 414–427 (2007)
5. Lee, J.Y., Cho, S.B.: Sparse Fitness Evaluation for Reducing User Burden in Interactive Algorithm. In: 1999 IEEE International Fuzzy Systems Conference, pp. 998–1003. IEEE Press, New York (1999)
6. Kim, H.S., Cho, S.B.: An Efficient Genetic Algorithm with Less Fitness Evaluation by Clustering. In: IEEE Congress on Evolutionary Computation, pp. 887–894 (2001)
7. Gong, D.W., Yuan, J., Ma, X.P.: Interactive Genetic Algorithms with Large Population Size. In: 2008 IEEE Congress on Evolutionary Computation, pp. 1678–1685. IEEE Press, New York (2008)
8. Gong, D.W., Hao, G.S., Zhou, Y., Guo, Y.N.: Theory and Applications of Interactive Genetic Algorithms. Defense Industry Press, Beijing (2007) (in Chinese)

A Unified Direct Approach to Image Registration and Object Recognition with a Hybrid Evolutionary Algorithm

Igor V. Maslov[1] and Izidor Gertner[2]

[1] Dept. of Intelligent Computer Technologies,
St.-Petersburg State Polytechnical University, 29 Polytechnicheskaya Street,
St.-Petersburg 195251, Russia
ivm3@columbia.edu
[2] Dept. of Computer Science,
The City College of New York, 138th Street at Convent Avenue, NAC 8/206,
New York, NY 10031, USA
gertner@cs.ccny.cuny.edu

Abstract. The paper proposes a unified direct approach to a number of problems arising in image processing. In particular, the areas of image registration, and object or pattern recognition are addressed when the images of interest display significant geometric distortion due to some physical or geometrical conditions. The proposed method performs a direct multi-objective search in image response space for an optimal piece-wise affine transformation of the images using a hybrid evolutionary algorithm. In its most general form, the entire algorithm works in two relatively independent passes. First, the global search attempts to find the optimal solution for the principal affine transformation. During the second pass, the correction procedure seeks for the optimal piece-wise approximation of the actual image transformation using the result of the first pass as the initial approximation.

Keywords: Hybrid evolutionary algorithm, image processing, piece-wise approximation, multi-objective optimization, local search.

1 Introduction

A number of real world applications in image processing, such as automatic target recognition; remote sensing; security systems; robotic and computer vision; medical imaging; and industrial control and detection have to deal with the problem of image registration and object recognition when images might undergo significant geometric distortion. Three examples of such a problem considered in the paper include human body recognition, 3D-object recognition in 2D space, and medical image registration.

Comprehensive surveys of numerous methods and techniques developed in the area of image registration, particularly in remote sensing and medical imaging, can be found in [1], [2]. One example of a difficult registration problem is the elastic registration of a series of medical images obtained from the MR or CT-scan. Various

D.-S. Huang et al. (Eds.): ICIC 2009, LNAI 5755, pp. 74–84, 2009.

approaches including evolutionary and particle swarm optimization have been developed that either use simplifying assumptions about the transformation, or attempt to approximate the organ shape with the known curves, e.g. splines [3], [4], [5], [6], [7].

Another example of a difficult problem is human body registration. The algorithms proposed in [8], [9], and [10] use evolutionary search based on motion analysis, in order to extract the image of the human body from video sequences. Here, motion analysis effectively reduces the computationally hard problem of global optimization to a more feasible problem of local search by spotting the location of the body. In the cases when motion analysis is infeasible or unavailable, e.g. in the process of recognition or registration of the still images, the entire feasible parameter space has to be explored by the search. The method proposed in this paper performs such a direct exploration of the global parameter space.

The direct application of image mapping to the task of 3D object recognition encounters two serious problems:

1. The object can be arbitrarily rotated in the 3D coordinate space of a scene, whereas available image templates typically show one or several 2D views of the object. Consequently, a single transformation can no longer correctly represent the sought mapping under the condition of incomplete or partial information.
2. Frequently used in object recognition features can lose their invariant properties when the object is observed from different points of view. Similarly, the direct comparison of the pixel values can rarely be used, since the different image viewpoints might result in the different pixel distributions. Therefore, during the search for a viable transformation between two images, Img_0 and Img_1, the Img_1 pixels might be erroneously mapped into wrong Img_0 pixels.

The approach proposed in this paper is based on the transformation of image local response [11], rather than on feature extraction or pixel comparison. Moreover, it uses a direct piece-wise affine approximation of the actual image transformation, which is applicable to a broad range of physically viable object transformations.

The purpose of this paper is to show that the commonalities shared by a number of seemingly different imaging problems allow one to look at their solutions from a single perspective. Namely, the paper considers the task of searching for the optimal mapping between the distorted images from a unified standpoint of multi-objective optimization of a piece-wise affine transformation using a hybrid evolutionary algorithm [12], [13].

The proposed approach uses the fact that all images of interest can be represented by their local responses: the entire search is conducted in image response space, rather than in the actual visual space. The algorithm intensively exploits local search to improve the quality of the evolving population of solutions. In order to increase the confidence about results, the algorithm implements a multi-objective optimization, such that different fitness functions are processed at the different stages of the search.

The structure of the paper is as follows. Section 2 describes the advanced image model based on local response. Section 3 deals with the global phase of the algorithm. Section 4 details the second phase of the algorithm - the search for the piece-wise approximation. Section 5 presents the results of the computational experiments. Section 6 concludes the paper with the summary of the proposed approach.

2 Advanced Image Model Based on Image Local Response

The model of an image participating in the evolutionary search has to be able to present the most important features of that image. Image local response defined in [11] provides such an essential image representation; it transforms the initial optimization problem in the real imaging space into the equivalent optimization problem in the response space. To further develop this approach, the advanced model used for every image participating in the search is described in this section.

The advanced image model is computed in accordance with the following algorithm:

- compute image local response R;
- compute histogram H of the response R and apply a threshold to reduce the noise;
- divide the image of R into k sections, such that every section can have its own transformation vector $\boldsymbol{V_k}$; this technique corresponds to a piece-wise approximation of the actual image transformation $A(\boldsymbol{V})$;
- decompose every section into a quadtree.

The algorithm assumes that the object presented in the template image has some prominent feature in the form of a body, or a trunk, to which all other parts of the object are attached. Throughout the paper, such a feature will be called *a hull*. The principal transformation of the hull can be defined by a vector $\boldsymbol{V_A}$ of the general affine transformation and a complementary vector $\boldsymbol{V_D}$ of elastic deformations. The latter describes the deviation of the actual hull transformation from the vector $\boldsymbol{V_A}$. The model of the hull includes the outline of the main part of the image represented as a list of nodes of a specified size and a set of internal black nodes of a specified size. The model can be built interactively by simply drawing the outline of the hull.

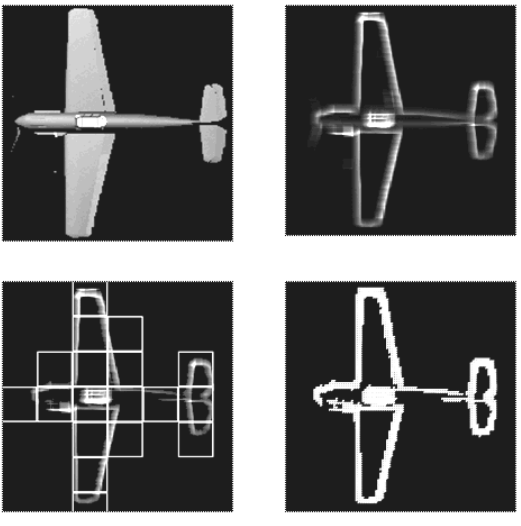

Fig. 1. Sequence of transformations of the response model of image template (*left to right, top to bottom*): original image, image local response, response histogram, final image quadtree

The hull has two important features participating in the fitness evaluation:

- the total length L_{HC} of the outer contour computed as the sum of all distances between the adjacent contour nodes;
- the area A_H covered by the hull and computed as the number of black nodes enclosed inside the hull.

To illustrate the process of building the advanced image model, Figure 1 shows the sequence of transformations performed in accordance with the stated algorithm. The original image has dimensions 210×210-pixel and contains the total of 44100 pixels. The threshold applied to the histogram defines the accuracy of the model. In Figure 1, the threshold is equal to 45, so only 1% of the larger gray values are retained in the histogram. The final quadtree model has 18 root blocks, or sections, and contains the total of 1314 nearly homogeneous nodes, each having the size of 2×2-pixel.

In order to accommodate multiple image templates, the advanced computational model uses multiple populations, such that every template is represented by its own independent population.

3 Global Search for the Optimal Hull Transformation

The first pass of the algorithm works with the image of the object hull. It is assumed that the full transformation T of the hull can be represented as a superposition of a general affine transformation A (i.e. the principal transformation), and a complementary elastic piece-wise transformation (i.e. deformation) D, as follows:

$$T = A + D\,. \tag{1}$$

The parameters of the principal affine transformation A are defined by the vector $\boldsymbol{V_A} = (DX, DY, \theta, SX, SY, SHX, SHY)$. Here, DX and DY are the translations along the x and y axes, θ is the rotation angle, SX and SY are the scaling factors along the x and y axes, and SHX and SHY are the shear factors along the x and y axes. The parameters DX, DY, and θ correspond to the rigid body transform, whereas the parameters SX, SY, SHX, and SHY define the global distortion of the image when the appropriate factors are non-isotropic, i.e. when $SX \neq SY$ and $SHX \neq SHY$.

The parameters of the complementary elastic piece-wise transformation D are defined by the vector $\boldsymbol{V_D} = (DX_{v1}, DY_{v1}, DX_{v2}, DY_{v2}, \ldots, DX_{vN}, DY_{vN})$. Here, every pair (DX_{vn}, DY_{vn}) is a partial deformation vector along the local normal v to the section n of the image template, and N is the total number of template sections. The vector $\boldsymbol{V_A}$ defines the principal transformation of the main hull, whereas the vector $\boldsymbol{V_D}$ describes possible local deviations of the actual hull shape from its principal transformation.

The multi-population and multi-objective global search for the optimal hull transformation starts with forming the initial population of chromosomes, i.e. individual solution vectors. The commonly used random generation of chromosomes is not well suited for the search that intensively uses the local optimization procedures, since the random placement of chromosomes inevitably creates many excessive and unnecessary individuals within the reach of the local search procedure. This consideration, together with the fact that the random generator does not provide a fair participation of all parameter ranges in the search (especially in relation to mutation) leads to the

need of expanding the mechanism of the mutation with memory [14] to the overall control over the process of forming the population. The managed creation of the chromosome population includes the following main features:

- breaking the entire parameter space into a set of regular cells whose size is limited by the capacity of the local search procedure;
- keeping track of the usage of every cell during the operations of crossover, mutation, and local search;
- leveraging the cell usage in such a way that all cells would eventually have a fair representation in the population;
- mixing parameter ranges in such a way that the population would have a greater diversity.

When two or more image templates are used in the search, the algorithm generates multiple chromosome populations, such that every template would have its own rather independent population. Since all such populations attempt to map the different templates onto the same reference image, the individual populations have to be "synchronized", i.e. aligned with each other. Note that the templates represent different views of the same object and, therefore, can generally have different values of *DX, DY, SX*, and *SY* of the principal transformation defined by the vector $\boldsymbol{V_A}$. However, if one requests that all templates have to be aligned on the rotation angle before the search begins, they have to retain their alignment throughout the search. It means that all template populations have to be synchronized on the rotation angle at the beginning of every global iteration when the new populations are generated.

Once the new chromosome population has been generated, the fitness values can be computed for all chromosomes. In the process of the global search, the following three objectives are simultaneously evaluated:

- F_{LEN} preserves the basic shape of the main hull;
- F_{MATCH} takes into account the distortion of the actual hull in relation to the principal affine transformation;
- F_{RATIO} evaluates the fraction of the total number of template quadtree nodes which have been successfully mapped onto the reference image. This is the final objective of the search that evaluates its overall success.

The results of the fitness evaluation are sorted in the increasing order of the fitness values F_{LEN}. The best fraction of the population is selected and inserted in the pool B_P of the fittest solutions. If $\boldsymbol{V^{curr}}$ is the current member of the pool and $\boldsymbol{V^{cand}}$ is a potential candidate for the insertion, then $\boldsymbol{V^{cand}}$ is inserted in place of $\boldsymbol{V^{curr}}$ only if the following conditions hold:

$$F_{LEN}^{cand} <= F_{LEN}^{curr} \quad \text{and} \quad F_{RATIO}^{cand} <= F_{RATIO}^{curr} \tag{2}$$

In order to improve the quality of the population, local search with the Downhill Simplex Method (DSM) [15] is utilized at the end of every global iteration. Typically, some chromosomes in the best pool B_P are located fairly close to each other; they can be clustered to form a single simplex that participates in the local search. Since every parameter is presented as a sequence of ranges, the algorithm can easily compute the Hamming distance between any two chromosomes in the pool B_P and

find close neighbors. The clustering operation is controlled with the maximum acceptable Hamming distance (threshold) L_R between any two ranges, within which these ranges can be considered close neighbors and selected as the vertices of the same DSM simplex.

Local search is conducted for all DSM simplexes generated from the best pool B_P. The quality of the individuals during the search is evaluated on the basis of their fitness values F_{LEN}. At the end of the search, every simplex produces one chromosome with the best fitness value F_{LEN}. All such chromosomes are selected into the second best pool, B_{LOC}. If there are a sufficient number of chromosomes, the matrix of Hamming distances is computed for the pool B_{LOC}. The chromosomes in the pool are clustered to form a new set of the DSM simplexes.

Since the best pool B_{LOC} is composed of the chromosomes that have best fitness values F_{LEN}, local search is conducted for the new DSM simplexes using the second fitness function, F_{MATCH}. At the end of the corresponding global iteration, the best pools B_P and B_{LOC} are sorted in the increasing order of their respective fitness values F_{LEN} and F_{MATCH}. The best chromosomes from the both pools are selected to form the final best pool B_{FIN}. The pool is sorted in the increasing order of the values of the third fitness function, F_{RATIO}. The specified number of chromosomes from the pool B_{FIN} are presented for the final evaluation. These chromosomes participate in the second phase of the algorithm – the local search for the optimal piece-wise affine transformation.

4 Search for the Optimal Piece-Wise Affine Transformation

The optimal final solutions found by the global hull optimization serve as the initial approximation for the piece-wise optimization of the entire image template. This phase of the search attempts to find a piece-wise affine transformation that can produce the best mapping from the image template onto the reference image in the response space. The image template is represented as a set of sections of specified dimensions, i.e. $Img_T = \{S_1, S_2, \ldots, S_M\}$, where M is the number of sections. Then, the sought transformation T of the entire template is represented in the form of superposition of the affine transformations A_k of individual sections S_k:

$$T = \sum_{k=1}^{M} A_k \tag{3}$$

where every individual affine transformation A_k is defined by the parameter vector $\boldsymbol{V_k} = (DX_k, DY_k, \theta_k, SX_k, SY_k, SHX_k, SHY_k)$.

The overall strategy of the multi-objective optimization of the piece-wise affine transformation of the image template in the response space is as follows. The response image of the template is divided into sections forming a hierarchical tree structure. The sections that are the closest to the template hull are placed at the top of the hierarchy; they form the base level of the tree. The sections that are adjacent to the base level form the next level of the tree. The process of building the section tree continues until all template sections are placed on their appropriate levels.

Once the section tree has been completed, the algorithm processes all sections sequentially, level after level, in the "peeling-off" manner. It starts from the base level

at the top of the hierarchy and moves down along the tree. The rationale behind this "peeling-off" technique is that the base sections adjacent to the hull have their transformation vectors close to the hull transformation vector. These vectors can be relatively easily computed using the hull transformation as the initial approximation.

Once the transformation of the base level has been found, the base sections are correspondingly transformed and eliminated from the further work of the algorithm, i.e. they are "peeled off". All following levels of the section tree have to be adjusted in accordance with the transformation of the base level. Next, the sections adjacent to the base level can be processed using the transformation of the base sections as the initial approximation for their own transformation vectors. The "peeling-off" process continues in this manner until all sections on all levels of the tree have been processed.

The final transformation $A_{S,LEV}$ of any individual section S_k located at some level *LEV* of the section tree is, therefore, a combination of the transformations of this section occurred at all previous levels:

$$A_{S,LEV} = A_{S,LEV-1} \times A_{S,LEV-2} \times \cdots \times A_{S,0} \tag{4}$$

Once all sections of the current tree level *LEV* have been processed, they undergo local DSM optimization using fitness function F_{LINK}. This function takes into account the relative position of the section among the adjacent parents and siblings and preserves the integrity of the template model. The best solutions are selected and ranked according to the second objective of the search defined as the fitness function F_{RATIO}. The latter evaluates the degree of the match between the sections of the template and the corresponding sections of the reference image in the response space.

The optimization phase of the piece-wise template transformation terminates when all sections at all levels of the section tree have been processed. The best final piecewise transformations of the template sections are presented to the decision maker for the final evaluation.

5 Computational Experiments

The validity of the proposed approach was examined on three sample imaging problems: human body recognition, 3D-object recognition in 2D space, and medical image registration.

5.1 Human Body Recognition

The setup for the problem of human body recognition is shown in Figure 2. The test set includes a 512×384 image of a street scene and two 128×256 templates of a human body. The templates are taken from different camera views and aligned with respect to their vertical angular position.

The results of the recognition are shown in Figure 3. The algorithm was able to find satisfactory results after iteration 6. The best match $r = 0.797$ occurs between the scene image and the side body template, whereas the back body template displays a slightly worse match of only $r = 0.670$. These values are supported by the visual evaluation of the image.

Fig. 2. A street scene (*left*) and human body templates (*right*)

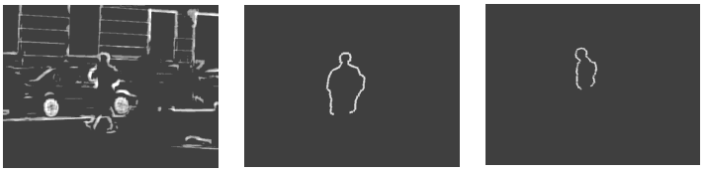

Fig. 3. Results of the recognition: the scene (*left*) and the templates (*center and right*)

5.2 Recognition of a 3D Object in the 2D Space

The possibility of extending the approach to the 3D object mapping was tested on a set of three grayscale images shown in Figure 4. The 300×300 reference image contains an object arbitrarily rotated in the 3D coordinate system. The templates are a 178×195 top view and a 185×66 left view of the same object.

Figure 5 shows the results of three different phases of the search: the global affine transformation of the template hulls, the respective transformation of the template sections, and the final piece-wise transformation of the template sections. As one can see, the global pass of the algorithm was able to find a fairly good approximation for the actual elastic transformations of the template hulls including their mutual angular alignment. The local pass of the algorithm found a good set of transformation vectors for the template sections – compare the rightmost column of the final piece-wise transformation in Figure 5 with the original image of the scene in Figure 4 (left image).

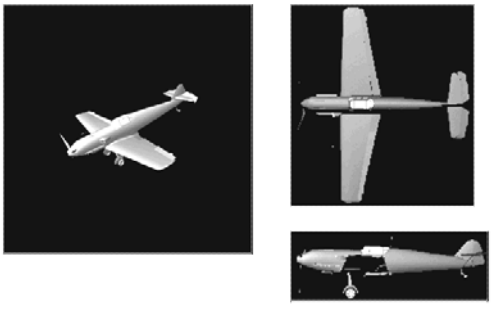

Fig. 4. A scene with the 3D object (left) and object templates (right)

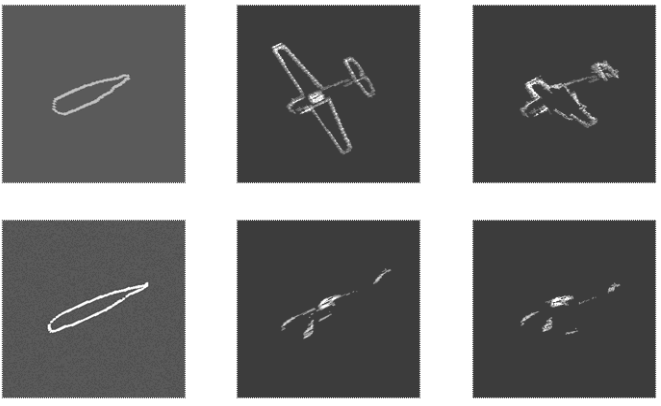

Fig. 5. Three phases of the algorithm for the top view (*top*) and the side view (*bottom*): global transformation of the hulls (*left*); initial transformation of the template sections (*center*); the final piece-wise transformation of the template sections (*right*)

5.3 Registration of Medical Images

This section presents the registration of a sample set of three medical images shown in Figure 6. One of the images (Figure 6, left) plays a role of the reference image, whereas the other two images (Figure 8, center and right) serve as templates that have to be mapped onto the reference image.

The following results of the algorithm are shown in Figure 7: the affine transformation of the template hulls at the end of the global pass, the corresponding transformation of the template sections at the beginning of the second pass, and the final piece-wise transformations of the template images. As one can see from the comparison of the results of the piece-wise transformation (Figure 7, the rightmost column) with the original reference image in Figure 6 (left), the algorithm was able to find a fairly good mapping from the templates onto the reference image.

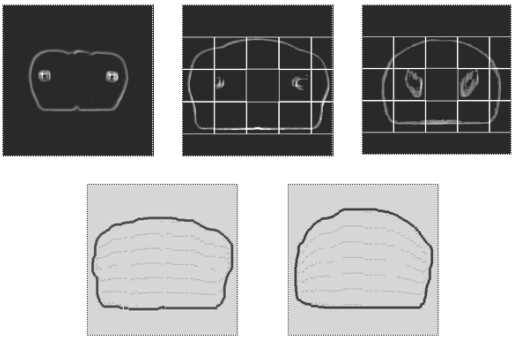

Fig. 6. Local responses of the reference image (*top, left*) and the templates (*top, center and right*); images of the template hulls with shown inner black nodes (*bottom*)

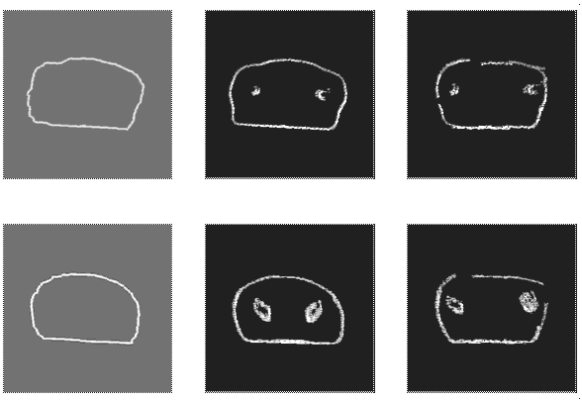

Fig. 7. Different phases of the algorithm for the templates 1 (*top*) and 2 (*bottom*): global transformation of the hulls (*left*); initial transformations of the template sections (*center*); the final piece-wise transformations of the template sections (*right*)

6 Conclusion

The main contribution of the paper is to propose a unified direct approach to a number of problems arising in image processing. In particular, the areas of image registration, and object or pattern recognition are addressed in the case when the images of interest display significant distortion due to some physical or geometrical conditions.

The proposed method does not imply any initial knowledge about the problem, nor does it impose constraints on the shape or smoothness of image transformation. Instead, it employs a direct multi-objective search in image response space for an optimal piece-wise affine transformation of the images using a hybrid evolutionary algorithm.

The search for the optimal solution is performed in two consecutive passes. During the first pass, the global optimization procedure seeks for a proper mapping of the main shape feature - image hull. During the second pass, the hull transformation is used as the initial approximation for the final piece-wise optimization.

Computational experiments on three sample imaging problems illustrate the potential of the proposed method and its ability to solve complex image mapping problems involving significant geometric distortions of the images.

References

1. Hallpike, L., Hawkes, D.J.: Medical Image Registration: an Overview. Imaging 14, 455–463 (2002)
2. Zitová, B., Flusser, J.: Image Registration Methods: a Survey. Image and Vision Computing 21, 977–1000 (2003)
3. Cordón, O., Damas, S., Santamaría, J.: A CHC Evolutionary Algorithm for 3D Image Registration. In: Fuzzy Sets and Systems — IFSA 2003, pp. 134–211 (2003)
4. Wachowiak, M.P., Smolíková, R., Zheng, Y., Zurada, J.M., Elmaghraby, A.S.: An Approach to Multimodal Biomedical Image Registration Utilizing Particle Swarm Optimization. IEEE Transactions on Evolutionary Computation 8, 289–301 (2004)

5. Han, J., Bhanu, B.: Hierarchical Multi-Sensor Image Registration Using Evolutionary Computation. In: Proceedings of the 2005 Conference on Genetic and Evolutionary Computation, Washington DC, USA, June 25-29, pp. 2045–2052 (2005)
6. Cordón, O., Damas, S., Santamaría, J.: Feature-Based Image Registration by Means of the CHC Evolutionary Algorithm. Image and Vision Computing 24, 525–533 (2006)
7. Khamene, A., Azar, F., Schwarz, L., Zikic, D., Navab, N., Rietzel, E.: A Unified and Efficient Approach for Free-Form Deformable Registration. In: IEEE 11th International Conference on Computer Vision - ICCV 2007, pp. 1–8 (2007)
8. Hu, C., Li, Q.Y.Y., Ma, S.: Extraction of Parametric Human Model for Posture Recognition Using Genetic Algorithm. In: Proc. of the Fourth IEEE International Conference on Automatic Face and Gesture Recognition, pp. 518–523 (2000)
9. Zhao, J., Li, L.: Human Motion Reconstruction from Monocular Images Using Genetic Algorithms. Comp. Anim. Virtual Worlds 15, 407–414 (2004)
10. Shen, S., Chen, W.: Probability evolutionary algorithm based human body tracking. In: Rothlauf, F., Branke, J., Cagnoni, S., Costa, E., Cotta, C., Drechsler, R., Lutton, E., Machado, P., Moore, J.H., Romero, J., Smith, G.D., Squillero, G., Takagi, H. (eds.) EvoWorkshops 2006. LNCS, vol. 3907, pp. 525–529. Springer, Heidelberg (2006)
11. Maslov, I.V., Gertner, I.: Using Image Local Response for Efficient Image Fusion with the Hybrid Evolutionary Algorithm. In: Sadjadi, F.A. (ed.) Automatic Target Recognition XIV: AeroSense 2004. Proc. SPIE, vol. 5426, pp. 326–333. SPIE, San Jose (2004)
12. Goldberg, D.E.: Genetic Algorithms in Search, Optimization, and Machine Learning. Addison-Wesley, Reading (1989)
13. Bäck, T.: Evolutionary Algorithms in Theory and Practice. Oxford University Press, New York (1996)
14. Gertner, I., Maslov, I.V.: Using Local Correction and Mutation with Memory to Improve Convergence of Evolutionary Algorithm in Image Registration. In: Automatic Target Recognition XII: AeroSense 2002. Proc. SPIE, vol. 4726, pp. 241–252. SPIE, San Jose (2002)
15. Nelder, J.A., Mead, R.: A Simplex Method for Function Minimization. Computer J. 7, 308–313 (1965)

Two Step Template Matching Method with Correlation Coefficient and Genetic Algorithm

Gyeongdong Baek and Sungshin Kim

School of Electrical Engineering, Pusan National University, Busan, Korea
{gdbaek,sskim}@pusan.ac.kr

Abstract. This paper presents a rotation invariant template matching method based on two step matching process, cross correlation and genetic algorithm. In order to improve the matching performance, the traditional normalized correlation coefficient method is combined with genetic algorithm. Normalized correlation coefficient method computes probable local position of the template in the scene image. And genetic algorithm computes global position and rotation of the template in the scene image. The experimental results show that this algorithm has good rotate invariance, and high precision property.

Keywords: Two step template matching, Correlation coefficient, Genetic algorithms.

1 Introduction

Image processing is used to detect and analyze the trouble of end-product in the industrial automation system. Template matching is crucial conditions in many machine vision systems such production line of fiducial alignment, and printed circuit board (PCB) [1-3]. Template matching is that given a reference image of a target object, searching whether that target object exists in a scene image under image processing, and find its location. The matching problem consists in determining the unknown transform parameters to map template image to match the source image. The unknown transform parameters are translation, rotation, scale, and skew of image. Traditional pattern matching research has many applications such as point correlation, chamfer matching, and sequential hierarchical scene matching [4-7]. But any misorientation of target object may lead to wrong analysis for reference based method. Mathematical morphology and fuzzy neural network can handle problems such as translation, scale and image rotation [8-9]. These methods need feature extraction process in given image.

Proposed template matching method consists of two parts as shown in Fig.1: cross correlation matching method and genetic algorithm (GA). Cross correlation matching provides local position of the object in the scene image. GA is especially appropriate for the optimization in the large search spaces. GA computes global position and rotation of the target object in a large optimization space. The main objective of this paper is to investigate the translation and rotation among template and scene image.

D.-S. Huang et al. (Eds.): ICIC 2009, LNAI 5755, pp. 85–90, 2009.

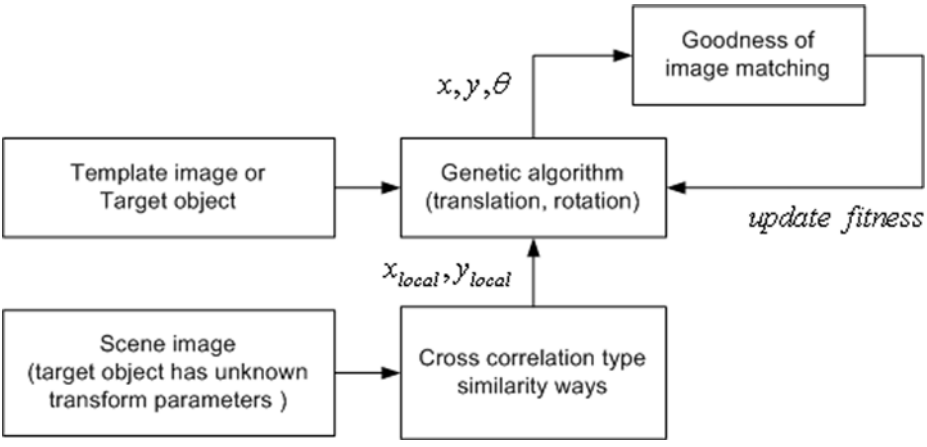

Fig. 1. Two step template matching diagram that consists cross correlation and genetic algorithm

The following section provides traditional template matching method for finding similar region and presents proposed two step template matching. Section 3 shows experimental result, and contains concluding remarks.

2 Proposed Two Step Template Matching Method

2.1 Traditional Image Matching Method for Finding Similar Region

Template matching implements a set of methods for finding the image regions that are similar to the given template. Similarity can be calculated in several ways: normalized squared difference, normalized cross correlation, and normalized correlation coefficient [10].

Normalized squared difference is defined as

$$S(x,y)=\frac{\sum_{y'=0}^{h-1}\sum_{x'=0}^{w-1}\left[T(x',y')-I(x+x',y+y')\right]^2}{\sqrt{\sum_{y'=0}^{h-1}\sum_{x'=0}^{w-1}T(x',y')^2\sum_{y'=0}^{h-1}\sum_{x'=0}^{w-1}I(x+x',y+y')^2}}, \tag{1}$$

where *I(x,y)* is the value of the image pixel in the location *(x,y)*, *T(x,y)* is the value of the template pixel in the location *(x,y)*. Given a source image with $W \times H$ pixels and a template with $w \times h$ pixels, the size of resulting image has $W-w+1 \times H-h+1$ pixels.

Normalized cross correlation is defined as

$$C(x,y)=\frac{\sum_{y'=0}^{h-1}\sum_{x'=0}^{w-1}T(x',y')I(x+x',y+y')}{\sqrt{\sum_{y'=0}^{h-1}\sum_{x'=0}^{w-1}T(x',y')^2\sum_{y'=0}^{h-1}\sum_{x'=0}^{w-1}I(x+x',y+y')^2}}, \tag{2}$$

where *I(x,y)* is the value of the image pixel in the location *(x,y)*, *T(x,y)* is the value of the template pixel in the location *(x,y)*.

Normalized correlation coefficient is defined as

$$R(x,y)=\frac{\sum_{y'=0}^{h-1}\sum_{x'=0}^{w-1}\tilde{T}(x',y')\tilde{I}(x+x',y+y')}{\sqrt{\sum_{y'=0}^{h-1}\sum_{x'=0}^{w-1}\tilde{T}(x',y')^2\sum_{y'=0}^{h-1}\sum_{x'=0}^{w-1}\tilde{I}(x+x',y+y')^2}}, \tag{3}$$

where $\tilde{T}(x',y')=T(x',y')-\overline{T}$, $\tilde{I}(x+x',y+y')=I(x+x',y+y')-\overline{I}(x,y)$, $\overline{T}$ stands for the average value of pixels in the template and $\overline{I}(x,y)$ stands for the average value of the pixels in the current window of the image.

In this paper, similarity is used the normalized correlation coefficient that is not sensitive to linear changes in light. After the similarity equations return the resultant image, probable position of the template in the image could be located as the local or global maximums of the resultant image brightness. But when target object is rotated, the method above is difficult to be used. The matched point is blurred in correlation coefficient map as shown in Fig.2.

2.2 Proposed Two Step Template Matching Method

Template image can be used to transform using translation, rotation, scale, and skew matrix. 2*X*2 matrix doesn't work for translation, so we need homogeneous coordinates in (4). The effect of skew and scale are limited in this paper, no-skew and scale is 1.

$$\begin{aligned}\begin{bmatrix}x'\\y'\\1\end{bmatrix}&=T\cdot S\cdot R\cdot\begin{bmatrix}x\\y\\1\end{bmatrix}\\&=\begin{bmatrix}1&0&t_x\\0&1&t_y\\0&0&1\end{bmatrix}\begin{bmatrix}s&0&0\\0&s&0\\0&0&1\end{bmatrix}\begin{bmatrix}\cos\theta&-\sin\theta&0\\\sin\theta&\cos\theta&0\\0&0&1\end{bmatrix}\begin{bmatrix}x\\y\\1\end{bmatrix},\end{aligned} \tag{4}$$

where T is translation matrix, S is scale matrix, and R is rotation matrix.

Translation parameter T_x, T_y and rotation parameter θ are used as fitness function for GA which then produces new sets of T_x, T_y, θ values which lead to better matching. The basic outline of the proposed algorithm is presented below.

Algorithm. Two Step Template Matching Method with Correlation Coefficient and Genetic Algorithm.

1. Input two 2D-images: scene image *I(x,y)*, and template image *T(x,y)*.
2. Compute normalized correlation coefficient map *R(x,y)*.
3. Find maximum brightness point (x_m, y_m) for the local location of template.
4. Initialize the location of template $(x, y) = (x_m, y_m)$.
5. Do thresholding

$$S(x,y)=\begin{cases}S(x,y), & if\ \left|I(x,y)-\overline{T}\right|<\varepsilon\\0\ , & otherwise\end{cases}, \tag{5}$$

where $I(x, y)$ is the value of the scene, $\bar{T}$ is the mean of the template. ε is a fixed threshold.

6. Create initial generation of M individuals (each individual representing a set of (t_x, t_y, θ)).
7. Compute fitness value for each individual.

$$fitness = \sum_{y}^{H}\sum_{x}^{W} S(x, y), \quad S(x, y) = \sum_{y'=0}^{h-1}\sum_{x'=0}^{w-1}\left|I(x+x', y+y') - T(x', y')\right|, \tag{6}$$

where $I(x,y)$ is the value of the scene, $T(x,y)$ is the value of the template. The less fitness value is, the higher precision property is.

8. Create new generation by reproduction, crossover, and mutation.
9. Until no fitness improvement is achieved, move 6.
10. Output the location and rotation of template image.

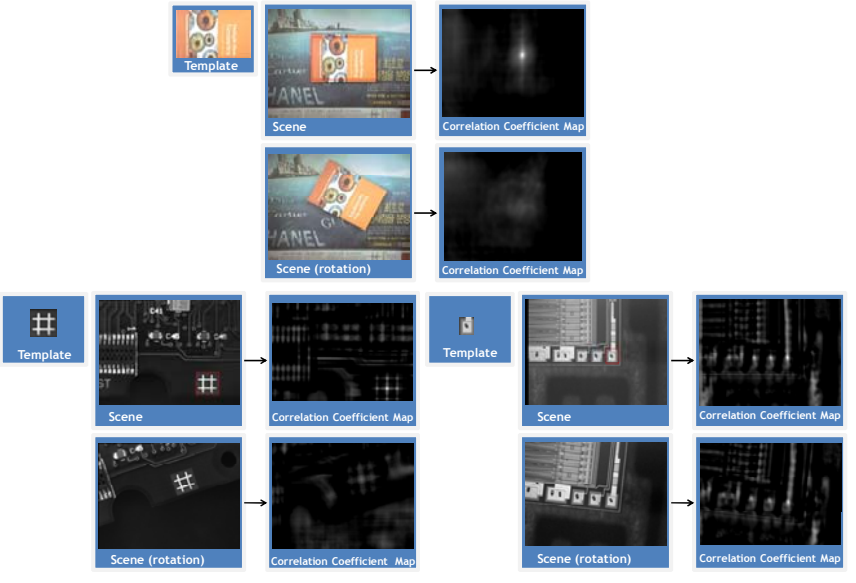

Fig. 2. The extracted probable position of the template in the scene and rotation images

3 Experimental Result and Discussion

We have tested in three rotation cases which are non-rotation and rotation scene image. When target object is rotated, it is difficult to show maximum brightness point as shown in Fig. 2. So we called the local location of template. From local information, we are searched translation, and rotation angle (T_x, T_y, θ) with genetic algorithm. From table 1, it is obvious that the results for the fitness values decrease in all cases and the precision property is better. Fig. 3 illustrates results for goodness of matching precision in three cases. The mean of movement point is (-5.6, -23.0) for the mean of rotation angle 18.0˚.

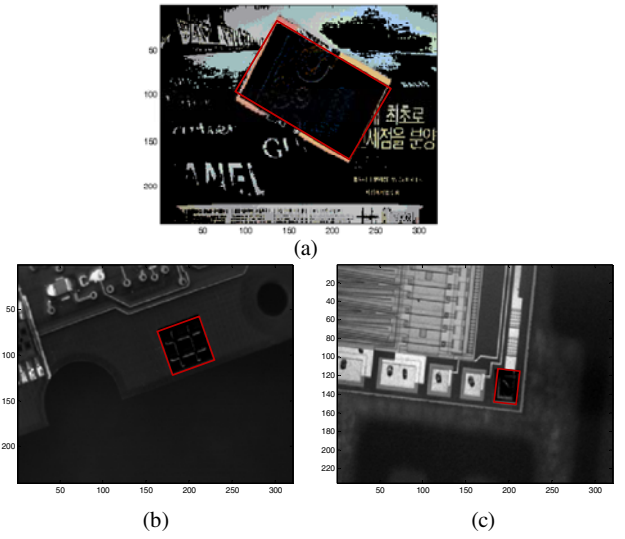

(a) (b) (c)

Fig. 3. The comparison of matching precision in three cases: (a) general case, (b) fiducial mark, (c) printed circuit board (PCB)

Table 1. Result of template matching: only normalized correlation coeff. (Local), combined method (Global)

Case	Position			Fitness		Rotation angle(°)
	Local	Global	Trans.	Local	Global	
A	(99, 75)	(92, 17)	(-7, -58)	49.7	43.1	-30.9
B	(170, 60)	(162, 52)	(-8, -8)	29.9	29.5	19.5
C	(181,114)	(179, 111)	(-2, -3)	66.4	66.3	-3.8

In this paper, we have developed two step template matching method with correlation coefficient and genetic algorithm. The method uses a genetic algorithm to find the transformation parameters. The experimental results show that this algorithm has good rotate invariance, and high precision property. In our future work matching of different kind of objects will be tested.

Acknowledgment

This work was supported by the Grant of the Korean Ministry of Education, Science and Technology (The Regional Core Research Program/Institute of Logistics Information Technology).

References

1. Syamsiah, M., Jonathan, R.E., Ahmet, T.E.: Automatic Gybrid Genetic Algorithm Based Printed Circuit Board Inspection. In: First NASA/ESA Conference on Adaptive Hardware and Systems, pp. 390–400 (2006)

2. Madhav, M., Fikret, E.: Segmentation of Printed Circuit Board Images into Basic Patterns. Computer Vision and Image Understanding 70, 74–86 (1998)
3. Tarnawski, W.: Colour Image Segmentation Algorithm in Vectoral Approach for Automated Optical Inspection in Eectronics. Opto-electronics Review 11, 197–202 (2003)
4. Liu, T., Zhu, G., Zhang, C., Hao, P.: Fingerprint Indexing Based on Singular Point Correlation. In: IEEE International Conference on Image Processing, Beijing, vol. 3, pp. 11–14 (2005)
5. András, H., Ioannis, P.: Optimal Approach for Fast Object-template Matching. IEEE Transactions on Image Processing 16, 8 (2007)
6. Gunilla, B.: Hierarchical Chamfer Matching: a Parametric Edge Matching Algorithm. IEEE Transaction on Pattern Analysis and Machine Intelligence 10, 6 (1988)
7. Shen, M., Song, H., Sheng, W., Liu, Z.: Fast Correlation Tracking Method Based on Circular Projection. In: Eighth ACIS International Conference on Software Engineering, Artificial Intelligence, Networking, and Parallel/Distributed Computing, Qingdao, vol. 1, pp. 235–238 (2007)
8. Sidnei, A.A., Kim, H.Y.: Rotation, Scale and Translation-invariant Segmentation-free Grayscale Shape Recognition Using Mathematical Morphology. In: Proceedings of the 8th International Symposium on Mathematical Morphology, vol. 2, pp. 61–62 (2007)
9. Patil, P.M., Sontakke, T.R.: Rotation, Scale and Translation Invariant Handwritten Devanagari Numeral Character Recognition Using General Fuzzy Neural Network. The Journal of Pattern Recognition 40, 2110–2117 (2007)
10. Open Source Computer Vision Library, `http://sourceforge.net/projects/opencvlibrary`

A Framework on Rough Set-Based Partitioning Attribute Selection

Tutut Herawan and Mustafa Mat Deris

Faculty of Information Technology and Multimedia,
Universiti Tun Hussein Onn Malaysia,
Parit Raja, 86400, Batu Pahat, Johor, Malaysia
tututherawan@yahoo.com, mmustafa@uthm.edu.my

Abstract. In this paper, we focus our discussion on the rough set-based partitioning attribute selection. Firstly, we point out that the statement of MMR technique is an extension of Mazlack's technique is unreasonable. We prove that the mean roughness of MMR technique is only the opposite of that Mazlack's TR technique. Secondly, we observe that the suggestion of MMR to achieve lower computational complexity using the roughness measurement based on relationship between an attribute $a_i \in A$ and the set defined as $A-\{a_i\}$ instead of calculating the maximum with respect to all $\{a_j\}$ where $a_i \neq a_j$, $1 \leq i, j \leq |A|$ only can be applied to a special type of information system and we illustrate this with an example. Finally, we propose an alternative technique for selecting partitioning attribute using rough set theory based on dependency of attributes in an information system. We show that the proposed technique is a generalization and has lower computational complexity than that of TR and MMR.

Keywords: Rough set theory; Dependency of attributes.

1 Introduction

Recently, there has been works in the area of applying rough set theory in the process of selecting partitioning attribute. Mazlack *et al.* [1] proposes two techniques to select partitioning attribute: i.e., Bi-Clustering (BC) technique based on bi-valued attributes and Total Roughness (TR) technique. Mazlack *et al.* suggested that BC technique will be attempted first in order to achieve low dissonance inside the partition. With this technique, there are three different approaches of selecting partitioning attribute, i.e. arbitrary, imbalanced, and balanced. For balanced or unbalanced partitioning approaches, it is likely that two kinds of problems may occur. First, it may have several candidates of bi-partitioning attributes. Then, a decision has to be made to which one should be chosen as the partitioning attribute. Second, no two-valued attribute can be found to form balance partitioning. At this point, partitioning on multiple valued attributes will be considered. Therefore, for selecting partitioning attribute for data set with multiple-valued attributes, Mazlack *et al.* proposed a technique using the average

D.-S. Huang et al. (Eds.): ICIC 2009, LNAI 5755, pp. 91–100, 2009.

of the accuracy of approximation (accuracy of roughness) in the rough set theory [2-4] called Total Roughness (TR). In other words, it is based on the average of mean roughness of an attribute with respect to the set of all other attributes in an information system, where the higher the total roughness is, the higher the accuracy of selecting partitioning attribute. In [5], Parmar *et al.* proposes a new technique called Min-Min Roughness (MMR) for categorical data clustering. In this technique, bi-valued and multi-valued attributes are equally treated and it's accuracy of approximation is measured using the well-known Marczeweski-Steinhaus metric [6-8] applied to the lower and upper approximations of a subset of the universe in an information system. However, the mean roughness MMR is only the opposite of that TR. Consequently, they produce the same accuracy and complexity for selecting partitioning attribute. In addition, with MMR technique, the complexity is however still an issue due to all attributes are considered to obtain the partitioning attribute. Further, we observe that the suggestion of MMR to achieve lower computational complexity using the roughness measurement based on relationship between an attribute $a_i \in A$ and the set defined as $A-\{a_i\}$ instead of calculating the maximum with respect to all $\{a_j\}$ where $a_i \neq a_j$, $1 \leq i, j \leq |A|$ only can be applied to a special type of information system and we illustrate this with an example. Therefore, there is a need for a technique in selecting partitioning attribute to improve the TR and MMR. One way to select partitioning attribute is to discover the relationship among attributes based on their dependencies. In this paper, a technique called Maximum Dependency of Attributes (MDA) is proposed. It is based on the dependency of attributes using rough set theory in an information system. A test case is considered to evaluate and compare the performance of MDA with TR and MMR techniques. We show that the proposed technique provides better performance with that of TR and MMR techniques.

The rest of this paper is organized as follows. Section 2 describes rough set theory. Section 3 describes the analysis and comparison of TR and MMR techniques. Section 4 describes the Maximum Dependency of Attributes (MDA) technique. A comparison test of MDA with BC, TR and MMR techniques is described in section 5. Finally, the conclusion of this work is described in section 6.

2 Rough Set Theory

An information system as in [4] is a 4-tuple (quadruple) $S=(U,A,V,f)$, where U is a non-empty finite set of objects, A is a non-empty finite set of attributes, $V=\bigcup_{a\in A} V_a$, V_a is the domain (value set) of attribute a, $f: U\times A \rightarrow V$ is a total function such that $f(u,a)\in V_a$, for every $(u,a)\in U\times A$, called information (knowledge) function.

Definition 1. *Two elements $x, y \in U$ are said to be B-indiscernible (indiscernible by the set of attribute $B \subseteq A$ in S) if and only if $f(x,a)=f(y,a)$, for every $a \in B$.*

Obviously, every subset of A induces unique indiscernibility relation. Notice that, an indiscernibility relation induced by the set of attribute B, denoted by $IND(B)$, is an

equivalence relation. The partition of *U* induced by $IND(B)$ is denoted by U/B and the equivalence class in the partition U/B containing $x \in U$, is denoted by $[x]_B$. The notions of lower and upper approximations of a set are defined as follows.

Definition 2. (See [4].) *The B-lower approximation of X, denoted by* $\underline{B}(X)$ *and B-upper approximations, denoted by* $\overline{B}(X)$ *of X, respectively, are defined by*

$$\underline{B}(X) = \{x \in U \mid [x]_B \subseteq X\} \text{ and } \overline{B}(X) = \{x \in U \mid [x]_B \cap X \neq \phi\}. \quad (1)$$

The accuracy of approximation (accuracy of roughness) of any subset $X \subseteq U$ with respect to $B \subseteq A$, denoted $\alpha_B(X)$ is measured by

$$\alpha_B(X) = |\underline{B}(X)| / |\overline{B}(X)|, \quad (2)$$

where $|X|$ denotes the cardinality of *X*. The higher of accuracy of approximation of any subset $X \subseteq U$ is the more precise (the less imprecise) of itself. The accuracy of roughness in equation (2) can also be interpreted using the well-known Marczeweski-Steinhaus (MZ) metric [6-8]. By applying the Marczeweski-Steinhaus metric to the lower and upper approximations of a subset $X \subseteq U$ in information system *S*, we have

$$D(\underline{R}(X), \overline{R}(X)) = 1 - \frac{|\underline{R}(X) \cap \overline{R}(X)|}{|\underline{R}(X) \cup \overline{R}(X)|} = 1 - \frac{|\underline{R}(X)|}{|\overline{R}(X)|} = 1 - \alpha_R(X). \quad (3)$$

Definition 3. *Let* $S = (U, A, V, f)$ *be an information system and let D and C be any disjoint subsets of A. Dependency attribute D on C in a degree k* $(0 \le k \le 1)$*, is denoted by* $C \Rightarrow_k D$*. The degree k is defined by*

$$k = \frac{\sum_{X \in U/D} |\underline{C}(X)|}{|U|}. \quad (4)$$

Attribute D is said to be fully depends (in a degree of k) on C if $k = 1$*. Otherwise, D is partially depends on C.*

Thus, *D* fully (partially) depends on *C*, if all (some) elements of the universe *U* can be uniquely classified to equivalence classes of the partition U/D, employing *C*. Based on Definition 3, we can select the partitioning attributes based on the maximum value of *k*.

3 The Analysis and comparison of TR and MMR Techniques

In this section, we analyze and compare the Total Roughness (TR) and Min-Min Roughness (MMR) techniques.

3.1 The TR Technique

The definition of information system is based on the notion of information system as stated in section 2. From the definition, suppose that attribute $a_i \in A$ has *k*-different values, say β_k, $k = 1,2,\cdots,n$. Let $X(a_i = \beta_k)$, $k = 1,2,\cdots,n$ be a subset of the objects having *k*-different values of attribute a_i. The roughness of TR technique of the set $X(a_i = \beta_k)$, $k = 1,2,\cdots,n$, with respect to a_j, where $i \neq j$, denoted by $\mathrm{R}_{a_j}(X|a_i = \beta_k)$, is defined by

$$\mathrm{R}_{a_j}(X|a_i = \beta_k) = \frac{\left|\underline{X}_{a_j}(a_i = \beta_k)\right|}{\left|\overline{X}_{a_j}(a_i = \beta_k)\right|} \quad k = 1,2,\cdots,n \tag{5}$$

From TR technique, the mean roughness of attribute $a_i \in A$ with respect to attribute $a_j \in A$, where $i \neq j$, denoted $\mathrm{Rough}_{a_j}(a_i)$, is evaluated as follows

$$\mathrm{Rough}_{a_j}(a_i) = \frac{\sum_{k=1}^{|V(a_i)|} \mathrm{R}_{a_j}(X|a_i = \beta_k)}{|V(a_i)|}, \tag{6}$$

where $V(a_i)$ is the set of values of attribute $a_i \in A$.

The total roughness of attribute $a_i \in A$ with respect to attribute $a_j \in A$, where $i \neq j$, denoted $\mathrm{TR}(a_i)$, is obtained by the following formula

$$\mathrm{TR}(a_i) = \frac{\sum_{j=1}^{|A|} \mathrm{Rough}_{a_j}(a_i)}{|A| - 1}. \tag{7}$$

As stated in Mazlack *et al.* [1], the highest value of TR, the best selection of partitioning attribute.

3.2 The MMR Technique

The definition of information system is based on the notion of information system as stated in section 2. From the definition, suppose that attribute $a_i \in A$ has *k*-different values, say β_k, $k = 1,2,\cdots,n$. Let $X(a_i = \beta_k)$, $k = 1,2,\cdots,n$ be a subset of the objects having *k*-different values of attribute a_i. The roughness of MMR technique of the set $X(a_i = \beta_k)$, $k = 1,2,\cdots,n$, with respect to a_j, where $i \neq j$, denoted by $\mathrm{R}_{a_j}(X|a_i = \beta_k)$, is defined by

$$\mathrm{MMR}_{a_j}(X|a_i = \beta_k) = 1 - \frac{\left|\underline{X}_{a_j}(a_i = \beta_k)\right|}{\left|\overline{X}_{a_j}(a_i = \beta_k)\right|}, \; k = 1,2,\cdots,n. \tag{8}$$

It is clear that MMR technique uses MZ metric to measure the roughness of the set $X(a_i = \beta_k)$, $k = 1,2,\cdots,n$, with respect to a_j, where $i \neq j$.

The mean roughness of MMR technique is defined by

$$\text{MMRough}_{a_j}(a_i) = \frac{\sum_{k=1}^{|V(a_i)|} \text{MMR}_{a_j}(X|a_i = \beta_k)}{|V(a_i)|}. \tag{9}$$

According to Parmar *et al.* [5], the least mean roughness, the best selection of partitioning attribute.

Proposition 4. *The value of roughness of MMR technique is the opposite of that TR technique.*

Proof. Since MMR technique uses MZ metric to measure the roughness of the set $X(a_i = \beta_k)$, $k = 1,2,\cdots,n$, with respect to a_j, where $i \neq j$, i.e.,

$$\text{MMR}_{a_j}(X|a_i = \beta_k) = 1 - \frac{\left|\underline{X}_{a_j}(a_i = \beta_k)\right|}{\left|\overline{X}_{a_j}(a_i = \beta_k)\right|},$$

then from (5) and (8), we have

$$\text{MMR}_{a_j}(X|a_i = \beta_k) = 1 - \text{R}_{a_j}(X|a_i = \beta_k). \tag{10}$$

Thus, the value of mean roughness of MMR technique (9) is also the opposite of that TR technique (6), i.e.,

$$\begin{aligned}
\text{MMRough}_{a_j}(a_i) &= \frac{\sum_{k=1}^{|V(a_i)|} \text{MMR}_{a_j}(X|a_i = \beta_k)}{|V(a_i)|} \\
&= \frac{\sum_{k=1}^{|V(a_i)|} \left(1 - \text{R}_{a_j}(X|a_i = \beta_k)\right)}{|V(a_i)|} \\
&= \frac{\sum_{k=1}^{|V(a_i)|} 1 - \sum_{k=1}^{|V(a_i)|} \text{R}_{a_j}(X|a_i = \beta_k)}{|V(a_i)|} \\
&= \frac{|V(a_i)|}{|V(a_i)|} - \frac{\sum_{k=1}^{|V(a_i)|} \text{R}_{a_j}(X|a_i = \beta_k)}{|V(a_i)|} \\
&= 1 - \text{Rough}_{a_j}(a_i), \text{ for } i \neq j.
\end{aligned} \tag{11}$$

The MMR technique is based on the minimum value of mean roughness in (11), without calculating total roughness (7). □

This analysis and comparison seems to show that TR and MMR are given the same result. On the other hand, with MMR technique, to achieve lower computational

complexity in selecting partitioning attribute in an information system $S=(U,A,V,f)$, it is suggested to measure the roughness based on relationship between an attribute $a_i \in A$ and the set defined as $A-\{a_i\}$ instead of calculating the maximum with respect to all $\{a_j\}$ where $a_i \neq a_j$. We observe this technique only can be applied in a very special data set. To illustrate this problem, we consider to the following example.

Example 5. We consider to the data set in illustrative example of Table 2 in [5]. The calculation of MMR is based on formulas in equations (8) and (9). According to Parmar *et al.* attribute a_1 is chosen as the clustering (partitioning) attribute. However, if we consider to measure the roughness of attribute $a_i \in A$ with respect to the set of attributes $A-\{a_i\}$, then we get the value of MMR as in Table 1.

Table 1. The modified MMR of all attributes in data set from [5]

Attribute w.r.t.	Mean Roughness	MMR
a_1	Rough $A-\{a_1\}$ 0	0
a_2	Rough $A-\{a_2\}$ 0	0
a_3	Rough $A-\{a_3\}$ 0	0
a_4	Rough $A-\{a_4\}$ 0	0
a_5	Rough $A-\{a_5\}$ 0	0
a_6	Rough $A-\{a_6\}$ 0	0

Based on Table 1, we cannot select a partitioning attribute. On the other hand, the suggested technique would lead a problem, i.e., after calculation of mean roughness of attribute $a_i \in A$ with respect to the set of attributes $A-\{a_i\}$, the value of MMR usually cannot preserve the original decision. Thus, this modified technique is not relevant to all type of data set.

In section 4, we introduce the Maximum Dependency of Attributes (MDA) technique to deal with the problem of selecting partitioning attribute.

4 Maximum Dependency of Attributes (MDA) Technique

The MDA technique for selecting partitioning attribute is based on the maximum degree of dependency of attributes. The justification that the higher of the degree of

dependency of attributes implies the more accurate for selecting partitioning attribute is stated in the Proposition 6.

Proposition 6. *Let* $S=(U,A,V,f)$ *be an information system and let D and C be any subsets of A. If D depends totally on C, then*

$$\alpha_D(X)\le\alpha_C(X), \text{ for every } X\subseteq U.$$

Proof. Let *D* and *C* be any subsets of *A* in information system $S=(U,A,V,f)$. From the hypothesis, we have $IND(C)\subseteq IND(D)$. Furthermore, the partitioning U/C is finer than that U/D, thus, it is clear that any equivalence class induced by $IND(D)$ is a union of some equivalence class induced by $IND(C)$. Therefore, for every $x\in X\subseteq U$, we have $[x]_C\subseteq[x]_D$. And hence, for every $X\subseteq U$, we have

$$\underline{D}(X)\subseteq\underline{C}(X)\subset X\subset\overline{C}(X)\subseteq\overline{D}(X).$$

Consequently

$$\alpha_D(X)=\frac{|\underline{D}(X)|}{|\overline{D}(X)|}\le\frac{|\underline{C}(X)|}{|\overline{C}(X)|}=\alpha_C(X). \qquad \square$$

Proposition 7. *MDA is a generalization of TR and MMR.*

Proof. In an information system, $S=(U,A,V,f)$, an attribute $a_i\in A$ may have several different values, say β_k, $k=1,2,\cdots,n$. Thus from equations (2) and (5), we can generalize the roughness of the sets as follows

$$R_{a_j}(X)=\frac{\left|\underline{(Xa_j(a_i=\beta_1))}\right|}{U}+\frac{\left|\underline{(Xa_j(a_i=\beta_2))}\right|}{U}+\cdots+\frac{\left|\underline{(Xa_j(a_i=\beta_n))}\right|}{U}$$
$$=\frac{\sum_{U/a_i}\left|\underline{X(a_i=\beta_k)}\right|}{U},\quad k=1,2,\cdots,n. \tag{12}$$

The formula in equation (12) is a degree of dependency of attribute a_j on attribute a_i, where $i\neq j$. Thus, MDA is a generalization of TR and MMR. $\square$

5 A Comparison Test

To this framework, a small-sized data set from [9] is considered to compare and evaluate the accuracy and the complexity of MDA with TR, MMR and in addition with BC techniques. To measure the accuracy of selecting partitioning attribute, we use the formula of mean roughness in equation (6) to represent all techniques. The higher the mean roughness is the higher the accuracy of the selecting partitioning attribute.

In Table 2, there are five categorical attributes: Magazine Promotion (MP), Watch Promotion (WP), Life Insurance Promotion (LIP), Credit Card Insurance (CCI) and Sex (S) and ten objects are considered. Notice that with the BC technique, the

attribute with the least distinct balanced-value will be selected as a partitioning attribute without consideration of the maximum value of total roughness of each attributes. Thus, for BC technique, attribute LIP will be chosen as a partitioning attribute. Meanwhile, the TR, MMR and MDA are based on calculations using formula (7), (9) and (4), respectively. The results of the calculation of TR, MMR and MDA of all attributes in Table 2 are summarized in Tables 3, 4 and 5, respectively.

Table 2. The Credit Card Promotion dataset from [9]

#	MP	WP	LIP	CCI	S
1	yes	no	no	no	male
2	yes	yes	yes	no	female
3	no	no	no	no	male
4	yes	yes	yes	yes	male
5	yes	no	yes	no	female
6	no	no	no	no	female
7	yes	no	yes	yes	male
8	no	yes	no	no	male
9	yes	no	no	no	male
10	yes	yes	yes	no	female

Table 3. The value of TR of all attributes

Attribute w.r.t.	TR mean roughness				TR
MP	WP	LIP	CCI	S	0.0875
	0	0.25	0.1	0	
WP	MP	LIP	CCI	S	0
	0	0	0	0	
LIP	MP	WP	CCI	S	0.0625
	0.15	0	0.1	0	
CCI	MP	WP	LIP	S	0.1500
	0.15	0	0.25	0.2	
S	MP	WP	LIP	CCI	0.02500
	0	0	0	0.1	

Table 4. The value of MMR of all attributes

Attribute w.r.t.	MMR mean roughness				MMR
MP	WP	LIP	CCI	S	0.75
	1	0.75	0.9	1	0.9
WP	MP	LIP	CCI	S	1
	1	1	1	1	
LIP	MP	WP	CCI	S	0.85
	0.85	1	0.9	1	
CCI	MP	WP	LIP	S	0.75
	0.85	1	0.75	0.8	0.8
S	MP	WP	LIP	CCI	0.9
	1	1	1	0.9	

As shown in Table 3, the value of TR of LIP, i.e. 0.0625 is lower than that TR of MP, i.e. 0.0875 and CCI, i.e. 0.15. Thus, the decision of BC technique to select LIP as a partitioning attribute is not the best. Based on Table 3, the TR technique selects CCI as the partitioning attribute. From Table 4, MMR selects attribute CCI as partitioning attribute. This is due to the fact that the second mean roughness of attribute CCI, i.e. 0.8 is less than that of the attribute IT, i.e. 0.9. Meanwhile, from Table 5, MDA selects attribute CCI is selected as the partitioning attribute.

Table 5. The degree of dependency of all attributes

Attribute depends on	Degree of dependency				MDA
MP	WP	LIP	CCI	S	0.5
	0	0.5	0.2	0	0.2
WP	MP	LIP	CCI	S	0
	0	0	0	0	
LIP	MP	WP	CCI	S	0.3
	0.3	0	0.2	0	
CCI	MP	WP	LIP	S	0.5
	0.3	0	0.5	0.4	0.4
S	MP	WP	LIP	CCI	0.2
	0	0	0	0.2	

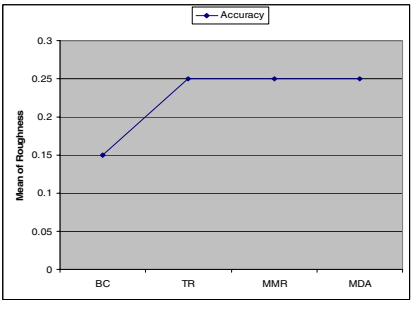

Fig. 1. The accuracy of BC, TR, MMR and MDA techniques

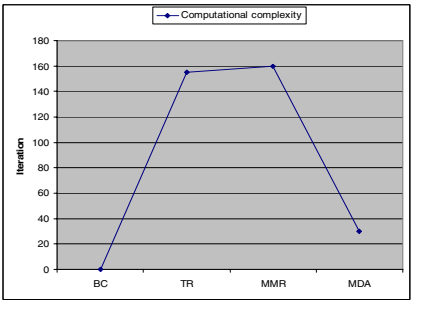

Fig. 2. The computational complexity of BC, TR, MMR and MDA techniques

Based on formula in equation (6), the accuracy of TR, MMR and MDA in selecting partitioning attribute is the same, i.e. 0.25. But, the accuracy of BC technique is 0.15. Additionally, since BC technique only select the partitioning attribute based on least distinct balanced-value of attribute, then BC need no computation. However, for the other techniques, MDA achieve lower computational complexity than that TR and MMR techniques.

6 Conclusion

In this paper, we have pointed out some unreasonable statements of MMR technique. We have proven that the mean roughness of MMR technique is only the opposite of that Mazlack's TR technique and shown that the idea of MMR to achieve lower computational complexity is not error free by an example. In order to solve these problems, MDA (Maximum of Dependency Attributes), an alternative rough set-based technique for selecting partitioning attribute by taking into account the dependency of attributes in an information system is proposed. We have proven that MDA technique is a generalization of TR and MMR techniques which achieve lower computational complexity and has higher accuracy than that BC technique. With this approach, we believe that some applications using dependency attributes in the theory of rough set in information system through this view will be applicable. For the future activities, we use the proposed technique for categorical data clustering and decision support systems in complex domain through larger data set likes the benchmark datasets from some standard UCI database.

Acknowledgement

This work was supported by the FRGS under the Grant No. Vote 0402, Ministry of Higher Education, Malaysia.

References

1. Mazlack, L.J., He, A., Zhu, Y., Coppock, S.: A rough set approach in choosing partitioning attributes. In: Proceedings of the ISCA 13th, International Conference, CAINE-2000, pp. 1–6 (2000)
2. Pawlak, Z.: Rough sets. International Journal of Computer and Information Science 11, 341–356 (1982)
3. Pawlak, Z.: Rough sets: A theoretical aspect of reasoning about data. Kluwer Academic Publisher, Dordrecht (1991)
4. Pawlak, Z., Skowron, A.: Rudiments of rough sets. Information Sciences. An International Journal 177(1), 3–27 (2007)
5. Parmar, D., Wu, T., Blackhurst, J.: An algorithm for clustering categorical data using rough set theory. Data and Knowledge Engineering 63, 879–893 (2007)
6. Yao, Y.Y.: Two views of the theory of rough sets in finite universes. Approximate Reasoning, An International Journal 15(4), 191–317 (1996)
7. Yao, Y.Y.: Constructive and algebraic methods of the theory of rough sets. Information Science, An International Journal 109(1-4), 21–47 (1998)
8. Yao, Y.Y.: Information granulation and rough set approximation. International Journal of Intelligent Systems 16(1), 87–104 (2001)
9. Roiger, R.J., Geatz, M.W.: Data Mining: A Tutorial-Based Primer. Addison Wesley, Reading (2003)

On Multi-soft Sets Construction in Information Systems

Tutut Herawan and Mustafa Mat Deris

Faculty of Information Technology and Multimedia
Universiti Tun Hussein Onn Malaysia
Parit Raja, 86400, Batu Pahat, Johor, Malaysia
tututherawan@yahoo.com, mmustafa@uthm.edu.my

Abstract. The "standard" soft set deals with a binary-valued information system. For a multi-valued information system $S=(U,A,V,f)$, where $V=\bigcup_{a\in A}V_a$, V_a is the domain (value set) of attribute a which has multi value $(|V_a|\geq 3)$, a decomposition can be made from S into $|A|$ number of binary-valued information systems $S=(U,A,V_{\{0,1\}},f)$. In this paper, we present the notion of multi-soft set representing S based on such decomposition. The AND and OR operations in multi-soft sets also presented.

Keywords: Multi-valued information system; Multi-soft set.

1 Introduction

Soft set theory [1], proposed by Molodtsov in 1999, is a new general method for dealing with uncertain data. What the soft set theory different with the traditional tool for dealing with uncertainties, such as theory of probability, theory of fuzzy set [2] and theory of rough set [3,4,5], is that it is free from the inadequacy of the parameterization tools of those theories as pointed out in [1]. In recent years, research on soft set theory has been active, and great progress has been achieved, including the works of fundamental soft set theory [6-8] and decision support systems [9-12]. Soft sets are called (binary, basic, elementary) neighborhood systems [13]. The "standard" soft set is a mapping from parameter to the crisp subset of universe. From such case, we may see the structure of a soft set is very simple i.e. the mapping only classify the objects into two classes (yes/1 or no/0). However, in the theoretical and practical researches of soft sets, the situations are usually very complex. In the real application, depending on the set of parameters, a given parameter may have different values (contain multiple grades). For example, the mathematics degree of student can be classified into three values; high, medium and low. In this situation, every parameter determines a partition of the universe which is contains more than two disjoint subsets. To this, we may represent a multi-valued information system to n binary-valued information system based on each attribute, where each soft set can be defined. Related to a multi-valued information system $S=(U,A,V,f)$, where U is a non-empty finite set of objects, A is a non-empty finite set of attributes, $V=\bigcup_{a\in A}V_a$, V_a is the domain

D.-S. Huang et al. (Eds.): ICIC 2009, LNAI 5755, pp. 101–110, 2009.

(value set) of attribute *a* which has multi value $(|V_a| \geq 3)$ and $f : U \times A \rightarrow V$ is a total function such that $f(u,a) \in V_a$, for every $(u,a) \in U \times A$, called information (knowledge) function, there are $|A|$ number of binary-valued information systems $S = (U, A, V_{\{0,1\}}, f)$ we can created, where $|A|$ denotes the cardinality of *A*. Consequently, the $|A|$ number of binary-valued information systems define multi-soft sets of the multi-valued information systems. In this paper, we present a construction and propose some operations of multi-soft sets based on multi-valued information systems.

The rest of this paper is organized as follows. Section 2 describes knowledge representation. Section 3 describes fundamental soft set theory. Section 4 describes a multi soft set construction in information systems. Finally, we conclude our works in section 5.

2 Knowledge Representation

In this section, we present the notion of a finite table representing knowledge, called an information system. An *information system* as in [5] is a 4-tuple (quadruple) $S = (U, A, V, f)$, where $U = \{u_1, u_2, u_3, \cdots, u_{|U|}\}$ is a non-empty finite set of objects, $A = \{a_1, a_2, a_3, \cdots, a_{|A|}\}$ is a non-empty finite set of attributes, $V = \bigcup_{a \in A} V_a$, V_a is the domain (value set) of attribute *a*, $f : U \times A \rightarrow V$ is an information function such that $f(u,a) \in V_a$, for every $(u,a) \in U \times A$, called information (knowledge) function. The complexity for computing an information system $S = (U, A, V, f)$ is $|U| \times |A|$ since there are $|U| \times |A|$ values of $f(u_i, a_j)$ to be computed, where $i = 1,2,3,\cdots,|U|$ and $j = 1,2,3,\cdots,|A|$. Note that *t* induces a set of maps, $t = f(u,a) : U \times A \rightarrow V$. Each map is a tuple $t_i = (f(u_i, a_1), f(u_i, a_2), f(u_i, a_3), \cdots, f(u_i, a_{|A|}))$, where where $i = 1,2,3,\cdots,|U|$. Note that, the tuple *t* is not necessarily associated with entity uniquely. In an information system, two distinct entities could have redundant tuple, which is not permissible in a relational database. Thus, the concept of an information system is a generalization of the concept of a relational database.

The notion of soft sets and its fundamental operations are given in the following section. Much of the definition and examples are quoted directly from [1,6,9].

3 Soft Set Theory

In this section, we present the notion of a standard soft set. Throughout this section *U* refers to an initial universe, *E* is a set of parameters, $P(U)$ is the power set of *U* and $A \subseteq E$.

Definition 1. *A pair* (F, A) *is called a soft set over U, where F is a mapping given by*

$$F : A \to P(U).$$

In other words, a soft set over U is a parameterized family of subsets of the universe U. For $\varepsilon \in A$, $F(\varepsilon)$ may be considered as the set of ε-elements of the soft set (F, A) or as the set of ε-approximate elements of the soft set. Clearly, a soft set is not a (crisp) set.

Example 2

a. Let we consider a soft set (F, E) which describes the "attractiveness of houses" that Mr. X is considering to purchase. Suppose that there are six houses in the universe U under consideration, $U = \{h_1, h_2, h_3, h_4, h_5, h_6\}$, and is a set of decision parameters $E = \{e_1, e_2, e_3, e_4, e_5\}$, where e_1 stands for the parameters "expensive", e_2 stands for the parameters "beautiful", e_3 stands for the parameters "wooden", e_4 stands for the parameters "cheap", e_5 stands for the parameters "in the green surrounding".

Consider the mapping $F : E \to U \times U$ given by "houses $(\cdot)$", where $(\cdot)$ is to be filled in by one of parameters $e \in E$. Suppose that $F(e_1) = \{h_2, h_4\}$, $F(e_2) = \{h_1, h_3\}$, $F(e_3) = \{h_3, h_4, h_5\}$, $F(e_4) = \{h_1, h_3, h_5\}$, $F(e_5) = \{h_1\}$. Therefore, $F(e_1)$ means "houses (expensive)", whose functional value is the set $\{h_2, h_4\}$. Thus, we can view the soft set (F, E) as a collection of approximations as below

$$(F, E) = \left\{ \begin{array}{c} \text{expensive houses} = \{h_2, h_4\}, \\ \text{beautiful houses} = \{h_1, h_3\}, \\ \text{wooden houses} = \{h_3, h_4, h_5\}, \\ \text{cheap houses} = \{h_1, h_3, h_5\}, \\ \text{in the green surrounding houses} = \{h_1\} \end{array} \right\}$$

Each approximation has two parts, a predicate *p* and an approximate value set *v*. For example, for the approximation "expensive houses $= \{h_2, h_4\}$", we have the predicate name of expensive houses and the approximate value set or value set if $\{h_2, h_4\}$. Thus, a soft set (F, E) can be viewed as a collection of approximations below:

$$(F, E) = \{p_1 = v_1, p_2 = v_2, p_3 = v_3, \cdots, p_n = v_n\}$$

b. Every rough set can be considered as a soft set.

The starting point of rough set theory is the indiscernibility relation, which is generated by information about objects of interest. Two objects in an information system are called indiscernible (indistinguishable or similar) if they have the same feature. Let $S = (U, A, V, f)$ be an information system and let $B \subseteq A$. Two elements $x, y \in U$ are said to be *B*-indiscernible (indiscernible by the set of attribute *B* in *S*) if only if $f(x, a) = f(y, a)$, for every $a \in B$. Obviously, every non-empty subset of *A* induces unique indiscernibility relation. Notice that, an indiscernibility relation induced by the

set of attribute B, denoted by $IND(B)$, is an equivalence relation. It is well known that, an equivalence relation induces unique partition. The partition of U induced by B is denoted by U/B and the equivalence class in the partition U/B containing $x \in U$, is denoted by $[x]_B$. The B-lower approximation of X, denoted by $\underline{B}(X)$ and B-upper approximations of X, denoted by $\overline{B}(X)$, are defined by $\underline{B}(X) = \{x \in U \mid [x]_B \subseteq X\}$ and $\overline{B}(X) = \{x \in U \mid [x]_B \cap X \neq \phi\}$, respectively.

Definition 3. *A rough approximation of a subset $X \subseteq U$ with respect to B is defined as a pair of lower and upper approximations of X, i.e. $\langle \underline{B}(X), \overline{B}(X) \rangle$.*

Let $\langle \underline{B}(X), \overline{B}(X) \rangle$ be the rough approximating a subset $X \subseteq U$. We define a mapping $\underline{B}, \overline{B} : P(U) \to P(U)$ as in Definition 3. Thus every rough set $\langle \underline{B}(X), \overline{B}(X) \rangle$ can be considered a pair of two soft sets $(F, U) = \left((\underline{B}, P(U)), (\overline{B}, P(U)) \right)$.

Table 1. Tabular representation of a soft set in the above example

U	e_1	e_2	e_3	e_4	e_5
h_1	0	1	0	1	1
h_2	1	0	0	0	0
h_3	0	1	1	1	0
h_4	1	0	1	0	0
h_5	0	0	1	1	0
h_6	0	0	0	0	0

4 On Multi-soft Sets Construction in Information Systems

4.1 Decomposition of Multi-valued Information Systems

In this sub-section we discuss a decomposition of a multi-valued information system $S = (U, A, V, f)$ into $|A|$ number of binary-valued information systems. The decomposition of $S = (U, A, V, f)$ is based on decomposition of $A = \{a_1, a_2, \cdots, a_{|A|}\}$ into the disjoint-singleton attribute $\{a_1\}, \{a_2\}, \cdots, \{a_{|A|}\}$. Here, we only consider for complete information systems. Let $S = (U, A, V, f)$ be an information system such that for every $a \in A$, $V_a = f(U, A)$ is a finite non-empty set and for every $u \in U$, $|f(u, a)| = 1$. For every a_i under i^{th}-attribute consideration, $a_i \in A$ and $v \in V_a$, we define the map $a_v^i : U \to \{0,1\}$ such that $a_v^i(u) = 1$ if $f(u, a) = v$, otherwise $a_v^i(u) = 0$. The next result, we define a binary-valued information system as a

quadruple $S^i = (U, a_i, V_{\{0,1\}}, f)$. The information systems $S^i = (U, a_i, V_{\{0,1\}}, f)$, $i = 1,2,\cdots,|A|$ is referred to as a decomposition of a multi-valued information system $S = (U, A, V, f)$ into $|A|$ binary-valued information systems, as depicted in Figure 1. Every information system $S^i = (U, a_i, V_{ai}, f)$, $i = 1,2,\cdots,|A|$ is a deterministic information system since for every $a \in A$ and for every $u \in U$, $|f(u,a)| = 1$ such that the structure of a multi-valued information system and $|A|$ number of binary-valued information systems give the same value of attribute related to objects.

U	a_1	a_2	…	a_k	…	$a_{\|A\|}$
u_1	$f(u_1,a_1)$	$f(u_1,a_2)$	…	$f(u_1,a_k)$	…	$f(u_1,a_{\|A\|})$
u_2	$f(u_2,a_1)$	$f(u_2,a_2)$	…	$f(u_2,a_k)$	…	$f(u_2,a_{\|A\|})$
u_3	$f(u_3,a_1)$	$f(u_3,a_2)$	…	$f(u_3,a_k)$	…	$f(u_3,a_{\|A\|})$
⋮	⋮	⋮	⋱	⋮	⋱	⋮
$u_{\|U\|}$	$f(u_{\|U\|},a_1)$	$f(u_{\|U\|},a_2)$	…	$f(u_{\|U\|},a_k)$	…	$f(u_{\|U\|},a_{\|A\|})$

Binary-valued information system-1

U	a_1					
	Va_{11}	Va_{12}	…	Va_{1k}	…	Va_{1n}
u_1	0	1	…	0	…	0
u_2	0	0	…	1	…	0
u_3	0	1	…	0	…	0
⋮	⋮	⋮	⋱	⋮	⋱	⋮
$u_{\|U\|}$	1	0	…	0	…	0

⋮

Binary-valued information system-$|A|$

U	$a_{\|A\|}$					
	$Va_{\|A\|1}$	$Va_{\|A\|2}$	…	$Va_{\|A\|k}$	…	$Va_{\|A\|n}$
u_1	0	0	…	1	…	0
u_2	0	0	…	0	…	1
u_3	0	1	…	0	…	0
⋮	⋮	⋮	⋱	⋮	⋱	⋮
$u_{\|U\|}$	1	0	…	0	…	0

Fig. 1. A decomposition of a multi-valued information system

Based on the definition of an information system and a soft set, in this section we show that a soft set is a special type of information systems, i.e., a binary-valued information system.

Proposition 4. *If* (F,E) *is a soft set over the universe U, then* (F,E) *is a binary-valued information system* $S=(U,A,V_{\{0,1\}},f)$.

Proof. Let (F,E) be a soft set over the universe U, we define a mapping

$$F=\{f_1,f_2,\cdots,f_n\},$$

where

$$f_i:U\to V_1 \text{ and } f_i(x)=\begin{cases}1, & x\in F(ei_1)\\ 0, & x\notin F(e_i)\end{cases}, \text{ for } 1\le i\le n.$$

Hence, if $A=E$, $V=\bigcup_{e_i\in A}V_{e_i}$, where $V_{e_i}=\{0,1\}$, then a soft set (F,E) can be considered as a binary-valued information system $S=(U,A,V_{\{0,1\}},f)$. □

From Proposition 4, it is easily to understand that a binary-valued information system can be represented as a soft set. Thus, we can make a one-to-one correspondence between (F,E) over U and $S=(U,A,V_{\{0,1\}},f)$.

4.2 Multi-soft Sets in Information Systems

Based on the notion of a decomposition of a multi-valued information system in the previous sub-section, in this sub-section we present the notion of multi-soft set representing multi-valued information systems. Let $S=(U,A,V,f)$ be a multi-valued information system and $S^i=(U,a_i,V_{ai},f)$, $i=1,2,\cdots,|A|$ be the $|A|$ binary-valued information systems. From Proposition 4, we have

$$S=(U,A,V,f)=\begin{cases}S^1=(U,a_1,V_{\{0,1\}},f) & \Leftrightarrow (F,a_1)\\ S^2=(U,a_2,V_{\{0,1\}},f) & \Leftrightarrow (F,a_2)\\ \quad\vdots & \quad\vdots \quad\vdots\\ S^{|A|}=(U,a_{|A|},V_{\{0,1\}},f) & \Leftrightarrow (F,a_{|A|})\end{cases}$$

$$=\left((F,a_1),(F,a_2),\cdots,(F,a_{|A|})\right)$$

We define $(F,E)=\left((F,a_1),(F,a_2),\cdots,(F,a_{|A|})\right)$ as a multi-soft set over universe U representing a multi-valued information system $S=(U,A,V,f)$.

Example 5. We consider to a multi-valued information system from Parmar *et. al.* [14].

Table 2. An information system from [14]

#	a_1	a_2	a_3	a_4	a_5	a_6
1	Big	Blue	Hard	Indefinite	Plastic	Negative
2	Medium	Red	Moderate	Smooth	Wood	Neutral
3	Small	Yellow	Soft	Fuzzy	Plush	Positive
4	Medium	Blue	Moderate	Fuzzy	Plastic	Negative
5	Small	Yellow	Soft	Indefinite	Plastic	Neutral
6	Big	Green	Hard	Smooth	Wood	Positive
7	Small	Yellow	Hard	Indefinite	Metal	Positive
8	Small	Yellow	Soft	Indefinite	Plastic	Positive
9	Big	Green	Hard	Smooth	Wood	Neutral
10	Medium	Green	Moderate	Smooth	Plastic	Neutral

The decomposition of Table 2 into multi-tables of binary-valued information systems is given in Table 3. From Table 3, we have the following corresponding soft sets

$$(F,a_1)=\{\text{Big}=\{1,6,9\},\text{Medium}=\{2,4,10\},\text{Small}=\{3,5,7,8\}\}$$
$$(F,a_2)=\{\text{Blue}=\{1,4\},\text{Red}=\{2\},\text{Yellow}=\{3,5,7,8\},\text{Green}=\{6,9,10\}\}$$
$$(F,a_3)=\{\text{Hard}=\{1,6,7,9\},\text{Moderate}=\{2,4,10\},\text{Soft}=\{3,5,8\}\}$$
$$(F,a_4)=\{\text{Indefinite}=\{1,5,7,8\},\text{Smooth}=\{2,6,9,10\},\text{Fuzzy}=\{3,4\}\}$$
$$(F,a_5)=\{\text{Plastic}=\{1,4,5,8,10\},\text{Wood}=\{2,6,9\},\text{Plush}=\{3\},\text{Metal}=\{7\}\}$$
$$(F,a_6)=\{\text{Negative}=\{1,4\},\text{Neutral}=\{2,5,9,10\},\text{Positive}=\{3,6,7,8\}\}$$

Thus the multi-soft set representing Table 2 is

$$(F,E)=((F,E_1),(F,E_2),(F,E_3),(F,E_4),(F,E_5),(F,E_6))$$

$$=\begin{pmatrix}\{\text{Big}=\{1,6,9\},\text{Medium}=\{2,4,10\},\text{Small}=\{3,5,7,8\}\},\\ \{\text{Blue}=\{1,4\},\text{Red}=\{2\},\text{Yellow}=\{3,5,7,8\},\text{Green}=\{6,9,10\}\},\\ \{\text{Hard}=\{1,6,7,9\},\text{Moderate}=\{2,4,10\},\text{Soft}=\{3,5,8\}\},\\ \{\text{Indefinite}=\{1,5,7,8\},\text{Smooth}=\{2,6,9,10\},\text{Fuzzy}=\{3,4\}\},\\ \{\text{Plastic}=\{1,4,5,8,10\},\text{Wood}=\{2,6,9\},\text{Plush}=\{3\},\text{Metal}=\{7\}\},\\ \{\text{Negative}=\{1,4\},\text{Neutral}=\{2,5,9,10\},\text{Positive}=\{3,6,7,8\}\},\end{pmatrix}$$

Notice that, from Example 5, the partition U/a_i and the corresponding soft set (F,a_i), for $1\le i\le 6$, they have the equivalent structures. Generally, a soft set (F,E) over U can be considered as a partition type of the universe U. We can define $F:E\to P(U)$ as the partition $\{F(e),U\setminus F(e)\}$, for every $e\in E$.

4.3 AND and OR Operations in Multi-soft Sets

The notions of AND and OR operations in multi-soft sets are given below.

Table 3. A decomposition of Table 2 into multi-tables

#	a_1		
	Big	**Med**	**Small**
1	1	0	0
2	0	1	0
3	0	0	1
4	0	1	0
5	0	0	1
6	1	0	0
7	0	0	1
8	0	0	1
9	1	0	0
10	0	1	0

#	a_4		
	Indefinite	**Smooth**	**Fuzzy**
1	1	0	0
2	0	1	0
3	0	0	1
4	0	0	1
5	1	0	0
6	0	1	0
7	1	0	0
8	1	0	0
9	0	1	0
10	0	1	0

#	a_2			
	Blue	**Red**	**Yellow**	**Green**
1	1	0	0	0
2	0	1	0	0
3	0	0	1	0
4	1	0	0	0
5	0	0	1	0
6	0	0	0	1
7	0	0	1	0
8	0	0	1	0
9	0	0	0	1
10	0	0	0	1

#	a_5			
	Plastic	**Wood**	**Plush**	**Metal**
1	1	0	0	0
2	0	1	0	0
3	0	0	1	0
4	1	0	0	0
5	1	0	0	0
6	0	1	0	0
7	0	0	0	1
8	1	0	0	0
9	0	1	0	0
10	0	0	0	0

#	a_3		
	Hard	**Moderate**	**Soft**
1	1	0	0
2	0	1	0
3	0	0	1
4	0	1	0
5	0	0	1
6	1	0	0
7	1	0	0
8	0	0	1
9	1	0	0
10	0	1	0

#	a_6		
	Negative	**Neutral**	**Positive**
1	1	0	0
2	0	1	0
3	0	0	1
4	1	0	0
5	0	1	0
6	0	0	1
7	0	0	1
8	0	0	1
9	0	1	0
10	0	1	0

Definition 6. *Let* $(F,E)=\{(F,a_i): i=1,2,\cdots,|A|\}$ *be a multi-soft set over U representing a multi-valued information system* $S=(U,A,V,f)$. *The* AND *operation between* (F,a_i) *and* (F,a_j) *is defined as*

$$(F,a_i)\text{AND}(F,a_j)=(F,a_i\times a_j),$$

where

$$H(Va_i, Va_j) = F(Va_i) \cap G(Va_j),\ \forall (Va_i, Va_j) \in a_i \times a_j,\ for\ 1 \le i, j \le |A|.$$

Example 7. From Example 5, let two soft-sets

$$(F, a_1) = \{\text{Big} = \{1,6,9\}, \text{Medium} = \{2,4,10\}, \text{Small} = \{3,5,7,8\}\}$$

and

$$(F, a_3) = \{\text{Hard} = \{1,6,7,9\}, \text{Moderate} = \{2,4,10\}, \text{Soft} = \{3,5,8\}\}.$$

Then, we have

$$(F, a_1)\text{AND}(F, a_3) = (F, a_1 \times a_3)$$

$$= \begin{pmatrix} (\text{Big}, \text{Hard}) = \{1,6,9\}, (\text{Big}, \text{Moderate}) = \phi, (\text{Big}, \text{Soft}) = \phi, \\ (\text{Medium}, \text{Hard}) = \phi, (\text{Medium}, \text{Moderate}) = \{2,4,10\}, (\text{Medium}, \text{Soft}) = \phi, \\ (\text{Small}, \text{Hard}) = \phi, (\text{Small}, \text{Moderate}) = \{2,4,10\}, (\text{Small}, \text{Soft}) = \{3,5,8\} \end{pmatrix}$$

Definition 8. *Let* $(F, E) = \{(F, a_i) : i = 1,2,\cdots,|A|\}$ *be a multi-soft set over U representing a multi-valued information system* $S = (U, A, V, f)$. *The* OR *operation between* (F, a_i) *and* (F, a_j) *is defined as*

$$(F, a_i)\text{OR}(F, a_j) = (F, a_i \times a_j),$$

where

$$F(Va_i, Va_j) = F(Va_i) \cup G(Va_j),\ \forall (Va_i, Va_j) \in a_i \times a_j,\ for\ 1 \le i, j \le |A|.$$

Example 9. From Example 5, let two soft-sets

$$(F, a_4) = \{\text{Indefinite} = \{1,5,7,8\}, \text{Smooth} = \{2,6,9,10\}, \text{Fuzzy} = \{3,4\}\}$$

and

$$(F, a_5) = \{\text{Plastic} = \{1,4,5,8,10\}, \text{Wood} = \{2,6,9\}, \text{Plush} = \{3\}, \text{Metal} = \{7\}\}$$

Then we have

$$(F, a_4)\text{OR}(F, a_5) = (F, a_4 \times a_5) =$$

$$= \begin{pmatrix} (\text{Indefinite}, \text{Plastic}) = \{1,4,5,7,8,10\}, (\text{Indefinite}, \text{Wood}) = \{1,2,5,6,7,8,9\}, \\ (\text{Indefinite}, \text{Plush}) = \{1,3,5,7,8\}, (\text{Indefinite}, \text{Metal}) = \{1,5,7,8\}, \\ (\text{Smooth}, \text{Plastic}) = \{1,2,4,5,6,8,9,10\}, (\text{Smooth}, \text{Wood}) = \{2,6,9,10\}, \\ (\text{Smooth}, \text{Plush}) = \{2,3,6,9,10\}, (\text{Smooth}, \text{Metal}) = \{2,6,7,9,10\}, \\ (\text{Fuzzy}, \text{Plastic}) = \{1,3,4,5,8,10\}, (\text{Fuzzy}, \text{Wood}) = \{2,3,4,6,9\}, \\ (\text{Fuzzy}, \text{Plush}) = \{3,4\}, (\text{Fuzzy}, \text{Metal}) = \{3,4,7\} \end{pmatrix}$$

Thus, both AND and OR operations in multi-soft set over U define a soft set over $U \times U$.

5 Conclusion

In this paper, we have presented the notion of a multi-sot sets representing a multi-valued information system. The idea is based on the decomposition of a multi-valued information system into binary-valued information systems. Since the "standard" soft set deals with a binary-valued information system, then we easily define the notion of multi-soft sets. The operations AND and OR in multi-soft sets also presented. Both AND and OR operations in multi-soft set over U define a soft set over $U \times U$.

Acknowledgements

This work was supported by the FRGS under the Grant No. Vote 0402, Ministry of Higher Education, Malaysia.

References

1. Molodtsov, D.: Soft Set Theory-first Fesults. Computers and Mathematics with Applications 37, 19–31 (1999)
2. Zadeh, L.A.: Fuzzy Set. Information and Control 8, 338–353 (1965)
3. Pawlak, Z.: Rough Sets. International Journal of Computer and Information Science 11, 341–356 (1982)
4. Pawlak, Z.: Rough Sets: A Theoretical Aspect of Reasoning about Data. Kluwer Academic Publisher, Dordrecht (1991)
5. Pawlak, Z., Skowron, A.: Rudiments of Rough Sets, Information Sciences. An International Journal 177(1), 3–27 (2007)
6. Maji, P.K., Biswas, R., Roy, A.R.: Soft Set Theory. Computers and Mathematics with Applications 45, 555–562 (2003)
7. Yang, C.F.: A Note on Soft Set Theory. Computers and Mathematics with Applications 56, 1899–1900 (2008)
8. Ali, M.I., Feng, F., Liu, X., Min, W.K., Shabir, M.: On Some New Operations in Soft Set Theory. Computers and Mathematics with Applications (2008), doi:10.1016/j.camwa.2008.11.009
9. Maji, P.K., Roy, A.R., Biswas, R.: An Application of Soft Sets in a Decision Making Problem. Computers and Mathematics with Applications 44, 1077–1083 (2007)
10. Chen, D., Tsang, E.C.C., Yeung, D.S., Wang, X.: The Parameterization Reduction of Soft Sets and its Applications. Computers and Mathematics with Applications 49, 757–763 (2005)
11. Zou, Y., Xiao, Z.: Data Analysis Approaches of Soft Sets Under Incomplete Information. Knowledge-Based Systems 21, 941–945 (2008)
12. Zhi, K., Gao, L., Wang, L., Li, S.: The Normal Parameter Reduction of Soft Sets and Its Algorithm. Computers and Mathematics with Applications 56, 3029–3037 (2008)
13. Yao, Y.Y.: Relational Interpretations of Neighbourhood Operators and Rough Set Approximation Operators. Information Sciences 111, 239–259 (1998)
14. Parmar, D., Wu, T., Blackhurst, J.: MMR: An Algorithm for Clustering Categorical Data Using Rough Set Theory. Data and Knowledge Engineering 63, 879–893 (2007)

Knowledge Representation and Consistency Checking in a Norm-Parameterized Fuzzy Description Logic

Jidi Zhao[1], Harold Boley[2], and Weichang Du[1]

[1] Faculty of Computer Science,
University of New Brunswick, Fredericton, Canada
{Judy.Zhao,wdu}@unb.ca
[2] Institute for Information Technology, National Research Council of Canada
Fredericton, NB, E3B 9W4 Canada
Harold.Boley@nrc.gc.ca

Abstract. This paper has its motivation in the occurrence of uncertain knowledge in different application areas, and introduces an expressive fuzzy description logic that extends classical description logics to many-valued logics. We represent, and reason with, uncertain knowledge in the description logic $\mathcal{ALCHIN}$ extended to an interval-based, norm-parameterized fuzzy logic. First, the syntax and the semantics of the proposed fuzzy description logic are addressed. Then the paper presents an algorithm for consistency checking of knowledge bases in the proposed language.

1 Introduction

The Semantic Web is an evolving extension of the World Wide Web in which the semantics of the information and services available on the Web are formally described, making it possible for machines to better understand and satisfy requests of people. The Web ontology language (OWL), built upon the logic-based knowledge formalisms known as Description Logics (DLs), has enabled machine interpretation of such semantics and become a W3C recommendation for ontology representation.

Description Logics (DLs) [1] are a family of logic-based formalisms designed to represent and reason about the conceptual knowledge of arbitrary domains. Elementary descriptions of DLs are atomic concepts and atomic roles. Complex concept descriptions and role descriptions can be built from the elementary descriptions according to construction rules. As a notational convention, in this paper we will use a, b, x for individuals, A for an atomic concept, C and D for concept descriptions, R and P for atomic roles. Different description languages of DLs are distinguished by the kind of concept and role constructors (such as conjunction, disjunction, and exists restriction) allowed in their description language and the kinds of axiom allowed in their terminologies. For example, the $\mathcal{ALCHIN}$ DL [5] extends the well-known $\mathcal{ALC}$ DL with inverse roles, role hierarchies (inclusion axioms), and number restrictions.

D.-S. Huang et al. (Eds.): ICIC 2009, LNAI 5755, pp. 111–123, 2009.

Standard DLs in use today are only suitable for representing and reasoning with crisp concepts, properties and constructors, but are not capable of dealing with uncertainty. To overcome this deficiency, considerable work has been carried out in integrating uncertain knowledge into DLs in the last decade. The approaches based on Fuzzy Set Theory and Fuzzy Logic, such as [7] [8] [6] [2], have proved very promising in various Semantic Web applications.

Fuzzy Set Theory was first introduced by Zadeh [9] as an extension to the classical notion of a set to capture the inherent vagueness (the lack of crisp boundaries of sets). Fuzzy Logic is a form of multi-valued logic derived from Fuzzy Set Theory to deal with reasoning that is approximate rather than precise. In Fuzzy Logic, the degree of truth of a statement can range between 0 and 1, and is not constrained to the two truth values $\{0, 1\}$ or $\{false, true\}$ as in classical predicate logic. Formally, a fuzzy set X with respect to a set of elements Ω (also called a universe) is characterized by a membership function $\mu(x)$ which assigns a value in the real unit interval [0,1] to each element x in X ($x \in X$), notated as $X : \Omega \rightarrow [0, 1]$. $\mu(x)$ gives us a degree of an element x belonging to a set X. Such degrees can be computed based on some specific membership function. A fuzzy relation R over two fuzzy sets X_1 and X_2 is defined by a function $R : \Omega \times \Omega \rightarrow [0, 1]$.

Fuzzy Logic extends the Boolean operations defined on crisp sets and relations in the context of fuzzy sets and fuzzy relations. These operations, such as complement, union, and intersection, are interpreted as mathematical functions over the unit interval [0,1]. The mathematical functions for fuzzy intersection are usually called t-norms ($t(\eta, \theta)$); those for fuzzy union are called s-norms ($s(\eta, \theta)$); and those for the fuzzy set complement are called negations ($\neg\eta$); here η, θ define the truth degrees of sets and relations and can range between 0 and 1. These functions usually satisfy certain mathematical properties. The most widely known operations in the Fuzzy Logic family of Zadeh Logic, Lukasiewicz Logic, Product Logic, and Gödel Logic, are summarized in Table 1.

Table 1. Fuzzy Operations

	Zadeh Logic	Lukasiewicz Logic	Product Logic	Gödel Logic
t-norm ($t(\eta, \theta)$)	$\min(\eta, \theta)$	$\max(\eta + \theta - 1, 0)$	$\eta \cdot \theta$	$\min(\alpha, \beta)$
s-norm ($s(\eta, \theta)$)	$\max(\eta, \theta)$	$\min(\eta + \theta, 1)$	$\eta + \theta - \eta \cdot \theta$	$\max(\eta, \beta)$
negation ($\neg\eta$)	$1 - \eta$	$1 - \eta$	if η=0 then 1 else 0	if η=0 then 1 else 0

In existing fuzzy extensions to DLs, most work is based on Zadeh logic (e.g. [6] [7]) and some work is based on Product logic (e.g. [2]). In this paper, we extend our work in [10], and propose a general, parameterized semantics for t-norms and s-norms as well as allowing Lukasiewicz negation in the fuzzy description logic

called $f\mathcal{ALCHIN}$, so that the interpretation of complex concept descriptions can cover different types of operations in the parameterized Fuzzy Logic family. Another effort considering different logic operations in Fuzzy Logic is due to Hájek [4], with the underlying DL language being $\mathcal{ALC}$. Furthermore, unlike other approaches based on Fuzzy Logic, which only deal with crisp subsumption of fuzzy concepts, our fuzzy description logic deals with fuzzy subsumption of fuzzy concepts and addresses its semantics. We argue that fuzzy subsumption of fuzzy concepts permits more adequate modeling of the uncertain knowledge existing in real world applications. The notion of fuzzy subsumption was first proposed in [8] and used in the forms $\geq l$ and $\leq u$, where l,u $\in$ [0,1], but it was left unsolved how to do reasoning on fuzzy knowledge bases. In this paper, we also define a unified interval form $[l, u]$ and present a reasoning algorithm.

2 A Norm-Parameterized Fuzzy Description Logic

2.1 Syntax and Semantics of $f\mathcal{ALCHIN}$

Concept descriptions in $f\mathcal{ALCHIN}$ are formed based on the following syntax:

$$C \rightarrow \top|\bot|A|\neg A|\neg C|C \sqcap D|C \sqcup D|\exists R.C|\forall R.C|\geq nR|\leq nR$$

We can see that the syntax of this fuzzy description logic is identical to that of the standard description logic $\mathcal{ALCHIN}$. The difference is that the concepts and roles in $f\mathcal{ALCHIN}$ are defined as fuzzy concepts (i.e. fuzzy sets) and fuzzy roles (i.e. fuzzy relations).

Similar to standard DLs, the semantics of the proposed $f\mathcal{ALCHIN}$ is based on the notion of interpretation. Classical interpretations are extended to the notion of fuzzy interpretations by using membership functions that range over the interval [0,1]. A fuzzy interpretation I is still a pair $I = (\Delta^I, \cdot^I)$ consisting of a domain Δ^I which is a non-empty set and of a fuzzy interpretation function $\cdot^I$ which maps each individual x into an element of Δ^I ($x \in \Delta^I$), each concept C into a membership function of $C^I : \Delta^I \rightarrow [0, 1]$, and each atomic role R into a membership function of $R^I : \Delta^I \times \Delta^I \rightarrow [0, 1]$.

The semantics of the top concept $\top$ is the greatest element in the domain Δ^I, that is, $\top^I = 1$ ($\forall x \in \Delta^I$). Note that, in standard DLs, the top concept $\top \equiv A \sqcup \neg A$, while in $f\mathcal{ALCHIN}$, $\top \neq A \sqcup \neg A$. As shown in Table 1, after applying the s-norms on $A \sqcup \neg A$, the result is no longer always equal to 1, so cannot be used as $\top$. Thus, we explicitly define the top concept, stating that the truth degree of x in $\top$ is 1. Similarly, the bottom concept $\bot$ is the least element in the domain, defined as $\bot^I = 0$ ($\forall x \in \Delta^I$).

In the Fuzzy Logic family, there exist two kinds of negation: Lukasiewicz negation and Gödel negation. We do not see much practical interest in the latter negation, and thus prefer to interpret the concept negation $\neg C$ based on Lukasiewicz negation, that is, $(\neg C)^I(x) = 1 - C^I(x)$. For example, if we have that the statement "John is young" has a truth value of greater than or equal to 0.8 ($Young(John)$ $[0.8, 1]$), then the statement "John is not young" is written as $\neg Young(John) = \neg[0.8, 1] = [0, 0.2]$.

The interpretation of concept conjunction is defined by a t-norm as $(C \sqcap D)^I(x) = t(C^I(x), D^I(x))$ $(\forall x \in \Delta^I)$. For example, if we have both $Young(John)$ $[0.8, 1]$ and $Tall(John)$ $[0.7, 1]$, and assume the product function in Product Logic is chosen as the t-norm, then the degree of truth that John is both young and tall is $(Young \sqcap Tall)(John) = t_P([0.8, 1], [0.7, 1]) = [0.56, 1]$.

The interpretation of concept disjunction is defined by an s-norm as $(C \sqcup D)^I(x) = s(C^I(x), D^I(x))$ $(\forall x \in \Delta^I)$. For example, if we have $Young(John)$ $[0.8, 1]$ and $Tall(John)$ $[0.7, 1]$, and the s-norm is the maximum function as in Zadeh logic or Gödel logic, then the degree of truth that John is young or tall is $(Young \sqcup Tall)(John) = \max([0.8, 1], [0.7, 1]) = [0.8, 1]$.

The semantics of exists restriction $\exists R.C$ is the result of viewing $\exists R.C$ as the open first order formula $\exists y.R(x, y) \wedge C(y)$ and the existential quantifier $\exists$ as a disjunction over the domain, defined as sup (supremum or least upper bound). Therefore, we define $(\exists R.C)^I(x) = \sup_{y \in \Delta^I}\{t(R^I(x, y), C^I(y))\}$.

A value restriction $\forall R.C$ is viewed as an implication of the form $\forall y \in \Delta^I, R^I(x, y) \rightarrow C^I(x)$. As proposed by Hájek [3], we interpret $\forall$ as inf (infimum or greatest lower bound). Furthermore, in classical logic, $a \rightarrow b$ is a shorthand for $\neg a \vee b$; we can thus interpret $\rightarrow$ as the Kleene-Dienes implication, and finally get its semantics as $(\forall R.C)^I(x) = \inf_{y \in \Delta^I}\{s(\neg R^I(x, y), C^I(y))\}$.

A fuzzy at-least restriction is of the form $\geq nR$, whose semantics

$$(\geq nR)^I(x) = \sup_{y_1,\ldots,y_n \in \Delta^I, y_i \neq y_j, 1 \leq i < j \leq n} t_{i=1}^n \{R^I(x, y_i)\}$$

is derived from its first order reformulation

$$\exists y_1, \ldots, y_n. \wedge_{i=1}^n R(x, y_i) \bigwedge \wedge_{1 \leq i < j \leq n} y_i \neq y_j.$$

The semantics states that there are at least n distinct individuals $(y_1, \ldots, y_n)$ all of which satisfy $R(x, y_i)$ to some degree.

Furthermore, as suggested by [8], we define the semantics of a fuzzy at-most restriction as

$$\begin{aligned}(\leq nR)^I(x) &= \neg(\geq (n+1)R)^I(x) \\ &= \inf_{y_1,\ldots,y_{n+1} \in \Delta^I, y_i \neq y_j, 1 \leq i < j \leq n+1} s_{i=1}^{n+1}\{\neg R^I(x, y_i)\}\end{aligned}$$

The semantics states that for $n + 1$ role assertions $R(x, y_i)$ $(1 \leq i \leq n + 1)$ that can be formed, at least one of them satisfies $\neg R(x, y_i)$ to some degree. More intuitively, we can directly view the semantics of a fuzzy at-most number restriction as there being at most n unique individuals $(y_1, \ldots, y_n)$ that satisfy $R(x, y_i)$ to some degree. For example, $(\leq 2R)(a)$ [0.8,1] means that there are at most two role assertions about the individual a: $R(a, b_1)$ and $R(a, b_2)$ $(b_1 \neq b_2)$. Assuming $x_{R(a,b_1)}$ is the truth degree of $R(a, b_1)$ and $x_{R(a,b_2)}$ is the truth degree of $R(a, b_2)$, then both $x_{R(a,b_1)}$=[0.8,1] and $x_{R(a,b_2)}$=[0.8,1] hold.

2.2 Knowledge Bases in *fALCHIN*

A fuzzy knowledge base $KB =< T, A >$ in *fALCHIN* consists of two parts: the terminological box (TBox T) and the assertional box (ABox A). The TBox has several kinds of axioms. A fuzzy concept inclusion axiom has the form of

$C \sqsubseteq D$ $[l, u]$ with $0 \leq l \leq u \leq 1$, which describes that the subsumption degree of truth between concepts C and D is from l to u.

For example, the axiom

$$Professor \sqsubseteq (\exists publishes.Journalpaper \sqcap \exists teaches.Graduatecourse)\ [0.8, 1]$$

states that the concept *professor* is subsumed by entities that *publish* journal papers and *teach* graduate courses with a truth degree of at least 0.8.

The FOL translation of a fuzzy concept inclusion axiom $C \sqsubseteq D$ has the form $\forall x.C(x) \rightarrow D(x)$; under the Kleene-Dienes implication, we thus define its semantics as

$$(C \sqsubseteq D)^I(x) = \inf_{x \in \Delta^I} C^I(x) \rightarrow D^I(x) = \inf_{x \in \Delta^I} \{s(\neg C^I(x), D^I(x))\}.$$

We also consider a fuzzy concept equivalence axiom of the form $C \equiv D$ $[l, u]$ with the semantics as $C^I = D^I$ $[l, u]$. In fact, concept equations ($C \equiv D$ $[l, u]$) are interchangeable with a pair of fuzzy concept inclusion axioms ($C \sqsubseteq D$ $[l, u]$ and $D \sqsubseteq C$ $[l, u]$).

A fuzzy role inclusion axiom has the form $R \sqsubseteq P$ $[l, u]$. Similarly to concept inclusion, the semantics of a role inclusion axiom $R \sqsubseteq P$ is defined as

$$(R \sqsubseteq P)^I(x, y) = \inf_{x,y \in \Delta^I} \{s(\neg R^I(x, y), P^I(x, y))\}.$$

A fuzzy role equivalence axiom is an expression of the form $R \equiv P$ $[l, u]$, i.e., a pair of fuzzy role inclusion axioms ($R \sqsubseteq P$ $[l, u]$ and $P \sqsubseteq R$ $[l, u]$).

There are three kinds of assertions in the ABox: concept individual, role individual, and individual inequality. A fuzzy concept assertion and a fuzzy role assertion are of the form $C(a)$ $[l, u]$ and the form $R(a, b)$ $[l, u]$, respectively. The semantics of assertions is interpreted as the assertion $C(a)$ $[l, u]$ (resp. $R(a, b)$ $[l, u]$) being satisfied by I iff $a^I \in C^I = [l, u]$ (resp. $(a^I, b^I) \in R^I = [l, u]$). An individual inequality in the ABox is identical to standard DLs and has the crisp form $a \neq b$ for a pair of individuals a and b, with the natural semantics.

3 Consistency Checking

The most important reasoning task for an $f\mathcal{ALCHIN}$ KB, as for any DL, is **consistency checking**, which refers to determining whether the KB is consistent or not. Here we first give formal definitions for $f\mathcal{ALCHIN}$ consistency, generalizing those for a standard DL KB consistency.

Definition 1 (Complete). Let A_i^ε be an extended ABox obtained by applications of the completion rules (given in Definition 7). An extended ABox A_i^ε is complete if no more completion rule can be applied to A_i^ε. □

Definition 2 (Solution). Let $\mathcal{C}$ be the constraint set obtained by applications of the completion rules. Let $Var(\mathcal{C})$ be the set of variables occurring in the constraint set $\mathcal{C}$. If the system of inequations in $\mathcal{C}$ is solvable, the result of the constraint set, i.e. the mapping $\Phi : Var(\mathcal{C}) \rightarrow [0, 1]$, is a solution. □

Definition 3 (Clash). We say there is a clash in the extended ABox A_i^ε iff one of the following situations occurs:

1. $\{\bot(a)\ [l,u]\} \subseteq A_i^\varepsilon$ *and* $0 < l \leq u$
2. $\{\top(a)\ [l,u]\} \subseteq A_i^\varepsilon$ *and* $l \leq u < 1$
3. $\{A(a)\ [l_1,u_1], A(a)\ [l_2,u_2]\} \subseteq A_i^\varepsilon$ *and* $(u_1 < l_2$ *or* $u_2 < l_1)$
4. $\{R(a,b)\ [l_1,u_1], R(a,b)\ [l_2,u_2]\} \subseteq A_i^\varepsilon$ *and* $(u_1 < l_2$ *or* $u_2 < l_1)$
5. $\{(\leq nR)(a)\ [l,u]\} \cup \{R(a,b_i)\ [l_i,u_i] | 1 \leq i \leq n+1\} \cup \{b_i \neq b_j | 1 \leq i < j \leq n+1\} \subseteq A_i^\varepsilon$ *and* $([l_i,u_i] \subseteq [l,u] | 1 \leq i \leq n+1)$ □

For example, if a knowledge base contains both assertions *Tall(John)* [0,0.2] and *Tall(John)* [0.7,1], since 0.2<0.7, the third clash trigger will detect this as an inconsistency.

Definition 4 (Model). Let A_i^ε be the extended ABox obtained by applications of the completion rules. Let $I = (\Delta^I, \cdot^I)$ be a fuzzy interpretation, $\Phi : Var(\mathcal{C}) \rightarrow [0,1]$ be a solution, x_α be the variable representing the truth degree of assertion α. The pair $< I, \Phi >$ is a model of the extended ABox A_i^ε if both of the following hold:

1. for each assertion $(C(a)\ x_{C(a)}) \in A_i^\varepsilon$, $(C^I(a) = x_{C(a)}) \in \Phi$.
2. for each assertion $(R(a,b)\ x_{R(a,b)}) \in A_i^\varepsilon$, $(R^I(a,b) = x_{R(a,b)}) \in \Phi$. □

Definition 5 (Consistency). Let $KB =< T, A >$ be an $f\mathcal{ALCHIN}$ knowledge base where T is the TBox and A is the ABox. Let $I = (\Delta^I, \cdot^I)$ be a fuzzy interpretation, and $\Phi : Var(\mathcal{C}) \rightarrow [0,1]$ be a solution. If there exists a model $< I, \Phi >$ for the extended ABox resulting from $KB =< T, A >$, we say the knowledge base $KB =< T, A >$ is consistent. If there is no such model, we call the knowledge base inconsistent. □

Note that the consistency checking of an $f\mathcal{ALCHIN}$ knowledge base is a crisp 'yes/no' decision.

As in standard DLs, the reasoning procedure for $f\mathcal{ALCHIN}$ tries to construct a model over the KB. Such a model has the shape of a forest, a collection of trees, with nodes corresponding to individuals, root nodes corresponding to named individuals, and edges corresponding to roles between individuals. Each node is associated with a node label, $\mathcal{L}$(individual). But unlike in standard DLs where a node is labeled only with concepts, each node in $f\mathcal{ALCHIN}$ is associated with a label that consists of two components: the concept assertions for this individual and the corresponding constraints. Furthermore, each edge is associated with an edge label, $\mathcal{L}$(individual1, individual2) which consists of two components: the role assertions between the two individuals and the corresponding constraints, instead of simply being labeled with roles as in standard DLs.

The tableau algorithm consists of the following steps.

1. Replace each axiom of the form $C \equiv D$ [l,u] with the following two subsumption axioms: $C \sqsubseteq D$ [l,u] and $D \sqsubseteq C$ [l,u]. Replace each axiom of the form $R \equiv P$ [l,u] with the following two subsumption axioms: $R \sqsubseteq P$ [l,u] and $P \sqsubseteq R$ [l,u]. Transform every axiom in the TBox into its normal form. That is, replace each axiom of the form $C \sqsubseteq D$ [l,u] with $\top \sqsubseteq \neg C \sqcup D$ [l,u], $R \sqsubseteq P$ [l,u] with $\top \sqsubseteq \neg R \sqcup P$ [l,u].
2. Augment the ABox A with respect to the TBox T. That is, for each individual a in A and each axiom $\top \sqsubseteq \neg C \sqcup D$ [l,u] in T, add $(\neg C \sqcup D)(a)$ [l,u] to A; for each role assertion $R(a, b)$ and each axiom $\top \sqsubseteq \neg R \sqcup P$ [l,u] in T, add $(\neg R \sqcup P)(a, b)$ [l,u] to A. The resulting ABox after finishing this step is called the initial extended ABox, denoted by A_0^ε. Initialize the set of constraints $\mathcal{C}_0$ to be the empty set.
3. Apply completion rules. Through applying these rules in arbitrary order, derived assertions are added to the extended ABox A_i^ε. At the same time, corresponding constraints that denote the semantics of the assertions are added to the constraint set $\mathcal{C}_j$ in the form of linear/non-linear inequations. This process stops when either A_i^ε contains a clash or no further rule can be applied to A_i^ε. If A_i^ε contains a clash, the knowledge base is inconsistent. If the complete ABox obtained this way does not contain a direct clash, the reasoning procedure continues to solve the inequations in the constraint set $\mathcal{C}_j$. If the system of these inequations is unsolvable, the knowledge base is inconsistent, and consistent otherwise. The values returned from the system of inequations, if solvable, serve as the truth degrees of the entailment problem.

The completion rules are a set of consistency-preserving transformation rules. Each rule either detects a clash or derives one or more assertions and constraints. In the reasoning procedure, the application of some completion rules, including the role existential restrictions and at-least number restrictions, may lead to nontermination. Therefore, we have to find some blocking strategy to ensure the termination of the reasoning procedure.

Definition 6 (Blocking). Let a, b be anonymous individuals in the extended ABox A_i^ε, $A_i^\varepsilon(a)$ (respectively, $A_i^\varepsilon(b)$) be all the assertions in A_i^ε that are related to a (respectively, b), $\mathcal{C}_j(a)$ (respectively, $\mathcal{C}_j(b)$) be all the constraints in $\mathcal{C}_j$ that are related to a (respectively, b), $\mathcal{L}(a) = \langle A_i^\varepsilon(a), \mathcal{C}_j(a)\rangle$ and $\mathcal{L}(b) = \langle A_i^\varepsilon(b), \mathcal{C}_j(b)\rangle$ be the node labels for a and b. An individual b is said to be *blocked* by its ancestor a if $\mathcal{L}(b) \subseteq \mathcal{L}(a)$, where '$\subseteq$' applies to both label components. □

Definition 7 (Completion Rules). Let T be the TBox in normal form, A_i^ε be an extended ABox which is initialized to be the initial extended ABox A_0^ε, and $\mathcal{C}_0$ be the initial constraint set. Let Γ be either a range of truth degrees or the variable x_α denoting the truth degree of an assertion α. The completion rules are as follows:

1. **The concept assertion rule**
   Condition:
   A_i^ε contains $A(a)$ Γ, $\{x_{A(a)} = \Gamma\} \nsubseteq \mathcal{C}_j$, and Γ is not the variable $x_{A(a)}$.
   Action: $\mathcal{C}_{j+1} = \mathcal{C}_j \cup \{x_{A(a)} = \Gamma\}$; if$\{x_{\neg A(a)} = \neg\Gamma\} \nsubseteq \mathcal{C}_j$, then $\mathcal{C}_{j+1} = \mathcal{C}_j \cup \{x_{\neg A(a)} = \neg\Gamma\}$.
2. **The role assertion rule**
   Condition:
   A_i^ε contains $R(a,b)$ Γ, $\{x_{R(a,b)} = \Gamma\} \nsubseteq \mathcal{C}_j$, and Γ is not the variable $x_{R(a,b)}$.
   Action: $\mathcal{C}_{j+1} = \mathcal{C}_j \cup \{x_{R(a,b)} = \Gamma\}$; if$\{x_{\neg R(a,b)} = \neg\Gamma\} \nsubseteq \mathcal{C}_j$, then $\mathcal{C}_{j+1} = \mathcal{C}_j \cup \{x_{\neg R(a,b)} = \neg\Gamma\}$.
3. **The concept negation rule**
   Condition: A_i^ε contains $\neg A(a)$ Γ.
   Action:
   If Γ is not the variable $x_{\neg A(a)}$ and A_i^ε does not contain $A(a)$ $\neg\Gamma$, then $A_{i+1}^\varepsilon = A_i^\varepsilon \cup \{A(a)\ \neg\Gamma\}$. If Γ is the variable $x_{\neg A(a)}$ and $\{x_{\neg A(a)} = 1 - x_{A(a)}\} \nsubseteq \mathcal{C}_j$, then $\mathcal{C}_{j+1} = \mathcal{C}_j \cup \{x_{\neg A(a)} = 1 - x_{A(a)}\}$.
4. **The role negation rule**
   Condition: A_i^ε contains $\neg R(a,b)$ Γ.
   Action:
   If Γ is not the variable $x_{\neg R(a,b)}$ and A_i^ε does not contain $R(a,b)$ $\neg\Gamma$, then $A_{i+1}^\varepsilon = A_i^\varepsilon \cup \{R(a,b)\ \neg\Gamma\}$. If Γ is the variable $x_{\neg R(a,b)}$ and $\{x_{\neg R(a,b)} = 1 - x_{R(a,b)}\} \nsubseteq \mathcal{C}_j$, then $\mathcal{C}_{j+1} = \mathcal{C}_j \cup \{x_{\neg R(a,b)} = 1 - x_{R(a,b)}\}$.
5. **The concept conjunction rule**
   Condition:
   A_i^ε contains $(C \sqcap D)(a)$ Γ, but it does not contain both $C(a)$ $x_{C(a)}$ and $D(a)$ $x_{D(a)}$. $\mathcal{C}_j$ does not contain $t(x_{C(a)}, x_{D(a)}) = \Gamma$.
   Action:
   $A_{i+1}^\varepsilon = A_i^\varepsilon \cup \{C(a)\ x_{C(a)}, D(a)\ x_{D(a)}\}$, $\mathcal{C}_{j+1} = \mathcal{C}_j \cup \{t(x_{C(a)}, x_{D(a)}) = \Gamma\}$.
6. **The role conjunction rule**
   Condition:
   $\mathcal{A}_i^\varepsilon$ contains $(R \sqcap P)(a,b)$ Γ, but $\mathcal{C}_j$ does not contain $t(x_{R(a,b)}, x_{P(a,b)}) = \Gamma$.
   Action:
   $\mathcal{C}_{j+1} = \mathcal{C}_j \cup \{t(x_{R(a,b)}, x_{P(a,b)}) = \Gamma\}$. If Γ is not the variable $x_{(R\sqcap P)(a,b)}$, $C_{j+1} = C_{j+1} \cup \{x_{(R\sqcap P)(a,b)} = \Gamma\}$. If $\mathcal{A}_i$ does not contain $R(a,b)$ $x_{R(a,b)}$, $\mathcal{A}_{i+1}^\varepsilon = \mathcal{A}_i^\varepsilon \cup \{R(a,b)\ x_{R(a,b)}\}$. If $\mathcal{A}_i$ does not contain $P(a,b)$ $x_{P(a,b)}$, $\mathcal{A}_{i+1}^\varepsilon = \mathcal{A}_i^\varepsilon \cup \{P(a,b)\ x_{P(a,b)}\}$.
7. **The concept disjunction rule**
   Condition: A_i^ε contains $(C \sqcup D)(a)$ Γ, but neither $C(a)$ $x_{C(a)}$ nor $D(a)$ $x_{D(a)}$. $\mathcal{C}_j$ does not contain $s(x_{C(a)}, x_{D(a)}) = \Gamma$.
   Action:
   $A_{i+1}^\varepsilon = A_i^\varepsilon \cup \{C(a)\ x_{C(a)}, D(a)\ x_{D(a)}\}$, $\mathcal{C}_{j+1} = \mathcal{C}_j \cup \{s(x_{C(a)}, x_{D(a)}) = \Gamma\}$.
8. **The role disjunction rule**
   Condition: A_i^ε contains $(R \sqcup P)(a,b)$ Γ, but neither $R(a,b)$ $x_{R(a,b)}$ nor $P(a,b)$ $x_{P(a,b)}$. $\mathcal{C}_j$ does not contain $s(x_{R(a,b)}, x_{P(a,b)}) = \Gamma$.
   Action: $A_{i+1}^\varepsilon = A_i^\varepsilon \cup \{R(a,b)\ x_{R(a,b)}, P(a,b)\ x_{P(a,b)}\}$,
   $\mathcal{C}_{j+1} = \mathcal{C}_j \cup \{s(x_{R(a,b)}, x_{P(a,b)}) = \Gamma\}$.

9. **The inverse role rule**
Condition: A_i^{ε} contains $R^{-}(a,b)\ \Gamma$, but it does not contain $R(b,a)\ \Gamma$.
Action: $A_{i+1}^{\varepsilon} = A_i^{\varepsilon} \cup \{R(b,a)\ x_{R(b,a)}\}$, $\mathcal{C}_{j+1} = \mathcal{C}_j \cup \{x_{R(b,a)} = \Gamma\}$.
10. **The exists restriction rule**
Condition: A_i^{ε} contains $(\exists R.C)(a)\ \Gamma$, and a is not blocked.
Action:
If there is no individual name b such that $C(b)\ x_{C(b)}$ and $R(a,b)\ x_{R(a,b)}$ are in A_i^{ε}, and $\mathcal{C}_j$ does not contain $t(x_{C(b)}, x_{R(a,b)}) = x_{(\exists R.C)(a)}$, then $A_{i+1}^{\varepsilon} = A_i^{\varepsilon} \cup \{C(b)\ x_{C(b)}, R(a,b)\ x_{R(a,b)}\}$, $\mathcal{C}_{j+1} = \mathcal{C}_j \cup \{t(x_{C(b)}, x_{R(a,b)}) = x_{(\exists R.C)(a)}\}$, for each axiom $\top \sqsubseteq \neg C \sqcup D\ [l,u]$ in the TBox, add $A_{i+1}^{\varepsilon} = A_{i+1}^{\varepsilon} \cup \{(\neg C \sqcup D)(b)\ [l,u]\}$.
If there exists an individual name b such that $C(b)\ x_{C(b)}$ and $R(a,b)\ x_{R(a,b)}$ are in A_i^{ε}, but $\mathcal{C}_j$ does not contain $t(x_{C(b)}, x_{R(a,b)}) = x_{(\exists R.C)(a)}$, then $\mathcal{C}_{j+1} = \mathcal{C}_j \cup \{t(x_{C(b)}, x_{R(a,b)}) = x_{(\exists R.C)(a)}\}$;
If Γ is not the variable $x_{((\exists R.C)(a)}$, then if there exists $x_{((\exists R.C)(a)} = \Gamma'$ in $\mathcal{C}_j$, then $\mathcal{C}_{j+1} = \mathcal{C}_{j+1} \backslash \{x_{((\exists R.C)(a)} = \Gamma'\} \cup \{x_{((\exists R.C)(a)} = sup(\Gamma, \Gamma')\}$, else add $\mathcal{C}_{j+1} = \mathcal{C}_{j+1} \cup \{x_{(\exists R.C)(a)} = \Gamma\}$.
11. **The value restriction rule**
Condition:
A_i^{ε} contains $(\forall R.C)(a)\ \Gamma$ and $R(a,b)\ \Gamma'$, but it does not contain $C(b)\ x_{C(b)}$.
$\mathcal{C}_j$ does not contain $s(x_{C(b)}, x_{\neg R(a,b)}) = x_{(\forall R.C)(a)}$.
Action:
$A_{i+1}^{\varepsilon} = A_i^{\varepsilon} \cup \{C(b)\ x_{C(b)}\}$, $\mathcal{C}_{j+1} = \mathcal{C}_j \cup \{s(x_{C(b)}, x_{\neg R(a,b)}) = x_{(\forall R.C)(a)}\}$.
If Γ is not the variable $x_{((\forall R.C)(a)}$, then if there exists $x_{((\forall R.C)(a)} = \Gamma'$ in $\mathcal{C}_j$, add $\mathcal{C}_{j+1} = \mathcal{C}_{j+1} \backslash \{x_{((\forall R.C)(a)} = \Gamma'\} \cup \{x_{((\forall R.C)(a)} = inf(\Gamma, \Gamma')\}$, otherwise, add $\mathcal{C}_{j+1} = \mathcal{C}_{j+1} \cup \{x_{(\forall R.C)(a)} = \Gamma\}$.
12. **The at-least rule**
Condition:
A_i^{ε} contains $(\geq nR)(a)\ \Gamma$, a is not blocked, and there are no individual names $b_1, \ldots, b_n$ such that $R(a,b_i)\ \Gamma_i$ $(1 \leq i \leq n)$ are contained in A_i^{ε}.
Action:
$A_{i+1}^{\varepsilon} = A_i^{\varepsilon} \cup \{R(a,b_i)\ x_{R(a,b_i)} | 1 \leq i \leq n\}$,
$\mathcal{C}_{j+1} = \mathcal{C}_j \cup \{t(x_{R(a,b_1)}, \ldots, x_{R(a,b_n)}) = \Gamma\}$.
13. **The at-most rule**
Condition:
A_i^{ε} contains $n+1$ distinguished individual names $b_1, \ldots, b_{n+1}$ such that $(\leq nR)(a)\ \Gamma$ and $R(a,b_i)\ \Gamma_i$ $(1 \leq i \leq n+1)$ are contained in A_i^{ε}, $b_i \neq b_j$ is not in A_i^{ε} for some $i \neq j$, and if Γ is not the variable $x_{\leq nR(a)}$ and for any i $(1 \leq i \leq n+1)$, Γ_i is not the variable $x_{R(a,b_i)}$, $\Gamma_i \subseteq \Gamma$ holds.
Action:
For each pair b_i, b_j such that $j > i$ and $b_i \neq b_j$ is not in A_i^{ε}, the ABox A_{i+1}^{ε} is obtained from A_i^{ε} and the constraint set $\mathcal{C}_{j+1}$ is obtained from $\mathcal{C}_j$ by replacing each occurrence of b_j by b_i, and if Γ_i is the variable $x_{R(a,b_i)}$, $\mathcal{C}_{j+1} = \mathcal{C}_{j+1} \cup \{x_{R(a,b_i)} = \Gamma\}$. □

4 Examples

In this section, we use two examples to explain the reasoning procedure presented in the above sections.

Example 1. In order to explain the importance of the blocking strategy, we consider a fuzzy knowledge base as follows, where we abbreviate the concept *CancerPatient* and the role *hasParent* by CP and hP, respectively.

$T = \{CP \sqsubseteq \exists hP.CP\ [0.5, 1]\}$, $A = \{CP(P002)\ [0, 0.5]\}$

The reasoning task is to check the consistency of this knowledge base. Assume we choose Zadeh Logic. First, we transform the axiom into its normal form $T = \{\top \sqsubseteq \neg CP \sqcup \exists hP.CP\ [0.5, 1]\}$.

After augmenting the ABox, we can initialize the extended ABox as $A_0^\varepsilon = \{CP(P002)\ [0, 0.5], (\neg CP \sqcup \exists hP.CP)(P002)\ [0.5, 1]\}$ and the initial constraint set as $\mathcal{C}_0 = \{\}$.

Next, we apply the relevant completion rules. For compactness, we use Table 2 to show the procedure steps.

The last row in the table shows the application of blocking. The fully expanded tree is shown in Figure 1. The notation in this figure is the same as in Table 2, where unlabeled dashed arrows connect an individual to its alterative branches when applying the concept disjunction rule. This illustrates how Table 2 leads to $A_4^\varepsilon(c) = A_2^\varepsilon(b)$, $A_5^\varepsilon(1)(c) = A_3^\varepsilon(1)(b)$, $A_5^\varepsilon(2)(c) = A_3^\varepsilon(2)(b)$, and $\mathcal{C}_9(C) = \mathcal{C}_6(b)$. Therefore, $\mathcal{L}(c) \subseteq \mathcal{L}(b)$, and the individual c is blocked by its ancestor b. We then stop applying the role existential restriction rule to A_5^ε and $\mathcal{C}_9$ at this point.

Table 2. Reasoning Procedure Applied to Example 1

$\mathcal{C}_1 = \{x_{CP(P002)} = [0, 0.5], x_{\neg CP(P002)} = [0.5, 1]\}$	The concept assertion rule
$A_1^\varepsilon(1) = A_0^\varepsilon \cup \{\neg CP(P002)\ x_{\neg CP(P002)}\}, A_1^\varepsilon(2) = A_0^\varepsilon \cup \{\exists hP.CP(P002)\ x_{\exists hP.CP(P002)}\}$	The concept disjunction rule
$\mathcal{C}_2 = \mathcal{C}_1 \cup \{\max(x_{\neg CP(P002)}, x_{\exists hP.CP(P002)}) = [0.5, 1]\}$	
$\mathcal{C}_3 = \mathcal{C}_2 \cup \{x_{\neg CP(P002)} = 1 - x_{CP(P002)}\}$	The concept negation rule
$A_2^\varepsilon = A_1^\varepsilon(2) \cup \{hP(P002, b)\ x_{hP(P002,b)}, CP(b)\ x_{CP(b)}, (\neg CP \sqcup \exists hP.CP)(b)\ [0.5, 1]\}$	The exists restriction rule
$\mathcal{C}_4 = \mathcal{C}_3 \cup \{\min(x_{CP(b)}, x_{hP(P002,b)}) = x_{\exists hP.CP(P002)}\}$	
$A_3^\varepsilon(1) = A_2^\varepsilon \cup \{\neg CP(b)\ x_{\neg CP(b)}\}, A_3^\varepsilon(2) = A_2^\varepsilon \cup \{\exists hP.CP(b)\ x_{\exists hP.CP(b)}\}$	
$\mathcal{C}_5 = \mathcal{C}_4 \cup \{\max(x_{\neg CP(b)}, x_{\exists hP.CP(b)}) = [0.5, 1]\}$	The concept disjunction rule
$\mathcal{C}_6 = \mathcal{C}_5 \cup \{x_{\neg CP(b)} = 1 - x_{CP(b)}\}$	The concept negation rule
$A_4^\varepsilon = A_3^\varepsilon(2) \cup \{CP(c)\ x_{CP(c)}, hP(b, c)\ x_{hP(b,c)}, (\neg CP \sqcup \exists hP.CP)(c)\ [0.5, 1]\}$	The exists restriction rule
$\mathcal{C}_7 = \mathcal{C}_6 \cup \{\min(x_{CP(c)}, x_{hP(b,c)}) = x_{\exists hP.CP(b)}\}$	
$A_5^\varepsilon(1) = A_4^\varepsilon \cup \{\neg CP(c)\ x_{\neg CP(c)}\}, A_5^\varepsilon(2) = A_4^\varepsilon \cup \{\exists hP.CP(c)\ x_{\exists hP.CP(c)}\}$	
$\mathcal{C}_8 = \mathcal{C}_7 \cup \{\max(x_{\neg CP(c)}, x_{\exists hP.CP(c)}) = [0.5, 1]\}$	The concept disjunction rule
$\mathcal{C}_9 = \mathcal{C}_8 \cup \{x_{\neg CP(c)} = 1 - x_{CP(c)}\}$	The concept negation rule
$\{\mathcal{L}(c) = \langle A_5^\varepsilon(c), \mathcal{C}_9(c)\rangle\} \subseteq \{\mathcal{L}(b) = \langle A_5^\varepsilon(b), \mathcal{C}_9(b)\rangle\}$	Blocking

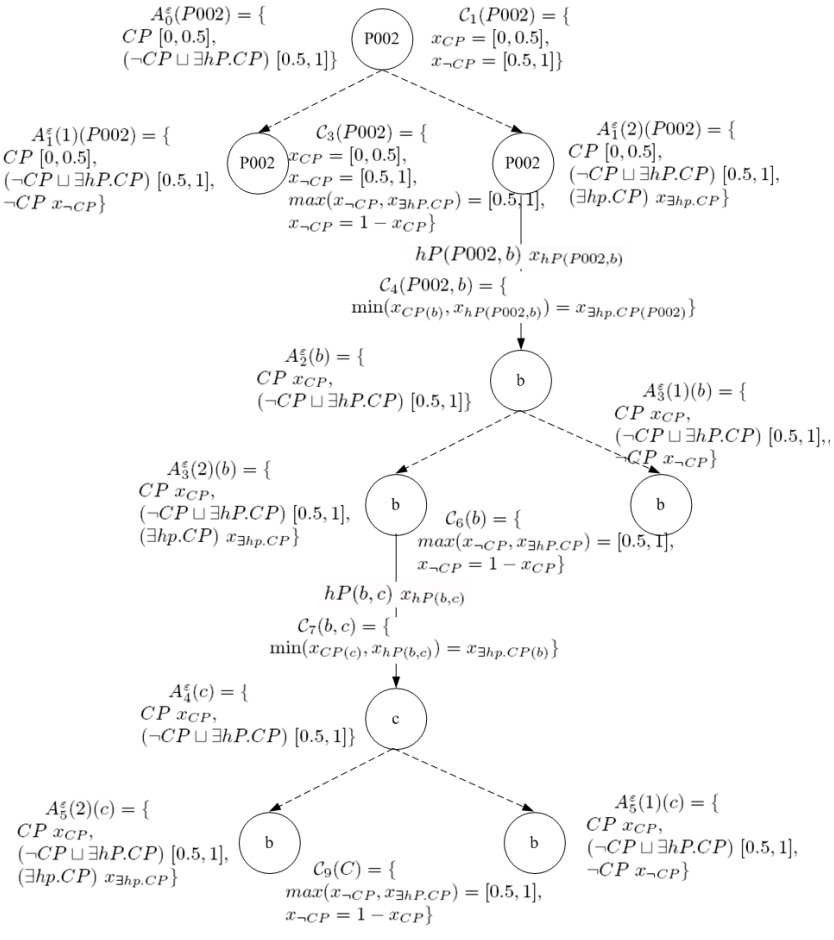

Fig. 1. Expanded Tree for Example 1

Next, we rewrite the constraint set into the following form:

$$\textit{subject to} \begin{cases} 0.5 \leq x_{CP(P002)} \leq 1 \\ 0 \leq x_{\neg CP(P002)} \leq 0.5 \\ 0.5 \leq \max(x_{\neg CP(P002)}, x_{(\exists hP.CP)(P002)}) \leq 1 \\ x_{\neg CP(P002)} = 1 - x_{CP(P002)} \\ \min(x_{hP(P002,b)}, x_{CP(b)}) = x_{(\exists hP.CP)(P002)} \\ 0.5 \leq \max(x_{\neg CP(b)}, x_{(\exists hP.CP)(b)}) \leq 1 \\ x_{\neg CP(b)} = 1 - x_{CP(b)} \\ \min(x_{hP(b,c)}, x_{CP(c)}) = x_{(\exists hP.CP)(b)} \end{cases}$$

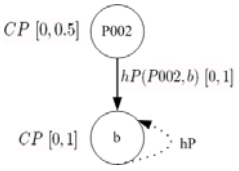

Fig. 2. A Model of Example 1

Using a linear/non-linear programming solver, e.g., the GLPK solver in our experiments (http://www.gnu.org/software/glpk/), it is easy to show that the constraint set is solvable. Thus, the interpretation includes $\triangle^I = \{P002, b\}$ united with $\{CP^I(P002)\ [0, 0.5], CP^I(b)\ [0, 1], hP^I(P002, b)\ [0, 1]\}$.

Figure 2 shows the model constructed for Example 1. The dotted arrow here indicates the blocking.

Therefore, we can draw the conclusion that the knowledge base is consistent.

Example 2. To explain the at-most role restriction rule and inverse role rule, let us consider the following simple fuzzy knowledge base:

$\{(\leq 1R)(a)\ [0.7, 1], R(a, b_1)\ [0.8, 1], R^-(b_2, a)\ [0.7, 1]\}$

By applying the inverse role rule, we add $R(a, b_2)\ [0.7, 1]$ to the extended ABox. By applying the at-most role restriction rule, we have

$\mathcal{A}_1^\varepsilon = \{(\leq 1R)(a)\ [0.7, 1], R(a, b_1)\ [0.8, 1], R^-(b_1, a)\ [0.7, 1], R(a, b_1)\ x_{R(a,b_1)}\}$
$\mathcal{C}_1 = \{x_{(\leq 1R)(a)} = [0.7, 1], x_{R(a,b_1)} = [0.8, 1], x_{R^-(b_1,a)} = [0.7, 1], x_{R(a,b_1)} = [0.7, 1]\}$

Using the GLPK solver, it can be shown that this constraint set is solvable. Therefore, we can draw the conclusion that the knowledge base is consistent. But if we had an extra assertion $b_1 \neq b_2$ in the knowledge base, then the at-most role restriction rule would not be applicable, and the knowledge base would be inconsistent because it contained a clash.

5 Conclusion and Future Work

In this paper we propose an extension to Description Logics based on Fuzzy Set Theory and Fuzzy Logic. The syntax and semantics of the proposed norm-parameterized Fuzzy Description Logic $f\mathcal{ALCHIN}$ are explained in detail. We then address the reasoning task of consistency checking on $f\mathcal{ALCHIN}$ knowledge bases. A reasoning procedure that always terminates and its completion rules are presented. As the examples suggest, the computational complexity of the reasoning procedure is usually high, which surfaces even for a relatively small knowledge base. Therefore, one of the main practical directions for future work is to investigate the core of the reasoning procedure and to develop strategies for reducing the computational complexity. Description Logics constitute a family of knowledge formalisms with different expressiveness. Our fuzzy Description Logic $f\mathcal{ALCHIN}$ extends fuzzy $\mathcal{ALC}$ taking into account inverse roles, role inclusion axioms, and number restrictions. For reasons of simplicity, it does not yet include

$\mathcal{SHIN}$-style transitive roles, nor nominals (i.e. collections of individuals) or datatypes. Future work will consider fuzzy extensions to these more expressive description languages.

References

1. Baader, F., Calvanese, D., Mcguinness, D., Nardi, D., Patel- Schneider, P.: The Description Logic Handbook: Theory, Implementation and Applications. Cambridge University Press, Cambridge (2003)
2. Bobillo, F., Straccia, U.: A fuzzy description logic with product t-norm. In: Proceedings of the IEEE International Conference on Fuzzy Systems (Fuzz IEEE 2007), pp. 652C–657C. IEEE Computer Society, Los Alamitos (2007)
3. Hájek, P.: Metamathematics of fuzzy logic. Kluwer, Dordrecht (1998)
4. Hájek, P.: Making fuzzy description logics more expressive. Fuzzy Sets Syst. 154(1), 1–15 (2005)
5. NETO, A.G.S.S.: Tableau algorithm for alchin consistency checking
6. Stoilos, G., Stamou, G., Pan, J., Tzouvaras, V., Horrocks, I.: Reasoning with very expressive fuzzy description logics. Journal of Artificial Intelligence Research 30, 273–320 (2007)
7. Straccia, U.: A fuzzy description logic. In: Proceedings of the 15th National Conference on Artificial Intelligence (AAAI 1998), pp. 594–599 (1998)
8. Straccia, U.: Towards a fuzzy description logic for the semantic web (Preliminary report). In: Gómez-Pérez, A., Euzenat, J. (eds.) ESWC 2005. LNCS, vol. 3532, pp. 167–181. Springer, Heidelberg (2005)
9. Zadeh, L.A.: Fuzzy sets. Information and Control 8(3), 338–353 (1965)
10. Zhao, J., Boley, H., Du, W.: Expressing Vague Knowledge in the Fuzzy Description Logic fALCHIN. In: Proc. of the Sixth Annual Research Exposition, p. 72 (2009), http://www.cs.unb.ca/itc/ResearchExpo/Expo2009-proceeding.pdf

Using Intelligent System for Reservoir Properties Estimation

Fariba Salehi[1] and Arnoosh Salehi[2]

[1] Department of Computer, Faculty of Science, Islamic Azad University, Karaj branch, Iran
[2] National Iranian Oil Company, Tehran, Iran
salehi_si@yahoo.com

Abstract. Reservoir description for simulation studies requires good knowledge of the permeability. Reliable permeability is only available from laboratory tests on cores, which are usually taken from a small percentage of the wells. In an offshore gas field only three wells have core data and all wells have full set of conventional log data. By using concept of hydraulic flow unit, statistical methods and intelligent systems is made a model for estimation of reservoir properties. Graphical statistical methods are applied for classification of hydraulic flow units. The Sugeno-type of fuzzy inference system conjunction with backpropagation network and subtractive clustering is used for prediction of flow zone indicator, permeability is then calculated from mean flow zone indicator value and corresponding porosity.

Keywords: Permeability, Hydraulic Flow Unit, Flow Zone Indicator, Fuzzy Inference System, Backpropagation Network, Subtractive Clustering.

1 Introduction

Rock permeability is an extremely important parameter in reservoir characterization and simulation, because its influence the hydrocarbon rate of production, ultimate recovery and optimal placement of wells. Thus, the proper determination of the permeability is paramount importance because it affects the economy of the whole venture of development and operation of a gas and oil field.

The most reliable data of local permeability are taken from laboratory analysis of cores. Core analysis is the direct method in dynamic condition. Extensive coring is very expensive and this expense becomes reasonable in very limited cases. In general, these core data are available only from some wells in the field, and for some intervals in each well. Then the permeability of the whole field is estimated from this sparse information.

The hydraulic flow unit (HFU) approach is a methodology for classification ofrock types and prediction of reservoir properties, based on sensible geological parameters and the physics of flow at pore scale. In this approach first flow zone indicator (FZI) is calculated by using core, log and petrophysical data. Permeability is related to the porosity and FZI values. Porosity in each point is derived from log data and

D.-S. Huang et al. (Eds.): ICIC 2009, LNAI 5755, pp. 124–133, 2009.

petrophysical evaluation. Major task in this approach is predication of FZI values. Traditional methods such as multivariate regression model cannot estimate FZI values because of scatter data. A hybrid technique combining fuzzy logic, backpropagation network and Subtractive clustering is used for estimating FZI values. Fuzzy inference system is trained by well log data in cored interval wells. FZI values of obtained from core analysis is observation data that is used as an output in fuzzy inference system. Then fuzzy inference system generates FZI from well log and petrophysical data. Finally permeability is calculated by mean FZI in each hydraulic flow unit (HFU). This methodology is applied for estimation of permeability in an offshore gas field as denoted OGC field. There are ten wells with conventional log data. Core measurement is available for three wells.

2 Permeability Estimation

Following is the methodology plan to perform all the tasks involved in this study.

2.1 HFU Concept [1] - [5]

A HFU is defined as the representative volume of total reservoir rock within which geological properties that control fluid flow are internally consistent and predictably different from properties of other rocks. Thus, a flow unit is a reservoir zone that is continuous laterally and vertically and has similar flow and bedding characteristics. HFU's are related to geological facies distribution but do not necessarily coincide with facies boundaries. The parameters that influence fluid flow are mainly pore-throat geometrical attributes. The pore geometry is turn controlled by mineralogy (type, abundance, location) and texture (grain size, grain shape, sorting, packing). Various combinations of these geological properties can lead to distinct rock flow units that have similar fluid transport properties. Therefore, a HFU can include several rock facies types, depending on their depositional texture and mineralogical content. The grouping of rocks based on their fundamental geological flow attributes in the basis of HFU classification.

If a porous medium is simulated as a bundle of straight capillary tubes, the following expression for rock permeability is obtained by combining Darcy's law for flow in porous media and Poiseuille's law for flow in tubes:

$$k = \left(r^2/8\right) \times \phi_e . \tag{1}$$

This is a simple but important relationship because it shows that the factor that relates permeability depends on the pore characteristics, which is geological feature of sedimentary rock. For a realistic model of a porous medium where the connected pore structure is not straight researchers added a tortusity factor and used mean pore radius in Equation 1. The mean pore radius is defined as the ratio of cross sectional area and wetted perimeter. This is related to the surface area per unit grain volume. The generalized Kozeny-Carman equation with these modifications to Equation 1 results in

$$k = \left(\phi_e^{\,3}/(\phi_e - 1)^2\right) \times \left(1/F_s \tau^2 S_{gv}^2\right), \tag{2}$$

Where k is in μm^2 and s_{vg} is in μm^{-1}. The effective porosity ϕ_e is obtained from core or appropriate log data. The constant $F_s\tau^2$ is known as the Kozeny constant. The variation in $F_s\tau^2$ is the main limitation for the universal use of model because in practice the Kozeny constant is not known for a given formation. The entire term $F_s\tau^2 S_{gv}$ is a function of geological characteristics of porous media and varies with changes in pore geometry. Thus, this term captures the geological aspect of HFU's. The determination and discrimination of the $F_s\tau^2 S_{gv}^2$ group is the central part of the HFU classification technique, which is described in the following. Equation 2 can be written in field units as

$$0.0314\left(k/\phi_e\right)^{1/2} = \left(\phi_e/1-\phi_e\right)\times\left(1/\sqrt{F_s}\tau.S_{gv}\right), \tag{3}$$

where the constant 0.0314 is the conversion factor form μm^2 to md define flow zone indicator (FZI) as

$$FZI = 1/\sqrt{F_s}\tau.S_{gv}. \tag{4}$$

and reservoir quality index (RQI) as

$$RQI = 0.0314\left(k/\phi_e\right)^{1/2}. \tag{5}$$

Then, Equation 3 becomes

$$RQI = \phi_z FZI, \tag{6}$$

or

$$\log(RQI) = \log(\phi_z) + \log(FZI), \tag{7}$$

where

$$\phi_z = \phi_e/1 - \phi_e. \tag{8}$$

Thus, FZI can be calculated from Equation 6 for each sample point where permeabilit y and porosity values are measured.

A plot of RQI versus ϕ_z on log-log coordinates will be a straight line with the slope equal of one if FZI is constant for all core samples.

Data samples with similar but not identical FZI values will be located around a single unit-slope straight line with a mean FZI value. Samples with significantly different FZI value is the intercept of a unit-slope line with the coordinate $\phi_z = 1$. The scatter of data about the straight lines is owing to measurement errors in core data analysis and minor fluctuations around main geological controls on pore throat characteristics of rock samples. The basic idea of HFU classification to identify groupings of data classes that from the unit-slope straight lines on log-log plot of RQI versus ϕ_z. Permeability of sample point is then calculated from a pertinent HFU using its mean FZI value and the corresponding sample porosity,

$$k = 1014\,(FZI_{mean})^2\,\phi_e{}^3/(1-\phi_e)^2\,. \tag{9}$$

It is interesting to note that the group k/ϕ_e has had a basic use in reservoir characterization in delineating layering based on the speed of flow in the layers. This provides an interesting link between the concept of HFU and the previously proven useful reservoir characterization method.

2.2 HFU Classification Using Core Data [3] - [5]

After calculating pore-throat related parameters of RQI and FZI from core information. HFU's can be identified based on FZI values. Although there should exist one single value for each HFU, a distribution for each FZI around its true mean results because of random measurement error in core analysis. When multiple groups exist, the overall FZI distribution function is a superposition of individual distribution functions around their mean FZI. Two methods histogram analysis and probability plot approach are used for clustering and classification of HFU.

Histogram Approach. [4], [5] Because of FZI distribution is a superposition of multiple log-normal distributions. A histogram of Log (FZI) should show "n" number of normal distributions for "n" number of HFU's. The convolved frequency distribution for a mixture of multiple Gaussian probability density function is described by

$$f = \sum_{i=1}^{N_U} \omega_i \Big/ \sqrt{2\pi\sigma_i^{\,2}}\,\exp\left[-(z-\bar{z}_i)^2/2\sigma_i^{\,2}\right] \tag{10}$$

and,

$$\sum_{i=1}^{N_U} \omega_i = 1\,. \tag{11}$$

Where the weight factors are for generalization purposes to emphasize some distribution functions, if desired. In general ω_i are themselves from a probability density function for equally weighted distributions,

$$\omega_i = 1/N_U \quad for \quad all \quad i = 1,\ldots,N_U. \tag{12}$$

When clusters are distinctly separate, the histogram clearly delineates each HFU and provides their corresponding FZI values. This is the easiest and the simplest approach. However, it is often difficult to separate the overlapped individual from a histogram plot. Therefore, this method is not suitable for most field applications because the transition zones between HFU's often clouds the judgment on their identity.

Probability Plot Approach. [4], [5] The probability plot or cumulative distribution function is the integral of histogram or probability density function, and, as such, it is a smoother plot than the histogram. The scatter in data is reduced on this plot and the identification of clusters becomes easier. The cumulative distribution function is given by

$$F = 1/2\left[1 + \sum_{i=1}^{N_U} \omega_i \, erf\left(z - \bar{z}_i\right)/2\sigma_i\right]. \tag{13}$$

A normal probability plot has a specially arranged coordinate system where a normal distribution forms a distinct straight line. Hence, the number of straight lines and the limiting boundary values of FZI or each HFU can be can be obtained from the probability plot of logarithm of FZI.

HFU Classification in OGC Field. (Case Study) The histogram of logarithm of FZI values from all cored wells shows superposition of a number of normal distributions. However, the exact number of HFU's and the threshold values between them are not distinguished easily because the individual distributions are not distinct enough. Figure 1 shows core derived histogram of log (FZI) distribution.

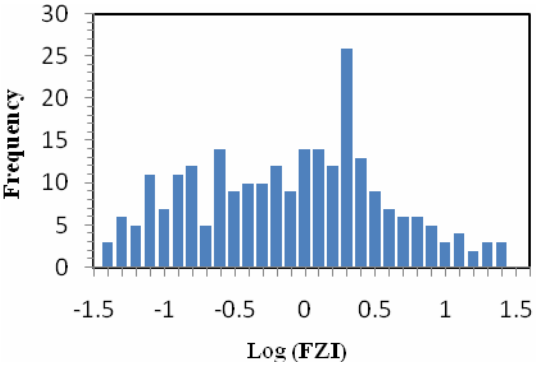

Fig. 1. Histogram of Log (FZI), core data

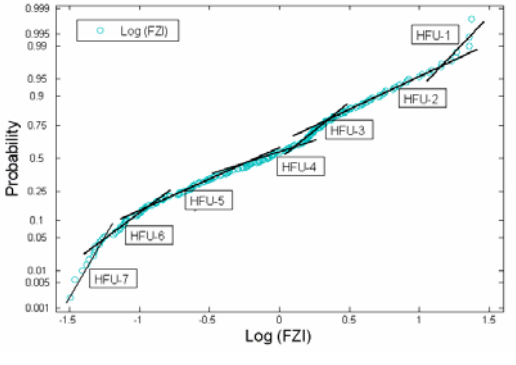

Fig. 2. Probability plot of Log (FZI), core data

Figure 2 shows core derived probability plot of log (FZI) distribution. Seven HFU's for the reservoir are identified, as seen by seven straight lines on Figure 2. Based on the HFU definition is obtained from the probability plot, a combined RQI versus ϕ_z graph was made for the wells and is shown in Figure 3. The unit slope lines

were drawn through segments of data according to mean FZI values calculated for each group data within the straight lines of Figure 3. The mean FZI values are used to fix the intercept with the $\phi_z = 1$ vertical line.

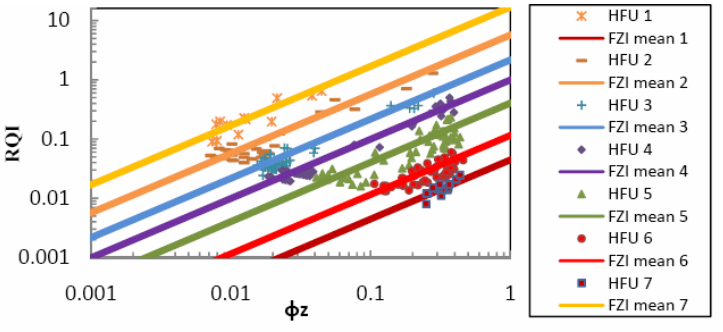

Fig. 3. RQI versus ϕ_z in a log-log plot for classification of HFU's and FZI mean determination

2.3 HFU Prediction Using Log Data [4], [5]

The major task is to predict HFU's in wells where only well log measurements and interpretation of petrophysical evaluation are available. This is an inverse process that requires a probabilistic approach. Three steps are needed for the inference of HFU distribution at logged wells.

Database Preparation. Prior to any prediction attempts, we first have to make sure that available logs were properly calibrated, environmentally corrected and both log and core data are accurately depth matched. Most of available log data were recorded using differently calibrated tools and had different scales. All logs are normalized using Equation 14 so that all log values will be lies between zero and one and become dimensionless.

$$N\delta = \delta - \delta_{\min} / \delta_{\max} - \delta_{\min} , \tag{14}$$

Where δ any is log, $\delta_{\min}$ and $\delta_{\max}$ is the minimum and maximum of reading δ log in all wells, $N\delta$ is the normalized δ log. Also the values of the normalized logs are extracted at the exactly the same depths as the core plugs.

Selection of Input Data for Model. In the intervals and wells without core the only available tool to reproduce the FZI model are the log curves and petrophysical evaluation. Normally models just need a small number of variables to attain reliability. There are full conventional log in all wells. Conventional logs such as gamma ray log (GR), sonic log (DT), compensated neutron log (CNL), formation density compensated log (FDC), latrolog deep (LLD), latrolog shallow (LLS) and finally effective porosity (ϕ_e) is obtained from interpretation of different logs. For selection of input data for generating FZI in uncored intervals and wells is used Pearson's correlation coefficient and Spearman's rank correlation. Table 1 shows correlation coefficient

between FZI and all variables available in wells. Table 1 shows the variables FDC, DT, and LLS have the highest correlation coefficients with FZI values. Also we carried out rank correlation analysis of log responses and core derived FZI values. Spearman's rank correlation calculates the degree of correlation between a set of measurement on two variables. Although the exact nature of variations in well log and core measurements are not considered in rank correlation, the procedure is extremely useful because it identifies well logs with poor correlation numbers effectively. Table 2 shows FZI has strongest relationship with DT, FDC, ϕ_e and LLS. Finally FDC, DT, ϕ_e and LLS are selected for predicting FZI values in uncored interval wells.

Table 1. Pearson's correlation coefficient of available data

	GR	DT	CNL	FDC	LLD	LLS	ϕ_e	FZI
GR	1.00							
DT	-0.12	1.00						
CNL	-0.05	0.45	1.00					
FDC	0.05	-0.74	-0.39	1.00				
LLD	0.03	-0.18	0.00	0.14	1.00			
LLS	0.20	-0.45	-0.22	0.26	0.61	1.00		
ϕ_e	-0.30	0.82	0.62	-0.84	-0.14	-0.45	1.00	
FZI	-0.17	-0.37	-0.04	0.44	0.22	0.23	-0.28	1.00

Table 2. Spearman's rank correlation of available data

data	GR	DT	CNL	FDC	LLD	LLS	ϕ_e
Rank -FZI	0.07	-0.57	-0.24	0.51	0.31	0.37	-0.49

FZI Prediction. Two methods are applied for estimation FZI from selected available variables data. First method is multiple linear regression. Figure 4 is a plot of log (FZI) calculated from core data and the log (FZI) obtained from regression model. The R-squared is 0.343. This model is not reliable for predicting FZI and permeability.

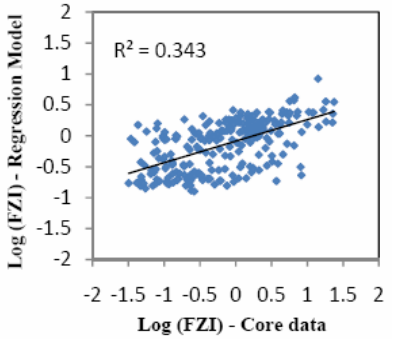

Fig. 4. Plot of Log (FZI) from core data versus Log (FZI) obtained from regression model

3 Intelligent System for FZI Prediction [6]-[10]

First order Sugeno-type system is used for fuzzy inference system in model. Briefly, Sugeno-type inference is a type of fuzzy inference in which the consequent of each rule is a linear combination of the inputs. The output is a weighted linear combination of the consequents. It is similar to the Mamdani method in many respects. The first two parts of the fuzzy inference process, fuzzifying the inputs and applying the fuzzy operator, are exactly the same. The main difference between Mamdani and Sugeno is that the Sugeno output membership functions are either linear or constant. A typical rule in a Sugeno fuzzy model in this model has the form:

If Input 1=N-DT and Input 2 = N-FDC and Input 3=N-LLS and Input 4 = N-ϕ_e

Then Output is z = *a N-DT + b N-FDC + c N-LLS+ d N-*ϕ_e *+ e.*

Where N-DT, N-FDC, N-LLS are normalized values of logs data of DT, FDC and LLS. N-ϕ_e is normalized value of effective porosity. Constant of model are *a, b, c, d* and *e*. All mentioned data have to calculate in each depth. The output level z_i of each rule is weighted by the firing strength w_i of the rule. For an *And* rule with Input 1, 2, 3 and 4, the firing strength is

w_i =*And Method (* F_1 *(N-DT),* F_2 *(N-FDC),* F_3 *(N-LLS),* F_4 *(N-*ϕ_e *))*

The final output of the system is the weighted average of all rule outputs, computed as

$$Final \quad Output = \sum_{i=1}^{N} w_i z_i \Big/ \sum_{i=1}^{N} w_i . \tag{15}$$

Subtractive clustering is used or generating fuzzy inference system and number of membership functions. Subtractive clustering is a technique for automatically generating fuzzy inference systems by detecting clusters in input-output training data.

Symmetric Gaussian function is used for fuzzifying input data. The symmetric Gaussian function depends on two parameters σ and c :

$$f(x,\sigma,c) = \exp(-(x-c)^2 / 2\sigma^2). \tag{16}$$

Adaptive neuro-fuzzy system is used for determination of parameters of membership function. Adaptive neuro-fuzzy system uses a hybrid learning algorithm to identify parameters of Sugeno-type fuzzy inference systems. It applies a combination of the least-squares method and the backpropagation gradient descent method for training of membership function parameters to emulate a given training data set. Figure 5 shows structure of fuzzy inference system with four input, 46 rules and one output.

Figure 6 is a plot of logarithm of FZI calculated from core data and the logarithm of FZI obtained from intelligent system. The R-squared is 0.936. This model can be reliable for predicting FZI and permeability. FZI obtained from intelligent model and then permeability is calculated by using Equation 9. Figure 7 shows porosity versus permeability distribution throughout the OGC field obtained from intelligent system by considering mean FZI in HFU approach.

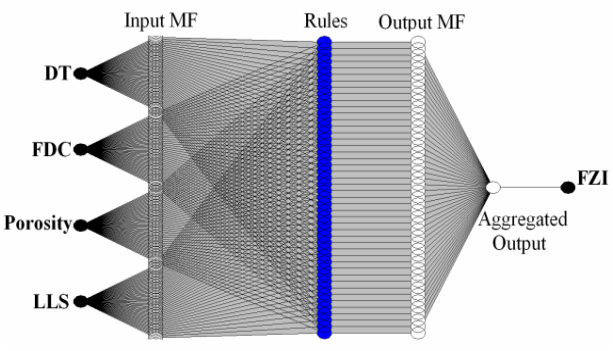

Fig. 5. Structure of intelligent system

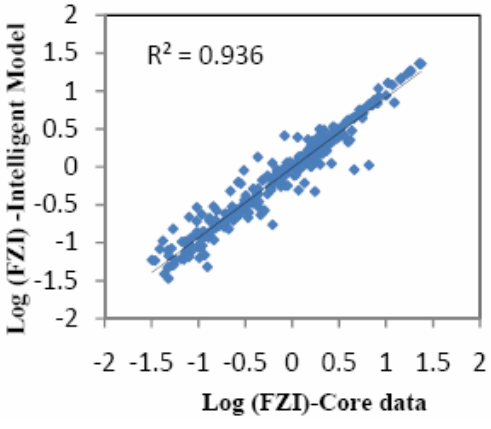

Fig. 6. Plot of Log (FZI) from core data versus Log (FZI) obtained from intelligent model

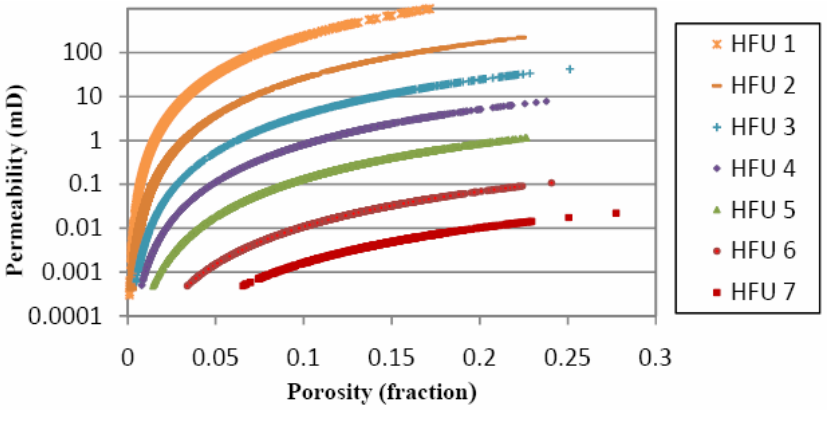

Fig. 7. Porosity versus permeability distribution throughout the field obtained from mean FZI-i ntelligent model according to HFU classification

4 Conclusions

Graphical clustering methods as histogram analysis and probability plot provide a visual image of an FZI distribution to determine the number of HFU's, their mean values, and their distribution types in a real case for an offshore gas filed as denoted OGC field. Analysis of Pearson's correlation coefficient and Spearman's rank correlation is rather benefit tools for selection input data from all available well log data and other data obtained from interpretation of petrophysical evaluation for training FZI model. The Sugeno-type fuzzy inference system conjunction with backpropagation network and subtractive clustering is useful tool for prediction of FZI from selected input data from available data.

Acknowledgements

The authors wish to thank Department of Computer, Faculty of Science, Islamic Azad University, Karaj branch for their support.

References

1. Kozeny, J.: Uber Kapillare Leitung des Wassers im Boden, Stizurgsberichte. Royal Academy of Science, Vienna, Proc. Class 1 136, 271–306 (1927)
2. Carmen, P.C.: Fluid Flow through Granular Beds. Trans. AIChE 15, 150–166 (1937)
3. Amaefule, J.O., Altunbay, M., Tiab, D., Kersey, D.G., Keelan, D.K.: Enhanced Reservoir Description: Using Core and Log Data to Identify Hydraulic (Flow) Units and Predict Permeability in Uncored Intervals/wells. In: Presented at 68th Ann. Tech. Conf. Houston, Tx (1993)
4. Abbaszadeh, M., Fujii, H., Fujimoto, F.: Permeability Prediction by Hydraulic Flow Units, Theory and Applications. SPE Formation Evaluation Journal, 263–271 (December 1996)
5. Anderberg, M.R.: Cluster Analysis for Applications. Academic Press, New York (1973)
6. Soto, B.R., Garcia, J.C., Torres, F., Perez, G.S.: Permeability Prediction Using Hydraulic Flow Units and Hybrid Soft Computing Systems. In: SPE 71455 (2001)
7. Jang, J.S.: ANFIS: Adaptive Network based Fuzzy Inference Systems. IEEE Transations on Systems, Man and Cybernetics 23(3), 665–685 (1993)
8. Chiu, S.: Fuzzy Model Identification Based on Cluster Estimation. Journal of Intelligent & Fuzzy Systems 2(3) (1994)
9. Zadeh, L.A.: Knowledge Representation in Fuzzy Logic. IEEE Transactions on Knowledge and Data Engineering 1, 89–100 (1989)
10. Sugeno, M.: Fuzzy Measures and Fuzzy Integrals: a Survey. In: Gupta, M.M., Saridis, G.N., Gaines, B.R. (eds.) Fuzzy Automata and Decision Processes, North-Holland, NY, pp. 89–102 (1977)

Fuzzy Support Vector Classification Based on Fuzzy Optimization*

Zhimin Yang[1], XiaoYang[2], and Bingquan Zhang[1,**]

[1] Zhijiang College, Zhejiang University of Technology, Hangzhou, P.R. China, 310024
[2] College of Business and Administration, Zhejiang University of Technology, Hangzhou, P.R. China, 310023
spaceicy@126.com

Abstract. This paper is concerned with the fuzzy support vector classification, in which both of the type of the output training point and the value of the final fuzzy classification function are triangle fuzzy number. First, the fuzzy classification problem is formulated as a fuzzy chance constrained programming. Then, we transform this programming into its equivalence quadratic programming. Final, a fuzzy support vector classification algorithm is proposed to deal with the problem. An example is presented to illustrate rationality of the algorithm.

Keywords: Machine learning, fuzzy support vector classification, possibility measure, triangle fuzzy number.

1 Introduction

Support vector machines (SVMs) proposed by Vapnik, is a novel method for machine learning ([1], [2], [3], [4], [11]). Due to its excellent learning capability, It has become a hot spot of the machine learning field and applied successfully to many application fields. But as an immature novel technique, it still needs further improvements; when it is concerned to solve the problem with fuzzy information, for instance, the output $y_j (j = 1, \cdots, l)$ of the training points in the training set $S = \{(x_1, y_1), \cdots, (x_l, y_l)\}$, are fuzzy. In 2002, Lin and Wang [8] proposed a Fuzzy Support Vector Machines(FSVM) technique, but they only added the fuzzy membership grade to the penalty parameters of the quadratic programming in the Fuzzy Support Vector classification rather than building up a Fuzzy Support Vector classification in terms of the algorithm's mathematical essentially. And the value of the final obtained classification functions (the output of the testing points) are still 1 or -1 (positive class or negative class). In 2004 and 2005, Tao Qing, Wang Jueand Lee K Y et.al. respectively proposed A New Fuzzy Support Vector Machine Based on the Weighted Margin（NFSVM）[9] and Possibilistic Support Vector Machine(PSVM) [10]. In NFSVM, the training points' fuzzy informations are represented by fuzzy member and fuzzy margin thus the fuzzy

* Supported by National Natural Science Pivot Foundation of China (No.10631070) and Natural Science Foundation of Zhejiang Province (No.Y606082).
** Corresponding author.

D.-S. Huang et al. (Eds.): ICIC 2009, LNAI 5755, pp. 134–143, 2009.

classification problem is transformed to a quadratic programming problem. In PSVM, the training points' fuzzy informations are represented by possibilistic member and possibilistic margin thus the fuzzy classification problem is also transformed to a quadratic programming problem. But the value of the final obtained classification functions (the output of the testing points) for both of the two techniques are still 1 or -1 (positive class or negative class).

In this paper, we study the fuzzy classification problem , in which the training points include the full fuzzy information, i.e., the input of the training points is the membership grades of the positive and negative class, the sum of which is 1. In this technique, both of the training points' output and the value of the constructed fuzzy optimal classification function are triangle fuzzy numbers. This technique is similar to the above three techniques for using the optimization method to solve the fuzzy classification problem in which the training points include fuzzy information. But the difference is that, in this method, the fuzzy optimization method is used to solve the fuzzy classification problem in which the training points include fuzzy information so that the fuzzy information in the training points are included naturally in the fuzzy programming and the obtained fuzzy optimal classification function is still fuzzy. That is to say, given an arbitrary testing point input, substitute it to the fuzzy optimal classification function, and the output are triangle fuzzy numbers. Thus the testing points and the training points are matched in the form and reach agreement in the logic. While the other three techniques are based on ordinary optimization method to solve the fuzzy classification problem with the training points including fuzzy information; thus the final obtained classification function is determinate (without fuzzy feature), which leads to the output of the testing points are determinate ,i.e., positive class or negative class, and not matched to form of the training points' output (fuzzy membership grades); so that the error would occur when the training points are used as testing points to make the **LOO** error estimation[11,12].

2 Fuzzy Support Vector Classification

A kind of special triangle fuzzy number is introduced as an extension of positive class symbol 1 or negative class symbol -1 .when the input of a training point is positive class membership grade $\delta^+(0.5 \le \delta^+ \le 1)$, we define the corresponding output as the following triangle fuzzy number[4,5] (eq.1)

$$\tilde{y} = (r_1, r_2, r_3) = (\frac{2(\delta^+)^2 + \delta^+ - 2}{\delta^+}, 2\delta^+ - 1, \frac{2(\delta^+)^2 - 3\delta^+ + 2}{\delta^+}), 0.5 \le \delta^+ \le 1 \qquad (1)$$

Similarly, when the input of a training point is negative class membership grade $\delta^-(0.5 \le \delta^- \le 1)$, the corresponding output triangle fuzzy number is

$$\tilde{y} = (r_1, r_2, r_3) = (\frac{2(\delta^-)^2 - 3\delta^- + 2}{-\delta^-}, -2\delta^- + 1, \frac{2(\delta^-)^2 + \delta^- - 2}{-\delta^-}), 0.5 \le \delta^- \le 1 \qquad (2)$$

Thus we can use $(x, \tilde{y})$ to represent a training point's input x and the output $\tilde{y}$, where $\tilde{y}$ is a triangle fuzzy number as shown in（1）or（2）. Also the following Corresponding relationship can be obtained.

$$\delta = \begin{cases} \delta^{+} & if\ x\ is\ positive \\ \delta^{-} & if\ x\ is negative \end{cases} \tag{3}$$

And (x, δ) also can be used to represent a training point's input x and the output δ.

Based on the above triangle fuzzy numbers, given the training set of classification is

$$S = \left\{(x_1, \tilde{y}_1), \cdots, (x_p, \tilde{y}_p), (x_{p+1}, \tilde{y}_{p+1}), \cdots, (x_l, \tilde{y}_l)\right\} \tag{4}$$

or

$$S_\delta = \left\{(x_1, \delta_1), \cdots, (x_p, \delta_p), (x_{p+1}, \delta_{p+1}), \cdots, (x_l, \delta_l)\right\} \tag{5}$$

where $x_j \in R^n$ is an usual input, $\tilde{y}_j\ (j = 1, \cdots, l)$ is a triangle fuzzy number as shown in (1) or (2), δ_j is shown in (3), $j = 1, \cdots, l$, $(x_t, \tilde{y}_t)$ and (x_t, δ_t) are fuzzy positive points ($t = 1, \cdots, p$), $(x_i, \tilde{y}_i)$ and (x_i, δ_i) are fuzzy negative points ($i = p+1, \cdots, l$).

Definition 1. Suppose a fuzzy training set as shown in (6) or (7), given a confidence level λ （$0 < \lambda \le 1$）, if there exist $w \in R^n$ and $b \in R$ so that

$$Pos\{\tilde{y}_j((w \cdot x_j) + b) \ge 1\} \ge \lambda,\ \ j = 1, \cdots, l \tag{6}$$

where $Pos\{\cdot\}$ is a feasibility estimate of the fuzzy event [4]. Then fuzzy training set (6) or (7)is considered to be fuzzy linearly separable, and the corresponding fuzzy classification problem be fuzzy linearly separable.

Theorem 1. Inequality (8) in **Definition 3** is equivalent to the following real inequalities:

$$\begin{cases} ((1-\lambda)r_{t3} + \lambda r_{t2})((w \cdot x_t) + b) \ge 1, t = 1, \cdots, p, \\ ((1-\lambda)r_{i1} + \lambda r_{i2})((w \cdot x_i) + b) \ge 1, i = p+1, \cdots, l. \end{cases} \tag{7}$$

Where r_{t2}, r_{t3} are the center and right end points of the fuzzy positive point $y_t (t = 1, \cdots, p)$ (triangular fuzzy number); r_{i2}, r_{i1} are the center and left end points of the fuzzy positive point $y_i (i = p+1, \cdots, l)$ (triangular fuzzy number) [12].

In inequalities (10), let

$$\begin{aligned} k_t &= \frac{1}{(1-\lambda)r_{t3} + \lambda r_{t2}}, \quad t = 1, \cdots, p \ ; \\ l_i &= \frac{1}{(1-\lambda)r_{i1} + \lambda r_{i2}}, i = p+1, \cdots, l \ , \end{aligned} \tag{8}$$

then （7） can be rewritten as:

$$\begin{cases} (w \cdot x_t) + b \geq k_t, t = 1, \cdots, p \\ (w \cdot x_i) + b \leq l_i, i = p+1, \cdots, l. \end{cases}$$

Definition 2. Considering the fuzzy linearly separability problem of fuzzy training set (6) or (7), the two parallel hyperplanes $(w \cdot x) + b = k^+$ and $(w \cdot x) + b = l^-$ are called as the support hyperplanes of the fuzzy training set (6) or (7). If

$$\begin{cases} (w \cdot x_t) + b \geq k_t, t = 1, \cdots, p \\ \min\limits_{t=1,\cdots,p} \{(w \cdot x_t) + b\} = k^+ \\ (w \cdot x_i) + b \leq l_i, i = p+1, \cdots, l \\ \max\limits_{i=p+1,\cdots,l} \{(w \cdot x_i) + b\} = l^-, \end{cases}$$

where $k_t (t = 1, \cdots, p)$, $l_i (i = p+1, \cdots, l)$ is as shown in （11 ） , $k^+ = \min\limits_{t=1,\cdots,p} \{k_t\}$, $l^- = \max\limits_{i=p+1,\cdots,l} \{l_i\}$.

then distance between the two support hyperplanes $(w \cdot x) + b = k^+$ and $(w \cdot x) + b = l^-$ is ：

$$\frac{| k^+ - l^- |}{\| w \|},$$

which is called as margin （where k^+ and l^- are constant and satisfy the condition that $k^+ > 0$ and $l^- < 0$） .Due to basic idea of Support Vector Machine, our goal is to maximize margin. Under the confidence level $\lambda (0 < \lambda \leq 1)$, fuzzy linearly separability problem of the fuzzy training set as shown in (6)or (7), can be transformed to fuzzy chance constrained programming with decision variable $(w, b,)^T$:

$$\begin{cases} \min\limits_{w,b} \dfrac{1}{2} \| w \|^2, \\ s.t. Pos\{\tilde{y}_j ((w \cdot x_j) + b) \geq 1\} \geq \lambda, j = 1, \cdots, l, \end{cases} \tag{9}$$

Theorem 2. Under the confidence level $\lambda(0<\lambda\le 1)$, the certain equivalence programming (common programming equivalent to(12) of the fuzzy chance constrained programming （13） is the quadratic programming:

$$\begin{cases} \min\limits_{w,,b} \dfrac{1}{2}\|w\|^2, \\ s.t.((1-\lambda)r_{t3}+\lambda r_{t2})((w\cdot x_t)+b)\ge 1, t=1,\cdots,p, \\ ((1-\lambda)r_{i1}+\lambda r_{i2})((w\cdot x_i)+b)\ge 1, i=p+1,\cdots,l. \end{cases} \tag{10}$$

Theorem 3. There exists an optimal solution of quadratic programming (10).

Theorem 4. The duality programming of quadratic programming (10) is quadratic programming with decision variable $(\beta,\alpha)^T$:

$$\begin{cases} \min\limits_{\beta,\alpha} \dfrac{1}{2}(A+2B+D)-(\sum\limits_{t=1}^{p}\beta_t+\sum\limits_{i=p+1}^{l}\alpha_i), \\ s.t.\sum\limits_{t=1}^{p}\beta_t((1-\lambda)r_{t3}+\lambda r_{t2})+\sum\limits_{i=p+1}^{l}\alpha_i((1-\lambda)r_{i1}+\lambda r_{i2})=0, \\ \beta_t\ge 0, t=1,\cdots,p, \\ \alpha_i\ge 0, i=p+1,\cdots,l, \end{cases} \tag{11}$$

where $A=\sum\limits_{t=1}^{p}\sum\limits_{s=1}^{p}\beta_t\beta_s((1-\lambda)r_{t3}+\lambda r_{t2})((1-\lambda)r_{s3}+\lambda r_{s2})(x_t\cdot x_s)$,

$$B=\sum_{t=1}^{p}\sum_{i=p+1}^{l}\beta_t\alpha_i((1-\lambda)r_{t3}+\lambda r_{t2})((1-\lambda)r_{i1}+\lambda r_{i2})(x_t\cdot x_i),$$

$$D=\sum_{i=p+1}^{l}\sum_{q=p+1}^{l}\alpha_i\alpha_q((1-\lambda)r_{i1}+\lambda r_{i2})((1-\lambda)r_{q1}+\lambda r_{i2})(x_i\cdot x_q),$$

$\beta=(\beta_1,\cdots,\beta_p)^T\in R_+^p$, $\alpha=(\alpha_{p+1},\cdots,\alpha_l)^T\in R_+^{l-p}$, $(\beta,\alpha)^T$ is decision variable.

Programming （14） is a convex quadratic programming. After getting its optimal solution $(\beta^*,\alpha^*)^T=(\beta_1^*,\cdots,\beta_p^*,\ \alpha^*{}_{p+1},\cdots\alpha^*{}_l)^T$, we can get the certain optimal classification hyperplane (see [11]):

$$(w^*\cdot x)+b^*=0, x\in R^n \tag{12}$$

where

$$w^* = \sum_{t=1}^{p} \beta_t^* ((1-\lambda) r_{t3} + \lambda r_{t2}) x_t + \sum_{i=p+1}^{l} \alpha_i^* ((1-\lambda) r_{i1} + \lambda r_{i2}) x_i ,$$

$$b^* = ((1-\lambda) r_{s3} + \lambda r_{s2}) - (\sum_{t=1}^{p} \beta_t^* ((1-\lambda) r_{t3} + \lambda r_{t2})(x_t \cdot x_s) + \sum_{i=p+1}^{l} \alpha_i^* ((1-\lambda) r_{i1} + \lambda r_{i2})(x_i \cdot x_s)),$$

$s \in \{s \mid \beta_s^* > 0\}$, or

$$b^* = ((1-\lambda) r_{q1} + \lambda r_{q2}) - (\sum_{t=1}^{p} \beta_t^* ((1-\lambda) r_{t3} + \lambda r_{t2})(x_t \cdot x_q) + \sum_{i=p+1}^{l} \alpha_i^* ((1-\lambda) r_{i1} + \lambda r_{i2})(x_i \cdot x_q)),$$

$q \in \{q \mid \alpha_q^* > 0\}$.

For the Fuzzy Support Vector classification, however, we expect to obtain an fuzzy optimal classification function whose value is a triangular fuzzy number $\tilde{y}_j$ as shown in (1) and (2), which can be achieved through $g(x) = (w^* \cdot x) + b^*$ and the following function (16):

$$\delta = \delta(u) = \begin{cases} \varphi_+(u), 0 < u \le \varphi_+^{-1}(1), \\ 1, u > \varphi_+^{-1}(1), \\ -\varphi_-(u), \varphi_-^{-1}(1) \le u < 0, \\ -1, u < \varphi_-^{-1}(1), \end{cases} \tag{13}$$

where $\varphi_+^{-1}(u)$ and $\varphi_-^{-1}(u)$ are respectively the inverse function of $\varphi_+(u)$ and $\varphi_-(u)$.

$\varphi_+(u)$ is a regression function (monotonous increasing function on u) obtained from the $\varepsilon-$support vector regression. And $\varepsilon-$ support vector regression is constructed by the following method.

(i) Build up the Construct training set of the regression problem

$$\{(g(x_1), \delta_1), \cdots, (g(x_p), \delta_p)\} \tag{14}$$

(ii) Use (17) as training set , and select appropriate $\varepsilon > 0$, penalty parameter $C > 0$,choose a linear kernel as the kernel function ,thus to construct $\varepsilon-$support vector regression.

Similarly, $\varphi_-(u)$ is a regression function (monotonous decreasing function on u) obtained from the $\varepsilon-$support vector regression which is constructed with the same method.

According to the corresponding relationship (3) and the transformation rules (1) and (2), the fuzzy optimal classification function will be achieved by transforming the function $\delta = \delta(g(x))$ in (16) to a triangular fuzzy number $\tilde{y} = \tilde{y}(x)$.

Given an arbitrary testing point input $\bar{x}$, substitute it to the fuzzy optimal classification function, and then obtain a output are triangle fuzzy numbers $\tilde{y}$ which is the output of the testing points and can objectively reflect the fuzzy classification situation of the testing points $(\bar{x}, \tilde{y})$ (shown the membership grade of the positive or negative testing input).

From the above discussion, we can achieve the following algorithm.

3 Algorithm

(i) Given a fuzzy training set (6) or (7) ,and select an appropriate confidence level $\lambda(\sigma \le \lambda \le 1)$, $C > 0$ and a kernel function $K(x, x')$,then construct quadratic programming:

$$\begin{cases} \min\limits_{\beta,\alpha} \dfrac{1}{2}(A_K + 2B_K + D_K) - (\sum\limits_{t=1}^{p} \beta_t + \sum\limits_{i=p+1}^{l} \alpha_i) \\ s.t. \sum\limits_{t=1}^{p} \beta_t((1-\lambda)r_{t3} + \lambda r_{t2}) + \sum\limits_{i=p+1}^{l} \alpha_i((1-\lambda)r_{i1} + \lambda r_{i2}) = 0 \\ 0 \le \beta_t \le C, t = 1, \cdots, p \\ 0 \le \alpha_i \le C, i = p+1, \cdots, l, \end{cases} \tag{15}$$

where $A_K = \sum\limits_{t=1}^{p}\sum\limits_{s=1}^{p} \beta_t \beta_s ((1-\lambda)r_{t3} + \lambda r_{t2})((1-\lambda)r_{s3} + \lambda r_{s2})K(x_t, x_s)$,

$$B_K = \sum_{t=1}^{p}\sum_{i=p+1}^{l} \beta_t \alpha_i ((1-\lambda)r_{t3} + \lambda r_{t2})((1-\lambda)r_{i1} + \lambda r_{i2})K(x_t, x_i),$$

$$D_K = \sum_{i=p+1}^{l}\sum_{q=p+1}^{l} \alpha_i \alpha_q ((1-\lambda)r_{i1} + \lambda r_{i2})((1-\lambda)r_{q1} + \lambda r_{i2})K(x_i, x_q),$$

$\beta = (\beta_1, \cdots, \beta_p)^T \in R_+^p$, $\alpha = (\alpha_{p+1}, \cdots, \alpha_l)^T \in R_+^{l-p}$, $(\beta, \alpha)^T$ is a decision variable.

(ii) Solve quadratic programming(18), get optimal solution

$(\beta^*, \alpha^*)^T = (\beta_1^*, \cdots, \beta_p^*, \alpha_{p+1}^*, \cdots, \alpha_l^*)^T$.

(iii) Select the positive component $\beta_s^* \in (0, C)$ of β^* ,or $\alpha_q^* \in (0, C)$ of α^* then compute

$$b^* = ((1-\lambda)r_{s3} + \lambda r_{s2}) -$$

$$(\sum_{t=1}^{p} \beta_t^* ((1-\lambda)r_{t3} + \lambda r_{t2})K(x_t, x_s) + \sum_{i=p+1}^{l} \alpha_i^* ((1-\lambda)r_{i1} + \lambda r_{i2})K(x_i, x_s))$$

or

$$b^* = ((1-\lambda)r_{q1} + \lambda r_{q2}) -$$

$$(\sum_{t=1}^{p} \beta_t^* ((1-\lambda)r_{t3} + \lambda r_{t2})K(x_t, x_q) + \sum_{i=p+1}^{l} \alpha_i^* ((1-\lambda)r_{i1} + \lambda r_{i2})K(x_i, x_q))$$

(iv) Construct function :

$$g(x) = \sum_{t=1}^{p} \beta_t^* ((1-\lambda)r_{t3} + \lambda r_{t2})K(x_t, x_s) + \sum_{i=p+1}^{l} \alpha_i^* ((1-\lambda)r_{i1} + \lambda r_{i2})K(x_i, x_s)$$

(v) Consider $\{(g(x_1), \delta_1), \cdots, (g(x_p), \delta_p)\}$ and $\{(g(x_{p+1}), -\delta_{p+1}), \cdots, (g(x_l), -\delta_l)\}$ as training set respectively, construct $\varepsilon -$ support vector regression (select appropriate $\varepsilon > 0$, penalty parameter $C > 0$,choose a linear kernel as the kernel function), then obtain regression functions $\varphi_+(u)$ and $\varphi_-(u)$,and construct function(16).

(vi) According to corresponding relationship (3) and the transformation rules (1) and (2), the fuzzy optimal classification function will be achieved by transforming the function $\delta = \delta(g(x))$ in (16) to a triangular fuzzy number $\tilde{y} = \tilde{y}(x)$.

If the outputs of all fuzzy training points in fuzzy training set(6) or (7) are all real number 1 or -1, then the fuzzy training set degenerates to the common training set, so the fuzzy support vector classification machine degenerates to the support vector classification machine.

4 Numerical Experiments

In order to make this method's superiority obvious, a numerical experiment is perfomed in the method based on the experiment data of Breast cancer, Heart, Banana, Diabetis, Flare-solar in Ref.[9] and Hungarian, Iris, Wine, Leukemia in Ref.[10]. and the experiment result has been compared with the result obtained through SVM, NFSVM and PSVM. The details as per table 1 and table 2.

Table 1. Average classification errors on the testing sets(%)

	SVM	**NFSVM**	proposed algorithm
Breast cancer	26.04	25.33	24.83
Heart	15.95	15.27	15.11
Banana	11.53	11.04	10.76
Diabetic	23.53	23.42	23.27
Flare-sola	32.43	32.38	32.34

Table 2. Mean accuracy of SVM, PSVM and proposed algorithm(%)

	SVM	PSVM.I	PSVM.II	proposed algorithm
Hungarian	72.83	75.70	76.59	77.37
Iris	96.33	98.37	98.37	98.56
Wine	93.15	95.28	95.17	96.02
Leukemia	65.79	94.21	96.84	96.89

In the result obtained from the algorithm proposed in this paper, the positive testing points are regarded as positive for and negative for those membership grades less than 0.5. from table 1 , it shows the Average classification errors of result obtained from the algorithm is smaller than that from SVM and NFSVM; and from table 2, it can been concluded that the Mean accuracy of the algorithm is higher than that of SVM and PSVM.

5 Conclusion

This paper builds up a Fuzzy Support Vector classification (algorithm) with the the fuzzy chance constraint programming based on the Support Vector classification. The reasonableness of the algorithm is shown by numerical experiments and the superiority is evident through the comparison with other algorithms of the same kind.

References

1. Vapnik, V.N.: The Nature of Statistical Learning Theory. Springer, New York (1995)
2. Cristianini, N.: Introduction to Support Vector Machines. Cambridge University Press, Cambridge (2000)
3. Mangasarian, O.L.: Generalized Support Vector Machines. In: Advances in Large Margin Classifiers, MIT Press, Cambridge (1999)
4. Zadeh, L.A.: Fuzzy Sets as a Basis for a Theory of Possibility. Fuzzy Sets and Systems 1(1), 3–28 (1978)
5. Zhang, W.X.: Foundation of Fuzzy Mathematics. Xi'an Jiaotong University Press, Xi'an (1995)
6. Liu, B.D.: Chance Constrained Programming with Fuzzy Parameters. Fuzzy Sets and Systems 94(2), 227–237 (1998)
7. Liu, B.D., Zhao, R.Q.: Random Programming and Fuzzy Programming. Tsinghua University Press, Beijing (1998)
8. Lin, C.F., Wang, S.D.: Fuzzy Support Vector Machines. IEEE Transactions on Neural Networks 13(2), 464–471 (2002)
9. Tao, Q., Wang, J.: A New Fuzzy Support Vector Machine Based on the Weighted Margin. Neural Procession Letters 20(3), 139–150 (2004)
10. Lee, K.Y., Kim, D.W., Lee, K.H., Lee, D.: Possibilistic Support Vector Machine. Pattern Rrcognition 38(3), 1325–1327 (2005)

11. Deng, N.Y., Tian, Y.J.: The New Method in Data Mining——Support Vector Machines. Science Press, Beijing (2004)
12. Yang, Z.M., Liu, G.L.: Principium and Applications of Uncertain Support Vector Machines. Science Press, Beijing (2007)
13. Yuan, Y.X., Sun, W.Y.: Optimal Theories and Methods. Science Press, Beijing (1997)

An FIS for Early Detection of Defect Prone Modules

Zeeshan Ali Rana, Mian Muhammad Awais, and Shafay Shamail

Department of Computer Science,
Lahore University of Management Sciences (LUMS),
Sector U, DHA Lahore, Pakistan
{zeeshanr,awais,sshamail}@lums.edu.pk

Abstract. Early prediction of defect prone modules helps in better resource planning, test planning and reducing the cost of defect correction in later stages of software lifecycle. Early prediction models based on design and code metrics are difficult to develop because precise values of the model inputs are not available. Conventional prediction techniques require exact inputs, therefore such models cannot always be used for early predictions. Innovative prediction methods that use imprecise inputs, however, can be applied to overcome the requirement of exact inputs. This paper presents a fuzzy inference system (FIS) that predicts defect proneness in software using vague inputs defined as fuzzy linguistic variables. The paper outlines the methodology for developing the FIS and applies the model to a real dataset. Performance analysis in terms of recall, accuracy, misclassification rate and a few other measures has been conducted resulting in useful insight to the FIS application. The FIS model predictions at an early stage have been compared with conventional prediction methods (i.e. classification trees, linear regression and neural networks) based on exact values. In case of the FIS model, the maximum and the minimum performance shortfalls were noticed for true negative rate ($TNRate$) and F measure respectively. Whereas for $Recall$, the FIS model performed better than the other models even with the imprecise inputs.

1 Introduction

Today software are used in almost every walk of life. The software development companies cannot risk their business by shipping poor quality software [10] as it results in customer dissatisfaction. Risk to business can be minimized by predicting the quality of the software in the early stages of the software development lifecycle (SDLC). This would not only keep the clients satisfied but also reduce the cost of correction of defects. It has been reported in [10] that the cost of defect correction is significantly high if the corrections are made after testing. An additional benefit of early prediction of software quality is better resource planning [21] and test planning [9], [21]. Therefore the key is to identify defect prone modules at an early SDLC stage. The importance of early software quality

D.-S. Huang et al. (Eds.): ICIC 2009, LNAI 5755, pp. 144–153, 2009.

prediction is evident from a number of studies conducted in this regard [10], [7], [19], [16], [18], [20]. A brief overview of the previous studies follows.

In order to keep the software corrections cost effective, defect proneness of software modules has been predicted earlier in the development phase using discriminant analysis [10]. In order to collect the defect proneness information as early as possible, studies have been conducted using requirements metrics [7]. This highlights the importance of prediction in very early phases of software lifecycle. Xing et al. have employed support vector machines for early quality prediction using design and static code metrics and have achieved correct classification rate of upto 90% [19]. Later, a study comparing design and code metrics suggests that design metrics combined with static code metrics can help get better defect prediction results [8]. But waiting until the development phase, when the code metrics are available, is late.

Attempts have been made to identify some rules useful in early stages of software lifecycle to predict defect proneness and reliability [20]. Yang et al. suggest the use of fuzzy self-adaptation learning control network (FALCON) which can predict the quality based on fuzzy inputs. Their work is similar to ours in the sense that they also intend to predict the quality when exact values of software metrics are not known and the domain knowledge and experience of the project managers can be used to approximate the metrics values. Furthermore, they also intend to find the rule set which has the capability to reason under uncertainty, which is a limitation of most of the quality prediction models [5]. This study also extracts some rules in an attempt to overcome the ceiling effect problem [14] in the defect prediction models.

Each of the existing studies has its limitations which restrict its use in the software industry. Limitations of studies cited in this paper are given in Table 1. The table also shows when does the prediction information becomes available, whether it is available just before the testing phase, just before the release or at some other stage. In some cases data used for the study is not publicly available [10], [16], [18] hence generating those models with the same results is not possible for other researchers. This refrains the researchers to take advantage of the existing work. The experiments conducted using public data can be replicated and the studies reporting such experiments are more useful. In other cases the predictions are made at a later stage in the SDLC as they use code metrics, thus reducing the benefits of early predictions [19], [7]. Such predictions are termed as 'Late' in Table 1. In [7] early prediction of software quality using requirements metrics has been tested without any promising results. Design and code metrics have been used to identify the defect prone modules with a high success rate [10], [18], [19], [7], [8]. Jiang et al. have compared the prediction models based on design and code metrics [8] and have asserted that the models based on code metrics usually perform better than the models based on design metrics. The combination of the design and code metrics gives better prediction results [8] but delays the defect prediction until the code metrics are available.

In this paper we suggest to use design and code metrics at the start of design phase, through defining the values of the metrics in fuzzy linguistic terms. The

Table 1. Limitations of relevant early quality prediction Studies

Reference	Metrics Used	Data	When?	Limitation
[10]	Design	Non Public	Prior to Testing	Data Unavailable. Late.
[16]	Design	Non Public	Prior to Release	Data Unavailable. Late.
[18]	Code	Non Public	Prior to Release	Data Unavailable Late.
[19]	Code	Non Public, Proprietary, Purchasable.	Prior to Testing	Only Complexity Metrics Used. Late.
[7]	Requirements, Code	Public	Prior to Testing	Late.
[20]	Design, Code	Synthetic	Prior to Testing	Data Synthetic. Late.

Prior to Testing = Predictions are available just before the start of testing phase
Data Unavailable = Data used for the study cannot be obtained publicly
Late = The prediction information is either available late in the SDLC or based on the metrics collected during or after development phase

reason for defining linguistic values is that the exact values of design and code metrics are not available at this stage. Initial resource plans are usually made at the start of the design phase, the prediction based on linguistic variables would help in tentative resource planning. The conventional prediction is more accurate but has a disadvantage of delayed prediction. Approximate prediction on the other hand can be a bit less accurate, but can be useful at early stages. The approach adopted here provides an approximate value of the conventional prediction made at the later stages of SDLC. It is envisaged that fuzzy linguistic based model can reach a certain level of accuracy, precision and recall. Expressing software metrics in fuzzy linguistic terms is a workable solution because the management responsible for preparing resource plans is usually experienced enough to provide the values of software metrics in linguistic terms such as very low, low, medium, high.

This paper attempts to develop a fuzzy inferencing system (FIS) using inputs represented in fuzzy linguistic terms. The fuzzy linguistic inputs have been used to generate an FIS that predicts the defect proneness of various modules of object oriented software. The paper uses kc1-class-level-data [3] for this purpose. First fuzzy c-means clustering [1] is applied on the input data to determine: 1) the membership functions for each input and 2) the number of rules to be generated. A Sugeno type FIS [11] is generated afterwards. The FIS based model proposed in this study has been compared with classification trees (CT) [15], linear regression (LR) [2] and neural networks (NN) [6] based prediction models so that a comparison of approximate prediction with the exact prediction can be made to see the extent of performance shortfall.

The rest of the paper is organized as follows: Section 2 describes the dataset used for the study, the FIS generation and the evaluation parameters for the comparison. Section 3 presents and discusses the experimental results. Section 4 identifies the future directions and concludes the paper.

2 Methodology

2.1 Dataset

The dataset used for the study is class-level data for kc1 available at PROMSIE website [3]. The dataset originally has 145 instances each with 95 parameters. Each instance represents a software class (or module). A classification parameter is used as output to indicate if the software class is defect prone (D) or not-defect prone (ND). The rest of the 94 parameters are software metrics calculated for that module and are divided into two groups. *Group A* has 10 parameters and *Group B* has 84 parameters. Values of the parameters in *Group A* are originally measured at module level whereas the values of the parameters in *Group B* are originally measured at method level and are later transformed to module level before making the dataset available at PROMSIE website [3]. No parameter from *Group B* (transformed to module level) has been selected for this study. From *Group A*, 8 most commonly used parameters identified in [13] have been selected to predict defect proneness and are listed in Table 2.

2.2 FIS Based Model

Our FIS based model is generated through a two phase process. The first phase performs fuzzy c-means clustering [1] to identify the membership functions for each input and the second phase then generates a fuzzy inference system that models the behavior of the data. Two types of fuzzy reasoning methods, i.e. Mamdani and Sugeno reasoning methods [11], can be applied in FIS implementations. Sugeno uses constant or linear functions as output functions whereas Mamdani uses fuzzy membership functions at the output resulting in higher computational costs [11]. In the present study Sugeno method has been applied

Table 2. *Group A* Parameters used for the study

Parameter	Abbreviation
Coupling Between Object classes	CBO
Depth of Inheritance Tree	DIT
Lack of Cohesion in Methods	LCOM
Number Of Children	NOC
Dependence on an a descendant	DOC
Count of calls by higher modules	FAN_IN
Response For a Class	RFC
Weighted Methods per Class	WMC

as the reasoning process simply because it is computationally efficient, and performance enhancement of this method can further be achieved through applying other optimization and adaptive techniques.

Phase 1: Performing Fuzzy C-Means Clustering. In order to generate the fuzzy rules, it is required to determine the total number of rules to be developed and the number of antecedent membership functions. Fuzzy c-means clustering (FC) [1] has been used to determine these two parameters. The total number of clusters given by FC are useful in determining the number of rules. FC algorithm outputs n clusters $C_{1\cdots n}$ and the membership value of each antecedent in each of the n clusters.

Phase 2: Generating FIS. We have generated a Sugeno type FIS using Matlab fuzzy toolbox. In a Sugeno type FIS, the consequent y of a rule is a crisp number which is computed as follows:

$$y = \sum_{i=1}^{k} \alpha_i x_i + \beta_i \tag{1}$$

where k is total number of antecedents (parameters predicting the defect proneness), α_i and β_i are co-efficients which can be different for each parameter x_i. The generated FIS has n rules and the j^{th} rule takes the form:

$$Rule_j : IF\ input_1\ in\ C_i\ AND\ \cdots\ AND\ input_k\ in\ C_i\ THEN\ output\ in\ C_i$$

where k is total number of input parameters and $i = 1 \cdots n$. For a binary class problem, two rule sets, $RuleSet_D$ and $RuleSet_{ND}$, are generated for classification of the D and ND modules respectively. When a certain rule, say $Rule_p$, is fired, the following $Rule_D$ and $Rule_{ND}$ classify the given module into class D and ND respectively:

$$Rule_D : IF\ Rule_p\ \epsilon\ RuleSet_D\ THEN\ D$$

$$Rule_{ND} : IF\ Rule_p\ \epsilon\ RuleSet_D\ THEN\ ND$$

where

$$RuleSet_D = \{Rule_q |\ Rule_q\ classifies\ the\ given\ module\ as\ D\},$$

$$RuleSet_{ND} = \{Rule_r |\ Rule_r\ classifies\ the\ given\ module\ as\ ND\}$$

and

$$RuleSet_D \cap RuleSet_{ND} = \Phi$$

Table 3. Evaluation parameters used for comparison

Evaluation Parameter	Abbreviation
True Negative Rate	$TNRate$
True Positive Rate (Recall)	$TPRate$ ($Recall$)
False Positive Rate	$FPRate$
False Negative Rate	$FNRate$
Accuracy	Acc
Precision	$Prec$
Misclassification Rate	$MCRate$
F-Measure	F

2.3 Comparison

The suggested FIS model has been compared with the prediction models such as classification tree (CT), linear regression (LR) and neural network (NN) based models. A binary CT is used in this study for comparison. The LR based model is a standard R-squared approach. The NN model is a single hidden layer feed forward back propagation based network having one neuron in the hidden layer. The NN model selected for comparison is obtained after exhaustive experimental runs. It was seen during the experiments that the more complicated NN models did not perform better than the single layer single neuron network for kc1-class-level data. The comparison of these models with the FIS based model not only identifies the best model for each evaluation parameter but also attempts to highlight the extent of performance shortfall for each evaluation parameter if fuzzy prediction model is used instead of the exact prediction models.

2.4 Evaluation Parameters for Comparison

The comparison mentioned above has been done in terms of the evaluation parameters listed in Table 3. $TNRate$, $TPRate$ or $Recall$, $FPRate$ and $FNRate$ are obtained while computing a confusion matrix. Acc, $Prec$ and $MC\ Rate$ are important and widely used model performance measures when confusion matrix is available. Acc is not considered a good performance measure for unbalanced datasets [12], therefore to deal with the unbalanced data F [17] is used. It is worthwhile to mention that performance in terms of $Recall$ (i.e. true positive rate) is significant as it helps in focusing on the problematic areas in the software and thus better resource planning can be done. Since our goal is to detect the defect prone modules, we consider $Recall$ as our primary measure of comparison. In addition to these parameters we have determined the position of each model on relative operating characteristic (ROC) graph [4] by plotting a ROC point for each model. This visualization is helpful in identifying a better model in terms of $Recall$. To see the effect of using fuzzy model, a percentage of performance shortfall is calculated for each evaluation parameter. An overall performance shortfall (maximum shortfall from all the parameters) is also recorded. This percentage is helpful in finding what are the benefits of using the fuzzy based prediction and what are its drawbacks over using the exact predictions.

3 Results and Discussion

Experiments were conducted with a split of training and test data as 67% to 33% respectively. For the CT a tree with 12 intermediate nodes was developed. The standard R-squared LR model was obtained using the training data. To train the NN, 100 epochs were used to obtain reasonable results. A larger number of epochs has not produced better results with the initial bias of 1 and the initial unit weights at each hidden layer. To develop the FIS, the membership functions for each input were assigned based on the frequency distribution of the data. A relationship between the distribution of all the input metrics and the membership functions (or clusters) for each input software metric is shown in Figure 1 and Figure 2 . There are more membership functions in Figure 2 for the more dense areas of the corresponding input metric in Figure 1. We have kept the shape of all the membership functions of the antecedents as gaussian and have used the information obtained from phase 1 to determine the rules that model the data behavior. Linear least squares estimation has been used to find the consequent

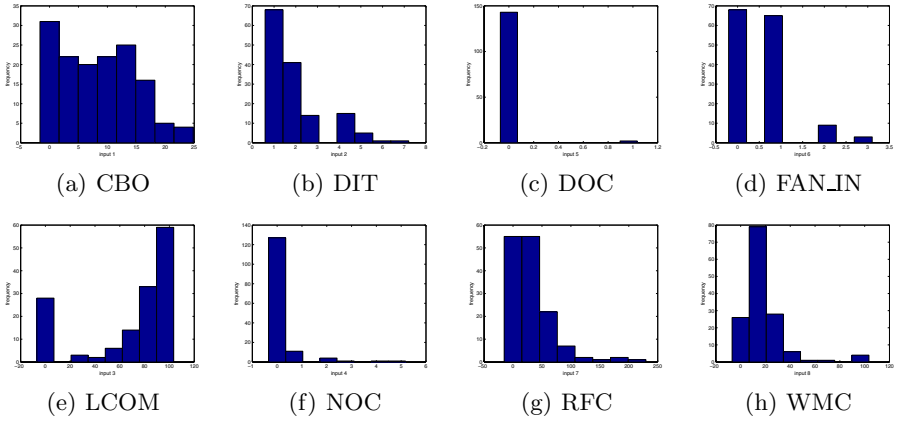

(a) CBO (b) DIT (c) DOC (d) FAN_IN

(e) LCOM (f) NOC (g) RFC (h) WMC

Fig. 1. Frequency distribution of all input metrics

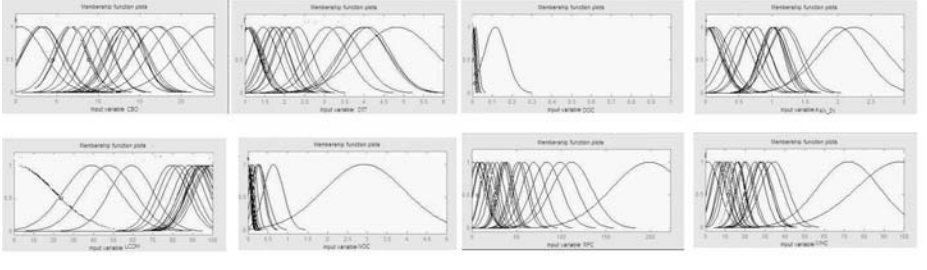

Fig. 2. Output of phase 1: clusters and membership functions for each input. (The plot of the membership functions for each input appear in the same order as the distribution of each input appears in Fig. 1).

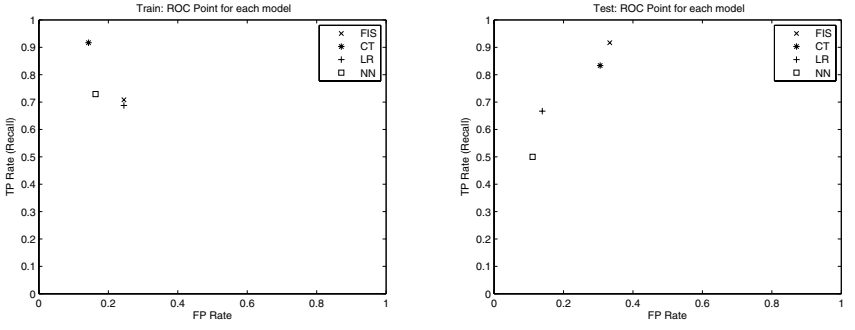

(a) Training (b) Testing

Fig. 3. ROC point for each model in training and testing

of each rule. When the FIS is generated, 21 conjunctive rules were generated. The decision whether a module is D or ND is made using $Rule_D$ and $Rule_{ND}$ respectively. In total, 21 clusters were obtained with clusters 1 to 11 belonging to ND class and clusters 12 to 21 belonging to D class.

A number of experiments were conducted and the optimal results for each model are reported in this paper. Despite being a simplest learner of all the other learners, CT has performed better in training phase. It has the best values for all the evaluation parameters including *Recall*. The FIS based model has the third best *Recall* during training as shown in Fig. 3(a) whereas it has the best *Recall* but a higher $FPRate$ in the testing phase as shown in Fig. 3(b). The testing phase performance reported in Table 4 indicates that the CT based model has failed to keep its performance due to overfitting the training data. The LR based model dominates in the test phase in terms of *Acc*, *Prec* and *MC Rate*. The NN based model turns out to be the best classifier for the ND modules. The FIS based model has the second best F value. It is worthwhile to mention that the results reported in Table 4 are for unbalanced test data which is dominated by ND classes. Hence the best *Recall* and the second best F value of the FIS based model is reasonable for a model developed using fuzzy inputs. These values can be improved if the membership functions are further fine tuned.

The effect of using fuzzy inputs have been measured in terms of performance shortfall. Maximum performance shortfall of 24.99% has been observed in case

Table 4. Testing performance measures

	$TNRate$	$TPRate/Recall$	$FPRate$	$FNRate$	*Acc.*	*Prec.*	$MCRate$	F
FIS	0.6667	**0.9167**	0.3333	**0.0833**	0.7292	0.4783	0.2708	0.6286
CT	0.6944	0.8333	0.3056	0.1667	0.7292	0.4762	0.2708	0.6061
LR	0.8611	0.6667	0.1389	0.3333	**0.8125**	**0.6154**	**0.1875**	**0.6400**
NN	**0.8889**	0.5000	**0.1111**	0.5000	0.7917	0.6000	0.2083	0.5455

of $TNRate$ and $FPRate$. For the rest of the evaluation parameters, the performance shortfalls have been 10.25%, 22.27%, 10.25% and 1.81% for Acc, $Prec$, $MCRate$ and F respectively. The observed performance shortfalls are reasonably low given the approximate nature of the inputs used for the FIS prediction model. Therefore the FIS based prediction can be used to identify the possible defect prone modules at an early stage of the SDLC. In order to get the exact prediction, the conventional prediction models can be used later in the SDLC when precise values are available.

4 Conclusions and Future Work

The conventional quality prediction models require exact values of their input parameters. This paper introduces a novel concept of getting approximate prediction of defect proneness when exact input values are not available, especially during early SDLC phases. These early predictions are needed for better resource planning, cost reduction and test planning. The paper suggests the use of fuzzy inputs to overcome the need for exact and precise input metric values. The prediction model introduced in this paper is fuzzy inference system based and requires imprecise estimates of input software metrics. This imprecision is introduced by defining inputs as fuzzy linguistic variables. The linguistic labels can be obtained from a domain expert. The paper identifies that predictions made through vague inputs are reasonably close to predictions obtained through the application of conventional models based on exact and precise inputs. In light of the analysis conducted in this paper, one can easily predict the defect proneness at an early stage without requiring exact measurements of the metrics.

This study needs to be extended for the validation using more datasets. We also plan to investigate if the rules extraction can be improved to establish a causal relationship between the values of software metrics and the defect proneness of software modules.

Acknowledgments

We are thankful to Higher Education Commission (HEC) of Pakistan and Lahore University of Management Sciences (LUMS) for funding this research.

References

1. Bezdek, J.C.: Pattern Recognition with Fuzzy Objective Function Algoritms. Plenum Press, New York (1981)
2. Bishop, C.M.: Pattern Recognition and Machine Learning (Information Science and Statistics). Springer, Heidelberg (2006)
3. Boetticher, G., Menzies, T., Ostrand, T.: Promise Repository of Empirical Software Engineering Data (2007)
4. Egan, J.P.: Signal Detection Theory and Roc Analysis. Series in Cognition and Perception (1975)

5. Fenton, N.E., Neil, M.: A Critique of Software Defect Prediction Models. IEEE Transactions on Software Engineering 25(5), 675–687 (1999)
6. Haykin, S.: Neural Networks: A Comprehensive Foundation. Macmillan, New York (1994)
7. Jiang, Y., Cukic, B., Menzies, T.: Fault Prediction Using Early Lifecycle Data. In: Proceedings of ISSRE 2007, TBF (2007)
8. Jiang, Y., Cukic, B., Menzies, T., Bartlow, N.: Comparing Design and Code Metrics for Software Quality Prediction. In: Proceedings of PROMISE 2008, ACM, New York (2008)
9. Khosgoftaar, T.M., Munson, J.C.: Predicting Software Development Errors Using Software Complexity Metrics. IEEE Journal On Selected Areas In Communications 8(2) (1990)
10. Khoshgoftaar, T.M., Allen, E.B., Kalaichelvan, K.S., Goel, N.: Early Quality Prediction: A Case Studv in Telecommunications. IEEE Software (1996)
11. Kosko, B.: Fuzzy engineering. Prentice-Hall Inc., Upper Saddle River (1997)
12. Kubat, M., Holte, R.C., Matwin, S.: Machine Learning for the Detection of Oil Spills in Satellite Radar Images. Machine Learning 30, 195–215 (1998)
13. Menzies, T., Stefano, J.S.D., Chapman, M.: Learning Early Lifecycle ivv Quality Indicators. In: Proceedings of IEEE Metrics 2003. IEEE, Los Alamitos (2003)
14. Menzies, T., Turhan, B., Bener, A., Gay, G., Cukic, B., Jiang, Y.: Implications of Ceiling Effects in Defect Predictors. In: Proceedings of the PROMISE 2008 (2008)
15. Mitchell, T.M.: Machine Learning. McGraw-Hill, New York (1997)
16. Quah, T.S., Thwin, M.M.T.: Application of Neural Network for Predicting Software Development Faults Using Object-Oriented Design Metrics. In: Proceedings of The 19th International Conference on Software Maintenance. IEEE Computer Society, Los Alamitos (2003)
17. Rijsbergen, C.J.V.: Information Retrieval, 2nd edn. Butterworth-Heinemann, Newton (1979)
18. Wang, Q., Yu, B., Zhu, J.: Extract Rules from Software Quality Prediction Model Based on Neural Network. In: Proceedings of The 16th IEEE International Conference on Tools with Artificial Intelligence, ICTAI 2004 (2004)
19. Xing, F., Guo, P., Lyu, M.R.: A Novel Method for Early Software Quality Prediction Based on Support Vector Machine. In: Proceedings of The 16th IEEE International Symposium on Software Reliability Engineering (2005)
20. Yang, B., Yao, L., Huang, H.Z.: Early Software Quality Prediction Based on a Fuzzy Neural Network Model. In: Proceedings of Third International Conference on Natural Computation (2007)
21. Yuan, X., Khoshgoftaar, T.M., Allen, E.B., Ganesan, K.: An Application of Fuzzy Clustering to Software Quality Prediction. In: Proceedings of The 3rd IEEE Symposium on Application-Specific Systems and Software Engineering Technology (2000)

Variable Precision Concepts and Its Applications for Query Expansion

Fei Hao[1] and Shengtong Zhong[2]

[1] Department of Computer Science
Korea Advanced Institute of Science and Technology
373-1, Guseong-Dong, Yuseong-Gu, Daejeon 305-701, Korea
fhao@islab.kaist.ac.kr
[2] Department of Computer and Information Science
Norwegian University of Science and Technology
NO-7491 Trondheim, Norway
shket@idi.ntnu.no

Abstract. One of the most important tasks of search engines is presenting more additional relevant web pages and reducing those pages which are useless for users. Query expansion is an efficient method for dealing with this task. In this paper, variable precision concept(VPC) based on formal concept analysis(FCA) is firstly proposed and its properties are discussed. Then a new strategy of expanding query terms based on VPC is proposed. According to this new strategy, users can set the query precision in terms of their interests and obtain the additional relevance web pages. Finally, application results show the efficiency and effectiveness of this method.

Keywords: FCA, variable precision concept, query expansion.

1 Introduction

Formal concept analysis(FCA) is a discipline that studies the hierarchical structures induced by a binary relation between a pair of sets. The structure, made up of the closed subsets ordered by set-theoretical including, satisfies the properties of a complete lattice and has been firstly mentioned in the work of Birkhoff [4]. The term concept lattice and FCA are due to Wille [5,6,7,8,9]. Later on, it has been the subject of an extensive study with many interesting results. As a classification tool, FCA has been used in several areas such as data mining, knowledge discovery, and software engineering. Today, there is a constantly growing number of studies in both theoretical and practical issues [11,12,13,14,15,16,17,18].

The space of the information retrieval system is very large, and the terms of natural language take on the ambiguities. In a search engine, a user query can be understood into several meanings, and search results are always in a long list of web pages for the user query, much of which are not always relevant to the users information needs[10]. Query expansion technology is an effective method for improving the query precision in the information retrieval field. And some search

D.-S. Huang et al. (Eds.): ICIC 2009, LNAI 5755, pp. 154–165, 2009.

engines have used it for improving the query precision[20]. Query expansion technology can improve the efficiency of the search engine by adding other terms which are closely related to the original query terms and disambiguate the user query.

Recently, some advanced data mining methods, especially association rules mining are used for query expansion. It can extract lots of potential correlations between query terms and non-query terms which user cannot find them out directly from a huge web page database. Using these potential correlations, more additional terms besides query terms can be gained. But unfortunately, the complexity of this problem is exponential to the size of the database. In the literature, efficient algorithms for mining association rules have been presented, such as Apriori algorithm [18]. In fact, the set of association rules contain a lot of redundancy, and can rapidly grow to be unwieldy, especially as we tackle large databases or lower the frequency requirements.

In this paper, we propose the variable precision concepts(VPC). And we are concerned with the conclusions based on VPC. A query expansion application based on VPC is given. In the next Section, some preliminaries knowledge are introduced. Section 3 is devoted to propose VPC. Some conclusions are given in Section 4, and we are concerned with the query expansion applications based on these conclusions. Conclusion is Section 5.

2 Preliminaries

Definition 1. *[1] Let an information system S=(U,A,V,f), where U is a non-empty finite set of objects, A is a non-empty finite set of attributes,* $V = \bigcup_{a \in A} V_a$ *and* V_a *is the domain of a,* $f : U \times A \to V$ *is information function.*

Theorem 1. *[3] S = (U, A, V, f) is an information system,* $\forall B \subseteq A$*,let*

$$R_B = \{(x_i, x_j) | f_l(x_i = f_l(x_j)(a_l \in B))\} \tag{1}$$

then R_B *is an equivalence relation based on U. Let*

$$[x_i]_B = \{x_j | (xi, x_j) \in R_B\} \tag{2}$$

then $U/R_B = \{[x_i] | x_i \in U\}$ *can be called the classes of U.*

Definition 2. *[2] A formal context is organized as (U,A,I), where* $U = \{x_1, x_2, \cdots, x_n\}$ *is the set of objects,* $A = \{a_1, a_2, \cdots, a_m\}$ *is the set of attributes, I is the binary relation between U and A. And* $I \subseteq U \otimes A$*,* $(x, a) \in I$ *denotes object x has the attribute a, and* $(x, a) \notin I$ *denotes object x does not have the attribute a, where* $x \in U, a \in A$*.*

Remark 1. Let 1 denotes $(x, a) \in I$, 0 denotes $(x, a) \notin I$. Then this formal context can be seen as an information system with only 0 or 1.

Definition 3. *[3] For a formal context (U, A, I), define operators* $\uparrow$ *and* $\downarrow$ *on* $X \subseteq U$ *and* $B \subseteq A$ *respectively:*

$$X^{\uparrow} = \{a \in A | \forall x \in X, (x, a) \in I\}, \tag{3}$$

$$B^{\downarrow} = \{x \in U | \forall a \in B, (x, a) \in I\}. \tag{4}$$

$\forall x \in U, let \{x\}^{\uparrow} = x^{\uparrow}$, *and* $\forall a \in A$, *let* $\{a\}^{\downarrow} \in a^{\downarrow}$

Definition 4. *[3] For a formal context (U, A, I), if* $x \in U$, $x^{\uparrow} \neq \emptyset, x^{\uparrow} \neq A$ *and* $\forall a \in A, a^{\downarrow} \neq \emptyset, a^{\downarrow} \neq U$, *then the formal context is called positive.*

Definition 5. *[2] For a formal context (U, A, I), if a pair (X,B) satisfies* $X^{\uparrow} = B$ *and* $B^{\downarrow} = X$, *then the pair (X,B) is a concept. Where X is called the extent of the concept, B is called the intent of the concept. And let L(U, A, I) denotes the set of all concepts with respect to (U, A, I).*

Theorem 2. *[3] For a formal context (U, A, I),* $\forall X_1, X_2, X \subseteq U, \forall B_1, B_2, B \subseteq A$, *we have these properties:*

- $X_1 \subseteq X_2 \Rightarrow X_2^{\uparrow} \subseteq X_1^{\uparrow}, B_1 \subseteq B_2 \Rightarrow B_2^{\downarrow} \subseteq B_1^{\downarrow}$;
- $X \subseteq X^{\uparrow\downarrow}, B \subseteq B^{\downarrow\uparrow}$
- $X^{\uparrow} = X^{\uparrow\downarrow\uparrow}, B^{\downarrow} = B^{\downarrow\uparrow\downarrow}$
- $X \subseteq B^{\downarrow} \Leftrightarrow B \subseteq X^{\uparrow}$
- $(X_1 \cap X_2)^{\uparrow} = X_1^{\uparrow} \cap X_2^{\uparrow}, (B_1 \cup B_2)^{\downarrow} = B_1^{\downarrow} \cup B_2^{\downarrow}$
- $(X_1 \cap X_2)^{\uparrow} \supseteq X_1^{\uparrow} \cup X_2^{\uparrow}, (B_1 \cap B_2)^{\downarrow} = B_1^{\downarrow} \cap B_2^{\downarrow}$
- $(X^{\uparrow\downarrow}, X^{\uparrow}) and (B^{\downarrow}, B^{\downarrow\uparrow})$ *are concepts*

Theorem 3. *[2,3] If* $(X_i, B_i), (i = 1, 2, \cdots, k)$ *are concepts, then*

$$(X_i, B_i) \wedge (X_j, B_j) = (X_i \wedge X_j, (B_i \cup B_j)^{\downarrow\uparrow}) \tag{5}$$

$$(X_i, B_i) \vee (X_j, B_j) = ((X_i \cup X_j)^{\uparrow\downarrow}, (B_i \cap B_j)) \tag{6}$$

$(i \neq j), 1 \leq i \leq k, 1 \neq j \neq k$ *and*

$$\bigvee_{i=1}^{k} (X_i, B_i) = ((\bigcup_{i=1}^{k} X_i)^{\uparrow\downarrow}, \bigcap_{i=1}^{k} B_i) \tag{7}$$

$$\bigwedge_{i=1}^{k} (X_i, B_i) = ((\bigcap_{i=1}^{k} X_i), (\bigcup_{i=1}^{k} B_i)^{\downarrow\uparrow}) \tag{8}$$

are all concepts.

Definition 6. *[3] Let L(U, A, I) denotes the set of all the concepts of the formal context (U, A, I). If* $(X_1, B_1), (X_2, B_2) \in L(U, A, I)$, *then let*

$$(X_1, B_1) \leq (X_2, B_2) \Leftrightarrow X_1 \subseteq X_2 (\Leftrightarrow B_1 \supseteq B_2) \tag{9}$$

then " $\leq$ " *is a partial relation of* $L(U, A, I)$.

3 Variable Precision Concepts

Definition 7. *(U,A,I) is a formal context, according to Definition 7.* $\forall x \in U, x^{\uparrow} = \{a \in A | (x,a) \in I\}$ *and* $\forall a \in A, a^{\downarrow} = \{x \in U | (x,a) \in I\}$*, for* β *in*$(0.5, 1]$*,* $X \subseteq U, B \subseteq A$ *let*

$$X_{\beta}^{\uparrow} = \{a \in A | \frac{|a^{\downarrow} \cap X|}{|X|} \geq \beta\} \tag{10}$$

$$B_{\beta}^{\downarrow} = \{x \in U | \frac{|x^{\uparrow} \cap B|}{|B|} \geq \beta\} \tag{11}$$

$\forall a \in A, \forall x \in U, \{a\}_{\beta}^{\downarrow} = a_{\beta}^{\downarrow}, \{x\}_{\beta}^{\uparrow} = x_{\beta}^{\uparrow}$

Note 1. If $X = \emptyset$, then $\forall a \in A$, denote $\frac{|\emptyset \cap a^{\downarrow}|}{|\emptyset|} = \frac{|\emptyset|}{|\emptyset|} = 1$ then $^{\uparrow} = A, \emptyset_{\beta}^{\downarrow} = U$

Definition 8. *For a formal context (U, A, I), if a pair* $(X, B)_{\beta}$ *can be called as a variable precision concept or* β *concept if and only if* $\exists(X^{'}, B^{'}) \in L(U, A, I)$*, s.t.,* $X^{'} \subseteq X \subseteq B_{\beta}^{'}, B^{'} = B, \frac{|X^{'}|}{|X|} \geq \beta or X^{'} = X, B^{'} \subseteq B \subseteq X_{\beta}^{'}, \frac{|B^{'}|}{|B|} \geq \beta$*. Where X is called the extent of the variable precision concept, B is called the intent of the variable precision concept. And let* $L_{\beta}(U, A, I)$ *denotes the set of all* β *concepts with respect to (U, A, I).*

Theorem 4. *For a formal context (U, A, I),* $(X, B) \in L_{\beta}(U, A, I) \Leftrightarrow \exists Y \subseteq U$*, s.t.,* $Y^{\uparrow\downarrow} \subseteq X \subseteq (Y^{\uparrow})_{\beta}^{\downarrow}, B = Y^{\uparrow}, \frac{|Y^{\uparrow\downarrow}|}{|X|} \geq \beta$ *or* $X = Y^{\uparrow\downarrow}, Y^{\uparrow} \subseteq B \subseteq (Y^{\uparrow\downarrow})_{\beta}^{\uparrow}, \frac{|Y^{\uparrow}|}{|B|} \geq \beta. Where, X \subseteq U, B \subseteq A.$

Proof. $\forall Y \subseteq U, if x \in Y^{\uparrow\downarrow} \Rightarrow \forall a \in Y^{\uparrow}, (x,a) \in I \Rightarrow \forall a \in Y^{\uparrow}, a \in x^{\uparrow} \Rightarrow Y^{\uparrow} \subseteq x^{\uparrow}, if x \notin (Y^{\uparrow})_{\beta}^{\downarrow} \Rightarrow \frac{|x^{\uparrow} \cap Y^{\uparrow}|}{|Y^{\uparrow}|} < \beta \Rightarrow \frac{|Y^{\uparrow}|}{|Y^{\uparrow}|} = 1 < \beta$, it is impossible. So, $\forall x \in Y^{\uparrow\downarrow} \Rightarrow x \in (Y^{\uparrow})_{\beta}^{\downarrow}, i.e., Y^{\uparrow\downarrow} \subseteq (Y^{\uparrow})_{\beta}^{\downarrow}$. If $a \in Y^{\uparrow\downarrow\uparrow} \Rightarrow \forall x \in Y^{\uparrow\downarrow}, (x,a) \in I \Rightarrow \forall x \in Y^{\uparrow\downarrow}, x \in a^{\downarrow} \Rightarrow Y^{\downarrow\uparrow} \subseteq a^{\downarrow} \Rightarrow \frac{|a^{\downarrow} \cap Y^{\uparrow\downarrow}|}{|Y^{\uparrow\downarrow}|} = \frac{|Y^{\uparrow\downarrow}|}{|Y^{\uparrow\downarrow}|} = 1 \geq \beta \Rightarrow a \in (Y^{\uparrow\downarrow})_{\beta}^{\uparrow}, i.e., Y^{\uparrow} = Y^{\uparrow\downarrow\uparrow} \subseteq (Y^{\uparrow\downarrow})_{\beta}^{\uparrow}$. □

Due to $\forall Y \subseteq U \Rightarrow (Y^{\uparrow\downarrow}, Y^{\uparrow})$ is a concept(according to Theorem 2), and $\forall (X, B) \in L(U, A, I) \Rightarrow \exists Y \subseteq U$ s.t., $Y^{\uparrow} = B, Y^{\uparrow\downarrow} = X$. Because, when Y=X, it holds obviously. Therefore, $(X, B) \in L(U, A, I) \Leftrightarrow \exists Y = X \subseteq U$, s.t., $(Y^{\uparrow\downarrow}, Y^{\uparrow}) \in L(U, A, I)$.

Then according to Definition 8, $(X, B)_{\beta} \in L_{\beta}(U, A, I) \Leftrightarrow \exists(X^{'}, B^{'}) \in L(U, A, I)$, s.t., $X^{'} \subseteq X \subseteq B_{\beta}^{'}, B^{'} = B, \frac{|X^{'}|}{|X|} \geq \beta$ or $X^{'} = X, B^{'} \subseteq B \subseteq X_{\beta}^{'\downarrow}, \frac{|B^{'}|}{|B|} \geq \beta \Leftrightarrow \exists Y \subseteq U$,s.t., $Y^{\uparrow\downarrow} \subseteq X \subseteq (Y^{\uparrow})_{\beta}^{\downarrow}, B = Y^{\uparrow}, \frac{|Y^{\uparrow\downarrow}|}{|X|} \geq \beta or X = Y^{\uparrow\downarrow}, Y^{\uparrow} \subseteq B \subseteq (Y^{\uparrow\downarrow})_{\beta}^{\uparrow}, \frac{|Y^{\uparrow}|}{|B|} \geq \beta$. Thus, this theorem holds.

Theorem 5. *For a formal context(U,A,I),if* $\beta = 1, X_{\beta}^{\uparrow} = B^{\downarrow}$.

Proof. When $\beta = 1, a \in X_\beta^\uparrow \Leftrightarrow \frac{|a^\downarrow \cap X|}{|X|} \geq \beta = 1 \Leftrightarrow |a^\downarrow \cap X| = |X| \Leftrightarrow X \subseteq a^\downarrow \Leftrightarrow \forall x \in X, x \in a^\downarrow \Leftrightarrow \forall x \in X, (x, a) \in I \Leftrightarrow a \in X^\uparrow$. Namely,$X_\beta^\uparrow = X^\uparrow$ holds. $B_\beta^\downarrow = B^\downarrow$ holds similarly. □

Remark 2. According to Definition 8 and Theorem 4,5, we can conclude that, β concepts are just generalized concepts.

Remark 3. For a formal context(U,A,I), Let β denotes a mood operator, such as "*most of*","*much of*"*etc.* So, β concepts can be contacted with linguistic value concepts. We can give a map between β_v and mood operator, namely, $f : \beta_v \rightarrow$ mood operator, where β_v is the domain of β, *i.e.*, $\beta_v \subseteq (0.5, 1]$.For example, we define:

- *f((0.5,0.6])="about half of"*,
- *f((0.6,0.7])="much of"*,
- *f((0.7,0.9])="most of"*,
- *f((0.9,1.0])="nearly all of"*,
- *f(1)="all of"*.

Theorem 6. *For a formal context (U,A,I),* $\forall (X, B)_\beta \in L_\beta(U, A, I)$*, we have*

$$\forall x \in X, \frac{|x^\uparrow \cap B|}{|B|} \geq \beta \tag{12}$$

$$\forall a \in B, \frac{|a^\downarrow \cap X|}{|X|} \geq \beta \tag{13}$$

Proof. According to Definition 8, $(X, B)_\beta \in L_\beta(U, A, I) \Leftrightarrow \exists (X^{'}, B^{'}) \in L(U, A, I)$, $s.t., X^{'} \subseteq X \subseteq B_\beta^{'\downarrow}\ B^{'} = B, \frac{|X^{'}|}{|X|} \geq \beta$ or $X^{'} = X, B^{'} \subseteq B \subseteq X_\beta^{'\downarrow}, \frac{|B^{'}|}{|B|} \geq \beta$. If $X^{'} \subseteq X \subseteq B_\beta^{'\downarrow}, B^{'} = B, \frac{|X^{'}|}{|X|} \geq \beta$, then $\forall x \in X, x \in B_\beta^{'\downarrow}$ so, $\frac{|x^\uparrow \cap B|}{|B|} = \frac{|x^\uparrow \cap B^{'}|}{B^{'}} \geq \beta$ and $\forall a \in B = B^{'}$, we have $X^{'} = B^{'\downarrow} \subseteq a^\downarrow$ and due to $X^{'} \subseteq X$ So,$\forall a \in B, X^{'} \subseteq X \cap a^\downarrow$ then $\forall a \in B, \frac{|a^\downarrow \cap X|}{|X|} \geq \frac{|X^{'}|}{|X|} \geq \beta$ If $X^{'} = X, B^{'} \subseteq B \subseteq X_\beta^{'\downarrow}, \frac{|B^{'}|}{|B|} \geq \beta$,similarity to prove. This problem holds. □

Example 1. According to Remark 3 and Theorem 6, Let $\beta = 0.8$, then we can describe a 0.8 concept as follows:

* $\forall a \in Y^\uparrow$, most of X have it;
* $\forall x \in Y^{\uparrow\downarrow}$,has most of elements of B.

Theorem 7. *For a formal context (U, A, I),* $\beta \in (0.5, 1], \forall Y \subseteq U$*, let*

$$\gamma = |(Y^\uparrow)_\beta^\downarrow| - |Y^{\uparrow\downarrow}| \tag{14}$$

$$\eta = |(Y^{\uparrow\downarrow})_\beta^\uparrow| - |Y^\uparrow| \tag{15}$$

$$\zeta = min\{\lfloor\frac{|Y^{\uparrow\downarrow}|}{\beta}\rfloor, |(Y^{\uparrow})^{\downarrow}_{\beta}|\} - |Y^{\uparrow}| \tag{16}$$

$$\xi = min\{\lfloor\frac{|Y^{\uparrow}|}{\beta}\rfloor, |(Y^{\uparrow\downarrow})^{\uparrow}_{\beta}|\} - |Y^{\uparrow}| \tag{17}$$

then

$$|L_{\beta}(U,A,I)| \leq |L(U,A,I)| + \sum_{(Y^{\uparrow\downarrow},Y^{\uparrow})\in L(U,A,I)} (\sum_{i=1}^{\zeta} C_{\gamma}^{i} + \sum_{j=1}^{\xi} C_{\eta}^{j}) \tag{18}$$

Where, $|(Y^{\uparrow})^{\downarrow}_{\beta}|$ *denotes the power of the set* $\frac{|Y^{\uparrow\downarrow}|}{\beta}$*) and when* $i > \gamma, C_{\gamma}^{i} = 0$.

Proof. According to Theorem 4, $(X,B) \in L_{\beta}(U,A,I) \Leftrightarrow \exists Y \subseteq U, s.t., Y^{\uparrow\downarrow} \subseteq X \subseteq (Y^{\uparrow})^{\downarrow}_{\beta}, B = Y^{\uparrow}, \frac{|Y^{\uparrow\downarrow}|}{|X|} \geq \beta$ or $X = Y^{\uparrow\downarrow}, Y^{\uparrow} \subseteq B \subseteq (Y^{\uparrow\downarrow})^{\uparrow}_{\beta}, \frac{|Y^{\uparrow}|}{B} \geq \beta$ so,$|Y^{\uparrow\downarrow}| \leq |X| \leq |(Y^{\uparrow})^{\downarrow}_{\beta}|, |Y^{\uparrow\downarrow}| \leq |X| \leq \frac{|Y^{\uparrow\downarrow}|}{\beta}, |B| = |Y^{\uparrow}|$ or $|Y^{\uparrow}| \leq |B| \leq |(Y^{\uparrow\downarrow})^{\uparrow}_{\beta}|, |Y^{\uparrow}| \leq |B| \leq \frac{|Y^{\uparrow}|}{\beta}, |X| = |Y^{\uparrow\downarrow}|, i.e., |Y^{\uparrow\downarrow}| \leq |X| \leq min\{\lfloor\frac{|Y^{\uparrow\downarrow}|}{\beta}\rfloor, |(Y^{\uparrow})^{\downarrow}_{\beta}|\}$, $|B| = |Y^{\uparrow}|$ or $|Y^{\uparrow}| \leq |B| \leq min\{\lfloor\frac{|Y^{\uparrow}|}{\beta}\rfloor, |(Y^{\uparrow\downarrow})^{\uparrow}_{\beta}|\}, |X| = |Y^{\uparrow\downarrow}|$. Then $\forall(Y^{\uparrow\downarrow}, Y^{\uparrow}) \in L(U,A,I)$, if $Y^{\uparrow\downarrow} \subseteq X \subseteq (Y^{\uparrow})^{\downarrow}_{\beta}, B = Y^{\uparrow}, |Y^{\uparrow\downarrow}| \leq |B| \leq min\{\lfloor\frac{|Y^{\uparrow\downarrow}|}{\beta}\rfloor$ $|(Y^{\uparrow})^{\downarrow}_{\beta}|\}$ or $X = Y^{\uparrow\downarrow}, Y^{\uparrow} \subseteq B \subseteq (Y^{\uparrow\downarrow})^{\uparrow}_{\beta}, |Y^{\uparrow\downarrow}| \leq |B| \leq min\{\lfloor\frac{|Y^{\uparrow}|}{\beta}\rfloor, |(Y^{\uparrow\downarrow})^{\uparrow}_{\beta}|\}$, $(X,B) \in L_{\beta}(U,A,I)$. Therefore, $\forall(Y^{\uparrow\downarrow}, Y^{\uparrow}) \in L(U,A,I)$, there are at most $(\sum_{i=1}^{\zeta} C_{\gamma}^{i} + \sum_{j=1}^{\xi} C_{\eta}^{j} + 1)$ variable precision concepts accordingly, where the added number 1 denotes the classical concept$(Y^{\uparrow\downarrow}, Y^{\uparrow})$. Thus, the theorem holds. □

Theorem 8. *For a formal context (U, A, I),* $\beta \in (0.5, 1], \forall a, b \in X^{\uparrow}_{\beta} \Rightarrow a^{\downarrow} \cap b^{\downarrow} \neq \emptyset; \forall x, y \in B^{\downarrow}_{\beta} \Rightarrow x^{\uparrow} \cap y^{\uparrow} \neq \emptyset$.

Proof. $\forall a, b \in X^{\uparrow}_{\beta} \Rightarrow \frac{|a^{\downarrow}\cap X|}{|X|} \geq \beta, \frac{|b^{\downarrow}\cap X|}{|X|} \geq \beta \Rightarrow \frac{|a^{\downarrow}\cap X|}{|X|} + \frac{|b^{\downarrow}\cap X|}{|X|} \geq 2\beta \Rightarrow \frac{|a^{\downarrow}\cap X|+|b^{\downarrow}\cap X|}{|X|} \geq 2\beta \Rightarrow \frac{|(a^{\downarrow}\cap X)\cup(b^{\downarrow}\cap X)|+|(a^{\downarrow}\cap X)\cap(b^{\downarrow}\cap X)|}{|X|} \geq 2\beta \Rightarrow \frac{|(a^{\downarrow}\cup b^{\downarrow})\cap X)|+|a^{\downarrow}\cap b^{\downarrow}\cap X|}{|X|} \geq 2\beta$ If $a^{\downarrow} \cap b^{\downarrow} = \emptyset$, then $\frac{|(a^{\downarrow}\cup b^{\downarrow})\cap X|}{|X|} \geq 2\beta > 1, i.e., |(a^{\downarrow} \cup b^{\downarrow})\cap X| > |X|$. It is inconsistent with $|(a^{\downarrow}\cup b^{\downarrow})\cap X| \leq |X|$. Therefore, $a^{\downarrow}\cap b^{\downarrow} \neq \emptyset$. The same to prove $\forall x, y \in B^{\downarrow}_{\beta} \Rightarrow x^{\downarrow} \cap y^{\downarrow} \neq \emptyset$. The theorem holds. □

Corollary 1. *For a formal context (U, A, I),* $\beta \in (0.5, 1], \forall a, b \in X^{\uparrow}_{\beta} \Rightarrow \exists x \in X, s.t., x \in a^{\downarrow}, x \in b^{\downarrow}; \forall x, y \in B^{\downarrow}_{\beta} \Rightarrow \exists a \in B, s.t., a \in x^{\uparrow}, a \in y^{\uparrow}$.

Proof. According to the Theorem 8, $\forall a, b \in X^{\uparrow}_{\beta} \Rightarrow \frac{|(a^{\downarrow}\cup b^{\downarrow})\cap X)|+|a^{\downarrow}\cap b^{\downarrow}\cap X|}{|X|} \geq 2\beta > 1$ If $a^{\downarrow} \cap b^{\downarrow} \cap X = \emptyset$ then $\frac{|(a^{\downarrow}\cup b^{\downarrow})\cap X|}{|X|} \geq 2\beta > 1, i.e., |(a^{\downarrow} \cup b^{\downarrow}) \cap X| > |X|$. It is inconsistent with $|(a^{\downarrow} \cup b^{\downarrow}) \cap X| \leq |X|$. Therefore, $a^{\downarrow} \cap b^{\downarrow} \cap X \neq \emptyset$. Namely, $\exists x \in X, s.t., x \in a^{\downarrow}, x \in B^{\downarrow}$. The same to prove $\forall x, y \in B^{\downarrow}_{\beta} \Rightarrow \exists a \in B, s.t., a \in x^{\uparrow}, a \in y^{\uparrow}$. □

Theorem 9. *For a formal context (U, A, I),*$\beta \in (0.5, 1]$ *if* $|X| \leq 2, a \in X_\beta^\uparrow \Leftrightarrow x \subseteq a^\downarrow$; *if* $|B| \leq 2, x \in B_\beta^\downarrow \Leftrightarrow B \subseteq x^\uparrow$.

Proof. When $|X| = 0, i.e., X = \emptyset$ then $a \in_\beta^\uparrow = A$. When $|X| = 1, a \in X_\beta^\uparrow \Leftrightarrow \frac{|a^{\downarrow} \cap X|}{|X|} \geq \beta \Leftrightarrow |a^{\downarrow} \cap X| \geq \beta |X| \geq \beta \Leftrightarrow |a^\downarrow \cap X| = 1 \Leftrightarrow X \subseteq a^\downarrow$. When $|X| = 2, a \in X_\beta^\uparrow \Leftrightarrow |a^\downarrow \cap X| \geq \beta |X| \geq 2\beta > 1 \Leftrightarrow |a^\downarrow \cap X| = 2 \Leftrightarrow X \subseteq a^\downarrow$. The same to prove if $|B| \leq 2, x \in B_\beta^\downarrow \Leftrightarrow B \subseteq x^\uparrow$. The theorem holds. □

Theorem 10. *For a formal context(U,A,I),* $\beta \in (0.5, 1]$ *if* $|X| \leq 2, X_\beta^\uparrow = X^\uparrow$; *if* $|B| \leq 2, B_\beta^\downarrow = B^\downarrow$.

Proof. According to Theorem 9, if $|X| \leq 2, \forall a \in X_\beta^\uparrow \Leftrightarrow X \subseteq a^\downarrow \Rightarrow a^{\uparrow\downarrow} \subseteq X^\uparrow$(according to Theorem 2), if $a \notin X^\uparrow$, then $a \notin a^{\downarrow\uparrow}$, it is inconsistent with Theorem 2, so, $a \in X^\uparrow, i.e., X_\beta^\uparrow \subseteq X^\uparrow$. Then $\forall b \in X^\uparrow \Rightarrow X^{\uparrow\downarrow} \subseteq b^\downarrow$(according to Theorem 2), and due to $X \subseteq X^{\uparrow\downarrow}$, so, $X \subseteq b^\downarrow$, then $\frac{|b^\downarrow \cap X|}{|X|} = \frac{|X|}{|X|} = 1 \geq \beta, i.e., b \in X_\beta^\uparrow$, namely,$X^\uparrow \subseteq X_\beta^\uparrow$. similarly to prove when $|B| \leq 2, B_\beta^\downarrow = B_\downarrow$. □

Example 2. For a formal context (U,A,I), where $U = \{document 1, 2, 3, 4\}, A = \{AI, ML, SVM, DM, NN\}, (d_1, AI) \in I$ denotes document 1 has keyword *"AI"*. In Table 1, there are six concepts (see Fig 1). According to Theorem 10, we only calculate $X_\beta^\uparrow$ when $|X| \geq 3$ and $B_\beta^\downarrow$ when$|B| \geq 3$. So, let $\beta = 0.6$, these equations obtained as follows:

$$U_{0.6}^\uparrow = \{AI, ML\}, \tag{19}$$

$$\{AI, ML, DM, NN\}_{0.6}^\downarrow = \{d_1\}, \tag{20}$$

$$\{d_1, d_2, d_4\}_{0.6}^\uparrow = \{AI, ML, SVM\}, \tag{21}$$

$$\{AI, ML, SVM\}_{0.6}^\downarrow = \{d_1, d_2, d_4\}, \tag{22}$$

$$A_{0.6}^\downarrow = \{d_1, d_2, d_4\}. \tag{23}$$

Then we can obtain one variable precision concept except for classical concepts as:$(\{d_1, d_2, d_4\}), \{AI, ML, SVM\}$. Because of for the classical concept $((\{d_1, d_2, d_4\}, \{AI, ML\})), \{d_1, d_2, d_4\}, \{AI, ML\} \subseteq \{AI, ML, SVM\} \subseteq \{d_1, d_2, d_4\}_{0.6}^\uparrow$ and $\frac{|\{AI,ML\}|}{|\{AI,ML,SVM\}|} = \frac{2}{3} \geq 0.6$.

Table 1. A formal context

$U \backslash A$	Artificial Intelligent(AI)	Machine Learning(ML)	Support Vector Machine(SVM)	Data Mining (DM)	Neural Network(NN)
document 1	×	×		×	×
document 2	×	×	×		
document 3				×	
document 4	×	×	×		

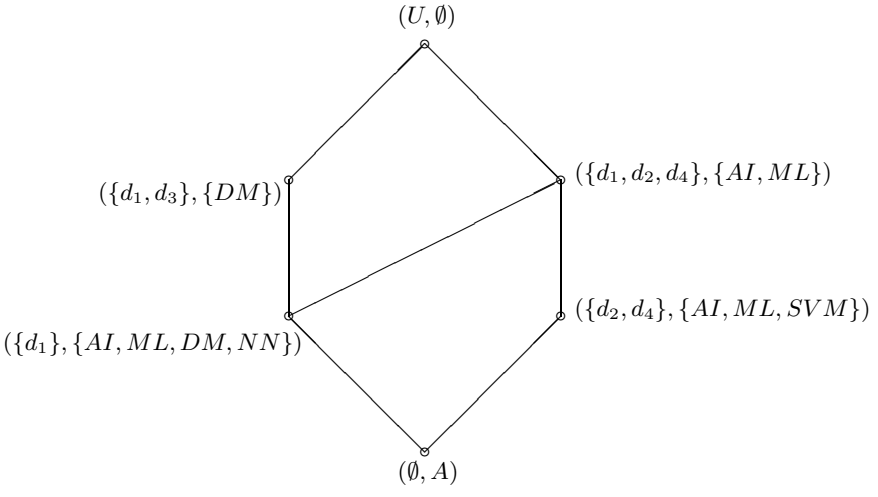

Fig. 1. The concepts Lattice of(U, A, I)

4 Applications Based on VPC

Theorem 11. *(U,A,I) is a formal context, and* $\beta \in (0.5, 1], \forall a \in A, a^{\downarrow} \subseteq (a^{\uparrow\downarrow})^{\downarrow}_{\beta}$, *and* $\forall x \in U, x^{\uparrow} \in U, x^{\uparrow} \subseteq (x^{\uparrow\downarrow})^{\uparrow}_{\beta}$.

Proof. $\forall a \in A$,if $a^{\downarrow}! \subseteq (a^{\downarrow\uparrow})^{\downarrow}_{\beta}$, then $\exists x \in a^{\downarrow}$ and $x \notin (a^{\downarrow\uparrow})^{\downarrow}_{\beta}, i.e., (x, a) \in I$ and $\frac{|x^{\uparrow} \cap a^{\downarrow\uparrow}|}{|a^{\downarrow\uparrow}|} < \beta$. Due to $x \in a^{\downarrow}$, then $a^{\downarrow\uparrow} \subseteq x^{\uparrow}$ (according to Theorem 2), $\frac{|x^{\uparrow} \cap a^{\downarrow\uparrow}|}{|a^{\downarrow\uparrow}|} = \frac{|a^{\downarrow\uparrow}|}{|a^{\downarrow\uparrow}|} = 1$, it is inconsistent with $\frac{|x^{\uparrow} \cap a^{\downarrow\uparrow}|}{|a^{\downarrow\uparrow}|} < \beta < 1$ Therefore, $a^{\downarrow} \subseteq (a^{\downarrow\uparrow})^{\downarrow}_{\beta}$. The same to prove $\forall x \in U, x^{\uparrow} \subseteq (x^{\uparrow\downarrow})^{\uparrow}_{\beta}$. □

Definition 9. *For a formal context (U,A,I),* $\forall x, y \in U$ *or* $\forall a, b \in A$, *We define their correlative degrees* $COR^{\uparrow}(x, y)$ *or* $COR^{\downarrow}(a, b)$ *as follows:*

$$COR^{\uparrow}(x, y) = \frac{|x^{\uparrow} \cap y^{\uparrow}|}{|x^{\uparrow} \cup y^{\uparrow}|}, \quad COR^{\downarrow}(a, b) = \frac{|a^{\downarrow} \cap b^{\downarrow}|}{|a^{\downarrow} \cup b^{\downarrow}|} \tag{24}$$

Theorem 12. *For a formal context (U,A,I),* $\forall X \subseteq U, B \subseteq A, if (X, B)_{\beta} \in L(U, A, I)_{\beta}$, *then* $\forall x, y \in X$, *or* $\forall a, b \in B$, *we obtain* $COR^{\uparrow}(x, y) \geq 0$, *or* $COR^{\downarrow}(a, b) \geq 0$.

Proof. According to Theorem 8, this theorem holds obviously. □

Definition 10. *For a formal context(U,A,I), we define* $\delta(\delta \in (0, 1])$ *correlative relations* $COR^{\uparrow}_{\delta}$ *and* $COR^{\downarrow}_{\delta}$ *as follows,*

$$COR^{\uparrow}_{\delta} = \{(x, y) \in U^2 | COR^{\uparrow}(x, y) \geq \delta\} \tag{25}$$

$$COR^{\downarrow}_{\delta} = \{(a, b) \in A^2 | COR^{\downarrow}(a, b) \geq \delta\} \tag{26}$$

Theorem 13. *Relations $COR_\delta^\uparrow$ and $COR_\delta^\downarrow$ are reflective and symmetrical, but not transitive.*

Proof. $\forall x \in U, \frac{|x^\uparrow \cap x^\uparrow|}{|x^\uparrow \cup x^\uparrow|} = 1 \geq \delta$, so $(x,x) \in COR_\delta^\uparrow, i.e., COR_\delta^\uparrow$ is reflective. $\forall (x,y) \in COR_\delta^\uparrow \Rightarrow COR^\uparrow(x,y) \geq \delta \Rightarrow \frac{|x^\uparrow \cap y^\uparrow|}{|x^\uparrow \cup y^\uparrow|} \geq \delta \Rightarrow COR^\uparrow(y,x) \geq \delta \Rightarrow (y,x) \in COR_\delta^\uparrow, i.e., COR_\delta^\uparrow issymmetrical$. If $x^\uparrow = \{a_1, a_2\}, y^\uparrow = \{a_2, a_3\}, z^\uparrow = \{a_3, a_4\}$, then $(x,y) \in COR_{0.3}^\uparrow, (y,z) \in COR_{0.3}^\uparrow$, but $(y,z) \notin COR_{0.3}^\uparrow$, namely, $COR_\delta^\uparrow$ is not transitive. Similarly to prove $COR_\delta^\downarrow$. □

Remark 4. According to Remark 1, a formal context (U, A, I) can be transformed into a information system $(U, A, \{0,1\}, f)$. Where $(x,a) \in I \Leftrightarrow f_a(x) = 1, (x,a) \notin I \Leftrightarrow f_a(x) = 0$, and $x \in U, a \in A$.

Theorem 14. *For a formal context (U, A, I) and its transform$(U, A, \{0,1\}, f)$, if $\delta = 1$, then $(x,y) \in COR_1^\uparrow \Leftrightarrow (x,y) \in COR_\delta^\uparrow \Leftrightarrow (x,y) \in R_A$, where, $x, y \in U$.*

Proof. $(x,y) \in COR_1^\uparrow \Leftrightarrow COR_1^\uparrow(x,y) \geq 1 \Leftrightarrow \frac{|x^\uparrow \cap y^\uparrow|}{|x^\uparrow \cup y^\uparrow|} \geq 1 \Leftrightarrow x^\uparrow = y^\uparrow \Leftrightarrow \forall a \in A, a \in x^\uparrow$ if and only if $a \in y^\uparrow \Leftrightarrow \forall a \in A, f_a(x) \Leftrightarrow (x,y) \in R_A$. The theorem holds. □

Definition 11. *For a formal context (U, A, I), $\forall x \in U$, or $\forall a \in A$, we define δ correlative classes $[x]_\delta^\uparrow$ or $[a]_\delta^\downarrow$ as follows:*

$$[x]_\delta^\uparrow = \{y \in U | (x,y) \in COR_\delta^\uparrow\} \tag{27}$$

$$[a]_\delta^\downarrow = \{b \in A | (a,b) \in COR_\delta^\downarrow\} \tag{28}$$

Theorem 15. *For a formal context (U, A, I) and its transform $(U, A, \{0,1\}, f)$, if $\delta = 1, [x]_\delta^\uparrow = [x]_{R_A}$, where, $x \in U$.*

Proof. When $\delta = 1, y \in [x]_\delta^\uparrow \Leftrightarrow (x,y) \in COR_\delta^\uparrow \Leftrightarrow R_A$(according to Theorem 14) $\Leftrightarrow y \in [x]_{R_A}$ (according to Theorem 1), so, $\forall x \in U, [x]_\delta^\uparrow = [x]_{R_A}$. □

Theorem 16. *For a formal context (U,A,I) and $\delta \in (0,1], \forall x \in U, x^\uparrow \subseteq \bigcup_{y \in [x]_\delta^\uparrow} y^\uparrow$, and $\forall a \in A, a^\downarrow \subseteq \bigcup_{b \in [a]_\delta^\downarrow} b^\downarrow$.*

Proof. $\forall x \in U, x \in [x]_\delta^\uparrow$, because of $\frac{|x^\uparrow \cap x^\uparrow|}{x^\uparrow \cup x^\uparrow} = 1 \geq \delta$, then $(x,x) \in COR_\delta^\uparrow, i.e., x \in [x]_\delta^\uparrow$. Therefore, $x^\uparrow \subseteq x^\uparrow \cup \bigcup_{y \in ([x]_\delta^\uparrow - x)} y^\uparrow$. The same to prove $\forall a \in A, a^\downarrow \subseteq \bigcup_{b \in [a]_\delta^\downarrow} b^\downarrow$. □

Theorem 17. *For a formal context (U, A, I), and $\beta \in (0.5, 1]$, $a \in A, a^\downarrow \subseteq \bigcup_{b \in (a^\downarrow)_\beta^\uparrow} b^\downarrow$, and $\forall x \in U, x^\uparrow \subseteq \bigcup_{y \in (x^\uparrow)_\beta^\downarrow} y^\uparrow$.*

Proof. Due to $\frac{|x^\uparrow \cap x^\uparrow|}{|x^\uparrow|} = 1 \geq \beta$, so,$\forall x \in U, x \in (x^\uparrow)_\beta^\downarrow$, then $x^\uparrow \subseteq x^\uparrow \cup \bigcup_{y \in ((x^\uparrow)_\beta^\downarrow - x)} y^\uparrow = \bigcup_{y \in (x^\uparrow)_\beta^\downarrow} y^\uparrow$. The same to prove $\forall a \in A, a^\downarrow \subseteq \bigcup_{b \in (a^\downarrow)_\beta^\uparrow} b^\downarrow$. □

Corollary 2. *According to Theorem11, Theorem 16 and Theorem 17, if we want to search some documents based on one or more keywords denoted by* $a_1, a_2, \cdots, a_r$. *Then we can provide the results as follows,*

$$\bigcup_{i=1}^{r}(a^{\downarrow\uparrow})_{\beta}^{\downarrow} \text{ or} \qquad \bigcup_{i=1}^{r}(\bigcup_{b\in[a_i]_{\delta}^{\downarrow}} b^{\downarrow}) \text{ or} \qquad \bigcup_{i=1}^{r}(\bigcup_{b\in(a_i^{\downarrow})_{\beta}^{\uparrow}} b^{\downarrow})$$

Where, β *and* δ *are both the threshold value. From this point, we can search the documents which contain some keywords we will search or do not contain any keyword but have many other keywords that have related with the searched keywords. Then we can use this documents better, and we can process fuzzy search.*

According to Corollary 2, we apply variable precision concepts in another area. In this application, we can give some better advices with respect to some special requirements.

Example 3. In Table 2, there are twelve mobile telephones as the set of objects. *i.e.*, U, and eight functions as the set of attributes, *i.e.*, A. Then let I is a binary relation between U and A, and $I \subseteq U \otimes A$. For example,$(document7, M) \in I$ denotes document 7 has keyword "*Mp3-player(M)*".

Table 2. A formal context about web documents

	JAVA (J)	Blue-Tooth (B)	Infrared (I)	FM-Radio (F)	Record (R)	Mp3-Player (M)	Camera (C)	GPRS (G)
document1	×				×		×	×
document2	×		×				×	×
document3					×			
document4	×				×		×	×
document5							×	
document6	×		×		×		×	×
document7		×			×	×	×	×
document8					×			
document9	×				×			×
document10	×		×	×	×			×
document11	×	×	×		×	×	×	×
document12	×	×			×	×	×	×

Remark 5. From a formal context, we can use some attributes to satisfy our requirements. And based on Corollary 2, we expand our results in order to satisfy our requirements better.

Based on the discussion of Remark 5, if someone want to search a web page which has some relevant web pages, as a search engine, it will provide some query expansion results.

Let $\delta = 0.35, \beta = 0.6$, we can obtain these equations as follows,

$$M^{\downarrow} = \{document7, document11, document12\} \tag{29}$$

$$(M^{\downarrow\uparrow})^{\downarrow}_{0.6} = \{document1, 4, 6, 7, 11, 12\} \tag{30}$$

$$\bigcup_{b \in [M]^{\downarrow}_{0.35}} b^{\downarrow} = \{document1, 2, 4, 5, 6, 7, 11, 12\} \tag{31}$$

$$\bigcup_{b \in (M^{\downarrow})^{\uparrow}_{0.6}} b^{\downarrow} = U \tag{32}$$

From these equations, the search engine gives users some results as follows,

- *document 7,11,12 will be given according to user's query.*
- *document 1,4, 6 are the extended web pages relevant to web pages 7,11,12.*
- *document 2, 5 are the extended web pages relevant to web pages 1,4,6,7,11,12.*

5 Conclusion

In this paper, we firstly proposed the variable precise concepts(VPC) in terms of classical definition of concepts can not describe something clearly. Some important properties and conclusions of VPC are discussed. To illustrate the advantage of our proposed new theory (VPC), we applied it into an application for query expansion in web pages database. The experiments show that VPC is efficient for expanding the relevant web pages for user's current query.

References

1. Pawlak, Z.: Rough Sets. International Journal of Computer and Information Science 11(5), 341–356 (1982)
2. Ganter, B., Wille, R.: Formal Concept Analysis. In: Mathematical Foundations. Springer, Heidelberg (1999)
3. Zhang, W.X., Qiu, G.F.: Uncertain Decision Making Based on Rough Sets, pp. 12–58. Tsinghua University Publisher, Beijing (2005) (in Chinese)
4. Birkhoff, B.: Lattice Theory. American Mathematical Society Colloquium Publ., Providence (1973) (revised edition)
5. Wille, R.: Restructuring the Lattice Theory: An Approach Based on Hierarchies of Concepts. In: Rival, I. (ed.) Ordered Sets, pp. 445–470. Reidel, Dordrecht (1982)
6. Wille, R.: Lattices in Data Analysis: How to Draw Them with a Computer. In: Algorithms and Order, pp. 33–58. Kluwer Acad. Publ., Dordrecht (1989)
7. Wille, R.: Concepe Lattices and Conceptual Knowledge Systems. Comput. Math. Apll. 23(6-9), 493–515 (1992)
8. Ganter, B., Stahl, J., Wille, R.: Concept Measurement and Many-Valued Contexts. In: Gaul, W., Schader, M. (eds.) Classification as a Tool of Research, pp. 169–176. Elsevier Science Publishers B.V, North-Holland (1986)
9. Ganter, B. (ed.): Two Basic Algorithms in Concept Analysis. Technische Hochschule, Darmstadt (1984)
10. Stumme, G., Taouil, R., Yves, B.C., Pasquier, N., Lakhal, L.: Computing Iceberg Concept Lattices with TITANIC. Data & Knowledge Engineering 42, 189–222 (2002)

11. Patrick, D.B.R., Derek, B.: Collaborative Recommending using Formal Concept Analysis. Knowledge-Based Systems 19(5), 309–315 (2006)
12. Kim, M., Tom, T.: Delving Source Code with Formal Concept Analysis. Computer Languages, Systems & Structures 31(3-4), 183–197 (2005)
13. Jitender, S.D., Jamil, S.: Monotone Concepts for Formal Concept Analysis. Discrete Applied Mathematics 144(1-2), 70–78 (2004)
14. Jiang, G.Q., Katsuhiko, O., Akira, E., Tsunetaro, S.: Context-Based Ontology Building Support in Clinical Domains using Formal Concept Analysis. International Journal of Medical Informatics 71(1), 71–81 (2003)
15. Susanne, P.: Formal Concept Analysis for General Objects. Discrete Applied Mathematics 127(2), 337–355 (2003)
16. Karl, E.W.: Concepts in Fuzzy Scaling Theory: Order and Granularity. Fuzzy Sets and Systems 132(1), 63–75 (2002)
17. Valtchev, P., Missaoui, R., Lebrun, P.: A Partition-Based Approach towards Constructing Galois(Concept) Lattices. Discrete Mathematics 256(3), 801–829 (2002)
18. Agrawal, R., Imielinski, T.: Mining Association Rules between Sets of Items in Large Databases. In: Proceedings of the 1993 ACM-SIGMOD Int. Conference, Management of Data, Washington, D. C., pp. 207–216 (1993)
19. Bhogal, J., Macfarlane, A., Smith, P.: A Review of Ontology based Query Expansion. Information Processing and Management 43, 866–886 (2007)
20. Jones, K.S.: Notes and References on Early Classification Work. SIGIR Forum 25(1), 10–17 (1991)

The Application of Intuitionistic Fuzzy Theory in Radar Target Identification

Hong Wang and Jie Wang

College of Mathematics and Computer Science,
Shanxi Normal University, Linfen, Shanxi 041004, P.R. China
wangh@sxnu.edu.cn

Abstract. By the fundamental notion in Atanassov's intuitionistic fuzzy sets (IFS), synthetically considering the effects of both the membership and the nonmember ship degrees, seven calculating methods of similarity degree for intuitionistic fuzzy, i.e., max-min, maximal-minimum, arithmetic mean minimum, geometric mean minimum, Hamming distance, Euclidean distance and correlative coefficient, are proposed and applied to radar target identification, this further developing the approaches to the calculating similarity degree in IFS.

Keywords: Fuzzy sets, Intuitionistic fuzzy sets, Radar target identification, Similarity degree.

1 Introduction

The theory of fuzzy sets, proposed by Zadeh (1965), has gained successful applications in various fields. Measures of similarity between fuzzy sets, as an important content in fuzzy mathematics, have gained attention from researchers for their wide applications in real world. Based on similarity measures that are very useful in some areas, such as pattern recognition, machine learning, decision making and market prediction, many measures of similarity between fuzzy sets have been proposed and researched in recent years. For example, Chen (1994) proposed a similarity function F to measure the degree of similarity between fuzzy sets. Then Chen (1995) also made a comparison of similarity measures of fuzzy values. Pappis and Karacatilides (1993) made an assessment of measures of similarity of fuzzy values. Hyung et al. (1994) presented two similarity measures between fuzzy sets and between elements. Wang (1997) proposed new fuzzy similarity measures on fuzzy sets and elements. Zwich et al. (1987) reviewed 19 similarity measures of fuzzy sets and compared their performance in an experiment. Santini and Jain (1999) proposed similarity measures based on fuzzy logic. With the research of fuzzy sets, Atanassov (1986, 1989, 1994a,b, 1995, 1999) presented intuitionistic fuzzy sets (IFSs) which are very effective to deal with vagueness. Gau and Buehere (1993) researched vague sets. On the basis of this, Bustince and Burillo (1996) pointed out that the notion of vague sets is same as that of IFSs by Atanassov. Taranli and Coker (2001) proposed several types of fuzzy connectedness in intuitionisitc fuzzy topological spaces. De et al. (2000) defined some operations on IFSs. Then De et al. (2001) discussed the Sanchez_s approach for

D.-S. Huang et al. (Eds.): ICIC 2009, LNAI 5755, pp. 166–173, 2009.

medical diagnosis and extended this concept with the notion of IFSs. As a matter of fact, IFSs are a generalized version of fuzzy sets. In some cases, IFSs can deal with problems more effectively. On the basis of IFSs, Chen (1988, 1994) and Chen and Tan (1994) proposed two similarity measures for measuring the degree of similarity between vague sets. Szmidt and Kacprzyk (2000) proposed distances between IFSs. Li and Cheng (2002) also proposed similarity measures of IFSs and applied similarity measures to pattern recognition.

Introduction Radar target identification can be grouped under three heads: discerning ourselves from the enemy, discerning categories, and types, all possessing complicated indefiniteness. There are a lot of ways to identify radar target. Until now, these is no all-round target identifying method, that is to say, these is still no such method that can be used at any cases to identify target because of radar target being complicated and the information obtained being incomplete. Under many conditions, the information acquired before target identification is more often than not very rough, inaccurate, incomplete and firsthand. A common way to be employed to identify target is frequently by taking advantage of the final distinguished rules resulted from the firsthand information and the target useful features. As to the same target, different radar station obtains different information; even the same radar may acquire different information at different moment. Furthermore, different distinguished result may be obtained with different method by utilizing the same data, and so on and so forth. Therefore, as such complicated problem is concerned; it is quite difficult to acquire a final correctly distinguished result. However, IFS can be used to deal with such complicated problem[1].

In this paper, the application of IFS to target identification and information processing is studied and employed to evaluate the distinguished effect of radar target.

2 Intuitionistic Fuzzy Sets (IFS)

IFS effectively broaden the indicative ability of Zacleh's Fuzzy Sets. Atanassov[2,3] defines IFS as follows:

Suppose X is the given universe of discourse, then in X one IFS A is

$$A = \{< x, \mu_A(x), \gamma_A(x) > \big| x \in X\}$$

Where, $\mu_A(x): X \to [0,1]$ and $\gamma_A(x): X \to [0,1]$ respectively stand for membership function $\mu_A(x)$ and nonmember ship function $\gamma_A(x)$, being tenable to

$$x \in X, 0 \le \mu_A(x) + \gamma_A(x) \le 1$$

When, X is continuous space, then $A = \int_A <\mu_A(x), \gamma_A(x) > / x, x \in X$;

When, $X = \{x_1, x_2, \cdots, x_n\}$ is discrete space, then

$$A = \sum_{i=1}^{n} < \mu_A(x_i), \gamma_A(x_i) > / x_i, x_i \in X, i = 1,2,...,n$$

IFS A can be sometimes as $A=<x,\mu_A,\gamma_A>$ or $A=<\mu_A,\gamma_A>/x$. Each common intuitionistic fuzzy subset corresponds to the fuzzy subset[4]

$$A=\{<x,\mu_A(x),1-\mu_A(x)>/x\in X\}.$$

As for each intuitionistic fuzzy subset among *X*, $\pi_A(x)=1-\mu_A(x)-\gamma_A(x)$ is named as the intuitionistic exponent of *X*, is also the measure of hesitation degree of *X* to *A*. Obviously, as to each $x\in X$ $0\le\pi_A(x)\le 1$ and to each common fuzzy subset *A* among *X*,

$$\gamma_A(x)=1-\mu_A(x),$$

then

$$\pi_A(x)=1-\mu_A(x)-[1-\mu_A(x)]=0,\forall x\in X.$$

As concerns a fuzzy set $A\in F(u)$, its single membership degree $\mu_A(x)$ includes not only evidence $\mu_A(x)$ which support *X*, but also evidence 1-$\mu_A(x)$ which opposes *X*, but it can in no way show the evidence of neutral stale that neither support nor opposes, or being neither this nor that stale. However, one IFS $A\in IFS(u)$, its membership degree is $\mu_A(x),\forall x\in U$. Nonmember ship degree $\gamma_A(x),\forall x\in U$ and the intuitionistic exponent $\pi_A(x),\forall x\in U$ can respectively indicate the degree of three evidences, support, opposition and neutrality which belong to IFS A with *X*, as the target. For instance, suppose IFS *A*=<*x,* 0.5, 0.3>, indicating its membership degree $\mu_A(x)$ =0.5, nonmember ship degree $\gamma_A(x)$ =0.3, the hesitation degree $\pi_A(x)$ =1-0.5-0.3=0.2, then indicating target *X* belongs to IFS A with the degree being 0.5; target *X* does not belong to IFS *A* with the degree being 0.3 and target *X* neither support nor opposes IFS with the neutral degree being 0.2.

In radar target identification we can explain set *A*=<*x,* 0.5, 0.3>. When target is *X*, target is judged as *X* by 50% , target is *X*, target is judged as *X* by 30%, target is in no way judged as whether it is X by 20%.

3 Similarity Degree of IFS

Suppose *A*, *B* and *C* are three arbitrarily intuitionistic fuzzy subsets in the universe of discourse U, similarity of A and B is written down as $f(A,B)$, then $f(A,B)$ possesses the following four features[8-10]:

1) $0\le f(A,B)\le 1$;
2) $A=B\Leftrightarrow f(A,B)=1$;
3) $f(A,B)=f(B,A)$;

4) If $A \subseteq B \subseteq C$, then $f(A,C) \le f(A,B)$ and $f(A,C) \le f(B,C)$

In this section, we firstly recall similarity measures proposed by Li and Cheng (2002). Then several examples are applied to show that the Li and Cheng_s method is not always reasonable in some cases. On the basis of this, we propose several new similarity measures on IFSs.

Assume that *A* and *B* are two IFSs and contain *n* elements respectively. Then *A* and *B* are denoted as follows:

$$A = \sum_{i=1}^{n} (\mu_A(x_i), \gamma_A(x_i))/x_i \quad , \quad B = \sum_{i=1}^{n} (\mu_B(x_i), \gamma_B(x_i))/x$$

Similarity measures are defined by Li and Cheng as follows:

$$f(A,B) = 1 - \frac{1}{\sqrt[p]{n}} \sqrt[p]{\sum_{i=1}^{n} \left(\frac{1+\mu_A(x_i)-\gamma_A(x_i)}{2} - \frac{1+\mu_B(x_i)-\gamma_B(x_i)}{2} \right)^p} \quad (1)$$

From $f(A,B)$, we consider the following fact. If median values $\frac{1+\mu(x_i)-\gamma(x_i)}{2}$ between IFSs are equal respectively, similarity measures between two IFSs are equal to 1. Intuitively, if =1, *A* and *B* should be identical. However, it is not the case in some conditions according to Li and Cheng's method. In the following, we give a simple example.

Example 1. Assume that there are three patterns denoted with IFSs in $U = \{1,2,3\}$. Three patterns are denoted as follows:

$A = \{(0.3,0.7),(0.2,0.8),(0.1,0.9)\};$
$B = \{(0.2,0.8),(0.2,0.8),(0.2,0.8)\};$
$C = \{(0.4,0.6),(0.4,0.6),(0.4,0.6)\};$

Assume that a sample $E = \{(0.3,0.7),(0.2,0.8),(0.1,0.9)\}$ is given. According to Li and Cheng's definition, $f(A,E) = 1; f(B,E) = 1; f(C,E) = 1$. From the above example, it is evident that *A* and *E* are identical. However, we cannot obtain correct results using the definition of (1). In other words, if we adopt the principle of maximum membership degree, the pattern *A* cannot be recognized from this group.

In order to deal with this problem, another definition of similarity measures between IFSs is proposed.

When the similarity of two IFS is calculated there is a great need to consider the composition of the membership function and non-membership function. To calculate the similarity, these are generally max-min, maximal-minimum, arithmetic mean minimum, geometric mean minimum, Hamming distance, Euclidean distance and correlative coefficient methods, which are respectively applied to different conditions. The degree of similarity of two IFS *A* and *B* is also addressed of matching *A* with *B*; the greater the degree, the more *A* matches *B*.

Suppose A and B are two intuitionistic fuzzy subsets in the universe of discourse U; A is written as $A = (\mu_A, \gamma_A)/x$, B as $B = (\mu_B, \gamma_B)/x$, the degree of similarity between them $f(A,B)$ can be calculated by the following formula:

1) Max-Min

$$f(A,B) = \frac{1}{2}\frac{\sum_U \min[\mu_A(x), \mu_B(x)]}{\sum_U \max[\mu_A(x), \mu_B(x)]} + \frac{1}{2}\frac{\sum_U [1 - \max(\gamma_A(x), \gamma_B(x))]}{\sum_U [1 - \min(\gamma_A(x), \gamma_B(x))]} \quad (2)$$

2) Maximal-Minimum

$$f(A,B) = \frac{1}{2}[A \cdot B + (1 - A \otimes B)] \quad (3)$$

Where, $A \cdot B = \frac{1}{2}\{\vee_u [\mu_A(x) \wedge \mu_\beta(x)] + \vee_u [(1-\gamma_A(x)) \wedge (1-\gamma_\beta(x))]\}$

$$A \otimes B = \frac{1}{2}\{\wedge_u [\mu_A(x) \vee \mu_\beta(x)] + \wedge_u [(1-\gamma_A(x)) \vee (1-\gamma_\beta(x))]\}$$

Here '$\vee$' stands for maximum, '$\wedge$' for minimum, $A \cdot B$ is named as the interior product of A and B, $A \otimes B$ as the exterior product of A and B.

3) Arithmetical Mean Minimum

$$f(A,B) = \frac{\sum_U \min[\mu_A(x), \mu_B(x)]}{\sum_U [\mu_A(x) + \mu_B(x)]} + \frac{\sum_U \min[1-\gamma_A(x), 1-\gamma_B(x)]}{\sum_U [2 - \gamma_A(x) - \gamma_B(x)]} \quad (4)$$

4) Geometric Mean Minimum

$$f(A,B) = \frac{1}{2}\frac{\sum_U \min[\mu_A(x), \mu_B(x)]}{\sum_U \sqrt{\mu_A(x) \times \mu_B(x)}} + \frac{1}{2}\frac{\sum_U \min[1-\gamma_A(x), 1-\gamma_B(x)]}{\sum_U \sqrt{(1-\gamma_A(x)) \times (1-\gamma_B(x))}} \quad (5)$$

5) Hamming Distance

$$f(A,B) = 1 - \frac{1}{2N}\sum_U [|\mu_A(x) - \mu_B(x)| + |\gamma_A(x) - \gamma_B(x)|] \quad (6)$$

Where, N stands for the cardinal number of universe of discourse U.

6) Euclidean Distance

$$f(A,B)=1-\left\{\frac{1}{2N}\sum_{U}\left(\left|\mu_A(x)-\mu_B(x)\right|^2+\left|\gamma_A(x)-\gamma_B(x)\right|^2\right)\right\}^{\frac{1}{2}} \tag{7}$$

7) Correlative Coefficient Mean

$$f(A,B)=\frac{1}{2}\left[\mu_A(x)*\mu_B(x)+(1-\gamma_A(x))*(1-\gamma_B(x))\right] \tag{8}$$

Where, $a*b$ stands for the correlative coefficient of two sequences a and b. Among the above-said seven definitions, the greater the $f(A,B)$, the more similar the two IFS A and B match each other. In actual application, when the degree of similarity is greater than a certain predetermined threshold value, the corresponding fuzzy conditions can be thought of matching the evidence. The above-mentioned seven definitions of degree of similarity can be applied to different circumstances.

4 Actual Application

Radar target identification is quite an uncertain problem, the key of which is whether the kernel information of the target to be identified can be got hold of, and by relying upon the kernel information to make judged identification. Under most circumstance, data information acquired from the detective equipment, such as various sensors, etc., is inaccurate, imperfect, inconsistent, and or rather coarse.

Since the coarse information gathering contains large amount of redundant information, even including some false message. Therefore, identified result acquired by taking advantage of different information and the identical discerning method is not usually the same; by employing the identical information and the different discerning method the identified result obtained by employing different information and different discerning method of the identified effect is better? It will be difficult if the traditional analysis method is used to deal with such problem. Applying IFS theory to the discerning field has put forward a new method in order to deal with such problem. On the premise of not losing the firsthand important information, by relying the IFS theory and by means of calculating the degree of similarity of the two IFS A and B, the distinguished of rules can be thereafter formed. The application of the IFS theory to target identification and information processing is studied in this paper.

Table 1. Four Different Types of Airplanes with Their Identification Results

Type of airplane	1		2		3		4	
Identified Result	Yes	No	Yes	No	Yes	No	Yes	No
A (One-D distance image)	0.64	0.23	0.70	0.20	0.80	0.10	0.82	0.12
B (Sound signal)	0.60	0.11	0.50	0.30	0.68	0.25	0.74	0.22
C (RCS)	0.57	0.14	0.43	0.50	0.58	0.30	0.65	0.24
D (Track, speed acceleration)	0.58	0.15	0.68	0.25	0.88	0.10	0.65	0.28
E (Ideal-case)	0.93	0.04	0.89	0.05	0.95	0.02	0.87	0.11

Radar target can be identified through one dimensional distance image, sound signal of radar target. C (RCS, reflex cross section) of radar target and the track, speed, acceleration of the garget. Table.1 indicates the identified result provided for a certain research unit to identify target with four different types of air-planes, of which A, B, C and D are the identified results obtained by using different actual data through four ways, while E being the identified result acquired by using the ideal(not actual) data.

The following is Table.1 being expressed as IFS gathering:

$$A = (0.64,0.23)/1 + (0.70,0.20)/2 + (0.80,0.10)/3 + (0.82,0.12)/4 \ ;$$
$$B = (0.60,0.11)/1 + (0.50,0.30)/2 + (0.68,0.25)/3 + (0.74,0.22)/4 \ ;$$
$$C = (0.57,0.14)/1 + (0.43,0.50)/2 + (0.58,0.30)/3 + (0.65,0.24)/4 \ ;$$
$$D = (0.58,0.15)/1 + (0.68,0.25)/2 + (0.88,0.10)/3 + (0.65,0.28)/4 \ ;$$
$$E = (0.93,0.04)/1 + (0.89,0.05)/2 + (0.95,0.02)/3 + (0.87,0.11)/4 \ .$$

1) To calculate by means of hamming distance, the degree of similarity among A, B, C and D will be

$$f(A,B)=0.886 \ ; \ f(A,C)=0.820 \ ; \ f(A,D)=0.922 \ ;$$
$$f(B,C)=0.926 \ ; \ f(B,D)=0.901 \ ; \ f(C,D)=0.868.$$

Since $f(B,C)=0.926$, being the maximum, IFS B is more similar to C, that is, B matcher C.

2) To calculate by means of hamming distance, the degree of similarity among A, B, C and D will be

$$f(A,B)=0.168 \ ; \ f(A,C)=0.255 \ ; \ f(A,D)=0.342 \ ;$$
$$f(B,C)=0.937 \ ; \ f(B,D)=0.281 \ ; \ f(C,D)=0.177.$$

Since $f(B,C)=0.937$, being the maximum, IFS B is more similar to C, that is to say, B matcher C.

3) To calculate by means of hamming distance, the degree of similarity among A, B, C and D will be

$$f(A,E)=0.8612 \ ; \ f(B,E)=0.7775 \ ; \ f(C,E)=0.7037 \ ; \ f(D,E)=0.8237.$$

Since $f(B,C)=0.8612$, being the maximum, IFS A is more similar to E, that is to say, E , i.e., A matcher E. And because of the identified result against E is most ideal, so in actual target identification, the distinguished effect against A is bettor, i.e., by employing one dimensional distance image the identified effect is better.

The calculating methods of other degrees of similarity among A, B, C, D and E can be also worked out according to the above formulas, there is no need to work out one by one.

In target identification system and the process of distinguish, the system must be continuously matched with the known target feature data and the feature data in data-bank. If the known feature data match a certain feature data in data-bank, the target identification can be carried out.

5 Conclusion

When the inaccurate imperfect and coarse information is analyzed and processed, the IFS theory is quite an effectively mathematical means, being the expansion and development of Zaclen's IFS gathering. The degree of similarity among IFS is an important feature volume in the intuitionistic fuzzy inference. When the degree of similarity is calculated, there is a great need to membership and nonmember ship degrees. In this paper, there are seven methods of calculating the degree of similarity, being respectively applied to different conditions, in addition, the similarity that is applied to identify radar target can make a comment on the discerning methods---whether they are good or bad.

Acknowledgment

This work was supported by the Natural Science Foundation of Shanxi Province in China (No. 2008011012).

References

1. Swiniarski, R.W. Skowron, A.: A Rough Set Methods in Feature Selection and Recognition. In: Pattern Recognition Letters, vol. 6, pp. 833–849 (2003)
2. Atanassov, K.: New Operations Defined Over the Intuitionistic Fuzzy Sets. Fuzzy Sets and Systems 61(1), 137–142 (1994)
3. Atanassov, K.T., Kacprzyk, J., Szmidt, E.: On Reparability of Intuitionistic Fuzzy Sets. LNCS (LNAI), vol. 2715, pp. 285–292 (2003)
4. Bustince, H., Burillo, P.: Vague Sets are Intuitionistic Fuzzy Sets. Fuzzy Sets and Systems 79(3), 403–405 (1993)
5. Glad, D., Kerre, E.E.: On the Relationship Between Some Extensions of Fuzzy Set Theory. Fuzzy Sets and Systems 133(2), 227–235 (2003)
6. Lei, Y.J., Wang, J.Y.: Technique for Intuitionistic Fuzzy Reasoning with Truth Qualification. Journal of Air Force Engineering University 6(1), 234–236 (2005)
7. Lei, Y.J., Wang, B.S.: On the Semantic Operators for Intuitionistic Fuzzy Logic. Computer Science 31(11), 4–6 (2004)
8. Liu, H.W.: Basic Theorems of the Intuitionistic Fuzzy Sets. Journal of mathematics for technology 16(1), 55–60 (2005)
9. Lei, Y.J., Wang, T., Zhao, Y.: On Semantic Distance and Near Compactness for Intuitionistic Fuzzy Match. Journal of Air Force Engineering University 6(1), 69–72 (2005)
10. Lei, Y.J., Zhao, Y.: On the Measurement of Similarity on Semantic Match for Intuitionistic Fuzzy. Journal of Air Force Engineering University 6(2), 83–86 (2005)
11. Lei, Y.J., Wang, B.: On the Equivalent Mapping Between Extensions of Fuzzy Set Theory. Systems Engineering and Electronics 26(10), 1414–1417 (2004)

On the Robustness of Type-1 and Type-2 Fuzzy Tests vs. ANOVA Tests on Means

Juan C. Figueroa García[1], Dusko Kalenatic[2], and Cesar Amilcar Lopez Bello[3]

[1] Universidad Distrital Francisco José de Caldas, Bogotá, Colombia*
[2] Universidad de la Sabana, Chia, Colombia**
[3] Universidad Distrital Francisco José de Caldas, Bogotá, Colombia***
jcfigueroag@udistrital.edu.co, duskokalenatic@yahoo.com,
clopezb@udistrital.edu.co

Abstract. This paper presents a simulation study on fuzzy tests vs. ANOVA test on means. Type-1, Interval Type-2 and ANOVA classical tests are compared through a simulated experiment for contrasting the stability of those approaches in front to a small change on sample.

We perform an experiment of comparing the means of three groups where the classical ANOVA test is very nearby to the rejection p-value and the fuzzy tests get more robust results. In this way, we use bootstrap concepts to simulate the change of a random value of the sample to view the behavior of each technique in front to these changes.

1 Introduction and Motivation

Recently, the use of fuzzy sets for involving uncertainty in the statistical analysis and its advantages has allowed the appearance of a new discipline called *Fuzzy Statistics*, in which many researchers are dedicating their efforts to the definition of correct expressions for solving different problems of data analysis.

James J. Buckley in [1] and [2] defines new probability concepts based on Type-1 fuzzy sets called *"Fuzzy Probabilities"* and therefore fuzzy test statistics. A. Mohammadpuor & A. Mahammad.Djafari in [3] propose a fuzzy test by using fuzzy relations and Bayesian concepts, showing their proposal converges to the best crisp test by using the *Neyman-Pearson Lemma*[1], B.F. Arnold in [7] proposes a similar work based on interval numbers and M. Last, A. Schenker & A. Kandel in [8] show an application to medical data.

We compare three hypothesis engines: ANOVA test, a Type-1 fuzzy logic system (T1FLS) proposed by Figueroa & Soriano in [9] and an Interval Type-2 fuzzy logic system (IT2FLS) proposed by Figueroa, Rodriguez & Sierra in [10] in order to view its behavior when the sample has been changed.

* Laboratory for Automation, Microlectronics and Computational Intelligence (LAMIC) and Mathematical Modelling Applied to Industry (MMAI) research group.
** Logistic Systems Research Group.
*** Mathematical Modelling Applied to Industry (MMAI) research group.
[1] For additional information see [4], [5] and [6].

D.-S. Huang et al. (Eds.): ICIC 2009, LNAI 5755, pp. 174–183, 2009.

This paper is divided as follows: Section 1 introduces the topic; Section 2 presents hypothesis testing; Section 3 describes the two fuzzy logic test systems; in Section 4 we present the methodology of simulation; Section 5 presents the results of the simulation and Section 6 gives some concluding remarks.

2 Hypothesis Testing

In many hypothesis-testing problems two hypothesis are discussed: The first, the hypothesis being tested, is called the *Null Hypothesis*, denoted by H_0, and the second is called the *Alternative Hypothesis*, denoted by H_a. The natural supposition is that if H_0 is false, then H_a is true. The H_0 outlined here is:

$$H_0 : \mu_1 = \mu_2 = \cdots = \mu_n \tag{1}$$
$$H_a : \textit{At least one mean is different from others.}$$

The multiple means case (1) is widely treated by using the ANOVA method. The Table 1 shows a brief description of the test.

Table 1. Test Statistics for multiple means

Null Hypothesis	Test Statistic
$H_0 : \mu_1 = \mu_2 = \cdots = \mu_n$	$F_0 = \dfrac{MS_{means}}{MS_E}$
Alternate Hypothesis	Reject Criterion
At least one mean is different from others.	Reject H_0 when $F_0 \leqslant F_{1-\alpha,a-1,N-a}$

Where a is the Amount of Data groups, n_i is the Number of observations of the i_{th} group, N is the Total number of observations, MS_{means} is the Mean Square of means, MS_E is the Mean Square of error, y_{ij} is the j_{th} observation for the i_{th} data group, $j = 1, 2, \cdots, n$, $\overline{y}_{i.}$ is the Mean of the i_{th} data group, $i = 1, 2, \cdots, a$ and $\overline{y}_{..}$ is the Mean of the complete data set. For more information see Scheffé in [11] and Searle in [12].

2.1 Decision Making

A crisp bilateral hypothesis test is a simple process that either rejects or accepts H_0 by using a pre-defined α confidence level (Usually $\alpha = 0.05$), assuming it as the correct one, based on any asymptotic test statistic. The usual reasoning is to Accept H_0 if the sample statistic is inside a *Confidence Interval*, that is:

$$\bar{y} \in [\, g_1(\mu_0); g_2(\mu_0) \,] \tag{2}$$

Where $g_1(\mu_0)$ and $g_1(\mu_0)$ are functions of μ_0 and $\bar{y}$ is the mean of the sample y. $P(g_1(\mu_0) < \mu < g_2(\mu_0)) = 1 - \alpha$. The classical hypothesis tests use only one rule to verify H_0, based on asymptotic properties (Or Normality) of the sample:

R_1: If $\overline{y} \in [\, g_1(\mu_0); g_2(\mu_0) \,]$ then H_0 is Accepted, otherwise H_0 is Rejected.

2.2 General Discussion about Sensibility of the ANOVA Test

Classical statistics are sensible to small perturbations of their samples, that is, the estimator of any parameter depends on the properties of the sample. In fact, an estimator is said to be *Sufficient* if it has an appropriate amount of information about the parameter. Now suppose that we change an observation y_{ij} in a random position of the sample by using the original distributional properties of the i_{th} group, then $MS_{means}, \overline{y}_{i\cdot}, \overline{y}_{\cdot\cdot}$ and MS_E change, in other words:

$$\lim_{\epsilon \to 0} \overline{y}_{i\cdot}(\epsilon) = \sum_{j=1}^{n_i} \frac{y_{ij} + \epsilon}{n_i} = \sum_{j=1}^{n_i} \frac{y_{ij}}{n_i} \tag{3}$$

$$\lim_{\epsilon \to x_{ij}} \overline{y}_{i\cdot}(\epsilon) = \sum_{j=1}^{n_i} \frac{y_{ij} + x_{ij}}{n_i} \neq \sum_{j=1}^{n_i} \frac{y_{ij}}{n_i} \tag{4}$$

Where ϵ is a perturbation of size x_{ij} obtained from the same distribution of the i_{th} group. It is clear that the test can be changed depending on the size of ϵ.

Now suppose that the ANOVA test is very close to the rejection p-value, that is, the F_0 statistic is very close to $F_{1-\alpha,a-1,N-a}$. It leads us to think that a small change ϵ on any group could generates the rejection or accepting of H_0, compromising the robustness of the method against perturbations. That is:

$$F_0 \approx F_{1-\alpha,a-1,N-a} \tag{5}$$

$$\lim_{\epsilon \to x_{ij}} F_0(\epsilon) \neq F_0 \tag{6}$$

In this way, the behavior of the ANOVA test is tested by changing a single observation on any group by a simulated value. To do so, we use bootstrap concepts for finding sufficient estimates of the parameters of each group. For further information see Efron in [13], [14], [15] and [16].

3 Type-1 and Interval Type-2 Fuzzy Hypothesis Testing

In this paper, we use the following definition of fuzzy randomness:

Definition 1 (Liu & Liu in [17]). *Let $(\Omega, \sum, P)$ be a probability space. A fuzzy random vector is a mapping $\xi : \Omega \to \mathfrak{F}_v$ such that for any closed subset C of $\mathbb{R}$.*

$$\xi(C)(\omega) = Pos\{\xi(\omega) \in C\} = \sup_{x \epsilon C} \mu_{\xi(\omega)}(x) \tag{7}$$

Is a measurable function of ω, where $\mu_{\xi(\omega)}$ is the distribution function of fuzzy variable $\xi(\omega)$. For simplicity, we avoid the use of $\xi(\omega)$ instead of any subset C.

First, a statistical transformation is used to standardize sample means namely $\{\overline{x}_i\}$. For known and unknown variances, the z and t transformations are:

$$z_i = \frac{\bar{y}_{i\cdot} - \mu_0}{\delta_i / \sqrt{n_i}} \quad or \quad t_i = \frac{\bar{y}_{i\cdot} - \mu_0}{s_i / \sqrt{n_i}} \tag{8}$$

$\overline{x}_i, \delta_i, s_i$ and n_i are the mean, population and sample variance of the i_{th} sample.

By using (7) and (8), both uncertainty and randomness are treated with either a T1FLS or IT2FLS whose methodology is presented in the Figure 1.

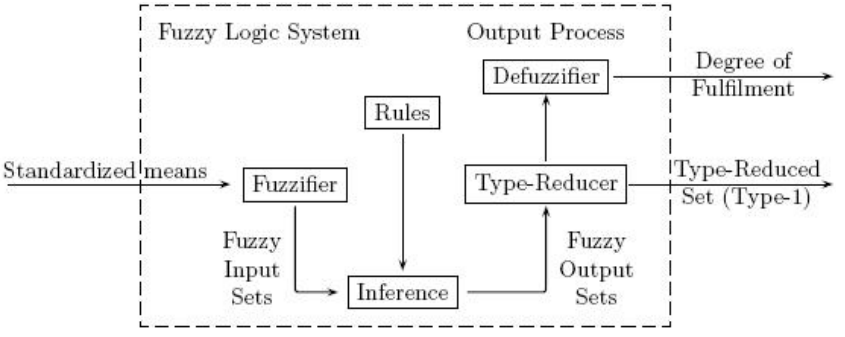

Fig. 1. Fuzzy Logic System design methodology

3.1 Fuzzy Input and Output Sets

According to Figueroa & Soriano in [9] and Figueroa, Rodriguez & Sierra in [10], we use only one input set called Central *(c)*. Three fuzzy output sets are defined as Low *(l)*, Medium *(m)* and High *(h)* fulfilment of H_0. f is the output of the FLS represented as a fulfilment degree, after firing all rules.

Gaussian membership functions were selected, due to its nonlinear behavior which is well known it is a good representation of the natural randomness of many variables. As always, there are many useful membership functions and the proposed method is adaptable with any of them.

3.2 Differences between the Type-1 and Type-2 Approach

Recall that the main differences between the T1FLS and IT2FLS are the handle of uncertainty through membership functions which are shown in the Figure 3, the Type-reduction process and deffuzzification process which is defined in (11).

The Input set "Central", $\mu_{\tilde{c}}$ is characterized by the standardized mean z_i or t_i according to (7), (8) and two membership functions: Its upper membership function $\bar{\mu}_{\tilde{c}}$ and its lower membership function $\underline{\mu}_{\tilde{c}}$.

The output sets "Low", "Medium" and "High", $\mu_{\tilde{l}}, \mu_{\tilde{m}}$ and $\mu_{\tilde{h}}$ are characterized by a fulfilment degree f and two membership functions for each set: Their upper membership functions $\bar{\mu}_{\tilde{l}}, \bar{\mu}_{\tilde{m}}$ and $\bar{\mu}_{\tilde{h}}$ and their lower membership functions $\underline{\mu}_{\tilde{l}}, \underline{\mu}_{\tilde{m}}$ and $\underline{\mu}_{\tilde{h}}$. Their graphical representation is shown in Figure 3.

A Type-2 fuzzy set has embedded an infinite amount of Type-1 fuzzy sets into its *Footprint of Uncertainty (FOU)*, so we use the simple average between the upper an lower membership functions of the IT2 fuzzy sets, that is:

$$\mu_A = \frac{\bar{\mu}_{\tilde{A}} + \underline{\mu}_{\tilde{A}}}{2}$$

For further details about either the T1FLS or IT2FLS, see Figueroa & Soriano in [9] and Figueroa, Rodriguez & Sierra in [10].

3.3 Rule Base for Multiple Means Tests

A multiple means test tries to verify $H_0 : \mu_1 = \mu_2 = \cdots = \mu_n$ by using the *"Mean of complete data"*, $\bar{y}_{..}$ namely μ_0 in (8):

$$\bar{y}_{..} = \sum_{i=1}^{a} \sum_{j=1}^{n} \frac{y_{ij}}{N} \tag{9}$$

If all means are similar among them, then $\overline{y}_{..}$ is close them, but if at least one differs from the rest, then $\overline{y}_{..}$ is biased regarding them. In this paper we compare a case with three data sets, so its respective rule base is presented:

R_1: if z_1, z_2 and z_3 are c, then output is h.
R_2: if z_1, z_2 and z_3 are not c, then output is l.
R_3: if z_1 is not c, z_2 is c and z_3 is c, then output is m.
R_4: if z_1 is c, z_2 is not c and z_3 is c, then output is m.
R_5: if z_1 is c, z_2 is c and z_3 is not c, then output is m.
R_6: if z_1 is not c, z_2 is not c and z_3 is c, then output is l.
R_7: if z_1 is not c, z_2 is c and z_3 is not c, then output is l.
R_8: if z_1 is c, z_2 is not c and z_3 is not c, then output is l.

3.4 Output of the FLS

The output of the T1FLS is the centroid of the outputs after firing all rules, f.

Definition 2. *The output after defuzzification is defined as the P_s-value named $\{P_sv\}$ of fulfillment of H_0, and it represents the possibility of fulfilling of H_0. It is a measure of the overall fulfilment of all means regarding H_0. Formally:*

$$P_sv = \frac{\int \mu_f(f) f \ df}{\int \mu_f(f) df} \tag{10}$$

The output of the IT2FLS is the centroid of the outputs after firing all rules.

Definition 3. *The output after Type-reduction and defuzzification is defined as the $P_s - value$ named $\{\tilde{P}_sv\}$ of fulfilment of H_0. It is a measure of the overall fulfilment of all means regarding H_0. Formally:*

$$\tilde{P}_sv = \int_{\mu_{f_1} \in J_{x_1}} \cdots \int_{\mu_{f_N} \in J_{x_N}} 1 \Big/ \frac{\sum_{i=1}^{N} \mu_{f_i} f_i \ df}{\sum_{i=1}^{N} \mu_{f_i} df} = \frac{c_l + c_r}{2} \tag{11}$$

Here, c_l is the left centroid and c_r is the right centroid after Type-reduction. The reader is kindly encouraged to review the theory of Type-2 fuzzy sets to get a better lecture. Remember that P_sv is a crisp value while $\tilde{P}_sv$ is an interval.

Remark 1 (Figueroa & Soriano in [9]). *The fuzzy test does not attempt to reject or accept H_0, only for a low P_sv degree ($P_sv < 0.3$) it suggests to contrast all samples by using other techniques, but for other P_sv degrees it does not reject H_0. For a medium P_sv degree ($0.3 \leqslant P_sv \leqslant 0.7$), it suggests the existence of small differences, and for a high P_sv degree ($P_sv > 0.7$), it accepts H_0.*

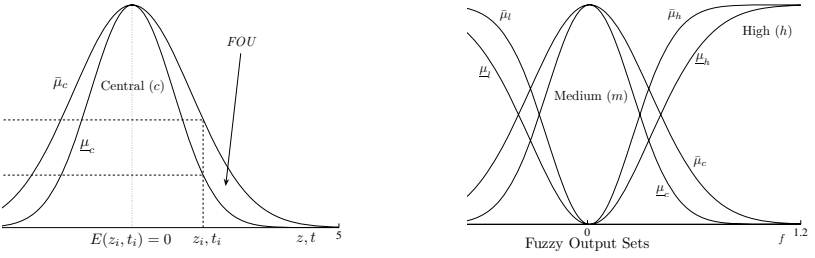

Fig. 2. IT2 Input and Output sets

The selected Type-reduction algorithm is the *IASCO* algorithm proposed by Melgarejo in [18] since it is faster than other algorithms as the *EKM* algorithm, proposed by Karnik & Mendel in [19].

4 Methodology of Simulation

The simulation methodology is presented below, including concepts of bootstrap and discrete events simulation to define the number of runs. First of all, an input analysis of data groups must be done to identify their distributional properties (See Law & Kelton in [20] and Luc Devroye in [21]).

Study Case: The main problem is the comparison of three data groups where their means are compared with the ANOVA method. The study case is interesting since the ANOVA test gets a p-value very close to the rejection value, that is $P(F_0 \geqslant F_{1-\alpha,a-1,N-a}) \approx 0.05$.

Random Number Generator: We select an element $\{\hat{y}_{ij}\}$ located on a random position (i, j) to be replaced by a new observation called $\{x_{ij}\}$ by using the same distribution of the j_{th} group and (8). It means that:

$$\hat{y}_{ij} = y_{ij} + \epsilon = x_{ij} \tag{12}$$

Number of Runs: According to Efron in [13], [14], [15] and [16] we simulate the experiment 10.000 times to ensure that the simulated values get sufficient information to obtain unbiased statistics.

Procedure 1. Simulation Methodology.

for $n = 1 \rightarrow 10000$ **do**
  Select a random element $\{\hat{y}_{ij}^n\}$
  Replace it with$\{x_{ij}^n\}$ {Use the *pdf* of the respective j_{th} group}
  return $\{\hat{y}_{ij}^n\}, \{x_{ij}^n\}, P_v, P_v k, P_s v, \tilde{P}_s v$
end for
return $(\max_{P_v}), (\max_{P_v k}), (\max_{P_s v}), (\max_{\tilde{P}_s v})$
return $\{x_{ij}^n\} \rightarrow \max_{P_v}, \{x_{ij}^n\} \rightarrow \max_{P_v k}, \{x_{ij}^n\} \rightarrow \max_{P_s v}, \{x_{ij}^n\} \rightarrow \max_{\tilde{P}_s v}$

Statistics of Interest: Some statistics about each test after replacing $\{\hat{y}_{ij}\}$ are collected: The results of the ANOVA test (P_v), the Kruskall-Wallis test (P_vk), the T1FLS (P_sv) and the IT2FLS ($\tilde{P}_sv$).

A brief description of the simulation is given in the Procedure 1. All computations are made in *MatLab® 2008b*.

5 Study Case and Simulation Results

We implement an experiment to contrast the equality on means hypothesis among three groups $\{H_0 : \mu_1 = \mu_2 = \mu_3\}$, obtaining the following results:

Table 2. Resultant experiment report

Group	Size (n)	Sum	Mean	Variance
1	30	602.952	20.098	28.567
2	30	522.690	17.423	15.403
3	30	601.666	20.056	24.736

The ANOVA test obtains $F = 3.076$ and a $p-value$ of 0.051 and the Kruskal-Wallis test obtains a $p-value$ of 0.0666. By using these results the analyst has no statistical evidence to reject H_0 and he would concludes that all means are equal. On the other hand, the $p-value$ is very close to 0.05, generating doubts around their significance. Additionally, the analyst points out measurement problems in the 2^{nd} group, identifying a source of uncertainty.

The T1FLS obtains a P_sv of 0.2721 and the IT2FLS obtains a $\tilde{P}_sv$ of 0.267 which indicate possible differences among groups. In both cases the analyst must compare all groups to detect real differences among means in order to either reject or accept H_0. Given these evidences, three comparison tests are implemented to verify H_0. Their results are shown in the Table 3.

Table 3. Comparison Tests for $\alpha = 0.05$

Test	Significance of the Subset.		
2-4	1	1-3	1-2-3
Duncan	—	0.972	—
Waller-Duncan	—	0.846	—
Gabriel	—	—	0.096
Fuzzy-Test	—	0.999	—

In this Table, each test groups the samples and later contrasts the significance of each group. The *Duncan* and *Waller-Duncan* tests suggests the existence of differences among the first group and the other ones. The Gabriel test does not reject the idea of equality on means with a $p-value$ of 0.096.

Table 4. Simulation Report

Technique	N_r	max	$x_{ij} \rightarrow$ max	min	$x_{ij} \rightarrow$ min	Mean	Variance
ANOVA	5313	0.1737	28.208	0.0154	8.5818	0.0526	0.0003
Kruskal-Wallis	8142	0,1790	28.208	0.0236	8.5818	0.0680	0.0004
T1FLS	759	0.4149	30.424	0.1781	30.744	0.2651	0.0007
IT2FLS	530	0.3600	30.424	0.1780	30.744	0.2381	0.0004

The Table 4 presents some interesting statistics: The times that each classical test rejects or accepts H_0 and the times that each fuzzy test recommends multiple comparisons (N_r), both max and min of $P_v, P_s v, \tilde{P}_s v$ and $P_v k$ and the simulated value x_{ij}. The Figure 3 shows 100 runs of the experiment.

The Figure 3 shows that the fuzzy tests have a very similar behavior compared to the classical statistics, increasing or decreasing its value depending on the sample. This confirms that the rule base is a correct emulation of the knowledge about data comparisons.

The fuzzy tests show more robustness in front to a small perturbation ϵ. While classical statistics show a high percent of accepted simulations ($> 50\%$), the T1FLS shows a 7% and the IT2FLS shows a 5% of acceptances, when the correct decision is to Reject H_0.

Classical tests do not reject H_0 in average, that is $\bar{P}_v = 0.0526$ and $\bar{P}_v k = 0.0680$ and their fuzzy counterparts $\bar{P}_s v = 0.02651$ and $\bar{\tilde{P}}_s v = 0.02651$ suggest an exhaustive comparison process to identify possible differences.

In this way, the fuzzy tests have more accurately results than classical tests since they are more robust in front to perturbations. Finally, we point out that the IT2FLS obtains more reduced values of fulfilment since their definition

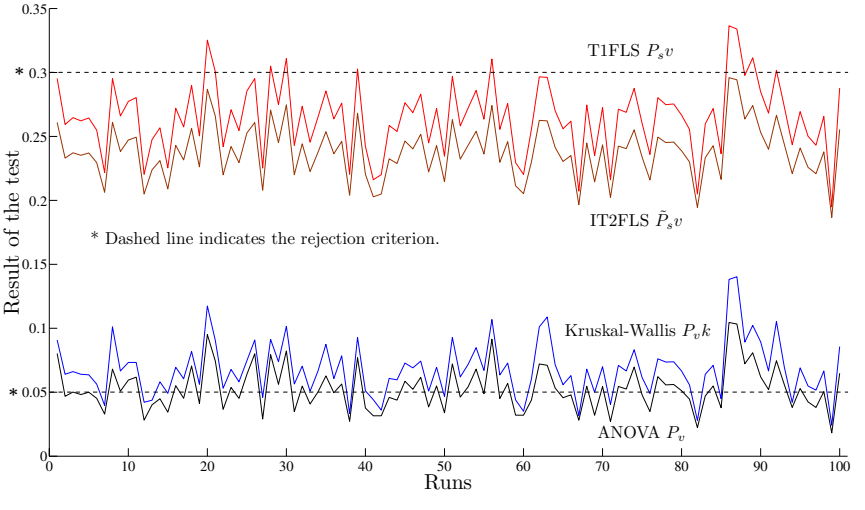

Fig. 3. Simulation Tests results

involves the uncertainty via interval Type-2 fuzzy sets. Additionally, the Type-reduction process ensures more robust results in front to extreme values, just like Wu & Mendel in [22] and Melgarejo in [23] have reported.

6 Concluding Remarks

Some concluding remarks of the study can be given.

- The most important conclusion is that Fuzzy tests are more robust in front to perturbations ϵ since they suggest making multiple comparisons to detect differences instead of classical tests which reject or not H_0.
- The number of runs is sufficient to conclude about H_0. Classical tests have tendency to accept H_0 while Fuzzy tests have tendency to make posterior comparison tests for identifying real differences among groups.
- Fuzzy hypothesis testing outperforms crisp tests in the sense that it recommends multiple comparisons instead of reject H_0, being a soft decision.
- The rule base of a fuzzy test emulates the knowledge of an expert about data. All tests have the same behavior but in different random spaces. This leads us to view the fuzzy tests as complementary tools for classical tests.
- It is important to recall that the sample size has an important effect into the inference. The classical estimation theory applies to fuzzy measurement theory in the sense that if the sample size is increased, then both the estimates and the hypothesis about samples are more accurate.

It is important to emphasize that the presented study evaluates the decision that an analyst should make based on a specific test, either a crisp or a fuzzy test. By this way, if a sample has been changed, fuzzy techniques offer additional information about data through soft decisions to avoid Type-2 errors.

Its applicability in many fields where the making of an incorrect decision has a prohibitive cost is wide. Many clinical, psychological, mechanical, financial and biological applications are candidates to be tested with the presented approach.

Dedicatory

Juan Carlos Figueroa García dedicates this work to the memory of Maria Ninfa García Bautista (*Rest in peace my angel*).

References

1. Buckley, J.J.: Fuzzy Probability and Statistics. Springer, Heidelberg (2004)
2. Buckley, J.J.: Fuzzy statistics: hypothesis testing. Soft Computing - A Fusion of Foundations, Methodologies and Applications 9, 512–518 (2005)
3. Mohammadpuor, A., Mahammad Djafari, A.: On classical, bayesian and fuzzy hypothesis testing. Metrika 17, 348–354 (2004)
4. Mood, A.M., Graybill, F.A., Boes, D.C.: Introduction to the Theory of Statistics. McGraw Hill Book Company, New York (1974)

5. Wilks, A.: Mathematical Statistics. John Wiley and Sons, New York (1962)
6. Huber, P.: Robust Statistics. John Wiley and Sons, New York (1981)
7. Arnold, B.: An approach to fuzzy hypothesis testing. Metrika 44, 119–126 (1996)
8. Last, M., Schenker, A., Kandel, A.: Applying fuzzy hypothesis testing to medical data. In: Zhong, N., Skowron, A., Ohsuga, S. (eds.) RSFDGrC 1999. LNCS, vol. 1711, pp. 221–229. Springer, Heidelberg (1999)
9. Figueroa García, J.C., Soriano Mendez, J.J.: A fuzzy logic approach to test statistical hypothesis on means. In: Huang, D.-S., Wunsch II, D.C., Levine, D.S., Jo, K.-H. (eds.) ICIC 2008. LNCS (LNAI), vol. 5227, pp. 316–325. Springer, Heidelberg (2008)
10. Figueroa, J.C., Rodriguez, D., Sierra, A.: An interval type-2 fuzzy logic system to test statistical hypothesis on means. In: Proceedings of NAFIPS 2009, vol. 28 (2009)
11. Scheffe, H.: The analysis of Variance. John Wiley and Sons, Chichester (1991)
12. Searle, S.R.: Linear Models. John Wiley and Sons, Chichester (1971)
13. DiCiccio, T.J., Efron, B.: Bootstrap confidence intervals. Statistical Science 11, 189–228 (1996)
14. Efron, B.: Bootstrap methods: Another look at the jackknife. The Annals of Statistics 7, 1–26 (1979)
15. Efron, B., Tibshirani, R.J.: Bootstrap methods for standard errors, confidence intervals, and other measures of statistical accuracy. Statistical Science 1, 54–77 (1986)
16. Efron, B., Tibshirani, R.j.: Introduction to the bootstrap. Chapman and Hall, New York (1993)
17. Liu, Y.K., Liu, B.: Fuzzy random variables: A scalar expected value operator. Fuzzy optimization and Decision Making 2, 143–160 (2003)
18. Melgarejo, M., Bernal, H., Duran, K.: Improved iterative algorithm for computing the generalized centroid of an interval type-2 fuzzy set. In: Proceedings of NAFIPS 2009, vol. 27, pp. 1–6 (2008)
19. Zeng, J., Liu, Z.Q.: Enhanced Karnik-Mendel algorithms for Interval Type-2 fuzzy sets and systems. In: Proceedings of NAFIPS 2007, vol. 26, pp. 184–189 (2007)
20. Law, A., Kelton, D.: Simulation System and Analysis. McGraw Hill International, New York (2000)
21. Devroye, L.: Non-Uniform Random Variate Generation. Springer, New York (1986)
22. Wu, D., Mendel, J.M.: Uncertainty measures for interval type-2 fuzzy sets. Information Sciences 177, 5378–5393 (2007)
23. Melgarejo, M.A.: Implementing Interval Type-2 Fuzzy processors. IEEE Computational Intelligence Magazine 2, 63–71 (2007)

Combining Global Model and Local Adaptive Neuro-Fuzzy Network

Yun-Hee Han and Keun-Chang Kwak

Dept. of Control, Instrumentation, and Robot Engineering, Chosun University
375 Seosuk-dong, Dong-gu, Gwangju, 501-759, Korea
kwak@chosun.ac.kr

Abstract. This paper is concerned with a method for combining global model with local adaptive neuro-fuzzy network. The underlying principle of this approach is to consider a two- step development. First, we construct a standard linear regression as global model which could be treated as a preliminary design capturing the linear part of the data. Next, all modeling discrepancies are compensated by a collection of rules that become attached to the regions of the input space in which the error becomes localized. The incremented neuro-fuzzy network is constructed by building a collection of information granules through some specialized fuzzy clustering, called context-based fuzzy c-means that is guided by the distribution of error of the linear part of its development. The experimental results reveal that the proposed method shows a good approximation and generalization capability in comparison with the previous works.

Keywords: global model, linear regression, local adaptive neuro-fuzzy network, information granules, context-based fuzzy c-means.

1 Introduction

During the past few years, the landscape of fuzzy modeling is overwhelmingly rich embracing numerous architectures, learning schemes, hybrid development strategies, and various interpretation mechanisms [1][6][7]. In spite of this profound diversity existing in the area, all fuzzy models share a surprisingly unified design viewpoint and rely on a single coherent methodological platform. Specially, Adaptive Neuro-Fuzzy Network (ANFN) has studied as the constituents of soft computing which is aimed at solving real-world decision making, modeling, and control applications [1][2]. Furthermore, ANFN has realized in the conception and design of hybrid intelligent systems based on their ability to incorporate human knowledge and to adapt their knowledge base. The design principle used in this study is that adopting a construct of a linear regression as a first-principle global model and then refine it through a series of local fuzzy rules that capture remaining and more localized nonlinearities of the system. More schematically, we could express the resulting ANFN by stressing the existence of the two contributing components through the relationship between linear regression and localized network. On the basis of this principle, we emphasize the tendency that in system modeling we always proceed with the simplest possible

D.-S. Huang et al. (Eds.): ICIC 2009, LNAI 5755, pp. 184–189, 2009.

version of the model, assess its performance and afterwards complete a series of required refinements. The localized network handling the residual part of the model is conveniently captured through some rules. The effectiveness of this incremental approach has been demonstrated on the combination of linear regression and linguistic model [3]. Based on the concept of this combination, we develop a new incremental approach by combining linear regression and ANFN as a global and local model, respectively. The ANFN is designed by the use of fuzzy granulation realized via context-based fuzzy c-means clustering. This clustering technique builds information granules in the form of fuzzy sets and develops clusters by preserving the homogeneity of the clustered patterns associated with the input and output space [4][5].

The paper is organized in the following manner. In Section 2, we present context-based clustering technique for extracting fuzzy if-then rules in the design of ANFN. The incremental approach and entire design process are presented in Section 3. The proposed model is applied to Boston Housing data [3] in Section 4. Conclusions are given in Section 5.

2 Context-Based Fuzzy C-Means

The proposed clustering supporting the design of information granules is completed in the space of the input data associated with the error of the linear regression part of the model while the build of the clusters is guided by a collection of some pre-defined fuzzy sets defined in the space of error. By taking into account the contexts, the clustering in the input space is focused by some predefined fuzzy sets of contexts. This helps reveal the relationships between the regions of the input space and the associated error and naturally leads to the formation of some web of connection between the information granules defined in the error space and constructed in the input space. The visualization of the principle of the context-based clustering is presented in Fig. 1.

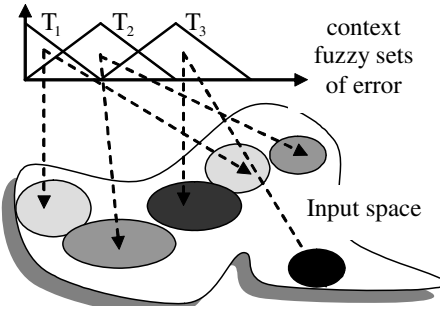

Fig. 1. The concept of context-based fuzzy c-means

For this context variable, we define a fuzzy set of linguistic context as follows

$$T : \mathrm{Z} \rightarrow [0,1] \tag{1}$$

where **Z** is a universe of discourse of output variable. We assume that the values of context for the given data are available. The $f_k = T(z_k)$ represents a level of involvement of the k 'th data in the assumed context (fuzzy set) of the output space. Here the value of f_k produced the membership degree between 0 and 1. For this reason, we modify the requirements of the membership matrix as follows

$$U(f) = \left\{ u_{ik} \in [0,1] \mid \sum_{i=1}^{c} u_{ik} = f_k \ \forall k \ and \ 0 < \sum_{k=1}^{N} u_{ik} < N \ \forall i \right\} \tag{2}$$

The modified membership matrix $U = [u_{ik}]$ is completed as follows [3-5]

$$u_{ik} = \frac{f_k}{\sum_{j=1}^{c} \left(\frac{\| x_k - c_i \|}{\| x_k - c_j \|} \right)^{\frac{2}{m-1}}} \tag{3}$$

where $m \in [1, \infty)$ is a fuzzification factor. The linguistic contexts to obtain f_k are generated through a series of triangular membership functions along the domain of an output variable and an 1/2 overlap between successive fuzzy sets. These contexts are automatically produced by probabilistic distribution of the output space. The context-based fuzzy clustering forms a backbone of the granular model forming the refinement of the regression model.

3 Combining Linear Regression with ANFN

In this section, we cover the fundamental concept of the construction of the incremental network. There are two essential phases: the development of the linear regression being followed by the construction of the local fuzzy rule-based network that attempt to eliminate errors produced by the regression part of the model. The fundamental scheme of the construction of the incremental network is covered in Fig. 2.

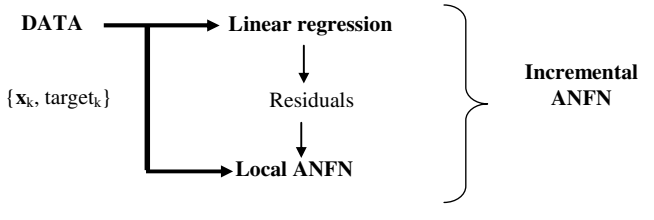

Fig. 2. A general flow of the development of the incremental ANFN

The experimental data under discussion are the pairs of the *n*-dimensional input-output data sets. They come in the following form {**x**(k), target(k)} k=1,2,…,N, where $\mathbf{x}(k) \in \mathbf{R}^n$ and target(k) $\in \mathbf{R}$. The first principle linear regression comes in the standard form of $z(k) = L(\mathbf{x}; \mathbf{b}) = \mathbf{a}^T\mathbf{x}(k) + a_0$ where the values of the coefficients of

the regression plane, denoted here by a_0 and **a**, namely $\mathbf{b} = [\mathbf{a} \quad a_0]^T$, are determined through the standard least-square error method. The enhancement of the model at which the ANFN part comes into the play is based on the transformed data $\{\mathbf{x}(k), e(k)\}$ where the residual part manifests through the expression $e(k) = \text{target} - z(k)$ which denotes the error of the linear model. In the sequel, those data pairs are used to develop an ANFN as the incremental rule-based part of the model. Here this rule-based augmentation of the model associates input data set with the error produced by the linear regression in the form of the rules "if input then error". The rules and the information granules are constructed by means of a specialized grouping.

In this section, we describe the architecture and learning rules of the ANFN based on context-based fuzzy clustering. We will discuss the ANFN with simple TSK (Takagi-Sugeno-Kang) type of fuzzy if-then rules. The TSK fuzzy type is by far the most popular candidate for data-driven fuzzy modeling. The network consists of five layers similar to Jang's model. While Jang's model often encounter "curse of dimensionality" problem that the number of fuzzy rules exponentially increases due to the grid partitioning of the input space, the ANFN can solve such a problem due to the flexible scatter partitioning of context-based fuzzy clustering. Summarizing, let us briefly recall the main design phases of the network, refer also to Fig. 3 showing how the two functional modules operate. First we decide upon the granularity of information to be used in the development of the network including the number of contexts and the number of clusters formed for each context. As shown in Fig. 3, the incremental part is designed by ANFN with TSK fuzzy type based on fuzzy granulation as a local model.

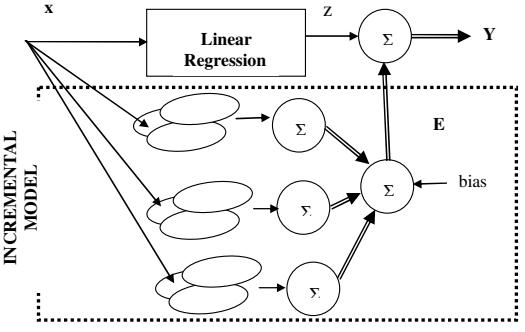

Fig. 3. The overall flow of processing the incremental networks

4 Experimental Results

In the experiment, we report on the development and performance of the proposed method that combines linear regression and local ANFN. We demonstrate how the ANFN part of the model builds the increments of the core of the linear regression. We shall use the Boston Housing data as an example. This data set concerns prices of real estate in the Boston area. The MEDV depends on 13 continuous attributes and 1 binary attribute. The data set consists of 506 examples. We divide the data set into

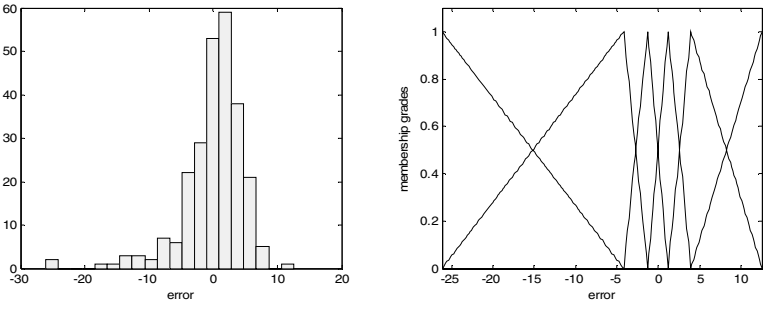

Fig. 4. Linguistic contexts (p=6)

Table 1. Performance comparison of RMSE

	RMSE (training data)	RMSE (checking data)
Linear regression	4.65	4.85
Pedrycz and Kwak [3] (p=6,c=6)	3.45	4.18
The proposed method (p=6,c=2)	2.88	3.92

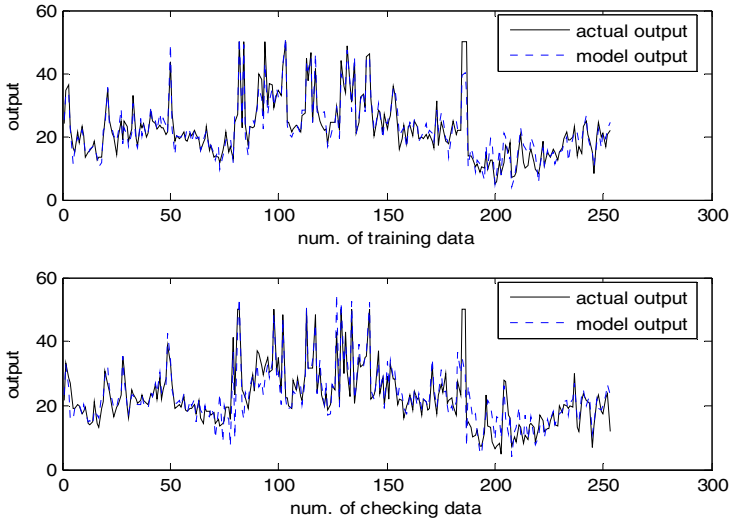

Fig. 5. Generalization capability (checking data)

training (odd number) and test data sets (even number) in the normalized space between 0 and 1, respectively. The training data set is used for model construction, while the test set is used for model validation. Thus, the resultant model is not biased toward the training data set and it is likely to have a better generalization capacity to new data. Fig. 4 shows the flexible linguistic contexts produced by probabilistic distribution of localized error. This error between the actual output and model output is obtained after performing linear regression on training data set. These discrepancies are locally estimated by ANFN realized via context-based fuzzy c-means clustering. Table 1 listed the experimental results regarding approximation and generalization capability, respectively. As listed in Table 1, the experimental results revealed that the proposed approach yielded a good performance in comparison with the conventional methods. Fig. 5 shows the approximation and generalization capability for training and checking data, respectively.

5 Conclusions

In this study, we have proposed an augmented design methodology of incremental ANFN. This methodology is quite different from the one commonly pursued in the realm of fuzzy models with the predominant concept of rule-based architectures. It is also worth stressing that one could view this design methodology as a way of augmenting some global model by a collection of local rule-based models. Therefore, we could express the resulting model by stressing the existence of the two contributing components through the relationship between linear regression and local ANFN. The same approach of the incremental ANFN could be fully explored in other domains such as pattern recognition and classification, in particular. For example, some local rule-based classifiers could seamlessly augment a certain global linear classifier. It is also worth stressing that one could view this design methodology as a way of augmenting some global model by a collection of local rule-based models.

References

1. Jang, J.S.R., Sun, C.T., Mizutani, E.: Neuro-Fuzzy and Soft Computing: A Computational Approach to Learning and Machine Intelligence. Prentice Hall, Englewood Cliffs (1997)
2. Kwak, K.C.: Adaptive Neuro-fuzzy Networks with the Aid of Fuzzy Granulation. IEICE Trans. on Information and Systems E88D(9), 2189–2196 (2005)
3. Pedrycz, W., Kwak, K.C.: The Development of Incremental Models. IEEE Trans. on Fuzzy Systems 15(3), 507–518 (2007)
4. Pedrycz, W.: Conditional Fuzzy Clustering in the Design of Radial Basis Function Neural Networks. IEEE Trans. on Neural Networks 9(4), 601–612 (1998)
5. Pedrycz, W., Vasilakos, A.V.: Linguistic Models and Linguistic Modeling. IEEE Trans. on Systems, Man, and Cybernetics – Part C 29(6), 745–757 (1999)
6. Abonyi, J., Babuska, R., Szeifert, F.: Modified Gath-Geva Fuzzy Clustering for Identification of Takagi-Sugeno Fuzzy Models. IEEE Trans. on Systems, Man, and Cybernetics 32(5), 612–621 (2002)
7. Chen, J.Q., Xi, Y.G., Zhang, Z.J.: A Clustering Algorithm for Fuzzy Model Identification. Fuzzy Sets and Systems 98, 319–329 (1998)

On Some Properties of Generalized Symbolic Modifiers and Their Role in Symbolic Approximate Reasoning

Saoussen Bel Hadj Kacem[1], Amel Borgi[2], and Moncef Tagina[1]

[1] National School of Computer Sciences, University campus Manouba, Manouba 2010, Tunisia
[2] National Institute of Applied Sciences and Technology, Centre Urbain Nord de Tunis, Tunis 1080, Tunisia
Saoussen.BHK@ieee.org, Moncef.Tagina@ensi.rnu.tn, Amel.Borgi@insat.rnu.tn

Abstract. Linguistic modifiers, defined by Zadeh in fuzzy logic context, are operators that transform a linguistic term to another linguistic term. Akdag and al. extend linguistic modifiers to symbolic multi-valued logic context, and called them *Generalized Symbolic Modifiers*. In this paper we propose a study which allows deepening the use of Generalized Symbolic Modifiers in soft computing applications. We focus on symbolic modifiers composition, and we give new properties. Then, we study modifiers order relation, based on a lattice that orders all the defined modifiers according to their parameters. Finally, we illustrate the utilities of our propositions, particularly in approximate reasoning based on linguistic modifiers.

Keywords: Linguistic modifiers, composition, order relation, symbolic multi-valued logic, multi-sets.

1 Introduction

The use of non classical logics became a necessity in intelligent applications. This is due to the imperfection of manipulated knowledge: they are often vague, imprecise, uncertain, etc. The most popular non classical logic is fuzzy logic, introduced by Zadeh [1]. According to this logic, every linguistic term, such as *large*, is presented by a *fuzzy-set*. In the other hand, multi-valued logic still have an important value despite the greet success of fuzzy logic. This is due to many reasons, as the fact that multi-valued logic allows representing qualitative terms whose domains are not numerical, which is not possible with fuzzy logic. Indeed, in fuzzy logic, each fuzzy set A is defined on a set of reference U which must be numerical. Some authors [2,3] have improved the multi-valued logic, and proposed to present every term by a *multi-set*.

In order to manage imperfect knowledge, several formalisms and tools were defined in symbolic context: linguistic modifiers [4,5], approximate reasoning [2,6,7], etc. In this symbolic context of multi-valued logic, we focus on linguistic modifiers.

D.-S. Huang et al. (Eds.): ICIC 2009, LNAI 5755, pp. 190–208, 2009.

Linguistic modifiers were introduced by Zadeh [8] in the fuzzy logic context. Their principle is to construct new fuzzy sets by applying a function to the membership of an original fuzzy set. As every fuzzy set presents a linguistic term, the new fuzzy set obtained by the linguistic modifiers presents new linguistic terms. For example, the modification of a primary term *tall* can lead to *very tall*, or *more or less tall*, etc. More generally, a linguistic modifier is a function that transforms a primary term in another term.

We are interested in this paper on linguistic modifiers in the multi-valued logic context. Since terms in the multi-valued logic are represented by multi sets, linguistic modifiers in the multi-valued logic transform a multi-set to a new multi-set. Propositions of linguistic modifiers in symbolic multi-valued framework were defined by Akdag and al. in [5], and were named *Generalized Symbolic Modifiers*. Since that, it appears that these modifiers are very efficient and have an interesting role in intelligent applications. Indeed, they were used in an application of Colorimetric [9,10], as well as aggregation of words [11]. Moreover, we used these modifiers in approximate reasoning [12,13]. They allowed a coherent and efficient inference result, checking the axiomatic of approximate reasoning [14,15,16,17]. One important result was that the use of linguistic modifiers has the particularity to allow gradual reasoning. In the present work we deepen the study of the symbolic modifiers, notably by focusing on their composition and comparison.

This paper is organized as follow. In section 2, we briefly present the symbolic multi-valued logic. Then, section 3 presents Generalized Symbolic Modifiers, proposed by Akdag and al [5]. In section 4, we propose additional composition and order relation properties of symbolic modifiers. In section 5, some utilities of the proposed properties in intelligent applications are given. Finally, section 6 concludes this work.

2 Symbolic Multi-valued Logic

In symbolic multi-valued logic, each linguistic term (such as *large*) is represented by a multi set [2]. To express the imprecision of a predicate, a qualifier v_α is associated to each multi set (such as *rather*, *little*, etc). When a speaker uses a statement "X is $v_\alpha A$", v_α is the degree to which X satisfies the predicate A[1]. A truth-degree τ_α must correspond to each adverbial expression v_α so that:

$$\begin{aligned} X \text{ is } v_\alpha A &\Longleftrightarrow \text{"}X \text{ is } v_\alpha A\text{" is true} \\ &\Longleftrightarrow \text{"}X \text{ is } A\text{" is } \tau_\alpha\text{-true} \end{aligned}$$

For example, the statement "John is rather tall" means that John satisfies the predicate *tall* with the degree *rather*. This theory of multi-sets can be seen as an axiomatization of the theory of fuzzy-sets. However, in multi-valued logic, membership degrees are symbolic terms of the natural language, and not reals belonging to $[0, 1]$ as in fuzzy logic.

[1] Denoted mathematically by "$X \in_\alpha A$": the object X belongs with a degree α to a multi-set A.

The set of symbolic truth-degrees forms an ordered list $\mathcal{L}_M = \{\tau_0, ..., \tau_i, ..., \tau_{M-1}\}$[2] with the total order relation: $\tau_i \leq \tau_j \Leftrightarrow i \leq j$, its smallest element is τ_0 (false) and the greatest is τ_{M-1} (true) [2]. In practice, the number of truth-degrees is often close to 7. The expert can even propose his own list of truth-degrees; the only restrictive condition is that they must be ordered. For example, the list of truth-degrees used in [2] for $M = 7$ is $\mathcal{L}_7 = \{$not-at-all, very-little, little, moderately, enough, very, completely$\}$.

In order to aggregate truth-degrees, T-norms[3], T-conorms[4] and implicators[5] are used as in fuzzy logic. In multi-valued logic, the aggregation functions of Lukasiewicz are often used. In this context and with M truth-degrees, they are defined by:

$$T_L(\tau_\alpha, \tau_\beta) = \tau_{max(0,\alpha+\beta-M+1)} \tag{1}$$

$$S_L(\tau_\alpha, \tau_\beta) = \tau_{min(M-1,\alpha+\beta)} \tag{2}$$

$$\mathcal{I}_L(\tau_\alpha, \tau_\beta) = \tau_{min(M-1,M-1-\alpha+\beta)} \tag{3}$$

3 Generalized Symbolic Modifiers

A multi-set is characterized by a degree τ_i and a base $\mathcal{L}_M$. Thus, to modify a data in multi-valued logic, one can just transform the degree rank i and/or the base size M of the multi set. Such modification operators were proposed by Akdag and al. in [4], they were generalized and formalized in [5] and named the *Generalized Symbolic Modifiers*.

A Generalized Symbolic Modifier (GSM) is a semantic triplet of parameters (*radius*, *nature*, *mode*). The *radius* represents the strength of the modifier, it is denoted ρ with $\rho \in \mathbb{N}^*$. The more ρ increases, the more the modifier is powerful [5]. The *nature* is the way to modify the scale basis (i.e dilation, erosion or conservation) and the *mode* is the sense of modification (i.e reinforcing, weakening or centring).

Definition 1. *Let us consider a symbolic degree τ_i with $i \in \mathbb{N}$ in a scale $\mathcal{L}_M$ of a base $M \in \mathbb{N}^* \setminus \{1\}$, and $i < M$. A GSM m with a radius ρ is denoted m_ρ. The modifier m_ρ is a function which applies a linear transformation to the symbolic degree τ_i to obtain a new degree $\tau_{i'} \in \mathcal{L}_{M'}$ (where $\mathcal{L}_{M'}$ is the linear transformation of $\mathcal{L}_M$) according to a radius ρ such as [5]:*

$$m_\rho : \mathcal{L}_M \rightarrow \mathcal{L}_{M'}$$
$$\tau_i \mapsto \tau_{i'}$$

[2] With M a positive integer not null.

[3] In multi-valued logic, a T-norm is any symmetric, associative, increasing $\mathcal{L}_M \times \mathcal{L}_M \rightarrow \mathcal{L}_M$ mapping T satisfying $T(\tau_{M-1}, \tau_\alpha) = \tau_\alpha \ \forall \ \tau_\alpha \in \mathcal{L}_M$.

[4] In multi-valued logic, a T-conorm is any symmetric, associative, increasing $\mathcal{L}_M \times \mathcal{L}_M \rightarrow \mathcal{L}_M$ mapping S satisfying $S(\tau_0, \tau_\alpha) = \tau_\alpha \ \forall \ \tau_\alpha \in \mathcal{L}_M$.

[5] In multi-valued logic, an implicator is any $\mathcal{L}_M \times \mathcal{L}_M \rightarrow \mathcal{L}_M$ mapping $\mathcal{I}$, whose first and second partial mappings are decreasing, respectively increasing, satisfying $\mathcal{I}(\tau_0, \tau_0) = \mathcal{I}(\tau_0, \tau_{M-1}) = \mathcal{I}(\tau_{M-1}, \tau_{M-1}) = \tau_{M-1}$.

The greatest degree in the base is denoted $MAX(\mathcal{L}_M) = M-1$. The scale position in the base is denoted $p(\tau_i) = i$. A proportion is associated to each symbolic degree within a base denoted $Prop(\tau_i) = \frac{p(\tau_i)}{MAX(\mathcal{L}_M)}$. As we can see, the proportion is the rate of the degree according to the base, and so $Prop(\tau_i) \in [0,1]$ $\forall i$ and $\forall M$. This proportion allows distinguishing a very important property of the defined modifiers. Indeed, by analogy with fuzzy modifiers, the authors proposed a classification of symbolic modifiers: weakening and reinforcing modifiers, and they added the family of central modifiers [5].

Weakening Modifiers: They weaken the notion expressed by the initial term. Formally, this weakening is remarked by a decrease on the initial value of $Prop(\tau_i)$, i.e. $Prop(\tau_{i'}) < Prop(\tau_i)$.

Reinforcing Modifiers: They reinforce the notion expressed by the initial term. Formally, this reinforcing is remarked by an increase on the initial value of $Prop(\tau_i)$, i.e. $Prop(\tau_{i'}) > Prop(\tau_i)$.

Central Modifiers: They do not change the notion expressed by the initial term. Formally, they transform the degree and the base such a way that the rate $Prop(\tau_i)$ remains unchanged. In other words, they act as a zoom on the scale.

The authors proposed three weakening modifiers, called EW, DW and CW for Eroded Weakening, Dilated Weakening and Conserved Weakening. In the same way, three reinforcing modifiers were defined: ER, DR and CR for Eroded Reinforcing, Dilated Reinforcing and Conserved reinforcing. The proposed central modifiers are EC (for Eroded Centring) and DC (for Dilated Centring). The definitions of the reinforcing, weakening and central modifiers are given in table 1[6], and examples of some modifiers are given in figure 1 [5]. One can notice that two kinds of Dilated Weakening modifiers were defined DW and DW', as well as two kinds of Eroded Reinforcing ER and ER'.

We add to this set of modifiers a new one denoted by CC (for *Conserved Centring*). This modifier does not make any changes on the degree and the base of the multi-set, in others words $CC(v_\alpha A) = v_\alpha A$. We have used this operator to insure classical reasoning in our symbolic approximate reasoning introduced in [12].

We notice that the operator ER' defined in [5] is incoherent. Indeed, when $\rho > M-1$ one obtains $M-\rho-1 < 0$, which gives $\tau_{i'} < \tau_0$. This result is illogical because a truth-degree can never be negative. We propose a new definition of this operator that we call ER'':

$$ER''_\rho = \begin{cases} \tau_{i'} = \tau_{max(0,min(i+\rho,M-\rho-1))} \\ \mathcal{L}_{M'} = \mathcal{L}_{max(2,M-\rho)} \end{cases}$$

This new definition ensures that the value of the resulted membership degree $\tau_{i'}$ is greater than or equal to τ_0. Moreover, the effect of this operator keeps the

[6] We made corrections in the definitions of some modifiers (ER, EW, EC) to meet the boundary conditions $M \geq 2$ and $i \in [0, M-1]$.

Table 1. Definitions of weakening, reinforcing and central modifiers

MODE / NATURE	Weakening	Reinforcing		Central	
Erosion	$\tau_{i'} = \tau_{max(0,i-\rho)}$ $\mathcal{L}_{M'} = \mathcal{L}_{max(2,M-\rho)}$	$\boxed{EW_\rho}$	$\tau_{i'} = \tau_i$ $\mathcal{L}_{M'} = \mathcal{L}_{max(2,i+1,M-\rho)}$ $\tau_{i'} = \tau_{min(i+\rho,M-\rho-1)}$ $\mathcal{L}_{M'} = \mathcal{L}_{max(2,M-\rho)}$	$\boxed{ER_\rho}$ $\boxed{ER'_\rho}$	$\tau_{i'} = \tau_{max(\lfloor \frac{i}{\rho} \rfloor,1)}$ $\mathcal{L}_{M'} = \mathcal{L}_{max(\lfloor \frac{M}{\rho} \rfloor+1,2)}$	$\boxed{EC_\rho}$*
Dilation	$\tau_{i'} = \tau_i$ $\mathcal{L}_{M'} = \mathcal{L}_{M+\rho}$ $\tau_{i'} = \tau_{max(0,i-\rho)}$ $\mathcal{L}_{M'} = \mathcal{L}_{M+\rho}$	$\boxed{DW_\rho}$ $\boxed{DW'_\rho}$	$\tau_{i'} = \tau_{i+\rho}$ $\mathcal{L}_{M'} = \mathcal{L}_{M+\rho}$	$\boxed{DR_\rho}$	$\tau_{i'} = \tau_{i\rho}$ $\mathcal{L}_{M'} = \mathcal{L}_{M\rho-\rho+1}$	$\boxed{DC_\rho}$
Conservation	$\tau_{i'} = \tau_{max(0,i-\rho)}$ $\mathcal{L}_{M'} = \mathcal{L}_M$	$\boxed{CW_\rho}$	$\tau_{i'} = \tau_{min(i+\rho,M-1)}$ $\mathcal{L}_{M'} = \mathcal{L}_M$	$\boxed{CR_\rho}$	$\tau_{i'} = \tau_i$ $\mathcal{L}_{M'} = \mathcal{L}_M$	$\boxed{CC}$

* $\lfloor . \rfloor$ is the floor function.

same modification in the multi-set than the operator ER', in the sense that it increases the degree by ρ units and decreases the base by ρ units.

4 Some Properties of GSM

This section is devoted to some properties of Generalized Symbolic Modifiers. First, we focus on composition of modifiers, and we introduce some new theorems. We then address order relation, and we give a lattice of modifiers order relation.

4.1 Composition

Composition of linguistic modifiers, denoted by $\circ$, allows extending linguistic modifiers defined in [5]. Indeed, every composition of two Generalized Symbolic Modifiers leads to a new degree in a new base, but this modification does not necessarily correspond to one of the Generalized Linguistic Modifiers defined in [5]. We first remind some definitions and results given in [18].

Definition 2 (Dual Operator). *Among the GSM defined in [5], there are some couples which are dual. They are* (EW, DR), (DW, ER), (DW', ER') *and* (CW, CR).

It can be seen that for two dual modifiers m and m' and two radiuses ρ and ρ', if $\rho = \rho'$ then the composition $m_\rho \circ m'_{\rho'}$ leaves the multi-set unchanged. For example, for CR_3 and CW_3, CR_3 increases the multi-set degree of 3 units, and CW_3 decreases the multi set degree of 3 units. So applying CR_3 then CW_3 on a multi set does not change it. In other words, one can remark from the previous definition that $m_\rho \circ m'_\rho = CC$.

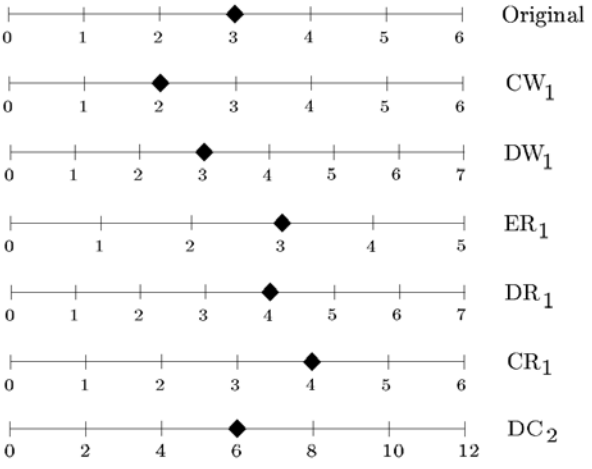

Fig. 1. Illustration of some symbolic linguistic modifiers

Definition 3 (Elementary Operators). *An elementary operator is a Generalized Symbolic Modifier that steadily increases or decreases the truth-degree of a unit, or it increases or decreases the base of a unit.*

Thus, among the Generalized Linguistic Modifiers, CR, CW, ER and DW with a radius 1 are elementary operators [18].

Theorem 1. *If m_1 is any weakening or reinforcing GSM with a radius ρ_1, and if m_2 is any GSM of the same family than m_1 with a radius ρ_2, ... and if m_n is any GSM of the same family than m_1 with a radius ρ_n, then $m_s = m_1 \circ m_2 \ldots \circ m_n$ is a GSM of the same mode than m_1, but with a radius ρ_s equal to the sum of the radiuses, i.e. $\rho_1 + \rho_2 + \ldots + \rho_n$.*

For example, $\forall \rho_1, \rho_2, \ldots \rho_n \in \mathbb{N}^*$, $DR_{\rho_1} \circ DR_{\rho_2} \circ \ldots \circ DR_{\rho_n} = DR_{\rho_1+\rho_2+\ldots+\rho_n}$.

Theorem 2. *If m_1 is any central GSM of the DC family with a radius ρ_1, and if m_2 is any GSM of the same family than m_1 with a radius ρ_2, ... and if m_n is any GSM of the same family than m_1 with a radius ρ_n, then $m_s = m_1 \circ m_2 \ldots \circ m_n$ is a GSM of the same mode than m_1, but with a radius ρ_s equal to the product of the radiuses, i.e. $\rho_1 * \rho_2 * \ldots * \rho_n$.*

New Properties of GSM Composition. We propose as a complement of the work given in [18] the following results:

Property 1. The operator CC is the neutral operator of composition.

Theorem 3. *Given m and m' two weakening or reinforcing modifiers with m the dual of m', and two radius ρ and ρ', then:*

$$m_\rho \circ m'_{\rho'} = \begin{cases} m_{\rho-\rho'} & \text{if } \rho > \rho'; \\ m'_{\rho'-\rho} & \text{if } \rho < \rho'; \\ CC & \text{else.} \end{cases}$$

Proof. We know that m is the dual of m', so $m_\rho \circ m'_\rho = CC$. One can distinguish three different cases: when $\rho = \rho'$, when $\rho > \rho'$ and when $\rho < \rho'$.

1st case: $\rho = \rho'$, so $m_\rho \circ m'_{\rho'} = m_\rho \circ m'_\rho = CC$.
2nd case: $\rho > \rho'$, so $m_\rho \circ m'_{\rho'} = m_{\rho-\rho'+\rho'} \circ m'_{\rho'}$
According to theorem 1 one obtains $m_\rho \circ m'_{\rho'} = m_{\rho-\rho'} \circ m_{\rho'} \circ m'_{\rho'} = m_{\rho-\rho'}$.
3nd case: $\rho < \rho'$, so $m_\rho \circ m'_{\rho'} = m_\rho \circ m'_{\rho+\rho'-\rho}$
According to theorem 1 one obtains $m_\rho \circ m'_{\rho'} = m_\rho \circ m'_\rho \circ m'_{\rho'-\rho} = m'_{\rho'-\rho}$.

We extend the concept of dual modifiers to central modifiers, but with boundary conditions, thus EC_ρ and DC_ρ are quasi-dual. This result is given by the following theorem:

Theorem 4

$$EC_\rho \circ DC_\rho = \begin{cases} m(i) = max(i, 1) \\ m(M) = M \end{cases}$$

Proof.

$$EC_\rho = \begin{cases} m(i) = max(\lfloor \frac{i}{\rho} \rfloor, 1) \\ m(M) = max(\lfloor \frac{M}{\rho} \rfloor + 1, 2) \end{cases} \quad DC_\rho = \begin{cases} m'(i) = i\rho \\ m'(M) = M\rho - \rho + 1 \end{cases}$$

$$EC_\rho \circ DC_\rho = \begin{cases} m(m'(i)) = max(\lfloor \frac{m'(i)}{\rho} \rfloor, 1) \\ m(m'(M)) = max(\lfloor \frac{m'(M)}{\rho} \rfloor + 1, 2) \end{cases} = \begin{cases} m(m'(i)) = max(\lfloor \frac{i\rho}{\rho} \rfloor, 1) \\ m(m'(M)) = max(\lfloor \frac{M\rho-\rho+1}{\rho} \rfloor + 1, 2) \end{cases}$$

$$= \begin{cases} m(m'(i)) = max(\lfloor i \rfloor, 1) \\ m(m'(M)) = max(\lfloor M - 1 + \frac{1}{\rho} \rfloor + 1, 2) \end{cases} = \begin{cases} m(m'(i)) = max(i, 1) \\ m(m'(M)) = max(M - 1 + \lfloor \frac{1}{\rho} \rfloor + 1, 2) \end{cases}$$

$$= \begin{cases} m(m'(i)) = max(i, 1) \\ m(m'(M)) = max(M + \lfloor \frac{1}{\rho} \rfloor, 2) \end{cases}$$

$$\rho \geq 2 \Rightarrow 0 \leq \tfrac{1}{\rho} \leq \tfrac{1}{2} \Rightarrow \lfloor \tfrac{1}{\rho} \rfloor = 0$$

$$EC_\rho \circ DC_\rho = \begin{cases} m(m'(i)) = max(i, 1) \\ m(m'(M)) = max(M, 2) \end{cases} = \begin{cases} m(m'(i)) = max(i, 1) \\ m(m'(M)) = M \end{cases}$$

Property 2. Every Generalized Linguistic Modifiers defined in [5] can be obtained by the composition of elementary operators.

The property 2 corresponds to a set of theorems that gives for every Generalized Linguistic Modifiers, the composition of elementary operators equivalent to it. Table 2 presents a summary of elementary operators composition. The demonstrations of these theorems are given in the appendix.

4.2 Order Relation

Symbolic linguistic modifiers have an order relation proposed by Truck and al. [10] and denoted by $\trianglelefteq$. This order relation is reflexive, transitive and antisymmetric as the order relation $\leq$.

Table 2. A summary of elementary operators composition (i a symbolic degree rank in a base of size M)

Operator	Composition
CR	Elementary
CW	Elementary
ER	Elementary
DW	Elementary
DR_ρ	$CR_\rho \circ DW_\rho$
EW_ρ	$ER_\rho \circ CW_\rho$
DW'_ρ	$DW_\rho \circ CW_\rho$
ER''_ρ	$CR_\rho \circ ER_\rho$ if $i+1 \leq M-\rho$
	$ER_\rho \circ CW_{\rho-M+i-1}$ else
DC_ρ	$CR_{i(\rho-1)} \circ DW_{(M-1)(\rho-1)}$
EC_ρ	$ER_{M-\lfloor \frac{M}{\rho} \rfloor -1} \circ CW_{i-\lfloor \frac{i}{\rho} \rfloor}$ if $\lfloor \frac{i}{\rho} \rfloor \geq 1$
	$ER_{M-\lfloor \frac{M}{\rho} \rfloor -1} \circ CW_{i-1}$ else

Definition 4. *Given two modifiers m and m', a truth-degree rank i and a base size M of a multi-set. $prop(m) = \frac{m(i)}{m(M)-1}$ is comparable to $prop(m') = \frac{m'(i)}{m'(M)-1}$ if and only if [10]:*

$$\begin{cases} prop(m) \leq prop(m'), \forall i \text{ and } \forall M; \\ or \\ prop(m') \leq prop(m), \forall i \text{ and } \forall M. \end{cases}$$

Definition 5 (Order Relation $\trianglelefteq$). *Two modifiers m and m' are comparable according to the order relation $\trianglelefteq$ if and only if $prop(m)$ is comparable to $prop(m')$. Formally, the order relation $\trianglelefteq$ is defined by [10]:*

$m \trianglelefteq m' \Leftrightarrow \forall\ i$ *and* M, $prop(m) \leq prop(m')$

Truck and al. [10] compared the different modifiers in pair with the same radius ρ, and establish a partial order relation between them that was expressed by a lattice. Figure 2 shows this lattice.

The modifier DW'_ρ is the weakest modifier, and ER''_ρ is the strongest one. We remark that this lattice is not complete. Indeed, one can see that the comparisons were realized between modifiers which have the same radius ρ. However, it is sometimes necessarily to compare modifiers that have different radius, for example ER_{ρ_1} and DW_{ρ_2} or DR_{ρ_1} and DR_{ρ_2} with $\rho_1 \neq \rho_2$. Moreover, central modifiers are not presented in the lattice. We introduce in figure 3 a lattice that is more complete than the one introduced in [10].

We can see that the modifier CC is also presented in this lattice, as well as ER'', the modification of ER'. The order relations in bold line present the original lattice of figure 2.

We remark from figure 3 that all weakening modifiers are decreasing, i.e. $m_{\rho+k} \trianglelefteq m_\rho$ where $k \in \mathbb{N}$. In addition, all reinforcing modifiers are increasing, i.e. $m_\rho \trianglelefteq m_{\rho+k}$ where $k \in \mathbb{N}$.

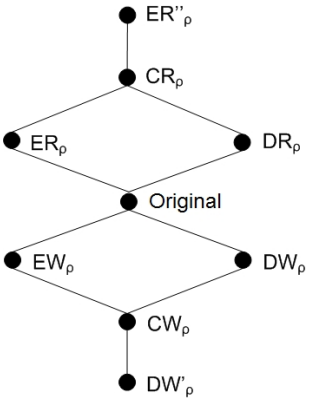

Fig. 2. Lattice for the relation $\trianglelefteq$

Dilated Centring modifier always keeps the proportion unchanged, and that for all radiuses. For this reason it is presented at the same level as CC. On the other hand, Eroded Centring modifiers is incomparable to all the modifiers. We have not presented it in the figure.

Consequently, the completed lattice is obtained according to:

- the initial lattice of figure 2, for two modifiers with the same radius (For example $DR_\rho \trianglelefteq CR_\rho$ implies $DR_{\rho+k} \trianglelefteq CR_{\rho+k}$).
- the radius and the family, for two modifiers from the same family but with different radius (For example $DR_\rho \trianglelefteq DR_{\rho+k}$ and $DW_{\rho+k} \trianglelefteq DW_\rho$).

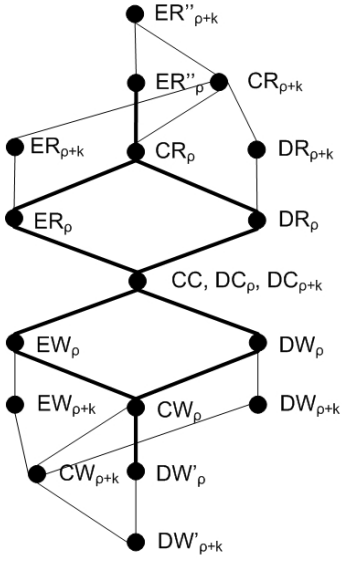

Fig. 3. New lattice for the relation $\trianglelefteq$

– the comparison of the modifiers proportions (for example $prop(DC_\rho) = prop(DC_{\rho+k})$).

We finally extract the two following new definitions:

Definition 6 (Weakest). *Given two modifiers m and m'. The weakest modifier between m and m', denoted by $weakest(m, m')$, is the greatest lower bound of m and m' in the lattice of figure 3.*

Definition 7 (Strongest). *Given two modifiers m and m'. The strongest modifier between m and m', denoted by $strongest(m, m')$, is the least upper bound of m and m' in the lattice of figure 3.*

5 Some Utilities of GSM

In this paragraph, we discuss some cases where Generalized Symbolic Modifiers are used in intelligent applications. Specifically, we choose to address the problem of knowledge management in knowledge based systems. Zadeh has introduced the concept of approximate reasoning [8,19] in order to reason with imperfect data. Approximate reasoning was firstly defined in a fuzzy logic context, since that some others versions were appeared in the symbolic multi-valued context [2,6,7, 20,21]. The principle of approximate reasoning is presented by a generalization of Modus Ponens knows as Generalized Modus Ponens. It can be expressed in standard form as follows:

$$\frac{\begin{array}{l}\text{If } X \text{ is } \mathcal{A} \text{ then } Y \text{ is } \mathcal{B} \\ X \text{ is } \mathcal{A}'\end{array}}{Y \text{ is } \mathcal{B}'} \tag{4}$$

where X and Y are two variables and $\mathcal{A}$, $\mathcal{A}'$, $\mathcal{B}$ and $\mathcal{B}'$ are predicates whose interpretation depends on the used logic. In the case of fuzzy logic, these predicates are fuzzy sets, and in the case of multi-valued logic, they are multi-sets.

We know that Modus Ponens triggers a rule if and only if the observation is exactly equal to rule premise. The generalized Modus Ponens allows inferring not only with an observation which is equal, but also approximately equal to the rule premise. Thus, having an observation "X is $\mathcal{A}'$" with $\mathcal{A}'$ is approximatively equal to $\mathcal{A}$, one can deduce that "Y is $\mathcal{B}'$" with $\mathcal{B}'$ is approximatively equal to $\mathcal{B}$. Hte problem is so the determine the predicate $\mathcal{B}'$.

In a previous works, we have studied axiomatic of approximate reasoning, and we have introduced new approximate reasoning based on linguistic modifiers in the multi-valued framework [12,13]. Its Generalized Modus Ponens in presented as follow:

$$\frac{\begin{array}{ll}\text{Rule} & \textbf{If } X \text{ is } v_\alpha A \textbf{ then } Y \text{ is } v_\beta B \\ \text{Observation} & X \text{ is } m(v_\alpha A)\end{array}}{\text{Conclusion} \qquad Y \text{ is } m'(v_\beta B)} \tag{5}$$

where X and Y are two variables, A and B are multi-sets, and v_α and v_β are symbolic degrees. The observation is modeled by a modification of the rule premise

$m(v_\alpha A)$, where m is a linguistic modifier. The inference conclusion is modeled by a modification of the rule conclusion $m'(v_\alpha B)$, where m' is a linguistic modifier which depends on m, i.e. $m' = f(m)$. To solve this inference, it is enough to determine the modifier m'.

Our hypothesis was that the obtained modifier m' is equal to m, i.e. $m' = m$. It translates effectively the graduality between the rule premise and the rule conclusion. Indeed, the modification observed on the rule premise will be applied with the same intensity to the rule conclusion. For example, given a rule $C \rightarrow D$ and an observation *very* C, the conclusion obtained is *very* D [16,7,15]. Thus, our Generalized Modus Ponens becomes as follows:

$$\begin{array}{ll} \text{Rule} & \textbf{If } X \text{ is } v_\alpha A \textbf{ then } Y \text{ is } v_\beta B \\ \text{Observation} & X \text{ is } m(v_\alpha A) \\ \hline \text{Conclusion} & Y \text{ is } m(v_\beta B) \end{array} \tag{6}$$

To determine the inference conclusion $m(v_\beta B)$, one must just determine the modifier m. After that, this same modifier m is applied to the rule conclusion $v_\beta B$. We will show later in this paper the way to determine this modifier.

The integration of linguistic modifiers in approximate reasoning [12,13] allows checking axiomatic of approximate reasoning [14,15], and has the particularity of providing a gradual reasoning based on the meta-knowledge: "the more the observation is a reinforcement (weakening) of the premise, the more the inference conclusion is a reinforcement (weakening) of the rule conclusion". We explain in this section the use of linguistic modifiers in different cases of approximate reasoning.

5.1 Computing the Transformation between Two Multi-sets

A modifier is a function that transforms a multi-set to another one. So, given two multi-sets, one can determine the modifier that transforms the first multi-set to the second one. There is no way to solve this problem in fuzzy logic. Indeed, the fuzzy sets structure is more complex than the multi-sets structure. It is very difficult, often impossible, to determine a specific operator that transform a whole membership function of a given fuzzy set to another one, especially if their universe of discourse is continuous.

To find a modifier which allows passing from a multi-set to another multi-set, it is easiest to use the elementary operators which are CR, CW, ER and DW [10] as well as the neutral operator CC [12].

Given two multi-sets $v_\alpha A$ and $v_{\alpha'} A'$, the modifier m which transform the first multi-set to the second one can be obtained with the algorithm defined in [12] and reminded here:

det_mod(multi-set $v_\alpha A$, multi-set $v_{\alpha'} A'$): modifier m
M_A and $M_{A'}$ are the basis of A and A' respectively.
- If $M_A = M_{A'}$ and $\alpha = \alpha'$ then $m = CC$.
- If $M_A = M_{A'}$ and $\alpha \neq \alpha'$, m is equal to the operator m_{ρ_1}, defined below, which allows to modify the degree τ_α.

- If $M_A \neq M_{A'}$ and $\alpha = \alpha'$, m is equal to the operator m_{ρ_2}, defined below, which allows to modify the base $\mathcal{L}_{M_A}$.
- If $M_A \neq M_{A'}$ and $\alpha \neq \alpha'$, m is equal to the composition of the two operators: $m_{\rho_1} \circ m_{\rho_2}$, with m_{ρ_1} is the operator allowing to modify the degree and m_{ρ_2} is the one allowing to modify the base.
- Determination of the operator m_{ρ_1} acting on the degree: the radius of the operator is $\rho_1 = |\alpha - \alpha'|$;
  - If $\alpha < \alpha'$ then the operator is CR_{ρ_1}.
  - If $\alpha > \alpha'$ then the operator is CW_{ρ_1}.
- Determination of the operator m_{ρ_2} acting on the base: the radius of the operator is $\rho_2 = |M_A - M_{A'}|$;
  - If $M_A < M_{A'}$ then the operator is DW_{ρ_2}.
  - If $M_A > M_{A'}$ then the operator is ER_{ρ_2}.

End of algorithm

This algorithm was used in our approximate reasoning with linguistic modifiers explained higher. Indeed, to solve the inference, one must determines the modifiers that transform the rule premise to lead to the observation. This modifier is obtained according to the algorithm *det_mod* given above.

Example 1. Given the list of truth-degrees $\mathcal{L}_7 = \{$not-at-all, very-little, little, moderately, enough, very, completely$\}$, and the rule:

"If a tomato is moderately red then it is enough ripe." ($\tau_\alpha = \tau_3$, $\tau_\beta = \tau_4$)
For the following fact: *"This tomato is little red."* ($\tau_{\alpha'} = \tau_2$)

the modifier m transforms "moderately" to "little", so we go from the truth-degree τ_3 to τ_2. Thus, $m = CW_1$ since the operator CW decreases truth-degrees. We apply this modifier to the rule conclusion.

$CW_1(enough) = moderately$. And so we deduce:

"This tomato is moderately ripe." ($\tau_{\beta'} = \tau_3$)

For the following fact: *"This tomato is enough red."*

the modifier which transform "moderately" to "enough" is CR_1. We apply this modifier to the rule conclusion: $CR_1(enough) = very$. We deduce:

"This tomato is very ripe."

We notice through this example that when the observation is a reinforcement (respectively weakening) of the premise ($enough > moderately$), the conclusion undergoes the same reinforcement (weakening) intensity as the premise.

5.2 Transforming the Basis of a Multi-set

In some applications, one needs to transform the basis of a given multi set, more precisely, to relax or to reduce the degrees scale and so to make it flexible. This is required when the intelligent system manipulates data whose multi-sets have not the same basis, for example when data are collected from different sources.

Formally, the problem consists on: given a multi-set in a base $\mathcal{L}_M$, how to transform this multi-set to another one whose base is $\mathcal{L}_{M'}$. To solve this problem, one can use central modifiers. Indeed, Central modifiers act as a zoom on a multi-set. They reduce or retract the basis. In the same time, they try to not change its proportion. So, the maximum degree of the new basis is a multiple of the original one $(M'-1) = (M-1).\rho$, or its quotient $(M'-1) = \lfloor (M-1)/\rho \rfloor$[7]. To relax the basis, Dilated Centering modifier DC id used. And to reduce the basis, Eroded Centering modifier EC is used. For example, given a degree τ_6 of a basis $\mathcal{L}_{19}$, the transformation of this degree to a basis $\mathcal{L}_{33}$ is obtained by DC_2, and its transformation to a basis $\mathcal{L}_{10}$ is obtained by EC_2.

Let's note that sometimes, reducing the basis allows an information loss. Indeed, the central modifiers EC don't always keep the proportion unchanged. According to [5] it happens when the basis becomes very small. We think that it is not due only to the size of the basis. Indeed, the use of the floor function is the cause of the information loss. Thus, to keep the proportion, one must verify that $(M-1)$ is a multiple of $(M'-1)$ and that i is a multiple of i', and so the use of the floor function is avoided. In other terms, according to the modifier definition (see table 1), to verify this condition the radius ρ must be a quotient of i and $M-1$.

The effect of a modifier on a multi-set is not necessarily the same effect on another multi-set. This is due to the following fact: the proportion variation suffered by a modifier varies from multi-set to another. Indeed, to apply for example CR_1 on the degree τ_6 of a basis $\mathcal{L}_{19}$ leads to a proportion increase of 6%, but applying the same modifier with the same radius on the degree τ_3 of a basis $\mathcal{L}_5$ leads to a proportion increase of 25%. For this reason, the hypothesis that $m' = m$ of the GMP (6) is preferable only when the manipulated multi-sets have the same basis. However, when the bases are different it is important to consider this heterogeneity in the inference process in order to keep a coherent result. Let's consider the following GMP:

$$\begin{array}{ll} \text{Rule} & \textbf{If } X \text{ is } v_\alpha A \textbf{ then } Y \text{ is } v_\beta B \\ \text{Observation} & X \text{ is } v_{\alpha'} A' \\ \hline \text{Conclusion} & Y \text{ is } v_{\beta'} B' \end{array} \tag{7}$$

The multi-set A' (respectively B') express the same linguistic term than A (respectively B), or a different term which have the same meaning. However, A' and B' don't necessarily have the same basis than A and B.

With this GMP, the user can choose of the multi-set of the inference conclusion A', contrarily to the GMP defined in [12] where the multi-set of the inference conclusion must be equal to the multi-set of the rule conclusion.

As the manipulated multi-sets have different bases ($\mathcal{L}_{M_A}$, $\mathcal{L}_{M_B}$, $\mathcal{L}_{M_{A'}}$ and $\mathcal{L}_{M_{B'}}$), the principle is first to normalize the basis: convert them all on the same basis $\mathcal{L}_M$. The base size M is obtained by the lowest common multiple of the original bases. Then, ones all the multi-sets represented on the same basis, the approximate reasoning based on linguistic modifiers of the previous section

[7] This results are reduced by 2.

can be applied: the algorithm *det_mod* is used to determine the modifier which allows passing from the rule premise to the observation, and then this modifier is applied on the rule conclusion. Thus, the multi-set obtained by the inference is compatible with the basis $\mathcal{L}_M$. However, the final conclusion is needed on another basis which is $\mathcal{L}_{M_{B'}}$. It is necessarily to convert it on the basis $\mathcal{L}_{M_{B'}}$. The different conversions of the multi-sets are made here by central modifiers, i.e. EC and DC.

The symbolic degree $\tau_{\beta'}$ in the base $\mathcal{L}_{M_{B'}}$ of the inference conclusion are determined as follow:

M_A, M_B, M'_A and M'_B are the basis sizes of respectively the multi-sets A, B, A' and B'. Given $M = LCM(M_A - 1, M_B - 1, M_{A'} - 1, M_{B'} - 1) + 1$[8], and the modifier $m = det\_mod(DC_{\frac{M-1}{M_A-1}}(v_\alpha A), DC_{\frac{M-1}{M_{A'}-1}}(v_{\alpha'} A'))$,

$v_{\beta'} B' = EC_{\frac{M-1}{M_{B'}-1}}(m(DC_{\frac{M-1}{M_B-1}}(v_\beta B)))$

Example 2. Given the lists of truth-degrees:

$\mathcal{L}_9$ = {not-at-all, very-little, little, almost, moderately, more or less, enough, very, completely},
$\mathcal{L}_7$ = {not-at-all, very-little, little, moderately, enough, very, completely},
$\mathcal{L}_5$ ={not-at-all, little, moderately, enough, completely},
$\mathcal{L}_3$ ={not-at-all, moderately, completely},

and the rule:

"If a tomato is more or less red then it is enough ripe."

with *red* and *ripe* are multi-sets in the basis $\mathcal{L}_9$ and $\mathcal{L}_7$ respectively (so $\tau_\alpha = \tau_5$ and $\tau_\beta = \tau_4$). The user gives the fact:

"This tomato is moderately scarlet."

with *scarlet* is a multi-set on the basis $\mathcal{L}_5$ (so $\tau_{\alpha'} = \tau_2$), and wants that the inference conclusion must be constructed with the multi-set *cultivatable* of the base $\mathcal{L}_3$.

We consider the mutli-set A which will be used in the normalisation of the multi-sets of this problem. The size basis of A is:

$M = LCM(2, 4, 6, 8) + 1 = 25$

The modifier which transforms the rule premise to the observation is:

$m = det\_mod(DC_{\frac{24}{8}}(\tau_5 \text{ red}), DC_{\frac{24}{4}}(\tau_2 \text{ scarlet})) = det\_mod(DC_3(\tau_5 \text{ red}), DC_6(\tau_2 \text{ scarlet})) = det\_mod(\tau_{15}A, \tau_{12}A)) = CW_3$
So, the inference conclusion is determined as follows:

$v_{\beta'} cultivatable = EC_{\frac{24}{2}}(m(DC_{\frac{24}{6}}(\tau_4 ripe))) = EC_{12}(CW_3(DC_4(\tau_4 \text{ ripe}))) = EC_{12}(CW_3(\tau_{16}A)) = EC_{12}(\tau_{13}A) = \tau_1$ cultivatable

[8] LCM is the least common multiple.

And so we deduce:

"This tomato is moderately cultivatable."

6 Conclusion

We have given in this paper a study of linguistic modifiers in a symbolic multi-valued context. We have introduced new properties and theorems in order to improve the use of linguistic modifiers. More precisely, composition of linguistic modifiers has been studied. We have demonstrated by a set of theorems that every symbolic modifier can be obtained by a composition of elementary symbolic modifiers. Then we have focused on order relation, and we have constructed a lattice that orders all the defined symbolic modifiers, with considering their parameters. We have also introduced new properties and definitions as a complement of this work. Finally, we have illustrated some utilities of symbolic modifiers in soft computing applications, principally in approximate reasoning. We have used the defined properties to deepen our approximate reasoning based on linguistic modifiers proposed in [12,13]. The new approximate reasoning based on linguistic modifiers offers more liberty and flexibility to the user. However, this approximate reasoning supports simple rule, i.e. the rule premise is a simple proposition. Our future work is to extend our approximate reasoning to infer with complex rules, i.e. rules whose premises are conjunctions or disjunctions of propositions.

References

1. Zadeh, L.A.: Fuzzy sets. Information and Control 8(3), 338–353 (1965)
2. Akdag, H., Glas, M.D., Pacholczyk, D.: A qualitative theory of uncertainty. Fundam. Inform. 17(4), 333–362 (1992)
3. Ginsberg, M.L.: Multivalued logics: a uniform approach to reasoning in artificial intelligence. Computational Intelligence 4(3), 265–316 (1988)
4. Akdag, H., Mellouli, N., Borgi, A.: A symbolic approach of linguistic modifiers. In: Information Processing and Management of Uncertainty in Knowledge-Based Systems, Madrid, 1713–1719 (2000)
5. Akdag, H., Truck, I., Borgi, A., Mellouli, N.: Linguistic modifiers in a symbolic framework. International Journal of Uncertainty. Fuzziness and Knowledge-Based Systems 9(suppl.), 49–61 (2001)
6. Khoukhi, F.: Approche logico-symbolique dans le traitement des connaissances incertaines et imprécises dans les systémes á base de connaissances. PhD thesis, Université de Reims, France (1996)
7. El-Sayed, M., Pacholczyk, D.: Towards a symbolic interpretation of approximate reasoning. Electr. Notes Theor. Comput. Sci. 82(4) (2003)
8. Zadeh, L.A.: The concept of a linguistic variable and its application to approximate reasoning - i - ii - iii. Information Sciences 8, 199–249, 8, 301–357, 9, 43–80 (1975)
9. Truck, I., Akdag, H., Borgi, A.: A symbolic approach for colorimetric alterations. In: Proceedings of the 2nd International Conference in Fuzzy Logic and Technology (EUSFLAT 2001), Leicester, UK, pp. 105–108 (2001)

10. Truck, I., Borgi, A., Akdag, H.: Generalized modifiers as an interval scale: Towards adaptive colorimetric alterations. In: Garijo, F.J., Riquelme, J.-C., Toro, M. (eds.) IBERAMIA 2002. LNCS, vol. 2527, pp. 111–120. Springer, Heidelberg (2002)
11. Truck, I., Akdag, H.: Manipulation of qualitative degrees to handle uncertainty: formal models and applications. Knowledge and Information Systems 9(4), 385–411 (2006)
12. Kacem, S.B.H., Borgi, A., Ghédira, K.: Generalized modus ponens based on linguistic modifiers in a symbolic multi-valued framework. In: Proceeding of the 38th IEEE International Symposium on Multiple-Valued Logic, Dallas, USA, pp. 150–155 (2008)
13. Borgi, A., Kacem, S.B.H., Ghédira, K.: Approximate reasoning in a symbolic multi-valued framework. In: Lee, R.Y., Kim, H.K. (eds.) Computer and Information Science. Studies in Computational Intelligence, vol. 131, pp. 203–217. Springer, Heidelberg (2008)
14. Baldwin, J., Pilsworth, B.: Axiomatic approach to implication for approximate reasoning with fuzzy logic. Fuzzy Sets and Systems 3(2), 193–219 (1980)
15. Fukami, S., Mizumoto, M., Tanaka, K.: Some considerations of fuzzy conditional inference. Fuzzy Sets and Systems 4(3), 243–273 (1980)
16. Lascio, H.D., Gisolfi, A., Cortés, U.: Linguistic hedges and the generalized modus ponens. International Journal of Intelligent Systems 14, 981–993 (1999)
17. Cornelis, C., Kerre, E.E.: Inclusion-based approximate reasoning. In: Alexandrov, V.N., Dongarra, J., Juliano, B.A., Renner, R.S., Tan, C.J.K. (eds.) ICCS-ComputSci 2001. LNCS, vol. 2074, pp. 221–230. Springer, Heidelberg (2001)
18. Truck, I.: Approches symbolique et oue des modificateurs linguistiques et leur lien avec l'agrégation. PhD thesis, Université de Reims, France (2002)
19. Zadeh, L.A.: A theory of approximate reasoning. Machine Intelligence 9, 149–194 (1979)
20. Schwartz, D.G.: A system for reasoning with imprecise linguistic information. Int. J. Approx. Reasoning 5(5), 463–488 (1991)
21. Chung, H.T., Schwartz, D.G.: A resolution-based system for symbolic approximate reasoning. Int. J. Approx. Reasoning 13(3), 201–246 (1995)

Appendix

Theorem 5. $DR_\rho = CR_\rho \circ DW_\rho$

Proof.

$$CR_\rho = \begin{cases} m(i) = min(i+\rho, M-1) \\ m(M) = M \end{cases} ; DW_\rho = \begin{cases} m'(i) = i \\ m'(M) = M+\rho \end{cases}$$

$$CR_\rho \circ DW_\rho = \begin{cases} m(m'(i)) = min(m'(i)+\rho, m'(M)-1) \\ m(m'(M)) = m'(M) \end{cases}$$

$$= \begin{cases} m(m'(i)) = min(i+\rho, M+\rho-1) \\ m(m'(M)) = M+\rho \end{cases} = \begin{cases} m(m'(i)) = i+\rho \\ m(m'(M)) = M+\rho \end{cases} = DR_\rho$$

Theorem 6. $EW_\rho = ER_\rho \circ CW_\rho$

Proof.

$$ER_\rho = \begin{cases} m(i) = i \\ m(M) = max(2, i+1, M-\rho) \end{cases} ; CW_\rho = \begin{cases} m'(i) = max(0, i-\rho) \\ m'(M) = M \end{cases}$$

$$ER_\rho \circ CW_\rho = \begin{cases} m(m'(i)) = m'(i) \\ m(m'(M)) = max(2, m'(i)+1, m'(M)-\rho) \end{cases}$$

$$= \begin{cases} m(m'(i)) = max(0, i-\rho) \\ m(m'(M)) = max(2, max(0, i-\rho)+1, M-\rho) \end{cases}$$

1st Case: $i - \rho \geq 0$
$i - \rho \geq 0 \Rightarrow m(m'(M)) = max(2, i-\rho+1, M-\rho)$
$i + 1 \leq M \Rightarrow i - \rho + 1 \leq M - \rho \Rightarrow m(m'(M)) = max(2, M-\rho)$
2nd Case: $i - \rho < 0$
$i - \rho < 0 \Rightarrow m(m'(M)) = max(2, M-\rho)$

Consequently: $ER_\rho \circ CW_\rho = \begin{cases} m(m'(i)) = max(0, i-\rho) \\ m(m'(M)) = max(2, M-\rho) \end{cases} = EW_\rho$

Theorem 7. $DW'_\rho = DW_\rho \circ CW_\rho$

Proof.

$$DW_\rho = \begin{cases} m(i) = i \\ m(M) = M+\rho \end{cases} ; CW_\rho = \begin{cases} m'(i) = max(0, i-\rho) \\ m'(M) = M \end{cases}$$

$$DW_\rho \circ CW_\rho = \begin{cases} m(m'(i)) = m'(i) \\ m(m'(M)) = m'(M)+\rho \end{cases} = \begin{cases} m(m'(i)) = max(0, i-\rho) \\ m(m'(M)) = M+\rho \end{cases} = DW'_\rho$$

Theorem 8

$$ER''_\rho = \begin{cases} CR_\rho \circ ER_\rho & \text{if } i+1 \leq M-\rho \\ ER_\rho \circ CW_{\rho-M+i-1} & \text{else} \end{cases}$$

Proof. **1st Case:** $i+1 \leq M-\rho$

$$CR_\rho = \begin{cases} m(i) = min(i+\rho, M-1) \\ m(M) = M \end{cases} ; ER_\rho = \begin{cases} m'(i) = i \\ m'(M) = max(2, i+1, M-\rho) \end{cases}$$

$$CR_\rho \circ ER_\rho = \begin{cases} m(m'(i)) = min(m'(i)+\rho, m'(M)-1) \\ m(m'(M)) = m'(M) \end{cases}$$

$$= \begin{cases} m(m'(i)) = min(i+\rho, max(2, i+1, M-\rho)-1) \\ m(m'(M)) = max(2, i+1, M-\rho) \end{cases} = \begin{cases} m(m'(i)) = min(i+\rho, max(2, M-\rho)-1) \\ m(m'(M)) = max(2, M-\rho) \end{cases}$$

$$= \begin{cases} m(m'(i)) = min(i+\rho, max(1, M-\rho-1)) \\ m(m'(M)) = max(2, M-\rho) \end{cases}$$

$i+\rho \geq 1 \Rightarrow min(i+\rho, max(1, M-\rho-1)) = min(i+\rho, M-\rho-1)$
$i+1 \leq M-\rho$ and $i \geq 0 \Rightarrow 1 \leq M-\rho$

$$CR_\rho \circ ER_\rho = \begin{cases} m(m'(i)) = max(0, min(i+\rho, M-\rho-1)) \\ m(m'(M)) = max(2, M-\rho) \end{cases} = ER''_\rho$$

2nd Case: $i+1 > M-\rho$. We note $\rho' = \rho - M + i + 1$.

$$ER_\rho = \begin{cases} m(i) = i \\ m(M) = max(2, i+1, M-\rho) \end{cases} ; CW_{\rho'} = \begin{cases} m'(i) = max(0, i-\rho') \\ m'(M) = M \end{cases}$$

$$ER_\rho \circ CW_{\rho'} = \begin{cases} m(m'(i)) = m'(i) \\ m(m'(M)) = max(2, m'(i)+1, m'(M)-\rho) \end{cases}$$

$$= \begin{cases} m(m'(i)) = max(0, i-\rho') \\ m(m'(M)) = max(2, max(0, i-\rho')+1, M-\rho) \end{cases}$$

$$= \begin{cases} m(m'(i)) = max(0, i-\rho+M-i-1) \\ m(m'(M)) = max(2, max(0, i-\rho+M-i-1))+1, M-\rho) \end{cases}$$

$$= \begin{cases} m(m'(i)) = max(0, M-\rho-1) \\ m(m'(M)) = max(2, max(0, M-\rho-1)+1, M-\rho) \end{cases}$$

$$= \begin{cases} m(m'(i)) = max(0, M-\rho-1) \\ m(m'(M)) = max(2, max(1, M-\rho), M-\rho) \end{cases} = \begin{cases} m(m'(i)) = max(0, M-\rho-1) \\ m(m'(M)) = max(2, M-\rho) \end{cases}$$

$M-\rho < i+1 \Rightarrow M-\rho-1 < i < i+\rho \Rightarrow min(i+\rho, M-\rho-1) = (M-\rho-1)$

$$ER_\rho \circ CW_{\rho'} = \begin{cases} m(m'(i)) = max(0, min(i+\rho, M-\rho-1)) \\ m(m'(M)) = max(2, M-\rho) \end{cases} = ER''_\rho$$

Theorem 9. $DC_\rho = CR_{i(\rho-1)} \circ DW_{(M-1)(\rho-1)}$

Proof. Let's remind that for central modifiers, $i > 1$[9]. We note $\rho_1 = i(\rho-1)$ and $\rho_2 = (M-1)(\rho-1)$.

[9] Otherwise, if $i = 0$ the obtained degree $m(i)$ with m a central modifier will remain $m(i) = 0$.

$$CR_{\rho_1} = \begin{cases} m(i) = min(i + \rho_1, M-1) \\ m(M) = M \end{cases} ; DW_{\rho_2} = \begin{cases} m'(i) = i \\ m'(M) = M + \rho_2 \end{cases}$$

$$CR_{\rho_1} \circ DW_{\rho_2} = \begin{cases} m(m'(i)) = min(m'(i) + \rho_1, m'(M) - 1) \\ m(m'(M)) = m'(M) \end{cases} = \begin{cases} m(m'(i)) = min(i + \rho_1, M + \rho_2 - 1) \\ m(m'(M)) = M + \rho_2 \end{cases}$$

$$= \begin{cases} m(m'(i)) = min(i + i(\rho-1), M + (M-1)(\rho-1) - 1) \\ m(m'(M)) = M + (M-1)(\rho-1) \end{cases} = \begin{cases} m(m'(i)) = min(i\rho, M\rho - \rho) \\ m(m'(M)) = M\rho - \rho + 1 \end{cases}$$

$(M\rho - \rho) - i\rho = \rho(M - 1 - i) \geq 0$ (because $i \leq M-1$)

$$\Rightarrow (M\rho - \rho) \geq i\rho \Rightarrow min(i\rho, M\rho - \rho) = i\rho \Rightarrow CR_{\rho_1} \circ DW_{\rho_2} = \begin{cases} m(m'(i)) = i\rho \\ m(m'(M)) = M\rho - \rho + 1 \end{cases} = DC_\rho$$

Theorem 10

$$EC_\rho = \begin{cases} ER_{M - \lfloor \frac{M}{\rho} \rfloor - 1} \circ CW_{i - \lfloor \frac{i}{\rho} \rfloor} & if \lfloor \frac{i}{\rho} \rfloor \geq 1 \\ ER_{M - \lfloor \frac{M}{\rho} \rfloor - 1} \circ CW_{i-1} & else. \end{cases}$$

Proof

$$ER_{\rho_1} = \begin{cases} m(i) = i \\ m(M) = max(2, i+1, M - \rho_1) \end{cases} ; CW_{\rho_2} = \begin{cases} m'(i) = max(0, i - \rho_2) \\ m'(M) = M \end{cases}$$

$$ER_{\rho_1} \circ CW_{\rho_2} = \begin{cases} m(m'(i)) = m'(i) \\ m(m'(M)) = max(2, m'(i) + 1, m'(M) - \rho_1) \end{cases}$$

$$= \begin{cases} m(m'(i)) = max(0, i - \rho_2) \\ m(m'(M)) = max(2, max(0, i - \rho_2) + 1, M - \rho_1) \end{cases}$$

1st Case: $\lfloor \frac{i}{\rho} \rfloor \geq 1$, we set $\rho_1 = M - \lfloor \frac{M}{\rho} \rfloor - 1$ and $\rho_2 = i - \lfloor \frac{i}{\rho} \rfloor$.

$$ER_{\rho_1} \circ CW_{\rho_2} = \begin{cases} m(m'(i)) = max(0, i - i + \lfloor \frac{i}{\rho} \rfloor) \\ m(m'(M)) = max(max(0, i - i + \lfloor \frac{i}{\rho} \rfloor) + 1, M - M + \lfloor \frac{M}{\rho} \rfloor + 1) \end{cases}$$

$$\begin{cases} m(m'(i)) = max(0, \lfloor \frac{i}{\rho} \rfloor) \\ m(m'(M)) = max(2, max(0, \lfloor \frac{i}{\rho} \rfloor) + 1, \lfloor \frac{M}{\rho} \rfloor + 1) \end{cases}$$

$$\lfloor \frac{i}{\rho} \rfloor \geq 1 \Rightarrow max(0, \lfloor \frac{i}{\rho} \rfloor) = \lfloor \frac{i}{\rho} \rfloor \Rightarrow ER_{\rho_1} \circ CW_{\rho_2} = \begin{cases} m(m'(i)) = \lfloor \frac{i}{\rho} \rfloor \\ m(m'(M)) = max(2, \lfloor \frac{i}{\rho} \rfloor + 1, \lfloor \frac{M}{\rho} \rfloor + 1) \end{cases}$$

$$i < M \Rightarrow \lfloor \frac{i}{\rho} \rfloor + 1 \leq \lfloor \frac{M}{\rho} \rfloor + 1 \Rightarrow ER_{\rho_1} \circ CW_{\rho_2} = \begin{cases} m(m'(i)) = max(\lfloor \frac{i}{\rho} \rfloor, 1) \\ m(m'(M)) = max(\lfloor \frac{M}{\rho} \rfloor + 1, 2) \end{cases} = EC_\rho$$

2nd Case: $\lfloor \frac{i}{\rho} \rfloor < 1$, we set $\rho_1 = M - \lfloor \frac{M}{\rho} \rfloor - 1$ and $\rho_2 = i - 1$.

$$ER_{\rho_1} \circ CW_{\rho_2} = \begin{cases} m(m'(i)) = max(0, i - i + 1) \\ m(m'(M)) = max(2, max(0, i - i + 1) + 1, M - M + \lfloor \frac{M}{\rho} \rfloor + 1) \end{cases}$$

$$= \begin{cases} m(m'(i)) = 1 \\ m(m'(M)) = max(2, \lfloor \frac{M}{\rho} \rfloor + 1) \end{cases} = \begin{cases} m(m'(i)) = max(\lfloor \frac{i}{\rho} \rfloor, 1) \\ m(m'(M)) = max(\lfloor \frac{M}{\rho} \rfloor + 1, 2) \end{cases} = EC_\rho$$

A New Differential Evolution Algorithm with Random Mutation*

Yuelin Gao and Junmei Liu

Institute of Information and System Science, North National University, Yinchuan, China, 750021
gaoyuelin@263.net

Abstract. This paper suggests a new differential evolution algorithm with a random mutation. In this algorithm, a new dynamically mutation rule is given through a linear descending weighted convex combination of two different mutation strategies of DE/rand/1 and DE/best/1, so as to use dynamically DE/rand/1 and DE/best/1 advantages, and an exponent increased crossover probability and a random mutation is introduced to further improve the global optimal capacity. The standard test functions tests show that the new algorithm has fast convergence and high accuracy, robustness stronger, more suitable for solving complex high-dimensional global optimization problem.

Keywords: Global optimization, Differential evolution algorithm, Weighted strategy, Exponent increased crossover probability, Random mutation.

1 Introduction

Differential evolution (DE) as a new evolution algorithm was first proposed by Storn and Price in 1995[1] and had been demonstrated to be the fastest one of evolution algorithms during the first international IEEE evolutionary algorithm race held in 1996[2]. Moreover, DE has a number of advantages over other famous stochastic algorithms, such as, fast convergence speed, strong stability and so on[3]. It starts from the original population to derive new population in constantly iterative calculation by several genetic manipulations i.e. mutation and crossover and selection, and guides the search process to approximate global optimal solution, and in accordance with each individual's fitness to retain the fine individual and out of poor-quality individuals. So far, DE has received extensive attention and applied to many areas successfully due to its simple evolutionary operators, less control parameters and easy to achieve.

However, DE also has drawback as other intelligent algorithms, such as slower convergence rate in iterative latter periods, even falling to local extremes. Many scholars have done lots of attempts to relieve these problems. After the algorithm fall into premature convergence, a chaotic mutation strategy was utilized in the literature

* The work is supported by the Social Science Foundation of China under Grant No.07XJY038 and the Natural Science Foundation of Ning xia under Grant No.NZ0848.

D.-S. Huang et al. (Eds.): ICIC 2009, LNAI 5755, pp. 209–214, 2009.

[4] to help the algorithm to escape from the local extremes; migrating and accelerating operators were joined into DE to improve diversity of population and convergence rate in the literature[5]; a fuzzy adaptive differential evolutionary algorithm was introduced in the literature[6].

We experiment dozens of mutation strategy which are proposed by Price and Storn. Results show that version DE/rand/1 has strong global search ability and version DE/best/1 has strong local search ability. Combining the advantages of the two versions, this paper suggests an improved differential algorithm (MDE), in which a new dynamically mutation rule is given through a linear descending weighted convex combination of the two different mutation strategies. We use linear annealing factor as a weighted factor [7], so that the initial phase of the algorithm has strong global search ability, and as far as possible to find many overall extreme points , and in the later stage should have a strong local search capabilities to enhance algorithm's accuracy and convergence rate. In the MDE algorithm, a crossover probability operator[8] and a random mutation[9] are used to further balance the global search ability and local search capabilities. The standard test functions' test results shows that MDE algorithm has fast convergence and high accuracy, robustness stronger, more suitable for solving complex high-dimensional global optimization problems .

This paper is organized as follows. In section 2, the standard DE and an indexed increased crossover probability are introduced. In section 3, a new improved evolution algorithm with random mutation is given. In section 4, Numerical experiments demonstrate the effectiveness of MDE algorithm. The concluding remarks are offered finally.

2 Based Differential Evolution Algorithm

Differential evolution algorithm contains the following operations: initialization, mutation, crossover and selection. DE algorithm creates new candidate solutions by combining the parent individual and several other individuals of the same population. A candidate replaces the parent only if it has better fitness value.

Assume that population size is N .D denotes dimension number . The i-th individual in the population could be presented with a D-dimension vector. The main operators in DE include:

- Initialization: Input scaling factor of difference vector $F \in [0,2]$,crossover control parameter $CR \in [0,1]$, and population size N . Then individuals in the first generation are generated randomly: $\overline{X}(0) = \{X_1(0), X_2(0), \cdots, X_N(0)\}$, $X_i(0) = (x_1^i(0), x_2^i(0), \cdots, x_D^i(0))$;
- Evaluation: For each individual $X_i(t)$, evaluate its fitness value $f(X_i(t))$;
- Mutation: For each individual $X_i(t)$,three different integers r_1 , r_2 , $r_3 \in \{1,2,\cdots,N\}$ are generated randomly, where $r_1 \neq r_2 \neq r_3 \neq i$.

For variant of version DE/rand/1 we have

$$v_j^i(t) = x_j^{r_1}(t) + \mathrm{F}(x_j^{r_2}(t) - x_j^{r_3}(t)), \quad j = 1,2,\cdots,D. \tag{1}$$

For variant of version DE/best/1 we have

$$v_i^t = x_{best}^t + F(x_{r2}^t - x_{r3}^t). \tag{2}$$

- Crossover: Crossover operator is designed to increase the diversity of the population. First, an integer $j_{rand} \in \{1,2,\cdots,D\}$ is generated randomly. Then, we have the trail vector $U_i(t) = (u_1^i(t), u_2^i(t), \cdots, u_D^i(t))$ by the following equation:

$$u_j^i(t) = \begin{cases} v_j^i(t) & if\ rand(0,1) \le \mathrm{CR}\ or\ j = j_{rand} \\ x_j^i(t) & otherwise \end{cases} \quad j = 1,2,\cdots,D. \tag{3}$$

- Selection: Selection operates by comparing the individuals' fitness to generate the next generation population.

$$X_i(t+1) = \begin{cases} X_i(t) & if\ f(X_i(t)) < f(U_i(t)) \\ U_i(t) & otherwise \end{cases}. \tag{4}$$

This paper introduces exponent increased crossover probability as follows:

$$CR = CR_{\min} + (CR_{\max} - CR_{\min})\exp(-a(1 - t/T_{\max})^b), \tag{5}$$

where a and b are constants, we set $a = 30, b = 3$, t denotes current iteration number, $T_{\max}$ denotes the largest iteration number, $CR_{\min}, CR_{\max}$ are depend on given problems. The exponent increased crossover can provide a good balance between the global exploration and local exploitation abilities.

3 Improved Differential Evolution Algorithm

3.1 Dynamically Mutation Operation

DE algorithm has dozens of the basic mutation versions, in which DE / rand / 1 is able to better maintain population diversity and global search capability, but be slow in convergence; DE/best/1 has better local search ability and faster convergence rate. We use linear combination of the two versions to produce a new dynamically mutation rule below:

$$v_i^t = \lambda x_{r1}^t + (1-\lambda)x_{best}^t + F(x_{r2}^t - x_{r3}^t), \tag{6}$$

where $\lambda \in [0,1]$, if $\lambda = 1$, then (6) is equivalent to (1); if $\lambda = 0$, then (6) is equivalent to (2). Generally speaking, a good algorithm has strong global search ability in the initial stage and has strong local search capabilities in the later stage. Thus in the evolutionary process of DE, λ can be gradually changed from 1 to 0 so as to realize to combine global search with local search. We make λ as

$$\lambda = (T_{\max} - t)/T_{\max}, \tag{7}$$

where $T_{\max}$ is the largest number of iterations and t is current iteration number.

3.2 Random Mutation Operation

In order to avoid stagnation phenomenon in the iteration late, we give next mutation mechanism:

$$\begin{aligned} &if\ F(x_i^t) = F(x_i^{t+1}) = F(x_i^{t+2}) = ... = F(x_i^{t+p})\ and\ F(x_i^t) \neq F^* \\ &then\ x_i^{t+p+1} = x_{\min} + rand(0,1) * (x_{\max} - x_{\min}) \end{aligned} \tag{8}$$

where F^* is the global minimum of the fitness function, p is the largest allowable number of stagnation , $(x_{\min}, x_{\max})$ is allowed the interval of search.

3.3 Description of New Algorithm

Step1. Initialize population size N , scaling factor F , upper bound and lower bound of crossover probability $CR_{\min}, CR_{\max}$, largest iterations number $T_{\max}$.
Step2. Let $t = 0$.
Step3. Update populations according to equations (5),(6),(7), (3),(4) respectively, set the best individual position to Xb , set the corresponding best fitness to Pb .
Step4. Judge whether stagnation or not; if it appears, implemation equation (8).
Step5. $t = t + 1$; if $t = T_{\max}$, then Output Xb , best fitness Pb ; otherwise go to step3.

4 Numerical test

In order to test the performance of MDE, we uses a series of benchmark functions in , and compares MDE with BDE and RDE as well as BRDE . Where BDE is DE algorithm with version DE/best/1, RDE is DE algorithm with version DE/rand/1, BRDE is DE algorithm with two versions' linear combination. Due to space restrictions，only four complex functions are listed in Table 1. f_1 is a high-dimensional single-peak function and is used to inspect convergence speed and convergence precision. And f_2, f_3, f_4 are high-dimensional complex multi-peak functions, this functions'

Table 1. Benchmark test functions

Benchmark function	range	dimension	theory optimal value
$f_1(x) = \sum_{i=1}^{n} \lvert x_i \rvert + \prod_{i=1}^{n} \lvert x_i \rvert$,	$\lvert x_i \rvert \le 10$	30	0
$f_2(x) = \frac{1}{4000} \sum_{i=1}^{n} x_i^2 - \prod_{i=1}^{n} \cos(\frac{x_i}{\sqrt{i}}) + 1$,	$\lvert x_i \rvert \le 600$	30	0
$f_3(x) = -20 \exp[-0.2\sqrt{\sum_{i=1}^{n} x_i^2 / n}]$ $-\exp(\sum_{i=1}^{n} \cos(2\pi x_i)/n) + 20 + e$,	$\lvert x_i \rvert \le 32$	30	0
$f_4(x) = 0.1\{\sin^2(3\pi x_1) + \sum_{i=1}^{n-1} (x_i - 1)^2 [1 +$ $\sin^2(3\pi x_{i+1})] + (x_n - 1)^2\} + \sum_{i=1}^{n} u(x, 5, 100, 4)$	$\lvert x_i \rvert \le 50$	30	0

Table 2. The results of benchmark test functions

function		best value	worst value	average value	standard deviation
f_1	BRDE	3.2282e-030	7.9054e-020	3.4937e-027	1.7482e-027
	BDE	1.8362e-029	2.7122e-019	2.0359e-024	1.0188e-024
	RDE	1.7645e-016	4.2655e-015	7.0515e-016	3.5286e-016
	MDE	4.6960e-031	4.2939e-026	3.2533e-029	1.6279e-029
f_2	BRDE	0	0	0	0
	BDE	0	0.9683	0.0981	0.0491
	RDE	0	0	0	0
	MDE	0	0	0	0
f_3	BRDE	3.3478e-010	0.0639	2.2130e-008	1.1374e-008
	BDE	6.2314	14.4369	7.5934	3.7998
	RDE	2.6334e-012	19.8664	6.5734e-012	1.3178e-012
	MDE	3.4007e-015	4.4409e-015	4.2188e-015	2.1111e-015
f_4	BRDE	2.7917e-032	2.8743e-025	1.5697e-020	7.3452e-021
	BDE	1.7044e-030	839.0652	61.3437	30.6966
	RDE	1.6683e-022	4.4924e-021	8.7014e-022	4.3542e-022
	MDE	1.0098e-032	3.8150e-032	1.2823e-032	6.4166e-033

local optiml solutions exponent increased with the dimesion. The multi-peak functions are used to test effectively the performance of global search of algorithms. The results are listed in Table 2 and Figure 1~4.

In MDE, $CR_{\min} = 0.1, CR_{\max} = 0.9$. In the others algorithms, $CR = 0.6$. F is taken as 0.6 the largest allowable number of stagnation $P = 20$, The population size of each algorithm is 60, The largest iteration number on f_1 is 2000, on the others is 1500. Set run 20 times for each test. Take the average of 20 times as the final result.

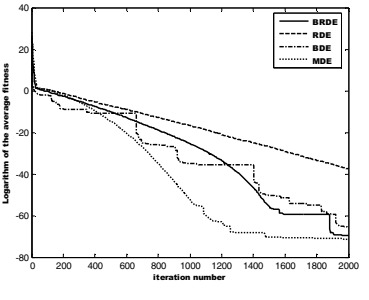

Fig. 1. Evolution curve of function f_1

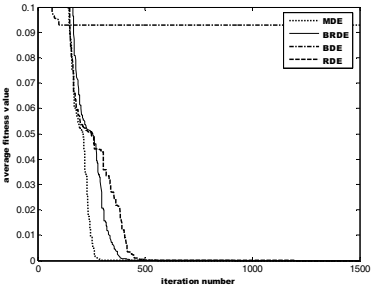

Fig. 2. Evolution curve of function f_2

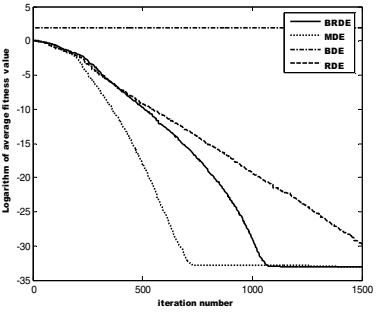

Fig. 3. Evolution curve of function f_3

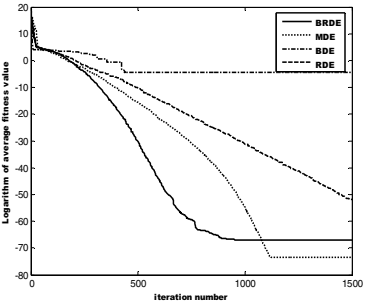

Fig. 4. Evolution curve of function f_4

5 Conclusion

This paper suggests a new DE algorithm with a random mutation. We used four standard test functions to test the performance of MDE Algorithm, and compares MDE with BDE and RDE as well as BRDE. Tested all results mentioned MDE for high-dimensional peak function has a good convergence rate, accuracy, robustness.

References

1. Storn, R., Price, K.: Differential evolution-a simple and efficient adaptive scheme for global optimization over continuous spaces. International Computer Science Institute (1995)
2. Storn, R., Price, K.: Differential evolution-a simple and efficient heuristic for global optimization over continuous spaces. Journal of Global Optimization 11, 341–369 (1997)
3. Hu, Z.B., Xiong, X.W.: Study of hybrid differential evolution based on simulated annealing. Computer Engineering and Design 28(9), 1989–1991 (2007)
4. Liu, J.M., Gao, Y.L.: Differential evolution algorithm based on chaos searching. Computer Engineering and Applications 44(12), 66–68 (2008)
5. Chiou, J.P., Wang, F.S.: A hybrid method of differential evolution with application to optimal control problems of a bioprocess system. In: Proc. of IEEE Int. Conf. on Evolutionary Computation, New York, pp. 627–632 (1998)
6. Liu, J., Lampinen, L.: A fuzzy adaptive differential evolution algorithm. In: IEEE Region 10 Conference on Computers, Communications, Control and Power Engineering, pp. 606–611 (2002)
7. Wu, L.H., Wang, Y.N., et al.: Differential Evolution for Nonlinear Constrained Optimization Using Non-stationary Multi-stage Assignment Penalty Function. Systems engineering —theory & practice 27(3), 128–133 (2007)
8. Deng, X.Z., et al.: A new differential evolution algorithm. Computer Engineering and Applications 44(24), 40–42 (2008)
9. Lua, L.J., Tan, L.J., Niu, P.: A new hybrid global optimization algorithm based on particle swarm optimization and differential evolution algorithm. Information and Control 36(6), 708–714 (2007)

An Improved Harmony Search Algorithm for the Location of Critical Slip Surfaces in Slope Stability Analysis

Liang Li[1], Guang-Ming Yu[1], Shi-Bao Lu[1], Guo-Yan Wang[1,2], and Xue-Song Chu[1]

[1] Qingdao Technological University, 11 Fu Shun Road, Qingdao, 266033, P.R. China
[2] Liao Ning Technical University, Fuxin, 123000, P.R. China
liangli14@yahoo.com.cn

Abstract. The harmony search algorithm was found to be sensitive to the parameters used in the algorithm. Although there is no theoretical method for the determination of values of the used parameters, a dynamic procedure for the values of parameters and a new substituting procedure are proposed in this study which will be demonstrated to be efficient for the location of critical slip surfaces of soil slopes in the slope stability analysis.

Keywords: Artificial intelligence, Engineering optimization, Harmony search algorithm, Slope stability analysis.

1 Introduction

The slope stability was usually performed by Finite Element method, limit analysis and limit equilibrium method. At present, Limit equilibrium method has been widely used by engineers and researchers for slope stability analysis because of its simplicity and extensive engineering experience. The uses of limit equilibrium for general problems required the selection of trial failure surfaces and minimization of the factor of safety for which many proposals have been used with success for simple problems. Some of the difficulties in the location of general critical non-circular failure surfaces are:

(1) The objective function of the safety factor f is usually non-smooth and non-convex. Gradient type optimization method may break down easily if 'failure to converge' (no solution for f for some combinations of control variables) is encountered which can happen for complicated ground condition with external loads.

(2) Chen and Shao [1] have found that multiple minima will exist in general and many solution methods can be trapped easily by the existence of local minimum.

(3) A good initial trial failure surface for global minimization is usually difficult to be estimated for general conditions with arbitrary loadings and geometry. Without a good initial trial, classical minimization methods may fail to locate the global minimum.

The increased complexities of slope stability analyses have drawn the attention of many researchers and engineers to find effective and efficient methods in determining

D.-S. Huang et al. (Eds.): ICIC 2009, LNAI 5755, pp. 215–222, 2009.

the global minimum factor of safety of complex problems. Baker and Gaber [2] used the calculus of variations to locate the critical slip surface and its associated factors of safety but this approach is too complicated for real engineering problems. Nguyen [3] employed simplex method as the technique to locate the critical slip surface. Celestino and Arai and Tagyo [4] utilized conjugate-gradient method for this problem. Baker [5] as well as Yamagami and Jiang [6] adopted dynamic programming to determine the critical slip surface. Greco [7] and Malawi [8] adopted Monte Carlo technique for searching the critical slip surface. Cheng [9] developed a procedure, which transformed the various constraints and requirement of a kinematically acceptable failure mechanism to the evaluation of upper and lower bounds of the control variables and employed simulated annealing algorithm to determine the critical slip surface. Zolfaghari [10] adopted genetic algorithm while Bolton [11] used leap-frog optimization technique to evaluate the minimum factor of safety.

Although there are several new artificial algorithms which have been adopted in the location of critical slip surfaces of soil slopes, for example, the ant colony algorithm [12] and artificial fish algorithm [13].the further research regarding the improvement of existing algorithms should be encouraged. A dynamic adaptation procedure and a new substituting method in the original harmony search algorithm were proposed in this paper which would be tested through case studies.

2 Procedure for Generating Slip Surfaces

The present study adopted the procedure provided by Cheng [9] which was shown in Fig.1. The slope geometry was represented by $y_l(x)$ and the bed rock line which controlled the minimum *y*-coordinates of points in the slip surfaces was represented by $R(x)$. Considering the slip surface subdivided into n slices, refer to Fig.1 ($n=5$), V_1 and V_6 were exit and entrance points of the slip surface, the horizontal distance between x_1 and x_{n+1} was subdivided into n equal segments using Equation. (1):

$$x_i = x_1 + \frac{x_{n+1} - x_1}{n} \times (i-1), i = 2,...,n, \tag{1}$$

Where the lower and upper bounds to $y_2 \ldots y_n$ were denoted as $y_{2\min}, y_{2\max} \ldots y_{n\min}, y_{n\max}$ respectively. The solution domains for variables x_1 and x_{n+1} could be defined easily by engineering experience or sufficiently wide domains could be specified by the engineers. It could be seen from Fig.1 that the value of x_1 varied from the lower bound x_l to upper bound x_u, the value of x_{n+1} varied from the lower bound x_L to upper bound x_U.

After the values of x_1 to x_{n+1} were determined, $y_{2\min}, y_{2\max}$ were identified by the geometry and bed rock line of the slope. y_2 was randomly generated within the range $[y_{2\min}, y_{2\max}]$. The line between V_{n+1} and V_2 intersected with the line $x = x_3$ at point G with the y-ordinates y_G, and the line passing through V_1 and V_2 was extended to intersect with the line $x = x_3$ at point H and *y*-ordinates y_H was received. $y_{3\min}, y_{3\max}$ were determined using Equation. (2):

$$y_{3\min} = \max\{y_H, R(x_3)\} \qquad y_{3\max} = \min\{y_G, y_1(x_3)\}, \tag{2}$$

$y_{4\min}, y_{4\max}, ..., y_{n\min}, y_{n\max}$ were obtained in a way similar to the above one. The slip surface was represented mathematically by the vector $V = [x_1, x_{n+1}, y_2, ..., y_n]$. The number of control variables in this study was $m = n + 1$.

The factor of safety which is the objective function in this study was calculated by using the unbalanced thrust method.

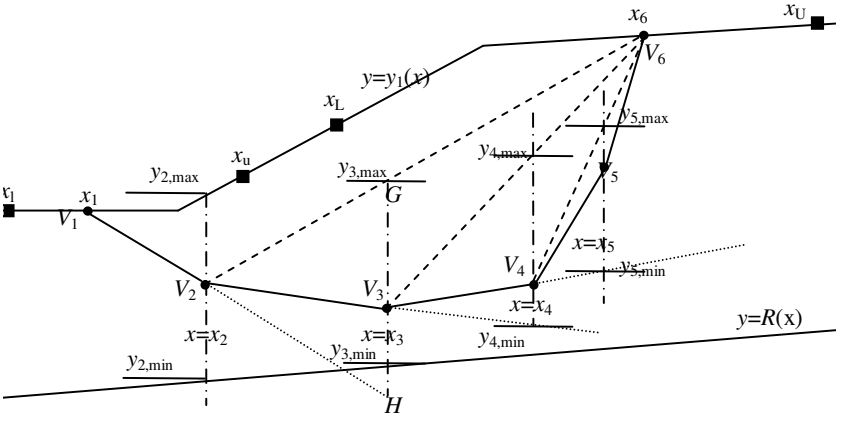

Fig. 1. Illustrating of procedure for generating slip surfaces

3 Improved Harmony Search Algorithm

3.1 Sketch of Original Harmony Search Algorithm

The harmony search algorithm[15,16] was original developed by Dr. Geem based on the musical process of searching for a perfect state of harmony. Musical performances sought to find pleasing harmony (a perfect state) as determined by an aesthetic standard, just as the optimization process sought to find a global solution as determined by an objective function. The harmony in music was analogous to the optimization solution vector, and the musician's improvisations were analogous to local and global search schemes in optimization techniques. The HS algorithm did not require initial values for the decision variables. Furthermore, instead of a gradient search, the HS algorithm used a stochastic random search that was based on the harmony memory considering rate H_r and the pitch adjusting rate P_r so that derivative of function was unnecessary during the analysis.

Harmony search algorithm was a population based search method. A harmony memory HM containing L harmonies was used to generate a new harmony which was probably better than the optimum in the current harmony memory. In present study, the harmony was analogous to the slip surface generated by procedure illustrated in Fig. 1. Consider $\mathrm{HM} = \{h_1 \quad h_2 \quad ,..., \quad h_L\}$, in which $h_i = (x_{i1}, x_{im}, y_{i2}..., y_{in})$ represented vector

V described above. The generation of a new harmony h_{L+1} was of importance to harmony search algorithm which would be described as follows:

Taking the first element x_1 in V for example, its lower and upper bound were x_l and x_u respectively. A random number r in the range of 0 to 1was generated, if $r \le H_r$, $x_{L+1,1}$ was randomly chosen from HM, i e., $x_{L+1,1} \in \{x_{11}, x_{21}, ..., x_{L1}\}$ then P_r was utilized to adjust $x_{L+1,1}$, at last $x_{L+1,1}$ was obtained; if $r > H_r$, $x_{L+1,1}$ was randomly generated from its lower and upper bound, the abovementioned procedure was applied to other elements in V thereby obtaining a new harmony h_{L+1}.

The iterative steps of harmony search algorithm are as follows:

Step1: initialize the algorithm parameters: H_r, P_r, L and randomly generate L harmonies (slip surfaces);

Step 2: generate a new harmony (as described above) and evaluate it, i.e calculate the factor of safety using unbalanced thrust force method;

Step 3: update the HM; i e., if the new harmony h_{N+1} was better than the worst harmony in the HM in terms of factor of safety, the worst harmony was replaced with the new harmony, thus one iteration was finished.

Step 4: repeat steps 2 and 3 until the termination criterion (number of iterations reached the maximum allowed value (see T_m)) was achieved. The values of parameters such as H_r, P_r were usually determined by the rule of thrum and there was no theoretical basis for the determination of these values, a dynamic adaptation procedure for the determination of these two values was proposed in improved harmony search algorithm. In addition, the substituting rule used by original harmony search algorithm was changed in improved harmony search algorithm.

3.2 Improved Harmony Search Algorithm

As mentioned above, there were two different procedures used in improved harmony search algorithm. The dynamic adaptation procedure for the determination of values of parameters was based on the convergence degree among all the harmonies. The convergence degree was represented by 'central distance' C_d of all the harmonies in the present HM which was calculated by Equation (3).

$$C_d = \sum_{i=1}^{L} D_i \qquad D_i = \sqrt{\sum_{j=1}^{m} \left(h_{ij} - C_j\right)^2} \qquad C_j = \frac{\sum_{i=1}^{L} h_{ij}}{L}. \tag{3}$$

$$\begin{cases} H_r = \dfrac{C_d}{M_d} & C_d \le M_d \\ H_r = 1.0 & C_d > M_d \end{cases}. \tag{4}$$

$$M_d = \eta . L . \sqrt{\sum_{j=1}^{m} \left(u_i - l_i\right)^2}. \tag{5}$$

When one iteration was completed, equation (4) was used to determine the value of H_r .Where M_d was the threshold value assigned by the researchers and it was defined in this study according to the lower and upper bounds to elements in vector V , assuming the lower and upper bounds to i^{th} element in vector V as l_i, u_i respectively, M_d was calculated by using equation (5). Where η was a coefficient varying from 0 to1 which was used to decrease the value of $L.\sqrt{\sum_{j=1}^{m}(u_i - l_i)^2}$.

The second improvement was the substituting rule. In the original harmony search algorithm, the worst harmony was replaced with the new generated harmony if the latter was better in terms of objective function than the former one. Such rule only considered the improvement of objective function, actually the new obtained harmony was always better than several ones in the current HM. A new substituting rule was proposed this study which defined the one yielding the maximum 'central distance' C_d to be replaced with the new obtained harmony. To put it in details, each of several harmonies which were worst than the new harmony was replaced with the new one respectively, the corresponding 'central distance' was obtained by Equation (3), the harmony yielding the maximum 'central distance' was replaced in the end.

The improved harmony search algorithm was implemented as follows:

(1) The harmony search algorithm with dynamic adaptation procedure functioned in the first half of total iterations prescribed by T_m ;

(2) The harmony search algorithm with new substituting rule functioned in the second half of total iterations prescribed by T_m , in this half H_r was equal to 1.0.

In the following case studies, 10 different values of parameter H_r were adopted for the original harmony search algorithm, while the value of P_r was identical for both the harmony search algorithms which was 0.1. The parameter T_m was 10000, the number of control variables for the generation of slip surface, i.e., m was 20, L was equal to $2m$.

4 Case Studies

The focused example was a slope in layered soil and genetic algorithm with Morgenstern and Price method was used by Zolfaghari [10]. The geometric layout of the slope was shown in Fig.2 while Table 1 gave the geotechnical properties for soil layers 1 to 4.

Table 1. Geotechnical parameters for example

Layers	γ (kN/m^3)	c (kPa)	ϕ (degree)
1	19.0	15.0	20.0
2	19.0	17.0	21.0
3	19.0	5.00	10.0
4	19.0	35.0	28.0

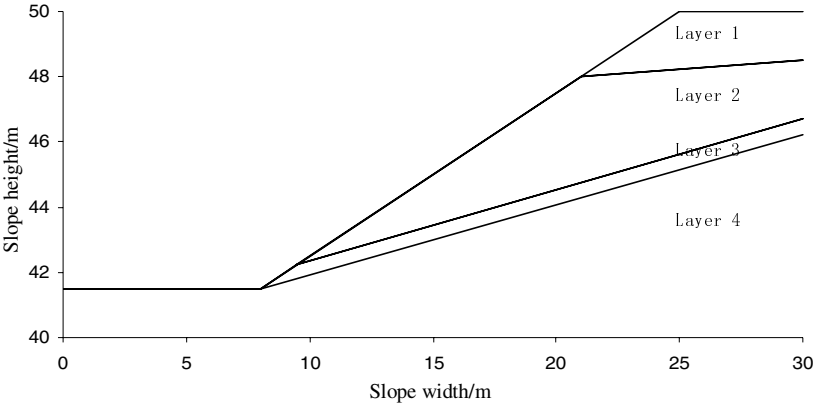

Fig. 2. Cross section of example slope

It was clearly noticed from Fig. 3 that in original harmony search algorithm different values of parameter H_r yielded different results varying from 1.103 to 1.145. However, one result of 1.102 was obtained by improved harmony search algorithm which avoided the determination of value of parameter H_r and considered the diversity of the HM during the iteration steps. The initial harmony memory HM was identical during the experimental analysis for ten different values of H_r and also during the implementation of improved harmony search algorithm, thus the noise situation has insignificant effect on the results obtained. The improved harmony search algorithm utilized different values of H_r according to the 'central distance' of present HM to avoid the probability of trap into the local minimum, whereas the original harmony search algorithm regarded H_r as one invariant regardless of the 'central distance' of present HM which was so small enough to lead the algorithm to the local minimum.

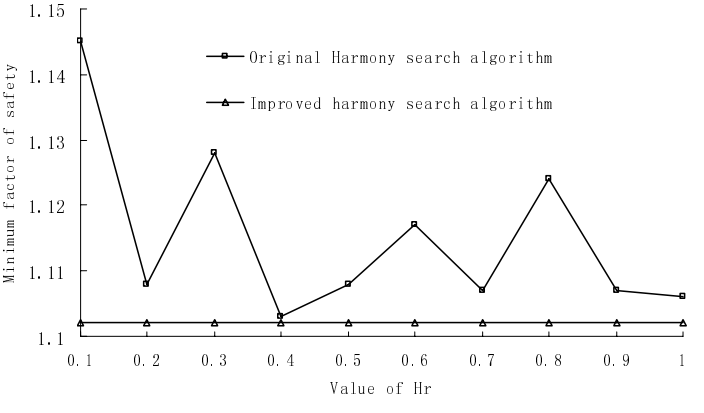

Fig. 3. The curves of minimum factors of safety found by different values of H_r

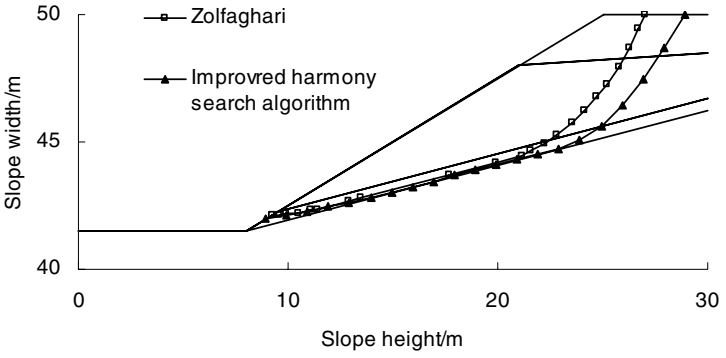

Fig. 4. The comparison of critical slip surfaces

Zolfghari [11] gave the factor of safety of 1.24 by using genetic algorithm, Although the number of slices used by Zolfaghari was not clearly stated, the differences in the factors of safety between the results by the authors and Zolfghari were not small and such differences could not be accounted for by different number of slices used for computation. Refer to Fig.4, it was noticed that greater portions of the failure surfaces by the authors lay within soil layer 3 as compared with the solution by Zolfghari. The lower factor of safety obtained by the authors was hence more reasonable than the solution by Zolfghari.

The comparison of the results proved that the improved harmony search algorithm was efficient and effective for this optimization problem which could also provide promising experience for other related fields.

5 Conclusions

In this study an improved harmony search algorithm was proposed to determine the value of parameter H_r which was usually defined by the rule of thrum. The improved harmony search algorithm also considered the diversity of the current HM which was possible to avoid the trap into the local minimum. The case studies demonstrated the improved harmony search algorithm was efficient within the same number of iterations.

Acknowledgments

The author would like to thank for the help from Project (50874064 and 50804026) supported by the National Natural Science Foundation of China and also from Key Project (Z2007F10) supported by the Natural Science Foundation of Shandong province.

References

1. Chen, Z., Shao, C.: Evaluation of Minimum factor of safety in Slope Stability Analysis. Canadian Geotechnical Journal 25, 735–748 (1988)
2. Baker, R., Garber, M.: Theoretical Analysis of the Stability of Slopes. Geotechnique 28, 341–395 (1978)

3. Nguyen, V.U.: Determination of Critical Slope Failure Surfaces. Journal of Geotechnical Engineering, ASCE 111, 238–250 (1985)
4. Arai, K., Tagyo, K.: Determination of noncircular slip surfaces giving the minimum factor of safety in slope stability analysis 21, 43–51 (1985)
5. Baker, R.: Determination of the critical slip surface in slope stability computations. International Journal of Numerical and Analytical Methods in Geomechanics, 333–359 (1980)
6. Yamagami, T., Jiang, J.C.: A Search for the Critical Slip Surface in Three-Dimensional Slope Stability Analysis. Soils and Foundations 37, 1–6 (1997)
7. Greco, V.R.: Efficient Monte Carlo technique for locating critical slip surface. Journal of Geotechnical Engineering 122, 517–525 (1996)
8. Malkawi Abdallah, I.H., Hassan, W.F., Sarma, S.K.: Global search method for locating general slip surface using Monte Carlo techniques. Journal of Geotechnical and Geoenvironmental Engineering 127, 688–698 (2001)
9. Cheng, Y.M.: Location of Critical Failure Surface and some Further Studies on Slope Stability Analysis. Computers and Geotechnics 30, 255–267 (2003)
10. Bolton Hermanus, P.J., Heymann, G., Groenwold, A.: Global search for critical failure surface in slope stability analysis. Engineering Optimization 35, 51–65 (2003)
11. Zolfaghari, A.R., Heath, A.C., McCombie, P.F.: Simple genetic algorithm search for critical non-circular failure surface in slope stability analysis. Computers and Geotechnics 32, 139–152 (2005)
12. Li, L., Chi, S.C., Lin, G.: The complex method based on ant colony algorithm and its application on the slope stability analysis. Chinese Journal of Geotechnical Engineering 26, 691–696 (2004)
13. Cheng, Y.M., Li, L., Chi, S.C.: Determination of the critical slip surface using artificial fish swarms algorithm. Journal of Geotechnical and Geoenvironmental Engineering 134, 244–251 (2008)
14. Geem, Z.W., Kim, J.H., Loganathan, G.V.: Harmony search. Simulation 76, 60–68 (2001)
15. Geem, Z.W.: Optimal cost design of water distribution networks using harmony search. Engineeering optimization 38, 259–280 (2006)

An Improved PSO Algorithm Encoding *a priori* Information for Nonlinear Approximation

Tong-Yue Gu, Shi-Guang Ju, and Fei Han

School of Computer Science and Telecommunication Engineering, Jiangsu University, Zhenjiang, Jiangsu, China
gtyglx@tom.com, jushig@ujs.edu.cn, hanfei1976@163.com

Abstract. In this paper, an improved PSO algorithm for nonlinear approximation is proposed. The particle swarm optimization is easy to lose the diversity of the swarm and trap into the local minima. In order to resolve this problem, in the proposed algorithm, when the swarm loses its diversity, the current each particle and its historical optimium are interrupted by random function. Moreover, the *a priori* information obtained from the nonlinear approximation problem is encoded into the PSO. Hence, the proposed algorithm could not only improve the diversity of the swarm but also reduce the likelihood of the particles being trapped into local minima on the error surface. Finally, two real data in chemistry field are used to verify the efficiency and effectiveness of the proposed algorithm.

1 Introduction

In past decades, feedforward neural networks (FNN) have been widely used to pattern recognition and function approximation [1-2]. There have many algorithms used to train the FNN, such as backpropagation algorithm (BP), genetic algorithm (GA) [3], particle swarm optimization algorithm (PSOA) [4], simulating annealing algorithm (SAA) [5], etc. Compared with genetic algorithm, PSO algorithm has some advantages. First, PSO algorithm has the memory, and the knowledge of good solution is retained by all the particles. As for the genetic algorithm, the good solutions will lose once the current iteration particle changes. Second, the particles in the PSO algorithm are interrelated with each other to share information. Third, the PSO algorithm can converge faster to the optimal solution, easy to implement, and does not require to encode/decode, hybrid, etc. Finally, the PSO algorithm can solve a lot of optimization problems, and its global search capabilities are much better [6]. Nevertheless, the PSO is easy to lose its diversity, and leads to converge very slowly around the global optimum, which is the phenomenon of the "premature convergence" [7-8].

In order to overcome the shortcoming of PSO, many corresponding algorithms have been proposed. In the literature [9], the passive PSO algorithm was proposed. In this algorithm, the particle tracked its historical optimal location and the global one, and on the mean time tracked the location of its neighbors to update the velocity and improved the diversity of particles. A hybrid PSO algorithm was proposed in the literature [10], and each particle would be given the propagation probability based on

D.-S. Huang et al. (Eds.): ICIC 2009, LNAI 5755, pp. 223–231, 2009.

predetermined criteria. In each iteration, according to the high and low propagation probability, some particles are chosen into a pool. The particles hybrid each other in the pool and generate the equal number of offspring particles, and the offspring particles replace his parent ones in order to keep the same number. In the literature [11], a social clustering PSO algorithm regarded some particles as center, and grouped some particle near from it, and then calculate the center of each cluster and replace the historical and global optimal position with it.

The algorithms mentioned above can improve the diversity of the swarm to some extent, but the particles in these algorithms still may be trapped into the local minima in the course of the training. In this paper, an improved PSO algorithm for nonlinear approximation is proposed. At the beginning of training, the *a priori* information will be encoded into initial particles. In the course of training, when the diversity of the swarm is lost, each particle and its historical optimum are interrupted by a random function, and on the mean time the *a priori* information of the involved problem is encoding into the interrupted particles. The proposed algorithm could not only improve the diversity of the swarm but also reduce the likelihood of the particles being trapped into local minima on the error surface., and the convergence performance of the proposed algorithm will be improved.

2 Particle Swarm Optimization Algorithm

In PSO, a point in the problem space is called a particle, which is initialized with a random position and search velocity. Each particle flies with a certain velocity and find the global best position after some iteration. At each iteration, each particle adjusts its velocity, based on its momentum and the influence of its best position (P_b) as well as the best position of its neighbors (P_g), and then computes a new position that the particle is to fly to. Supposing the dimension for a searching space is m, the total number of particles is n, the position of the ith particle can be expressed as $X_i = (x_{i1}; x_{i2}...; x_{im})$; the best position of the ith particle being searching until now is denoted as $P_i=(p_{i1}; p_{i2}...p_{im})$; and the best position of the total particle swarm being searching until now is denoted as $P_g=(p_{g1}; p_{g2}...p_{gm})$; the velocity of the ith particle is represented as $V_i = (v_{i1}; v_{i2};...; v_{im})$. Then the original PSO is described as:

$$V_i(t+1) = V_i(t) + c_1 * r * (P_i(t) - X_i(t)) + c_2 * r * (P_g(t) - X_i(t)) \quad (1)$$

$$X_i(t+1) = X_i(t) + V_i(t+1) \quad (2)$$

where c_1, c_2 are the acceleration constants worth positive values; *rand()* is a random number between 0 and 1; w is the inertia weight. In addition to the parameter c_1, and c_2 parameters, the implementation of the original algorithm also requires placing a limit on the velocity (v_{max}). After adjusting the parameters w and v_{max}, the PSO can achieve the best ability.

The adaptive particle swarm optimization (APSO) algorithm is based on the original PSO algorithm, firstly proposed by Shi and Eberhart in 1998[12].The APSO can be described as follows:

$$V_i(t+1) = W(t) * V_i(t) + c_1 * r * (P_i(t) - X_i(t)) + c_2 * r * (P_g(t) - X_i(t)) \quad (3)$$

$$X_i(t+1) = X_i(t) + V_i(t+1) \quad (4)$$

where w is a new inertial weight. This algorithm by adjusting the parameter w can make w reduce gradually as the generation increases, In the searching process of the PSO algorithm, the searching space will reduce gradually as the generation increase. The APSO algorithm is more effective, because the searching space reduces step by step nonlinearly. In this paper, we also use this strategy to modify the inertia weight w. When the PSO algorithm is used to modified the weights, each particle $X_i = (w_{1j}^{2i}, \ w_{j1}^{3i}),\ j = 1, 2, \ldots, n$ is defined as the connected weights in the feedforward neural networks which is shown in the Fig.1.

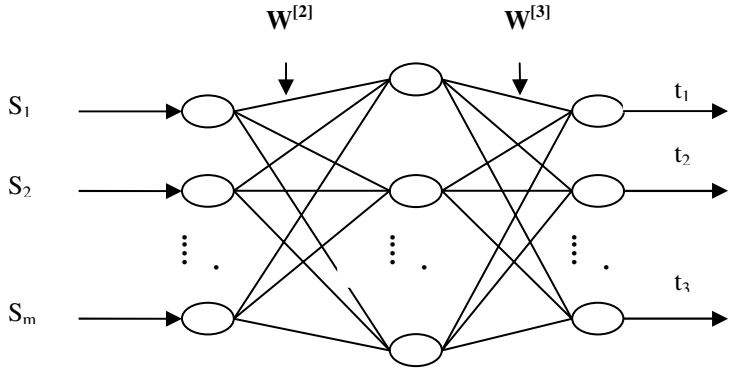

Fig. 1. The scheme of single hidden layer feedforward nural networks

3 The Proposed Algorithm

The standard PSO algorithm has good global search ability, but the particle swarm is also easy to lose its diversity and trap into the local minimum. The reason why the loss of diversity is because that the current particle not only tracks its historical *pbest* position, but also tracks the *gbest* to find its own better position *pbest*. Therefore, *pbest* will close to the *gbest*, and bounds to lose the diversity. In this paper the proposed algorithm named as IDP-PSO algorithm, applies a random function to interrupt the current iteration particle and its *pbest* so that the current particles disperse around the global optimum [13]. As the iteration number increases, the optimal position is nearer to the global optimum obtained by PSO algorithm, so a constrained function is used to control the scope of the current particles dispersed. At the same time, the scope of particle swarm dispersed gradually becomes smaller, so that it could improve the convergence accuracy and rate. Because there are lots of local minima in the error surface, the particles are apt to be trapped into these local minima. In this paper the improved PSO algorithm is used to approximate the nonlinear monotonic functions. The *a priori* information of the monotonicity is encoded into the each particle.

In this paper, the diversity of the swarm is defined as follows [14]:

$$S(t) = \frac{1}{n}\sum_{i=1}^{n}\sqrt{\sum_{j=1}^{n}(x_{ij}(t) - \overline{x_j(t)})^2} \tag{5}$$

where t is the tth generation of the current particle evolution; $S(t)$ is the convergent degree of the current particle swarm and the its historical best particle; n is the total number of the swarm; i is the jth dimension of the ith; $X_{ij}(t)$ is the jth dimension value of the ith particle; $\overline{x_j(t)}$ is the average value of the jth dimension over all particle. When the value of the diversity is less than the value of $S(t)$, the random function is used to disturb current particle and its own P_b.

The function which controls the scope of particle dispersed is defined as follows:

$$X_{ij}(iter) = X_{ij}(iter) + \frac{rand}{e^{\arctan(iter)}} \tag{6}$$

Where $iter$ is the $iter$ th iteration times; $X_{ij}(iter)$ is the i th dimension value of the j th particle; $rand$ stands for the generated values randomly between 0 and 1. In the literature [15], Joerding and Meador presented J.PF method to impose the increasing monotonicity on weights. In their method, a sufficient (but not necessary) condition to satisfy the increasing monotonicity is deduced:

$$w_{j1}^{[2]} w_{1j}^{[3]} > 0,\ j = 1, 2, ..., n, \tag{7}$$

Based on this, J.PF method utilizes the following performance function to eliminate the nonmonotonic intervals in network models:

$$PE(w) = SSE(w) + L(w) \tag{8}$$

$$L(w) = \sum_j u(\theta w_{j1}^{[2]} w_{1j}^{[3]})(e^{\theta w_{j1}^{[2]} w_{1j}^{[3]}} - 1) \tag{9}$$

$$u(\theta w_{j1}^{[2]} w_{1j}^{[3]}) = \begin{cases} 0 & \theta w_{j1}^{[2]} w_{1j}^{[3]} > 0 \\ 1 & otherwise \end{cases} \tag{10}$$

where θ is a modulatory constant. In practice, due to the introduction of the penalty function, J.PF's approximation accuracy and prediction ability are not very good. In this paper, in order to satisfy the priori information, C.P.G method is presented that the position of current iteration particle is obtained from the its own *pbest* and the *gbest*. The current particle is: $X_i = (w_{1j}^{2i},\ w_{j1}^{3i}),\ j = 1, 2, ..., n$. The global optimal position is $P_g = (w_{1j}^{2g}, w_{j1}^{3g})\ j = 1, 2, ..., n$. The historical optimal position of each particle is $P_i = (w_{1j}^{2pi}, w_{j1}^{3pi})\ j = 1, 2, ..., n$. If the weights of current iteration is $w_{1j}^{2i}.w_{j1}^{3i} < 0$ (supposed that $\left|w_{1j}^{2i}\right| > \left|w_{j1}^{3i}\right|$) then set $w_{j1}^{3i} = {w_{j1}^{3g} + w_{j1}^{3pi}}/{2}$. It must satisfy the following penalty:

$$w_{j1}^{3i} = \begin{cases} -(w_{j1}^{3g} + w_{j1}^{3pi}/2) & \operatorname{sgn}(w_{j1}^{3i}) * \operatorname{sgn}(w_{j1}^{3g} + w_{j1}^{3pi}/2) < 0 \\ w_{j1}^{3g} + w_{j1}^{3pi}/2 & \operatorname{sgn}(w_{j1}^{3i}) * \operatorname{sgn}(w_{j1}^{3g} + w_{j1}^{3pi}/2) > 0 \end{cases} \tag{11}$$

Fig.2 shows the concret steps of the IDP-PSO algorithm

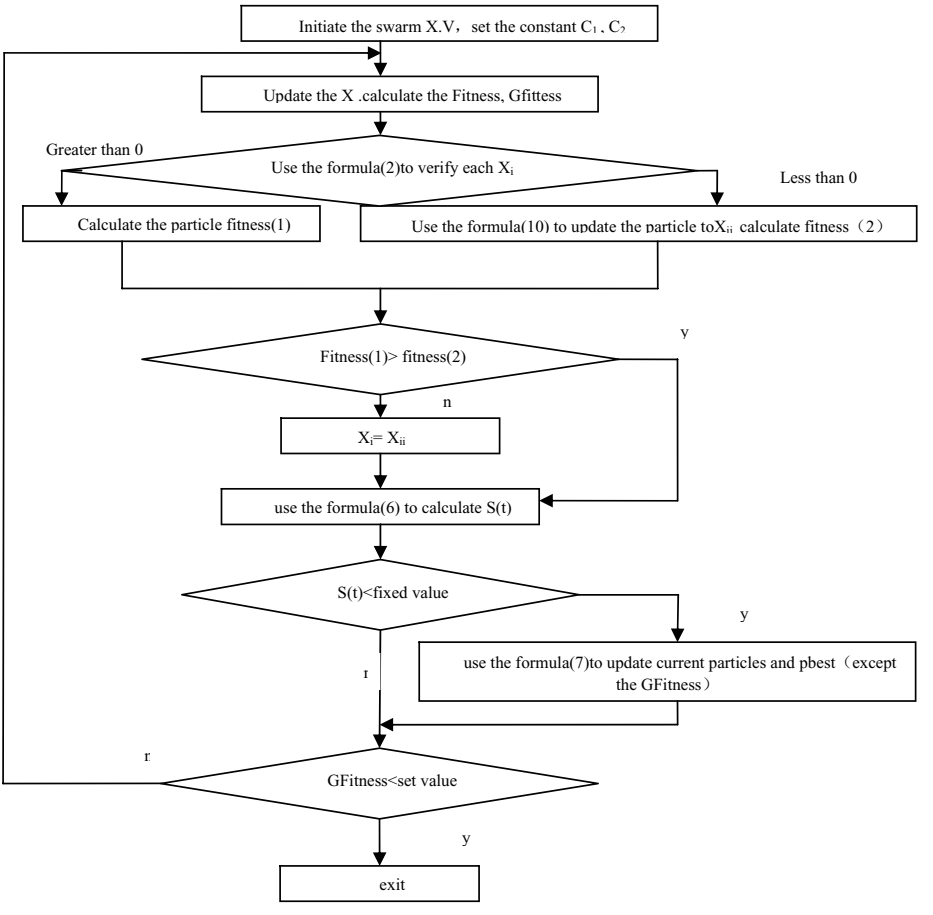

Fig. 2. The flow chart of the IDP-PSO algorithm

4 Experimental Result and Discussion

To demonstrate the improved convergence performance of our proposed algorithm, in this section we shall do two experiments. The proposed algorithm will be compared with BP andPSO. Since a neural network with single nonlinear hidden layer is capable of forming an arbitrarily close approximation of any continuous nonlinear mapping [16], our discussion will be limited to such networks. The transfer functions of

the neurons in all layers are selected as tangent sigmoid function. Every initial particle is a set of weights of FNN generated at random in the range of [0, 1]. Let the initial inertial weight *w* be 1.5, the acceleration constants, *c1* and *c2* both be 1.50, *r1* and *r2* be two random values in the range of [0,1], respectively. The maximum velocity is 5.0 and the minimum velocity is -5.0. The initial velocities of the particles are generated randomly in the range of [0, 1].

In the first experiment, the true boiling point curve of crude oil is plotted by taking the mass percentage of distilled component and the distilled temperature. The curve can reflect the composition of the distilled crude oil. To build a model that takes the mass percentage of distilled component as the independent variable and the distilled temperature as the dependent variable is an important problem in petrochemical industry[17]. In the second experiment, we also verify the methods by modeling the curve of effect of pressure on entropy. The curve of crude oil is plotted by takes the effect of pressure as the independent variable and the entropy as the dependent variable [18]. In the two experiments, the number of hidden neurons and the size of PSO are selected as 8 and 45 respectively. The true boiling point curve of crude oil modeled by the IDP-PSO algorithm is shown at Fig. 3. Fig. 5 shows the curve of effect of pressure on entropy modeled by the IDP-PSO algorithm.

In the two experiments, the one-leave-out method is employed to verify the approximation accuracy and prediction ability of the proposed algorithm and each experiment is conducted 28 times. The corresponding results are shown in Table 1-2.

From the Table 1 it also can be seen that the IDP-PSO algorithm exhibits good approximation accuracy and outstanding prediction ability. Both its $\overline{|r_e|}$ and $|\delta_{r_e}|$ are the smallest among the different methods, which implies that it can predict with high accuracy and stability. Fig. 4 shows the relations between the training error and the iteration number with three learning algorithms. It is evident that the IDP-PSO algorithm is better than the other algorithms in convergence speed and accuracy.

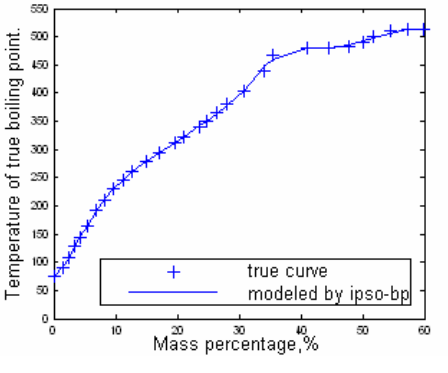

Fig. 3. The true boiling point curve of crude oil modeled by the IPSO-BP algorithm

Table 1. The $\overline{MSE}$, $\overline{|r_e|}$ and the $|\delta_{r_e}|$ on the testing data for modeling the true boiling point curve of crude oil with three algorithms

Learning algorithm	Meanof approximation accuracy($\overline{MSE}$)	Mean of relative prediction error $\overline{|r_e|}$	Standard deviation of relative prediction error $|\delta_{r_e}|$
BP algorithm	2.8061e-003	0.0578	0.0712
PSO algorithm	7.2535e-004	0.0321	0.0623
IDP-PSO algorithm	2.3415e-004	0.0145	0.0056

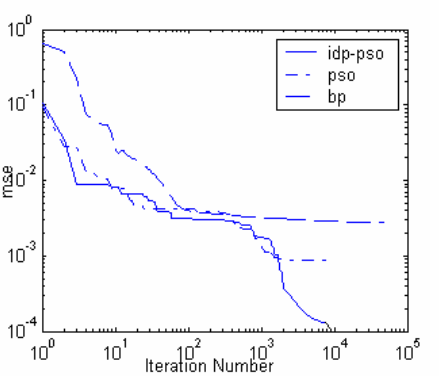

Fig. 4. The relations between the training errors and the iteration number for modeling the true boiling point curve of crude oil with three learning algorithms

Table 2. The $\overline{MSE}$, $\overline{|r_e|}$ and the $|\delta_{r_e}|$ on the testing data for modeling the curve of effect of pressure on entropy with three algorithms

Learning algorithm	Mean of approximation accuracy($\overline{MSE}$)	Mean of relative prediction error $\overline{|r_e|}$	Standard deviation of relative prediction error $|\delta_{r_e}|$
BP algorithm	4.2132e-003	0.0108	0.0053
PSO algorithm	9.6242e-004	0.0073	0.0041
IDP-PSO algorithm	2.4911e-004	0.0032	2.0527e-003

From the Table 2 it also can be seen that the IDP-PSO algorithm also exhibits good approximation accuracy and outstanding prediction ability. Both its $\overline{|r_e|}$ and $|\delta_{r_e}|$ are the smallest among the different methods, which implies that it can predict with high accuracy and stability. Likely, Fig. 6 shows the relations between the training error and the iteration number with four learning algorithms. It is evident that the IDP-PSO algorithm is better than the other algorithms in convergence speed and accuracy.

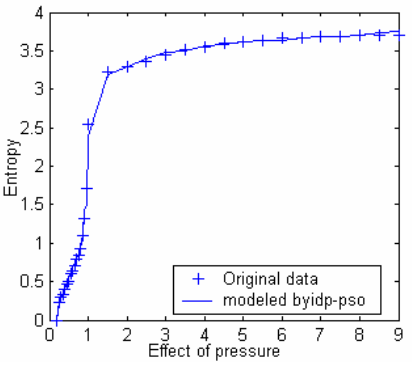

Fig. 5. The curve of effect of pressure on entropy modeled by the IDP-PSO algorithm

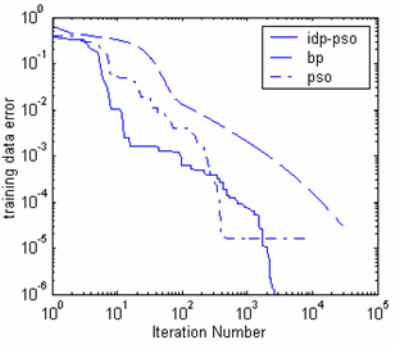

Fig. 6. The relations between the training errors and the iteration number for modeling the curve of effect of pressure on entropy with three learning algorithms

5 Conclusions

In this paper, an improved PSO algorithm for nonlinear approximation was proposed. First, the *a priori* information was encoded into initial particles. Second, in the course of training, when the diversity of the swarm was lost, each particle and its historical optimum were interrupted by a random function, and on the mean time the *a priori* information of the involved problem was encoding into the interrupted particles. The proposed algorithm could not only improve the diversity of the swarm but also reduce the likelihood of the particles being trapped into local minima on the error surface., and the convergence performance of the proposed algorithm were improved. Simulation results were given to verify the efficiency and effectiveness of the proposed approach In future research works, we shall focus on how to apply this improved algorithm to solve more numerical problems.

Acknowledgement

This work was supported by the National Science Foundation of China (No. 60702056) and the Initial Funding of Science Research of Jiangsu University (No. 07JDG033).

References

1. Han, F., Ling, Q.H., Huang, D.H.: Modified Constrained Learning Algorithms Incorporating Additional Functional Constraints Into Neural Network. Information Sciences 178(3), 907–919 (2008)
2. Lin, C.J., Chen, C.H., Lee, C.Y.: A Self-adaptive Quantum Radial Basis Function Network for Classification Applications. In: Proc. of 2004 IEEE International Joint Conference on Neural Networks, pp. 3263–3268 (2004)
3. Angeline, P.J., Sauders, G.M., Pollack, J.B.: An Evolutionary Algorithm that Constructs Recurrent Neural Networks. IEEE Trans, Neural Networks 5(1), 54–65 (1994)
4. Zhang, C.K., Shao, H.H., Li, Y.: Particle Swarm Optimization for Evolving Artificial Neural Network. In: Proc. of IEEE Int. Conf. on System, Man, and Cybernetics, pp. 2487–2490 (2000)
5. Shaw, S., Kinsner, W.: Chaotic Simulated Annealing in Multilayer Feedforward Networks. In: Proc. of Canadian Conf. on Electrical and Computer Engineering, 265–269 (1996)
6. Kennedy, J., Eberhart, R.C.: Swarm Intelligence. Morgan Kaufmann Publishers, San Francisco (2001)
7. Eberhart, R.C., Shi, Y.: Particle Swarm Optimization: Developments Applications and Resources. In: Proc. of 2001 Congress on Evolutionary Computation, pp. 81–86. IEEE Press, Piscataway (2001)
8. Shi, Y., Eberhart, R.C.: A Modified Particle Swarm Optimizer. In: Proceedings of the IEEE International Conference on Evolutionary Computation, pp. 69–73. IEEE Press, Piscataway (1998)
9. He, S., Wu, Q.H., Wen, J.Y.: A Particle Swarm Optimizer with Passive Congregation. BioSystem 78, 135–147 (2004)
10. Naka, S.: A Hybrid Particle Swarm Optimization for Distribution State Estimation. IEEE Transactions on Power Systems 18(1), 60–68 (2003)
11. Kennedy, J.: Stereotyping: Improving Particle Swarm Performance with Cluster Analysis. In: Proceedings of the 2000 Congress on Evolutionary Computation, pp. 1507–1512. IEEE, Piscataway (2000)
12. Shi, Y.H., Eberhart, R.C.: A Modified Particle Swarm Optimizer. In: Proc. of the IEEE Congress on Evolutionary Computation, pp. 69–73. IEEE Press, Piscataway (1998)
13. Gu, T.Y., Ju, S.G., Han, F.: A PSO Algorithm with the Improved Diversity for Feedforward Neural Networks. In: Proc. of Second International Symposium, Moscow, 23-25 January, pp. 123–127 (2009)
14. Engelbrecht, A.P.: Fundamentals of Computational Swarm Intelligence. John Wiley&Sons Ltd., West Sussex (2005)
15. Joerding, W.H., Meador, J.L.: Encoding a Priori Information in Feedforward Networks. Neural Networks 4, 847–856 (1991)
16. Chen, C.W., Chen, D.Z.: An Improved Differential Evolution Algorithm in Training and Encoding Prior Knowledge into Feedforward Networks with Application in Chemistry. Chemometrics and Intelligent Laboratory Systems (2002)
17. Meng, J.L., Sun, Z.Y.: Application of Combined Neural Networks in Nonlinear Function Approximation. In: Proceedings of the Third World Congress on Intelligent Control and Automation, Hefei, pp. 839–841 (2000)
18. American Pertroleum Institute: Technical Data Book—PetroleumRefining, pp. 7–198. Port City Press, Washington (1970)

Multi-objective Oriented Search Algorithm for Multi-objective Reactive Power Optimization*

Xuexia Zhang and Weirong Chen

School of Electrical Engineering, Southwest Jiaotong University, Chengdu 610031, China
zxxswjtu@gmail.com,
wrchen@home.swjtu.edu.cn

Abstract. This paper presents a novel algorithm, multi-objective oriented search algorithm (MOOSA), to deal with the problem of multi-objective reactive power optimization in power system. The multi-objective oriented search algorithm has strong ability to search optimal solutions and well-distributed solutions in Pareto front. The results show that the proposed algorithm is able to balance the multi objects in multi-objective reactive power optimization through the simulations on IEEE 30-bus testing system. The paper concludes that MOOSA is an effective tool to handle the problem of multi-objective reactive power optimization.

Keywords: MOOSA, Pareto-optimal solutions, Pareto front, multi-objective reactive power optimization.

1 Introduction

Reactive power optimization in power system is a crucial way to improve voltage quality, decrease active power losses and increase voltage stability margin. In single-objective reactive power optimization problem, we consider only one objective function, for example, minimizing the active power losses. However, with the development of power market, we need to take account of the voltage quality, the active power losses and the voltage stability margin simultaneously. This paper introduces the mathematic model of multi-objective reactive power optimization, which includes three objective functions to be optimized, such as minimal active power losses, minimal voltage deviations and maximal voltage stability margin.

Multi-objective reactive power optimization is a non-linear, multi-constraint, non-convex, mixed discrete-continuous problem. Many methods have been explored to deal with this problem, mainly including linear programming, non-linear programming and mixed discrete-continuous methods [1-3]. Recently, researchers

* Project Supported by National Natural Science Foundation of China (60870004).

D.-S. Huang et al. (Eds.): ICIC 2009, LNAI 5755, pp. 232–241, 2009.

have focused on computing intelligent technology to handle multi-objective reactive power optimization, for instance, genetic algorithm [4-7], SPEA [8], chaos optimization algorithm [9], immune algorithm [10], particle swarm optimization algorithm [11-12] etc.

Multi-objective oriented search algorithm (MOOSA) stems from single-objective oriented search algorithm [13]. This paper proposes MOOSA to optimize multi-objective reactive power flow and to obtain Pareto front. Through testing on IEEE 30-bus power system, the simulations show that MOOSA can balance different objective functions and make the Pareto front well-distributed. In order to prove the validity of MOOSA, the performances of MOOSA are compared with those of NSGA-II [6]. The comparison results confirm that MOOSA is an efficiency tool applied in multi-objective reactive power optimization.

2 Mathematic Model of Multi-objective Reactive Power Optimization

In the mathematic model of multi-objective reactive power optimization, the multi-objective functions are minimal active power losses P_{loss}, minimal voltage deviations du and maximal voltage stability margin V_{SM}. These multi-objective functions are followed as:

$$\begin{cases} P_{loss} = \sum_{b=1}^{N_L} G_{b(i,j)}[U_i^2 + U_j^2 - 2U_iU_j\cos\delta_{ij}] \\ \min dV = du = \sum_{l=1}^{N_l} \left| \dfrac{U_l - U_l^{spec}}{\Delta U_l^{\max}} \right|^2 \\ \max V_{SM} = \delta_{\min} \end{cases} \tag{1}$$

Equation constraint

$$\begin{cases} P_{Gi} - P_{Li} = U_i \sum_{j=1}^{n} U_j (G_{ij}\cos\delta_{ij} + B_{ij}\sin\delta_{ij}) \\ Q_{Gi} + Q_{Ci} - Q_{Li} = U_i \sum_{j=1}^{n} U_j (G_{ij}\sin\delta_{ij} - B_{ij}\cos\delta_{ij}) \end{cases} \tag{2}$$

Control variables constraint

$$\begin{cases} U_{Gi\min} \le U_{Gi} \le U_{Gi\max} & i = 1,...,N_G \\ T_{Ti\min} \le T_{Ti} \le T_{Ti\max} & i = 1,...,N_T \\ Q_{Ci\min} \le Q_{Ci} \le Q_{Ci\max} & i = 1,...,N_C \end{cases} \tag{3}$$

Dependent variables constraint

$$\begin{cases} U_{Li\min} \le U_{Li} \le U_{Li\max} & i = 1,...,N_l \\ Q_{Gi\min} \le Q_{Gi} \le Q_{Gi\max} & i = 1,...,N_G \end{cases} \tag{4}$$

N_L, N_G, N_T, N_C, N_l denote the number of branch, the number of generator, the number of transformer, the number of capacitor, the number of load-bus, respectively. $G_{b(i,j)}$ denotes the conductance between bus *i* and bus *j* of branch *b*. $\delta_{\min}$ denotes minimal singular value of Jacobin matrix in conventional convergence power flow. U_l , U_l^{spec} , $\Delta U_l^{\max}$ ($\Delta U_l^{\max} = U_l^{\max} - U_l^{\min}$) denote the actual voltage, the specific voltage and the maximal voltage deviations of load-bus *l*, respectively. $U_{Gi}, T_{Ti}, Q_{Ci}, U_{Li}, Q_{Gi}$ denote the generator voltage, the transformer ratio, the shunt capacitors, the load-bus voltage, the generator reactive power. The multi-objective reactive power optimization problem is defined as:

$$\min(F) = \min(P_{loss}, du, -V_{SM})^T \tag{5}$$

3 Multi-Objective Oriented Search Algorithm (MOOSA)

The proposed algorithm, multi-objective oriented search algorithm (MOOSA), is derived from the single-objective oriented search algorithm (OSA) [13]. In nature, single-objective optimization is different from multi-objective optimization, especially in updating strategy and fitness evaluation aspects.

3.1 MOOSA Conceptual Model

In MOOSA, Pareto-optimal solutions of the objective functions, that is, the search-objects, could be regarded as intelligent agents which can transmit information to search-individuals; search-individual simulates the random search behavior of human who could find the intelligent agents as soon as possible when he receives the information. The current search-object transmits the oriented information, which acts as the oriented-neighbor-space of the next walk. According to the oriented-neighbor-space, search-individuals set search-neighbor-space and generate stochastic search steps and search directions. Thus, the interactive action between oriented-neighbor-space and search-neighbor-space models the communication between search-individuals and the search-object.

It should be noticed that the current search-object in MOOSA is different from that in OSA. In MOOSA, the current search-object is one solution chosen randomly from current Pareto-optimal solutions saved in external archive (explicated in later section), while the current search-object in OSA is the current optimal-solution of the objective function. Moreover, these two algorithms are not similar to the oriented-neighbor-space and the search-neighbor-space. The conceptual model of MOOSA is described in the following.

Search-individual
Search-individual simulates the act of human stochastic search. The position of each search-individual is initialized at random, and is formulated as:

$$x_{0ji} = X_{\min i} + (X_{\max i} - X_{\min i}) * random(0,1) \tag{6}$$

Where $random(0,1)$ is a random value between 0 and 1; $X_{\min i}$ and $X_{\max i}$ are the search space bounds; i=1,…, n ,n is the number of dimensions; j=1,…, m, m is the size of population.

Search-object
In each walk, every search-individual achieves multi current search-objects which are saved in external archive P. The external archive saves and updates well-spread non-dominated solutions that would be the Pareto-optimal solutions when the algorithm converges to the Pareto front. For different search-individual, the position of the current search-object is x_{tp} selected randomly in external archive. The current search-object adaptively transmits the oriented information which acts as the oriented-neighbor-space of the next walk. According to the oriented-neighbor-space, search-individuals set search-neighbor-space, and generate stochastic search steps and search directions.

Oriented-neighbor-space
The oriented-neighbor-space is a stochastic neighbor-space built on current search-object adjusting its position adaptively. Correspondingly, oriented information, produced by the current search-object moving adaptively, is the position information of the current search-object. Besides, with the oriented information varying, the oriented-neighbor-space varies accordingly. Different search-individual has different oriented-neighbor-space in each walk, and the same search-individual can have distinct oriented-neighbor-space in different walks. For the whole optimization process, the range of the oriented-neighbor-space is reduced gradually with search-individuals approaching to the search-object, and becomes one certain position until search-individuals achieve the search-object. The oriented-neighbor-space is formulated as: $x_{tp} * (1 + w * randn(0,1))$, where $randn(0,1)$ is a random value of normal distribution between 0 and 1. The parameter w is a variable which can adjust the variable trend of oriented-neighbor-space. $w = w_{\max} - t * (w_{\max} - w_{\min}) / G$, t is the current step, G is maximal generation.

Search-neighbor-space, Search Direction and Step Updating Strategy
During each search walk, each search-individual explores in its own search-neighbor-space while the search direction and step updating strategy depend on the variable oriented-neighbor-space. Different search-individual has dissimilar direction and step.

Exploration Process
The strategy of updating:

$$\Delta x_{tji} = (x_{tp} * (1 + w * randn(0,1)) - x_{tji}) * random(0,1) \tag{7}$$

Explore new position of search-individuals:

$$x_{(t+1)ji} = x_{tji} + \Delta x_{tji} \tag{8}$$

External Archive [14]
In evolution process, MOOSA applies external archive to serve several purposes. First, it saves and updates well-spread non-dominated solutions that would be the Pareto-optimal solutions when the algorithm converges to the Pareto front. Second, it is used as an aid to choose between current Pareto-optimal solutions and previous Pareto-optimal solutions when they do not dominate each other. Finally, this paper explores external archive as a pool to select the x_{tp} .

Evaluation Criteria
The evaluation criteria display difference in nature between single-objective algorithm and multi-objective algorithm. In MOOSA, we comply with Pareto relationship criteria: If individual A dominates individual B; or individual A and individual B are non-dominated with each other, but A is less crowded than individual B, then individual A is better than individual B.

Selecting Excellent Individual
Evaluate the search-object $f_{(t+1)j} = f(\mathbf{x}_{(t+1)j})$, and compare $f_{(t+1)j}$ with f_{tj} , the search-object nearest to $f_{(t+1)j}$ in the solution space. If f_{tj} dominates $f_{(t+1)j}$, discard $f_{(t+1)j}$. If $f_{(t+1)j}$ dominates f_{tj} , replace f_{tj} with $f_{(t+1)j}$ and update external archive P_t . If $f_{(t+1)j}$ and f_{tj} are non-dominated with each other, choose less crowded one to be the new search-object and update external archive P_t .

$f_{(t+1)j}$ will enter the external archive if it is not dominated by the solutions of the external archive: If $f_{(t+1)j}$ dominates some solutions of the external archive, it will enter into the external archive, and the dominated solutions of the external archive will be deleted; or if $f_{(t+1)j}$ and the solutions of the external archive are non-dominated with each other, $f_{(t+1)j}$ will also enter the external archive.

In order to keep the maximal numbers of the external archive, we select the less crowded individuals according to harmonic average distance [14].

3.2 MOOSA for Multi-objective Reactive Power Optimization

The chart of multi-objective reactive power optimization based on MOOSA is described as figure 1:

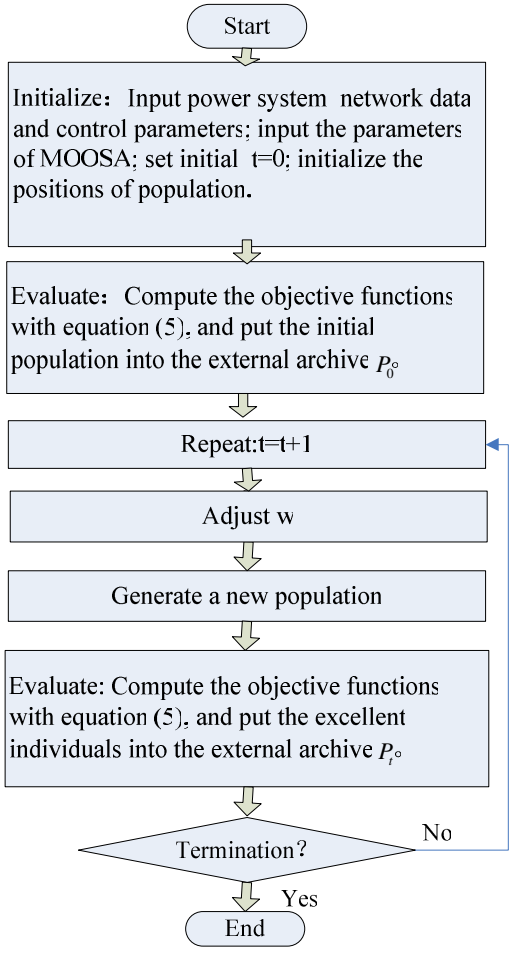

Fig. 1. Flow chart of multi-objective reactive power optimization based on MOOSA

The multi-objective reactive power optimization problem is formulated as equation (5), the position of the search-individual **x** denotes the control values, formulated as equation (9). MOOSA utilizes continuous variables for generator voltages and discrete variables for transformer taps and shunt capacitors, respectively.

$$\mathbf{x} = [U_{G1} \ldots U_{GN_G}, T_{T1} \ldots T_{TN_T}, Q_{C1} \ldots Q_{CN_C}]^T \tag{9}$$

The reactive power optimization based on MOOSA can be described in the following steps.

Step 1 Initialize: Input power system network data and control parameters; input the parameters of MOOSA; set initial t=0; initialize the positions of population.
Step 2 Evaluate: Compute the objective functions with equation (5), and put the initial population into the external archive P_0 .
Step 3 Repeat: t=t+1.

a) Adjust the parameter w to change the oriented-neighbor-space. Where $w = w_{\max} - t*(w_{\max} - w_{\min})/G$.

b) Generate a new population.

c) Evaluate: Compute the objective functions with equation (5), and put the excellent individuals into the external archive P_t .

Step 4 Go to ***Step 3*** until a criterion is met, a maximal number of generation is the termination condition.

4 Numerical Results

4.1 Simulation Setting

In all experiments, the settings are same: the same maximal number of generation is $G = 200$, total 10 runs are made. The initial size of population is $N = 100$. The parameters of the NSGA-II [6] are these: crossover ratio is 0.9, mutation ratio is 0.1; the parameters of the MOOSA are these: w , the one decreased from 0.01 to 0 with increasing generation, and the external archive size is 100. All experiments run in the Lenovo PC of Pentium 4 CPU 2.93GHz, 512MB memory with MATLAB 7.0.

The IEEE 30 and 57-bus power systems are tested. From the results, MOOSA shows well ability of searching. Considering the requirement of paper pages, we present the reactive power optimization results of IEEE 30-bus power system [13] by MOOSA to compare with those by NSGA-II. The transformer taps and the reactive power source installation are discrete variables with the change step of 0.01 and 0.048, respectively. The initial active power loss is 0.06031p.u, the initial voltage deviation is 1.25 and the initial voltage stability margin is 0.2124. The comparative results of average values of optimization are listed in table 1 and table 2, besides, figure 2 and figure 3 show the 3-D Pareto front.

4.2 IEEE 30-Bus Power System Case

The network of IEEE 30-bus power system consists of 41 branches, six generator-buses and 21 load-buses. Four branches, (6, 9), (6, 10), (4, 12) and (27, 28), are under load tap setting transformer branches. The possible reactive power source installation buses are 3, 10 and 24. The comparison results are given as follows:

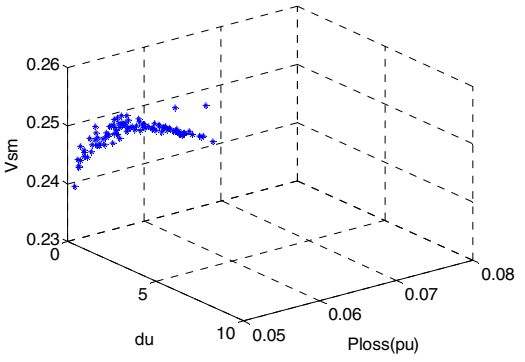

Fig. 2. Pareto front distribution of optimal solutions of reactive power based on MOOSA in IEEE 30-bus system

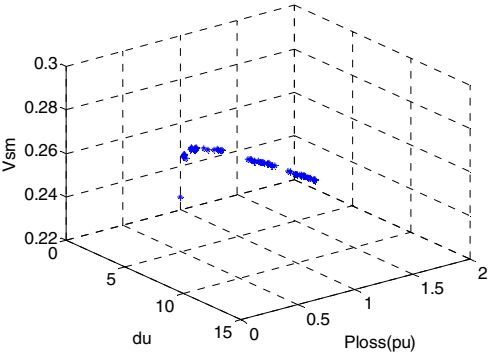

Fig. 3. Pareto front distribution of optimal solutions of reactive power based on NSGA-II in IEEE 30-bus system

Table 1. Comparsion average of optimization in IEEE 30-bus system based on MOOSA with that of in IEEE 30-bus system based on NSGA-II

Algorithm	P_{loss} (p.u.)	du	V_{SM}
MOOSA	0.05125	0.53167	0.24652
NSGA-II	0.05654	0.57411	0.24493

Table 2. Comparsion average optimal rate of optimization in IEEE 30-bus system based on MOOSA with that of in IEEE 30-bus system based on NSGA-II

Algorithm	Saving Percent of P_{loss} (%)	Decreasing Percent of du (%)	Increasing Percent of V_{SM} (%)
MOOSA	15.02	57.47	16.06
NSGA-II	6.25	54.07	15.32

From table 1 and table 2, it can be concluded that the average values of three objective functions (P_{loss} , du and V_{SM}) achieved by MOOSA are better than those achieved by NSGA-II. Also figure 2 and figure 3 identify that MOOSA could obtain well distributed Pareto front and has the ability to balance different objective functions.

In a word, from the perspective of the statistic index of average values, and the single run index of three objective functions values as well, MOOSA is better than NSGA-II.

5 Conclusion

The multi-objective oriented search algorithm is an improved algorithm based on single-objective oriented search algorithm. In the present paper, MOOSA is firstly proposed to apply to multi-objective reactive power dispatch, and is designed to run to achieve multi-optimal solutions (Pareto-optimal solutions) at one time. Therefore, the decision-maker could make a choice from the set of Pareto-optimal solutions. The simulations on IEEE 30-bus power system conclude that MOOSA is an efficient method to dispatch multi-objective reactive power flow.

Acknowledgments. Sincere thanks go to the project supported by National Natural Science Foundation of China（60870004）.

References

1. Momoh, J.A., Adapa, R., El-Hawary, M.E.: A Review of Selected Optimal Power Flow Literature to 1993. I. Nonlinear and Quadratic Programming Approaches. IEEE Trans on Power Systems 14, 96–104 (1999)
2. Momoh, J.A., El-Hawary, M.E., Adapa, R.: A Review of Selected Optimal Power Flow Literature to 1993. II. Newton, Linear Programming and Interior Point Methods. IEEE Trans on Power Systems 14, 105–111 (1999)
3. Liu, M.B., Yang, Y.: Optimal Reactive Power Planning Incorporating Steady State Voltage Stability Constraints. Automation of Electric Power Systems 29, 21–25 (2005)
4. Zhang, W.J., Ye, J.F., Liang, W.J.: Multi-objective Reactive Power Optimization Based on Improved Genetic Algorithm. Power System Technology 28, 67–71 (2004)
5. Lou, S.H., Li, Y., Wu, Y.W.: Multi-objective Reactive Power Optimization Using Quantum Genetic Algorithm. High Voltage Engineering 31, 69–83 (2005)
6. Feng, S.G., Ai, Q.: Application of Fast and Elitist Non-dominated Sorting Generic Algorithm in Multi-objective Research Power Optimization. Transactions of China Electrotechnical Society 28, 146–151 (2007)
7. Liu, F., Yan, W., Yu, D.C.: A Hybrid Strategy Based on GA and IPM for Optimal Reactive Power Flow. Proceedings of the CSEE 25, 67–72 (2005) (in Chinese)
8. Shigang, F., Qian, A.: Multi-objective Reactive Power Optimization Using SPEA2. High Voltage Engineering 33, 115–119 (2007)
9. Lou, S.H., Wu, Y.W., Xiong, X.Y.: Mutative Scale Chaos Optimization Algorithm for Reactive Power Optimization of Power System. Power System Technology. 29, 20–24 (2005)

10. Xiong, H.G., Cheng, H.Z., Hu, Z.C.: A Hybrid Algorithm Based on Chaos Optimization Algorithm and Immune Algorithm for Multi-objective Optimal Reactive Power Flow. Power System Technology 31, 33–37 (2007) (in Chinese)
11. Liu, J., Li, D., Gao, L.Q.: Vector Evaluated Adaptive Particle Swarm Optimization Algorithm for Multi-objective Reactive Power Optimization. Proceedings of the CSEE 28, 22–28 (2008)
12. Lou, S.H., Wu, Y.W., Xiong, X.Y.: Application of Multi-Objective Particle Swarm Optimization Algorithm in Power System Reactive Power Optimization Based on Evaluation of Distance in Fitness Space. Power System Technology 31, 41–46 (2007)
13. Zhang, X.X., Chen, W.R., Dai, C.H.: Application of Oriented Search Algorithm in Reactive Power Optimization. In: The Third International Conference Electric Utility Deregulation and Restructuring and Power Technologies, pp. 2856–2861 (2008)
14. Huang, V.L., Suganthan, P.N., Qiin, A.K.: Multi-objective Differential Evolution with External Archive and Harmonic Distance-based Diversity Measure. Technical Report, Nanyang Technological University (2005)

Combined Discrete Particle Swarm Optimization and Simulated Annealing for Grid Computing Scheduling Problem

Ruey-Maw Chen[1], Der-Fang Shiau[2,*], and Shih-Tang Lo[3]

[1] Department of Computer Science and Information Engineering, National Chin-yi University of Technology, Taichung, 411, Taiwan, R.O.C.
[2] Department of Information Management, Fooyin University, Kaohsiung, Taiwan, R.O.C.
Fax: +886 7 7821301
ft041@mail.fy.edu.tw
[3] Department of Information Management, Kun-Shan University, Tainan, Taiwan, R.O.C.
raymond@mail.ncut.edu.tw, ft041@mail.fy.edu.tw, edwardlo@mail.ksu.edu.tw

Abstract. The grid scheduling problem is concerted with some tasks assigning to a grid distributed system that the relative tasks have to exchange information on different grids. In the original particle swarm optimization (PSO) algorithm, particles search solutions in a continuous solution space. Since the solution space of the grid scheduling problem is discrete. This paper presents a discrete particle swarm optimization (PSO) that combines the simulated annealing (SA) method to solve the grid scheduling problems. The proposed discrete PSO uses a population of particles through a discrete space on the basis of information about each particle's local best solution and global best solution of all particles. For generating the next solution of each particle, the SA is adopted into the discrete PSO. The objective is to minimize the maximum cost of the grid, which includes computing cost and communication cost. Simulation results show that the grid scheduling problem can be solved efficiently by the proposed method.

Keywords: Particle Swarm Optimization, Simulated annealing, Grid Computing, Task Assignment, Meta-heuristic.

1 Introduction

Many applications involve the concepts of scheduling, such as communications, routing, production planning and task assignment in multi-processor system. Most problems in these applications are categorized into the class of NP-complete or combinatorial problems. This means that it would take amount of computation time to obtain an optimal solution, especially for a large-scale scheduling problem. A large variety of approaches have been applied to scheduling problems, such as simulated annealing, neural network, genetic algorithm, heuristic, tabu search, ant system and

* Corresponding author.

D.-S. Huang et al. (Eds.): ICIC 2009, LNAI 5755, pp. 242–251, 2009.

particle swarm optimization. This study incorporates the simulated annealing (SA) algorithm into the discrete particle swarm optimization (PSO) algorithm to solve the scheduling problem of grid computing.

Grid is a service for sharing computer power and data storage capacity over the Internet. The grid systems do better than simple communication between computers and aims ultimately to turn the global network of computers into one vast computational resource. Grid computing can be adopted in many applications, such as high-performance applications, large-output applications, data-intensive applications and community-centric applications. These applications major concern to efficiently schedule tasks over the available processor environment provided by the grid. The efficiency and effectiveness of grid resource management greatly depend on the scheduling algorithm [1]. Generally, in the grid environment, these resources are different over time, and such changes will affect the performance of the tasks running on the grid. In grid computing, tasks are assigned among grid system [2]. Furthermore, the dynamic situations are not considered in this study.

2 The Task Assignment Problem in Grid

The scheduling problem discussed in this study was proposed by the Salman et al. [2]. A meta-heuristic algorithm that is based on the principles of discrete particle swarm optimization (PSO) is proposed for solving the grid scheduling problem. The traditional assignment problems are only concerned to minimize the total processing cost, and there is no communication cost between these tasks and grids.

In homogeneous system, a grid environment can be represented as task interaction graph (TIG) G (V, E), where $V \in \{1, 2, \ldots, M\}$ is the set of the tasks and E are the interaction between these tasks. The M and N are the total number of tasks and the total number of grids, respectively. The total amount of transmission data weight e_{ij} denotes the information exchange (interactive) data between tasks i and j. The p_i is the processing time (cost) corresponding to the work load to be performed by task i on grid. In the example of TIG problem shown in Figure 1, the tasks 2 and 5 are processed on the grid 2 (p2). This means that there is no communication between the two tasks. In addition, each task i has memory requirement m_i to be processed on one grid, and each grid requires enough memory to run their tasks.

For example, the processing time of task 1 is 15 and scheduled on grid 1. The task 1 has to exchange data with the tasks 2, 4 and 5. However, the tasks 2 and 4 are on different grids, this means that there is communication cost with task 1. Furthermore, tasks 1 and 5 are on the same grid and there is no communication cost required between them. Therefore, the total cost for grid 1 is (15) + (5 * 2 + 1 * 2 + 4 * 1) = 31. Moreover, task 1 satisfies the memory constraint; that is, the memory requirement is 20 for task 1, which is less than the memory available of 25 for grid 1. The communication cost is computed by the communication distance multiplies the edge weight. The simulation results can be found in section 5.

The grid system can be represented as a grid environment graph (GEG) G (P, C), where $P = \{1, 2, \ldots, N\}$ is the set of grids in the distributed system. The C represents the set of communication cost between these grids. The d_{ij} between grids i and j

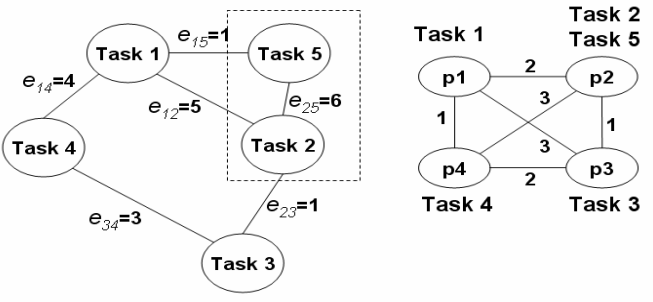

Grid #	1	2	3	4
Memory Available	25	40	30	25

Task #	1	2	3	4	5
Process Time	15	10	20	30	15
Memory Requirement	20	30	25	20	10

Fig. 1. The TIG example proposed by [2]

represents the link cost between the grids. The problem of this study is to assign these tasks in V to the set of grids P. The objective function is to minimize the maximum total execution time required by each grid and the communication cost among all the interactive tasks that satisfies the memory constraint on different grids. The problem can be defined as:

$$\text{Minimize } \{\max (C_{exe}(k)+C_{com}(k))\}, k \in \{1, 2, \ldots, N\} \tag{1}$$

Where

$$C_{exe}(k) = \sum_{i \in A_k} p_i \quad , A_k \text{ is the set of tasks assigned to grid } k \tag{2}$$

$$C_{mem}(k) = \sum_{i \in A_k} m_i \quad , A_k \text{ is the set of tasks assigned to grid } k \tag{3}$$

$$C_{com}(k) = \sum_{i \in A_k} \sum_{j \notin A_k} d_{kp} \cdot e_{ij} \quad \text{,for all grids } p \neq k, p=1 \text{ to } N; i, j=1 \text{ to } M \tag{4}$$

Subject to

$$C_{mem}(k) \leq MemAvail(k) \tag{5}$$

where $C_{exe}(k)$ be the total execution time of all tasks assigned to grid k and $C_{com}(k)$ be the total communication cost between tasks assigned to grid k. Those relative tasks are assigned to other grids in an assignment. The $C_{mem}(k)$ be the total memory requirement of all tasks assigned to grid k, for which the value of $C_{mem}(k)$ have to less than or equal than the total available memory of grid k (Eq. 5) The objective of the task assignment problem is to find an assignment schedule that the cost is minimized

of one grid for a given TIG on a given GEG. In this study, the penalty function is adopted in the proposed algorithms.

$$Penalty(k) = C_{mem}(k) - MemAvail(k) \quad (6)$$

3 Background

3.1 Simulated Annealing Algorithm

Simulated annealing (SA) was introduced by Metropolis in 1953 [3]. SA is one of the efficient methods to solve widely complex problems and a lot of solution combinations [4]. The original SA could be performed by the following algorithm.

Initial a solution S, compute E

Set the initial T, k, r

While $E <> 0$

S' = Generate the new solution

Compute energy E' and $\Delta E = E' - E$

if $\Delta E<0$ then accept $S = S', E = E'$

else Compute the $\delta = e^{-\frac{\Delta E}{kT}}$

Accept the new solution when random number < δ

decrease the temperature $T = T * r$

Fig. 2. Simulated annealing algorithm

where E is defined as $\{\max (C_{exe}(k) + C_{com}(k))\} + Penalty(k)$, $k \in \{1, 2, \ldots, N\}$.

3.2 Particle Swarm Optimization

The particles swarm optimization (PSO) is first proposed by Kennedy and Eberhart [5]. The original PSO is applied in real variable number space. And there are a lot of related works have been introduced in recent years [6-10]. These works indicated that the problems are set in a space featuring of continuous. However, the combination problems are most of discrete or qualitative variables [11]. Kennedy and Eberhart developed a discrete version of PSO in 1997 [12]. The discrete PSO essentially differs from the original PSO in two characteristics. Firstly, the particle is composed of the binary variable. Secondly, the velocity is represented the probability of the binary variable taking the value of one, i. e., the probability of task i is assigned to grid k in this study ($i \in \{1, 2, \ldots, M\}$; $k \in \{1, 2, \ldots, N\}$).

The particle swarm optimization is a multi-agent general meta-heuristic method, and can be applied extensively in solving many NP-complete or combinatorial problems. The PSO consists of a swarm of particles in the space; the position of a particle is indicated by a vector which presents a potential solution. PSO is initialized with a population of particles and searches for the best position (solution or schedule). In every generation or iteration, the local bests and global bests are determined through evaluating the performances, i.e., the fitness values of current population of particles. A particle moves to a new position obtaining a new solution guided by the velocity (a vector). Hence, the velocity plays an important role in affecting the characters of creating new solution. There are two experience positions are used in the PSO; one is the global experience position of all particles, which memorizes the global best solution obtained from all positions (solutions) of all particles; the other is the individual experience position of each particle, which memorizes the local best solution acquired from the positions (solutions) of the corresponding particle has been at. These two experience positions and the inertia weight of the previous velocities used to determine the impact on the current velocity. The velocity retains part of prior velocity (the inertia) and driving particle toward the direction based on the global experience position and the individual experience position. Thus, the particles can derive new positions (solutions) by their own inertia and experience positions.

In traditional PSO, the search space is D dimension space (the number of dimension is corresponding to the parameters of solutions) and the population consists of N_p particles. For the ith particle ($i = 1, \ldots, N_p$), the position consists of M components $X_i = \{ X_{i1}, \ldots, X_{iM} \}$, X_{ij} is the jth component of the position for task j (j=1, . . . , M). The velocity $V_i = \{V_{i1},\ldots,V_{iM} \}$, where V_{ij} is the velocity of component X_{ij}, and the individual experience is a position $L_i = \{ L_{i1}, \ldots, L_{iM} \}$, the local best solution for the ith particle. Additionally, $G = \{G_1, \ldots, G_M \}$ represents the global best experience shared among all the population of particles achieved so far. The mentioned parameters above are used to calculate the updating of the jth component of the position and velocity for the ith particle, as shown in Eq. (7).

$$\begin{cases} V_{ij}^{new} = wV_{ij} + c_1 r_1 (L_{ij} - X_{ij}) + c_2 r_2 (G_j - X_{ij}) \\ X_{ij}^{new} = X_{ij} + V_{ij}^{new} \end{cases} \tag{7}$$

where w is an inertia weight used to determine the influence of the previous velocity to the new velocity. The c_1 and c_2 are learning factors used to derive how the ith particle approaching the position closes to the individual experience position or global experience position respectively. Furthermore, the r_1 and r_2 are the random numbers uniformly distributed in [0, 1], influencing the tradeoff between the global and local exploration abilities during search.

The discrete PSO is adopted by generating solutions for updating the particle's position and velocity vectors to solve the task scheduling problem in parallel machines [13-15]. Another similar to the discrete PSO optimization technique developed by Laskari et al. [16], which is based on the truncation of the real values to their nearest integer. In this study, we introduce discrete PSO equations, which were introduced by Kennedy and Eberhard, to solve the task assignment problem. They also used the

discrete PSO to solve the flowshop scheduling problem, and performed very well in the computation result. This study conducts the discrete PSO method introduced by Liao et al. [11] and combines the SA algorithm for solving the grid system assignment problems. The task assignment problem will be showed in next section.

4 The Proposed Discrete PSO Method

There are N_p particles, and each particle searches for $D = M \times N$ dimension space (the number of tasks and grids). For the hth particle ($h = 1, \ldots, N_p$), the position consists of $M \times N$ components $X_h = \{X_{h11}, \ldots, X_{hMN}\}$, $X_{hij} \in \{0,1\}$is the ith task assigned to grid j for particle h ($i = 1, \ldots, M$; $j = 1, \ldots, N$). The velocity $V_h = \{V_{h11}, \ldots, V_{hMN}\}$, where V_{hij} is the velocity of component X_{hij}, and the individual experience is a position $L_h = \{L_{h11}, \ldots, L_{hMN}\}$, the local best solution for the hth particle. Additionally, $G = \{G_{11}, \ldots, G_{MP}\}$ represents the global best experience shared among all the population of particles achieved so far. The mentioned parameters in above are used to calculate the updating of the V_h component of the position. The velocity for the ith particle is shown in Eq. (8).

$$V_{hij}^{new} = wV_{hij} + c_1 r_1 (L_{hij} - X_{hij}) + c_2 r_2 (G_{ij} - X_{hij}) \tag{8}$$

According to Eq. (8), each particle moves according to its new velocity. As mentioned in Section 3.2, particles are represented by binary variables. Kennedy and Eberhart claim that the higher velocity value is more likely to choose 1, while lower value favors the value of 0. Furthermore, they restrict the velocity values to the interval [0, 1] by using the following sigmoid function:

$$s(V_{hij}) = \frac{1}{1 + \exp(-V_{hij})} \tag{9}$$

where $s(V_{hij})$ is defined as representing the probability of $X_{hij} = 1$. To avoid the value of $s(V_{hij})$ approaching 0 or 1, a constant V_{max} is used to limit the range of V_{hij}. In practice, V_{max} is often set at 4, i.e., $V_{hij} \in [-V_{max}, +V_{max}]$. For task assignment problem, each task can only be assigned to one grid. In the proposed algorithm, each particle h places the unassigned job i to grid j according to the following probability [11]:

$$q_h(i, j) = \frac{s(V_{hij})}{\sum_{j \in U} s(V_{hij})}, \quad U \text{ is the set of unscheduled tasks} \tag{10}$$

Based on the pseudo code of discrete PSO given by the Kennedy et al. [12], the proposed algorithm is showed in Fig. 3. The computation steps of the proposed algorithm in the simulation system can be summarized as: (1) Initialize the parameters and input the problem data. (2) Generate the initial particle solution, including velocity matrix ($V_{N_p MN}$), and then transform the velocity to a matrix of $s(V_{hij})$, and use Eq. (10) to generate the matrix ($X_{N_p MN}$), and set the local best and global best solution. (3) use Eq. (8) to generate the velocity of particles for the next generation until a specified stopping criterion is reached.

```
Initialize and generate each particle solution of X_h matrix and velocity V_h
  Set L_h =X_h, h=1,…, N_p, G = X_1
  Loop
  //find the global best solution
  For h= 1 to N_p
      If Z(X_h)<Z(G) then       // Z( ) objective function
         g = h  //g is the index of the global best G
      End if
  Next h
  For h= 1 to N_p
    Update the velocity matrix V_h based on Eq. (8)
        subject to V_hij ∈ [−Vmax,+Vmax]
    Update the assignment matrix X_h based on Simulated annealing
      E = Z(X_h)-Z(L_h)
    if  E<0 then
        L_h = X_h
    else
        Compute the δ = e^(−ΔE/kT)
        L_h = X_h  when Pa<
     End if
  Next h
  // find the local best solution
    For h = 1 to N_p
      If Z(X_h)<Z(L_h) then          // Z( ) objective function
         L_h = X_h // L_h is the best so far for particle h
      End if
    Next h
   decrease the temperature T
Until the end of criterion is reached
```

Fig. 3. The proposed discrete PSO combined with SA

5 Simulation Results

The simulations use the cases of 5 and 10 tasks to verify the performance of the proposed algorithm. According to Fig. 1, the 5-task case only uses 4 grids and suffers the heavy loading from the computation effort in which the processing time is much more than the communication cost. For the 10-task case, the setting of processing time is in the range of [5, 10], and it needs more communications than the processing cost. The other parameters in this study are set as following: The temperature T was set to 100 and decrease interval was set to 0.99, i.e., $T = T * 0.99$, $w = 0.7$, $c_1 = c_2 = 1$ and $V_{max} = 4$. There are 10 or 20 particles involved in simulation tests. The interactive matrix is symmetrical matrix as the grid distance matrix.

Table 1. The simulation data with 10 tasks

Task #	1	2	3	4	5	6	7	8	9	10
Process time	10	9	8	7	6	5	5	9	8	10
Memory Requirement	10	15	10	20	10	10	20	15	20	10

Table 2. The interaction cost matrix for 5 tasks

Task #	1	2	3	4	5
1	0	5	0	4	1
2	5	0	1	0	6
3	0	1	0	3	0
4	4	0	3	0	0
5	1	6	0	0	0

Table 3. Memory available for 5 grids

Grid #	1	2	3	4	5
Memory Available	100	90	130	90	100

Table 4. The interaction cost matrix for 10 tasks

Task #	1	2	3	4	5	6	7	8	9	10
1	0	1	2	3	4	5	5	4	3	4
2	1	0	5	1	2	3	4	3	5	4
3	2	5	0	3	2	1	0	1	2	3
4	3	1	3	0	4	5	4	3	2	1
5	4	2	2	4	0	1	2	3	4	5
6	5	3	1	5	1	0	4	3	2	1
7	5	4	0	4	2	4	0	2	3	4
8	4	3	1	3	3	3	2	0	5	1
9	3	5	2	2	4	2	3	5	0	2
10	4	4	3	1	5	1	4	1	2	0

Table 5. The distance cost matrix for 5 grids

Grid #	1	2	3	4	5
1	0	2	3	1	5
2	2	0	1	3	3
3	3	1	0	2	4
4	1	3	2	0	6
5	5	3	4	6	0

Table 6. The distance cost matrix for 4 grids

Grid #	1	2	3	4
1	0	2	3	1
2	2	0	1	3
3	3	1	0	2
4	1	3	2	0

In the example of 5-task and 4-grid, the best solution can be found in Table 7. Task 4 is assigned to grid 4, task 1 is assigned to grid 1, and so on. The total processing cost for task 4 on grid 4 is 30. Based on Tables 2 and 6, task 4 has interaction with tasks 1 and 3, and the communication cost to tasks 1 and 3 is 1*4 + 2*3 = 10. Thus, the total cost is 40.

Table 7. The assignment result for 5 tasks and 4 grids

	Grid #			
Task #	1	2	3	4
1	1	0	0	0
2	0	1	0	0
3	0	0	1	0
4	0	0	0	1
5	0	1	0	0

Table 8. The assignment result for 10 tasks and 5 grids

	Grid #				
Task #	1	2	3	4	5
1	0	1	0	0	0
2	0	0	1	0	0
3	0	0	1	0	0
4	0	1	0	0	0
5	0	1	0	0	0
6	0	0	1	0	0
7	0	0	1	0	0
8	0	0	1	0	0
9	0	1	0	0	0
10	0	0	1	0	0

Table 9. The simulation results

(Task, Grid)	Number of particles				
	10		20		
	# of iterations		# of iterations		
	100	300	100	300	500
20,6	1967	1888	1946	1872	1818
20,8	1619	1611	1611	1608	1569
20,12	1308	1249	1263	1241	1163
30,8	3347	3325	3329	3325	3315
30,12	2514	2359	2470	2359	2359
30,15	1998	1998	1998	1957	1957
40,12	4276	4276	4276	4276	4276
40,15	4008	3808	3808	3562	3562
50,15	5157	5157	5741	5157	5156

Table 8 shows the result of 10-task case that the more grids can not decrease the total cost due to the communication cost. In Table 9, the total numbers of tasks were set 20 to 50, the processing times of tasks are uniform distribution of [5, 10] and the memory requirement is also uniform distribution of [50, 100]. The numbers of grids are from 6 to 15, the total available memory is uniform distribution of [200, 400]. The interactive data between of tasks are varying from 1 to 10, and the communications between grids are varied uniform distribution from 1 to 10. Table 9 also shows that more grids can not decrease the total cost. Moreover, simulation results demonstrate that more iterations or number of particles can obtain the better solution.

6 Conclusion

This study has investigated the discrete PSO method for solving a distributed grid system. We also incorporated the SA algorithm into discrete PSO to improve solution

quality. The simulation results demonstrate that the proposed approach yields an efficient solution in the simulation cases. In the future, we suggest that the more complicated cases have to be considered, such as more realistic examples and more tasks involved. Further research encourages that the extension of the discrete PSO incorporating other meta-heuristic maybe is more effective for other scheduling problems.

References

1. Lee, L.T., Tao, D.F., Tsao, C.: An Adaptive Scheme for Predicting the Usage of Grid Resources. Comput. Electr. Eng. 33(1), 1–11 (2007)
2. Salman, A., Ahmad, I., Al-Madani, S.: Particle Swarm Optimization for Task Assignment Problem. Microprocessors and Microsystems 26, 363–371 (2002)
3. Metropolis, N., Rosenbluth, A.W., Rosenbluth, M.N., Teller, A.H., Teller, E.: Equation of State Calculations by Fast Computing Machines. J. of Chem. Phys. 21(6), 1087–1092 (1953)
4. Kirkpatrick, S., Gelatt, C.D., Vecchi, M.P.: Optimization by Simulated Annealing. Science 220, 671–680 (1983)
5. Kennedy, J., Eberhard, R.C.: Particle Swarm Optimization. In: Proceedings IEEE International Conference on Neural Networks, pp. 1942–1948 (1995)
6. Kuo, I.H., Horng, S.J., Kao, T.W., Lin, T.L., Lee, C.L., Terano, T., Pan, Y.: An Efficient Flow-shop Scheduling Algorithm based on a Hybrid Particle Swarm Optimization Model. Expert Syst. Appl. (2009) doi:10.1016/j.eswa.2008.08.054
7. Sha, D.Y., Hsu, C.Y.: A Hybrid Particle Swarm Optimization for Job Shop Scheduling Problem. Comput. Ind. Eng. 51, 791–808 (2006)
8. Bokhari, S.H.: Assignment Problems in Parallel and Distributed Computing. Kluwer Academic Publishers, Boston (1987)
9. Chaudhary, V., Aggarwal, J.K.: A Generalized Scheme for Mapping Parallel Algorithms. IEEE Trans. Parallel Distrib. Syst. 4, 328–346 (1993)
10. Norman, M.G., Thanisch, P.: Models of Machines and Computation for Mapping in Multicomputers. ACM Comput. Surv. 25, 263–302 (1993)
11. Liao, C.J., Tseng, C.T., Luarn, P.: A Discrete Version of Particle Swarm Optimization for Flowshop Scheduling Problems. Comput. Oper. Res. 34(10), 3099–3111 (2007)
12. Kennedy, J., Eberhard, R.C.: A Discrete Binary Version of the Particle Swarm Algorithm. In: Proceedings of IEEE Conference on Systems, Man, and Cybernetics, Piscataway, NJ, pp. 4104–4109 (1997)
13. Kashan, A.H., Karimi, B.: A Discrete Particle Swarm Optimization Algorithm for Scheduling Parallel Machines. Comput. Ind. Eng. 56(1), 216–223 (2009)
14. Kashan, A.H., Karimi, B., Jenabi, M.: A Hybrid Genetic Heuristic for Scheduling Parallel Batch Processing Machines with Arbitrary Job Sizes. Comput. Oper. Res. 35, 1084–1098 (2008)
15. Lee, W.C., Wu, C.C., Chen, P.: A Simulated Annealing Approach to Makespan Minimization on Identical Parallel Machines. Int. J. Adv. Manuf. Technol. 31, 328–334 (2006)
16. Laskari, E.C., Parsopoulos, K.E., Vrahatis, M.N.: Particle Swarm Optimization for Integer Programming. In: Proceedings of the IEEE Congress on Evolutionary Computation, Honolulu, pp. 1582–1587 (2002)

Profile Based Algorithm to Topic Spotting in Reuter21578

Taeho Jo

School of Computer and Information Engineering, Inha University
230 Yonghyundong Namgu Incheon 402-751 South Korea
tjo018@inha.ac.kr
http://tjo018.inha.ac.kr

Abstract. This research proposes an alternative approach to machine learning based ones for categorizing online news articles in Reuter21578. For using machine learning based approaches for any task of text mining or information retrieval, documents should be encoded into numerical vectors; two problems, huge dimensionality and sparse distribution, caused by encoding so. Although there are various tasks of text mining such as text categorization, text clustering, and text summarization, the scope of this research is restricted to text categorization. The idea of this research is to avoid the two problems by encoding a document or documents into a table, instead of numerical vectors. Therefore, the goal of this research is to improve the performance of text categorization by avoiding the two problems.

Keywords: Categorical Profile, Text Categorization.

1 Introduction

Even if there are many approaches to text categorization, as the scope of the exploration on previous research, we will mention only four representative approaches: KNN (K Nearest Neighbor), NB (Naive Bayes), SVM (Support Vector Machine), and MLP (Multi Layers Perceptron). Concerning KNN, Massand et al applied it initially to automatic categorization of news articles in 1992 [5], and Yang recommended it as one of best approaches to text categorization in 1999 [6]. Concerning NB, Mitchell mentioned the case of applying it to a task of text categorization in his textbook in 1997 [7]. Concerning SVM, it was recently regarded as a popular approach to text categorization; Joachim initially applied it to text categorization in 1998 [1], Drucker et al proposed SVM for filtering spam mail as the practical instance of text categorization in 1999 [2], and Cristianini and Shawe-Taylor mentioned SVM as a typical approach to text categorization in their textbook in 2000 [8]. MLP was also regarded as one of popular approaches to text categorization; Wiener initially proposed it for text categorization in 1995 [9], and Ruiz and Srinivasan proposed a hierarchical combination of MLPs for the task in 2002 [10].

For using one of traditional approaches, documents should be encoded into numerical vectors, and encoding documents so causes the two main problems.

D.-S. Huang et al. (Eds.): ICIC 2009, LNAI 5755, pp. 252–257, 2009.

The first problem is huge dimensionality where documents must be encoded into very large dimensional numerical vectors. In general, documents must be encoded at least into several hundreds dimensions of numerical vectors in previous literatures [1][2][3]. This problem causes very high costs for processing each numerical vector representing a document in terms of time and system resources. Furthermore, much more training examples are required proportionally to the dimension for avoiding over-fitting.

The second problem from encoding documents so is sparse distribution where each numerical vector has zero values dominantly. In other words, more than 90% of its elements have zero values in each numerical vector. The discrimination among numerical vectors may be degraded by the problem. This causes poor performance of text categorization. In order to improve performance of text categorization, the two problems should be addressed.

There was a previous attempt to solve the two problems. In 2002, Lodhi et al proposed a kernel function of two raw texts for using SVM for text categorization [4]. An output value of their proposed kernel function indicates a syntactic similarity between two raw texts as two long strings. In other words, they proposed a modified version of SVM which is free from the two problems, and its advantage is that the modified version is applicable to text categorization independently of natural language. However, their proposed version of SVM failed to be better than the traditional version of SVM [4].

In this paper, the proposed approach to text categorization is called table based matching algorithm. The approach is defined as the text categorization algorithm where a document or documents are encoded into a table and they are classified by comparing tables with each other. Since documents are encoded into alternative forms to numerical vectors, the two problems are avoided in using the proposed approach. Thanks to the avoidance, we can expect the performance of text categorization to be improved. Additionally, since tables representing documents are more transparent in terms of their contents than numerical vectors, it may be easier to trace why unseen documents are classified into their own categories.

2 Document Encoding

The first step of the process is tokenization as shown in figure 1.

The output of the first step is transferred to the next step, 'stemming and exception handling' to as its input. In this step, each token is converted into its root form. Before doing that, rules of stemming and exception handling are saved into a file. When the process of encoding documents is triggered, all rules saved as a file are loaded into memory and the corresponding one among them is applied to each token. The output of this step is a list of tokens in their root forms.

The last step of the process is to remove stop words as illustrated in figure 1. Here, stop words are defined as words which perform only grammatical functions irrelevantly to content of their document; articles (a, an, or the), prepositions

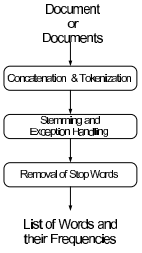

Fig. 1. The Process of Extracting a List of Words and Their Frequencies

(in, on, into, or at), pronoun (he, she, I, or me), and conjunctions (and, or, but, and so on) belong to this kind of words. It is necessary to remove the kind of words for efficient document processing, whether the given task belong to text mining or information retrieval. This step is carried out by loading a list of stop words from a file. Therefore, counting frequencies of words except of stop words and a list of words and their frequencies is generated as a table representing a document or documents.

Although there are various schemes of assigning weights to words, we will mention only three representative schemes. First, we can assign zero or one to words as their weights, depending on their frequencies. Second, the frequencies of words themselves may be used as their weights. For third, we can assign values computed by equation (1) to words as their weights,

$$weight_i(w_k) = tf_i(w_k)(log_2 D + log_2 df(w_k) + 1, \quad (1)$$

where $weight_i(w_k)$ indicates a weight of the word, , which indicates its content based importance in the document, i, $tf_i(w_k)$ indicates the frequency of the word, w_k, in the document, i, $df(w_k)$ is the number of documents including the word, w_k, and D is the total number of documents in a given corpus. In this research, we adopted the third one as the scheme for assigning weights to words.

3 Profile Based Algorithm

Figure 2 illustrates the process of building categorical profiles as the learning process and categorizing an unseen document in the proposed scheme. In the previous section, the process of encoding a document or documents into a table was already described. Therefore, the scope of this section is restricted to the learning process and classification of unseen documents.

In the proposed scheme, the learning process is defined as the construction of tables corresponding to predefined categories. The tables are called categorical profiles in this research, since they are reference for classifying unseen documents. A group of sample labeled documents is given as input of this process. The group is partitioned into subgroups depending on their target labels. Documents in each subgroup are encoded into a table consisting of words and their weights by the process which was described in section 2.

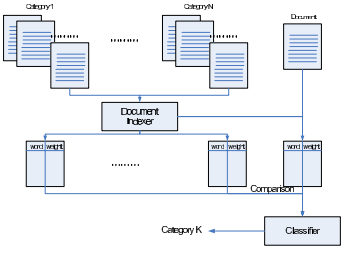

Fig. 2. Learning Process and Classification of Unseen Document in the Proposed Scheme

Once categorical profiles are constructed by the learning process, unseen documents are classified based on the profiles. As shown in figure 2, a single unseen document is given as the input. The document is encoded into a table, and it is compared with each categorical profile. In matching the table with each categorical profile, common words are generated altogether with their weights , and they are summed into a categorical score. The category corresponding to the maximum categorical score is selected as the label of an unseen document, and becomes the output of this process.

4 Experiments and Results

The test bed is Reuter21578, which is a typical standard test bed for evaluating approaches to text categorization. Each news article is given as a document in SGML format, while each news article is given as a plain text in the previous test beds. In the experiment, we selected the most frequent ten categories and table 1 shows the ten categories and a number of documents in each category. The partition of the test bed into training set and test set follows the version, ModApte, which is the standard partition of Reuter 21578 for evaluating text classifiers [11]. The difference of this test bed from 20NewsGroups is that in this test bed each news article is labeled with more than one category, while in the previous test bed each news article is labeled with only one category.

We can implement a text categorization system with decomposing a text categorization task into several binary classification tasks. There are given classifiers as many as predefined categories; ten classifiers are given in this set of experiments. The reason is that each document is labeled softly with more than one category. Each classifier answers whether an unseen document belongs to its corresponding category or not. Instead of accuracy, we adopt F1 measure as the scheme for evaluating the performance of the participating approaches.

F1 measure is the combination of precision and recall with their identical portions. The detail explanation of precision and recall is given in the literature, [12]. Each classifier corresponds to a category one to one; ten classifiers are given according to the number of predefined categories. There are two ways for averaging F1 measures of the ten classifiers: micro averaged F1 and macro-averaged F1. The two kinds of F1 measure are explained in detail in the literatures, [12].

Table 1. Training and Test Set in the Test Bed: Reuter21578

Category Name	Training Set	Test Set	Total
Acq	1452	672	2124
Corn	152	57	209
Crude	328	203	531
Earn	2536	954	3490
Grain	361	162	523
Interest	296	135	431
Money-Fx	553	246	799
Ship	176	87	263
Ship	335	160	495
Wheat	173	76	249
Total	6362	2752	9114

The left side of figure 3 illustrates the results of evaluating the proposed approach with the four options. The right side illustrates results of evaluating the four approaches: three machine learning based approaches and the proposed approach with the most optimal option. The left side of figure 3 shows that the third option where weights of common words in the side of categorical profiles are adopted is optimal in both micro and macro averaged F1 measures. The right side of figure 3 shows that the proposed approach with the third option works better than any of the three machine learning based approaches. Therefore, from this set of experiments, it is judged that once the optimal option is adopted, the proposed one may work better than any of the three popular approaches.

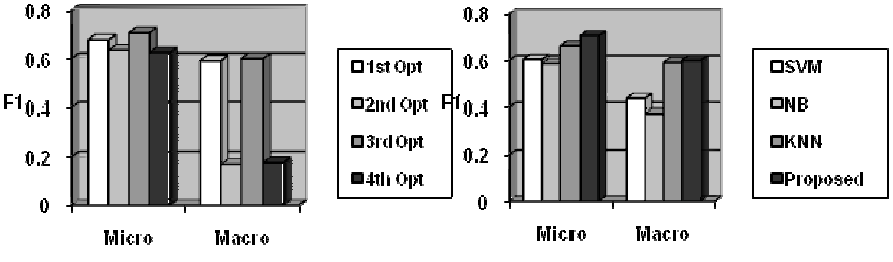

Fig. 3. Results of Four Options of the Proposed Approach and ML based Approaches in Reuter21576

5 Conclusions

This section describes the proposed scheme for categorizing This research proposes an alternative approach to machine learning based ones to text categorization. In the proposed approach, a document or documents are encoded into a table, instead of a numerical vector or numerical vectors. In other words, we can avoid the two main problems in encoding documents into numerical vectors:

huge dimensionality and sparse distribution. The performance of the proposed approach was validated in the previous section using the test beds: Reuter21578. Since the two problems are solved, the proposed approach is shown to work better than machine learning based ones for text categorization.

References

1. Joachims, T.: Text Categorization with Support Vector Machines: Learning with many Relevant Features. In: The Proceedings of 10th European Conference on Machine Learning, pp. 143–151 (1998)
2. Drucker, H., Wu, D., Vapnik, V.N.: Support Vector Machines for Spam Categorization. IEEE Transaction on Neural Networks 10, 1048–1054 (1999)
3. Androutsopoulos, I., Koutsias, K., Chandrinos, K.V., Spyropoulos, C.D.: An Experimental Comparison of Naive Bayes and Keyword-based Anti-spam Filtering with personal email message. In: The Proceedings of 23rd ACM SIGIR, pp. 160–167 (2000)
4. Lodhi, H., Saunders, C., Shawe-Taylor, J., Cristianini, N., Watkins, C.: Text Classification with String Kernels. Journal of Machine Learning Research 2, 419–444 (2002)
5. Massand, B., Linoff, G., Waltz, D.: Classifying News Stories using Memory based Reasoning. In: The Proceedings of 15th ACM International Conference on Research and Development in Information Retrieval, pp. 59–65 (1992)
6. Yang, Y.: An evaluation of statistical approaches to text categorization. Information Retrieval 1, 67–88 (1999)
7. Mitchell, T.M.: Machine Learning. McGraw-Hill, New York (1997)
8. Cristianini, N., Shawe-Taylor, J.: Support Vector Machines and Other Kernel-based Learning Methods. Cambridge University Press, Cambridge (2000)
9. Wiener, E.D.: A Neural Network Approach to Topic Spotting in Text. The Thesis of Master of University of Colorado (1995)
10. Ruiz, M.E., Srinivasan, P.: Hierarchical Text Categorization Using Neural Networks. Information Retrieval 5, 87–118 (2002)
11. Sebastiani, F.: Machine Learning in Automated Text Categorization. ACM Computing Survey 34, 1–47 (2002)
12. Jackson, P., Mouliner, I.: Natural Language Processing for Online Applications: Text Retrieval. In: Extraction and Categorization. John Benjamins Publishing Company, Amsterdam (2002)

Training Neural Networks for Protein Secondary Structure Prediction: The Effects of Imbalanced Data Set

Viviane Palodeto[1], Hernán Terenzi[2], and Jefferson Luiz Brum Marques[1]

[1] IEB – Biomedical Engineering Institute, Federal University of Santa Catarina, Florianópolis, SC, Brazil
{viviane,jmarques}@ieb.ufsc.br
[2] Biochemistry Department, Federal University of Santa Catarina, Florianópolis, SC, Brazil
hterenzi@ccb.ufsc.br

Abstract. Protein secondary structure prediction (PSSP) is one of the main tasks in computational biology. During the last few decades, much effort has been made towards solving this problem, with various approaches, mainly artificial neural networks (ANN). Generally, in order to predict the protein secondary structure, the ANN training process is performed using CB513 data set. Like protein structures databases, this data set is imbalanced and it can cause a low error rate for the majority class and an undesirable error rate for the minority class. In this paper we evaluate the effects of an imbalanced data set in training and learning of neural networks when they are applied to predict protein secondary structure. For this we applied resampling methods to tackle the imbalance class problem. Results show that imbalanced data sets decrease the helixes predictions rates. Although, protein data set distribution does not affect significantly the global accuracy (Q_3).

Keywords: Imbalanced data, Protein secondary structure prediction, Artificial neural network training.

1 Introduction

The prediction of protein structure is one of the main tasks in computational biology. Since protein structure is related to its function [1]. Determining the three-dimensional structure of a protein is a very hard task due to most reliable results are produced by experimental approaches such as nuclear magnetic resonance and X-ray crystallography [2]. However, such approaches are expensive and can require years to produce the structure of a single protein [3]. So, the gap between the amount of protein structures stored in international repositories (such as, PDB – Protein Data Bank) and the number of known proteins sequences is increasing exponentially [4]. Despite all efforts, the computational methods to determine the protein structure are still unreliable [5].

The protein secondary structure prediction (PSSP) allows a simplification of the protein structure prediction. Furthermore, it provides information about domains and classification of proteins into families [2,4]. PSSP consists in to assign to each amino acid from

D.-S. Huang et al. (Eds.): ICIC 2009, LNAI 5755, pp. 258–265, 2009.

protein sequences one of the three secondary structure states: helixes, strand or coils/others. During the last few decades, much effort has been made towards solving this problem, with various approaches including: statistical information [6-8], nearest-neighbour algorithms [9,10] and support vector machine [11,12]. Nevertheless, the most applied approach to predict the secondary structure of a protein is artificial neural networks [13-26].

Protein databases used for artificial neural networks training to solve PSSP are imbalanced [27]. Imbalanced data sets are often encountered in real-world applications; they may distort the performance of classification [28]. This problem can cause a low error rate for the majority class and an undesirable higher error rate for the minority class [27]. Despite the imbalanced class problem in protein databases was previously reported [28], Radivojac *et al.* (2004) analysed the effects of imbalanced protein databases for protein classification and showed that training classifiers especialized to the class distributions of each cluster resulted in a further decrease in classification error for the problem of classifying proteins into families.

In this paper we investigate the effects of an imbalanced data set for training neural networks when they are applied to solve the problem of predicting the secondary structure of proteins.

2 Methods

In this section we describe the methodology applied to study the effects of the imbalanced class problem to the protein secondary structure prediction. First, we discuss the protein database used. Then, we present the characteristics topology of the neural artificial network and the methods employed for tackling the class imbalance problem. Finally, Section 2.4 describes the accuracy measurements carried out to asses the effects of using imbalanced data sets for training ANN in PSSP.

2.1 Data Set

In 1993, Rost and Sander selected a set of 126 proteins (RS126) that was used to train and test secondary structure prediction algorithms based on ANN [15]. The sequences chosen were defined as non-redundant that mean that no two proteins in the set share more than 25% sequence identity. Although, RS126 set contains pairs of proteins that presents clearly sequence similarity [29]. As reported, similarity can overestimate prediction results [30]. In order to ensure no sequence similarity, Cuff and Barton (1999) selected a new set of protein sequences, called CB396. Similar sequences between RS126 and CB396 were removed and the remaining sequences were joined to compose CB513 [29]. This data set was chosen because it is applied for testing many protein secondary structure predictions methods [22,24].

Mostly real-world data are imbalanced [28]. Particularly, secondary structure classes in globular proteins have a very uneven distribution [31]. Particulary, CB513 has the following distribution: 36.04% helixes, 22.91% strands, and 41.05% coil/loop or other structures. Similar distribution is observed in protein structure repositories like (PDB – http://www.rscb.org.pdb) [30]. This imbalance can affect the performance of the protein secondary structure predictors.

2.2 Artificial Neural Networks

The major goal in this study is the analysis of the effects of the data set imbalance problem. Therefore, we implemented a simple multi-layer feed-forward neural network with one hidden layer, since this topology provide a universal approximation function [32].

As suggested by Rost and Sander [17] evolutionary information is obtained performing multiple sequence alignments. A sequence profile with the amino acid frequencies of each of the 20 amino acid residue at a given position in the sequence is derived from multiple sequence alignments. The ANN input layer consist of w multiplied by 20 units where w is the window length, i.e. the length of the sliding window around the central amino acid residue analyzed.

The input signal is propagated through a network with input, hidden and output layers. The output layer has three units corresponding to the three secondary-structure states: helix, strand, and coil/other.

2.3 Schemes for Dealing with Imbalanced Data sets

Many approaches can be tried to solve the class imbalance problem. These can be divided into two groups (1) resampling methods and (2) modifications of existing learning algorithms [33]. Here we are not focused in developing modifications on artificial neural networks learning algorithms. Therefore, we focus in the resampling methods: over-sampling and under-sampling.

The simplest method to increase the size of the minority class corresponds to random over-sampling, i.e., a non-heuristic method that balances the class distribution through the random replication of minority class examples [28, 33]. Nevertheless, this method can increase the likelihood of over fitting, since it makes exact copies of the minority class instances [28,33]. Chawla et al. [34] proposed a technique for over-sampling the minority class and, instead of merely replicating cases belonging to the minority class, this generates new synthetic minority instances by interpolating between several positive examples that lie close together. This method, allows the classifier to build larger decision regions that contain nearby instances from the minority class.

Random under-sampling [28,33] aims at balancing the data set through the random removal of majority class examples. Despite its simplicity, it has empirically been shown to be one of the most effective resampling methods [28]. The major problem of this technique is that it can discard data potentially important for the classification process.

2.4 Accuracy Measurements

In order to assess the accuracy of a PSSP method is considered the percentage of correct prediction for a given secondary structure state (Q_h for helixes, Q_s for strands or Q_c coil/other) as the ratio of the total number of residues correctly predicted to be in a secondary structure state (c) and the total number of residues in that state (N) multiplied by 100 (Eq. 1).

$$Q_{\{h,s,c\}} = \frac{c_{\{h,s,c\}}}{N_{\{h,s,c\}}} \times 100 . \quad (1)$$

Also, we calculate Q_3 that defines the percentage of correct prediction as the ratio of total residues correctly predicted (c) to the total number of the amino acid residues in the protein sequence (Eq. 2).

$$Q_3 = \frac{\sum_{i=1}^{3} ci}{N} \times 100 , \quad (2)$$

where *i* is one of the three secondary structure states helix, strand or coil/other.

3 Results and Discussion

The CB513 data set was balanced using two resampling methods: random over- sampling and random under-sampling. Thus, sets for ANN training, validation and testing were selected from the two resulting balanced data sets.

We also select imbalanced sets in order to evaluate the ANN performance in both cases, dealing with balanced data or not. Imbalanced data sets (for ANN training, validation and testing processes) were selected randomly and are composed 36.39% of helixes, 22.82% of strands, and 40.79% of coil/other (almost like CB513 distributions).

Neural network was trained using backpropagation learning algorithm and under cross-validation conditions.

Typically, PSSP methods that uses ANN consider windows sizes from 13 to 21 adjacent residues [15-17,20,22,24]. We carried out tests with different windows lengths: 11 to 27.

For each set of parameters (such as window length, ANN learning rate and data set type) we carried out 1000 experiments (ANN random initialization, training, validation and test).

Table 1 presents Q3 values achieved even when imbalanced data (second column) or balanced data (third column) was applied for ANN training, validation and testing. The results achieved in training ANN with imbalanced data and testing ANN with balanced data are showed in the 4th column. The last column presents ANN training process with balanced data and testing with imbalanced data.

Differences between imbalanced and balanced accuracy results in Table 1 are not statistically significant (p=0.05). Hence, we can conclude that the protein data set distribution does not affect significantly the global accuracy (Q3) of secondary structure predictions by neural networks.

Since the neural networks were trained we can evaluate predictions accuracies for each class of protein secondary structure (Q_h, Q_s and Q_c), using imbalanced and balanced data sets (Table 2).

Individual class results (Table 2) show that the accuracy for helixes prediction (Qh) drops when we used imbalanced data sets. As expected, Qc predictions rates are higher when we used imbalanced data sets due to the distribution of coils/other class

Table 1. Comparative of Q_3 values for imbalanced and balanced data sets. First column shows window length, i. e. the number of residues considered in the input layer of the neural network. Columns 2 and 3 present the prediction accuracy (Q_3) for imbalanced and balanced data, respectively. The results achieved in training ANN with imbalanced data and testing ANN with balanced data are showed in the 4th column. The last column presents ANN training process with balanced data and testing with imbalanced data.

Window Size	Imbalanced ANN Training		Balanced ANN Training	
	Imbalanced ANN Testing – Q_3	Balanced ANN Testing - Q_3	Imbalanced ANN Testing - Q_3	Balanced ANN Testing - Q_3
11	63.67%	63.52%	62.65%	62.85%
13	70.84%	70.15%	68.92%	68.92%
15	69.10%	65.36%	66.62%	68.58%
17	68.39%	64.77%	67.24%	67.27%
19	68.24%	65.83%	66.18%	67.88%
21	69.96%	64.44%	66.03%	69.24%
23	68.22%	64.45%	68.58%	69.67%
25	68.31%	63.92%	64.90%	67.57%
27	67.70%	63.54%	64.01%	68.71%

Table 2. Prediction accuracy achieved for individual secondary structure class

Window Size	Balanced Data			Imbalanced Data		
	Q_h	Q_s	Q_c	Q_h	Q_s	Q_c
11	69.83%	47.85%	70.87%	70.05%	48.87%	72.09%
13	74.15%	58.60%	74.02%	75.77%	60.84%	75.92%
15	72.38%	52.48%	74.48%	59.31%	47.72%	90.25%
17	76.82%	54.53%	72.94%	58.32%	48.95%	79.91%
19	75.34%	54.02%	76.88%	65.27%	51.98%	83.54%
21	73.44%	53.32%	72.76%	61.92%	45.32%	84.73%
23	79.91%	46.73%	72.88%	55.52%	48.95%	87.57%
25	73.56%	51.47%	72.54%	56.27%	48.07%	81.04%
27	74.00%	58.56%	67.88%	52.97%	46.76%	87.91%

in the protein data set (40.79%), i.e. the majority class showed a lower error rate. Also, Qs decreases poorly when we compare balanced and imbalanced. This result are not statically meaningful (p=0.05).

During the experiments, the accuracy measured using either over-sampling or under-sampling methods was very similar (p=0.5). Thus, in Table 1 and Table 2, the results reported as achieved with balanced data refer to the average of the Q3 using both resampling methods.

As reported by others PSSP methods based on ANN, the best accuracy was achieved using a window of 13 residues [17, 20].

4 Conclusions

In this study we evaluated the effects of imbalanced data set problem in protein secondary structure prediction using artificial neural networks. For this purpose we select a balanced data set from CB513 by applying over-sampling and under-sampling methods. From both, balanced and imbalanced data, we select sets in order to train, validate and test the ANNs.

Prediction results were measured following the accuracy metrics in protein secondary structure prediction area, i.e. Q3. Afterwards, results achieved from balanced and imbalanced data sets where compared.

Despite there is not significant differences in global predictions results (Q3), when we observed individual results for secondary structure class (Qh, Qs and Qc) we noticed a meaningful disparity between balanced and imbalanced data. In imbalanced data training predictions accuracy were at least 10 percent worst for helixes predictions (Qh).

Due to the distribution of the coil/others class secondary structure in protein data set (40.79%), Qc rates are higher when we used imbalanced data set. For both balanced and imbalanced data set, strands are predicted rather poorly due to their non local folding characteristic. Low Qs rates are reported for many PSSP methods [30].

We present a discussion about imbalanced data problem for protein secondary structure prediction, using methods most commonly applied as for protein secondary structure prediction (ANN) as for data resampling. Nevertheless, additional experiments can be performed in order to evaluate the imbalanced data set problem in PSSP using others resampling methods and machine learning methods for classification.

Acknowledgments

We wish to thanks to CNPq for the VP scholarship.

References

1. Nelson, D.L., Cox, M.M.: Lehninger Principles of Biochemistry. W H Freeman, New York (2005)
2. Mount, D.W.: Bioinformatics: Sequence and Genome Analysis. Cold Spring Harbor Laboratory, New York (2004)
3. Isaev, A.: Introduction to Mathematical Methods in Bioinformatics. Springer, Heidelberg (2006)
4. Tramontano, A.: Protein Structure Prediction. Wiley-VCH, Weinheim (2006)
5. Bourne, P.E., Weissig, H.: Structural Bioinformatics. Wiley-Liss, New Jersey (2003)
6. Garnier, J., Osguthorpe, D.J., Robson, B.: Analysis of the Accuracy and Implications of Simple Methods for Predicting the Secondary Structure of Globular Proteins. Journal of molecular Biology 120, 97–120 (1978)
7. Gibrat, J.F., Garnier, J., Robson, B.: Further Developments of Protein Secondary Structure Prediction Using Information Theory. Journal of Molecular Biology 198, 425–443 (1987)
8. Biou, V., Gibrat, J.F., Levin, J.M., Robson, B., Garnier, J.: Secondary Structure Prediction: Combination of Three Different Methods. Prot. Engin. 2, 185–191 (1988)

9. Yi, T.M., Lander, E.S.: Protein Secondary Structure Prediction Using Nearest-Neighbor Methods. Journal of Molecular Biology 232, 1117–1129 (1993)
10. Salamov, A.A., Solovyev, V.V.: Prediction of Protein Secondary Structure by Combining Nearest-Neighbor Algorithms and Multiple Sequence Alignment. Journal of Molecular Biology 247, 11–15 (1995)
11. Chen, C., Chen, L., Zou, X., Cai, P.: Prediction of protein secondary structure content by using the concept of Chou's pseudo amino acid composition and support vector machine. Protein and Peptides Letters 16, 27–31 (2009)
12. Nguyen, M.N., Rajapakse, J.C.: Prediction of Protein Secondary Structure with two-stage multi-class SVMs. International Journal in Data Mining and Bioinformatics 1, 248–269 (2007)
13. Yi, T.M., Lander, E.S.: Protein Secondary Structure Prediction Using Nearest-Neighbor Methods. Journal of Molecular Biology 232, 1117–1129 (1993)
14. Bohr, H., Bohr, J., Brunak, S., Cotterill, R., Lautrup, B.: Protein Secondary Structure and Homology by Neural Networks. FEBS Letter 241, 223–228 (1988)
15. Qian, N., Sejnowski, T.J.: Predicting the Secondary Structure of Globular Proteins Using Neural Network Models. Journal of Molecular Biology 202, 865–884 (1988)
16. Holley, H.L., Karplus, M.: Protein Secondary Structure Prediction with a Neural Network. Proceedings of the National Academy of Sciences of U.S.A. 86, 152–156 (1989)
17. Rost, B., Sander, C.: Prediction of Protein Secondary Structure at Better than 70% Accuracy. Journal of Molecular Biology 232, 584–599 (1993)
18. Maclin, R., Shavlik, J.W.: Using Knowledge-Based Neural Networks to Improve Algorithms: Refining the Chou-Fasman Algorithm for Protein Folding. Machine Learning 11, 195–215 (1993)
19. Chandonia, J.-M., Karplus, M.: Neural Networks for Secondary Structure and Structural Class Predictions. Protein Science 4, 275–285 (1995)
20. Baldi, P., Brunak, S., Frasconi, P., Soda, G., Pollastri, G.: Exploiting the Past and the Future in Protein Secondary Structure Prediction. Bioinformatics 15, 937–946 (1999)
21. Jones, D.T.: Protein Secondary Structure Prediction Based on Position-Specific Scoring Matrices. Journal of Molecular Biology 292, 195–202 (1999)
22. Ouali, M., King, R.D.: Cascaded Multiple Classifiers for Secondary Structure Prediction. Protein Science 9, 1162–1176 (2000)
23. Pollastri, G., Przybylski, D., Baldi, P.: Improving the Predicition of Protein Secondary Structure in Three and Eight classes using recurrent neural networks and profiles. Proteins: Structure, Function and Genetics 47, 228–235 (2002)
24. Yao, X.Q., Zhu, H., She, Z.S.: A Dynamic Bayesian Network Approach to Protein Secondary Structure Prediction. BMC Bioinformatics 9 (2008)
25. Liu, K.H., Xia, J.F., Li, X.: Efficient Ensemble Schemes for Protein Secondary Structure Prediction. Protein and Peptides Letters 15, 488–493 (2008)
26. Malekpour, S.A., Naghizadeh, S., Pezeshk, H., Sadeghi, M., Eslahchi, C.: Protein secondary structure prediction using three neural networks and a segmental semi Markov model. Mathematical Biosciences 217, 145–150 (2008)
27. Radivojac, P., Chawla, N.V., Dunker, A.K., Obradovic, Z.: Classification and Knowledge Discovery in Protein Databases. Journal of Biomedical Informatics 37, 224–239 (2004)
28. Chawla, N.V., Japkowicz, N., Kolcz, A.: Editorial: Special Issue on Learning from Imbalanced Data Set. Sigkdd Explorations 6, 1–6 (2004)
29. Cuff, J.A., Barton, G.: Evaluation and Improvement of Multiple Sequence Methods for Protein Secondary Structure Prediction. Proteins: Structure, function and Genetics 34, 508–519 (1999)

30. Rost, S.: Review: Protein Secondary Structure Continues to Rise. Journal of Structural Biology 134, 204–218 (2001)
31. Rost, B., Sander, C.: Improved Prediction of Protein Secondary Structure by Use of Sequence Profiles and Neural Networks. Proceedings of the National Academy of Sciences 90, 7558–7562 (1993)
32. Haykin, S.: Neural Networks: a Comprehensive Foundation. Prentice Hall, New York (1999)
33. Japkowicks, N., Stephen, S.: The Class imbalance Problem: a Systematic Study. Intelligent Data Analysis 6, 429–449 (2002)
34. Chawla, N.V., Bowyer, K.W., Hall, L.O., Kegelmeyer, W.P.: SMOTE: Synthetic Minority Over-Sampling Technique. Journal of Artificial Intelligence Research 16, 321–357 (2002)

Rough Set Theory in Pavement Maintenance Decision

Ching-Tsung Hung[1], Jia-Ruey Chang[2], Jyh-Dong Lin[3], and Gwo-Hshiung Tzeng[4]

[1] Department of Logistics & Shipping Management, Kainan University
cthung@mail.knu.eud.tw
[2] Department of Civil Engineering, Minghsin University of Science and Technology
jrchang@must.edu.tw
[3] Department of Traffic Engineering and Management, Feng Chia University
shc@fcu.edu.tw
[4] Department of Business and Entrepreneurial Management, Kainan University
cthung@mail.knu.eud.tw

Abstract. The decision tree models based on pavement experts' experiences are usually used to derive pavement maintenance decisions. Because experiences are very difficult to obtain completely, some importance condition attributes in decision tree model are easily to be lost. With the prevailing of the computer, Case Base Reasoning (CBR) or Data Mining approach are used to process a large number of historical pavement maintenance records. But, the shortcoming is all condition attributes have to be included in the analyses.Rough Set Theory was proposed in 1982. Rough Set Theory can reduce the condition attributes and decision rules without changing the accuracy. The provincial and county roads located in north Taiwan are used as the empirical study. With the same accuracy, Rough Set Theory can reduce thirteen condition attributes to eight. Thus, RST is suitable for pavement maintenance decisions.

1 Introduction

How to determining the repair method depending on pavement condition is a critical problem in pavement management system (PMS). Because the maintenance strategy considers the whole road network condition and history record to supply engineer making appropriate strategy in limited budget. It is the final result in PMS. A good strategy makes people to understand the PMS's value easier. But most factors used in selecting one treatment and the wide range of factors that may control the process, so the knowledge form expert is hardly acquisition.

So many factor including current condition of the pavement, the functional classification of the road, traffic volume, and type of distress is depending on various maintenance demand. Most research chooses the pavement distress in decision process[1]. Some acquirement method had developed in recent year, but it is still some problem like the vague decision knowledge in approaching real world. The Rough Set theory is a new method to solve complex and vague problem.

D.-S. Huang et al. (Eds.): ICIC 2009, LNAI 5755, pp. 266–275, 2009.

2 Critical Review of Pavement Maintenance Decision

2.1 Decision Trees-Matrices

Decision trees-matrices establish a set of rule for selecting a particular type of treatment through the use of branches that define various sets of decisions. This method need survey with experienced experts and collect full condition. First, the panel must deal type of distress and research aim to make a appropriate question. The experts will select the appropriate maintenance treatment in various pavement conditions in their experience. Through the interactive with expert and research worker, it will produce a clear result to apply in pavement strategy. This general approach of pooling the expertise into a group consensus is called the Delphi technique. Figure presents a typical decision tree developed employing the Delphi technique and incorporated into the Mississippi Department of Transportation (MDOT) PMS.

The same way also used in Minnesota Department of Transportation (MnDOT) and Montana Department of Transportation. MnDOT consider more factors including type of surface, type of distress and condition rating.

With the factors increases, the decision tree-matrices become much more complex. Evan any change, the decision tree-matrices must be reconstruction. The process of establishing a tree is costly.

2.2 Knowledge Base Expert system

Knowledge Base Expert system is a system utilizing the computer procedure to simulate expert solve partial field. It can succeed in changing expert's knowledge and experience in the specific field. The development of its basic expert system of knowledge needs to go through the question and defines, knowledge pick fetching, five steps that knowledge expresses, carrying out and verifying expanding, etc. Problem its define step to let definition of problem clear and can make knowledge basic expert system looks on solving problem than have efficiency to the traditional method. The second step is to carry on the knowledge result to the expert. It is usually the knowledge of the respect of combining documents, discussing the result and expert and judging etc. But exactly closing surfacing with will both meet and fail to have problem that will be dealt with of method of a set of structured to set up law to make policy in knowledge. It is expressed that the knowledge obtained is changed into a rule system with the procedure language, and carry out with the computer procedure. After the procedure finishes, need passing the expert's test and affirmation. As to the thing that shop front maintain knowledge basic expert system of decision have SCEPTRE, EXPEAR, ROSE tree[2].

Knowledge basic restriction of expert system lies in to judge can usage express expert. Need to spend more time and cost to bigger problem. Similarly, take an exam of change which measures the parameter and also need to write the procedure again in any, and this system is unable to deal with the indeterminate, dim and information inconsistent.

3 Methods of Decision Rule

3.1 Artificial Neural Network

The ANN is a simulation of the function of the human nervous system, exhibiting abilities such as learning, generalization, and abstraction [1]. Neural nets can learn associative patterns and approximate the functional relationship between a set of inputs and outputs. The simple artificial neuron called a perception.

Neural network have the potential to provide some of the human characteristics of problem-solving ability that are difficult to simulate using the logical. For example, neural network can analyse large quantities of data to establish patterns and characteristics for situations in which rules are not now and can often make sense of incomplete or noisy data. There capabilities have so far provided too difficult for the traditional symbolic or logic approaches [3]. With the neural network approach, there no need for the information to be programmed since there is no need for a predefined knowledge base. The system creates its own knowledge system based on inputs and outputs to which it is exposed.

Other advantages of using a neural network include the following:

- Any change in the problem do not reprogramming: the system simply retrains itself on the basis of the new information.
- The ANN is very good at filtering out noise and isolating useful input information.
- A well-trained ANN, for example, may be able to discern patterns that human experts would miss and to recognize with a high degree of consistency.

3.2 Rough Set Theory

3.2.1 Background

The rough sets theory introduced by Pawlak [4, 5] has often proved to be an excellent mathematical tool for the analysis of a vague description of objects (called actions in decision problems). The vague, referring to the quality of information, means inconsistency or ambiguity which follows from information granulation. The rough sets philosophy is based on the assumption that with every object of the universe there is associated a certain amount of information (data, knowledge), expressed by means of some attributes used for object description. Objects having the same description are indiscernible (similar) with respect to the available information. The indiscernible relation thus generated constitutes a mathematical basis of the rough sets theory; it induces a partition of the universe into blocks of indiscernible objects, called elementary set, which can be used to build knowledge about a real or abstract world. The use of the indiscernible relation results in information granulation.

Some important characteristics of the rough set approach make of this a particularly interesting tool in a number of problems and concrete applications. With respect to the input information, it is possible to deal with both quantitative and qualitative data, and inconsistencies need not to be removed prior to the analysis. With reference to the output information, it is possible to acquire a posteriori information regarding the relevance of particular attributes and their subsets to the quality of approximation considered in the problem at hand, without any additional inter-attribute preference

information. Moreover, the final result in the form of ``if..., then..." decision rules, using the most relevant attribute, are easy to interpret.

3.2.2 Methodology

The original concept of approximation space in rough set can be described as follows.

Given an approximation space

$$apr = (U, A)$$

where U is the universe which is a finite and non-empty set, and A is the set of attributes. Then based on the approximation space, we can define the lower and upper approximations of a set.

Let X be a subset of U and the lower approximation of X in A is

$$\overline{apr}(A) = \{x \mid x \in U, U / ind(A) \subset X\} \tag{1}$$

The upper approximation of X in A is

$$\underline{apr}(A) = \{x \mid x \in U, U / ind(A) \cap X \neq \phi\} \tag{2}$$

Where

$$U / ind(a) = \{(x_i, x_j) \in U \cdot U, f(x_i, a) = f(x_j, a) \tag{3}$$

$$\forall a \in A\}$$

Eq. (1) represents the least composed set in A containing X, called the best upper approximation of X in A, and Eq. (2) represents the greatest composed set in A contained in X, called the best lower approximation.

After constructing upper and lower approximations, the boundary can be represented as

$$BN(A) = \overline{apr}(A) - \underline{apr}(A) \tag{4}$$

According to the approximation space, we can calculate reducts and decision rules. Given an information system $I = (U, A)$ then the reduct, $RED(B)$, is a minimal set of attributes $B \subseteq A$ such that $r_B(U) = r_A(U)$ where

$$r_B(U) = \frac{\sum card(\underline{B}X_i)}{card(U)} \tag{5}$$

denotes the quality of approximation of U by B.

Once the reducts have been derived, overlaying the reducts on the information system can induce the decision rules. A decision rule can be expressed as $\phi \Rightarrow \theta$,

where ϕ denotes the conjunction of elementary conditions, $\Rightarrow$ denotes 'indicates', and θ denotes the disjunction of elementary decisions.

The advantage of the induction based approaches is that it can provide the intelligible rules for decision-makers (DMs). These intelligible rules can help DMs to realize the contents of data sets.

3.2.3 Rough Set Theory Used in Pavement Management Process

Pavement condition collection plays an important role in pavement management process. The appropriate M&R strategies are decided according to correct condition information. Although the current decision support techniques can acquire valuable information from enormous data, the systematized analytic process is needed for the significant improvement of accuracy and efficiency. Systematized decision support system for pavement management must accomplish the following functions [6]:

1. Discover pavement management database to induce correct M&R rules
2. Screen the redundant and useless data
3. Simplify the database if too much useless information exists
4. Describe the association between distress and M&R strategy as decision rules

According to literature reviews, data mining techniques actually applied to engineering issues are limited, especially RST application is extremely rare. RST provides a new direction for pavement knowledge discovery and decision table analysis. RST can be used in pavement database primarily to deduct attributes, remove redundant records, simplify decision table, and induce M&R rules. Attoh-Okine demonstrated the feasibility of RST to M&R decision induction and suggested more reality data for verification is required. Attoh-Okine [7] further explored the potential applications of rough set theory and neural networks in concrete-faulting-performance modelling. The key characteristic of the proposed method is that the new decision table created by using the rough set analysis will free the neural network paradigm from redundancy.

4 Empirical Study: A Case of Pavement M&R Strategy

4.1 Pavement Distress Survey and M&R Strategy

Pavement distress survey is conducted for the purpose of monitoring the existing pavement condition and making the appropriate M&R activities. Generally, the severity and coverage should be separately identified and recorded for each distress type. For accurate, consistent, and repeatable distress surveys, one distress survey manual is required for clarifying the definition, severity, and coverage of each distress type. In the empirical study, pavement distress survey was carried out primarily following the Distress Identification Manual for the Long-Term Pavement Performance Program issued by FHWA. Furthermore, the adopted M&R strategy for each distress was

identified according to the standardized M&R Guidance used in Taiwan Highway Bureau (THB).

Problem description

Pavement distress surveys were conducted on seven county roads in Chung-Li Engineering Section of THB by 8 experienced pavement engineers in 1999. The collected 2,348 records (2,115 records were randomly selected for rule induction; the rest of 233 records were for rule verification) are utilized in the empirical study. The seven county roads are 110, 112, 112A, 113, 113A, 114 and 115. Engineers were carrying surveys by walking or driving and recording the distress information and their corresponding M&R strategy. Then, the data are integrated as Table 1. The first column in Table 1 shows the record numbers, column 2 to column 19 illustrate the distress types, and the last column refers to the adopted M&R strategy. The details are described as the following:

This study explores 18 common distress types in Taiwan, which are represented from D1 to D18: D1. Alligator Cracking, D2. Block Cracking, D3. Longitudinal Cracking, D4. Transverse Cracking, D5. Edge Cracking, D6. Reflection Cracking, D7. Pothole, D8. Bleeding, D9. Rutting, D10. Corrugation, D11. Lane/Shoulder Drop-off, D12. Depression, D13. Structure Drop-off, D14. Utility Cut Patching, D15. Shoving, D16.Manhole Drop-off, D17. Patching Deterioration, D18. Ravelling.

The severity levels of distress are classified as L (low), M (moderate), and H (high).The coverage levels of distress are classified as A (local), B (medium), and C (extensive). Therefore, there are nine combinations (LA, LB, LC, MA, MB, MC, HA, HB, HC) of severity and coverage which are represented by number 1 to 9 respectively, and plus 0 represents no distress. For example, "D1 = 2" denotes Alligator Cracking occurs with low severity and medium coverage.

M&R strategies used in the empirical study are classified as four types, which are represented as number 1 to 4 referring to no M&R required, preventive M&R, localized M&R and global M&R respectively.

M&R rules induction and verification

This section will illustrate the RST application on M&R strategy induction and rules verification. Rough Set Exploration System (RSES) is employed to execute analyses. RSES is a software tool that provides the means for analysis of tabular data sets with use of various methods, in particular those based on RST.

4.2 Rules Induction

Firstly, M&R rules are induced by using 2,115 records before attributes are deducted. The induced 435 rules are shown in Table 2. The first and second row in Table 2 represent the first and second rule, which match with 419 records (most records) and 205 records, respectively:

If (D1=1) & (D2=0) & (D3=0) & (D4=0) & (D5=0) & (D6=0) &(D7=0) & (D8=0) & (D9=0) & (D10=0) & (D11=0) & (D12=0) & (D13=0) & (D14=0) (That is, Alligator Cracking occurs with low severity and local coverage, and no other distress occurs.)Then the adopted M&R strategy might be no M&R required (448 records) or preventive M&R (11 records)

Table 1. Analytic Database

Table: Modeling

2115 / 19	D1	D2	D3	...	...	...	...	...	...	...	...	...	...	...	...	D16	D17	D18	M&R
0:1	2	0	0	0	0	0	0	0	0	0	0	0	0	0	0	5	0	0	1
0:2	1	0	0	0	0	0	0	0	0	0	0	0	0	6	0	0	0	0	1
0:3	2	1	1	0	0	0	0	0	0	1	0	0	1	0	0	0	0	0	1
0:4	2	1	0	0	0	0	0	0	0	1	0	0	1	0	0	0	0	0	1
0:5	2	0	0	0	1	0	0	0	0	0	0	0	1	0	0	0	0	0	1
0:6	1	0	1	0	0	0	0	0	0	0	0	0	1	0	0	0	0	0	1
0:7	1	0	1	0	0	0	0	0	0	0	0	0	1	0	0	0	0	0	1
0:8	2	0	1	0	0	0	0	0	0	0	0	0	1	0	0	0	0	0	1
0:9	1	0	0	0	0	0	0	0	0	0	0	0	1	0	0	0	0	0	1
0:10	1	0	0	0	0	0	0	0	0	0	0	0	1	0	0	0	0	0	1
0:11	2	0	0	0	0	0	0	0	0	0	0	0	1	0	0	0	0	0	1
0:12	4	0	0	0	0	0	0	0	0	0	0	0	1	0	0	0	0	0	1
0:13	5	0	0	0	0	0	0	0	0	0	0	0	2	0	0	0	0	0	1
0:14	2	0	0	0	0	0	0	0	0	0	2	0	0	0	0	0	0	0	1
0:15	1	0	0	0	0	0	1	0	0	1	0	0	0	0	0	0	0	0	1
0:16	1	0	1	0	1	0	0	0	0	1	0	0	0	0	0	0	0	0	1
0:17	1	0	1	0	1	0	0	0	0	1	0	0	0	0	0	0	0	0	1
0:18	1	0	0	0	1	0	0	0	0	1	0	0	0	0	0	0	0	0	1
0:19	1	0	0	0	1	0	0	0	0	1	0	0	0	0	0	0	0	0	1
0:20	1	0	0	0	1	0	0	0	0	1	0	0	0	0	0	0	0	0	1
0:21	1	0	0	0	1	0	0	0	0	1	0	0	0	0	0	0	0	0	1
0:22	1	0	0	0	1	0	0	0	0	1	0	0	0	0	0	0	0	0	1
0:23	1	0	0	0	1	0	0	0	0	1	0	0	0	0	0	0	0	0	1
0:24	1	0	0	0	1	0	0	0	0	1	0	0	0	0	0	0	0	0	1
0:25	1	0	0	0	1	0	0	0	0	1	0	0	0	0	0	0	0	0	1
0:26	1	0	0	0	1	0	0	0	0	1	0	0	0	0	0	0	0	0	1
0:27	1	0	0	0	1	0	0	0	0	1	0	0	0	0	0	0	0	0	1
0:28	1	0	0	0	1	0	0	0	0	1	0	0	0	0	0	0	0	0	1
0:29	1	0	0	0	1	0	0	0	0	1	0	0	0	0	0	0	0	0	1
0:30	1	0	0	0	1	0	0	0	0	1	0	0	0	0	0	0	0	0	1
0:31	1	0	0	0	1	0	0	0	0	1	0	0	0	0	0	0	0	0	1
0:32	1	0	0	0	1	0	0	0	0	1	0	0	0	0	0	0	0	0	1
0:33	1	0	0	0	1	0	0	0	0	1	0	0	0	0	0	0	0	0	1
0:34	1	0	0	0	1	0	0	0	0	1	0	0	0	0	0	0	0	0	1
0:35	1	0	0	0	1	0	0	0	0	1	0	0	0	0	0	0	0	0	1
0:36	1	0	0	0	1	0	0	0	0	1	0	0	0	0	0	0	0	0	1
0:37	1	0	0	0	1	0	0	0	0	1	0	0	0	0	0	0	0	0	1
0:38	2	0	0	0	1	0	0	0	0	1	0	0	0	0	0	0	0	0	1
0:39	2	0	0	0	1	0	0	0	0	1	0	0	0	0	0	0	0	0	1
0:40	4	0	0	0	1	0	0	0	0	1	0	0	0	0	0	0	0	0	1
0:41	1	0	1	5	0	0	0	0	0	1	0	0	0	0	0	0	0	0	1
0:42	1	1	1	0	0	0	0	0	0	1	0	0	0	0	0	0	0	0	1
0:43	1	0	1	0	0	0	0	0	0	1	0	0	0	0	0	0	0	0	1
0:44	1	0	1	0	0	0	0	0	0	1	0	0	0	0	0	0	0	0	1
0:45	1	0	1	0	0	0	0	0	0	1	0	0	0	0	0	0	0	0	1

If (D1=1) & (D5=1) (That is, both Alligator Cracking occurs with low severity and local coverage and Edge Cracking occurs with low severity and local coverage.) Then the adopted M&R strategy will be no M&R required (205 records).

Then, RST is utilized to carry out reduced analysis for 18 attributes. Two groups of reduced set with 14 size attributes are shown below:

D1, D2, D3, D4, D5, D6, D7, D8, D9, D10, D11, D13, D14, D16
D1, D2, D3, D4, D5, D6, D7, D8, D10, D11, D13, D14, D15, D16

The 13 attributes (cores) obtained from intersection of the above two reduced sets are D1, D2, D3, D4, D5, D6, D7, D8, D9, D10, D11, D13, D14, D16. It is found that D12 (Depression), D17(Patching Deterioration) and D18(Raveling) is not shown in both reduce sets.

M&R rules are induced again by using 2,115 records based on the reduced attributes. We could obtain 332 rules. Fewer rules are obtained than what of before attributes reduction. It demonstrated that RST can eliminate redundant attributes to improve the efficiency of rule induction. The rule which matches with the most records (208 records) is shown below:

Table 2. The Induced 435 Rules with No Attribute Deduction

Rule set: Modeling

(1-435)	Match	Decision rules
1	419	(D1=1)&(D2=0)&(D3=0)&(D4=0)&(D5=0)&(D6=0)&(D7=0)&(D8=0)&(D10=0)&(D13=0)&(D14=0)=>(M&R={1[408],2[11]})
2	205	(D1=1)&(D5=1)=>(M&R={1[205]})
3	176	(D1=1)&(D2=0)&(D3=1)&(D4=0)&(D5=0)&(D6=0)&(D7=0)&(D8=0)&(D10=0)&(D13=0)=>(M&R={1[174],2[2]})
4	128	(D1=0)&(D2=0)&(D3=0)&(D4=1)&(D5=0)=>(M&R={2[128]})
5	83	(D1=2)&(D3=1)=>(M&R={1[83]})
6	67	(D1=1)&(D10=1)=>(M&R={1[67]})
7	62	(D1=0)&(D2=0)&(D3=1)&(D4=0)&(D5=0)&(D6=0)&(D8=0)&(D10=0)=>(M&R={1[1],2[61]})
8	55	(D1=5)&(D2=0)&(D3=0)&(D4=0)&(D5=0)&(D7=0)&(D8=0)&(D10=0)&(D13=0)=>(M&R={1[2],2[34],3[19]})
9	50	(D1=2)&(D2=0)&(D3=0)&(D4=0)&(D5=0)&(D6=0)&(D10=0)&(D11=0)&(D13=0)&(D16=0)=>(M&R={1[49],2[1]})
10	50	(D1=2)&(D2=0)&(D3=0)&(D4=0)&(D5=0)&(D8=0)&(D10=0)&(D11=0)&(D13=0)&(D16=0)=>(M&R={1[49],2[1]})
11	46	(D1=2)&(D5=1)=>(M&R={1[46]})
12	38	(D1=0)&(D2=0)&(D3=0)&(D4=0)&(D5=1)&(D6=0)&(D8=0)&(D10=0)&(D14=0)=>(M&R={1[1],2[21],3[16]})
13	33	(D1=0)&(D2=0)&(D3=1)&(D4=1)&(D5=0)&(D6=0)&(D13=0)=>(M&R={2[29],3[4]})
14	32	(D1=4)&(D2=0)&(D3=0)&(D4=0)&(D5=0)&(D7=0)&(D8=0)&(D13=0)=>(M&R={2[23],3[9]})
15	28	(D1=0)&(D3=1)&(D5=1)=>(M&R={2[28]})
16	28	(D1=0)&(D3=1)&(D4=1)&(D5=0)&(D6=0)&(D7=0)&(D13=0)=>(M&R={2[27],3[1]})
17	26	(D1=1)&(D2=0)&(D3=0)&(D4=1)&(D5=0)&(D7=0)=>(M&R={1[23],2[3]})
18	25	(D1=0)&(D3=5)&(D4=1)&(D7=5)=>(M&R={2[2],3[23]})
19	25	(D1=0)&(D3=5)&(D7=5)&(D8=0)=>(M&R={2[2],3[23]})
20	25	(D1=0)&(D3=5)&(D7=5)&(D10=0)=>(M&R={2[2],3[23]})
21	24	(D1=1)&(D8=1)=>(M&R={1[24]})
22	22	(D1=1)&(D2=1)=>(M&R={1[22]})
23	21	(D1=0)&(D3=1)&(D6=0)&(D10=1)=>(M&R={2[21]})
24	20	(D1=0)&(D2=5)&(D3=5)&(D7=5)=>(M&R={2[1],3[19]})
25	20	(D1=0)&(D2=5)&(D4=1)&(D7=5)=>(M&R={2[1],3[19]})
26	20	(D1=0)&(D2=5)&(D7=5)&(D10=0)=>(M&R={2[1],3[19]})
27	17	(D1=5)&(D2=5)&(D5=0)&(D6=0)=>(M&R={2[17]})
28	17	(D1=0)&(D2=0)&(D3=5)&(D4=0)&(D5=0)=>(M&R={2[17]})
29	17	(D1=0)&(D2=0)&(D3=5)&(D4=0)&(D7=0)=>(M&R={2[17]})
30	16	(D1=2)&(D10=1)=>(M&R={1[16]})
31	16	(D1=0)&(D2=1)&(D3=0)=>(M&R={2[16]})
32	15	(D1=2)&(D3=2)&(D7=0)=>(M&R={1[15]})
33	15	(D4=0)&(D5=6)&(D6=0)=>(M&R={2[15]})
34	15	(D1=0)&(D3=0)&(D4=1)&(D5=1)=>(M&R={2[8],3[7]})
35	13	(D1=1)&(D7=1)=>(M&R={1[13]})
36	13	(D1=0)&(D3=0)&(D4=4)&(D8=0)=>(M&R={2[13]})
37	13	(D1=0)&(D2=0)&(D3=0)&(D5=0)&(D10=1)=>(M&R={2[12],3[1]})
38	13	(D1=0)&(D2=0)&(D3=5)&(D4=1)=>(M&R={2[8],3[5]})
39	12	(D1=5)&(D2=5)&(D3=5)&(D6=0)=>(M&R={2[12]})
40	12	(D1=0)&(D5=1)&(D10=1)=>(M&R={2[12]})
41	12	(D1=5)&(D2=5)&(D4=5)=>(M&R={2[12]})
42	12	(D1=0)&(D3=0)&(D4=2)&(D5=0)&(D11=0)=>(M&R={2[11],3[1]})
43	12	(D1=0)&(D3=0)&(D4=2)&(D11=0)&(D14=0)=>(M&R={2[11],3[1]})
44	12	(D1=0)&(D2=1)&(D3=1)&(D4=0)&(D8=0)&(D10=0)=>(M&R={2[11],3[1]})

If (D1=1) & (D2=0) & (D3=0) & (D4=0) & (D5=0) & (D6=0) & (D7=0) & (D8=0) & (D9=0) & (D10=0) & (D11=0) & (D12=0) & (D13=0) & (D16=0) (That is, Alligator Cracking occurs with low severity and local coverage.)

Then adopted M&R strategy might be no M&R required (204 records) or fragment M&R required (4 records).

In addition, RST is able to carry out the shortening of reduces. One shortening ratio has to be assigned. This coefficient is between 0 and 1, which determines how "aggressive" the shortening procedure should be. The coefficient equals to 1.0 means that no shortening occurs. If shortening ratio is near zero, RST attempts to maximally shorten reduces. In the study, four shortening ratios - 1.0 (no shortening), 0.9, 0.7, and 0.5 - are selected to establish four shorten models for further verification and then 332, 89, 72, and 58 rules are obtained, respectively.

Additional 233 records are used to conduct verification analyses in the light of three shorten models and one no-shorten model. The results are shown in Table 3.

Table 3. Verification Results of Shortening Ratio = 1.0 (No Shortening, 332 Rules)

		predicted						
		1	2	3	4	No. of obj.	Accuracy	Coverage
Actual	1	123	0	1	0	135	0.992	0.919
	2	3	45	15	0	74	0.714	0.851
	3	0	0	15	0	18	1	0.833
	4	0	0	0	5	6	1	0.833
	True positive rate	0.98	1	0.48	1			
Total number of tested objects:233 Total accuracy:0.908 Total coverage:0.888								

5 Discussion

In the same case, we also use the decision tree and neural network method to solve problem. At the accuracy, rough set theory is better than other method. Under the same accuracy, Rough set theory uses 14 attributes to generate decision rule. So it can decrease the survey cost in feature. We can find the Rough set theory application pavement maintenance strategy is suitable.

Table 4. Compare with ANN and Decision Tree method

	Rough Set Theory	Decision Tree	Neural Network
Accuracy			
Training Set	93.6%	87.0%	92.2%
Testing Set	88.0%	83.0%	67.1%
Generation Rules	72	101	-
Consider Attribute	14	18	18

6 Conclusion

Pavement distress survey can assist engineers in M&R strategy decisions. Proper M&R strategy can save long-term expense and keep the pavement above an acceptable serviceability. RST is used to induce M&R strategies by using 2,348 actual data (2,115 records for rule induction, and 233 records for rule verification). On the basis of the verification results, total accuracy for the induced rules is as high as 93.6%, which illustrates that RST certainly can assist engineers to easily remove redundant records, reduce attributes, discover association, and induce the most appropriate M&R strategy when they deal with the enormous pavement distress data. In the future, the database can be further extended for inducing more proper M&R strategies.

Acknowledgments

This study is partial results of project NSC 93-2211-E-159-003. The authors would like to express their appreciations to National Science Council of Taiwan for funding support.

References

1. Prechaverakul, S., Hadipriono, F.C.: Using a Knowledge-based Expert System and Fuzzy Logic for Minor Rehabilitation Projects in Ohio. Transportation Research Record 1497, 19–26 (1995)
2. Hajek, J.J., Chong, G.J., Phang, W.A., Haas, R.: ROSE, A Knowledge Based Expert System for Routing and Sealing. In: 2nd North American Conference on Managing Pavement (1987)
3. Medsker, L.: Design and Development of Expert Systems and Neural networks. Macmillan College Publishing, USA (1994)
4. Pawlak, Z.: Rough Set. International Journal of Computer and Information Science 11(5), 341–356 (1982)
5. Pawlak, Z.: Rough Sets: Theoretical Aspects of Reasoning about Data. Kluwer Academic Publisher, Dordrecht (1991)
6. Attoh-Okine, N.O.: A Rough Set Application to Data Mining Principles in Pavement Management Database. ASCE Journal of Computing in Civil Engineering 11(4), 231–237 (1997)
7. Attoh-Okine, N.O.: Combining Use of Rough Set Theory and Artificial Neural Networks in Doweled Performance Modeling: A Hybrid Approach. ASCE Journal of Transportation Engineering 128(3), 270–275 (2002)

Using Control Theory for Analysis of Reinforcement Learning and Optimal Policy Properties in Grid-World Problems

S. Mostapha Kalami Heris[1], Mohammad-Bagher Naghibi Sistani[2], and Naser Pariz[2]

[1] Control Engineering Department, Faculty of Electrical Engineering,
K. N. Toosi University of Technology, Tehran, Iran
[2] Electrical Engineering Department, Faculty of Engineering,
Ferdowsi University of Mashhad, Mashhad, Iran
kalami@ee.kntu.ac.ir, mb-naghibi@um.ac.ir, n-pariz@um.ac.ir

Abstract. Markov Decision Process (MDP) has enormous applications in science, engineering, economics and management. Most of decision processes have Markov property and can be modeled as MDP. Reinforcement Learning (RL) is an approach to deal with MDPs. RL methods are based on Dynamic Programming (DP) algorithms, such as Policy Evaluation, Policy Iteration and Value Iteration. In this paper, policy evaluation algorithm is represented in the form of a discrete-time dynamical system. Hence, using Discrete-Time Control methods, behavior of agent and properties of various policies, can be analyzed. The general case of grid-world problems is addressed, and some important results are obtained for this type of problems as a theorem. For example, equivalent system of an optimal policy for a grid-world problem is dead-beat.

Keywords: Dynamic Programming, Discrete-Time Control Systems, Markov Decision Process, Reinforcement Learning, Stochastic Control.

1 Introduction

A grid-world problem is a special case of Markov Decision Process (MDP). MDP is introduced and studied by Bellman (1957) for the first time, and studied in more detail by Howard (1960) [1]. First registered application of MDP is Road Management in Arizona State (1978) [1]. Wild-life Management, Manufacturing Management, Inventory and Transportation, are examples of MDP applications [1]. A full list of MDP applications is gathered by Puterman [1], Cassandra [2], Pyeatt [3], Hu et al. [18] and Soo et al. [19].

Obtaining an optimal policy for a MDP is one of most discussable problems in optimization and control theories. To solve this problem, Linear Programming (LP) and Dynamic Programming (DP) methods are used [1,5,8,18,19]. Basic DP algorithms to deal with MDPs, are Policy Evaluation, Policy Iteration and Value Iteration, which are studied in [1], [4], [5], [6] and [7], in detail. Use of these methods, yields accurate solutions to MDPs, and also inexact solutions with specific accuracy can be obtained. Existence of solutions for these methods, is proved using various methods and Exact

D.-S. Huang et al. (Eds.): ICIC 2009, LNAI 5755, pp. 276–285, 2009.

conditions for the existence of optimal solution for MDP, are gathered and studied in detail [5,6,7,16]. Curse of Dimensionality, which is introduced by Bellman, causes critical problems with the use of DP algorithms within large-scale problems. So approximate and fast algorithms are developed in the framework of Reinforcement Learning (RL) [5,7,9] and Neural-Dynamic Programming [4,8,9].

The approaches deployed for improvement of the procedure used to solve MDP are dividable into four major groups. Methods of group one use structural properties of the problem to facilitate procedure of achieving solution or optimal policy [11,12,26]. Other methods in opposition to methods discussed in group one, do not lead to optimal results for the problem. Hence these results are sub-optimal [10,15]. Approaches in group two could be divided into two sub categories. In methods of first sub-group, simplified models are used to solve the problem and sub-optimal solutions are found for main problem [10,15]. In the second sub-group methods, the structure of the policy is being assumed in a particular form and therefore a kind of simplification is implemented [4,6,10,15]. The third group of approaches is obtained through approximation of State Value Functions and State-Action Value Function, and equations of DP [4,5,7,9,10,13,14]. Methods in the fourth group are defined and used in policy space such as classic method of Policy Iteration. These approaches are aimed to speed up formation of optimal policy using special methods and consequently the overall process of problem solution is accelerated.

One of suggested methods in order to speed up the process of solution of MDP, is utilization of a method called Policy Reuse, which is used to accelerate the learning and categorization of information obtained on later experiences [20-23]. Also optimization of policy iteration algorithm has resulted in appropriate consequences. We can refer to [1], [6], [7], [19], [24], [25] and [26] as examples.

Many approaches are introduced to improve functionality and speed of DP algorithms and also RL algorithms in MDPs. The main difficulty in most of problems is absence of knowledge about optimal result. There is no simple and fast criterion to compare two policies and to identify an optimal policy. It means that the policy must be utilized by the agent to evaluate it, based on the return. In spite of many researches carried on to improve functionality of algorithms related to solution of MDP problems, no method is proposed to mathematical analysis of optimal policy in MDP problems, up to now. For this reason there is no criterion to analyze performance of the agent, which obeys particular policy, but time consuming algorithms.

In this paper the procedure of solving MDP problem using Dynamic Programming method is stated as a discrete-time or digital dynamical system. Obtained digital system is consistent with proposed solution for this problem. It is possible to identify related solution properties by analyzing control characteristics of the equivalent system and guessing quality of final solution. Utilizing this equalization leads to the possibility of analyzing functionality of RL in Markovian environments.

Other sections of this paper are as follows. In the section 2, Reinforcement Learning and its main ideas are discussed briefly. Section 3 studies primary definitions of MDP and DP methods, which are used to solve this type of problems, are represented. In section 4, policy evaluation algorithm is proposed as a discrete-time dynamical system. In section 5, two sample problems are investigated based on contents of section 4 and analysis and control methods of discrete-time dynamical

systems. Section 6 consists of general statements on grid-world problems and optimal policy related to this type of problems. Finally, conclusion is done in section 7.

2 Reinforcement Learning

In Reinforcement Learning the main purpose of learning is performing duties or reaching some target without the case that the agent is fed by direct external information. In this method the only way of informing agent is through one reward or penalty signal. The one thing that gets across to agent via reward signal is whether appropriate decision is made or not. In this method of learning the agent is never told that which the correct action in each state is, and just it is being told that how much each action is good or bad. A generic Reinforcement Learning problem is shown in Fig. 1. Learning agent achieves some descriptions of environment through sensors. Information relevant to the environment is fed to the agent as sensory information. When the agent performs an action, it earns a reward which could be positive or negative based on whether the action was good or bad. The target of the agent in learning is equivalent to maximization of reward in a specific range of time. These two targets are consistent and satisfaction of each one will result in satisfaction of the other. In this way the agent learns appropriate way of operation via focus on earned rewards. This is possible through finding a mapping between states and actions doable by the agent. This mapping which is called policy tells the agent what to perform when run into different states.

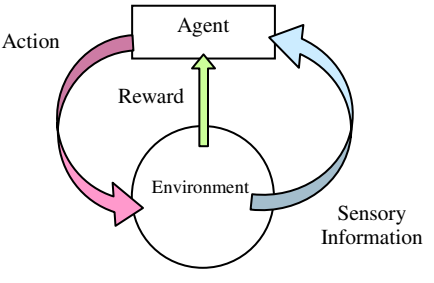

Fig. 1. One Reinforcement Learning problem and the way agent and environment interact

3 Markov Decision Processes

One major assumption in most of works on Reinforcement Learning is that the interaction between agent and surrounding environment could be modeled as a Markov Decision Process (MDP). A MDP is a stochastic and discrete-time process which is often defined as quadruple like $(\mathbb{S}, \mathbb{A}, \mathcal{P}, \mathcal{R})$.

$\mathbb{S} = \{s^1, s^2, \ldots, s^n\}$ is state space of the process and consists of all possible states that deciding agent encounter and the agent must make a decision. $\mathbb{A} = \{a^1, a^2, \ldots, a^m\}$ is set of actions which could be selected by the agent. $\mathcal{P}$ models transition and change

of states. If the process is in state s and action a is selected by the agent, the probability that the state of process change to s' is defined as $\mathcal{P}_{ss'}^{a}$. Generally speaking, $\mathcal{P}$ is a mapping of the form $\mathcal{P}:\mathbb{S}\times\mathbb{A}\times\mathbb{S}\to[0,1]$. This model has the Markov property. If s_t and a_t indicate process state and selected action in discrete time t respectively, then Markov property could be defined as below:

$$\mathcal{P}_{s_t s_{t+1}}^{a_t} = \Pr\{s_{t+1}\,|\,s_t, a_t\} = \Pr\{s_{t+1}\,|\,s_t, a_t, s_{t-1}, a_{t-1}, \ldots\} \ . \tag{1}$$

$\mathcal{R}$ defines expectation of reward. If the agent is in state s and goes to state s' by choosing action a, the value of reward will be a random number with expectation of $\mathcal{R}_{ss'}^{a}$. Generally speaking, reward function is a mapping such as $\mathcal{R}:\mathbb{S}\times\mathbb{A}\times\mathbb{S}\to\mathbb{R}$. Function $\mathcal{R}$ has the Markov property and the value of $\mathcal{R}_{ss'}^{a}$ is just dependent to present state s and present action a and next state s' and is totally independent of previous states or actions.

The probability that action a is selected by the agent in state s is being defined as a mapping such as $\pi:\mathbb{S}\times\mathbb{A}\to[0,1]$, such that $\Pr\{a_t = a\,|\,s_t = s\} = \pi(s,a)$. The mapping π is known as policy and is the main unknown of a Reinforcement Learning problems or every other decision making problem [1,5,7,14].

In order to compare different policies with each other, it is possible to define a criterion to measure them. This criterion is the value that each policy returns in each state of process and is called as policy return in mentioned state. The return of one policy is the value that is obtained during consecutive decisions and obeying that policy. Solving a Reinforcement Learning problem is to find optimal policy of π^* in the way that maximizes the return of policy or the value of each state [5,7,14]. If a constant discount factor is defined as $\gamma\in[0,1]$, then the value of state s could be calculated by:

$$V^{\pi}(s) = \mathbb{E}^{\pi}\{r_{t+1} + \gamma r_{t+2} + \cdots\,|\,s_t = s\} = \sum_{a\in\mathbb{A}}\pi(s,a)\sum_{s'\in\mathbb{S}}\mathcal{P}_{ss'}^{a}\left(\mathcal{R}_{ss'}^{a} + \gamma V^{\pi}(s')\right) \ , \tag{2}$$

in which $\mathbb{E}^{\pi}$ is the operator of expectation. Super-indices π are written to emphasize that the agent obeys policy π. Equation (2) is known as Bellman optimality equation [1,4,14,18,19]. One of the methods being used to solve this equation and finding values of all states is to change the equations into recurrent mode. This method, which is based on fixed-point theorem [17], and it is suggested to rewrite the equation (2) as following form[17]:

$$V_{k+1}^{\pi}(s) = \sum_{a\in\mathbb{A}}\pi(s,a)\sum_{s'\in\mathbb{S}}\mathcal{P}_{ss'}^{a}\left(\mathcal{R}_{ss'}^{a} + \gamma V_{k}^{\pi}(s')\right) \ , \tag{3}$$

in which $V_k^{\pi}(s)$ is k^{th} estimation of actual value of $V^{\pi}(s)$. Based on the fact that $|\gamma|<1$, we can infer $V_{k+1}^{\pi}(s)$ is related to $V_k^{\pi}(s)$ through a contraction mapping [17] and this mapping has a unique fixed-point which is the solution of equation and:

$$V^{\pi}(s) = \lim_{k\to\infty} V_k^{\pi}(s) \ . \tag{4}$$

4 Modeling the Policy Evaluation algorithm

Assume a vector defined as follows:

$$v^{\pi} = [V^{\pi}(s^1) \quad V^{\pi}(s^2) \quad \cdots \quad V^{\pi}(s^n)]^T \ . \tag{5}$$

This vector consists of all values for states of a model. Therefore recurrent equation of (3) could be rewritten for all states and changed to a joint equation:

$$v_{k+1}^{\pi} = \gamma \mathcal{P} v_k^{\pi} + \mathcal{R} = \gamma \begin{bmatrix} \mathcal{P}_{s^1 s^1} & \cdots & \mathcal{P}_{s^1 s^n} \\ \vdots & \ddots & \vdots \\ \mathcal{P}_{s^n s^1} & \cdots & \mathcal{P}_{s^n s^n} \end{bmatrix} v_k^{\pi} + \begin{bmatrix} \mathcal{R}_{s^1} \\ \vdots \\ \mathcal{R}_{s^n} \end{bmatrix}, \tag{6}$$

in which elements of matrices $\mathcal{P}$ and $\mathcal{R}$ are defined as follows:

$$\mathcal{P}_{ss'} = \sum_{a \in \mathbb{A}} \pi(s,a) \mathcal{P}_{ss'}^{a} \ , \text{ and} \tag{7}$$

$$\mathcal{R}_s = \sum_{a \in \mathbb{A}} \sum_{s' \in \mathbb{S}} \pi(s,a) \mathcal{P}_{ss'}^{a} \mathcal{R}_{ss'}^{a} = \sum_{a \in \mathbb{A}} \pi(s,a) \mathcal{R}_s^{a} \ . \tag{8}$$

Equation (6) could be rewritten in the form of $v_{k+1}^{\pi} = \gamma \mathcal{P} v_k^{\pi} + \mathcal{R} u_k$, in which it is assumed that u_k is discrete-time unit step, which is equals to 1 for $k \geq 0$ [27]. Equation $v_{k+1}^{\pi} = \gamma \mathcal{P} v_k^{\pi} + \mathcal{R} u_k$, is state equation of a discrete-time linear system [27], which its state variables are values of the process states. Stability condition for this system is that, all eigenvalues of matrix $\gamma \mathcal{P}$, are located inside unit circle [27]. To satisfy this condition, discount factor must agree the following inequality:

$$\gamma < \frac{1}{\max\limits_{1 \leq i \leq n} |\lambda_i(\mathcal{P})|} = \frac{1}{\rho(\mathcal{P})} \ , \tag{9}$$

in which $\lambda_i(\mathcal{P})$ is the i^{th} eigenvalue and $\rho(\mathcal{P})$ is spectral radius of square matrix $\mathcal{P}$. It can be seen that the condition $\gamma \leq 1$ does not necessarily ensure existence of finite solution for (2). Equation (9) states more accurate condition for γ .

5 Solving and Investigating a Problem

Assume a table such as Fig. 2. In this problem the agent is located in one of white cells again and it is required to reach one of gray cells moving up, down, left and right. Moving in each direction has a reward of -1 which shows the cost to move in each state. The movements which cause agent exit the table has no effect on the location of the agent. The agent must learn to reach one of target cells earning maximum reward (minimum penalty). If so the agent has reach target in minimum number of movements. This problem could be stated as a MDP.

s^0	s^1	s^2	s^3
s^4	s^5	s^6	s^7
s^8	s^9	s^{10}	s^{11}
s^{12}	s^{13}	s^{14}	s^0

Fig. 2. The table relevant to the problem in section 5.2

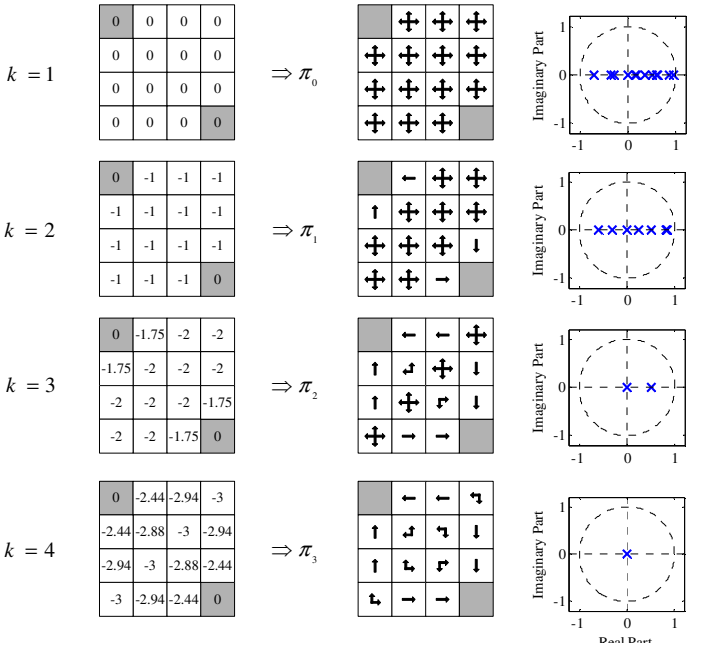

Fig. 3. Steps of policy evaluation algorithm for π_0 and inferred policies in each step with the diagram of equivalent dynamic system poles

In order to deploy policy evaluation method, initial value of all cells are assumed to be zero. The policy deployed up to the end of evaluation, is random policy. It means that in all cells of the table the probability of movements in all directions are the same and all equal to 0.25. In Fig. 3 some iterations of Eq. (3) are shown.

Based on the results of each step, a greedy policy could be formed. It means that the agent must move in the direction which has the most value. The policy obtained using the results yielded in step k^{th} is shown as π_k . π_0 is the random policy. π_3 and all of policies after that, are identical and this fact is referred to by $\pi_3 = \pi_\infty$. Assume matrix $\mathcal{P}$ in equation (6) equals $\mathcal{P}_i$ for policy π_i . Spectral radius of all mentioned matrixes are calculated and shown as follows:

$$\rho(\mathcal{P}_0) \simeq 0.9468, \quad \rho(\mathcal{P}_1) \simeq 0.8431, \quad \rho(\mathcal{P}_2) = 0.5, \quad \rho(\mathcal{P}_3) = \rho(\mathcal{P}_\infty) = 0 \tag{10}$$

It can obviously be seen that more optimal the policy, the least the greatest eigenvalue of state matrix is. Specially for policy π_3, all eigenvalues are zero. Consequently upper bound for discount coefficient value of γ are as follows respectively: 1.0562, 1.1861, 2, ∞. So the Eq. (2) has finite solutions for all values of γ, for the policy π_3.

The poles of system (6) are identical to eigenvalues of matrix $\gamma\mathcal{P}$. It can be seen that the poles of the system equal to policy π_∞ are all located at the origin, the system is dead-beat and has the fastest response among the systems with the same degree. Defining the value of all states as the output, transfer function of all systems could be found as $G_i(z) = (zI - \gamma\mathcal{P}_i)^{-1}\mathcal{R}_i$. This transfer function models a system with one input and 14 outputs. Each output is related to the value of one cell in the grid. Frequency response of four systems are shown in Fig. 4 for cell s^3.

The scaling of vertical axis is not set to dB and mentioned values are real values. The frequency response shown in Fig. 4 contains very important information about the environment and the policy implemented by the agent. In this figure, steady state response of the systems in cell s^3 can be observed. Steady state response of these systems is identical to the value of frequency response in frequency zero. It can be seen that the amplitude of frequency response in frequency zero for policies π_0, π_1, π_2 and π_3 is respectively 22, 9, 4 and 3. These are mean costs that agent pays to reach each of target cells starting from s^3. According to the definition of reward for this problem the value of penalty is the number of movements which the agent does to reach target cells. It can be seen that the minimum number of movements is achieved for π_3. Fig. 4 shows that the systems equivalent to better policies have wider bandwidth. Based on the fact that the bandwidth is a criterion of response speed, it can be inferred that for better policies response speed of systems is faster. This is the point we expect from a good policy for present problem.

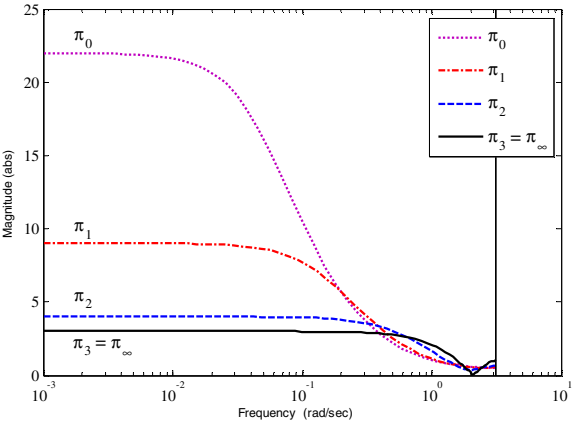

Fig. 4. Frequency response of systems obeying policies π_0 to π_3 in cell s^3 of table in Fig. 2

6 General Investigation of Grid-World Problems

The results obtained in this section are related to grid-world problem or other similar problems. Common characteristics of the problems for which the results of this section are applicable, are listed:

- The problem must be representable in the form of MDP.
- There must be one or more final state that reaching them means end of process.
- All movements have cost as negative reward.
- The target of the problem is to find a schedule to reach final state paying minimum cost or yielding minimum negative reward. Total cost is defined as discounted summation of rewards obtained by the agent.

Assume a grid-world problem with one or more target cells. All target cells are assumed as one joint state. The value of state relevant to target cells is always assumed to be zero and dismissed from the vector of state values. Each movement has a cost modeled as a -1 reward. For each state s, at least one path could definitely be found in a way that has the least penalty. This path has the least possible movements and for the state s this number of movements is indicated by $m(s)$. Under these assumptions, it is possible to state a theorem about grid-world and similar problems.

Theorem. Dynamical system equal to optimal policy evaluation system of a table problem has the properties as follows:

- The system is a dead-beat one and the component relevant to state s has exactly $m(s)$ poles at the origin of z plane.
- Frequency response of this system in frequency zero has the least value. If $\gamma = 1$, the magnitude of frequency relevant to state s in $\omega = 0$ will be equal to $m(s)$. This value equals to the final value of state s with negative sign.
- This system is stable for all values of discount factor γ. □

Proof. If the agent obeys optimal policy, it will pass an optimal path starting from state s and will reach target cell exactly after doing $m(s)$ movements and finally will have a total reward equal to $-m(s)$. If we assume $\gamma = 1$ the value of cell s after movement k^{th} will be summation of rewards gained by the agent up to k^{th} movement. Therefore the value of state s could be defined as a function of discrete time as:

$$V_k(s) = \begin{cases} 0 & ,k < 0 \\ -k & ,0 \le k \le m(s) \\ -m(s) & ,k > m(s) \end{cases} . \tag{11}$$

Note that the time in definition above is equal to the number of iteration in policy evaluation algorithm. The function above is one of outputs for equivalent system to optimal policy evaluation. z transform of mentioned value function is as follows:

$$\mathcal{Z}\{V_k(s)\} = V_s(z) = -\sum_{k=1}^{m(s)} k z^{-k} - m(s) \sum_{k=m(s)+1}^{\infty} z^{-k} . \tag{12}$$

At the other hand, based on the proposed contents, the input of the system equal to policy evaluation is always assumed to be unit step. Therefore the transfer function relevant to state s could be calculated through following equation:

$$V_s(z) = G_s(z)U(z) = \frac{1}{1-z^{-1}}G_s(z) \ . \tag{13}$$

Therefore the transfer function relevant to value of state s, is defined by $G_s(z) = (1-z^{-1})V_s(z)$. Substituting (12) yields:

$$G_s(z) = -\sum_{k=1}^{m(s)} z^{-k} = -\frac{z^{m(s)-1}+\cdots+z+1}{z^{m(s)}} = -\frac{z^{m(s)}-1}{z^{m(s)}(z-1)} \ . \tag{14}$$

It can be seen that the transfer function relevant to state s has exactly $m(s)$ poles on the origin of z plane, and $G_s(z)$ is a dead-beat system. Also zeros of $G_s(z)$ are always located on the unit circle and all of them are $m(s)^{\text{th}}$ roots of 1. Note that $z=1$ is not a zero of $G_s(z)$. ■

7 Conclusion

In this paper having a survey on Reinforcement Learning (RL), Markov Decision Process (MDP) and Dynamic Programming (DP), equations related to solution of one MDP using DP are rewritten and concluded as a discrete-time dynamical system. This approach provides the possibility of solving and analyzing a Reinforcement Learning problem in Markovian environment in the form of a discrete-time dynamical system. Therefore it is possible to use Discrete-Time Control methods to analyze a learning process. The main subject of this paper is on a kind of problems called grid-world problems. The results show that the optimal policies for this type of problem could be defined as dead-beat system in the framework of Discrete-Time Control systems. Generalization of these results into other problems and defining a duality between decision making space and Discrete-Time Control system space are of completing researches and studies could be imagined.

References

1. Puterman, M.L.: Markov Decision Processes: Discrete Stochastic Dynamic Programming. Wiley, Chichester (2005)
2. Cassandra, A.: Exact and Approximate Algorithms for Partially Observable Markov Decision Processes. Ph.D. Thesis, Brown University (1998)
3. Pyeatt, L.: Integration of Partially Observable Markov Decision Processes and Reinforcement Learning for Simulated Robot Navigation. Ph.D. Thesis, Colorado State University (1999)
4. Bertsekas, D.P., Tsitsiklis, J.N.: Neuro-Dynamic Programming. Athena Scientific (1996)
5. Sutton, R.S., Barto, A.G.: Reinforcement Learning: An Introduction. The MIT Press, Cambridge (1998)

6. Lew, A., Mauch, H.: Dynamic Programming: A Computational Tool. Springer, Berlin (2007)
7. Reynolds, S.I.: Reinforcement Learning with Exploration. Ph.D. Thesis, School of Computer Science, University of Birmingham, UK (2002)
8. Van Roy, B.: Neuro-Dynamic Programming: Overview and Recent Trends. In: Feinberg, E.A., Schwartz, A. (eds.) Handbook of Markov Decision Processes: Methods and Applications. Kluwer Academic, Dordrecht (2002)
9. Si, J., et al.: Handbook of Learning and Approximate Dynamic Programming. Wiley InterScience, Hoboken (2004)
10. Soo Chang, H., et al.: A survey of some Simulation-Based Algorithms for Markov Decision Processes. Communications in Information and Systems 7(1), 59–92 (2007)
11. Smith, J.E., Mc Cardle, K.F.: Structural Properties of Stochastic Dynamic Programs. Operations Research 50, 796–809 (2002)
12. Fu, M.C., et al.: Monotone optimal policies for queuing staffing problem. Operations Research 46, 327–331 (2000)
13. Givan, R., et al.: Bounded Markov Decision Processes. Artificial Intelligence 122, 71–109 (2000)
14. Kaelbling, L.P., Littman, M.L., Moore, A.W.: Reinforcement Learning: A Survey. Journal of Artificial Intelligence Research 4, 237–285 (1996)
15. Gordon, G.J.: Approximate Solution to Markov Decision Processes. Ph.D. Thesis, School of Computer Science, Carnegie Mellon University (1999)
16. de Farias, D.P., Van Roy, B.: On the Existance of Fixed-points for Approximate Value Iteration and Temporal-Difference Learning. Journal of Optimization theory and Applications 105(3), 589–608 (2000)
17. Royden, H.: Real Analysis, 3rd edn. Prentice Hall, Englewood Cliffs (1988)
18. Hu, Q., Yue, W.: Markov Decision Processes with Their Applications. Springer Science+Busines Media, LLC (2008)
19. Soo, H., et al.: Simulation-based Algorithms for Markov Decision Processes. Springer, London (2007)
20. Fernandez, F., Veloso, M.: Exploration and Policy Reuse. Technical Report, School of Computer Science, Carnegie Mellon University (2005)
21. Fernandez, F., Veloso, M.: Probabilistic Reuse of Past policies. Technical Report, School of Computer Science, Carnegie Mellon University (2005)
22. Fernandez, F., Veloso, M.: Building a Library of Policies through Policy Reuse. Technical Report, School of Computer Science, Carnegie Mellon University (2005)
23. Bernstein, D.S.: Reusing Old Policies to Accelerate Learning on New Markov Decision Processes. Technical Report, University of Massachusetts (1999)
24. Zhang, N.L., Zhang, W.: Speeding Up the Convergence of Value Iteration in Partially Observable Markov Decision Processes. Journal of Artificial Intelligence Research 14, 29–51 (2001)
25. Hansen, E.A.: An Improved Policy Iteration for Partially Observable Markov Decision Processes. In: Proceedings of 10th Neural Information Processing Systems Conference (1997)
26. Sallans, B.: Reinforcement Learning for Factored Markov Decision Processes. Ph.D. Thesis, Graduate Department of Computer Science, University of Toronto (2002)
27. Ogata, K.: Discrete-Time Control Systems, 2nd edn. Prentice Hall, Englewood Cliffs (1994)

Adaptive Chaotic Cultural Algorithm for Hyperparameters Selection of Support Vector Regression

Jian Cheng[1,2], Jiansheng Qian[1], and Yi-nan Guo[1]

[1] School of Information and Electrical Engineering, China University of Mining and Technology, 221116, Xu Zhou, China
[2] Department of Automation, Tsinghua University, 100084, Beijing, China
chjpaper@126.com

Abstract. The hyperparameters selection has a great affection on accuracy of support vector regression (SVR). In order to determine the hyperparameters of SVR, an adaptive chaotic cultural algorithm (ACCA) is employed for the optimal hyperparameters including kernel parameters σ of Gaussian kernel function, regular constant γ and ε in the ε -insensitive loss function. Based on this, a learning algorithm with two-stage is constructed to realize the objective. Firstly, the initialization search spaces of hyperparameters are determined according to their influence on the performance of support vector regression. Secondly, optimal hyperparameters are selected using ACCA. ACCA adopt dual structure in cultural algorithm and adaptive chaotic mutation in evolution induction functions, and uses implicit knowledge extracted from evolution process to control mutation scale, which inducts individuals escaping from local best solutions. Taken the forecasting of gas concentration as example, experiment results indicate optimal hyperparameters can be obtained through above strategy.

1 Introduction

The support vector machine (SVM) that proposed by Vapnik and his research groups is a novel approach for solving the problems of classification [1]. The structural risk minimization principle is based on the fact that the generalization error is bounded by the sum of training error and a confidence interval term that dependents on the Vapnik-Chervonenkis (VC) dimension. Originally, the SVM has been developed for pattern recognition problems. However, with the introduction of Vapnik's ε -insensitive loss function, the SVM has been extended to solve a nonlinear regression estimation problem that has been shown to excellent performance [2]. In addition, the support vector regression (SVR) with proper kernel function can be also viewed as a constructive learning procedure employed to implement a variety of representations.

In order to obtain a better performance, some parameters, which are called hyperparameter in the SVR must be chosen carefully. In this paper, the Gaussian function shown in (1) with kernel parameter σ is used as kernel function that often used in the literature. So the hyperparameters include the kernel parameter σ, ε in Vapnik's ε -insensitive loss function and regular constant γ.

D.-S. Huang et al. (Eds.): ICIC 2009, LNAI 5755, pp. 286–293, 2009.

$$K(x_u, x_v) = \exp(-\|x_u - x_v\|^2 / 2\sigma^2) . \quad (1)$$

In [3], authors review some of possible hyperparameter selection methods such as cross-validation methods, bootstrapping and Bayesian methods. Making use of a validation set is still not a structured way to select the hyperparameters as this iterative process involves expensive computation. In order to simply the problems of hyperparameters, a new method with adaptive chaotic cultural algorithm (ACCA) is proposed to determine the σ, ε and γ in this paper.

ACCA uses the dual evolution structure of cultural algorithm, and a self adaptive chaotic mutation based on knowledge guiding is adopted. A chaotic clone evolutionary programming algorithm that was proposed in literature [4] used chaotic mutation in clone selection algorithm [5]. But it lacks in utilizing the effective implicit information of evolution process. This paper combines the chaotic clone evolutionary programming algorithm with cultural algorithms. In the influence of knowledge, the mutation step-size and chaotic factor can be self adaptive adjusted. It has been proved that implicit knowledge extracted from evolution process can be used to induce evolution operators so as to improve the performance of algorithms.

The rest of this paper is organized as follows. In Section 2, adaptive of chaotic cultural algorithm is shown. The proposed architecture and algorithm are given in Section 3. Section 4 presents the results and discussions on the experimental validation. Finally, some concluding remarks are drawn in Section 5.

2 Adaptive Chaotic Cultural Algorithm

2.1 Algorithm Description

It has been proved that implicit knowledge extracted from evolution process can be used to induce evolution operators so as to improve the performance of algorithms. Based on above theory, a novel evolutionary algorithm with chaotic mutation induced by implicit knowledge is proposed.

In the method, various knowledge are extracted and utilized by adopting dual evolution structure in culture algorithms in order to improve the evolution performance and decrease computation complexity. The structure of the adaptive chaotic cultural algorithm (ACCA) is shown in Figure 1.

In population space, evolution operators, including selection, crossover and mutation, are implemented. Each path is evaluated and their feasibility is judged and repaired. In belief space, samples are selected from evaluated individuals in population space by sample-selection function. Evolution knowledge are extracted from samples by knowledge-extraction function and stored in the evolution-knowledge database. They influence the evolution process by evolution- inducing function. In common sense database, integrated information about environment are stored. They are used to evaluate the length of the paths.

It is obvious that the keys of the method are how to describe, extract and utilize knowledge and how to judge and repair the infeasible individuals.

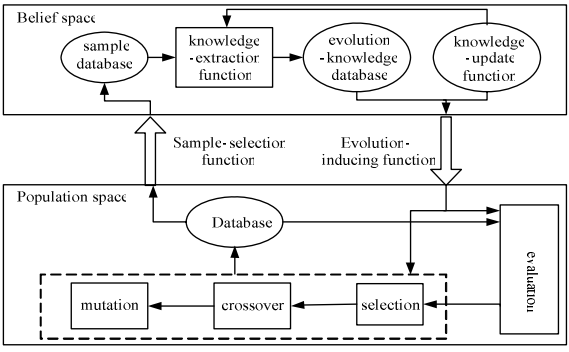

Fig. 1. The structure of adaptive chaotic cultural algorithm

2.2 Extraction and Update of Knowledge

Knowledge expressed by bintree are extracted and updated according to the distribution of individuals with largest fitness in each iteration.

Definition 1: increment of information ΔI_j

$$\Delta I_j = \frac{f(p_{best}(t)) - f(p_{best}(t-1))}{p_{best,j}(t) - p_{best,j}(t-1)}, \tag{2}$$

where $p_{best}(t)$ denotes the best individual in tth iteration. It is obvious that increment of information expresses the fitness gradient in each dimension.

Definition 2: bintree of knowledge Sk

$$\begin{aligned} Sk &= [sp_1, sp_2, \cdots sp_{N_s}], \\ sp_k &= \frac{1}{2}(p_{best,j}(t) - p_{best,j}(t-1)), j = \arg\max_{j=1,2,\cdots,n} \Delta I_j, \end{aligned} \tag{3}$$

where sp_k is the split point in bintree. It divides the search space into two parts along the dimension with largest increment of information so as to shrink the feasible search space. That is

$$\begin{cases} \Omega_{k1}(t) : \underline{C_j^{K1}}(t) = \underline{C_j}(t-1), \overline{C_j^{K1}}(t) = sp_k, \\ \Omega_{k2}(t) : \underline{C_j^{K2}}(t) = sp_k, \overline{C_j^{K2}}(t) = \overline{C_j}(t-1), \end{cases} \tag{4}$$

$$\Omega(t-1) = \Omega_{k1}(t) \cup \Omega_{k2}(t), \tag{5}$$

where $\underline{C_j^{K1}}(t)$, $\overline{C_j^{K1}}(t)$ denote lower and upper limits of the dominant space $\Omega_{k1}(t)$.

2.3 Knowledge-Based Chaotic Mutation

The scale of mutation is adaptively adjusted based on chaotic sequence according to current knowledge describing the dominant space, shown in (6).

$$c_{ij}(t+1)=\begin{cases}\underline{C_j}(t)+(\overline{C_j}(t)-\underline{C_j}(t))a_{ij}^{l}(t), & p_i(t)\notin\Omega_{k1}(t),\\ c_{ij}(t)+\exp(\dfrac{-\alpha t}{T})\times(\overline{C_j^{K1}}(t)-\underline{C_j^{K1}}(t))\times a_{ij}^{l}(t), & p_i(t)\in\Omega_{k1}(t),\end{cases} \tag{6}$$

where $a_{ij}^{l}(t)$ is the value of Logistic chaotic sequence.

$$a_{ij}^{l+1}=\mu a_{ij}^{l}(1-a_{ij}^{l}),l=0,1,2,\cdots Lm\,, \tag{7}$$

where Lm is the length of sequence. $a_{ij}^{0}\in[0,1]$ is a random number. $\mu\in[3,4]$ is the chaotic factor. The ergodicity of a chaotic sequence is different when μ and Lm is different. Here, implicit knowledge is introduced to decide the value of μ.

$$\mu(t)=3.5+0.5\times\frac{\overline{c_j}(t)-\underline{c_j}(t)}{\overline{c_j}(0)-\underline{c_j}(0)}\,. \tag{8}$$

It is obvious that the possible value of $\mu(t)$ is between 3.5 and 4. When the span of current dominant space is shrunken, the value of μ is smaller. It will decrease the ergodicity of the chaotic sequence and the complexity of computation in the algorithm. In a word, the scale of mutation is in inverse proportion to iteration and in proportion to the span of the dominant space so as to ensure the diversity of population in evolution process.

3 The Proposed Architecture and Algorithm

The Basic idea is to use ACCA to select the optimal hyperparameters and apply SVR for gas concentration forecasting. Figure 2 shows how the model is built.

Up to here the process of forecasting gas concentration is completed. The detailed step of algorithm is illustrated as the following:

Step 1. For a gas concentration original input data x_k, some trails are applied to assign the initialization search space of hyperparameters with kernel parameter σ, regular constant γ and ε in the ε-insensitive loss function.

Step 2. The optimal hyperparameters are determined through adaptive chaotic cultural algorithm.

Step 3. Through the former two steps, the structure of SVR model with the optimal hyperparameters is built for gas concentration forecasting.

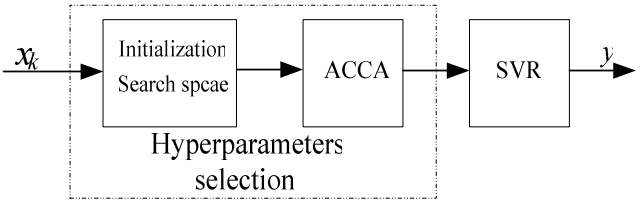

Fig. 2. The structure of the proposed model

4 Experiment Analysis

4.1 Gas Concentration Forecasting

Gas concentration (CH_4) is a very complex dynamic phenomenon which is affected by many factors, and is also one of key factors which influence safe production of coal mine. It is very important to forecast gas concentration accurately for ensuring the coal mine safety. Gas concentration is nonlinear and chaotic time series in essence, so it can be forecasted using the method of chaotic time series model [6].

Nonlinear and chaotic time series prediction is a practical technique which can be used for studying the characteristics of complicated systems based on recorded data [7]. As a result, the interests in chaotic time series prediction have been increased, however, most practical time series are of nonlinear and chaotic nature that makes conventional, linear prediction methods inapplicable [8]. Although the neural networks is developed in chaotic time series prediction [9], some inherent drawbacks, e.g., the multiple local minima problem, the choice of the number of hidden units and the danger of over fitting, etc., would make it difficult to put the neural networks into some practice.

SVR has demonstrated its success in chaotic time series analysis. However, little work has been done in coal mine gas concentration forecasting. The objective of this paper is to propose a SVR method for gas concentration forecasting in coal mine.

4.2 Phase Space Reconstruction and Nonlinear Function Approximation

Chaos occurs as a feature of orbits $x(t)$ arising from systems of differential equations of $dx(t)/dt = F(x(t))$ with three or more degrees of freedom or invertible maps of $x(t+1) = F(x(t))$. As a class of observable signals $x(t)$, chaos lies logically between the well-studied domain of predictable, regular, or quasi-periodic signal and the totally irregular stochastic signals [9]. In many systems the interaction between the underlying physical processes that are responsible for the evolution of system behavior are unknown. In addition, it is seldom that one has information about all the relevant dynamic variables. Instead, one usually tries to construct a multivariate phase space in which the dynamics unfold using system output measurements of a single time series by converting the time series to a multidimensional phase space. In phase space reconstruction, a scalar time series $\{x_t\}$, $t = 1, \cdots, N$, with sampling time Δt, is converted to its phase space using the method of delays:

$$X_t = [x_t, x_{t+1}, \cdots, x_{t+(d-1)}], \tag{9}$$

where $t = 1, 2, \cdots, N-(d-1)T/\Delta t$, d is the embedding dimension, and T is the delay time. In other words, phase space reconstruction techniques convert a single scalar time series to a state-vector representation using the embedding dimension (d) and delay time (T). This reconstruction is required for both characterization and forecasting. In this study, SVR will be employed to capture the dynamics depicted in (21) with the purpose of producing reliable predictions: $X_{t+T} = f(X_t)$,

$$f : (x_t, x_{t+1}, \cdots, x_{t+(d-1)}) \to (x_{t+T}, x_{t+1+T}, \cdots, X_{t+(d-1)+T}), \tag{10}$$

so $\hat{y} = X_{t+(d-1)+T} = g(x_t, x_{t+1}, \cdots, x_{t+(d-1)})$. The training data consists of a d-dimensional vector, $x \in R^d$, and the response or output, $y \in R$. The goal of the learning machine, then, is to estimate an unknown continuous, real-valued function $g(x)$ that is capable of making accurate predictions of an output y, for previously unseen values of x, thus utilizing information about the dynamics of system behavior in the phase space representation to make forecasts of future system states in observation space. T is the prediction step. In this paper, we try applying SVR to estimate the unknown function $g(x)$.

4.3 Gas Concentration Data Acquesting

From the Luling coal mine, located in north of Anhui province, a gas concentration, Ⅱ816-working face T0, is researched. This experiment selects 2000 samples from the industrial field. Through the industrial field empirical knowledge and several trials, the phase space parameters are selected as following: the embedding dimension $d = 10$, and the prediction step $T = 6$. Then the first 1600 samples are used for training the model, while the remaining 400 samples are used for testing the identified model only.

The prediction performance is evaluated using by the root mean squared error (*RMSE*) as follows:

$$RMSE = \sqrt{\frac{1}{n}\sum_{i=1}^{n}(y_i - \hat{y}_i)^2}, \tag{11}$$

where n represents the total number of data points in the test set, y_i and $\hat{y}_i$ are the actual value, prediction value and the mean of the actual values respectively.

4.4 Simulation Results

In the first, the initialization search space of hyperparameters are determined through several trails, that $\sigma = [0.1, 0.6]$, $\gamma = [1, 200]$ and $\varepsilon = [0.002, 0.05]$. Secondly, main parameters used in ACCA are listed in Table 1.

Table 1. Main parameters of adaptive chaotic cultural algorithm

Population size	Run times	Crossover probability	Lm	m	Mutation probability
50	20	0.4	30	30	0.02

Using above ACCA, the optimal hyperparameters are obtained, that σ, γ and ε are, respectively, fixed at 0.467, 98.963 and 0.006812. So the SVR model is constructed with the optimal hyperparameters. The simulation results are shown in Figure 3 and Figure 4, and the training and testing *RMSE* are 0.0364 and 0.0512 respectively.

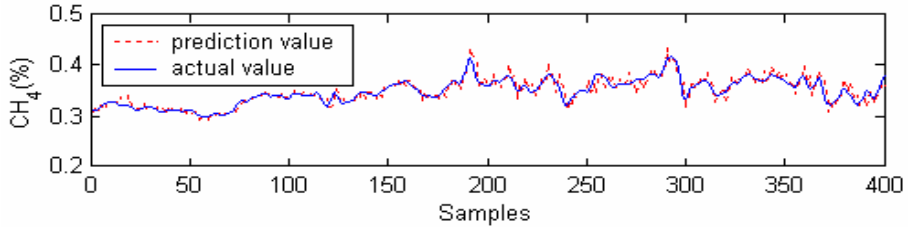

Fig. 3. The output of the proposed model (solid line is actual value and dashed line is prediction value)

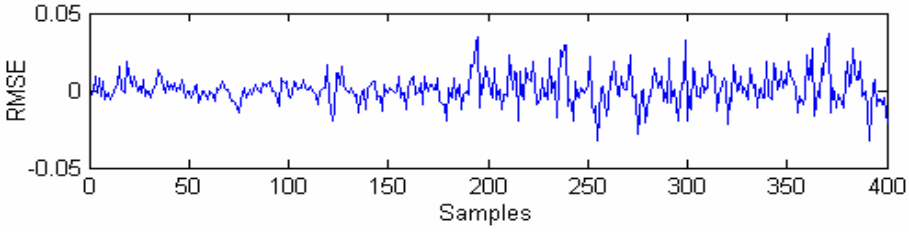

Fig. 4. Prediction error of the proposed model

5 Conclusions

Gas concentration forecasting is very important for coal mine safety. This paper describes a novel methodology, a optimal SVR based on adaptive chaotic cultural algorithm, to model and predict gas concentration. In order to achieve the optimal solution effectively, a novel evolutionary algorithm with knowledge-based chaotic mutation is proposed. Utilizing the ergodicity of chaotic, the scale of mutation is adaptively adjusted based on Logistic chaotic sequence according to current implicit knowledge. It also can improve the speed of convergence and have better computation stability. Firstly, the initialization search space of hyperparameters are determined by several trials. Secondly, the optimal hyperparameters can be obtained by adaptive chaotic cultural algorithm. Based on the efficiently structured way for

chosen hyperparameters, the results of the proposed approach in the SVR can closely to optimum hyperparameters region and provides a promising alternative for gas concentration forecasting in coal mine.

Acknowledgements

This research is supported by National Natural Science Foundation of China under grant 70533050 and Young Science Foundation of CUMT under grant 2006A010.

References

1. Vapnik, V.N.: An Overview of Statistical Learning Theory. IEEE Transactions Neural Networks 10(5), 988–999 (1999)
2. Li, D., Mersereau, R.M., Simske, S.: Blind image deconvolution through support vector regression. IEEE Transactions on Neural Networks 18(3), 931–935 (2007)
3. Chapelle, O., Vapnik, V.N., Bousquet, O., Mukherjee, S.: Choosing Multiple parameters for support vector machines. Machine Learning 46(1), 131–159 (2002)
4. Du, H.F., Gong, M.G., Liu, R.C., et al.: An Adaptive Chaotic Clone Evolutionary Programming. Science in China Ser. E Information Science 35(8), 817–829 (2005)
5. Xidong, J., Reynolds, R.G.: Using Knowledge-based Evolutionary Computation to Solve Nonlinear Constraint Optimization Problems: a Cultural Algorithm Approach. In: IEEE Congress on Evolutionary Computation, pp. 1672–1678 (1999)
6. Cheng, J., Bai, J.Y., Qian, J.S., Li, S.Y.: Short-term forecasting method of coal mine gas concentration based on chaotic time series. Journal of China University of Mining and Technology 10(2), 231–235 (2008)
7. Cao, L.J., Tay, F.E.H.: Support vector machine with adaptive parameters in financial time series forecasting. IEEE Transactions on Neural Networks 14(6), 1506–1518 (2003)
8. Han, M., Xi, J.H., Xu, S.G., Yin, F.L.: Prediction of chaotic time series based on the recurrent predictor neural network. IEEE Transactions on Signal Processing 52(12), 3409–3416 (2004)
9. Leung, H., Lo, T., Wang, S.: Prediction of noisy chaotic time series using an optimal radial basis function neural network. IEEE Transactions on Neural Networks 12(5), 1163–1172 (2001)

Application of a Case Base Reasoning Based Support Vector Machine for Financial Time Series Data Forecasting

Pei-Chann Chang[1], Chi-Yang Tsai[2], Chiung-Hua Huang[3,4,*], and Chin-Yuan Fan[5]

[1] Department of Information Management, Yuan Ze University, Taoyuan 32026, Taiwan
[2] Department of Industrial Engineering and Management, Yuan Ze University, Taoyuan 32026, Taiwan
[3] Department of Industrial Engineering and Management, Yuan Ze University, Taoyuan 32026, Taiwan
[4] Department of Business Innovation and Development, Ming Dao University, Changhua 52345, Taiwan
[5] Department of Information Management, Yuan Ze University, Taoyuan 32026, Taiwan
hch@thit.edu.tw

Abstract. This paper establishes a novel financial time series-forecasting model, by clustering and evolving support vector machine for stocks on S&P 500 in the U.S. This forecasting model integrates a data clustering technique with Case Based Reasoning (CBR) weighted clustering and classification with Support Vector Machine (SVM) to construct a decision-making system based on historical data and technical indexes. The future price of the stock is predicted by this proposed model using technical indexes as input and the forecasting accuracy of the model can also be further improved by dividing the historic data into different clusters. Overall, the results support the new stock price predict model by showing that it can accurately react to the current tendency of the stock price movement from these smaller cases. The hit rate of CBR-SVM model is 93.85% the highest performance among others.

Keywords: case base reasoning, support vector machine, financial time series data, forecasting; clustering, classification.

1 Introduction

Data mining stock market trend is challengeable because of its high volatility and tumultuous environment. Many factors, such as political issues, general economic conditions, and traders' expectations, affect the performance of the stock market. High accurate classification is difficult to achieve although stocks and futures traders have relied heavily upon various types of intelligent systems to make trading decisions, the performances have been a disappointment [1].

* Corresponding author.

D.-S. Huang et al. (Eds.): ICIC 2009, LNAI 5755, pp. 294–304, 2009.

The key to stock traders is the development of a well-timed and precise trading decision-making tool. New techniques and appliances are essential for dealing with noise and non-linearity of the stock price predictions since the stock price series is influenced by a mixture of deterministic and random factors [2]. Support Vector Machine (SVM), an up-to-date and efficient way for time series analysis, aims to seek out the latent regularity in a large amount of data. There are also other approaches have been shown to be interpretable, operative and able to treat large-scale applications. However, regarding minor perturbations in the training data, some of those are recognized as instability. SVM provides solutions to these contradictions.

In this research, we try to reckon the movement of the stock price via analyzing and deriving some information from available data (i.e., Technical indicators) with proper clustering procedures and SVM. In financial markets, technical analysis is widely used to contrive suitable trades. Follow with the price fluctuations, a great diversity of indicators and patterns provide forcible timings for trades. A number of studies since the 1980s imply that some combinations of technical indicators can successfully detect the reversals of financial market and hence make more profit than a simple buy-and-hold strategy [7] and [9]. In addition, it is considered technical indicators to be major inputs; the step of clustering will gather similar data according to the stock price movement profile (standardized stock price movement) and weight of each input variable. Consequently, SVM is utilized to detect interpretable rules between the direction of price change and the input variables with each cluster.

2 Literature Survey

Conventional research addressing the stock forecasting problem has generally relied on time series analysis techniques, i.e., mixed auto regression moving average (ARMA) as well as multiple regression models. However, the assumptions of these methods may come out with ineffective results since a number of missing factors, such as macro economical or political effects may seriously influence stock tendencies.

Artificial neural networks (ANNS) have begun applied to this area (refer to Ref. [2] [4] [7] [9] [11]). However, these models are still restricted to tremendous noise and complex stock price data. Moreover, data quality itself may interfere with data input variables and this will lead the results to be inconvincible.

It has been a new tendency that combining the soft computing (SC) technologies of NNs, fuzzy logic (FL) and genetic algorithms (GAs) may significantly improve an analysis. These approaches are based on using quantitative inputs, as technical indexes, and qualitative factors, as political effects, to make stock market forecast and trend analysis automatically. A novel intelligent algorithm Support Vector Machine (SVM) is developed by Cristianini et al. [5]. SVM is applied to avoid local minima and over fitting of traditional neural network models. Not like traditional Neural Network (NN) models, SVM carry the structural risk minimization out. The former seeks to minimize the misclassification error or deviation from correct solution of the training data but the latter searches to minimize an upper bound of generalization error. [6] A lot of researchers resort to this model while forecasting financial time series data trend. Kim. [8] forecast the trend of stock price exchange by using traditional SVM and technical index; the result shows that SVM is a better than both BPN neural

network and case based reasoning. Regard GA as variable selection to reduce the model complexity, Yu et al. [13] improves the efficiency of the traditional SVM. [13] Combines SVM with wavelet soft threshold demising model to categorize the noise data into stochastic trend, and this improves the forecast accuracy of traditional SVM. These researches prove that SVM is more popular in financial time series forecasts, especially doing stock trend prediction; nevertheless, there are still some limitations of SVM. According to Cristianini et al. [5] an important and practical problem, the selection of the kernel function parameters - for Gaussian kernels the width parameter σ and the value of ε in the ε-insensitive loss function, is not yet entirely solved. And this problem causes three label data cannot be identified by SVM effectively.

3 Development of a CBR-SVM Model

A Case based reasoning weighted clustering model was developed by Shiu.et al. [10]. This clustering model applies a data matrix to find the similarity weighted data, and use Gradient method to find the clustering groups. Un-like other traditional clustering methods (K-means), A case based reasoning weight clustering model (CBR weighted model) will automatically find the clustering groups and derive a better accuracy rate when compared with other clustering models.

In this research, a novel financial time series-forecasting model is developed by clustering and evolving support vector machine for stocks on S&P 500. The S&P500 index is a well-known indicator of the economic condition in US. Therefore, the S&P500 index selected for studying. This forecasting model integrates a data clustering technique Case based reasoning (CBR) weighted clustering and support vector machine(SVM) to construct a decision-making system based on historical data and technical indexes. The forecasting accuracy of the model can also be further improved.

3.1 Technical Indexes

Aim to reflect the trend of stock prices, the technical indexes are calculated by using a specific equation with the information of trading prices, volumes and time. And it is especially useful for judging the trading points and phenomena of overbuying and overselling. Listed in Table 1, are technical indexes, like KD, RSI, MACD, MA and BIAS and so on. A set of technical indices affecting the stock price movement have been identified by Chang, et al. [3]. These input factors will be further selected using Stepwise Regression Analysis (SRA) model.

3.2 Case Based Reasoning Weight Clustering Model

Derive from yahoo.com.tw is a stock historic case library that is applied to develop the weighted distance metric and similarity measure used as followings. The first is to assume a Stock Library equal to $SL=\{e_1,e_2,.....,e_N\}$. According to an index of corresponding features, each case in the library can be recognized; in addition, to be made for each stock's current performance, it is with an associated action either a holding,

Table 1. Technical indexes applied as input variables

Technical index	Technical Index (input in our system)	Explanation
Moving Average(MA)	5MA,6MA,10MA, 20MA	Moving averages are used to emphasize the direction of a trend and smooth out price and volume fluctuations that can confuse interpretation.
Bias (BIAS)	5BIAS, 10BIAS	The difference between the closing value and moving average line, which uses the stock price nature of returning back to average price to analyze the stock market.
relative strength index (RSI)	6RSI,12RSI	RSI compares the magnitude of recent gains to recent losses in an attempt to determine overbought and oversold conditions of an asset
nine days Stochastic line (K, D)	KD	The stochastic line K and line D are used to determine the signals of over-purchasing, over-selling, or deviation.
Moving Average Convergence and Divergence (MACD)	9 MACD	MACD shows the difference between a fast and slow exponential moving average (EMA) of closing prices. Fast means a short-period average, and slow means a long period one.
Williams %R (pronounced "percent R")	12W%R	Williams %R is usually plotted using negative values. For the purpose of analysis and discussion, simply ignore the negative symbols. It is best to wait for the security's price to change direction before placing your trades.

selling or buying decision. We formally use a collection of features $\left\{F_j\left(j=1,.....,n\right)\right\}$ to stand for the cases and a variable V to denote the action. The i-th case e_j in the library symbolize a n+1-dimensional vector, i.e. $e_j=\left(x_{i1},x_{i2},.....,x_{in},y_i\right)$. Where x_j c coordinate the value of feature $F_j\left(1\le j\le n\right)$ and y_i coordinate the action $\left(i=1,.....,N\right)$ to be taken and this will be clarified later. Presume that each j $(1 \le j \le n)$ a weight $wj_{(w_j\in[0,1])}$ has been assigned to the j-th feature to signify the importance of the feature. Then, any pairs of cases e_p and e_q in the library, a weighted distance metric can be defined as below:

$$d_{pq}^{(w)} = d^{(w)}\left(e_p, e_q\right) = \left(\sum_{j=1}^{n} w_j^2 \left(x_{pj} - x_{qj}\right)^2\right)^{1/2} = \left(\sum_{j=1}^{n} w_j^2 x_j^2\right)^{1/2}. \quad (1)$$

When all the weights are same as 1 the distance metric that has been defined above synchronize the Euclidean measure, denote by $d_{pq}^{(1)}$.

A similarity measure between two cases, $SM_{pq}^{(w)}$, can be defined as follows according to the weighted distance defined in equation (1):

$$SM_{pq}^{(w)} = \frac{1}{1+\alpha \cdot d_{pq}^{(w)}}. \quad (2)$$

When all weighs take value 1 the similarity measure is denoted by $SM_{pq}^{(1)}$, "α" is a positive parameter.

After introducing the weighted distance metric and the similarity measure, the methodology of weighted clustering will be further described as below:

Phase One: Finding weighted feature values from important Technical Indexes.

This is a step that applies the gradient method to find weighted values from important Technical Indexes and a feature evaluation function is also defined. The evaluation value is smaller and the corresponding features are better; thus, we would like to find out the weights such as the evaluation function attains its minimum.

The details processes are as below:

Step 1. Select the parameter α and the learning rate η .

Step 2. Initialize w_j with random values in [0, 1].

Step 3. Compute Δw_j for each j using equation (3):

$$\Delta w_j = -\eta \frac{\partial E}{\partial w_j} \quad . \tag{3}$$

In this equation, *E* is defined as equation (4):

$$E(w) = \frac{2 * \left[\sum_{pq} \sum_{(q<p)} \left(SM_{pq}^{(w)} \left(1 - SM_{pq}^{1}\right) + SM_{pq}^{1} \left(1 - SM_{pq}^{(w)}\right) \right) \right]}{N * (N-1)} \quad . \tag{4}$$

Where N is the number of cases in the *SL* base.

Step 4. Update w_j with $w_j + \Delta w_j$ for each j.

Step 5. Repeat step 3 and step 4 until convergence, i.e., until the value of E becomes less, equal to a given threshold or until the number of iterations exceeds a certain predefined number.

Phase Two: Dividing the SL (Stock library) into Several Clusters

By using distance metric with the weights learned in the previous section, this phase aims to divide the Stock library into several clusters. Many methods such as K-Means clustering and Kohonen' self-organizing network can be used to divide the case library since the features are regarded as real-value. However, only a typical approach, using only the information of similarity between the cases, of clustering by Shiu.et al. [10] is adopted in this research. First, transform the similarity matrix to an equivalent matrix and then reckon the cases are equivalent to each other as one cluster. This idea is similar to the view of Shiu.et al. [10] , the relation clustering. The detail procedures of the algorithm are as below:

Step 1. Give a significant level (threshold) $\beta \in (0,1]$.

Step 2. Determine the similarity matrix $SM = \left(SM_{pq}^{(w)}\right)$ based on equation (2) and (1) .

Step 3. Compute $SM1 = SM$.

Step 4. If $SM1 \subset SM$ then go to step 5, or replace SM $SM = \left(s_{pq}\right)$

Where $s_{pq} = \max_k \left(\min \left(sm_{pk}^{(w)}, sm_{kq}^{(w)} \right) \right)$ with SM1 and go to step 3.

Step 5. Determine several clusters according to the rule, "case p and case q" belongs to the same cluster if and only if $s\,pq \geq \beta$.

The cases library will be divided into various sub-clusters via a series of weighted and clustering steps. In terms of the features and action of each data point, the data will be more similar in patterns from each sub-cluster. At that time, these case bases are ready for further application of stock price movement forecast.

3.3 Support Vector Machine in Classification

The support vector machine (SVM) is a very useful method in data classification, pattern recognition, regression estimation problems, and as well as in forecasting. Consider a classification problem in which a set of training data with p features, denoted by $\mathbf{X} = \{\mathbf{x}_1, \mathbf{x}_2, \ldots, \mathbf{x}_N\}$, where N is the number of samples, associated with label $y_i = 1$ or -1, i=1, 2, …, N. Suppose the classification problem is nonlinear separable, the nonlinear SVM can be applied by introduced a transformation function $\varphi(\mathbf{x}) = \{\varphi_i(\mathbf{x}), i = 1, 2, ..., M, M >> N\}$ and determines an "optimal separating hyperplane" $\mathbf{w}^{\mathrm{T}}\mathbf{x} + b = 0$ by maximizing the margin of separating subspaces.

Vapnik [12] show finding the maximum margin for classification is equivalent to solve a QP problem with bound constraints and linear equality constraints, the problem is shown in:

$$\text{Min } \frac{1}{2}\|\mathbf{w}\|^2 \tag{5}$$

subject to

$$y_i\left[w^T \varphi(\mathbf{x}_i) + b\right] \geq 1 \qquad i = 1,2,\ldots,n \ . \tag{6}$$

Since even the transformation is applied, in many real-world practical problems, the data may not be completely separable. The SVM can be generalized to handle the none the non-separable case, by introducing slack variable ξ_i , i=1, 2, …, N, and a regularization parameter C. The slack variable ξ_i indicates the distance between the margin when x_i lying on the wrong side of the margin, and C is used to control the tradeoff between the training error and the margin. Accordingly, the problem can formulated as

$$\min \phi(w\xi) = \frac{1}{2}\mathbf{w}^T\mathbf{w} + C\sum_{i=1}^{N}\xi_i \tag{7}$$

subject to

$$y_i\left[\mathbf{w}^T \varphi(\mathbf{x}_i) + b\right] \geq 1 - \xi_i \qquad i = 1,2,\ldots,N \tag{8}$$

$$\xi_i \geq 0 \qquad i = 1,2,\ldots,N \ . \tag{9}$$

The revised formulations can be solved similarly by minimizing its Lagrange and the Karush-Kuhn-Tucker (KKT) conditions. Then the equivalent Lagrange dual form is

$$\text{Max } L_D = \sum_{i=1}^{N} \alpha_i - \frac{1}{2}\sum_{i=1}^{N}\sum_{j=1}^{N} \alpha_i \alpha_i y_i y_j \varphi^T(\mathbf{x}_i)\varphi(\mathbf{x}_j) \tag{10}$$

subject to

$$\sum_{i=1}^{N} \alpha_i y_i = 0, \qquad i = 1, 2, \ldots, N \tag{11}$$

$$0 \le \alpha_i \le C \qquad i = 1, 2, \ldots, N \tag{12}$$

$$\alpha_i \left[y_i (w^T \varphi(\mathbf{x}_i) + b) - 1 + \xi_i \right] = 0 \tag{13}$$

$$\mu_i \xi_i = 0. \tag{14}$$

Where the term $\varphi^T(\mathbf{x}_i)\varphi(\mathbf{x})$ can be replaced by a kernel function $K(\mathbf{x}_i, \mathbf{x}_j) = \varphi^T(\mathbf{x}_i)\varphi(\mathbf{x}_j)$ and the elegance of using the kernel function is usually unnecessary to explicitly know the $\varphi(\mathbf{x})$ explicitly. Many kernel functions have been mentioned in the literature. Gaussian radial basis kernel function (RBF) is one most frequently applied and is defined as

$$K(\mathbf{x}, \mathbf{y}) = \exp(-|\mathbf{x} - \mathbf{y}|^2 / \sigma^2) \tag{15}$$

where σ is the width of the Gaussian function. Finally, for an unknown data $\mathbf{x}$ can be classified by the following decision function:

$$f(\mathbf{x}) = \sum_{i \in SV} \alpha_i y_i \varphi^T(\mathbf{x}_i)\varphi(\mathbf{x}) + b^* \tag{16}$$

and

$$\mathbf{x} \in \begin{cases} \text{class } 1, & \text{if } f(\mathbf{x}) \ge 0 \\ \text{class } 2, & \text{otherwise} \end{cases}. \tag{17}$$

4 Experimental Results

As discussed in section 3, the S&P500 index selected for studying. We performed extensive experiments based on the historical data we got from the finance section of Yahoo. The whole data set covers the period from January 1, 2000 to December 31, 2004, a total of 1255 observations. The data set is divided into two parts. The first part which has 1190 observations is trained to determine the specification of the model and parameters. The second part which has 65 observations is reserved for out-of-sample testing and comparison of performances. The main purpose of instance selection is to emphasis the importance of stock screening. Another purpose is to show that the proposed model can have a robust performance even under different type of stock trends. Then different input factors for S&P500 index are selected according to

stepwise regression analysis. Detailed procedures of CBR-SVM applied are explained in the following:

4.1 Stepwise Regression Analysis

Stepwise regression analysis (SRA) is applied to determine the set of independent variables that most closely affect the dependent variable. This is accomplished by the repetition of a variable selection procedure.

A set of important technical factors as shown in Table 2 which will affect the forecasting results have been identified by Chang et al.[4]. These important input factors which have 24 ones will be further selected 12 factors through Stepwise Regression Analysis (SRA) model in this research. The result is shown in Table 2 as follows.

Table 2. Input factors selected by Stepwise Regression Analysis

Input Factors	
Total Number of Technical Indexes	5MA、5BIAS、6MA、10MA、9K、9D、6RSI、9MACD、12W%R、20MA、12RSI、K_D、10BIAS
Total Number of difference of Technical Indexes	5MA difference、6MA difference、10MA difference、5BIAS difference、10BIAS difference、6RSI difference、9K difference、9D difference、12RSI difference、9MACD difference、12W%R difference
Factors selected by Stepwise Regression Analysis	
Technical Indexes	5MA、5BIAS、10MA、12W%R、10BIAS
Difference of Technical Indexes	5MA difference、6MA difference、10MA difference、5BIAS difference、10BIAS difference、6RSI difference、9K difference

4.2 Case Based Reasoning Weighted Clustering Method

Taguchi experimental method is applied to decide the best parameter setting. This research chooses three levels for these five factors, i.e., α, Learning Rate, β, Phase-one running times, Phase-two running times. Table 3 shows detail experimental design, i.e., three levels of these five factors. In addition, a final output of S&P500 from Taguchi experimental method is shown in Figure 1, i.e., level 3 for factor A stand for α, level 3 for factor B stand for Learning Rate, level 3 for factor C stand for Phase-one running times, level 3 for factor D stand for Phase-two running times, and level 1 for factor E stand for β. Final output for each stock from Taguchi experimental method is shown Table 4 which is a best combination of parameter settings.

Table 3. Experimental parameter design：five factors each at three levels

Parameter setting	**level 1**	**level 2**	**level 3**
α	0.6	0.8	**1**
Learning Rate	0.01	0.05	**0.1**
β	**0.003**	0.094	0.135
Phase-one running times	5000	3000	**1000**
Phase-two running times	30	20	**10**

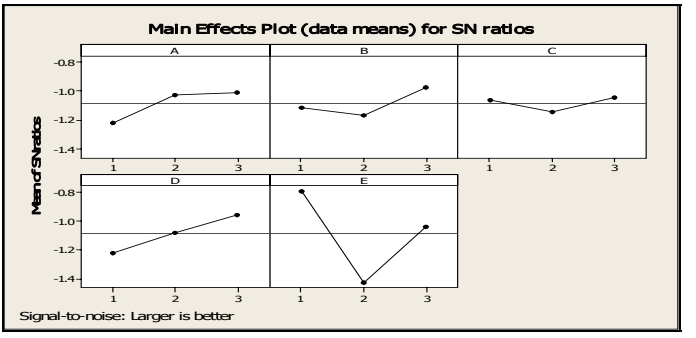

Fig. 1. The larger the better S/N ratio selection in Taguchi's method

Table 4. Best parameter setting from Taguchi experimental method

Parameter setting	S&P 500
α	1
Learning Rate	0.1
β	0.003
Phase-one running times	1000
Phase-two running times	10

4.3 Results and Method Comparisons

In this research, there are 12 important input factors will be further selected through Stepwise Regression Analysis (SRA). The gamma value of SVM is equal to 1/12 which standing for 12 input factors. After setting up the parameters of the experiments, the CBR-SVM is compared with other 2 models, i.e., SVM and K-mean-SVM. As shown in Table 5, we can see CBR-SVM much better than other models in hit rate performance. Due to CBR-SVM model with only for 4 cases which is smaller than k-mean-SVM model with 6 cases, so it may be a better mining model.

Table 5. Hit rate of S&P500 from 3 model in this research

Mining model	Hit Rate (%)	Parameter setting
SVM	90.769	SVM : **Gamma=1/k =0.0833 (k =12)**
K-mean-SVM	92.31	K-mean : **Cases = 6** SVM : **Gamma=1/k =0.0833**
CBR-SVM	93.85	CBR : **α=1, η=0.1, β=0.003,** **N_1= 1000, N_2=10 (cluster→ Cases = 4)** SVM : **Gamma=1/k =0.0833**

In addition, to evaluate the forecasting ability of CBR-SVM model, we illustrate S&P500 which is shown in Table 6 proposed by Kim. [8] and Yu et al. [13] to compare their performance. The comparison results show that CBR-SVM outperforms the other classification methods. The hit rate of SVM model in this research is better than the benchmark's one, the improvement is done by SRA. Taguchi experimental

method is applied to decide the best parameter setting for a CBR to divide the case base into a smaller case. Next, the SVM derives the best decision from each case. Hence, the combining model performs best among all the forecasting methods.

Table 6. Comparison of hit rates for CBR-SVM with other benchmark models in S&P500

Mining model	Hit Rate (%)
RW	51.06
ARIMA	56.13
BPNN	69.78
SVM*	78.65
GASVM	84.57
CBR-SVM	**93.85**

5 Conclusion

This research proposes using a CBR-based SVM data mining model that combines a case base reasoning and support vector machine to predict the stock price movement. First, a step-wise regression (SRA) method is applied to select the most important factors from the set of inputs. Next, a case base reasoning (CBR) weighted clustering method is adopted to divide the case base into a smaller case. Within each case, a more homogeneous data are grouped into together. Therefore, these data can be more effectively react to the current stock price movement. Finally, the support vector machine (SVM) derives the best decision from each case. Through a series of experimental tests, the CBR-SVM outperforms other forecasting methods with a hit rate around 93.85%. It is the highest among the literature published up to present. The Hit-ratio (buy or sell) of the future stock price movement can be applied to help investors to make better decision in trading stocks.

References

1. Aiken, M., Bsat, M.: Forecasting Market Trends with Neural Networks. Inf. Syst. Manage 16(4), 42–48 (1994)
2. Chi, S.C., Chen, H.P., Cheng, C.H.: A Forecasting Approach for Stock Index Future Using Grey Theory and Neural Networks. In: IEEE International Joint Conference on Neural Networks, pp. 3850–3855 (1999)
3. Chang, P.C., Fan, C.Y., Liu, C.H.: Integrating a Piecewise Linear Representation Method and a Neural Network Model for Stock Trading Points Prediction. IEEE Transactions on Systems, Man and Cybernetics Part C: Applications and Reviews (December 2008); Online available
4. Chang, P.C., Liao, T.W.: Combing SOM and Fuzzy Rule Base for Flow Time Prediction in Semiconductor Manufacturing Factory. Appl. Soft. Comput. 6(2), 198–206 (2006)
5. Cristianini, N., John, S.T.: Support Vector Machine and Other Kernel-Based Learning Methods. Cambridge University Press, Cambridge (2000)
6. Huang, W., Nakamori, Y., Wang, S.Y.: Forecasting Stock Market Movement Direction with Support Vector Machine. Computers and Operations Research 32(10), 2513–2522 (2005)

7. Kimoto, T., Asakawa, K.: Stock Market Prediction System with Modular Neural Network. In: IEEE. Int. Join. Conf. Neural Network, pp.1–6 (1990)
8. Kim, K.J.: Financial Time Series Forecasting Using Support Vector Machines. Neurocomputing 55, 307–319 (2003)
9. Lee, J.W.: Stock Price Prediction Using Reinforcement Learning. In: IEEE. Int. Join. Conf. Neural Network, pp. 690–695 (2001)
10. Shiu, S.C.K., Sun, C.H., Wang, X.Z., Yeung, D.S.: Maintaining Case-Based Reasoning Systems Using Fuzzy Decision Trees. In: Proc. 5th Euro. Work. Case-based Reasoning (EWCBR2K), Trento, Italy, vol. 5, pp. 285–296 (2000)
11. Tsang, E.C.C., Wang, X.Z., Yeung, D.S.: Improving Learning Accuracy of Fuzzy Decision Trees by Hybrid Neural Networks. IEEE Trans. Fuzzy Syst. 8, 601–614 (2000)
12. Vapnik, V.N.: The Nature of Statistical Learning Theory. Springer, New York (1995)
13. Yu, L., Wang, S.-Y., Lai, K.K.: Mining stock market tendency using GA-based support vector machines. In: Deng, X., Ye, Y. (eds.) WINE 2005. LNCS, vol. 3828, pp. 336–345. Springer, Heidelberg (2005)

Cost-Sensitive Supported Vector Learning to Rank Imbalanced Data Set

Xiao Chang[1,2], Qinghua Zheng[1,2], and Peng Lin [1,2]

[1] Dept. Computer Science and Engineering, Xi'an Jiaotong University
[2] Shaanxi Key Lab. of Satellite and Computer Network
No.28 Xianning West Road, Xi'an, Shaanxi, 710049, P.R. China
{changxiao,qhzheng}@mail.xjtu.edu.cn,
ice-spider@163.com

Abstract. In recent years, the algorithms of learning to rank have been proposed by researchers. Most of these algorithms are pairwise approach. In many real world applications, instances of ranks are imbalanced. After the instances of ranks are composed to pairs, the pairs of ranks are imbalanced too. In this paper, a cost-sensitive risk minimum model of pairwise learning to rank imbalance data sets is proposed. Following this model, the algorithm of cost-sensitive supported vector learning to rank is investigated. In experiment, the convention Ranking SVM is used as baseline. The document retrieval data set is used in experiment. The experimental results show that the performance of cost-sensitive supported vector learning to rank is better than Ranking SVM on the document retrieval data set.

Keywords: Cost-sensitive learning, Supported vector learning, Learning to rank, Imbalanced data set.

1 Introduction

The problem of learning ranking function attracted much attention from machine learning community in recent years. This task is referred to as "Learning to Rank" in this field. "Learning to Rank" resides between multi-classes classification and metric regression in the area of supervised learning. In "Learning to Rank" problem, the samples are labeled with a set of discrete ranks which the size is larger than or equal to two. The task of learning to rank is to find a model on samples data set, which can predict the order of new instances. In information retrieval, for example, the retrieval results can be rated by giving the grades to the results on the relevant to user's query.

Many methods of "Learning to Rank" have been proposed [1] [2] [3] [4] [5] [6] [7] [8] [9] [10]. Most of these recent algorithms are based on the pairwise preference framework [1] [2] [5] [6] [9] [10], in which instead of taking instances in isolation, instances pairs are used as instances in the learning process. The idea of pairwise preference learning to rank is to minimize the number of misordered pairs.

In practice, the data are imbalanced among ranks in many real world applications. In information retrieval, for example, the most relevant results occupy only a small

D.-S. Huang et al. (Eds.): ICIC 2009, LNAI 5755, pp. 305–314, 2009.

part of candidates set. However, the problem of imbalanced data set is not considered in most of the proposed algorithms of learning to rank. Only one approach is proposed to addressing the problem of imbalanced queries data with cost-sensitive supported vector learning approach [11]. However, the problem of imbalance among ranks is not considered in this approach. A binary classification model is used in it to learn ranking function.

In this paper, the cost-sensitive learning approach is proposed to learn the data set that is imbalanced among ranks. One class supported vector model is employed to learn ranking function as convention Ranking SVM [12].

The performance of the approach proposed in this paper is compared with the convention Ranking SVM on one real world dataset. The experimental results show that the performance of our approach is significant better than convention Ranking SVM to learn imbalance data.

The rest of this paper is organized as follows. The related work is presented in section 2. The problem analysis of imbalance among ranks is given in section 3. An approach of cost sensitive supported vector learning to rank imbalance data is proposed in section 4. The experimental results and discussion are given in section 5. Section 6 is the conclusion of this paper.

2 Related Work

2.1 Pairwise Learning to Rank

Pairwise approach of learning to rank is an important strategy followed by many researchers. The strategy of this approach is transfer ranking instances to classifying the instance pairs. The classification algorithm is the basis of pairwise approach of learning to rank. For example, supported vector machine is adopted to learn ranking function, which is called Ranking SVM [12]. Ranking SVM is a state-of-the-art method for learning to rank and has been empirically demonstrated to be effective. A boosting algorithm called RankBoost is developed [1]. A probability loss of preference relation prediction is proposed and a two layers net is used to learn a ranking function [5]. Fidelity in physical field is employed as the loss function and a boosting algorithm is suggested to learn ranking function [9]. Preference learning with Gaussian process is shown in [6]. Regularized least-squares approach is used to learn to rank function in [10].

2.2 Cost-Sensitive Learning to Rank

Cost-sensitive strategy of learning to rank is first proposed in [11]. The SVM learning to rank is re-formalized as that of minimizing loss function as the form

$$\min_{\mathbf{w}} \sum_{i=1}^{l} \tau_{k(i)} \mu_{q(i)} \left[1 - z_i \left\langle w, \mathbf{x}_i^{(1)} - \mathbf{x}_i^{(2)} \right\rangle \right]_+ + \lambda \|\mathbf{w}\|^2 , \tag{1}$$

where $\mathbf{x}_i^{(1)}$ and $\mathbf{x}_i^{(2)}$ denotes two instances in a data pair, z_i denotes the preference relation of two instances in a data pair ($z_i \in \{-1,+1\}$), $k(i)$ denotes the type of ranks of instance pair i, $\tau_{k(i)}$ denotes the rank parameter for $k(i)$, $\mathrm{q}(i)$ denotes the query of

instance pair i, and $\mu_{q(i)}$ denotes the query parameter for $q(i)$. The penalty received by the i-th pair is determined by $\tau_{k(i)}\mu_{q(i)}$. With the parameter $\mu_{q(i)}$, this model can more penalize the errors on the queries with fewer instance pairs.

Although the performance of cost-sensitive Ranking SVM is better than that of standard Ranking SVM on experiments is shown in this paper, there are some drawbacks.

Binary classification model is employed in this model. However, one class model is used in convention Ranking SVM [12]. The instance in dataset can be combined with same preference relation by the strategy of combining data pairs. In this case, the pairs label with only one class will be learned. The problem of learning imbalance data is avoided.

The imbalance among ranks is not considered. In real world dataset, the number of instances of ranks is different. To different ranks, the pairs combined with the instances will be imbalance too. These pairs are the imbalanced data to be learned. This case is not considered in model (1).

3 Problem Analysis

3.1 Learning to Rank Statement

In preference learning problem, given an i.i.d training sample set $S=\{(\mathbf{x}_i,y_i)\}_{i=1}^{N}$, each instance $\mathbf{x}_i\in\mathbb{R}^n$ is associated with a label y_i. $R=\{R_1,R_2,\ldots,R_k\}$ is a label space, the object in it can be ranked as $R_k\succ_R\cdots\succ_R R_2\succ_R R_1$. ($\succ_R$ denotes the order among ranks). R_i is the label of rank i.

Given π is a set of pairs, i.e. $\pi=\{\pi_i\mid i=1,\ldots,M\}$. π_i is a couple (d_i,r_i) where d_i denotes a pair of instances (x,x'), and r_i denotes x in preference than x' or not. $r_i\in\{-1,+1\}$

The goal of preference learning to rank is to learning a model from sample set π to rank the instances with right preference relation.

Assuming the model space of mapping object to real number is $\mathscr{H}=\{f(\cdot):X\mapsto\mathbb{R}\}$. Each f in $\mathscr{H}$ creates an order $\succ_X$ in input space $X\subset\mathbb{R}^n$, according to the rule

$$\mathbf{x}_i\succ_X\mathbf{x}_j\Leftrightarrow f(\mathbf{x}_i)>f(\mathbf{x}_j), \tag{2}$$

which means that there is an unobservable latent function value $f(\mathbf{x}_i)\in\mathbb{R}$ associated with each training sample $\mathbf{x}_i$, and that the preference relation between any two instances dependents on the latent function values of them. The rules of deducing the preference label r_i^* of pair d_i take the form

$$r_i^*=\begin{cases}+1, f(x)>f(x')\\ 0, f(x)=f(x')\\ -1, otherwise\end{cases}. \tag{3}$$

The task of learning to rank is to find a model f^* in space $\mathscr{H}$, which takes the minimum error of predicting the preference relation of the instances in training dataset.

When r_i is not equal to r_i^*, the loss of the prediction error of model $f(\cdot)$ can be denoted as the form $l_{pref}(d_i, r_i, r_i^*)$. $l_{pref}(\cdot)$ is the loss function. The empirical risk of prediction error of $f(\cdot)$ to all pairs in set π is given as the form

$$R_{emp}(f;\ \pi) = \frac{1}{M}\sum_{i=1}^{M} l_{pref}(d_i, r_i, r_i^*) \cdot \tag{4}$$

The goal of learning to rank is to find an optimal model f_{pref}^* which takes the minimum empirical risk of prediction error as the form

$$f_{pref}^* = \underset{f}{\operatorname{argmin}}\ R_{emp}(f;\ \pi) \cdot \tag{5}$$

3.2 Ranks Imbalance Analysis

The instance pair d_i can be labeled with the rank label of one of two instances. The formal rule of labeling the pair is given in Definition 1.

Definition 1: A pair $d = \left(d^{(1)}, d^{(2)}\right)$ can be labeled with a rank label r following the rule as form:

$$r = \begin{cases} \mathrm{y}_{d^{(1)}}, & \text{if } \mathrm{y}_{d^{(1)}} \succ \mathrm{y}_{d^{(2)}} \\ \mathrm{y}_{d^{(2)}}, & \text{if } \mathrm{y}_{d^{(1)}} \prec \mathrm{y}_{d^{(2)}} \end{cases}, \tag{6}$$

where $\mathrm{y}_{d^{(\mathrm{i})}}$ is the label of *i*-th instance in the pair d. $(i \in \{1,2\})$ The pair d can be called a pair of rank r.

According to the result of labeling the pairs in the set π following Definition 1, the empirical risk function $R_{emp}(f;\ \pi)$ can be decomposed into $k-1$ sub-items as the form

$$R_{emp}(f;\pi) = \frac{1}{M}\underbrace{\sum_{i=1}^{N_k} l_{pref}(d_i, r_i, r_i^*)}_{R_k} + \cdots + \frac{1}{M}\underbrace{\sum_{i=1}^{N_2} l_{pref}(d_i, r_i, r_i^*)}_{R_2}, \tag{7}$$

where N_i denotes the number of instances of rank i $(i = 2,...,\mathrm{k})$, k is the number of ranks and R_i denotes the risk of prediction error of rank *i*.

In real world dataset, the number of instances of ranks is different. Usually, the instance of the '*important*' rank is fewest, followed by '*possible important*' rank, and the instance of the '*no important*' rank is most. Combining these instances to pairs and labeled with Definition 1. The pairs of ranks will be imbalance too. In this condition, the risk of the most important rank will occupies a fewer proportion in the total risk $R_{emp}(f;\pi)$ than that of minor ranks. The optimal result f_{pref}^* of (5) will bias to the

rank of occupying the larger proportion in the total risk. The minimum prediction error can not be attained on the sample pairs of most important rank.

Unfortunately, the most of real world datasets are imbalanced. So, researching the approach to improve the optimization result in this case should be a valuable work.

4 Cost-Sensitive Supported Vector Learning to Rank Imbalance Data

4.1 Cost-Sensitive Risk Model of Learning to Rank

The strategy of learning imbalance data is to modify the error cost of pairs of ranks. Following the Definition 1, the dataset labeled with k ranks is split into k-1 pairs subsets. The error cost of pairs of a rank is adjusted by the proportion occupied by them in π . The cost-sensitive risk model is written as the form

$$R_{emp}(f;\pi) = \frac{1}{M}\eta_2 \sum_{i=1}^{N_2} l_{pref}(d_i, r_i, r_i^*) + \cdots + \frac{1}{M}\eta_K \sum_{i=1}^{N_K} l_{pref}(d_i, r_i, r_i^*), \tag{8}$$

where η_r is a cost parameter of pairs of rank *r*, which is used to adjust the error cost of pairs of rank *r*. The cost parameters η_r can be computed by the formula as the form

$$\eta_r = e_r \cdot N_m / N_r \quad , \quad r = 2,...,\mathrm{k}\ , \tag{9}$$

where e_r is a enlargement factor to the cost of pairs of rank *r*, rank *m* is the rank with the most pairs which takes the form

$$\mathrm{m} = \arg\max_r (N_r), \quad \mathrm{r} = 2,...,\mathrm{k}\cdot \tag{10}$$

The error risk of pairs of a rank in $R_{emp}(f;\ \pi)$ can be adjusted by changing the value of e_r .

4.2 Cost-Sensitive One-Class Supported Vector Learning to Rank

In model (1), a binary classification model is employed. Following the rules (3), the pairs will be labeled as two classes. However, the pairs can be label with one class by changing the order of two instances in a pair. In this case, only the data of one class will be learned. Therefore, the cost-sensitive One-Class supported vector learning to rank is given as the form

$$\min_w \sum_{r=2}^{\mathrm{K}} \sum_{\mathrm{j}=1}^{\mathrm{N_r}} \eta_r \left[1 - \left\langle w, \Phi\left(\mathrm{d}_j^{(1)}\right) - \Phi\left(\mathrm{d}_j^{(2)}\right) \right\rangle \right]_+ + \lambda \|w\|^2 , \tag{11}$$

where $\Phi(\cdot)$ mapping a sample pair d_i from input space into feature space.

The model in (11) is equal to a quadratic programming model as the form

$$\begin{aligned} &\min_{w} \ \frac{1}{2}\|w\|^2 + \sum_{i=1}^{\mathrm{M}} C_i \cdot \xi_i \\ &\quad subject\ to \\ &\quad \left\langle w, \Phi\left(\mathrm{d}_j^{(1)}\right) - \Phi\left(\mathrm{d}_j^{(2)}\right) \right\rangle \geq 1 - \xi_i, \quad i = 1, \cdots, \mathrm{M} \\ &\quad \xi_i \geq 0, \quad i = 1, \cdots, \mathrm{M} \end{aligned}, \tag{12}$$

which is used in computation.

Proposition 1: The problems in (11) and (12) are equivalent, when $C_i = \frac{\eta_{\mathrm{r}}}{2\lambda}$ where the pair d_i belongs to rank r.

The Lagrange method is used to solve the quadratic programming problem (12). The Lagrange dual form of problem (12) takes the form

$$\begin{aligned} &\min_{\alpha} \ \frac{1}{2}\sum_{i=1}^{\mathrm{M}}\sum_{i'=1}^{\mathrm{M}} \alpha_i \alpha_{i'} \left\langle \Phi\left(\mathrm{d}_i^{(1)}\right) - \Phi\left(\mathrm{d}_i^{(2)}\right), \Phi\left(\mathrm{d}_{i'}^{(1)}\right) - \Phi\left(\mathrm{d}_{i'}^{(2)}\right) \right\rangle \\ &\quad subject\ to \\ &\quad 0 \leq \alpha_i \leq C_i, \ i = 1, \cdots, \mathrm{M} \\ &\quad \sum_{i=1}^{\mathrm{M}} \alpha_i = 1 \end{aligned}, \tag{13}$$

where C_i is the upper limit of the value of α_i. The upper limit C_i of the value of the Lagrange coefficient of the pairs of rank r will increase with the increasing of the enlargement factor e_r. It is possible that a large value is assigned to α_i that corresponds to a large C_i.

5 Experiments

In experiment, the performance of the approach of cost-sensitive supported vector learning to rank proposed in this paper, is called CSRankSVM, is compared with convention Ranking SVM. The convention Ranking SVM is called RankSVM.

OHSUMED [13], a dataset for document retrieval research, is used in the experiment. It has been processed and included in LETOR [14], a Benchmark dataset build by MSAR for ranking algorithm research. This dataset is imbalanced. CSRankSVM and RankSVM are trained and tested on both of the two datasets.

The linear kernel function is employed in two algorithms in our experiment, which takes the form $\kappa\left(\mathbf{x}, \mathbf{x}'\right) = \mathbf{x}^{\mathrm{T}} \bullet \mathbf{x}'$. The trade-off parameter ' λ ' is set to 0.5 for two algorithms.

The normalized discounted cumulative gain (NDCG) [15] is used as evaluation measure, which has been widely used by researchers in recent years. NDCG can be used to evaluate the performance of ranking method on the dataset that is labeled with more than two ranks.

$$\mathrm{NDCG@k} = \mathrm{N(k)} \bullet \sum_{j=1}^{k} \frac{2^{r(j)}-1}{\log(1+j)}, \tag{14}$$

where N(k) is the NDCG at *k*-th position of ideal ranking list. It is used as a normalization factor of the NDCG at k of ranking list of prediction result.

5.1 Experiment on Document retrieval

The OHSUMED collection is used in document retrieval research. This dataset has been used in information filtering task of TREC 2000. The relevance judgments of documents in OHSUMED are either 'd' (*definitely relevant*), 'p' (*possibly relevant*), or 'n' (*not relevant*). Rank 'n' has the largest number of documents, followed by 'p' and 'd'. The original OHSUMED collection consists of 348,566 records from 270 medical journals. There are 106 queries. For each query, there are a number of documents associated.

The OHSUMED has been collected into a Benchmark dataset LETOR for ranking algorithm research. In this dataset, each instance is represented as a vector of features, determined by a query and a document. Every vector consists of 25 features. The value of features has been computed.

The 20 folds experimental dataset is obtained by running following strategy 20 times: selecting the instances of two query randomly as training data, the instances of one half of remained queries as validate data and that of another half of queries as test data.

The average instances number of three ranks in 20 folds is given in Table 1. The rank 2, 1 and 0 denote the rank of '*definitely relevant'*, '*possibly relevant'* and *'not relevant'* respectively. The rank 0 has the most instances, followed by rank 1 and 2.

Table 1. Instances number of ranks

	Rank 0	Rank 1	Rank 2
Instance Number	38	4	3

Following the Definition 1, instance of three ranks are combined to the pairs of two ranks. The average pair number of two ranks is given in Table 2.The pairs of rank 2 is few than rank 1. All of the pairs of Rank 1 and Rank 2 are assigned to one class: +1.

Table 2. Pairs number of ranks

	Total Number of Pairs of A Rank
Rank 1	159.5
Rank 2	138.3

The training pairs are fallen into two most relevant ranks. The error risk of prediction can be decomposed into two parts. A two dimensions enlargement factor vector $\mathbf{E} = (e_1, e_2)$ is used in this experiment. e_1 is the enlargement factor of rank 1. e_2 is

enlargement factor of rank 2, i.e. '*definitely relevant*' rank. Document retrieval problem is focused on the prediction precision of '*definitely relevant*' rank. In experiment, therefore, e_1 is set to 1 and e_2 is adjusted from 1 to 5. The experimental results are given in Fig.1. It can be seen that when e_2 is set to 1 to 5 the value of NDCG of CSRankSVM all are higher than that of RankSVM significant.

The value of NDCG is increased when e_2 is set from 1 to 4. But when change the value of e_2 from 4 to 5, the change of the value of NDCG is not monotony.

The trend of the value of NDCG changing with the augment of e_2 can be seen more obvious in Fig. 2. When e_2 is increased from 1 to 4, the value of NDCG is improved significantly. When e_2 is set to large than 4 the change of NDCG is not significant.

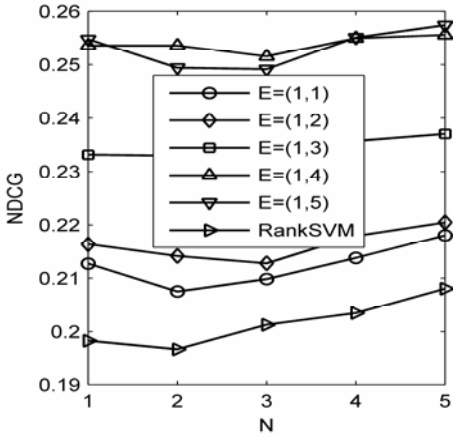

Fig. 1. The results of CSRankSVM an RankSVM on OHSUMED

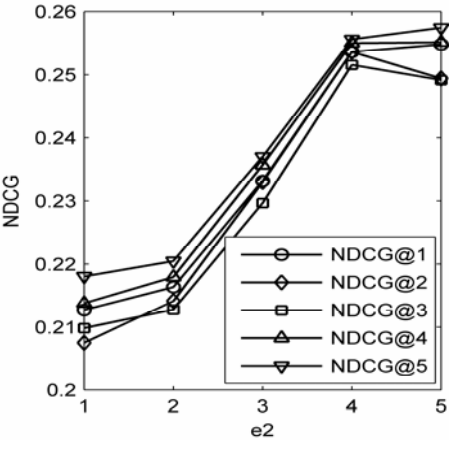

Fig. 2. NDCG at 1 to 5 vs. e_2 of CSRankSVM on OHSUMED

This mean that the prediction model will not be improved significantly when e_2 is larger than a certain value. The optimal setting to vector **E** can be found by cross-validate approach.

6 Conclusion

In this paper, a cost-sensitive risk minimum model is proposed to learning to rank imbalance data. In this model, the enlargement factors are used to adjust the error cost of ranks. Following this model, a cost-sensitive supported vector learning approach is developed. The performance of the approach proposed in this paper is compared with convention Ranking SVM in experiment. The experimental results on two real world dataset show that the performance of our approach is better than that of convention Ranking SVM to learn imbalanced data.

In this paper, a simple way is employed to improve the Ranking SVM to learn imbalance data more efficient. In the future work, some advanced techniques which have been used in SVM classification imbalance data will be adopted to learning to rank imbalance data [16] [17].

Acknowledgement

The research was supported by the National High-Tech R&D Program of China under Grant No.2008AA01Z131, the National Science Foundation of China under Grant Nos.60825202, 60803079, 60633020, the National Key Technologies R&D Program of China under Grant Nos. 2006BAK11B02, 2006BAJ07B06.

References

1. Freund, Y., Iyer, R., Schapire, R.E., Singer, Y.: An Efficient Boosting Algorithm for Combining Preferences. In: 15th International Conference on Machine Learning, pp. 170–178 (1998)
2. Herbrich, R., Graepel, T., Obermayer, K.: Support Vector Learning for Ordinal Regression. In: Nineth Ann. Conf. Artificial Neural Networks (ICANN 1999), pp. 97–102 (1999)
3. Crammer, K., Singer, Y.: Pranking with Ranking. In: Fourteenth Ann. Conf. Neural Information Processing Systems, NIPS 2001 (2001)
4. Shashua, A., Levin, A.: Ranking with Large Margin Principle: Two Approaches. In: 16th Ann. Conf. Neural Information Processing Systems (NIPS 2003), pp. 961–968 (2003)
5. Burges, C., Shaked, T., Renshaw, E., Lazier, A., Deeds, M., Hamilton, N., Hullender, G.: Learning to Rank Using Gradient Descent. In: The 22nd International Conference on Machine Learning, pp. 89–96 (2005)
6. Chu, W., Ghahramani, Z.: Preference Learning with Gaussian Processes. In: 22nd International Conference on Machine Learning, pp. 137–144 (2005)
7. Chu, W., Ghahramani, Z.: Gaussian Processes for Ordinal Regression. Journal of Machine Learning Research 6, 23 (2005)
8. Lin, H.-T., Li, L.: Large-margin thresholded ensembles for ordinal regression: Theory and practice. In: Balcázar, J.L., Long, P.M., Stephan, F. (eds.) ALT 2006. LNCS, vol. 4264, pp. 319–333. Springer, Heidelberg (2006)
9. Tsai, M.-F., Liu, T.-Y., Qin, T., Chen, H.-H., Ma, W.-Y.: FRank: A Ranking Method with Fidelity Loss. In: The 30th Annual International ACM SIGIR Conference (2007)
10. Pahikkala, T., Tsivtsivadze, E., Airola, A., Boberg, J., Salakoski, T.: Learning to rank with pairwise regularized least-squares. In: The 30th International Conference on Research and Development in Information Retrieval -Workshop on Learning to Rank for Information Retrieval, pp. 27–33 (2007)
11. Cao, Y., Xu, J., Liu, T.Y., Li, H., Huang, Y., Hon, H.-W.: Adapting Ranking SVM to Document Retrieval. In: 29th Annual International ACM SIGIR Conference on Research and Development in Information Retrieval, pp. 186–193 (2006)
12. Joachims, T.: Optimizing Search Engines Using Clickthrough Data. In: The ACM Conference on Knowledge Discovery and Data Mining, pp. 133–142 (2002)
13. Hersh, W., Buckley, C., Leone, T.J., Hickam, D.: OHSUMED: An Interactive Retrieval Evaluation and New Large Test Collection for Research. In: Seventeenth Ann. ACM-SIGIR Conf. Research and Development in Information Retrieval (SIGIR 1994), pp. 192–201|358 (1994)

14. Liu, T.Y., Xu, J., Qin, T., Xiong, W., Li, H.: Letor: Benchmark Dataset for Research on Learning to Rank for Information Retrieval. In: SIGIR 2007 Workshop on Learning to Rank for Information Retrieval (2007)
15. Kekalainen, J.: Binary and Graded Relevance in IR Evaluations - Comparison of the Effects on Ranking of IR Systems. Information Processing & Management 41, 1019–1033 (2005)
16. Raskutti, B., Kowalczyk, A.: Extreme re-balancing for SVMs: a Case Study. ACM SIGKDD Explorations Newsletter 6, 60–69 (2004)
17. Tao, Q., Wu, G.W., Wang, F.Y., Wang, J.: Posterior Probability Support Vector Machines for Unbalanced Data. IEEE Transactions on Neural Networks 16, 1561–1573 (2005)

A Biologically Plausible Winner-Takes-All Architecture*

Sebastian Handrich, Andreas Herzog, Andreas Wolf, and Christoph S. Herrmann

Otto-von-Guericke-University Magdeburg
Institute for Psychology II
Department for Biological Psychology
Universitätsplatz 2
39106 Magdeburg Germany
sebastian.handrich@ovgu.de

Abstract. Winner-takes-all (WTA) is an important mechanism in artificial and biological neural networks. We present a biologically plausible two layer WTA architecture with biologically plausible spiking neuron model and conductance based synapses. The excitatory neurons in the WTA layer receive spiking signals from an input layer and can inhibit other excitatory WTA neurons via related inhibitory neurons. The connections from the input layer to WTA layer can be trained by Spike-Time-Dependent Plasticity to discriminate between different classes of input patters. The overall input of the WTA neurons are controlled by synaptic scaling.

1 Introduction

For some purposes, it is desirable to have exactly one out of a number of neurons fire while others remain silent, e.g. for binary classifications. The so called winner-takes-all (WTA) architecture ensures this behavior. The WTA mechanism occurs in biological neural systems and has become an important part of artificial neural networks. Due to variations of input or variations in the first processing steps (input accumulation, different weights) a single neuron is activated, while all other neurons or populations are inactive. In a more liberal version, called k-winner-take-all, a limited number (k) of neurons are activated while the others remain inactive [1]. The WTA mechanism is the basis of many algorithms for perceptual decision making [2], selection of attention [3], and pattern classification.

In the field of classical artificial neural networks, WTA architectures are widely used in unsupervised learning, e.g. in self-organizing-maps [4], and as post-processing for supervised learning (classifiers). In these cases, the WTA mechanism can easily be realized via a formal maximum search.

In more complex networks, the WTA behavior can be an intrinsic network property, implemented by recurrent connections, like lateral inhibition. Such networks can be used to sharpen inputs in visual systems [5] and auditory systems [6].

WTA mechanisms have also been realized by spiking networks with integrate and fire neurons. Oster and Liu show a hardware implementation of 64 integrate and fire neurons

* This work was supported by the DFG HE 3353/6-1 Forschungsverbund 'Electrophysiological Correlates of Memory and their Generation', SFB 779, and by BMBF Bernstein-group 'Components of cognition: small networks to flexible rules'.

D.-S. Huang et al. (Eds.): ICIC 2009, LNAI 5755, pp. 315–326, 2009.

in an analog VLSI array [7] with instantaneous non-conductance based synapses. The recurrently connected neuron array works like a filter. Only the neuron with the highest input firing rate passes its activity onto the next layer.

However, when implementing WTA architectures in more complex networks, a number of problems arise. If we consider the output of a neuron as a mean spiking rate, the dynamic of such WTA networks can be analyzed analytically [8,9]. Mao and Massaquoui [9] investigate the WTA dynamics with lateral inhibition in an abstract model of only inhibitory neurons under the assumption that all output connections of an inhibitory neuron have the same weight. They found that a strong lateral inhibition improves the contrast between winner and losers, but it does not guarantee the neuron with the largest input to win, because of the possible existence of multiple stable equilibria. In contrast, a weak lateral inhibition may guarantee the uniqueness of an equilibrium but has relative poor WTA behavior.

An additional aspect is the dynamics of the inhibition. Ermentrout [10] discusses the complex dynamics in WTA networks with slow inhibition. The neurons can synchronize to a global periodic solution, which are stable under certain conditions but they can also start to oscillate.

Taken together, there are two major problems, if we realize a WTA with lateral inhibition based on biologically plausible neurons and synaptic connections: (I) there is no guarantee that one of the excitatory neurons will fire during an input, and (II) the delay between the firing of the first excitatory neuron and the time inhibition requires to shut down other neurons lead up to the problem that an other excitatory neuron may fire during the delay [11].

A possibility to overcome the delay problem is given in [12]. A part of the inhibitory neurons gets a direct input parallel to the excitatory neurons and reacts to an input signal without the delay of the excitatory to inhibitory connection. This works fine on predefined connection weights, but it is unclear how the parallel learning of the parallel connections to inhibitory and excitatory can be performed.

In this paper, we introduce biologically plausible WTA (bpWTA) in a network of spiking neurons based on the model of Izhikevich [13]. The network consists of an input layer and a bpWTA output layer (see Methods). When training networks by Spike-Time-Dependent Plasticity (STDP) [14], bpWTA is a prerequisite when reward is supposed to modulate STDP learning [15]. In recurrent networks STDP can synchronize or desynchronize the activity, depending of the network connectivity and additional plasticity mechanisms [16]. In the presented paper we train feed forward connections from input layer to WTA layer and have to ensure that there is a relevant number of nearly coincident spikes on the pre- and postsynaptic side of the WTA output layer neurons.

2 Methods

2.1 Network Configuration

Our network architecture consists of two different layers, the input- and the WTA-layer (see Fig. 1). The input layer is used to receive the external stimulus as described below. It is composed of 64 excitatory neurons, which are not laterally connected. The WTA layer consists of two excitatory neurons, which on the one hand integrate their inputs

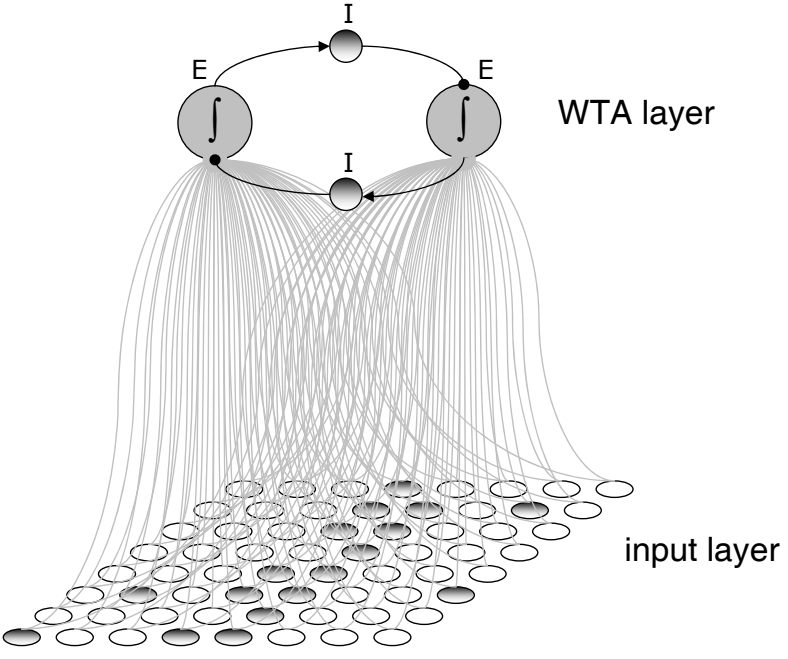

Fig. 1. Network structure of the proposed WTA architecture. The input layer is activated by stimuli (filled circles). Within the WTA layer, the two excitatory neurons (E) inhibit each other via an inhibitory neuron (I).

received from the input layer, and on the other hand inhibit each other via two inhibitory neurons. This results in a binary categorization after some time which allows to compute an error signal for a possible subsequent learning algorithm. Each input neuron i is connected to each excitatory WTA neuron j, with initial synaptic weights $c_{ij} = r^2/64$, where r is randomly chosen from the uniform distribution within the interval of $[0, 0.5]$. In the WTA layer all synaptic weights are set to $c_{WTA} = 1$.

There are two types of input to our network. The first one is the stimulation of the input layer defined by a grid of 8x8 sensitive areas that can be stimulated by the input patterns. Those patterns, if considered as images, show randomly distributed noise superimposed onto vertical or horizontal bars (Fig. 5). Each sensitive area can excite the corresponding input neuron by a spike train (firing-rate $f_s = 50$Hz), which is either uniformly- (synchronous input) or Poisson-distributed. The two patterns are presented alternately for one second with an inter-stimulus-interval (ISI) of one second. Additionally, each neuron receives thalamic background activity, which is generated by a Poisson-point process with a mean firing rate of $\lambda = 1$Hz.

2.2 Neuron Model

We used the neuron model by Izhikevich [13], which reduces the biophysically accurate Hodgkin-Huxley model to a two-dimensional system of ordinary differential equations. The advantages of this model are the fast computation and the configuration of

different behaviors via a few parameters. So, it is widely used e.g. to apply simulations of network development [17].

The neurons of the input layer and the inhibitory ones of the WTA-layer were modeled by:

$$\begin{aligned} \dot{v} &= 0.04v^2 + 5v + 140 - u - I_{syn}, \\ \dot{u} &= a\left(bv - u\right), \end{aligned} \tag{1}$$

where v is the membrane potential, u the recovery variable and I_{syn} is the total synaptic current. The parameter a determines the decay of the recovery-variable and b defines the sensibility of u to the membrane potential. If v reaches a threshold of 30 mV, v and u are reset to c and d, respectively (see [13] for more detail). The dimensionless model parameters a, b, c, d are used to generate typical firing patterns, observed in neocortical neurons.

To implement an integrator characteristic, we adapt the constants for the excitatory neurons of the WTA-layer [18]:

$$\begin{aligned} \dot{v} &= 0.04v^2 + 4.1v + 108 - u - I_{syn}, \\ \dot{u} &= a\left(bv - u\right). \end{aligned} \tag{2}$$

The standard time step is 0.1 ms.

2.3 Neuron Types

In our study, we used three different types of neurons:

1. *Glutamate (excitatory) neurons* with, according to the simulations in [19]:
   $(a, b) = (0.02, 0.2)$ and $(c, d) = (-65, 8) + (15, -6)\, r^2$, where r is randomly selected from the uniform distribution in the interval $[0, 0.5]$ to obtain a behavior between regular spiking (RS, $r = 0$) and intrinsically bursting (IB, $r = 0.5$). The square of r biases the distribution towards the RS cells.
2. *GABAergic (inhibitory) neurons:*
   $(a, b) = (0.02, 0.25)$ and $(c, d) = (-65, 2)$, to get low-threshold spiking (LTS) neurons.
3. *Input-integrating(excitatory) neurons:*
   $(a, b) = (0.02, -0.1)$ and $(c, d) = (-55, 6)$, used in the WTA-layer (Fig 2).

2.4 Synapse Model

The synaptic input current in a neuron is calculated in each time step by:

$$\begin{aligned} I_{syn} = {} & g_{AMPA}\left(v - 0\right) \\ & + g_{NMDA} \frac{\left[\left(v + 80\right)/60\right]^2}{1 + \left[\left(v + 80\right)/60\right]^2} \left(v - 0\right) \\ & + g_{GABA_A}\left(v + 70\right) \\ & + g_{GABA_B}\left(v + 90\right), \end{aligned} \tag{3}$$

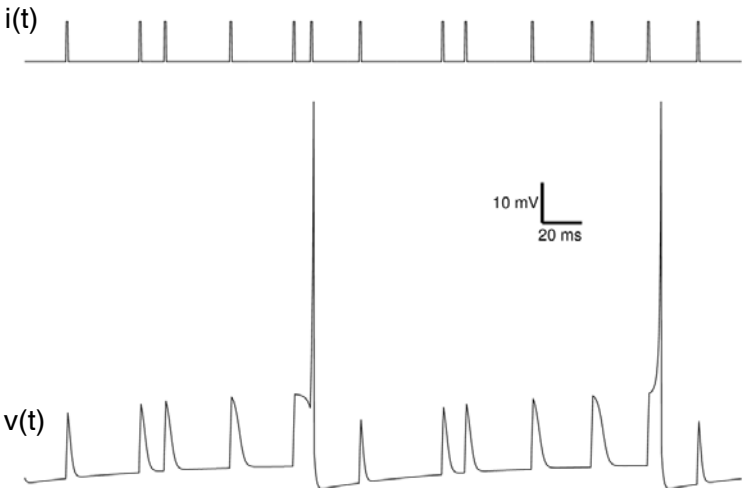

Fig. 2. Excitatory neurons of the WTA-Layer are parametrized as integrator. A slow spike train (upper trace) from a single input neuron excites the membrane potential (lower trace) and results in an action potential only after some input spikes have been integrated.

where g_k is the time dependent synaptic conductance and v the actual membrane potential. The conductances change by first-order linear kinetics

$$\dot{g}_k = -\frac{g_k}{\tau_k}, \tag{4}$$

with time constants $\tau_k = 5$, 150, 6 and 150 ms for the simulated $AMPA$, $NMDA$, $GABA_A$ and $GABA_B$ receptors, respectively [19]. The rise time of currents is typically short and neglected.

If a spike is transmitted from presynaptic neuron i to postsynaptic neuron j, after a delay-time t_{Delay}, the conductances are updated depending on the type of presynaptic neuron, the synaptic efficiency $R_i \cdot w_i$ and the synaptic weight c_{ij}:

$$g_k \leftarrow g_k + c_{ij}, \tag{5}$$

The transmission-delay t_{Delay} results from the Euclidean distance between the neurons and an additional latency of 0.5 ms. It is set in the WTA layer (all connections) to 1 ms, and from the input layer to WTA layer to 10 ms. The relation of $AMPA$ to $NMDA$ channels and $GABA_A$ to $GABA_B$ channels is set to one.

2.5 Synaptic Plasticity

Learning in neural circuits is considered as a change of synaptic strengths. To implement this, we used a well known form of hebbian learning, the Spike-Time-Dependent

Plasticity (STDP) [14], in which the temporal order of presynaptic and postsynaptic spike determines, whether a synapse is potentiated (LTP) or weakened (LTD):

$$\Delta c_{ij} = \begin{cases} A_+ e^{\frac{-|\Delta t|}{\tau_+}}(1 - c_{ij}) - \frac{A_+}{10} & \text{if } \Delta t > 0 \\ A_- e^{\frac{-|\Delta t|}{\tau_-}} c_{ij} & \text{if } \Delta t \leq 0 \end{cases}, \tag{6}$$

with $A_+ = 0.005$, $A_- = 0.009$, $\tau_+ = 15ms$ and $\tau_- = 20ms$. This fullfills the equation $A_+\tau_+ \leq A_-\tau_-$, which ensures, that uncorrelated pre- and postsynaptic spikes lead to an overall synaptic weakening [20]. The term $\frac{A_+}{10}$ causes LTD, if the temporal difference between pre- and postsynaptic spike is too large, i.d. there is a postsynaptic spike without a preceding presynaptic one.

The use of plastic synapses may end in an unconstrained feedback-cycle due to the fact, that correlated pre- and postsynaptic firing leads to LTP which again increases that correlation [21]. In biological neural networks this stability problem is avoided through a mechanism called *homeostatic-synaptic-scaling*, which changes the number of AMPA and NMDA receptors of the postsynaptic neuron in dependence of its activity [22]. This leads to a competitive scaling of the afferent synapses. In our model we achieved this competitive scaling by keeping the cumulative weight $\sum_j^n c_{ij}$ of the synapses leading onto the same excitatory WTA-neuron i at a constant level c_0:

$$c_{ij} \leftarrow c_{ij} \cdot \frac{c_0}{\sum_j^n c_{ij}} \; \forall i. \tag{7}$$

The STDP mechanism and the synaptic scaling interact dynamically. During the stimulation of the network with input patterns, the STDP increased the synaptic weights between stimulated neurons in the input layer and the winner neuron. The synaptic scaling prevents the winner neuron from excessive firing and down-regulates the weights of unused connections.

3 Results

The goal of the proposed WTA mechanism is the generation of an error signal for a learning mechanism. The learning should be performed by the Spike-Time Depended Plasticity (STDP) [14]. Only if a fast computation from the onset of a stimulus to the decision of the winner is achieved, it can be guaranteed that enough pairs of pre- and postsynaptic spikes can be computed at the winner neuron.

The weights c_{ij} of the connections from the 64 input neurons to the two excitatory WTA neurons are initialized randomly. The input patterns stimulate both excitatory WTA neurons. Due to the different weights and different stimulation, there are different input currents to the excitatory WTA neurons. This is demonstrated in Fig. 3 (upper trace) by showing the integrated input currents received by each excitatory WTA neuron (reseted to zero on each stimulus onset).

The excitatory WTA neuron with the highest input fires first (e.g in Fig. 3 first trial, neuron E2), the related inhibitory neuron (I2) is activated with a short transmission delay and inhibits the opposite excitatory neuron (E1). During the presentation of the

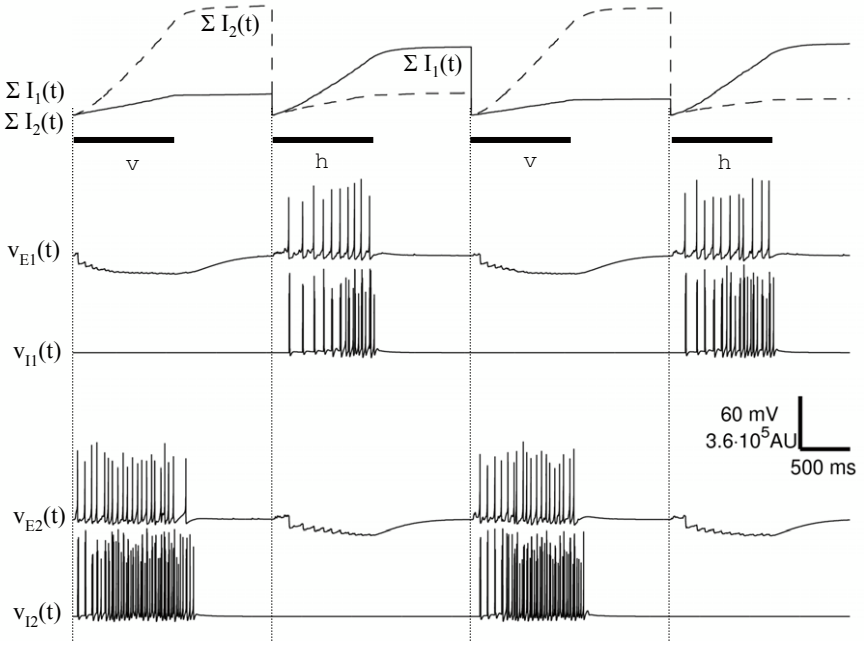

Fig. 3. The WTA mechanism. Upper traces show the integrated input current of excitatory WTA neurons in arbitrary units (AU) (reset to zero at each stimulus onset). The black bars indicate the stimulation with a vertical (v) or horizontal (h) bar. Other traces show the membrane potential of the WTA neurons. Note that only one excitatory neuron (E) is active at a time, i.e. the WTA requirement is fulfilled.

first input pattern, the neurons E1/I1 fire and the neurons E2/I2 are silent. This is the required WTA behavior.

Thus, in each trial only one of the excitatory WTA neurons is activated. Therefore, there is a simultaneous activation of the input neurons, which are stimulated by the specific input pattern, and the winner of the excitatory WTA neurons resulting in an adaptation of the weights by STDP. While the input stimulation continues, the other neuron has no chance to fire until the input stops or the input pattern changes.

There is a chance that both excitatory WTA neurons are stimulated nearly identically, so that they fire nearly synchronously. The feedback delay from the first firing of the winner neuron to an inhibitory postsynaptic potential (IPSP) in the other neuron is approximately 2.5 ms. If the delay between the firing of the first and second excitatory neuron is smaller than the inhibition feedback, both WTA neurons fire a short burst and potentially inhibit each other after that.

However, such synchronous activation is unlikely and happens only on the first trials after a random initialization of the weights. Due to the noisy input patterns, a sequence with more than one coincident activation of both excitatory WTA-neurons is extreme unlikely, and one single bad trial has not much influence on STDP learning.

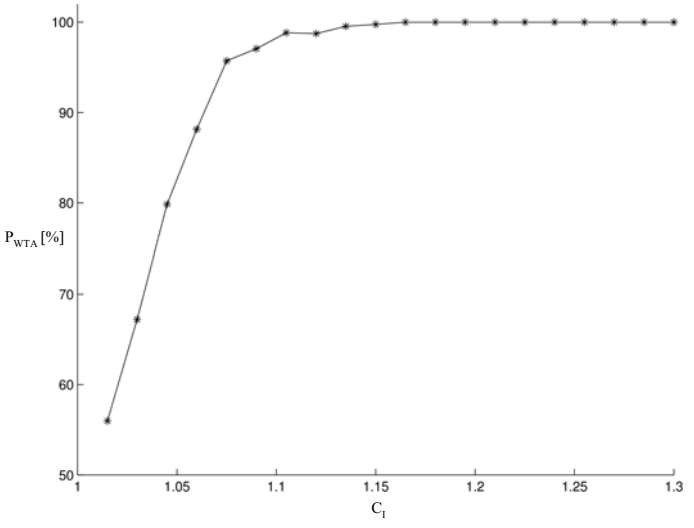

Fig. 4. Performance of the WTA network on low input contrasts. The network is untrained, the weights are randomly initialized.

In order to quantify the performance of our WTA architecture, we consider its response in relation to the input contrast. The WTA response in each trial is defined as relative number of spikes of the winner neuron:

$$P_{WTA} = \frac{n_{HI}}{n_{HI} + n_{LI}}, \tag{8}$$

where n_{HI} and n_{LI} are the number of spikes generated by the WTA neurons, which received the higher and lower input respectively. The input contrast C_I is defined as

$$C_I = \frac{I_{max} - I_{min}}{I_{max} + I_{min}}, \tag{9}$$

where I_{min} is the minimal and I_{max} is the maximal cumulative current which is received by the WTA neurons. The cumulative current of each WTA neuron is integrated from the stimulus onset t_0 to the firing time t_{w0} of the first spike of the winner neuron:

$$I = \int_{t_0}^{t_{w0}} i(t). \tag{10}$$

Figure 4 depicts the performance P_{WTA} of an untrained WTA network (weights randomly initialized) in dependence of the input contrast C_I. Contrast is divided into bins (width: 0.015 units). Performance of all trials (N=2700) in each bin is averaged. With rising contrast, the probability rapidly increases that the neuron, which received a higher input, fires more frequently. If the contrast is larger than 1.15, in every trial only the winner neuron is activated. Even if there is a very low input contrast (first bin from 1.0 to 1.015) there is a preference to the correct neuron. Thus, if STDP mechanism is applied, the synapses onto the correct WTA neuron are strengthened. This again leads to a higher input contrast.

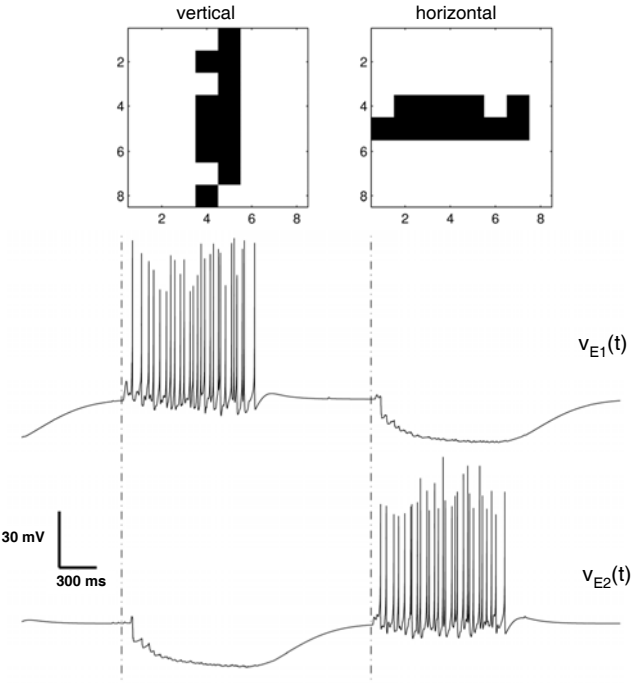

Fig. 5. Network response after training. Vertical and horizontal patters are discriminated correctly by activation of either E1 (vertical) or E2 (horizontal).

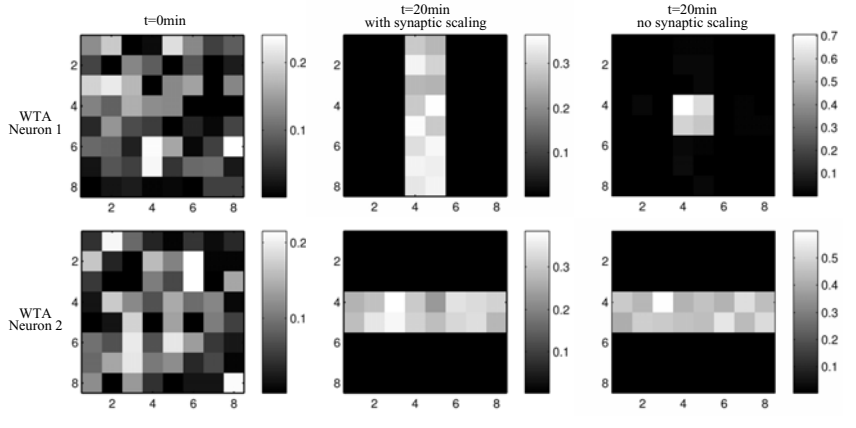

Fig. 6. Weight matrix of excitatory WTA neurons. Left: random initialization. Middle and right: after 20 min training, with synaptic scaling (middle), without synaptic scaling (right).

Fig. 5 shows the behavior of the network after 20 minutes of learning. Vertical patterns activate neuron E1 and horizontal patterns activate E2. The mapping is not fixed but depends on initialization of weights and the noise of the input pattern. During the training the weights are adapted by the STDP rule. The matrix of input weights for each excitatory WTA neuron reflects the input pattern (Fig 6, left and middle column).

However, the unsupervised classification of overlapping and noisy patterns are not unambiguous. There are two general problems. The first is the generalization: If the two patterns can be discriminated during the training by only one single pixel, it may be possible that the final classification is based only on this single pixel and only one very hight synaptic weight. The second problem is, that the overlapping area itself can be interpreted as an additional pattern (Fig 6, right column). Both problems can be solved by an additional synaptic mechanism, the synaptic scaling (eq. 7).

4 Discussion and Conclusion

We show a WTA architecture with a biologically plausible neuron model and conductance based synaptic connections.

The input and output signals to the neurons in the WTA layer in our model are spikes (events). So we have to define the winner in an event driven environment. Many models use as input a value, which is considered as a mean firing rate of a population or single cells (see e.g. [11,23,10]) and the winner is defined as the neuron or population with the highest mean firing rate. Thus, on short intervals in the vicinity of the interspike distance, a mean firing rate can not be defined, although some models, like the Wilson-Cowan oscillator, suggest there are. We have designed a biologically plausible model with spikes to compare it with biological EEG experiments via time frequency representations [24]. Therefore, we need a spiking implementation and have used STDP as learning mechanism. The selected integrator characteristic of the WTA neurons is biologically plausible and combines the mean firing rate of earlier spikes with a fast computation of present spikes (see Fig. 2). This means the winner is the excitatory WTA neuron which receives the most input from many selective areas within an integration time. The integration time depends on synaptic components (NMDA time constant) and neuron components (integrator).

An additional point is the design of the synaptic transmission and the synaptic plasticity. All firing rate models and simpler spiking models use a strict superposition of the input signals. The values of input are weighted and integrated as continuous values (firing rate) or current pulses (spikes). Real biological systems are nonlinear. We use conductance based synapses which take the actual membrane potential into account. The effect of a spike depends on the synaptic time constants, the actual membrane potential, and the reversal potential of the synapses.

In contrast to other model studies, we did not use a single global inhibitor neuron and no self-excitation of excitatory WTA neurons. Instead, every excitatory WTA neuron has its own inhibitory neuron. Authors of global inhibition argument that there is a higher number of excitatory than inhibitory neurons in the cortex [11]. Hence, some excitatory neurons have to share one inhibitory neuron. This may be correct for the entire cortex, but circuits with WTA mechanisms may be very small parts and it is possible

that for those small parts a one to one relation can be assumed. If we do not consider single neurons in WTA, but small populations of neurons, one population of excitatory neurons can be connected to one (smaller) population of inhibitory neurons [25]. However, a global inhibition requires a self excitation of the winner neuron to prevent it from inhibition. The parametrization of such recurrent networks are a difficult optimization problem with complex dynamics to prevent unstable behavior. It can be solved for a larger number of neurons by estimating the weights via a mean field model. Based on the working memory simulations of Brunel and Wang [26], Zylberberg et al. [27] present a network model of 2000 neurons with a global inhibition and self excitation of input selective excitatory populations which can work as a WTA network. The network provides load and retrieval mechanisms with a top-down control for two different inputs. But if we assume a larger number of input sources (e.g. the 8x8 input layer), which cause a higher input variability and a large number of weights for each of the excitatory WTA neurons, it seems more useful to use single neurons in the WTA layer instead of large populations.

The input weights of each excitatory WTA neuron directly reflect the discriminated input pattern. We show that a WTA network consisting only of an input layer and a WTA layer can be trained in an unsupervised fashion to discriminate simple patterns with small areas of overlap. This network can be extended to different tasks. With one or more hidden layers it should be possible to discriminate more complex (spatiotemporal) input patterns, e.g. with more overlap. The hidden layer transforms the input pattern into another coordinate space. An unsupervised training of such a multilayer network by STDP requires a coincident activation of the WTA output neuron with the input neurons which can be a problem when input patterns are presented briefly. In [15] we show a network architecture with an additional feedback layer to extend the firing of the input layer after the end of external stimulation resembling the function of the hippocampus.

The presented WTA architecture can also be applied for supervised learning by an external activation of the (winner) excitatory WTA neuron or activation of the opposite (non winner) inhibitory WTA neuron. It gives the chance to integrate supervised and unsupervised learning algorithm into a single mechanism (STDP) in one network architecture.

References

1. Yuille, A.L., Geiger, D.: Winner-take-all networks. In: Arbib, M.A. (ed.) The Handbook of Brain Therory and Neural Networks, 2nd edn., pp. 1228–1231. MIT Press, Cambridge (2003)
2. Salzman, C.D., Newsome, W.T.: Neural mechanisms for forming a perceptual decision. Science 264(5156), 231–237 (1994)
3. Lee, D.K., Itti, L., Koch, C., Braun, J.: Attention activates winner-take-all competition among visual filters. Nat. Neurosci. 2(4), 375–381 1097-6256 (Print) Journal Article (1999)
4. Kohonen, T.: Self-organizing maps. Springer, Heidelberg (2001)
5. Blakemore, C., Carpenter, R.H., Georgeson, M.A.: Lateral inhibition between orientation detectors in the human visual system. Nature 228(5266), 37–39 (1970)
6. Wu, G.K., Arbuckle, R., hua Liu, B., Tao, H.W., Zhang, L.I.: Lateral sharpening of cortical frequency tuning by approximately balanced inhibition. Neuron 58(1), 132–143 (2008)

7. Oster, M., Liu, S.: Spiking inputs to a winner-take-all network. In: Weiss, Y., Schölkopf, B., Platt, J. (eds.) Advances in Neural Information Processing Systems, vol. 18, pp. 1051–1058. MIT Press, Cambridge (2005)
8. Maass, W.: On the computational power of winner-take-all. Neural Computation 12(11), 2519–2535 (2000)
9. Mao, Z.H., Massaquoi, S.: Dynamics of winner-take-all competition in recurrent neural networks with lateral inhibition 18(1), 55–69 (2007)
10. Ermentrout, B.: Complex dynamics in winner-take-all neural nets with slow inhibition. Neural Networks 5, 415–431 (1992)
11. Coultrip, R., Granger, R., Lynch, G.: A cortical model of winner-take-all competition via lateral inhibition. Neural Networks 5(1), 47–54 (1992)
12. Jin, D.Z.: Spiking neural network for recognizing spatiotemporal sequences of spikes. Phys. Rev. E 69(2), 021905 (2004)
13. Izhikevich, E.M.: Simple model of spiking neurons. IEEE Transactions on neural networks 14(6), 1569–1572 (2003)
14. Bi, G.Q., Poo, M.M.: Synaptic modifications in cultured hippocampal neurons: dependence on spike timing, synaptic strength, and postsynaptic cell type. J. Neurosci. 18(24), 10464–10472 (1998)
15. Handrich, S., Herzog, A., Wolf, A., Herrmann, C.S.: Prerequisites for integrating unsupervised and reinforcement learning in a single network of spiking neurons. In: IJCNN (2009) (in press)
16. Kube, K., Herzog, A., Michaelis, B., de Lima, A., Voigt, T.: Spike-timing-dependent plasticity in small world networks. Neurocomputing 71, 1694–1704 (2008)
17. Herzog, A., Kube, K., Michaelis, B., de Lima, A.Baltz, T., Voigt, T.: Contribution of the gaba shift to the transition from structural initializationto working stage in biologically realistic networks. Neurocomputing, 1134–1142 (2008)
18. Izhikevich, E.M.: Dynamical Systems in Neuroscience: The Geometry of Excitability and Bursting. The MIT Press, Cambridge (2006)
19. Izhikevich, E.M., Gally, J.A., Edelman, G.M.: Spike-timing dynamics of neuronal groups. Cerebral Cortex 14, 933–944 (2004)
20. Song, S., Miller, K., Abbott, L.: Competitive hebbian learning through spike-timing-dependent synaptic plasticity. Nat. Neurosci. 3(9), 919–926 (2000)
21. Abbott, L., Nelson, S.: Synaptic plasticity: taming the beast. Nat. Neurosci. 3(suppl.), 1178–1183 (2000)
22. Turrigiano, G.: The self-tuning neuron: synaptic scaling of excitatory synapses. Cell 135(3), 422–435 (2008)
23. Brandt, S., Wessel, R.: Winner-take-all selection in a neural system with delayed feedback. Biol. Cybern. 97(3), 221–228 (2007)
24. Fründ, I., Schadow, J., Busch, N., Naue, N., Körner, U., Herrmann, C.: Anticipation of natural stimuli modulates eeg dynamics: physiology and simulation. Cogn. Neurodyn. 2, 89–100 (2008)
25. Lumer, E.D.: Effects of spike timing on winner-take-all competition in model cortical circuits. Neural Comput. 12(1), 181–194 (2000)
26. Brunel, N., Wang, X.: Effects of neuromodulation in a cortical network model of object working memory dominated by recurrent inhibition. J. Comput. Neurosci. 11(1), 63–85 (2001)
27. Zylberberg, A., Dehaene, S., Mindlin, G., Sigman, M.: Neurophysiological bases of exponential sensory decay and top-down memory retrieval: a model. Front Comput. Neurosci. 3, 4 (2009)

Minimum Sum-of-Squares Clustering by DC Programming and DCA

Le Thi Hoai An[1] and Pham Dinh Tao[2]

[1] Laboratory of Theoretical and Applied Computer Science
UFR MIM, University of Paul Verlaine - Metz, Ile du Saulcy, 57045 Metz, France
[2] Laboratory of Modelling, Optimization & Operations Research,
National Institute for Applied Sciences - Rouen, BP 08, Place Emile Blondel
F 76131 Mont Saint Aignan Cedex, France
pham@insa-rouen.fr, lethi@uni-metz.fr

Abstract. In this paper, we propose a new approach based on DC (Difference of Convex functions) programming and DCA (DC Algorithm) to perform clustering via minimum sum-of-squares Euclidean distance. The so called Minimum Sum-of-Squares Clustering (MSSC in short) is first formulated in the form of a hard combinatorial optimization problem. It is afterwards recast as a (continuous) DC program with the help of exact penalty in DC programming. A DCA scheme is then investigated. The related DCA is original and very inexpensive because it amounts to computing, at each iteration, the projection of points onto a simplex and/or onto a ball, that all are given in the explicit form. Numerical results on real word data sets show the efficiency of DCA and its great superiority with respect to K-means, a standard method of clustering.

Keywords: clustering, MSSC, Combinatorial optimization, DC programming, DCA, Nonsmooth nonconvex programming, Exact penalty.

1 Introduction

Clustering, which aims at dividing a data set into groups or clusters containing similar data, is a fundamental problem in unsupervised learning and has many applications in various domains. In recent years, there has been significant interest in developing clustering algorithms to massive data sets (see e.g. [2] - [11], [17], [18], [23], [24] and the references therein). Two main approaches have been used for clustering: statistical and machine learning based on mixture models (see e.g. [2], [6]) and the mathematical programming approach that considers clustering as an optimization problem (see e.g. [3], [4], [7], [17], [18], [22], [26], [28], [32] and the references therein).

The general term "clustering" covers many different types of problems. All consist of subdividing a data set into groups of similar elements, but there are many measures of similarity, many ways of measuring, and various concepts of subdivision (see [11] for a survey). Among these criteria, a widely used one is the minimum sum of squared Euclidean distances from each entity to the centroid of

D.-S. Huang et al. (Eds.): ICIC 2009, LNAI 5755, pp. 327–340, 2009.

its cluster, or minimum sum-of-squares (MSSC) for short, which expresses both homogeneity and separation.

The MSSC problem consists in partitioning a given set of n entities into c clusters in order to minimize the sum of squared distances from the entities to the centroid of their cluster. This problem may be formulated mathematically in several ways, which suggest different possible algorithms. The two most widely used models are a bilevel programming problem and a mixed integer program. Many early studies were focused on the well-known K-means algorithm ([8],[10]) and its variants (see [29] for a survey). More recently, several works in optimization approaches have been developed for the MSSC with the mixed integer programming formulation (see e.g. [4], [24], [26], [32]). There are some attempts to solve this problem exactly through the branch and bound or cutting methods via reformulation-linearization techniques, 0-1 SDP formulation. However, these methods are not available for massive data sets (large number of samples and large number of features).

We investigate in this paper an efficient nonconvex programming approach for the mixed integer programming formulation of the MSSC problem. Our method is based on DC (Difference of Convex functions) programming and DCA (DC Algorithms) that were introduced by Pham Dinh Tao in a preliminary form in 1985. They have been extensively developed since 1994 by Le Thi Hoai An and Pham Dinh Tao (see [13], [14], [15], [27] and the references therein). They are classic now, and used by many researchers (see e.g. [20] , [21], [25], [30], [31]). Our walk is motivated by the fact that DCA has been successfully applied to many (smooth or nonsmooth) large-scale nonconvex programs in various domains of applied sciences (see [13] - [21], [25], [27], [30] - [33] and the references therein), in particular in Machine Learning ([17] - [21], [25], [30] - [33]) for which they provide quite often a global solution and proved to be more robust and efficient than the standard methods. In [17] an efficient DCA scheme has been developed to MSSC problem with a bilevel programming formulation.

The purpose of this paper is to demonstrate that, as shown for previous studies in Machine Learning, DCA is a promising approach for the MSSC problem with a mixed integer programming formulation. Using an exact penalty result in DC programming we reformulate the considered MSSC problem in the form of a DC program. A so-called DC program is that of minimizing a DC function

$$f = g - h \text{ (with } g \text{ and } h \text{ being convex functions)}$$

over a convex set. The construction of DCA involves the convex DC components g and h but not the DC function f itself. Moreover, a DC function f *has infinitely many DC decompositions* $g - h$ *which have a crucial impact on the qualities* (speed of convergence, robustness, efficiency, globality of computed solutions,...) of DCA. We propose in this work a nice DC program for a continuous formulation of the MSSC problem and develop the corresponding DCA scheme. We show that the effect of the DC decomposition is meaningful.

Experimental results on several biomedical data sets show clearly the effectiveness of the proposed algorithms and their superiority with respect to the standard K-means algorithm in both running-time and accuracy of solutions.

The remainder of the paper is organized as follows. Section 2 is devoted to the mathematical formulation of the MSSC problem and a continuous reformulation via an exact penalty technique. DC programming and DCA for solving the resulting MSSC problem are developed in Section 3. Finally, numerical experiments are reported in Section 4.

2 Mathematical Formulations of the MSSC Problem

2.1 Mixed Integer Program

Let $X := \{x_1, x_2, ..., x_n\}$ denote n entities to be partitioned into c $(2 \leq c \leq n)$ homogeneous clusters $C_1, C_2, ..., C_c$ where $x_k \in \mathbb{R}^d$ $(k = 1, ..., n)$ represents a multidimensional data vector. Let $U = (u_{i,k}) \in \mathbb{R}^{c\times n}$ with $i = 1, \ldots, c$ and $k = 1, \ldots, n$ be the matrix defined by:

$$u_{i,k} := \begin{cases} 1 & \text{if} \quad x_k \in C_i \\ 0 & \text{otherwise} \end{cases} .$$

Then a straightforward formulation of MSSC is

$$\begin{cases} \min f(U,V) := \sum\limits_{k=1}^{n} \sum\limits_{i=1}^{c} u_{i,k} ||x_k - v_i||^2 \\ s.t. \quad u_{i,k} \in \{0,1\} \text{ for } i = 1, .., c \quad k = 1, .., n \\ \sum\limits_{i=1}^{c} u_{i,k} = 1, \ k = 1, .., n \end{cases} . \tag{1}$$

where $\|.\|$ is, in this paper, the Euclidean norm in $\mathbb{R}^d$, and V the $(c \times d)$ - matrix whose i^{th} row is $v_i \in \mathbb{R}^d$, the center of C_i. In the sequel to simplify related computations we will work on the vector space $\mathbb{R}^{c\times n} \times \mathbb{R}^{c\times d}$ of real matrices. The variables are then $(U, V) \in \mathbb{R}^{c\times n} \times \mathbb{R}^{c\times d}$, where $U \in \mathbb{R}^{c\times n}$ whose k^{th} column is denoted U^k and $V \in \mathbb{R}^{c\times d}$ whose i^{th} row is denoted V_i or v_i (v_i is a row-vector in $\mathbb{R}^d$).

The last constraint ensures that each point x_k is assigned to one and only one group. This is a mixed integer program where the objective function is nonconvex. It has recently been shown in [1] that the problem is NP-hard. Moreover, it is a global optimization problem with possibly many local minima. In real applications this is a very large scale problem (*high* dimension and *large* data set, i.e. d and n are very large), that is why global optimization approaches such as Branch & Bound, Cutting algorithms can't be used. Most of the methods for the model (1) are pure heuristics that can only locate a "good" local solution.

In some previous works , by rewriting the center v_i of the cluster C_i as $v_i = \frac{\sum_{l=1}^{n} u_{i,l} x_l}{\sum_{l=1}^{n} u_{i,l}}$ one considered the following problem where only U is variable:

$$\min \left\{ \sum_{k=1}^{n} \sum_{i=1}^{c} u_{i,k} \left\| x_k - \frac{\sum_{l=1}^{n} u_{i,l} x_l}{\sum_{l=1}^{n} u_{i,l}} \right\|^2 : \ u_{i,k} \in \{0,1\}, \sum_{i=1}^{c} u_{i,k} = 1, \ k = 1, .., n \right\}.$$

In this work we maintain the model (1) because it is quite convenient for using DCA: (1) is a nice DC program having an appropriate DC decomposition to which the corresponding DCA is simple and inexpensive. Moreover DCA computes separately U and V, so the use of both variables U and V do not increase actually the complexity of DCA.

For applying DCA we reformulate (1) as a continuous optimization problem. First of all, since $u_{i,k} \in \{0,1\}$ we can replace $u_{i,k}$ by $u_{i,k}^2$ and rewritte the objective function of (1) by

$$f(U,V) := \sum_{k=1}^{n}\sum_{i=1}^{c} u_{i,k}^2 ||x_k - v_i||^2.$$

We will see on the next that using $u_{i,k}^2$ instead to $u_{i,k}$ is uselful for getting a good DC decomposition and the resulting DCA is interesting.

2.2 A Continuous Reformulation

Our reformulation technique is based on the following results developed in [16]

Lemma 1. *([16]) Let K be a nonempty bounded polyhedral convex set, f be a DC function on K and p be a nonnegative concave function on K. Then there exists $t_0 \geq 0$ such that for all $t > t_0$ the following problems have the same optimal value and the same solution set:*

$$\begin{aligned} (P) \qquad & \alpha = \inf\{f(x) : x \in K, p(x) \leq 0\} \\ (P_t) \qquad & \alpha(t) = \inf\{f(x) + tp(x) : x \in K\}. \end{aligned}$$

For applying this result in the reformulation of (1) we first show that $f(U,V)$ is a DC function.

Using the equation $2f_1f_2 = (f_1+f_2)^2 - (f_1^2+f_2^2)$ we can express $f(U,V)$ as

$$\begin{aligned} f(U,V) &= \sum_{k=1}^{n}\sum_{i=1}^{c} u_{i,k}^2 \|x_k - v_i\|^2 \\ &= \tfrac{1}{2}\sum_{k=1}^{n}\sum_{i=1}^{c} \left(u_{i,k}^2 + \|x_k - v_i\|^2\right)^2 - \tfrac{1}{2}\left(u_{i,k}^4 + \|x_k - v_i\|^4\right). \end{aligned}$$

Hence the following DC decomposition of $f(U,V)$ seems to be natural:

$$f(U,V) := G_1(U,V) - H_1(U,V) \tag{2}$$

where

$$G_1(U,V) = \frac{1}{2}\sum_{k=1}^{n}\sum_{i=1}^{c} \left(u_{i,k}^2 + \|x_k - v_i\|^2\right)^2 \tag{3}$$

and

$$H_1(U,V) = \frac{1}{2}\sum_{k=1}^{n}\sum_{i=1}^{c} \left(u_{i,k}^4 + \|x_k - v_i\|^4\right) \tag{4}$$

are clearly convex functions.

In the problem (1) the variable U is a priori bounded in $\mathbb{R}^{c\times n}$. One can also find a constraint for bound the variable V. Indeed, let $x_{k,j}$ be the j^{th} component, $j = 1, ..., d$, of the vector x_k and let

$$\alpha_j := \min_{k=1,...,n} x_{k,j},\ \beta_j := \max_{k=1,...,n} x_{k,j}.$$

Hence $v_i \in \mathcal{T}_i := \Pi_{j=1}^{d} [\alpha_j, \beta_j]$ for all $i = 1, ..., c$. For each $k \in \{1, ..., n\}$ let Δ_k be the $(c-1)$-simplex in $\mathbb{R}^c$ defined by

$$\Delta_k := \left\{ U^k := (u_{i,k})_i \in [0,1]^c : \sum_{i=1}^{c} u_{i,k} = 1 \right\}$$

and $\Delta := \Pi_{k=1}^{n} \Delta_k, \mathcal{T} := \Pi_{i=1}^{c} \mathcal{T}_i$. The problem (1) can be rewritten as:

$$\min \left\{ f(U,V) : U \in \Delta \cap \{0,1\}^{c\times n}, V \in \mathcal{T} \right\}. \tag{5}$$

Consider the function p defined on $\mathbb{R}^{c\times n}$ by

$$p(U) := \sum_{i=1}^{c}\sum_{k=1}^{n} u_{i,k}(1-u_{i,k}).$$

Clearly that p is finite concave on $\mathbb{R}^{c\times n}$, nonnegative on Δ, and

$$\Delta \cap \{0,1\}^{c\times n} := \left\{ u_{i,k} \in \{0,1\}^{c\times n} : \sum_{i=1}^{c} u_{i,k} = 1 \right\} = \{U \in \Delta :\ p(U) = 0\} = \{U \in \Delta :\ p(U) \le 0\}.$$

Using the Lemma above we can now write (5) in the form of the following nonconvex program in continuous variables:

$$\min \{F(U,V) := f(U,V) + tp(U) : (U,V) \in \Delta \times \mathcal{T}\}, \tag{6}$$

where $t > t_0$ is called penalty parameter.

In the sequel we will consider the MSSC problem via the continuous formulation (6) with t being sufficiently large. We will develop DC programming and DCA for solving (6).

3 DC Programming and DCA for Solving MSSC Problem

For facilitate the readers we give below a brief introduction to DC programming and DCA.

3.1 Outline of DC Programming and DCA

DC programming and DCA constitute the backbone of smooth/nonsmooth nonconvex programming and global optimization. They address the problem of minimizing a function f which is the difference of two convex functions on the whole

space $\mathbb{R}^d$ or on a convex set $C \subset \mathbb{R}^d$. Generally speaking, a DC program is an optimisation problem of the form :

$$\alpha = \inf\{f(x) := g(x) - h(x) : x \in \mathbb{R}^d\} \qquad (P_{dc})$$

where g, h are lower semi-continuous proper convex functions on $\mathbb{R}^d$. Such a function f is called a DC function, and $g - h$ a DC decomposition of f while g and h are the DC components of f. The convex constraint $x \in C$ can be incorporated in the objective function of (P_{dc}) by using the indicator function on C denoted by χ_C which is defined by $\chi_C(x) = 0$ if $x \in C$, and $+\infty$ otherwise:

$$\inf\{f(x) := g(x) - h(x) : x \in C\ \} = \inf\{\chi_C(x) + g(x) - h(x) : x \in \mathbb{R}^d\}.$$

Let

$$g^*(y) := \sup\{\langle x, y\rangle - g(x) : x \in \mathbb{R}^d\}$$

be the conjugate function of a convex function g. Then, the following program is called the dual program of (P_{dc}):

$$\alpha_D = \inf\{h^*(y) - g^*(y) : y \in \mathbb{R}^d\}. \qquad (D_{dc})$$

One can prove that $\alpha = \alpha_D$, and there is the perfect symmetry between primal and dual DC programs: the dual to (D_{dc}) is exactly (P_{dc}). For a convex function θ, the subdifferential of θ at $x_0 \in \mathrm{dom}\ \theta := \{x \in \mathbb{R}^d : \theta(x_0) < +\infty\}$, denoted by $\partial\theta(x_0)$, is defined by

$$\partial\theta(x_0) := \{y \in \mathbb{R}^n : \theta(x) \geq \theta(x_0) + \langle x - x_0, y\rangle, \forall x \in \mathbb{R}^d\}. \qquad (7)$$

The subdifferential $\partial\theta(x_0)$ generalizes the derivative in the sense that θ is differentiable at x_0 if and only if $\partial\theta(x_0) \equiv \{\bigtriangledown_x\theta(x_0)\}$.

DCA is based on the local optimality conditions of (P_{dc}), namely

$$\partial h(x^*) \cap \partial g(x^*) \neq \emptyset \qquad (8)$$

(such a point x^* is called a *critical point* of $g - h$), and

$$\emptyset \neq \partial h(x^*) \subset \partial g(x^*). \qquad (9)$$

Note that (9) is a necessary local optimality condition for (P_{dc}). For many classes of the DC program, it is also a sufficient optimality condition (see [14], [15]).

The idea of DCA is simple : each iteration l of DCA approximates the concave part $-h$ by its affine majorization (that corresponds to taking $y^l \in \partial h(x^l)$) and minimizes the resulting convex function (that is equivalent to determining a point $x^{l+1} \in \partial g^*(y^l)$).

DCA scheme

Initialization: Let $x^0 \in \mathbb{R}^d$ be a best guess, $0 \leftarrow l$.

Repeat

- Calculate $y^l \in \partial h(x^l)$

– Calculate $x^{l+1} \in \arg\min\{g(x) - h(x^l) - \langle x - x^l, y^l\rangle : x \in \mathbb{R}^d\}$ (P_l)
– $l + 1 \leftarrow l$

Until convergence of $\{x^l\}$.
Note that (P_l) is a convex optimisation problem and in so far "easy" to solve. Convergence properties of DCA and its theoretical basis can be found in ([13], [14], [15], [27]). For instance it is important to mention that

– DCA is a descent method: the sequences $\{g(x^l)-h(x^l)\}$ and $\{h^*(y^l)-g^*(y^l)\}$ are decreasing (*without linesearch*).
– If the optimal value α of problem (P_{dc}) is finite and the infinite sequences $\{x^l\}$ and $\{y^l\}$ are bounded, then every limit point x^* (resp. $\widetilde{y}$) of the sequence $\{x^l\}$ (resp. $\{y^l\}$) is a critical point of $g - h$ (resp. $h^* - g^*$), i.e. $\partial h(x^*) \cap \partial g(x^*) \neq \emptyset$ (resp. $\partial h^*(y^*) \cap \partial g^*(y^*) \neq \emptyset$).
– DCA has a *linear convergence* for DC programs.

For a complete study of DC programming and DCA the reader is referred to [13], [14], [15], [27] and the references therein. The solution of a nonconvex program (P_{dc}) by DCA must be composed of two stages: the search of an *appropriate* DC decomposition of f and that of a *good* initial point. We shall apply *all these DC enhancement features* to solve problem (1) with the help of some equivalent DC program given in the next section.

We note that the convex concave procedure (CCCP) for constructing discrete time dynamical systems mentioned in [33] is nothing else than a special case of DCA. In the last five years DCA has been successfully applied in several studies in Machine Learning e.g., for SVM-based Feature Selection[19], [25], for improving boosting algorithms [12], for implementing-learning [20], [31], [21], for Transductive SVMs [30] and for unsupervised clustering [17], [18].

3.2 DC Reformulation for the MSSC Model (6)

We first remark that, if f is a DC function with DC components G and H then the function $F(U, V) := f(U, V) + tp(U)$ is DC too with DC components G and $H - tp$ (remember that p is concave function). Hence, the natural DC decomposition (2) of f involves the next DC decomposition of F:

$$F(U, V) := G_1(U, V) - [H_1(U, V) - tp(U)]. \tag{10}$$

However, from numerical point of views, the DCA scheme corresponding to this DC decomposition is not interesting because it requires an iterative algorithm for solving a convex program at each iteration. In an elegant way we introduce a nice DC reformulation of the problem (6) for which the resulting DCA is explicitly determined via a very simple formula. Firstly, we determine a ball of radius r and center $0 \in \mathbb{R}^d$ containing necessarily the optimum centers v_i. The necessary first order optimality conditions for (U, V) imply that $\nabla_V F(U, V) = 0$, i.e.,

$$\partial_{v_i} F(U, V) = \sum_{k=1}^{n} u_{i,k} 2(v_i - x_k),\ i = 1, ..., c,\ k = 1, ..., n$$

or $v_i \sum_{k=1}^{n} u_{i,k} = \sum_{k=1}^{n} u_{i,k} x_k$. On the other hand, the condition that cluster should not be empty imposes that $\sum_{k=1}^{n} u_{i,k} > 0$ for $i = 1, ..., c$. Hence

$$\|v_i\|^2 \leq \frac{(\sum_{k=1}^{n} u_{i,k}\|x_k\|)^2}{(\sum_{k=1}^{n} u_{i,k})^2} \leq \sum_{k=1}^{n} \|x_k\|^2 := r^2.$$

Let R_i $(i = 1, ..., c)$ be the Euclidean ball centered at the origin and of radius r in $\mathbb{R}^d$, and let $\mathcal{C} := \Pi_{i=1}^{c} R_i$. We can reformulate the problem (6) as:

$$\min \{F(U, V) : (U, V) \in \Delta \times \mathcal{C}\}. \tag{11}$$

A nice DC decomposition of F is inspired by the following result.

Theorem 1. *There exists $\rho > 0$ such that the function*

$$H(U, V) := \frac{\rho}{2} \|(U, V)\|^2 - f(U, V) \tag{12}$$

is convex on $\Delta \times \mathcal{C}$.

Proof. Let us consider the function $h : \mathbb{R} \times \mathbb{R} \to \mathbb{R}$ defined by

$$h(x, y) = \tfrac{\rho}{2} x^2 + \tfrac{\rho}{2n} y^2 - x^2 y^2. \tag{13}$$

The Hessian of h is given by:

$$J(x, y) = \begin{pmatrix} \rho - 2y^2 & -4xy \\ -4xy & \frac{\rho}{n} - 2x^2 \end{pmatrix}. \tag{14}$$

For all (x, y), $0 \leq x \leq 1, | y | \leq \alpha$, we have for the determinant of $J(x, y)$ (denoted $| J(x, y) |$):

$$\begin{aligned} | J(x, y) | &= \left(\rho - 2y^2\right)\left(\tfrac{\rho}{n} - 2x^2\right) - 16x^2y^2 \\ &= \tfrac{1}{n}\rho^2 - \left[\tfrac{2}{n} y^2 + 2x^2\right] \rho - 16x^2y^2 \\ &\geq \tfrac{1}{n}\rho^2 - \left(\tfrac{2}{n}\alpha^2 + 2\right) \rho - 16\alpha^2 \end{aligned}$$

provided that $\alpha > 0$ and ρ is larger than the upper zero of this quadratic function, i.e., for

$$\rho \geq n \left[\tfrac{1}{n}\, \alpha^2 + 1 + \sqrt{\left[\tfrac{1}{n}\, \alpha^2 + 1\right]^2 + \tfrac{16}{n}\alpha^2}\right]. \tag{15}$$

It is clear that $\rho > 0$. With ρ as large as in (15), the function h is convex on $[0, 1] \times [-\alpha, \alpha]$. Therefore, for $x \to u_{i,k}$ and $y \to \|x_k - v_i\|^2$, the functions

$$\theta_{i,k}(u_{i,k}, v_i) := \frac{\rho}{2}\, u_{i,k}^2 + \frac{\rho}{2n} \|x_k - v_i\|^2 \; - u_{i,k}^2 \|x_k - v_i\|^2$$

are convex on $\{0 \leq u_{i,k} \leq 1, \|v_i\| \leq r\}$ with ρ as in (15) and

$$\alpha = r + \max_{1 \leq k \leq n} \|x_k\| . \tag{16}$$

As a consequence, the function $h_{i,k}$ defined by

$$h_{i,k}(u_{i,k}, v_i) = \theta_{i,k}(u_{i,k}, v_i) + \frac{\rho}{n}\langle x_k, v_i\rangle - \frac{\rho}{2n}\|x_k\|^2$$

is convex on $(u_{i,k}, v_i)$. Finally, since $H(U,V) := \frac{\rho}{2}\|(U,V)\|^2 - f(U,V) = \sum_{k=1}^{n}\sum_{i=1}^{c} h_{i,k}(u_{i,k}, v_i)$, the function $H(U,V)$ is convex on $\Delta \times \mathcal{C}$ with ρ as in (15) and $\alpha = r + \max_{1 \leq k \leq n} \|x_k\|$. ■

In the sequel, the function H is defined with a ρ satisfying the condition (15). According to the proposition above we can express our second DC decomposition of as follows:

$$F(U,V) := G_2(U,V) - H_2(U,V) \tag{17}$$

with

$$G_2(U,V) := \frac{\rho}{2}\|(U,V)\|^2 , \; H_2(U,V) := H(U,V) - tp(U)$$

being clearly convex functions . Now, the optimisation problem (11) can be written as

$$\min\left\{\chi_{\Delta\times\mathcal{C}}(U,V) + \frac{\rho}{2}\|(U,V)\|^2 - H_2(U,V) : (U,V) \in (U,V) \in \mathbb{R}^{c\times n} \times \mathbb{R}^{c\times d}\right\}. \tag{18}$$

3.3 DCA Applied to (18)

For designing a DCA according the general DCA described above, we first need the computation of $(Y^l, Z^l) \in \partial H_2(U^l, V^l)$ and then have to solve the convex program

$$\min\left\{\frac{\rho}{2}\|(U,V)\|^2 - \langle (U,V), (Y^l, Z^l)\rangle : (U,V) \in \Delta \times \mathcal{C}\right\}. \tag{19}$$

The function H_2 is differentiable and its gradient at the point (U^l, V^l) is given by:

$$(Y^l, Z^l) = \nabla H_2(U^l, V^l) \quad \text{where}$$

$$\begin{aligned} Y^l &= \left(\left(\rho u_{i,k}^l - 2u_{i,k}^l\right)\|x_k - V_i^l\|^2 + 2tu_{i,k}^l - t\right)_{i=1,\ldots c}^{k=1,\ldots n}, \\ Z^l &= \left(\rho V_i^l - 2\sum_{k=1}^{n}(V_i^l - x_k)(u_{i,k}^l)^2\right)_{i=1,\ldots c}. \end{aligned} \tag{20}$$

The solution of the auxiliary problem (19) is explicitly computed as (Proj stands for the projection)

$$\left(U^{l+1}\right)^k = \text{Proj}_{\Delta_k}\left(\left(Y^l\right)^k\right) \quad k = 1, ...n, \quad V_i^{l+1} = \text{Proj}_{R_i}\left(\frac{1}{\rho}(Z^l)_i\right) \quad i = 1, ...c. \tag{21}$$

The algorithm can be described as follows. **DCA: DCA Applied to (18)**

Initialization: Choose the memberships U^0 and the cluster centers V^0. Let $\epsilon > 0$ be sufficiently small, $0 \leftarrow l$.
Repeat

- Compute Y^l and Z^l via (20).
- Define (U^{l+1}, V^{l+1}) by setting:

$$\left(U^{l+1}\right)^k = \text{Proj}_{\Delta_k}\left(\left(Y^l\right)^k\right) \text{ for } k = 1, ...n,$$

$$V_i^{l+1} = \text{Proj}_{R_i}\left(\frac{1}{\rho}(Z^l)_i\right) = \begin{cases} \frac{(Z^l)_{i,.}}{\rho} \text{ if } \|(Z^l)_{i,.}\| \leq \rho r \\ \frac{(Z^l)_{i,.}\, r}{\|(Z^l)_i\|} \text{ otherwise} \end{cases}, (i = 1, .., c).$$

- $l + 1 \leftarrow l$

Until $\|(U^{l+1}, V^{l+1}) - (U^l, V^l)\| \leq \epsilon$.

Remark 1. The DC decomposition (17) is interesting because the resulting DCA is simple: each iteration of DCA consists of computations of the projection of points onto a simplex and/or onto a ball, that all are explicitly computed. So DCA do not require an iterative method at each iteration as in the DCA scheme applied to the fist DC decomposition (10).

4 An Interpretation of DCA: Why DCA Is Better than K-Means?

In the MSSC formulation (1) the variable U corresponds to the affectation of objects to clusters while the variable V stands for centers of clusters. The computation of U^{l+1} at iteration l of DCA can be interpreted as the affectation of objects to clusters with centers V_i^l, $i = 1, ..., c$ (that are defined at iteration $l-1$) while the calculation of V^{l+1} is nothing but the determination of the new center of clusters. There are actually some similarities between DCA and the K-means algorithm. However DCA enjoys two main advantages that might explain why DCA is better than K-means.

i) Firstly, the sequence $\{(U^l, V^l)\}$ in DCA is determined in the way that the sequence of objective function of (1), say $\{f(U^l, V^l)\}$ (the cluster cost at iteration l), is decreasing. It means that each iteration of DCA improves certainly the clustering.

ii) Secondly, in DCA U^{l+1} and V^{l+1} are separately but simultaneously computed in the way that U^{l+1} as well as V^{l+1} depend on both U^l and V^l, while K-means determines them alternatively and V^{l+1} depends on U^{l+1}. In other words DCA determines at the same time the clusters and their centers.

5 Numerical Experiments

Our algorithms are coded in C++, and run on a Pentium 2.930GHz of 1024 DDRAM. We have tested our code on 8 real data sets.

• "PAPILLON" is a well known dataset called "jeux de papillon". Several articles on clustering have discussed this dataset (see Revue Modulad - Le Monde Des Utilisateurs de L'Analyse de Données, numéro 11, 1993, 7-44).
• "IRIS" is the classical IRIS dataset which is perhaps the best known dataset found in pattern recognition literature. The dataset consists of 3 classes, 50 instances each and 4 numeric attributes where each class refers to a type of iris plant, namely Iris Setosa, Iris Versicolor, Iris Verginica. The first class is linearly separable from the other ones while that latter ones are not linearly separable. The measurements consist of the sepal and petal lengths and widths in centimeters.
• "GENE" is a Gene Expression dataset containing 384 genes that we get from http://faculty.washington.edu/kayee/cluster/.
• "VOTE" is the Congressional Votes dataset (Congressional Quarterly Almanac, 98th Congress, 2nd session 1984, Volume XL: Congressional Quarterly Inc. Washington, D.C., 1985), it consists of the votes for each of the U.S. House of Representative Congressmen, for 16 key votes, on different subjects (handicap, religion, immigration, army, education, . . .). For each vote, three answers are possible: yes, nay, and unknown. The individuals are separated into two clusters: democrats (267) and republicans (168).
• "ADN" is the ADN dataset (ftp://genbank.bio.net) that consists of 3186 genes, described by 60 DNA sequel elements, called nucleotides or base pairs, with 4 possible modalities (A, C, G or T). These genes are divided into three different clusters: "intron → exon" or ie (sometimes called donors, 767 objects), "exon → intron" or ei (sometimes called acceptors, 765 objects), and "neither", noted as n objects).
• "YEAST" is composed of 2945 genes in the space of 15 dimensions and can be downloaded from http://genomics.stanford.edu.
• "SERUM" is composed of 517 genes in the space of 12 dimensions; the entire dataset is available at http://genome-www.stanford.edu/serum.
• "HUMAN CANCER " is composed of 60 human cancer cell lines in the space of 768 dimensions and is available at http://discover.nci.nih.gov/nature2000/.

We used the following parameters in our code: the exact penalty parameter t is in the interval $[10, 100]$ while the accuracy ϵ is equal to 10^{-6}. The starting point V^0 is randomly chosen in the ball $\mathcal{C}$ and $U^0_{i,k}$ corresponds to the assignment of the point x_k to closest cluster center v^0_i.

In Tables 1 we present the comparative numerical results provided by our algorithms and K-means which is available on the web site: http://www.fas.umonteral.ca/biol/legendre/. Here "iter"denotes the number of iterations. All CPU are computed in seconds.

Table 1. Comparative results between **DCA** and **K-means**. PWPO (in the first five problems where the clustering is known a priori) means the percentage of the well placed objects. J_c (in the last three problems) denotes the so termed "cluster cost", say $J_c := \sum_{i=1..n} \min_{k=1..c} \|x_i - v_k\|^2$.

Real Data				K-means			DCA		
	n	p	c	iter	CPU	PWPO / J_c	iter	CPU	PWPO / J_c
PAPILLON	23	4	5	3	0.01	97%	10	0.002	100%
IRIS	150	4	3	4	0.81	92%	5	0.01	99.33%
GENE	384	17	5	24	0.73	75%	8	0.20	91.55%
VOTE	435	16	2	4	0.03	82%	3	0.01	98.34%
ADN	3186	60	3	15	1.95	79%	8	0.62	94.52
YEAST	2945	15	16	156	6.36	43424.88	28	7.81	43032.01
SERUM	517	12	8	120	50.98	6199.56	39	4.50	6009.37
HUMAN CANCER	768	60	9	118	44.3	139696.02	65	16.03	129622.05

From the numerical experiments we observe that

- **DCA** is better than **K-means** in both the running-time and quality of solutions.
- DCA is efficient for all datasets: for PAPILLON dataset, DCA gives exactly the right clustering; for IRIS dataset only one element is misclassified; likewise, for all other datasets the percentage of well placed objects is large.

6 Conclusion

We have proposed, for solving the MSSC problem a new and efficient approach based on DC programming and DCA. The hard combinatorial optimization MSSC model has been recast as a DC program in its elegant matrix formulation and with a nice DC decomposition, in order to make simpler and so much less expensive the computations in the resulting DCA. It fortunately turns out that the corresponding DCA consists in computing, at each iteration, the projection of points onto a simplex and/or a ball, that all are given in the explicit form. Preliminary numerical experiments on real world database show the efficiency and the superiority of DCA with respect to the K-means. Moreover it is possible to better still improve the DCA (on both the quality of solution and time consuming) by investigating efficient procedures to get a good starting point for DCA. On the other hand, DCA may be interesting for a kernelized version of MSSC model. Works in these directions are in progress.

References

1. Aloise, D., Deshpande, A., Hansen, P., Popat, P.: Np-hardness of Euclidean Sum-of-squares Clustering, Cahiers du GERAD, G-2008-33 (2008)
2. Arora, S., Kannan, R.: Learning Mixtures of Arbitrary Gaussians. In: Proceedings of the 33rd Annual ACM Symposium on Theory of Computing, pp. 247–257 (2001)

3. Bradley, B.S., Mangasarian, O.L.: Feature Selection via Concave Minimization and Support Vector Machines. In: Shavlik, J. (ed.) Machine Learning Proceedings of the Fifteenth International Conferences (ICML 1998), pp. 82–90. MorganKaufmann, San Francisco (1998)
4. Brusco, M.J.: A Repetitive Branch-and-bound Procedure for Minimum Within-cluster Sum of Squares Partitioning. Psychometrika 71, 347–363 (2006)
5. Dhilon, I.S., Korgan, J., Nicholas, C.: Feature Selection and Document Clustering. In: Berry, M.W. (ed.) A Comprehensive Survey of Text Mining, pp. 73–100. Springer, Heidelberg (2003)
6. Duda, R.O., Hart, P.E.: Pattern classification and Scene Analysis. Wiley, Chichester (1972)
7. Feder, T., Greene, D.: Optimal Algorithms for Approximate Clustering. In: Proc. STOC (1988)
8. Fisher, D.: Knowledge Acquisition via Incremental Conceptual Clustering. Machine Learning 2, 139–172 (1987)
9. Forgy, E.: Cluster Analysis of Multivariate Date: Efficiency vs. Interpretability of Classifications. Biometrics, 21–768 (1965)
10. Jancey, R.C., Botany, J.: Multidimensional Group Analysis. Australian, 14–127 (1966)
11. Jain, A.K., Murty, M.N., Flynn, P.J.: Data Clustering: a Review. ACM Comput. Surv. 31(3), 264–323 (1999)
12. Krause, N., Singer, Y.: Leveraging the Margin More Carefully. In: International Conference on Machine Learning ICML (2004)
13. Le, T.H.A.: Contribution à l'optimisation non convexe et l'optimisation globale: Théorie, Algoritmes et Applications, Habilitation à Diriger des Recherches, Université de Rouen (1997)
14. Le, T.H.A., Pham, D.T.: Solving a Class of Linearly Constrained Indefinite Quadratic Problems by DC Algorithms. Journal of Global Optimization 11, 253–285 (1997)
15. Le, T.H.A., Pham, D.T.: The DC (Difference of Convex Functions) Programming and DCA Revisited with DC Models of Real World Nonconvex Optimization Problems. Annals of Operations Research 133, 23–46 (2005)
16. Le, T.H.A., Pham, D.T., Huynh, V.: Ngai, Exact penalty in DC Programming, Technical Report. LMI, INSA-Rouen (2005)
17. Le, T.H.A., Belghiti, T., Pham, D.T.: A New Efficient Algorithm Based on DC Programming and DCA for Clustering. Journal of Global Optimization 37, 593–608 (2007)
18. Le, T.H.A., Le, H.M., Pham, D.T.: Optimization Based DC Programming and DCA for Hierarchical Clustering. European Journal of Operational Research (2006)
19. Le, T.H.A., Le, H.M., Nguyen, V.V., Pham, D.T.: A DC Programming Approach for Feature Selection in Support Vector Machines Learning. Journal of Advances in Data Analysis and Classification 2, 259–278 (2008)
20. Liu, Y., Shen, X., Doss, H.: Multicategory ψ-Learning and Support Vector Machine: Computational Tools. Journal of Computational and Graphical Statistics 14, 219–236 (2005)
21. Liu, Y., Shen, X.: Multicategoryψ -Learning. Journal of the American Statistical Association 101, 500–509 (2006)
22. Mangasarian, O.L.: Mathematical Programming in Data Mining. Data Mining and Knowledge Discovery 1, 183–201 (1997)

23. MacQueen, J.B.: Some Methods for Classification and Analysis of Multivariate Observations. In: Proceedings of 5-th Berkeley Symposium on Mathematical Statistics and Probability, vol. 1, pp. 281–297. University of California Press, Berkeley (1967)
24. Merle, O.D., Hansen, P., Jaumard, B., Mladenovi'c, N.: An Interior Point Algorithm for Minimum Sum of Squares Clustering. SIAM J. Sci. Comput. 21, 1485–1505 (2000)
25. Neumann, J., Schnörr, C., Steidl, G.: SVM-based feature selection by direct objective minimisation. In: Rasmussen, C.E., Bülthoff, H.H., Schölkopf, B., Giese, M.A. (eds.) DAGM 2004. LNCS, vol. 3175, pp. 212–219. Springer, Heidelberg (2004)
26. Peng, J., Xiay, Y.: A Cutting Algorithm for the Minimum Sum-of-Squared Error Clustering. In: Proceedings of the SIAM International Data Mining Conference (2005)
27. Pham, D.T., Le, T.H.A.: DC Optimization Algorithms for Solving the Trust Region Subproblem. SIAM J. Optimization 8, 476–505 (1998)
28. Hansen, P., Jaumard, B.: Cluster analysis and mathematical programming. Mathematical Programming 79, 191–215 (1997)
29. Hartigan, J.A.: Clustering Algorithms. Wiley, New York (1975)
30. Ronan, C., Fabian, S., Jason, W., Léon, B.: Trading Convexity for Scalability. In: International Conference on Machine Learning ICML (2006)
31. Shen, X., Tseng, G.C., Zhang, X., Wong, W.H.: ψ -Learning. Journal of American Statistical Association 98, 724–734 (2003)
32. Sherali, H.D., Desai, J.: A global Optimization RLT-based Approach for Solving the Hard Clustering Problem. Journal of Global Optimization 32, 281–306 (2005)
33. Yuille, A.L., Rangarajan, A.: The Convex Concave Procedure (CCCP). In: Advances in Neural Information Processing System, vol. 14. MIT Press, Cambrige (2002)

An Effective Hybrid Algorithm Based on Simplex Search and Differential Evolution for Global Optimization

Ye Xu, Ling Wang, and Lingpo Li

Tsinghua National Laboratory for Information Science and Technology (TNList),
Department of Automation, Tsinghua University, Beijing, 100084, P.R. China
{xuye05,llp03}@mails.tsinghua.edu.cn,
wangling@mail.tsinghua.edu.cn

Abstract. In this paper, an effective hybrid NM-DE algorithm is proposed for global optimization by merging the searching mechanisms of Nelder-Mead (NM) simplex method and differential evolution (DE). First a reasonable framework is proposed to hybridize the NM simplex-based geometric search and the DE-based evolutionary search. Second, the NM simplex search is modified to further improve the quality of solutions obtained by DE. By interactively using these two searching approaches with different mechanisms, the searching behavior can be enriched and the exploration and exploitation abilities can be well balanced. Based on a set of benchmark functions, numerical simulation and statistical comparison are carried out. The comparative results show that the proposed hybrid algorithm outperforms some existing algorithms including hybrid DE and hybrid NM algorithms in terms of solution quality, convergence rate and robustness.

Keywords: global optimization, Nelder-Mead simplex search, differential evolution, hybrid algorithm.

1 Introduction

Global optimization has always gained extensive research and applications in science and a variety of engineering fields [1]. During the past two decades, evolutionary computation has been a hot topic in the fields of Operations Research and Computer Science and has been a kind of promising tool for global optimization. As a comparatively new optimization algorithm, Differential evolution (DE) is with less control parameters than other evolutionary algorithms like Genetic Algorithm (GA) [2], [3], [4]. DE performs its search process under the instruction of swarm intelligence produced by cooperation and competition between individual vectors in the species. Also, the specific memory ability of DE makes it possible to track the current search situation dynamically to adjust the search strategy. Although having some advantages in finding global optimum, the local search ability of DE is weak and sometimes the searching process of DE may be trapped in local minima [5]. As a direct search method, Nelder-Mead simplex search method [6] is easy to implement and has been widely applied to unconstrained optimization problems with low dimensions.

D.-S. Huang et al. (Eds.): ICIC 2009, LNAI 5755, pp. 341–350, 2009.

However, it has been shown that the performance of NM simplex search depends on the initial simplex and especially it is difficult to achieve good results for multi-dimensional problems [7], [8].

Recently, Memetic algorithms that reasonably combine evolutionary algorithms with local search have shown good performances for both combinatorial optimization and numerical optimization. In this paper, the NM simplex-based geometric search and the DE-based evolutionary search are hybridized within a reasonable framework. In particular, the NM simplex search is modified and incorporated into DE to enhance and to balance the exploration and exploitation abilities. By merging these two approaches with different searching mechanisms, the hybrid algorithm is of good performances in terms of solution quality, convergence rate and robustness. Numerical simulation and statistical comparison are carried out based on a set of benchmarks, which verifies the superiority of the proposed hybrid algorithm.

The remainder of the paper is organized as follows: DE and NM simplex methods are briefly introduced in Section 2. In Section 3, the NM-DE hybrid algorithm is proposed. Computational results and comparisons are provided in Section 4. Finally, we end the paper with some conclusions in Section 5.

2 Introduction to DE and NM Simplex Method

2.1 Problem Statement

Generally, an unconstrained optimization problem is formulated as follows [9]:

$$\min \quad f(X),\ X=[x_1,...,x_n],\ \ s.t. \quad x_j \in [a_j,b_j],\ j=1,2,...,n\ , \tag{1}$$

where f is the objective function, and X is the decision vector consisting of n variables, and a_j and b_j are the lower and upper bounds for each decision variable, respectively.

2.2 Differential Evolution

Differential Evolution is a population-based stochastic optimization technique [10]. According to the comprehensive study in [11], DE outperforms many other optimization methods like GA in terms of convergence speed and robustness over some benchmark problems and real-world applications. While DE shares some similarities with other evolutionary algorithms, it differs significantly in the sense that distance and direction information from the current population is used to guide the search process [12]. The DE denoted as $DE/rand/1/bin$ is adopted in this paper, whose searching power is accredited to parent choice (selection), differential operator (mutation), discrete crossover (crossover) and greedy selection (decision) [13].

Selection: All the individuals in the population have the same chance to generate candidate individuals. For each individual X_i, three other individuals are randomly selected from current population such that the four individuals are different from each other. Thus, a pool of four parents is formed.

Mutation: A mutated individual V_i is generated with the three individuals randomly chosen by Selection as follows:

$$V_i = X_{r1} + F(X_{r2} - X_{r3}) \quad , \tag{2}$$

where $r1, r2, r3 (r1 \neq r2 \neq r3 \neq i)$ are three distinct indexes randomly selected, F is a positive real number that is usually less than 1.0.

Crossover: A trial individual T_i is formed by recombination of the elements of X_i and V_i one by one as follows:

$$t_{i,j} = \begin{cases} v_{i,j} & if\ r \leq cr\ or\ j = sn \\ x_{i,j} & otherwise \end{cases} \quad j = 1, \ldots, n \quad , \tag{3}$$

where $t_{i,j}$ is the j th element of the trial individual T_i, r is a uniformly random number between 0 and 1, cr is a real number between 0 and 1 to control the ratio of selection between of the parent and mutated vector, and sn is an index randomly chosen to ensure that at least one element of V_i will be inherited.

Decision: Greedy selection between the trial vector T_i and X_i is applied and the one with better function value f_i will be promoted to the next generation.

The procedure of the DE is illustrated in Fig. 1.

```
Step 1: Initialize the population randomly and find the
     best individual X^best;
Step 2: For each individual X_i in the population:
     Step 2.1: Randomly selected three indexes r1, r2, r3;
     Step 2.2: Get the mutation vector V_i by Eqn. (2);
     Step 2.3: Get trial vector T_i by Eqn. (3);
     Step 2.4: Greedy selection between T_i and X_i.
Step 3: Go back to Step 2 if the stopping criterion is
     not satisfied, else stop.
```

Fig. 1. Procedure of DE

2.3 The Nelder-Mead Simplex Search Method

The Nelder-Mead simplex search method is a direct search method designed for unconstrained optimization without using gradient information [14]. The procedure of this method is to rescale the simplex based on the local behavior by using four basic operators: reflection, expansion, contraction and shrink. With these operators, the simplex can successfully improve itself and get closer to the optimum. The original NM simplex procedure is outlined in Fig. 2, where all the steps are described as follows.

```
Step 1: Randomly Initialize n+1 individuals, and order
        them s.t. f(X_1) ≤ f(X_2) ... ≤ f(X_{n+1});
Step 2: Calculate the reflection point X_r;
        If f(X_1) ≤ f(X_r) < f(X_n), accept X_r and terminate;
        If f(X_r) < f(X_1), go to Step 3;
        If f(X_r) ≥ f(X_n), go to Step 4;
Step 3: generate X_e;
        If f(X_e) ≤ f(X_r), accept X_e and terminate;
          If f(X_e) > f(X_r), accept X_r and terminate;
Step 4: If f(X_r) < f(X_{n+1}), generate X_c;
           If f(X_c) ≤ f(X_r), accept X_c and terminate;
           Else, go to Step 5;
        If f(X_r) ≥ f(X_{n+1}), generate X_c;
             If f(X_c) ≤ f(X_{n+1}), accept X_c and terminate;
           Else, go to Step 5;
Step 5: For each individual i except 1 in population:
        evaluate V_i = X_1 + δ(X_i - X_1) and set X = V;
```

Fig. 2. Procedure of NM simplex method

Initialization: To minimize a function with n variables, create n+1 vertex points randomly to form an initial n-dimensional simplex. Evaluate the function value at each vertex point and order the n+1 vertices to satisfy $f(X_1) \le f(X_2) \ldots \le f(X_{n+1})$.

Reflection: Calculate the reflection point X_r as follows:

$$X_r = \bar{X} + \alpha(\bar{X} - X_{n+1}) \ , \tag{4}$$

where $\bar{X} = \sum_{i=1}^{n} X_i / n$ is the centroid of the n best points (all vertices except for X_{n+1}), and α (α >0) is the reflection coefficient. If $f(X_1) \le f(X_r) < f(X_n)$, then accept the reflected point X_r and terminate the iteration.

Expansion: If $f(X_r) < f(X_1)$, then calculate the expansion point as follows:

$$X_e = \bar{X} + \beta(X_r - \bar{X}) \ , \tag{5}$$

where β (β >1) is the expansion coefficient. If $f(X_e) \le f(X_r)$, then accept the expanded point X_e and terminate the iteration; otherwise accept X_r and terminate the iteration.

Contraction: If $f(X_r) \ge f(X_n)$, then perform a contraction between $\bar{X}$ and the better of X_{n+1} and X_r.

(a) If $f(X_r) < f(X_{n+1})$, then perform outside contraction:

$$X_c = \overline{X} + \gamma(X_r - \overline{X}) \quad , \tag{6}$$

where γ ($1>\gamma>0$) is the contraction coefficient. If $f(X_c) \le f(X_r)$, then accept X_c and terminate the iteration; otherwise go to Shrink step.

(b) If $f(X_r) \ge f(X_{n+1})$, then perform inside contraction:

$$X_c = \overline{X} - \gamma(\overline{X} - X_{n+1}) \quad . \tag{7}$$

If $f(X_c) \le f(X_{n+1})$, then accept X_c and terminate the iteration; otherwise go to Shrink step.

Shrink: Shrink operator is performed as follows:

$$V_i = X_1 + \delta(X_i - X_1) \quad , \quad i = 2, \ldots, n+1 \ , \tag{8}$$

where δ ($1>\delta>0$) is the shrinkage coefficient. The simplex obtained by shrink is denoted as $V = \{X_1, V_1, V_2, ..., V_{n+1}\}$ for the next iteration.

3 Hybrid NM-DE Algorithm

To fuse the searching behaviors of the NM and DE methods, we propose a hybrid search framework illustrated in Fig. 3. It can be seen from Fig. 3 that NM simplex search and DE-based evolutionary search are hybridized. During each generation, the population will be improved both by differential evolution and simplex search. The information of the best individuals is well used to guide the local search of the algorithm. Thus, the advantages of these two methods could be utilized together. Moreover, the classic NM simplex search is modified, which is used to guide the search towards promising region, which can enhance the local search ability.

Suppose the population size is *P*, the initial *P* points are randomly generated from the *n*-dimensional space. First, the *P* individuals are ranked from best to worse according to the objective values. Then, the top *Q* individuals are used to calculate the initial simplex centroid for the NM method. For the left *P*-*Q* individuals, each will perform an iteration of simplex search with the calculated centroid:

$$\overline{X} = \sum_{i=1}^{Q} X_i / Q \quad . \tag{9}$$

When dealing with the shrink step, just shrink the single point to the best point until it reaches a better objective value while keeping the positions of the other points fixed instead of shrinking all simplex points as original NM simplex method does. For example, for the point X_j, generate the shrink point as follows:

$$V_j = X_1 + \delta(X_j - X_1) \quad . \tag{10}$$

If $f(V_j) \le f(X_j)$, then accept V_j, otherwise, keep on shrinking operation until the termination condition is satisfied.

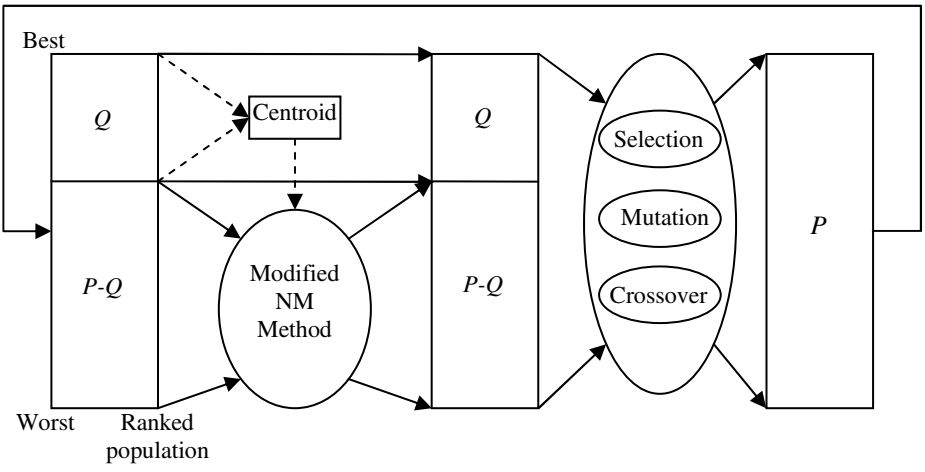

Fig. 3. Schematic representation of the NM-DE hybrid algorithm

After performing the modified NM simplex search method, P-Q new individuals are generated. Then the P-Q new individuals and the original Q individuals from the initial population are merged to form the initial population of DE-based evolutionary search. Via a generation of DE-based search, P new individuals are generated. After ranking these new individuals, the modified NM simplex search is performed once again. The above interactive search process based on simplex search and DE based search is repeated until a predefined stopping criterion is satisfied.

By combining the NM simplex search and DE search, the exploration and exploitation searching abilities could be enhanced and balanced, which may result in a more effective optimization algorithm for global optimization.

4 Numerical Simulation and Comparisons

4.1 Experiment Setup

In this section, the proposed hybrid algorithm is tested based on ten benchmarks [13] as shown in Table.1. These benchmarks are widely used to test and compare the performances of newly designed optimization algorithms. Moreover, to compare our algorithm with hybrid DE and hybrid NM methods, we compare NM-DE with the recent hybrid DEahcSPX algorithm and DE in [13] and NM-PSO in [6]. For the NM-DE algorithm, we set F=0.7, Cr=0.2, α=1, β=1.5, γ=0.5, δ=0.5, Q=n. As for the stopping criterion, we set the maximum number of function evaluations as 10000*n, which is the same as that in [13]. The experiments were carried out on Intel Pentium Processor 1600MHZ and 2GB-RAM in Visual Studio 2005 environment. For each problem, the NM-DE is independently run 50 times.

In addition, an accuracy level is set as 1e-6 for all the functions. That is, a test is viewed as a successful run if the derivation between the obtained function value by the algorithm and the theoretical optimal value is less than the level.

Table 1. Test testing functions [13]

Function number	Function name	Optimal OBJ value
1	Sphere Function	0
2	Rosenbrock's Function	0
3	Ackley's Function	0
4	Griewank's Function	0
5	Rastrigin's Function	0
6	Generalized Schwefel's Problem 2.26	0
7	Salomon's Function	0
8	Whitely's Function	0
9	Generalized Penalized Function 1	0
10	Generalized Penalized Function 2	0

4.2 Simulation Results and Comparisons

Firstly, we compare the NM-DE (P=2n) with DE and the hybrid DEahcSPX.

For all the testing problems with 30 dimensions, the resulted average function values and variance values of DE, DEahcSPX and NM-DE are listed in Table 2. In addition, the average evaluation times and the time of successful run (data in the bracket) of these algorithms are summarized in Table 3.

Table 2. Comparison of DE, DEahcSPX, NM-DE (n =30)

Function no.	DE [13]	DEahcSPX [13]	NM-DE
1	5.73E-17±2.03E-16	1.75E-31±4.99E-31	**4.05E-299±0.00E+00**
2	5.20E+01±8.56E+01	4.52E+00±1.55E+01	9.34E+00±9.44E+00
3	1.37E-09±1.32E-09	**2.66E-15±0.00E+00**	8.47E-15±2.45E-15
4	2.66E-03±5.73E-03	2.07E-03±5.89E-03	**8.87E-04±6.73E-03**
5	2.55E+01±8.14E+00	2.14E+01±1.23E+01	**1.41E+01±5.58E+00**
6	4.90E+02±2.34E+02	4.70E+02±2.96E+02	3.65E+03±7.74E+02
7	2.52E-01±4.78E-02	**1.80E-01±4.08E-02**	1.11E+00±1.91E-01
8	3.10E+02±1.07E+02	3.06E+02±1.10E+02	**4.18E+02±7.06E+01**
9	4.56E-02±1.31E-01	2.07E-02±8.46E-02	**8.29E-03±2.84E-02**
10	1.44E-01±7.19E-01	**1.71E-31±5.35E-31**	2.19E-04±1.55E-03

From Table 2, it can be seen that for most problems NM-DE outperforms DE and DEahcSPX in terms of average value and variance. So, it is concluded that the proposed NM-DE is of better searching quality and robustness.

Table 3. Comparison of DE, DEahcSPX, NM-DE in terms of average evaluation times and time of successful runs

Fun. no.	DE [13]	DEahcSPX [13]	NM-DE
1	148650.8 (50)	87027.4 (50)	**8539.4 (50)**
2	-	299913.0 (2)	**74124.9 (40)**

Table 3. (*continued*)

Fun. no.	DE [13]	DEahcSPX [13]	NM-DE
3	215456.1 (50)	129211.6 (50)	**13574.7 (29)**
4	190292.5 (38)	121579.2 (43)	**9270.2 (36)**
9	160955.2 (43)	96149.0 (46)	**7634.3 (44)**
10	156016.9 (48)	156016.9 (48)	**7996.1 (42)**

From Table 3, it can be found that the NM-DE costs much less computational effort than DE and DEahcSPX while the time of successful run of NM-DE is close to that of DEahcSPX. So, it is concluded that NM-DE is more efficient than the comparative algorithms.

Secondly, we compare NM-DE with NM-PSO [6] that combines the NM simplex search with particle swarm optimization (PSO). Since only three high-dimensional functions were used to test NM-PSO in [6], here we compare our NM-DE with NM-PSO by using those problems. The population size is set $3n+1$ as the same as that in [6]. The results are summarized in Table 4. From the table it can be clearly seen that the average performance NM-DE is superior to that of NM-PSO. Comparing with the pure PSO and NM methods, our NM-DE is of much better performance.

Table 4. Comparison of NM, PSO, NM-PSO, NM-DE

Function no.	Dimension	NM [6]	PSO [6]	NM-PSO [6]	NM-DE
2	10	2.429e-8	1013.251	3.378e-9	**9.783e-21**
1	30	726.704	4824.621	2.763e-11	**4.516e-155**
4	50	1.230	6.575	9.969e-12	**1.184e-16**

Finally, we test the effect of population size on the performance of algorithms with the fixed total evaluation times (300000). From Table 5, it can be seen that with the growth of the population size, the performances of DE and DEahcSPX gradually get worse while the population size has little effect on the performance of NM-DE. That is, our NM-DE is much robust on population size. All in all, the proposed hybrid algorithm is a potentially powerful tool for global optimization.

Table 5. Comparison of DE, DEahcSPX, NM-DE with different population size

	PopSize=50		
Fun. no.	DE [13]	DEahcSPX [13]	NM-DE
1	2.31E-02±1.92E-02	6.03E-09±6.86E-09	**8.46E-307±0.00E+00**
2	3.07E+02±4.81E+02	4.98E+01±6.22E+01	**2.34E+00±1.06E+01**
3	3.60E-02±1.82E-02	1.89E-05±1.19E-05	**8.26E-15±2.03E-15**
4	5.00E-02±6.40E-02	1.68E-03±4.25E-03	2.12E-03±5.05E-03
5	5.91E+01±2.65E+01	2.77E+01±1.31E+01	**1.54E+01±4.46E+00**
6	7.68E+02±8.94E+02	**2.51E+02±1.79E+02**	3.43E+03±6.65E+02
7	8.72E-01±1.59E-01	**2.44E-01±5.06E-02**	1.16E+00±2.36E-01
8	8.65E+02±1.96E+02	4.58E+02±7.56E+01	**3.86E+02±8.39E+01**

Table 5. (*continued*)

		PopSize=50	
9	2.95E-04±1.82E-04	1.12E-09±2.98E-09	**4.48E-28±1.64E-31**
10	9.03E-03±2.03E-02	**4.39E-04±2.20E-03**	6.59E-04±2.64E-03
		PopSize=100	
Fun. no.	DE [13]	DEahcSPX [13]	NM-DE
1	3.75E+03±1.14E+03	3.11E+01±1.88E+01	**1.58E-213±0.00E+00**
2	4.03E+08±2.59E+08	1.89E+05±1.47E+05	**2.06E+01±1.47E+01**
3	1.36E+01±1.48E+00	3.23E+00±5.41E-01	**8.12E-15±1.50E-15**
4	3.75E+01±1.26E+01	1.29E+00±1.74E-01	**3.45E-04±1.73E-03**
5	2.63E+02±2.79E+01	1.64E+02±2.16E+01	**1.24E+01±5.80E+00**
6	6.56E+03±4.25E+02	6.30E+03±4.80E+02	3.43E+03±6.65E+02
7	5.97E+00±6.54E-01	1.20E+00±2.12E-01	**8.30E-01±1.27E-01**
8	1.29E+14±1.60E+14	3.16E+08±4.48E+08	**4.34E+02±5.72E+01**
9	6.94E+04±1.58E+05	2.62E+00±1.31E+00	**6.22E-03±2.49E-02**
10	6.60E+05±7.66E+05	4.85E+00±1.59E+00	**6.60E-04±2.64E-03**
		PopSize=200	
Fun. no.	DE [13]	DEahcSPX [13]	NM-DE
1	4.01E+04±6.26E+03	1.10E+03±2.98E+02	**5.05E-121±2.44E-120**
2	1.53E+10±4.32E+09	1.49E+07±7.82E+06	**2.04E+01±8.49E+00**
3	2.02E+01±2.20E-01	9.11E+00±7.81E-01	**7.83E-15±1.41E-15**
4	3.73E+02±6.03E+01	1.08E+01±2.02E+00	**3.45E-04±1.73E-03**
5	3.62E+02±2.12E+01	2.05E+02±1.85E+01	**1.23E+01±6.05E+00**
6	6.88E+03±2.55E+02	6.72E+03±3.24E+02	4.61E+03±6.73E+02
7	1.34E+01±8.41E-01	3.25E+00±4.55E-01	**6.36E-01±9.85E-02**
8	2.29E+16±1.16E+16	5.47E+10±6.17E+10	**4.16E+02±5.40E+01**
9	2.44E+07±7.58E+06	9.10E+00±2.42E+00	**4.48E-28±1.55E-31**
10	8.19E+07±1.99E+07	6.18E+01±6.30E+01	**4.29E-28±2.59E-31**
		PopSize=300	
Fun. no.	DE [13]	DEahcSPX [13]	NM-DE
1	1.96E+04±2.00E+03	6.93E+02±1.34E+02	**5.55E-86±7.59E-86**
2	3.97E+09±8.92E+08	5.35E+06±2.82E+06	**2.25E+01±1.16E+01**
3	1.79E+01±3.51E-09	7.23E+00±4.50E-01	**7.19E-15±1.48E-15**
4	1.79E+02±1.60E+01	7.26E+00±1.74E+00	**6.40E-04±3.18E-03**
5	2.75E+02±1.27E+01	2.03E+02±1.49E+01	**1.30E+01±7.48E+00**
6	6.87E+03±2.72E+02	6.80E+03±3.37E+02	4.41E+03±6.41E+02
7	1.52E+01±5.43E-01	3.59E+00±4.54E-01	**5.32E-01±8.19E-02**
8	2.96E+16±1.09E+16	1.83E+11±1.72E+11	**4.28E+02±5.47E+01**
9	3.71E+07±1.29E+07	1.09E+01±3.76E+00	**4.48E-28±1.64E-31**
10	1.03E+08±1.87E+07	3.42E+02±4.11E+02	**4.29E-28±5.44E-43**

5 Conclusion

In this paper, NM simplex method and DE were reasonably hybridized for global optimization. With the local search via the modified NM method and the evolutionary search via DE, NM-DE algorithms got better results than some existing hybrid DE and hybrid NM algorithms in terms of searching quality, convergence rate and robustness. The future work is to develop the hybrid algorithm with adaptive mechanism and to apply the algorithm to some engineering problems.

Acknowledgments

This research is partially supported by National Science Foundation of China (Grant No. 60774082, 70871065, 60834004) and the National 863 Program under the grant number 2007AA04Z155 as well as the Project-sponsored by SRF for ROCS, SEM.

References

1. Nash, S.G., Sofer, A.: Linear and Nonlinear Programming. McGraw-Hill, New York (1996)
2. Huang, F.Z., Wang, L.: A Hybrid Differential Evolution with Double Populations for Constrained Optimization. In: IEEE CEC, pp. 18–25. IEEE Press, New York (2008)
3. Price, K., Storn, R.M., Lampinen, J.A.: Differential Evolution: A Practical Approach to Global Optimization. Springer, New York (2005)
4. Rahman, S., Tizhoosh, H.R., Salama, M.M.A.: Opposition-Based Differential Evolution. IEEE Transactions on Evolutionary Computation 12(1), 64–79 (2008)
5. Isaacs, A., Ray, T., Smith, W.: A Hybrid Evolutionary Algorithm with Simplex Local Search. In: IEEE CEC, pp. 1701–1708. IEEE Press, New York (2007)
6. Fan, S.K.S., Zahara, E.: A Hybrid Simplex Search and Particle Swarm Optimization for Unconstrained Optimization. European J. Operational Research 181, 527–548 (2007)
7. Nelder, J.A., Mead, R.: A Simplex Method for Function Minimization. Computer J. 7(4), 308–313 (1965)
8. Lagarias, J.C., Reeds, J.A., Wright, M.H., Wright, P.E.: Convergence Properties of the Nelder-Mead Simplex Method in Low Dimensions. SIAM J. Optimization 9(1), 112–147 (1999)
9. Ali, M.M.: Differential Evolution With Preferential Crossover. European J. Operational Research 181, 1137–1147 (2007)
10. Storn, R., Price, K.: Differential Evolution - A Simple and Efficient Heuristic for Global Optimization Over Continuous Spaces. J. Global Optimization 11(4), 341–359 (1997)
11. Czajkowski, K., Fitzgerald, S., Foster, I., Kesselman, C.: Real-Parameter Optimization with Differential Evolution. Evolutionary Computation 2(1), 506–513 (2005)
12. Omran, M.G.H., Engelbrecht, A.P., Salman, A.: Bare Bones Differential Evolution. European J. Operational Research 196(1), 128–139 (2009)
13. Noman, N., Iba, H.: Accelerating Differential Evolution Using an Adaptive Local Search. IEEE Transactions on Evolutionary Computation 12(1), 107–125 (2008)
14. Cohen, G., Ruch, P., Hilario, M.: Model Selection for Support Vector Classifiers via Direct Simplex Search. In: FLAIRS Conference, Florida, pp. 431–435 (2005)

Differential Evolution with Level Comparison for Constrained Optimization

Ling-po Li, Ling Wang, and Ye Xu

Tsinghua National Laboratory for Information Science and Technology (TNList),
Department of Automation, Tsinghua University, Beijing, 100084, P.R. China
{llp03,xuye05}@mails.tsinghua.edu.cn, wangling@tsinghua.edu.cn

Abstract. The effectiveness of a constrained optimization algorithm depends on both the searching technique and the way to handle constraints. In this paper, a differential evolution (DE) with level comparison is put forward to solve the constrained optimization problems. In particular, the α (comparison level) constrained method is adopted to handle constraints, while the DE-based evolutionary search is used to find promising solutions in the search space. In addition, the scale factor of the DE mutation is set to be a random number to vary the searching scale, and a certain percentage of population is replaced with random individuals to enrich the diversity of population and to avoid being trapped at local minima. Moreover, we let the level increase exponentially along with the searching process to stress feasibility of solution at later searching stage. Experiments and comparisons based on the 13 well-known benchmarks demonstrate that the proposed algorithm outperforms or is competitive to some typical state-of-art algorithms in terms of the quality and efficiency.

Keywords: differential evolution, level comparison, constrained optimization.

1 Introduction

Generally speaking, a constrained optimization problem is described as follows:

$$\begin{aligned} &\text{Find } X \text{ to minimize } f(X) \\ &\text{Subject to: } g_i(X) \le 0 \quad i = 1,2,\ldots,m, \\ &h_j(X) = 0 \quad j = 1,2,\ldots,q, \\ &l_k \le x_k \le u_k \quad k = 1,2,\ldots,d \ , \end{aligned} \tag{1}$$

where $X = [x_1, x_2, \ldots, x_d]^T$ denotes a d-dimensional solution vector, m denotes the number of inequality constraints, and p denotes the number of equality constraints, and u_k and l_k are the upper bound and the lower bound of x_k, respectively.

During the past two decades, much attention has been attracted to solve constrained optimization problems via evolutionary algorithms (EAs) [1], [2]. For constrained optimization, it is known that the balance of searching between the objective and constraints greatly affects the effectiveness of the algorithm. However, there is no

D.-S. Huang et al. (Eds.): ICIC 2009, LNAI 5755, pp. 351–360, 2009.

any theoretical metric criterion on this subject. Numerous methods have been proposed for handling constraints, such as adaptive penalty approach based on genetic algorithm (GA) [3], co-evolutionary particle swarm optimization (PSO) [4], multi-objective optimization [5], comparison criteria [6], stochastic-rank (SR) based method [7], and α constrained method [8].

As a population based EA, Differential evolution (DE) [9] is of simple concept, easy implementation and quick convergence. So far, DE has been successfully applied to a variety of unconstrained optimization problems and real world applications, such as filter design [10], production scheduling [11]. Since the work by Lampinen [12], DE has gained increasing attention in the field of constrained optimization [13], [14], [15]. In this paper, a DE with level comparison is put forward for constrained problems. In particular, the α constrained method is adopted to handle constraints, while DE is used to perform evolutionary search in the search space. In addition, some modifications are made to DE to enhance global searching ability and to enrich the diversity of population. Moreover, we set the level varying with the searching process to stress the feasibility of solutions to different extent. Experiments and comparisons based on the 13 well-known benchmarks are carried out, and the results demonstrate that the proposed algorithm outperforms or is competitive to some effective state-of-art algorithms in terms of the quality and efficiency.

The remaining content is organized as follows. The DE and the α constrained method are briefly introduced in Section 2 and Section 3, respectively. In Section 4, the DE with level comparison is proposed. Simulation results and comparisons are presented in Section 5. Finally, we conclude the paper in Section 6.

2 Differential Evolution

Differential Evolution is a population-based stochastic optimization technique proposed for unconstrained problem [16]. According to the comprehensive study [9], DE outperforms many other EAs like GA in terms of convergence speed and robustness over common benchmark problems and real-world applications. Many variants of the classic DE have been proposed. The DE denoted as $DE/rand/1/bin$ [16] is adopted in this paper, whose key operators are introduced as follows.

The mutation operator is performed by the following way:

$$u_i = X_{r1} + F(X_{r2} - X_{r3}) \ , \tag{2}$$

where $u_i = [u_{i1}, u_{i2}, \ldots, u_{id}]$ is the trial individual, X_{r1}, X_{r2}, X_{r3} are three different individuals in the population, and F is a scale factor between 0 and 1.

The crossover is performed as follows:

$$v_{ij} = \begin{cases} u_{ij} & if\ (rand(j) \le cr)\ or\ j = sn \\ x_{ij} & ohterwise \end{cases} \quad j = 1,2,\ldots,d \ , \tag{3}$$

where cr is a real parameter between 0 and 1 to control the crossover rate of the trial individual and the old individual, sn is a random integer number in $\{1,2,\ldots,d\}$ to

assure that at least one component of the new individual is inherited from the trial individual, and v_{ij} is the jth dimension of the new individual V_i.

After crossover, a greedy selection is performed as follows:

$$X_{g+1} = \begin{cases} X_g & if\ (f(X_g) \le f(v_g)) \\ V_g & if\ (f(v_g) > f(X_g)) \end{cases}, \tag{4}$$

where X_{g+1} denotes the individual in the next generation, X_g denotes the old individual and V_g denotes the new individual.

The main procedure of DE is summarized as follows:

```
Step 1: Initialize a population of individuals with
random solutions.
Step 2: Evaluate all individuals.
Step 3: For each individual:
Step 3.1: Perform mutation;
Step 3.2: Perform crossover;
Step 3.3: Greedy selection.
Step 4: If a stopping criterion is met, then output
best solution found so far, otherwise go back to Step 3.
```

3 α Constrained Method

Inspired by the fuzzy control rules, Takahama and Sakai [17] proposed the α constrained method by introducing the level comparison to compare the search solutions based on a predefined satisfaction level. Using level comparison, the constrained problem is converted to an unconstrained problem. Thus, unconstrained optimization techniques can be applied.

3.1 Satisfaction Level of Constraints

The satisfaction level of constraints is used to indicate how well a solution satisfies the constraints, which is defined as follows:

$$\begin{cases} \mu(x) = 1 & f(g_i(x) \le 0 \text{ and } h_j(x) = 0) \text{ for all } i, j \\ 0 \le \mu(x) \le 1 & \text{otherwise} \end{cases}. \tag{5}$$

To define a satisfaction level, the level of each constraint should be defined and combined. For example, each constraint in Eqn. (1) can be transformed into one of the following satisfaction levels defined by piecewise linear functions on g_i and h_j.

$$\mu_{g_i}(X)=\begin{cases}1 & \text{if } g_i(x)\le 0\\ 1-\dfrac{g_i(X)}{b_i}, & \text{if } 0\le g_i(x)\le b_i\\ 0 & \text{otherwise}\end{cases}, \tag{6}$$

$$\mu_{h_j}(X)=\begin{cases}1-\dfrac{h_j(X)}{b_j} & \text{if } |h_j(x)|\le b_j\\ 0 & \text{otherwise}\end{cases}. \tag{7}$$

where b_i and b_j are proper positive fixed numbers.

The satisfaction level of the solution is obtained by combining the satisfaction levels of all constraints. In this paper, the levels are combined as follows:

$$\mu(X)=\min_{i,j}\{\mu_{g_i}(X),\mu_{h_j}(X)\}\ . \tag{8}$$

3.2 The α Level Comparison

The α level comparison is defined as the order relationship on the set of solutions to be used in the tournament selection as the Deb's rules [6]. If the satisfaction level of a solution is less than 1, it is viewed as infeasible. The α level comparisons are defined by a lexicographic order in which $\mu(X)$ precedes $f(X)$, because the feasibility is more important than the minimization of objective value.

Let f_1, f_2 and μ_1, μ_2 be the function values and the satisfaction levels of two solutions X_1, X_2. Then, for any α satisfying $0\le\alpha\le 1$, the α level comparisons $\le_\alpha$ and $<_\alpha$ between (f_1,μ_1) and (f_2,μ_2) are defined as follows:

$$(f_1,\mu_1)\le_\alpha(f_2,\mu_2)\Leftrightarrow\begin{cases}f_1\le f_2, & \text{if } \mu_1,\mu_2\ge\alpha\\ f_1\le f_2, & \text{if } \mu_1=\mu_2\\ \mu_1\le\mu_2, & \text{otherwise}\end{cases}, \tag{9}$$

$$(f_1,\mu_1)<_\alpha(f_2,\mu_2)\Leftrightarrow\begin{cases}f_1< f_2, & \text{if } \mu_1,\mu_2\ge\alpha\\ f_1< f_2, & \text{if } \mu_1=\mu_2\\ \mu_1<\mu_2, & \text{otherwise}\end{cases}. \tag{10}$$

In the case of $\alpha=0$, the α level comparison is equivalent to ordinal comparison of objective value. Meanwhile, in the case of $\alpha=1$, the α level comparison is equivalent to Deb's rules.

4 Differential Evolution with Level Comparison (αDE)

It is well known that the effectiveness of a constrained optimization algorithm depends on both the searching technique and the way to handle constraints. Due to the

good performance of DE for unconstrained optimization and the superiority of α constrained method in handling constraints, it is reasonable to combine the DE with the α constrained method to form a DE with level comparison for constrained optimization. The procedure of the algorithm is illustrated in Fig. 1. For convenience, we name the algorithm as α DE.

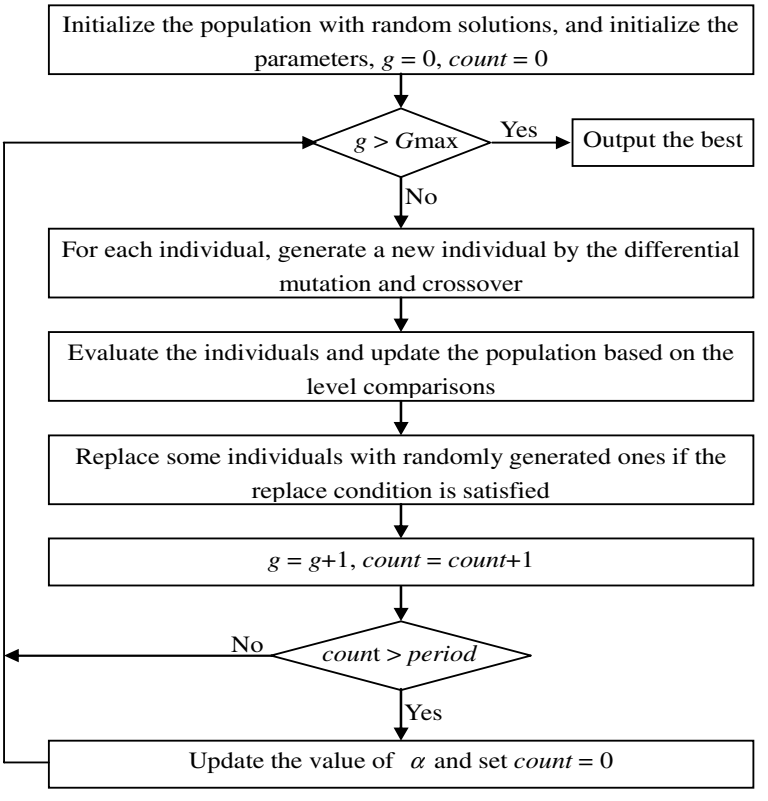

Fig. 1. The Flowchat of α DE

As shown in Fig. 1, the α DE has the similar procedure as traditional DE. In particular, a population is initialized with random individuals and the differential mutation and crossover operators are almost the same as those of traditional DE. To diversify the mutation operator, the scale factor is set as a random value between 0.2 and 0.9, which is different from the classic DE with the fixed factor. The selection in α DE is based on the α level comparison. To take advantage of the information of infeasible solutions at earlier searching stage while stress feasibility at later searching stage, the value of α is dynamically updated by Eqn. (11). In addition, the level is adjusted with period T_p from an initial value.

$$\alpha(g)=\begin{cases}(\max(\mu)+\text{average}(\mu))/2 & g=0\\ (1-\beta)\alpha(g-1)+\beta & g\%T_p=0, g<G\max/2\\ \alpha(g-1) & g\%T_p\neq 0, g<G\max/2\\ 1 & g\geq G\max/2\end{cases}, \tag{11}$$

where g denotes the number of generation, $G\max$ is the maximum generation number, β is used to control increasing rate of α, % denotes modulus operator.

In order to avoid converging to infeasible local optima when the value of α is less than 1, a few individuals of the population are replaced with randomly generated individuals after certain generations. In our procedure, the population is divided into two parts. The first part contains feasible individuals, where the individuals with the largest objective value are eliminated. The second part contains infeasible individuals, where the individuals with the lowest satisfaction level are eliminated. In the following simulation, 1/3 solutions of each part will be eliminated.

5 Experiments and Comparisons

In order to verify the effectiveness and efficiency of α DE, we carry out some experiments based on the 13 well-known benchmarks for constrained optimization [18]. These benchmarks are widely used to test and compare the performances of the newly designed algorithms. In our experiments, we set population size $N=50$, $G\max=4500$ (i.e., the total evaluation time is 225000), $cr=0.9$ as commonly used in the literature, $T_p=5$, β=0.05. The fixed number b_i, b_j to define the α level of each constraint is set as the median value of the initial constraint violations. Moreover, it is limited to $1e4$ if the value is too large, and it is set as the length of search space if the value is 0. Simulation is carried out in MATLAB2008b on AMD Athlon 64 Processor 2800+1.81GHz with 1G-RAM. Each problem is independently run 30 times.

5.1 Performances of α DE

The statistical results of α DE are summarized in Table 1, which include the best, median, mean, worst, and standard deviation of the objective values.

Table 1. Performances of α DE

f	Optimal	best	median	mean	worst	std
g01	-15.000	-15.00000	-15.00000	-15.00000	-15.00000	6.3364E-15
g02	0.803619	0.803619	0.785274	0.7785236	0.694402	2.5319E-02
g03	-1.000	-1.0000	-1.0000	-1.0000	-1.0000	3.3599E-07
g04	-30665.539	-30665.539	-30665.539	-30665.539	-30665.539	2.0108E-11
g05	5126.498	5126.4981	5126.4981	5126.4981	5126.4981	1.8736E-07
g06	-6961.814	-6961.814	-6961.814	-6961.814	-6961.814	4.9548E-11

Table 1. (*continued*)

f	Optimal	best	median	mean	worst	std
g07	24.3062	24.3062	24.3062	24.3062	24.3062	6.7723E-06
g08	-0.95825	-0.095825	-0.095825	-0.095774	-0.094043	3.2510E-04
g09	680.630	680.6301	680.6301	680.6301	680.6301	2.8946E-13
g10	7049.248	7049.2480	7049.2480	7049.2480	7049.2480	1.1030E-05
g11	0.7500	0.7500	0.7500	0.7500	0.7500	1.9259E-11
g12	-1.000	-1.0000	-1.0000	-1.0000	-1.0000	0.0000E+00
g13	0.053950	0.05395	0.05395	0.05395	0.05395	1.6332E-11

It can be seen from the Table that the best solution is almost equivalent to the optimal solution for every problem, even for g13 containing three equality constraints that is regarded as very hard to optimize. For g01 g04 g06 g07 g09 g10 g12, the optimal solutions can be found consistently in all 30 runs. For g03, g05, g11 and g13 with equality constraints, the result obtained is very close to the optimal value. For g02, the optimal solutions could not be consistently found since there are many local optima with high peak near the global optimum. For g08, we find that the optimal solution can be found in 29 runs out of 30 runs.

5.2 Comparison with Other Approaches

Next, we compare α DE with some typical state-of-art approaches, including the Improved Stochastic Ranking (ISR) [18], Simple Multimember Evolution Strategy (SMES) [19], the Diversity DE (DDE) [20], DE with Dynamic Stochastic Selection (MDESS) [11] and the α simplex [8]. The main parameter setting of the six approaches are illustrated in Table 2. Note that the equality constraints should be converted to inequality constraints with a certain tolerance when using ISR, SMES, DDE, MDESS, while the conversion is not needed when using α DE and α simplex.

Table 2. The main parameters of the algorithms for comparisons

Approach	Total evaluation times	Run times	Tolerance	Population size
ISR	350,000	100	0.0001	400
SMES	240,000	30	0.0004	300
DDE	225,000	100	0.0001	450
MDESS	225,000	100	0.0001	250
α simplex	290,000~330	30	0	90
α DE	225,000	30	0	50

The results of all the algorithms are listed in Table 3. From Table 3, it is clear that α DE outperforms or competitive to other five algorithms in terms of the quality and efficiency except for g08, where α DE was trapped at local optimum in 1 out of the 30 runs. All the six algorithms can find the optima consistently for g01, g04, g06, g07, g09, g10 and g12. As for g02, α DE was able to find the same optima as the other five algorithms, whereas the worst result of α DE is the worst among the six algorithms. However, the "mean" of α DE is better than that of ISR, SMES and

α simplex. For problem g03, g05 and g11, ISR, MDESS and α simplex found better results than the optima because of using the tolerance to treat the equality constraints, SEMS could not find the optima consistently, whereas α DE was capable to find the real optima consistently. With respect to g 13, only α DE can find the optima consistently, ISR, SMES, DDE and α simplex were trapped in the local optima, MDESS could only find the optima consistently after relaxing the equality constraints. As for the computational costs, the maximum number of function evaluations (NFE) of our algorithm is 225,000, whereas those of ISR, SEMS, DDE, MDESS and α simplex are 350,000, 240,000, 225,000, 225,000 and 330,000. The computation cost of our algorithm is the smallest one. Thus, our algorithm is a potentially promising tool for constrained optimization, especially for problems with equality constraints.

Table 3. Comparisons between different algorithms

f	Sta	ISR[18]	SMES[19]	DDE[20]	MDESS[13]	α simplex[8]	α DE
g01	best	**-15.000**	**-15.000**	**-15.000**	**-15.000**	**-15.000**	**-15.000**
	mean	**-15.000**	**-15.000**	**-15.000**	**-15.000**	**-15.000**	**-15.000**
	worst	**-15.000**	**-15.000**	**-15.000**	**-15.000**	**-15.000**	**-15.000**
	std	5.8E-14	0	1.0E-09	1.3E-10	6.4E-06	6.3E-15
g02	best	**0.803619**	**0.803619**	**0.803619**	**0.803619**	**0.803619**	**0.803619**
	mean	0.782715	0.785238	**0.798079**	0.786970	0.7841868	0.785274
	worst	0.723591	0.751322	0.751742	0.728531	**0.7542585**	0.694402
	std	2.2E-02	1.7E-02	1.1E-02	1.5E-02	1.3E-02	2.5E-02
g03	best	1.001	**1.000**	**1.000**	1.0005	1.0005	**1.000**
	mean	1.001	**1.000**	**1.000**	1.0005	1.0005	**1.000**
	worst	1.001	**1.000**	**1.000**	1.0005	1.0005	**1.000**
	std	8.2E-09	2.1E-04	0	1.9E-08	8.5E-14	3.36E-07
g04	best	**-30665.539**	**-30665.539**	**-30665.539**	**-30665.539**	**-30665.539**	**-30665.539**
	mean	**-30665.539**	**-30665.539**	**-30665.539**	**-30665.539**	**-30665.539**	**-30665.539**
	worst	**-30665.539**	**-30665.539**	**-30665.539**	**-30665.539**	**-30665.539**	**-30665.539**
	std	1.1E-11	0	0	2.7E-11	4.2E-11	2.0E-11
g05	best	5126.497	5126.599	5126.497	5126.497	5126.497	**5126.498**
	mean	5126.497	5174.492	5126.497	5126.497	5126.497	**5126.498**
	worst	5126.497	5304.167	5126.497	5126.497	5126.497	**5126.498**
	std	7.2E-13	5.0E+01	0	0	3.5E-11	1.9E-07
g06	best	**6961.814**	**6961.814**	**6961.814**	**6961.814**	**6961.814**	**6961.814**
	mean	**6961.814**	**6961.284**	**6961.814**	**6961.814**	**6961.814**	**6961.814**
	worst	**6961.814**	**6952.482**	**6961.814**	**6961.814**	**6961.814**	**6961.814**
	std	1.9E-12	1.9E+00	0	0	1.3E-10	5.0E-11
g07	best	**24.306**	24.327	**24.306**	**24.306**	**24.306**	**24.306**
	mean	**24.306**	24.475	**24.306**	**24.306**	**24.306**	**24.306**
	worst	**24.306**	24.843	**24.306**	**24.306**	**24.307**	**24.306**
	std	6.3E-05	1.3E-01	8.22E-09	7.5E-07	1.3E-04	6.8E-06
g08	best	**0.095825**	**0.095825**	**0.095825**	**0.095825**	**0.095825**	**0.095825**
	mean	**0.095825**	**0.095825**	**0.095825**	**0.095825**	**0.095825**	0.095774
	worst	**0.095825**	**0.095825**	**0.095825**	**0.095825**	**0.095825**	0.094043
	std	2.7E-17	0	0	4.0E-17	3.8E-13	3.3E-04

Table 3. (*continued*)

f	Sta	ISR[18]	SMES[19]	DDE[20]	MDESS[13]	α simplex[8]	α DE
g09	best	**680.630**	**680.632**	**680.630**	**680.630**	**680.630**	**680.630**
	mean	**680.630**	**680.643**	**680.630**	**680.630**	**680.630**	**680.630**
	worst	**680.630**	680.719	**680.630**	**680.630**	**680.630**	**680.630**
	std	3.2E-13	1.6E-02	0	2.9E-13	2.9E-10	2.9E-13
g10	best	**7049.248**	**7049.248**	**7049.248**	**7049.248**	**7049.248**	**7049.248**
	mean	**7049.248**	**7049.248**	**7049.248**	**7049.248**	**7049.248**	**7049.248**
	worst	**7049.248**	**7049.248**	**7049.248**	**7049.248**	**7049.248**	**7049.248**
	std	3.2E-03	1.4E-02	4.45E-02	1.4E-03	4.7E-06	1.1E-05
g11	best	**0.7500**	**0.7500**	**0.7500**	**0.7499**	**0.7499**	**0.7500**
	mean	**0.7500**	**0.7500**	**0.7500**	**0.7499**	**0.7499**	**0.7500**
	worst	**0.7500**	**0.7500**	**0.7500**	**0.7499**	**0.7499**	**0.7500**
	std	1.1E-16	1.5E-04	0	0	4.9E-16	1.9E-11
g12	best	**1.000**	**1.000**	**1.000**	**1.000**	**1.000**	**1.000**
	mean	**1.000**	**1.000**	**1.000**	**1.000**	**1.000**	**1.000**
	worst	**1.000**	**1.000**	**1.000**	**1.000**	**1.000**	**1.000**
	std	1.2E-09	0	0	0	3.9E-10	0
g13	best	0.053942	0.053986	0.053941	0.053942	0.053942	**0.53950**
	mean	0.06677	0.166385	0.069336	0.053942	0.066770	**0.53950**
	worst	0.438803	0.468294	0.438803	0.053942	0.438803	**0.53950**
	std	7.0E-02	1.8E-01	7.58E-02	1.0E-13	6.9E-02	1.6E-11

6 Conclusion

In this paper, level comparison was combined with differential evolution to develop an approach for constrained optimization. To the best of our knowledge, this was the first report to incorporate α constrained method into DE for constrained optimization. Simulation results based on some well-known benchmarks and comparisons with some typical state-of-art approaches demonstrated the effectiveness and efficiency of our algorithm. The future work is to further improve the algorithm by incorporating diversity maintains and adaptive mechanism and to apply the algorithm for some constrained engineering design problems.

Acknowledgments

This research is partially supported by National Science Foundation of China (Grant No. 60774082, 70871065, 60834004) and the National 863 Program under the grant number 2007AA04Z155 as well as the Project-sponsored by SRF for ROCS, SEM.

References

1. Wang, L.: Intelligent Optimization Algorithms with Application. Tsinghua University & Springer Press, Beijing (2001)
2. Coello, C.A.C.: Theoretical and Numerical Constraint-Handling Techniques Used with Evolutionary Algorithms: A Survey of the State of the Art. Comput. Methods Appl. Mech. Eng. 191, 1245–1287 (2002)

3. Rasheed, K.: An Adaptive Penalty Approach for Constrained Genetic-Algorithm Optimization. In: Genetic Programming 1998. Proceedings of the Third Annual Conference, Madison, WI, USA, pp. 584–590 (1998)
4. He, Q., Wang, L.: An Effective Co-evolutionary Particle Swarm Optimization for Constrained Engineering Design Problems. Eng. Appl. Artif. Intell. 20, 89–99 (2007)
5. Cai, Z., Wang, Y.: A Multiobjective Optimization-Based Evolutionary Algorithm for Constrained Optimization. IEEE Trans. Evol. Comput. 10, 658–675 (2006)
6. Deb, K.: An Efficient Constraint Handling Method for Genetic Algorithms. Comput. Methods Appl. Mech. Eng. 186, 311–338 (2000)
7. Runarsson, T.P., Yao, X.: Stochastic Ranking for Constrained Evolutionary Optimization. IEEE Trans. Evol. Comput. 4, 284–294 (2000)
8. Takahama, T., Sakai, S.: Constrained Optimization by Applying the Alpha Constrained Method to the Nonlinear Simplex Method with Mutations. IEEE Trans. Evol. Comput. 9, 437–451 (2005)
9. Price, K., Storn, R.M., Lampinen, J.A.: Differential Evolution: A Practical Approach to Global Optimization (Natural Computing Series). Springer, New York (2005)
10. Storn, R.: Designing Nonstandard Filters with Differential Evolution. IEEE Signal Process. Mag. 22, 103–106 (2005)
11. Qian, B., Wang, L., Huang, D., Wang, X.: Multi-objective Flow Shop Scheduling Using Differential Evolution. LNCIS, vol. 345, pp. 1125–1136 (2006)
12. Lampinen, J.: A Constraint Handling Approach for the Differential Evolution Algorithm. In: Proceedings 2002 IEEE Congress on Evolutionary Computation, Honolulu, Hawaii, pp. 1468–1473 (2002)
13. Zhang, M., Luo, W., Wang, X.: Differential Evolution with Dynamic Stochastic Selection for Constrained Optimization. Inf. Sci., 3043–3074 (2008)
14. Huang, F.Z., Wang, L., He, Q.: An Effective Co-evolutionary Differential Evolution for Constrained Optimization. Appl. Math. Comput. 186, 340–356 (2007)
15. Becerra, R.L., Coello, C.A.C.: Cultured Differential Evolution for Constrained Optimization. Comput. Meth. Appl. Mech. Eng. 195, 4303–4322 (2006)
16. Storn, R., Price, K.: Differential Evolution - A Simple and Sfficient Heuristic for Global Optimization Over Continuous Spaces. J. Glob. Optim. 11, 341–359 (1997)
17. Takahama, T., Sakai, S.: Tuning Fuzzy Control Rules by Alpha Constrained Method Which Solves Constrained Nonlinear Optimization Problems. Trans. Inst. Elect. Inf. Commun. Eng. 82-A, 658–668 (1999)
18. Runarsson, T.P., Yao, X.: Search Biases in Constrained Evolutionary Optimization. IEEE Trans. Syst., Man, Cybern. C, Appl. Rev. 35, 233–243 (2005)
19. Mezura-Montes, E., Coello, C.A.C.: A Simple Multimembered Evolution Strategy to Solve Constrained Optimization Problems. IEEE Trans. Evol. Comput. 9, 1–17 (2005)
20. Mezura-Montes, E., Velazquez-Reyes, J., Coello, C.A.C.: Promising Infeasibility and Multiple Offspring Incorporated to Differential Evolution for Constrained Optimization. In: Proceedings of the Genetic and Evolutionary Computation Conference (GECCO 2005), New York, pp. 225–232 (2005)

Tactical Aircraft Pop-Up Attack Planning Using Collaborative Optimization

Nan Wang, Lin Wang, Yanlong Bu, Guozhong Zhang, and Lincheng Shen

Mechatronics and Automation School of National University of Defense Technology, 410073, Changsha, China
xlaser2003@yahoo.com.cn

Abstract. This paper proposes a collaborative optimization based method for tactical aircraft pop-up attack planning. First, the planning problem is described by four laws: delivery maneuver, ballistics, survivability and detection. Then the collaborative optimization (CO) framework is introduced to model the complex coupled problem, in which the problem is divided into two levels: system level optimization and laws level optimization. Following the planning procedure of CO, the genetic algorithm combined with response surface method is used to solve the above optimization problem. Finally, the proposed method is validated through experiments and appears to be effective and feasible to solve the pop-up attack planning problem.

Keywords: pop-up attack, weapon delivery, planning, law, collaborative optimization, response surface.

1 Introduction

Nowadays air-to-ground attack is playing a more and more important role in modern wars. Given current surface-to-air threat capabilities, pop-up attack (Fig. 1) is widely used by pilots to engage well-protected targets. Before executing, the attack profile should be deliberately planned to ensure the survivability of the plane and the success of engagement, which includes determination and evaluation of the attack parameters (ingress height, speed, dive angle, release height, etc).

To solve the pop-up attack planning (PAP) problem, two difficulties must be faced. First, the design space, formed by the attack parameters, is large and heterogeneous. There are more than 20 variables to be determined and evaluated, some of which are continuous, and some are discrete, with different bounds. Second, the analysis and evaluation is performed by different laws: the delivery maneuver law, the ballistics law, the survivability law and the sensor detection law. Each law computes its own constrains and objects and is coupled with each other, making the total problem a complex multi-objective, multidisciplinary optimization problem.

In this paper, the collaborative optimization (CO) method combined with evolutionary optimization techniques is introduced to solve the pop-up attack planning problem. Detailed algorithms and experimental results are also presented.

D.-S. Huang et al. (Eds.): ICIC 2009, LNAI 5755, pp. 361–370, 2009.

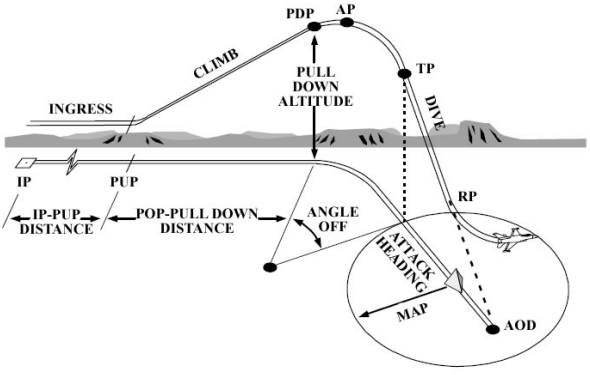

Fig. 1. Typical profile of pop-up attack

2 Problem Formulation

As described above, the PAP problem contains four laws (Fig. 2): ①delivery maneuver; ②ballistics; ③survivability; ④sensor detection. Table 1 lists the design variables and their bounds in the problem. Table 2 lists the state variables and their relations with each law. When the laws are considered as disciplines, the pop-up attack planning is inherently a multidisciplinary process. Traditionally multidisciplinary optimization (MDO) methods have focused on disciplines within the field of engineering analysis, such as aerodynamics, solid mechanics and so on. However, in planning domain, similar problem encounters, and may become a potential application domain to be explored.

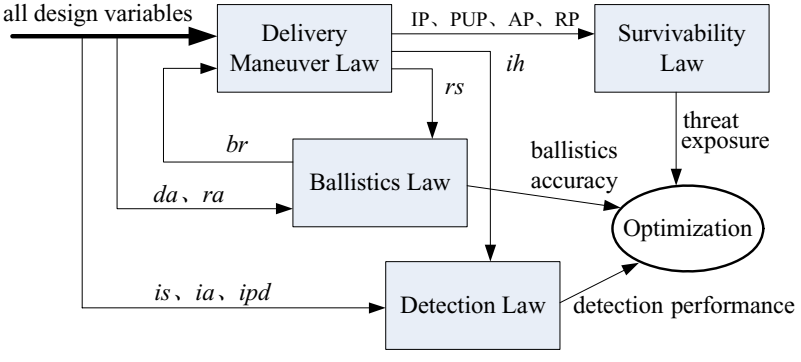

Fig. 2. Structure of the pop-up planning problem, where IP, PUP, AP and RP stand for the key positions in the attack profile

2.1 Delivery Maneuver Law

In the delivery maneuver law, the attack profile is calculated based on the attack parameters, which are treated as design variables, such as *is*, *ia*, *ipd*, *da*, etc. The output

Table 1. List of design variables in PAP problem

	Name (Unit)	Bound
is	ingress speed (KTAS)	[300, 550]
ia	ingress altitude (ft)	[150, 500]
ipd	IP-PUP distance (nm)	[1, 5]
da	dive angle (°)	[10, 45]
lf	load factor (G)	{3, 4, 5}
tt	tracking time (s)	[1, 10]
ra	release altitude (ft)	[2000, 8000]
ah	attack heading (°)	[0, 360)
tu	turn	{left, right}

Table 2. List of state variables in PAP problem

	Name (Unit)	Output From	Input to
IP	initial point position	DML	SL
PUP	pop-up point position	DML	SL
AP	apex point position	DML	SL
RP	release point position	DML	SL
tet	threat exposure time (s)	SL	
sp	survivability (%)	SL	
rs	release speed (m/s)	DML	BL
ba	ballistic accuracy (%)	BL	
br	bomb range (ft)	BL	DML
ih	ingress heading (°)	DML	DL
dp	detection probability (%)	DL	

profile contains variables used by other laws, which are treated as state variables, such as *rs*, *ih*, etc. The calculation is based on the pop-up formulas in [1].

2.2 Ballistic Law

The ballistic law analyzes the release parameters (*da*, *ra*, *rs*) and calculates the bomb range *br* as well as the ballistic accuracy *ba*. The aod, which is input to the delivery maneuver law to calculate the RP position and *ra*, is calculated through simulation of the delivered bomb trajectory using (1), where v is the value of bomb velocity, θ is the obliquity angle of bomb axis, x and y are the horizontal and vertical distance traveled by the bomb.

$$\begin{cases} \dfrac{dv}{dt} = g\sin\theta - a_R \\ \dfrac{d\theta}{dt} = g\cos\theta / v \end{cases} \qquad \begin{cases} \dfrac{dx}{dt} = v\cos\theta \\ \dfrac{dy}{dt} = v\sin\theta \end{cases} \tag{1}$$

The ballistic accuracy ba is attained by looking up the statistical table of typical bombing errors under different release parameters for special bomb types and delivery types, and is one of the objects to be optimized (minimized) in the PAP problem.

2.3 Survivability Law

The survivability law takes the IP, PUP, AP, RP position and altitude into calculation and outputs the *tet*. In the survivability law, threats are modeled as 3-D envelopes. As the threats in the target area are mainly A-A guns and short range missiles, detection and engagement areas are no distinguished.

The tet is attained by analyzing the IP-PUP, PUP-AP, AP-RP segment respectively. The average speed v_i in each segment is calculated and is considered constant through the analysis. In the analyzing procedure, dichotomy is used to calculate the threat exposure trajectory length L_i in each segment. Then the *tet* is calculated as follows, which is another object to be minimized.

$$tet = \sum L_i / v_i \tag{2}$$

2.4 Detection Law

Before carrying out the delivery maneuver, the target must be found and locked, and these are done in the ingress phase. In the detection law, the detection performance (*dp*, *rt*) during the ingress is calculated using sensor detection and observer search models. For EO sensors, the resolvable cycles across the target δ is used to evaluate the imaging quality in slope range *R*, which is calculated as follows, where L_b is the resolving line number, and S_e is the target equivalent dimension, f_c is the camera focus, b_c is the imaging surface height. The line-of-sight between the plane and the target should be maintained during the detection course, otherwise the detection is considered to be failed.

$$\delta = L_b \times S_e \times f_c / (b_c \times R) \tag{3}$$

For different targets, δ_M represents the minimum resolvable cycles needed to find the target with 50%, which is the function of target sizes and orientations. The instantaneous probability of detection is the function of δ and δ_M, as shown in (4). And the ensemble detection probability P_N by time step *N* can be calculated by (5). Then *dp* can be calculated based on the ingress time and the expected detection probability, and dp^{-1} is the third object to be minimized.

$$P_i = f(\delta / \delta_M) \tag{4}$$

$$P_N = 1 - \prod_{i=1}^{N} (1 - P_i) \tag{5}$$

3 Methodology

The structure of the PAP problem makes it difficult to be solved by conventional planning methods. First, the design space is large, highly non-linear and contains different variable types, both continuous and discrete. And due to the complex battle environment, local minima are inevitable. Second, the problem involves complex analysis and evaluation procedures carried out by different laws, and laws are coupled

with each other. This leads to the time-consuming analysis and iteration in planning procedures.

Inherently, the PAP problem is a complex design problem with a set of design variables to be determined. If the laws are considered as disciplines, the PAP problem is inherently a MDO problem. Therefore, the collaborative optimization (CO) method is adopted to determine the optimal solution of this complicated problem. The collaborative optimization method is first proposed by Kroo et al., [3] and Balling and Sobieszczanski-Sobieski [4], and has been successfully applied to a number of different MDO problems. CO is a two level optimization method specifically created for large-scale distributed-analysis applications. The basic architecture of CO is made up by two-level optimizers (Fig. 3), which facilitates concurrent optimization at the discipline design level. In CO, variables are divided into shared design variables x_{sh}, local variables x_i, state variables y_i and auxiliary variables $(x_{aux})_{ij}$. Auxiliary variables are introduced as additional design variables to replace the coupling variables (y_{ij}) output from disciplinary i and input to disciplinary j, so that the analyses in disciplines i and j can be executed concurrently. Interdisciplinary compatibility constraints d are added to ensure that consistency such that $(x_{aux})_{ij}=y_{ij}$. The system level optimizer attempts to minimize the design objectives function F while satisfying all the compatibility constrains d. The system level design variables x_{sys} consist of not only the variables x_{sh} but also the auxiliary variables x_{aux}, which are specified by the system level optimizer and sent down to subspaces as targets to be matched. Each subspace, as a local optimizer, operates on its local design variables x_i with the goal of matching target values posed by the system level as well as satisfying local constraints g_i. The optimization procedure runs through the iteration between the system level and subspace optimizers, and the optimal solution is found when the design variables converge.

When applying the CO method to solve the PAP problem, a system optimizer is founded and an optimizer is integrated within each law. The resulting framework rigorously simulates the existing relationship of the laws in the PAP problem as shown in Fig. 4. The design and state variables are organized as follows.

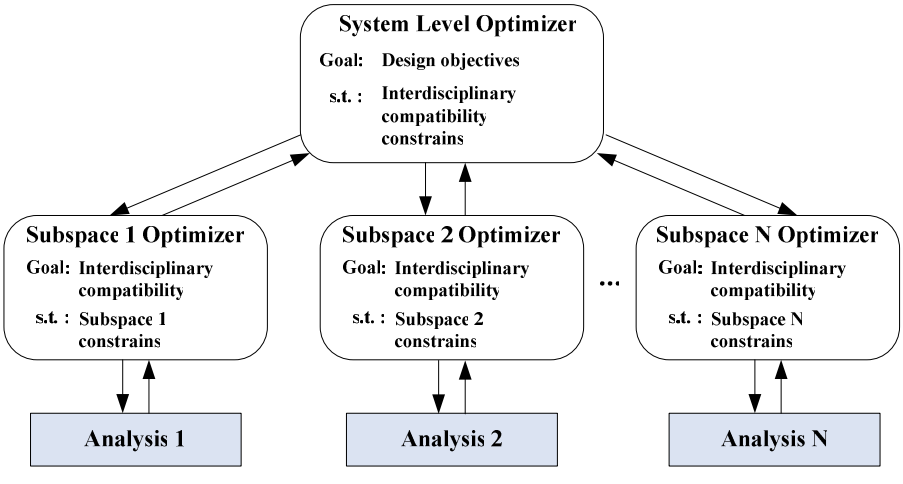

Fig. 3. Basic collaborative optimization architecture (Braun et al., [5])

Table 3. Design vectors and functions for PAP problem

	Vector or Function	Variables or Content
	x_{sh}	{*is, ia, ipd, da, ra*}
	x_{aux}	{IP, PUP, AP, RP, *rs, ih, aod*}
CA1	targets to be matched	$(x_{sys}^{0})_1$={*is, ia, ipd, da, ra, aod*}
	x_1	{*lf, tt, ah, tu*}
	$(x_{sh})_1$	{*is, ia, ipd, da, ra*}
	$(x_{aux})_1$	empty set
	analysis	{IP, PUP, AP, RP, *rs, ih*}
CA2	targets to be matched	$(x_{sys}^{0})_2$={*da, ra, rs*}
	x_2	empty set
	$(x_{sh})_2$	{*da, ra*}
	$(x_{aux})_2$	{*rs*}
	analysis	{*ba, aod*}
CA3	targets to be matched	$(x_{sys}^{0})_3$={IP, PUP, AP, RP}
	x_3	empty set
	$(x_{sh})_3$	empty set
	$(x_{aux})_3$	{IP, PUP, AP, RP}
	analysis	{*tet*}
CA4	targets to be matched	$(x_{sys}^{0})_4$={*is, ia, ipd, ih*}
	x_4	empty set
	$(x_{sh})_4$	{*is, ia, ipd*}
	$(x_{aux})_4$	{*ih*}
	analysis	{*dp, dt*}

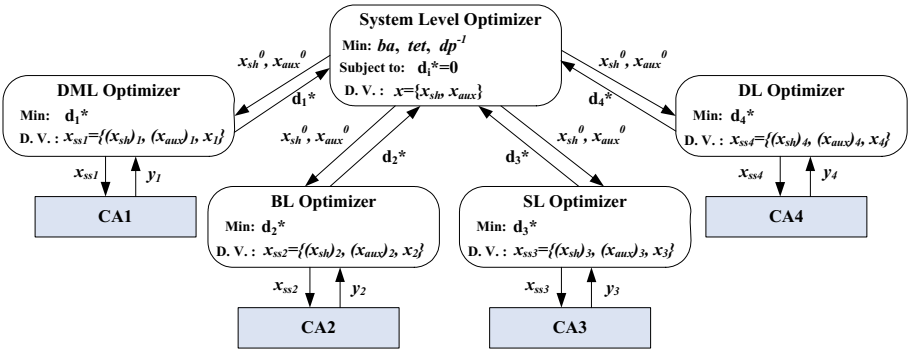

Fig. 4. The PAP problem collaborative optimization framework

In the CO optimization process, the system level optimizer adjusts the design variables to minimize the objectives while satisfies the compatibility constrains. The system objectives are scaled by weight factors, as shown in (6), where each weight represents the significance of the corresponding objective. Due to the non-linear characteristic of the problem, the genetic algorithms (GA) are used to solve the optimization needs in both system and laws level. However, the fitness evaluation is based on the analyses results of the laws, which may cause intolerable evaluation time during

iteration. The most common way to handle it in MDO is to calculate the post-optimal sensitivities at the subspace optimum as the gradients of the system level objectives and constrains. However, when the problem is highly non-linear, the calculation gradients fails to work. For a better choice, the response surface method (RSM) is used to approximate the fitness (state variables) changes in response to the design variable variation [rsearico]. There are several techniques in building the response surface, including polynomial, variable complexity modeling (VCM) and neural networks (NN). In this article, the RBF neural network is adopted. Details of the RSM methods are provided in [6][7][8].

$$f_{obj} = w_1 \times be + w_2 \times tet + w_3 \times dt^{-1} \tag{6}$$

The planning procedure of the PAP problem using CO is as follows:

Procedure: *Collaborative Optimization based PAP with RSM*

(1) *Construct response surface*
(2) *Initialize system level decide variables*
(3) ***Repeat***
(4) ***For*** *i=1 to 4*
(5) *Send system design variables* $[x_{sh}^{\ i}\ x_{aux}^{\ i}]$ *to ith law*
(6) ***End For***
(7) *Perform laws level optimization respectively*
(8) ***For*** *i=1 to 4*
(9) *Return ith law objective value* d_i^* *to system level*
(10) ***End For***
(11) *Update response surface*
(12) *Perform system level optimization using response surface*
(13) ***Until*** *all compatibility constrains are satisfied or terminal iteration condition is reached*

4 Experiments and Results

The introduced CO method is tested in two different PAP planning scenarios, as shown in Figure 5. The simulation is run by Matlab on a standard PC with Pentium 4 CPU of 2.8GHz. The main parameters' values are shown in Table 4.

The training samples for building the RBF network are randomly selected among the design space. The output of the network includes the optimization objectives (*tet*, *ba*, dp^{-1}) as well as the compatibility constrains (d_1-d_4). The initial number of training samples is as small as 37, and the network is updated through every iteration in the optimization process. The average running time of the proposed method with RSM is compared to that without a RSM as shown in Table 6. It can be seen that using the RBF network a significant improvement in planning speed is achieved.

The results found by the CO method are shown in Table 5, and the delivery maneuver trajectory is shown in Figure 6. The quality of the results is compared with general GA methods in which all design variables are searched on a single level (all-at-once). From the comparison results, we can find that the proposed CO method can find out better solutions while maintain efficiency in solving the PAP problem.

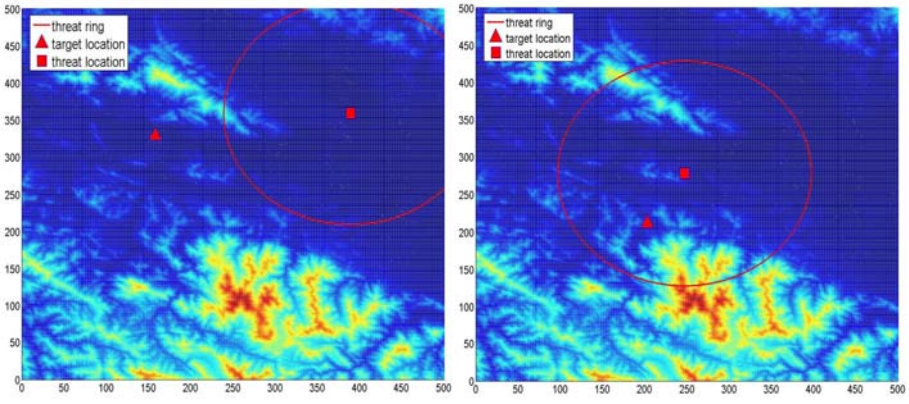

(a) (b)

Fig. 5. Two different scenarios for pop-up attack weapon delivery tasks

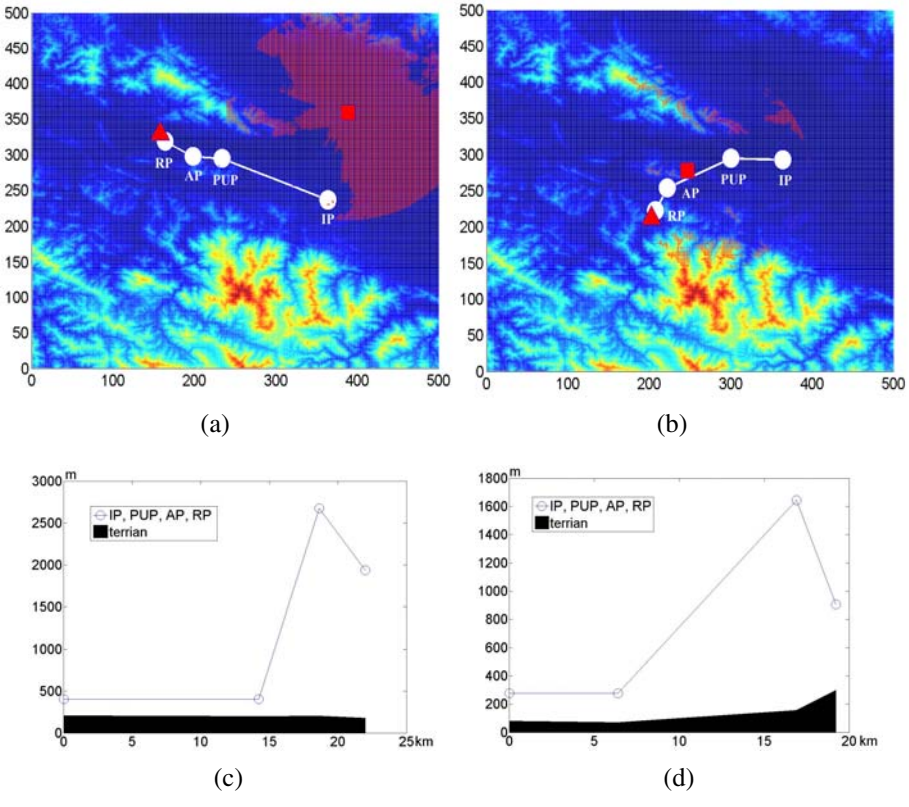

(a) (b)

(c) (d)

Fig. 6. The result delivery maneuver trajectory found by the CO method. Subfigure (a) and (b) show the plane profile and subfigure (c) and (d) show the vertical profile in different scenarios. The area in red shows the terrain mask to threat at ingress altitude

Table 4. The main parameters' values used by the experiments

Parameters	Values	Units	Parameters	Values	Units
L_b	400	/	b_c	9.6	mm
f_c	120	mm	δ_M	4	/

Table 5. The results found by the CO method

Design variables	Scenario a	Scenario b
is	400	357
ia	410	170
ipd	7.686	2.67
da	17	24
lf	3	3
tt	8	5
ra	5429	2229
ah	328	205
tu	right	right

Table 6. The running time of the method with and without RSM

	Scenario a	Scenario b
with RSM	35s	40s
without RSM	250s	291s

Table 7. Comparison of the proposed CO method and general GA

	proposed CO method		general GA	
	Scenario a	Scenario b	Scenario a	Scenario b
tet	0	12	0	10
ba	79.9%	60.70%	69.7%	49.9%
dp	100%	100%	100%	92%
constrains	satisfied	satisfied	satisfied	satisfied
iteration rounds	711	791	1002	1122
planning time	35s	40s	120s	133s

5 Conclusion

In this paper, four different laws (DML, BL, SL, and DL) are presented to describe the tactical aircraft pop-up attack planning problem. Then, to solve the aforementioned problem, a collaborative optimization method with response surface is designed and implemented. And the efficiency of the method is verified by simulations. The simulation results demonstrate that the proposed method do well in PAP planning. Further, based on the proposed method, we can implement parallel algorithm to further improve the method for near real-time planning, which can make the algorithm more practical for the applications of tactical aircraft mission planning and is an important direction for our research.

References

1. F-16 combat aircraft fundamentals. HQ ACC/DOT (1996)
2. Yang, M.Z., Yin, J., Yu, L.: Research on Operation Distance of TV Homer. Electronics Optics & Control 10, 27–30 (2003) (in Chinese)
3. Kroo, I., Altus, S., Braun, R.: Multidisciplinary Optimization Methods for Aircraft Preliminary Design. In: AIAA-96-4018, 5th AIAA Symposium on Multidisciplinary Analysis and Optimization (1994)
4. Balling, R.J., Sobieski, J.: Optimization of Coupled Systems: A Critical Overview of Approaches. In: AIAA-94-4330-CP, 5th AIAA Symposium on Multidisciplinary Analysis and Optimization (1994)
5. Braum, R.D., Gage, P., Kroo, I.M., Sobieski, I.P.: Implementation and Performance Issues in Collaborative Optimization. In: AIAA 94-4325-CP, 6th AIAA Symposium on Multidisciplinary Analysis and Optimization (1994)
6. Sobieski, I.P., Manning, V.M.: Response surface estimation and refinement in collaborative optimization. In: AIAA-98-4758, pp. 359–370 (1998)
7. Sobieski, I.P., Kroo, I.M.: Collaborative Optimization Using Response Surface Estimation. In: AIAA Aerospace Sciences Meeting (1997)
8. Marc, A.S., Stephen, M.B.: Neural network approximation of mixed continuous discrete systems in multidisciplinary design. In: AIAA-98-0916, 36th Aerospace Science Meeting and Exhibit (1998)
9. Luis, V.S., Victor, A.S., Carlos, A.: Coello Coello: Use of Radial Basis Functions and Rough Sets for Evolutionary Multi-Objective Optimization (2007)
10. Rana, A.S., Zalzala, A.M.S.: A Neural Networks Based Collision Detection Engine for Multi-Arm Robotic Systems. In: International conference on artificial neural networks 5th, pp. 140–145 (1997)
11. Jon, C.L., Ronald, G.D.: Surveillance and Reconnaissance Imaging Systems. Artech House Publishers, Beijing (2007)
12. Russell, D.N.: Evaluation of Air-to-Ground Weapon Delivery Systems Performance. Naval Air Test Center Report, TM 80-1 SA (1980)
13. Gu, X.Y., John, E.R., Leah, M.A.: Decision-Based Collaborative Optimization. Journal of Mechanical Design 124 (2002)
14. Kroo, I.M., Manning, V.M.: Collaborative optimization - Status and directions. In: AIAA-2000-4721, 8th AIAA Symposium on Multidisciplinary Analysis and Optimization (2000)
15. Garza, A.D., Darmofa, D.L.: An all-at-once approach for multidisciplinary design optimization. AIAA (1998)

Stereo Vision Based Motion Parameter Estimation

Xinkai Chen

Department of Electronic and Information Systems,
Shibaura Institute of Technology,
307 Fukasaku, Minuma-ku, Saitama-shi, Saitama 337-8570, Japan
chen@shibaura-it.ac.jp

Abstract. The motion parameter estimation for a class of movements in the space by using stereo vision is considered by observing a group of points. The considered motion equation can cover a wide class of practical movements in the space. The observability of this class of movement is clarified. The estimation algorithm for the motion parameters which are all time-varying is developed based on the second method of Lyapunov. The assumptions about the perspective system are reasonable and have apparently physical interpretations. The proposed recursive algorithm requires minor *a priori* knowledge about the system. Experimental results show the proposed algorithm is effective even in the presence of measurement noises.

Keywords: Stereo vision, motion parameter, estimation.

1 Introduction

Estimation of the motion and the structure of a moving object in the space by using the image data with the aid of CCD camera(s) has been studied recently. The motion treated in the literature field is composed of a rotation part and a translation part. A very typical method is the application of the extended Kalman filter (EKF) [5][13][14]. Numerous successful results have been reported until now where the formulation is based on a discrete expression of the motion, and the observability conditions are derived based on the perspective observations of a group of points [1][4]. Such a recursive algorithm obviously alleviates the noises in the image data in contrast to the non-recursive methods [9] based on solving a set of nonlinear algebraic equations. It should be mentioned that some theoretical convergence conditions of discrete EKF have been established both as observer and filter [11].

For continuous time perspective systems, the observation problem has been studied in the point of view of dynamical system theory in [2][3][7][10]. A necessary and sufficient condition for the perspective observability is given in [6] for the case that the motion parameters are constants. For the movements with piecewise constant motion parameters, the perspective observability problems are clarified in [13] for the cases of observing one point or a group of points. Furthermore, for the observer design, some simple formulations for observing the position of a moving object are proposed in [2][3][8]. The proposed observers are guaranteed to converge in an arbitrarily large (but bounded) set of initial conditions, and since the convergence is

D.-S. Huang et al. (Eds.): ICIC 2009, LNAI 5755, pp. 371–380, 2009.

exponential it is believed that the performance of the new observers are reliable, robust and would quickly compute the position on real data.

This paper considers the problem of motion parameter estimation for a class of movements under perspective observation. Naturally, the motions are formulated in continuous-time settings and the so-called motion parameters are assumed to be all time-varying. The motion parameters are estimated by using image data observed through pin-hole camera with constant focal length (normalized to unity). The basic and important idea is to analyze the extent to which we can develop a scheme that is guaranteed to converge by observing minimum number of points. A dynamical systems approach is employed since it provides us with powerful mathematical tools, and a nonlinear observer is developed based on the second method of Lyapunov [12].

In this paper, the considered motion equation can cover a wide class of practical movements in the space. The observability of this class of movement is clarified by observing at least three points. The estimation algorithm of the motion parameter is developed. The formulated problem can be converted into the observation of a dynamical system with nonlinearities. It should be noted that smoothened image data instead of the measured one is used in the proposed formulation in order to alleviate the noises in the image data. The assumptions about the perspective system are reasonable, and the convergence conditions are intuitive and have apparently physical interpretations. The attraction of the new method lies in that the algorithm is very simple, easy to be implemented practically. Furthermore, the proposed method requires minor *a priori* knowledge about the system and can cope with a much more general class of perspective systems. It should be noted that the changing of focal length is not considered in this paper. Experimental results show the proposed algorithm is effective.

2 Problem Statement

Consider the movement of the object described by

$$\frac{d}{dt}\begin{bmatrix} x_1(t) \\ x_2(t) \\ x_3(t) \end{bmatrix} = \begin{bmatrix} 0 & \omega_1(t) & \omega_2(t) \\ -\omega_1(t) & 0 & \omega_3(t) \\ -\omega_2(t) & -\omega_3(t) & 0 \end{bmatrix} \begin{bmatrix} x_1(t) \\ x_2(t) \\ x_3(t) \end{bmatrix} + \begin{bmatrix} b_1(t) \\ b_2(t) \\ b_3(t) \end{bmatrix}, \tag{1}$$

where $x(t) = [x_1, \ x_2, \ x_3]^T$ is the position; $\omega_i(t)$ and $b_i(t)(i = 1,2,3)$ are the motion parameters.

It is supposed that the observed position by Camera 1 is defined by

$$y(t) = [y_1(t), \quad y_2(t)] = \left[\frac{x_1}{x_3}, \quad \frac{x_2}{x_3}\right], \tag{2}$$

and the observed position by Camera 2 is defined by

$$y^*(t) = [y_1^*(t), \quad y_2^*(t)] = \left[\frac{x_1 - m}{x_3}, \quad \frac{x_2 - n}{x_3}\right], \tag{3}$$

where m and n are constants. The perspective observations are defined in (2) and (3). The combination of the observations in (2) together with (3) is called "stereo vision".

In this paper, we make the following assumptions.

(A1). m and n are known constants with $m^2 + n^2 \neq 0$.

(A2). The motion parameters $\omega_i(t)$ and $b_i(t)(i = 1, 2, 3)$ are bounded.

(A3). $x_3(t)$ meets the condition $x_3(t) > \eta > 0$, where η is a constant.

(A4). $y(t)$ and $y^*(t)$ are bounded.

Remark 1. It is easy to see that assumptions (A3) and (A4) are reasonable by referring to the practical systems.

The purpose of this paper is to estimate the motion parameters $\omega_i(t)$ and $b_i(t)(i = 1, 2, 3)$ by using the perspective observations.

3 Formulation of the Motion Identification

Define

$$y_3(t) = \frac{1}{x_3(t)}. \tag{4}$$

Then, equation (1) can be transformed as

$$\begin{cases} \dot{y}_1(t) = \omega_2 + \omega_1 y_2 + \omega_2 y_1^2 + \omega_3 y_1 y_2 + b_1 y_3 - b_3 y_1 y_3 \\ \dot{y}_2(t) = \omega_3 - \omega_1 y_1 + \omega_2 y_1 y_2 + \omega_3 y_2^2 + b_2 y_3 - b_3 y_2 y_3 \\ \dot{y}_3(t) = \omega_2 y_1 y_3 + \omega_3 y_2 y_3 - b_3 y_3^2 \end{cases}. \tag{5}$$

Let

$$\theta(t) = [b_1,\ b_2,\ b_3,\ \omega_1,\ \omega_2,\ \omega_3]^T \triangleq [\theta_1,\ \theta_2,\ \theta_3,\ \theta_4,\ \theta_5,\ \theta_6]^T, \tag{6}$$

and

$$\phi(t) = \begin{bmatrix} \phi_1(t) \\ \phi_2(t) \end{bmatrix} = \begin{bmatrix} y_3 & 0 & -y_1 y_3 & y_2 & 1 + y_1^2 & y_1 y_2 \\ 0 & y_3 & -y_2 y_3 & -y_1 & y_1 y_2 & 1 + y_2^2 \end{bmatrix}. \tag{7}$$

Thus, the first two equations in (5) can be rewritten as

$$\begin{bmatrix} \dot{y}_1(t) \\ \dot{y}_2(t) \end{bmatrix} = \phi(t) \cdot \theta(t). \tag{8}$$

Similarly, for $y^*(t)$, it gives

$$\begin{bmatrix} \dot{y}_1^*(t) \\ \dot{y}_2^*(t) \end{bmatrix} = \phi^*(t) \cdot \theta(t). \tag{9}$$

with

$$\phi^*(t)=\begin{bmatrix}\phi_1^*(t)\\ \phi_2^*(t)\end{bmatrix}$$

$$=\begin{bmatrix} y_3 & 0 & -y_1^* y_3 & y_2^*+ny_3 & 1+y_1^*(y_1^*+my_3) & y_1^*(y_2^*+ny_3)\\ 0 & y_3 & -y_2^* y_3 & -y_1^*-my_3 & y_2^*(y_1^*+my_3) & 1+y_2^*(y_2^*+my_3)\end{bmatrix}, \tag{10}$$

From (2) and (3), $y_3(t)$ can be calculated by the average

$$y_3(t)=m\frac{y_1-y_1^*}{m^2+n^2}+n\frac{y_2-y_2^*}{m^2+n^2}. \tag{11}$$

Thus, $\phi(t)$ and $\phi^*(t)$ are available.

In the following, the vectors $\phi(t)\cdot\theta(t)$ and $\phi^*(t)\cdot\theta(t)$ are estimated in section 3.1 by using the perspective observations defined in (2) and (3). Then, the motion parameters $\omega_i(t)$ and $b_i(t)(i=1,2,3)$ are estimated in section 3.2 by using the stereo observation of at least three points.

3.1 Identification of $\phi(t)\theta(t)$ and $\phi^*(t)\theta(t)$

In the following, the observer of system (8) is formulated. We consider the system described by

$$\begin{bmatrix}\dot{\hat{y}}_1(t)\\ \dot{\hat{y}}_2(t)\end{bmatrix}=\begin{bmatrix}w_1(t)\\ w_2(t)\end{bmatrix},\ \begin{bmatrix}\hat{y}_1(0)\\ \hat{y}_2(0)\end{bmatrix}=\begin{bmatrix}y_1(0)\\ y_2(0)\end{bmatrix}, \tag{12}$$

$$\dot{w}_i(t)=-(f_i+\alpha_i)w_i(t)+\hat{\lambda}_i(t)\cdot sign(y_i-\hat{y}_i)+f_i\alpha_i(y_i-\hat{y}_i), \tag{13}$$

$$\hat{\lambda}_i(t)=\beta_i\left(|y_i-\hat{y}_i|+\alpha_i r_i(t)\right), \tag{14}$$

$$\dot{r}_i(t)=|y_i-\hat{y}_i|, \tag{15}$$

where f_i,α_i,β_i are positive constants, $w_i(0)$ can be any small constants, and $r_i(0)$ is chosen as $r_i(0)=0$.

Let

$$w(t)=\begin{bmatrix}w_1(t)\\ w_2(t)\end{bmatrix}. \tag{16}$$

The next theorem is obtained.

Theorem 1. All the generated signals in (12)-(15) are uniformly bounded and $w(t)$ is the asymptotic estimate of $\phi(t)\cdot\theta(t)$, i.e.

$$\lim_{t\to\infty}\left(\phi(t)\cdot\theta(t)-w(t)\right)=0. \tag{17}$$

Proof. For simplicity, we only give the proof for i=1. Let

$$e_1(t)=y_1(t)-\hat{y}_1(t). \tag{18}$$

Differentiating $e_1(t)$ yields

$$\dot{e}_1(t)=\phi_1(t)\cdot\theta(t)-w_1(t),\ \ e_1(0)=0. \tag{19}$$

Now, define

$$r_1(t)=\dot{e}_1(t)+\alpha_1 e_1(t). \tag{20}$$

Differentiating $r(t)$ yields

$$\dot{r}_1(t)=\frac{d}{dt}\left(\phi_1\theta-w_1\right)+\alpha_1\left(\phi_1\theta-w_1\right)=\eta_1(t)-\left(f_1 r_1(t)+\hat{\lambda}_1(t)sign(e_1)\right), \tag{21}$$

with

$$\eta_1(t)=\frac{d}{dt}\left(\phi_1\theta\right)+\left(f_1+\alpha_1\right)\left(\phi_1\theta\right). \tag{22}$$

The uniformly boundedness of $\eta_1(t)$ and $\dot{\eta}_1(t)$ can be easily derived by using the assumptions. Thus, there exist constants $\lambda_1>0$ such that

$$\left|\eta_1\right|+\frac{1}{\alpha_1}\left|\dot{\eta}_1\right|<\lambda_1. \tag{23}$$

Now, consider the Lyapunov candidate

$$V(t)=\frac{1}{2}r_1^2(t)+\frac{1}{2\beta_1}\left(\hat{\lambda}_1(t)-\lambda_1\right)^2. \tag{24}$$

Differentiating $V(t)$ yields

$$\begin{aligned}\dot{V}(t)&=r_1(t)\left(\eta_1(t)-f_1 r_1(t)-\hat{\lambda}_1(t)\cdot sign(e_1(t))\right)\\&\quad+\left(\hat{\lambda}_1(t)-\lambda_1\right)\left(\dot{e}_1(t)\cdot sign(e_1(t))+\alpha_1\left|e_1(t)\right|\right)\\&=-f_1 r_1^2(t)+r_1(t)\eta_1(t)-\left(\dot{e}_1(t)+\alpha_1 e_1(t)\right)\hat{\lambda}_1(t)\cdot sign(e_1(t))\\&\quad+\left(\hat{\lambda}_1(t)-\lambda_1\right)\left(\dot{e}_1(t)\cdot sign(e_1(t))+\alpha_1\left|e_1(t)\right|\right)\\&=-f_1 r_1^2(t)+r_1(t)\eta_1(t)-\lambda_1\dot{e}_1(t)\cdot sign(e_1(t))-\alpha_1\lambda_1\left|e_1(t)\right|\end{aligned} \tag{25}$$

Integrating the both sides of (25) from 0 to t yields

$$\begin{aligned} V(t) &= V(0) - f_1 \int_0^t r_1^2(\tau) d\tau + \int_0^t \left(\dot{e}_1(\tau) + \alpha_1 e_1(\tau)\right) \eta_1(\tau) d\tau \\ &\quad - \lambda_1 |e_1(t)| - \alpha_1 \lambda_1 \int_0^t |e_1(\tau)| d\tau \\ &= V(0) - f_1 \int_0^t r_1^2(\tau) d\tau + e_1(t)\eta_1(t) - e_1(0)\eta_1(0) \\ &\quad + \int_0^t e_1(\tau)\left(-\dot{\eta}_1(\tau) - \alpha_1 \eta_1(\tau)\right) d\tau - \lambda_1 |e_1(t)| - \alpha_1 \lambda_1 \int_0^t |e_1(\tau)| d\tau \\ &\le V(0) - f_1 \int_0^t r_1^2(\tau) d\tau + |e_1(t)|\left(|\eta_1(t)| - \lambda_1\right) \\ &\quad - e_1(0)\eta_1(0) + \int_0^t |e_1(\tau)|\left(|\dot{\eta}_1(\tau)| + \alpha_1 |\eta_1(\tau)| - \alpha_1 \lambda_1(\tau)\right) d\tau \\ &\le V(0) - f_1 \int_0^t r_1^2(\tau) d\tau - e_1(0)\eta_1(0) \end{aligned} \tag{26}$$

Thus, it can be seen that $V(t)$ and the integral $\int_0^t r_1^2(\tau) d\tau$ are bounded. Therefore, $r_1(t) \to 0$ as $t \to \infty$. By the definition of $r_1(t)$, it gives $e_1(t) \to 0$ and $\dot{e}_1(t) \to 0$ as $t \to \infty$. The theorem is proved.

Similarly to (10), construct the equation

$$\dot{\hat{y}}^*(t) = \begin{bmatrix} \dot{\hat{y}}_1^*(t) \\ \dot{\hat{y}}_2^*(t) \end{bmatrix} = \begin{bmatrix} w_1^*(t) \\ w_2^*(t) \end{bmatrix}, \quad \begin{bmatrix} \hat{y}_1^*(0) \\ \hat{y}_2^*(0) \end{bmatrix} = \begin{bmatrix} y_1^*(0) \\ y_2^*(0) \end{bmatrix}, \tag{27}$$

where $\begin{bmatrix} w_1^*(t) \\ w_2^*(t) \end{bmatrix} \triangleq w^*(t)$ can be defined by referring (13)-(15) by using the obtained image data $y^*(t)$ from Camera 2. Similar to Theorem 1, it can be concluded that $w^*(t)$ is uniformly bounded and

$$\lim_{t \to \infty} \left(\phi^*(t) \cdot \theta(t) - w^*(t)\right) = 0, \tag{28}$$

i.e. $w^*(t)$ is the asymptotic estimate of $\phi^*(t)\theta(t)$.

3.2 Identification of $\theta(t)$

Relations (17) and (28) tell us that, by observing one point via stereo vision, four relations about $\theta(t)$ can be obtained. It can be easily checked that the rank of the matrix $\begin{bmatrix} \phi(t) \\ \phi^*(t) \end{bmatrix}$ is three. It can be argued that the relations about $\theta(t)$ can be increased by increasing the observation points. Since there are six entries in $\theta(t)$, it can be argued that at least two points are needed to get a solution of $\theta(t)$.

Now, suppose p points are observed. For the j-th point, we denote the obtained $\begin{bmatrix} \phi(t) \\ \phi^*(t) \end{bmatrix}$ and $\begin{bmatrix} w(t) \\ w^*(t) \end{bmatrix}$ as $\begin{bmatrix} \phi^{(j)}(t) \\ \phi^{*(j)}(t) \end{bmatrix}$ and $\begin{bmatrix} w^{(j)}(t) \\ w^{*(j)}(t) \end{bmatrix}$, respectively.

Define

$$\boldsymbol{\Phi}(t) = \begin{bmatrix} \phi^{(1)}(t) \\ \phi^{*(1)}(t) \\ \vdots \\ \phi^{(p)}(t) \\ \phi^{*(p)}(t) \end{bmatrix}, \quad W(t) = \begin{bmatrix} w^{(1)}(t) \\ w^{*(1)}(t) \\ \vdots \\ w^{(p)}(t) \\ w^{*(p)}(t) \end{bmatrix}. \tag{29}$$

By Theorem 1, it gives

$$\lim_{t\to\infty}\left(\boldsymbol{\Phi}(t)\cdot\theta(t) - W(t)\right) = 0\,. \tag{30}$$

About the rank of the matrix $\boldsymbol{\Phi}(t)$, we have the next lemma.

Lemma 1. The matrix $\boldsymbol{\Phi}(t)$ is of full rank if and only if at least three points are not on a same line.

Proof. First, it can be easily checked that $rank\begin{bmatrix} \phi^{(j)}(t) \\ \phi^{*(j)}(t) \end{bmatrix} = 3$. Then, by some basic calculations, it can be concluded that $rank\begin{bmatrix} \phi^{(i)}(t) \\ \phi^{*(i)}(t) \\ \phi^{(j)}(t) \\ \phi^{*(j)}(t) \end{bmatrix} = 5$ if the i-*th* point and the j-*th* points are not same. Then, by some calculations, the lemma can be proved.

Lemma 1 means that at least three points are needed in the proposed formulation.

Theorem 2. If at least three observed points are not on a same line, then the motion parameters are observable and it holds

$$\lim_{t\to\infty}\left\{\theta(t) - \left(\boldsymbol{\Phi}^T(t)\boldsymbol{\Phi}(t)\right)^{-1}\boldsymbol{\Phi}^T(t)W(t)\right\} = 0\,, \tag{31}$$

i.e. $\left(\boldsymbol{\Phi}^T(t)\boldsymbol{\Phi}(t)\right)^{-1}\boldsymbol{\Phi}^T(t)W(t)$ is the asymptotic estimate of the vector $\theta(t)$.

Since the image data is directly used in $\boldsymbol{\Phi}(t)$, the measurement noise will directly influence the accuracy of the estimation. In the practical application of the proposed algorithm, the image data $y^{(j)}(t)$ and $y^{*(j)}(t)$ can be respectively replaced by the generated smooth signals $\hat{y}^{(j)}(t)$ and $\hat{y}^{*(j)}(t)$, since $y^{(j)}(t) - \hat{y}^{(j)}(t) \to 0$ and $y^{*(j)}(t) - \hat{y}^{*(j)}(t) \to 0$. As to the value of $y_3^{(j)}(t)$ in $\boldsymbol{\Phi}(t)$, although it can be

calculated in (11) by using the image data, we use a smoothed signal $\hat{y}_3^{(j)}(t)$ to replace it in order to mitigate the influence of measurement noises. The signal $\hat{y}_3^{(j)}(t)$ is generated as follows.

$$\dot{\hat{y}}_3^{(j)} = \hat{\lambda}_3^{(j)}(t) sign\left(m\frac{y_1^{(j)} - y_1^{*(j)}}{m^2+n^2} + n\frac{y_2^{(j)} - y_2^{*(j)}}{m^2+n^2} - \hat{y}_3^{(j)} \right), \tag{32}$$

$$\dot{\hat{\lambda}}_3^{(j)}(t) = \gamma \cdot \left| m\frac{y_1^{(j)} - y_1^{*(j)}}{m^2+n^2} + n\frac{y_2^{(j)} - y_2^{*(j)}}{m^2+n^2} - \hat{y}_3^{(j)} \right|, \tag{33}$$

where γ is a positive constant. It can be easily proved that $\hat{y}_3^{(j)}(t)$ and $\hat{\lambda}_3(t)$ are uniformly bounded and $\lim_{t\to\infty}\left(y_3^{(j)}(t) - \hat{y}_3^{(j)}(t)\right) = 0$.

The recursive algorithms of deriving $\hat{y}^{(j)}(t)$, $\hat{y}^{*(j)}(t)$ and $\hat{y}_3^{(j)}(t)$ obviously alleviate the noises in the image data. By replacing $y^{(j)}(t)$, $y^{*(j)}(t)$ and $y_3^{(j)}(t)$ in the matrix $\boldsymbol{\Phi}(t)$ with $\hat{y}^{(j)}(t)$, $\hat{y}^{*(j)}(t)$ and $\hat{y}_3^{(j)}(t)$ recpectively, we get a matrix $\hat{\boldsymbol{\Phi}}(t)$. If $\boldsymbol{\Phi}(t)$ is of full rank, then $\hat{\boldsymbol{\Phi}}(t)$ is of full rank when *t* is large enough. Then, the relation (31) still holds if $\boldsymbol{\Phi}(t)$ is replaced by $\hat{\boldsymbol{\Phi}}(t)$.

4 Experimental Results

In the experiment, an object is fixed on the tip of robot manipulator. The motion of the object is observed by two cameras. The generated motion of the object is described by

$$\frac{d}{dt}\begin{bmatrix} x_1(t) \\ x_2(t) \\ x_3(t) \end{bmatrix} = \begin{bmatrix} 0 & 0.3 & 0.4 \\ -0.3 & 0 & -0.6 \\ -0.4 & 0.6 & 0 \end{bmatrix}\begin{bmatrix} x_1(t) \\ x_2(t) \\ x_3(t) \end{bmatrix} + \begin{bmatrix} \text{- 35.9 - 3cos(2t)} \\ \text{62.4 + 0.1sin(t)} \\ \text{11.8} \end{bmatrix}. \tag{34}$$

The image data is obtained every 0.06 seconds. Four points starting at $[23, 13, 98]^T$, $[23, -13, 98]^T$, $[-23, 13, 98]^T$, and $[-23, -13, 98]^T$ are observed.

The differences between the estimated parameters and the corresponding genuine parameters are shown in Figures 1-2. The simulation results of the differences $\omega_1(t) - \hat{\omega}_1(t)$ and $\omega_2(t) - \hat{\omega}_2(t)$ are very similar to that in Figure 1. The simulation results of $b_1(t) - \hat{b}_1(t)$ and $b_3(t) - \hat{b}_3(t)$ is very similar to that in Fig. 2. It can be seen that very good estimates for the motion parameters are obtained based on the obtained image data.

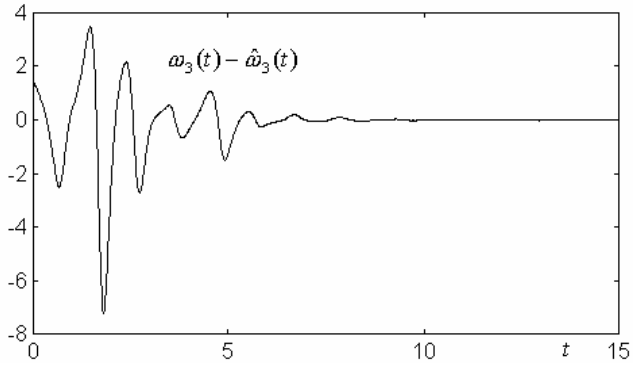

Fig. 1. The difference between $\omega_3(t)$ and $\hat{\omega}_3(t)$

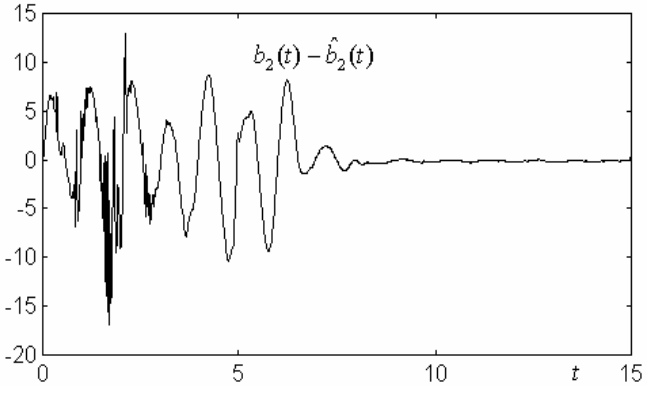

Fig. 2. The difference between $b_2(t)$ and $\hat{b}_2(t)$

5 Conclusions

The motion parameter estimation for a class of movements in the space by using stereo vision has been considered based on the observation of multiple (at least three) points. The considered motion equation can cover a wide class of practical movements in the space. The estimations of the motion parameters which are all time-varying have been developed based on the second method of Lyapunov. The assumptions about the perspective system are reasonable, and the convergence conditions are intuitive and have apparently physical interpretations. The proposed method requires minor *a priori* knowledge about the system and can cope with a much more general class of perspective systems. Experimental results have shown that the proposed algorithm is effective.

References

1. Calway, A.: Recursive estimation of 3D motion and surface structure from local affine flow parameters. IEEE Trans. on Pattern Analysis and Machine Intelligence 27, 562–574 (2005)
2. Chen, X., Kano, H.: A new state observer for perspective systems. IEEE Trans. Automatic Control 47, 658–663 (2002)
3. Chen, X., Kano, H.: State Observer for a class of nonlinear systems and its application to machine vision. IEEE Trans. Aut. Control 49, 2085–2091 (2004)
4. Chiuso, A., Favaro, P., Jin, H., Soatto, S.: Structure from motion causally integrated over time. IEEE Trans Pattern Analysis & Machine Intelligence 24, 523–535 (2002)
5. Doretto, G., Soatto, S.: Dynamic shape and appearance models. IEEE Trans. on Pattern Analysis and Machine Intelligence 28, 2006–2019 (2006)
6. Dayawansa, W., Ghosh, B., Martin, C., Wang, X.: A necessary and sufficient condition for the perspective observability problem. Systems & Control Letters 25, 159–166 (1994)
7. Ghosh, B.K., Inaba, H., Takahashi, S.: Identification of Riccati dynamics under perspective and orthographic observations. IEEE Trans. on Automatic Control 45, 1267–1278 (2000)
8. Jankovic, M., Ghosh, B.K.: Visually guided ranging from observation of points, lines and curves via an identifier based nonlinear observer. Systems & Control Letters 25, 63–73 (1995)
9. Kanatani, K.: Group-Theoretical Methods in Image Understanding. Springer, Heidelberg (1990)
10. Loucks, E.P.: A perspective System Approach to Motion and Shape Estimation in Machine Vision. Ph.D Thesis, Washington Univ. (1994)
11. Reif, K., Sonnemann, F., Unbehauen, R.: An EKF-based nonlinear observer with a prescribed degree of stability. Automatica 34, 1119–1123 (1998)
12. Satry, S., Bodson, M.: Adaptive Control, Stability, Convergence, and Robustness. Prentice Hall, Englewood Cliffs (1989)
13. Soatto, S.: 3-D structure from visual motion: Modelling, representation and observability. Automatica 33, 1287–1321 (1997)
14. Xirouhakis, Y., Delopoulos, A.: Least squares estimation of 3D shape and motion of rigid objects from their orthographic projections. IEEE Trans. on Pattern Analysis and Machine Intelligence 22, 393–399 (2000)

Binary Sequences with Good Aperiodic Autocorrelations Using Cross-Entropy Method

Shaowei Wang[1], Jian Wang[1], Xiaoyong Ji[1], and Yuhao Wang[2]

[1] Department of Electronic Science and Engineering, Nanjing University, Nanjing, Jiangsu, 210093, P.R. China
[2] Information Engineering School, Nanchang University, Nanchang, Jiangxi, 330031, P.R. China
{wangsw,wangj,jxy}@nju.edu.cn, yuhao@gmail.com

Abstract. Cross Entropy (CE) has been recently applied to combinatorial optimization problems with promising results. In this short paper a CE based algorithm is presented to search for binary sequences with good aperiodic autocorrelation properties. The algorithm proposed can explore and exploit the solution space efficiently. In most cases, it can frequently find out binary sequences with higher merit factor and lower peak sidelobe level very quickly.

1 Introduction

A binary sequence S of length n is an $n-\texttt{tuple}(s_0, s_1, \ldots, s_{n-1})$, where each s_i takes the value -1 or $+1$. The aperiodic autocorrelation of the binary sequence S at shift k is given by the autocorrelation function (ACF)

$$R_k = \sum_{i=0}^{n-k-1} s_i s_{i+k}, \quad \texttt{for} \quad k = 0, 1, ..., n-1. \tag{1}$$

Generally, binary sequences whose aperiodic autocorrelations are collectively as small as possible are suitable for application in synchronization, pulse compression and especially radar. Researchers endeavor to search for such sequences since the 1950s. Barker sequence [1], which has the peak sidelobe level (PSL) of unity ($|R_k| = 1$ for $0 < k < n-1$), is obviously the perfect one. But the longest Barker sequence found by now is of length 13. It has long been conjectured that no other Barker sequence exists [2].

Since it is unlikely to achieve the ideal behavior given by a Barker sequence when the length of a binary sequence is beyond 13, attentions turned to other measures of how closely the aperiodic autocorrelations of a binary sequence of length can collectively approach the ideal behavior. There are two measures which are commonly used to evaluate the merit figures of the ACF. One is PSL mentioned above, which is the maximum magnitude of the out of phase ACF

$$\texttt{PSL}(S) = \max_{0<k<n} |R_k|. \tag{2}$$

D.-S. Huang et al. (Eds.): ICIC 2009, LNAI 5755, pp. 381–385, 2009.

The other measure is the merit factor(MF) introduced by Golay in 1977 [3]

$$\mathtt{MF}(S) = \frac{n^2}{2\sum_{i=0}^{n-1} R_k^2} \quad \mathtt{for} \quad n > 1. \tag{3}$$

In many applications, it requires to make the PSL as small as possible and the MF as great as possible.

In order to compute the PSL or MF numerically to find out the best sequences for a given length n, it requires testing 2^n different sequences in the most naive manner. Some efficient algorithms can reduce the exponential term of the computation complexity from $\boldsymbol{O}(2^n)$ to about $\boldsymbol{O}(\sqrt{2^n})$[4]. Obviously it is impossible to search for the best sequences when n is large. As far as I know, the minimum PSL has been computed up to $n = 70$ with exhaustive search [4]. And for length n up to 60 binary sequences with the maximum MF were reported in [5]. For longer length some heuristic methods, such as neural networks, evolutionary algorithms (EAs) and so on, were proposed to search for the suboptimum binary sequences with good aperiodic autocorrelation properties [6-7].

In this paper, we use a cross entropy (CE) method to search for the desired binary sequences. The CE based algorithm generates a set of random binary sequences with series of parameters and updates them using the sample set to amend the data in the next iteration. The algorithm converges very quickly. The computational complexity is much lower than that of the other heuristic algorithms. Moreover, it can frequently produce good aperiodic autocorrelation binary sequences for given length discussed.

2 Cross Entropy Based Algorithm

The Cross Entropy (CE) method was first proposed to estimate probabilities of rare events in complex stochastic networks involving variance minimization [8]. Then it was used to solve difficult combinatorial optimization problems [9]. Generally the CE based algorithm is an iterative procedure which covers two phases. First, generate a random data sample according to the characteristics of a given problem. Then update the pre-defined dynamic parameters to produce a better sample in the next iteration.

The optimization problem in this work is to maximize the fitness function defined as following.

$$f(S) = \frac{\mathtt{MF}(S)}{\mathtt{PSL}(S)}. \tag{4}$$

The procedure of the CE based algorithm for searching binary sequences with good aperiodic autocorrelation is illustrated in Table 1, where

$$I_{f(S_i \geq \gamma_t)} = \begin{cases} 1, & \text{if } f(S_i) \geq \gamma_t \\ 0, & \text{otherwise} \end{cases}. \tag{5}$$

N is set to 150 in this work.

Table 1. Pseudo Code of CE Based Algorithm

Initialization:

Set a fraction $\rho = 0.1$, an n dimension probability vector P^0=(0.5,0.5,...,0.5), $t = 1$.

Repeat:

Generate a sample set $S_i \in \{-1, +1\}^n$, $i = 1, 2, ..., N$, where the kth element s_i^k of S_i is assigned to -1 or +1 with probability p_k^{t-1};

Calculate the fitness value $f(S_i)$ for all i;

Rank $f(S_i)$ in descending order, the new set satisfy $f(S_1) \leq f(S_2) \leq ... \leq f(S_N)$;

Let γ_t be the $1 - \rho$ sample quantile of the performance $\gamma_t = f(S_{\lceil (1-\rho)N \rceil})$;

Use the same sample to calculate $P^t := (p_1^t, p_2^2, ..., p_n^t)$ in the following way:

$$p_k^t = \frac{\sum_{i=1}^{N} I_{f(S_i) \geq \gamma_t} I_{s_i^k = 1}}{\sum_{i=1}^{N} I_{f(S_i) \geq \gamma_t}}, \; k = 1, 2, ..., n;$$

Then $t = t + 1$.

Until: Pre-assigned number of iterations or $\max p_k^t : k = 1, 2, ..., n \leq 0.001$.

Table 2. Binary Sequences of This Work

n	MF	MF in Ref.6	Min PSL	Min PSL in Ref.7	Example Sequence
71	4.9325	4.8942	6	7	2192ef67ec2b3e5587
72	4.3784	5.0233	6	7	24CF25EC7E1019550E
73	4.7243	4.0417	6	6	19884B7EADF8BA79971
74	4.5863	4.2450	6	7	3C03DF76D4E8B0C4CA6
75	4.5881	4.2040	6	6	51508217ACD21F330F9
76	4.5552	4.9283	6	7	82D03EF948B18455312
77	4.1288	4.2474	6	6	1110DBC60B8EB95B36A
78	4.2075	4.4023	6	7	1657259F87E8084D18A1
79	4.3160	3.8861	6	7	4E1F1D43FF335499492A
80	4.4693	3.4335	6	8	0896C5E86378E8CBA91
81	5.2237	4.2494	6	7	1F97804E42254CAB28E34
82	4.4179	3.5880	6	7	1E3994A0F26EDAFD445EF
83	4.2368	3.4138	6	7	3DD3D5F728317B396CC1B
84	4.0739	3.6522	6	7	F5380B005DC2471B2B26A
85	4.3524	4.1145	6	7	80F371FCEF96553B734A3
86	4.0952	3.3285	6	7	1874CDA909F508844A2FA7
87	4.7365	3.4688	6	8	7EF790CB7A1772E39170D5
88	4.5660	3.5328	6	7	4400CFC5D167189CA965AC
89	4.1602	4.3049	7	7	12EC2748DC1406152FB431D
90	4.6180	3.7886	7	8	D03EE618D4AA3B79B3D79
91	4.6575	3.9774	7	7	34D377644F21EF7E552B8D0
92	4.1736	4.0268	7	7	EBE13C2EEE6C61B4413AD2A
93	4.7943	4.1343	7	9	9E4E3E5FC245ABABFECDE8
94	4.7050	3.3600	7	8	3C6836C88E7ACD9BD7F4AE
95	4.0040	4.3939	7	8	3890BF182539C154268DB6F
96	4.1439	3.8658	7	10	F043F2951A7B190410662E99
97	4.0004	3.6300	7	9	137C639F8AA5B1284B47EB26
98	4.5089	4.0251	7	8	1CA1BC236B6CA62F368182055
99	4.1354	4.4188	7	8	62B90DFC57CF0224506465AD
100	4.6211	3.3829	7	8	B3B07A43DC9466D5229E7D7E7

3 Numerical Results

The numerical results obtained by the CE based algorithm are listed in Table 2 placed at the end of this paper. To simplify the denotation of a binary sequence, all -1's in a sequence are represented by 0's. The hexadecimal numbers denote the least significant bits of a given length binary sequences. From Table 2 we can see the MF of the binary sequence of a given length is greater than that of [6] in most cases. The PSL is less than that of [7] at the same given length.

Since it is usually difficult to analyze the exact computational complexity of a heuristic algorithm, we use the CPU time to compare the computation cost of different heuristic methods (MATLAB programming environment, 2.66-GHz Pentium(R) D CPU and 1GB of RAM). The CE based algorithm proposed here needs several seconds to converge with the given parameters in Table 1 for all length discussed in this work. However, the evolutionary algorithm [6] and neural networks [7] usually cost more than several hours to find a relatively good binary sequence of a given length.

4 Conclusions

We proposed a cross entropy method to search for the low autocorrelation binary sequence of a given length. Experimental results show that the CE based algorithm is more efficient as compared with other heuristic methods. It can find out binary sequences with good aperiodic autocorrelation properties very quickly. Some primary results are listed in this paper. In the following stage, we will analyze the characteristics of the problem and modify the parameters of the algorithm to improve the performance.

Acknowledgment

This work was supported by a grant from Natural Science Foundation of Jiangsu Province, China (No.BK2008261) and National Natural Science Foundation of China (No.60762005).

References

1. Barker, R.H.: Group Synchronizing of Binary Digital Systems. In: Jackson, W. (ed.) Communication Theory, pp. 273–287. Academic Press, New York (1953)
2. Turyn, R.J.: Sequences with Small Correlation. In: Mann, H.B. (ed.) Error Correcting Codes, pp. 195–228. Wiley, New York (1968)
3. Golay, M.J.E.: Sieves for Low Autocorrelation Binary Sequences. IEEE Transactions on Information Theory 23, 43–51 (1977)
4. Coxson, G.E., Russo, J.: Efficient Exhaustive Search for Optimal Peak-sidelobe Binary Codes. IEEE Transactions on Aerospace and Electronic Systems 41, 302–308 (2005)

5. Jedwab, J.: A survey of the merit factor problem for binary sequences. In: Helleseth, T., Sarwate, D., Song, H.-Y., Yang, K. (eds.) SETA 2004. LNCS, vol. 3486, pp. 30–55. Springer, Heidelberg (2005)
6. Deng, X., Fan, P.: New Binary Sequences with Good Aperiodic Autocorrelations Obtained by Evolutionary Algorithm. IEEE Communications Letters 3(10), 288–290 (1999)
7. Hu, F., Fan, P.Z., Darnell, M., Jin, F.: Binary Sequences with Good Aperiodic Autocorrelation Functions Obtained by Neural Network Search. Electronics Letters 33(8), 688–690 (1997)
8. Rubinstein, R.Y.: Optimization of Computer Simulation Models with Rare Events. European Journal of Operations Research 99, 89–112 (1997)
9. Rubinstein, R.Y.: Combinatorial Optimization, Cross-entropy, Ants and Rare Events. In: Uryasev, S., Pardalos, P.M. (eds.) Stochastic Optimization: Algorithms and Applications, pp. 304–358. Kluwer, Dordrecht (2001)

Agent Based Modeling of Atherosclerosis: A Concrete Help in Personalized Treatments

Francesco Pappalardo[1,2], Alessandro Cincotti[3], Alfredo Motta[4], and Marzio Pennisi[2]

[1] Institute for Computing Applications 'M. Picone', National Research Council (CNR), Rome, Italy
[2] University of Catania, Catania, Italy
[3] School of Information Science
Japan Advanced Institute of Science and Technology, Japan
[4] Politecnico di Milano
Milano, Italy
{francesco,mpennisi}@dmi.unict.it, cincotti@jaist.ac.jp,
motta.lrd@gmail.com

Abstract. Atherosclerosis, a pathology affecting arterial blood vessels, is one of most common diseases of the developed countries. We present studies on the increased atherosclerosis risk using an agent based model of atherogenesis that has been previously validated using clinical data. It is well known that the major risk in atherosclerosis is the persistent high level of low density lipoprotein (LDL) concentration. However, it is not known if short period of high LDL concentration can cause irreversible damage and if reduction of the LDL concentration (either by life style or drug) can drastically or partially reduce the already acquired risk. We simulated four different clinical situations in a large set of virtual patients (200 per clinical scenario). In the first one the patients lifestyle maintains the concentration of LDL in a no risk range. This is the control case simulation. The second case is represented by patients having high level of LDL with a delay to apply appropriate treatments; The third scenario is characterized by patients with high LDL levels treated with specific drugs like statins. Finally we simulated patients that are characterized by several oxidative events (smoke, sedentary life style, assumption of alcoholic drinks and so on so forth) that effective increase the risk of LDL oxidation. Those preliminary results obviously need to be clinically investigated. It is clear, however, that SimAthero has the power to concretely help medical doctors and clinicians in choosing personalized treatments for the prevention of the atherosclerosis damages.

1 Introduction

Atherosclerosis, a disease affecting arterial blood vessels, is one of most common disease of the developed countries. It is, in large part, due to the deposition of low density lipoproteins (LDLs), i.e., plasma proteins carrying cholesterol and

D.-S. Huang et al. (Eds.): ICIC 2009, LNAI 5755, pp. 386–396, 2009.

triglycerides, that determine the formation of multiple plaques within the arteries [8,14]. The origin of atherosclerosis is still not fully understood. However there are risk factors which increase the probability of developing atherosclerosis in humans. Some of these risk factors are beyond a person's control (smoking, obesity), others seem to have genetic origin (familial hypercholesterolemia, diabetes, hypertension) [13]. Common denominator in all the form of atherosclerosis is the elevated level of LDL, which is subject to oxidation becoming ox-LDL, that promotes an inflammatory response and immune activation in the artery walls [4]. The formation of atherosclerotic plaques in the arteries reduces both the internal diameter of vessels and the blood flux leading to a number of serious pathologies [20]. Early studies demonstrated that ox-LDL can induce activation of monocytes/macrophages, endothelial cells and T cells. Ox-LDLs engulfed by macrophages form the so called foam cells [17]. These cells represent the nucleus of the plaques formation. Ox-LDL promotes also immune activation of B cells inducing the production of specific anti ox-LDL antibody (OLAB).

Atherosclerosis and its anatomical consequences cause severe problems. Stenosis (narrowing) and aneurysm of the artery are chronic, slowly progressing and cumulative effects indicating the progression of atherosclerotic disease. In both case the result is an insufficient blood supply to the organ fed by the artery. Most commonly, soft plaque suddenly ruptures, causes the formation of a thrombus that will rapidly slow or stop blood flow, leading to death of the tissues fed by the artery. This catastrophic event is called infarction and is not predictable. The most common event is thrombosis of the coronary artery causing infarction (a heart attack): However, since atherosclerosis is a body wide process, similar events also occur in the arteries of the brain (stroke attack), intestines, kidneys, etc. Those atherosclerosis associated events often cause dead or serious invalidating diseases and require preventive treatments. Vaccine research for atherosclerosis is a hot pharmaceutical topic.

Recently we proposed a model based on the Agent Based Model (ABM) paradigm [12] which reproduces clinical and laboratory parameters associated to atherogenesis. The model and its computer implementation (SimAthero simulator) considers all the relevant variables that play an important role in atherogenesis and its induced immune response, i.e., LDL, ox-LDL, OLAB, chitotriosidase and the foam cells generated in the artery wall.

In this paper we will analyze four different situations over a time scale of two years. Patients with an LDL level considered normal, where no foam cells are formed; patients having high level of LDL with a delay to apply appropriate treatments; patients that have high LDL levels, treated with specific drugs aiming at reducing total LDL (statins); patients that are characterized by several oxidative events (smoke, sedentary life style, assumption of alcoholic drinks and so on so forth) that effective increase the risk of LDL oxidation.

The plan of the paper is the following. In §2 we briefly describe the biological scenario we modeled and the computer implementation of the simulator. In §3 we describe our simulated patients and we show the simulator results. We briefly draw conclusions and future extension of this work in §4.

2 The Model and Its Computer Implementation

2.1 The Biological Scenario

Exogenous and endogenous factors induce in humans a very small, first oxidative process of blood circulating native LDLs (minimally modified LDLs or mm-LDLs). In endothelium mm-LDLs are extensively oxidized from intracellular oxidative products and then recognized by the macrophage scavenger receptor. High level and persistent in time LDLs lead to macrophages engulfment and their transformation in foam cells. Contrary, low level of LDLs and their oxidized fraction, lead to the internalization of the oxidized low density lipoproteins and subsequent presentation by major histocompatibility complex class II at the macrophages surface. Recognition of ox-LDL by macrophages and naive B cells leads, by T helper lymphocytes cooperation, to the activation of humoral response and production of OLAB. When the OLAB/ox-LDL immune complexes are generated in the vascular wall, the macrophages catch them by the Fc receptor or via phagocytosis and destroy ox-LDL in the lysosome system. During this process, the activated macrophage releases chitotriosidase enzyme, that is then used as a marker of macrophage activation.

2.2 SimAthero

To describe the above scenario one needs to include all the crucial entities (cells, molecules, adjuvants, cytokines, interactions) that biologists and medical doctors (MD) recognize to be relevant in the game. Having this in mind we realized an Agent based model, described [12], that contains all the entities and interactions considered mandatory by biologists and MD to correctly reproduce the process.

Atherosclerosis is a very complex phenomenon which involves many components, and some of them are not yet fully understood. In the present version of the simulator we considered only the immune system processes (IS) that control atherogenesis. These processes may occur in IS organs, like lymph nodes, or locally, in the artery endothelium. To describe the Immune processes we considered both cellular and molecular entities.

Cellular entities can take up a state from a certain set of suitable states and their dynamics is realized by means of state-changes. A state change takes place when a cell interacts with another cell, with a molecule or with both of them. We considered the relevant lymphocytes that play a role in the atherogenesis-immune system response, B lymphocytes and helper T lymphocytes. Monocytes are represented as well and we take care of macrophages. Specific entities involved in atherogenesis are present in the model: low density lipoproteins, oxidized low density lipoproteins, foam cells, auto antibodies anti oxidized low density lipoproteins and chitotriosidase enzyme. Cytotoxic T lymphocytes are not taken into consideration because they are not involved in the immune response (only humoral response is present during atherogenesis).

Molecular entities The model distinguishes between simple small molecules, like interleukins or signaling molecules in general, and more complex molecules like immunoglobulins and antigens, for which we need to represent the specificity.

We only represent interleukin 2, necessary for the development of T cell immunologic memory which is one of the unique characteristics of the immune system and depends upon the expansion of the number and function of antigen-selected T cell clones.

For what is related to the immunoglobulins, we represent only type IgG. This just because at the actual state we don't need to represent other classes of Ig and because IgG is the most versatile immunoglobulin since it is capable of carrying out all of the functions of immunoglobulins molecules. Moreover IgG is the major immunoglobulin in serum (75% of serum Ig is IgG) and IgG is the major Ig in extra vascular spaces.

The actual model does not consider multi-compartments processes and mimics all processes in a virtual region in which all interactions take place. Our physical space is therefore represented by a 2D domain bounded by two opposite rigid walls and left and right periodic boundaries. This biological knowledge is represented using an ABM technique. This allows to describe, in a defined space, the immune system entities with their different biological states and the interactions between different entities. The evolution of the system in space and in time is generated from the interactions and diffusion of the entities. Compared to the complexity of the real biological system our model is still very naive and it can be extended in many aspects. However, the model is sufficiently complete to describe the major characteristics of the atherogenesis-immune system response phenomenon.

The computer implementation of the model (SimAthero hereafter) has two main classes of parameters: the first one refers to values known from standard immunology literature [1,9]; the second one collects all the parameters with unknown values which we arbitrarily set to plausible values after performing a series of tests (*tuning phase*).

The simulator takes care of the main interactions that happens during an immune response against atherogenesis.

Physical proximity is modeled through the concept of lattice-site. All interactions among cells and molecules take place within a lattice-site in a single time step, so that there is no correlation between entities residing on different sites at a fixed time. The simulation space is represented as a $L \times L$ hexagonal (or triangular) lattice (six neighbors), with periodic boundary conditions to the left and right side, while the top and bottom are represented by rigid walls. All entities are allowed to move with uniform probability between neighboring lattices in the grid with equal diffusion coefficient. In the present release of the simulator chemotaxis is not implemented.

LDLs values can be fixed in order to simulate different patients both in normolipidic condition and in hypercholesterolemic condition. The same applies to ox-LDLs. However human habits change with time and personal life style. A normolipidic patient can change its attitude becoming an hypercholesterolemic one and vice versa. For this reason we allow the simulator to accept varying life style conditions and preventive actions to decrease risk factors.

3 Results

SimAthero includes the possibility of mimicking biological diversity of patients. The general behavior of a class of virtual patients arise from the results of a suitable set of patients, i.e., the mean values of many runs of the simulator of different patients under the same conditions. The class of virtual patients described by the model were tuned against *human* data data collected by [6,7] where different conditions, such as normal and hypercholesterolemic patients were analyzed.

In this section we analyze the behavior of the same patients in four broad classes of clinical conditions to show how SimAthero could be used to analyze and predict the effects of various LDL levels in the host. Humoral immune system response is also highlighted: it represents the main protective counterattack that the host can mount against atheromatous plaques formation.

The normal patient simulation is used as control experiment for the other simulations. The differences among these four clinical conditions depend on the LDL level and the time interval which occurs between the time in which concentration of LDL rise above normal level and the time in which the patient takes appropriate measures (lifestyle or drug) to reduce it to normal level.

A patient with a LDL level of roughly 950-970 ng/μl of blood is considered normal in clinical practice and he will develop atheromatous plaques with very low probability. Results obtained by SimAthero for a mean virtual normal patient (Figure 1) show that he will not support the formation of foam cells and, as a consequence, the beginning of the atherogenesis process is absent or negligible. The humoral response is absent due to limited level of oxidized LDL that in this situation is completely controlled by the liver cleaning mechanism.

We then simulated a scenario in which a normal virtual patient leads its LDL level at 1900 ng/μl, keeping it up between 1650 and 1750 ng/μl. Looking at figure 2 one can observe about 20 foam cells per μl at the end of in silico follow up. This leads to a small atherogenesis process due to the high level of LDL and therefore high level of oxidized LDL. Ox-LDL in this situation stimulates the immune system humoral response through macrophages presentation. Even if antibodies anti-Ox-LDL are present, they are not completely able to keep under control the foam cells formation that will lead to atheromatous plaques accumulation in artery walls.

Figure 3 represents a microphotograph-like snapshot of the simulated artery wall section. We took four snapshots, one every 6 months of the in silico follow-up period.

The third case represents a virtual patient that, for some reason depending on his own life style or linked with some pathology (genetic hypercholesterolemia, diabetes), rises up the LDL level to 1900-2000 ng/μl. The virtual patient is immediately treated with statins, a class of drugs that lower cholesterol levels in people with or at risk of cardiovascular disease. These treatments lower cholesterol by inhibiting the enzyme HMG-CoA reductase, which is the rate-limiting enzyme of the mevalonate pathway of cholesterol synthesis. Inhibition of this enzyme in the liver results in decreased cholesterol synthesis as well as increased

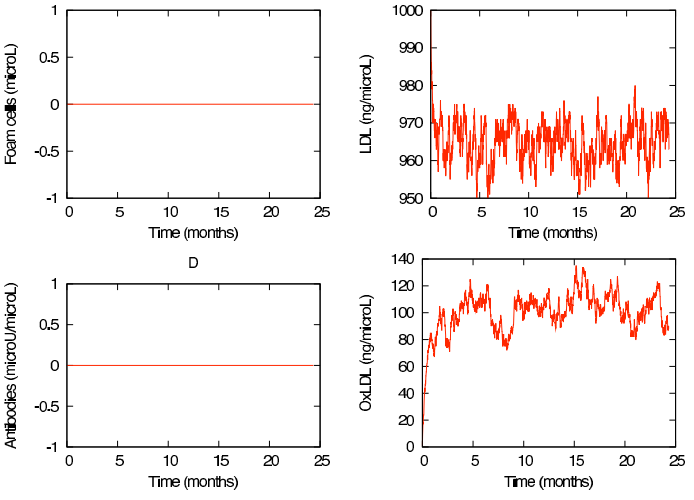

Fig. 1. Simulation results of a virtual patient with level of LDL considered normal. The follow-up period is two years. The figure shows that foam cells formation is absent in this patient. Also immune system response is absent because the oxidized part of LDL is kept under control by the cleaning mechanism of the liver.

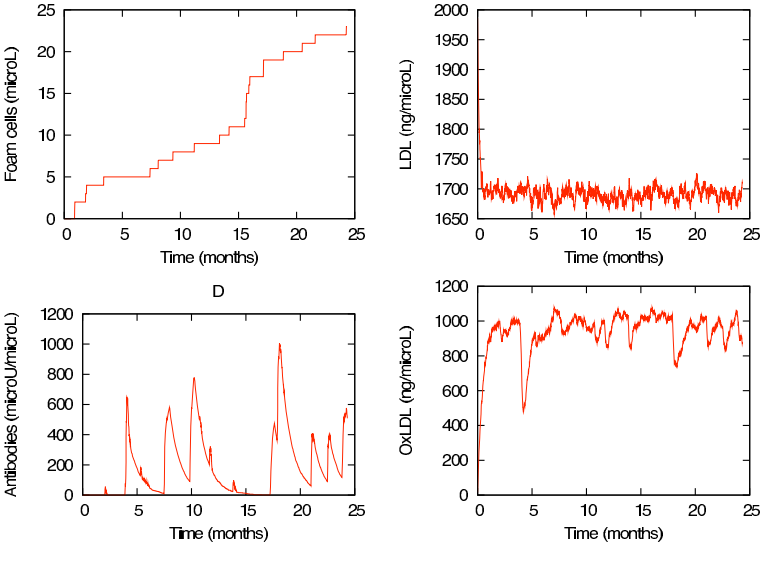

Fig. 2. Simulation results of a virtual patient with level of LDL considered at high risk. The follow-up period is two years. The figure shows that foam cells formation is present, leading to an atherogenesis process. Specific antibodies anti-oxLDL, due to humoral immune system response, are not sufficient to protect the host from the initial atherosclerosis damage.

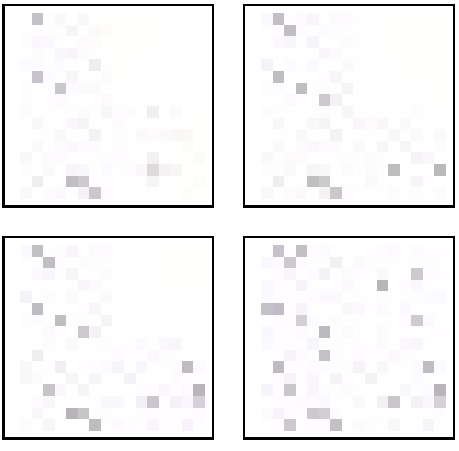

Fig. 3. Simulation results of an artery wall section microphotograph-like. Pictures are taken (clockwise sense) at 6, 12, 18, 24 months of the observed period. From the analysis of this figure, one can observe that atheromatous plaques formation increases during the follow-up period, reducing the total volume of the artery.

synthesis of LDL receptors, resulting in an increased clearance of LDL from the bloodstream [10]. We interrupted the treatment at month 14. Figure 4 shows that initial rise of foam cells is blocked soon after the statin treatment begins. The foam cells formation is then stopped until statins are administered. Between two sessions of treatment, we put about two weeks of rest in which one can observe returning peaks of LDL. From this simulation, important facts can be deduced. Firstly drugs that concretely lower the total LDL level could be effective in preventing foam cells formation and, as a consequence, they are able to limit atherosclerosis induced damage. Secondly, periods of rest did not influence the benefits of the treatment. This can be explained looking at the humoral immune system response in figure 4. Peaks of antibodies anti-Ox-LDL are able to keep ox-LDL relatively low, inducing an effective removal of antibodies anti-Ox-LDL and Ox-LDL immunocomplexes by macrophages. Thirdly, if the treatment is suspended and the LDL returns to an unacceptable level, foam cells formation starts again.

Figure 5 shows tha artery wall section during the follow-up period of the hypercholesterolemic patient treated with statins.

Finally we simulated a mean virtual patient that keeps both LDL and ox-LDL levels high due to oxidative relative scenarios. This means wrong life styles habits linked to smoke, diet or drinks. This is the worst scenario we simulated, from the clinical point of view. Looking at figure 6, one can observe that even if a strong humoral immune system is present (due to high levels of ox-LDL) the foam cells formation is very high (about 70 foam cells per μl at the end of the follow-up period). This indeed leads to a high risk situation in which all related atherosclerosis consequences can arise.

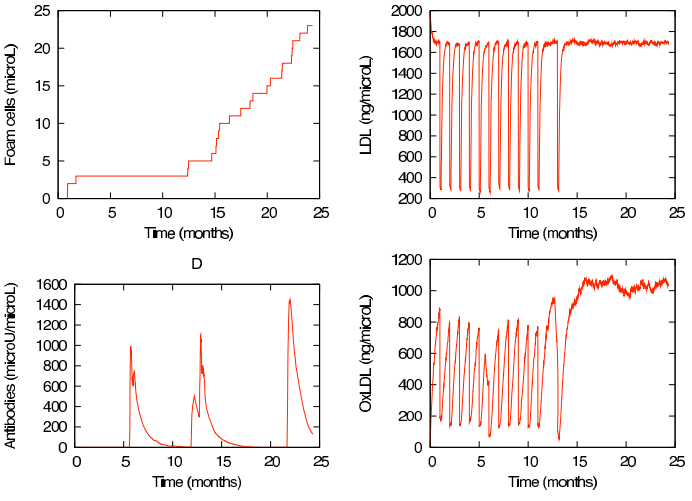

Fig. 4. Simulation results of a virtual patient with level of LDL considered at high risk, treated with statins. The follow-up period is two years. The figure shows that foam cells formation is initially present but is kept under control by statin treatment. During periods of rest, humoral immune system response is able to maintain ox-LDL level relatively low. After month 14 the treatment is suspended. Soon after the interruption of treatment, LDL and consequently its oxidized part, start to rise up again, leading to an atherogenesis process.

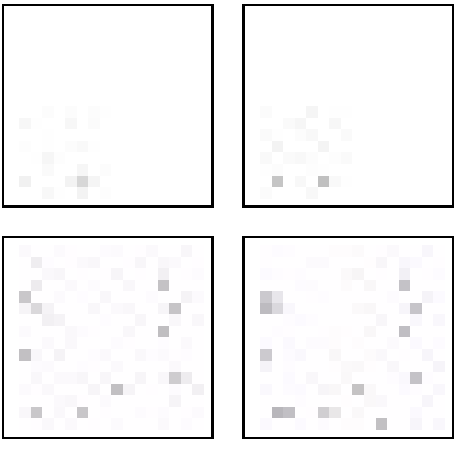

Fig. 5. Simulation results of an artery wall section microphotograph-like. Pictures are taken (clockwise sense) at 6, 12, 18, 24 months of the observed period. From the analysis of this figure, one can observe that atheromatous plaques formation is kept under control during the statin treatment. After month 14, LDL level starts to increase again, reducing the total volume of the artery.

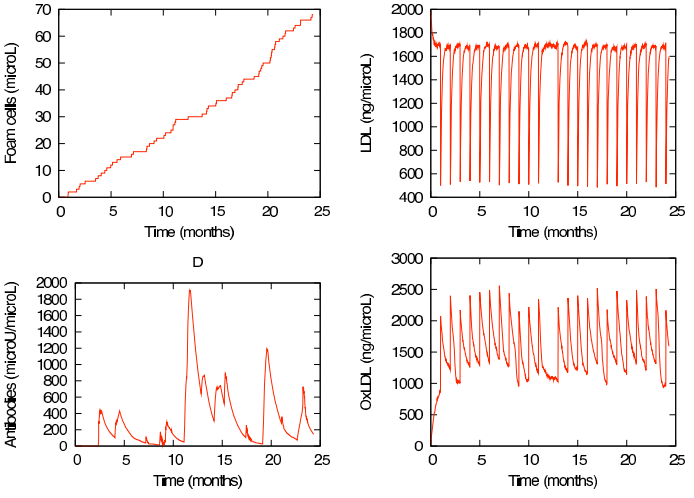

Fig. 6. Simulation results of a virtual patient with level of both LDL and ox-LDL very high. The follow-up period is two years. The figure shows that foam cells formation rise up and continue to grow. Even if a strong humoral immune system response is present, the atherogenesis process continues, leading to severe consequences.

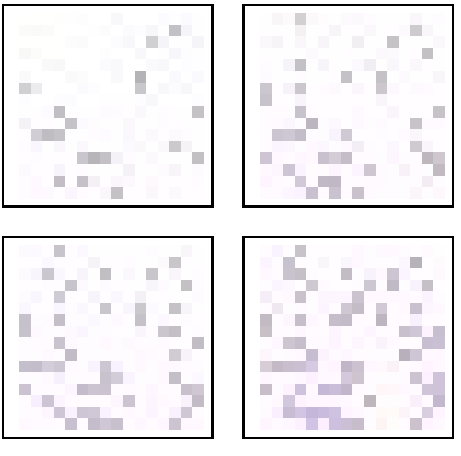

Fig. 7. Simulation results of an artery wall section microphotograph-like. Pictures are taken (clockwise sense) at 6, 12, 18, 24 months of the observed period. From the analysis of this figure, one can observe that atheromatous plaques formation is promoted due to wrong life style linked habits. The total volume of the simulated artery wall section is concretely reduced.

Figure 7 shows the damage caused by foam cells formation to the simulated artery wall section.

4 Conclusions

Atherosclerosis is a pathology where the immune control plays a relevant role. In this article, we presented studies on the increased atherosclerosis risk using an ABM model of atherogenesis and its induced immune system response in humans.

It is well known that the major risk in atherosclerosis is persistent high level of LDL concentration. However it is not known if short period of high LDL concentration can cause irreversible damage and if reduction of the LDL concentration (either by lfe style or drug) can drastically or partially reduce the already acquired risk.

Using an ABM cellular model describing the initial phase of plaque formation (atherogenesis) we are able to simulate the effect of life style which increases the risk of atherosclerosis. We were also capable to simulate one of the best known treatment against high levels of cholesterol, based on statin drugs.

It is clear that SimAthero can concretely help both clinicians and medical doctors to better understand the atherosclerosis process and, after needed clinical validation, can help to better design a treatment dosage, in the possible view of personalized medicine.

References

1. Abbas, A.K., Lichtman, A.H., Pillai, S.: Cellular and molecular immunology, 6th edn. Saunders, Philadelphia (2007)
2. Artieda, M., Cenarro, A., Gañàn, A., Jericó, I., Gonzalvo, C., Casado, J.M., Vitoria, I., Puzo, J., Pocoví, M., Civeira, F.: Serum chitotriosidase activity is increased in subjects with atherosclerosis disease. Arterioscler. Thromb. Vasc. Biol. 23, 1645–1652 (2003)
3. Artieda, M., Cenarro, A., Gańàn, A., Lukic, A., Moreno, E., Puzo, J., Pocoví, M., Civeira, F.: Serum chitotriosidase activity, a marker of activated macrophages, predicts new cardiovascular events independently of C-Reactive Protein. Cardiology 108, 297–306 (2007)
4. Berliner, J.A., Heinecke, J.W.: The role of oxidized lipoproteins in atherogenesis. Free Radic. Biol. Med. 20(5), 707–727 (1999)
5. Brizzi, P., Isaja, T., D'Agata, A., Malaguarnera, A., Malaguarnera, M., Musumeci, S.: Oxidized LDL antibodies (OLAB) in patients with beta-thalassemia major. J. Atheroscler. Thromb. 9(3), 139–144 (2002)
6. Brizzi, P., Tonolo, G., Carusillo, F., Malaguarnera, M., Maioli, M., Musumeci, S.: Plasma Lipid Composition and LDL Oxidation. Clin. Chem. Lab. Med. 41(1), 56–60 (2003)
7. Brizzi, P., Tonolo, G., Bertrand, G., Carusillo, F., Severino, C., Maioli, M., Malaguarnera, L., Musumeci, S.: Autoantibodies against oxidized low-density lipoprotein (ox-LDL) and LDL oxidation status. Clin. Chem. Lab. Med. 42(2), 164–170 (2004)
8. Hanson, G.K.: Inflammation, atherosclerosis, and coronary artery disease. N. Engl. J. Med. 352(16), 1685–1695 (2005)
9. Klimov, A.N., Nikul'cheva, N.G.: Lipid and Lipoprotein Metabolism and Its Disturbances. Piter Kom, St. Petersburg (1999)

10. Law, M.R., Wald, N.J., Rudnicka, A.R.: Quantifying effect of statins on low density lipoprotein cholesterol, ischaemic heart disease, and stroke: systematic review and meta-analysis. BMJ 326(7404), 1423 (2003)
11. Orem, C., Orem, A., Uydu, H.A., Celik, S., Erdol, C., Kural, B.V.: The effects of lipid-lowering therapy on low-density lipoprotein auto-antibodies: relationship with low-density lipoprotein oxidation and plasma total antioxidant status. Coron. Artery Dis. 13(1), 56–71 (2002)
12. Pappalardo, F., Musumeci, S., Motta, S.: Modeling immune system control of atherogenesis. Bioinformatics 24(15), 1715–1721 (2008)
13. Romero-Corral, A., Somers, V.K., Korinek, J., Sierra-Johnson, J., Thomas, R.J., Allison, T.G., Lopez-Jimenez, F.: Update in prevention of atherosclerotic heart disease: management of major cardiovascular risk factors. Rev. Invest. Clin. 58(3), 237–244 (2006)
14. Ross, R.: Atherosclerosis–an inflammatory disease. N. Engl. J. Med. 340(2), 115–126 (1999)
15. Shaw, P.X., Hörkkö, S., Tsimikas, S., Chang, M.K., Palinski, W., Silverman, G.J., Chen, P.P., Witztum, J.L.: Human-derived anti-oxidized LDL autoantibody blocks uptake of oxidized LDL by macrophages and localizes to atherosclerotic lesions in vivo.t Arterioscler. Thromb. Vasc. Biol. 21(8), 1333–1339 (2001)
16. Shoji, T., Nishizawa, Y., Fukumoto, M., Shimamura, K., Kimura, J., Kanda, H., Emoto, M., Kawagishi, T., Morii, H.: Inverse relationship between circulating oxidized low density lipoprotein (oxLDL) and anti-oxLDL antibody levels in healthy subjects. Atherosclerosis 148(1), 171–177 (2000)
17. Steinberg, D.: Low density lipoprotein oxidation and its pathobiological significance. J. Biol. Chem. 272(34), 20963–20966 (1997)
18. Tinahones, F.J., Gomez-Zumaquero, J.M., Rojo-Martinez, G., Cardona, F., Esteva de Antonio, I.E., Ruiz de Adana, M.S., Soriguer, F.K.: Increased levels of anti-oxidized low-density lipoprotein antibodies are associated with reduced levels of cholesterol in the general population. Metabolism 51(4), 429–431 (2002)
19. Tinahones, F.J., Gomez-Zumaquero, J.M., Garrido-Sanchez, L., Garcia-Fuentes, E., Rojo-Martinez, G., Esteva, I., Ruiz de Adana, M.S., Cardona, F., Soriguer, F.: Influence of age and sex on levels of anti-oxidized LDL antibodies and anti-LDL immune complexes in the general population. J. Lipid Res. 46(3), 452–457 (2005)
20. Vinereanu, D.: Risk factors for atherosclerotic disease: present and future. Herz, Suppl. 3, 5–24 (2006)

MotifMiner: A Table Driven Greedy Algorithm for DNA Motif Mining

K.R. Seeja[1], M.A. Alam[1], and S.K. Jain[2]

[1] Department of Computer Science
[2] Department of Biotechnology, Hamdard University, NewDelhi, India
seeja@jamiahamdard.ac.in, aalam@jamiahamdard.ac.in,
skjain@jamiahamdard.ac.in

Abstract. DNA motif discovery is a much explored problem in functional genomics. This paper describes a table driven greedy algorithm for discovering regulatory motifs in the promoter sequences of co-expressed genes. The proposed algorithm searches both DNA strands for the common patterns or motifs. The inputs to the algorithm are set of promoter sequences, the motif length and minimum Information Content. The algorithm generates subsequences of given length from the shortest input promoter sequence. It stores these subsequences and their reverse complements in a table. Then it searches the remaining sequences for good matches of these subsequences. The Information Content score is used to measure the goodness of the motifs. The algorithm has been tested with synthetic data and real data. The results are found promising. The algorithm could discover meaningful motifs from the muscle specific regulatory sequences.

Keywords: Regulatory motif, Greedy approach, Information content, Motif discovery.

1 Introduction

Regulatory motifs are short patterns of nucleotides, usually 5-20 bp long, found common in the promoter region of set of co-expressed genes. Co-expressed genes are considered to be co-regulated which in turn considered to have common binding sites. The regulatory motifs control the expression or regulation of genes. Usually they describe the transcription factor binding sites in the upstream of a gene's transcription start site. Identification of these motifs gives insight into the regulatory mechanism of genes. Motif discovery algorithms aim to discover these common patterns. Identification of DNA motifs is complex due to mutations and substitutions which make them weekly conserved patterns. A motif discovery algorithm has to identify these patterns which may present in either strand of the DNA double helix. This paper describes an enumerative table driven algorithm which is a variant of the (l,d) motif discovery problem where l is the length of the motif and d is the maximum number of allowed mutations of the original motif. Enumerative algorithms generate all 4^l possible combinations of {A, C, G, T} of length l. By considering each of this generated sequence as original

D.-S. Huang et al. (Eds.): ICIC 2009, LNAI 5755, pp. 397–406, 2009.

motif, these algorithms try to find all motifs with a maximum of *d* mutations of original motif. Here the complexity increases exponentially with increase in *l*. The proposed algorithm is a kind of enumerative algorithm. But the algorithm does not generate all the 4^l possible combinations of {A, C, G, T}. Instead of this, the algorithm takes the shortest input sequence and generates all *l*-mers. These *l*-mers and their reverse complements become the original motif candidates. Since the co-expressed genes are assumed to have common transcription factor binding sites, atleast one motif will be common in all sequences. The proposed algorithm makes use of this valid assumption and considers only the *l*-mers of the shortest sequence and their reverse complement instead of all 4^l combinations. In the proposed algorithm, the user can specify the minimum information content *I,* whose value is between 0 and 2 instead of *d*. The more the value of *I* is close to 2, the more the corresponding motif is relevant. The output generated by MotifMiner is the set of motifs whose Information Content is greater than or equal to the user defined minimum Information Content *I*. The algorithm uses a table to store the motif instances discovered so far. At each step the algorithm selects the motif with highest information content greedily. The performance of the algorithm has been tested with synthetic datasets and real datasets.

2 Motif Discovery Problem

The basic form of a regulatory motif discovery problem can be defined as follows. Given a set of promoter sequences of co-expressed genes, which are believed to share some common pattern, the problem is to identify these common patterns. The motif discovery algorithms can be classified into two as enumerative and probabilistic. Enumerative algorithms generate all possible motifs which are subsequences of length *l*. Then, it performs exhaustive search over the generated search space for significant motifs. This exhaustive enumeration is an NP-hard problem. The second class of algorithms uses statistical models of Position Frequency Matrix (PFM) and Position Weight Matrix (PWM). The proposed algorithm is a combination of both enumerative as well as probabilistic approaches.

2.1 Motif Score and Motif Representation

In DNA motif discovery exact matching patterns are rare due to mutations. The motif discovery algorithms return sets of similar patterns. One way to find which motif is better than other is by counting the number of mismatched nucleotides. But this count is not biologically valid always. Many scores like p-value, z-score and Information Content are suggested to evaluate the motifs. MotifMiner uses the Information Content score to find the goodness of the discovered motifs.

The motifs can be represented in many ways like consensus sequence, Position Weight Matrix, and sequence logo.

3 Related Work

Many algorithms and scores have been suggested for motif discovery. Oligoanalysis [1] is a word enumeration algorithm which performs a brute force search over all

possible motifs of length *l*. Though the algorithm is simple, memory requirement is high. Later another word based algorithm Yeast Motif Finder (YMF)[2] which uses z-score and a background model based on Markov chain has been suggested. There are some other word based approaches [3],[4],[5] which use suffix trees and its variants to represent sequences. WINNOWER [6] is another word based algorithm which uses graph theory concepts.

Consensus [7] is a greedy probabilistic algorithm which tries to find highest information content motif. Most of the probabilistic algorithms use statistical techniques like expectation maximization (EM) and Gibbs sampling. MEME [8] is a famous motif discovery algorithm which uses EM. Gibbs sampler [9] is another heavily used probabilistic algorithm which is a Markov Chain Monte Carlo approach. Later many algorithms like AlignACE [10], Motif Sampler[11], Bioprospector [12] and GibbsST [13] have been developed by extending Gibbs Sampling.

Many researchers have explored the use of machine learning techniques like genetic algorithm [14],[15] and neural networks[16] in motif discovery. Some algorithms [18],[19] based on phylogenetic foot printing[17] instead of promoter sequences of co-expressed genes have been proposed. Also a hybrid approach of phylogenetic foot printing and other enumerative [20] and probabilistic approaches [21], [22], [23] have been suggested.

4 Proposed Algorithm

The proposed algorithm is a word based algorithm. The inputs are set of promoter sequences *S*, the length of the motif *l* and the minimum information content *I*. The assumption made is that each sequence contains at least one instance of the motif. This assumption is valid since the co-expressed genes share some common binding sites. The algorithm checks both DNA strands for the motif instances.

The Information Content is the score used for finding best motifs. We have used the greedy approach similar to that of Consensus [7] and used the same score suggested in the original Gibbs sampler[9] which is given below.

Let Q is the Position Specific Scoring Matrix defined as

$$q_{i,j} = \frac{c_{i,j}}{c_i}, \tag{1}$$

where $c_{i,j}$ is the observed count of base j at position i and is the sum of $c_{i,j}$ over the alphabets{A,C,T,G}.

The Information content IC is defined as,

$$IC = \frac{1}{l} \times \sum_{i=1}^{l} \sum_{j=1}^{4} \left[q_{i,j} \times \log_2 \left(\frac{q_{i,j}}{P_j} \right) \right]. \tag{2}$$

Here p_j is the probability of base j occurring in the back ground sequences. It is calculated as the number of base j in the motif instances divided by total number of bases in the motif instances.

The logarithm base 2 is taken to express the information content in bits between 0 and 2 (weakest motif to strongest motif).

The algorithm takes the shortest sequence from the set of given promoter sequences. Let it be the first sequence. Then it generates all the substrings of size equal to the length of the motif, *l* using sliding window approach. Then create a table of size equal to twice the number of subsequences. Add all the subsequences and their reverse complements into the table. Add the subsequence, its staring position, + or - (represent forward strand and complementary strand) and the sequence number into the attached list associated with each table entry. The shortest sequence is selected to reduce the size of this table. Consider the first entry in the table. Then take second sequence from the remaining sequences and generate subsequences of length *l*. Calculate the information content IC for each combination of the sequences in the list associated with the first entry in the table and each subsequence of the second sequence. Select the subsequence in the second sequence whose combination with the table entry gives the highest IC. If this highest IC is less than the specified minimum information content *I*, delete the corresponding entry from the table. Otherwise, add the corresponding information such as the subsequence, its starting position, + or – to represent forward or complimentary strand and sequence number to the list attached to that table entry. Now take the remaining input sequences one by one and repeat the process. After calculating all instances of the first motif, go to the second entry in the table and repeat the procedure. After repeating the procedure for all sequences and all table entries, the table will contain all instances of all motifs whose IC is greater than or equal to *I*.

4.1 Pseudo Code

Input: The DNA sequences S, length of the motif *l*, Minimum information content *I*.

Output: Motif (s)

```
Motif discovery(S,I,l)
{
   Let S[1] is the shortest sequence;
   Length=strlen(S[1]);
   For i= 1 to length-l do
   {
          X=S[1][i]….S[1][i+l];
          X'= reverse complement of X;
          Add X and X' to the end of the list associated
            with Table[i] and Table [(length-l) +i]
               respectively;
   }
10:For each j in the table do
```

```
    {
            For each sequence S_i do
            {
              Generate l-mers from the sequence S_i;
              Calculate IC from the sequences in the list
                associated with table[j] and each l-mers
                (and its reverse complement);
          Select the highest IC;
        If IC<I then delete table[j]and goto 10;
        Else
               Add the l-mer corresponds to highest IC
                 to the list associated with table[j];
            }
      }
}
```

4.2 Data Structure

The table is implemented as list of list. Both lists are implemented as linked list since memory allocation is dynamic with linked list. Each node in the main list has two pointer parts: a pointer to the next node in the main list and the start pointer to the associated list. The associated list has an element part and a pointer part. The element part contains the information about a motif instance such as the subsequence, its staring position, + or – to represent forward or complimentary strand and sequence number. The pointer part contains the pointer to the next node in the associated list. After execution, the associated lists contain all the instances of the motifs having IC greater than or equal to *I*.

4.3 Running Time

Running time of the algorithm depends on the number of promoter sequences n , their length m and the length of the motif l. The inner for loop repeats for $n \times (m-l)$ times. The outer for loop repeats for $2\times (m-l)$ times. Therefore the total running time, $T(n) = O(n\times (m-l)^2)$.

4.4 Memory Requirement

The main list contains $2\times(m-l)$ nodes initially. Since linked list is used for implementation, the memory occupied by the main list node and its associated list can be deallocated when ever delete operation is performed. The worst case is that there is a motif instance for each of the initial $2\times (m-l)$ subsequences in all the sequences. In

that case each of the associated list will have *n* nodes. Thus, in the worst case memory is needed to store 2× (m-*l)* main list nodes and 2*n*× *(*m-*l)* associated list nodes.

5 Performance Evaluation

The performance of the algorithm has been evaluated with synthetic data and real data. The algorithm is implemented in C++ in a system with 1GB RAM. In order to find best motifs, run the program with different values of *I* (between 0 and 2), starting from 2.

5.1 Synthetic Data

The synthetic data set is created by implanting a common motif with varying degrees of conservation at random positions into six DNA sequences each of length=52. We have created six synthetic DNA sequences containing some instance of the pattern '**CCGATTACCGA**' [24] and are given in figure 1. We ran the algorithm with *I*=2,1.5,1 etc. There were no motif instances for *I* value 2 and only one motif instance for *I* value 1.5. The information content of this motif is 1.53909. This is the best motif and is underlined in figure 1.

GAATTCATACCAGATCAC**CGGATTCCCGA**CTCCAAATGTGTCCCCCTCACAC
TCCC**CCGATTACCGT**CTTCTGCTCTTAGACCACTCTACCCTATTCCCCACACT
CACCGGAGCCAAAGCCGCGGCCCTTCCGTT**CCGATTACCGA**AAAGACCCCA
CCCGTAGGTGGCAAGCTAGCTTAAGTAACGCCACT**TCGATTAACGA**GGAAA
AATACATAACTGA**CCTATTATCGA**GTTCAGATCAAGGTCAGGAACAAAGAA
ACA**CCGATTACCGT**AACCGTAAGATAGTGGTATCGATACGTAGACAGTTTA

Fig. 1. Synthetic DNA sequences and the discovered motifs

5.2 Real Data

In order to evaluate the performance of the algorithm on real biological data, the algorithm is applied to two real datasets.

5.2.1 Tissue Specific Data

Wasserman-Fickett's collection of 43 muscle specific promoter sequences [25] has been selected for this experiment. This dataset is known to contain multiple motifs. The best motifs we got are evaluated with the help of TOMTOM motif comparison tool[27]. TOMTOM searches the TRANSFAC Database of known motifs for a match for the motifs identified by MotifMiner. Position specific scoring matrix of the identified motif is the input to TOMTOM. TOMTOM gave many motif matches for the identified motifs. In that, there are previously known muscle specific motifs also. The sequence logos of the previously known muscle specific motif which best matches the query motif are shown in figure 2. The MyoD from myogenin family is a known transcription factor binding site essential for regulating gene expression in muscle. Figure 2 shows the output generated by TOMTOM.

Some other known muscle specific motifs are identified using JASPAR database[28] and is shown in Figure 3 to 5. Myf is a muscle-specific transcription factor that can induce myogenesis. Serum response factor (SRF) controls the transcription of muscle genes. Sp1 inhibits proliferation and induces apoptosis in vascular smooth muscle cells. MyoD, Myf, SRF and Sp1[15],[26] are known muscle specific transcription factor binding sites in Wasserman-Fickett's collection of muscle specific promoter sequences. MotifMiner could identify these motifs from Wasserman-Fickett's set.

1. Information content =1.26281
   Target motif= MyoD(M00001)
   Length=8

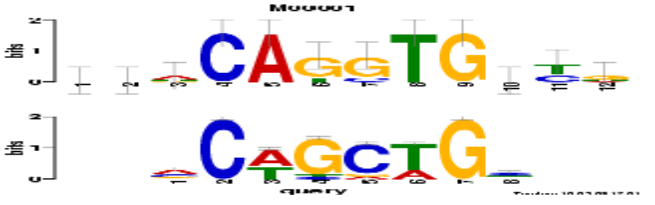

Fig. 2. MyoD Vs discovered motif

2. Information content=1.05466
   Target motif= Myf(MA0055)
   Length=10

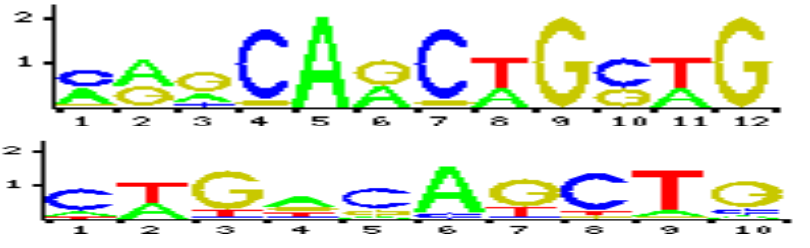

Fig. 3. Myf Vs discovered motif

3. Information content=1.02779
   Target motif=SRF (MA0083)
   Length=10

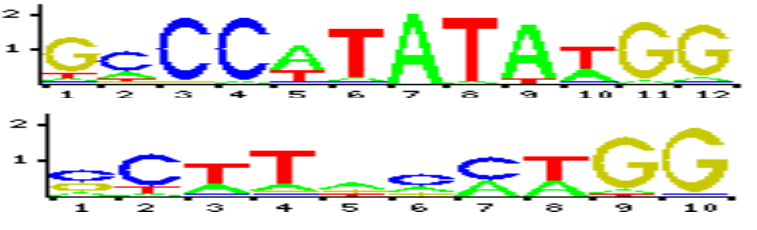

Fig. 4. SRF Vs discovered motif

4. Information content=1.24054
   Target Motif=Sp1 (MA009)
   Length=7

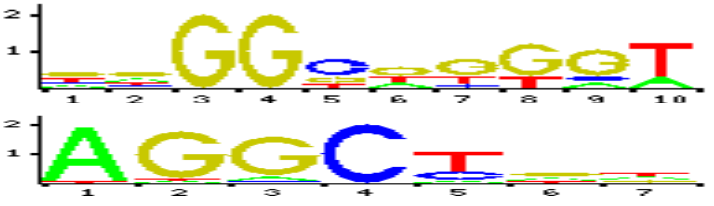

Fig. 5. Sp1 Vs discovered motif

5.2.2 CRP Motif

CRP motif sequences are downloaded from Purdue university website[29]. Six sequences are selected and applied to MotifMiner. The best motif identified by MotifMiner is evaluated by using TOMTOM motif comparison tool. It is found that the discovered motif matches the CRP motif (M0022) and is shown in figure 6. This is the expected result and thus validated the correctness of MotifMiner.

Information content=1.2145
Length=15

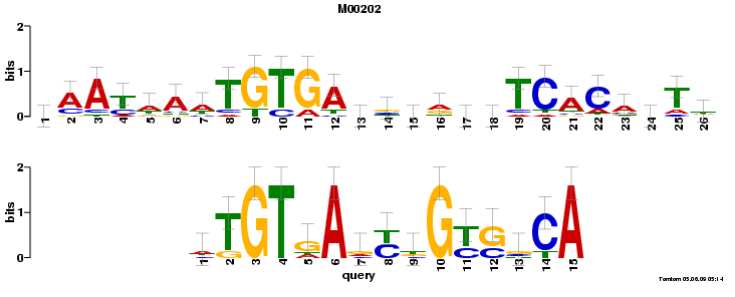

Fig. 6. CRP motif Vs discovered motif

6 Conclusion

In this paper, we have proposed a table driven greedy algorithm for DNA motif discovery. It is a word based enumerative algorithm. The greedy approach and the user defined minimum information content provide efficient pruning of the search space. The performance of the algorithm is evaluated with different data sets and the algorithm could give expected results. However, the problem of local optimum associated with the greedy approach is possible in this algorithm also. In future, we will try to improve this algorithm by exploring the possibility of local optimum elimination to get a global optimum result.

References

1. Helden, J.V., Andre, B., Collado-Vides, J.: Extracting Regulatory Sites from the Upstream Region of Yeast Genes by Computational Analysis of Oligonucleotide Frequencies. J. Mol. Biol. 281(5), 827–842 (1998)
2. Sinha, S., Tompa, M.: Discovery of Novel Rranscription Factor Binding Sites by Statistical Overrepresentation. Nucleic Acids Res. 30(24), 5549–5560 (2002)
3. Sagot, M.F.: Spelling Approximate Repeated or Common Motifs Using a Sufix Tree. In: Proceedings of the Third Latin American Symposium on Theoretical Informatics, pp. 374–390. Springer, Heidelberg (1998)
4. Pavesi, G., Mauri, G., Pesole, G.: An Algorithm for Finding Signals of Unknown Length in DNA Sequences. Bioinformatics 17(suppl. 1), S207–S214 (2001)
5. Eskin, E., Pevzner, P.A.: Finding Composite Regulatory Patterns in DNA Sequences. Bioinformatics 18(suppl.1), 354–363 (2002)
6. Pevzner, P., Sze, S.: Combinatorial Approaches to Finding Subtle Signals in DNA Sequences. In: Proc. Int. Conf. Intell. Syst. Mol. Biol., vol. 8, pp. 269–278 (2000)
7. Hertz, G.Z., Hartzell, G.W., Stormo, G.D.: Identification of Consensus Patterns in Unaligned DNA Sequences Known to be Functionally Related. Comput. Appl. Biosci. 6, 81–92 (1990)
8. Bailey, T.L., Elkan, C.: Unsupervised Learning of Multiple Motifs in Biopolymers Using Expectation Maximization. Machine Learning 21, 51–80 (1995)
9. Lawrence, C.E., Altschul, S.F., Boguski, M.S., Liu, J.S., Neuwald, A.F., Wootton, J.C.: Detecting Subtle Sequence Signals: a Gibbs Sampling Strategy for Multiple Alignment. Science 262, 208–214 (1993)
10. Roth, F.P., Hughes, J.D., Estep, P.W., Church, G.M.: Finding DNA Regulatory Motifs within Unaligned Noncoding Sequences Clustered by Whole-genome mRNA Quantitation. Nature Biotechnology 16, 939–945 (1998)
11. Thijs, G., Marchal, K., Moreau, Y.: A Gibbs Sampling Method to Detect Over-represented Motifs in Upstream Regions of Co-expressed Genes. RECOMB 5, 305–312 (2001)
12. Liu, X., Brutlag, D.L., Liu, J.S.: BioProspector: Discovering Conserved DNA Motifs in Upstream Regulatory Regions of Co-expressed Genes. In: Proceedings of the Sixth Pacific Symposium on Biocomputing, pp. 127–138 (2001)
13. Shida, K., Gibbs, S.T.: A Gibbs Sampling Method for Motif Discovery with Enhanced Resistance to Local Optima. BMC Bioinformatics 7, 486 (2006)
14. Liu, F.F.M., Tsai, J.J.P., Chen, R.M., Chen, S.N., Shih, S.H.: Finding Motifs by Genetic Algorithm. In: Fourth IEEE Symposium on Bioinformatics and Bioengineering, p. 459 (2004)
15. Michael, A., Andy, M.: Tyrrell, Regulatory Motif Discovery Using a Population Clustering Evolutionary Algorithm. IEEE/ACM Transactions on Computational Biology and Bioinformatics 4(3), 403–414 (2007)
16. Liu, D., Xiong, X., Das Gupta, B., Zhang, H.: Motif Discoveries in Unaligned Molecular Sequences Using Self-organizing Neural Network. IEEE Transactions on Neural Networks 17, 919–928 (2006)
17. McCue, L., Thompson, W., Carmack, C., Ryan, M., Liu, J., Derbyshire, V., Lawrence, C.: Phylogenetic Footprinting of Transcription Factor Binding Sites in Proteobacterial Genomes. Nucleic Acids Res. 29, 774–782 (2001)
18. Berezikov, E., Guryev, V., Plasterk, R.H.A., Cuppen, E.: CONREAL: Conserved Regulatory Elements Anchored Alignment Algorithm for Identification of Transcription Factor Binding Sites by Phylogenetic Footprinting. Genome Res. 14, 170–178 (2004)

19. Cliften, P., Sudarsanam, P., Desikan, A., Fulton, L., Fulton, B., Majors, J., Waterston, R., Cohen, B.A., Johnston, M.: Finding Functional Features in Saccharomyces Genomes by Phylogenetic Footprinting. Science 301, 71–76 (2003)
20. Wang, T., Stormo, G.D.: Combining Phylogenetic Data with Coregulated Genes to Identify Regulatory Motifs. Bioinformatics 19, 2369–2380 (2003)
21. Sinha, S., Blanchette, M., Tompa, M.: PhyME: A probabilistic Algorithm for Finding Motifs in Sets of Orthologous Sequences. BMC Bioinformatics 5, 170 (2004)
22. Moses, A., Chiang, D., Eisen, M.: Phylogenetic Motif Detection by Expectation-maximization on Evolutionary Mixtures. In: Proceedings of the Ninth Pacific Symposium on Biocomputing, pp. 324–335 (2004)
23. Siddharthan, R., Siggia, E.D., Van, N.E.: PhyloGibbs: A Gibbs Sampling Motif Finder That Incorporates Phylogeny. PLoS Comput. Biol. 1, 534–556 (2005)
24. Chandan, K.R., Weng, Y.C., Chiang, H.D.: Refining Motifs by Improving Information Content Scores Using Neighborhood Profile Search. Algorithms for Molecular Biology 1, 23 (2006)
25. Wasserman, W.W., Fickett, J.W.: Identification of Regulatory Regions Which Confer Muscle-specific Gene Expression. Journal of Molecular Biology 278, 167–181 (1998)
26. Andrew, D.S., Pavel, S., Zhang, M.Q.: Identifying Tissue-selective Transcription Factor Binding Sites in Vertebrate Promoters. PNAS 102(5), 1560–1565 (2005)
27. TOMTOM motif comparison tool, `http://meme.sdsc.edu/meme4_1/cgi-bin/tomtom.cgi`
28. JASPAR, `http://jaspar.cgb.ki.se/`
29. CRP Motif sequences, `http://dragon.bio.purdue.edu/pmotif/`

A New Method of Morphological Associative Memories

Naiqin Feng, Xizheng Cao, Sujuan Li, Lianhui Ao, and Shuangxi Wang

College of Computer & Information Technology, Henan Normal University, 453007, Xinxiang, China
fengnaiqin@163.com

Abstract. The morphological associative memories (MAM) have many attractive advantages. However, they can not give a guarantee that morphological hetero-associative memories are perfect, even if input patterns are perfect. In addition, the problem with the associative memory matrixes $\boldsymbol{W}_{XY}$ and $\boldsymbol{M}_{XY}$ is that $\boldsymbol{W}_{XY}$ is incapable of handling dilative noise while $\boldsymbol{M}_{XY}$ is incapable of effectively handling erosive noise. In this paper, the new methods of MAM, ${}^{+}\boldsymbol{W}_{XY}$ and ${}^{+}\boldsymbol{M}_{XY}$ are proposed. The certain qualifications that make ${}^{+}\boldsymbol{W}_{XY}$ and ${}^{+}\boldsymbol{M}_{XY}$ be perfect memories are analyzed and proved. As far as the hetero-associative memories are concerned, although ${}^{+}\boldsymbol{W}_{XY}$ and ${}^{+}\boldsymbol{M}_{XY}$ are not perfect, they are complements to original $\boldsymbol{W}_{XY}$ and $\boldsymbol{M}_{XY}$. ${}^{+}\boldsymbol{W}_{XY}$ is capable of handling dilative noise while ${}^{+}\boldsymbol{M}_{XY}$ is capable of effectively handling erosive noise. Therefore they can be put together with original $\boldsymbol{W}_{XY}$ and $\boldsymbol{M}_{XY}$ to learn from others' strong points to offset ones' own weakness and to make the effect of hetero-associative memories and pattern recognition better. The calculation results demonstrate that both ${}^{+}\boldsymbol{W}_{XY}$ and ${}^{+}\boldsymbol{M}_{XY}$ are effectual.

Keywords: Morphological associative memories, Auto-associative memories, Hetero- associative memories.

1 Introduction

The concept of morphological neural networks was advanced by Davidson and Ritter in 1990 [1]. Ritter and Sussner point out that this is a novel type of artificial neural networks and they are capable of solving any conventional computational problem [2]. In 1998, Ritter and his partners put forward the concept of morphological associative memories (MAM) [3]. MAM is essentially different to traditional neural networks. Its stimulus rules of neurons, associative rules, and so on differ from traditional neural networks. It can process not only two value-patterns, but also real patterns, such as processing and recognition of grey pictures. At the same time, MAM has unlimited storage capacity, one-shot recall speed, good noise-tolerance to single erosive or dilative noise. Its strong vitality and broad application prospects in pattern recognition and other areas arouse the attention of some scholars.

In 2002, complex morphological associative memory model is advanced by Chen [4], so MAM is extended to complex number domain. Wang Min and her partners put forward a new fuzzy morphological associative memory (FMAM) model in 2003[5]. Wang and Chen propose another enhanced FMAM (EFMAM) in 2005[6]. In the same year,

D.-S. Huang et al. (Eds.): ICIC 2009, LNAI 5755, pp. 407–416, 2009.

Wu and Wang research on fuzzy morphological bidirectional associative memories (FMBAM) and its robust analysis for random noise [7]. Also, they give the novel approach of gray image processing using FMBAM [8]. Sussner and Valle focus on FMAM and give a general framework of FMAM [9][10][11]. Feng and his partners tried to bring forward a unified framework of morphological associative memories in 2006[12]. However, so far only a handful of people research into morphological associative memories, especially on hetero-associative memories. At present, auto-associative MAM is perfect for inputs of no noise, but when hetero-associative MAM is concerned, it can not guarantee perfect recall even if input patterns are perfect. It is hard to enhance the performance of morphological hetero-associative memories. In addition, morphological associative memory $\boldsymbol{W}_{XY}$ is incapable of handling dilative noise while morphological associative memory $\boldsymbol{M}_{XY}$ is incapable of effectively handling erosive noise.

Aiming at these problems mentioned above, this paper researches deeply on MAM. We analyze the operation method in MAM, and point out the operation feature which reverse operations exist between the memory and recall of MAM. The new methods of morphological associative memories, ${}^{+}\boldsymbol{W}_{XY}$ and ${}^{+}\boldsymbol{M}_{XY}$ are proposed. The qualifications that make ${}^{+}\boldsymbol{W}_{XY}$ or ${}^{+}\boldsymbol{M}_{XY}$ be perfect recall memories under the conditions that the inputs are complete or distorted are given in theorem. The research shows that this method is valid for hetero-associative MAM. ${}^{+}\boldsymbol{W}_{XY}$ is capable of handling dilative noise while ${}^{+}\boldsymbol{M}_{XY}$ is capable of handling erosive noise. So they are complements to original $\boldsymbol{W}_{XY}$ and $\boldsymbol{M}_{XY}$, and also necessary complements to the existing morphological hetero-associative methods. The computing with the new method demonstrates the effectiveness of morphological associative memories ${}^{+}\boldsymbol{W}_{XY}$ and ${}^{+}\boldsymbol{M}_{XY}$, and good application prospect of complement methods of MAM.

2 Morphological Associative Memories

Traditional artificial neural network models are specified by the network topology, node characteristics, and training or learning rules. The basic algebraic system used in these models is the set of real numbers R together with the operations of addition and multiplication and the laws governing these operations. This algebraic system is called a ring, and is commonly denoted by $(R,+,\times)$. The standard mathematical model of traditional artificial neural networks is expressed as follows:

$$\tau_i(t+1) = \sum_{j=1}^{n} a_j(t).w_{ij}\,, \tag{1}$$

$$a_i(t+1) = f(\tau_i(t+1) - \theta_i)\,, \tag{2}$$

Where $a_j(t)$ denotes the value of the jth neuron at time t, n represents the number of neurons in the network, w_{ij} the synaptic connectivity value between the ith neuron and the jth neuron, $\tau_i(t+1)$ the next total input effect on the ith neuron, θ_i the threshold of the ith neuron, and f the next state function which usually introduces a nonlinearity into the network.

Differing from the traditional neural networks, the basic computations occurring in the morphological neural networks are based on the algebraic lattice structure $(R,\wedge,\vee,+)$, where the symbols $\wedge$ and $\vee$ denote the binary operations of minimum

and maximum, respectively. The basic computation model in the morphological neural network is given by

$$\tau_i(t+1) = \bigwedge_{j=1}^{n} a_j(t) + w_{ij}, \tag{3}$$

and

$$a_i(t+1) = f(\tau_i(t+1) - \theta_i), \tag{4}$$

or

$$\tau_i(t+1) = \bigvee_{j=1}^{n} a_j(t) + w_{ij}, \tag{5}$$

and

$$a_i(t+1) = f(\tau_i(t+1) - \theta_i). \tag{6}$$

Eq.(3) and Eq.(5) represent the erosive operation and the dilative operation which form the foundation of mathematical morphology, respectively.

For simulating associative memories, Ritter defines two basic memory matrixes $\boldsymbol{W_{XY}}$ and $\boldsymbol{M_{XY}}$: assume that $\boldsymbol{X}$ and $\boldsymbol{Y}$ are a couple of pattern matrixes, where $\boldsymbol{X}$ is an $n \times p$ input pattern matrix, $\boldsymbol{Y}$ is an $m \times p$ associative pattern matrix, $\boldsymbol{Z = X'}$ is a $p \times n$ matrix. Then the minimum product memory of $\boldsymbol{X}$ and $\boldsymbol{Y}$ is denoted by

$$\boldsymbol{W_{XY}=Y\triangle(-Z)} \tag{7}$$

Where the i,jth entry of $\boldsymbol{W_{XY}}$ is given by

$$w_{ij} = \bigwedge_{k=1}^{p} y_{ik} - z_{kj} = (y_{i1} - z_{1j}) \wedge \cdots \wedge (y_{ip} - z_{pj}). \tag{8}$$

The maximum product memory of $\boldsymbol{X}$ and $\boldsymbol{Y}$ is denoted by

$$\boldsymbol{M_{XY}=Y\nabla(-Z)}, \tag{9}$$

Where the i, jth entry of $\boldsymbol{M_{XY}}$ is given by

$$m_{ij} = \bigvee_{k=1}^{p} y_{ik} - z_{kj} = (y_{i1} - z_{1j}) \vee \cdots \vee (y_{ip} - z_{pj}). \tag{10}$$

When we provide the input pattern matrix $\boldsymbol{X}$ for the network, the associative output pattern matrix $\boldsymbol{Y_o}$ is denoted by

$$\boldsymbol{Y_o=W_{XY}\nabla X} \tag{11}$$

and the i, jth entry of $\boldsymbol{Y_o}$ is given by

$$y_{ij} = \bigvee_{k=1}^{p} w_{ik} + x_{kj} = (w_{i1} + x_{1j}) \vee \cdots \vee (w_{ip} + x_{pj}), \tag{12}$$

or

$$\boldsymbol{Y_o=M_{XY}\triangle X} \tag{13}$$

and the i,jth entry of $\boldsymbol{Y_o}$ is given by

$$y_{ij} = \bigwedge_{k=1}^{p} m_{ik} + x_{kj} = (m_{i1} + x_{1j}) \wedge \cdots \wedge (m_{ip} + x_{pj}). \tag{14}$$

We say that $\boldsymbol{W_{XY}}$, $\boldsymbol{M_{XY}}$ are perfect recall memories when $\boldsymbol{Y_o=Y}$.

3 Analysis on Morphological Associative Memories

We notice that there are two couples of reverse operations in the MAM presented by Ritter: one is $(+,-)$, and the other is $(\triangle,\triangledown)$.

For auto-associative MAM, Ritter proves that MAM can give a perfect recall on the condition without any noises. He proves the following theorem:

Theorem 0: $\boldsymbol{W_{XX}\triangledown X=X}$, $\boldsymbol{M_{XX}\triangle X=X}$.

However, we still notice that when it comes to hetero-associative MAM, it can not give a guarantee of perfect recall memories for any pattern matrix even if there is no noise.

Example 1: Assume that

$$\boldsymbol{x}^1=\begin{pmatrix}1\\2\\3\end{pmatrix},\boldsymbol{y}^1=\begin{pmatrix}1\\0\\0\end{pmatrix};\boldsymbol{x}^2=\begin{pmatrix}2\\3\\4\end{pmatrix},\boldsymbol{y}^2=\begin{pmatrix}0\\-1\\-1\end{pmatrix};\boldsymbol{x}^3=\begin{pmatrix}3\\4\\1\end{pmatrix},\boldsymbol{y}^3=\begin{pmatrix}0\\1\\0\end{pmatrix}.$$

If Ritter's method is adopted, then

$$\boldsymbol{W}_{XY}=\boldsymbol{Y}\triangle(-\boldsymbol{X}')'=\bigwedge_{\xi=1}^{3}[\boldsymbol{y}^{\xi}\triangle(-\boldsymbol{x}^{\xi})']$$

$$=\begin{pmatrix}0&-1&-2\\-1&-2&-3\\-1&-2&-3\end{pmatrix}\wedge\begin{pmatrix}-2&-3&-4\\-3&-4&-5\\-3&-4&-5\end{pmatrix}\wedge\begin{pmatrix}-3&-4&-1\\-2&-3&0\\-3&-4&-1\end{pmatrix}=\begin{pmatrix}-3&-4&-4\\-3&-4&-5\\-3&-4&-5\end{pmatrix},$$

$$\boldsymbol{M}_{XY}=\boldsymbol{Y}\triangledown(-\boldsymbol{X}')'=\bigvee_{\xi=1}^{3}[\boldsymbol{y}^{\xi}\triangledown(-\boldsymbol{x}^{\xi})']$$

$$=\begin{pmatrix}0&-1&-2\\-1&-2&-3\\-1&-2&-3\end{pmatrix}\vee\begin{pmatrix}-2&-3&-4\\-3&-4&-5\\-3&-4&-5\end{pmatrix}\vee\begin{pmatrix}-3&-4&-1\\-2&-3&0\\-3&-4&-1\end{pmatrix}=\begin{pmatrix}0&-1&-1\\-1&-2&0\\-1&-2&-1\end{pmatrix},$$

$$\boldsymbol{W}_{XY}\triangledown\boldsymbol{X}=\begin{pmatrix}-3&-4&-4\\-3&-4&-5\\-3&-4&-5\end{pmatrix}\triangledown\begin{pmatrix}1&2&3\\2&3&4\\3&4&1\end{pmatrix}=\begin{pmatrix}-1&0&0\\-2&-1&0\\-2&-1&0\end{pmatrix}\neq\boldsymbol{Y},$$

$$\boldsymbol{M}_{XY}\triangle\boldsymbol{X}=\begin{pmatrix}0&-1&-1\\-1&-2&0\\-1&-2&-1\end{pmatrix}\triangle\begin{pmatrix}1&2&3\\2&3&4\\3&4&1\end{pmatrix}=\begin{pmatrix}1&2&0\\0&1&1\\0&1&0\end{pmatrix}\neq\boldsymbol{Y}.$$

So both $\boldsymbol{W_{XY}}$ and $\boldsymbol{M_{XY}}$ are not perfect recall.

4 The New Method of MAM

Assume that $\boldsymbol{X}$ and $\boldsymbol{Y}$ are a couple of pattern matrixes, and $\boldsymbol{X}$ is an $n\times p$ input pattern matrix, $\boldsymbol{Y}$ is an $m\times p$ associative pattern matrix, $\boldsymbol{Z=X'}$ is a $p\times n$ matrix, ${}^{+}\boldsymbol{W_{XY}}$ and ${}^{+}\boldsymbol{M_{XY}}$ denote the new morphological associative memories.

Definition 1: The morphological minimum product associative memory ${}^{+}\boldsymbol{W_{XY}=Y}\triangle\mathrm{Z}$, and its element w_{ij} is defined by

$$w_{ij}=\bigwedge_{k=1}^{p}y_{ik}+z_{kj}=(y_{i1}+z_{1j})\wedge\cdots\wedge(y_{ip}+z_{pj})\cdot \tag{15}$$

Definition 2: The morphological maximum product associative memory ${}^{+}\boldsymbol{M}_{XY}=\mathrm{Y}\bigtriangledown\mathrm{Z}$, and its element m_{ij} is defined by

$$m_{ij}=\bigvee_{k=1}^{P} y_{ik}+z_{kj}=(y_{i1}+z_{1j})\vee\cdots\vee(y_{ip}+z_{pj}). \tag{16}$$

As far as the hetero-associative memories are concerned, in general, because $\boldsymbol{W}_{XY}$ and $\boldsymbol{M}_{XY}$ are not perfect for any ($\boldsymbol{X}$, $\boldsymbol{Y}$), so when ${}^{+}\boldsymbol{W}_{XY}$ and ${}^{+}\boldsymbol{M}_{XY}$ are added, they may be complements to original $\boldsymbol{W}_{XY}$ and $\boldsymbol{M}_{XY}$. Experiments show that this idea is correct and it can enhance the effect of hetero-associative memories and pattern recognition.

Example 2: Assume that

$$\boldsymbol{X}=\begin{pmatrix}1&2&3\\2&3&4\\3&4&1\end{pmatrix},\quad \boldsymbol{Y}=\begin{pmatrix}1&0&0\\0&-1&1\\0&-1&0\end{pmatrix}$$

By example 1, we know that neither $\boldsymbol{W}_{XY}$ nor $\boldsymbol{M}_{XY}$ can give a perfect recall for the ($\boldsymbol{X}$, $\boldsymbol{Y}$). However, by means of the new method of MAM we can obtain

$${}^{+}\boldsymbol{W}_{XY}=\boldsymbol{Y}\,\Delta\,\boldsymbol{X}'=\begin{pmatrix}1&0&0\\0&-1&1\\0&-1&0\end{pmatrix}\Delta\begin{pmatrix}1&2&3\\2&3&4\\3&4&1\end{pmatrix}=\begin{pmatrix}2&3&1\\1&2&2\\1&2&1\end{pmatrix},$$

$${}^{+}\boldsymbol{M}_{XY}=\boldsymbol{Y}\,\nabla\,\boldsymbol{X}'=\begin{pmatrix}1&0&0\\0&-1&1\\0&-1&0\end{pmatrix}\nabla\begin{pmatrix}1&2&3\\2&3&4\\3&4&1\end{pmatrix}=\begin{pmatrix}3&4&4\\4&5&3\\3&4&3\end{pmatrix},$$

$${}^{+}\boldsymbol{W}_{XY}\nabla(-\boldsymbol{X})=\begin{pmatrix}2&3&1\\1&2&2\\1&2&1\end{pmatrix}\nabla\begin{pmatrix}-1&-2&-3\\-2&-3&-4\\-3&-4&-1\end{pmatrix}=\begin{pmatrix}1&0&0\\0&-1&1\\0&-1&0\end{pmatrix}=\boldsymbol{Y},$$

$${}^{+}\boldsymbol{M}_{XY}\Delta(-\boldsymbol{X})=\begin{pmatrix}3&4&4\\4&5&3\\3&4&3\end{pmatrix}\Delta\begin{pmatrix}-1&-2&-3\\-2&-3&-4\\-3&-4&-1\end{pmatrix}=\begin{pmatrix}1&0&0\\0&-1&1\\0&-1&0\end{pmatrix}=\boldsymbol{Y}.$$

This example shows that, sometimes, perfect recall for hetero-associative memories can be obtained by ${}^{+}\boldsymbol{W}_{XY}$ and ${}^{+}\boldsymbol{M}_{XY}$, which compensate for the weakness of Ritter's methods.

Obviously, in order to be perfect recall, ${}^{+}\boldsymbol{W}_{XY}$ and ${}^{+}\boldsymbol{M}_{XY}$ must satisfy some conditions. The conditions can be described as follows:

Theorem 1: ${}^{+}\boldsymbol{W}_{XY}$ is a perfect recall memory for ($\boldsymbol{X}$,$\boldsymbol{Y}$), if and only if each row of the matrix $[\mathbf{y}^{\xi}\triangle(\mathrm{x}\xi)']-+\boldsymbol{W}_{XY}$ contains a zero entry for each ξ=1,…,k.

Proof: ${}^{+}\boldsymbol{W}_{XY}$ is the perfect recall memory for ($\boldsymbol{X}$, $\boldsymbol{Y}$)

$$\Leftrightarrow [{}^{+}\boldsymbol{W}_{XY}\nabla(-\boldsymbol{x}^{\xi})]_{\mathrm{i}}=y_i^{\xi},\ \forall\xi=1,\cdots,k\ \text{ and }\ \forall i=1,\cdots,m$$
$$\Leftrightarrow y_i^{\xi}-[{}^{+}\boldsymbol{W}_{\mathrm{XY}}\nabla(-\boldsymbol{x}^{\xi})]_{\mathrm{i}}=0,\ \forall\xi=1,\cdots,k\ \text{ and }\ \forall i=1,\cdots,m$$
$$\Leftrightarrow y_i^{\xi}-\bigvee_{j=1}^{n}(w_{ij}-x_j^{\xi})=0,\ \forall\xi=1,\cdots,k\quad\text{and}\quad\forall i=1,\cdots,m$$
$$\Leftrightarrow y_i^{\xi}+\bigwedge_{j=1}^{n}(x_j^{\xi}-w_{ij})=0,\ \forall\xi=1,\cdots,k\quad\text{and}\quad\forall i=1,\cdots,m$$

$$\Leftrightarrow \wedge_{j=1}^{n}(y_i^{\xi} + x_j^{\xi} - w_{ij}) = 0, \forall \xi = 1, \cdots, k \quad \text{and} \quad \forall i = 1, \cdots, m$$

$$\Leftrightarrow \wedge_{j=1}^{n}([\boldsymbol{y}^{\xi} \Delta (\boldsymbol{x}^{\xi})'] - {}^{+}\boldsymbol{W}_{XY})_{ij} = 0, \forall \xi = 1, \cdots, k \quad \text{and} \quad \forall i = 1, \cdots, m .$$

The last set of equations is true if and only if the ith row of the matrix $[\boldsymbol{y}^{\xi} \triangle (\boldsymbol{x}^{\xi})'] - {}^{+}\boldsymbol{W}_{XY}$ contains at least one zero entry for each ξ=1,…,k and each i=1,…,m.

Theorem 2: ${}^{+}\boldsymbol{M}_{XY}$ is a perfect recall memory for $(\boldsymbol{X},\boldsymbol{Y})$ if and only if each row of the matrix ${}^{+}\boldsymbol{M}_{XY} - [\boldsymbol{y}^{\xi} \triangledown (\boldsymbol{x}^{\xi})']$ contains a zero entry for each ξ=1,…,k.

Proof: The proof of theorem 2 is similar to the proof of theorem 1.

Experiments demonstrate that ${}^{+}\boldsymbol{W}_{XY}$ and ${}^{+}\boldsymbol{M}_{XY}$ are capable of handling dilative noise and erosive noise.

Example 3: Suppose that $\tilde{\boldsymbol{X}}$ denotes a distorted version of $\boldsymbol{X}$

$$\boldsymbol{X} = \begin{pmatrix} 1 & 2 & 2 \\ 4 & 2 & 2 \\ 4 & 2 & 4 \end{pmatrix}, \quad \boldsymbol{Y} = \begin{pmatrix} 2 & 4 & 2 \\ 4 & 4 & 4 \\ 2 & 3 & 2 \end{pmatrix}, \quad \tilde{\boldsymbol{X}} = \begin{pmatrix} 1 & 2 & 1 \\ 2 & 2 & 2 \\ 4 & 2 & 4 \end{pmatrix},$$

$${}^{+}\boldsymbol{W}_{XY} = \boldsymbol{Y} \Delta \boldsymbol{X}' = \begin{pmatrix} 2 & 4 & 2 \\ 4 & 4 & 4 \\ 2 & 3 & 2 \end{pmatrix} \Delta \begin{pmatrix} 1 & 4 & 4 \\ 2 & 2 & 2 \\ 2 & 2 & 4 \end{pmatrix} = \begin{pmatrix} 3 & 4 & 6 \\ 5 & 6 & 6 \\ 3 & 4 & 5 \end{pmatrix},$$

$${}^{+}\boldsymbol{M}_{XY} = \boldsymbol{Y} \nabla \boldsymbol{X}' = \begin{pmatrix} 2 & 4 & 2 \\ 4 & 4 & 4 \\ 2 & 3 & 2 \end{pmatrix} \nabla \begin{pmatrix} 1 & 4 & 4 \\ 2 & 2 & 2 \\ 2 & 2 & 4 \end{pmatrix} = \begin{pmatrix} 6 & 6 & 6 \\ 6 & 8 & 8 \\ 5 & 6 & 6 \end{pmatrix},$$

$${}^{+}\boldsymbol{W}_{XY} \nabla (-\boldsymbol{X}) = \begin{pmatrix} 3 & 4 & 6 \\ 5 & 6 & 6 \\ 3 & 4 & 5 \end{pmatrix} \nabla \begin{pmatrix} -1 & -2 & -2 \\ -4 & -2 & -2 \\ -4 & -2 & -4 \end{pmatrix} = \begin{pmatrix} 2 & 4 & 2 \\ 4 & 4 & 4 \\ 2 & 3 & 2 \end{pmatrix} = \boldsymbol{Y},$$

$${}^{+}\boldsymbol{M}_{XY} \Delta (-\boldsymbol{X}) = \begin{pmatrix} 6 & 6 & 6 \\ 6 & 8 & 8 \\ 5 & 6 & 6 \end{pmatrix} \Delta \begin{pmatrix} -1 & -2 & -2 \\ -4 & -2 & -2 \\ -4 & -2 & -4 \end{pmatrix} = \begin{pmatrix} 2 & 4 & 2 \\ 4 & 4 & 4 \\ 2 & 3 & 2 \end{pmatrix} = \boldsymbol{Y},$$

$${}^{+}\boldsymbol{W}_{XY} \nabla (-\tilde{\boldsymbol{X}}) = \begin{pmatrix} 3 & 4 & 6 \\ 5 & 6 & 6 \\ 3 & 4 & 5 \end{pmatrix} \nabla \begin{pmatrix} -1 & -2 & -1 \\ -2 & -2 & -2 \\ -4 & -2 & -4 \end{pmatrix} = \begin{pmatrix} 2 & 4 & 2 \\ 4 & 4 & 4 \\ 2 & 3 & 2 \end{pmatrix} = \boldsymbol{Y},$$

$${}^{+}\boldsymbol{M}_{XY} \Delta (-\tilde{\boldsymbol{X}}) = \begin{pmatrix} 6 & 6 & 6 \\ 6 & 8 & 8 \\ 5 & 6 & 6 \end{pmatrix} \Delta \begin{pmatrix} -1 & -2 & -1 \\ -2 & -2 & -2 \\ -4 & -2 & -4 \end{pmatrix} = \begin{pmatrix} 2 & 4 & 2 \\ 4 & 4 & 4 \\ 2 & 3 & 2 \end{pmatrix} = \boldsymbol{Y}.$$

So both ${}^{+}\boldsymbol{W}_{XY}$ and ${}^{+}\boldsymbol{M}_{XY}$ are perfect for not only perfect input pattern $\boldsymbol{X}$, but also distorted input pattern $\tilde{\boldsymbol{X}}$. Even for the severely erosive pattern

$$\tilde{\boldsymbol{X}} = \begin{pmatrix} -10 & 2 & 1 \\ 0 & 0 & -20 \\ 4 & -30 & 4 \end{pmatrix},$$

${}^{+}\boldsymbol{M}_{XY}$ can still give a perfect recall memory for $\boldsymbol{Y}$, showing the good capability of handling erosive noise. And for following severely dilative (and also some erosive) input pattern

$$\tilde{\boldsymbol{X}} = \begin{pmatrix} 100 & 200 & 100 \\ 2 & 2000 & 2 \\ 4000 & 2 & 40 \end{pmatrix},$$

${}^{+}\boldsymbol{W}_{\boldsymbol{XY}}$ can give a perfect recall for $\boldsymbol{Y}$, too, showing the good capability of handling dilative noise.

Theorem 3 and theorem 4 provide the needed boundary conditions, which guarantee ${}^{+}\boldsymbol{M}_{\boldsymbol{XY}}$ and ${}^{+}\boldsymbol{W}_{\boldsymbol{XY}}$ are perfect recall on condition that input patterns are distorted.

Theorem 3: Assume that $\tilde{\boldsymbol{x}}^{\gamma}$ is a distorted version of the pattern $\boldsymbol{x}^{\gamma}$. Then ${}^{+}\boldsymbol{M}_{\boldsymbol{XY}} \triangle (-\tilde{\boldsymbol{x}}^{\gamma}) = \boldsymbol{y}^{\gamma}$ if and only if

$$\tilde{x}_j^{\gamma} \le x_j^{\gamma} \vee \bigwedge_{i=1}^{m} \left[\bigvee_{\xi \ne \gamma} (y_i^{\xi} - y_i^{\gamma} + x_j^{\xi}) \right] \quad \forall j = 1, \cdots, n. \tag{17}$$

At the same time, for each row index $i \in \{1,\ldots,m\}$, there exists a column index $j_i \in \{1,\ldots,n\}$, such that

$$\tilde{x}_{j_i}^{\gamma} = x_{j_i}^{\gamma} \vee \left[\bigvee_{\xi \ne \gamma} (y_i^{\xi} - y_i^{\gamma} + x_{j_i}^{\xi}) \right]. \tag{18}$$

Proof: 1) Assume that $\tilde{\boldsymbol{x}}^{\gamma}$ denotes a distorted version of the pattern $\boldsymbol{x}^{\gamma}$ and for γ=1,…, k, ${}^{+}\boldsymbol{M}_{\boldsymbol{XY}} \triangle (-\tilde{\boldsymbol{x}}^{\gamma}) = \boldsymbol{y}^{\gamma}$, then

$$y_i^{\gamma} = \left[{}^{+}\boldsymbol{M}_{\boldsymbol{XY}} \Delta (-\tilde{\boldsymbol{x}}^{\gamma}) \right]_i = \bigwedge_{l=1}^{n} (m_{il} - \tilde{x}_l^{\gamma}) \le m_{ij} - \tilde{x}_j^{\gamma},$$
$$\forall i = 1, \cdots, m \quad \text{和} \quad \forall j = 1, \cdots, n.$$

Therefore

$$\begin{aligned}
&\tilde{x}_j^{\gamma} \le m_{ij} - y_i^{\gamma} \quad \forall i = 1, \cdots, m \quad \text{and} \quad \forall j = 1, \cdots, n \\
\Leftrightarrow\ & \tilde{x}_j^{\gamma} \le \bigwedge_{i=1}^{m} (m_{ij} - y_i^{\gamma}) \quad \forall j = 1, \cdots, n \\
\Leftrightarrow\ & \tilde{x}_j^{\gamma} \le \bigwedge_{i=1}^{m} \left[\bigvee_{\xi=1}^{k} (y_i^{\xi} + x_j^{\xi}) - y_i^{\gamma} \right] \quad \forall j = 1, \cdots, n \\
\Leftrightarrow\ & \tilde{x}_j^{\gamma} \le \bigwedge_{i=1}^{m} \left[\bigvee_{\xi \ne \gamma} (y_i^{\xi} + x_j^{\xi}) \vee (y_i^{\gamma} + x_j^{\gamma}) - y_i^{\gamma} \right] \forall j = 1, \cdots, n \\
\Leftrightarrow\ & \tilde{x}_j^{\gamma} \le \bigwedge_{i=1}^{m} \left[\bigvee_{\xi \ne \gamma} (y_i^{\xi} - y_i^{\gamma} + x_j^{\xi}) \vee x_j^{\gamma} \right] \quad \forall j = 1, \cdots, n \\
\Leftrightarrow\ & \tilde{x}_j^{\gamma} \le x_j^{\gamma} \vee \bigwedge_{i=1}^{m} \left[\bigvee_{\xi \ne \gamma} (y_i^{\xi} - y_i^{\gamma} + x_j^{\xi}) \right] \quad \forall j = 1, \cdots, n.
\end{aligned}$$

This means that the inequalities given by (17) are satisfied. It also follows that

$$\tilde{x}_j^{\gamma} \le x_j^{\gamma} \vee \left[\bigvee_{\xi \ne \gamma} (y_i^{\xi} - y_i^{\gamma} + x_j^{\xi}) \right] \quad \forall j = 1, \cdots, n \quad \text{and} \quad \forall i = 1, \cdots, m.$$

Suppose that the set of inequalities given by (17) does not contain an equality for i=1,…,m, namely, assume that there exists a row index $i \in \{1,\ldots,m\}$, such that

$$\tilde{x}_j^{\gamma} < x_j^{\gamma} \vee \left[\bigvee_{\xi \neq \gamma} (y_i^{\xi} - y_i^{\gamma} + x_j^{\xi}) \right] \quad \forall j = 1, \cdots, n.$$

Then

$$\begin{aligned}
\left[{}^{+}\boldsymbol{M}_{XY} \Delta (-\tilde{\boldsymbol{x}}^{\gamma}) \right]_i &= \bigwedge_{j=1}^{n} (m_{ij} - \tilde{x}_j^{\gamma}) \\
&> \bigwedge_{j=1}^{n} \left[m_{ij} - x_j^{\gamma} \vee \left(\bigvee_{\xi \neq \gamma} [y_i^{\xi} - y_i^{\gamma} + x_j^{\xi}] \right) \right] \\
&= \bigwedge_{j=1}^{n} \left[m_{ij} - \left(\bigvee_{\xi=1}^{k} [y_i^{\xi} - y_i^{\gamma} + x_j^{\xi}] \right) \right] \\
&= \bigwedge_{j=1}^{n} \left[m_{ij} + \left(\bigwedge_{\xi=1}^{k} [y_i^{\gamma} - y_i^{\xi} - x_j^{\xi}] \right) \right] \\
&= \bigwedge_{j=1}^{n} \left[m_{ij} + y_i^{\gamma} - \bigvee_{\xi=1}^{k} (y_i^{\xi} + x_j^{\xi}) \right] \\
&= \bigwedge_{j=1}^{n} [m_{ij} + y_i^{\gamma} - m_{ij}] \\
&= y_i^{\gamma}.
\end{aligned}$$

That is ${}^{+}\boldsymbol{M}_{XY} \triangle(-\tilde{\boldsymbol{x}}^{\gamma}) > \boldsymbol{y}^{\gamma}$. This contradicts the hypothesis that ${}^{+}\boldsymbol{M}_{XY} \triangle(-\tilde{\boldsymbol{x}}^{\gamma}) = \boldsymbol{y}^{\gamma}$. Therefore, for each row index $i \in \{1,\ldots,m\}$ there must exist a column index $j_i \in \{1,\ldots,n\}$ satisfying equality (18).

2) Suppose that

$$\tilde{x}_j^{\gamma} \leq x_j^{\gamma} \vee \bigwedge_{i=1}^{m} \left(\bigvee_{\xi \neq \gamma} [y_i^{\xi} - y_i^{\gamma} + x_j^{\xi}] \right) \quad \forall j = 1, \cdots, n.$$

By the first part of the proof, we can know that this inequality is true if and only if

$$\tilde{x}_j^{\gamma} \leq m_{ij} - y_i^{\gamma} \quad \forall i = 1, \cdots, m \quad \text{and} \quad \forall j = 1, \cdots, n,$$

or, equivalently, if and only if

$$\begin{aligned}
& m_{ij} - \tilde{x}_j^{\gamma} \geq y_i^{\gamma} \quad \forall i = 1, \cdots, m \quad \text{and} \quad \forall j = 1, \cdots, n \\
\Leftrightarrow \quad & \bigwedge_{j=1}^{n} \left(m_{ij} - \tilde{x}_j^{\gamma} \right) \geq y_i^{\gamma} \quad \forall i = 1, \cdots, m \\
\Leftrightarrow \quad & \left[{}^{+}\boldsymbol{M}_{XY} \Delta (-\tilde{\boldsymbol{x}}^{\gamma}) \right]_i \geq y_i^{\gamma} \quad \forall i = 1, \cdots, m.
\end{aligned}$$

Which means that ${}^{+}\boldsymbol{M}_{XY} \triangle(-\tilde{\boldsymbol{x}}^{\gamma}) \geq \boldsymbol{y}^{\gamma}, \quad \forall \gamma = 1, \cdots, k$.

If we can prove ${}^{+}\boldsymbol{M}_{XY} \triangle(-\tilde{\boldsymbol{x}}^{\gamma}) \leq \boldsymbol{y}^{\gamma}, \quad \forall \gamma = 1, \cdots, k$, further, we must obtain that ${}^{+}\boldsymbol{M}_{XY} \triangle(-\tilde{\boldsymbol{x}}^{\gamma}) = \boldsymbol{y}^{\gamma}, \quad \forall \gamma = 1, \cdots, k$. Let $\gamma \in \{1, \cdots, k\}$ and $i \in \{1, \cdots, m\}$ be arbitrarily chosen. Then

$$\begin{aligned}
\left[{}^{+}\boldsymbol{M}_{XY} \Delta (-\tilde{\boldsymbol{x}}^{\gamma}) \right]_i &= \bigwedge_{j=1}^{n} \left(m_{ij} - \tilde{x}_j^{\gamma} \right) \\
&\leq m_{ij_i} - \tilde{x}_{j_i}^{\gamma} \\
&= m_{ij_i} - \left[x_{j_i}^{\gamma} \vee \bigvee_{\xi \neq \gamma} (y_i^{\xi} - y_i^{\gamma} + x_{j_i}^{\xi}) \right]
\end{aligned}$$

$$
\begin{aligned}
&= m_{ij_i} + \left[\bigwedge_{\xi=1}^{k} (y_i^\gamma - y_i^\xi - x_{j_i}^\xi) \right] \\
&= m_{ij_i} + y_i^\gamma - \bigvee_{\xi=1}^{k} (y_i^\xi + x_{j_i}^\xi) \\
&= m_{ij_i} + y_i^\gamma - m_{ij_i} \\
&= y_i^\gamma .
\end{aligned}
$$

This shows that ${}^{+}\boldsymbol{M}_{XY} \triangle (-\tilde{\boldsymbol{x}}^{\gamma}) \leq \boldsymbol{y}^{\gamma}$.

Theorem 4. Assume that $\tilde{\boldsymbol{x}}^{\gamma}$ denotes a distorted version of the pattern $\boldsymbol{x}^{\gamma}$, then ${}^{+}\boldsymbol{W}_{XY} \triangledown (-\tilde{\boldsymbol{x}}^{\gamma}) = \boldsymbol{y}^{\gamma}$ if and only if

$$
\tilde{x}_j^\gamma \geq x_j^\gamma \wedge \bigvee_{i=1}^{m} \left(\bigwedge_{\xi \neq \gamma} [y_i^\xi - y_i^\gamma + x_j^\xi] \right) \quad \forall j = 1, \cdots, n.
$$

Meanwhile, for each row index $i \in \{1,\ldots,m\}$, there exists one column index $j_i \in \{1,\ldots,n\}$, such that

$$
\tilde{x}_{j_i}^\gamma = x_{j_i}^\gamma \wedge \left(\bigwedge_{\xi \neq \gamma} [y_i^\xi - y_i^\gamma + x_{j_i}^\xi] \right).
$$

Proof: The proof of theorem 4 is similar to the proof of theorem 3.

5 Conclusions

Aiming at the weakness of MAM with adopting reverse thinking, we present the new methods of morphological associative memories, ${}^{+}\boldsymbol{W}_{XY}$ and ${}^{+}\boldsymbol{M}_{XY}$. Our research proves that ${}^{+}\boldsymbol{W}_{XY}$ and ${}^{+}\boldsymbol{M}_{XY}$ are effective for hetero-associative MAM. As far as hetero-associative MAM and perfect inputs are concerned, ${}^{+}\boldsymbol{W}_{XY}$ and ${}^{+}\boldsymbol{M}_{XY}$ can give a perfect recall memory on the condition which is given by theorem 1 and theorem 2. In addition, ${}^{+}\boldsymbol{M}_{XY}$ can handle the erosive noise and its noise margin for perfect recall is given by theorem 3. And ${}^{+}\boldsymbol{W}_{XY}$ can handle the dilative noise and its noise margin for perfect recall is given by theorem 4. ${}^{+}\boldsymbol{W}_{XY}$, ${}^{+}\boldsymbol{M}_{XY}$, $\boldsymbol{W}_{XY}$ and $\boldsymbol{M}_{XY}$ are complementary to each other, therefore they can combined together to improve the effect of practical applications, for example, pattern recognition, image processing, and so on.

Acknowledgments

This work is supported by the Project of Science and technology of Henan Province, China and the Doctor Fund of Henan Normal University, China.

References

1. Davidson, J.L., Ritter, G.X.: A theory of morphological neural networks. In: Digital Optidal Computing II, vol. 1215, pp. 378–388 (1990)
2. Ritter, G.X., Sussner, P.: An introduction to morphological neural networks. In: Proc 13th Int. Conf. Pattern Recognition, Vienna, Austria, pp. 709–717 (1996)

3. Ritter, G.X., Sussner, P., Diaz-de-Leon, J.L.: Morphological Associative Memories. IEEE Transactions on Neural Networks 9(2), 281–292 (1998)
4. Chen, S.C., Liu, W.L.: Complex Morphological Associative Memories and Their Performance Analysis. Journal of Software (in Chinese) 13(3), 453–459 (2002)
5. Wang, M., Wang, S.T., Wu, X.J.: Initial Results on Fuzzy Morphological Associative Memories. Acta Electronica Sinica (in Chinese) 31(5), 690–693 (2003)
6. Wang, M., Chen, S.C.: Enhanced FMAM Based on Empirical Kernel Map. IEEE Transactions on Neural Networks 16(3), 557–564 (2005)
7. Wu, X.S., Wang, S.T.: Bidirectional fuzzy morphological associative memory and its robust analysis for random noise. Pattern Recognition and Artificial Intelligence (in Chinese) 18, 257–262 (2005)
8. Wu, X.S., Wang, S.T.: Fuzzy morphological associative memories and their application in storing and recalling cell images. Journal of Image and Graphics (in Chinese) 11(10), 1450–1455 (2006)
9. Sussner, P., Valle, M.E.: Gray-scale Morphological Associative Memories. IEEE Transactions on Neural Networks 17(3), 559–570 (2006)
10. Sussner, P., Valle, M.E.: Implicative Fuzzy Associative Memories. IEEE Transactions on Fuzzy Systems 14(6), 793–807 (2006)
11. Valle, M.E., Sussner, P.: A general framework for fuzzy morphological associative memories. Fuzzy Sets and Systems 159(7), 747–768 (2008)
12. Feng, N.Q., Qiu, Y.H., Wang, F., et al.: A Unified Framework of Morphological Associative Memories. In: Huang, D.S., Li., K. (eds.) Intelligent Control and Automation. Lecture Notes in Control and Information Sciences, vol. 344, pp. 1–11. Springer, Heidelberg (2006)

A New Method of Color Map Segmentation Based on the Self-organizing Neural Network

Zhenqing Xue and Chunpu Jia

Department of Information Science and Engineering, Shandong Business Institute, Yantai 264000, China
zhenqingxue@yahoo.com.cn, jiaonanjia@163.com

Abstract. Segmentation is a key step of the map self-identification. This paper put forward a color map segmentation method based on the self-organizing neural network and realized it. This self-segmentation of the map was excellent in no manual intervention. The paper also put forward the way of accelerating the process, which is tested effective.

Keywords: self-organizing, Neural network, Color map segmentation.

1 Introduction

With the rapid development of geo-information technologies, the demand for the map information processed is more and more urgent for the people. It becomes an important subject for the people that how to make paper-maps imported into the computer automatically. To realizing the recognition of the map, what the first we should do is the color map segmentation.

Color map segmentation is similar to color image segmentation. People have many methods to deal with segmentation of color image. These methods are mainly based on pattern recognition technology. It relies on the hypothesis of the distribution of sample data. The effect of segmentation depends on accuracy of assumptions. However the spatial distribution of the color in the map is influenced by many factors. The statistical law of distribution is difficult to estimate. The map is imported into the computer by scanning. the image will appear cross-color and color noise. Moreover, with the restriction of the print technology, there is some of color error in the map, so the traditional segmentation method is difficult to apply.

SOM network have the feature that it can study autonomous, SOM network can divide training sample into different category in each neuron's competition. The division reflects essence distinguishes of the sample set. This classification method reduce the human factors about uniform criterion, we make SOM network trained as a classifier. So we can make color map segmentation.

2 Description of the Network

The result of the research indicates that the information of the brain cerebral cortex have two obvious characters: Firstly, the topological mapping structure is not constructed by reassembly of the nerve cells, but be consisted of each nerve cell which is on excitation;

D.-S. Huang et al. (Eds.): ICIC 2009, LNAI 5755, pp. 417–423, 2009.

secondly, the structure of this topology has the characteristics of self-organization. Kohonen's SOM has the same information mapping character as human brain at the process of forming the topology by input external information.

SOM have two layers, showed as Fig.1. Input layer simulate the retina apperceiving external information, output layer simulate the brain cerebral cortex. Each node in the input layer(nerve cell) assemble external information to the each nerve cell in the output layer by weight vectors. The format of input layer is the same as BP neural network, the number of the node is assigned N which equals the dimension of the sample. Output layer is the competition layer, the node have several formations, for example, one-dimensional linear matrix, two-dimensional plane matrix and three-dimensional grad matrix, etc. Stratified map often use two-dimension which have node M=m×m. The relationship of input layer and output layer is entire inter-connected, each node of output layer is connected lateral inhibitory. So there are two different connections in the neural network, one is the weight between node and external input, another is the weight between nodes which can control the interaction among nodes.

SOM network carries on in output layer below:

We suppose that there has N input pattern, for some input pattern, by competition, which gradually converges to the center of K subsets that are divided from sample space. When an output node is given max stimulus, just the winner node which can indicate respective area of the mode, and the nodes close to the winner node are given bigger excitation. When using another input mode, the winner area moves to another. For the winner node j, the nodes nearly area $N_j(t)$ are varying degrees of excitement, and the nodes out of the $N_j(t)$ area are inhibitory, this area often are square. Just as Fig.2, $N_j(t)$ is the function of t which stands for time, as time increases, the area of

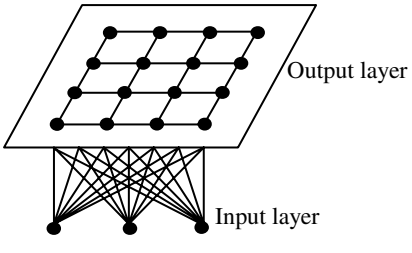

Fig. 1. The structure of SOM

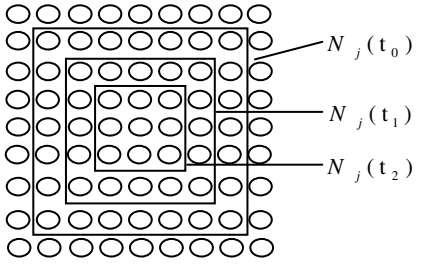

Fig. 2. The relation between $N_i(t)$ and time t

$N_j(t)$ proportionally decreases, at last just one node or a group of nodes are left, which reflect a kind of samples.

For any input node i and output node j:

i = {1, 2, … , N}, j = {1, 2, … , M}, and $Y_j = \sum_{i=1}^{N} \omega_{ij} X_i$

3 Traditional Step for Segmentation

(1) Initialization. We assigned a small random number to the weight vector on out layer, and took normalization, and obtained ωij(0) = r; i = 0, 1, …, N-1, j = 0, 1, …, M-1, r∈(0,1). Gave the output node an initial winning neighborhood Nj(0); to confirm the initial value which names learning rate η(0); Input layer was a one-dimensional vector N=3,corresponded to each pixel value which was R、G、B. Output layer was a two-dimensional matrix which size was decided in accordance with the specific issue.

(2) Accepting input

Select a pixel From the map randomly and Put its R、G、B value as input mode and normalize:

$$X^p = (a_1^p, a_2^p, ..., a_N^p), \quad p \in \{1,2,...,P\} \tag{1}$$

P stands for sample number, and N=3

(3) Looking for the winner node

Computed the dot matrix Xp and Wj, Chose the winning node j* which the dot matrix was biggest. If you were not normalized the input mode you should calculate the Euclidean distance in accordance with the following formula:

$$d_j = \left\| X^p - W_j \right\| = [\sum_{i=1}^{N} (a_i^p - \omega_{ij})^2]^{1/2} \tag{2}$$

(4) Definition of the superior neighborhood $N_j(t)$.

Took j^* as the center and determine the adjustment field of weight in time t. In general initial neighborhood was $N_j(0)$ which was bigger.

$N_j(t)$contracted gradually along with the training time. We could represent superior neighborhood size by neighborhood radius r(t). $r(t) = C_1 e^{-B_1 t/t_m}$,C_1 is normal number with node number of output layer, B_1 is a constant which is greater than zero, t_m was the biggest training number.

(5) Adjust weights

We adjusted all node weights in superior neighborhood:

$$\omega_{ij}(t+1) = \omega_{ij}(t) + \eta(t,N)[x_i^p - \omega_{ij}(t)] \quad i = 1,2,...N; j \in N_j(t) \tag{3}$$

η(t, N) stands for a function. We can calculate with: $\eta(t, N) = \eta(t)e^{-N}$; η(t) is the study rate in the SOM in time t. η(t) should be assigned a great value in the beginning,

Afterward, to be smaller in a rapid rate, When it reaches a small value, it declines slowly to zero. This may adjust the weight precisely to accord to the distribution structure of the sample space.

(6) To End Inspection

Judged weather η(t) declines to a small decimal scheduled or t=t+1. If didn't satisfy the termination condition, we make t=t+1 and go to step (2).

4 Improvement of Algorithm

4.1 Selection of Color Space

During the stratification processing, the selection of the color space was very important, the color space RGB or HLS was generally used. During the use of RGB colors space, the R, G, B components have a strong correlation between these three components, at the same time, these three components all have lightness, hue, saturation, so it was difficult to deal with. During the use of HLS space, although its three components are relatively independent, you can overcome those shortcomings above. But its H-component has no meaning when R=G=B (singular point), and more importantly, the paper quality (such as color cast, etc.) and illumination impacts H-component and S-component very seriously. Additionally, HLS is the nonlinear transform of RGB, and the volume of calculating is very large. During the use of RGB colorful space, its R, G, B components all have strong brightness factor and they related between each other.

Linear transformation of RGB colorful space and its expression is:

$$I_1 = (R + G + B)/3 \tag{4}$$

$$I_2 = R - B \tag{5}$$

$$I_3 = (2G - R - B)/2 \tag{6}$$

Among them, I_1 is the brightness of colorful space, I_2 can distinguish brown and blue effectively, I_3 can prominent green.

4.2 To Determine the Initial Value about Weight Vector

The weight of the SOM neural network is often initialized as lower random number, to make the initial position of the weight vector distribute in the sample space randomly. The weight vector nearest the sample space must be adjusted during training, but the vector far away from the sample space can't be adjusted for ever. So the result of training may make the sample into one kind. To solve this problem, we can make the initial position of the weights coincide with the distribution of input sample. So the training can't take the sample into one kind, and the training speed can be improved. According to the thinking above an easy method is that calculate the center vector of the whole sample:

$$\bar{X} = \frac{1}{P}\sum_{p=1}^{P} X^{p} \tag{7}$$

Then add a small random number to $\bar{X}$ as the initial value of weight vector, so the initial value could be in the sample space.

The distance between two vectors are not related with the two vectors' modulus values but related to the direction of the two vectors. So normalize the weight vector Wj as the formula below:

$$\bar{w} = \frac{W_j}{\|W_j\|} = \frac{(\omega_{1j}, \omega_{2j}, ..., \omega_{Nj})}{\sqrt{\omega_{ij}^2 + \omega_{2j}^2 + ... + \omega_{Nj}^2}} \quad j = 1, 2, \ldots, M \tag{8}$$

After these processes, there is just the direction of the vector W_j rest, so this can shorten the training time of the network, adjust the direction of W_j faster to accordance with the direction of X^p. When the input mode X^p is normalized, we can gain the shortest path by using the inner product of X^p and W_j.

4.3 Learning Rate

At present, there is none universal math method to choose the training rate from self-organization neural network, but the practice showed the simulated annealing function can make the stratification better.

$$\eta(t) = \begin{cases} \eta_0, & t \le t_p \\ \eta_0 (1 - \dfrac{t - t_p}{t_m - t_p}), & t > t_p \end{cases} \tag{9}$$

t_p is the initial value of simulated annealing, t_m is the end value, $0 < \eta_0 \le 1$. At the beginning of training, in order to gain the probability structure of input sample space fast, so when the training time $t \le t_p$,choose max rate η_0 from $\eta(t)$.when $t > t_p$, make $\eta(t)$ into 0 uniform to adjust the weight subtly, to accordance the probability structure of sample space.

5 Results And Discussions

In this paper we took segmentation to a color map using the above algorithm improved. In this operation we selected I1-I2-I3 as Color space, and took I1-I2 -I3 as input mode. We used 8X8 matrix on output layer, Fig.3 was a scanning color map which had been erase noise. Fig.4 and Fig.5 were the results of segmentation.

We may draw the following conclusions from the above segmentation results:

(1) The competition learning network structure and the learning algorithm are simpler, the calculation is high efficiency when we took segmentation to the color map, small interference by the noise, and better accuracy.

(2) The competition learning network is sometimes unstable. And longer time study. The experiment indicates that the competition learning network improved overcome this flaw in a certain extent.

(3) When we used the SOM algorithm to take segmentation to the color map, Majority of pixels could be effectively distinguished. But some individual category division is not to be good. It is mainly because the samples are not typical, not many, etc

Fig. 3. Color map

Fig. 4. Blue element

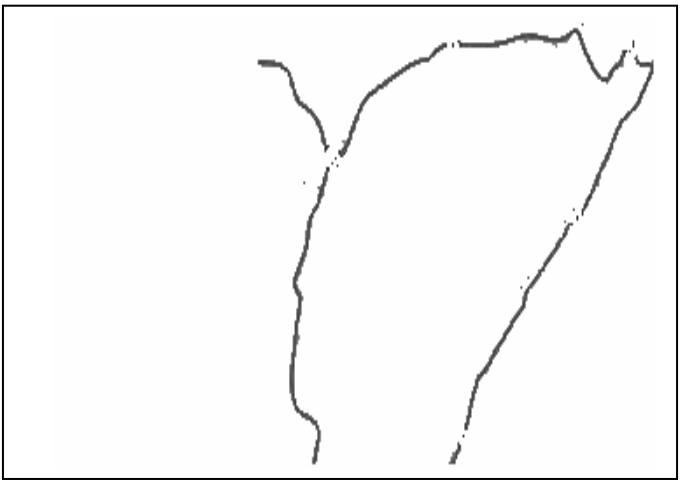

Fig. 5. Brown element

Acknowledgment

We wish to extend our heartfelt thanks to Sen Yang, Wenjun Yang, Wenli Zhang who devoted considerable time to this thesis, knowing that they would derive very little in the way of tangible benefits in return.

References

1. Li, H.J.: SOM network in the Image Segmentation. Computing Technology and Automation, 19(3), 21–25(2000)
2. Moreira, J., Costa, L.D.F.: Neural-based Color Image Segmentation and Classification using Self-organizing Maps. In: Anais do IX SIBGRAPI 1996, pp. 47–54 (1996)
3. Kohonen, T.: Self-organized formation of topologically correct feature maps. Biological Cybernetics 43(1), 59–69 (1982)
4. Liqun, H.: Artificial neural network theory. Design and Application, 63–72 (2002)
5. Vesanto, J.: Data mining techniques based on the self-organizing map, Finland, pp. 4–10 (1997)
6. Hagan, M.T.: Neural network design, 14th edn., pp. 12–16. China Machine Press (2002)
7. Ohta, Y.C.: Color Information for Recog Segmentation. Computer Graphics and Image Processing 13, 222–241 (1990)
8. Martin, T., Hagan Howard, B., Demuth, M.B.: Neural Network Design. China Machine Press, 14(12)–14(16) (2002)

A Quantum Particle Swarm Optimization Used for Spatial Clustering with Obstacles Constraints

Xueping Zhang[1,2], Jiayao Wang[1,3], Haohua Du[4], Tengfei Yang[1], and Yawei Liu[1]

[1] School of Information Science and Engineering, Henan University of Technology, Zhengzhou 450052, China
[2] Key Laboratory of Spatial Data Mining & Information Sharing of Ministry of Education, Fuzhou University, Fuzhou, 350002, China
[3] School of Surveying and Mapping, PLA Information Engineering University, Zhengzhou 450052, China
[4] School of computer science and engineering, Beihang University,Beijing 100191, China
zhang_xpcn@yahoo.com.cn

Abstract. In this paper, a more effective Quantum Particle Swarm Optimization (QPSO) method for Spatial Clustering with Obstacles Constraints (SCOC) is presented. In the process of doing so, we first proposed a novel Spatial Obstructed Distance using QPSO based on Grid model (QPGSOD) to obtain obstructed distance, and then we developed a new QPKSCOC based on QPSO and K-Medoids to cluster spatial data with obstacles constraints. The contrastive experiments show that QPGSOD is effective, and QPKSCOC can not only give attention to higher local constringency speed and stronger global optimum search, but also get down to the obstacles constraints and practicalities of spatial clustering; and it performs better than Improved K-Medoids SCOC (IKSCOC) in terms of quantization error and has higher constringency speed than Genetic K-Medoids SCOC.

Keywords: Spatial clustering, Obstacles constraints, Quantum particle swarm optimization, Spatial obstructed distance.

1 Introduction

Spatial clustering has been an active research area in the data mining community. Spatial clustering is not only an important effective method but also a prelude of other task for Spatial Data Mining (SDM). As reported in surveys on data clustering, clustering methods can be classified into Partitioning approaches, Hierarchical methods, Density-based algorithms, Probabilistic techniques, Graph theoretic, Grid-based algorithms, Model-based approaches, Genetic Algorithms, Fuzzy methods, Rough Set methods etc. Some algorithms have also integrated two or three kinds of clustering methods. As pointed out earlier, these techniques have focused on the performance in terms of effectiveness and efficiency for large databases. However, few of them have taken into account constraints that may be present in the data or constraints on the clustering. These constraints have significant influence on the results of the clustering

D.-S. Huang et al. (Eds.): ICIC 2009, LNAI 5755, pp. 424–433, 2009.

process of large spatial data. In order to improve the practicability of spatial clustering, studying spatial clustering with constraints is essential, and moreover, has important practical meaning. Its achievements will have more practical value and extensive application prospect.

Spatial clustering with constraints has two kinds of forms [1]. One kind is Spatial Clustering with Obstacles Constraints (SCOC).An obstacle is a physical object that obstructs the reach ability among the data objects, such as bridge, river, and highway etc. whose impact on the result should be considered in the clustering process of large spatial data. As an example, Fig.1 shows clustering data objects in relation to their neighbors as well as the physical obstacle constraints. Ignoring the constraints leads to incorrect interpretation of the correlation among data points. The other kind is spatial clustering with handling operational constraints [2], it consider some operation limiting conditions in the clustering process. In this paper, we mainly discuss SCOC. Handling these obstacles constraints can lead to effective and fruitful data mining by capturing application semantics [3-8].

Since K.H.Tung put forward a clustering question COE (Clustering with Obstacles Entities) [3] in 2000, a new studying direction in the field of clustering research have been opened up. To the best of our knowledge, only three clustering algorithms for clustering spatial data with obstacles constraints have been proposed very recently:

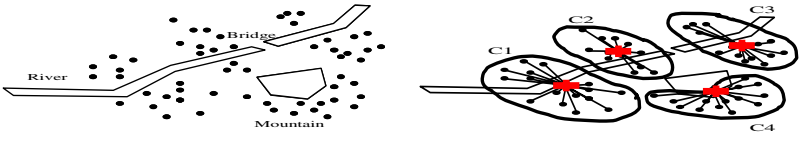

(a) Data objects and constraints (b) Clusters ignoring constraints

Fig. 1. Clustering data objects with obstacles constraints

COD-CLARANS [3] based on the Partitioning approach of CLARANS, AUTOCLUST+ [4] based on the Graph partitioning method of AUTOCLUST, and DBCluC [5]-[8] based on the Density-based algorithm. Although these algorithms can deal with some obstacles in the clustering process, many questions exist in them. COD-CLARANS algorithm inherits the shortcoming of CLARANS algorithm, which only gives attention to local constringency. AUTOCLUST+ algorithm inherits the limitation of AUTOCLUST algorithm, which builds a Delaunay structure to cluster data points with obstacles costly and is unfit for a large number of data. DBCluC inherits the shortcoming of DBSCAN algorithm, which cannot run in large high dimensional data sets etc. We proposed GKSCOC (Genetic K-Medoids Spatial Clustering with Obstacles Constraints) based on Genetic algorithms (GAs) and IKSCOC (Improved K-Medoids Spatial Clustering with Obstacles Constraints) in the literature [9]. The experiments show that GKSCOC is effective but the drawback is a comparatively slower speed in clustering.

Particle Swarm Optimization (PSO) is relatively a newer addition to a class of population based search technique for solving numerical optimization problems. PSO has undergone a plethora of changes since its development in 1995. One of the recent developments in PSO is the application of Quantum laws of mechanics to observe the

behavior of PSO. Such PSO's are called Quantum PSO (QPSO), and has faster convergence and global optima [10-13]. Recently, QPSO has been applied to data clustering [14].

In this paper, we presented a more effective QPSO method for SCOC. In the process of doing so, we first proposed a novel Spatial Obstructed Distance using QPSO based on Grid model (QPGSOD) to obtain obstructed distance, and then we developed QPKSCOC algorithm based on QPSO and K-Medoids to cluster spatial data with obstacles constraints. The contrastive experiments show that QPGSOD is effective, and QPKSCOC is better than IKSCOC in terms of quantization error and has higher constringency speed than GKSCOC.

The remainder of the paper is organized as follows. Section 2 introduces QPSO algorithm. QPGSOD is developed in Section 3. Section 4 presents QPKSCOC. The performances of QPKSCOC are showed in Section 5, and Section 6 concludes the paper.

2 Quantum Particle Swarm Optimization

2.1 Classical PSO

The Particle Swarm Optimization (PSO) is a population-based optimization method first proposed by Kennedy and Eberhart [15]. In order to find an optimal or near-optimal solution to the problem, PSO updates the current generation of particles (each particle is a candidate solution to the problem) using the information about the best solution obtained by each particle and the entire population. In the context of PSO, a swarm refers to a number of potential solutions to the optimization problem, where each potential solution is referred to as a particle. The aim of the PSO is to find the particle position that results in the best evaluation of a given fitness (objective) function. Each particle has a set of attributes: current velocity, current position, the best position discovered by the particle so far and, the best position discovered by the particle and its neighbors so far. The user can define the size of the neighborhood.

The mathematic description of PSO is as the following. Suppose the dimension of the searching space is D, the number of the particles is n. Vector $X_i = (x_{i1}, x_{i2}, \ldots, x_{iD})$ represents the position of the i^{th} particle and $pbest_i = (p_{i1}, p_{i2}, \ldots, p_{iD})$ is its best position searched by now, and the whole particle swarm's best position is represented as $gbest = (g_1, g_2, \ldots, g_D)$. Vector $V_i = (v_{i1}, v_{i2}, \ldots, v_{iD})$ is the position change rate of the i^{th} particle. Each particle updates its position according to the following formulas:

$$v_{id}(t+1) = wv_{id}(t) + c_1 rand()[p_{id}(t) - x_{id}(t)] + c_2 rand()[g_d(t) - x_{id}(t)] \quad (1)$$

$$x_{id}(t+1) = x_{id}(t) + v_{id}(t+1), \ 1 \le i \le n, \ 1 \le d \le D \quad (2)$$

where c_1 and c_2 are positive constant parameters, $Rand()$ is a random function with the range [0, 1], and w is the inertia weight.

Equation (1) is used to calculate the particle's new velocity, then the particle flies toward a new position according to equation (2). The performance of each particle is

measured according to a predefined fitness function, which is usually proportional to the cost function associated with the problem. This process is repeated until user-defined stopping criteria are satisfied. A disadvantage of the global PSO is that it tends to be trapped in a local optimum under some initialization conditions [16].

2.2 Quantum PSO

The development in the field of quantum mechanics is mainly due to the findings of Bohr, de Broglie, Schrödinger, Heisenberg and Bohn in the early twentieth century. Their studies forced the scientists to rethink the applicability of classical mechanics and the traditional understanding of the nature of motions of microscopic objects [17].

As per classical PSO, a particle is stated by its position vector X_i and velocity vector V_i, which determine the trajectory of the particle. The particle moves along a determined trajectory following Newtonian mechanics. However if we consider quantum mechanics, then the term trajectory is meaningless, because X_i and V_i of a particle cannot be determined simultaneously according to uncertainty principle. Therefore, if individual particles in a PSO system have quantum behavior, the performance of PSO will be far from that of classical PSO [18].

In the quantum model of a PSO, the state of a particle is depicted by wave function $\psi(x,t)$, instead of position and velocity. The dynamic behavior of the particle is widely divergent from that of the particle in traditional PSO systems. In this context, the probability of the particle's appearing in position X_i from probability density function $|\psi(x,t)|^2$, the form of which depends on the potential field the particle lies in [10]. The particles move according to the following iterative equations[11-13]:

$$\begin{aligned} x(t+1) &= p + \beta * |mbest - x(t)| * In(1/u) \quad if \quad \mathrm{k} \geq 0.5 \\ x(t+1) &= p - \beta * |mbest - x(t)| * In(1/u) \quad if \quad \mathrm{k} \prec 0.5 \end{aligned}, \tag{3}$$

where

$$p = (c_1 p_{id} + c_2 p_{gd})/(c_1 + c_2) \tag{4}$$

$$mbest = \frac{1}{M}\sum_{i=1}^{M} P_i = (\frac{1}{M}\sum_{i=1}^{M} P_{i1}, \frac{1}{M}\sum_{i=1}^{M} P_{i2}, \ldots, \frac{1}{M}\sum_{i=1}^{M} P_{iD}). \tag{5}$$

Mean best of the population is defined as the mean of the best positions of all particles, u, k, c_1 and c_2 are uniformly distributed random numbers in the interval [0, 1]. The parameter β is called contraction-expansion coefficient.

The QPSO is presented as follows:

1. Initialize population;
2. For $t = 1$ to $t_{\max}$ do {
3. Calculate *mbest* by equation (5)
4. Update particles position using equation (3);
5. Evaluate fitness of particle;
6. Update *Pbest* ;
7. Update *Pgbest* }

3 Spatial Obstructed Distance Using QPSO

To derive a more efficient algorithm for SCOC, the following definitions are first introduced.

*Definition 1. (Obstructed distance)*Given point p and point q, the obstructed distance $d_o(p,q)$ is defined as the length of the shortest Euclidean path between two points p and q without cutting through any obstacles.

Spatial obstructed distance using QPSO can be divided into two stages, that is, first establishes environment modeling based on grid model, and then adopts QPSO to get shortest obstructed path.

3.1 Environment Modeling Based on Grid Model

The basic thought is that the space area is divided into many small areas which have the same size, and every small area is considered as a grid. If the obstructed area is irregular shape, we can fill up the obstacles within verges. The grid considered as a free grid if it has no obstacles, otherwise an obstructed grid. Every grid has a corresponding coordinate and a sequence number, which represents coordinate uniquely. Grid model divided the space area into two-valued grids, number 0 represents the free grid and number 1 represents the obstructed grid. An example is shown in Fig.2 (a), 20*20 grid model, the shadow areas indicate the obstructed grid, and the number in the grid is the sequence number.

The relationship between coordinate (x_p, y_p) and sequence number P is defined as follows:

$$\left\{\begin{array}{l} x_p = \left[(p-1) \bmod m\right] + 1 \\ y_p = \operatorname{int}\left[(p-1)/m\right] + 1 \end{array}\right\}, \tag{6}$$

where m is the number of grid in every line. Our task is to search a route avoiding obstacles from point S to point E .The objective function can be revised as:

$$L = \sum_{i=2}^{n_p} \sqrt{(x_i - x_{i-1})^2 + (y_i - y_{i-1})^2}, \tag{7}$$

where (x_i, y_i) express the information of route point, n_p is the number of route point.

3.2 Obstructed Distance by QPSO

In the system of PSO, each particle represents a route from starting point to target point, for an example, $x_i = (x_{i1}, x_{i2}, \cdots x_{iD})$, where D is the dimension of particle. The dimension of every particle represents a grid, the first dimension express the sequence number of the starting grid and the last one is the sequence number of target grid. Thus it can form a route when the sequence numbers are connected by the ascending order. The fitness function is defined as follows:

$$f = \Big/ \left(1+\frac{1}{\sqrt{n-1}}\right)L, \tag{8}$$

where n is the number of the route grid passed, L is the sum distance between the two sequence number, it can be calculated according to equation (7).

The QPGSOD is developed as follows.

1. Establish the environment model by grid model;
2. Initialize each particle, and make any particle's position is free grid;
3. For $t=1$ to $t_{\max}$ do {
4. Calculate *mbest* by equation (5)
5 Update particles position using equation (3);
6. Evaluate fitness of particle according to equation (8);
7. Update *Pbest* ;
8. Update *Pgbest* }
9. Output obstructed distance.

The simulation result is in Fig.2 (b) and the solid line represents the optimal obstructed path obtained by QPGSOD.

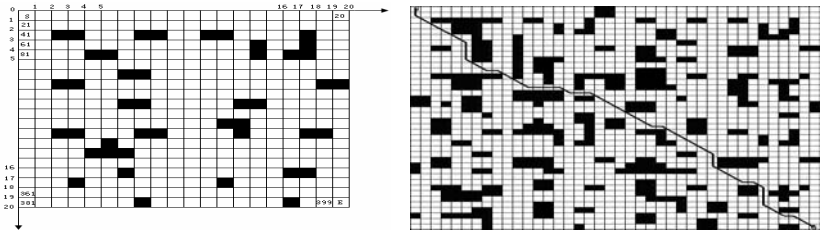

(a) Environment modeling (b) Obstructed path by QPGSOD

Fig. 2. Spatial Obstructed Distance using QPSO

4 Spatial Clustering with Obstacles Constraints Using QPSO

4.1 IKSCOC Based on K-Medoids

Typical partitioning-base algorithms are K-Means, K-Medoids and CLARANS. Here, K-Medoids algorithm is adopted for SCOC to avoid cluster center falling on the obstacle.Square-error function is adopted to estimate the clustering quality, and its definition can be defined as:

$$E = \sum_{j=1}^{N_C} \sum_{p \in C_j} (d(p, m_j))^2 \quad , \tag{9}$$

where N_C is the number of cluster C_j, m_j is the cluster centre of cluster C_j, $d(p,q)$ is the direct Euclidean distance between the two points p and q.

To handle obstacle constraints, accordingly, criterion function for estimating the quality of spatial clustering with obstacles constraints can be revised as:

$$E_o = \sum_{j=1}^{N_c} \sum_{p \in C_j} (d_o(p, m_j))^2 \tag{10}$$

where $d_o(p,q)$ is the obstructed distance between point p and point q.

The method of IKSCOC is adopted as follows [5].

1. Select N_C objects to be cluster centers at random;
2. Distribute remain objects to nearest cluster center;
3. Calculate E_o according to equation (10);
4. While (E_o changed) do {Let current $E = E_o$;
5. Select a not centering point to replace the cluster center m_j randomly;
6. Distribute objects to the nearest center;
7. Calculate E according to equation (9);
8. If $E >$ current E , go to 5;
9. Calculate E_o ;
10. If $E_o <$ current E , form new cluster centers}.

While IKSCOC still inherits two shortcomings, one is selecting initial value randomly may cause different results of the spatial clustering and even have no solution, the other is that it only gives attention to local constringency and is sensitive to an outlier.

4.2 QPKSCOC Based on QPSO and K-Medoids

QPSO has been applied to data clustering [12]. In the context of clustering, a single particle represents the N_C cluster centroid. That is, each particle X_i is constructed as follows:

$$X_i = (m_{i1}, ..., m_{ij}, ..., m_{iN_c}) \tag{11}$$

where m_{ij} refers to the j^{th} cluster centroid of the i^{th} particle in cluster C_{ij}. Here, the objective function is defined as follows:

$$f(x_i) = 1 / J_i \tag{12}$$

$$J_i = \sum_{j=1}^{N_c} \sum_{p \in C_{ij}} d_o(p, m_j) \tag{13}$$

The QPKSCOC is developed as follows.

1. Execute the IKSCOC algorithm to initialize one particle to contain N_C selected cluster centroids;

2. Initialize the other particles of the swarm to contain N_c selected cluster centroids at random;
3. For $t = 1$ to $t_{\max}$ do {
4. For i = 1 to no_of_particles do {
5. For each object p do {
6. Calculate $d_o(p, m_{ij})$;
7. Assign object p to cluster C_{ij} such that $d_o(p, m_{ij}) = \min \forall c = 1, ..., N_c \{d_o(p, m_{ic})\}$;
8. Calculate the fitness according to equation (12) }
9. Calculate *mbest* by equation (5)
10. Update particles position using equation (3);
11. Update *Pbest* ;
12. Update *Pgbest* }
13. Select two other particles j and k ($i \neq j \neq k$) randomly;
14. Optimize new individuals using IKSCOC}
15. Output.

where $t_{\max}$ is the maximum number of iteration for QPSO. STEP 14 is to improve the local constringency speed of QPSO.

5 Results and Discussion

We have made experiments separately by K-Medoids, IKSCOC, GKSCOC, and QPKSCOC. $n = 50$, $c_1 = c_2 = 2$, $t_{\max} = 100$.

Fig.3 shows the results on real Dataset. Fig.3 (a) shows the original data with river obstacles. Fig.3 (b) shows the results of 4 clusters found by K-Medoids without considering obstacles constraints. Fig.3(c) shows 4 clusters found by IKSCOC. Fig.3 (d) shows 4 clusters found by GKSCOC. Fig.3 (e) shows 4 clusters found by QPKSCOC. Obviously, the results of the clustering illustrated in Fig.3(c), Fig.3 (d) , and Fig.3 (e) have better practicalities than that in Fig.3 (b), and the ones in Fig.3 (e) and Fig.3 (d) are both superior to the one in Fig.3(c). So, it can be drawn that QPKSCOC is effective and has better practicalities.

Fig.4 is the value of J showed in every experiment on Dataset1 by IKSCOC and QPKSCOC respectively. It is showed that IKSCOC is sensitive to initial value and it constringes in different extremely local optimum points by starting at different initial value while QPKSCOC constringes nearly in the same optimum points at each time.

Fig. 5 is the constringency speed in one experiment on Dataset1. It is showed that QPKSCOC constringes in about 12 generations while GKSCOC constringes in nearly 25 generations. So, it can be drawn that QPKSCOC is effective and has higher constringency speed than GKSCOC. Therefore, we can draw the conclusion that QPKSCOC has stronger global constringent ability than IKSCOC and has higher convergence speed than GKSCOC.

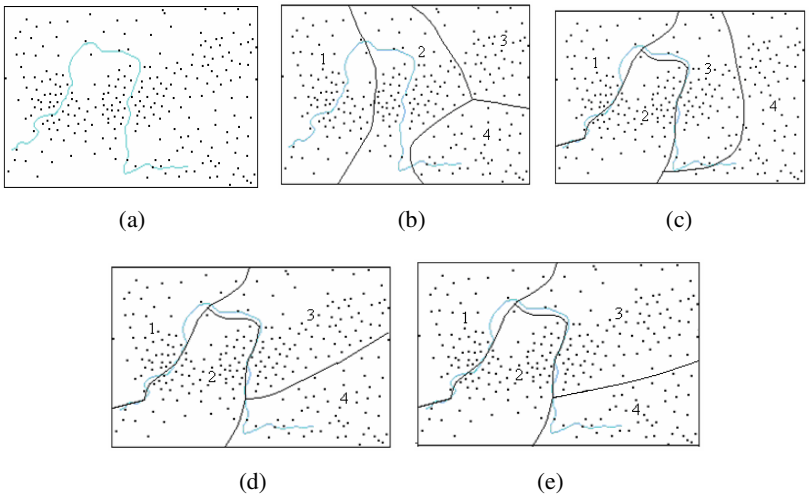

Fig. 3. Clustering Dataset

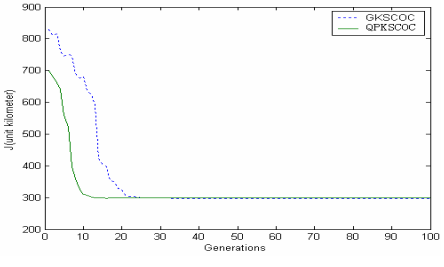

Fig. 4. QPKSCOC vs. IKSCOC

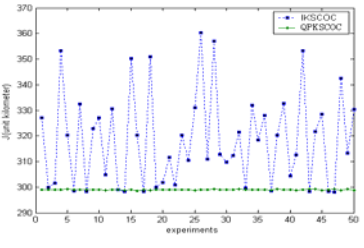

Fig. 5. QPKSCOC vs. GKSCOC

6 Conclusions

In this paper, we developed a more effective Quantum Particle Swarm Optimization (QPSO) for Spatial Clustering with Obstacles Constraints (SCOC) by proposing a novel spatial obstructed distance using QPSO and the QPKSCOC algorithm. The proposed method is also compared with some other algorithms to demonstrate its efficiency and the experimental results are satisfied.

Acknowledgments

This work is partially supported by Program for New Century Excellent Talents in University (NCET-08-0660),the Supporting Plan of Science and Technology Innovation Talent of Colleges in Henna Province (Number: 2008HASTIT012),and the Opening Research Fund of Key Laboratory of Spatial Data Mining & Information Sharing of Ministry of Education (Number:200807).

References

1. Tung, A.K.H., Han, J., Lakshmanan, L.V.S., Ng, R.T.: Constraint-based clustering in large databases. In: Van den Bussche, J., Vianu, V. (eds.) ICDT 2001. LNCS, vol. 1973, pp. 405–419. Springer, Heidelberg (2000)
2. Tung, A.K.H., Ng, R.T., Lakshmanan, L.V.S., Han, J.: Geo-spatial Clustering with User-Specified Constraints. In: Proceedings of the International Workshop on Multimedia Data Mining (MDM/KDD 2000), Boston USA, pp. 1–7 (2000)
3. Tung, A.K.H., Hou, J., Han, J.: Spatial Clustering in the Presence of Obstacles. In: Proceedings of International Conference on Data Engineering (ICDE 2001), Heidelberg Germany, pp. 359–367 (2001)
4. Castro, V.E., Lee, I.J.: AUTOCLUST+: Automatic Clustering of Point-Data Sets in the Presence of Obstacles. In: Proceedings of the International Workshop on Temporal, Spatial and Spatial-Temporal Data Mining, Lyon France, pp. 133–146 (2000)
5. Zaïane, O.R., Lee, C.H.: Clustering Spatial Data When Facing Physical Constraints. In: Proceedings of the IEEE International Conference on Data Mining (ICDM 2002), Maebashi City Japan, pp. 737–740 (2002)
6. Wang, X., Hamilton, H.J.: DBRS: A Density-Based Spatial Clustering Method with Random Sampling. In: Proceedings of the 7th PAKDD, Seoul Korea, pp. 563–575 (2003)
7. Wang, X., Rostoker, C., Hamilton, H.J.: DBRS+: Density-Based Spatial Clustering in the Presence of Obstacles and Facilitators (2004), `http://Ftp.cs.uregina.ca/Research/Techreports/2004-09.pdf`
8. Wang, X., Hamilton, H.J.: Gen and SynGeoDataGen Data Generators for Obstacle Facilitator Constrained Clustering (2004), `http://Ftp.cs.uregina.ca/Research/Techreports/2004-08.pdf`
9. Zhang, X.P., Wang, J.Y., Fang, W., Fan, Z.S., Li, X.Q.: A Novel Spatial Clustering with Obstacles Constraints Based on Genetic Algorithms and K-Medoids. In: Proceedings of the Sixth International Conference on Intelligent Systems Design and Applications (ISDA 2006) [C], Jinan Shandong China, pp. 605–610 (2006)
10. Liu, J., Sun, J., Xu, W.-b.: Quantum-behaved particle swarm optimization with adaptive mutation operator. In: Jiao, L., Wang, L., Gao, X.-b., Liu, J., Wu, F. (eds.) ICNC 2006. LNCS, vol. 4221, pp. 959–967. Springer, Heidelberg (2006)
11. Sun, J., Feng, B., Xu, W.: Particle Swarm Optimization with particles having Quantum Behavior. In: Proceedings of Congress on Evolutionary Computation, Portland, OR, USA, pp. 325–331 (2004)
12. Liu, J., Sun, J., Xu, W.-b.: Improving quantum-behaved particle swarm optimization by simulated annealing. In: Huang, D.-S., Li, K., Irwin, G.W. (eds.) ICIC 2006. LNCS (LNBI), vol. 4115, pp. 130–136. Springer, Heidelberg (2006)
13. Sun, J., Lai, C.H., Xu, W.-b., Chai, Z.: A novel and more efficient search strategy of quantum-behaved particle swarm optimization. In: Beliczynski, B., Dzielinski, A., Iwanowski, M., Ribeiro, B. (eds.) ICANNGA 2007. LNCS, vol. 4431, pp. 394–403. Springer, Heidelberg (2007)
14. Chen, W., Sun, J., Ding, Y.R., Fang, W., Xu, W.B.: Clustering of Gene Expression Data with Quantum-Behaved Particle Swarm Optimization. In: Proceedings of IEA/AIE 2008, vol. I, pp. 388–396 (2008)
15. Kennedy, J., Eberhart, R.C.: Particle Swarm Optimization. In: Proceedings of IEEE International Conference on Neural Networks, Perth, Australia, vol. IV, pp. 1942–1948 (1942)
16. van de Frans, B.: An Analysis of Particle Swarm Optimizers. Ph.D. thesis, University of Pretoria (2001)
17. Pang, X.F.: Quantum mechanics in nonlinear systems. World Scientific Publishing Company, River Edge (2005)
18. Feng, B., Xu, W.B.: Adaptive Particle Swarm Optimization Based on Quantum Oscillator Model. In: Proceedings of the 2004 IEEE Conf. on Cybernetics and Intelligent Systems, Singapore, pp. 291–294 (2004)

Fuzzy Failure Analysis of Automotive Warranty Claims Using Age and Mileage Rate

SangHyun Lee and KyungIl Moon

Department of Computer Engineering, Honam University, Korea
Leesang64@gmail.com, kimoon@honam.ac.kr

Abstract. There are many situations where several characteristics are used together as criteria for judging the eligibility of a failed product. The warranty analysis characterized by a region in a two-dimensional plane with one axis representing age and the other axis representing mileage is known as warranty plan. A classical warranty plan requires crisp data obtained from strictly controlled reliability tests. However, in a real situation these requirements might not be fulfilled. In an extreme case, some warranty claims data come from users whose reports are expressed in a vague way. It might be caused by subjective and imprecise perception of failures by a user, by imprecise records of warranty data, or by imprecise records of the rate of mileage. This paper suggests different tools appropriate for modeling a two-dimensional warranty plan, and a suitable fuzzy method to handle some vague data.

Keywords: Mileage accumulation ratio, Use period, Warranty claims reoccurrence, Fuzzy reasoning.

1 Introduction

Manufacturers in developing products, production process, as well as available on the market after the sale and use of products sold to users and to verify the reliability of assessment is emerging as an important issue. Development in the life of products made in the lab for testing and accurate results of the data, but takes a lot of the costs, as well as does not reflect the actual use environment is a disadvantage. But the actual use of the warranty claims data obtained from the scene contains inaccurate data, but cost less and entering an environment that reflects the actual use and is the biggest advantage. The product of the post-warranty claims to collect data that can be generated with the system growing companies, the use of these warranty claims data is more demanding. Automotive warranty claims are usually obtained from afterservice center, in which are included some repairs of product failure and warranty data. Using these data, the failure of the product failure occurred at the point of extraction period on sales is defined as the period minus the period of use.

Kaleisch et al. (1991) proposed a log-linear Poisson model using a number of warranty claims. But, Baxter (1994) pointed out that it can not see the first product use to estimate some distributions of its life table. This model can be applied only if the product is the same of each period. For the accumulation of mileage warranty, Lawless et al.

D.-S. Huang et al. (Eds.): ICIC 2009, LNAI 5755, pp. 434–439, 2009.

(1995) suggested an optimal model based on data and supplementary information. Hu and Lawless (1996) developed non-parametric estimation of means and rates of occurrences from truncated recurrent event data. Suzuki(1985) examined the efficiency of a consistent estimator relative to maximum likelihood estimator when along with complete record of failure; partial record of non-failures can also be obtained. Nelson (1988, 1995) gave simple graphical methods for analyzing repairable systems data based on number and costs of repair and also provided confidence limits for the same.

Automotive warranty claims related databases using the actual useful data about product performance in environments without feedback is a very rich resource of information. Failure mode and failure is loosely based on that report incorrect data belongs to the warranty period of uncertainly and mileage inaccurate because of features can occur. In this paper data from previous model year vehicle available through automotive warranty database will be used for the assessment. Sub-system of the vehicle mileage and the warranty claims data used to arrive at estimates for the time period using the fuzzy system provides a simple methodology. Also, the estimate of the vehicle's warranty coverage period and mileage to evaluate the impact of the change in imports is used to help. In this paper, we received from the car company's warranty data from actual field use and the mileage on the part of the fuzzy system using the product as opposed to a bad rate.

2 The Estimation of Warranty Claims

We develop a method to estimate number of claims for a specific sub-system of a vehicle at various combinations of use period and mileage limits of warranty. Although the method focuses on analysis at component and sub-system level, the estimates at system or vehicle level can be easily obtained by pooling of component, sub-system level estimates. A main objective of the estimation method being discussed is to be able to assess the impact of changes in time and/or mileage limits on number of claims. For this purpose, in the following section, we discuss some issues of mileage accumulation, repeat failures, and claims per thousand vehicles sold.

Let M_i denote time (in months from the sale of the automobile) and K_i denote mileage for the i-th (i =1, 2,…, N) automobile in a population of same type of vehicles. Let (in miles per month) denote mileage accumulation of i-th automobile. Let and be the distribution function (df) and probability density function (pdf), respectively, for. Estimating the parameters of pdf and df is a crucial step in the analysis. A warranty database usually contains mileage accumulation data for only those cars that fail within the warranty period. Repeat claims could be the result of either a new failure or difficulty in root cause elimination during the previous repair. The expected number of total claims can be obtained by combining estimates of repeat claims with the estimates for the first claims. Repeat claims as a proportion of the first claims can be estimated using following formula.

$$\hat{p}_{rc,m/k_0} = \frac{n(m) - n_f(m)}{n_f(m)}.$$

1) $p_{rc,m/k_0}$: estimate of repeat claims as a proportion of the first claims at month-in-service and K_0 mileage warranty limit.

2) $n(m)$: total number of claims up to m month-in-service value

3) $n_f(m)$: number of first claims up to m_0 month-in-service or number of cars with at least one claim up to m_0 month-in-service.

When increments of 5 or 10 month-in-service are used for arriving at $p_{rc,m/k_0}$ values, the curve fitted to the data points can be used to arrive at intermediate $p_{rc,m/k_0}$ values. Using $\hat{p}_{rc,m/k_0}$ and parameters of $G(\alpha)$, $\hat{p}_{rc,m/unlimited}$ is estimated as:

$$\hat{p}_{rc,m/unlimited} = \frac{x - \upsilon}{p[\alpha_i \le \frac{K_0}{M_0} | m]}.$$

3 Fuzzy Reasoning of Age/Mileage Failure Rate

Fuzzy logic was originally introduced by Zadeh as a mathematical way to represent vagueness in everyday life. The proposed overall procedure for approximating the impact of corrective actions on two-dimensional warranty is shown in Fig. 1, which consists of four components, namely, fuzzy rule base, fuzzy inference process, fuzzification process, and defuzzification process.

The basic unit of any fuzzy system is the fuzzy rule base. All other components of the fuzzy logic system are used to implement these rules in a reasonable and efficient manner.

Fuzzy rules are usually formulated as IF-THEN statements, with one or more antecedents connected to a consequent via operators like AND, OR, etc. IF (Antecedent$_1$) OP (Antecedent$_2$) … OP (Antecedent$_n$) THEN (Consequent) (w).

Where n is an integer, OP stands for operators like AND, OR, etc., and w represents a weight value indicating the importance of a rule.

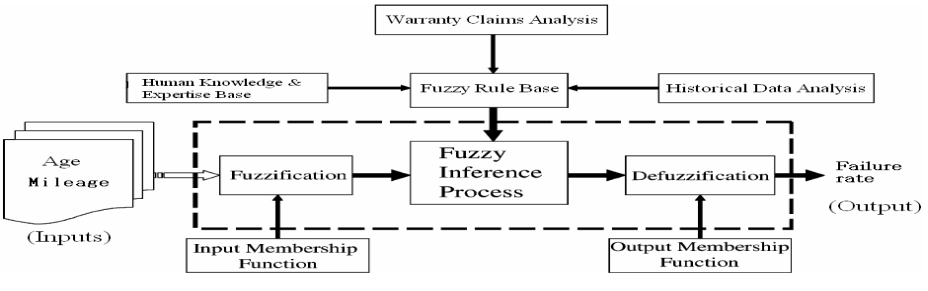

Fig. 1. An overview of fuzzy logic system for a failure rate

Now, imagine a fuzzy rule where 2 antecedents apply to the same consequent (n = 2). Further, let Antecedent$_1$ be activated to a degree of 0.8, and Antecedent$_2$ to a degree of 0.7. The weight value is usually 1.0, and OP is usually an OR operator defined as:

Consequent = max[Antecedent$_1$, Antecedent$_2$]. In this situation, Consequent would be activated to a degree of max[0.8, 0.7] = 0.8. There is nothing extraordinary here. The process described is a standard process. Now imagine a more complex scenario where 5 antecedents apply to a Consequent (n = 5). A possible scenario may look like: Consequent = max[0.7, 0.8, 0.6, 0.5, 0.9] = 0.9. In this situation, we probably are less confident in the applicability and usefulness of the rule. Furthermore, as there are many different weights indicating the importance of the rule, an aggregation of the consequents across the rules is probably less confident. The formulation of rules showing such complexity, however, might be common in some domains. To approach the problem, this paper presents a method that aims to include each activated rule antecedent more actively in the reasoning process of the fuzzy rule base.

OP is usually an OR operator defined as: Consequent = max[Antecedent1, Antecedent2]. IF an AND operator is defined, Consquent=min[Antecedent1, Antecedent2].

To explain the method, we describe a simple fuzzy rule system where two antecedents (Age, Mileage) relate to an output (Failure rate). The following two rules shall be included in the fuzzy rule system:

IF (Mileage) IS (*normal*) OR (Age) IS (*normal*) THEN (Number of Warranty Claim) is (*normal*)

IF (Mileage) IS (*low*) OR (Age) IS (*low*) THEN (Number of Warranty Claim) is (*low*)

Further, both rules shall carry the weight 1.0, and the OR operator employed shall be the same as it was used before.

4 The Automotive Example

The result of estimation of stress failure rate is obtained by two-way fuzzy analysis of the mileage and the age data. In this example, the vehicle information regarding particular model year, vehicle, sub-system name, and failure mode is not disclosed to protect proprietary nature of the information. Tables 1 summarize the number and amount of warranty claims issued against vehicle A shipped out in the 2004~2005 year.

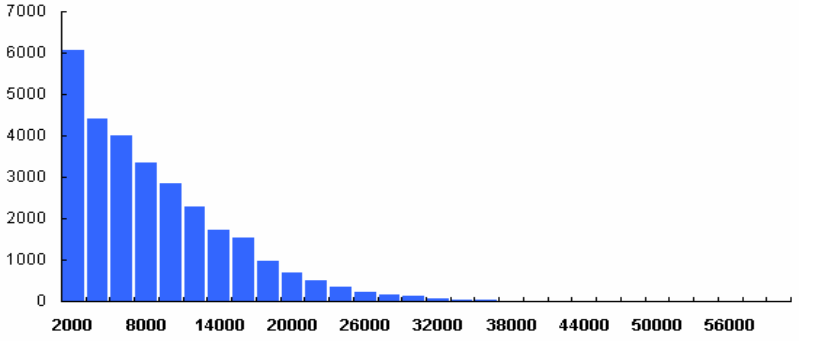

Fig. 2. Mileage distribution

Using reliability analysis mileage to the production and sales by month and claims analysis to the claims data can accurately mapping. However, the number of vehicles

in production and difficult to calculate mileage. But, [figure 2 and Table 1] the total mileage claims came as the number of vehicles used to estimate the reliability of the mileage-based function can be calculated.

Table 1. Mileage reliability analysis

$$\sum M_{0\sim 2000} = \hat{m}_{0\sim 2000}(\%) \times \sum Sale$$

mileage	Ratio	Target vehicle be estimated	Be failures	Failure rate	Cumulative failure rate
2000	0.2231	12896	52	0.00403	0.00403
4000	0.1475	9362	49	0.00523	0.00927
6000	0.1338	8497	55	0.00647	0.01574
8000	0.1121	7116	41	0.00576	0.02150
10000	0.096	6095	37	0.00607	0.02757
12000	0.0773	4910	29	0.00591	0.03348
14000	0.0582	3692	29	0.00785	0.04133
16000	0.0519	3297	28	0.00849	0.04982
18000	0.0336	2136	24	0.01124	0.06106
20000	0.0238	1510	24	0.01589	0.07696
22000	0.0173	1095	25	0.02282	0.09978
24000	0.0123	780	16	0.02050	0.12028
26000	0.0087	554	11	0.01985	0.14013
28000	0.0065	410	10	0.02437	0.16451
30000	0.0054	345	12	0.03481	0.19932
32000	0.0033	211	4	0.01891	0.21824
34000	0.0024	152	5	0.03284	0.25107
36000	0.0018	116	7	0.06018	0.31126
38000	0.0014	87	3	0.03460	0.34586
40000	0.0013	82	4	0.04850	0.39436
42000	0.0007	44	1	0.02252	0.41688
44000	0.0005	30	0	0.00000	0.41688
46000	0.0002	13	1	0.07881	0.49569

Total stress can be defined as a function of mileage and age. Here, a stress and the failure rate of production are analyzed. Using the proposed fuzzy reasoning, the stress failures are estimated in 40000 and 60000km [figure 3].

$$Stress(\%) = \frac{\sum Claim_{ij}}{\sqrt{\sum Sale_i \times \sum Mileage_j}} \times 100(\%) \quad i = a \quad Age, l = a \quad Mileage$$

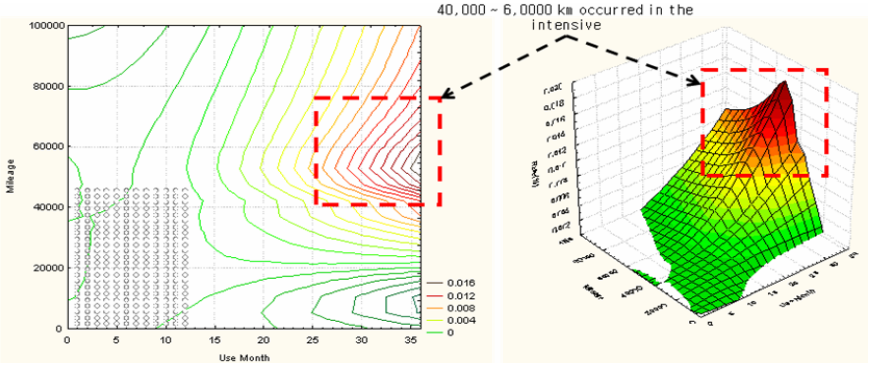

Fig. 3. Estimation of stress failure rate

5 Conclusion

In this study, the change in age and the limit for usage are critical elements for evaluating the effect on the number and failure rate of the warranty claims. In general, when the accumulated ratio of mileage is high, the expectation of the warranty claim

is higher than when the ratio is low. In the conventional method for the estimation of the failure rate for warranty claims, the result is relatively higher. However, the method for the analysis of age and mileage warranty based on fuzzy deduction shows more reasonable results. In other words, the rate of an increase in the number of claims changes more rapidly while the accumulated ratio of Mileage is higher. Finally, since there exist various elements affecting warranty claims and it is necessary to perform a multi-dimensional analysis in consideration of these elements simultaneously, there is room for future improvements on this study. It is critical to probe deeply into the formation of the fuzzy groups in terms of input and output variables. In addition, it is desirable to obtain more accurate measurements for the weighted ratio of this fuzzy rule.

References

1. Baxter, L.A.: Estimation from Quasi Life Table. Biometrika 81(3), 567–577 (1994)
2. Kalbfleisch, J.D., Lawless, J.F., Robinson, J.A.: Methods for the Analysis and Prediction of Warranty Claims. Technometrics 33(3), 273–285 (1991)
3. Lawless, J.F., Hu, J., Cao, J.: Methods for the estimation of failure distributions and rates from automobile warranty data. Lifetime Data Anal., 227–240 (1995)
4. Suzuki, K.: Estimation of lifetime parameters from incomplete field data. Technometrics 27, 263–271 (1985)
5. Hu, X.J., Lawless, J.F.: Estimation of rate and mean functions from truncated recurrent event data. J. Am. Statist. Assoc. 91, 300–310 (1996)
6. Nelson, W.: Graphical analysis of system repair data. J. Qual. Technol. 20, 24–35 (1988)
7. Nelson, W.: Confidence limits for recurrence data applied to cost or number of product repairs. Technometrics 37, 147–157 (1995)

A Fuzzy-GA Wrapper-Based Constructive Induction Model

Zohreh HajAbedi[1,*], and Mohammad Reza Kangavari [2]

[1] Science and Research branch, Islamic Azad University, Tehran, Iran
[2] Department of Computer, Iran University of Scince and Technology, Tehran, Iran

Abstract. Constructive Induction is a preprocessing step applied to representation space prior to machine learning algorithms and transforms the original representation with complex interaction into a representation that highlights regularities and is easy to be learned. In this paper a Fuzzy-GA wrapper-based constructive induction system is represented. In this model an understandable real-coded GA is employed to construct new features and a fuzzy system is designed to evaluate new constructed features and select more relevant features. This model is applied on a PNN classifier as a learning algorithm and results show that integrating PNN classifier with Fuzzy-GA wrapper-based constructive induction module will improve the effectiveness of the classifier.

Keywords: Constructive induction, Feature construction, Feature selection, Fuzzy, GA.

1 Introduction

One of the most fundamental machine-learning tasks is inductive machine learning where a generalization is obtained from a set of samples, and it is formalized using different techniques and models. The ability of an inductive learning algorithm to find an accurate concept description depends strongly on the representation space [6]. Representation space is a space in which, training samples, hypotheses and domain knowledge are represented. Learning algorithms encounter difficulties when data is complex and includes irrelevant features, high accuracy in values and correlated features. If the representation space is well-designed, then learning results will tend to be satisfactory with almost any method [11].

As the importance of the representation space for machine learning problems was proved, the idea of CI was introduced by Michalski in 1986 [3]. Gradually, this idea was expanded and different artificial intelligent tools were employed to implement it.

A learning process that includes two phases, one for constructing best representation space and the other for generating best hypothesis in new space, is known as CI. Most CI methods such as GALA[1] [26], LFC [27] [2] and MRP[3] [28], apply a greedy search to

* Corresopnding author.
[1] Lookahead Feature Construction.
[2] Multidimensional Relational Projection.
[3] Similarity Based Learning Algorithm.

D.-S. Huang et al. (Eds.): ICIC 2009, LNAI 5755, pp. 440–449, 2009.

find new features. Due to the attributes interaction, the search space for constructing new features has more variation, and therefore, a greedy method may find a local optimal solution. Recent works on problems with interaction show that a global search strategy such as GA[4] is more likely to be successful in searching through the intractable and complicated search spaces. Moreover, GA provides the ability to construct and evaluate several features as one single individual. Evaluating a combination of features is essential for the success of a CI method when complex interactions among several subsets of attributes exist.

Some CI methods such as Fringe, SymFringe and DCFringe [30] use hypotheses that are generated with an SBL. These methods rely strongly on generated hypotheses. In cases where representation space is very complex, A SBL cannot learn effective hypotheses and as a result, CI methods depended on these hypotheses, cannot generate optimized representation space. Other CI methods such as CITRE [5] and Fringe are applicable for specific learning algorithm such as decision trees.

Many earlier methods such as GALA use greedy approaches to implement CI and as we know greedy methods may be converged to local optima in complex search spaces. Evolutionary approaches are successful global search strategies in complex spaces. In recent works, evolutionary algorithms are employed to implement constructive induction. One example of these systems is MFE2/GA [4] system. In this system a GA-based Constructive Induction method is applied to representation space and satisfactory result are taken. Another example of evolutionary based constructive induction systems is GAP [13] system. In this system Genetic Programming and a Genetic Algorithm to pre-process data before it is classified using the C4.5 decision tree learning algorithm. Genetic Programming is used to construct new features from those available in the data, a potentially significant process for data mining since it gives consideration to hidden relationships between features. A Genetic Algorithm is used to determine which set of features is the most predictive.

In this paper, a Fuzzy-GA wrapper-based approach is employed to implement CI. This model uses a simple and understandable real coding scheme for encoding chromosomes; it is also applicable for all types of learning algorithms. This model is tested on a PNN classifier and the results reveal that with the present CI module, PNN classifier accuracy can be increased considerably.

The organization of this paper is as follows: section 2 introduces constructive induction, a brief explanation of fuzzy is represented in section 3, section 4 represents GA briefly, section 5 discusses Fuzzy-GA wrapper-based constructive induction system, in section 6 implementation results are illustrated and section 7 concludes the paper.

2 Constructive Induction

Learning algorithms depend on information which is provided by user, in order to construct descriptions and hypotheses from data. So data analyst should determine adequate features for the learner. Features will be inadequate for learning if they are

[4] Probabilistic Neural Network.

weakly or indirectly inter relevant or if they are not measured correctly and with appropriate accuracy.

As the importance of the representation space for machine learning problems was proved, the idea of CI was introduced by Michalski [3] in 1986. Gradually, this idea was expanded and different artificial intelligent tools were employed for implementing it.

CI is the process of transforming the original representation of hard concepts with complex interaction into a representation that highlights regularities [4]. The basic premise of research on CI is that results of a learning process directly depend on the quality of the representation space. If the representation space is well-designed, then learning results will be satisfactory with almost any method [11].

Similarity-Based Learning methods learn concepts by discovering similarities. They achieve high accuracy when the data representation of the concept is good enough to maintain the closeness of instances of the same class. Hard concepts with complex interaction are difficult to be learned by an SBL. Interaction means the relation between one feature and the target concept depends on another feature[19]. Due to interaction, each class is scattered through the space, and therefore, regularities are hidden to the learner. The interaction problem arises when shortage of domain knowledge exists and only low-level primitive features are available to represent data.

In the previous works, CI concentrated only on constructing new goal relevant features. Later it was revealed that constructing new features is only one of the ways to optimize representation space. In fact, constructing new features is one type of expanding the space. Feature selection and features' values abstraction are types of destruction of representation space. More recent works have viewed CI more generally, as a double-search process, in which one search is for an improved representation space and the other for best hypothesis in this space [11].

Operations for improving representation space for learning are: removing irrelevant features, constructing new goal relevant features and abstracting features' values. We can also define constructive induction as a preprocessing process that is applied on representation space before learning algorithm, to provide a more suitable space for the learner.

Place of CI is demonstrated in Fig. 1 [8].

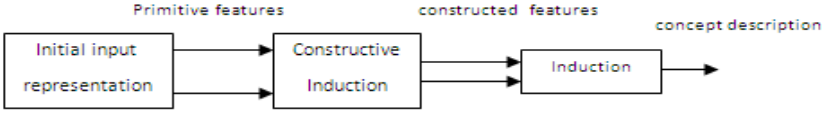

Fig. 1. Place of CI process

Constructive induction can be divided into a filter approach or a wrapper [3]. In the filter approach feature selection is performed as a pre-processing step to induction. Because it is separated from the induction algorithm, filters are fast, they can be used with any induction algorithms once filtering is done, and can be used on large datasets. However, they may not agree on the relevancy of certain features with the induction algorithm. Methods for filtering mostly include those based on information theory or probabilistic methods. The wrapper approach uses the induction algorithm itself to make estimates of the relevance of the given features.

3 Fuzzy-GA Wrapper-Based Constructive Induction Model

In this paper a wrapper-based constructive induction model is designed and implemented using a hybrid method by combination of GA and fuzzy logic. As we know, fuzzy set theory has been widely used to represent uncertain or flexible information in many types of applications, such as scheduling, engineering design, and optimization problems. It may provide an alternative and convenient framework for handling uncertain parameters, while there is lack of certainty in data or even lack of available historical data. In this model a genetic algorithm is also employed. A genetic algorithm is a problem-solving technique motivated by Darwin's theory of natural selection in evolution [22]. A basic framework of GAs was established by Holland [21]. Most of the optimization problems are complex and solving them with classic methods is difficult or impossible. Genetic algorithms are powerful tools for these kinds of problems. In the presented model we combine fuzzy and GA as a hybrid model to use the premiums of both.

The model presented in this paper discrete features' values, constructs new goal relevant features and select best features and thus provide a improved representation space for learning algorithms. In the Fig. 2 a block diagram of wrapper-based FGACI[5] model is illustrated.

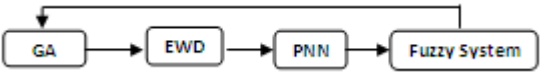

Fig. 2. Wrapper Based FGACI Model block diagram

As it is demonstrated in the Fig. 2, in the first step a real coded genetic algorithm is employed for constructing new features. Data set is updated on the basis of new features' formulas. EWD[6] discretization algorithm is applied on new data set and feature's values are discretizied.EWD is a simple discretization algorithm that discretes features' values into a predefined number of intervals [18]. In the next step, a PNN[7] classifier is applied on data set and classifier precision is considered as a criterion for evaluating the new features. PNN [29] is a two-layer feed forward neural network that is used widely in classification applications.

In Fuzzy-GA wrapper-based CI model a fuzzy system is designed for final evaluation of feature's sets. This fuzzy system has two inputs and one output. Fuzzy system inputs are "PNN classifier" and "average length of features". Fuzzy system output represents the quality of features sets.

3.1 GA Coding Scheme

In wrapper-based FGACI model a real coding scheme is considered. Real coding in comparison to binary coding has faster convergence [20]. In this model each

[5] Fuzzy GA Constructive Induction.
[6] Equal Width Discretization.
[7] Probabilistic Neural Network.

chromosome has a structure as shown in Fig. 3.a. As it is depicted in Fig. 3.a, chromosome structure is in matrix form. In this matrix, the number of rows determines the number of new constructed features and the number of columns determines the length of constructed features.

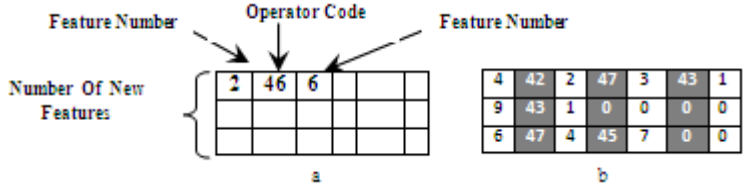

Fig. 3. a: FGACI Chromosome Structure, b: A RGACI chromosome example

Each chromosome, i.e. a problem solution, includes one set of new features. Each row in chromosome matrix is a new feature formula. The number of new features varies and is determined randomly. Also the length of each feature formula and as a result, number of original features that take part in constructing new features varies and selected at random. In this matrix structure, odd columns contain original feature's number and even columns contain operator's code. Arithmetic operators, i.e. +,-,/,*, are used to construct new features.

As an example, a row similar to Fig. 4, means 8^{th} feature's value must be subtracted from value of 7^{th} feature to construct a new feature.(45 is subtraction code).

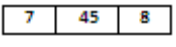

Fig. 4. A new feature formula

As another example, consider the Fig. 3.b.

In this chromosome, the number of rows is 3 and thus we have 3 new features. Each row represents a new feature formula. Length of first new feature (row no. 1) is seven, length of second new feature (row no. 2) is 3 and length of third new feature (row no. 3) is 5. Features' length are variable and thus in each row, extra cells are illustrated with zero.

3.2 GA Crossover Operator

In FGACI, one-point crossover[1] is employed. Depending on crossover rate, a number of chromosomes are selected as parents. Parent chromosomes are selected two by two at random. In the next step, in each parent, one row is selected randomly as a crossover point. Ultimately parent chromosomes' rows are exchanged from crossover points.

In different applications, various types of crossover operators are being used. In FGACI model, a one-point crossover operator is employed.

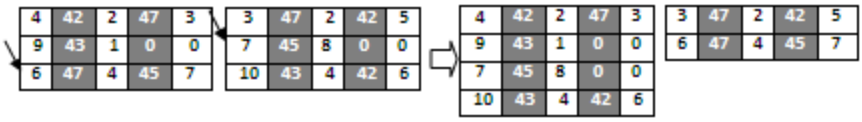

Fig. 5. Crossover operator

Crossover operation is illustrated in Fig. 5. As depicted in Fig. 7, first parent is a feature subset of five new features that consists of five new features' formula. Second parent consists of three new features' formula. In the first parent, fifth row is selected as crossover point and in the second parent, second row is selected. Parents' rows are exchanged through the crossover points and two offsprings are generated that have six and two rows, respectively.

3.3 GA Mutation Operator

Mutation is used to transform the chromosome by the means of randomly changing one of the genes [23]. In FGACI, one chromosome is selected randomly. In the matrix of selected chromosome, one cell is selected. If column number of this cell is odd, selected cell contains a feature number and therefore it is replaced by a new feature number. If column number is even, it will be replaced by a new operator code.

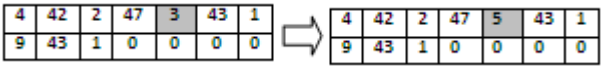

Fig. 6. Mutation operator

As it is demonstrated in Fig. 6, cell with row number of three and column number of five is selected. Column number of this cell is odd and therefore the feature number of seven is replaced by five.

3.4 GA Selection Method

The selection operation determines which parent chromosomes participate in producing offsprings for the next generation. Usually members are selected with a probability proportional to their fitness value [1].

In FGACI model, %90 percent of next generation population is selected in proportion to their fitness values and %10 percent of population is selected randomly. So in addition to providing strong solutions with more chance of being selected, weak solutions have still some chance to be included and improved in the next generation.

3.5 GA Fitness Function

A genetic algorithm uses a fitness function to calculate the degree of fitness of a chromosome [24].

Within every generation, a fitness function should be used to evaluate the quality of every chromosome to determine the probability of its surviving to the next generation; usually the chromosomes with larger fitness have a higher survival probability [25].

In wrapper-based FGACI, fitness of each chromosome is evaluated with the fuzzy system designed for this purpose. This fuzzy system has two inputs and one output. Two inputs are "average length of features" and "PNN classifier accuracy". The output variable determines the quality of features set based on "average length of features" and "PNN classifier accuracy".

"PNN classifier accuracy" is calculated by applying PNN on new data set. "Average length of features" is a criterion that estimates the complication of features sets. For calculating this criterion, sum of new features' formulas length are calculated through each feature set and this summation is divided on the number of features in the features set. As an example consider the chromosome in the Fig.7.

Feature1	4	42	2	47	3	43	1
Feature2	9	43	1	0	0	0	0
Feature3	6	47	4	45	7	0	0

Fig. 7. A chromosome with 3 features formula

Fig.10 displays a feature set with 3 features. First feature length is 7, second feature length is 3, third feature length is 5. Average length of features in this feature set is calculated as below:

$$average\ of\ features\ length = \frac{7+3+5}{3} = 5 \quad (1)$$

This fuzzy system is a mamdani fuzzy system that has two inputs and one output, Its inputs are " PNN Classifier Precision" and " Average length of features " and its output is " Quality of features set ".

This fuzzy system rulebase has 25 fuzzy rules that some of them are listed below:

If (ClassifierPrecision is very low) and (length is very short) then (Performance is Xpoor)
If (ClassifierPrecision is medium) and (length is very short) then (Performance is XXgood)
If (ClassifierPrecision is high) and (length is very short) then (Performance is excellent)

The wrapper-based FGACI model is applied on five data sets and results are shown in the following section.

4 Implementation Results

Five well-known data sets are used from the UCI repository to examine the wrapper-based FGACI performance. These data sets Information are shown in table 1.

Table 1. Datasets Information

DataSet	Features	Samples	Classes
Glass Identification	10	214	7
Wine	13	178	3
Pima	8	768	2
Ionosphere	34	354	2
Ecoli	7	336	8

Table 2, displays the results of running PPN classifier, prior to integrating it with wrapper-based FGACI module and after integrating it with the model. Datasets are divided to train and test data. In each dataset, 60% of data are used as train data and 40% are used as test data. In Table 2, accuracy columns show classifier accuracy on test data.

GA parameters, i.e. population size, max epoch, crossover rate and mutation rate, are selected through a trial and error approach.

Table 2. PNN classifier accuracy prior to integrating it with wrapper-based FGACI module and after integrating it with the model

Population Size = 50 , Max Epochs Number = 50 , Crossover rate = 0.1 , Mutation rate = 0.1									
	Wrapper Based FGACI Model						PNN Classifier		
Data Set	epoch	F.N.	A.F.L.	A.T.P.	A.F.N.	precision	precision	A.T.P.	A.F.N.
Ionosphere	32	11	31	60	15	%80.13	%74.17	56	19
Wine	31	7	10	26	0	%100	%71.79	18	7
Glass	39	7	10	13	0	%100	%90.42	12	1
Ecoli	43	15	5	15	1	%89.70	%85.29	14	2
Pima	30	3	6	151	33	%79.06	%37.77	69	114

F.N. : Features Number , A.F.L : Average Features Length , A.T.P. : Average True Positive , A.F.N. : Average False Negative

As illustrated in Table 2, in "Wine" and "Glass" data set, classifier accuracy is increased up to 100% and thus AFN, i.e. the average number of samples that are labeled negative incorrectly, is zero.

Number of samples in “Ionosphere” dataset is 354, 60% of this data, i.e. 212 samples, are used for training and 142 samples are used for testing the system. Number of classes in “Ionosphere” dataset is 2.In order to calculate ATP[8], in each class, the number of samples that are predicted positive truly, is accounted and an average over the 2 classes is calculated and introduced as ATP. The calculating procedure of AFN[9] is the same as ATP; the difference is in that for calculating AFN, in each class, then number of samples that are predicted negative falsely is accounted. As it is shown in Table 2, in “Ionosphere” dataset, AFN is decreased from 19 to 15, after integrating PNN with constructive induction module.

Results reveal that classifier accuracy is increased considerably after applying FGACI module.

In table 3, results of applying wrapper-based FGACI on datasets are compared with results of a system, named GAP [13]. As it is noted in Introduction section, in GAP, a GP[10] is used for constructing features and a GA is employed for feature selection.

Table 3. Comparison of Fuzzy-GA wrapper-base CI with GAP

Data set	wrapper-based FGACI	GAP System
Ionosphere	90.06%	89.38%
Wine	100%	94.68%
Glass	98.93%	73.74%
Pima	79.08%	73.50%

[8] Average True Positive.
[9] Average False Negative.
[10] Genetic Programming.

As it is shown in table 3 in most cases Fuzzy-GA wrapper-based CI system represents better solutions. Furthermore, in this system, features complexity is also considered for evaluating but in GAP system only the learning algorithm accuracy is considered to evaluate the features sets.

5 Conclusion

In this paper a Fuzzy-GA wrapper-based model is represented for constructive induction. In this model we employed fuzzy and GA in combination to take advantages of both to conquer the optimization problem of finding the best representation space for learning algorithms. Wrapper-based approaches use the induction algorithm itself to make estimates of the relevance of the given features and therefore we employed the wrapper-based approach to get better results. This model is applied to data sets prior to learning algorithms and improves learning algorithm accuracy by optimizing representation space. In this work, a PNN classifier is selected as learning algorithm and PNN classifier accuracy is evaluated before and after integrating it with represented constructive induction model. Results reveal that classifier accuracy will improved after integrating PNN classifier with Fuzzy-GA wrapper-based constructive induction module.

References

1. Kantardzic, M.: Data Mining: Concepts, Models, Methods, and Algorithms. John Wiley & Sons, Chichester (2003)
2. Zhou, E., Khotanzad, A.: Fuzzy Classifier Design Using Genetic Algorithms. Elsevier, Pattern Recognition 40 (2007)
3. Bloedorn, E.: Multistrategy Constructive Induction. George Mason University in Partial Fulfillment of the Requirements for the Degree of Doctor of Philosophy (1996)
4. Shila, S.L., Pérez, E.: Constructive Induction and Genetic Algorithms for Learning Concepts with Complex Interaction. ACM, New York (2005)
5. Matheus, C., Rendell, L.: Constructive Induction On Decision Tree. University of Illinois at Urbana-Champaign (1989)
6. Hu, Y., Kibler, D.: A Wrapper Approach For Constructive Induction. University of California (1993)
7. Callan, J.: Knowledge-Based Feature Generation for Inductive Learning. University of Massachusetts (1993)
8. Fawcett, T.: Feature Discovery for Inductive Concept Learning. University of Massachussets (1993)
9. Yang, S.: A Scheme for Feature Construction and a Comparison of Empirical Methods. University of Illinois (1991)
10. Rendell, L., Ragavan, H.: Improving the Design of Induction Methods by Analyzing Algorithm Functionality and Data-Based Concept Complexity. University of Illinois (1993)
11. Bloedorn, E., Michalski, R.: The AQ17-DCI System for Data-Driven Constructive Induction and Its Application to the Analysis of World Economic. In: Ninth International Symposium on Methodologies for Intelligent Systems (ISMIS-1996), Zakopane, Poland, June 10–13 (1996)

12. Gang, Q., Garrison, W., Greenwood, D., Liu, C., Sharon, H.: Searching for Multiobjective Preventive MaintenanceSchedules: Combining Preferences with Evolutionary Algorithms. Elsevier, European Journal of Operational Research (2007)
13. Ghosh, A., Jain, L.C.: Evolutionary Computation in Data Mining. Springer, Heidelberg (2005)
14. Thomas, B.B.: Evolutionary Computation in Data Mining. Springer, Heidelberg (2006)
15. Theodoridis, S.: Pattern Recognition, 2nd edn. Elsevier, Amsterdam
16. Fukunaga, K.: Introduction to Statistical Pattern Recognition. Purdue University (2003)
17. Wesley, C., Tsau, Y.L.: Foundations and Advances in Data Mining. Springer, Heidelberg (2005)
18. Yang, Y., Webb, G.I.: A Comparative Study of Discretization Methods for Naive-Bayes Classifiers. In: The 2002 Pacific Rim Knowledge Acquisition Work-shop, Tokyo, Japan (2002)
19. Watanabe, L., Rendell, L.: Learning Structural Decision Trees From Examples. University of Illinois (1991)
20. Cho, H.J., Wang, B.H.: Automatic Rule Generation for Fuzzy Controllers Using Genetic Algorithms: a Study on Representation Scheme and Mutation rate. In: IEEE World Congress on Computational Intelligence Fuzzy Systems (1998)
21. Holland, J.: Adaption in Natural and Artificial. SystemsUniversity of Michigan Press (1975)
22. Whitley, D.: A genetic algorithm tutorial (1994)
23. Guo, Z.X., Wong, W.K., Leung, S.Y.S., Fan, J.T., Chan, S.F.: Genetic Optimization of Order Scheduling with Multiple Uncertainties. Elsevier, Expert Systems with Applications 35 (2008)
24. Chen, S.M., Huang, C.M.: A New Approach to Generate Weighted Fuzzy Rules Using Genetic Algorithms for Estimating Null Values. Elsevier, Expert Systems with Applications 35 (2008)
25. Chen, L.H., Hsiao, H.D.: Feature Selection to Diagnose a Business Crisis by Using a Real GA-based Support Vector Machine: An Eempirical Study. Elsevier, Expert Systems with Applications 35 (2008)
26. Hu, Y., Kibler, D.F.: Generation of Attributes for Learning Algorithms. In: Proc. of the Thirteenth National Conference on Artificial Intelligence, pp. 806–811. AAAI, The MIT Press (1996)
27. Ragavan, H., Rendell, L.A.: Lookahead Feature Construction for Learning Hard Concepts. In: Proc. Of the Tenth International Conference on Machine Learning, June 1993, pp. 252–259. University of Massachusetts, Amherst, MA, USA (1993)
28. Perez, E.: Learning Despite Complex Interaction: An Approach Based on Relational Operators. PhD thesis, university of Illinois, Urbana-Champaign (1997)
29. Specht, D.F.: Probabilistic Neural Networks and the Polynomial Adaline as Complementary Techniques for Classification. IEEE Transactions on Neural Networks 1, 111–121 (1990)
30. Pagallo, G.: Adaptive Decision Tree Algorithms for Learning from Examples. PhD thesis, University of California at Santa Cruz (1990)

Warning List Identification Based on Reliability Knowledge in Warranty Claims Information System

SangHyun Lee[1], ByungSu Jung[2], and KyungIl Moon[1]

[1] Department of Computer Engineering, Honam University, Korea
[2] Department of Computer and Electric Information, Nambu University, Gwangju, Korea
Leesang64@gmail.com, bsjung@nambu.ac.kr, kimoon@honam.ac.kr

Abstract. The purpose of this paper is to propose process, method and knowledge for identifying warning lists objectively based on reliability knowledge in warranty claims information system. This study was designed with literature (process, method, knowledge) and case study. Firstly, process, method and knowledge for identifying were proposed and then applied to an automobile manufacturing firm. An identifying process was used three kinds of reliability knowledge composed of false alarm knowledge of warranty claims, inventory knowledge of products and variation knowledge due to warranty claims factors. Based on the case study of an automobile manufacturing firm, we found that the identification of warning lists using reliability knowledge results in the improvement in the production process of units. The main idea has been applied to a single practical case, an automobile manufacturing firm. For warning list identification of warranty claims, this paper uses three kinds of knowledge from a warranty claims system, which have not been treated before, including false warning possibility, inventory aspects and variation knowledge among warranty claims factors.

Keywords: Warranty claims information system, Reliability knowledge, Warning list identification, VIN list.

1 Introduction

Warranty claims are knowledge obtained by analyzing field data. The field data provides important information used to evaluate reliability, to assess new design and manufacturing changes, to identify causes of failure and to compare designs, vendors, materials, or manufacturing methods. The age-specific analysis of product failure data has engendered considerable interest in the literature. Field data is usually obtained from requests for repair or replacement when failures occur within the warranty period. For example, if an automobile under warranty fails, it is repaired by the original manufacturer, and the manufacturer obtains information such as failure times, causes of failures, manufacturing characteristics of items (e.g., model, place or time of manufacture, etc.), and environmental characteristics during use (e.g., personal characteristics of users, climatic conditions, etc.) (Junga and Bai, 2007).

D.-S. Huang et al. (Eds.): ICIC 2009, LNAI 5755, pp. 450–457, 2009.

Many factors contribute to product failures in the warranty claims. The most important factors are the age (the time in service, etc.) of the product and the effects of the manufacturing characteristics, time of manufacture and the operating seasons or environments. The main problem is knowledge related to age-based warranty claims, which is obtained by analyzing the unanticipated failure modes, a harsher than expected operating environment, an unknown change in raw material properties or supplier quality, an improperly verified design change, etc (Wu and Meeker, 2001). The age-based analysis has several problems in statistically estimating the reliability. In particular, the calculation of the false alarm probability can be unreasonable in aggregated warranty claims analysis.

Majeske (2003) proposes a general mixture model framework for automobile warranty data that includes parameters for product field performance, the manufacturing and assembly process, and the dealer preparation process. Identifying warning lists in a warranty claims system is a sort of warranty planning system that needs reliability knowledge (tolerance error of fraction nonconforming, degree of error variation, deviance of control limit, etc.) and artificial intelligence in the reasoning of system risk. There are many studies in connection with this problem: Data mining modeling in the automotive industry (Hotz et al., 1999); warranty claims process modeling of the automobile (Hipp and Lindner, 1999); software cost model for quantifying the gain and loss associated with warranty claims (Teng and Pham, 2004); software-based reliability modeling (Jeske and Zhang, 2005). These studies are related to forecasts of warranty claims. Sometimes warranty claims may depend on knowledge such as manufacturing conditions or the environment in which the product is used (such as production or operating periods). In regard to this problem, how to detect change points using adjacent distribution of warranty data in terms of identifying sub-units of the product serviceable during the warranty period is a reasonable and useful method (Karim and Suzuki, 2005). In warranty claims analysis using these covariates, inventory knowledge can be extended in the usual way to allow covariate analysis. Inventory knowledge for countable data such as claims is required in forecasting warranty claims.

There are three problems in warning list identification of warranty claims data. The first is to exclude it even if there is a possibility that the warranty claims data may be wrong. The second is to identify the warning list by using only a known quantity of production. Thus, there is not reasonable in practical application. The final is to include variation due to chance of warranty claims variations. In this study, we provide a focus for these problems. The warning list identification of warranty claims is similar to data mining for identifying the reliability knowledge.

2 Reliability-Based Warning List Identification Procedure

Many factors contribute to product failures that result in warranty claims. The most important factors are the age (the time in service) of the product and the effects of the manufacturing characteristics, time of manufacture and the operating seasons or environments. Thus, the age-specific analysis of product failure data has engendered considerable interest in the warranty system development. Specifically, the age-specific analysis is related to reliability knowledge discovery which can be defined as the nontrivial extraction of implicit, unknown, and potentially useful information from the

warranty claims system. The reliability knowledge is very important to early warning/detection of bad design, poor production process, defective parts, poor materials, etc. Thus, this section describes a process of the reliability knowledge discovery in the warranty claims system and represents a reliability-based procedure for warning list identification.

2.1 Reliability Knowledge in Warranty Claims System

The reliability of warranty claims data can be measured by operation group and parts group. Figure 1 represents a process for measuring reliability in each operation group. The applied unit contains unit code, previous models, applicability of previous models and point of application. New units interlock the number of units and that of warranty claims with each other in the previous model to identify data. Unit sales data includes unit number, classification code, model code, model index and point of production and sales. Filtering engine outputs an XML or any other formatted document that contains claim ID, age (in days), usage (in hours), failure mode, downtime (in days), repair cost (adjusted), etc. Application discovery defines some terminology and concepts of group reliability, which are related to life, failure mode, repair and downtime (the time elapsed between the occurrence of failure and the completion of repair). The warranty claims count is very important to group reliability characterization. The warranty claims count by operation typically shows use period, number of warranty claims and total sales amount. The purpose of operation data is to multiply the number of individual operations that comprise the operation group by the number of units sold for the sake of correcting defective percentages. Group reliability characterization includes model codes, operation codes, points of production, and the shape and scale parameter of probability distribution as the reliability function. A standardization of Fraction nonconforming is frequently used in the reliability definition.

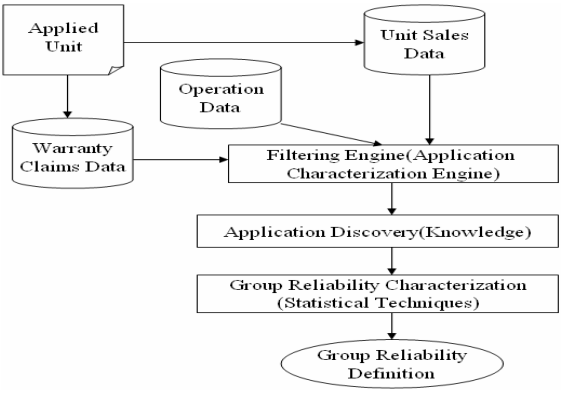

Fig. 1. The process of reliability discovery by the operation group

Figure 1. The reliability discovery by each parts group is similar to figure 1 except that parts group data file is used instead of the operation data. The parts data file includes unit division, parts group, parts code and parts name. Warranty claims count

per parts group includes unit division, model code, model index, group code, use duration and number of warranty claims. As the reliability characterization, a function of time in service and fraction nonconforming is usually used, and it is represented as a Poisson model or a Weibull distribution. In particular, the Weibull distribution is frequently used in the case that the failure rate is increasing according to worn-out. So, the Weibull distribution is most suitable for the warning/detection problem of the warranty claims. To estimate the parameters of the Weibull distribution for each operation group, data must be identified under the assumption of stable quality over a constant past period.

2.2 Reliability-Specific Warranty Claims Identification Process

Figure 2 shows a method for analyzing and predicting warranty claims using the reliability knowledge discovery. In the reliability knowledge discovery, some incorrect facts are regarded as random variables. From this viewpoint, the false warning (alarm) problem of the warranty claims is included in reliability analysis. The second step is to build up a warranty claims table through an appropriate estimation of inventory period. In most cases, the warranty claims table is based on production and marketing level with no regard to inventory period. It makes the deviation between production amount and marketing amount remarkable, and thus leads to the significant error in the reliability sense. The third step is to provide early-warning lists of the warranty claims and to improve the imperfect units. Past warranty repair units are checked, and improvement effects are analyzed. The analysis of improvement effect is equivalent to the reduced operation of fraction nonconforming based on the warranty claims. Here, safety and security units are excluded. The fourth step is to apply variation knowledge due to disturbing factors. Thus, a desirable warning degree of the warranty claims can be determined.

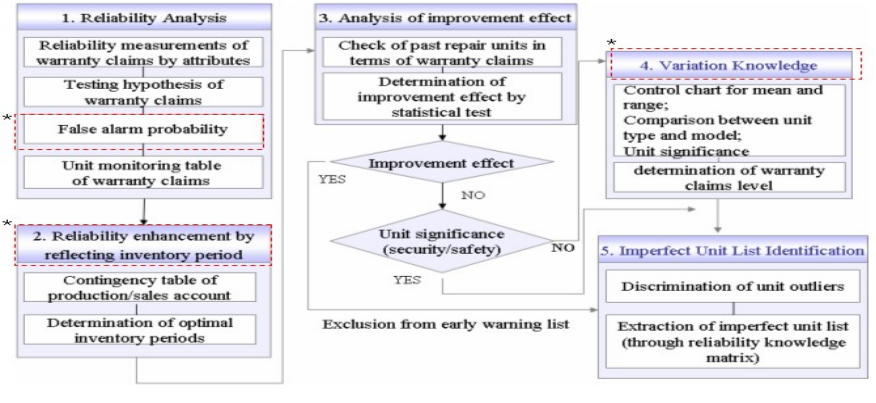

Fig. 2. Reliability-specific procedure for waning list identification

3 Constructing Reliability Knowledge Matrix

A reliability-specific procedure is to objectify the current failure state and to predict any future states. Basically, this procedure requires the modules which regard certain

failure phenomenon as random variable and calculate the failure distribution. Also, a method of sales amount prediction is needed for every warning activity of the warranty claims, and it is usually accomplished by using time series analysis. Here, there are several problems such that a possibility that the warranty claims data may be wrong, to set aside the inventory aspects, not to apply improvement effect and to include variation due to chance of warranty claims variations. In this section, a reliability knowledge matrix is proposed to resolve these problems.

3.1 False Warning Knowledge of Warranty Claims

Suppose that n_i is the unit number produced at period i ; n_{ij} is the unit number produced at period i and sold at period $i+(j-1)$; and R_{ijk} is the number of warning reports at k-th period with regard to certain warranty claims codes under consideration. The warranty claims monitoring is based on the nonconforming fraction of the past warranty claims. It is necessary to allocate a power function that allows us to answer questions about the service life of different. Let R_{ijk} is subject to a Poisson distribution with independent parameter, $n_{ij}\ \lambda_k$. Here, λ_k means the number of units reported during the k -th serviceable period for the certain warranty claims code under consideration. λ_R^0 equivalent to the reference value of λ_k may be obtained on the basis of past reports. The process of detecting lower reliability refers to testing a hypothesis $\lambda_1 \le \lambda_1^0, \lambda_2 \le \lambda_2^0, \cdots, \lambda_M \le \lambda_M^0$. In terms of overall error alarm rate, the increase of M must turn to decrease the power function. Since R_{ijk} is independent of $R_{ijl}(\ l \ne k\ )$, the test for hypothesis $\lambda_1 \le \lambda_1^0, \cdots, \lambda_M \le \lambda_M^0$ may be conducted to form of an individual test. The test for a hypothesis $\lambda_1 \le \lambda_1^0$ (corresponding to a report during the first serviceable period) can come to the conclusion that $\lambda_1 > \lambda_1^0$ at period $i+1$, if $R_{i11} \ge C_{i11}$ for appropriate critical values. During the follow-up period, additional information can be still be accumulated on the basis of this information. In general, if $S_{ij1} \ge C_{ij1}$ at period $i+j$, we can come to the conclusion that $\lambda_1 > \lambda_1^0$. Here, S_{il1} is equivalent to the cumulative frequency of warranty claims reported during the first serviceable period in terms of units manufactured at period i . The probability of type 1 error can be expressed in the following:

$$\alpha_1^* = 1 - p[s_{i11} < c_{i11,} \cdots, s_{iM1} < C_{iM1}]. \tag{1}$$

This is less than or equal to the probability of actual type 1 errors. At j-th period after information is available at service time k , a hypothesis $\lambda_k \le \lambda_k^0$ can be accepted, if $S_{ijk} \ge C_{ijk}$. So, type 1 error can be expressed as the following:

$$\alpha_k^* = 1 - P[\, S_{j1k} < C_{i1k}, \cdots, S_{i,M-K+1,K} < C_{i,M-k+1,k}\ ] \le \alpha_k . \tag{2}$$

Thus, the false warning probability is calculated as follows:

$$\alpha^* = 1 - \prod_{K=1}^{M}(1-\alpha_K^*) \le 1 - \prod_{K=1}^{M}(1-\alpha_K) = \alpha \,. \tag{3}$$

To present this probability concept easily, it can be used a monitoring chart of specific warranty claims codes (see Wu and Meeker, 2001). The monitoring chart shows alarms arising during the first service period from units manufactured at the second production period. As the production period passes by, monitoring goes on, but something terminates. Here, there is an unacceptable problem. It is that $1-\prod\alpha^*$ becomes zero in the sense that when there are a few number of units sold even without any warranty claims. In particular, the poisson probability detection is not desirable. This problem can be solved by applying Z-test method for failure rate in parallel with the Poisson test so as to calculate the optimal interval of production and sales based on inventory point.

3.2 Warning List Identification

Which it requires aggregate information such as point of production, use period and frequency report of warranty claims data. The warning list of warranty claims is obtained as the way of calculating the statistical power function and predicting the fraction nonconforming by using this knowledge. A poisson distribution is usually used to the fraction nonconforming. First, the differences of poisson parameter(λ) are calculated based on previous and current warranty claims. Next, the product of the differences and the statistical significance level is calculated.

The warning list can be obtained as the following rule: IF $\sum C(R_{ijk}) > \alpha^*$

More accurate warning list is to reflect the improvement effect analysis, and to rewrite as the following rule: *IF* (*AV_Ratio*> threshold value) and (average of pre-improvement > average of post-improvement) *then* positive effects=Yes, *else* positive effects=No.

Here, AV_Ratio refers to pure variation of improvement effect in terms of warranty claims variations; it is the ratio of reproducibility variation in warranty claims data. And the threshold value refers to a value offered by users.

4 The Automotive Example

This section discusses the practical cases of applying the warning list identification. The warning list identification is the same as that of VIN(Vehicle Identification Number) list in the case of the automobile company. To extract the VIN list, this study used warranty claims data for report an automobile Company. In particular, warranty claims related to a pad kit – front disk as parts of the front brake system of cars; dating from September 2004 to August 2005. Figure 4 shows warranty claims data loaded from the point of view of production and sales and the serviceable point with regard to pad kit. By estimating parameters of the Weibull distribution, it is found that m = 2.0056, η = 44.6, and the intercept value of least square regression line, t_0 = 2031.98. By using these parametric values, we can get average life cycle = 11 months, the viability in 3 years (t =36) = 47.8% and the time for multiple failures

= 2.6 years. Poisson probability detection is disadvantageous in the sense that when there are a few number of units sold even without any warranty claims, $1-\prod\alpha^{*}$ becomes zero, as discussed in the above Section 3.

Ref. failure rate : λ_0	Use period	Statistics	sep. 04			oct. 04			nov. 04		
0.000793	2months	No. of claims	8			2					
		Z-value	2.45	-1	-1.1	-1.4	-0.7	-0.9	-1.9	-1.1	-1.6
		Z_{Δ}	0.01	0.83	0.87	0.92	0.76	0.8	0.97	0.87	0.95
		$Z_{\beta\Delta}$	0.00518			0.56677			0.80145		
		Poisson %	0.99	0.39	0.29	0.10	0.60	0.48	0.03	0.27	0.07
		P_{Δ}	0.01	0.61	0.71	0.90	0.40	0.52	0.97	0.73	0.93
		$P_{S\Delta}$	0.003915			0.187245			0.654592		
0.000793	1month	No. of claims	1						2		
		Z-value	-0.6	-0.7	-0.8	-1.6	-0.5	-0.6	0.2	-0.8	-1.2
		Z_{Δ}	0.71	0.76	0.78	0.95	0.7	0.73	0.42	0.79	0.88
		$Z_{\beta\Delta}$	0.42354			0.48097			0.29185		
		Poisson %	0.48	0.62	0.54	0.07	0.77	0.69	0.75	0.52	0.26
		P_{Δ}	0.52	0.38	0.46	0.93	0.23	0.31	0.25	0.48	0.74
		$P_{S\Delta}$	0.091682			0.066283			0.090036		
Inventory Period			7Days<	14days<	14days>	7Days<	14days<	14days>	7Days<	14days<	14days>
Production/Sales Account			4353	1186	1547	6656	647	926	4317	1643	3338
			7086			8229			9298		

Fig. 3. Optimal interval of production and sales using inventory knowledge

Use 1 Month	0.064%											
Use 2 Month	0.098%	0.008%										
Use 3 Month	0.107%	0.019%	0.001%									
Use 4 Month	0.089%	0.021%	0.012%	0.000%								
Use 5 Month	0.065%	0.015%	0.010%	0.005%	0.000%							
Use 6 Month	0.055%	0.004%	0.007%	0.003%	0.000%	0.000%						
Use 7 Month	0.030%	0.009%	0.004%	0.003%	0.011%	0.000%	0.002%					
Use 8 Month	0.036%	0.000%	0.002%	0.007%	0.000%	0.000%	0.000%	0.000%				
Use 9 Month	0.032%	0.007%	0.000%	0.004%	0.000%	0.000%	0.000%	0.000%	0.000%			
Use 10 Month	0.088%	0.013%	0.008%	0.000%	0.000%	0.000%	0.000%	0.000%	0.000%	0.000%		
Use 11 Month	0.060%	0.013%	0.000%	0.000%	0.000%	0.000%	0.000%	0.000%	0.000%	0.000%	0.000%	
Use 12 Month	0.014%	0.000%	0.022%	0.000%	0.000%	0.000%	0.000%	0.000%	0.000%	0.000%	0.035%	0.000%
	2004-09	2004-10	2004-11	2004-12	2005-01	2005-02	2005-03	2005-04	2005-05	2005-06	2005-07	2005-08

Fig. 4. Results of improvement effect analysis

To complement this demerit, this study applied the Z-test method for failure rate in parallel with the Poisson test so as to calculate the optimal interval of production and sales based on inventory point in regard to 1- to 2-month period of use, see Figure 5.

Finally, figure 6 shows a VIN list on the reliability knowledge matrix based on the production month and use month. The corresponding warning rule is the following.

$$If\ (\%AV > 30\%)\ \text{and}(\overline{X}_{pre-improvement} > \overline{X}_{post-improvement})\ then$$
$$improvement\ effect = Yes$$
$$else\quad improvement\ effect = No$$

The VIN list shows that all units produced appeared in warning status at a certain point just after 7-months of use, which indicates considerable faults in reliability. Follow-up ongoing process improvement has contributed to a remarkably better quality of units produced since October 2004.

Use 1 Month	Alert											
Use 2 Month	Alert											
Use 3 Month	Alert											
Use 4 Month	Alert											
Use 5 Month	Alert											
Use 6 Month	Alert											
Use 7 Month	Alert											
Use 8 Month												
Use 9 Month												
Use 10 Month	Alert											
Use 11 Month	Alert											
Use 12 Month												
	2004-09	2004-10	2004-11	2004-12	2005-01	2005-02	2005-03	2005-04	2005-05	2005-06	2005-07	2005-08

Fig. 5. VIN list extraction

5 Conclusion

In this paper, we presented a process for identifying the warning lists of the warranty claims based on the reliability knowledge. This knowledge is related to the incorrect warning of the warranty claims. As practical application for identifying the warning list, we represented the VIN list from the warranty claims database in an automobile manufacturing firm. The result showed that the proposed process was better than using the existing identification lists of the warranty claims data.

References

1. Bai, J., Pham, H.: Repair-limit Risk-free Warranty Policies with Imperfect Repair. IEEE Transactions on Systems, Man, and Cybernetics Part A 35(6), 765–772 (2005)
2. Jeske, D.R., Zhang, X.: Some Successful Approaches to Software Reliability Modeling in Industry. Journal of Systems and Software 74(1), 85–99 (2005)
3. Junga, M., Bai, D.S.: Analysis of field data under two-dimensional warranty. Reliability Engineering & System Safety 92, 135–143 (2007)
4. Karim, M.R., Suzuki, K.: Analysis of Warranty Claim Data: A Literature Review. International Journal of Quality & Reliability Management 22(7), 667–686 (2005)
5. Majeske, K.D.: A mixture model for automobile warranty data. Reliability Engineering & System Safety 81(1), 71–77 (2003)
6. So, M.W.C., Sculli, D.: The role of trust, quality, value and risk in conducting e-business. Industrial Management & Data Systems 102(9), 503–512 (2002)
7. Teng, X., Pham, H.: A Software Cost Model for Quantifying the Gain with Considerations of Random Field Environments. IEEE Trans. Computers 53(3), 380–384 (2004)
8. Wu, H., Meeker, W.Q.: Early Detection of Reliability Problems Using Information from Warranty Databases. Technometrics 44(2), 120–133 (2001)

Cluster Analysis and Fuzzy Query in Ship Maintenance and Design

Jianhua Che[1], Qinming He[1], Yinggang Zhao[2], Feng Qian[1], and Qi Chen[1]

[1] College of Computer Science and Technology, Zhejiang University, Hangzhou 310027, China
{chejianhua,hqm,qfeng,chenqi}@zju.edu.cn
[2] College of Computer Science and Technology, Henan Polytechnic University, Jiaozuo 454003, China
ygz129@163.com

Abstract. Cluster analysis and fuzzy query win wide-spread applications in modern intelligent information processing. In allusion to the features of ship maintenance data, a variant of hypergraph-based clustering algorithm, i.e., Correlation Coefficient-based Minimal Spanning Tree(CC-MST), is proposed to analyze the bulky data rooting in ship maintenance process, discovery the unknown rules and help ship maintainers make a decision on various device fault causes. At the same time, revising or renewing an existed design of ship or device maybe necessary to eliminate those device faults. For the sake of offering ship designers some valuable hints, a fuzzy query mechanism is designed to retrieve the useful information from large-scale complicated and reluctant ship technical and testing data. Finally, two experiments based on a real ship device fault statistical dataset validate the flexibility and efficiency of the CC-MST algorithm. A fuzzy query prototype demonstrates the usability of our fuzzy query mechanism.

Keywords: Cluster Analysis; Fuzzy Query; Data Mining; Ship Maintenance and Design.

1 Introduction

Cluster analysis and fuzzy query are always the pivotal arts in data mining and information retrieval. In recent decades, they have received a lot of focus by community researchers. Cluster analysis is often applied in data compression and vector quantization, image processing and pattern recognition, business analysis and bioinformatics mining [13] etc. Clustering, in nature, is a kind of unsupervised classification process, which partitions a given set of patterns(observations, data items, or feature vectors) into disjoint groups(clusters), and makes the proximity between patterns in the same group maximal, the proximity between patterns in different groups minimal [7]. The proximity between patterns may be figured out according to their diversified properties, and distance between patterns is one of the most common measures. However, clustering is also a difficult

D.-S. Huang et al. (Eds.): ICIC 2009, LNAI 5755, pp. 458–467, 2009.

problem for its efficiency and agility in different applications. For example, there are a mass of devices fault statistic data in ship maintenance, which holds the features such as devices type diversity, data scale density and so on. At the same time, ship maintainers often need to examine various clustering results to find out the indeed fault causes. Many traditional clustering algorithms fail to offer an agile and convenient manner for ship maintainers. The appropriate clustering algorithms will be helpful for this peculiar application.

On the other hand, fuzzy query plays an important role in intelligent information processing, especially in intelligent information retrieval [11]. Designed to run in conjunction with plain database management systems(DBMSs), fuzzy query explores the endless possibilities in database and shows the approximate candidates that best meet a given criteria so as to conduct the next level of information analysis. By setting an elastic threshold that relaxes or restricts how deeply into the data that query process probes, fuzzy query can provide information beyond the harsh restrictions of algebra and crisp relational operators. But similar to cluster analysis, fuzzy query currently suffers from two issues: 1) How to compute the similarity degree of database record properties to the criteria record properties; 2) How to compute the similarity degree of database records to the criteria record according to the similarity degree of their homologous properties. Therefore, it's requisite to design a reasonable fuzzy query mechanism for those basilica applications.

This paper presents a variant of hypergraph-based clustering algorithm for ship maintainers to analyze the existed fault data, an unbiased and usable fuzzy query mechanism for ship designers to retrieve the helpful data records. Specifically, the contributions of this paper consist in: 1) we have proposed a hypergraph-based clustering algorithm-Correlation Coefficient-based Minimal Spanning Tree(CC-MST) to group the peculiar ship maintenance data by investigating their features, the CC-MST algorithm owns merits such as intuition, flexibility and efficiency, etc. 2) we have designed an unbiased and serviceable fuzzy query mechanism to find the most similar data records to a given criteria record. This fuzzy query mechanism efficiently resolves two issues, i.e., computing the similarity degree of different properties data such as numeric, character, boolean and the similarity degree of database records to the given criteria record.

The rest of this paper is organized as follows. We begin in Section 2 with related work. Then, we introduce the taxonomy of common cluster algorithms and our proposed Correlation Coefficient-based Minimal Spanning Tree(CC-MST) algorithm in Section 3 and our proposed fuzzy query mechanism in Section 4. In Section 5, we describe the experiment setup and result evaluation. Finally, we conclude with discussion in Section 6.

2 Related Work

Cluster analysis and fuzzy query in common applications have been studied extensively for decades, and lots of clustering algorithms and fuzzy query mechanisms have been brought forward [6,12,10,3,13,5,2]. Tapas Kanungo et al. [6]

gives a detailed introduction to the analysis and implementation of K-MEANS clustering algorithm. Hui Xiong et al. [12] investigates how data distributions can have impact on the performance of K-means clustering, and provides a necessary criterion to validate the clustering results, i.e., the coefficient of variation(CV). Pavan and Pelillo [10] present a new graph-theoretic approach for clustering and segmentation. Inderjit S. Dhillon et al. [3] develops a fast high-quality multilevel algorithm that directly optimizes various weighted graph clustering objectives to achieve the weighted graph cuts without eigenvectors. Rui Xu and Donald Wunsch II [13] survey the scope of cluster analysis, popular clustering algorithms and their applications in some benchmark data sets, and disscuss several tightly related topics like proximity measure and cluster validation. Hoque et al. [5] designs a sample fuzzy database and shows that fuzzy query costs the same time as classical query on classical database, but the less time on the sample fuzzy database. Charalampos Bratsas et al. [2] provide an extension of the ontology-based model to fuzzy logic, as a means to enhance the information retrieval(IR) procedure in semantic management of Medical Computational Problems(MCPs).

As for cluster analysis of ship model design and industry information, Li et al. [8] propose a fuzzy c-mean clustering algorithm to detect ships using fully polarimetric SAR data. Fang et al. [4] explores the application of key data mining technologies in computer aided conceptual design of ship engine room through analyzing the principle and way of ship engine room conceptual design. Benito et al. [1] analyzes the roles of each section in Norway marine industry and their influence on the whole industry with clustering algorithms. Liu and Wu [9] have analyzed the human operational factors in all investigation reporters of shipwreck to find the relation between shipwreck and human misoperations. All of these works are classic and significant. However, they do not involve the devices fault analysis with clustering method in ship maintenance and the ship model design with fuzzy query in ship design. At present, there are little work on cluster analysis in ship maintenance and fuzzy query in ship design.

3 Cluster Analysis in Ship Maintenance

In ship maintenance, there exists amount of statistic data about various device faults. For example, marine pump is an important unit to pump water and oil, and its reliability impacts directly the quality of ship products. Each type of marine pumps may occur various fault phenomena, which arise by some design and fabrication factors, types selection or human operations. When maintaining them, it is hard to properly classify these phenomena and identify the fault causes. Cluster analysis is an efficient resolution to do active precaution, diagnose arisen failure and improve original design.

3.1 Classification of Clustering Algorithms

Multitudinous algorithms have been proposed in the literature for clustering. These algorithms can be divided into seven categories: *hierarchical methods*, *partitional methods*, *grid-based methods*, *constraint-based methods*, *co-occurrence*

categorical data-based methods, *methods used in machine learning*, and *methods for high dimensional data* [13]. Further, hierarchical methods can be classified into *agglomerative algorithms* and *divisive algorithms*, which agglomerative algorithms contain *single-link algorithms*, *complete-link algorithms* and *minimum-variance algorithms*(e.g., BIRCH, CURE, ROCK, CHAMELEON). Partitional method includes also *squared error clustering*(e.g., SNN, PAM, CLARA, CLARANS, X-means), *probabilistic clustering*(e.g., EM), *density-based clustering*(e.g., DBSCAN, DENCLUE, OPTICS, DBCLASD, CURD), *graph-theoretic clustering*, and *mode-seeking clustering*. Grid-based methods includes STNG, STNG+, CLIQUE, Wave-Cluster, etc. Constraint-based methods includes COD and so on. Methods used in machine learning enclose *artificial neural network*(ANN)(e.g., SOM, LVQ) and *evolutionary algorithms*(e.g., SNICC). Methods for high dimensional data include *subspace clustering*(e.g., CACTUS), *projection techniques* and *co-clustering techniques*.

3.2 Correlation Coefficient-Based Minimal Spanning Tree

In all clustering algorithms, hypergraph-based clustering algorithms hold the simple, intuitive and flexible properties [10]. Taking into account the special characteristic of devices fault data in ship maintenance, we propose a variant of hypergraph-based clustering algorithms, i.e., Correlation Coefficient-based Minimal Spanning Tree(CC-MST). The primary philosophy of CC-MST includes two steps: building a minimal spanning tree and partitioning it into clusters. To build the minimal spanning tree, we select randomly an observation and start from it to compute the correlation coefficient between any two observations, and then take each observation as node, the correlation coefficient between two observations as the weight value of their edge to connect all observations. The obtained connected graph is a hypergraph, which has many minimal spanning trees. By comparing the edge weight value sum of all minimal spanning trees, a minimal spanning tree with all nodes and the smallest edge weight value will be used for clustering. After that, one or more connected subgraph can be obtained by partitioning the minimal spanning tree according to a given threshold value $\lambda(\lambda \in [0,1])$, and all observations in a connected subgraph make up of a cluster. To cluster all observations, we firstly need to figure out the proximity degree of all observations.

Definition 1: To assume that domain $U = \{X_1, X_2, ..., X_n\}$ is the set of observations, and element X_i represents an observation. Each observation X_i has m feature indices that can be denoted by a vector: $X_i = (x_{i1}, x_{i2}, ..., x_{im})$, where $i = 1, 2, ..., n$. In CC-MST, we use the correlation coefficient method to compute the proximity degree of two observations as follow:

$$R_{ij} = r(X_i, X_j) = \frac{\sum_{k=1}^{m} |x_{ik} - \overline{x}_i||x_{jk} - \overline{x}_j|}{\sqrt{\sum_{k=1}^{m} (x_{ik} - \overline{x}_i)^2} \sqrt{\sum_{k=1}^{m} (x_{jk} - \overline{x}_j)^2}} \tag{1}$$

where $\overline{x}_i = \frac{1}{m}\sum_{k=1}^{m} x_{ik}$, $\overline{x}_j = \frac{1}{m}\sum_{k=1}^{m} x_{jk}$. If R_{ij} is negative, then adjust the values of all R_{ij} with $\hat{R_{ij}} = \frac{R_{ij}+1}{2}$ to ensure $\hat{R_{ij}} \in [0, 1]$.

Algorithm. Correlation Coefficient-based Minimal Spanning Tree(CC-MST)

Input: $X_i = (x_{i1}, x_{i2}, ..., x_{im})$ and λ; //The feature data sequence of observations and partitioning threshold value

Proc: 1) Compute the proximity $r(X_i, X_j)$ of all observations with equation (11), and build the feature proximity matrix Λ;

2) Take each observation as node, connect all observations according to the value of $r(X_i, X_j)$ in Λ with descending order, mark each $r(X_i, X_j)$ as the weight value of edges and extract the minimal spanning tree with all nodes;

3) Traverse the minimal spanning tree, delete all edges that the weight values are smaller than λ (i.e., $r(X_i, X_j) < \lambda$) and obtain one or more connected subgraphs, which each subgraph means a cluster;

Output: one or more clusters;

From the algorithm, we can find that the clustering results will be different according to different λ values. This presents an opportunity for ship maintainers to make a comparison between multiple categories of clustering results without any additional computation. The λ is often set to 0.5 as default.

4 Fuzzy Query in Ship Design

As is well known, shipbuilding has a long history. Large-scale technical data about various types of ships and devices have been piled up during their design and manufacture. From another perspective, ship designers often want some reference data to improve or renew their original design after determining the fault causes. The massive legacy data will give a lot of help at the moment. For example, when designing a bow, the technical and testing data of shape-alike bows own a high reference value. But, these technical data of ships and devices hold very complicated structure and characteristics, how to get the relevant data for ship designers from a large database? Fuzzy query is an ideal resolution.

In fuzzy query, we call the criteria data record presented by ship designers as criteria object, and the data record existed in the database as query object, which both have the same property(i.e., field in a database) structure. A key difficulty is how to compute the similarity degree between query object and criteria object. In our proposed mechanism, we first compute the similarity degree of each property between query object and criteria object, and then figure out the similarity degree between both with a weighting method. Note that the algorithms to compute the similarity degree between different types of properties data will be

diverse, because the properties field of record objects may be numeric, character or boolean, etc.

4.1 Similarity Computing of Numeric Property Data

For numeric property data, we compute the similarity degree with gray correlation coefficient method. To assume that the criteria object presented by ship designers is $X_0 = (x_0(1), x_0(2), ..., x_0(n))$, and the query object existed in data table is $X_i = (x_i(1), x_i(2), ..., x_i(n))(i = 1, 2, ..., n)$, where $x_i(1), x_i(2), ..., x_i(n)$ are the property fields corresponding to $x_0(1), x_0(2), ..., x_0(n)$, i.e., both have the same numeric property structure. The similarity degree of numeric property data between X_0 and X_i is:

$$s(x_0(k), x_i(k)) = \frac{\min\limits_i \min\limits_k |x_0(k) - x_i(k)| + \varepsilon \max\limits_i \max\limits_k |x_0(k) - x_i(k)|}{|x_0(k) - x_i(k)| + \varepsilon \max\limits_i \max\limits_k |x_0(k) - x_i(k)|}$$

Where ε is the resolution ratio and $\varepsilon = 0.5$ as default. In addition, we can normalize all numeric property data of query object and criteria object by initialization, equalization and reciprocal transformation to ensure the value of $s(x_0(k), x_i(k))$ falling into $[0, 1]$.

4.2 Similarity Computing of Character Property Data

For character property data, we design a compromised algorithm *STRCOMPAR* to compute the similarity degree of character property data. The algorithm deals with two cases:

1. If the character property data in criteria object is the abbreviation or synonym of the one in query object(or vice verse), then the similarity degree of both is set to 1;
2. If the character property data in criteria object is not the abbreviation or synonym of the one in query object(or vice verse), then the similarity degree of both is:

$$r(S_1, S_2) = \frac{STREQUAL(S_1, S_2)}{MAX(S_1, S_2)} \times 100\%$$

Where $STREQUAL(S_1, S_2)$ returns the number of same characters in S_1 and S_2, $MAX(S_1, S_2)$ returns the maximal character number of S_1 and S_2.

4.3 Similarity Computing of Boolean Property Data

Compared with numeric and character property data, the similarity computing of boolean property data is intuitive: if the boolean property data values of query objects are equal to criteria object, then the similarity degree of both is set to 1; otherwise, it is set to 0.

After figuring out the similarity degree of each property data in query objects and criteria object with three above methods, the similarity degree of query objects and criteria object can be computed by superimposing the similarity degree of each property data with allowing for their weight values in the whole record object. Finally, all record data are listed for ship designers according to the descending order of their similarity degrees.

5 Experiments Setup and Evaluation

To validate the agility and efficiency of CC-MST algorithms, we have conducted two experiments based on a real ship device fault statistic dataset. These ship devices fault statistic data originates from the historical records of maintaining various conked ship devices by ship maintainers. As limited by the privacy of these data, we have just taken a part of this dataset and made some undamaged processing. The probability data is shown in Figure 1, where $P1 \sim P4$ represents four type of marine propellers, and $X1 \sim X20$ denotes twenty kind of faults, e.g., the first ten kind of faults (namely $X1 \sim X10$) mean respectively *an over-tightly enclosed swivel*, *a loose collar bearing*, *the break-away of axis traction rod*, *a powerless drawbar pull*, *the unstable rotation of swivel*, *the intermittent rotation of propeller blades*, *the stopping rotation of propeller blades*, *an attrited swivel*, *the abnormally slow gyration of swivel*, and *some slack coping bolts for propeller blades*. For the sake of a clear look, we just show a minimal spanning tree with 10 nodes and edges that the weight value λ is bigger than 0.5 as Figure 2. With our CC-MST algorithm, different granular clusters can be gained by setting different λ values. For example, Figure 3 and Figure 4 show two different clustering results corresponding to two λ values. The result clusters are $\{X1, X3, X8, X9\}$, $\{X2, X5\}$, $\{X4, X6, X7, X10\}$ with $\lambda = 0.7$ and $\{X1, X8, X9\}$, $\{X3\}$, $\{X2, X5\}$, $\{X4, X6\}$, $\{X7, X10\}$ with $\lambda = 0.8$. These results will contribute a lot for ship maintainers to discover the fault causes. Further, the value of λ for an optimized clustering result may be set by ship maintainers with their experimental knowledge, or computed automatically with a machine learning method based on those existed fault diagnosis data. In the second experiment, we have compared the clustering speed of CC-MST against the classic K-MEANS algorithm based on different size parts of the whole dataset as Figure 5. The CPU times for each data size demonstrate that CC-MST is faster than K-MEANS, especially when the dataset is getting bigger.

In addition, we have implemented our fuzzy query mechanism based on a practical database of ship model technic and performance data, which derives from the practice process of designing and testing numerous ship models. By carrying through many times of fuzzy queries for different criteria objects, we compute the real distance between the obtained fuzzy query objects and the criteria object by hand and compare the real distance with the similarity degree computed by fuzzy query engine. The consistency of both proves the availability of our fuzzy mechanism.

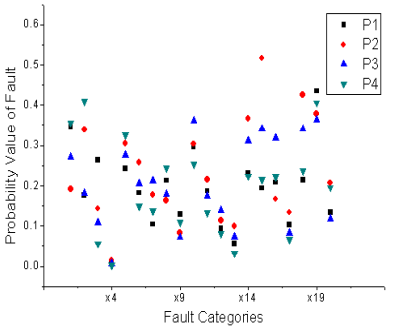

Fig. 1. The fault probability data of four ship bows

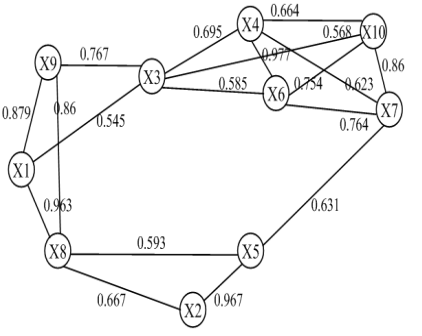

Fig. 2. The MST with only 10 nodes and $\lambda = 0.5$

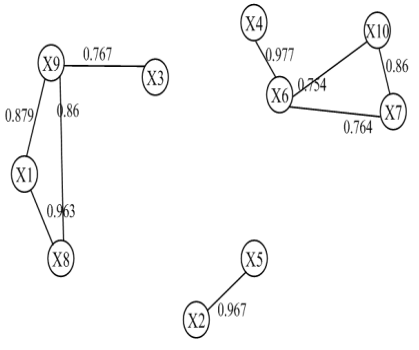

Fig. 3. The clustering result of CC-MST with $\lambda = 0.7$

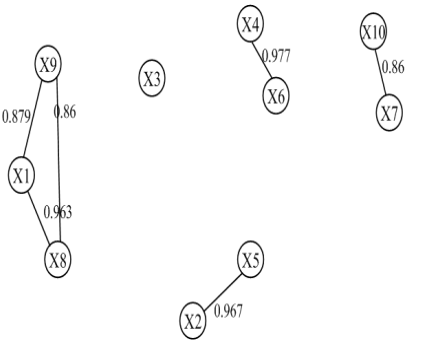

Fig. 4. The clustering result of CC-MST with $\lambda = 0.8$

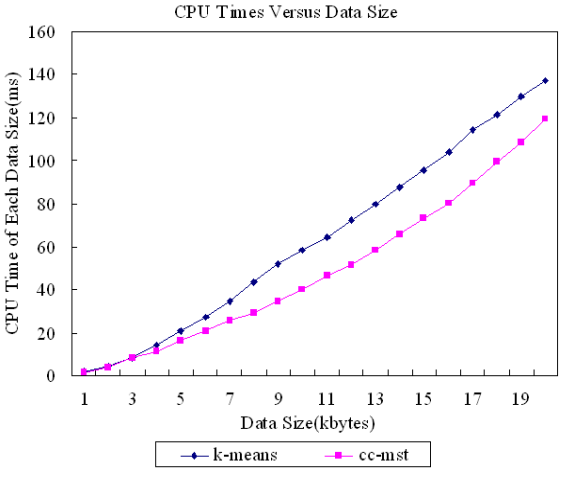

Fig. 5. Running time versus data size of CC-MST and K-MEANS

6 Conclusion and Future Work

The existed clustering algorithms are competent for most applications, but not agile enough for some special field such as ship maintenance data analysis. This paper proposed a hypergraph-based clustering algorithm namely Correlation Coefficient based-Minimal Spanning Tree(CC-MST) to diagnose the causes of ship device faults based on the detailed analysis of ship maintenance data features. The algorithm holds the intuitive, flexible and efficient properties. Two experiments on a real ship maintenance dataset indicates the agility and efficiency of the CC-MST algorithm. In addition, we also design a fuzzy query mechanism to retrieve the most proximate ship technical and testing data records for ship designers to assist their design. Its unbiasedness and usability are verified by matching two kind of similarity degrees computed by hand and fuzzy query engine. In the future, we will go further into computing the weight value of each property in fuzzy query with machine learning methods.

References

1. Benito, G.R.G., Berger, E., Shum, J.: A Cluster Analysis of the Maritime Sector in Norway. International Journal of Transport Management, 203–215 (2003)
2. Bratsas, C., Koutkias, V., Kaimakamis, E., Bamidis, P., Maglaveras, N.: Ontology-Based Vector Space Model and Fuzzy Query Expansion to Retrieve Knowledge on Medical Computational Problem Solutions. In: IEEE of the 29th Annual International Conference on Engineering in Medicine and Biology Society, pp. 3794–3797 (2007)
3. Dhillon, I.S., Guan, Y., Kulis, B.: Weighted Graph Cuts without Eigenvectors a Multilevel Approach. IEEE Transactions on Pattern Analysis and Machine Intelligence, 1944–1957 (2007)
4. Fang, X.F., Wu, H.T.: Application of Data Mining Technology to Concept Design of Ship Engine Room. Shipping Engineering, 28–30 (2003)
5. Hoque, A.H.M., Sajedul, M.S., Aktaruzzaman, M., Mondol, S.K., Islam, B.: Performance Comparison of Fuzzy Queries on Fuzzy Database and Classical Database. In: International Conference on Electrical and Computer Engineering, ICECE 2008, pp. 654–658 (2008)
6. Kanungo, T., Mount, D.M., Netanyahu, N.S., Piatko, C.D., Silverman, R., Wu, A.Y., Center, A.R., San Jose, C.A.: An Efficient K-means Clustering Algorithm: Analysis and Implementation. IEEE Transactions on Pattern Analysis and Machine Intelligence, 881–892 (2002)
7. Kotsiantis, S.B., Pintelas, P.E.: Recent Advances in Clustering: A Brief Survey. WSEAS Transactions on Information Science and Applications, 73–81 (2004)
8. Li, H., He, Y., Shen, H.: Ship Detection with the Fuzzy C-mean Clustering Algorithm Using Fully Polarimetric SAR. In: IEEE International Geoscience and Remote Sensing Symposium, pp. 1151–1154 (2007)
9. Liu, Z.J., Wu, Z.L.: Data Mining to Human Factors Based on Ship Collision Accident Survey Reports. Navigation of China, 1–6 (2004)
10. Pavan, M., Pelillo, M.: A New Graph-Theoretic Approach to Clustering and Segmentation. IEEE Computer Society Conference on Computer Vision and Pattern Recognition (2003)

11. Ribeiro, R.A., Moreira, A.M.: Fuzzy Query Interface for a Business Database. International Journal of Human-Computer Studies, 363–391 (2003)
12. Xiong, H., Wu, J., Chen, J.: K-means Clustering versus Validation Measures: A Data Distribution Perspective. In: Proceedings of the 12th ACM SIGKDD international conference on Knowledge discovery and data mining, pp. 779–784 (2006)
13. Xu, R., Wunsch II, D.: Survey of Clustering Algorithms. IEEE Transactions on Neural Networks, 645–678 (2005)

A Semantic Lexicon-Based Approach for Sense Disambiguation and Its WWW Application

Vincenzo Di Lecce[1,*], Marco Calabrese[1], and Domenico Soldo[2]

[1] Polytechnic of Bari, II Faculty of Engineering – DIASS, Taranto, 74100, Italy
[2] myHermes S.r.l., Taranto, 74100, Italy
{v.dilecce,m.calabrese}@aeflab.net,
domenico.soldo@myhermessrl.com

Abstract. This work proposes a basic framework for resolving sense disambiguation through the use of Semantic Lexicon, a machine readable dictionary managing both word senses and lexico-semantic relations. More specifically, polysemous ambiguity characterizing Web documents is discussed. The adopted Semantic Lexicon is WordNet, a lexical knowledge-base of English words widely adopted in many research studies referring to knowledge discovery. The proposed approach extends recent works on knowledge discovery by focusing on the sense disambiguation aspect. By exploiting the structure of WordNet database, lexico-semantic features are used to resolve the inherent sense ambiguity of written text with particular reference to HTML resources. The obtained results may be extended to generic hypertextual repositories as well. Experiments show that polysemy reduction can be used to hint about the meaning of specific senses in given contexts.

Keywords: semantic lexicon, sense disambiguation, WordNet; polysemy, Web Mining.

1 Introduction

Since its origin, the World Wide Web (hereinafter WWW or simply the Web) has quickly increased in number of available resources. Most of current search engines however seem not to keep the pace with this evolution due to low-semantics information retrieval approaches they implement. Everyone has experience of it when, in the search for a Web resource, he/she specifies an ambiguous (polysemous or general purpose) query word. The access to high-quality information on the Web may be thus problematic for unskilled users.

Several approaches have been proposed in the literature with the purpose of semantically organizing Web knowledge from Web resources. In many cases they require the human experience to control a part (i.e. semi-supervised techniques) of knowledge process or the whole (i.e. supervised techniques) of it. Research on the Semantic Web still remains far from the Tim Berners Lee's vision [1] appearing achievable only in

* Corresponding author.

D.-S. Huang et al. (Eds.): ICIC 2009, LNAI 5755, pp. 468–477, 2009.

the long run. In the short term instead Web ontology representation in restricted domains can be a better target to follow.

Web ontologies have to deal with a large range of questions spanning from language inherent ambiguity to context dependency, presence of incoherent statements, difficulty in ontology matching and so on. Nevertheless, it seems that these issues comprise both the semantic (concept) level and the lexical (language) level. This observation hints the need of tackling with both conceptual and linguistic aspects when engineering knowledge. Currently, a good mean between the two approaches seems to be represented by the new emerging golden standard-based ontologies [2][3] represented by a particular type of enhanced thesaurus called Semantic Lexicon (SL for short). SL proves to be highly feasible and reliable thanks to the recent progress in developing broad-coverage dictionaries like WordNet [4]. WordNet is a broadly used tool for Natural Language Processing (NLP) that, as it will be shown further in the text, is particularly suited for Word Sense Disambiguation (WSD) task. WSD is an ontology-based technique that consists in assigning the correct semantic interpretation to ambiguous words in a given context.

This work proposes a model for resolving sense disambiguation using WordNet taxonomy. In particular the adopted knowledge-based system refers to the IS-A hierarchy, i.e. hyponymy/hypernymy semantic relation. The model is based on the taxonomical and ontological layers of the SL. The information retrieval system uses a recently published procedure to extract relevant information from website documents. It was introduced in other authors' works [5][6][7], highlighting the innovation of the proposed system ensured by the good quality of the experiment results.

The outline of this paper is as follows: Section 2 sketches some well-known methods particularly used to disambiguate word senses in text; Section 3 introduces some theoretical aspects of word sense ambiguity; Section 4 presents the proposed WSD framework; Section 5 shows experiments; Section 6 reports the conclusions.

2 Related Work

It is noteworthy in the literature that the supervised learning from examples is a valid approach in WSD. It consists of statistical or Machine Learning classification models induced from semantically annotated corpora [8].

In [9] a system that uses a statistical language model to evaluate the potential substitutions in a given context is presented. Through this model the likelihoods of the various substitutes are used to select the best sense for the analyzed word. Always studying the statistical substitution model for WSD some authors [10][11] evaluated the use of related monosemous words, resulting in extensive labelled examples for the semi-supervised techniques. Instead an unsupervised system has been proposed in [12], evaluating the relevance of the sense gathered by the substitution model for the analyzed word by means of the query responses of a search engine. Moreover they have extended the statistical model to its uses for polysemy ambiguity.

In [13] another WSD method used to disambiguate polysemous word for a given context by means of dictionary definitions is presented. This technique consists in counting the number of common words between the "context bag" (i.e. the set of words presented in the definitions of other context words) and each "sense bag"

(i.e. the set of words presented in the definition of a single sense) for a specific word. The sense gaining the maximum common words is considered as the "winner" sense.

In [14] Sussna's WSD method is based on the use of a semantic distance between topics in WordNet. In [15] a WSD method grounded on the idea of conceptual density in WordNet is proposed. In text representation domain authors in [16] propose a technique based on the representation in terms of the synsets through the IS-A relations of the tokenized words from text. Scott's model presents a pre-filtering module aiming at the sense disambiguation. In [17] a noun disambiguation method also using IS-A relations was presented. The method evaluates the semantic similarity between two words and gives back the most informative common subsumer from hypermym hierarchy of both words. A similar method was presented in [18][19]. They proposed a measure of the semantic similarity by calculating the length of the path between the two nodes in the hierarchy. Some of the above systems were evaluated in a real-word spelling correction system in [20].

3 Managing Word Sense Ambiguity

In a dictionary any lexical element refers to one or more senses and typically for each sense some examples are reported. The word "sense" is generally defined as the meaning of a word or phrase in a specific context. This implies that, a word can be used with different senses depending on the context in which it is used (giving the polysemous ambiguity) or different words can be used with the same sense (driving to the synonymous ambiguity). A human user of a dictionary is generally able to find the correct word form in a context only by means of information gathered from a thesaurus: this task appears instead challenging for a machine.

WordNet provides the following definitions for the two types of before mentioned ambiguities:

- *Polysemy*: the ambiguity of an individual word or phrase that can be used (in different contexts) to express two or more different meanings;
- *Synonymy*: the semantic relation between two words that can (in a given context) express the same meaning.

Starting by these definitions, it is clear that the meaning of a word is tightly related to the meanings of the surrounding elements, which in turn may be ambiguous. It is interesting enough referring to [21] underlining that the meaning is highlighted by means of mutual sense reinforcement of possibly ambiguous words. Then, for the sense definition the concept of *context* is of paramount importance. This is what WordNet reports for "context":

- *Sense #1*: discourse that surrounds a language unit and helps to determine its interpretation;
- *Sense #2*: the set of facts or circumstances that surround a situation or event.

3.1 Lexico-Semantic Synthesis: Sense Matrix

In the aim of formalizing the concept of sense two distinct entities can be identified. The first one is the lexical element (i.e. lexicon) and the second one is the semantic

element (i.e. concept). According to WordNet 3.0 data model, the sense is the relation existing between a lexical entity and a concept. The concept is derived by the semantic relations. Then, the sense collection can be represented by a matrix whose rows and columns are lexical set and semantic set respectively. This matrix is known in the literature [22][23] as *lexical* matrix. Referring to the sense concept we prefer to call it *sense* matrix. Table 1 depicts an example of a sense matrix. The sense matrix element can be expressed as a binary relation between a word form and a concept.

Table 1. Example sense matrix. Senses are defined as matches between lexical entities (rows) and concepts (columns).

Sense Matrix		**Concepts**			
		c1	*c2*	*c3*	*c4*
Lexicon	*l1*	0	1	0	1
	l2	0	0	0	1
	l3	1	1	0	0
	l4	1	0	1	1
	l5	0	0	1	0

3.2 Semantic Relations: Core Ontology

The semantic relation between concepts has been represented in the literature through a particular type of direct acyclic graph (DAG) known as single-rooted tree. In [24] the authors use this DAG to define Core Ontology and formalize the concept of taxonomy. The structure CO := (C, c_{root}, $\leq_C$) is called core ontology. C is a set of conceptual entities and $c_{root} \in C$ is a designated root concept for the partial order, $\leq_C$ on C. This partial order is called concept hierarchy or taxonomy. The relation $\forall c \in C: c \leq_C c_{root}$ holds for this concept hierarchy. Hence, Core Ontology refers to the semantic level, while it lacks any mention to lexical entities.

3.3 Semantic Lexicon and Lexico-Semantic Features

Sense matrix and Core Ontology are widely used in knowledge-based systems. In addition, the SL is the third relevant concept in this application domain. SL can be simply defined as the join between the lexical and concept sets (the sense matrix) on the one hand and the set of recursive relations on concept set on the other hand. Lexical recursive relations may be considered as well but, for the sake of simplicity, they are not considered in the proposed model.

In a previous work [7] the concept of Web minutia was defined as a sub-graph extracted from the above mentioned SL. Minutiae are actually lexico-semantic features (relevant senses) for the explored Web site and represent an effective way to deal with WSD in Web documents.

4 Proposed WSD Model

The authors have chosen WordNet 3.0. as SL. WordNet is one of the most adopted golden standard-based ontologies in knowledge-based systems. Furthermore, it is a

broad-coverage dictionary purposely engineered for text mining and information extraction.

WordNet is based on the concept of synset; in version 3.0, its data model is developed around the concept of sense, i.e. the one-to-one relation between the synset and the lexical entity. In WordNet data model (part of which is depicted in Figure 1) one group of tables ('word', 'sense' and 'synset') is related to lexico-semantic meaning and another one ('lexlinkref', 'semlinkref' and 'linkdef') is related to lexico-semantic relations. The underpinning knowledge structure is then represented by context-dependent lexico-semantic chains organized according to given hierarchies (e.g. hypernymy). In this work only semantic relations are adopted to disambiguate word forms retrieved by a semantic feature extractor. The other elements provided by the WordNet data model have not been considered and will be examined in future research: Fragos et al. for example use WordNet relations to disambiguate tokenized text by means of the WordNet glosses.

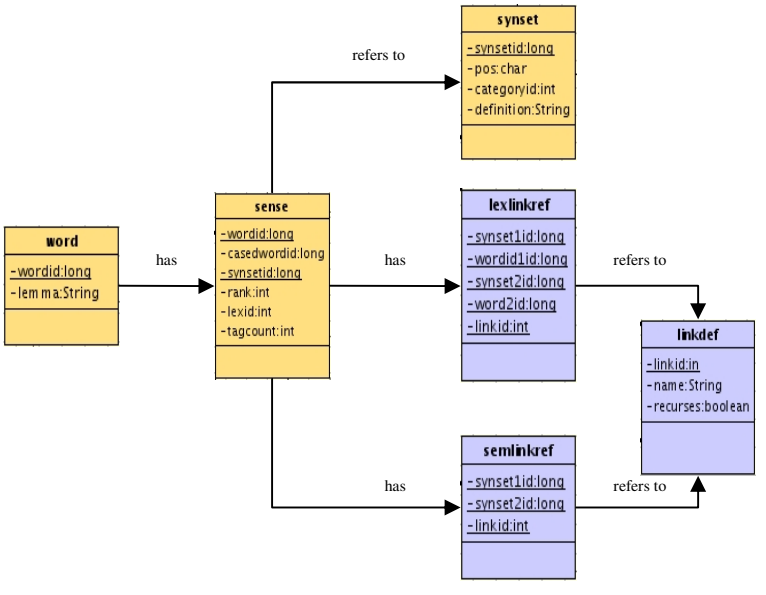

Fig. 1. An extract of WordNet data model

4.1 WSD Abstract Architecture

Figure 2 shows the proposed architecture. Two main blocks can be identified:

1. Lexical entity extraction: it is composed of a crawling/parsing system to retrieve texts from website.
2. Sense disambiguation: it carries out the WSD task. The lexical entity array is the input buffer for the feature extraction process.

First some considerations are necessary to understand the WSD process. A synchronous switch pairs controlled by the semantic feature extractor (SFE for short) drive data flow to/from the sense matrix.

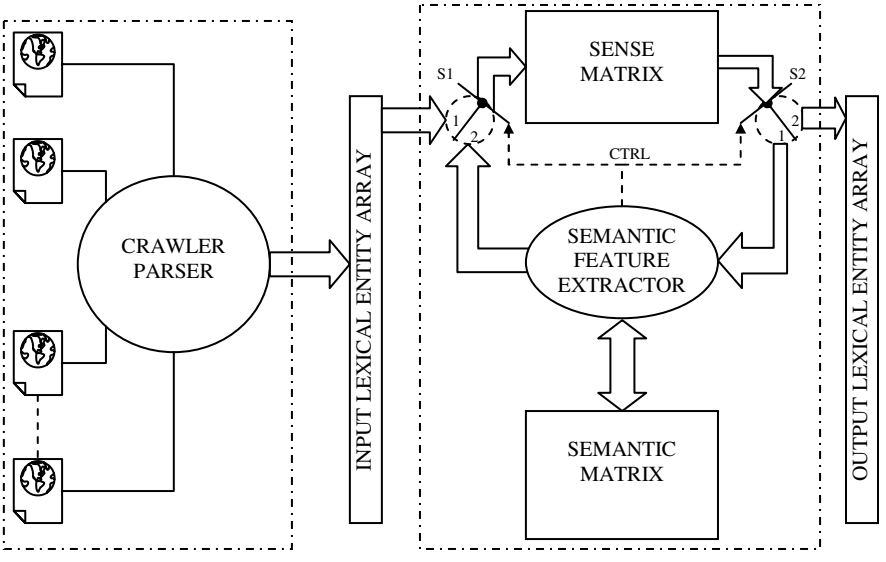

Fig. 2. Proposed WSD abstract architecture. It can be divided into a lexical entity extraction module (left side) and a sense disambiguation module (right side). The sense disambiguation module takes lexical entities parsed from Web sites as input and returns disambiguated lexical entities in a given context. The sense disambiguation is resolved by the two-step interaction between the SFE and the Sense Matrix.

Lexical entries deriving from the parsing phase act as triggers for the WSD system. These inputs (rows in the sense matrix) intercept concepts (columns in the sense matrix) when there is a match between lexical entity and concept (corresponding to a unit value in the example matrix shown in Table 1). When the match occurs, the retrieved concepts are used as inputs for the SFE. SFE iterates on recursive semantic relations (i.e. hypernymy) until it finds stop conditions depending on the implemented procedures. Web minutiae are an example of such procedures [7]. This process ends with a set of newly found concepts, which are fed back to the sense matrix (e.g. column entries) in order to intercept new lexical entries. All the matches found during these steps produce a *subset* of the original sense matrix. This subset can be statistically analyzed to infer on polysemy by simply assessing the number of retrieved senses (reduced core ontology) for each retrieved lexical entity (reduced vocabulary). It is interesting to note that the proposed architecture is very scalable since it adopts WordNet semantic-lexicon taxonomies as the indexing structure. This structure of course does not increase as the amount of indexed documents increases.

According to the proposed model, WordNet can be decomposed into the blocks depicted in Figure 3. It is plain that the “sense table” and the “synset relation table” refer exactly to the corresponding tables in WordNet E-R model (named ‘sense’ and ‘semlinkref’ in WordNet 3.0).

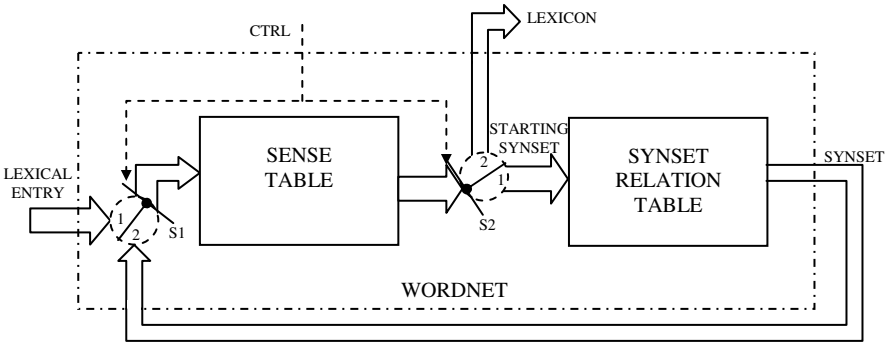

Fig. 3. SL instance using WordNet

5 Experiments and Results

Several websites have been crawled to test the proposed model. We have purposely pre-clustered these sites in four distinct semantic contexts reported in Table 2.

Table 2. Semantic contexts and number of inspected websites for each one

Semantic Context	# inspected websites
University	17
Airport	13
Low-cost Airline	10
Seaport	8

The crawling and parsing processes have been limited to the analysis of the first one hundred crawled webpages for each website. The authors consider this limit enough to demonstrate the ability of the presented model. The semantic matrix depicted in Figure 2 represents the IS-A relations (i.e. hypernym/hyponym hierarchy). The maximum number of iterations on the semantic matrix has been fixed to 5 for reasons of two orders:

1. higher depth level in taxonomy returns context-independent concepts;
2. computational effort may increase considerably as depth level increases.

As mentioned in Section 4 the input for the proposed disambiguation system is the set of lexical entity extracted from webpages; while the output is the set of disambiguated input lexical entities. Thus given a word form having different senses in WordNet the system returns the same word possibly with a reduced number of senses. This reduction is more evident when a word form is strongly context-dependent. Figure 4 depicts a part of the results that have been carried out about Web minutiae extracted by the "university" context. It is clearly visible that increasing the number of iterations in the WordNet taxonomy the system shows lower WSD performances. This consideration can be deduced by analyzing the hypernym hierarchy, which has been used at the

base of the Web minutiae feature extraction process. In fact, crossing the IS-A hierarchy in hypernymy direction represents a shift towards generalized synsets (the maximum abstraction for any lexical entity is considered in WordNet with the "entity" synset).

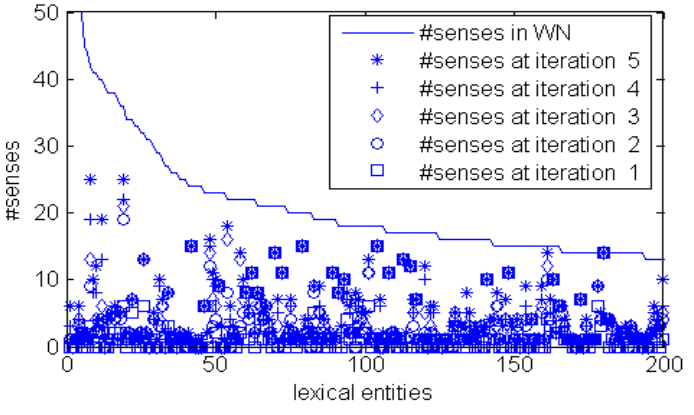

Fig. 4. Plot over first 200 most polysemous lexical entities in the 'university' benchmark. Icons account for different number of iterations used in minutiae feature extraction process

Table 3 reports the average ratio obtained dividing, for any lexical entity, the number of senses retrieved by the proposed WSD system with the number of all senses of that lexical entity in WordNet. Results are grouped according to the chosen contexts and number of iterations on the synset relation table. It highlights the relevant performance of the proposed system with one iteration and for two contexts even with two iterations. In these cases, the disambiguated senses result to be on average as about the 85% of their whole.

Table 3. Polysemy ratios experiment results

#iteration	University	Airport	Low-cost Airline	Seaport
1	0,18	0,23	0,10	0,13
2	0,30	0,34	0,17	0,18
3	0,35	0,36	0,27	0,28
4	0,41	0,38	0,37	0,38
5	0,48	0,41	0,47	0,45

6 Conclusions

A basic framework for resolving WSD (polysemy in particular) through the exploitation of a Semantic Lexicon has been presented as an extension of a semantic approach firstly

presented in [6]. The here proposed WSD framework enables sense disambiguation without human intervention.

The authors used the WordNet 3.0 dictionary as Semantic Lexicon. The model is suitable for any kind of hypertextual dataset. In this work the system has been tested on different contexts datasets. The system is highly modular and suitable for distributed knowledge extraction because it relies on a well-studied layered architecture. The system can be adapted for using some other relations or modules of WordNet, thus obtaining a possible increase of its performance.

Furthermore, the proposed model is sufficiently robust to be extended to other languages than English, without affecting the system generality. In this sense, the studies on multi-lingual dictionaries employing the WordNet structure are being currently carried out by some authors [25, 26].

As future works, further experiments will be conducted on a more extensive set of different contexts in order to better define dependency between Web minutiae and context lexical descriptors.

References

1. Berners-Lee, T., Hendler, J., Lassila, O.: The Semantic Web. Scientific American (2001)
2. Zavitsanos, E., Paliouras, G., Vouros, G.A.: A Distributional Approach to Evaluating Ontology Learning Methods Using a Gold Standard. In: Proc. of 3rd Workshop on Ontology Learning and Population (OLP3) at ECAI 2008, Patras, Greece (2008)
3. Farrar, S., Langendoen, D.T.: A Linguistic Ontology for the Semantic Web. GLOT International 7(3), 97–100 (2003)
4. Fellbaum, C.: WordNet: An Electronic Lexical Database. MIT Press, Cambridge (1998)
5. Di Lecce, V., Calabrese, M., Soldo, D.: Mining context-specific web knowledge: An experimental dictionary-based approach. In: Huang, D.-S., Wunsch II, D.C., Levine, D.S., Jo, K.-H. (eds.) ICIC 2008. LNCS (LNAI), vol. 5227, pp. 896–905. Springer, Heidelberg (2008)
6. Di Lecce, V., Calabrese, M., Soldo, D.: Fingerprinting Lexical Contexts over the Web. Journal of Universal Computer Science 15(4), 805–825 (2009)
7. Di Lecce, V., Calabrese, M., Soldo, D.: Semantic Lexicon-Based Multi-agent System for Web Resources Markup. In: The Fourth International Conference on Internet and Web Applications and Services (ICIW 2009), Mestre, Italy, pp. 143–148 (2009)
8. Màrquez, L., Escudero, G., Martínez, D., Rigau, G.: Supervised Corpus-Based Methods for Wsd. In: Agirre, E., Edmonds, P. (eds.) Word Sense Disambiguation: Algorithms and Applications. Text, Speech and Language Technology, vol. 33, Springer, Heidelberg (2007)
9. Yuret, D.: KU: Word Sense Disambiguation by Substitution. In: Proc. of the 4th International Workshop on Semantic Evaluations (SemEval 2007), Prague, Czech Republic, pp. 207–214 (2007)
10. Mihalcea, R.: Bootstrapping Large Sense Tagged Corpora. In: Proc. of the 3rd International Conference on Languages Resources and Evaluations (LREC 2002), Las Palmas, Spain, pp. 1407–1411 (2002)
11. Leacock, C., Chodorow, M., Miller, G.: Using Corpus Statistics and WordNet Relations for Sense Identification. Computational Linguistics 24(1), 147–165 (1998)

12. Martinez, D., Agirre, E., Wang, X.: Word Relatives in Context for Word Sense Disambiguation. In: Proc. of the 2006 Australasian Language Technology Workshop (ALTW 2006), Sydney, Australia, pp. 42–50 (2006)
13. Lesk, M.: Automatic Sense Disambiguation Using Machine Readable Dictionaries: How to Tell a Pine Cone from an Ice Cream Cone. In: Proc. of the of the 5th Annual International Conference on Systems Documentation (SIGDOC 1986), New York, USA, pp. 24–26 (1986)
14. Sussna, M.: Word Sense Disambiguation for Free-Test Indexing Using a Massive Semantic Network. In: Proc. of the 2nd International Conference on Information and Knowledge Management (CIKM 1993), Arlington, Virginia, USA, pp. 67–74 (1993)
15. Agirre, E., Rigau, G.: Word Sense Disambiguation Using Conceptual Density. In: Proc. of the 16th International Conference on Computational Linguistics (COLING 1996), Copenhagen, Denmark, vol. 1, pp. 16–22 (1996)
16. Scott, S., Matwin, S.: Text Classification Using the WordNet Hypernyms. In: Proc. of the Workshop on Usage of the WordNet in Natural Language Processing Systems (COLING-ACL 1998), Montreal, Canada, pp. 45–52 (1998)
17. Resnik, P.: Using Information Content to Evaluate Semantic Similarity in a Taxonomy. In: Proc. of the 14th International Joint Conference on Artificial Intelligence (IJCAI 1995), Montreal, Canada, pp. 448–453 (1995)
18. Lee, J., Kim, H., Lee, Y.: Information Retrieval Based on Conceptual Distance in IS-A Hierarchies. Journal of Documentation 49(2), 188–207 (1993)
19. Leacock, C., Chodorow, M.: Combining Local Context and WordNet5 Similarity for Word Sense Disambiguation. In: [6]
20. Budanitsky, A., Hirst, G.: Semantic Distance in WordNet: An Experimental, Application-Oriented Evaluation of Five Measures. In: Proc. of the Workshop on WordNet and Other Lexical Resources, Second Meeting of the North American Chapter of the Association for Computational Linguistics (NAACL 2001), Pittsburgh, PA, USA, pp. 29–34 (2001)
21. Ramakrishnanan, G., Bhattacharyya, P.: Text Representation with WordNet Synsets Using Soft Sense Disambiguation. In: Proc. of the 8th International Conference on Application of Natural Language to Information Systems (NLDB 2003), Burg, Germany, pp. 214–227 (2003)
22. Ruimy, N., Bouillon, P., Cartoni, B.: Inferring a Semantically Annotated Generative French Lexicon from an Italian Lexical Resource. In: Proc. of the Third International Workshop on Generative Approaches to the Lexicon, Geneva, Switzerland, pp. 27–35 (2005)
23. Magnini, B., Strapparava, C., Ciravegna, F., Pianta, E.: A Project for the Construction of an Italian Lexical Knowledge Base in the Framework of WordNet. IRST Technical Report #9406-15 (1994)
24. Dellschaft, K., Staab, S.: On how to perform a gold standard based evaluation of ontology learning. In: Cruz, I., Decker, S., Allemang, D., Preist, C., Schwabe, D., Mika, P., Uschold, M., Aroyo, L.M. (eds.) ISWC 2006. LNCS, vol. 4273, pp. 228–241. Springer, Heidelberg (2006)
25. Ramanand, J., Ure, A., Singh, B.K., Bhattacharyya, P.: Mapping and Structural Analysis of Multilingual Wordnets. IEEE Data Engineering Bulletin 30(1) (2007)
26. Ordan, N., Wintner, S.: Representing Natural Gender in Multilingual Lexical Databases. International Journal of Lexicography 18(3), 357–370 (2005)

The Establishment of Verb Logic and Its Application in Universal Emergency Response Information System Design

Jian Tan and XiangTao Fan

Laboratory of Digital Earth Sciences, Center for Earth Observation and Digital Earth, Chinese Academy of Sciences, Beijing, 100101, China
Tanjian1998@gmail.com

Abstracts. It is always a challenge to build up a stable and high-level integrated system capable of different types of emergencies. The biggest obstacle is how to build a universal work flow mode for the different events. To solve the problem, our research adopts an unusual way based on the self-evident truth that full text description of phenomena is a whole map of it. Then the system analysis' subject can be altered from the real emergency response to the text description of it. Therefore semantic annotation which uses the semantic labels in propbank can be employed in the analysis process. The annotation subjects are the documents that each of them described a full emergency response process of different emergency type. After classification and statistic, three linguistic rules are found out. First, every sentence have a predicate verb which indicate an executable action and it belongs to a fixed set, second, each verb coexists with semantic role Arg0(actor), third, all the complement roles of predicate verbs converge into a fixed subset of semantic roles ,these conclusions are named together as verb logic. It is a high abstract semantic model, for it not only contains domains but also tell the relations among domains. Based on verb logic, universal work flow mode is constructed, and a universal emergency response system can be built up. The design of the system is also stated in this paper.

Keywords: Universal emergency response system, Verb logic, Semantic annotation, Propbank.

1 Introduction

Emergency system involved researches are booming since the 9.11 attack which is a reminder to the necessity of efficient integrated emergency response. Most of the researches of computer aided emergency response derived from the former expert decision systems, which focused on decision models extraction from domain ontology and knowledge. The others contribute to the technology of system construction in special event type. But these solutions are not integrated in a universal framework yet, because the business logics differ in different types of emergency, and the relations between these emergency response systems are not stable, if the business logic changed in one of the collaborated systems, the integration would be broken.

D.-S. Huang et al. (Eds.): ICIC 2009, LNAI 5755, pp. 478–491, 2009.

So the basic challenge is the construction of a universal emergency response work flow mode.

In the practice to build a first emergency response system which must integrate with other emergency systems for national security department of china, we have to consider the compatibility in prior in the system design.

Originally, the first step of software design in OO programming era is extracting the object from concrete business process, for they can be redefined and saved in computer format. this procedure commonly only existed in the mind of designer who digest the business flow and then figure it out in ways that are more familiar to the programmer, like UML.

Until R.A. Meersman I in his research put forward an semantic way to speed this procedure up ,in his work, a "global" common ontology (lexicon, thesaurus) is conjectured, and some desirable properties are proposed[1], He argue nevertheless that large public lexicons should be simple, suggest their semantics become implicit by agreement among "all" users, and ideally completely application independent. In short, the lexicon or thesaurus then becomes the semantic domain for all applications. In designing these lexicons whose grammar can be conceived by computer and expression in natural language. eg. choosing “has a”.” of a” on behalf of the relation between an ontology object and its property. While other words or phrase used for the rest in domain ontology.

One following similar research by Meenakshi is about extracting domain ontology entities through semantic web. His research used an ontology database which can aid in entity extraction in web document, after a disambiguation process, the semantic annotation result could be formatted like this: *<Enilty id="494S05" class="company"> Henietl-Packard </Enitty> <Entity id="3'7S349" class="tickerSymi'ol"> IYPQ</Entity>: up <Regexp type="money"> $0.J3 </Regexp> to <Rogexp type="r>ton0y">SlS.O3</Regexp>*[2]. In the form of XML,it can be delivered and processed through different systems for object reconstruction.

The researches mentioned above are both innovative, despite of their different methods and results they all use semantic annotation to extract domain model to facilitate other application automatically perceiving and integrating the meaningful entity. In the other hand, either of them can not figure out the interoperation details between entities yet, because there are uncountable relations which couldn’t be unambiguously identified. This fault makes the results not suitable for system design but class construction.

In our research, firstly the construction of a universal emergency response system is the goal, second, based on the axiom that full text description of an phenomena is a whole map of it, as well as a full work flow of the same phenomena executed in computer, then the system analysis’ subject can be altered to the text description which act as an agent of the real phenomena. This way may be indirect but could find some useful rules that can not be found out in ordinary ways, therefore analysis is directly taken on the linguistic descriptions of emergency response process in our research, and semantic annotation also adopted, which use the semantic labels in propbank.

The subjects are some documents that each of them described a full emergency response process. After the annotation, statistic is tried, finally three linguistic rules are found out, first, every sentence have a predicate verb, second, each predicate verb coexists with semantic role Arg0(actor), third, all the complement roles of predicate

verbs converge into a fixed subset of semantic roles ,we call them together as verb logic. It is a higher abstract semantic model than domain ontology, for it is not only across domains but also tell the relations among entities. So based on verb logic, the universal emergency response system can be built up.

In this paper, first the process of verb logic is stated, second the system design based on it is described, and then the system's capability is discussed, finally three cases of different event type are used to demonstrate its capability.

2 Verb Logic

2.1 Semantic Labels and Propbank

Representing the predicate-argument structure has been one of the focal points in recent efforts to develop semantic resources. This is generally achieved by specifying the semantic roles for the arguments anchored by the predicate, but the specific semantic role labels used differ from project to project. They range from very general role labels such as agent, theme, beneficiary adopted in the VerbNet(Kipper et al. 2000; Kipper et al. 2004; Kipper et al. 2006) and the semantic component of the Sinica Treebank (Chen et al. 2004), to labels that are meaningful to a specific situation, like the role labels used in the FrameNet (Bakeret al. 1998) and the Salsa Project for German (Burchardt et al. 2006), to predicate specific labels used in the English PropBank (Palmer et al. 2005) and the Nombank (Meyers et al. 2004). The difference between the various approaches can be characterized in terms of levels of abstraction. The Propbank style of annotation can be considered to be the least abstract, as it uses argument labels (Arg0, Arg1, etc.) that are meaningful only with regard to a specific predicate.

Table 1. Semantic roles in Propbank

Core semantic role	labels	Arg0	Arg1	Arg2	Arg3	Arg4	Arg5						
	meaning	Agent, Experiencer	Theme ,Topic, Patient	Recipient, Extent, Predicate	Asset, Theme2, Recipient	Beneficiary	Destination						
Additional Semantic Role	labels	ArgM -ADV	ArgM -BNE	ArgM -CND	ArgM -DIR	ArgM -DGR	ArgM -EXT	ArgM -TMP	ArgM -TPC	ArgM -PRP	ArgM -FRQ	ArgM -LOC	ArgM -MNR
	meaning	Adverbials	Beneficiary	Condition	Direction	Degree	Extent	Temporal	Topic	Purpose or Reason	Frequency	Locative	Manner

2.2 Statistic and Analysis

There are many kinds of Linguistic documents described emergency response process such as Emergency Processing Conclusion, Counterplan or Exercise instruments, even journalistic reports can provide the detail of response.

In our study, we collect 16 different kinds' documents.

As table 2 show, each of them has at least 30 sentences and fully covers an emergency response process whether finished or just in preparation.

Table 2. The subject documents

Index	Event type	Document type	Source organization	The number of sentence
1	Fire incident	Handling norms	Community property companies	52
2	Drug trafficking	Handling norms	Public security bureau	33
3	smuggling	counterplan	Border Corps	75
4	Public health crisis	Handling norms	Health Department	46
5	Bombings	counterplan	Public security Department	118
6	earthquake	counterplan	Seismological Bureau	81
7	Refugees	counterplan	Border Corps	87
8	Human smuggling	Processing Conclusion	Border Corps	48
9	smuggling	Processing Conclusion	Border Corps	103
10	Human smuggling	Exercise instruments	Border Corps	35
11	Drug trafficking	Exercise instruments	Coast guard	105
12	Robberies	Processing Conclusion	Public security bureau	74
13	power grids damaged	counterplan	Power company	36
14	First aid	Handling norms	medical emergency center	66
15	Fire incident	Processing Conclusion	Fire Squadron	64
16	Mass riots	Handling norms	Public security Department	79

Because samples are of a small quantity, manually semantic annotations could be done in acceptable time, and no existed program affords the unambiguous work, for the frequently phenomena that one sense is multiple referenced in forms as verb Nominalizations phrase in documents. Then we assign semantic role labels which are defined in propbank system to the constituents by ourselves.

Fig. 1 is illustrating the annotation of an isolated sentence. It is not difficult to judge the semantic roles in a single sentence, but in a written document some semantic roles are often omitted for the context implicitly provides their meaning. This phenomenon will introduce errors into the statistic work. So we take a pretreatment that regenerate the documents to make each sentence can describe a complete and unambiguous meaning independently by appending the implicit roles from context.

When the annotation work finished, we count each semantic role present times in all samples and get table 3. In this table, we confirm that these documents consist of predicate centered sentences, and each verb always coexists with an Arg0 role which denotes the doer of the action. But no discipline of other arguments can be told yet.

Little was raveled from detailed statistic which has been done in different ways until we classify the annotation by the sense of core verb. While the same meaning can be expressed in different forms, so to simplify the statistic we choose the most common expression of each independent meaning and name it as predicate verb (PV) and filter out the roles conveying dispensable meaning and of unremarkable present frequency like Arg4 ArgM –EXT , Next step is do the statistic of appearance frequency

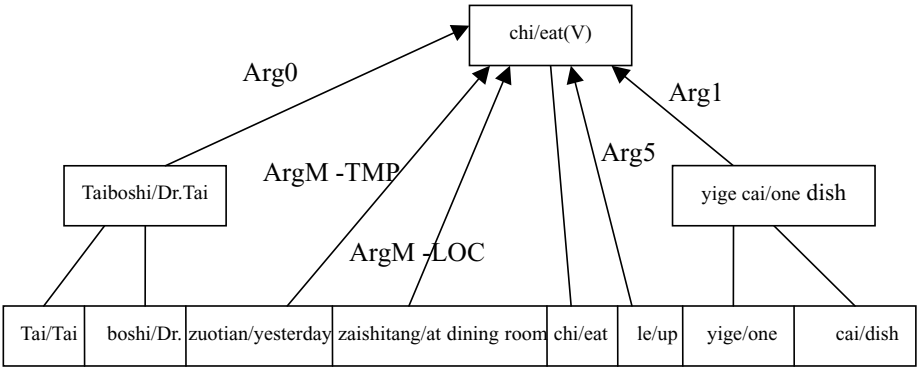

Fig. 1. Semantic annotation in propbank labels

Table 3. Appearance frequency of all semantic roles

Semantic role	Meaning	Appearance frequency	Possibility of appearance in a sentence(total of sentences: 1102)
V	Verb	1102	1
Arg0	Agent, Experiencer	1102	1
Arg1	Theme ,Topic, Patient	484	0.439201
Arg2	Recipient, Extent, Predicate	327	0.296733
Arg3	Asset, Theme2, Recipient	59	0.053539
Arg4	Beneficiary	4	0.00363
Arg5	Destination	75	0.068058
ArgM -ADV	Adverbials	0	0
ArgM -BNE	Beneficiary	0	0
ArgM -CND	Condition	0	0
ArgM -DIR	Direction	5	0.004537
ArgM -DGR	Degree	0	0
ArgM -EXT	Extent	2	0.001815
ArgM -FRQ	Frequency	0	0
ArgM -LOC	Locative	752	0.682396
ArgM -MNR	Manner	5	0.004537
ArgM -PRP	Purpose or Reason	0	0
ArgM -TMP	Temporal	578	0.524501
ArgM -TPC	Topic	0	0
ArgM -CAU	Cause	0	0
ArgM -NEG	Negation	0	0
ArgM -MOD	Modal	0	0

of the PV's complement roles, then we find one PV and its coherent semantic roles have a fixed relationship. The part of result is shown in table 4.

Table 4. Appearance frequency of some verb's coexisted roles

Predicate verb	Semantic role	Meaning	Coexist frequency	Predicate verb frequency	P(V|Arg*)
ganfu/go for	Arg0	Agent, Experiencer	123	123	1
	Arg5	Destination	123	123	1
	ArgM -LOC	Locative	123	123	1
	ArgM -TMP	Temporal	123	123	1
jiuhu/ cure	Arg0	Agent, Experiencer	75	75	1
	Arg2	Recipient, Extent, Predicate	75	75	1
	Arg3	Asset, Theme2, Recipient	75	75	1
	ArgM -LOC	Locative	75	75	1
sushan/evacuate	Arg0	Agent, Experiencer	18	18	1
	Arg1	Theme ,Topic, Patient	18	18	1
	ArgM -LOC	Locative	18	18	1
	ArgM -TMP	Temporal	18	18	1
daibu/arrest	Arg0	Agent, Experiencer	37	37	1
	Arg1	Theme ,Topic, Patient	37	37	1
	ArgM -LOC	Locative	37	37	1
	ArgM -TMP	Temporal	37	37	1
fengshuo/ Blockade	Arg0	Agent, Experiencer	53	53	1
	ArgM -LOC	Locative	53	53	1
	ArgM -TMP	Temporal	53	53	1

Given the result, the semantic roles which have the possibility to coexist with one particular predicate verb can be limited, and all of them must show up with the predicate verb while the other roles absent. Now we confirm the conclusion that each predicate verb must coherent with several fixed semantic roles to express a complete and independent meaning. Furthermore, we collect all presented semantic roles, and the result is interesting that the complement roles is not the rest roles exclude Verb, the complement roles converged into seven types: Arg-tmp Arg-loc Arg0 Arg1 Arg2 Arg3 Arg5. That means in description of emergency response process, fixed types of arguments must be addressed, in other words, these types is enough for linguistic description of a whole response process of any event type.

But why these roles are necessary to the documents? Why not the others? Some points are presented.

First, Arg0 is the actor and Arg1 is the objects or persons that received or affected by the action of the predicate verb. In rescue and response process, every action must executed by special persons or forces and the action must have specific effect to objects, otherwise the action is of no meaning.

Second, Arg2 is the influence or goal of the action of the predicate verb, it is a basic complements of lasting actions to work for ,and implicitly for emergency manager estimate effect to decide the action' going on or not.

Third, Arg3 is the equipments or methods that took by the actions. it is reasonable that response team could not accomplish mission with empty hand and they must make preparation for the different situations in the spot.

Fouth, Arg-TMP is the argument indicate temporal period or point in a sentence. Emergency response has the basic require for proceeding in an efficient time-ordered manner. So the time point when action take place or finished is remarkable important to the accuracy in the whole process.

Fifth, Arg5 is the Destination and Arg-LOC is about the location. Actually they are the most important complement to a response action, because both emergency and its response are spatial, which means any event has its limited effective area in the whole life cycle. Their spatial properties is the foundation of where the response actions implements. Furthermore they are the necessary elements of most decision-making models which can tell the suitable route that emergency troop takes to reach the spot or other target place.

2.3 Expression of VL

As a summary of statistics above, three useful points are stated.

First, the emergency response describe documents compose of sentences which has a core predicate verb without exceptions.

Second, with each verb the appearance of the semantic role Arg0 is a certainty.

Third, all the complement semantic roles in the documents converge into a fixed and countable set that has seven members of roles in propbank. Enumerated as: Arg-tmp Arg-loc Arg0 Arg1 Arg2 Arg3 Arg5.

We name these points together as verb logic in emergency response, VL for abbreviation. It is an semantic abstraction which is in a higher level than domain ontology, because the discipline has nothing to do with the specific type of events, neither fixed analytic model nor fixed reader or users, while in domain ontology, both the entities and their relations are concrete and can not extend to other domain that make the systems based on them hardly interoperate with each other.

So VL is the rules of all kinds of emergency response. And it can be the foundation of universal emergency response system design,

3 Universal Emergency Response System Design

Before the system design, in review of the former emergency response systems, it is obvious that they are almost aiming at one type of emergency and only a little can handle several kinds of emergency. The reason is every concrete emergency itself is a part of specific domain ontology, and involved with other entities in the domain. In

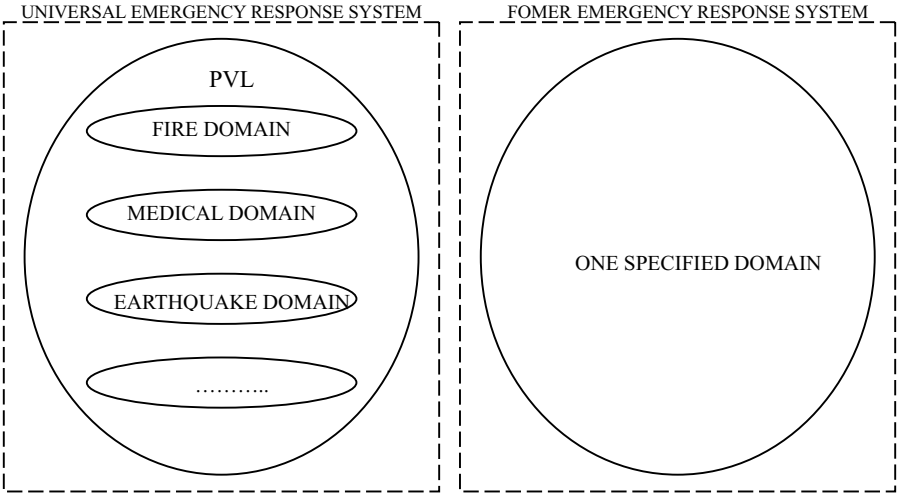

Fig. 2. System coverage comparison

other words, the domain ontology which includes a specific emergency event determines the concrete property of the event and its relatives.

In the contrary, the VL is not domain specified; because it is a higher abstraction of all domains and can apply to any emergency response. It can be regard as the meta-data of every emergency domain, while one type of domain ontology can be regard as the metadata of a concrete emergency response.

So the system which implements VL must have the capacity of any emergency domain. That is the theory foundation of the capability in the universal emergency response system.

3.1 First Any Concrete Emergency Itself Is belong to a Domain

Since every concrete emergency has domain ontology as its metadata, classifying emergent events by their superior domain is a right-on taxonomy which is the foundation of the universal emergency response system to keep it providing the particularity while in capable of every kinds of emergency.

To build up these classes in practice, a tree structure, which has a root node named abstract emergency as the parent of any emergency, is helpful. And child nodes of the tree can be specific domain and other emergency type, but only the domain node can have descendants. If a concrete emergency happened, there must be a sole domain node can contain it and all it's involved, that indicate the type of the emergency. And if an emergency is complex, also there is a high level domain node, which includes other detailed domains, can be the superior.

In addition, the events belonging to one same domain should be grouped by its quantitative property such as numbers of involved persons. Acreage of the spot etc. for the superior domain ontology is more of qualitative classification.

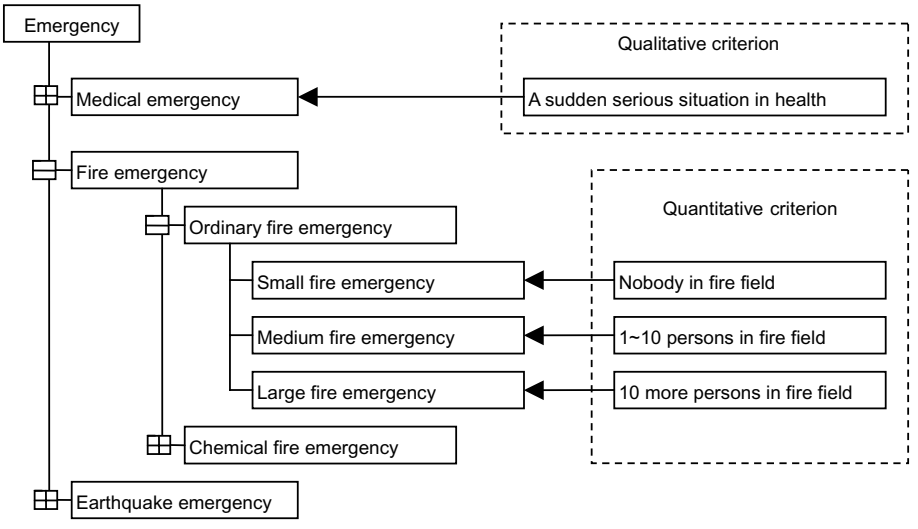

Fig. 3. Emergency classification

3.2 The Core Verb Turns to Emergency Command

Emergency response and rescue is not a civilian affair, always implement by government. And all the actions are implicitly taken by force and press which is guaranteed by government or military power.

The other point is that no civilian is responsible for handling emergency; they are the passive and supposed to obey the commands.

The response actions is unconditional executed for the firemen, military troops, medical teams and civilian, so we call the core verb as emergency command, by analogy of military command, we also can extract an unambiguous abbreviation, which is a single word or short phrase, for any specific action. It could be easily defined and stored as string data type in computer.

The emergency command is the center conception in universal emergency response system, because it has been stated in VL that the response work flow can be considered as a set of actions arranged in parallel or series.

3.3 The Arg0 Turns to Task Force

The semantic role Arg0, which means the actor or sponsor of the predicate, always coexists with core verb and indicates who took the actions. In real world, they are correspond to the persons or special equipments which can implement the response and rescue actions, for instance a medical team can rescue (the injure). A battle plane can destroy (enemy), a salvage corps can extinguish (fire).

Arg3 is the role which indicate the tools taken by the action, and don't appear for sure in those sentences. But any time it shows off, it actually means that the tools and

equipments must be used or handled by men who may be not mentioned. Like this sentence, a battle plane is going to lock the hijacked plane by Air-to-air missile. It implicates at least one battle plane、one missile and one pilot to do the "lock" job together.

From these arguments, we make a definition of any inseparable group, which buildup by organized person and special equipment, and which also can implement at least one response action interpedently, as task force, TF for short.

Despite of the clear definition, it is hardly to directly integrate all TF in response system for there are various TF, which made up of different Persons and equipments, and also no uniform format available of these domain entities. So by analogy to the emergency type classification, tree is the most suitable structure to organize all types of TF in one emergency response system.

The TF tree has the same domain node to emergency type tree, each domain node could have descendants included detailed domain nodes and TF node, and the TF node is also can find a sole superior node marked specific domain.

Also the leaf nodes can be group into different class by the measurable properties of their members and equipments like regimental battalion company, battery in military classification.

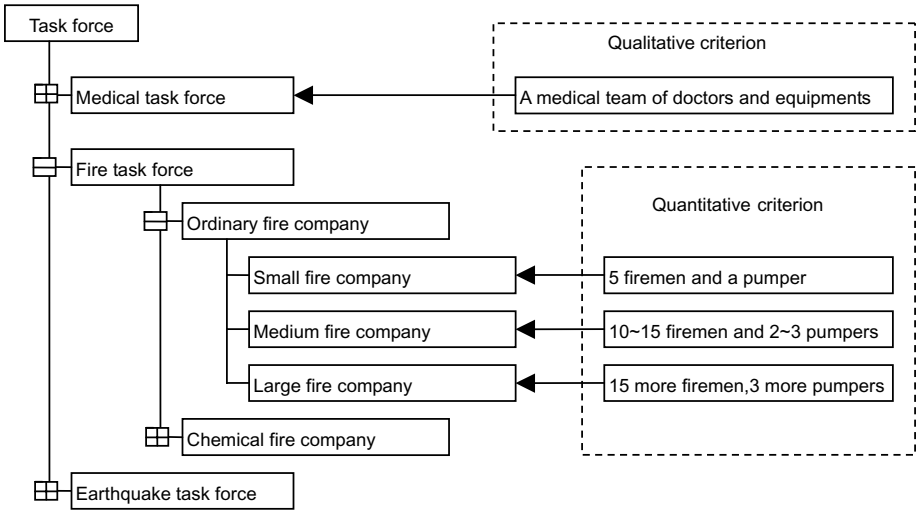

Fig. 4. Task force classification

3.4 The arg-1…n Collected as Command Arguments

There are some important complement roles to a response action in documents as arg-tmp arg-loc arg1 arg2 arg5. By the information they conveyed, what the concrete action is .can be determined, both for the documents reader and the TF who need to execute the action. So we call them action arguments, the variables to produce an real action.

In an order of clarity and comprehensibility, we map them into our universal emergency response system.

First, the Atg-Tmp is a time point or period, which can be easily stored by numbered Date type parameters, commonly one for time point and two for period.

Second, the Arg-loc and Arg5 are both indicating the location. In geographic information system, location can be defined by three types of spatial data, point\arc (line)\polygon, and these spatial data types already have their perfect definition after long time development in geographic field.

Third, the Arg2 is the influence or target of an action. It is a bit more variable description than other arguments, for it can be qualitative or quantitative and it is action depended.

Though it is hardly to directly extract a class from it, but we can use its original appearance in documents, which can be easily saved in computer as String Type, to make the expression and we call it Description. That is the best way by far.

Fourth, Arg1 are substantives or persons that received or affected by the action of the predicate verb. We can not use a simple class as their deputy, and it is more difficult to build a composition model of persons and substantives which we can't tell until the emergency occurs.

Then a compromise class named Action object, which has the compulsory fields included name, description and an optional field location, can fulfill the roles. Name is the basic property of any object, while the description can be the container of its individual characteristics or can be regarded as the serialized result of concrete character at runtime. And occupation of a space is the implicit property of substance or person, and it is always useful in emergency response, so the optional location can be assigned whenever required,

Briefly speaking, all the emergency command arguments in the universal emergency response system can be realized by these classes: TimePoint, Location, Description, ActionSubject, these classes are the super classes of any concrete emergency command argument and they are compose of the essential data types as String, point arc (line) polygon, Date. In this way the essential data types are able to transplant to different hardware and guarantee the capability of the response system.

3.5 Count Plan or Precaution Plan Is a Set or List of Actions

After the mapping work of the VL, the main benefit of the universal emergency response system should be reviewed. It is that keeping the storage of involved information and assists the response process.

Though the emergency involved semantic roles are stored, it is not enough for emergency manager to make decision in the scene, there is even no sufficient time to search for the information fragments to choose an action. The real efficient and needed is the preparation for every emergency---counterplan. Counterplan is the suppositional response process of a type of emergency, which could tell when\ where\ who to do something for emergency rescue in advance, but it must have the capability of the uncertainty during the emergency life cycle, otherwise could be useless. As argued in the semantic analysis section. The response process can be wholly described in predicate verb centered sentences. That means the process is made up of actions without exception. Then counterplan is also made up of actions. The capability of the

emergency uncertainty can be regard as some conditional options covered all the possibility of the scene. These options are also actions and at end of each of them there could also be a set of conditional options, in the angle of workflow the counter-plan can be defined as a list of actions, arranged in series and parallel. More clearly, one set of parallel actions named as Emergency Step in our system.

Then the design work of counter plan in universal emergency response system is, defining a step firstly, add actions secondly, in succession defining its next step for each action, and go through the approach in iteration until the response supposed finished. The fundamental action, which can be defined by limited semantic roles, disassembled into computer capable classes: emergency command task force and command arguments. So we can build up counterplan from bottom to top.

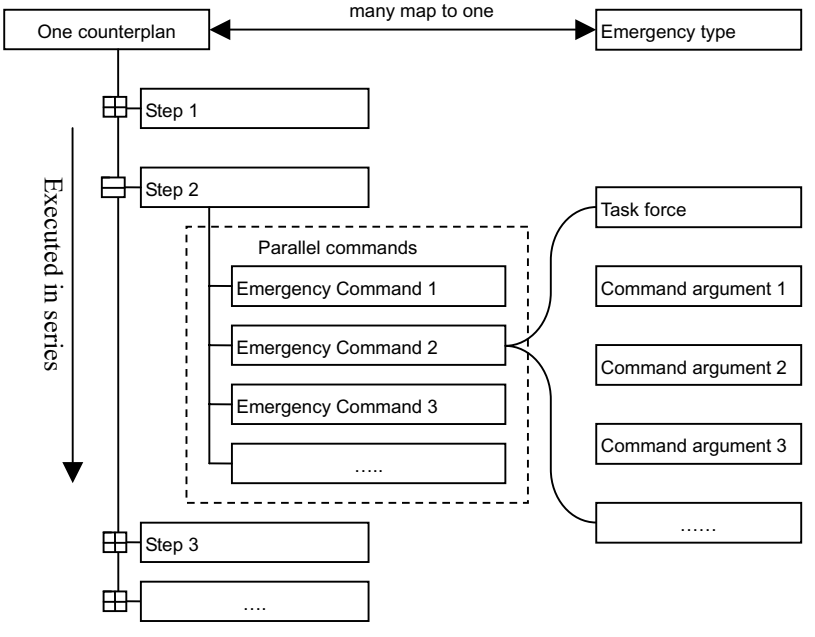

Fig. 5. Structure of counterplan

4 Integration of Decision Models

Decision models in emergency response are not the main theme of this paper, but they have been developed for years and a lot of them are fruitful. As well as emergency itself, the decision model is domain related for its inputs and arithmetic is altered among domains.

But decision models are all quantitative process, their results are quantitative too. And these results must be used in emergency response process that in according to VL only have quantitative semantic roles of Arg-TMP,Arg-LOC,Arg5. Furthermore

the three roles have been defined as command arguments in universal emergency response system.

So it can be deduced that all results of decision models in emergency response are command arguments. This conclusion means decision models can be stored as plug-ins and applied in the moment that command arguments needs to be assigned. That is the way to integrate any decision models.

5 The Work Flow of a Concrete Emergency Response

After the preparation listed above, the work flow of a concrete emergency response can be constructed as following.

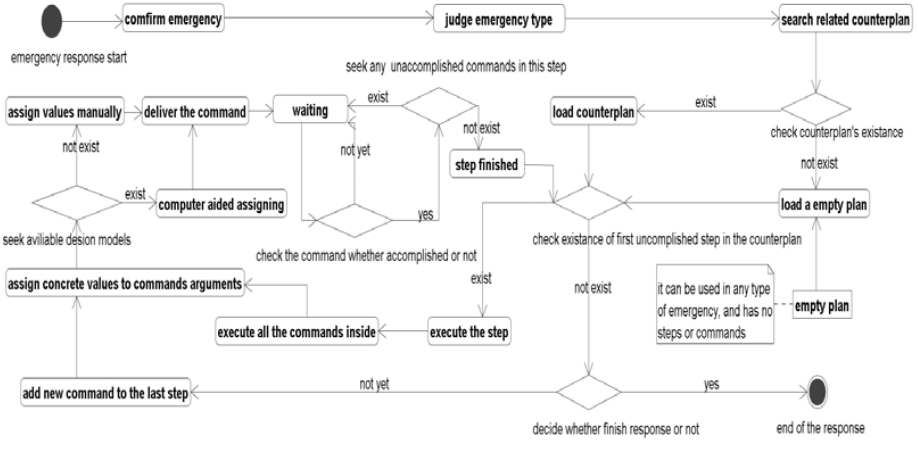

Fig. 6. Workflow in universal emergency response system

6 Conclusion

In front of the challenge of complexity of emergency, path divides. Most of emergency response system researches focus on the interoperation among different information systems which aiming at one type of emergency or one part of the response procedure. But we choose the construction of a universal emergency response system, and are enlightened by the semantic analysis which has make lots of achievements in build up domain ontology or semantic web; we research on the documents in which the response process wholly described, using methods of semantic annotation.

After statistic and analysis, we put forward three somatic rules as VL, which indicate the inner logic of all kinds of emergency responses. Then on the base of VL, the detailed design of universal emergency response system is made out, this design is capable of storing all the information fragments in emergency response process, even more it is capable of all types of emergency and related decision models.

7 Future Issues

First, VL is extracted from limited samples; it could be of more persuasion if more documents of other kinds of emergency be analyzed.

Second, mapping the semantic roles into computer could be more accurate and quantitative, in the system, the semantic roles that the goal and the object of action using String to provide for compatibility. The assumption that deeper semantic analysis of the predicate verb's arguments could bring some new consequence to define the arguments more accurate and quantitative needs proof,

Third, software engineering technology could make the system development more convenience. In our programming some design patterns and aspect oriented programming are adopted to provide the flexibility. Some other efficient technical methods need to be found out.

Acknowledgements

We gratefully acknowledge the financial support of National Basic Research Program of China (973 Program, NO. 2009CB723906) and CAS Knowledge Innovation Program, NO.092101104A.

References

1. Meersman, R.A.: Semantic Ontology Tools in IS Design. In: Proceedings of the 11th International Symposium on Foundations of Intelligent Systems, vol. 1609, pp. 30–45 (1999)
2. Nagarajan, M., Scale, L.: Semantic Annotations in Web Services. Semantic Web Services. In: Semantic Web Services Processes and Applications, ch.2. Springer, Heidelberg (2003)
3. Xue, N.: A Chinese Semantic Lexicon of Senses And Roles. Language Resources and Evaluation 40, 3–4 (2006)
4. Abdalla, R., Tao, C.V., Li, J.: Challenges for the Application of GIS Interoperability in Emergency Management Geomatics Solutions for Disaster Management, pp. 389–405. Springer, Heidelberg (2007)
5. Allen, E., Edwards, G., Bedard, Y.: Qualitative causal modeling in temporal GIS. Spatial Information Theory 988, 397–412 (1995)
6. Bishr, Y.: Overcoming the Semantic And Other Barriers to GIS Interoperability. International Journal of Geographical Information Science 12(4), 299–314 (1998)
7. Briggs, D.: The Role of GIS: Coping with Space (and Time) in Air Pollution Exposure Assessment. Journal of Toxicology and Environmental Health-Part a-Current Issues 68 (13-14), 1243–1261 (2005)
8. Christakos, G., Bogaert, P., Serre, M.: Temporal GIS: Advanced Field-Based Applications, p. 217. Springer, Heidelberg (2002)
9. ElAwad, Y., Chen, Z., et al.: An Integrated Approach for Flood Risk Assessment for the Red River in Southern Manitoba. In: Annual Conference of the Canadian Society for Civil Engineering, Toronto (2005)
10. Erharuyi, N., Fairbairn, D.: Mobile Geographic Information Handling Technologies to Support Disaster Management. Geography 88, 312–318 (2003)
11. Farley, J.: Disaster Management Scenarios. Univ. of Arkansas, OGC Discussion Paper (1999)

An AIS-Based E-mail Classification Method*

Jinjian Qing[1], Ruilong Mao[1], Rongfang Bie[1,**], and Xiao-Zhi Gao[2]

[1] College of Information Science and Technology, Beijing Normal University, Beijing 100875, P.R. China
[2] Department of Electrical Engineering, Helsinki University of Technology, Espoo 02150, Finland
rfbie@bnu.edu.cn

Abstract. This paper proposes a new e-mail classification method based on the Artificial Immune System (AIS), which is endowed with good diversity and self-adaptive ability by using the immune learning, immune memory, and immune recognition. In our method, the features of spam and non-spam extracted from the training sets are combined together, and the number of false positives (non-spam messages that are incorrectly classified as spam) can be reduced. The experimental results demonstrate that this method is effective in reducing the false rate.

Keywords: Artificial Immune System (AIS), Spam, E-mail Classification.

1 Introduction

During the past decade, the flood of e-mail spam has been becoming extremely severe. It can take up a lot of resources like transmission, storage, and computation, cause the mail servers congested, spread pornography, publish reactionary remarks, deceive money, mislead the public, and make our social security jeopardized. It also affects the economics both directly and indirectly, bringing about inestimable loss in the countries all over the world. To fight against the e-mail spam, researchers have proposed numerous methods to distinguish spam messages [1, 2, 3], such as black list, manual rule sets [4], challenge response system, honeypot, etc. In general, these methods have restricted the spread of spam to a certain degree. However, due to their self-imposed limitations as well as the constant variation of spam characteristics, their performances in practice are not so satisfactory.

Recently, Artificial Immune Systems (AIS) have been used for fault detection [13], spam detection [11, 12] and email classification [7]. This paper designs and implements a new e-mail classification method based on the Artificial Immune System (AIS). Firstly, it generates a set of spam detectors by training. Secondly, it generates non-spam detectors so as to optimize the detection space. After these two steps, it can classify emails by utilizing the non-spam and spam detectors successively and achieve

* Supported by National Natural Science Foundation of China (90820010) and the Academy of Finland under Grant 214144.
** Corresponding author.

D.-S. Huang et al. (Eds.): ICIC 2009, LNAI 5755, pp. 492–499, 2009.

the goal of reducing the false rate. In our experiments, we choose standard Chinese e-mail samples from the CERNET Computer Emergency Response Team (CCERT), and compare our optimized classification method with traditional technique. The experimental results show that this new method is effective in reducing the number of false positives.

2 Background

2.1 Artificial Immune System

Inspired by the biological immune system, the Artificial Immune System [5, 6] (AIS) is an emerging learning technique, which can provide evolutionary learning mechanism, such as noise tolerance, non-supervised learning, self-organization, and memorizing. It combines certain advantages of computational intelligence methods like neural networks, machine learning, etc. The AIS has been endowed with many features, e.g., diversity, adaptability, initiative, dynamics and robustness.

When we use the AIS to deal with textual classification, we define information of interest as self and non-interest as non-self [7]. The classification scheme includes two stages. One is learning phase, in which the system constructs a series of information detectors based on the determined samples. The other is application phase, where we compare the new information considered as an intruding antigen with detectors generated previously so that we can determine whether it is self or non-self.

2.2 Evaluation Indicators of E-mail Classification Methods

Generally, the recall rate and false rate are two evaluation indicators that can be used to assess any e-mail classification method. The following definitions are given. *totalSum* denotes the total number of e-mails we will check, among which the number of spam is *spamSum*, and that of non-spam is *hamSum*. The number of non-spam, which is falsely classified as spam is represented by *falseSpamNum*, and *rightHamNum* for legitimate e-mails correctly classified. Similarly, *rightSpamNum* indicates the number of spam with correct categorization, and *falseHamNum* denotes the number of spam, which is considered legitimate. According to these definitions, the recall rate and false rate are defined as below:

a. recall rate:

$$P_{recall} = \frac{rightSpamNum}{spamSum} \times 100\%, \tag{1}$$

b. false rate:

$$P_{vir} = \frac{falseSpamNum}{hamSum} \times 100\%. \tag{2}$$

2.3 E-mail Classification Method Based on AIS

E-mail classification is a special textual problem with two categories. In general, an AIS-based classification method includes the following phases.

Phase I: Pre-processing. It consists of code transformation, text body and header separation, Chinese word segmentation, and e-mail vector extraction. The extraction is the process of choosing a vector set, which best reflects the message characteristics [8]. The components of a vector can be the words in message, the size of text and attachments, the property that whether it is HTML coded, etc. The components are assigned with distinct weights according to their different importance, and they can represent the characteristics of e-mails.

Phase II: Training. Generate a set of spam detectors based on the determined spam, i.e., find the most representative spam. A detector has a center and a radius, whose values can be adjusted during several experiments to find the most appropriate ones. We compare each new coming e-mail with the existing detectors to decide whether to add it to the detector set or not. If it is too close to a center of any detector, it is disregarded. The purpose of this approach is to make the detectors have the largest coverage while avoid their excessive aggregation.

Because the length of an e-mail vector is indeterminate, it is difficult to calculate the affinity of two variable-length vectors. Generally, their affinity can be defined as follows:

$$aff\,(e[i], e[j]) = \frac{e[i] \cap e[j]}{minL(e[i], e[j])}\ , \tag{3}$$

aff($e[i]$, $e[j]$) represents the affinity of e-mail i and j, $e[i] \cap e[i]$ indicates the number of matching components of these two vectors, and the value of *minL*($e[i]$, $e[i]$) denotes the shorter length between them. Apparently, Equation (3) ensures the affinity ranges in [0, 1]. When two vectors have the same length, it works well, and the results are satisfactory. However, it becomes less effective, if the difference between their lengths becomes larger.

Phase III: Application. The incoming e-mails are classified with the trained detectors. When a new e-mail arrives, its feature vector can be obtained after pre-processing, and the affinity between this e-mail and the detectors is calculated. If the affinity is greater than the threshold, it is a spam; otherwise non-spam.

Phase IV: Feedback. It includes the manual intervention by the users, error correction, and re-training. This phase can guarantee the accuracy and timeliness of the detectors.

To summarize, the AIS-based method utilizes the spam detectors in a straightforward way. In the detection space, only the e-mails falling within the radius range of a detector can be classified as spam.

3 Our Approach – An Optimized E-mail Classification Method Based on AIS

As we know, the evaluation of an e-mail classification method depends on not only the recall rate, but also the false rate, which is an even more important indicator. From the users' point of view, it is unacceptable to categorize the legitimate messages as spam. Hence, how to reduce the false rate of e-mail classification becomes an important research topic.

In this paper, we design a new classification method, which employs two detector sets. One consists of non-spam detectors and the other spam detectors. By using both the non-spam and spam detectors successively, we can achieve efficient e-mail classification, and reduce the false rate. With the deployment of the non-spam detectors, this method divides the whole detection space into three parts, which are non-spam region, spam region, and blank region. Figure 1 shows the detection spaces of the traditional AIS-based and our classification methods.

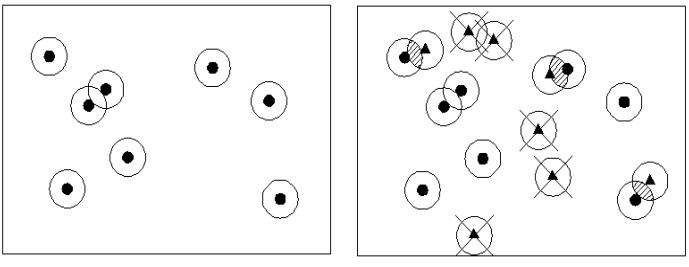

(a) (b)

Fig. 1. Detection spaces of traditional AIS-based and our classification methods. (a) Detection space of traditional AIS-based method: *spam detector* (*circle with a round as its center*), *spam region* (*inside the circles*) and *non-spam region* (*outside the circles*). (b) Detection space of our optimized method: *spam detector* (*circle with a round as its center*), *non-spam detector* (*circle with a triangle as its center*), *spam region* (*inside the round center circles except shaded parts*), *non-spam region* (*inside the triangle center circles*), and *blank region* (*outside all the circles*). Circles marked by "╳" are meaningless, which can be eliminated.

Figure 1(a) represents the detection space of a traditional AIS-based method. Here, a circle denotes a spam detector. The spam region is within the circle, while the outside is the area of non-spam. Figure 1(b) is the detection space of our classification

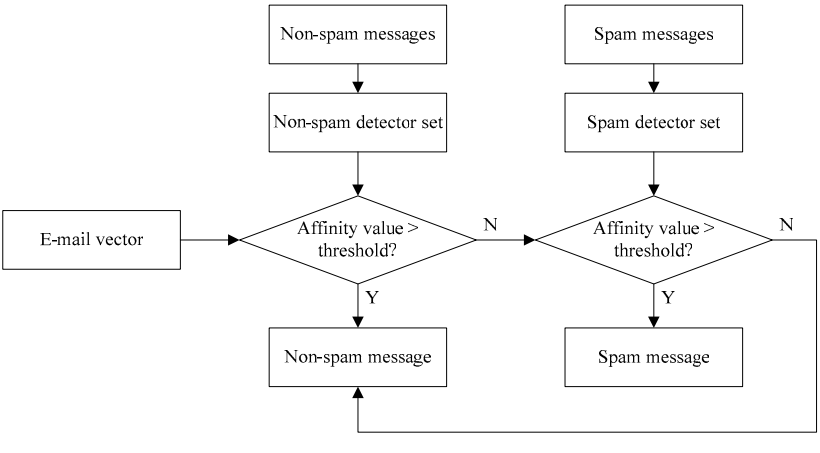

Fig. 2. Data flow chart of the optimized method

method, where a spam detector is denoted by a circle with a round as its center and a non-spam detector with a triangle. More precisely, we use the non-spam detectors to do the first tier classification, and the second tier with the spam detectors. This ensures the cross parts of spam and non-spam is considered as the non-spam region instead of spam region. That is to say, the spam detectors can give priority to those non-spam detectors. In summary, during the training procedure, two sets of spam and non-spam detectors are generated. The flow chart is given in Fig. 2.

4 Experiments

4.1 Background

We choose the e-mail sample set 2005-Jun (2005-Jun.tar.gz) as the experimental samples from the CCERT, which includes 25,088 spam and 9,272 non-spam. Lucene2.0 and IK_Canalyzer1.4 can be used as segmentation instruments for the Chinese words in our experiments.

We check from the 1st to the 9,000th spam, dividing them into spamGroup1 to spamGroup9 with 1,000 messages each. For the non-spam, the same pre-processing is made, except that the group label is from hamGroup1 to hamGroup9. By training our scheme with spamGroup1 and hamGroup1, we finally generate 100 spam detectors and no more than 100 non-spam detectors. The detailed procedures are described as follows.

We first generate a set of spam detectors by training. For example, select an e-mail from spamGroup1 for word segmentation, and generate an undetermined detector (denoted by *det*), which consists of a word list (*wordList*), the number of matched e-mail (*matchedCount*) and the number of e-mail already detected (*detedCount*). We calculate the affinity on property *wordList* between *det* and every *det*[*i*] in detector set (*detGroup*). If it is greater than the threshold, add one to *matchedCount* of *det*[*i*]. Meanwhile, *detedCount* of *det*[*i*] should be increased, no matter whether their affinity is less or greater than the threshold. If the number of *detGroup* is less than 100, directly add *det* in; if it equals 100, add *det* to the set after eliminating the detector with the smallest weight.

Next, we generate a set of non-spam detectors. Similar to the previous step, we circularly select an e-mail once from hamGroup1 for word segmentation, and generate an undetermined detector (also denoted by *det*). With regard to the affinity, the object to be compared with *det* is every spam detector generated previously rather than the non-spam. If any of the value is greater than the threshold, add *det* to the non-spam detector set. In particular, we point out that the reason why comparing a non-spam detector with the spam detectors is that we aim at searching for the detectors, which are similar to spam but actually belong to non-spam. Thus, we can discover the overlapping parts shown in Fig. 1(b).

The definition of the weights is given as follows:

$$pValue = \frac{matchedCount}{detedCount} \quad . \tag{4}$$

For each detector newly added, its initial weight that is set to 1/20 has a close relationship with the quality of the detector sets. During the training process, to avoid excessive aggregation, we have to ensure that the over-similar detectors should not be added to the set simultaneously. After training, we carry out the other eight experiments for testing by using these trained detectors and sixteen remaining groups.

4.2 Results and Analysis

The experimental results from the optimized classification method and traditional AIS-based method are as follows: the optimized one has a best recall rate of 83.1%,

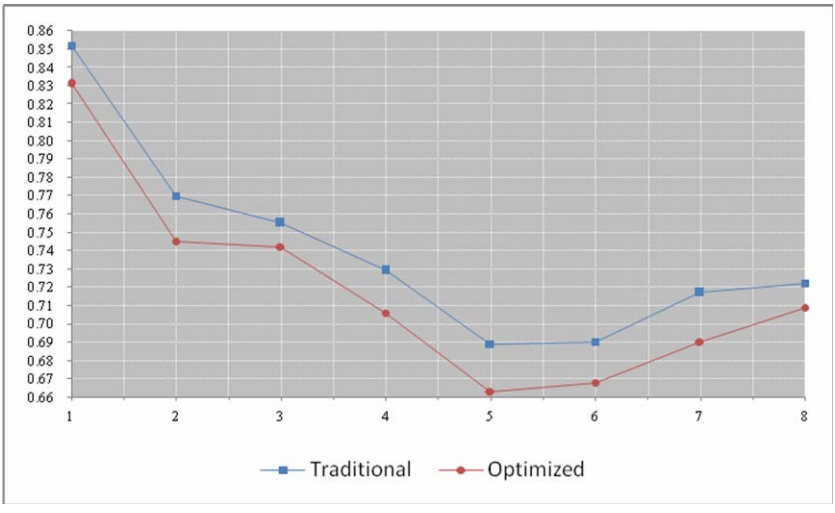

Fig. 3. Recall rates of classification

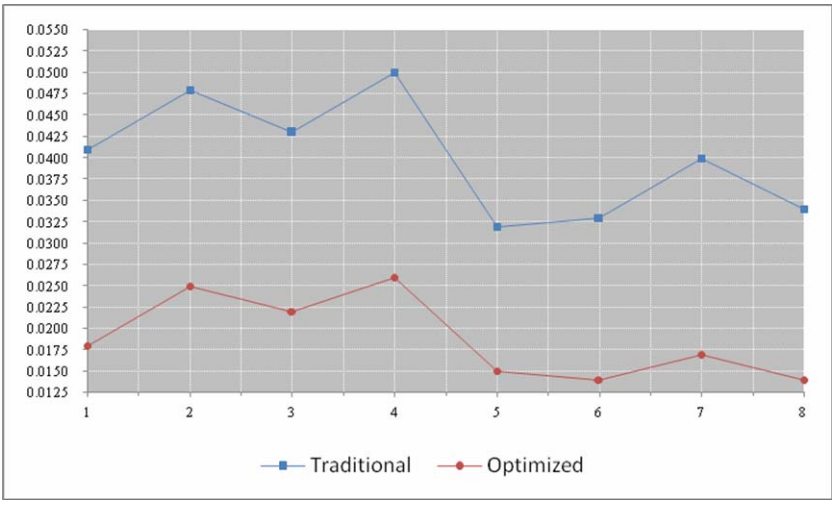

Fig. 4. False rates of classification

the worst 66.3%, and the average 71.93%. Concerning its false rate, the best is 1.4%, the worst 2.6%, and the average 1.89%. As for the traditional AIS-based classification method, the best recall rate is 85.2%, the worst 68.9%, and the average 74.05%. The corresponding best, worst, and average false rates are 3.2%, 5.0%, and 4.01%, respectively. Figure 3 shows the performance comparison between the optimized and traditional methods with respect to their recall rates, and the comparison of the false rates is demonstrated in Fig. 4. Figure 3 shows that in our eight experiments, the recall rate of the optimized classification method is lower than that of the traditional one. The range is from 0.4% to 2.3%, and the average drops to 75.2% from 76.4%. Figure 4 shows the false rate of the optimized classification method also decreases in varying degrees. The range is from 2% to 4%, and the average drops from 4.76% to 2.18%.

5 Conclusions

This paper proposes a new e-mail classification method based on the AIS, which is endowed with good diversity and self-adaptive ability. Our method makes use of both the spam and non-spam from training sets, and the number of false positives is reduced. Based on the experiments and analysis, it is very effective in reducing the false rate. However, the disadvantage is that it also decreases the recall rate. How to make an appropriate trade-off between the false rate and recall rate will be a future research topic.

References

1. Ahmed, K.: An Overview of Content-based Spam Filtering Techniques. Informatica 31, 269–277 (2007)
2. Oda, T., White, T.: Developing an Immunity to Spam. In: Cantú-Paz, E., Foster, J.A., Deb, K., Davis, L., Roy, R., O'Reilly, U.-M., Beyer, H.-G., Kendall, G., Wilson, S.W., Harman, M., Wegener, J., Dasgupta, D., Potter, M.A., Schultz, A., Dowsland, K.A., Jonoska, N., Miller, J., Standish, R.K. (eds.) GECCO 2003. LNCS, vol. 2723, pp. 231–242. Springer, Heidelberg (2003)
3. Graham, P.: Better Bayesian Filtering. In: Proceedings of 2003 Spam Conference (2003)
4. SpamAssasin public corpus, `http://spamassassin.apache.org`
5. De Castro, L.N., Timmis, J.: Artificial Immune Systems: a New Computational Intelligence Approach. Springer, London (2002)
6. Freitas, A., Timmis, J.: Revisiting the foundations of artificial immune systems: A problem-oriented perspective. In: Timmis, J., Bentley, P.J., Hart, E. (eds.) ICARIS 2003. LNCS, vol. 2787, pp. 229–241. Springer, Heidelberg (2003)
7. Andrew, S., Freitas, A., Timmis, J.: AISEC: An Artificial Immune System for E-mail Classification. In: Proceedings of the IEEE Congress on Evolutionary Computation, Canberra, Australia, pp. 131–139 (2003)
8. Burim, S., Ohm, S.: Artificial Immunity-based Feature Extraction for Spam Detection. In: Eighth ACIS Conference on Software Engineering, Artificial Intelligence, Networking, and Parallel/Distributed Computing, Qingdao, P.R. China, pp. 359–364 (2006)
9. Chen, C.-L., Gong, Y.-C., Bie, R., Gao, X.Z.: Searching for interacting features for spam filtering. In: Sun, F., Zhang, J., Tan, Y., Cao, J., Yu, W. (eds.) ISNN 2008, Part I. LNCS, vol. 5263, pp. 491–500. Springer, Heidelberg (2008)

10. Bie, R., Jin, X., Xu, C., Chen, C.-L., Xu, A., Shen, X.: Global and local preserving feature extraction for image categorization. In: de Sá, J.M., Alexandre, L.A., Duch, W., Mandic, D.P. (eds.) ICANN 2007. LNCS, vol. 4669, pp. 546–553. Springer, Heidelberg (2007)
11. Oda, T., White, T.: Increasing the Accuracy of a Spam-detecting Artificial Immune System. In: Proceedings of the Congress on Evolutionary Computation, Canberra, Australia, vol. 1, pp. 390–396 (2003)
12. Oda, T., White, T.: Immunity from spam: An analysis of an artificial immune system for junk email detection. In: Jacob, C., Pilat, M.L., Bentley, P.J., Timmis, J.I. (eds.) ICARIS 2005. LNCS, vol. 3627, pp. 276–289. Springer, Heidelberg (2005)
13. Gao, X.Z., Ovaska, S.J., Wang, X., Chow, M.Y.: A Neural Networks-based Negative Selection Algorithm in Fault Diagnosis. Neural Computing and Applications, 17(1), 91–98 (2008)

A New Intrusion Detection Method Based on Antibody Concentration

Jie Zeng, Tao Li, Guiyang Li, and Haibo Li

School of Computer Science, Sichuan University, Chengdu 610065, China
zengjie_0_2001@163.com

Abstract. Antibody is one kind of protein that fights against the harmful antigen in human immune system. In modern medical examination, the health status of a human body can be diagnosed by detecting the intrusion intensity of a specific antigen and the concentration indicator of corresponding antibody from human body's serum. In this paper, inspired by the principle of antigen-antibody reactions, we present a New Intrusion Detection Method Based on Antibody Concentration (NIDMBAC) to reduce false alarm rate without affecting detection rate. In our proposed method, the basic definitions of self, nonself, antigen and detector in the intrusion detection domain are given. Then, according to the antigen intrusion intensity, the change of antibody number is recorded from the process of clone proliferation for detectors based on the antigen classified recognition. Finally, building upon the above works, a probabilistic calculation method for the intrusion alarm production, which is based on the correlation between the antigen intrusion intensity and the antibody concentration, is proposed. Our theoretical analysis and experimental results show that our proposed method has a better performance than traditional methods.

Keywords: Antibody concentration, Antigen intrusion intensity, Antigen-antibody reactions, Intrusion detection, False alarm rate, Detection rate.

1 Introduction

Intrusion detection is a process used to identify abnormal activities in a computer system. Both of Detection Rate (DR) and False Alarm Rate (FAR) are two key attributions for evaluating the performance of Intrusion Detection System (IDS). Generally, traditional methods often sacrifice their FAR to strengthen DR, which means much time and many system resources have to be wasted for dealing with these flooding false alarms [1]. Therefore, finding an effective way to reduce FAR is significant for promoting IDS accuracy.

Recently, many techniques have been proposed for reducing FAR. In 2007, Hamsici et al. [2] proposed a detector training method relied on Naive Bayes (NB). It provides the one-dimensional subspace, where the detection rate error is minimized for intrusion detection problem with homoscedastic Gaussian distribution. In 2008, Hu et al. [3] presented an intrusion detection algorithm based on Multilevel Classifier (AdaBoost). In this algorithm, decision stumps are used as weak classifier. The decision rules are provided for both categorical and continuous features. By combing the

D.-S. Huang et al. (Eds.): ICIC 2009, LNAI 5755, pp. 500–509, 2009.

weak classifier for categorical features into a strong classifier, the relations between these two different types of features are handled naturally, without forced conversions between continuous and categorical features. In 2009, Hu et al. [4] presented an anomaly detection method using Hidden Markov Model (HMM). It has been studied with emphasis placed on system call-based HMM training. An enhanced incremental HMM training framework has been proposed that incorporates a simple data preprocessing method for identifying and removing similar and false subsequences of system calls in real-time.

In order to reduce FAR, the above methods aim at the optimization for detector lifecycle to fit the change of network running environment. However, all of them are lack of anomaly tolerance mechanism: their intrusion alarm is produced by "once detected, once triggering" strategy, which means IDS produces intrusion alarm immediately when an anomaly is detected by system. As a result, system will treat every detected anomaly as the harmful intrusion and increase FAR rapidly. Furthermore, without considering the intrusion destructive effect and the invaded computer importance, system will produce a lot of low accurate intrusion alarms that causing for FAR.

There has a satisfied effect on reducing FAR when the ideas of immunology in Human Immune System (HIS) are used into the intrusion detection domain [5]. In 1994, Forrest et al. [6] presented a Negative Selection Algorithm (NSA) for simulateing the tolerance process of new immune cell in HIS to avoid matching any normal activity. In 2002, Kim [7] proposed an algorithm of Dynamic Clonal Selection (DynamiCS), where the self definition can be changed in real-time and has greatly promoted the research of FAR reduction. In 2005, Li [8] provided an Immune based Dynamic Intrusion Detection model (Idid). Compared with traditional methods, Idid has a better adaptability to the change of network running environment and a lower FAR result.

In modern medical examination, the health status of a human body can be diagnosed by detecting the intrusion intensity of a specific antigen and the concentration indicator of the corresponding antibody from a human body's serum [9]. This diagnosis method is established based on Burnet's Clonal Selection Theory [10]: the HIS consists of a complex set of cells and molecules that protect organs against infection. With many different kinds of lymphocytes (B cell, T cell and so on) distributing all over the human body, the HIS can distinguish nonself from self and then eliminate nonself [11]. Once the affinity that a B cell matches to antigen comes up to a certain threshold, the B cell activates. At this moment, the concentration level of corresponding antibody is so low that human body does not appear any symptom. With expansion at the antigen intrusion intensity, the B cell will clone itself and secrete a lot of antibodies to catch more antigens, resulting in a rapid increase of antibody concentration. When the antibody concentration reaches at a certain level, human body appears some symptoms to warn of the disease, such as cough, inflammation and fever. After the elimination of antigens, the clone proliferation process is suppressed and the antibody concentration is decreased simultaneously [12]. After that, the human body restores its rehabilitation. Therefore, the health status of a human body can be diagnosed by combing the intrusion intensity of all types of antigens and the concentration of all kinds of antibodies. In this paper, inspired by this immune response in HIS, we present a New Intrusion Detection Method Based on Antibody Concentration (NIDMBAC) to reduce FAR without affecting DR. Our method takes advantage

of three processes, including the intrusion confirmation, the harmful intrusion confirmation and the intrusion alarm production whose results are coming from the correlation between the antigen intrusion intensity and the antibody concentration. The method is evaluated using the DARPA intrusion detection dataset [13]. Compared with NB, AdaBoost and HMM, the FAR of our proposed method is reduced by 8.66%, 4.93% and 6.36%, respectively. Our experimental results show that our proposed method has a better performance than previous methods.

The rest of the paper is organized as follows. In Section 2 we describe the definitions and proposed model of NIDMBAC that we have established. Section 3 presents the experimental results of NIDMBAC, followed by conclusions.

2 Definitions and Proposed Model of NIDMBAC

Certain of basic terms employed in this paper are defined below:

Definition 1. *Antigen* (*Ag*) are defined as the n-dimensional vectors of network activity features composed of Internet Protocol (IP) addresses, port number, protocol type, TCP/UDP/ICMP fields, the length of IP packets, etc. The structure of an antibody is the same as that an antigen. It is given by

$$Ag = \{a \mid a \subset f, f = \{f_1, f_2, \cdots, f_n\}^l, f_n \in [0,1], l > 0\}. \tag{1}$$

Definition 2. *Self antigens* (*Self*) are normal elements in IP packets, including normal sanctioned network service transaction dataset, no malicious background clutter dataset and so on. It is given by

$$Self = \{< s, rd > \mid s \in f, rd \in \mathbb{R}\}, \tag{2}$$

where s is a n-dimensional vector of network activity features, rd is the self radius and $\mathbb{R}$ is the real number set. System allows variability of each self element is specified by its self radius.

Definition 3. *Nonself antigens* (*Nonself*) are intrusions in IP packets. We have

$$Nonself = \{< s, rd > \mid s \in f, rd \in \mathbb{R}\}, \tag{3}$$

where s is a n-dimensional vector of network activity features, rd is the nonself radius and $\mathbb{R}$ is the real number set, such that

$$Self \bigcup Nonself = Ag, \tag{4}$$

$$Self \bigcap Nonself = \varnothing. \tag{5}$$

Definition 4. *Detector set* (*D*) simulates B cells in HIS for detecting antigens defined

$$\begin{aligned} D = \{< ab, rd, aff, den, cos, count, age > \mid ab \in f, \\ (rd, aff, den, cos) \in \mathbb{R}, (count, age) \in \mathbb{N}\}, \end{aligned} \tag{6}$$

where *ab* is the antibody that represents a n-dimensional vector of network activity features, *rd* is the detection radius of detector, *aff* is the affinity of detector, *den* is the density of detector, *cos* is the costimulation of detector, *count* is the antigen number matched by *ab*, *age* is the age of detector, $\mathbb{R}$ is the real number set and $\mathbb{N}$ is the natural number set. The above parameters are calculated in our previous work (see the ref. [14]).

2.1 Antigen Classified Recognition

The task of antigen classified recognition is discriminating intrusion (nonself antigen) from normal element (self antigen) by the primary immune response in NIDMBAC.

Detector Maturation. In order to avoid matching any self antigen, newly created detectors in an immature detector population should be tested by a negative selection operator immediately after their birth. As seen in the related work, a negative selection operator to given self antigens. From this comparison, if an immature detector matches to any self antigen during a predefined time period, this immature detector should be removed from an immature detector population. After that, the detector is matured. The process of detector maturation is given by Equation (7).

$$Mature(x) = \begin{cases} 1, & x.age > \omega \wedge \forall y \in Self \wedge \sqrt{\sum_{k=1}^{n} (x.ab_k - y.s_k)^2} > x.rd, \\ 0, & otherwise, \end{cases} \tag{7}$$

where $x \in D$ and ω is the predefined time period for the process of detector maturation. Equation (7) shows if the function $Mature(x)$ is equal to 0, in which the detector lies within the range of normal space, the detector is invalid and should be removed. Let T be the mature detector population given by

$$T = \{x \mid x \in D, Mature(x) = 1\}. \tag{8}$$

Detector Activation. Mature detectors, which have gained tolerance against self antigens. Each mature detector attempts to match to new antigens but when a mature detector matches any new antigen, it does not immediately regard the detected antigen as nonself. Instead, it continues attempting to match more new antigens until it matches to a sufficient number of new antigens. After that, the detector is activated. When detectors are activated, they send "anomaly appearance" signals to other detectors. The process of detector activation is given by Equation (9).

$$Activate(x) = \begin{cases} 1, & x.age \le \sigma \wedge x.count \ge \tau, \\ 0, & otherwise, \end{cases} \tag{9}$$

where $x \in T$ and σ is the predefined time period for the process of detector activation and τ is the detector activation threshold. If the antigen matched count satisfies the activation threshold before the age of a mature detector reaches the predefined time period, the mature detector activates.

Detector Memorization. Activated mature detector provides an anomaly detection signal and the detected antigens to system for further checking. If the detector receives a costimulation signal from system is greater than a specified value within a limited time, the mature detector immediately become memory one. After that, memory detector can recognize this anomaly as a type of nonself antigen definitely. The process of detector memorization is given by Equation (10).

$$Memorize(x) = \begin{cases} 1, & x.age \le \theta \wedge x.cos \ge \lambda, \\ 0, & otherwise, \end{cases} \tag{10}$$

where $x \in T$ and θ is the predefined time period for the process of detector memorization and λ is the detector memorization threshold. Let M be the memory detector population given by

$$M = \{x \mid x \in D, Mature(x) = 1 \wedge Activate(x) = 1 \wedge Memorize(x) = 1\}. \tag{11}$$

At the same time, we have

$$T \cup M = D, \tag{12}$$

$$T \cap M = \varnothing. \tag{13}$$

2.2 The Change of Antibody Number

According to this secondary immune response in HIS, we present a calculation method to compute the change of antibody number in real-time. We divide the secondary immune response into two phases, including antibody number accumulation and antibody decrement. In NIDMBAC, when memory detector clones, we increase its antibody number. However, if a memory detector does not match any antigen during antibody number maintaining period (γ), its antibody number will be decreased to zero, which means this type of intrusion has been eliminated. However, if a memory detector matches an antigen again during a period of γ, its antibody number will be accumulated, which means this type of intrusion increases continually.

Antibody Number Accumulation. If intrusions are continuous, the antibody number rapidly accumulates under the exciting process of clone proliferation in the memory detector population.

Consider a system composed of detector subpopulations, D_i, $i = 1, \cdots, n$. Each subpopulation when memorized grows according to

$$\frac{\partial D_i}{\partial t} = S_{new} + S_{clone} R_{mem} D_i, \tag{14}$$

where S_{new} is the rate of generation of new D_i detectors in system, S_{clone} is the memory detectors clone rate and R_{mem} is the memorization ratio of D_i.

When memorized, D_i secretes antibody ab_i, at rate $S_i(t)$. Because there is a memorization period before antibody secretion, we assume

$$\frac{\partial S_i}{\partial t} = S_{mem}(S_{max\_secrete}R_{mem} - S_i), \tag{15}$$

where $S_{max\_secrete}$ is the maximum rate of antibody secretion and S_{mem} determines the rate of memorization. At times long compared with $1/S_{mem}$, the secretion rate is approximately $S_{max\_secrete}R_{mem}$.

According to the definition of the density of detector, the antibody number, num_i, accumulation of ab_i is given by Equation (16).

$$\frac{\partial num_i}{\partial t} = S_i D_i - S_{abb} den_i num_i, \tag{16}$$

where S_{abb} is the rate of ab_i that bound by other antibodies. From Equations (14) to (16), we know that the larger and the more diversified memory detector population has, the more specific antibodies can be secreted to eliminate antigens.

Antibody Number Decrement. If intrusions are stop, the antibody number decreased under the suppressed process of clone proliferation in the memory detector population. The antibody number, num_i, decrement of ab_i is given by Equation (17).

$$\frac{\partial num_i}{\partial t} = (1 - \frac{1}{\gamma - age_i})num_i, \tag{17}$$

where age_i is the age of D_i.

2.3 Intrusion Alarm Production

In modern medical examination, the health status of a human body can be diagnosed by detecting the intrusion intensity of a specified antigen and the concentration indicator of the corresponding antibody from a human body's serum. Synthesizing the intrusion intensity of all types of antigens and the concentration of all kinds of antibodies, a disease can be analyzed. According to this relationship between the antigen intrusion intensity and the antibody concentration, a probabilistic calculation method for intrusion alarm production is established.

The probability of intrusion alarm production is related to four factors, including the antibody concentration of memory detector, the antigen matched count of memory detector, the intrusion destructive effect and the invaded computer importance. At time *t*, the probability of intrusion alarm production is given by Equation (18), where *v* is the adjusted coefficient, *con(t)* is the antibody concentration of memory detector population at time *t* and *intru(t)* is the antigen matched count of memory detector population at time *t*.

$$P_{alarm}(t) = \min\{1 : \upsilon \cdot con(t) \cdot intru(t)\}, \tag{18}$$

where $con(t)$ and $intru(t)$ is shown in Equations (19) and (20).

$$con(t) = \frac{2}{1 + e^{-\mu \sum_{j=1}^{m} x_j \sum_{i=1}^{n} y_i num_i(t)}} - 1, \tag{19}$$

where μ is the antibody concentration adjusted coefficient, x_j is the weight of *jth* invaded computer importance, y_i is the weight of *ith* type intrusion destructive effect.

$$intru(t) = \sum_{j=1}^{m} \sum_{i=1}^{n} \sum_{x \in M_i} x.count(t), \tag{20}$$

where M_i is the *ith* type of memory detector population.

3 Experimental Results

The simulation experiments are carried on the DARPA intrusion detection dataset to test the performance of IDS.

3.1 The Change of Antibody Concentration Experiment

The NIDMBAC monitors three computers (computer1, computer2, computer3), which are given the invaded computer importance as x_1 is equal to 0.6, x_2 is equal to 0.1 and x_3 is equal to 0.3. We launch LAND intrusion (y_1 is equal to 0.6) to computer1 and computer2, at the same time, computer3 is assaulted by DoS intrusion (y_2 is equal to 0.4). Figs. 1 to 4 show the change of antibody concentration, which is produced from the stimulation of these intrusions and a specific intrusion that the whole network and a specific computer face, is calculated by Equation (19). From Figs. 1 to 4, we see that, when the antigen intrusion happens and the antigen intrusion intensity increases, the corresponding antibody concentration also increases synchronously. Furthermore, when the antigen intrusion intensity decreases, the corresponding antibody concentration also decreases synchronously

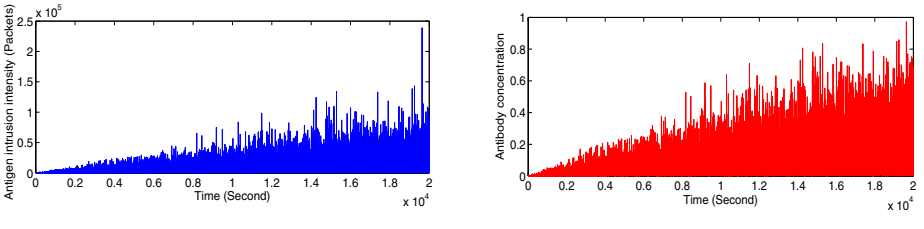

(a) (b)

Fig. 1. (a) Antigen intrusion intensity on Computer1, (b) Antibody concentration on Computer1

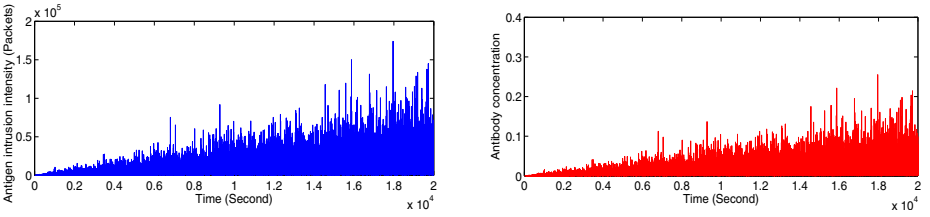

(a) (b)

Fig. 2. (a) Antigen intrusion intensity on Computer2, (b) Antibody concentration on Computer2

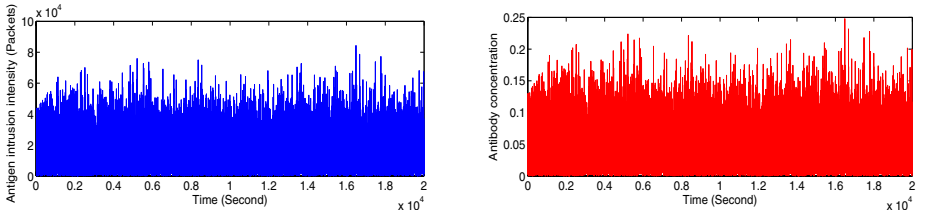

(a) (b)

Fig. 3. (a) Antigen intrusion intensity on Computer3, (b) Antibody concentration on Computer3

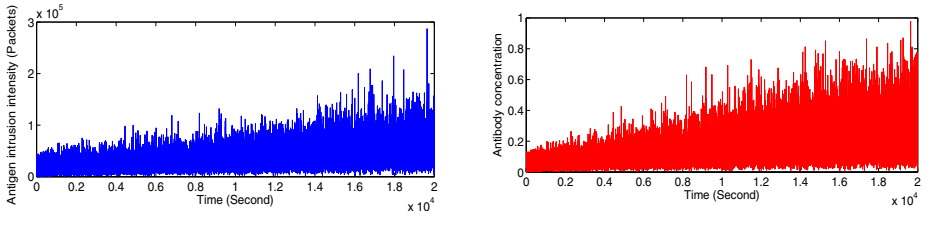

(a) (b)

Fig. 4. (a) Antigen intrusion intensity on Network, (b) Antibody concentration on Network

3.2 Intrusion Alarm Production Experiment

We calculate the probability of intrusion alarm from the experimental results of Section 3.1 according to Equation (18). The probability of intrusion alarm production on invaded computers, intrusions and the whole network are shown in Figs. 5 to 8, whose curve tendency is changing with the antibody concentration and the antigen intrusion intensity. According to the experimental results, we know that the antibody concentration and the antigen intrusion intensity can provide reliable evidence for producing intrusion alarm.

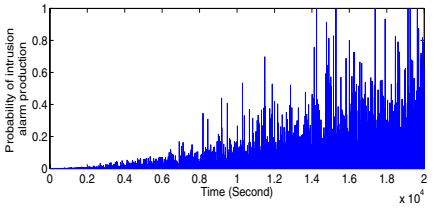

Fig. 5. Probability of intrusion alarm production on Computer1

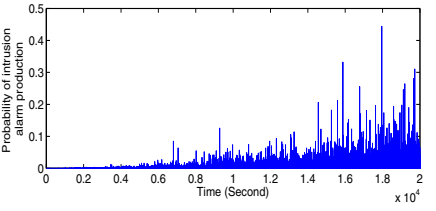

Fig. 6. Probability of intrusion alarm production on Computer2

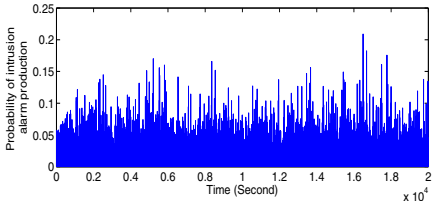

Fig. 7. Probability of intrusion alarm production on Computer3

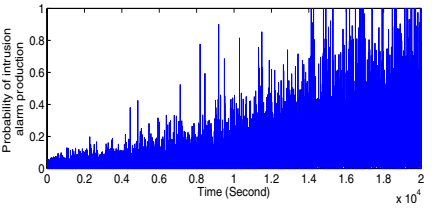

Fig. 8. Probability of intrusion alarm production on Network

3.2 FAR Reduction Experiment

We do the comparison experiment to prove NIDMBAC can reduce FAR effectively. Table 1 shows the comparison experimental results among NIDMBAC, NB, AdaBoost and HMM, the FAR of NIDMBAC is reduced by 8.66%, 4.93% and 6.36%.

Table 1. The comparison between NIDMBAC and other methods on FAR

Method	*Detection Rate*	*False Alarm Rate*
NIDMBAC	95.62% ~ 96.06%	1.95% ~ 4.04%
NB	96.81% ~ 97.21%	7.94% ~ 12.70%
AdaBoost	90.04% ~ 90.88%	6.55% ~ 8.97%
HMM	95.16% ~ 96.00%	1.33% ~ 10.40%

4 Conclusions

In NIDMBAC, the concept of antibody concentration in HIS has been abstracted and extended, and a new method based on antibody concentration for intrusion detection has been presented. In contrast to the traditional methods, NIDMBAC not only has the intrusion detection ability while system is invaded, but also can effectively reduce false alarm rate without affecting detection rate and has strong ability for detecting DoS intrusion. Concretely, Our proposed method can calculate the types, number and intensity of intrusion quantitatively in real-time, produce intrusion alarm signal

according to the correlation between the antibody concentration and the antigen intrusion intensity to warn of the harmful intrusion, avoid alarm flood that caused by the "once detected, once triggering" strategy of traditional methods.

Acknowledgements

This paper was supported by the National Natural Science Foundation of China (Nos. 60573130, 60502011 and 60873246), the National High-Tech Research and Development Plan of China (No. 2006AA01Z435) and the National Research Foundation for Doctoral Program of Higher Education of China (No. 20070610032).

References

1. Kemmerer, R.A., Vigna, G.: HI-DRA: Intrusion Detection for Internet Security. IEEE Transactions on Signal Processing 93, 1848–1857 (2005)
2. Hamsici, O.C., Martinez, A.M.: Bayes Optimality in Linear Discriminant Analysis. IEEE Transactions on Pattern Analysis and Machine Intelligence 30, 647–657 (2008)
3. Hu, W.H., Hu, W., Maybank, S.: Adaboost-Based Algorithm for Network Intrusion Detection. IEEE Transactions on Systems, Man and Cybernetics. 38, 577–583 (2008)
4. Hu, J.K., Yu, X.H., Qiu, D.: A Simple and Efficient Hidden Markov Model Scheme for Host-Based Anomaly Intrusion Detection. IEEE Network 23, 42–47 (2009)
5. Forrest, S., Hofmeyr, S.A.: Computer Immunology. Communications of the ACM 40, 88–96 (1997)
6. Forrest, S., Perelson, A.S.: Self-nonself Discrimination in a Computer. In: 1994 IEEE International Symposium on Security and Privacy, pp. 202–212. IEEE Press, Oakland (1994)
7. Kim, J., Bentley, P.: Toward an Artificial Immune System for Network Intrusion Detection: An Investigation of Dynamic Clonal Selection. In: 2002 IEEE Congress on Evolutionary Computation, pp. 1015–1020. IEEE Press, Honolulu (2002)
8. Li, T.: An Immune Based Dynamic Intrusion Detection Model. Chinese Science Bulletin 50, 2650–2657 (2005)
9. Mullighan, C.G., Philips, L.A., Su, X.P.: Genomic Analysis of the Clonal Origins of Relapsed Acute Lymphoblastic Leukemia. Science 322, 1377–1380 (2008)
10. Burnet, F.M.: The Clonal Selection Theory of Acquired Immunity. Cambridge University Press, New York (1959)
11. Han, B.R., Herrin, B.R., Cooper, M.D.: Antigen Recognition by Variable Lymphocyte Receptors. Science 321, 1834–1837 (2008)
12. Wrammert, J., Smith, K., Miller, J.: Rapid Cloning of High Affinity Human Monoclonal Antibodies against Influenza Virus. Nature 453, 667–672 (2008)
13. Aydin, M.A., Zaim, A.H., Ceylan, K.G.: A Hybird Intrusion Detection System Design for Computer Network Security. Computers and Electrical Engineering 35, 517–526 (2009)
14. Zeng, J., Zeng, J.Q.: A Novel Immunity-Based Anomaly Detection Method. In: 2008 International Seminar on Future Biomedical Information Engineering, pp. 195–198. IEEE Press, Wuhan (2008)

Research of the Method of Local Topography Rapid Reconstructed

Minrong Zhao[1], Shengli Deng[2], and Ze Shi[1]

[1] The Science Institute, Air-Force Engineering University, Xi'an, 710038, China
[2] Air-Force 93861 Army, Sanyuan, 713800, P.R. China
zhaominrong1965@sina.com

Abstract. For fast and convenient access to the environment based on the geomorphic characteristics of camouflage regional model for the complexity of topography, this article analyzes a variety of terrain modeling method's advantages and limitations, discussed a variety of modeling methods in the set up of the study of basic on the hybrid modeling method and the integrated use of research results to generate the details of the existing landform characteristics can be controlled on all-terrain results. Generate local terrain adaptive modeling method, as a regional model disguised form with the local terrain topography of the region to adapt to a good camouflage effect.

Keywords: Terrain model, Surface integration, Fractal model, Disturbance.

1 Introduction

Three-dimensional terrain accurate modeling to environment for all-terrain, are one of the key technologies in simulation and virtual, that is widely used in various different areas of the terrain model needs.

With the development of means of reconnaissance and surveillance technologies enhance traditional methods of camouflage for protection can easily be identified and targeted by precision-guided weapons, people have begun to study the method of camouflage based on the environmental characteristics the topography. Express, accurate, efficient generation and positions around the geomorphic environment integration and can be camouflaged with the object of the camouflage to match the regional geomorphology, the guidance of weapons and equipment for self-adaptive camouflage of great significance.

Traditional methods because of disguised algorithm and the technology itself the characteristics and limitations, together with the positions at the complexity of topography and irregular, and the existing topography of the simulation algorithm are under certain conditions or against some object that has applicability .

To this end in accordance with the characteristics of landform position, combined with existing algorithms and technologies, A fractal technology directly to the existing methods used to generate the surface disturbance, with the surrounding environment to generate topography camouflage integration model to meet the needs of a good camouflage.

D.-S. Huang et al. (Eds.): ICIC 2009, LNAI 5755, pp. 510–516, 2009.

2 Currently Used Methods of Terrain Modeling Analysis

2.1 Mathematical Characteristics of the Real Terrain

So far, none has a theory derived from a purely mathematical characteristics of the real terrain Ways, many geophysicists summed up the real terrain and math-related characteristics from across the wide range of temporal and spatial scales of topographic data analysis [1], there are as follows:

- the fractal dimension;
- multi-level fractal.
- anisotropy.
- must scale the scope of statistical self-similarity

$$p(X(t) < x) = p(X(\gamma t) < \gamma^a x.$$

- variation Satisfied bad $E[X(t+h) - X(t)]^2 = k|h|^{2a}$.
- profile power spectral density Satisfied $G(\omega) = 2\pi k\omega^{-a}$.
- non-stationary process.
- incremental smooth.

Topography simulation problem to be solved is how to construct the terrain model, so that the model as much as possible with the above characteristics, or math with the practical application of the field of math required characteristics.

2.2 Commonly Used Methods of Terrain Modeling [2]

1) The simplest data model of mountains are sparse distribution of points from some of the elevation value of the triangle pose a number of easy-plane to form a topographic framework, according to the triangle affixed to mountains texture map. This method can be controlled through the location of sparse the point acheived the purpose of control, but because of the formation of the framework was too sketchy and cartoon graphics finally make very obvious effects, felt the impact of the real terrain.

2) Fractal geometry with infinite details and statistical self-similarity of the typical characteristics, it is using the recursive algorithm to make complex features that simple rules can be used to generate, in a variety of existing fractal Brownian motion method implementation, MPD method because algorithm is simple, easy to implement and achieve faster and been widely used. Surface Fitting Method

3) With spline interpolation and surface fitting method for fitting data points to form a smooth connection, can improve the effect, but the lack of details of the irregular terrain description, which is characterized by realistic terrain where.

4) Improved algorithm

In order to increase the realistic effects, in fitting out to be perturbations on the surface, forming a more realistic surface topography. Perturbation method used in one of those who shape interpolation and multi-resolution stochastic approach (mulrtiesolutinostoehastie relaxtion) and so on. One of sub-J-zhen interpolation method is the use of IFS (Iteration Funetion Sysrem) Ways constructed fractal interpolation

function. Multiresolution stochastic relaxation method combining the spline surfaces of the structure, requires energy optimization method structure spline surfaces to achieve a large quantity of calculation, more complex.

A variety of modeling methods study to the development of topographic maps to build had a positive impact, and for further research provides a theoretical reference and methods of drawing. But there are some inadequacies and weaknesses, mainly embodied in the following ways:

l) With a method for different types of lack of systematic geomorphology. The vast majority of modeling algorithms are targeted at specific regions and applications launched, but the actual terrain is often a variety, different landforms on the model of the requirements are not the same, so how can we reasonably effective use of these methods has become Can not not consider the question.

2) To different modeling methods lack of research of adaptive law. There has been no response to a landform type, using the same modeling algorithm to examine the geomorphological type of modeling algorithm for determination of what is best. There is therefore necessary to study the adaptability of the law of modeling side of the terrain modeling for the future provide a valuable reference.

3 FBM Mathematical Characteristics [3]

We demand that the camouflage regional topography Analog pursue FBM incremental are stable and self-similarity, the product of such of its statistical topography is consistent. FBM are defined in a probability space on a stochastic process X : $[0,\infty] \to R$, and meet the following conditions:

(a) With probability 1, $X(1)$ continuous and X (0) = 0.

(b) for any $t \geq 0$ and $h \geq 0$, $X(t+h) - X(t)$ subject to the following distribution:

$$p((X(t+h) - X(t) < x) = 1 \tag{1}$$

$$p((X(t+h) - X(t)) < \frac{1}{\sqrt{\pi h^a}} \int_{-\infty}^{1} \exp[\frac{-u^2}{2h^{2a}}]du \quad 0 < \alpha < 1 \tag{2}$$

1) FBM steady incremental

Eqn.(1) shows that the distribution $X(t+h) - X(t)$ has nothing to *t*, so the conclusions that PBM with the establishment of steady incremental

2) FBM statistical self-similarity

$$\begin{aligned} p((X(t+h) - X(t) < x) &= \frac{-u^2}{\sqrt{2\pi h^{2a}}} \int_{-\infty}^{1} \exp[\frac{-u^2}{2h^{2a}}]du \\ &= \frac{1}{\sqrt{2\pi(\gamma h)^a}} \int_{-\infty} \exp[-\frac{u_1^2}{2(\gamma h)^{2a}}]du = p((\gamma t + \gamma h) - X(\gamma h) < \gamma^a x) \end{aligned} \tag{3}$$

Type on both sides of the check t = 0, then h will be replacement for t:

$$p(X(t) < x) = p(X(\gamma t) < \gamma^a x \tag{4}$$

Namely the so-called statistical self-similarity.

In addition, FBM have five at the nature of the terrain to meet the actual characteristics of the math. herefore, from the principle of speaking, using the method of fractal interpolation surface generated FBM Analog terrain has a good degree of realism and confidence. However, because of the fractal with infinite details and statistical self-similarity of the typical characteristics, but also that it is using the recursive algorithm allows complex scenes to use the law to generate easy, but the real terrain are anisotropic, according to the above-mentioned principle of simulated terrain are isotropic and, therefore, necessary to further study how to construct there is the direction of the characteristics of simulation methods; real terrain fractal features are globally inconsistent, but the principle of simulation of the topographical features are globally consistent, therefore, required further study DEM data sets for the sub-block, taken from the various local characteristics of the fractal in order to achieve some form terrain Analog Board.

Surface reconstruction is how to ensure that the reconstruction of the surface by the object can best reflect the actual shape; how to speed up the rate of surface reconstruction. Any single modeling method meets difficultly this demand. Therefore, we discuss the application of a variety of hybrid modeling method, mixed modeling method set up in front of the basis of the study, including research findings on the use of the General.

4 Modeling Methods and Results of the Integrated Use of Methods

Realistic terrain and topography are generated controllability study the direction of two parallel, if a combination of both well and may be better to describe the natural shape of the complexity and irregularity. Although MPD and surface modeling method can achieve built on the surface model of control in a way, but because of MPD with the increasing iterative the levels constantly Express generated terrain details can not be reached on the overall shape of the control, but also because of surface modeling method while on the surface of the model set up to achieve the overall control but unable to achieve the purposes of local thinning slightly less than the reason, thus to consider the implementation of both the organic integration ,take full advantage of modeling method of different landscape characteristics, and generated the corresponding source surface as the control surfaces, and the MPD-generated terrain Ways to integration, to achieve the data model of the terrain and topography can control the details of the purpose, that is both controllable randomness yet again is a completely controllable between the generation and randomly generated between the methods. Use this source more or less the shape and surface refinement noodle MPD could be ups and varying the terrain shape, can achieve the purpose of a combination of both, that is, the integration surface methodology.

1 Integration of the basic principles of [2]

At more or less has been with the shape of surface topography, how to integrate MPD into one of Ways? In the usual two-dimensional MPD approach, if a point $X(x, y)$ based data gridin, the elevation of value $Z(x, y)$, then

$$Z(x, y) = f(x, y) + D(x, y) \tag{5}$$

where $D(x, y)$ is one the random of points (x, y) are offset, it is a mean 0, variance σ^2 for the Gaussian random variable. But $f(x, y)$ is the average of point (x, y) around the neighborhood points

$$F(x, y) = \frac{Z(x-1, y+1) + Z(x+1, y+1) + Z(x-1, y-1) + Z(x+1, y-1)}{4} \tag{6}$$

Now has roughly the shape of the surface topography as a locus of control surfaces, and ensure that it and eventually want to generate the data model matrix with the same number of ranks.

MPD at two-dimensional methods, if Matrix is generated based $n \times n$, (n for the ranks of a few) Iteration $n = 2^{\max level} + 1$ is n and the total rise $\max level$ is the relationship between, This control surface with the MPD source of the data points are one-to-one, so that to achieve true integration, rather than a simple superposition of the two surfaces.

Set of control surfaces for the data matrix Y, Its up to a certain point $Y(x, y)$, MPD methods with the corresponding data generated by the existence of a deviation of this difference for the set, that is,

$$offset = Y(x, y) - Z(x, y) \tag{7}$$

$X(x, y)$ Are finally point elevation values, ω are the right factors. Clearly, then $\omega \to 0$ surface near MPD surface, $\omega \to 1$ which means the surface will eventually get closer to the control surface. When ω near l / 2, the surface for the control of the control sources and two-dimensional surface of the mean MPD.

5 Examples of FBM Terrain Topography and Several Terrain Modeling to Generate Integration

The following are examples that separately for different terrain features to take the corresponding methods to generate the surface with MPD ways to generate of conduct disturbance.

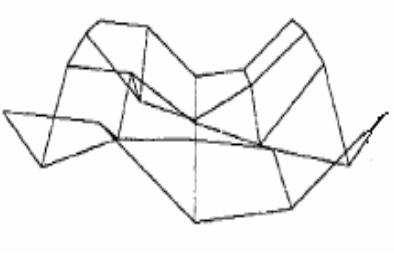

Fig. 1. The MPD graph when Iteration level mxaIveel = 2

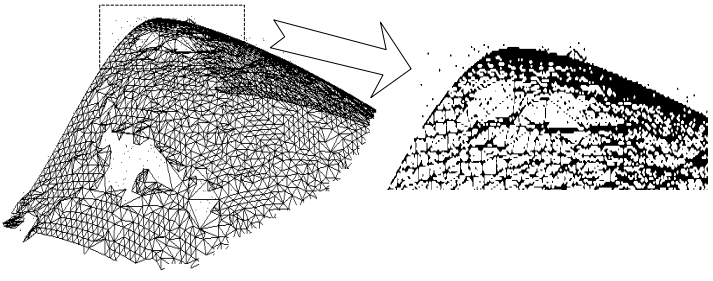

Fig. 2. Drawing Spaces scattered point cloud map

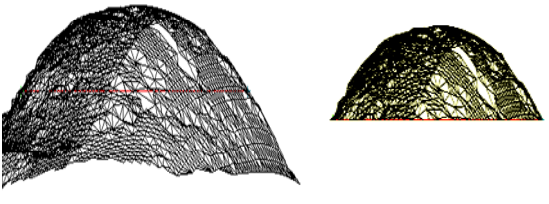

Fig. 3. After integration of graphics

Fig. 4. Gaussian law of the source drawing surface

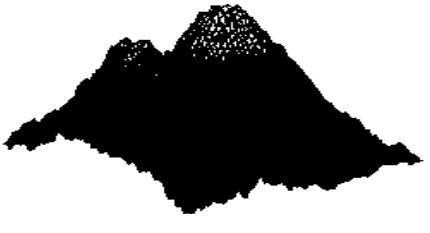

Fig. 5. Surface integration

Fig. 1 for the iteration when the level $\max level = 2$ of MPD map, Immediately at this time of the source grid surface Fig. 2 into the one of the data matrix, which uses gridded surface data matrix of Fig. 2, alternative methods are usually produced by MPD Fig. 1 the elevation data, and then, on the basis of continue iteration until it reaches the required depth of the iteration until after Fig. 3 for the integration of graphics. Fig. 4 is the control of the source surface modeling method with Gaussian-generated graphics, Fig. 5 are the result of graphical integration with MPD Fig. 1.

6 Experiment

Environment for all-terrain three-dimensional terrain accurate modeling, are one of the key technologies in the simulation and virtual. For the complexity of topography and non-regularity, in order to meet the needs of different areas of the terrain model of the demand made up for with the iterative method ,because of MPD increased levels continuously Express to generate topographic details could not be reached on the overall shape of the control status, also overcome the surface modeling method while on the surface of the model set up to achieve the overall control but unable to achieve the purpose of local refinement, so the more rapid, accurate, and convenient access to the surrounding environment combining geomorphic model to meet the good camouflage camouflage needs.

7 Conclusion

This paper analyzes a variety of terrain modeling method's advantages and limitations, discussed a variety of modeling methods in the set up of the study of basic on the hybrid modeling method and the integrated use of research results to generate the details of the existing landform characteristics can be controlled on all-terrain results. Generate local terrain adaptive modeling method, as a regional model disguised form with the local terrain topography of the region to adapt to a good camouflage effect.

References

1. She, L.H.: FBM-based Fractal Terrain Simulation Principle Study. Aviation Journal (1999)
2. Kang, X.Q.: MPD-based Method of Study of Mountain Terrain Generation. Northwestern Polytechnical University Master's degree thesis (2005)
3. Qin, X.Y., Bu, B.: Based on Fractal Theory of Micro-topography Reconstruction. National University of Defense Technology Journal 25(5) (2003)
4. Xu, D., Jin, B.: Scattered Points Based on Grid-based Topographic Maps Controllable Technology [J]. Journal of Engineering Graphics 26(4), 119–123 (2005)
5. Falconer, K.: Fractal Geometry-mathematical Foundations and Applications. John Wiley &Sons, New York (1990)

A Novel User Created Message Application Service Design for Bidirectional TPEG

Sang-Hee Lee and Kang-Hyun Jo

School of Electrical Engineering, University of Ulsan,
102 Daehakro Nam-gu, Ulsan, Korea
{shlee,jkh2009}@islab.ulsan.ac.kr

Abstract. The T-DMB (Terrestrial-Digital Multimedia Broadcasting) is the national service, currently successful in use in Korea since 2008. Among other services, TPEG (Transport Protocol Experts Group) service has been spotlighted in the aspects of creating earnings. At present, TPEG service is not so popular as it fails to satisfy the user's demands on various aspects. Thus, the variety of services including bidirectional service is necessary in stage of DMB2.0. In this paper, the limitations of existing TPEG-POI (Point of Interest) application service using the wireless communication network are indicated. To overcome such limitations, we propose a business model for TPEG-UCM (User Created Message) application service which uses individual bidirectional media. The experiment shown in this paper proves the usability and operability of the proposed method, suggesting that the implementation of the proposed method would be overcome a lack of variety and unidirectional of existing TPEG application.

Keywords: TPEG, TTI, DMB, Bidirectional, Interactive.

1 Introduction

The T-DMB (Terrestrial–Digital Multimedia Broadcasting) is an ETSI (European Telecommunication Standard Institute) standard which extends the Eureka-147 Digital Audio Broadcasting (DAB) standard to improve the capability of the mobile video streaming service [1-3]. The world's first commercial T-DMB service has been launched around Seoul metropolitan area of Korea in December 1, 2005 with a hope for a future growth engine. At the present of 2009, the T-DMB service has covered national region with full-scale service. The number of receiver has reached 15 million since August 2008, and is estimated to reach 20 million by 2009 [4, 5]. As the dramatic uprising in the population, the T-DMB service itself is regarded quite successful in the market.

In spite of that, T-DMB service providers carry a considerable amount of financial burden, as the T-DMB service is free of charge with advertisement as main source of income. As a result, it makes difficult to survive in the market. Thus, T-DMB data services have been spotlighted in the aspects of creating earnings. Especially, TPEG (Transport Protocol Experts Group) service is proposed as a killer application among other data services.

D.-S. Huang et al. (Eds.): ICIC 2009, LNAI 5755, pp. 517–526, 2009.

The TPEG is an international protocol in order to provide TTI service and was developed by EBU (European Broadcasting Union) [6]. TPEG application services based on the T-DMB in Korea has been commercialized by main service providers in Seoul metropolitan area of Korea since the second half of 2005 [7-10]. At present, TPEG service is not so popular as it fails to satisfy the user's demands on various aspects. Accordingly TPEG forum in Korea have pronounced the TPEG-POI (Point of Interest) application service to deliver new TTI service [11]. However, there are several limitations in existing TPEG-POI application service using the wireless communication network.

First, the TPEG-POI application service includes the contents of interesting points for drivers or travelers such as roads, restaurants, hotels, hospitals, banks, etc [12]. As its service sphere is too wide, it is necessary to develop a specialized service user-friendly within the limited travel information sphere. Second, in order to update seamlessly the POI data on service provider side, it is necessary to put additional cost and time. Web has many contents and is updating seamlessly even in now and future. Thus, if a service provider uses the LBS (Location Based Service) website such as the panoramio of google, the story map of cyworld, etc, the POI data may be updated seamlessly with small cost and time.

In this paper, we propose a new TPEG-UCM (User Created Message) application service as a business model combined T-DMB with wireless communication network like CDMA (Code Division Multiple Access) or WiBro (Wireless Broadband) [13]. The proposed TPEG-UCM service may overcome a lack of variety of existing TPEG application services and it is realized the bidirectional interactive TPEG service on T-DMB in stage of DMB2.0 as in the sphere of Web2.0.

This paper is organized as follows. In section 2, we present a scenario, and a system structure of business model for TPEG-UCM application service. In section 3, we propose a structure of proposed application service protocol which is interoperable with existing TPEG application services. In section 4, experimental results are provided by showing an example of the authoring tool and the decoding tool suitable for the TPEG-UCM application service in mobile phone. Finally, the brief conclusion on the effectiveness of the proposed service and the future work on another interactive service contents by user such as UCC (User Created Contents) are given in section 5.

2 The Proposed Business Model for TPEG-UCM Application Service

2.1 The Scenario of TPEG-UCM Application Service

The service flow of the proposed business model for TPEG-UCM application service is shown in detail in Figure 1. The proposed business model for TPEG-UCM application service consists of contents provider layer, DMB service layer, return channel layer, and DMB user layer.

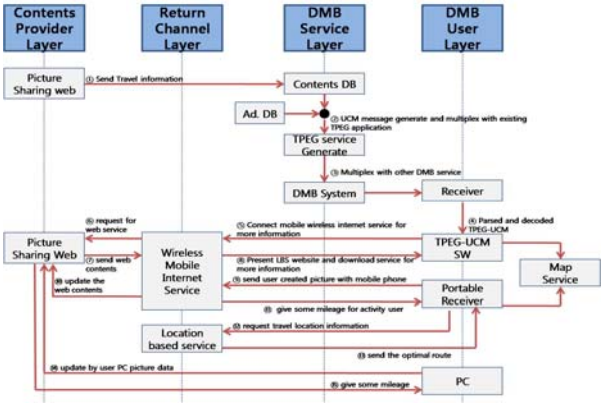

Fig. 1. The service flow of the proposed business model for TPEG-UCM application service. The proposed business model for TPEG-UCM application service consists of contents provider layer, DMB service layer, return channel layer, and DMB user layer [13].

The LBS information created by the user of the contents provider layer is transferred to the DMB service layer, and the information is saved in the database by the proposed protocol for TPEG-UCM application service. Then DMB service layer reads data from this contents database and banner ad database for creating earnings, and encodes them into the proposed UCM message. TPEG-UCM message is transferred to DMB user layer with video and audio service, other data services, and existing TPEG services.

The DMB user layer use TPEG-UCM application service parsed and decoded in the receiver. According to the request from the user, the additional information is sent to the receiver through the wireless communication internet service of the return channel layer. More active users transfer newly created travel information to the contents provider layer. They can also easily find the required location by optimal route service with inner map of the receiver. In the following, the example of service scenario is further explained.

A businessman in Seoul has an appointment to do a business presentation for his client in Ulsan, which is approximately 300km southeast from Seoul. He arrived around half an hour earlier than the appointment. For his ice-breaking, he wanted to take a short trip around in Ulsan to view scenery. He started TPEG-UCM application service with his car navigation. After searching the lists, he selected to see around 'spring news in Ulsan'. The list presented a travel information such as beautiful spring flower pictures of 'The theme botanic gardens and arboretum', writer, region, date, etc. Below the list, it showed the banner ad of local area.

He clicked 'view more' menu to view other pictures, and connected to the wireless communication internet service. He then searched LBS websites, like the story map of Korean popular mini-blog cyworld. After searching for more pictures which were taken at 'The theme botanic gardens and arboretum' in Ulsan, he decided to visit

there. Henceforth, he clicked 'map' menu to fine routes. He knew a few of routes with the transferred location information and with the car navigation inner map, he was able to visit 'The theme botanic gardens and arboretum' in Ulsan.

There he appreciated the well arranged and gardened beautiful flowers. Thus, he took a picture with his mobile phone incorporated camera. He wanted to upload the pictures at LBS websites and used wireless internet service in his mobile phone, and transferred the location information, picture, and travel information. Consequently, LBS website data was updated instantly. In addition, the pictures sent by the user acquired some mileage from the website, and he had many benefits such as getting some discounts on the phone bill. The return channel layer bills to the user for wireless internet service. This fee shares the return channel layer, the DMB service layer, and the contents provider layer. Also, DMB service layer creates benefits from hosting new ad using sending the banner ad of local area.

As shown in the above scenario, the travel information created by the user on the LBS website is transferred by TPEG application service on T-DMB. And the mobile communication meets use's request for more information. As a result, it may be overcome a lack of variety of existing TPEG application services, and realized the bidirectional interactive T-DMB service in stage of DMB2.0.

2.2 The System Structure of TPEG-UCM Application Service

The whole system of the business model for TPEG-UCM application service is shown in Figure 2. The contents provider layer is the LBS website such as the panoramio of google, the story map of cyworld etc. The user created data is transferred into DMB service layer, and is saved in the contents database by the proposed protocol for TPEG-UCM application service. In this paper, data is manually collected. However, it is necessary to further develop the collecting method.

The DMB service layer system for TPEG application service consists of data source, TPEG encoder, streamer, and DMB transmission system [12]. Data source module generates TPEG message such as RTM (Road Traffic Message), CTT (Congestion and Travel Information), SDI (Safety Driving Information), POI, NWS (NeWS information), etc including the proposed UCM message.

The UCM data source module consists of contents database, banner ad database, and UCM authoring tool. The contents database makes database from data transferred at the contents provider layer. The ad database is the banner ad of local area. The UCM authoring tool converts data from the contents database and ad database into binary UCM message, and saves in the message database. The UCM messages generated by its authoring tool are transferred to the TPEG encoder with existing TPEG message. TPEG encoder module reads TPEG messages data from the database made with authoring tool and encodes them into TPEG binary stream according to TPEG application specifications [12]. Also, UCM message is encoded according to TPEG-UCM application specification as proposed in this paper. Streamer module repeatedly transfers TPEG message including UCM message with user specified data rate by the form of a carousel to the DMB transmission system. And then send it by the T-DMB transmitter [12].

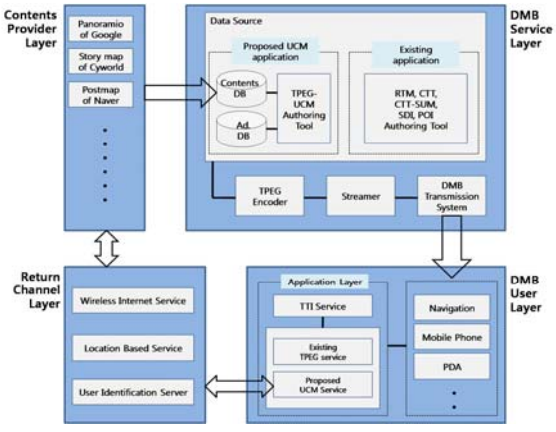

Fig. 2. The whole system of the proposed business model for TPEG-UCM application service. The proposed model consists of contents provider layer, DMB service layer, DMB user layer, and return channel layer [13].

The DMB user layer is the receiver such as navigator, mobile phone, etc. The received TPEG stream from the DMB receiver is parsed and decoded before they are used in the navigation application. All the service type RTM, POI, SDI, NWS, etc will be decoded separately and provided to application layer. Also, the parsed UCM message data is saved the database in the receiver and implemented near real-time service.

The return channel layer is the wireless communication network such as CDMA, WiBro, etc. The user's request in the DMB user layer for and response to more information is provided through the wireless mobile internet service of the return channel layer. Also if user created picture in the DMB user layer is sent, the data is uploaded to the contents provider layer for updating website contents by this layer.

3 The Proposed UCM Message Protocol Structure

In the previous section, we propose a business model for the TPEG-UCM application service on T-DMB. Among these components, the data source module for UCM message at the DMB service layer is firstly necessary to develop for the proposed service. Thus in this section, we propose the UCM message protocol structure and event coding in detail.

The hierarchical transport frame structure including the UCM message is shown in Figure 3, and it is also compatible to the existing TPEG application services [7-10]. The TPEG application service is identified by service component identifier of service component frame level. Application data is included in the component data field of service component frame level [14, 15]. The new UCM message defined in this paper is included in the component data field. The TPEG-UCM application service proposed in this paper is designed to deliver UCM message using three containers such

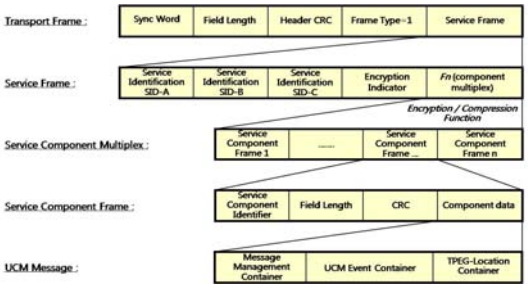

Fig. 3. The transport frame structure for the TPEG- UCM application service. It is completely compatible with existing TPEG protocol [14, 15].

as the message management container to manage the UCM in the receiving side, the event container for transmitting UCM information, and TPEG-location container having the geographical position information [6, 16]. The message management container and the TPEG-Location container of three TPEG-UCM application service data field are identical that of TPEG-POI application service [17]. In this paper, only event container component frame is designed and proposed.

As shown in Figure 4, the detailed structure of TPEG-UCM event container proposed in this paper consists of two kinds of elements such as story and info. The story element contains title and picture. The title of story element describes in detail for travel site. The picture of story element presents a thumbnail picture which is created by the user. The info element is defined for more information about travel site. It contains author, date, site, and banner ad of local area for new earnings source. Among the info element, the travel site information is newly defined in UCM10 table for increasing the transfer efficiency [13].

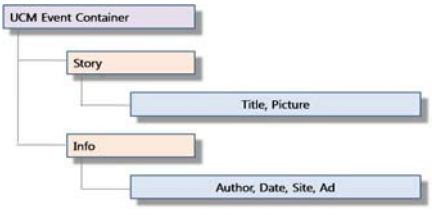

Fig. 4. The detailed event container structure of UCM message consists of two components, story and info, including newly defined UCM10 table [13]

Figure 5 shows the syntactical representation for encoding the story and the info element of UCM message. All information of TPEG-UCM application service message protocol proposed in this paper is coded by grammar and concept which is defined at TPEG Specification 'Part 2: Syntax, Semantics, and Framing structure' [13, 15].

a. Story

<UCM_component(80)>:=	: Story event class
<intunti> (id),	: Identifier, id=80 hex
<intunli> (n),	: Length of component data in bytes, n
m*<story_component()>;	: Story component

a.1 Story component template

<story_component(x)>:=	: Story component template
<intunti> (id),	: Identifier, id=x hex
<intunli> (n),	: Length of component data in bytes, n
n*<byte>;	: Component data

a.2 Title

<story_component(00)>:=	: Title of story component
<intunti> (id),	: Identifier, id=00 hex
<intunli> (n),	: Length of component data in bytes, n
<short_string>;	: Title of information

a.3 Picture

<story_component(01)>:=	: Picture of story compo- nent
<intunti> (id),	: Identifier, id=01 hex
<intunli> (n),	: Length of component data in bytes, n
<graph_type>,	: Picture format
m*byte;	: Picture file

b. info

<ucm_component(81)>:=	: Info event class
<intunti> (id),	: Identifier, id=81 hex
<intunli> (n),	: Length of component data in bytes, n
m*<info_component()>;	: Info component

b. 1 Info component template

<info_component(x)>:=	: Info component template
<intunti> (id),	: Identifier, id=x hex
<intunli> (n),	: Length of component data in bytes, n
n*<byte>;	: Component data

b.2 Site

<info_component(00)>:=	: Site of info component
<intunti> (id),	: Identifier, id=00 hex
<intunli> (n),	: Length of component data in bytes, n
<ucm10>;	: Site, TPEG table ucm10

b.3 Author

<info_component(01)>:=	: Author of info component
<intunti> (id),	: Identifier, id=01 hex
<intunli> (n),	: Length of component data in bytes, n
<short_string>;	: Author

b.4 Date

<info_component(02)>:=	: Date of info component
<intunti> (id),	: Identifier, id=02 hex
<intunli> (n),	: Length of component data in bytes, n
<date>;	: Date

b.5 Ad

<info_component(03)>:=	: Ad of info component
<intunti> (id),	: Identifier, id=03 hex
<intunli> (n),	: Length of component data in bytes, n
<graph_type>,	: Picture format
m*byte;	: Picture file

Fig. 5. The syntactical representation for the UCM message event container for TPEG-UCM application service [13-15]

4 The Simulation of TPEG-UCM Application Service

The interoperability of the TPEG-UCM application service must be verified through incorporating smooth the current existing TPEG application service and implementing in broadcasting. Thus, the proposed TPEG-UCM application service protocol is necessary to verify the stability by the experimental simulation. However, it is, in fact, difficult to prove its stability on T-DMB full system including the broadcasting. Instead, in this paper, the stability and capability using the example of the authoring tool and the decoding tool for service are proposed as shown in Figure 6. The collected travel information database and the ad database with banner ad of local area is encoded by file method making '*.bin' file as 'Guideline for TPEG on the internet (B/TPEG PG02/080)', not stream method [18].

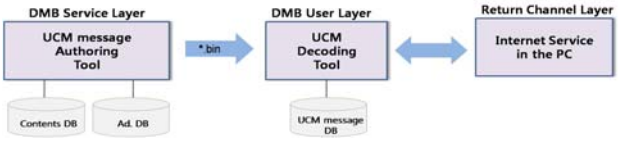

Fig. 6. The simulation of the TPEG-UCM application service. It is encoded by file method, not stream method [13].

4.1 The UCM Message Authoring Tool

The authoring tool convert a UCM message information to data file in the format of '*.bin' which is suitable for the proposed specification in this paper. The hardware of the developed authoring tool is PC of Pentium 4 dual core 1.87GHz and the software is implemented by the dialog based MFC (Microsoft Foundation Class) with the Visual Studio 2005 C++. The collected travel information database is implemented by Microsoft Access 2007. The feature of GUI (Graphic User Interface) is an easily and intuitively operable authoring tool interface as shown in Figure 7.

Pictures use jpg format among jpg, pna, and mng in TPEG specification and resolution is 320x240. Thus, the capacity of UCM message is about 55Kbytes per one message. At the present, the receiver of car navigation or mobile phone is over 1GB capacity in storage area. The proposed service requires 1,000 messages more for thinking receiver storage capacity and information value. As a result, the transferring whole capacity becomes about 55Mbyte.

The result shows the best receiving rate when it is transferred under 2Kbytes which is MSC (Main Service Channel) data group basic size by TPEG application service matching test [19]. The TPEG-UCM application service message is split into 2Kbytes parts by multiplexing the existing TPEG application service and the form of a carousel. The TPEG-UCM service is a non real-time service. Thus, we think suitable that its update duration is a week and it is received in background mode in the receiving side.

4.2 The UCM Message Decoding Tool

The hardware basis of the developed decoding tool is identical that of the authoring tool. Data transferred from UCM message authoring tool is made database by Microsoft Access 2007 and stored in hard disk. The easy and simple GUI example for mobile phone user is shown in Figure 7.

Fig. 7. The example of the UCM message authoring tool (left) and the UCM message decoding tool and the implementation by PC internet service (right) [13]

If user selects the title want to view, the receiver displays the additional information such as title, site, writer, date, etc. In the low part, it displays the transferred banner ad of local area disrupting the travel information. As a result, we may have the ad effect. If user click 'more view' menu for more picture or information, it is connected the story map of cyworld by PC internet service [20]. Also, if the user knows the route to the destination, user clicks 'map' menu, which prompts optimal route shown by the inner map of the receiver with travel site location information. The example shown in Figure 7 is the optimal route of the almap in the PC internet service [21].

5 Conclusions

In this paper, we propose a business model for the TPEG-UCM application service on T-DMB, which effectively transfers the information of LBS website to the user. The effectiveness of the proposed service is expected to acquire a variety of TPEG application services, and come true the bidirectional interactive service in the stage of DMB 2.0. The T-DMB service provider side also easily obtains the new information as broadcast contents, and creates the new source of income from banner ad of local area. As a result, the T-DMB service has acquired the robust position as new media in the future convergence period of broadcasting and communication.

It is necessary to further develop another TPEG service which transfers user created movie contents like UCC. Besides picture, a movie clip is large data size. Thus as future work, it is necessary to set up new business model which transfers the movie thumbnail as well as the link information at the UCC web site to the TPEG application service, and the whole movie can be downloaded with the return channel of the wireless communication network.

Acknowledgments. The authors would like to thank to Ulsan Metropolitan City, MKE and MEST which have supported this research in part through the NARC, the Human Resource Training project for regional innovation through KOTEF, and post BK21 at University of Ulsan.

References

1. Kim, J., Jang, H., Yun, J., Bae, B.: Design and Implementation of DMBonIP Gateway to Provide Internet Based DMB service. IEEE Transactions on Consumer Electronics 53(1), 2 (2007)
2. Bae, B., Kim, W., Ahn, C., Lee, S.I., Sohng, K.I.: Development of a T-DMB Extended WIPI Platform for Interactive Mobile Broadcasting Services. IEEE Transactions on Consumer Electronics 52(4), 11 (2006)
3. Jeong, Y., Kim, S., Cho, S., Geon, K., Ahn, C., Lee, S.: Bidirectional Location Based Services using Terrestrial-DMB and Wireless Communication Network. IEEE Transactions on Consumer Electronics 52(4), 11 (2006)
4. The number of DMB receivers reaches 15 million, Korea Economic Daily, 9. 25 (2008)
5. Yoon, N.: DMB Bidirectional Service in DMB2.0. Institute for Information Technology Advancement Focus 1354 (July 9, 2008)

6. Lv, W.F., Zhou, L., Cui, W.: A Novel SAI Application Based on TPEG: Second International Symposium on Intelligent Information Technology. Application of IEEE (2008)
7. KBS Mozen TPEG, http://www.kbs-mozen.com
8. SBS Roadi TPEG, http://www.sbsroadi.com
9. YTN DMB 4Drive, http://www.4drive.co.kr
10. MBC DMB Drive, http://www.dmbdrive.com
11. Kim, S., Jeong, Y., Cho, S., Kim, G., Ahn, C.H., Lee, S.: Delivery of New TTI services over Terrestrial DMB and a Bidirectional Network: IEEE (2007)
12. Jeong, Y., Kim, S.C., Cho, S.: Design and Implementation of POI Service based on Terrestrial-DMB. In: The Korean Society of Broadcasting Engineers Conference (2005)
13. Lee, S.H., Jo, K.H.: TPEG-based User Created Message Service Model Design for Terrestrial DMB. The journal of broadcasting engineering 13(6), 817–827 (2008)
14. KS X 6917-1 TPEG Part1: TPEG-INV (Introduction, Numbering and Version)
15. KS X 6917-2 TPEG Part2: TPEG-SSF (Syntax, Semantics and Framing structure)
16. KS X 6917-6 TPEG Part6: TPEG-LOC (Location)
17. TTAS.KO-07.0036 Specification of the TTI Point-of-Interest (POI) information service for DMB to Mobile, Portable and Fixed receivers
18. B/TPEG: Guidelines for TPEG on the Internet (B/TPEG Plenary Group)
19. Kwon, D., Chae, Y.: Design and Implementation of the Traffic and Travel Information Service for terrestrial DMB system. The journal of broadcasting engineering 12(3), 203–213 (2007)
20. The story map of cyworld, http://map.cyworld.com/
21. The almap of eastsoft, http://www.almap.co.kr/

An Empirical Study of the Convergence of RegionBoost

Xinzhu Yang, Bo Yuan, and Wenhuang Liu

Graduate School at Shenzhen, Tsinghua University, Shenzhen 518055, P.R. China
yangxz03@mails.tsinghua.edu.cn,
{yuanb,liuwh}@sz.tsinghua.edu.cn

Abstract. RegionBoost is one of the classical examples of Boosting with dynamic weighting schemes. Apart from its demonstrated superior performance on a variety of classification problems, relatively little effort has been devoted to the detailed analysis of its convergence behavior. This paper presents some results from a preliminary attempt towards understanding the practical convergence behavior of RegionBoost. It is shown that, in some situations, the training error of RegionBoost may not be able to converge consistently as its counterpart AdaBoost and a deep understanding of this phenomenon may greatly contribute to the improvement of RegionBoost.

Keywords: Boosting, RegionBoost, Convergence, kNN, Decision Stumps.

1 Introduction

Since ensemble learning can help improve the accuracy of a single learning model, it has been an active topic in supervised learning for more than two decades. An ensemble of classifiers refers to a set of classifiers whose individual decisions are combined in some way to determine the class labels of unknown samples [1]. As a result, how to combine the individual classifiers is a key question in ensemble learning. In the past, many strategies have been developed, such as unweighted voting in Bagging [2] and Random Forests [3], weighted voting in Boosting [3], learning a combiner function [4] and stacking [5].

In addition to the static weighting methods, various dynamic weighting schemes have also been proposed in recent years, which take the features of input samples into consideration. Typical examples include dynamic voting(DV), dynamic selection(DS), and dynamic voting selection(DVS) [6]. Some of these schemes are independent of the underlying ensemble algorithms. For example, DV, DS, DVS have been applied to Bagging, Boosting and Random Forests respectively [6, 7]. Other strategies focus on specific ensemble methods, among which Boosting is the most popular one.

Boosting [8] encompasses a family of successful ensemble mechanisms by sequentially producing a series of classifiers and combining them using weighted voting. The training set used for each classifier is chosen based on the performance of the earlier classifier(s) in the series [9]. AdaBoost [10] is a one of the most commonly used Boosting algorithms. In the training process, AdaBoost decreases the weights of training samples classified correctly by the current classifier and increases the weights of those classified incorrectly to create a new training set for the next iteration.

D.-S. Huang et al. (Eds.): ICIC 2009, LNAI 5755, pp. 527–535, 2009.

When combining the decisions, AdaBoost assigns a single value weight α_t to each basic classifier $h_t(x)$ based on its error on the corresponding weighted training set, which means that the weights of classifiers are constant and will not change for different new input samples. Obviously, this approach ignores the inherent performance variability of classifiers on new samples with different feature values. In fact, the same basic classifier may not be as effective at classifying samples in some areas of the feature space as in other areas.

This issue has been addressed by several improved Boosting algorithms independently, which replace the fixed weighting methods with dynamic weighting schemes, including RegionBoost [9], DynaBoost [11], iBoost [12], WeightBoost [13] and local Boost [14]. A crucial factor of these schemes is how to dynamically adjust the weights with regard to the input samples.

Apart from some limited progresses, theoretical analysis on ensemble mechanisms has shown to be a very challenging task. For the dynamic weighting schemes, both theoretical analysis and comprehensive empirical studies have been rare in the literature. The purpose of this paper is to conduct a preliminary investigation of the practical behavior of Boosting with dynamic weighting schemes with focus on RegionBoost in order to gain deeper insights into these algorithms.

2 Dynamic Weighting Schemes

One of the major advantages of ensemble learning over a single model is that an ensemble approach allows each basic model to cover a different aspect of the dataset. When combined together, they are able to explain the whole dataset more thoroughly. Therefore, in order to take the full strength of ensemble learning, a good combination strategy should be able to examine the input pattern and only invoke the basic models that are appropriate for the input pattern [13].

2.1 Framework

A number of Boosting methods with dynamic weighting schemes have been proposed independently with proven superior performance over standard Boosting algorithms. However, the essential ideas are very similar: the basic classifiers should be weighted based on not only the training error but also the sample to be classified.

Although the implementation details are more or less different, the framework of Boosting with dynamic weighting schemes can be illustrated as Fig. 1. An extra learner $\alpha_t(x)$ is introduced for every classifier $h_t(x)$ as a competency predictor to evaluate the dynamic input-dependent weights for each classifier. Generally speaking, the extra learner is trained to simulate the performance of each basic classifier on the sample space. In other words, this extra learner is used to indicate whether a certain basic classifier is likely to yield accurate results given an unknown sample.

Many of the commonly used classification methods have been employed as the competency predictors such as k-Nearest Neighbor (RegionBoost), Neural Networks (RegionBoost) and Decision Trees (iBoost). It is clear that one of the key issues in Boosting with dynamic weighting schemes is how to construct the competency predictors in order to appropriately determine the weights, which can significantly affect the performance of the combined classifiers.

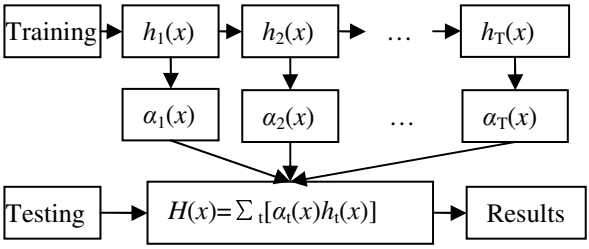

Fig. 1. The framework of Boosting with dynamic weighting schemes

2.2 RegionBoost

In this paper, we used RegionBoost as the representative example of Boosting with dynamic weighting schemes in the empirical analysis. The main idea behind RegionBoost is to build an extra model upon each basic classifier based on its training results (whether a training sample is classified correctly or not). By doing so, this new model is able to estimate the accuracy or the competency of the classifier for each new sample.

One of the intuitive approaches to estimating model competency is to use the kNN (*k*-Nearest Neighbor) method to find the *k* points in the training set nearest to the new sample to be classified and use the performance of each classifier on these *k* points as the measurement [9]. More specifically, the weight of each classifier for this new sample to be classified is determined by the percentage of points (out of *k* points) correctly classified by this classifier [9].

RegionBoost has been reported having better performance compared to AdaBoost in terms of accuracy on a number of UCI benchmark datasets (though it makes little difference on certain datasets) [9]. It should be mentioned that, in AdaBoost, the value of α_t is selected so that the overall error on the training set is minimized. In the meantime, the overall training error enjoys a proven upper bound that consistently decreases during iterations [10]. By contrast, in RegionBoost, $\alpha_t(x)$ depends on the local error of the basic classifier $h_t(x)$ on the specific x. As a result, the convergence behavior of RegionBoost can no longer be explained according to the existing theoretical work on AdaBoost.

3 Convergence of RegionBoost

This section presents some interesting phenomena of the convergence of RegionBoost on a synthesized dataset as well as a few UCI benchmark datasets. A detailed analysis is also given to provide some deeper insights into the mechanism of RegionBoost.

3.1 The Triangle Dataset

First of all, a simple 2D dataset called Triangle as shown in Fig. 2(a) was used to illustrate the convergence behavior of RegionBoost. The dataset with 1000 samples ("○" vs. "x") was randomly divided into training set and testing set of equal sizes. The

decision stumps model was used as the basic classifier, which is a weak classification method and can only split along a single attribute (a simplified decision tree model). An ensemble of 200 classifiers was created (the process of creating basic models in RegionBoost is the same as that in AdaBoost) and kNN (k=5) was used to determine the dynamic weights for each basic classifier.

When comparing the training error curves of RegionBoost and AdaBoost shown in Fig. 2(b), we found two distinctly different patterns. The training errors of Adaboost decreased consistently and reached zero in about 120 iterations. In contrast, the training errors of RegionBoost decreased faster at the beginning, but quickly flattened out after about 10 iterations.

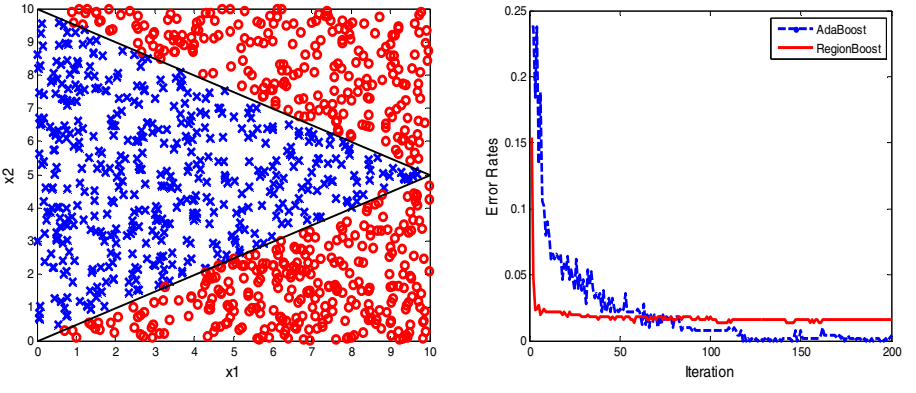

(a) (b)

Fig. 2. (a) The Triangle Dataset. (b) The training errors of AdaBoost and RegionBoost.

Since RegionBoost employs an extra parameter k compared to AdaBoost, additional experiments were conducted to examine the influence of different k values. Table 1 shows the results of RegionBoost with stumps and kNN with k = 3, 5, 7, 9 respectively. It is interesting to see that the training errors of RegionBoost with stumps were very close to those of kNN with the same k values.

Table 1. The training errors of RegionBoost and kNN (The Triangle Dataset)

K	RegionBoost	kNN
3	0.0340	0.0340
5	0.0220	0.0220
7	0.0200	0.0220
9	0.0240	0.0260

3.2 Analysis of the Triangle Dataset

Since it was observed that the training error of RegionBoost did not converge to zero and instead it was quite close to the error of kNN, it is reasonable to hypothesize that

the convergence of RegionBoost has a strong relation with the accuracy of kNN, which is used to determine the weights of basic classifiers. In this section, we will give some explanations of this relationship from three aspects.

Firstly, let's take a look into the classification process of a single sample. Given a query point (denoted by a star), depending on the locations of its neighbors and the decision boundary, there are two possible situations. In the first one, the boundary divides the neighborhood of the sample into two parts, as shown in Fig. 3(a), which is called "Split" pattern for that sample. In the second one, the boundary does not go through the neighborhood, which is called "Non-Split" pattern, as shown in Fig. 3(b).

In Fig. 3, suppose that the star belongs to "x". In the "Non-Split" pattern, if the left side of the boundary is classified as "○", the query point will be classified as "○" with weight 0.6 (3 out of 5). On the flip side, the query point will be classified as "x" with weight 0.4 (2 out of 5). By combining the above two classifiers, the query point will be misclassified as "○", which is the same as kNN. As a result, if within a large number of iterations, the numbers of the two types of classifiers are close, the results of RegionBoost should be identical to kNN.

However, there is another situation that can make RegionBoost different from kNN. In Fig. 3(a), the classifier will either make the 5 neighbors all right or all wrong. When all neighbors are classified correctly, the query point will be correctly classified as "x" and the weight of the classifier is 1. On the flip side, the query point will be incorrectly classified as "○" but the weight is 0, making no negative effect on the overall decision at all. Consequently, in this situation, RegionBoost can always classify the query point correctly while kNN will make a wrong decision. This is an important reason that RegionBoost may reach lower training errors than kNN.

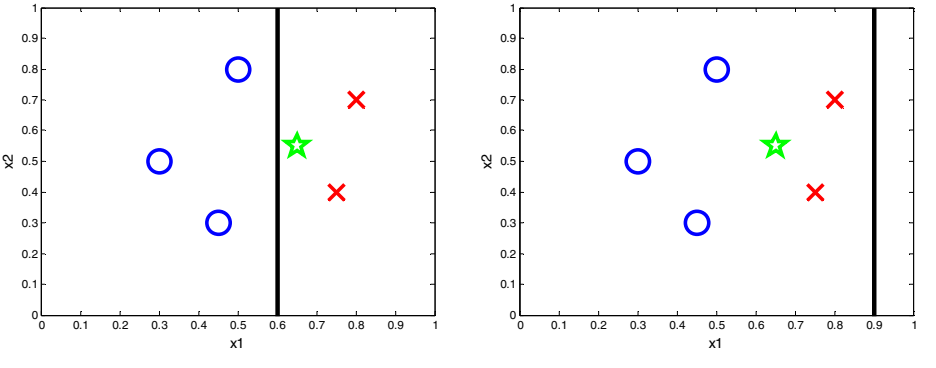

(a) Split Pattern (b) Non-Split Pattern

Fig. 3. Relationships of the neighborhood of a query point and the decision boundary

Note that in the "Non-Split" case, if all neighbors are of the same class label as the true class label of the query point, the weight of the basic classifier will be 1 if it makes the right decision (0 if it is wrong). As a result, RegionBoost can make the right decision on these query points immediately after a correct classifier is created. By contrast, in AdaBoost, multiple correct classifiers may be required to overturn the

wrong classification results made by a previous classifier. This fact explains the faster convergence speed of RegionBoost at the beginning of training.

Secondly, we analyzed the influence of proportions of the two patterns on the convergence of RegionBoost. Let $NS(i)$ and $S(i)$ be the number of "Non-Split" pattern classifiers and the number of "Split" pattern classifiers for the ith sample respectively. Fig. 4(a) shows the histogram of $p(i)=NS(i)/T$ (T=200). It is clear that for most samples, "Non-Split" pattern classifiers accounted for more than 90% of the classifiers.

Let $NS_+(i)$ be the number of "Non-Split" classifiers that produce the same result as kNN on the ith sample and $NS\_(i)$ be the number of the rest "Non-Split" classifiers.

$$D(i) = (NS_+(i) - NS\_(i))/NS(i) \tag{1}$$

The minimum $D(i)$ that can guarantee the consistence between RegionBoost and kNN can be calculated as follows. For k=5, the minimum weight of a classifier is 0.6 if it produces the same result as kNN (e.g., the query point is classified as "○"and there are three neighbors belonging to "○") while the maximum weight of a classifier is 0.4 if it produces the opposite result as kNN. As a result, it is easy to see that, as long as $D(i)$ is greater than -0.2 (i.e., 40% or more for NS_+ vs. 60% or less for $NS\_$), the set of "Non-Split" classifiers will be functionally identical to kNN.

Fig. 4(b) shows the distribution of $D(i)$ indicating that all $D(i)$ values were greater than -0.2. So the classification results from the ensemble of "Non-Split" classifiers were exactly the same as those of kNN.

Finally, the classification results from the ensemble of "Non-Split" classifiers, the ensemble of "Split" pattern and the overall results were compared. It turns out that the overall results of 498 out of 500 samples were the same as the results from the ensemble of "Non-Split" classifiers, which have been shown to be identical to kNN. In other words, the performance of RegionBoost was dominated by "Non-Split" classifiers and its training error should be close to the error of kNN (instead of converging towards 0).

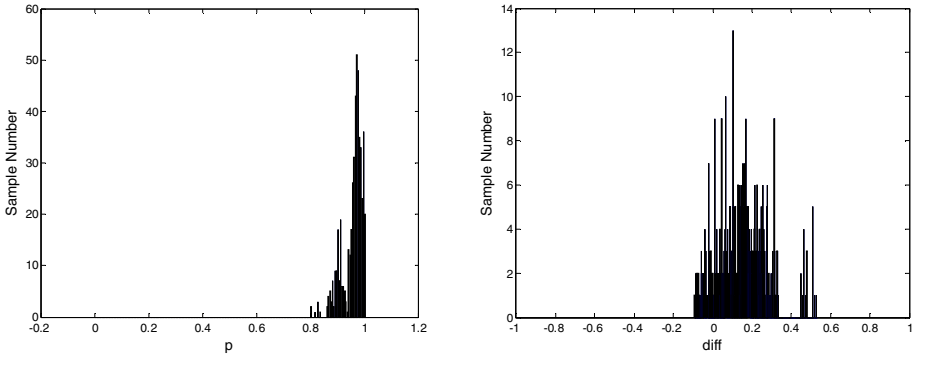

(a) (b)

Fig. 4. The Triangle Dataset (a) The distribution of $p(i)$. (b) The distribution of $D(i)$.

3.3 Validation on UCI Data

This section presents validation experiments on three commonly used UCI datasets: Pima, Credit Aus and Sonar [15]. The experimental settings were the same as in the Triangle dataset (50% samples were used as the training set). The training errors of AdaBoost, RegionBoost and kNN (k=5) are shown in Table 2. More specifically, on Pima and Credit Aus, the performance of RegionBoost was very close to kNN. In fact, the overall results of 383 out of 384 samples in Pima and 342 out of 345 samples in Credit Aus were the same as the results from the ensembles of "Non-Split" classifiers.

However the Sonar dataset showed something different. The training error of RegionBoost reached zero but the error of kNN was 0.1154. A closer look at the experimental results on Sonar showed that the final classification results of samples in Sonar were largely determined by the "Split" classifiers, which correctly classified 103 out of 104 samples. Note that the number of samples in Sonar is quite small (208) compared to its dimensionality (60). As a result, the neighbors of a query point are expected to be much sparser that in other cases and thus are more likely to be separated by the decision boundaries.

Table 2. The training errors on three UCI datasets

Dataset	AdaBoost	RegionBoost	kNN
Pima	0.1328	0.1771	0.1797
Credit Aus	0.0667	0.0812	0.0899
Sonar	0	0	0.1154

4 The Effect of Basic Learners

The reason that the training errors of RegionBoost did not converge to zero in the experiments above may be partially due to the power of the basic learner in use. Since the decision stumps model can only create very simple decision boundaries, the neighbors of most query points may belong to the "Non-Split" category. In this section, we chose the decision trees model as the basic classifiers. The experimental results of AdaBoost, RegionBoost and kNN are shown in Table 3, showing that the training errors of RegionBoost with trees were much lower than with stumps. In the meantime, the results of RegionBoost with trees became apparently different from kNN, which may be due to the increasing percentage of the "Split" classifiers.

Table 3. A comparison of the training errors (Trees vs. Stumps)

Dataset	AdaBoost (Trees)	RegionBoost (Trees)	AdaBoost (Stumps)	RegionBoost (Stumps)	kNN
Triangle	0	0.0120	0	0.0220	0.0220
Pima	0	0.0547	0.1328	0.1771	0.1797
Credit Aus	0	0.0087	0.0667	0.0812	0.0899
Sonar	0	0	0	0	0.1154

5 Conclusions

In this paper, we empirically investigated the convergence of a typical Boosting algorithm with dynamic weighting schemes called RegionBoost, which employs kNN as the competency predictor of its basic classifiers. The major motivation was to provide one of the first attempts to better understand the behavior of RegionBoost.

Experimental results showed that the training errors of RegionBoost decreased faster than those of AdaBoost at the beginning of iterations but could not converge to 0 in some cases. Through detailed analysis, we showed that the reason lies in the fact that the training errors of RegionBoost are largely influenced by the accuracy of kNN, especially when the basic learners are very weak. We also demonstrated that the performance of RegionBoost can be enhanced with basic learners capable of creating more sophisticated decision boundaries.

In addition to the preliminary results presented here, there is still a huge open area for future work. For example, competency predictors other than kNN may also be used with RegionBoost and its convergence behavior in the new situation needs to be formally investigated and we hope that the techniques used in this paper may still be helpful to some extend. In the meantime, it is also important to think about the strategy for purposefully creating a set of basic classifiers that are better suited to the weighting schemes of RegionBoost.

References

1. Dietterich, T.G.: Machine Learning Research: Four Current Directions. AI Magazine 18(4), 97–136 (1997)
2. Breiman, L.: Bagging Predictors. Machine Learning 24(2), 123–140 (1996)
3. Breiman, L.: Random Forests. Machine Learning. 45(1), 5–32 (2001)
4. Jordan, M.I., Jacobs, R.A.: Hierarchical Mixtures of Experts and the EM Algorithm. Neural Computation 6(2), 181–214 (1994)
5. Ting, K.M., Witten, I.H.: Issues in Stacked Generalization. Journal of Artificial Intelligence Research 10, 271–289 (1999)
6. Tsymbal, A., Puuronen, S.: Bagging and boosting with dynamic integration of classifiers. In: Zighed, D.A., Komorowski, J., Żytkow, J.M. (eds.) PKDD 2000. LNCS (LNAI), vol. 1910, pp. 116–125. Springer, Heidelberg (2000)
7. Tsymbal, A., Pechenizkiy, M., Cunningham, P.: Dynamic integration with random forests. In: Fürnkranz, J., Scheffer, T., Spiliopoulou, M. (eds.) ECML 2006. LNCS (LNAI), vol. 4212, pp. 801–808. Springer, Heidelberg (2006)
8. Schapire, R.E.: The Strength of Weak Learnability. Machine Learning 5(2), 197–227 (1990)
9. Maclin, R.: Boosting Classifiers Regionally. In: The 15th National Conference on Artificial Intelligence, Madison, WI, pp. 700–705 (1998)
10. Freund, Y., Schapire, R.E.: A Decision-Theoretic Generalization of On-Line Learning and an Application to Boosting. Journal of Computer and System Sciences 55(1), 119–139 (1997)
11. Moerland, P., Mayoraz, E.: DynaBoost: Combining Boosted Hypotheses in a Dynamic Way. In: IDIAP-RR, Switzerland (1999)

12. Kwek, S.S., Nguyen, C.: iBoost: Boosting using an instance-based exponential weighting scheme. In: Elomaa, T., Mannila, H., Toivonen, H. (eds.) ECML 2002. LNCS (LNAI), vol. 2430, pp. 245–257. Springer, Heidelberg (2002)
13. Jin, R., Liu, Y., Si, L., Carbonell, J., Hauptmann, A.G.: A New Boosting Algorithm Using Input-Dependent Regularizer. In: The 20th International Conference on Machine Learning, Washington, DC (2003)
14. Zhang, C.-X., Zhang, J.-S.: A Local Boosting Algorithm for Solving Classification Problems. Computational Statistics & Data Analysis 52, 1928–1941 (2008)
15. Asuncion, A., Newman, D.J.: UCI Machine Learning Repository. University of California, School of Information and Computer Science (2007), http://www.ics.uci.edu/~mlearn/MLRepository.html

Towards a Better Understanding of Random Forests through the Study of Strength and Correlation

Simon Bernard, Laurent Heutte, and Sébastien Adam

Université de Rouen, LITIS EA 4108
BP 12 – 76801 Saint-Etienne du Rouvray, France
{simon.bernard,laurent.heutte,sebastien.adam}@univ-rouen.fr

Abstract. In this paper we present a study on the Random Forest (RF) family of ensemble methods. From our point of view, a "classical" RF induction process presents two main drawbacks : (i) the number of trees has to be *a priori* fixed (ii) trees are independently, thus arbitrarily, added to the ensemble due to the randomization. Hence, this kind of process offers no guarantee that all the trees will well cooperate into the same committee. In this work we thus propose to study the RF mechanisms that explain this cooperation by analysing, for particular subsets of trees called sub-forests, the link between accuracy and properties such as Strength and Correlation. We show that these properties, through the Correlation/Strengh^2 ratio, should be taken into account to explain the sub-forest performance.

Keywords: Classification, Ensemble Method, Ensemble of Classifiers, Classifier Selection, Random Forests, Decision Trees.

1 Introduction

Random Forest is a family of classifier ensemble methods that use randomization to produce a diverse pool of individual classifiers, as for Bagging [1] or Random Subspaces methods [2]. It can be defined as a generic principle of classifier combination that uses L tree-structured base classifiers $\{h(x, \Theta_k),\ k = 1, ...L\}$ where $\{\Theta_k\}$ is a family of independent identically distributed random vectors, and x is an input data. The particularity of this kind of ensemble is that each decision tree is built from a random vector of parameters. A Random Forest can be built for example by randomly sampling a feature subset for each decision tree (as in Random Subspaces [2]), and/or by randomly sampling a training data subset for each decision tree (as in Bagging [1]). Since they have been introduced in 2001, RF have been studied in many ways, both theoretically and experimentally [3,4,5,6]. In most of those works, it has been shown that RF are particularly competitive with one of the most efficient learning principles, i.e. boosting [4,7,8]. However, the mechanisms that explain the good performance of RF are not clearly identified. For example, it has been theoretically proved in [4] and experimentally confirmed in [6], that above a certain number of trees, adding more trees in the forest does not improve the accuracy. Yet, no research work has studied the way each tree contributes to the performance of a RF, and how they cooperate.

In this paper we propose to go one step further in the understanding of RF mechanisms, by studying properties of different subsets of decision trees, with different performance. Thus our aim is not to find better subsets of trees that can outperform a larger

D.-S. Huang et al. (Eds.): ICIC 2009, LNAI 5755, pp. 536–545, 2009.

ensemble of trees, but rather to study properties that can explain those differences in the sub-RF performance. Therefore, as we will discuss in section 3, we have decided to use a sub-optimal classifier selection technique, *i.e.* SFS (Sequential Forward Selection), to generate different sub-RF that exhibit better accuracies on a test set than the initial forest from which sub-RF have been obtained. By monitoring the accuracies and by focusing on some particular properties shared by these sub-forests, we bring some primary responses for explaining the differences in performance. Strength and correlation properties, as defined in [4], have been chosen to study the evolution of sub-RF accuracy during the classifier selection process. We show that these properties, through the Correlation/Strengh^2 ratio, are important criteria that should be taken into account for explaining the performance evolution according to the number of trees in the sub-RF.

The paper is thus organized as follows: we recall in section 2 the Forest-RI principles; in section 3, we first explain our approach for studying the RF mechanisms, and then describe our experimental protocol, the datasets used, and the results obtained. We finally draw some conclusions and future works in the last section.

2 The Forest-RI Algorithm

One can see Random Forests as a family of methods, made of different decision trees ensemble induction algorithms, such as the Breiman Forest-RI method often cited as the reference algorithm in the literature. In this algorithm the Bagging principle is used with another randomization technique called Random Feature Selection. The training step consists in building an ensemble of decision trees, each one trained from a bootstrap sample of the original training set — *i.e.* applying the Bagging principle — and with a decision tree induction method called Random Tree. This induction algorithm, usually based on the CART algorithm [9], modifies the splitting procedure for each node, in such a way that the selection of the feature used for the splitting criterion is partially randomized. That is to say, for each node, a feature subset is randomly drawn, from which the best splitting criterion is then selected.

To sum up, in the Forest-RI method, a decision tree is grown by using the following process :

- Let N be the size of the original training set. N instances are randomly drawn with replacement, to form the bootstrap sample, which is then used to build the tree.
- Let M be the dimensionality of the original feature space, and K a preliminary fixed parameter so that $K \in [1..M]$. For each node of the tree, a subset of K features is randomly drawn without replacement, among which the best split is then selected.
- The tree is thus built to reach its maximum size. No pruning is performed.

With the introduction of randomization in the RF induction, one hopes to take benefits of complementarities of individual trees, but there is no guarantee that adding a tree in a RF will allow to improve the performance of the ensemble. One can even imagine that some trees of a RF make the accuracy of the ensemble decrease. This idea has led us to study how trees cooperate in the same committee to ensure a better accuracy.

In the literature, only few research works have focused on the way trees have to be grown in a RF. When introducing RF formalism in [4], Breiman demonstrated that

above a certain number of trees, adding more trees does not allow to improve the performance. Precisely he stated that for an increasing number of trees in the forest, the generalisation error converges to a maximum. This result indicates that the number of trees in a forest does not have to be as large as possible to produce an accurate RF. The works of Latinne et al. in [6], and of Bernard et al. in [3] experimentally confirm this statement. However, noting that above a certain number of trees no improvement can be obtained by adding more "arbitrary" trees in the forest does not mean obviously that the optimal performance has been reached. It does neither give explanation of the good cooperation of trees in the ensemble. Thus the idea of our experimental work is to lead an analysis of the evolution of accuracies, in order to understand this cooperation. We present in the next section our experimental approach for those purposes.

3 Analysing Strength and Correlation in Sub-RF

The principle of our experiments is to generate different subsets of trees and to evaluate their accuracies on the same test set so that it will be possible to examine some properties shared by the "best" sub-RF regarding the performance of the initial RF. The idea is firstly to use a classifier selection technique to generate those sub-RF and then to measure and monitor the properties on which we have decided to focus on.

As we intend to find a correlation between properties and accuracy, classifiers have been selected by optimizing the accuracy on a test set — i.e. minimizing the error rate. It is obvious that using the test set for the selection criterion, rather than an independent validation set, does not allow to evaluate the generalisation error rate of the resulting subsets and thus will not allow to conclude on the overall performance of the sub-RF comparing to the initial forest. However our goal is not actually to perform classifier selection to find better sub-RF in terms of generalisation capacities, but rather to focus on a possible link between accuracy and some properties regarding a particular prediction set.

Concerning the selection method, for the reasons mentioned above, the optimality of the selection method is not a priority here. That is the reason why the well-known classifier selection algorithm SFS (Sequential Forward Selection) has been chosen. This method is known to be sub-optimal because the sequential process makes each iteration depend on the previous one, and finally not all the possible solutions are explored. However it presents the advantage to be fast and simple. This selection technique iteratively builds a sub-optimal subset from an ensemble of classifiers according to a given criterion. At each iteration of the SFS process, each remaining classifier is added to the current subset and the one that optimizes the performance of the ensemble is retained. The stopping criterion in such an iterative process is commonly based on the convergence of the accuracy. For our experiments we have decided to let the selection algorithm explore all the possible iterations, *i.e.* for a number L', from 1 to L, of trees in the final subset, where L is the size of the original RF.

Then, our goal is thus to bring elements of explanation for this evolution of accuracy. In [4], Breiman introduced two crucial notions for inducing accurate RF : the *strength*, noted s, and the *correlation*, noted $\overline{\rho}$. The definition of the *strength* is based on the margin function of a RF, that measures the extent to which the average number of votes for the right class exceeds the average vote for any other class. The strength is consequently defined as the expectation of the margin function over all the training samples.

The *correlation* is the "classical" pairwise correlation, averaged over all the pairs of decision trees in the forest. This pairwise correlation is however computed through the raw margin function of each tree which gives three possible answers for a given training sample: 1 if the tree predicts the right label; −1 if the tree predicts the most popular of the wrong label; and 0 if the tree does not predict any of these two labels.

Breiman proved that an upper bound of the generalisation error of RF is given thanks to the ratio $\frac{\bar{\rho}}{s^2}$. He conjectured that *in understanding the functioning of random forests, this ratio will be a helpful guide — the smaller it is, the better*. We thus propose to experimentally study this statement by measuring this ratio for each of the sub-RF obtained during the selection process. This would allow to match this property with the accuracy, and to determine whether or not it can totally or partially explain its evolution.

We first describe in the following subsection the datasets used. We then detail our experimental protocol and results in the next two subsections.

3.1 Datasets

The 18 datasets that have been used in these experiments are described in Table 1. The first 13 datasets have been selected from the UCI repository [10], because they concern different machine learning issues in terms of number of classes, number of features and number of samples. Twonorm and Ringnorm are two synthetic datasets designed by Breiman and described in [11]. Three additional datasets on different handwritten digit recognition problems have been used: (i) the well-known MNIST database [12] with a 85 multiresolution density feature set ($1 + 2 \times 2 + 4 \times 4 + 8 \times 8$) built from greyscale mean values as explained in [3]; (ii) Digits and DigReject both described in [13], on which a 330-feature set has been extracted, made from three state-of-the-art kinds of descriptors.

Table 1. Datasets description

Dataset	Size	Features	Classes	Dataset	Size	Features	Classes
Digits	38142	330	10	Mnist	60000	84	10
DigReject	14733	330	2	Musk	6597	166	2
Gamma	19020	10	2	Pendigits	10992	16	10
Letter	20000	16	26	Ringnorm	7400	20	2
Madelon	2600	500	2	Segment	2310	19	7
Mfeat-factors	2000	216	10	Spambase	4610	57	2
Mfeat-fourier	2000	76	10	Twonorm	7400	20	2
Mfeat-karhunen	2000	64	10	Vehicle	946	18	4
Mfeat-zernike	2000	47	10	Waveform	5000	40	3

3.2 Experimental Protocol

First, each dataset has been divided into a training and a testing subset, with respectively two thirds of the samples used for training, and the other third for testing. We denote this split by $T = (T_r, T_s)$ where T_r and T_s stand respectively for the training set and the testing set. Then, a RF is grown from T_r, with a number L of trees fixed

to 300. The value of the hyperparameter K has been fixed to $\sqrt{M}$, which is a default value commonly used in the literature. An experimental work on the parametrization of RF, presented in [14], has shown that this value of K is a good compromise to induct accurate RF. Thus, SFS method is applied on the RF, so that at each iteration the tree to add is the one that allows to obtain the most accurate sub-forest on the test set. For each of these sub-RF three measures have been monitored : (i) the error rate measured on T_s (ii) the strength value (iii) and the correlation value.

Finally a statistical test of significance has been performed at each iteration of the selection procedure, in order to state whether or not the resulting subset outperforms the initial forest regarding to a particular prediction set. For that purpose we lean on the comparison of five approximate statistical tests, compared in [15]. In this paper, it is recommended to use McNemar's test [16], for which it is shown that it better suits to experimental protocols like ours. This test is used here to determine whether or not two learning algorithms differ significantly according to their sets of predictions. Three answers can thus be obtained through the McNemar test: (i) H_0 is rejected and $n_{01} > n_{10}$: Algorithm B produces significantly more accurate classifiers than algorithm A, (ii) H_0 is rejected and $n_{01} < n_{10}$: Algorithm A produces significantly more accurate classifiers than algorithm B, (iii) H_0 is accepted: The two algorithms do not produce classifiers significantly different in term of accuracy.

This procedure has been run for all the sub-RF in order to determine whether or not they outperform the initial RF on the test set. Algorithm 1. summarizes the whole experimental protocol applied to each dataset. Results are presented and discussed in the next subsection.

Algorithm 1. Experimental Protocol

Input: N: # samples in the original dataset.
Input: M: # features in the original dataset.
Input: L: # trees in the original forest.
Output: $\epsilon[L]$: 1D table for storing error rates.
Output: $s[L]$: 1D table for storing strength values.
Output: $\rho[L]$: 1D table for storing correlation values.
Output: $\mathcal{M}[L]$: 1D table for storing McNemar test answers.

Randomly draw without replacement $\frac{2}{3} \times N$ samples from the original dataset to form the training subset T_r. The remaining samples form the testing subset T_s.

$h \leftarrow$ Forest-RI($L = 300, K = \sqrt{M}, T_r$).

$h^{(0)}_{SFS} \leftarrow \emptyset$.

for $i = 1$ *to* L **do**

$h^{(i)}_{SFS} \leftarrow h^{(i-1)}_{SFS} \cup h(k)$ where $k = argmin_{h(j) \notin h^{(i-1)}_{SFS}} \{\text{error}(h^{(i-1)}_{SFS} \cup h(j), T_s)\}$.

$\epsilon(i) \leftarrow$ Test $h^{(i)}_{SFS}$ on T_s.

$s(i) \leftarrow$ compute strength for $h^{(i)}_{SFS}$ on T_s.

$\rho(i) \leftarrow$ compute correlation for $h^{(i)}_{SFS}$ on T_s.

$\mathcal{M}(i) \leftarrow$ run a McNemar test of significance with classifiers $(h, h^{(i)}_{SFS})$ on the testing set T_s

end for

3.3 Results

Table 2 presents the best error rates obtained during the selection process on each dataset, and the number of trees of the corresponding subset. Figure 1 presents 18 diagrams of our results for the 18 datasets used. For each of them, a curve has been plotted, representing the error rate obtained during the selection procedure, according to the number of trees in the subset. For comparison, a line has also been drawn on each diagram that represents the error rate obtained with the initial forest of 300 trees. Finally the McNemar test results have also been plotted on the same diagrams. For each sub-RF of each size a McNemar answer has been obtained that indicates whether or not the sub-RF has outperformed the initial forest. If so, a mark has been drawn on the x-axis of the diagrams. In that way sub-RF with significant improvement over the initial RF are highlighted.

Table 2. Best error rates and number of trees of the corresponding selected subsets

Dataset	SFS		Forest-RI	Dataset	SFS		Forest-RI
	error rates	# trees	300 trees		error rates	# trees	300 trees
Digits	1.68	101	2.18	MNIST	4.44	109	4.92
DigReject	5.27	43	6.52	Musk	1.13	35	2.36
Gamma	11.14	76	12.45	Pendigits	0.41	41	0.96
Letter	3.17	83	4.15	Ringnorm	2.47	99	3.73
Madelon	18.13	59	26.67	Segment	0.65	11	1.83
Mfeat-fac	1.21	70	2.42	Spambase	2.73	58	4.56
Mfeat-fou	10.60	51	15.76	Twonorm	1.74	82	3.01
Mfeat-kar	0.60	73	2.57	Vehicle	16.07	31	26.79
Mfeat-zer	16.06	102	21.21	Waveform	11.35	138	14.48

One can first observe from Table 2 that in spite of the sub-optimality of SFS, it always finds a subset of trees that exhibits a lower error rate on the test set than the initial RF, induced with Forest-RI. Results of McNemar statistical test presented in Figure 1 strongly confirm this statement. Though it does not concern generalisation performance, a surprising result is that the number of trees in the "best" subset found during the selection process is often very small regarding to the size of the initial forest, sometimes even approaching 30% of the amount of available trees (Musk, Segment and Vehicle). Classifier selection has already shown to be a powerful tool for obtaining significant improvement with ensemble of classifiers, but this result leads us to think that it would be interesting to further focus on the number of trees that have to be grown in a forest to obtain significant improvement comparing to RF induced with Forest-RI, and rather according to generalisation accuracy.

Additional diagrams are then presented in Figures 2 and 3: (i) the 9 diagrams in figure 2 represent the error rates according to the ratio $\frac{\bar{\rho}}{s^2}$ (ii) The 9 diagrams in figure 3 represent this ratio according to the size of the sub-RF obtained during the selection process. In a concern to be clearer, only 9 of the 18 datasets have been used to illustrate our results, but tendencies discussed in this section can be expanded to the rest of the datasets since all the curves obtained follow the same global behavior.

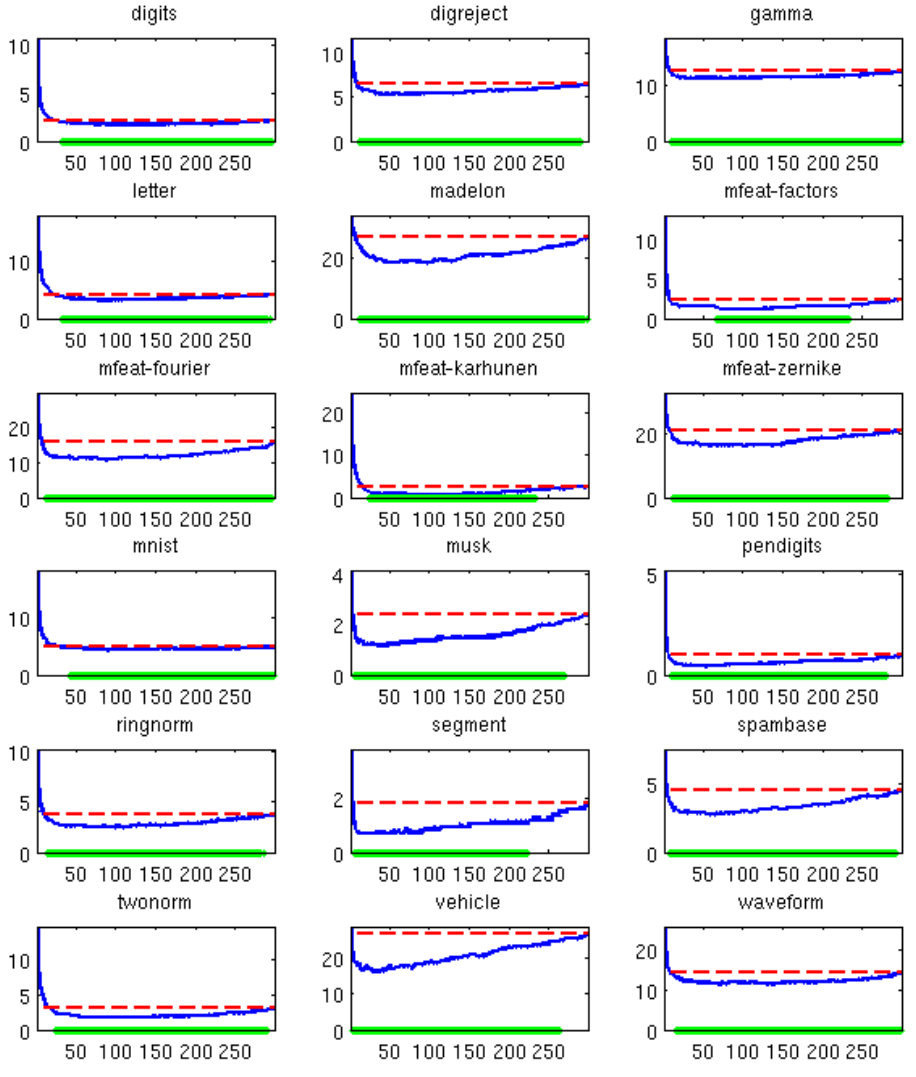

Fig. 1. Error Rates obtained during the selection process on the 18 datasets, according to the number of trees in the subsets. The dashed lines represent the error rates obtained with the initial RF made of 300 trees. The marks on the x-axis represent the sub-RFs for which McNemar test indicates that the accuracy improvement is statistically significant.

Figure 2 highlights the link between $\frac{\overline{p}}{s^2}$ and RF accuracy. One can firstly remark that the points on these diagrams follow the same global distribution for all the datasets, with a strong rise of error rates for increasing values of the ratio. From our point of view, this illustrates the fact that error rates are strongly related to the ratio and that this former measure tends to explain, at least partially, the variation of performance from a sub-RF to another. However, according to Breiman's theoretical results, the values

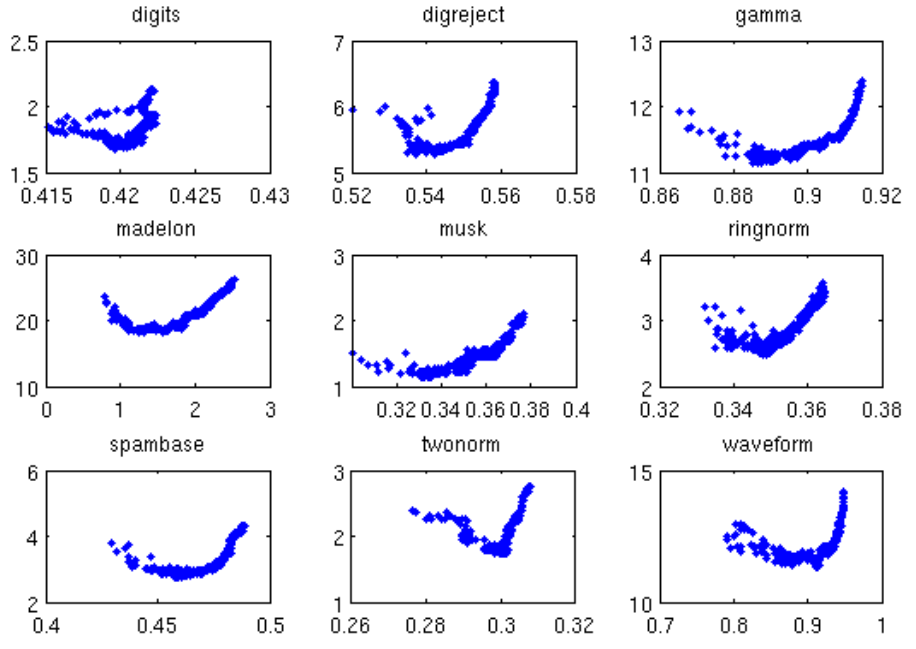

Fig. 2. Error rates according to the ratio $\frac{\bar{\rho}}{s^2}$

of this ratio should decrease jointly with the error rate, and one can observe that it is not strictly the case in these diagrams. The minimal error rate is never reached for the minimal value of $\frac{\bar{\rho}}{s^2}$, and a small rise is obtained for decreasing values on the x-axis. It seems to us that those few points for which the ratio is weak but for which the error rate is not minimal as expected, are particular cases for which the ratio computation has been biased. An explanation of these few points that do not fit with Breiman's theoretical results can probably be found in figure 3. One can notice indeed that all the curves in this figure surprisingly tend to monotonically decrease as the number of trees in sub-RF decreases. This decreasement is firstly consistent with our previous results that show that best error rates are obtained for a small subset of trees. But values of $\frac{\bar{\rho}}{s^2}$ seem particularly unstable for sub-RF made of less than about 50 trees, and this unstability has systematically been obtained for all the datasets used in our experiments. We think in the light of these results that the size of the sub-forests obtained during the selection process plays a role in the explanation of performance variations. Although the SFS method is interesting for evaluating the extent to which RF performance can be enhanced by selecting particular subsets of trees, the sequentiality of such a procedure seems to introduce a bias in the computation of Strength and Correlation measures. To continue the analysis of RF mechanisms via the study of sub-RF and of their accuracy evolution, we think that it would be more judicious to use a selection method such as Genetic Algorithm and to fix the number of trees selected, so that resulting sub-RF would be of the same size.

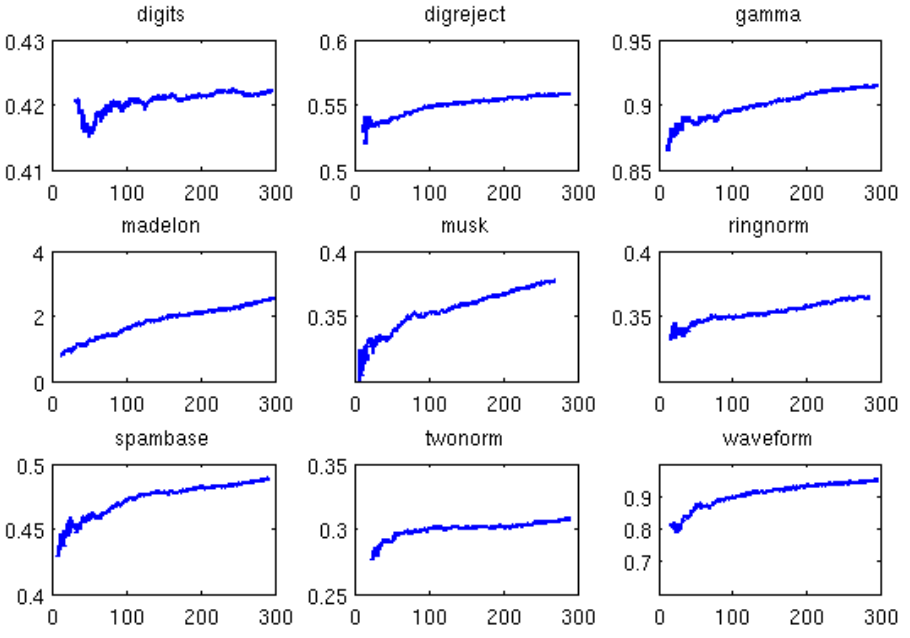

Fig. 3. The ratio $\frac{\bar{\rho}}{s^2}$ according to the size of the sub-RF

4 Conclusions

In this paper different sub-RF have been generated from a pool of random trees, in order to analyse RF mechanisms that could explain performance variation from a forest to another. A classifier selection method, *i.e.* the Sequential Forward Selection method (SFS), has been used for generating those sub-forests. The goal was firstly to obtain subsets of trees that exhibit lower error rates than the initial forest on a particular test set, in an attempt to correlate *strength* and *correlation* properties with those performance variations. A surprising result is that the "best" subsets of decision trees on the test set have shown to contain a small number of trees regarding to the amount of trees available in the initial forest, *i.e.* sometimes about 30%. Though this result is not significant in terms of generalisation performance, this statement gives the intuition that in a "traditional" RF induction algorithm several trees may deteriorate the performance of the ensemble, and that improvement could be obtained by inducing decision trees in a less arbitrary way in order to build accurate RF.

However for being able to design a RF induction procedure that could avoid this deterioration, it is essential to firstly identify and understand mechanisms that could explain the variations in sub-RF performance. We have thus propose in this paper a primary analysis that aimed at studying Strength and Correlation properties according to sub-RF accuracy obtained during the selection process on a particular test set. This experimental work has shown that the ratio $\frac{\bar{\rho}}{s^2}$, introduced by Breiman in [4], is linked to performance variation of RF. The nature of this link still remains an open issue but

we believe that this classifier selection approach will be very helpful in future works to identify it and to better understand Random Forest mechanisms.

References

1. Breiman, L.: Bagging predictors. Machine Learning 24(2), 123–140 (1996)
2. Ho, T.: The random subspace method for constructing decision forests. IEEE Transactions on Pattern Analysis and Machine Intelligence 20(8), 832–844 (1998)
3. Bernard, S., Heutte, L., Adam, S.: Using random forests for handwritten digit recognition. In: International Conference on Document Analysis and Recognition, pp. 1043–1047 (2007)
4. Breiman, L.: Random forests. Machine Learning 45(1), 5–32 (2001)
5. Geurts, P., Ernst, D., Wehenkel, L.: Extremely randomized trees. Machine Learning 36(1), 3–42 (2006)
6. Latinne, P., Debeir, O., Decaestecker, C.: Limiting the number of trees in random forests. In: Kittler, J., Roli, F. (eds.) MCS 2001. LNCS, vol. 2096, pp. 178–187. Springer, Heidelberg (2001)
7. Cutler, A., Zhao, G.: Pert - perfect random tree ensembles. Computing Science and Statistics 33 (2001)
8. Rodriguez, J., Kuncheva, L., Alonso, C.: Rotation forest: A new classifier ensemble method. IEEE Transactions on Pattern Analysis and Machine Intelligence 28(10), 1619–1630 (2006)
9. Breiman, L., Friedman, J., Olshen, R., Stone, C.: Classification and Regression Trees. Chapman and Hall (Wadsworth, Inc.), New York (1984)
10. Asuncion, A., Newman, D.: UCI machine learning repository (2007)
11. Breiman, L.: Arcing classifiers. The Annals of Statistics 26(3), 801–849 (1998)
12. LeCun, Y., Bottou, L., Bengio, Y., Haffner, P.: Gradient-based learning applied to document recognition. In: Proceedings of the IEEE, vol. 86(11), pp. 2278–2324 (1998)
13. Chatelain, C., Heutte, L., Paquet, T.: A two-stage outlier rejection strategy for numerical field extraction in handwritten documents. In: International Conference on Pattern Recognition, Honk Kong, China, vol. 3, pp. 224–227 (2006)
14. Bernard, S., Heutte, L., Adam, S.: Forest-rk: A new random forest induction method. In: International Conference on Intelligent Computing, pp. 430–437 (2008)
15. Dietterich, T.: Approximate statistical tests for comparing supervised classification learning algorithms. Neural Computation 10, 1895–1923 (1998)
16. Everitt, B.: The Analysis of Contingency Tables. Chapman and Hall, London (1977)

Learning Hereditary and Reductive Prolog Programs from Entailment*

Shahid Hussain[1] and M.R.K. Krishna Rao[2,**]

[1] Computer Science & Engineering Department,
Bahria University, Karachi 75260, Pakistan
[2] Information & Computer Science Department,
King Fahd University of Petroleum and Minerals,
Dhahran 31261, Saudi Arabia

Abstract. In this paper we study exact learning of Prolog programs from entailment and present an algorithm to learn two rich classes of Prolog programs namely hereditary and reductive Prolog programs. These classes contain standard Prolog programs with and without recursion like `append`, `merge`, `split`, `delete`, `member`, `prefix`, `suffix`, `length`, `add`, etc. Additionally our algorithm learns the hereditary Prolog programs in polynomial time.

1 Introduction

The problem of learning logic program from examples and queries based on works of Shapiro [3,4] has attracted a lot of attention in the last 25 years. Several techniques and systems for learning logic programs are developed and used in many applications. See [5] for a survey. In this paper, we consider the framework of *learning from entailment* [6,7,8,9,10,11,12,13] and present an algorithm to learn two classes of logic programs without local variables and include many program from Sterling and Shapiro's book [14].

The framework of *learning from entailment* has been introduced by Angluin [7] and Frazier and Pitt [9] to study the learnability of propositional Horn sentences. In recent times the framework has been used in learning first order Horn programs and many results have been published in [8,12,11,15]. In this framework, an Oracle (a teacher, a program, a machine, etc) is employed that answers the following types of queries from the learner. The Oracle answers "yes" to an *entailment equivalence query* EQUIV(H) if H is equivalent to the target program H_*, i.e., $H \models H_*$ and $H_* \models H$. Otherwise it produces a clause C such that $H_* \models C$ but $H \not\models C$ or $H_* \not\models C$ but $H \models C$. A *subsumption query* SUBSUME(C) produces an answer "yes" if the clause C is subsumed by a clause in H_*, otherwise answers 'no'. Furthermore, the learner might *ask* the Oracle for *hints*. If a clause $C : A \leftarrow B_1, \ldots, B_n$ such that $H_* \models C$, the request-for-hint

* This work is based upon first author's previous work as described in [1] and [2].
** Second author is currently with Lakshami Enterprises (Aust) Pty Ltd and Balaji Real Estate Pty Ltd, 22 Norinda Std, Sunnybank, QLD 4109, Australia.

D.-S. Huang et al. (Eds.): ICIC 2009, LNAI 5755, pp. 546–555, 2009.

query REQ(C) returns (a) an answer 'subsumed' if $A \leftarrow B_1, \ldots, B_n$ is subsumed by a clause in H_*, otherwise returns (b) an atom (the hint) B in the proof of $H_* \models C$. The framework of learning from entailment is employed in learning first order Horn programs by Page [10] and Arimura [8].

In this paper, we extend the results of Arimura [8] for two classes of Prolog programs namely *hereditary* and *reductive* Prolog programs. We show that hereditary and reductive programs are exactly learnable from entailment. Furthermore, the algorithm learns the hereditary programs in polynomial time.

The class of hereditary programs contains the class of acyclic-constrained horn programs. Furthermore, Krishna Rao in [16] shows that every hereditary Prolog program is a reductive program [16]. Both hereditary and reductive programs are also learnable from positive data alone.

The rest of the paper is organized as follows. The next section discusses the preliminaries required for this paper. Sections 3 and 4 describe the hereditary and reductive programs in detail, respectively. Section 5 presents the learning algorithm. The next two section i.e, Sections 6 and 7 analyze and prove the correctness of the learning algorithm for hereditary and reductive programs, respectively. Finally this paper ends with the conclusion in Section 8.

2 Preliminaries

We assume that the reader is acquainted with the basic terminology of first order logic and logic programming as described by Lloyd [17] or Apt [18]. Following is the discussion of some important results and definitions in the sequel.

2.1 Subsumption and Entailment

Definition 1. *Let C_1 and C_2 be two clauses $H_1 \leftarrow Body_1$ and $H_2 \leftarrow Body_2$ respectively. Then the clause C_1* subsumes *the clause C_2 denoted as $C_1 \succeq C_2$ (or $C_2 \preceq C_1$) if there exists a substitution θ such that $H_1\theta \equiv H_2$ and $Body_1 \subseteq Body_2$.*

Definition 2. *A program P_1 is a refinement of a program P_2, denoted as $P_1 \sqsubseteq P_2$ if $(\forall C_1 \in P_1)(\exists C_2 \in P_2)$ such that $C_2 \succeq C_1$. Further, P_1 is a* conservative refinement *of P_2 if P_1 is a refinement of P_2 and each C in P_2 has at most one $C' \in P_1$ such that $C \succeq C'$.*

Definition 3. *A program P* entails *a clause C, denoted as $P \models C$, if C is a logical consequence of P.*

The relation between subsumption and entailment is discussed below.

Definition 4. *A* derivation *of a clause C from a program P is a finite sequence of clauses $C_1, \ldots, C_k = C$ such that C_i is either an instance of a clause in P or a resolvent of two clauses in $C_1, \ldots, C_{i-1}$. If such a derivation exists, we write $P \vdash_d C$.*

Following theorem is proved in Nienhuys-Cheng and de Wolf [19]

Theorem 1 (Subsumption Theorem [19]). *Let P be a program and C be a clause. Then $P \models C$ if and only if one of the following holds:*

1. *C is a tautology or*
2. *there exists a clause D such that $P \vdash_d D$ and D subsumes C.*

When C is ground, the above theorem can be reformulated as follows.

Theorem 2. *Let P be a program and C be a ground clause $A \leftarrow B_1, \ldots, B_n$. Then $P \models C$ if and only if one of the following holds:*

1. *C is a tautology.*
2. *C is subsumed by a clause in P.*
3. *There is a minimal SLD-refutation of $P' \cup \{\leftarrow A\}$, where*

$$P' = P \cup \{B_i \leftarrow \mid i \in [1, n]\}$$

Definition 5. *An SLD-refutation is* minimal *if selected atoms are resolved with unit clauses whenever possible.*

Lemma 1. *If C_1 and C_2 are two clauses then $C_1 \succeq C_2$ is decidable in polynomial time over the sizes of C_1 and C_2.*

2.2 The Oracle

We assume that there exists an Oracle that answers following queries correctly.

- Entailment equivalence queries,
- Subsumption queries, and
- Request-for-hint queries.

Definition 6. *An* entailment equivalence query*, denoted as EQUIV(H), returns "yes" if H is equivalent to the target program H_*, i.e., $H \models H_*$ and $H_* \models H$. Otherwise it produces a ground atom A such that $H_* \models A$ but $H \not\models A$ or $H_* \not\models A$ but $H \models A$.*

Definition 7. *A* subsumption query*, denoted as SUBSUME(C), returns "yes" if the clause C is subsumed by a clause in H_*, otherwise "no".*

Definition 8. *A* request for hint query*, denoted as REQ(C) (when C is a ground clause $A \leftarrow B_1, \ldots, B_n$), returns an answer "subsumed" if C is subsumed by a clause in H_*, otherwise returns an atom (a hint) $B\theta$ in a minimal SLD-refutation of $H' \cup \{\leftarrow A\}$ with answer substitution θ such that $B\theta \notin \{B_1, \ldots, B_n\}$, where $H' = H_* \cup \{B_i \leftarrow \mid i \in [1, n]\}$.*

Lemma 2. *The query SUBSUME(C) can be answered in polynomial time over the size of the target program and the size of C.*

Proof. Follows from Lemma 1. □

Lemma 3. *The query EQUIV(H) can be answered in polynomial time over the size of the target program and the size of H.*

Proof. This can be done by checking that each clause in H is subsumed by a clause in the target program H_* and each clause in H_* is subsumed by a clause in H. Each such subsumption check can be done in polynomial time and hence EQUIV(H) can be answered in polynomial time. □

3 Hereditary Programs

A definite clause

$$p(t_1, \ldots, t_n) \leftarrow q_1(s_{1_1}, \ldots, s_{1_{n_1}}), \ldots, q_k(s_{k_1}, \ldots, s_{k_{n_k}})$$

is hereditary if each s_{i_j} is a subterm of some t_l for $i \in [1, k]$, $j \in [1, n_i]$, and $l \in [1, n]$. A logic program is called hereditary if all clauses in it are hereditary.

Consider following hereditary program from [16]:

$$p(h(f(\mathbf{X}), g(\mathbf{Y})), \mathbf{Z}) \leftarrow q(f(\mathbf{X}), g(\mathbf{Y}), \mathbf{Z})$$
$$q(\mathbf{X}, \mathbf{X}, g(\mathbf{Y}), \mathbf{Z}) \leftarrow$$

Following theorem appears in [13] for finely-moded programs and also in [16] in a slightly different form for hereditary programs.

Theorem 3. *Let P be an hereditary program and Q be a ground query $\leftarrow p(\mathbf{s})$. Then every term of any atom $q(\mathbf{u})$ in an SLD-derivation of $P \cup \{Q\}$ is a subterm of a term in $\mathbf{s}$.*

Definition 9. *A clause C is a saturation of an example E w.r.t. a theory (program) H if and only if C is a reformulation of E w.r.t. H and $C' \Rightarrow C$ for every reformulation C' of E w.r.t. H. A clause D is reformulation of E w.r.t. H if and only if $H \wedge E \Leftrightarrow H \wedge D$.*

A saturation of an example $E \equiv p_0(\mathbf{s}_0)$ w.r.t. a hereditary program H is defined as $E \leftarrow Closure_H(E)$, where $Closure_H(E) = \{p(\mathbf{s}) \mid$ each term in $\mathbf{s}$ is a subterm of a term in $\mathbf{s}_0$ and $H \models p(\mathbf{s})\}$.

Definition 10 (Least General Generalization). *Let C_1 and C_2 be two hereditary clauses $A_1 \leftarrow Body_1$ and $A_2 \leftarrow Body_2$, respectively. The* least general generalization *(LGG) $C_1 \sqcup C_2$ is defined as a clause $A \leftarrow Body$ such that:*

- *$A \equiv p_0(\mathbf{s}_0)$ is the least general generalization of A_1 and A_2 and $A_i \equiv A\sigma_i$, $i \in [1, 2]$.*
- *$Body = \{p(\mathbf{s}) \mid p(\mathbf{s})\sigma_i \in Body_i, i \in [1, 2]$, each term in $\mathbf{s}$ is a subterm of a term in $\mathbf{s}_0\}$.*

The least general generalization of two hereditary clauses defining the same predicate (i.e., predicate symbol of the two heads is same) is unique and its length is bounded by the lengths of the clauses. It can be computed in polynomial time in the sizes of the clauses (time complexity is $\mathcal{O}(m_1 \cdot m_2)$, where m_1 and m_2 are the number of atoms in the two clauses C_1 and C_2).

4 Reductive Programs

A definite clause

$$p(t_1, \ldots, t_n) \leftarrow q_1(s_{1_1}, \ldots, s_{1_{n_1}}), \ldots, q_k(s_{k_1}, \ldots, s_{k_{n_k}})$$

is reductive if for each argument s_{i_j} in the body, there is an argument t_l in the head such that $|t_l\sigma| \geq |s_{i_j}\sigma|$ for every substitution σ. A logic program is called reductive if all classes in it are reductive.

Theorem 4 (Krishna Rao [16]). *It is decidable whether a given logic programs is reductive or not.*

Theorem 5 (Krishna Rao [16]). *Let P be a reductive logic program and Q be a ground query such that n is greater than the size of every argument in Q. Then n is greater than the size of every argument of every atom in every SLD-derivation of $P \cup \{Q\}$.*

Definition 11. *A clause C is a saturation of an example E w.r.t. a theory (program) H if and only if C is a reformulation of E w.r.t. H and $C' \Rightarrow C$ for every reformulation C' of E w.r.t. H. A clause D is reformulation of E w.r.t. H if and only if $H \wedge E \Leftrightarrow H \wedge D$.*

A saturation of an example $E \equiv p(t_1, \ldots, t_n)$ w.r.t. a reductive program H is defined as $E \leftarrow \mathit{Closure}_H(E)$, where $\mathit{Closure}_H(E) = \{q(s_1, \ldots, s_m) \mid$ for every term s_i there is a term t_j such that $|s_i| \leq |t_j|\}$.

Definition 12 (Least General Generalization). *Let C_1 and C_2 be two reductive clauses $A_1 \leftarrow \mathit{Body}_1$ and $A_2 \leftarrow \mathit{Body}_2$, respectively. The* least general generalization *(LGG) $C_1 \sqcup C_2$ is defined as a clause $A \leftarrow \mathit{Body}$ such that:*

- *$A \equiv p(t_1, \ldots, t_n)$ is the least general generalization of A_1 and A_2 and $A_i \equiv A\sigma_i$, $i \in [1, 2]$.*
- *$\mathit{Body} = \{q(s_1, \ldots, s_m) \mid q(s_1, \ldots, s_m)\sigma_i \in \mathit{Body}_i, i \in [1, 2]$,and each term s_i is q, there is a term t_j in p such that $|s_i|\theta| \leq |t_j\theta|\}$.*

The least general generalization of two reductive clauses defining the same predicate (i.e., predicate symbol of the two heads is same) is unique and its length is bounded by the lengths of the clauses. It can be computed in polynomial time in the sizes of the clauses (time complexity is $\mathcal{O}(m_1 \cdot m_2)$, where m_1 and m_2 are the number of atoms in the two clauses C_1 and C_2).

5 Learning Algorithm

Following is a learning algorithm that can be used for both hereditary program as well as reductive programs. However, the working, complexity analyses, and correctness proofs are different for the two classes, as discussed in their respective sections.

Algorithm 1. Learn

```
begin
    H := ∅;
    while EQUIV(H) ≠ "yes" do
        A := counterexample;
        C := A ← Closure_H(A);
        while REQ(C) returns a hint B do
            C := B ← Closure_H(B);
        end
        C := Reduce(C);
        if SUBSUME(C ⊔ D) returns "yes" for some clause D ∈ H then
            generalize H by replacing D with Reduce(C ⊔ D);
            else generalize H by adding C to H
        end
    end
    Return(H);
end
```

Algorithm 2. Reduce$(A \leftarrow Body)$

```
begin
    for each atom B ∈ Body do
        if SUBSUME(A ← (Body − {B}) then
            Body := (Body − {B});
        end
    end
    Return(A ← Body);
end
```

6 Learning Hereditary Programs

6.1 Correctness Proof

In the following, k denotes the number of predicate symbols in Π and k' denotes the maximum arity of predicate symbols in Π.

Lemma 4. *If A is a ground atom then $|Closure_H(A)|$ is bounded by a polynomial over $|A|$ and can be computed in polynomial time over $|A|$.*

Proof. Let $n = |A|$. By definition each term of an atom $p \in Closure_H(A)$ is a subterm of a term of A. The number of subterms of a term is bounded by its size. The number of atoms $p \in Closure_H(A)$ is bounded by $k \cdot n^{k'}$, a polynomial in n and can be computed in polynomial time over $|A|$. □

Lemma 5. *Let A be either a positive example returned by an equivalence query or a hint returned by a request-for-hint query. The query $REQ(A \leftarrow Closure_H(A))$ can be answered in polynomial time over the size of the target program and the size of A.*

Proof. It is easy to see that $H_* \models A$ if A is a positive example or A is a hint returned by a request-for-hint query. Therefore, there is an SLD-refutation of $H_* \cup \{\leftarrow A\}$, say with an answer substitution θ. Theorem 3 asserts that every term of each atom $p(\mathbf{u})$ in such an SLD-refutation is a subterm of a term in A.

Let S be the set of all atoms $p(\mathbf{u})$ such that $H_* \models p(\mathbf{u})$ and each term in $\mathbf{u}$ is a subterm of a term in A. Since the number of subterms of a term is bounded by its size, $|S|$ is bounded by a polynomial over the size of A and S can be computed in polynomial time over the size of A in a bottom-up fashion. Now, an SLD-refutation of $H_* \cup \{\leftarrow A\}$ can be constructed in polynomial time by resolving each selected atom with a ground instance of a clause whose body atoms are members of S. □

Let H_* represent the target program to be learned from the algorithm **Learn**, $H_0, H_1, \ldots$, be the sequence of hypotheses proposed in the equivalence queries and $A_1, A_2, \ldots$, be the sequence of counterexamples returned by those queries.

Theorem 6. *For each $i \geq 0$, hypothesis H_i is conservative refinement of H_* and counterexample A_{i+1} is positive.*

Proof. Induction on i (the iteration).

Basis Step: For $i = 0$, $H_i = \emptyset$ and theorem trivially holds.

Induction Hypothesis: Assume that the theorem holds for $i = m - 1$.

Induction Step: Now establish that it holds for $i = m$. Consider the m-th iteration of the main **while** loop. Since A is positive counterexample, $H_* \models A$ and hence $H_* \models A \leftarrow \mathit{Closure}_{H_{m-1}}(A)$. Each hint B is an atom in an SLD-refutation of $H' \cup \{\leftarrow A\}$ where $H' = H_* \cup \{B' \leftarrow | B' \in \mathit{Closure}_{H_{m-1}}(A)\}$. By induction hypothesis, H_{m-1} is a conservative refinement of H_* and hence $H_* \models B'$ for each $B' \in \mathit{Closure}_{H_{m-1}}(A)$. Therefore, each hint B is an atom in an SLD-refutation of $H_* \cup \{\leftarrow A\}$ and $H_* \models B \leftarrow \mathit{Closure}_H(B)$. By definition, $H_{m-1} \not\models B$ for any hint B. That is, $H_* \models C$ and $H_{m-1} \not\models C$ for each clause C at the exit of the inner **while** loop. We have two cases:

(a) there is a clause $D \in H_{m-1}$ such that $C \sqcup D$ is subsumed by a clause $C_* \in H_*$ and $H_m = H_{m-1} \cup \{\mathbf{Reduce}(C \sqcup D)\} - D$, or
(b) there is no such clause D and $H_m = H_{m-1} \cup \{C\}$.

By induction hypothesis, H_{m-1} is a conservative refinement of H_* and its is easy to see that H_m is a conservative refinement of H_* in case (b). Consider case (a) now. Since H_{m-1} is a conservative refinement of H_*, D is the unique clause in H_{m-1} subsumed by C_*. As H_m is obtained from H_{m-1} by replacing D with $\mathbf{Reduce}(C \sqcup D)$, it is clear that H_m is a conservative refinement of H_*. Since each hypothesis is a refinement, each counterexample is positive. □

Lemma 6. *If C is a clause of size n, then the sequence $C = C_0 \succ C_1 \succ C_2 \succ \cdots$ is of length no more than $2n$.*

Proof. When $C_i \prec C_{i+1}$, one of the following holds: (1) $\mathit{size}(C_{i+1}) = \mathit{size}(C_i)$ and $|\mathit{Var}(C_{i+1})| > |\mathit{Var}(C_i)|$, i.e., a constant or an occurrence of a variable

(which occurs in C_i more than once) is replaced by a new variable or (2) $size(C_{i+1}) < size(C_i)$. The change (1) can occur at most n times as the number of variables in a clause is less than its size. Change (2) can occur at most n times as the size of any clause is positive. □

Theorem 7. *For any counterexample A of size n, the inner **while** loop of **Learn** iterates for no more than $k \cdot n^{k'}$ times.*

Proof. Since each hint B is an atom in an SLD-refutation of $H_* \cup \{\leftarrow A\}$, the terms of B are subterms of the terms of A by Theorem 3. There are at most $k \cdot n^{k'}$ such atoms. As the target program H_* is a terminating program, no atom B is returned as hint more than once. Therefore, the inner **while** loop iterates for no more than $k \cdot n^{k'}$ times. □

Theorem 8. *The algorithm **Learn** exactly identifies any hereditary program with m clauses in a polynomial time over m and n, where n is the size of the largest counterexample provided.*

Proof. Termination condition of the main **while** loop is $H \Leftrightarrow H_*$. Therefore **Learn** exactly identifies the target program H_* if **Learn** terminates. Following is the proof that the number of iteration of the main **while** loop is bounded by a polynomial over m and n.

By Theorem 6, H is always a conservative refinement of H_* and hence H has at most m clauses. By Lemma 4, the size of each clause in H is bounded by a polynomial in n. Each iteration of the main **while** loop either adds a clause to H or generalizes a clause in H. By Lemma 6, the number of times a clause can be generalized is bounded by twice the size of the clause. Therefore, the number of iterations of the main **while** loop is bounded by $m \cdot poly(n)$, where $poly(n)$ is a polynomial in n. Each iteration takes polynomial time as:

- saturation and least-general generalization are polynomial time computable,
- each query is answered in polynomial time, and
- by Theorem 7, the number of iterations of the inner **while** loop is bounded by a polynomial in n.

Therefore **Learn** exactly identifies hereditary programs with m clauses in a polynomial time over m and n. □

7 Learning Reductive Programs

7.1 Correctness Proof

Lemma 7. *Let A be either a positive example returned by an equivalence query or a hint returned by a request-for-hint query. The query $REQ(A \leftarrow Closure_H(A))$ is decidable.*

Proof. It is easy to see that $H_* \models A$ if A is a positive example or A is a hint returned by a request-for-hint query. Therefore, there is an SLD-refutation of $H_* \cup \{\leftarrow A\}$, say with an answer substitution θ. Theorem 5 asserts that the size of every term of each atom $p(u_1, \ldots, u_m)$ in such an SLD-refutation is less than or equal to that of a term in A.

Let S be the set of all atoms $p(u_1, \ldots, u_m)$ such that $H_* \models p(u_1, \ldots, u_m)$ and the size of each term in p is less than or equal to that of a term in A. Obviously $|S|$ is finite. Now, an SLD-refutation of $H_* \cup \{\leftarrow A\}$ can be constructed by resolving each selected atom with a ground instance of a clause whose body atoms are members of S. □

Let H_* represent the target program to be learned from the algorithm **Learn**, $H_0, H_1, \ldots$, be the sequence of hypotheses proposed in the equivalence queries and $A_1, A_2, \ldots$, be the sequence of counterexamples returned by those queries.

Theorem 9. *For each $i \geq 0$, hypothesis H_i is conservative refinement of H_* and counterexample A_{i+1} is positive.*

Proof. Similar as proof for Theorem 6 □

Theorem 10. *For any counterexample A, the inner **while** loop of **Learn** terminates.*

Proof. Similar as proof for Theorem 7 □

Theorem 11. *The algorithm **Learn** exactly identifies any reductive program.*

Proof. Termination condition of the main **while** loop is $H \Leftrightarrow H_*$. Therefore **Learn** exactly identifies the target program H_* if **Learn** terminates. Following is the proof that the algorithm **Learn** terminates.

By Theorem 9, H is always a conservative refinement of H_* and hence H has at most m clauses. Each iteration of the main **while** loop either adds a clause to H or generalizes a clause in H. By Lemma 6, the number of times a clause can be generalized is bounded by twice the size of the clause. Therefore, the number of iterations of the main **while** loop is finite and the algorithms is decidable as:

- saturation and least-general generalization are polynomial time computable,
- each query is decidable, and
- by Theorem 10, the inner **while** loop terminates.

Therefore **Learn** exactly identifies reductive programs. □

8 Conclusion

In this paper we considered exact learning of logic programs from entailment and present an algorithm that learns hereditary and reductive programs. Furthermore, the algorithm exactly learns the hereditary programs in polynomial time.

References

1. Hussain, S.: Learnability Results for Elementry Formal Systems. Ms thesis, King Fahd University of Petroleum and Minerals (2007)
2. Hussain, S.: Learnability Results for Elementary Formal Systems: EFS and Prolog programs. VDM Verlag Dr. Müller (2009)
3. Shapiro, E.Y.: Inductive Inference of Theories from Facts. Technical Report RR 192, Yale University (1981)
4. Shapiro, E.: Algorithmic Program Debugging. MIT Press, Cambridge (1983)
5. Muggleton, S., Raedt, L.: Inductive logic programming: Theory and methods. Journal of Logic Programming 19(20), 629–679 (1994)
6. Angluin, D.: Learning with hints. In: COLT 1988: Proceedings of The Second Annual Workshop on Computational Learning Theory, pp. 167–181 (1988)
7. Angluin, D.: Queries and Concept Learning. Machine Learning, 2(4), 319–342 (1988)
8. Arimura, H.: Learning Acyclic First-order Horn Sentences from Entailment. In: Li, M. (ed.) ALT 1997. LNCS, vol. 1316, pp. 432–445. Springer, Heidelberg (1997)
9. Frazier, M., Pitt, L.: Learning from Entailment: An Application to Propositional Horn Sentences. In: ICML 1993: Proceedings of International Conference on Machine Learning, pp. 120–127 (1993)
10. Page Jr., C.D., Frisch, A.: Generalization and Learnability: A Study of Constrained Atoms. In: Muggleton, S.H. (ed.) Inductive Logic Programming., pp. 29–61. Academic Press, London (1992)
11. Reddy, C., Tadepalli, P.: Learning first order acyclic Horn programs from entailment. In: ILP 1998: Proceedings of Internaional Workshop on Logic Programming, pp. 23–37 (1998)
12. Krishna Rao, M.R.K., Sattar, A.: Learning Linearly-moded Programs from Entailment. In: Lee, H.-Y. (ed.) PRICAI 1998. LNCS (LNAI), vol. 1531, pp. 482–493. Springer, Heidelberg (1998)
13. Krishna Rao, M.R.K., Sattar, A.: Polynomial-time Learnability of Logic Programs with Local Variables from entailment. Theoretical Computer Science 268, 179–198 (2001)
14. Sterling, L., Shapiro, E.: The Art of Prolog, 2nd edn. MIT Press, Cambridge (1994)
15. Arias, M., Khardon, R.: Learning Closed Horn Expressions. Information and Computation 178(1), 214–240 (2002)
16. Krishna Rao, M.R.K.: Some Classes of Prolog Programs Inferable from Positive Data. Theoretical Computer Science 241, 211–234 (2000)
17. Lloyd, J.: Foundations of Logic Programming. Springer, Berlin (1984)
18. Apt, K.R.: Logic programming. In: Handbook of Theoretical Computer Science: Formal Models and Semantics, vol. B, pp. 493–574. MIT Press, Cambridge (1990)
19. Nienhuys-Cheng, S.H., De Wolf, R.: The Subsumption Theorem for Several Forms of Resolution (1995)

A Novel Local Sensitive Frontier Analysis for Feature Extraction

Chao Wang[1,2], De-Shuang Huang[1], and Bo Li[1,2]

[1] Intelligent Computing Lab, Institute of Intelligent Machine,
Chinese Academy of Science, P.O. Box1130, Hefei, Anhui, 230031, China
dshuang@iim.ac.cn
[2] Department of Automation, University of Science and Technology of China,
Hefei, Anhui, 230027, China
wangchaopike@yahoo.com.cn, libo1975@163.com

Abstract. In this paper, an efficient feature extraction method, named local sensitive frontier analysis (LSFA), is proposed. LSFA tries to find instances near the crossing of the multi-manifold, which are sensitive to classification, to form the frontier automatically. For each frontier pairwise, those belonging to the same class are applied to construct the sensitive within-class scatter; otherwise, they are applied to form the sensitive between-class scatter. In order to improve the discriminant ability of the instances in low dimensional subspace, a set of optimal projection vectors has been explored to maximize the trace of the sensitive within-class scatter and simultaneously, to minimize the trace of the sensitive between-class scatter. Moreover, with comparisons to some unsupervised methods, such as Unsupervised Discriminant Projection (UDP), as well as some other supervised feature extraction techniques, for example Linear Discriminant Analysis (LDA) and Locality Sensitive Discriminant Analysis (LSDA), the proposed method obtains better performance, which has been validated by the results of the experiments on YALE face database.

Keywords: Dimensionality Reduction, LDA, LSFA, SVM, UDP, LSDA.

1 Introduction

Nowadays, manifold learning based methods have been put forward to explore the inherent structure of manifold data. For example, Isometric Maps (ISOMAP) [1], Local Linear Embedding (LLE)[2, 3], Laplacian Eigenmaps (LE) [4, 5], Local Tangent Space Alignment (LTSA) [6], Maximum Variance Unfolding (MVU) [7, 8, 9], and Riemannian Manifold Learning (RML) [10] are six representative manifold learning algorithms. Among all those, the most widely used one is LE, which is also a spectral mapping method. Usually, LE aims to find a low dimensional representation that preserves the local properties of the data lying on a low dimensional manifold. However, LE is a nonlinear dimensionality reduction technique, whose generalization ability is very weak. That is to say, the projection results in low dimensional space of the test image can not be easily obtained. This problem is also called out-of-sample problem. So far, linearization, kernelization, tensorization and other tricks have been

D.-S. Huang et al. (Eds.): ICIC 2009, LNAI 5755, pp. 556–565, 2009.

introduced to avoid the problem [2, 10]. Locality Preserving Projections (LPP) [11, 12] is a linear approximation to LE. Due to introducing of linearization, LPP shows its excellent properties such as low computational cost and robustness to noise and outliers [13]. Recently, Yang et al. proposed Unsupervised Discriminant Projection (UDP) algorithm [14], which is capable of characterize the local scatter and the non-local scatter. Moreover, UDP seeks to find a linear projection that can not only maximize the non-local scatter but also minimize the local scatter. And it must be noted that both LPP and UDP are the unsupervised, linear approximations to the manifold learning approaches without taking the class information into account. However, it has been shown that the class information has much to do with discriminative features that are optimal for classification**.** Therefore some supervised methods have been developed, such as Marginal Fisher Analysis (MFA) [15], Locality Sensitive Discriminant Analysis (LSDA) [16], Average Neighborhood Margin Maximization (ANMM)[17], Locally Linear Discriminant Embedding[LLDE][18], and Nonparametric Margin Maximization Criterion (NMMC) [19] etc. In MFA, two different graphs are constructed, one is the penalty graph constructed based on the instances from different classes, the other is the intrinsic graph where the instances from the same class are involved. Moreover, when constructing the graphs, the number of the nearest neighbors is differently selected in order to acquire a better prediction result. This weakness makes it difficult to be applied. Another similar method named Average Neighborhood Margin Maximization (ANMM) [17], which aims at pulling the neighboring points with the same class label towards each other as near as possible, while simultaneously pushing the neighboring points with different labels away from each other as far as possible. This algorithm also needs to define two neighborhood radiuses. Qiu et al. [19] proposed a Nonparametric Margin Maximization Criterion (NMMC) for learning the projection vectors, which tries to maximize the difference of the distance between each nearest neighbor of the different class to the distance among its furthest neighbor in the same class. The problem is that only using the nearest (or furthest) neighbor for defining the margin may cause the algorithm sensitive to outlier. In terms of implementation, MFA, ANMM, and NMMC have two radiuses to be set which could be time consumption. Unlike the last three methods, only one KNN criterion is introduced to define the neighborhood graph in Locality Sensitive Discriminant Analysis (LSDA) [16], which was proposed by Cai. et al. In this algorithm the neighborhood graph was constructed first, the instances from the k nearest neighbors with the same class label are considered as the within-class neighbors, while the others from different class considered as the between-class neighbors. Then LSDA aims to find a projection that can make the within-class neighbor more compact and the between-class neighbor more separate. However, this algorithm only focuses on the neighborhood, and the same class instances which are far from each other also play important contribution to the classification. Here, a more effective method which avoid the weakness of the former algorithm and inherit their advantages presented.

1) Only one KNN criterion has been constructed, which specifies two radiuses such as in-this-KNN patch and out-of-the-KNN patch. In the KNN patch if it has instance from different classes, it will become sensitive between class instances. Otherwise, instances from the same class but belong to different KNN

patches are sensitive within class instances. Only one KNN criterion to be set saves the time consumption and makes it easy to practical use.

2) The classification contribution weights are defined. Those weights take consideration of the local density and it could be weaken the assumption that the data of each class must be Gaussian distributed.
3) The within class intrinsic structure is protected well through leaving the instance of the same KNN patch from the same class unchanged, and set the instance's classification weight according to the position of its distribution. This disposal could preserve the data set's intrinsic structure well.

This paper is organized as follows: Section 2 introduces and elaborates the proposed algorithm local sensitive frontier analysis (LSFA). Section 3 presents the experimental results of the proposed algorithm in comparison with other popular algorithms. Finally, we summarize the work in Section 4.

2 Local Sensitive Frontier Analysis

2.1 Construction of the Nearest Neighborhood Matrix

To construct the nearest neighbor, an adjacency graph $G=(V,H)$ is constructed. Generally, there are two ways for constructing the nearest neighbor patch, either $k-neighborhood$ or $\varepsilon-ball$. $\varepsilon-ball$ method is used to construct the nearest neighbors in most cases, however, if the instances scattered much sparsely in some part of the high dimensional space or the instances from different classes are scattered much farther than ε . Under this circumstance, the sensitive between class instance of LSFA could not be correctly detected, therefore the method of $k-neighborhood$ is adopted in LSFA. The binary value to represent the instance belongs to other instance's KNN patch or not. Two kinds of criteria to define the nearest neighbor matrix are employed as follows:

$$H_{i,j}=\begin{cases}1 & if\ X_j\in K(X_i),\\ 0 & else.\end{cases} \tag{1}$$

$$H_{i,j}=\begin{cases}1 & if\ \|X_i-X_j\|\le\varepsilon\\ 0 & else\end{cases} \tag{2}$$

In the above function, ε is a parameter which can be set according to the average distance of the dataset, and $\|X_i-X_j\|$ is the Euclidean distance between instance X_i and instance X_j .

2.2 Label Neighborhood Relation Matrix

In the following, we introduce a label neighborhood relation matrix L to describe the class information of those instances. If instance X_i and instance X_j are belong to the

same class, the element L_{ij} equals to 1, and otherwise equals to 0. Formally, the elements of the label neighborhood relation matrix L are given as follows:

$$L_{i,j} = \begin{cases} 1 & X_j, X_i \in c_k, \\ 0 & X_j \in c_l, X_i \in c_k \text{ and } l \neq k \end{cases} \tag{3}$$

c_k is the sets of the instance belong to the class k.

2.3 Detection of the Sensitive Instances

After the nearest neighbor graph is constructed, the sensitive instance can be detected based on the adjacency graph and the label information. The instance which has the other classes' instances in its KNN patch is the sensitive inter-class instance. The sensitive inter-class instance can be formally defined as follows:

$$S_{SI_{ij}} = (ee^T - L_{ij}) \otimes H_{ij} \tag{4}$$

where $e = (1,1\cdots,1)^T$ is a N dimensional vector. In the matrix S_{SI}, if the row vector S_{SIi} has nonzero elements, the corresponding instance X_i is the sensitive inter-class instance and its classification contribution weight is equal to the number of nonzero elements in the row vectors S_{SIi}. Here symbol '$\otimes$' means the Hadamard product. On the other hand, those which are not contented in the same KNN patch but belong to the same class are named sensitive within-class instances. The sensitive within-class instances can be detected by the following function:

$$S_{SW_{ij}} = (ee^T - H_{ij}) \otimes L_{ij} \tag{5}$$

If the row vector S_{Swi} has nonzero element S_{Swij}, the corresponding instances X_i and X_j will be defined as the sensitive within-class instances and the classification contribution weight of X_i is equal to the number of nonzero elements in the row vectors S_{Swi}. The sensitive inter-class instances should be used to construct the sensitive inter-class graph and the sensitive within-class instances are taken to construct the sensitive within-class graph.

2.4 Characterization of the Sensitive within-Class Graph and Sensitive Inter-class Graph

After the sensitive instances were detected, the covariance matrix corresponding to those instances is computed. In order to fulfill the idea which is designed to make the sensitive inter-class instance much farther from each other after projection, this can be practically performed by maximizing the trace of the sensitive inter-class scatter matrix. In order to make those sensitive within-class instances more compact to its class center, the trace of the scatter matrix corresponding to the sensitive within-class

instances will be minimized after projection. Based on it, the following objective function can be constructed:

$$\begin{aligned}\max_w \quad J_{LL}(w) &= \frac{1}{2}\frac{1}{N}\frac{1}{N}\sum_{i=1}^{N}\sum_{j=1}^{N} S_{SIij}\left\|Y_i - Y_j\right\|^2 \\ &= \frac{1}{2}\frac{1}{N}\frac{1}{N}\sum_{i=1}^{N}\sum_{j=1}^{N} S_{SIij}\left\|w^T X_i - w^T X_j\right\|^2 \\ &= w^T\left[\frac{1}{2}\frac{1}{N}\frac{1}{N}\sum_{i=1}^{N}\sum_{j=1}^{N} S_{SIij}(X_i - X_j)(X_i - X_j)^T\right]w \\ &= w^T\left[\frac{1}{2}\frac{1}{N}\frac{1}{N}\sum_{i=1}^{N}\sum_{j=1}^{N} S_{SIij}\overline{X_i}\,\overline{X_j}^T\right]w \\ &= w^T S_{LL} w\end{aligned} \tag{6}$$

$$\begin{aligned}\min_w \quad J_{NL}(w) &= \frac{1}{2}\frac{1}{N}\frac{1}{N}\sum_{i=1}^{N}\sum_{j=1}^{N} S_{SWij}\left\|Y_i - Y_j\right\|^2 \\ &= \frac{1}{2}\frac{1}{N}\frac{1}{N}\sum_{i=1}^{N}\sum_{j=1}^{N} S_{SWij}\left\|w^T X_i - w^T X_j\right\|^2 \\ &= w^T\left[\frac{1}{2}\frac{1}{N}\frac{1}{N}\sum_{i=1}^{N}\sum_{j=1}^{N} S_{SWij}(X_i - X_j)(X_i - X_j)^T\right]w \\ &= w^T\left[\frac{1}{2}\frac{1}{N}\frac{1}{N}\sum_{i=1}^{N}\sum_{j=1}^{N} S_{SWij}\overline{X_i}\,\overline{X_j}^T\right]w \\ &= w^T S_{NL} w\end{aligned} \tag{7}$$

where $\overline{X}$ denotes the centralized instance. w represents the project vector, Y_i is the corresponding projected instance, i.e., $Y_i = w^T X_i$ .The matrices S_{LL} and S_{NL} represent the sensitive inter-class graph and the sensitive within-class graph, respectively, which are stated as follows:

$$\begin{aligned}S_{LL} &= \frac{1}{2}\frac{1}{N}\frac{1}{N}\sum_{i=1}^{N}\sum_{j=1}^{N} S_{SIij} X_i X_j^T = \frac{1}{2}\frac{1}{N}\frac{1}{N}\sum_{i=1}^{N}\sum_{j=1}^{N}(1-L_{ij})H_{ij} X_i X_j^T \\ &= \frac{1}{2}\frac{1}{N}\frac{1}{N}\sum_{i=1}^{N}\sum_{j=1}^{N} H_{ij} X_i X_j^T - \frac{1}{2}\frac{1}{N}\frac{1}{N}\sum_{i=1}^{N}\sum_{j=1}^{N} H_{ij} L_{ij} X_i X_j^T \\ &= S_L - \frac{1}{2}\frac{1}{N}\frac{1}{N}\sum_{i=1}^{N}\sum_{j=1}^{N} H_{ij} L_{ij} X_i X_j^T\end{aligned} \tag{8}$$

$$\begin{aligned}S_{LL} &= \frac{1}{2}\frac{1}{N}\frac{1}{N}\sum_{i=1}^{N}\sum_{j=1}^{N} S_{SIij} X_i X_j^T = \frac{1}{2}\frac{1}{N}\frac{1}{N}\sum_{i=1}^{N}\sum_{j=1}^{N}(1-L_{ij})H_{ij} X_i X_j^T \\ &= \frac{1}{2}\frac{1}{N}\frac{1}{N}\sum_{i=1}^{N}\sum_{j=1}^{N} H_{ij} X_i X_j^T - \frac{1}{2}\frac{1}{N}\frac{1}{N}\sum_{i=1}^{N}\sum_{j=1}^{N} H_{ij} L_{ij} X_i X_j^T \\ &= S_L - \frac{1}{2}\frac{1}{N}\frac{1}{N}\sum_{i=1}^{N}\sum_{j=1}^{N} H_{ij} L_{ij} X_i X_j^T\end{aligned} \tag{9}$$

Note that one sensitive instance may be contained in several other classes' instances' KNN patch, and then it will be computed several times. In other words, the sensitive instance's contribution weight is equal to the number of other classes' instance's KNN patch it belongs to. The sensitive within-class instance's contribution weight is equal to the number of the-same-class instances' KNN patches it does not belong to.

2.5 Justification

In order to make the sensitive instances from different classes much farther and at the same time to make the sensitive instances from the same class more compact to its class center**,** the objective function can be defined as follows:

$$\max_{W} J(w) = tr((W^T S_{LL} W)^T (W^T S_{NL} W)) \tag{10}$$

Note that this objective function puts more consideration on the local sensitive instances so as to define the projection matrix [19], however this may be trapped into overtraining. In other words, this projection matrix will be too sensitive. In order to avoid the overtraining, the statistical properties of the training dataset are taken into consideration. The between-class scatter is taken to define the globally classifying hyperplane, and the within-class scatter with the same definitions as Linear Discrimanant Analysis (LDA) is taken to define the center of the class. In the technique report of hybrid generalized fisher framework (HGFF) [21], it can be found that the class center information play an important part in the objective function, and a better projection orientation w can be acquired under a proper scale of the statistical property to the graph property. And the appendix A displays the connection of both properties. Therefore the objective function in Eqn. (16) can be modified to:

$$\max_{W} J(w) = \max_{W} tr(W^T (S_B + S_{LL})^{-1} (S_W + S_{NL}) W) \tag{11}$$

By substituting Eqns. (14) and (15) into Eqn.(17) , the following equation can be derived:

$$\max_{W} J(W) = \max_{W} tr(W^T (S_B + S_L - S_W S_L)^{-1} (S_W + S_W - S_W S_L) W) \tag{12}$$

where $S_W S_L$ are defined as follows:

$$S_W S_L = \frac{1}{2} \frac{1}{N} \frac{1}{N} \sum_{i=1}^{N} \sum_{j=1}^{N} (H_{ij} \odot L_{ij}) X_i X_j^T$$

Finally, the optimization problem is deduced into the following eigen-decomposition problem:

$$\left(S_B + S_L - 2S_W\right) W_k = \lambda_k W_k \tag{13}$$

Here, we assume that the leading eigenvectors of Eqn. (13), consisted optimal projection vectors of the trace quotient problem of Eqn. (12) [22]. So the eigenvectors associated with the top d eigenvalues are selected to project the instances to the subspace.

The outline of the LSFA algorithm is summarized as follows:

Step 1: Construct the neighborhood graph according to Eqn. (1).

Step 2: Detect the sensitive instances. If more than one class's instances are included in a KNN patch, all the instances in this patch are defined as sensitive instance. Eqn. (5) is used to detect the sensitive within-class instance.

Step 3: The sensitive within-class graph and the sensitive inter-class graph are constructed by Eqns. (8) and (9).

Step 4: The statistic information and the graph information are merged together in Eqn. (11). Then the project orientations can be computed by solving the eigen-decomposition of Eqn. (12).

3 Experiments

In this Section, the performance of LSFA algorithm will be evaluated on three different data sets and compared with the performances of Eigenface (PCA) [23], Fisherface (PCA+LDA) [24], Unsupervised Discriminant Projection (UDP) [14] and Local Sensitive Discriminant Analysis (LSDA) [16]. In all the experiments, a preprocessing method is performed to crop the original images. For face data, the original images were normalized such that the two eyes were aligned at the same position, then the facial areas were cropped into the final images for matching. The size of each cropped image in all the experiments is 32×32 pixels, with 256 gray levels per pixel. Thus, each image is represented by a 1024-dimensional vector in image space.

3.1 YALE Face Database

The Yale face database [25] was constructed at the Yale Center for Computation Vision and Control. There are 165 images about 15 individuals in YALE face data sets, where each person has 11 images. The images demonstrate variations in lighting condition (left-right, center-light, right-light), facial expression (normal, happy, sad, sleepy, surprised and wink), and with or without glasses. Each image is cropped to be the size of 32×32. Figure 6 shows the cropped images of two persons in Yale face database.

Fig. 1. The cropped sample face images from Yale database

We selected the l=2, 3, 4, 5, 6, 7, 8 instances of each class as training sets, respectively, and the rest $(11-l)$ of each class for testing. For each value of l, 50 runs were performed with different random partitions between training set and test set. The optimized recognition rates and its corresponding dimensions were chose from the 50 runs for different feature extraction methods, which are shown in TABLE.1. It can be found that the proposed method outperforms the other techniques. In different training samples the proposed algorithm can acquire better recognition rate, especially for the case of the 8 training samples. In real applications, how to set the parameter k is an open problem. In this experiment we set it at around about $3n_i/2$, where n_i is the number of the training set instances in each class.

Table 1. The comparison of The maximal recognition rates and the corresponding dimensions using Baseline, Eignfaces (PCA), Fisherfaces (PCA+LDA),UDP, LSDA and LSFA on Yale face database

Method		2 TRAIN	3 TRAIN	4 TRAIN	5 TRAIN	6 TRAIN	7 TRAIN	8 TRAIN
Baseline	PR(%)	58.52%	61.67%	64.76%	66.67%	70.67%	70.0%	75.56%
	D	1024	1024	1024	1024	1024	1024	1024
Eignfaces	PR(%)	54.81%	58.33%	60.95%	67.78%	68.0%	70.0%	77.78%
	D	32	44	60	64	16	104	28
Fisher-faces	PR(%)	49.63%	66.67%	76.19%	82.0%	85.33%	88.3%	91.11%
	D	8	8	12	12	18	18	18
UDP	PR(%)	**63.7%**	75.0%	80.0%	**84.44%**	88.0%	90.0%	91.11%
	D	**14**	14	14	**16**	18	14	14
LSDA	PR(%)	55.6%	75.83%	80.95%	**84.44%**	**89.33%**	90.00%	91.11%
	D	14	14	14	**16**	**14**	16	14
LSFA	PR(%)	**63.7%**	**76.67%**	**81.9%**	**84.44%**	**89.33%**	**91.67%**	**95.56%**
	D	**15**	**17**	**15**	**12**	**13**	**17**	**14**

In order to evaluate the performance of the LSFA algorithm in different dimensions, the recognition rate according to different dimensions are shown in Figure 7, where for each class 8 instances were selected as training set while two samples were used as test set.

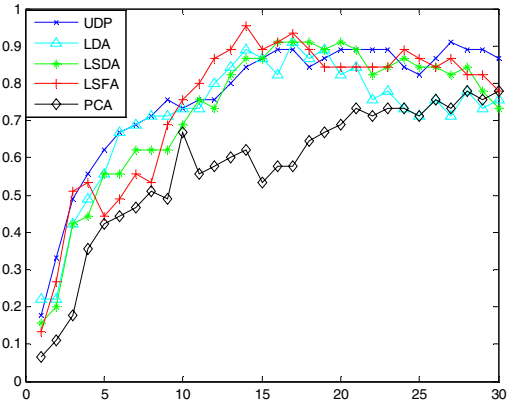

Fig. 2. The comparison of recognition rates at different dimensions for five methods

In Figure 7 the lateral axis is the dimension and the vertical axis represents the recognition rate. From Figure 7 we find that the recognition rate of the proposed algorithm raises very quickly when dimension is larger than 10, at dimension 14 it reaches its top 95.56%. Until dimension 17 it still keeps higher recognition rate than other methods. The recognition rates of LSFA algorithm decrease very fast after dimension 17. This is the common property of most nonlinear dimensionality reduction methods.

4 Conclusions

In this paper we proposed a new local sensitive froniter analysis (LSFA) algorithm, which is focused on the instances which are sensitive to the classification task. The

k-nearest neighbor (KNN) technique is used to detect the sensitive instances. One fixed KNN criteration can be used to determine the withinclass sensitive map and between-class sensitive map, unlike Local PCA should determine different number of local instance and also unlike MFA need define two kinds of KNN patches based on between class and within class. Unlike LSDA it use only one KNN patch and the sensitive within class scatter and the sensitive between class scatter are constructed in the KNN patch with same radius. The main difference from Nonparametric Margin Maximization Criterion (NMMC) is that our algorithm selects the sensitive within-class instances from the same class set and did not belong to the same KNN patch. Based on this unique viewpoint, LSFA could project the instance into a low subspace in which it is easier to classify.

Acknowledgement

This work was supported by the grants of the National Science Foundation of China, Nos. 60873012 & 60805021, the grants from the National High Technology Research and Development Program of China (863 Program), No.2007AA01Z167, the grant of the Guide Project of Innovative Base of Chinese Academy of Sciences (CAS), No.KSCX1-YW-R-30.

References

1. Tenenbaum, J.B., Silva, V., Langford, J.C.: A Global Geometric Framework for Nonlinear Dimensionality Reduction. Science 290, 2319–2323 (2000)
2. Roweis, S.T., Saul, L.K.: Nonlinear Dimensionality Reduction By Locally Linear Embedding. Science 290, 2323–2326 (2000)
3. Zhang, J.P., Shen, H.X., Zhou, Z.H.: Unified Locally Linear Embedding and Linear Discriminant Analysis Algorithm for Face Recognition. LNCS (2004)
4. Belkin, M., Niyogi, P.: Laplacian Eigenmaps and Spectral Techniques For Embedding And Clustering. In: Dietterich, T.G., Becker, S., Ghahramani, Z. (eds.) Advances in Neural Information Processing Systems, vol. 14, pp. 585–591. MIT Press, Cambridge (2002)
5. Belkin, M., Niyogi, P.: Laplacian Eigenmaps for Dimensionality Reduction and Data Representation. Neural Computation 15(6), 1373–1396 (2003)
6. Zhang, Z., Zha, H.: Principal Manifolds and Nonlinear Dimension Reduction via Local Tangent Space Alignment. SIAM J. Scientific Computing 26(1), 313–338 (2005)
7. Weinberger, K., Saul, L.: Unsupervised Learning of Image Manifolds by Semidefinite Programming. In: Proc. IEEE Int'l Conf. Computer Vision and Pattern Recognition, vol. 2, pp. 988–995 (2004)
8. Vandenberghe, L., Boy, S.P.: Semidefinite Programming. SIAM Review 38(1), 49–95 (1996)
9. Weinberger, K.Q., Saul, L.K.: Unsupervised Learning of Image Manifolds by Semidefinite Programming. International Journal of Computer Vision 70(1), 77–90 (2006)
10. Lin, T., Zha, H.B.: Riemannian Manifold Learning. IEEE Trans. Pattern Analysis and Machine Intelligence 30(5), 796–809 (2008)
11. Saul, L.K., Roweis, S.T.: Think Globally, Fit locally: Unsupervised Learning of Low Dimensional Manifolds. J. Mach. Learning Res. 4, 119–155 (2003)

12. He, X., Niyogi, P.: Locality Preserving Projections. In: Advances in Neural Information Processing Systems 16, Vancouver, Canada (2003)
13. He, X., Yang, S., Hu, Y., Niyogi, P., Zhang, H.J.: Face Recognition Using Laplacianfaces. IEEE Trans. Pattern Analysis and Machine Intelligence 27(3), 328–340 (2005)
14. Yang, J., Zhang, D., Yang, J.Y., Niu, B.: Globally Maximizing, Locally Minimizing: Unsupervised Discriminant Projection with Application to Face and Palm Biometrics. IEEE Trans. Pattern Analysis and Machine Intelligence 29(4), 650–664 (2007)
15. Yan, S.C., Xu, D., Zhao, B.Y., Zhang, H.J., Yang, Q., Lin, S.: Graph Embedding and Extensions: A General Framework for Dimensionality Reduction. IEEE Transactions On Pattern Analysis and Machine Intelligence 29(1), 40–51 (2007)
16. Cai, D., He, X., Zhou, K., Han, J., Bao, H.: Locality Sensitive Discriminant Analysis. In: Proceedings of the Twentieth International Joint Conference on Artificial Intelligence (2007)
17. Wang, F., Zhang, C.S.: Feature Extraction by Maximizing the Average Neighborhood Margin. In: IEEE Conference on Computer Vision and Pattern Recognition, pp. 1–8 (2007), doi:10.1109/CVPR.2007.383124
18. Li, B., Zheng, C.H., Huang, D.S.: Locally Linear Discriminant Embedding: An Efficient Method for Face Recognition. Pattern Recognition 41(12), 3813–3821 (2008)
19. Qiu, X., Wu, L.: Face Recognition by Stepwise Nonparametric Margin Maximum Criterion. In: Tenth IEEE International Conference on Computer Vision 2005, ICCV 2005, vol. 2(17-21), pp. 1567–1572 (2005)
20. Burris, S., Sankappanavar, H.P.: A Course in Universal Algebra, http://www.math.uwaterloo.ca/~snburris/htdocs/UALG/univ-algebra.pdf
21. Huang, D.S., Li, B., Wang, C.: A Hybrid Generalized Fisher Framework for Dimensionality Reduction. Technical Report of Intelligent Computing Laboratory
22. Yan, S.C., Tang, X.: Trace Quotient Problems Revisited. In: ECCV (2), pp. 232–244 (2006)
23. Turk, M., Pentland, A.: Eigenfaces for Recognition. Journal of Cognitive Neuroscience 3(1), 71–76 (1991)
24. Peter, N., Belhumeur, J.P., Hepanha, K.D.J.: Eigenface vs. Fisherfaces: Recognition Using class Specific Linear Projection. IEEE Transactions on Pattern Analysis and Machine Intelligence 19(7), 711–720 (1997)
25. Yale Univ. Face Database (2002), http://cvc.yale.edu/projects/yalefaces/yalefaces.html

Locality Preserving Discriminant Projections

Jie Gui[1,2,*], Chao Wang[1,2], and Ling Zhu[1,2]

[1] Intelligent Computing Lab, Institute of Intelligent Machine, Chinese Academy of Science, P.O. Box 1130, Hefei, Anhui, 230031, China
[2] Departments of Automation, University of Science and Technology of China, Hefei, Anhui, 230027, China
guijiejie@gmail.com

Abstract. A new manifold learning algorithm called locality preserving discriminant projections (LPDP) is proposed by adding between-class scatter matrix and within-class scatter matrix into locality preserving projections (LPP). LPDP can preserve locality and utilize label information in the projection. It is shown that the LPDP can successfully find the subspace which has better discrimination between different pattern classes. The subspace obtained by LPDP has more discriminant power than LPP, and is more suitable for recognition tasks. The proposed method was applied to USPS handwriting database and compared with LPP. Experimental results show the effectiveness of the proposed algorithm.

Keywords: Manifold learning, locality preserving discriminant projections, locality preserving projections.

1 Introduction

In the past few years, the computer vision and pattern recognition community has witnessed the rapid growth of a new kind of feature extraction method, namely, manifold learning. Locally linear embedding (LLE) [1-3], isometric feature mapping (Isomap) [4, 5], and Laplacian eigenmap [6, 7] are the three most famous manifold learning algorithms. But these approaches have limitations and are not suitable for pattern recognition because they cannot give an explicit subspace mapping and thus cannot deal with the out-of-sample problem directly.

Many linear approaches have been proposed for dimensionality reduction, such as principal component analysis (PCA) [8, 9], multidimensional scaling (MDS) [10] and so on. All of these methods are easy to implement. At the same time, their optimizations are well understood and efficient. Because of these advantages, they have been widely used in visualization and classification. Unfortunately, they have a common inherent limitation that they all deemphasize discriminant information, which is important in recognition problem.

He et al. [11] proposed a new linear dimensionality reduction method named locality preserving projections (LPP) and applied it in pattern recognition tasks successfully [12]. LPP is originally derived by the linear approximation of the Laplace Beltrami

* Corresponding author.

D.-S. Huang et al. (Eds.): ICIC 2009, LNAI 5755, pp. 566–572, 2009.

operator on a compact Riemannian manifold. However, LPP suffers from a limitation that it does not encode discriminant information while discriminant information is important for recognition task.

By introducing between-class scatter and within-class scatter into the objective function of LPP, we propose a locality preserving discriminant projections (LPDP) algorithm which not only considers the local information but also emphasizes the discriminant information. Experimental results show it is more suitable for recognition tasks with labeled information.

The remainder of this paper is organized as follows: Section 2 reviews manifold learning algorithms; Experiments and results are presented in Section 3; Conclusions are given in Section 4.

2 Mainfold Learning

The algorithm of linear dimensionality reduction finds a transformation matrix V that maps these N samples to a set of weight vectors $Y = [y_1, y_2, \cdots y_N]$, where Y is $d \times N$ matrix($d \ll D$). A reasonable criterion for choosing a 'good' map is to minimize an objective function [6].

2.1 Locality Preserving Projections (LPP)

The objective function of LPP [11, 12] is defined as:

$$\min \sum_{ij} \left\| Y_i - Y_j \right\|^2 W_{ij} \quad , \tag{1}$$

where $Y_i = V^T X_i$ and the matrix $W = \left(W_{ij} \right)$ is a similarity matrix. The weight W_{ij} incurs a heavy penalty when neighboring points X_i and X_j are mapped far apart. Therefore, minimizing the objective function is an attempt to ensure that if X_i and X_j are "close" then Y_i and Y_j are close as well. A possible way of defining W is as follows:

$W_{ij} = 1$, if X_i is among k nearest neighbors of X_j or X_j is among k nearest neighbors of X_i, otherwise, $W_{ij} = 0$. k is the number of neighbors. The justification for this choice of weights can be traced back to [6].

Suppose V is a transformation matrix, that is, $Y = V^T X$. By simple algebra formulation, the objective function can be reduced to:

$$\begin{aligned} &\frac{1}{2}\sum_{ij} \left\| Y_i - Y_j \right\|^2 W_{ij} = \frac{1}{2} trace(\sum_{ij} (V^T x_i - V^T x_j)(V^T x_i - V^T x_j)^T W_{ij}) \\ &= trace(\sum_{ij} V^T x_i D_{ii} x_i^T V - \sum_{ij} V^T x_i W_{ij} x_j^T V) = trace(V^T X (D - W) X^T V) \end{aligned} \quad , \tag{2}$$

where $X=[x_1,x_2,\cdots x_N]$, D is a diagonal matrix and D_{ii} is column (or row) sum of W, $D_{ii}=\sum_j W_{ij}$, $L=D-W$ is the Laplacian matrix.

In addition, a constraint is proposed as $V^T XDX^T V=I$.

Finally, the minimization problem reduces to finding:

$$\begin{aligned} &\arg\ \min \operatorname{trace}(V^T XLX^T V) \\ &V^T XDX^T V=I \end{aligned} \quad . \tag{3}$$

The transformation matrix that minimizes the objective functions is given by the minimum eigenvalues solution to the generalized eigenvalues problem:

$$XLX^T v=\lambda XDX^T v \quad . \tag{4}$$

It is easy to show that the matrices XLX^T and XDX^T are symmetric and positive semidefinite. The vectors υ_i that minimize the objective function are given by minimum eigenvalues solutions to the generalized eigenvalues problem. Let the column vectors $\upsilon_0,\upsilon_1,\cdots\upsilon_{d-1}$ be the solutions of Eq. (4), ordered according to their eigenvalues, $\lambda_0,\lambda_1,\cdots\lambda_{d-1}$. Thus, the embedding is as follows

$$x_i \to y_i=V^T x_i, V=[\upsilon_0,\upsilon_1,\cdots\upsilon_{d-1}] \quad . \tag{5}$$

Where y_i is a d-dimensional vector, and V is a $D\times d$ matrix.

2.2 Maximizing Margin Criterion (MMC)

Recently, MMC [13, 14] was proposed to determine the optimized subspace, which can maximize the average margin between classes after dimensionality reduction and can also successfully conquer the SSS (small sample size) problem. The objective function of MMC is written as:

$$\text{J=max}\left\{\sum_{ij} p_i p_j \left(d\left(m_i,m_j\right)-s\left(m_i\right)-s\left(m_j\right)\right)\right\} \quad . \tag{6}$$

Where p_i and p_j are the prior probability of class i and class j, m_i and m_j are the centroids of class i and class j. $d\left(m_i,m_j\right)$, $s\left(m_i\right)$ and $s\left(m_j\right)$ have the following definitions:

$$d\left(m_i,m_j\right)=m_i-m_j \quad , \tag{7}$$

$$s\left(m_i\right)=tr\left(S_i\right) \quad , \tag{8}$$

$$s\left(m_j\right)=tr\left(S_j\right) . \tag{9}$$

Thus the optimized function can be derived as follows:

$$J=max\,tr\left(S_b\text{ - }S_w\right) . \tag{10}$$

The matrix S_b is called between-class scatter matrix and S_w is called within-class scatter matrix.

2.3 Locality Preserving Discriminant Projections (LPDP)

If the linear transformation obtained by LPP can satisfy Eq. (3) simultaneously, the discriminability of the data will be improved greatly. Thus the problem can be represented as the following multi-objective optimized problem:

$$\begin{cases}\min\ \text{trace}\left(V^T XLX^T V\right)\\ \max\ \text{trace}\left(V^T\left(S_b-S_w\right)V\right)\end{cases} \tag{11}$$
$$s.t.\ \ V^T XDX^T V=I$$

It can be changed into the following constrained problem:

$$\begin{aligned}&\min\ \text{trace}\left(V^T\left(XLX^T-\alpha\left(S_b-S_w\right)\right)V\right)\\ &s.t.\ \ V^T XDX^T V=I\end{aligned} \tag{12}$$

The parameter α can adjust the contributions of maximizing margin criterion and the local structure according to different data sets. The transformation matrix V that minimizes the objective function can be obtained by solving the generalized eigenvalue problem:

$$\left(XLX^T-\alpha\left(S_b-S_w\right)\right)V=\lambda XDX^T V . \tag{13}$$

3 Experimental Results

The proposed algorithm is here applied to USPS handwriting database. The USPS handwriting digital data [6] include 10 classes from "0" to "9". Each class has 1100 examples. In our experiment, we select a subset from the original database. We cropped each image to be size of 16×16. There are 100 images for each class in the subset and the total number is 1000.

For each digit, *l*= (30, 40, 50, 60, 70) data are randomly selected for training and the rest are used for testing. In the PCA phase of LPP and LPDP, we kept 100 percent energy. The K-nearest neighborhood parameter k in LPP and LPDP was taken to be 5. The parameter α was taken to be 1. Finally, a nearest neighbor classifier with

Euclidean distance is employed to classify in the projected feature space. For each given l, we repeated this process for 20 times. Table 1 shows the best result obtained in the optimal subspace and the corresponding dimensionality. The best mean recognition rates for 20 times, standard deviation, and the corresponding dimensionality are also shown in Table 1. Fig. 1 displays the mean recognition rate curves versus the subspace dimensions when l= (30, 40, 50, 60).

Table 1. The maximal recognition rates, maximal average recognition rates, the corresponding standard deviations (percent) with the reduced dimensions for LPP, LPDP on USPS handwriting database (a nearest neighbor classifier with Euclidean distance)

Method	Accuracy (%)	30 Train	40 Train	50 Train	60 Train	70 Train
LPP	max(dimension)	43.86(20)	64.83(22)	74(12)	78.5(16)	84(24)
	average(dimension)	39.01(20)	58.58(20)	68.41(16)	74.49(20)	78.38(14)
	std	2.75	2.17	1.6	2.41	2.16
LPDP	max(dimension)	49.86(10)	70.67(12)	78.8(12)	83.25(14)	87.33(14)
	average(dimension)	46.44(10)	65.29(12)	73.5(12)	79.51(14)	82.32(14)
	std	2.54	2.54	1.64	2.04	2.01

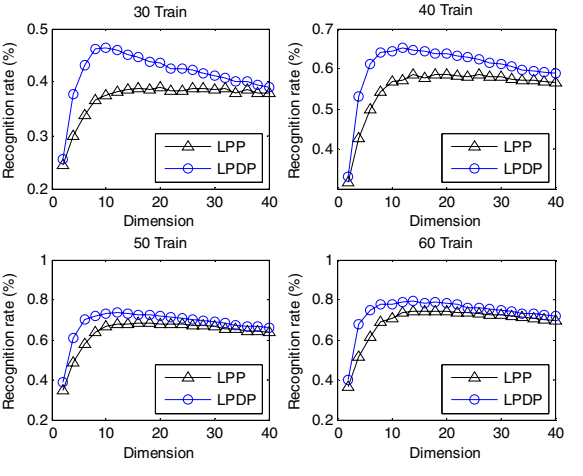

Fig. 1. The performance comparison of average recognition rates using LPP and LPDP by varying the dimensions for 30 Train, 40 Train, 50 Train, 60 Train (a nearest neighbor classifier with Euclidean distance)

If we employ a nearest neighbor classifier with cosine distance, the results will be better than a nearest neighbor classifier with Euclidean distance. This is consistent with the observation in [15]. We did not show them here due to limited space. If we employ a nearest neighbor classifier with cosine distance and normalize each image to be a unit vector, the results will be the best of all. The best results are reported in Table 2 and Figure 2.

Table 2. The maximal recognition rates, maximal average recognition rates, the corresponding standard deviations (percent) with the reduced dimensions for LPP, LPDP on USPS handwriting database (a nearest neighbor classifier with cosine distance)

Method	Accuracy(%)	30 Train	40 Train	50 Train	60 Train	70 Train
LPP	max(dim)	53.14(32)	73.00(40)	81.00(22)	84.50(30)	88.67(38)
	avg(dim)	48.01(40)	66.84(32)	75.65(36)	79.97(36)	84.07(30)
	std	2.27	1.73	1.85	2.49	1.93
LPDP	max(dim)	57.14(24)	75.50(22)	82.80(34)	88.00(28)	91.00(40)
	avg(dim)	51.24(36)	71.33(30)	79.46(26)	83.41(34)	86.98(26)
	std	2.96	1.52	1.42	2.24	1.76

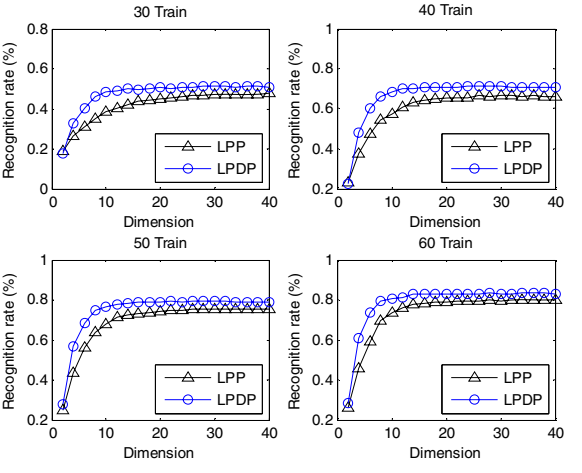

Fig. 2. The performance comparison of average recognition rates using LPP and LPDP by varying the dimensions for 30 Train, 40 Train, 50 Train, 60 Train (a nearest neighbor classifier with cosine distance)

Both Table 1,2 and Fig. 1,2 show that our LPDP algorithm performed better than LPP for all cases.

4 Conclusion

A novel method called LPDP is proposed. The new method adds the maximum margin criterion into the target function of LPP. The experiments on USPS handwriting database show that LPDP can improve the performance of LPP remarkably.

Acknowledgments

This work was supported by the grant from the National Basic Research Program of China (973 Program), No. 2007CB311002.

References

1. Roweis, S.T., Saul, L.K.: Nonlinear Dimensionality Reduction by Locally Linear Embedding. Science 290(5500), 2323–2326 (2000)
2. Saul, L.K., Roweis, S.T.: Think Globally, Fit Locally: Unsupervised Learning of Low Dimensional Manifolds. Journal of Machine Learning Research 4(2), 119–155 (2004)
3. Li, B., Zheng, C.H., Huang, D.S.: Locally Linear Discriminant Embedding: An Efficient Method for Face Recognition. Pattern Recognition 41(12), 3813–3821 (2008)
4. Tenenbaum, J.B., de Silva, V., Langford, J.C.: A Global Geometric Framework for Nonlinear Dimensionality Reduction. Science 290(5500), 2319–2324 (2000)
5. Li, B., Huang, D.S., Wang, C.: Improving the Robustness of ISOMAP by De-noising. In: Proceedings of 2008 IEEE World Congress on Computational Intelligence (WCCI 2008), Hong Kong, pp. 266–270 (2008)
6. Belkin, M., Niyogi, P.: Laplacian Eigenmaps and Spectral Techniques for Embedding and Clustering. In: Advances in Neural Information Processing Systems 14, vols. 1, 2, pp. 585–591 (2002)
7. Belkin, M., Niyogi, P.: Laplacian Eigenmaps for Dimensionality Reduction and Data Representation. Neural Computation 15(6), 1373–1396 (2003)
8. Belhumeur, P.N., Hespanha, J.P., Kriegman, D.J.: Eigenfaces vs. Fisherfaces: Recognition Using Class Specific Linear Projection. IEEE Transactions on Pattern Analysis and Machine Intelligence 19(7), 711–720 (1997)
9. Martinez, A.M., Kak, A.C.: PCA versus LDA. IEEE Transactions on Pattern Analysis and Machine Intelligence 23(2), 228–233 (2001)
10. Williams, C.K.I.: On a Connection between Kernel PCA and Metric Multidimensional Scaling. Machine Learning 46(1-3), 11–19 (2002)
11. He, X.F., Niyogi, P.: Locality Preserving Projections. Advances in Neural Information Processing Systems 16 16, 153–160 (2004)
12. He, X.F., Yan, S.C., Hu, Y.X., et al.: Face Recognition Using Laplacianfaces. IEEE Transactions on Pattern Analysis and Machine Intelligence 27(3), 328–340 (2005)
13. Liu, J., Cheri, S.C., Tan, X.Y., et al.: Comments on Efficient and Robust Feature Extraction by Maximum Margin Criterion. IEEE Transactions on Neural Networks 18(6), 1862–1864 (2007)
14. Li, H.F., Jiang, T., Zhang, K.S.: Efficient and Robust Feature Extraction by Maximum Margin Criterion. IEEE Transactions on Neural Networks 17(1), 157–165 (2006)
15. Yang, J., Zhang, D., Yang, J.Y., et al.: Globally Maximizing, Locally Minimizing: Unsupervised Discriminant Projection with Applications to Face and Palm Biometrics. IEEE Transactions on Pattern Analysis and Machine Intelligence 29(4), 650–664 (2007)

Using Bayesian Network and AIS to Perform Feature Subset Selection

Boyun Zhang[1,2]

[1] School of Information Science and Engineering, Central South University, Changsha, 410083, P.R. China
[2] Department of computer Science, Hunan Public Security College, Changsha, 410138, P.R. China
hnjxzby@hotmail.com

Abstract. Bayesian networks have been widely applied to the feature selection problem. The proposed methods learn a Bayesian network from the available dataset and utilize the Markov Blanket of the target feature to select the relevant features. And we apply an artificial immune system as search procedure to the Bayesian network learning problem. It find suitable Bayesian networks that best fit the dataset. Due to the resulting multimodal search capability, several subsets of features are obtained. Experimental results were carried out in order to evaluate the proposed methodology in classification problems and the subsets of features were produced.

Keywords: Feature selection, Bayesian network, Artificial immune system.

1 Introduction

The selection of features that play important role in characterizing a concept has been received growing attention over the last decades. Algorithms for feature selection fall into one of two broad categories: wrapper approaches and filter approaches[1]. In the wrapper approach, the model is previously specified and several subsets of features are generated by means of a heuristic search, given the space of all subsets. Each candidate subset is taken as the input vector and the resulting performance of the model is used to assign a relative score to the corresponding subset of features. On the other hand, the filter approaches compute a score for each feature based on some correlation metric involving the candidate feature and the target feature. The features with score above a given threshold are then selected to compose the input vector. Since filter algorithms do not depend on the model, they are in general less computationally expensive than wrapper approaches.

Among the filters, an appealing approach consists of learning a Bayesian network from the dataset aiming at determining the relationship among the features. The next step is to identify and remove the features that stay outside the Markov Blanket of the target feature, i.e., the features that have no direct causal relationship with the target feature. This approach helps to understand how a given feature behaves under the influence of other features. Besides, Koller etc have shown in their work [2] that the Markov Blanket criterion helps to remove features that are really unnecessary.

D.-S. Huang et al. (Eds.): ICIC 2009, LNAI 5755, pp. 573–580, 2009.

The Bayesian network learning can be viewed as a search and optimization procedure, where a scoring metric is used to attribute a relative merit to each candidate solution based on the likelihood, and a search mechanism is responsible for identifying networks with the highest scores throughout the search space.

Immune-inspired algorithms are inherently capable of dealing with large and multimodal search spaces by maintaining diversity and adjusting automatically the size of the population in response to the demands of the problem [3]. Computational experiments have pointed to the suitability of the methodology, with not only one but several high-quality Bayesian networks being obtained. In this paper we investigate the suitability of AIS and Bayesian network for the feature selection problem. Experiments were carried out aiming at evaluating the proposed algorithm in classification problems.

The paper is organized as follows. In Section 2 we introduce related work about feature selection. Section 3 states some basic concepts of Bayesian network and its application to feature selection. In Section 4 we present the artificial immune system utilized to learn the structure of Bayesian networks. The experimental results are outlined in Section 5. Finally, in the last Section we draw some concluding remarks of the research.

2 Related Work

Feature selection is considered to be a relevant subject in data analysis and constitutes an important preprocessing step in many areas in which datasets with several features are available [4]. The feature subset selection problem refers to the task of identifying and selecting a useful subset of features to be used to represent patterns from a larger set, possibly containing redundant and irrelevant features. By identifying irrelevant features, we can not only save a great amount of computational cost in future analysis, but often build a more accurate model. Besides, feature selection can improve the comprehensibility of the resulting model and clarify the relationships among features.

Algorithms that perform feature selection can be placed into one of two main broad categories [1]: the wrapper approach and the filter approach. Wrapper approaches look for features according to their usefulness to a given model. The feature selection problem is also considered as a search and optimization process. A wide range of heuristics can be used such as genetic algorithms [5], artificial immune systems [6] and estimation of distribution algorithms [7]. Usual models are decision trees, k-nearest neighbors, rules, naive Bayes, neural networks and fuzzy systems. Advantages of wrapper approaches include the ability to take into account many kind of feature dependencies and the possibility of customizing the subset of features according to the peculiarities of the adopted model. A common drawback of these techniques is that they have a higher risk of overfitting than filter techniques and are computationally intensive, particularly when the building of the model involves a high computational cost.

On the other hand, filter approaches are independent of the model to be used afterward. Filters only look at the intrinsic properties of the data and compute a feature relevance score such as correlation, mutual information or cross-entropy of each candidate feature with the target feature. Hence, low-scoring features are removed. As a result, feature selection needs to be performed only once, and then different models can

be evaluated. Other advantages of filter approaches are their low computational cost and their capability to easily scale to high-dimensional datasets. For example two classical examples of filter algorithms are FOCUS [8] and RELIEF [9].

3 Background

Aiming at a better understanding of this work, we outline the basic foundations of Bayesian networks and their application to the feature selection problem.

3.1 Bayesian Network

Bayesian networks are graphical models that encode the joint probability distribution of a set of random variables as nodes connected by directed edges in a graph. A Bayesian network for a set of variables $X = \{x_1, x_2, ..., x_n\}$ is a pair $B = (DAG, \Pr ob)$. Where *DAG* is a directed acyclic graph whose nodes are variables of the problem and the edges indicate dependence relationships between the connected variables. For example, if there is an edge from node x_1 to node x_2, we say that variable x_1 is parent of variable x_2 and, the value of x_2 is conditionally dependent on the value of x_1. The second component *Prob* is a set containing the probability distributions associated with each variable x_i, $i = 1, ..., n$. If a variable x_i has a set of parents, denoted by Γ_{x_i}, its probability distribution is said to be conditional and is expressed by $P(x_i \mid \Gamma_{x_i})$. The probability distribution of a variable x_j which has no parents is expressed by its marginal distribution $P(x_j)$.

3.2 Markov Blanket

In Bayesian networks, the Markov Blanket of a given node is the set of nodes that have influence on its conditional distribution [10]. As a consequence, the Markov Blanket of a node is the only knowledge needed to predict the behavior of that node. Therefore, the nodes outside the Markov Blanket of a specific node do not alter its probability.

The Markov Blanket of a node *A* consists of the parents and children of *A* and the parents of the children of *A*. Node *A* is dependent of all nodes included in its Markov Blanket. For classification tasks, after building the Bayesian network from the dataset, the Markov Blanket of the node that represents the outcome variable (class) can be used as the feature selection.

3.3 Bayesian Network Learning

The problem of Bayesian network learning reduces to the problem of searching for a model that yields the highest score, given the observed data. As the number of variables of the problem increases, the set of all possible Bayesian networks also grows leading

to an *NP*-hard problem [11]. Hence we should avoid any kind of exhaustive search. Alternatively, we can apply a heuristic search procedure to accomplish this task.

Usually, the heuristic search begins with an initial network generated at random. Next, the probability distribution of each variable is estimated using the dataset, and the score of the network is computed. The search process generally proposes small changes to the current structure in order to obtain a network with higher score than the previous one. These small changes can be accomplished by adding or deleting an edge, or reversing the edge direction. Every time a change is made it is necessary to compute the probability distribution of the variables for the modified network. Among the several measures proposed to score competing networks, the most frequently adopted is the Bayesian Information Criterion (*BIC*) [12]. The *BIC* metric for some network *B* modeling a dataset *D* of size *N*, denoted by *BIC*(*B*), is expressed in equation (1). It combines the likelihood of the network with a penalty related to the complexity of the structure.

$$BIC(B) = \log P(D \mid B) - \log N.\dim(B)/2 \tag{1}$$

where,

$$P(D \mid B) = \prod_{i=1}^{n} \prod_{j=1}^{q_i} (r_i - 1)!/(N_{ij} + r_i - 1)! \prod_{k=1}^{r_i} N_{ijk}!$$

where n is the number of instances, q_i denotes the number of possible instances of parents of x_i, r_i is the number of possible values of x_i, N_{ijk} is the number of cases where x_i takes the k-th value with its parents taking their j-th value, and $N_{ij} = \sum_{k=1}^{r_i} N_{ijk}$. The $\dim(B)$ is the dimension of the network, which is the number of parameters needed to specify the model.

4 Using AIS to Learn the Structure of Bayesian Networks

The artificial immune system (AIS) is based mainly on two immune principles, that is clonal selection and immune network. The clonal selection theory states that when an antigen invades the organism, some antibodies that recognize this antigen start proliferating. During proliferation, the clones suffer mutation with rates proportional to their affinity with antigens: the higher the affinity, the smaller the mutation rate. The other important concept is the so-called immune network theory, which proposes that antibodies are not only capable of recognizing antigens, but they are also capable of recognizing each other. When an antibody is recognized by another one, it is suppressed.

The initial population is generated randomly and its size can grow and shrink dynamically. In the cloning step, each antibody of the population gives origin to a number of clones. These clones suffer a mutation inversely proportional to their fitness: clones with higher fitness will be submitted to lower mutation rates. After the insertion of clones into the population, all antibodies interact with each other in a network. If two or more antibodies present a degree of similarity above a given threshold, all but one are removed from the population. Individuals with low fitness are also excluded.

In our method, we apply the AIS as search procedure to the Bayesian network learning problem. Starting from a sample dataset, the proposed method applies an immune-inspired algorithm to find suitable Bayesian networks that best fit the data. The components of the algorithm such as the coding scheme, the fitness function etc is detailed as follow.

In the proposed the algorithm, each candidate network is an antibody while the dataset represents an antigen. For a fixed domain with *n* variables, a Bayesian network structure is coded as an $n \times n$ binary matrix, where its entries, $v_{ij}, i, j = 1,...,n$ assume the values:

$$v_{ij} = \begin{cases} 1 & if\ j\ is\ a\ parent\ node\ of\ node\ i \\ 0 & otherwise \end{cases}$$

The initial population is randomly generated. It is formed by random matrices whose entries can assume values 0 or 1, with the constraint of generating acyclic graphs.

The fitness function used to evaluate the quality of the generated solutions is the *BIC* scoring metric, which expressed in equation (1). We adopte this scoring metric because it presents the interesting characteristic of expressing a trade-off between quality and complexity, favoring networks with higher likelihood and simpler structures.

During the cloning step, identical copies of existing antibodies are created. Then, each generated clone suffers a mutation process. The clone mutation rate is inversely proportional to its fitness. The mutation rate is given by:

$$P_{mut}(A_i) = \max\_P_{mut} \cdot \frac{\max\_Fitness - Fitness(A_i)}{\max\_Fitness - \min\_Fitness}$$

where $P_{mut}(A_i)$ is the mutation rate for clone *i*; $\max\_P_{mut}$ is the highest value that mutation rate can assume; $Fitness(A_i)$ is the fitness of clone *i*, $\max\_Fitness$ is the highest fitness value found in the current iteration, and $\min\_Fitness$ is the lowest fitness value found in the current iteration.

The hyper mutation operator is subject to the constraint of avoiding cycles. After performed the hyper mutation operation, the search for cycles in the novel Bayesian network is then accomplished. For each identified cycle, a connection chosen at random is removed.

5 Experimental Results

During the experiments, we considered five benchmarks from UCI Repository of Machine Learning Databases [13]: Bupa, Pima, Chess, Sonar, Card. Table 1 summarizes the characteristics of each one, giving the total number of instances, the number of attributes and number of classes.

Table 1. Dataset in Experiment

Dataset	Number of Sample	Number of Attr	Number of class
Bupa	345	6	2
Pima	768	8	2
Chess	3196	36	2
Sonar	208	60	2
Card	690	15	2

Empirically we set the parameters of the AIS as follows. The initial population contains 16 antibodies, the number of clones per antibody is 6, the maximum mutation rate is 0.3, and the stopping condition of the algorithm is the maximum number of generations, defined here as 200. Firstly, we apply the immune algorithm to the datasets in order to obtain suitable Bayesian networks that best fit the data. The probability for categorical features is estimated from data using the maximum likelihood estimation. To synthesize the classifiers, the datasets were partitioned as 50% for training and 50% for test. To test the selected subset of features, the Support Vector Machine is used as the classifiers.

In the experiments the comparative analysis were carried out taking into account $K2\chi^2$ algorithms[14]. For the two algorithms, we set their parameters aiming at achieving subsets with reduced number of features. Table 2 shows the average results for the 5 datasets, when using all the features and when using only the selected features. From Table 2 we can observe that the performance of the classifiers produced a significant improvement by using the selected features when compared with their performance using all features.

The number of selected features is similar for both $K2\chi^2$ and our proposal. However, the classifier using the features selected by our proposal presented a slight superior performance for most of the cases in terms of accuracy. This occurs maybe due to the efficient mechanism of exploration of the *AIS*s.

Table 2. Classification Rates

Dataset	All Feature(%)	Proposed Method(%)	$K2\chi^2$ Algorithm(%)
Bupa	70.3	74.6	72.2
Pima	73.5	75.2	72.6
Chess	93.2	97.1	96.4
Sonar	70.6	76.8	77.5
Card	78.7	83.4	81.9

Table 3 shows the subset of features selected by our proposal for each dataset. From the perspective of the search process, we notice an characteristic of the immune-based algorithm that it is able to generate not only one but several different solutions in a single execution. Using the SVM classifier with each different subsets of selected features we obtained the slight different classification rates.

Table 3. The selection subsets feature of Dataset

Dataset	Subset Feature
Bupa	2 3 4 5
Pima	1 6 7 8
Chess	2 3 10 14 16 18 20 32 33 35
Sonar	6 8 9 10 15 17 27 28 31 34 35 44 45 46 50 53 58
Card	4 6 8 10 11 13 14 15

6 Conclusion

In this paper a filter approach to feature subset selection in classification is proposed. The methodology considers a Bayesian network to represent the relationship among the features and takes the Markov Blanket of the target feature as the selected features. In our methodology, we have adopted an artificial immune system as the search mechanism capable of proposing multiple Bayesian networks. To evaluate our method, we have applied it to some UCI datasets and compared the obtained results with those produced by the $K2\chi^2$ algorithms. The experiment results show the performance in terms of classification score points favorably to our proposed method.

Acknowledgments

This work was partially supported by the Application of Innovation Plan Fund of the Ministry of Public Security under grand No. 2007YYCXHNST072 and the Postdoctoral Science Foundation of Central South University.

References

1. Kohavi, R., John, G.H.: Wrappers for feature subset selection. Artificial Intelligence 97(1-2), 273–324 (1997)
2. Koller, D., Sahami, M.: Toward Optimal Feature Selection. Int. Conf. on Machine Learning, 284–292 (1996)
3. de Castro, L.N., Timmis, J.: Artificial Immune Systems: A New Computational Intelligence Approach. Springer, Heidelberg (2002)
4. Guyon, I., Elisseeff, A.: An introduction to variable and feature selection. Journal of Machine Learning Research 3, 1157–1182 (2003)
5. Siedlecki, W., Sklansky, J.: A note on genetic algorithms for large-scale feature selection. Pattern Recogn. Lett. 10(5), 335–347 (1989)
6. Castro, P.A.D., Von Zuben, F.J.: Feature subset selection by means of a Bayesian Artificial Immune System. In: Proc. of the 8th Int. Conf. on Hybrid Intelligent Systems, pp. 561–566 (2008)
7. Inza, I., Larraaga, P., Etxeberria, R., Sierra, B.: Feature subset selection by Bayesian network-based optimization. Artificial Intelligence 123, 157–184 (2000)
8. Almuallim, H., Dietterich, T.G.: Learning with many irrelevant features. In: Proc. of the 9th National Conf. on Artificial Intelligence, vol. 2, pp. 547–552 (1991)

9. Saeys, Y., Inza, I., Larrañaga, P.: A review of feature selection techniques in bioinformatics. Bioinformatics 23(19), 2507–2517 (2007)
10. Pearl, J.: Probabilistic reasoning in intelligent systems: networks of plausible inference. Morgan Kaufmann Publishers Inc., San Francisco (1988)
11. Chickering, D., Heckerman, D., Meek, C.: Large-sample learning of Bayesian networks is NP-Hard. Journal of Machine Learning Research 5, 1287–1330 (2004)
12. Schwarz, G.: Estimating the dimension of a model. Annals of Statistics 6, 461–465 (1978)
13. Blake, C.L., Merz, C.J.: UCI repository of machine learning databases, http://www.ics.uci.edu/~mlearn/MLRepository
14. Hruschka Jr., E.R., Hruschka, E.R., Ebecken, N.F.F.: Feature selection by bayesian networks. In: Tawfik, A.Y., Goodwin, S.D. (eds.) Canadian AI 2004. LNCS (LNAI), vol. 3060, pp. 370–379. Springer, Heidelberg (2004)

Construction of the Ensemble of Logical Models in Cluster Analysis

Vladimir Berikov*

Sobolev Institute of mathematics,
Koptyg av. 4, 630090 Novosibirsk, Russia
berikov@math.nsc.ru
http://www.math.nsc.ru

Abstract. In this paper, the algorithm of cluster analysis based on the ensemble of tree-like logical models (decision trees) is proposed. During the construction of the ensemble, the algorithm takes into account distances between logical statements describing clusters. Besides, we consider some properties of the Bayes model of classification. These properties are used at the motivation of information-probabilistic criterion of clustering quality. The results of experimental studies demonstrate the effectiveness of the suggested algorithm.

Keywords: cluster analysis, ensemble of logical models, decision trees, distance between logical statements, adaptive planning, Bayes models.

1 Introduction

An actual problem in cluster analysis is the processing of information described by heterogeneous (quantitative or qualitative) features. In heterogeneous feature space, one is met the methodological problem of determination appropriate metric. Another actual problem is the increasing of stability of grouping decisions. In the majority of cluster analysis algorithms, the results can be powerfully changed depending on the choice of initial conditions, order of objects, parameters settings etc. It is known that the stability of decisions can be increased by using the ensembles of algorithms. There exist a number of ensemble clustering algorithms, e.g. [1,2,3]. These algorithms process numerical attributes only. In the coordination of clusters, they use the results ("knowledge"), obtained by different algorithms, or by the same algorithm, but with different parameter adjustments, in different feature subspaces etc. The construction of the collective decision is done after the design of the ensemble.

One of the perspective approaches in cluster analysis is based on logical models. Such types of models are broadly used in recognition and forecasting problems. It can be explained by good interpretability of the results, being in the form of logical regularities, high forecasting ability in noisy environment, possibility

* The author was supported by the Russian Foundation for Basic Research, project 08-07-00136a.

D.-S. Huang et al. (Eds.): ICIC 2009, LNAI 5755, pp. 581–590, 2009.

to process heterogeneous variables and select the most important factors. The algorithm for construction the logical models in cluster analysis was proposed, e.g., in [4]. In [6], the method for building logical functions in cluster analysis, based on the recursive algorithm of decision tree construction, was suggested. This algorithm allows, by the increase of depth of search, to find more complex logical regularities describing cluster structure. In [9], the clustering algorithm based on random decision forest was offered. The statistical modeling showed that usage of ensemble allows to improve significantly the quality of classification, in comparison with "uncoordinated" trees.

In the given work, the novel algorithm of construction the ensemble of logical models is suggested. At the coordination of base decisions, the algorithm takes into account distances between logical statements describing clusters. Besides, we offer new information-probabilistic criterion of grouping quality, based on the Bayes model of recognition on a finite set of events. Finally, the results of statistical modeling and experiments with real data are given.

2 Basic Notions

In standard cluster analysis problem, it is required to construct relatively small number of groups of objects ("clusters", "classes") which are close to each other in the same group, but far in different groups.

Let us consider the problem from the probabilistic point of view. Suppose that there exists a latent variable determining the class attribute for each object. The purpose is to classify observations as correctly as possible. Because the goal variable is unobservable, the quality of classification can be evaluated with some undirect method (with use of some model etc).

Let there be given a sample of objects $s = \{o^{(1)}, \ldots, o^{(N)}\}$ selected from general collection. It is required to form $K \geq 2$ classes; K can be either chosen beforehand or not determined (in the last case the optimum number of groups should be found automatically). Each object is described by features (variables) $X = (X_1, \ldots, X_n)$. The set of features can include variables of different types (quantitative and qualitative, under which we shall understand categorical and Boolean; ordinal). Let D_j denotes the set of values of variable X_j. Denote $x_j^{(i)} = X_j(o^{(i)})$ the value of j-th variable for i-th object, $i = 1, \ldots, N$, $j = 1, \ldots, n$.

Under the *grouping decision* we shall understand the partition $G = \{C^{(1)}, \ldots, C^{(K)}\}$, where $C^{(k)} = \{o^{(i_1)}, \ldots, o^{(i_{N_k})}\}$, N_k is number of objects belonging to k-th cluster, $k = 1, \ldots, K$. The *grouping decision function* will be the mapping $f : s \to \{1, \ldots, K\}$.

Under the *logical model* of data clustering we shall understand the tree with each internal node corresponding to a certain variable X_j; and branch, coming out of the given node corresponding to a certain statement "$X_j(o) \in E_j^{(q)}$", where o is an object, $q = 1, \ldots, r$, $r \geq 2$ is number of branches coming out of the given node. The set $E_j^{(1)}, \ldots, E_j^{(r)}$ is a partition of D_j. Each m-th leaf of the tree corresponds to the group of sample objects satisfying the chain of statements

coming from root node to this leaf. The given chain can be matched to logical statement of the type

$$\text{"If } X_{j_1}(o) \in E_{j_1}^{(i_1)} \text{ and } \ldots \text{ and } X_{j_{q_m}}(o) \in E_{j_{q_m}}^{(i_{q_m})},$$
$$\text{then } o \text{ belongs to } m\text{-th group"},$$

where q_m is length of the given chain, $m = 1, \ldots, M$. The described tree shall be called the *grouping decision tree*. This tree corresponds to the partition of feature space on M disjoint subregions $E^{(1)}, \ldots, E^{(M)}$, so that each m-th leaf is matched to subregion $E^{(m)}$. The partition of feature space, in its turn, corresponds to the partition of sample on subsets $C^{(1)}, \ldots, C^{(M)}$.

Let us consider an arbitrary group of objects $C^{(m)}$. By the *description* of this group we shall understand the following collection of statements:

$$X_1(o) \in T_1^{(m)}, \ldots, X_n(o) \in T_n^{(m)},$$

where $T_j^{(m)}$ is the interval $[\min\limits_{o \in C^{(m)}} X_j(o); \max\limits_{o \in C^{(m)}} X_j(o)]$ in case of quantitative or ordinal variable X_j, or set of values $\{X_j(o) |\ o \in C^{(m)}\}$ in case of qualitative variable. The subregion of feature space $T = T_1 \times \cdots \times T_n$ corresponding to the description of the group shall be called *taxon*. By the *relative power* of j-th projections of taxon T we shall understand the value $\delta_j = \frac{|T_j|}{|D_j|}$, where $|T_j|$ is the length of interval (in case of quantitative or ordinal variable X_j) or the cardinality of corresponding subset in case of qualitative variable X_j, $j = 1, \ldots, n$. Under taxon's *volume* we shall understand the value $\delta = \prod\limits_{j=1}^{n} \delta_j$.

In [6], two variants of algorithm that performs the directed search for optimum tree were suggested, provided that the quality criterion be given.

In the first variant, the top-down procedure of binary decision tree construction is implemented. In each step, it divides current group into two new subgroups so that the total volume of new taxons is minimal. The taxon with maximal volume is regarded as the most perspective for further division. The process stops then the required number of clusters is reached.

In the second variant, it is necessary to find a compromise between total volume of taxons and their number: the criterion $Q = \sum \delta_m + \alpha K/N$ should be minimized, where δ_m is m-th taxon volume, α is a certain parameter ($\alpha = 1$ was chosen in our experiments). Recursive R-method is used for the directed search for optimal tree (see details in [5]).

3 Ensemble of Logical Models

Let us form a number of variants of base grouping decisions $G^{(l)}$, $l = 1, \ldots, L$. Each variant is constructed in some random subspace of variables. It is required to construct the coordinated grouping decision. The stable regularities, revealed at the construction of separate decisions, must be mutually confirmed

("strengthen"), and unstable – "weakened". The theoretical analysis of collective classification and clustering (e.g., [2,7,8]), affirms that under certain conditions the quality of ensemble improves with the increase in number of base classifiers.

For the choice of the best coordination function, various principles can be used. A number of works uses the principle of calculating the coordinated matrix of differences between objects (e.g., [1,3]). Let us consider the following binary matrix $S^{(l)} = \{S^{(l)}(i,q)\}$ of dimensionality $N \times N$

$$S^{(l)}(i,q) = \begin{cases} 0, \text{ if } o^{(i)} \text{ and } o^{(q)} \text{ belongs to the same cluster;} \\ 1, \text{ otherwise,} \end{cases}$$

where $i, q = 1, \ldots, N$, $l = 1, \ldots, L$. After constructing L grouping decisions, it is possible to form the coordinated matrix of differences $S = \{S(i,q)\}$, where

$$S(i,q) = \frac{1}{L} \sum_{l=1}^{L} S^{(l)}(i,q).$$

The value $S(i,q)$ is the frequency of classifying the objects $o^{(i)}$ and $o^{(q)}$ into different groups in a set of clusterings. The value close to zero means that the given objects have a large chance of being in the same class. The value $S(i,q)$ close to one tells that the chance of being in the same group is small.

In this paper, similar principle is suggested, however instead of binary matrix $S^{(l)}$ that reflects the events of the type "belong" (or "not belong") of a pair into the same group, more informative matrix of the distances between clusters is used. For calculating the distances in heterogeneous feature space, the notion of the distance between logical expert statements [6] is utilized.

Let $T^{(s)}$, $T^{(q)}$ be different taxons. Then the distance between them is defined as follows:

$$\rho(T^{(s)}, T^{(q)}) = \left(\sum_{j=1}^{n} \rho_j^2(T^{(s)}, T^{(q)}) \right)^{1/2},$$

where $\rho_j(T^{(s)}, T^{(q)})$ is the distance between j-th projections. If X_j is categorical variable, then the distance between two sets is defined as the weighted measure of their symmetrical difference:

$$\rho_j(T_j^{(s)}, T_j^{(q)}) = \frac{|T_j^{(s)} \Delta\, T_j^{(q)}|}{|D_j|}.$$

Let X_j be quantitative or ordinal variable, the interval $T_j^{(s)} = [a^{(s)}, b^{(s)}]$, and $T_j^{(q)} = [a^{(q)}, b^{(q)}]$. Then

$$\rho_j(T_j^{(s)}, T_j^{(q)}) = \frac{|a^{(s)} - a^{(q)}| + |b^{(s)} - b^{(q)}|}{2|D_j|}.$$

For finding the overall variant of clustering, after calculation the coordinated differences matrix, the standard hierarchical method of dendrogram construction

is used. As input information, this algorithm employs the pair-wise distances between objects (the distances between groups are calculated using the principle of "average link").

4 The Bayes Model of Classification

In [10] and some earlier works, the Bayes model of recognition on a finite set of events was introduced. The model can be used for the evaluation of optimal complexity of logical function class, and is not oriented on the most "unfavorable" distribution and asymptotic case. It allows to take into account the expert knowledge about the applied problem. In the given paragraph, we consider some properties of the models, related to the information-probabilistic criterion of logical functions quality in cluster analysis problem.

Let there be given certain grouping decision tree, with corresponding partition of variable space into M subregions. In this setting, number of classes $K = M$. Denote $\theta = (p_1^{(1)}, \ldots, p_M^{(K)})$, where $p_m^{(k)}$ is the probability of falling into m-th subregion, determined for randomly chosen object of k-th class. Let $\mathbf{\Theta}$ be the set of possible values of θ. We shall consider the Bayes model of recognition on a finite set of events that correspond to the subregions of the partition. With this model, we assume that a random quantity Θ is defined on $\mathbf{\Theta}$, having a priori Dirichlet distribution $\theta \sim Dir(\mathbf{d})$, where $\mathbf{d} = (d_1^{(1)}, \ldots, d_M^{(K)})$ is a vector of distribution parameters. The works [6,10] suggest a way for the parameters setting, by means of the expert estimation of the degree of "intersection" between classes. In the absence of a priori knowledge, it is possible to use uniform a priori distribution ($d_m^{(k)} \equiv 1$).

Let us denote the entropy of vector θ as $H(\theta) = -\sum\limits_{k,m} p_m^{(k)} \ln p_m^{(k)}$. Consider the mathematical expectation $\mathrm{E}H(\Theta)$, where the averaing is done over the set $\mathbf{\Theta}$.

Theorem 1. *The following equality holds:*

$$\mathrm{E}H(\Theta) = \Psi(D+1) - \frac{1}{D}\sum_{k,m} d_m^{(k)} \Psi(d_m^{(k)} + 1),$$

where $\Psi(z)$ is digamma function: $\Psi(z) = \frac{d}{dz} \ln \Gamma(z)$, and $D = \sum\limits_{k,m} d_m^{(k)}$.

The proof is given in the Appendix.

Let the sample be transformed into the set of supposed frequencies of objects of latent classes in the subregions: $s = \{n_1^{(1)}, \ldots, n_M^{(K)}\}$, where $n_m^{(k)} = 0$ for $k \neq m$, and $n_m^{(k)} > 0$ for $k = m$, $m = 1, \ldots, M$. By the property of the Dirichlet distribution, a posteriori distribution $\Theta|s \sim Dir(\mathbf{d}+s)$. It follows from Theorem 1 that the *expected entropy* in classified sample

$$\mathrm{E}H(\Theta|s) = \Psi(D+N+1) - \frac{1}{D+N}\sum_{k,m} (d_m^{(k)} + n_m^{(k)}) \Psi(d_m^{(k)} + n_m^{(k)} + 1).$$

We shall call the quatity

$$I(s) = \mathrm{E}H(\Theta) - \mathrm{E}H(\Theta|s)$$

the *expected amount of information* in classified sample. This notion can be used as a criterion of quality for grouping decision function. The optimal variant corresponds to the maximum value of criterion.

5 Experimental Results

The statistical modeling and the analysis of real data sets are used to test the performance of the algorithm. At the modeling, the algorithm repeatedly analyzes randomly generated samples from mixtures of given distributions. Let P_{cor} be the estimation of correct classification probability. This quantity is calculated in each experiment using 100 random trials (the standard deviation of estimates was no more than 0.01 in our experiments).

Example 1. The Gauss multivariate distribution with diagonal covariance matrix $\Sigma = \sigma I$ is specified for each of $K = 2$ classes, where σ takes its values from $\{0.01; 0.04; 0.1; 0.5; 1\}$. The number of variables $n = 100$; half of them are continuous, and half – Boolean. Distribution means are chosen from vertices of unit hypercube at random. For Boolean variables, the values obtained by the random generator, are rounded to closest integer in $\{0; 1\}$. The sample size for each class equals 25, the number of trees in ensemble $L = 10$. Each of base trees is designed in a randomly chosen variable space of dimensionality $n_e = 2$. Table 1 shows estimated accuracies for different σ. The last row of table consists of averaged accuracies for "uncoordinated" trees.

Table 1. Accuracy of algorithms

P_{cor}	$\sigma = 0,01$	$\sigma = 0,04$	$\sigma = 0,1$	$\sigma = 0,5$	$\sigma = 1$
ensemble	1	1	0,9992	0,85	0,75
tree	1	0,87	0,85	0,65	0,61

Example 2. In the next experiment, we follow the above-mentioned scheme, but with $K = 3$, $\Sigma = (\sigma_{i,j})$, where $\sigma_{i,j} = 3$. The distribution means are chosen from set $\{1, 2, \ldots, 10\}^n$ at random. All variables are continuous. Figure 1 shows the dependence of P_{cor} from number of trees in ensemble. For the comparison, the results for analogous algorithm based on binary dissimilarity matrix are given.

Example 3. The procedure of statistical modeling is used for the comparison of tree ensemble clustering algorithm, k-means algorithm and the algorithm of single decision tree construction. The last two algorithms work in space of all variables (all features are continuous); number of classes $K = 2$. Additionally, we set that 90 of 100 variables are noisy (their numbers are chosen at random). For the remaining variables, we take $\Sigma = 0.25I$. The results (dependence of P_{cor} from L) are given in Figure 2.

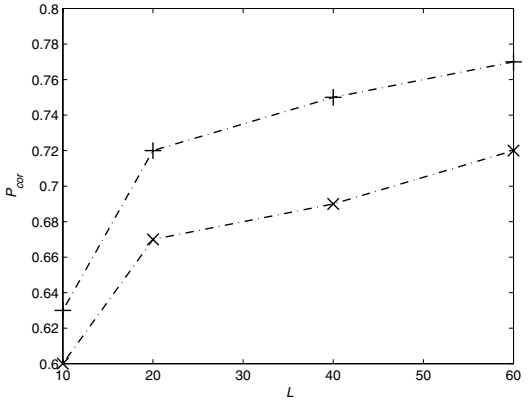

Fig. 1. Performance of algorithms: "+" – using distances between taxons; "×" – based on binary dissimilarity matrix

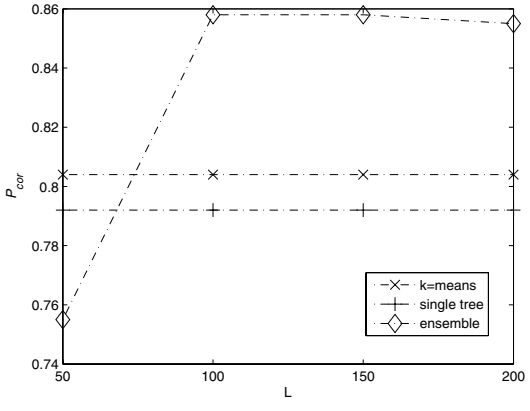

Fig. 2. Comparison of tree ensemble, k-means and single tree clustering algorithms

Example 4. The proposed algorithm was tested on real data, obtained either from specialists in applied areas, or from UCI Machine Learning Repository [11]. Each data set has known class attribute which allows to evaluate the classification accuracy (naturally, this attribute is excluded from cluster analysis). Note that such a priori partition of objects into "groups" not always completely coincides with the "objective" classification. However, it can be used for evaluating the approximate quality of algorithm.

1. Data set "anthropology" includes the descriptions of 252 anthropological findings of the neolith epoch on the territory of South-West Siberia. The objects are described by 23 variables, being the measurements of linear and angular sizes

of skeleton bones. The anthropological objects belong to two anthropological branches of the Mongoloid and the Europeoid race.

2. Data set "arrow heads" describes a collection of 102 arrow heads discovered in ancient cultural monuments on the territory of Novosibirsk region in Siberia. Each arrow head is described by 8 numeric and 4 categorical variables (the number of the categories varies from 2 to 10). The monuments belong to two main types of the cultures.

3. Data set "echocardiogramma.data" is from UCI repository. The data includes 7 variables (one of them is non-numeric), describing the results of echocardiogramma for 74 patients having heart attack recently. The patients belong to one of two classes: having survived a year or more after the attack; having not survived.

4. Data set "credit.data" is from UCI repository. The table has 6 numeric and 10 categorical variables (the maximum number of categories is 14) describing 690 anonymous credit card applicants. For each applicant it is specified, whether the decision was positive or not.

The results of the analysis are given in Table 2. Here P_{ans} is the frequency of correct classification in ensemble, L is the number of base classifiers, n_e is the dimensionality of feature subspace, $\overline{P}_{tree}$ is the average frequency of correct classification for uncoordinated tree.

Table 2. The results of the analysis of four data sets

Data set	P_{ans}	L	n_e	$\overline{P}_{tree}$
anthropology	0.74	40	2	0.61
arrow heads	0.83	40	2	0,63
echocardiogramma	0.76	10	3	0.68
credit	0.86	40	4	0.66

The experiments demonstrate the increase in classification accuracy for grouping decision tree ensemble algorithm.

6 Conclusions

The suggested algorithm of construction the ensemble of logical models, unlike other clustering ensembles algorithms, allows to process heterogeneous data and takes into account distances between logical regularities describing clusters. The experiments show that the algorithm can increase the quality of classification in comparison with "uncoordinated" decision tree and k-means clustering algorithms. We plan to continue the research of clustering ensembles methodology, and the information-probabilistic criteria for clustering quality, particularly, in the framework of the Bayesian analysis.

References

1. Strehl, A., Ghosh, J.: Clustering Ensembles - a Knowledge Reuse Framework for Combining Multiple Partitions. The Journal of Machine Learning Research 38, 583–617 (2002)
2. Topchy, A., Law, M., Jain, A., Fred, A.: Analysis of Consensus Partition in Cluster Ensemble. In: Fourth IEEE International Conference on Data Mining (ICDM 2004), pp. 225–232 (2004)
3. Hong, Y., Kwong, S.: To Combine Steady-state Genetic Algorithm and Ensemble Learning for Data Clustering. Pattern Recognition Letters 29(9), 1416–1423 (2008)
4. Michalski, R., Stepp, R., Diday, E.: Automated Construction of Classifications: Conceptual Clustering versus Numerical Taxonomy. IEEE Trans. Pattern Anal. Mach. Intell. PAMI-5. 5, 396–409 (1983)
5. Lbov, G.S., Berikov, V.B.: Recursive Method of Formation of the Recognition Decision Rule in the Class of Logical Functions. Pattern Recognition and Image Analysis 3(4), 428–431 (1993)
6. Lbov, G.S., Berikov, V.B.: Stability of Decision Functions in Problems of Pattern Recognition and Analysis of Heterogeneous Information (in Russian). Institute of mathematics, Novosibirsk (2005)
7. Kuncheva, L.: Combining Pattern Classifiers. In: Methods and Algorithms. John Wiley & Sons, Hoboken (2004)
8. Breiman, L.: Random Forests. Machine Learning 45(1), 5–32 (2001)
9. Berikov, V.B.: Cluster Analysis by the Ensemble of Decision Trees. In: 9-th International Conference on Pattern Recognition and Image Analysis: New Information Technologies (PRIA-9-2008), Nizhni Novgorod, vol. 1, pp. 51–54 (2008)
10. Berikov, V., Lbov, G.: Bayesian model of recognition on a finite set of events. In: Darzentas, J., Vouros, G.A., Vosinakis, S., Arnellos, A. (eds.) SETN 2008. LNCS (LNAI), vol. 5138, pp. 339–344. Springer, Heidelberg (2008)
11. http://archive.ics.uci.edu/ml/
12. Abramowitz, M., Stegun, I.A.: Handbook of Mathematical Functions. NBS, Washington (1972)

Appendix: Proof of Theorem 1

The probability density function of the Dirichlet distribution is $p(\theta) = \frac{1}{Z}\prod_{k,m}(p_m^{(k)})^{d_m^{(k)}-1}$, where $Z = \frac{\prod_{k,m}\Gamma(d_m^{(k)})}{\Gamma(D)}$ is normalizing constant. We have

$$\mathrm{E}_\Theta H(\Theta) = -\frac{1}{Z}\int_{\boldsymbol{\Theta}} \sum_{k,m} p_m^{(k)} \ln p_m^{(k)} p(\theta) d\theta$$

$$= -\frac{1}{Z}\sum_{k,m}\int_0^1 (p_m^{(k)})^{d_m^{(k)}} \ln p_m^{(k)} \int_{\boldsymbol{\Theta}_m^{(k)}} \prod_{l,q\in I_m^{(k)}} (p_q^{(l)})^{d_q^{(l)}-1} \prod_{l,q\in I_m^{(k)}} dp_q^{(l)} dp_m^{(k)},$$

where $I_m^{(k)} = \{(l,q)|(l,q) \neq (k,m),\ l,q = 1,\ldots,M\}$, $\mathbf{\Theta}_m^{(k)} = \{p_q^{(l)}| \sum\limits_{q,l \in I_m^{(k)}} p_q^{(l)} = 1 - p_m^{(k)}\}$, $k,m = 1,\ldots,M$. Using the Dirichlet integral formula:

$$\int\limits_{\substack{x_1,\ldots,x_{m-1}:\\ x_1+\ldots+x_{m-1}\leq 1\\ x_i\geq 0}} x_1^{d_1-1}\ldots x_{m-1}^{d_{m-1}-1}(1-x_1-\ldots-x_{m-1})^{d_m-1}dx_1\ldots dx_{m-1}$$

$$= \frac{\Gamma(d_1)\ldots\Gamma(d_m)}{\Gamma(d_1+\ldots+d_m)},$$

where $d_1,\ldots,d_m$ are positive reals, we obtain:

$$\mathrm{E}H(\Theta) = -\frac{1}{Z}\sum_{k,m}\int\limits_0^1 (p_m^{(k)})^{d_m^{(k)}}\ln p_m^{(k)}\frac{\prod\limits_{l,q}\Gamma(d_q^{(l)})}{\Gamma(\sum\limits_{l,q} d_q^{(l)})}(1-p_m^{(k)})^{\sum\limits_{l,q} d_q^{(l)}-1}dp_m^{(k)}$$

$$= -\frac{1}{Z}\sum_{k,m}\frac{\prod\limits_{l,q}\Gamma(d_q^{(l)})}{\Gamma(D-d_m^{(k)})}\int\limits_0^1 (p_m^{(k)})^{d_m^{(k)}}(1-p_m^{(k)})^{D-d_m^{(k)}-1}\ln p_m^{(k)}dp_m^{(k)}.$$

Let us use the following integral formula [12]:

$$\int\limits_0^1 x^{\mu-1}(1-x)^{\nu-1}\ln x dx = B(\mu,\nu)[\Psi(\mu)-\Psi(\mu+\nu)],$$

where $B(\cdot,\cdot)$ is beta function, $\mu,\nu > 0$. Thus, we have

$$\mathrm{E}H(\Theta) = -\tfrac{1}{Z}\sum\limits_{k,m}\frac{\prod\limits_{l,q}\Gamma(d_q^{(l)})}{\Gamma(D-d_m^{(k)})}B(d_m^{(k)}+1, D-d_m^{(k)})[\Psi(d_m^{(k)}+1)-\Psi(d_m^{(k)}+1+D-d_m^{(k)})].$$

Using the property $B(x,y) = \frac{\Gamma(x)\Gamma(y)}{\Gamma(x+y)}$, after transformations we get finally

$$\mathrm{E}H(\Theta) = -\frac{\Gamma(D)}{\Gamma(D+1)}\sum_{k,m}\frac{\Gamma(d_m^{(k)}+1)}{\Gamma(d_m^{(k)})}[\Psi(d_m^{(k)}+1)-\Psi(D+1)]$$

$$= \Psi(D+1) - \frac{1}{D}\sum_{k,m} d_m^{(k)}\Psi(d_m^{(k)}+1).$$

Ordinal Regression with Sparse Bayesian

Xiao Chang [1,2], Qinghua Zheng[1,2], and Peng Lin[1,2]

[1] Dept. Computer Science and Engineering, Xi'an Jiaotong University
[2] Shaanxi Key Lab. of Satellite and Computer Network
No.28 Xianning West Road, Xi'an, Shaanxi, 710049, P.R. China
{changxiao,qhzheng}@mail.xjtu.edu.cn,
ice-spider@163.com

Abstract. In this paper, a probabilistic framework for ordinal prediction is proposed, which can be used in modeling ordinal regression. A sparse Bayesian treatment for ordinal regression is given by us, in which an automatic relevance determination prior over weights is used. The inference techniques based on Laplace approximation is adopted for model selection. By this approach accurate prediction models can be derived, which typically utilize dramatically fewer basis functions than the comparable supported vector based and Gaussian process based approaches while offering a number of additional advantages. Experimental results on the real-world data set show that the generalization performance competitive with support vector-based method and Gaussian process-based method.

Keywords: Ordinal regression, Sparse bayesian, Automatic relevance determination.

1 Introduction

Ordinal regression resides between multiclass classification and metric regression in the area of supervised learning. In ordinal regression problem, the samples are labeled with a set of discrete ranks, which the size is larger than or equal to two. The task of learning in ordinal regression is to find a model on samples data, which can predict the rank of new instance.

Several approaches for ordinal regression were proposed in recent years from a machine learning perspective. One popular idea is to transform the ordinal scales into numeric values, and then solve the problem as a standard regression problem [1] [2] [3] [4] [5] [6] [7] [8] [9].

The supported vector based and Gaussian process based approaches are two state-of-the-art methods for ordinal regression, which all are based on sound learning theories and outperform most of other approaches. Kernel method is used in both of them. Their performance is competitive with other methods. However, the two approaches have some shortcomings respectively.

In this paper, a probabilistic sparse kernel model is proposed to ordinal regression. A Bayesian treatment is employed to ordinal regression. A prior over the weights governed by a set of hyperparameters is imposed. One hyperparameter associated with each weight.

D.-S. Huang et al. (Eds.): ICIC 2009, LNAI 5755, pp. 591–599, 2009.

This approach is inspired by the relevance vector machine [10] which has been proved its usefulness in learning (metric) regression and classification. RVM regression model has been adopted, e.g., to Visual Tracking [11], recovering 3D human body pose [12], medical image analysis [13, 14]. RVM classification model has been adopted , e.g., to the medical image analysis [15] and classifying gene expression problem [16].

The most compelling feature of our approach is that, while capable of generalization performance comparable to a supported vector based method, it typically utilizes dramatically fewer kernel functions. Furthermore, the probabilistic prediction can be derived from it, no parameter need to be estimated after learning and the kernel function must satisfy Mercer's condition.

The experiment has been done on real world dataset, and performance is compared with the approaches of ordinal regression with supported vector and Gaussian process methodology. Experimental results verify the usefulness of this approach. Experimental results demonstrate that the algorithm proposed in this paper usually outperforms the algorithm based on Gaussian process, and have comparable performance to supported vector based algorithms.

This paper is organized as follows. The proposed sparse Bayesian framework for ordinal regression is derived in Section 2. The learning technique is discussed in Section 3. The experimental results are shown in Section 4. In Section 5, the conclusion of this paper are given.

2 Sparse Bayesian Framework for Ordinal Regression

In ordinal regression problem, given an i.i.d training sample set $S = \{(\mathbf{x}_i, r_i)\}_{i=1}^{N}$, each instance $\mathbf{x}_i$ is associated with a label r_i. Here $\mathbf{x}_i$ is an observation vector, i.e. $\mathbf{x}_i \in \mathbb{R}^n$. Given $R = \{R_1, R_2, \ldots, R_k\}$ is a label space, the object in it can be ranked as $R_k \succ_R \cdots \succ_R R_2 \succ_R R_1$. ($\succ_Y$ represents the order among ranks). R_i is the label of rank *i*. The goal of ordinal regression is to find a model that predicts the rank of an input vector **x**.

In our approach, we assume that there is an unobservable latent function value $f(\mathbf{x}_i) \in \mathbb{R}$ associated with each training sample $\mathbf{x}_i$, and that the ordinal variable r_i dependents on the function values $f(\mathbf{x}_i)$ by modeling the ranks as intervals on the real line as introduce in section 2. Then we employ an appropriate likelihood function to learn from sample instances labeled with ranks, and impose a zero-mean Gaussian prior on these latent function values. The Bayesian framework is described with more details in the following.

2.1 Latent Function Model

Assuming the model space of mapping object to rank is $\mathscr{H} = \{f(\cdot) : X \mapsto \mathbb{R}\}$. Each f in $\mathscr{H}$ creates an order $\succ_X$ in input function $X \subset \mathbb{R}^n$, according the rule

$$\mathbf{x}_i \succ_X \mathbf{x}_j \Leftrightarrow f(\mathbf{x}_i) \succ_Y f(\mathbf{x}_j) . \tag{1}$$

The task of ordinal regression is to find a model f^* in space $\mathscr{H}$ and the thresholds of ranks, which take the minimum prediction error of predicting the ranks of the instances in training dataset.

Assuming the model f in $\mathscr{H}$ is a linear model as the form

$$f(\mathbf{x}) = \sum_{i=1}^{M} w_i \cdot \phi_i(\mathbf{x}), \tag{2}$$

where M is the number of the vectors used in prediction. This model is intended to mirror the structure of the support vector machine.

In particular, the basis functions are given by kernels, with one kernel associated with each of the data points from the training set. The general expression (2) then takes the supported vector machine (SVM) liked form

$$f(\mathbf{x}) = \sum_{i=1}^{M} w_i \cdot \kappa(\mathbf{x}, \mathbf{x}_i) = \mathbf{w}^T \bullet \phi(\mathbf{x}), \tag{3}$$

where $\kappa(\mathbf{x}, \mathbf{x}_i)$ is the kernel function. It is the result of inner product of instance $\mathbf{x}$ and a sample instance $\mathbf{x}_i$. In contrast to the SVM, there is no restriction to positive definite kernels, nor are the basis functions tied in either number or location to the training data points. $\phi(\mathbf{x})$ is a vector of kernel functions with the form $\phi(\mathbf{x}) = \left(\kappa(\mathbf{x}, \mathbf{x_1}), \kappa(\mathbf{x}, \mathbf{x_2}), \ldots, \kappa(\mathbf{x}, \mathbf{x_M})\right)^T$. The dimension of the vector $\phi(\mathbf{x})$ equals to the number of basis functions.

2.2 Prior Probability

The weight vector $\mathbf{w}$ of the latent function model can be found by maximum likelihood. In this case, however, the most of elements of weight vector $\mathbf{w}$ will not be zero. Therefore, we encode a preference for smoother function with a zero-mean Gaussian prior distribution [17, 18] over $\mathbf{w}$ like in [10], which is used to automatic relevance determination (ARD). The prior distribution is given as the form

$$p(\mathbf{w} \mid \boldsymbol{\alpha}) = \prod_{i=0}^{N} \mathrm{N}\left(w_i \mid 0, \alpha_i^{-1}\right) = (2\pi)^{-\frac{N}{2}} |\mathrm{A}|^{\frac{1}{2}} \exp\left(-\frac{1}{2}\mathbf{w}^{\mathrm{T}}\mathrm{A}\mathbf{w}\right), \tag{4}$$

where $\boldsymbol{\alpha}$ is a vector of N hyperparameters. There is an individual hyperparameter associated independently with every weight. All hyperparameters are collected into a diagonal matrix $\mathrm{A}=\mathrm{diag}(\alpha_1, \alpha_2, \ldots, \alpha_N)$.

2.3 Likelihood for Ordinal Variables

Input vector $\mathbf{x}$ is mapped to a real number by latent function. The conditional distribution that a rank target variable r is drew from, given an input vector $\mathbf{x}$, can takes the form

$$p\left(r \middle| \mathbf{x}, \mathbf{w}\right) = \delta(\theta_r - f(\mathbf{x})) - \delta(\theta_{r-1} - f(\mathbf{x})) \cdot \tag{5}$$

The likelihood of target vector $\mathbf{r}$ on dataset S can be written as the form

$$\begin{aligned} p(\boldsymbol{r} \mid \mathrm{X}, \mathbf{w}) &= \prod_{i=1}^{N} p\left(r_i \mid \mathbf{x_i}, \mathbf{w}\right) \\ &= \prod_{i=1}^{N} \left(\delta(\theta_{r_i} - f(\mathbf{x_i})) - \delta(\theta_{r_i-1} - f(\mathbf{x_i}))\right) \end{aligned}, \tag{6}$$

where N is the size of training dataset, δ can be the probabilistic function that relate a real number to probability, for example sigmoid function as form

$$p(l \mid \theta_{r_i} - f(\mathrm{x_i})) = \frac{1}{1+\exp\left(-l \cdot \left(\theta_{r_i} - f(\mathrm{x_i})\right)\right)}, \tag{7}$$

where $l \in \{-1, +1\}$.

2.4 Posterior Probability

Given hyperparameter vector $\boldsymbol{\alpha}$ and thresholds vector $\boldsymbol{\theta}$, the posterior parameter distribution conditioned on the data is given by combining the likelihood and prior within Bayes' rule. The posterior probability can then be written as the form

$$p(\mathbf{w} \mid \mathbf{r}, \boldsymbol{\alpha}, \boldsymbol{\theta}) = \frac{p(\mathbf{r} \mid \mathrm{X}, \mathbf{w}, \boldsymbol{\theta})\, p(\mathbf{w} \mid \boldsymbol{\alpha})}{p(\mathbf{r})}, \tag{8}$$

where the prior $p(\mathbf{w} \mid \boldsymbol{\alpha})$ is defined as in (4), the likelihood function $p(\mathbf{r} \mid \mathrm{X}, \mathbf{w}, \boldsymbol{\theta})$ is defined as in (6).

The vector $\mathbf{w}$ is the parameter vector of Bayesian framework that we described above, which is generally called the weights of latent function. The Bayesian framework is conditional on the hyperparameters including the kernel parameters κ in some kernel function that control the kernel shape, the threshold parameters $\{\theta_1, \theta_2, \ldots, \theta_{K-1}\}$ and the variance in prior function (4). All these hyperparameters can be collected into $\boldsymbol{\tau}$, which is the hyperparameter vector. The normalization factor $p(\mathbf{r})$ in (8), more exactly $p(\mathbf{r} \mid \boldsymbol{\tau})$, is known as the evidence for $\boldsymbol{\tau}$, a yardstick for model selection. In the next section, we discuss techniques for parameter and hyperparameter learning.

3 Learning

First, given the initial value of hyperparameter vector $\boldsymbol{\tau}$, the weight of latent function model is found by maximize the weight posterior $p(\mathbf{w} \mid \mathbf{r}, \boldsymbol{\tau})$. Then we applied the Laplace approximation [19] in evidence evaluation. The hyperparameters are computed by maximize "evidence for the hyperparameters".

3.1 Maximum a Posteriori (MAP) Estimate

The MAP estimate on the latent functions is referred to find a $\mathbf{w_{MAP}} \in \mathscr{H}$ which maximize the weight $\mathbf{w}$ posteriori probability of given hyperparameter vector $\boldsymbol{\tau}$. The form of MAP estimate is given as the form

$$\begin{aligned}\mathbf{w}_{\mathbf{MAP}} &= \arg\max_{\mathbf{w}} p(\mathbf{w} \mid \mathbf{r}, \boldsymbol{\tau}), \\ &\propto \arg\max_{\mathbf{w}} p(\mathbf{r} \mid \mathrm{X}, \mathbf{w}, \boldsymbol{\theta})\, p(\mathbf{w} \mid \boldsymbol{\alpha}).\end{aligned} \tag{9}$$

The problem in (9) is equivalent to the minimum of negative logarithm of $p(\mathbf{w} \mid \mathbf{r}, \boldsymbol{\tau})$ as form

$$\mathbf{w}_{\mathbf{MAP}} = \arg\min_{\mathbf{w}} \mathrm{E}(\mathbf{w}), \tag{10}$$

where $\mathrm{E}(\mathbf{w})$ is written as the form

$$\begin{aligned}\mathrm{E}(\mathbf{w}) &= -\ln p(\mathbf{r} \mid \mathbf{w}, \mathrm{X})\, p(\mathbf{w} \mid \boldsymbol{\alpha}) \\ &= -\sum_{i=1}^{N} \ln p(r_i \mid \mathbf{x}_i, \mathbf{w}) + \frac{1}{2}\mathbf{w}^T \mathrm{A}\mathbf{w} - \frac{1}{2}\log|\mathrm{A}| + \frac{N}{2}\log 2\pi\end{aligned}. \tag{11}$$

The iteratively-reweighted least-squares algorithm method is adapted to find $\mathbf{w}_{\mathbf{MAP}}$ as in [10].

3.2 Model Selection

The optimal hyperparameters is inferred by maximizing the evidence as the form

$$\boldsymbol{\tau}^* = \arg\max_{\boldsymbol{\tau}} p(\mathbf{r} \mid \boldsymbol{\tau}). \tag{12}$$

The evidence can be calculated analytically after applying the Laplace approximation [19] at the MAP estimate.. Using the Laplace approximation the evidence can be computed analytically as the form

$$\begin{aligned}p(\mathbf{r} \mid \boldsymbol{\tau}) &= \int p(\mathbf{r} \mid \mathbf{w}, \mathrm{X})\, p(\mathbf{w} \mid \boldsymbol{\tau}) d\mathbf{w} \\ &\approx [\, p(\mathbf{r} \mid \mathbf{w}, \mathrm{X})\, p(\mathbf{w} \mid \boldsymbol{\tau})]\Big|_{\mathbf{w}=\mathbf{w}_{\mathrm{MAP}}} (2\pi)^{N/2} |\Sigma|^{1/2}\end{aligned}, \tag{13}$$

where $\Sigma = \left(\dfrac{\partial^2 \mathrm{E}(\mathbf{w})}{\partial^2 \mathbf{w}} \right)^{-1}$.

The problem in (12) is equivalent to the minimum of negative logarithm of $p(\mathbf{r} \mid \boldsymbol{\tau})$, which can be written as the form

$$\min_{\boldsymbol{\tau}} \mathrm{E}(\mathbf{w}_{MAP}) - \frac{1}{2}\ln|\Sigma| \quad , \tag{14}$$

subject to

$$\mathbf{w} \bullet \phi(\mathbf{x}_i) - \theta_{r_i\text{-}1} > 0, \; i = 1, 2, \ldots N, \tag{15}$$

$$\mathbf{w} \bullet \phi(\mathbf{x}_i) - \theta_{r_i} \le 0, \; i = 1, 2, \ldots N, \tag{16}$$

$$\theta_j - \theta_{j-1} > 0, \; j = 1, \ldots, K-1. \tag{17}$$

The constraint condition (15), (16) and (17) should be attached to the optimization object (14). These constraint conditions are important to ensure the right $\boldsymbol{\theta}$ can be obtained in searching procedure.

For $\boldsymbol{\alpha}$, the derivatives of (14) equating to zero and rearranging, following the approach of [19] , gives the form:

$$a_i^{\text{new}} = \frac{1 - a_i \Sigma_{ii}}{w_i^2}, \tag{18}$$

where w_i is the *i*-th posterior mean weight, Σ_{ii} is the *i*-th diagonal element of the posterior weight covariance.

4 Experiments

4.1 Experiment Setting

In experiments, the performance of the algorithm proposed in this paper is compared with two proposed state-of-the-art ranking algorithms: SVMOR [6] and GPOR [9]. This algorithm is called SBOR.

The kernel method is used for all of three algorithms. The linear kernel function is employed in the three algorithms in our experiment, which takes the form $\kappa(\mathbf{x}, \mathbf{x}') = \mathbf{x}^{\mathrm{T}} \bullet \mathbf{x}'$. There is not parameter in linear kernel function.

For SVMOR, the optimal trade-off parameter is searched on linearly space by 0.2 in the region of $\{-2 \le \log_{10} C \le 2\}$.

One real world dataset included in LETOR [20] , a popular Benchmark dataset, is used in this experiment. OHSUMED [21], a dataset for document retrieval research.

Two measures for information retrieval evaluation are used in the experiment to compare the performance of algorithms.

The first measure is P@N . The strategy of this measure is to compute the precision at *N*-th position in the list of ranking result. It takes the form

$$\text{P@N} = \frac{\text{number of relevent instances for query in first N instances}}{\text{N}}. \tag{19}$$

$\text{P@N} \in [0,1]$. The higher the value of the algorithm is, the better the performance of it is. P@N can be used for the dataset labeled with two ranks. When it is used for the dataset label with more than two ranks, some ranks have to be combined to one rank.

The second measure is NDCG [22], which has been widely used by researchers in recent years. NDCG can be used to evaluate the performance of ranking method on the dataset that is labeled with more than two ranks, which takes the form

$$\text{NDCG @ k} = \text{N(k)} \bullet \sum_{\text{j=1}}^{\text{k}} \frac{2^{\text{r(j)}} - 1}{\log(1 + \text{j})}, \tag{20}$$

where $\text{N}(k)$ is the NDCG at *k* of ideal ranking list. It is used as a normalization factor of the NDCG at *k* of ranking list of prediction result.

4.2 Experiment on OHSUMED Data

The OHSUMED collection is used in document retrieval research. This dataset has been used in information filtering task of TREC 2000. The relevance judgments of documents in OHSUMED are either 'd' (*definitely relevant*), 'p' (*possibly relevant*), or 'n' (*not relevant*). Rank 'n' has the largest number of documents, followed by 'p' and 'd'. The original OHSUMED collection consists of 348,566 records from 270 medical journals. There are 106 queries. For each query, there are a number of documents associated.

The OHSUMED has been collected into a Benchmark dataset LETOR for ranking algorithm research. In this dataset, each instance is represented as a vector of features, determined by a query and a document. Every vector consists of 25 features. The value of features has been computed.

The 20 folds experimental dataset is obtained by running following strategy 20 times: selecting the instances of two query randomly as training data, the instances of one half of remained queries as validate data and that of another half of queries as test data.

When P@N is used in evaluation, all of the instances of rank 'p' and 'n' are combined into rank 'n'.

The experimental results of four algorithms on OHSUMED are given in Fig. 1.

From the experimental results in Fig. 1, we can see that the performance of SBOR significantly outperforms that of the SVMOR and GPOR in two measures. Therefore, we can consider that experimental results indicate that the generalization performance of SBOR algorithm outperforms that of supported vector based and Gaussian process based approach on OHSUMED data.

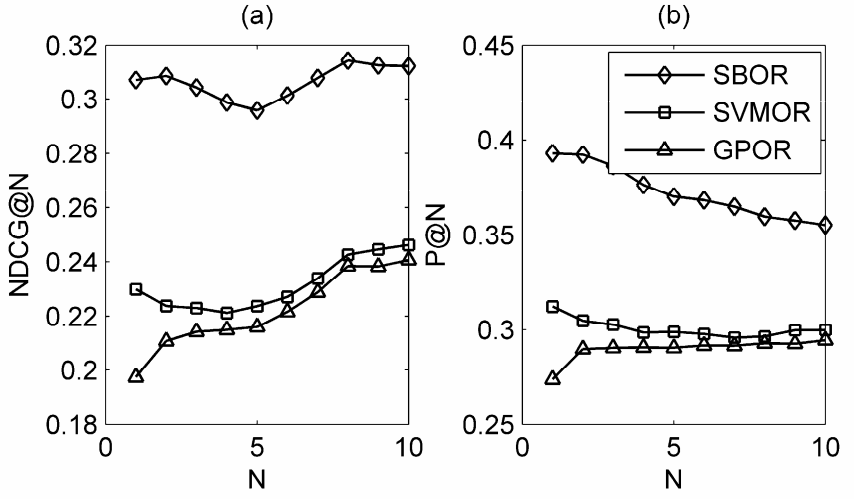

Fig. 1. The experiment results on OHSUMED data. In graph (a) is the evaluation result on NDCG@N. In graph (b) is the evaluation result on P@N.

5 Conlusion

In this paper a probability framework for ordinal prediction is proposed and the sparse Bayesian treatment to ordinal regression is given. The conditional probabilistic function of ordinal variables can be developed by using the binary classification probabilistic function in the probabilistic framework. The probabilistic sparse kernel model overcomes many of the limitations of the previous support vector based ordinal regression methods, while retaining the highly desirable property of sparseness. The property of sparseness is not owned by Gaussian process based method. Experiments on the real-world data set show that the generalization performance of sparse Bayesian ordinal regression is competitive with support vector based method Gaussian process based method.

Acknowledgement

The research was supported by the National High-Tech R&D Program of China under Grant No.2008AA01Z131, the National Science Foundation of China under Grant Nos.60825202, 60803079, 60633020, the National Key Technologies R&D Program of China under Grant Nos. 2006BAK11B02□2006BAJ07B06.

References

1. Kramer, S., Widmer, G., Pfahringer, B., DeGroeve, M.: Prediction of Ordinal Classes Using Regression Trees. Fundamenta Informaticae, 1–13 (2001)
2. Frank, E., Hall, M.: A Simple Approach to Ordinal Classification. In: Proceedings of the European Conference on Machine Learning, pp. 145–165 (2001)
3. Crammer, K., Singer, Y.: Pranking with Ranking. In: Proceedings of the conference on Neural Information Processing Systems (2001)
4. Harrington, E.F.: Online Ranking/Collaborative Filtering Using the Perceptron Algorithm. In: Proceedings of the Twentieth International Conference on Machine Learning, pp. 250–257 (2003)
5. Shashua, A., Levin, A.: Ranking with Large Margin Principle: Two Approaches. Advances In Neural Information Processing Systems, 961–968 (2003)
6. Chu, W., Keerthi, S.S.: New Approaches to Support Vector Ordinal Regression. In: Proceedings of the 22nd International Conference on Machine Learning, pp.145–152 (2005)
7. Shevade, S.K., Chu, W.: Minimum Enclosing Spheres Formulations for Support Vector Ordinal Regression. In: Proceedings of IEEE International Conference on Data Mining, ICDM, pp. 1054–1058 (2007)
8. Li, L., Lin, H.: Ordinal Regression by Extended Binary Classification. Advances In Neural Information Processing Systems 19, 865 (2007)
9. Chu, W., Ghahramani, Z.: Gaussian Processes for Ordinal Regression. Journal of Machine Learning Research 6, 23 (2005)
10. Tipping, M.E.: Sparse Bayesian Learning and the Relevance Vector Machine. Journal of Machine Learning Research 1, 211–244 (2001)
11. Williams, O., Blake, A., Cipolla, R.: Sparse Bayesian Learning for Efficient Visual Tracking. IEEE Transactions on Pattern Analysis and Machine Intelligence 27, 1292–1304 (2005)

12. Agarwal, A., Triggs, B.: 3D Human Pose from Silhouettes by Relevance Vector Regression. In: Proceedings of the 2004 IEEE Computer Society Conference on Computer Vision and Pattern Recognition, vol. 2, pp. 882–888 (2004)
13. Cawley, G.C., Talbot, N.L.C., Janacek, G.J., Peck, M.W.: Sparse Bayesian Kernel Survival Analysis for Modeling the Growth Domain of Microbial Pathogens. IEEE Transactions on Neural Networks 17, 471–481 (2006)
14. Peng, J.Y., Aston, J.A.D., Gunn, R.N., Liou, C.Y., Ashburner, J.: Dynamic Positron Emission Tomography Data-driven Analysis Using Sparse Bayesian Learning. IEEE Transactions on Medical Imaging 27, 1356–1369 (2008)
15. Wei, L.Y., Yang, Y.Y., Nishikawa, R.M.: A relevance Vector Machine Technique for Automatic Detection of Clustered Microcalcifications, pp. 831–839 (2005)
16. Li, Y., Campbell, C., Tipping, M.: Bayesian Automatic Relevance Determination Algorithms for Classifying Gene Expression Data. Bioinformatics 18, 1332–1339 (2002)
17. MacKay, D.J.C.: Bayesian Nonlinear Modeling for the Prediction Competition. ASHRAE Transactions 100, 1053–1062 (1994)
18. Neal, R.M.: Bayesian Learning for Neural Networks. Springer, Heidelberg (1996)
19. MacKay, D.J.C.: A Practical Bayesian Framework for Backpropagation Networks. Neural Computation 4, 448–472 (1992)
20. Liu, T.Y., Xu, J., Qin, T., Xiong, W., Li, H.: Letor: Benchmark Dataset for Research on Learning to Rank for Information Retrieval. In: Proceedings of SIGIR 2007 Workshop on Learning to Rank for Information Retrieval (2007)
21. Hersh, W., Buckley, C., Leone, T.J., Hickam, D.: OHSUMED: An Interactive Retrieval Evaluation and New Large Test Collection for Research. In: Proceedings of the Seventeenth Annual International ACM-SIGIR Conference on Research and Development in Information Retrieval, vol. 358, pp. 192–201 (1994)
22. Kekalainen, J.: Binary and Graded Relevance in IR Evaluations - Comparison of the Effects on Ranking of IR Systems. Information Processing & Management 41, 1019–1033 (2005)

GLRT Based Fault Detection in Sensor Drift Monitoring System

In-Yong Seo[1], Ho-Cheol Shin[1], Moon-Ghu Park[1], and Seong-Jun Kim[2]

[1] Korea Electric Power Research Institute,
65, Munji-Ro, Yuseong-Gu, Daejeon, Korea
[2] Kangnung National University,
120 Gangneung Daehangno, Gangneung-shi, Gangwon-do, Korea
iyseo@kepri.re.kr, sjkim@kangnung.ac.kr

Abstract. In a nuclear power plant (NPP), periodic sensor calibrations are required to assure sensors are operating correctly. However, only a few faulty sensors are found to be calibrated. For the safe operation of an NPP and the reduction of unnecessary calibration, on-line calibration monitoring is needed. This paper presents an on-line sensor drift monitoring technique, based on a Generalized Likelihood Ratio Test (GLRT), for detecting and estimating mean shifts in sensor signal. Also, principal component-based Auto-Associative support vector regression (AASVR) is proposed for the sensor signal validation of the NPP. Response surface methodology (RSM) is employed to efficiently determine the optimal values of SVR hyperparameters. The proposed model was confirmed with actual plant data of Kori NPP Unit 3. The results show that the accuracy of the model and the fault detection performance of the GLRT are very competitive.

Keywords: PCA, SVR, GLRT, NPP.

1 Introduction

For the past two decades, the nuclear industry has attempted to move toward a condition-based maintenance philosophy using new technologies developed to monitor the condition of plant equipment during operation. The traditional periodic maintenance method can lead to equipment damage, incorrect calibrations due to adjustments made under nonservice conditions, increased radiation exposure to maintenance personnel, and possibly, increased downtime. In fact, recent studies have shown that less than 5% of the process instruments are found in degraded condition that require maintenance. Therefore, plant operators are interested in finding ways to monitor sensor performance during operation and to manually calibrate only the sensors that require correction. Hence, in this study we developed an on-line calibration monitoring model for sensor validation.

Considerable research efforts have been made to develop on-line calibration monitoring algorithms. The application of artificial intelligence techniques to nuclear power plants were investigated for instrument condition monitoring [1]. The Multivariate State Estimation Technique (MSET) was developed in the late 1980s [2], and

D.-S. Huang et al. (Eds.): ICIC 2009, LNAI 5755, pp. 600–609, 2009.

the Plant Evaluation and Analysis by Neural Operators (PEANO) was developed in [3]. PEANO uses auto-associative neural networks (AANN) and applies them to the monitoring of nuclear power plant sensors.

The SVR algorithm that was developed by Vapnik [4] is based on the statistical learning theory. The SVM method was applied for the data-based state estimation in nuclear power reactors [5, 6]. In these papers, the Vector State Estimation Technique (VSET) kernel and Hermitian kernel were implemented with promising results.

We developed a principal component-based AASVR for on-line monitoring and signal validation. It utilizes the attractive merits of principal component analysis (PCA) for extracting predominant feature vectors and AASVR because it easily represents complicated processes that are difficult to model with analytical and mechanistic models [7]. The research presented in this paper primarily focuses on the integration of GLRT into a principal component based Auto-Associative support vector regression (PCSVR) system which can be used as an operator decision aid for PWR. The proposed PCSVR model and GLRT were confirmed with actual plant data of Kori Nuclear Power Plant Unit 3.

2 PC-Based AASVR

The outputs of an auto-associative model are trained to emulate its inputs over an appropriate dynamic range. An auto-associative model will estimate the correct input values using the correlations embedded in the model during its training. The estimated correct value from the auto-associative model can then be compared to the actual process parameter to determine if a sensor has drifted or has been degraded by another fault type. Fig. 1 shows the schematic diagram of the proposed PCSVR method for modeling measurements in an NPP.

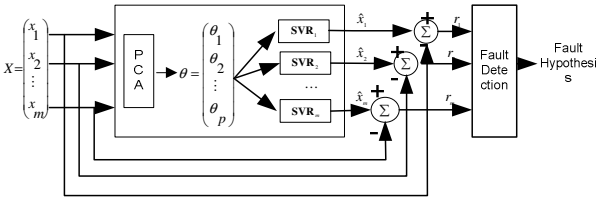

Fig. 1. The schematic diagram of PCSVR

2.1 AASVR Based upon Principal Components

In this paper, an SVM regression method is used for signal validation of the measurements in NPPs. The SVM regression is to nonlinearly map the original data into a higher dimensional feature space. Hence, given a set of data $\{(X_i, y_i)\}_{i=1}^{n} \in R^m \times R^m$ where $\mathbf{x}_i$ is the input vector to support vector machines, $\mathbf{y}_i$ is the actual output vector and n is the total number of data patterns. The multivariate regression function for each output signal is approximated by the following function,

$$y_k = f_k(\boldsymbol{x}) = \boldsymbol{w}_k{}^T \boldsymbol{\phi}(\boldsymbol{x}) + b_k \,, \tag{1}$$

where $\boldsymbol{w}_k = [w_1, w_2, \cdots, w_n]^T$, $\phi = [\phi_1, \phi_2, \cdots, \phi_n]^T$, $k = 1,2,\cdots,m$ and m is the number of sensor measurements. Also, the function $\phi_i(\boldsymbol{x})$ is called the feature. Equation (1) is a nonlinear regression model because the resulting hyper-surface is a nonlinear surface hanging over the m-dimensional input space. The parameters **w** and b are a support vector weight and a bias that are calculated by minimizing the following regularized risk function:

$$R(\boldsymbol{w}_k) = \frac{1}{2}\boldsymbol{w}_k{}^T \boldsymbol{w}_k + C_k \sum_{i=1}^{n} L_k(y_{k,i}) \,, \tag{2}$$

where

$$L_k(y_{k,i}) = \begin{cases} 0, & \left| y_{k,i} - f_k(\boldsymbol{x}) \right| < \varepsilon_k \\ \left| y_{k,i} - f_k(\boldsymbol{x}) \right| - \varepsilon_k, & otherwise \end{cases} \,, \tag{3}$$

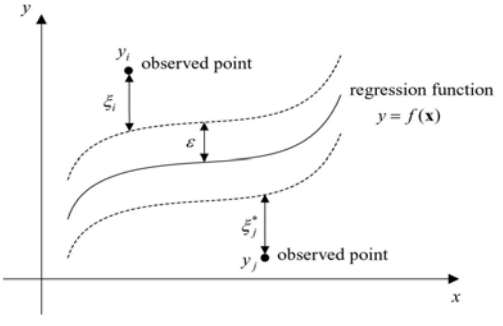

Fig. 2. The Parameters for the AASVR Models

The first term of Equation (2) characterizes the complexity of the SVR models. C_k and ε_k are user-specified parameters and $L_k(y_{k,i})$ is called the ε-insensitive loss function [8]. The loss equals zero if the estimated value is within an error level, and for all other estimated points outside the error level, the loss is equal to the magnitude of the difference between the estimated value and the error level. That is, minimizing the regularized risk function is equivalent to minimizing the following constrained risk function:

$$\text{Minimize} \quad R(\boldsymbol{w}, \xi, \xi^*) = 1/2\,\boldsymbol{w}_k{}^T \boldsymbol{w}_k + C_k \sum_{i=1}^{n} (\xi_{k,i} + \xi_{k,i}^*) \,, \tag{4}$$

$$\text{Subject to} \quad \begin{aligned} & y_{k,i} - \mathbf{w}_k^T \boldsymbol{\phi}(\mathbf{x}) - b_k \le \varepsilon_k + \xi_{k,i} \\ & \mathbf{w}_k^T \boldsymbol{\phi}(\mathbf{x}) + b_k - y_{k,i} \le \varepsilon_k + \xi_{k,i}^* \\ & \varepsilon_k, \xi_{k,i}, \xi_{k,i}^* \ge 0 \quad for\ i = 1,2,\cdots,n \end{aligned} \,, \tag{5}$$

where the constant C determines the trade-off between the flatness of $f(\boldsymbol{x})$ and the amount up to which deviations larger than ε are tolerated, and ξ and ξ^* are slack variables representing upper and lower constraints on the outputs of the system and are positive values.

The constrained optimization problem can be solved by applying the Lagrange multiplier technique to (4) and (5), and then by using a standard quadratic programming technique. Finally, the regression function of (1) becomes

$$y_k = \sum_{i=1}^{n} (\lambda_{k,i} - \lambda_{k,i}^*) \boldsymbol{K}(\boldsymbol{x}_i, \boldsymbol{x}) + b_k^* \quad , \tag{6}$$

where $\boldsymbol{K}(\boldsymbol{x}_i, \boldsymbol{x}) = \phi^T(\boldsymbol{x}_i)\phi(\boldsymbol{x})$ is called the kernel function.

By using different kernel functions for inner product evaluations, various types of nonlinear models in the original space could be constructed. It has been shown that, in general, radial-basis function (RBF) is a reasonable first choice of kernel functions since it equips with more flexibility and less parameters. The RBF kernel function used in this paper is expressed as

$$K(\mathbf{x}, \mathbf{x}_i) = \exp\left\{ -\frac{(\mathbf{x} - \mathbf{x}_i)^T (\mathbf{x} - \mathbf{x}_i)}{2\sigma^2} \right\} , \tag{7}$$

where σ is the kernel function parameter. The bias, b, is calculated as follows:

$$b_k^* = -\frac{1}{2} \sum_{i=1}^{n} (\lambda_{k,i} - \lambda_{k,i}^*)[K(\mathbf{x}_r, x_i) + K(\mathbf{x}_s, x_i)] , \tag{8}$$

where $\mathbf{x}_r$ and $\mathbf{x}_s$ are called support vectors (SVs) and are data points positioned at the boundary of the ε-insensitivity zone. By replacing principal component $\boldsymbol{\theta}$ with **x,** we can combine PC and AASVR as follows:

$$y_k = f_k(\theta) = \sum_{i=1}^{n} (\lambda_{k,i} - \lambda_{k,i}^*) \boldsymbol{K}(\theta_i, \theta) + b_k^* \quad , \tag{9}$$

$$b_k^* = -\frac{1}{2} \sum_{i=1}^{n} (\lambda_{k,i} - \lambda_{k,i}^*)[K(\theta_r, \theta_i) + K(\theta_s, \theta_i)] \quad .$$

The three most relevant design parameters for the AASVR model are the insensitivity zone, ε, the regularization parameter, C, and the kernel function parameter, σ. An increase in the insensitivity zone, ε, reduces the accuracy requirements of the approximation and allows a decrease in the number of SVs. In addition, an increase in the regularization parameter, C, reduces larger errors, thereby minimizing the approximation error. The kernel function parameter, σ, determines the sharpness of the radial basis kernel function.

2.2 GLRT

In sensor monitoring, at every new sample of a signal, a new mean and a new variance of the signals may be required to check the health of the sensor. The Sequential Probability Ratio Test (SPRT) which can detect a sensor fault without having to calculate a new mean and a new variance at each sample was used in the past [9]. But

with the development of computer the computation speed (burden) is not a significant factor for the on-line sensor monitoring any more in these days. The GLRT used in this paper is a statistical model developed by Kay [10].

The objective of sensor monitoring is to detect the failure as soon as possible with a very small probability of making a wrong decision. In the application of sensor diagnostics, the GLRT uses the residual signal that means the difference between the measured value and the estimated value. The sensor degradation or fault can be stated in terms of a change in the mean m_i or a change in the variance σ_i^2, which means the change of the probability distribution. Therefore, the GLRT detects a change of sensor health by sensing the alteration of the probability distribution. The basis for the GLRT lies in the likelihood ratio.

Let's consider the following hypothesis test for the application to the sensor drift;

$$H_0 : \mu = \mu_0, \quad H_1 : \mu \neq \mu_0 , \tag{11}$$

H_0 represents a hypothesis that the sensor is normal and H_1 represents a hypothesis that the sensor is degraded. Thus, the GLRT decides H_1 if

$$L_G(x) = \frac{p(x; \hat{\mu}_1, H_1)}{p(x; \hat{\mu}_0, H_0)} > \gamma , \tag{12}$$

where $\hat{\mu}_1$ is the maximum likelihood estimate (MLE) of μ_1 assuming H_1 is true, and $\hat{\mu}_0$ is the MLE of μ_0 assuming H_0 is true.

When the variance of residual is known, the MLE of μ is $\hat{\mu} = \sum_{i=1}^{n} x_i / n = \bar{x}$ and GLR statistic is

$$\ln \frac{p(\hat{H}_1)}{p(\hat{H}_0)} = \frac{n(\bar{x})^2}{2\sigma^2} , \tag{13}$$

or we decide H_1 if $|\bar{x}| > \gamma'$

When the variance of residual is unknown, the MLE of μ and σ_1^2 which satisfy $\partial p(H_1)/\partial \mu = 0$ and $\partial p(H_1)/\partial \sigma^2 = 0$ at the same time are $\hat{\mu} = \sum_{i=1}^{n} x_i / n = \bar{x}$, $\hat{\sigma}_1^2 = \frac{1}{n}\sum_{i=1}^{n}(x_i - \bar{x})^2$, $\hat{\sigma}_0^2 = \frac{1}{n}\sum_{i=1}^{n} x_i^2$ and GLR statistic is

$$\ln \frac{p(\hat{H}_1)}{p(\hat{H}_0)} = \frac{n}{2} \ln \left(1 + \frac{(\bar{x})^2}{\hat{\sigma}_1^2} \right) . \tag{14}$$

In this case, we decide the sensor is degraded when $(\bar{x})^2 / \hat{\sigma}_1^2 > \gamma$

One possibility for implementing the GLRT would be, at time t, to test for faults occurring at all prior timesteps. The computational expense, however, would be excessive. A more manageable approach taken in this paper is to test only for faults occurring in a window of length *w* (a user defined quantity), i.e., between timesteps *t-w+1* and the current time *t*. Thus, to implement the test one need only consider the *w* most recent residuals.

The null hypothesis is that no fault has occurred, and each of the *w* alternative hypotheses is that the fault occurred at one of the N timesteps within the window.

At current time *t*, the Generalized Likelihood Ratio (GLR) statistic, for the case that variance of residual is known, associated with the hypothesis that the fault occurred at time *t-k +1*(*k*= 1, 2, . . ., *w*) is given by

$$\begin{aligned} G_t &= \max[GLR_t(k), \quad 1 \le k \le w] \\ &= \max[k(\bar{x}_t(k))^2 / \sigma^2, \quad 1 \le k \le w] \end{aligned}, \tag{15}$$

where $GLR_t(k) = k \cdot (\bar{x}_t(k))^2 \Big/ \sigma^2$ and $\bar{x}_t(k) = \sum_{i=t-k+1}^{t} x_i / k$ with a user defined threshold γ chosen to provide a desired in control Average Run Length (ARL). If $G_t < \gamma$ it is concluded that no drift has occurred. If $G_t > \gamma$ it is concluded that the drift occurred at time k^*, where k^* is the value of *k* that maximizes (15). To implement the GLRT, the user must select the test parameters *w* and γ. For all examples in this paper *w*=50 was chosen. The required γ which produces a desired in-control ARL will depend on the fault signature and *w*. But Monte Carlo simulations for determining γ cannot be used because the data are acquired from the real nuclear power plant during startup period.

3 Application to the NPP Measurements

3.1 Experimental Data

The proposed algorithm was confirmed with the real plant startup data of the Kori Nuclear Power Plant Unit 3. These data are the values measured from the primary and secondary systems of the NPP. The data is derived from the following 11 types of measured signals: the reactor power (the ex-core neutron detector signal, Sensor 1); the pressurizer water level (Sensor 2); the SG steam flow rate (Sensor 3); the SG narrow range level (Sensor 4); the SG pressure (Sensor 5); the SG wide-range level (Sensor 6); the SG main feedwater flow rate (Sensor 7); the turbine power (Sensor 8); the charging flow rate (Sensor 9); residual heat removal flow rate (Sensor 10); and the reactor head coolant temperature (Sensor 11).

The data were sampled at a rate of 1 minute for about 38 hours. The total observation number of measurement data is 2,290 which is divided into five subsets of equal size, i.e., one training subset, one test subset and three optimization subsets. Total data set was indexed using Arabic numerals, i.e., i = 1,2,. . ., 2,290. 458 patterns with the indices, i=5j+3, j=0,1,…,457, named KR3 were used to train SVR to capture the quantitative relation between 11 inputs and outputs. KR1 which has indices of 5j+1, j=0,1,…,457, used for the test of the model, while the remaining three subsets (KR2, KR4, KR5) for the optimization.

Let $(\theta_1, \theta_2, \cdots, \theta_{11})$ denote principal components (PCs) obtained by applying PCA to the above plant data. As mentioned earlier, variance is used in selecting dominant PCs. We found that θ_1 is the most dominant PC and explains about 84.12% of total

variation in the original data. However, in order to minimize loss of information, the first seven PCs are considered in this study. The selected PCs explain more than 99.98% of total variation. The loss of information is less than 0.1%.

Parameter regularization is an important step in AASVR modeling. There are three parameters to be determined in AASVR. They are bandwidth of Gaussian radial basis kernel (σ), insensitive band of loss function (ε), and regularization parameter (C). In this study, they are assumed common in every model of AASVR. This paper adopts a statistical design of experiments called response surface methodology (RSM), which has been widely used in the fields of product design and process optimization.

From subsequent analysis results, it is shown that σ and ε have a significant effect on MSE, while C is of little significance. A response surface plot of $\log(MSE)$ versus σ and ε is depicted in Fig. 4. The optimum point of the response surface is obtained as $(\sigma, \varepsilon, C) = (1.4, 0.0005, 6.8)$.

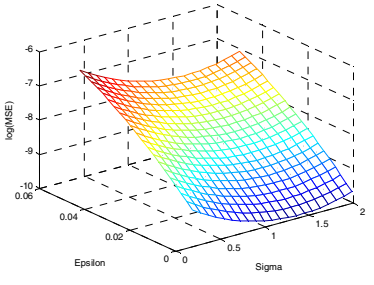

Fig. 3. Response surface plot of $\log(MSE)$ versus σ and ε

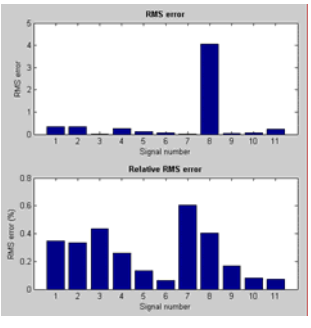

Fig. 4. RMS of estimated sensors

3.2 Test Results

Empirical model building is now done using PCSVR proposed in this paper. The numbers of support vectors needed for each SVR are 381 (83.2%), 230 (50.2%), 381 (83.2%), 108 (23.6%), 333 (72.7%), 206 (45.0%), 420 (91.7%), 384 (83.8%), 163 (35.6%), 105 (22.9%), and 436 (95.2%). The average number of support vectors is 286.1 (62.5%).

Fig. 5 shows root mean square (RMS) for the test data of each sensor representing PCSVR model accuracy. The relative RMS errors for all sensors are compared with their rated values: 100%, 100%, 2.0Mkg/hr, 100%, 100%, 100, 2.0Mkg/hr, 1000Mw, 30m^3/hr, 100m^3/hr, 330^{o}C.

For the feedwater flow rate the relative RMS errors compared with the rated value (2.0Mkg/hr) are 0.3856%, 0.4791%, and 0.5621% for the training data, the optimization data, and the test data, respectively.

In order to verify the failure detection algorithm, we artificially degraded the SG main feed water flow rate signal in test data KR1. The degraded signal is shown in

Fig. 7 (a) which linearly increases at a rate of 3.14% per day from the first observation, i.e. 5% positive drift at the end of the observation. The estimated feedwater flow rate is almost the same as the actual feedwater flow rate although the measured feedwater flow rate is degraded (see Fig. 7(a)). Residuals which were used for GLRT are shown in Fig. 6(b) and Fig. 7(b) for the normal and degraded sensor, respectively. The mean and standard deviation of H_0 residual are -0.0011 and 0.0108, respectively.

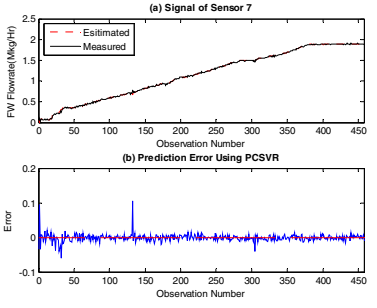

Fig. 5. Model output for normal state (a) Sensor signal (b) residual

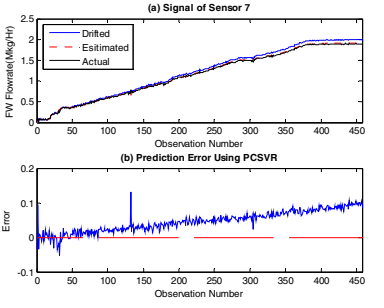

Fig. 6. Model output for drift state (a) Sensor signal (b) residual

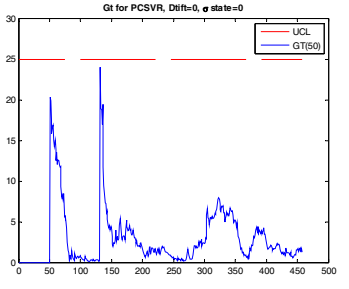

(a) Gt for normal, σ known

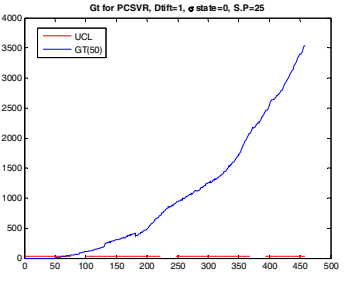

(b) Gt for drift, σ known

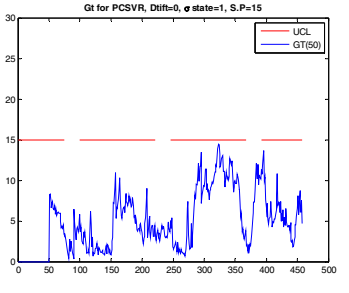

(c) Gt for normal, σ unknown

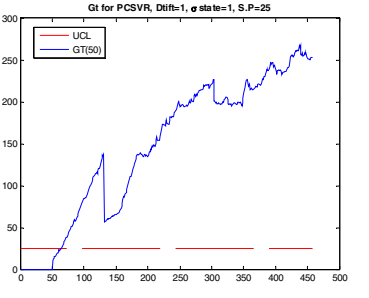

(d) Gt for drift, σ unknown

Fig. 7. Gt statistics for four cases

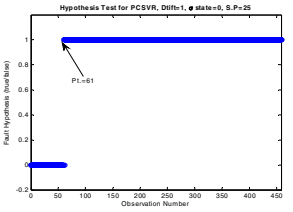

(a) Case 1 (σ known)

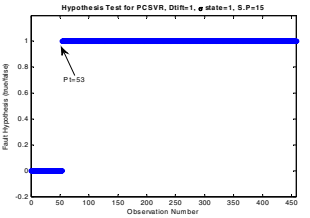

(b) Case 2 (σ unknown)

Fig. 8. Hypothesis test results

Fig. 8 shows Gt statistics for four cases. While Gt statistics for the normal sensor are shown in the left column, the right column is for the drift case. The upper row is Gt statistics for the σ known case and the lower row is for the σ unknown case. From the figure we can notice that Gt statistics for σ known cases are bigger than those for σ unknown cases. Especially when the drift occurs the Gt statistic for variance known case increases exponentially while for variance unknown case it increases linearly. In this example we choose 25 and 15 as the upper control limits (UCL) for σ known and unknown case, respectively. If Gt is greater than the UCL we decide the sensor is degraded.

Fig. 9 shows hypothesis test results which are decided by the UCLs. The drift was detected at 61 and 53 timesteps which correspond to 0.67% and 0.59% in drift amount for σ known (case 1) and unknown case (case 2), respectively. The fault detection point for case 1 occurs 8 timesteps, i.e, 40 minutes in time, earlier than case 2 does.

We can conclude that GLRT can be used for the detection of sensor degradation in NPP. Moreover, we can detect the sensor drift earlier by assuming the variance of residual is unknown than by assuming it is known.

4 Conclusions

In this work, a PCSVR which utilizes PCA for extracting predominant feature vectors and Auto-Associative SVR for databased statistical learning, and the GLRT algorithm were used for the signal validation and calibration monitoring of NPP.

The proposed PCSVR model was applied to the data of Kori Nuclear Power Plant Unit 3. The input signals into the AASVR are preprocessed by the principal component analysis. The first seven feature components are used as its input signals. The averaged relative RMS error for all predicted test output signals is about 0.3%. This error is so small enough. The model residual was tested for several cases using GLRT method. We can conclude that GLRT can be used for the detection of sensor degradation in NPP. Moreover, we can detect the sensor drift earlier by assuming the variance of residual is unknown than by assuming it is known.

Though we need Monte Carlo simulation to get the better in-control ARL and UCL it is impossible in real NPP. For the future work we need to test using several sets of real plant startup data instead of Monte Carlo simulation.

References

1. Upadhyaya, B.R., Eryurek, E.: Application of Neural Networks for Sensor Validation and Plant Monitoring. Nuclear Technology 97, 170–176 (1992)
2. Mott, Y., King, R.W.: Pattern Recognition Software for Plant Surveillance. U.S. DOE Report
3. Fantoni, P., Figedy, S., Racz, A.: A Neuro-Fuzzy Model Applied to Full Range Signal Validation of PWR Nuclear Power Plant Data. In: FLINS-1998, Antwerpen, Belgium (1998)
4. Cortes, C., Vapnik, V.: Support Vector Networks. Machine Learning 20, 273–297 (1995)
5. Zavaljevski, N., Gross, K.C.: Support Vector Machines for Nuclear Reactor State Estimation. In: ANS International Topical Meeting 7, Pittsburgh, USA (2000)
6. Gribok, A.V., Hines, J.W., Uhrig, R.E.: Use of Kernel Based Techniques For Sensor Validation In Nuclear Power Plants. In: NPIC&HMIT, Washington, DC (November 2000)
7. Seo, I.Y., Kim, S.J.: An On-line Monitoring Technique Using Support Vector Regression and Principal Component Analysis. In: CIMCA 2008, Vienna, Austria, pp. 10–12 (2008)
8. Vapnik, V.N.: The Nature of Statistical Learning Theory. Springer, New York (1995)
9. Chien, T.T., Adams, M.B.: A Sequential Failure Detection Technique and Its Application. IEEE Trans. Autom. Contr. 21, 750–757 (1976)
10. Steven, M.K.: Fundamentals of Statistical Signal Processing. Prentice Hall, Englewood Cliffs (1993)

A Support System for Making Archive of Bi-directional Remote Lecture – Photometric Calibration –

Naoyuki Tsuruta, Mari Matsumura, and Sakashi Maeda

Department of Electronics Engineering and Computer Science, Fukuoka University
8-19-1 Nanakuma Jonan-ku, Fukuoka, 814-0180, Japan
tsuruta@fukuoka-u.ac.jp, {matumura,maeda}@mdmail.tl.fukuoka-u.ac.jp
http://www.tl.fukuoka-u.ac.jp/~tsuruta/

Abstract. We are developing a system that supports making lecture movie archive. This system enables us to combine CG or another movie with a lecture scene movie by using intelligent computer vision techniques, and supports us to generate an effective lecture archive. In this paper, we concentrate on a scenario to generate a movie that seems to be like a lecture done in one lecture room based on two movies of lectures done in different remote lecture rooms. Because the source movies are captured on the different camera work and the different illumination condition, not only geometric calibration but also photometric calibration are important to make the target movie realistic. To overcome this problem, we propose a photometric calibration technique based on "fast separation of direct and global components" method. By using this method, estimation of color of illumination on the scene becomes more stable than our conventional method.

Keywords: Mixed Reality, Computer Vision, Computer Graphics, Lecture Archive.

1 Introduction

Realistic content including real image and computer graphics is well known as mixed reality. Fig.1 shows an example of mixed reality that used in a certain TV news program. The display panel synthesized by CG is shown in geometrically correct position even when camera moved. The reason why mixed reality is frequently used in TV program is that mixed reality is very effective for giving people information. This effectiveness must be also applicable to teaching aid such as lecture movie archive.

On the other hand, requirement of providing lecture movie archive becomes very high to enable students study whenever and wherever they want. Fig.2 shows an example of automatic lecture archive generator [1]. By using intelligent computer vision technology, this system automatically generates a summary

D.-S. Huang et al. (Eds.): ICIC 2009, LNAI 5755, pp. 610–617, 2009.

Fig. 1. An example of mixed reality used in a TV news program

Fig. 2. An example of automatic lecture archive generator

movie from original lecture video captured by a HDTV camera. Additionally, there are several researches that study lecture support system by using intelligent computer vision technology[4] [5].

We are developing a system that supports making lecture archive. This system enables us to combine CG or another movie with a lecture scene movie by using intelligent computer vision techniques, and supports generating an effective lecture archive. In this paper, we concentrate on a scenario to generate a movie that seems to be like a lecture done in one lecture room based on two lecture movies done in different remote lecture rooms. Because the source movies are captured on the different illumination condition and different camera work, not only geometric calibration but also photometric calibration are important to make the target movie realistic. To overcome this problem, we propose a photometric calibration technique based on "fast separation of direct and global components" method. By using this method, estimation of color of illumination on the scene becomes more stable than our conventional method.

In section 2, we describe a brief of overview of archive generator. After that, we focus on the photometric calibration, in section 3, and discuss about our conventional method and its problem. Then we clarify the necessarily of "separation of direct and global components" technique, and propose a new method. In section 4, we show experiment results that compare the conventional method and proposed method.

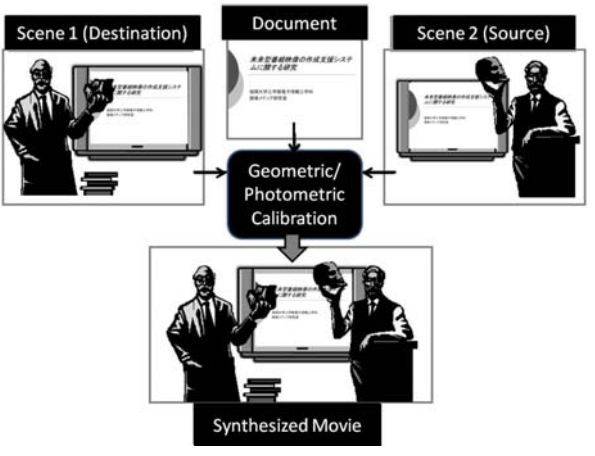

Fig. 3. A scenario of bi-directional remote lecture and how to make archive of it

2 Overview of Archive Generator

2.1 Scenario

As an example of bi-directional remote lecture, let us consider a scenario described in Fig. 3. In this scenario, two lecturers discuss staying in their each lecture room and pointing out their own screen on which the same content is projected. Two movies are captured for making an archive. If two archives are generated from each movie respectively, resolutions of them might be low and it is difficult for students to watch them spontaneously. Then, we consider combining those into a movie that seems to be like a lecture done in one lecture room. To do this, we need two techniques, that is, geometric calibration and photometric calibration. The geometric calibration is applied to one movie so that it can be overlapped onto a geometrically correct region in another movie. The photometric calibration is applied to equalize color of illumination of two scenes.

2.2 Giometric Calibration

Projection transformation is applied to a source image. Projection parameters are estimated from more than four pairs of corresponding points, which are selected from source and destination images, respectively. After this transformation, background subtraction is applied to the source image, and image regions of the lecturer are detected. Then finally, the source image is overlaid onto the destination image. If camera that was used to capture the source image moved during lecture, the source image is also geometrically transformed by using saved pan and tilt camera parameters. This transformation is done based on panorama generation technique for fixed focus camera [2].

3 Photometric Calibration

3.1 A Conventional Method

For the photometric calibration, we must know the color of global illumination lighting the target scene. A total radiance L measured at a camera pixel is given by the equation:

$$L = NI, \tag{1}$$

where N and I could be an object color and an illumination color measured at a camera pixel, respectively. If we know the object color N at each pixel, we can calculate I from the input image L. But, generally, N is unknown. So, we use the known controllable light P. If we use a digital projector as P, we can estimate its light color in advance. When we add the light P, input image N' is given by the equation:

$$L' = N(I + P). \tag{2}$$

From subtraction equation (1) from equation (2), N is given by following equations:

$$(L' - L) = N(I + P) - NI = NP, \tag{3}$$

$$N = (L' - L)/P. \tag{4}$$

Once N is estimated, L is given by the equation (1). Then, inferred Image L_2 captured under vartial illumination I_2 can be calculated from N and L_2 by the equation:

$$L_2 = NI_2. \tag{5}$$

However, the projector ray might actually reflect to the wall and be indirectly irradiated on the area for taking the movie, when the area is on the corner of the room as shown in Fig. 4. In this case, illumination color irradiated by the

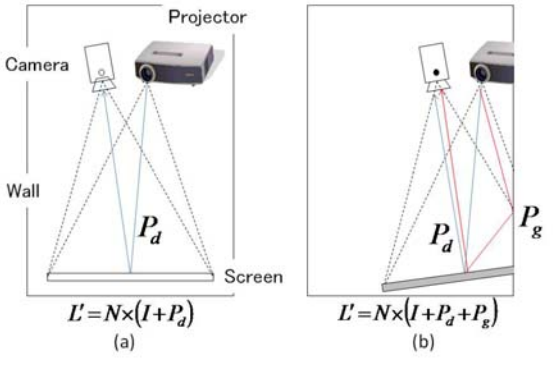

Fig. 4. A problem on estimation of global illumination based on auxiliary light. (a):A condition that our conventional method supposed. (b):Irregular conditions frequently occurred.

projector light on the area is not known. Illumination is described by $(P_d + P_g)$, where P_d and P_d are direct component and indirect (global) component of the projector light, respectively. Then, it is necessary to separate the illumination into an a direct component and global component.

3.2 Separation of Direct Compornent and Global Compornent

This method[3] restricts us to the use of a single camera and a digital projector as a single light source. A total radiance measured L at a camera pixel is the sum of the direct component and global component:

$$L = L_d + L_g, \tag{6}$$

where L_d and L_g are direct component and global component, respectively. Each point of the surface lit by the source scatters rays in the direction of the camera. Then the radiance of the point measured by the camera is referred to as the direct component L_d. The remaining radiance measured by the camera pixel is caused by inter-reflections and is referred to as the global component L_g.

Let us divide the surface into a total of N patches that corresponds to a single pixel of the source. We denote the radiance of the patch i measured by the camera c as $L[c;i]$, and its two components as $L_d[c;i]$ and $L_g[c;i]$, so that $L[c;i] = L_d[c;i] + L_g[c;i]$. The global component of i due to inter-reflections from all other surface patches can be written as:

$$L_g[c;i] = \sum_{j \in P} A[i;j] L[i;j], \tag{7}$$

where $P = \{j | 1 \leq j \leq N, j \neq i\}$ is the radiance of patch j in the direction of patch i and $A[i;j]$ incorporates the BRDF of i as well as the relative geometric configuration of the two patches.

Now let us assume that a half of the projector's pixels are activated and that these activated pixels are well-distributed over the entire scene to produce a high frequency illumination pattern, such as a checker flag pattern shown in Fig. 5.

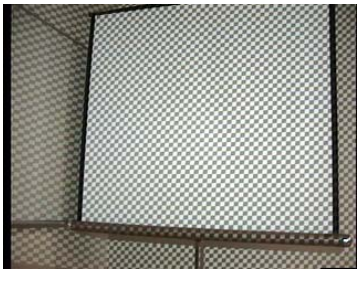

Fig. 5. An example of checker flag pattern used in the "Separation of Direct Compornent and Global Compornent" method

Then, consider two captured images of the scene, where, in the first image L^+ the scene is lit with high frequency illumination that has fraction $1/2$ activated projector pixels and in the second image L^- it is lit with the complementary illumination that has fraction $(1-1/2)$ activated projector pixels. If the patch i is lit directly by the projector in the first image then it is not lit by the projector in the second image, and we get:

$$L^+[c;i] = Ld[c;i] + \frac{1}{2}Lg[c;i]. \tag{8}$$

$$L^-[c;i] = (1-1/2)Lg[c;i]. \tag{9}$$

Therefore, if we subtract L^- from L^+, then we have L_d. Furthermore, by subtracting L_d from L_+, we have $\frac{1}{2}L_g$.

3.3 Proposed Method

By replacing L in equation (1) and L' in equation (2) by L^- and L^+, respectively, we can get correct object color N:

$$L^- = N(I + \frac{1}{2}P_g), \tag{10}$$

$$L^+ = N(I + P_d + \frac{1}{2}P_g), \tag{11}$$

$$(L^+ - L^-) = N(I + P_d + \frac{1}{2}P_g) - N(I + \frac{1}{2}P_g) = NP_d, \tag{12}$$

$$N = (L^+ - L^-)/P_d. \tag{13}$$

As mentioned above, P_d is observable if we use a digital projector as a auxiliary light.

4 Experimental Results

In this section, we describe two experimental results. In the first experiment, we estimated accuracy of illumination color estimation. Target area is a corner

Fig. 6. Environments for Experiment

of our lecture room. We estimated illumination color respectively twice for both conventional method and proposed method. The first estimation was done under the regular condition shown in the left image of Fig. 6. The second estimation was done under the same target area, the same illumination condition and the same camera position with the first one, except for wall color. The second environment is shown in the right image of Fig. 6.

Therefore, the illumination color measured in both conditions must be same. Table 1 shows RGB component and brightness of measured illumination color in both environments. The leftist column shows the difference between the estimations. Obviously, the difference for the proposed method is smaller than the conventional method.

In the second experiment, we synthesized a bi-directional remote lecture movie. For simplification of scenario, we used a scene, in which two lecturers played OX game. Fig. 7 shows views of different lecture room. The brightness, color of illumination and geometrical aspect were different. Fig. 8 shows results of synthesize by both conventional photmetric calibration method without geometric calibration (left side) and proposed method (right side). In the left image, the region of right lecturer is too bright and pointing position is also wrong. On the other hand, the right image is subjectively better than the left one.

Table 1. Comparison Accuracy of Proposed Method with Comventional Method. (Conv. Method:Conventional Method, Prop. Method: Proposed Method, Env.1: Environment 1, Env.2: Environment 2, Diff=—Env.1-Env.2—, V: Brightness).

Method	Color	Estimation		Diff
		Env.1	Env.2	
Conv. Method	R	0.58	0.63	0.05
	G	0.55	0.51	0.04
	B	0.59	0.53	0.06
	V	1.74	3.58	1.84
Prop. Method	R	0.54	0.51	0.03
	G	0.60	0.60	0.00
	B	0.58	0.59	0.01
	V	1.22	1.12	0.10

Fig. 7. Environments for Experiment

Fig. 8. Synthesized images. The left image is synthesized by conventional photometric calibration without geometric calibration. The right image is synthesized by proposed method.

5 Conclusion

In this paper, we described a scenario to generate a lecture movie that seems to be like a lecture done in one room based on two lecture movies done in remote different lecture rooms. In this scenario, the original movies are captured on the different illumination condition and different camera work. To make the target movie realistic, we proposed a photometric calibration technique based on "fast separation of direct and global components" method. In the experiment result, we showed that estimation of color of illumination on the scene became more stable than our conventional method.

References

1. http://www.i-collabo.jp/autorec/
2. Wada, T.: Fixed Viewpoint Pan-Tilt-Zoom Camera and Its Applications. The Transactions of the Institute of Electronics, Information and Communication Engineers J81DII(6), 1182–1193 (1998)
3. Nayar, S.K., Krishnan, G., Grossberg, M.D., Raskar, R.: Fast Separation of Direct and Global Components of a Scene using High Frequency Illumination. In: Proceedings of ACM SIGGRAPH, pp. 935–944 (2006)
4. Marutani, T., Nishiguchi, S., Kakusho, K., Minoh, M.: Making a lecture content with deictic information about indicated objects in lecture materials. In: The 3rd AEARU Workshop on Network Education, pp. 70–75 (2005)
5. Yueh, H.P., Liu, Y.L., Lin, W.J., Shoji, T., Minoh, M.: Integrating face recognition techniques with blog as a distance education support system (DESS) in international distance learning. In: Sixth International Conference on Advanced Learning Technologies (IEEE ICALT2006), pp. 507–511 (2007)

Conflict-Free Incremental Learning

Rong-Lei Sun

The State Key Laboratory of Digital Manufacturing Equipment and Technology
Huazhong University of Science and Technology, Wuhan 430074, China
ronglei@mail.hust.edu.cn

Abstract. Most machine learning algorithms are essentially generalized learning schemes. When used incrementally, conflict between the concepts already learned and the new events to be learned need be eliminated. This paper presents a new incremental learning scheme that divides induction into two phases: incrementally accurate learning and generalization. The new learning scheme is conflict-free thus it is suitable for incremental induction.

Keywords: Incremental induction, Machine learning, Artificial intelligence, Boolean algebra.

1 Introduction

Machine learning, being an efficient mean of acquiring knowledge such as if-then rules, attracts a lot of researchers. Theoretical studies regarding machine learning demonstrate that inductive learning is a NP-hard problem; that is, the computing complexity is increased exponentially with the complexity of the learning problem. Consider the problem on the contrary one can conducts that the computing complexity will decrease exponentially subject to the drop of complexity of the learning problem. Therefore it is easy to deal with a machine learning problem if the problem complexity is limited. Incremental learning strategy provides one of potential solutions to solve complicated real-world learning problems due to limit complexity of each learning epoch [1]. For AQ-family incremental learning [2], the new observed events used in the following learning epochs may conflict to the concept already learned. Therefore consistency maintenance becomes one of the central problems in the incremental learning fashion.

The concept confliction problem results from the *generalized learning* scheme, i.e., generalizing while learning in each learning epoch. To deal with the problem Sanchez [4] presents an incremental learning algorithm for constructing Boolean functions from positive and negative examples. Sun [5] proposed a non-expandable DNF (disjunctive normal form) for accurate incremental learning. However the generalization problem is missing.

This paper presents a generalization principle and a generalization algorithm, which making the non-expandable DNF be a real conflict-free incremental learning model. The rest of the paper is organized as follows. First in the next section, the methodology and basic concepts adopted in the article are introduced through a simple learning example. Incremental learning algorithm and generalization algorithm are introduced in

D.-S. Huang et al. (Eds.): ICIC 2009, LNAI 5755, pp. 618–626, 2009.

section 3 and 4, respectively. A simple but illustrative example is used to demonstrate the conflict-free incrementally inductive learning algorithm in section 5. Finally in the last section, we conclude the whole paper.

2 Basic Concepts and Methodology

Generalized learning is such a scheme that learning and generalization are tightly coupled. That is, generalization is performing when learning is conducting. Because generalization introduces learning errors, concept consistency becomes a core problem when used incrementally. To address the problem, we divide the learning procedure into two separated phases: *accurate learning* and *generalization*. The aim of accurate learning is to record the observed events exactly and simplify the learning results. This procedure emphasizes the logical equivalency between the learning results and the observed events. The results obtained are called *accurate concepts*. After the events available at the current learning epoch have been learned, the generalization procedure starts and the *generalized concepts* are obtained. The learning system keeps both the accurate concepts and the generalized concepts. When new observed events are available, new learning epoch starts with the accurate concepts and learns the new events in the incremental fashion. The updated accurate concepts are then to be generalized. Because of the logical equivalency between the accurate concepts and the observed events, the proposed incremental learning model can certainly maintain the consistency over all observed events. It is a conflict-free learning algorithm for incremental induction.

Consider a concept that can be described using attribute-valued pairs. Further more, as most attributes are discrete or with limited accuracy, we can use Boolean set containing two different elements to represent each of them. For example, suppose that an attribute F has 4 possible values, it can be characterized by two Boolean variables a_1 and a_2, each of which belongs to the Boolean set. When performing such a transformation, a *concept* can be represented as a DNF over the simplest Boolean set. Consequently the above accurate learning and generalization are transformed to simplification and generalization of Boolean expressions, respectively.

For simplification of complex Boolean expressions, it is ordinary to adopt Quine-McCluskey procedure [3]. This method, however, can not be used incrementally. In this paper we deal with the problem as following: each time only one observed event is accessed. When the event is added to the learning system, the Boolean expression is simplified immediately.

Before introducing the accurate learning algorithm and generalization algorithm, a simple example is used to demonstrate the principle of the proposed learning algorithm.

Example 1. Suppose that a concept can be expressed by four binary attributes. Let $\boldsymbol{e}_1 = 0101$, $\boldsymbol{e}_2 = 0000$, $\boldsymbol{e}_3 = 0111$, $\boldsymbol{e}_4 = 1111$, $\boldsymbol{e}_5 = 1101$ be *observed events* that are represented by *Boolean products* or *vectors*. The aim of the accurate learning is to simplify the Boolean expression $(\boldsymbol{e}_1 + \boldsymbol{e}_2 + \boldsymbol{e}_3 + \boldsymbol{e}_4 + \boldsymbol{e}_5)$, where + represents Boolean sum.

Suppose that the initial concept **R** is an empty set. The incremental learning procedure is illustrated as follows.

(1) Learn $\boldsymbol{e}_1$ thus $\mathbf{R} = \boldsymbol{e}_1 = 0101$.
Denote 0101 by $\boldsymbol{r}_1$ so we have $\mathbf{R} = \boldsymbol{r}_1$.
(2) Learn $\boldsymbol{e}_2$ thus $\mathbf{R} = \boldsymbol{r}_1 + \boldsymbol{e}_2 = 0101 + 0000$.
Denote 0000 by $\boldsymbol{r}_2$ so we have $\mathbf{R} = \boldsymbol{r}_1 + \boldsymbol{r}_2$.
(3) Learn $\boldsymbol{e}_3$ thus $\mathbf{R} = \boldsymbol{r}_1 + \boldsymbol{r}_2 + \boldsymbol{e}_3 = 0101 + 0000 + 0111 = 01{*}1 + 0000$.
Denote $01{*}1$ by $\boldsymbol{r}_3$ so we have $\mathbf{R} = \boldsymbol{r}_3 + \boldsymbol{r}_2$.
(4) Learn $\boldsymbol{e}_4$ thus $\mathbf{R} = \boldsymbol{r}_3 + \boldsymbol{r}_2 + \boldsymbol{e}_4 = 01{*}1 + 0000 + 1111 = 01{*}1 + 0000 + {*}111$.
Denote ${*}111$ by $\boldsymbol{r}_4$ so we have $\mathbf{R} = \boldsymbol{r}_3 + \boldsymbol{r}_2 + \boldsymbol{r}_4$.
(5) Learn $\boldsymbol{e}_5$ thus $\mathbf{R} = \boldsymbol{r}_3 + \boldsymbol{r}_2 + \boldsymbol{r}_4 + \boldsymbol{e}_5 = 01{*}1 + 0000 + {*}111 + 1101 = {*}1{*}1 + 0000$.
Denote ${*}1{*}1$ by $\boldsymbol{r}_5$ so we have $\mathbf{R} = \boldsymbol{r}_5 + \boldsymbol{r}_2$.

In the above example $*$ represents the corresponding variable does not occur in a Boolean product. The number of $*$ occurring in a vector $\boldsymbol{r}$ is defined as *degree of the vector*, denoted by degree($\boldsymbol{r}$).

Each time when learning a new event $\boldsymbol{e}$, it generates at least one new Boolean product, such as $\boldsymbol{r}_1 \sim \boldsymbol{r}_5$ in the example. Each new product must include the new observed event being learned. It should also include events already learned as many as possible so as to obtain a simpler concept expression. According to its relations to the original products of $\mathbf{R}$, a new product can be classified into two categories.

(1) If a new product includes original product(s) of $\mathbf{R}$, it is called a *covering product*. For example, after $\mathbf{R}$ learns $\boldsymbol{e}_3$, the new product $\boldsymbol{r}_3$ includes original product $\boldsymbol{r}_1$ of $\mathbf{R}$; after $\mathbf{R}$ learns $\boldsymbol{e}_5$, the new product $\boldsymbol{r}_5$ includes the original product $\boldsymbol{r}_3$ and $\boldsymbol{r}_4$ of $\mathbf{R}$.
(2) If a new product does not include any product of $\mathbf{R}$, it is called a *cross product*. For example, after $\mathbf{R}$ learns $\boldsymbol{e}_4$, the new product $\boldsymbol{r}_4$ includes neither $\boldsymbol{r}_2$ nor $\boldsymbol{r}_3$ of $\mathbf{R}$.

Definition. Let $a, b \in \{0, 1, *\}$. Define *generally equality* (denoted by $a \Leftrightarrow b$) as follows.

$0 \Leftrightarrow 0$, $1 \Leftrightarrow 1$, $* \Leftrightarrow *$,
$0 \Leftrightarrow *$, $1 \Leftrightarrow *$

Note that general equality is not *transitivity*.

Define the *general distance* (or *distance* for short) between a and b as:

$$\mathrm{dist}(a,b) = \mathrm{dist}(b,a) = \begin{cases} 0, & a \Leftrightarrow b \\ 1, & \text{otherwise} \end{cases}$$

Let $\boldsymbol{r}_1 = a_1 a_2 \ldots a_n$ and $\boldsymbol{r}_2 = b_1 b_2 \ldots b_n$ be two vectors. The *general distance* between $\boldsymbol{r}_1$ and $\boldsymbol{r}_2$ is defined as:

$$\mathrm{dist}(\boldsymbol{r}_1, \boldsymbol{r}_2) = \mathrm{dist}(\boldsymbol{r}_2, \boldsymbol{r}_1) = \sum_{i=1}^{n} \mathrm{dist}(a_i, b_i) .$$

The non-expandable DNF, maximally cross vector, intsect($\boldsymbol{v}$, $\boldsymbol{r}$), N($\boldsymbol{e}$|$\mathbf{R}$), S($\boldsymbol{e}$|$\mathbf{R}$), and other relative concepts for the incremental learning can be found in [5].

3 Accurate Learning Algorithm

In the incremental learning, new products belong to only one of the two categories: covering product or maximally cross vector. To obtain a more concise concept expression it is the first choice to produce the covering product whenever it is possible. In this case the new product not only learns (or includes) the event but also absorbs at least one original product of **R**, which makes **R** more concise. If no covering product is produced it needs to generate a maximally cross product so as to make the new product simplest. Therefore the core problems for the incremental learning is to generate the covering products or the maximally cross product while maintaining the concept expressed by DNF to be non-expandability.

Consider the following accurate learning problem.

Given:

(1) Initial concept **R** (expressed with non-expandable DNF) about a concept **C**.

(2) Observed event set **E** about concept **C** and $\mathbf{E} \cap \mathbf{R} = \varnothing$.

Find:

A concept expressed with non-expandable DNF, which is logically equivalent to (**R** + **E**).

We will adopt the following strategy to solve the learning problem. The learning procedure is divided into a series of learning epochs. Each epoch deals with only one observed event. When learning an event $\boldsymbol{e}$, the non-expandability of ($\mathbf{R}+\boldsymbol{e}$) must be kept.

Let $\mathbf{R} = \boldsymbol{r}_1 + \boldsymbol{r}_2 + \ldots + \boldsymbol{r}_m$ be the initial concept expressed with non-expandable DNF. Without loss of generality, suppose that $\forall\ 1 \le i < j \le m$, degree($\boldsymbol{r}_i$) ≥ degree($\boldsymbol{r}_j$). For a given event $\boldsymbol{e} \in \mathbf{E}$, let $k = |\mathbf{S}(\boldsymbol{e}|\mathbf{R})|$. The accurate algorithm of incremental learning is described as following [5].

```
for (select an event e ∈ E){ //each learning epoch
deals with only one event
for (i = 1 to m){ //test for each vector of R if it can
produce a covering vector
if (dist(e, r_i) >1) {continue;}  //can not produce a
covering vector including r_i
if (degree(r_i) ≥ k) {continue;}  //can not produce a
covering vector including e
construct a vector v including both e and r_i according
to the theorem 3 [5].
if (v is a covering vector){
add v to R.
delete from R all the vectors included in v.
delete e from E.
modify m accordingly.
}
else {discard v}
}
```

```
if (no covering vector is obtained){ //produce the
maximally cross vector
for (i = k to 1, k = k-1){
construct all vectors with degree i according to the
theorem 5 [5]. Denote each of them by v.
for (each v){
if (v is a cross vector){
add v to R.
delete e from E.
m = m+1.
break;
}
}
if(cross vector is obtained) {break;}
}
}
re-order the vectors of R according to their degrees.
}
```

It can be shown that, each time after learning an event according to the above learning algorithm, the **R** obtained is still a non-expandable DNF.

4 Generalization Algorithm

The aim of inductive learning is to abstract general formulas from the observed events so as to obtain the essential concepts, which are more universal and cover more events. Therefore the generalization is a crucial aspect of inductive learning. Now let us deal with the generalization aspect based on the accurate concepts obtained by the learning algorithm described in the last section.

Let $\mathbf{R}^+ = \boldsymbol{r}_1^+ + \boldsymbol{r}_2^+ + \ldots + \boldsymbol{r}_m^+$ represents accurate concept obtained from positive events; a_{ik}^+ represents kth component of ith vector of $\mathbf{R}^+$. Let $\mathbf{R}^- = \boldsymbol{r}_1^- + \boldsymbol{r}_2^- + \ldots + \boldsymbol{r}_l^-$ represents accurate concept obtained from negative events; a_{ik}^- represents kth component of ith vector of $\mathbf{R}^-$. Generalization algorithm is described as following.

(1) If $\exists k \in \{1, 2, \ldots, n\}$, such that: $\forall i, j \in \{1, 2, \ldots, l\}$, $a_{ik}^- \Leftrightarrow a_{jk}^-$.
And if $\exists h \in \{1, 2, \ldots, m\}$, such that $\forall i \in \{1, 2, \ldots, l\}$, $a_{hk}^+ \Leftrightarrow a_{ik}^-$.
Then perform generalization operation: $a_{hk}^+ = *$.
Suppose that the generalized vector is denoted by $\boldsymbol{r}_h^+$.
Delete from $\mathbf{R}^+$ those vectors being included in $\boldsymbol{r}_h^+$.

(2) If $\exists k \in \{1, 2, \ldots, n\}$, such that: $\forall i, j \in \{1, 2, \ldots, m\}$, $a_{ik}^+ \Leftrightarrow a_{jk}^+$.
And if $\exists h \in \{1, 2, \ldots, l\}$, such that: $\forall i \in \{1, 2, \ldots, m\}$, $a_{hk}^- \Leftrightarrow a_{ik}^+$.
Then perform generalization operation: $a_{hk}^- = *$.

Suppose that the generalized vector is denoted by $\boldsymbol{r}_h^-$.
Delete from $\mathbf{R}^-$ those vectors being included in $\boldsymbol{r}_h^-$.

(3) Repeat step(1) and step(2) until $\mathbf{R}^+$, $\mathbf{R}^-$ can not be generalized any more.

It is clear that the generalized $\mathbf{R}^+$ and $\mathbf{R}^-$ are not intersectant. That is, $\mathbf{R}^+ \cap \mathbf{R}^- = \varnothing$. The concepts learned are completeness and consistency over the observed event set **E**.

5 Numerical Example

An illustrative example is used to demonstrate the incrementally inductive learning algorithm based on the non-expandable DNF.

Example 2. Suppose that people can be characterized using three kinds of features, each of which has discrete attribute values.

Height ∈ {Short, Tall};
Hair ∈ {Blond, Black, Red};
Eyes ∈ {Blue, Dark, Gray}.

There are nine persons who are divided into two groups according to their features (see Table 1-a). Find concept descriptions using the incremental learning algorithm.

Table 1. Positive and negative observed events with different features

(a) Original observed events (b) Coded events

No.	Height	Hair	Eyes	Class	a_1	$a_2\,a_3$	$a_4\,a_5$
1	Short	Blond	Blue	+	0	00	00
2	Tall	Red	Blue		1	10	00
3	Tall	Blond	Blue		1	00	00
4	Short	Blond	Gray		0	00	10
5	Tall	Blond	Dark		1	00	01
6	Short	Black	Blue	-	0	01	00
7	Tall	Black	Blue		1	01	00
8	Tall	Black	Gray		1	01	10
9	Short	Blond	Dark		0	00	01

First we formulate the problem using the following Boolean variables.

Let a_1 represents Height: $a_1 = 0$ means Height = Short;
$a_1 = 1$ means Height = Tall.
Let a_2a_3 represent Hair: $a_2a_3 = 00$ means Hair = Blond;
$a_2a_3 = 01$ means Hair = Black;
$a_2a_3 = 10$ means Hair = Red.
Let a_4a_5 represent Eyes: $a_4a_5 = 00$ means Eyes = Blue;
$a_4a_5 = 01$ means Eyes = Dark;
$a_4a_5 = 10$ means Eyes = Gray.

The coded events are listed in Table 1-b.

Learning

Let **R** be an empty set.

First consider the positive events listed in Table 1.

(1) Learn the event $\boldsymbol{e}$ = 00000.

00000 → **R**.

R = 00000 = $\boldsymbol{r}_1$.

(2) Learn the event $\boldsymbol{e}$ = 11000.

∵ dist($\boldsymbol{e}$, $\boldsymbol{r}_1$) = dist(11000, 00000) = 2.

∴ Covering vector $\boldsymbol{v}$ including $\boldsymbol{r}_1$ can not be produced after learning $\boldsymbol{e}$ = 11000.

11000 → **R**.

R = 00000+11000 = $\boldsymbol{r}_1 + \boldsymbol{r}_2$.

(3) Learn the event $\boldsymbol{e}$ = 10000.

∵ dist($\boldsymbol{e}$, $\boldsymbol{r}_1$) = dist(10000, 00000) = 1,

dist($\boldsymbol{e}$, $\boldsymbol{r}_2$) = dist(10000, 11000) = 1.

∴ Construct vectors: $\boldsymbol{v}$ = ∗0000, $\boldsymbol{v}$ = 1∗000.

Let us consider $\boldsymbol{v}$ = ∗0000 first.

$\boldsymbol{v}_1$ = intsect($\boldsymbol{v}$, $\boldsymbol{r}_1$) = intsect(∗0000, 00000) = 00000.

$|\boldsymbol{v}| - |\boldsymbol{e}| - |\boldsymbol{v}_1| = |*0000| - |10000| - |00000| = 2 - 1 - 1 = 0$.

∴ $\boldsymbol{v}$ = ∗0000 is a covering vector.

∗0000 → **R**.

∵ $\boldsymbol{r}_1$ = 00000 ⊂ ∗0000.

Delete from **R** the vector included in ∗0000 and rename the vectors of **R**, we have:

R = ∗0000+11000 = $\boldsymbol{r}_1 + \boldsymbol{r}_2$.

Similarly, we can verify that $\boldsymbol{v}$ = 1∗000 is also a covering vector.

1∗000 → **R**.

∵ $\boldsymbol{r}_2$ = 11000 ⊂ 1∗000.

Deleting from **R** the vector included in 1∗000 and rename the vectors of **R**, we have:

R = ∗0000 + 1∗000 = $\boldsymbol{r}_1 + \boldsymbol{r}_2$.

(4) Learn the event $\boldsymbol{e}$ = 00010.

∵dist($\boldsymbol{e}$, $\boldsymbol{r}_1$) = dist(00010, ∗0000) = 1,

dist($\boldsymbol{e}$, $\boldsymbol{r}_2$) = dist(00010, 1∗000) = 2.

∴ Construct a vector: $\boldsymbol{v}$ = ∗00∗0.

Let $\boldsymbol{v}_1$ = intsect($\boldsymbol{v}$, $\boldsymbol{r}_1$) = intsect(∗00∗0, ∗0000) = ∗0000;

$\boldsymbol{v}_2$ = intsect($\boldsymbol{v}$, $\boldsymbol{r}_2$) = intsect(∗00∗0, 1∗000) = 10000;

$\boldsymbol{v}_{12}$ = intsect($\boldsymbol{v}_1$, $\boldsymbol{v}_2$) = intsect(∗0000, 10000) = 10000.

$|\boldsymbol{v}| - |\boldsymbol{e}| - |\boldsymbol{v}_1| - |\boldsymbol{v}_2| + |\boldsymbol{v}_{12}| = |*00*0| - |00010| - |*0000| - |10000| + |10000|$

$= 4 - 1 - 2 - 1 + 1 = 1 \neq 0$.

∴ $\boldsymbol{v}$ = ∗00∗0 is not a covering vector and should be discarded.

Now let us find the maximally cross vector.

∵**N**($\boldsymbol{e}$|**R**) = **N**(00010|**R**) = {00000}.

∴ |**S**($\boldsymbol{e}$|**R**)| = |**S**(00010|**R**)| = |{00000}| = 1.

So the maximal degree of the cross vector equals to one. The vector including observed event $\boldsymbol{e}$ = 00010 and its neighboring event (00000) is with the form: $\boldsymbol{v}$ = 000∗0.

In a manner similar to that used in (3), we can verify that $\boldsymbol{v}$ = 000∗0 is a cross vector.
000∗0 → **R**.
∴**R** = ∗0000 + 1∗000 + 000∗0.
Denote **R** by $\mathbf{R}^+ = \boldsymbol{r}_1^+ + \boldsymbol{r}_2^+ + \boldsymbol{r}_3^+$ = ∗0000 + 1∗000 + 000∗0.

Likewise, the negative events listed in Table 1 can also be learned, and we have:
$\mathbf{R}^- = \boldsymbol{r}_1^- + \boldsymbol{r}_2^- + \boldsymbol{r}_3^-$ = ∗0001 + ∗0100 + 101∗0.

Generalization
Let a_{ik}^+ represents *k*th component of *i*th vector of $\mathbf{R}^+$; a_{ik}^- represents *k*th component of *i*th vector of $\mathbf{R}^-$. Generalization for the above accurate concepts is as following.

∵$a_{11}^- \Leftrightarrow 1$, $a_{21}^- \Leftrightarrow 1$, $a_{31}^- \Leftrightarrow 1$ and $a_{21}^+ \Leftrightarrow 1$.
∴Generalize $\boldsymbol{r}_2^+$ as: $\boldsymbol{r}_2^+$ = ∗∗000.

Deleting from $\mathbf{R}^+$ all the vectors included in (∗∗000) and rename the vectors, we have:

$\mathbf{R}^+ = \boldsymbol{r}_1^+ + \boldsymbol{r}_2^+$ = ∗∗000 + 000∗0.

∵$a_{12}^- = a_{22}^- = a_{32}^- = 0$ and $a_{22}^+ = 0$.
∴Generalize $\boldsymbol{r}_2^+$ as: $\boldsymbol{r}_2^+$ = 0∗0∗0.

Deleting from $\mathbf{R}^+$ all the vectors included in (0∗0∗0) and rename the vectors, we have:

$\mathbf{R}^+ = \boldsymbol{r}_1^+ + \boldsymbol{r}_2^+$ = ∗∗000 + 0∗0∗0.

∵$a_{14}^- \Leftrightarrow 0$, $a_{24}^- \Leftrightarrow 0$, $a_{34}^- \Leftrightarrow 0$ and $a_{14}^+ \Leftrightarrow 0$.
∴Generalize $\boldsymbol{r}_1^+$ as: $\boldsymbol{r}_1^+$ = ∗∗0∗0.

Deleting from $\mathbf{R}^+$ all the vectors included in (∗∗0∗0) and rename the vectors, we have:

$\mathbf{R}^+ = \boldsymbol{r}_1^+$ = ∗∗0∗0.

The negative concept $\mathbf{R}^-$ can be generalized in the same way as which is used for positive concept. The generalized negative concept is:

$\mathbf{R}^- = \boldsymbol{r}_1^- + \boldsymbol{r}_2^-$ = ∗∗∗∗1 + ∗∗1∗∗.
Expressing the above concepts using attribute-valued pairs, we have:
$\mathbf{R}^+$ = (Hair = Blond or Red) and (Eyes = Blue or Gray).
$\mathbf{R}^-$ = (Hair = Black) or (Eyes = Dark).

6 Conclusions

For most learning algorithms, learning and generalization are tightly coupled. The learning procedure is also a generalization procedure. Such a learning scheme is

called generalized learning in this paper. The generalized learning results in concept inconsistency when used in incremental induction. To deal with the problem this paper divides the learning procedure into two separate phases: accurate incremental learning and generalization. The accurate learning procedure is to record the observed events exactly and simplify the learning results in incremental fashion. This phase emphasizes the logical equivalency between learning results and observed events. When learning is completed, generalization starts. Because of the logical equivalency between accurate concept and observed events, the proposed incremental learning method can maintain the consistency over all observed events. It is a conflict-free learning algorithm and thus it is more suitable for incremental induction.

Acknowledgement

The research work is supported by the National Nature Science Foundation of China (Grant No. 50575079, 50875100) and the National Key Technology R&D Program of China (Grant No. 2008BAI50B04).

References

1. Maloof, M.A., Michalski, R.S.: Incremental learning with partial instance memory. Artificial Intelligence 154, 95–126 (2004)
2. Kaufman, K.A., Michalski, R.S.: An adjustable description quality measure for pattern discovery using the AQ methodology. J. of Intelligent Information Systems 14, 199–216 (2000)
3. Rosen, K.H.: Discrete mathematics and its applications. McGraw-Hill, Inc., New York (1988)
4. Sanchez, S.N., Triantaphyllou, E., Chen, J., Liao, T.W.: An incremental learning algorithm for constructing Boolean functions from positive and negative examples. Computers and Operations Research 29, 1677–1700 (2002)
5. Sun, R.-L.: Study on the non-expandability of DNF and its application to incremental induction. In: Xiong, C.-H., Liu, H., Huang, Y., Xiong, Y.L. (eds.) ICIRA 2008. LNCS (LNAI), vol. 5314, pp. 699–706. Springer, Heidelberg (2008)

Supervised Isomap for Plant Leaf Image Classification

Minggang Du[1], Shanwen Zhang[2], and Hong Wang[1]

[1] Shanxi Normal University, Linfen 041004, China
[2] Faculty of Science, Zhongyuan University of Technology, Zhengzhou, 450007, China
wangh@sxnu.edu.cn

Abstract. Plant classification is very important and necessary with respect to agricultural informization, ecological protection and plant automatic classification system. Compared with other methods, such as cell and molecule biology methods, classification based on leaf image is the first choice for plant classification. Plant recognition and classification is a complex and difficult problem, and is very important in Computer-Aided Plant Species Identification technology. The feature extraction is a key step to plant classification. This paper presents a method to extract discriminant features for plant leaf images by using supervised Isomap. Experiments on the leaf image dataset have been performed. Experimental results show that the supervised Isomap is very effective and feasible.

Keywords: Plant classification, Isomap, Supervised Isomap, Plant leaf image, K-nearest neighbor.

1 Introduction

As the development of digital image processing and pattern recognition, the plant species identification based on computer is likely to be accessed. Since the characteristics can be obtained in the forms of numerical images, the efficiency of plant species classification can be improved with image processing and pattern recognition. Computer-Aided Plant Species Identification technology tries to recognize the known plant species by the salient features of the leaf. The focus of system is to extract the stable features of the plants, which are discriminable from others, then to classify and recognize plant species. It acts significantly on plant digital museum system and systematic botany which is the groundwork for research and development of plant.

Plants are basically classified according to shapes, colors and structures of their leaves and flowers. However, if we want to recognize the plant based on 2D images, it is difficult to analyze shapes and structures of flowers since they have complex 3D structures. On the other hand, the colors of leaves are always green; moreover, shades and the variety of changes in atmosphere and season cause the color feature having low reliability. The plant leaf shape feature is one of the most important features for characterizing a plant, which is commonly used in plant recognition, matching and registration. In addition, the plant leaf recognition is also an important part of machine intelligence that is useful for both decision-making and data processing.

D.-S. Huang et al. (Eds.): ICIC 2009, LNAI 5755, pp. 627–634, 2009.

More importantly, the plant recognition based on plant leaf shape feature is also a central problem in those fields such as pattern recognition, image technology and computer vision, etc., which have received considerable attention of agricultural scientist in recent years. Plant recognition, leaf image preprocessing, computer vision, handwriting analysis, and medical diagnosis, etc., are some of the common application areas of plant leaf shape recognition. For plant leaf shape recognition, there have been a wide range of methods proposed [1,2] structural methods organizing local features into graphs, trees, or strings, such as Fuzzy methods, Statistical methods, Transform methods, Fourier transform [3] or Hough transforms, Neural networks methods [4]. But most of these approaches are confined to specific image types and require that all plant leaf shapes must be preprocessed before recognition. Therefore, we decided to recognize various plants by the grey-level leaf image of plant. The leaf of plant carry useful information for classification of various plants, for example, aspect ratio, shape and texture. Some recent work [5-8] has focused on leaf feature extraction for recognition of plant et al. [5] used a hierarchical polygon approximation representation of leaf shape to recognize the Acer family variety. Wang et al. [6] presented the combination of different shape-based feature sets such as centroid-contour distance curve, eccentricity, and angle code histogram and adopted fuzzy integral for leaf image retrieval. Moreover, Saitoh et al. [7] required two pictures, a frontal flower image and a leaf image to recognize the plant. According to features utilized in object recognition, past research can be broadly classified into two categories [9]: contour-based [10,11] and region-based approaches [12-14]. Most plant recognition methods [5-8] used contour-based features. The disadvantage of the contour-based features is that correct curvature points are hard to find. Thus, our method adopts region-based approach. Although there are plenty of region-based features [12-15], projection used in optical character recognition and object recognition are effective because its recognition performance is good and can be computed in real time [13,14]. This study tries to adopt projection as shape feature.

Dimensionality reduction is an essential step involved in many research areas such as gene expression data analysis, face recognition and leaf images processing. It is a procedure of finding intrinsic low dimensional structures hidden in the high dimensional observations. Dimension reduction can be achieved by keeping only the most important dimensions, i.e, the ones that hold the most useful information for the task at hand, or by projecting the original data into a lower dimensional space that is most express for the task. For example, the goal of dimensionality reduction for visualization is to map a set of observations into a (two or three dimensiona1) space that preserves as much as possible. Three methods have been proposed to tackle the nonlinear dimensionality reduction problem, namely Laplacian Eigenmaps (LE), Isomap and Local Linear Embedding (LLE) [16-18], which are the extension of MDS with the assumption that only the distance of two local points can be approximated by Euelidean distance and the distance of two points far away from each other should be inferred from local distances. Among all those, the most widely used one is LE, which is also a spectral mapping method. Usually, LE aims to find a low dimensional representation that preserves the local properties of the data lying on a low dimensional manifold. However, LE is a nonlinear dimensionality reduction technique, whose

generalization ability is very weak. That is to say, the projection results in low dimensional space of the test image can not be easily obtained. Learning a kernel matrix for dimensionality reduction is another proposed method which is to learn a kernel matrix whose implicit mapping into feature space "unfolds" the manifold from which the data was sampled. Both of these methods attempt to preserve as well as possible the local neighborhood of each object while trying to obtain highly nonlinear embeddings. The central idea of Local Embeddings is using the locally linear fitting to solve the globally nonlinear problems, which is based on the assumption that data lying on a nonlinear manifold can be viewed as linear in local areas. Although, both Isomap and LLE have been used in visualization and classification, they are unsupervised and not so powerful when confronted with noisy data, which is often the case for real-world problems. In this paper, a supervised Isomap method based on the idea of Isomap is proposed to deal with such situation. Unlike the unsupervised learning scheme of Isomap, supervised Isomap follows the supervised learning scheme, i.e. it uses the class labels of the input data to guide the manifold learning.

The rest of the paper is organized as follows. Section 2 introduces Isomap and supervised Isomap. Experimental results and analysis are illustrated in Section 3. A conclusion is given in Section 4.

2 Isomap and Supervised Isomap

For data lying on a nonlinear manifold, the "true distance" between two data points is the geodesic distance on the manifold, i.e. the distance along the surface of the manifold, rather than the straight-line Euclidean distance. The main purpose of Isomap is to find the intrinsic geometry of the data, as captured in the geodesic manifold distances between all pairs of data points. The approximation of geodesic distance is divided into two cases. In case of neighboring points, Euclidean distance in the input space provides a good approximation to geodesic distance. In case of faraway points, geodesic distance can be approximated by adding up a sequence of "short hops" between neighboring points. Isomap shares some advantages with PCA, LDA and MDS, such as computational efficiency and asymptotic convergence guarantees, but with more flexibility to learn a broad class of nonlinear manifolds. The Isomap algorithm takes as input the distances $d(x_i, x_j)$ between all pairs x_i, x_j from N data points in the high-dimensional input space. The algorithm outputs coordinate vectors y_i in a d-dimensional Euclidean space that best represent the intrinsic geometry of the data. The detailed steps of Isomap are listed as follows:

Step 1. Construct neighborhood graph: Define the graph G over all data points by connecting points x_i, x_j if they are closer than a certain distance ε, or if x_i is one of the K nearest neighbors of x_j. Set edge lengths equal to $d(x_i, x_j)$.

Step 2. Compute shortest paths: Initialize $d_G(x_i, x_j) = d(x_i, x_j)$ if x_i, x_j are linked by an edge; $d_G(x_i, x_j) = +\infty$ otherwise. Then for each value of k=1,2,…,N in turn, replace all entries $d_G(x_i, x_j)$ by min $\{ d_G(x_i, x_j), d_G(x_j, x_k) + d_G(x_k, x_j) \}$. The matrix of

final values $D_G(x_i, x_j) = \{d_G(x_i, x_j)\}$ will contain the shortest path distances between all pairs of points in *G* (This procedure is known as Floyd's algorithm).

Step 3. Construct *d*-dimensional embedding: Let λ_p be the *p*-th eigenvalue (in decreasing order) of the matrix $\tau(D_G)$. The operator τ is defined by $\tau(D) = -HSH/2$, where $\boldsymbol{S}$ is the matrix of squared distances $\{S_{ij} = D_{ij}^2\}$, and *H* is the "centering matrix" $\{H_{ij} = \delta_{ij} - 1/N\}$, δ_{ij} is the Kronecker delta function. [7]), and V_p^i be the *i*-th component of the *p*-th eigenvector. Then set the *p*-th component of the *d*-dimensional coordinate vector y_i equal to $\sqrt{\lambda_p} V_p^i$ .This is actually a procedure of applying classical MDS to the matrix of graph distance D_G.

There may be two reasons to extend the Isomap. First, the real-world data are often noisy, which can weaken the mapping procedure of Isomap. Second, the goal of the mapping in classification is different from that in visualization. In visualization, the goal is to faithfully preserve the intrinsic structure as well as possible, while in classification, the goal is to transform the original data into a feature space that can make classification easier, by stretching or constricting the original metric if necessary. Both reasons indicate that some modification should be made on Isomap for the tasks of classification. We presented a supervised Isomap. First a new distance metric is designed as follows:

$$D(x_i, x_j) = \left\| x_i - x_j \right\| + \lambda \cdot \max_{i,j} \left(\left\| x_i - x_j \right\| \right) \cdot (1 - S(x_i, x_j)) \tag{1}$$

where λ is adjustable parameter, $0 \le \lambda \le 1$, $S(X_i, X_j)$ is expressed as follows

$$S(X_i, X_j) = \begin{cases} 1 & \text{If both } X_i \text{ and } X_j \text{ are } k \text{ nearest neighbors each other and have the same label;} \\ \exp\left(-\dfrac{\left\| X_i - X_j \right\|^2}{\beta}\right) & \text{If both } X_i \text{ and } X_j \text{ are } k \text{ nearest neighbors each other and have different labels;} \\ 0 & \text{otherwise} \end{cases}$$

Based on above distance metric, we proposed a supervised Isomap, the steps as follows:

(1) Build a sparse graph with *K*-nearest neighbors, where above distance metric is adopted.
(2) Infer other interpoint distances by finding shortest paths on the graph (Dijkstra's algorithm).
(3) Build a low dimensionality embedded space to best preserve the complete distance matrix.

The error function is expressed: $E = \left\| \tau(D_G) - \tau(D_Y) \right\|$, where $\tau(D_G)$ is inner product distances in graph, $\tau(D_Y)$ is inner product distances in new coordinate system.

Solution: set points Y to top eigenvectors of D_G. The shortest distance on a graph is easy to compute. It is shown in Fig1 (see www.combinatorica.com).

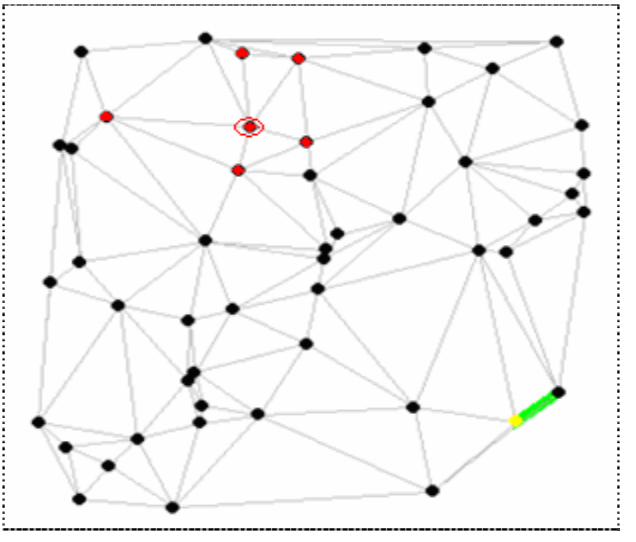

Fig. 1. The sketch map of Dijkstra's algorithm

3 Experiments

The purpose of image segmentation is to separate leaf objects from background so that we can extract leaves' shape features exactly in the later procedures, and the output of image segmentation is a binary image in which the leaf objects are numerically displayed with 1 and the background is with 0. After segmentation we can locate the leaf objects in binary images. Notice that there exist some variance on length and curvature of leafstalks. To keep the precision of shape features extraction these leafstalks should be removed. Therefore, we consider applying opening operation of mathematical morphology to binary images, which is defined as an erosion operation followed by a dilation operation using a same structuring element. By performing opening operation several times, we can successfully remove the leafstalks while preserving the main shape characteristics of leaf objects.

There are many kinds of leaf image features such as shape features, color features and texture features, etc, which can be used for leaf images classification. In our experiments, we use supervised Isomap to extract classification features from leaf images which have been pre-processed including segmentation, denoising.

In our work, a leaf image sub-database is used in the following experiment, which was collected and built by segmentation in our lab. This database includes 20 species of different plants. Each species includes at least 100 leaves images, 50 of which are used as training samples, the rest as testing set. The leaf images of 20 species are shown in Fig.2. Generally speaking, plant classification depends not only on the class

distribution but also on the classifier to be used. The combining classifiers are commonly used for plant recognition. The 1-NN classifier is adopted for its simplicity.

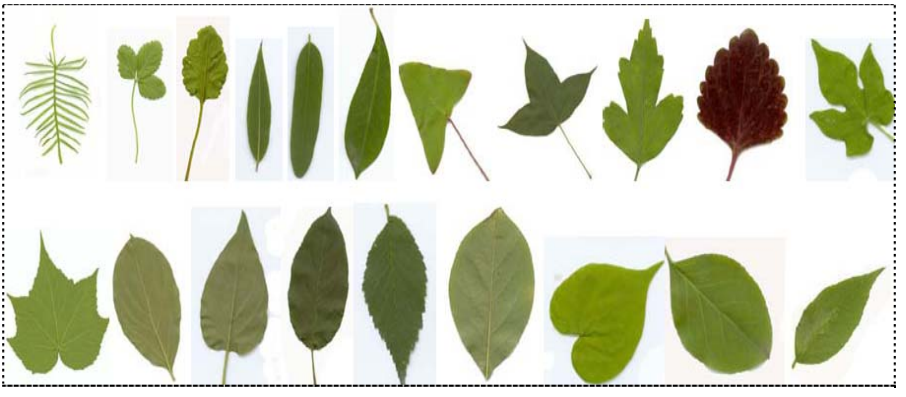

Fig. 2. The leaf images of 20 kinds of plants

Then k nearest neighbor criterion is adopted to construct the adjacency graph and k is set to 3 to 10 with step 0.1, the adjustable parameter λ is set to 0.1 to 1 with step 0.1. After supervised Isomap has been applied to extract feature, the 1-NN classifier is adopted to predict the labels of the test data. The statistical experimental result is shown in Table 1 comparing with the other classification methods.

The algorithm is programming with Matlab 6.5, and run on Pentium 4 with the clock of 2.6 GHz and the RAM of 256M under Microsoft Windows XP environment.

Table 1. Classification rate of plant

Method	Reference [19]	Reference [20]	Our proposed
Classification rate (%)	88.89	89.47	92.25

4 Conclusion

The plant leaf shape feature is one of the most important features for characterizing a plant, which is commonly used in plant recognition, matching and registration. In this paper, a plant recognition method is presented. The proposed method produces better classification performance. The experimental result illustrates the effectiveness of this method. The result of the proposed algorithm not only takes a further step to the technique of computer-aided plant species identification, but also remarkably enhances the correct rate of computer-aided plant species identification. At the end of this paper we have a prospect of technique of computer-aided plant species identification. The extensive application in the future of the plant species identification technique will also attracts more algorithms.

Future work should be directed to the following topics. (1) More difference leaf images in variety cases should be collected to generalize the proposed classification method. (2) More features of leaf should be included to improve the classification performance of the proposed method. Further study should be study a supervised robust feature extraction algorithm for plant classification. (3) The features of different leaf classes in the world should be taken into account to improve the classification accuracy. (4) The proposed method should be extended to handle distortion problems such as broken leaves and oriented leaves.

Acknowledgment

This work was supported by the grant of the National Natural Science Foundation of China, No. 60805021, the grant from the National Basic Research Program of China (973 Program), No.2007CB311002.

References

1. Loncaric, S.: A Survey of Shape Analysis Techniques. Pattern Recognition 31(8), 983–1001 (1998)
2. Zhang, D.S., Lu, G.J.: Review of Shape Representation and Description Techniques. Pattern Recognition 37(1), 1–19 (2004)
3. Rui, Y., She, A.C., Huang, T.S.: Modified Fourier Descriptors for Shape Representation-a practical Approach. In: First International Workshop on Image Databases and Multi Media Search, Amsterdam, The Netherlands (August 1996)
4. Papadourakis, G.C., Bebis, G., Orphanoudakis, S.: Curvature Scale Space Driven Object Recognition with an Indexing Scheme Based on Artificial Neural Networks. Pattern Recognition 32(7), 1175–1201 (1999)
5. Im, C., Nishida, H., Kunii, T.L.: Recognizing Plant Species by Leaf Shapes—a Case Study of the Acer Family. Proc. Pattern Recognition 2, 1171–1173 (1998)
6. Wang, Z., Chi, Z., Feng, D.: Fuzzy Integral for Leaf Image Retrieval. Proc. Fuzzy Systems 1, 372–377 (2002)
7. Saitoh, T., Kaneko, T.: Automatic Recognition of Wild Flowers. Proc. Pattern Recognition 2, 507–510 (2000)
8. Wu, S.G., Bao, F.S., et al.: Recognition Algorithm for Plant Classification Using Probabilistic Neural Network. arXiv:0707 4289 (2007)
9. Huang, D.S.: Systematic Theory of Neural Networks for Pattern Recognition. Publishing House of Electronic Industry of China, Beijing (1996)
10. He, Y., Kundu, A.: 2-D Shape Classification Using Hidden Markov Model. IEEE Transaction on Pattern Recognition and Machine Intelligence 13(11), 1172–1184 (1991)
11. Nishida, H.: Matching and Recognition of Deformed Closed Contours Based on Structural Transformation Models. Pattern Recognition 31(10), 1557–1571 (1998)
12. Agazzi, O.E., Kuo, S.S.: Hidden Markov Model Based Optical Character Recognition in the Presence of Deterministic Transformations. Pattern Recognition 26(12), 1813–1826 (1993)
13. Landraud, A.M.: Image Restoration and Enhancement of Characters Using Convex Projection Methods. Computer Vision, Graphics and Image Processing 3, 85–92 (1991)

14. Fuh, C.S., Liu, H.B.: Projection for Pattern Recognition. Image and Vision Computing 16, 677–687 (1998)
15. McCollum, A.J., Bowman, C.C., Daniels, P.A., Batchelor, B.G.: A Histogram Modification Unit for Real-time Image Enhancement. Computer Vision, Graphics and Image Processing 12, 337–398 (1988)
16. Dietterich, T.G., Becker, S., Ghahramani, Z.: Advances in Neural Information Processing Systems, vol. 14, pp. 585–591. MIT Press, Cambridge (2002)
17. Roweis, S.T., Saul, L.K.: Nonlinear Dimensionality Reduction by Locally Linear Embedding. Science 290, 2323–2326 (2000)
18. Tenenbaum, J.B., Silva, V., de Langford, J.C.: A Global Geometric Framework for Nonlinear Dimensionality Reduction. Science 290, 2319–2323 (2000)
19. Gu, X., Du, J.-X., Wang, X.-F.: Leaf recognition based on the combination of wavelet transform and gaussian interpolation. In: Huang, D.-S., Zhang, X.-P., Huang, G.-B. (eds.) ICIC 2005. LNCS, vol. 3644, pp. 253–262. Springer, Heidelberg (2005)
20. Wang, X.-F., Du, J.-X., Zhang, G.-J.: Recognition of leaf images based on shape features using a hypersphere classifier. In: Huang, D.-S., Zhang, X.-P., Huang, G.-B. (eds.) ICIC 2005. LNCS, vol. 3644, pp. 87–96. Springer, Heidelberg (2005)

Integration of Genomic and Proteomic Data to Predict Synthetic Genetic Interactions Using Semi-supervised Learning

Zhuhong You[1,2], Shanwen Zhang[1], and Liping Li[3]

[1] Intelligent Computing Lab, Hefei Institute of Intelligent Machines, Chinese Academy of Sciences, P.O. Box 1130, Hefei Anhui 230031, China
[2] Department of Automation, University of Science and Technology of China, Hefei 230027, China
[3] The Institute of Soil and Water Conservation of Gansu, Lanzhou 730020, China
zhuhongyou@gmail.com, wjdw716@163.com, LipingLi@gmail.com

Abstract. Genetic interaction, in which two mutations have a combined effect not exhibited by either mutation alone, is a powerful and widespread tool for establishing functional linkages between genes. However, little is known about how genes genetic interact to produce phenotypes and the comprehensive identification of genetic interaction in genome-scale by experiment is a laborious and time-consuming work. In this paper, we present a computational method of system biology to analyze synthetic genetic interactions. We firstly constructed a high-quality functional gene network by integrating protein interaction, protein complex and microarray gene expression data together. Then we extracted the network properties such as network centrality degree, clustering coefficient, etc., which reflect the local connectivity and global position of a gene and are supposed to correlate with its functional properties. Finally we find relationships between synthetic genetic interactions and function network properties using the graph-based semi-supervised learning which incorporates labeled and unlabeled data together. Experimental results showed that Semi-supervised method outperformed standard supervised learning algorithms and reached 97.1% accuracy at a maximum. Especially, the semi-supervised method largely outperformed when the number of training samples is very small.

Keywords: Genetic Interaction, Functional Gene network, Network Property, Semi-supervised learning.

1 Introduction

In the post-genomic era, one of the most important steps in modern molecular biology is to understand how gene products or proteins, interact to perform cellular functions. In [1] the proteins in the same pathway tend to share similar synthetic lethal partners, therefore for two genes the number of common genetic interaction partners can be used to measure the probability of physical interaction or sharing a biological function. Therefore, identifying gene pairs which participated in synthetic genetic interaction

D.-S. Huang et al. (Eds.): ICIC 2009, LNAI 5755, pp. 635–644, 2009.

(SGI), especially synthetic sick and lethal (SSL), is very important for understanding cellular interaction and determining functional relationships between genes. However, little is known about how genes interact to produce phenotypes. We can experimentally test the phenotype of all double concurrent perturbation to identify whether pairs of gene have the relation of SGI [1]. However, the comprehensive identification of SGI in genome-scale by experiment is a laborious and time-consuming work. Therefore, it is crucial that SGI is predicted using the computational method.

In this paper, we proposed a novel in-silico model to predict the synthetic genetic interaction gene pairs. Specifically, we firstly constructed a systematic functional gene network by integrating protein interaction data, protein complex data and microarray gene expression data together and employed the tool of network analysis to address the issue of SGI prediction.

To predict synthetic genetic interactions gene pairs, we choose data source which will be helpful in identifying the SGI. For example, protein interaction data or microarray gene expression data can provide a great deal of information about the functional relationship between genes. The protein complex data also contain rich information about functional relationship among involved proteins. PPI data can be modeled as a connectivity graph in which the nodes represent proteins and the edges represent physical interactions. In PPI network, the interactions reflect the direct collaboration of proteins. Gene expression profiles do not describe direct physical interaction but measure the expression levels of certain gene in whole genome scale. Protein complexes means groups of proteins perform a certain cellular task together. In previous work [2], it has proven that genes corresponding to the interacting proteins tend to have similar expression patterns. Following this observation, a natural idea is to integrate PPI data, protein complex data and microarray gene expression data to utilize more information for genetic interaction prediction.

In recent years, it has been a growing and hot topic to integrate diverse genomic data to protein-protein network and improve the coverage and accuracy of the network. Previous works which integrate diverse of data source indeed proved that such integrated function network is more reliable than network just based on a single data source [3]. However, most previous works for SGI prediction only consider protein interaction data or microarray gene expression data [4, 5]. In our study, we integrated genomic and proteomic data to build a biological network. Comparing with previous work, one contribution of our method is to build a probabilistic functional network where a probabilistic weight is assigned to each edge based on the projected functional linkage.

Network analysis is a quantitative method, which originates from the social science, to study the nodes' properties related to connectivity and position in the network. It has become increasingly popular to be applied to diverse areas, such as molecular biology, computational biology, etc. Network analysis is a powerful tool that allows one to study the relationships between two nodes in the network, providing information on the relationship that two nodes have similar properties. In this work, we extracted the network properties such as network centrality degree, clustering coefficient, betweenness centrality, etc., which reflect the local connectivity and global position of a gene and are supposed to correlate with its functional properties. Then we find relationships between synthetic genetic interactions and function network properties based on the machine learning algorithms.

Many machine learning algorithms including support vector machine (SVM), probabilistic decision tree have been developed to predict the SGI of gene pairs. However, most of previously mentioned learning algorithms predict the SGI only from labeled samples. When the number of labeled samples which used as training set is small, these traditional approaches do not work well. Usually obtaining unlabeled samples is much easier than getting labeled samples. Therefore, it is very desirable to develop a predictive learning algorithm to achieve high performance using both labeled samples and unlabeled samples. In this study, we proposed a method for predicting the genetic interactions based on the functional gene network which integrated genomic and proteomic data. The prediction of SGI is performed by using the graph-based semi-supervised learning which incorporates labeled and unlabeled data together and overcomes all the drawbacks mentioned above.

To sum up, we presented a computational method of system biology to analyze synthetic genetic interactions. This in-silico model can be used to find relationships between synthetic genetic interactions and function network properties. The proposed semi-supervised method only needs a few number of labeled training data and can approach a high performance. Experimental results showed that Semi-supervised method outperformed standard supervised learning algorithms, i.e., SVM, and reached 97.1% accuracy at a maximum. Especially, the semi-supervised method largely outperformed when the number of training samples is very small.

2 Methodology

2.1 General Procedure

In our approach, we first combined protein interaction data, protein complex data and microarray gene expression profiles of *saccharomyces cerevisiae* to build a high coverage and high precision weighted biological network.

Specifically, PPI and protein complex data are used to determine the topology of the network. The weights of the interaction are calculated based on the gene expression profile. The weights are assigned as the confidence score that represents their functional coupling of the biological network in this way. Secondly several graph-based network properties are extracted based on the biological network. Then these network properties which correspond to single gene or gene pair, the experimentally obtained gene pairs which have been confirmed to have or not have the synthetic genetic interaction are inputted to a semi-supervised classifier to prediction some other unknown interaction gene pairs. The overall workflow is illustrated in Fig. 1. The details of above procedure will be described as below.

2.2 Multiple Data Sources

Although each kind of genome or proteome data source can provide information on gene function insights, each data always contain severe noise and only reflect certain information. Therefore integrating different kinds of data source to build a network has been a hot topic and is expected to provide more and reliant information. The high-throughput data such as microarray gene expression data, protein interaction data and protein complexes data are becoming essential resource for understanding the dynamics of the cell. In this study, these three data source were integrated into a functional biology network.

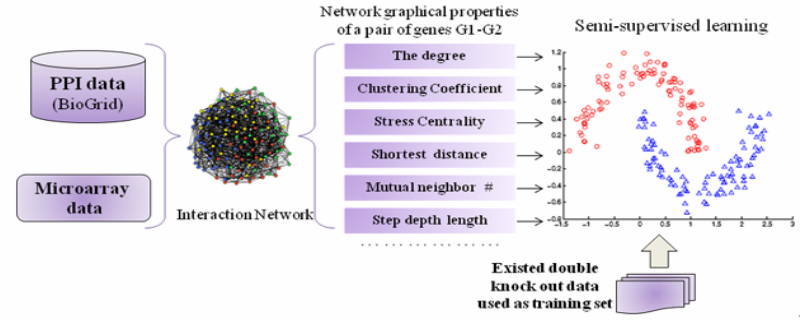

Fig. 1. Schematic diagram for predicting the Synthetic Genetic Interactions by integrating of Genomic and Proteomic Data. The Semi-supervised Learning is used to utilize both labeled samples and unlabeled samples.

2.2.1 Protein–Protein Interaction Data

Proteins play crucial roles, such as transferring signals, controlling the function of enzymes, in cellular machinery. One protein interacts with other proteins, DNA or other molecules. The Protein–protein interaction (PPI) data is believed to contain valuable insight for the inner working of cells; therefore it may provide useful clues for the function of individual proteins or signaling pathways. In our work, all the PPI data of yeast are from the BioGrid database [6]. The BioGrid contains many protein and genetic interaction curated from other literatures or databse. To study the protein interaction from a global perspective, we generated the PPI by extracting physical interactions reported in BioGrid, altogether with 12990 unique interactions among 4478 proteins.

2.2.2 Protein Complexes

In the protein complexes, although it is unclear which proteins are in physical contact, the protein complex data contain rich information about functional relationship among involved proteins. For simplicity, we assigned binary interactions between any two proteins participating in a complex. Thus in general, if there are n proteins in a protein complex, we add $n(n\text{-}1)/2$ binary interactions. We got the protein complex data from [7, 8]. Altogether about 49000 interactions are added to the protein interaction network.

2.2.3 Microarray Gene Expression Data

Protein-protein interaction data produced by current state of art methods contain many false positives, which can influence the analyses needed to derive biological insights. One way to address this problem is to assign confidence scores that reflect the reliability and biological significance of each interaction. Most previously described scoring methods use microarray gene expression data as another data source [9, 10]. Gene expression profile contains information on regulation between regulators and their targets. For this study we downloaded gene expression microarrays from the

Gene Expression Omnibus (GEO) database at the NCBI. This database contains data from over 300 large-scale microarray and SAGE experiments. However, when selecting datasets a tradeoff between reliability and computational costs has to be made. In this work we use 76 experimental conditions for all the genes in yeast related to cell regulation and migration. For each experiment, if there was a missing point, we substituted its gene expression ratio to the reference state with the average ratio of all the genes under that specific experimental condition.

2.3 Construction of Probabilistic Functional Network

As mentioned above each node pair linkage in a FGN carries a confidence score to represent the functional coupling between the two biological entities that it represents. The successful applications of integrating heterogeneous data have proved that integrating PPI and microarray gene expression data is superior to methods which just use PPI data [11]. For the protein-protein interaction, the interaction reflects the directly physical interaction of proteins to implement certain function. However, the PPI data is flooded with many false positive or false negative interaction mistakes. Therefore the prediction of synthetic genetic interactions just based on PPI data is often not very accurate and can not approach good performance. We suppose that genes with similar expression profiles are involved in the control of the same transcriptional factors and thus functional associated. The microarray gene expression data can provide useful information

Following the previous work [9, 10], we calculated the weighted score of two genes which indicate the function similarity based on different kinds of high-throughput data. We consider a microarray gene expression data set as $X=\{x_1,x_2,\ldots,x_M\}$, where $x_i=\{x_{i1},x_{i2},\ldots,x_{iM}\}$ is a N dimensional vector representing gene i with N conditions. We firstly use the clustering algorithm to group the genes into S different clusters $C_1,C_2,\ldots,C_S$. Specifically, the Pearson Correlation Coefficient (PCC) is adopted to measure the similarity or dissimilarity of the expression pattern of two genes. Let us consider genes x_i and x_j and the PCC can be calculated as

$$PPC(x_i,x_j)=\frac{\sum_{k=1}^{N}(x_{ik}-\overline{x_i})(x_{jk}-\overline{x_j})}{\sqrt{\sum_{k=1}^{N}(x_{ik}-\overline{x_i})^2\sum_{k=1}^{N}(x_{jk}-\overline{x_j})^2}} \tag{1}$$

where x_{ik} and x_{jk} are the expression values of the kth condition of the ith and jth genes respectively. $\overline{x_i},\overline{x_j}$ are the mean values of the ith and jth genes respectively. PCC is always in the range [-1,1]. A positive value of PCC means that the two genes are coexpressed and negative value denotes that they are the opposite expressed gene pairs. As proposed in [12], we used the Pearson correlation coefficient as a measure of similarity or dissimilarity to cluster genes with similar or different expression patterns, which means genes with coexpressed pattern are assigned to same cluster and vice versa. At first, all genes of the microarray data are considered in a single cluster and the cluster is partitioned into two disjoint clusters. Partitioning is done in such a way that x_i and x_j which have the most negative value of PCC will be assigned in two

different clusters. Genes having larger value of PCC with x_i compared with x_j are assigned in the cluster that contains x_i . Otherwise, they are placed in the cluster that contain x_j. In the next iteration, a cluster having a pair of gene (x_i, x_j) with the most negative PCC value will be selected and the above partitioning procession is repeated until there is no negative PCC value present between any pair of genes inside any cluster. This kind of cluster method ensures that all pairs of genes in any cluster are only positively correlated. In [12] it has been proven that this method is able to obtain clusters with higher biological significance than that obtained by some other algorithms such as Fuzzy K-means, GK and PAM clustering methods.

Based on the above obtained gene expression profile which has been partitioned into a couple of clusters, we calculated the weight scores of the interactions between two proteins as below formula:

$$W(x_i, x_j) = L_1 * (\left\| X_i - C_{x_i} \right\|^2 + \left\| X_j - C_{x_j} \right\|^2) + (1 - L_1) * \left\| C_{x_i} - C_{x_j} \right\|^2 \quad (2)$$

where x_i and x_j represent genes i and j with N conditions respectively. C_{x_i}, C_{x_j} denote the centroids of the clusters in which genes x_i and x_j located respectively. $\|.\|$ denotes the Euclidean distance. In equation (2), the constant L_1 is a trade-off parameter used to tune the ratio of the first and second term in the weight function. According to we chose L_1=0.3 because we supposed that the distance between centroids of two cluster more significant comparing with the distance of each gene from its centroid. The outcome of the integration method is a weighted undirected graph and the graph-based properties will be extracted and then be used to predict the synthetic genetic interaction.

2.4 The Properties of Probabilistic Functional Network for Predicting SGI (Synthetic Genetic Interaction)

Graph theory enables us to analyze structural properties of the network and link them to other information, such as function. The construction of a validated probabilistic functional network allows an in-depth analysis of the local connectivity and global position of a gene, which supposed to correlate with its functional properties. Here the network properties of the PFN, such as local connectivity and global position, are examined with the aim of discover the relationship between the network properties of a pair of genes and the existence of a synthetic genetic interactions relationship. We used graph-based semi-supervised classifier to model the correlation between the network properties of a pair of genes and the existence of a synthetic genetic interactions relationship. Several network properties of one gene or gene pair are input to the semi-supervised classifier.

In this study, we integrated microarray gene expression , protein-protein interaction and protein complexes data of Saccharomyces cerevisiae in the form of an undirected weighted graph G (V, E), which formally consists of a set of vertices V and edges E between them. An edge e_{ij} connects vertex i with vertex j. Most previous works only consider the topological aspects of the protein interaction network and ignore the underlying functional relationships which can be reflected by the microarray gene expression data [5]. Therefore, in this work we extend the concepts of network

properties in unweighted network to weighted network. The network properties such as Centrality degree, clustering coefficient, betweenness centrality, closeness centrality and eigenvector centrality was used in this study.

All of the above properties are properties of single nodes in a network. The first two are sensitive only to the local network structure around the node, while all the others are sensitive to the global network topology. Furthermore, the last two properties depend not only on shortest paths through the network, but on other paths as well. In addition to the above single-node properties, we also computed a set of two-node properties, for example the inverse of shortest distance $d(p,q)$ between proteins p and q, number of mutual neighbors between proteins p and q.

2.5 Graph-Based Semi-supervised Classifier

Generally speaking, to predict the synthetic genetic interaction based on biological network is challenging for two reasons. Firstly, only a small number of synthetic genetic interaction or non-interaction gene pairs have experimentally provided, which means the available knowledge of labels is usually very sparse. Therefore, it is difficult to obtain sufficient training data set for the supervised algorithm. Secondly, biological network integrated by heterogeneous data is inherently very noisy, which let the methods that exploit the network properties prone to noise propagation. In this study, we address these two issues by proposing a graph-based semi-supervised learning to synthetic genetic interaction prediction from functional biological network based on the network properties analysis.

Semi-supervised learning (SSL) is halfway between supervised and unsupervised learning. In this study, the prediction of synthetic genetic interaction is modeled as a classification problem. The candidate gene pairs are considered as points with a couple of features, which correspond to the properties of these two genes in the biological network. Consider the data set which can be denoted by $\mathcal{X}=(\mathcal{X}_l,\mathcal{X}_u)$ of labeled inputs $\mathcal{X}_l=\{x_1,x_2,\ldots,x_l\}$ and unlabeled inputs $\mathcal{X}_u=\{x_{l+1},x_{l+2},\ldots,x_n\}$ along with a small portion of corresponding labels $\{y_1,y_2,\ldots,y_l\}$. In our study the labels are binary: $y_l\in\{1,0\}$, Consider a connected weighted graph $G=(V,E)$ with vertex V corresponding to above n data points, with nodes $L=\{1,2,\ldots,l\}$ corresponding to the labeled points with labels $y_1,y_2,\ldots,y_l$ and $U=\{l+1,l+2,\ldots,n\}$ corresponding to unlabeled points. For semi-supervised learning, the objective is to infer the labels $\{y_{l+1},y_{l+2},\ldots,y_n\}$ of the unlabeled data $\{x_{l+1},x_{l+2},\ldots,x_n\}$, typically $l<<n$.

In our study, we use semi-supervised classifier (SSC) to model correlations between network properties and the existence of a synthetic genetic interaction. Various graph-theoretical properties (local as well as global) of two proteins in a PIN are fed as inputs to the SS classifier, which is schematically represented in Figure 1. The output of the SS classifier is a score that measures if the two corresponding genes to partake in a synthetic genetic interaction. The approach can be described as follows:

Firstly, the $n\times n$ symmetric weight matrix W on the edges of the graph can be

$$W_{ij}=\begin{cases}\exp\left(-\dfrac{\left\|x_i-x_j\right\|^2}{2\sigma^2}\right), & \text{if } i\neq j\\ 0, & \text{if } i=j\end{cases}$$

where x_i and x_j denote the different points in the graph G. The constant σ is a length scale hyperparameter. Therefore nearby points in Eucilidean space are assigned large edge weight, and vice versa.

Secondly, we build the matrix $S=D^{-1/2}WD^{-1/2}$ where D is a diagonal matrix with the (i,i) -elements equal to the sum of the ith row of W. Then take the iteration $F(t)=aSF(t+1)+(1-a)Y$ until the similarity matrix F converges, where a is a predefined constant which ranges from 0 to 1.

Thirdly, let F^* represent the limit of the sequence $\{F(t)\}$. Label each point x_i as a label $y_i = \arg\max_{j\le C} F_{ij}^*$. Because $0<a<1$ and the eigenvalues of S rangs from -1 to 1, $F^* = \lim_{n\to\infty} F(t) = \lim_{n\to\infty}(aS)^{t-1}Y + (1-a)\lim_{n\to\infty}\sum_{i=0}^{t-1}(aS)^i Y$ .Then the classification matrix can be calculated as: $F^* = (1-aS)^{-1}Y$. As in [13], F^* can be obtained without iteration.After above several steps, the labels of unlabeled data $\{x_{l+1},x_{l+2},\ldots,x_n\}$ will be assigned.

The full prediction system has 12 inputs lumped into a single vector. The graph-based semi-supervised methods define an undirected graph represented by G.

3 Computational Experiments and Results

All of above mentioned network properties, i.e., centrality degree, clustering coefficient, betweenness centrality, closeness centrality, eigenvector centrality, which correspond to single gene or gene pair, are constructed as a feature vector and inputted to the classifier. We also inputted the experimentally obtained gene pairs which have been confirmed to have or not have the synthetic genetic interaction to classifier as the training set. The next step we use the SVM and semi-supervised classifier to predict other unknown interaction gene pairs, i.e. to distinguish SSL and non-SSL pairs. Figure 2 shows the performance of our method, where the x axis denotes the number of training gene pairs and the y axis presents the average error rata. The red line and blue line denote the performance of SVM and SSL respectively. We can see both of the classifier can get the good performance.

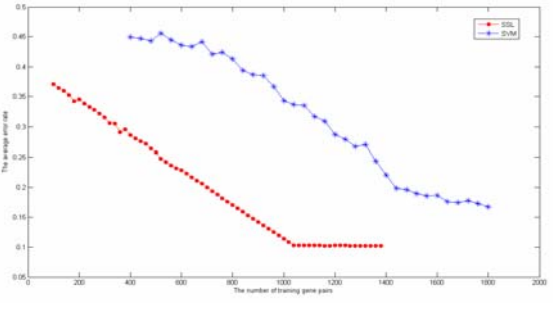

Fig. 2. Comparison of the average error rate for semi-supervised learning and SVM classifiers

We also compared the results where SVM classifier and Semi-supervised learning was used respectively. We can see from Figure 2 that the accuracy of SSL method

appears higher than the SVM classifier. Further, the accuracy obtained by SSL is significantly higher than obtained by SVM classifier when labeled training data set is very small.

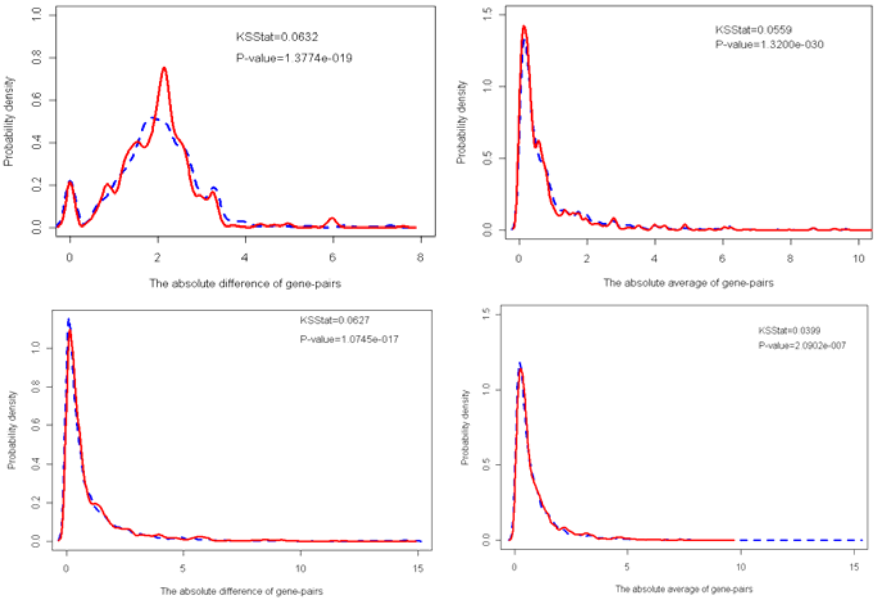

Fig. 3. The distribution of network properties for the SGI and Non-SGI gene pairs in the functional gene network. Numbers in each plot indicate the D-statistic associated with the Kolmogorov -Smirnov test for the difference between the two distributions and the corresponding P-value. The distribution of centrality degree, clustering coefficient, betweenness centrality, closeness centrality were shown in the figure.

Our results clearly demonstrate that the biological network integrating of protein interaction data, protein complex data and gene expression data can be used to predict the synthetic genetic interactions. We show that graph-based properties of gene in biological network serve as compelling and relatively robust determinants for the existence of synthetic interaction between their gene counterparts.

In order to assess the suitability of each of the network properties in classifying SSL gene pairs and non-SSL pairs, we drew the distributions of probability density for these properties across SSL pairs and non-SSL pairs. For certain property, we plotted the distribution of the absolute difference of that property across the two genes. Most properties studied here show statistically significant but small distributional differences between SGI pairs and non-SGI pairs (see Figure 3). The distributions of the difference of each property across two proteins in case of SGI pairs (red lines) and non-SGI pairs (blue lines) are displayed. We used the Kolmogorov-Smirnov statistic to compare the distributions of the two distributions. We can see that when viewed as part of a functional gene network, SSL pairs as compared to non-SSL ones tend to have higher average degree, higher average closeness centrality, higher

average information centrality and higher number of mutual neighbors. This can explain why it is reasonable using the network properties to predict the synthetic interaction.

Acknowledgements

The authors would like to thank the anonymous reviewers for helpful comments on this paper. This work was supported by the grants of the National Science Foundation of China, No. 30700161, the grant of the Guide Project of Innovative Base of Chinese Academy of Sciences (CAS), No.KSCX1-YW-R-30, and the grant of Oversea Outstanding Scholars Fund of CAS, No.2005-1-18.

References

1. Tong, A.H.Y., Lesage, G., Bader, G.D., Ding, H.M., Xu, H., Xin, X.F., Young, J., Berriz, G.F., Brost, R.L., Chang, M.: Global Mapping of the Yeast Genetic Interaction Network. Science 303(5659), 808–813 (2004)
2. Jansen, R., Greenbaum, D., Gerstein, M.: Relating Whole-genome Expression Data with Protein-protein Interactions. Genome Research 12(1), 37–46 (2002)
3. Zheng, H., Wang, H., Glass, D.H.: Integration of Genomic Data for Inferring Protein Complexes from Global Protein-protein Interaction Networks. IEEE Trans Syst Man Cybern B Cybern 38(1), 5–16 (2008)
4. Lezon, T.R., Banavar, J.R., Cieplak, M., Maritan, A., Fedoroff, N.V.: Using the Principle of Entropy Maximization to Infer Genetic Interaction Networks from Gene Expression Patterns. Proceedings of the National Academy of Sciences of the United States of America 103(50), 19033–19038 (2006)
5. Paladugu, S.R., Zhao, S., Ray, A., Raval, A.: Mining Protein Networks for Synthetic Genetic Interactions. Bmc Bioinformatics (2008)
6. Stark, C., Breitkreutz, B.J., Reguly, T., Boucher, L., Breitkreutz, A., Tyers, M.: BioGRID: a General Repository for Interaction Datasets. Nucleic Acids Res 34(Database issue), D535–D539 (2006)
7. Gavin, A.C., Bosche, M., Krause, R., Grandi, P., Marzioch, M., Bauer, A., Schultz, J., Rick, J.M., Michon, A.M., Cruciat, C.M.: Functional Organization of the Yeast Proteome by Systematic Analysis of Protein Complexes. Nature 415(6868), 141–147 (2002)
8. Ho, Y., Gruhler, A., Heilbut, A., Bader, G.D., Moore, L., Adams, S.L., Millar, A., Taylor, P., Bennett, K., Boutilier, K.: Systematic Identification of Protein Complexes in Saccharomyces Cerevisiae by Mass Spectrometry. Nature 415(6868), 180–183 (2002)
9. Segal, E., Wang, H., Koller, D.: Discovering Molecular Pathways From Protein Interaction and Gene Expression Data. Bioinformatics 19(suppl.1), i264–i271 (2003)
10. Tu, K., Yu, H., Li, Y.X.: Combining Gene Expression Profiles and Protein-protein Interaction Data to Infer Gene Functions. J. Biotechnol 124(3), 475–485 (2006)
11. Troyanskaya, O.G., Dolinski, K., Owen, A.B., Altman, R.B., Botstein, D.: A Bayesian Framework for Combining Heterogeneous Data Sources for Gene Function Prediction (in Saccharomyces cerevisiae). Proc. Natl. Acad. Sci. USA 100(14), 8348–8353 (2003)
12. Bhattacharya, A., De, R.K.: Divisive Correlation Clustering Algorithm (DCCA) for Grouping of Genes: Detecting Varying Patterns in Expression Profiles. Bioinformatics 24(11), 1359–1366 (2008)
13. Zhou, D., Bousquet, O., Lal, T.N., et al.: Learning with Local and Global Consistency. Advances in Neural Information Processing Systems 16, 321–328 (2004)

A Method of Plant Leaf Recognition Based on Locally Linear Embedding and Moving Center Hypersphere Classifier

Jing Liu[1], Shanwen Zhang[2], and Jiandu Liu[3]

[1] The Science Institute, Air-Force Engineering University, Xi' an, 710051, China
[2] Zhongyuan University of Technology, Zhengzhou, 450007, P.R. China
[3] Missile Institute, Air-Force Engineering University, Sanyuan, 713800, P.R.
liu_2007email@126.com

Abstract. This paper introduces a approach of plant leaf recognition. The classifier moving center hypersphere classifier is adopted for its classification validity. The features of plant leaf are extracted and processed by locally linear embedding to form the input vector of the classifier. The experimental results indicate that our algorithm is workable with the average correct recognition rate is up to 92 percent. Compared with other methods, this algorithm is fast in execution, efficient in recognition and easy in implementation. Future work is under consideration to improve it.

Keywords: Plant leaf image, Locally linear embedding (LLE), Moving center hypersphere classifier, Plant classification.

1 Introduction

The plant and human as well as the environment relations are closest in earth all living thing. A great quantity of plant maintenance their equilibrium of oxygen and carbon dioxide in atmosphere, and it is essential resources for mankind's produce and living. But the different produces were great damage its ecological environment in recent years, and then have been causing decrease of quantity of plant and even deracinate of species. It is felicitate that mankind have been conscious of this conjuncture and have been protecting plant gradually. Studying of classify for plant is the important precondition for protecting plant. The technique of image treatment and identification have been gradually applying for this studying along with the high-speed development of computer technique in recent years, and then the computer aided plant identification, the computer identification of plant leaf form etc. Plant leaf feature is the important scientific basis for plant classification and recognition, thus extracting the leaf image feature from plant's leaves would provide method and basis for plant's classify and recognition. On account of differ in thousands of ways for getting plant leaf image and it contains a great background component, therefore we must preprocessing before analyze the leaf image firstly. The preprocessing of leaf image affects directly feature extraction of the plant leaf image, so it is very important

D.-S. Huang et al. (Eds.): ICIC 2009, LNAI 5755, pp. 645–651, 2009.

that choose a good method of preprocessing. Mathematical morphology is a branch of biology which is new method of image treatment and pattern recognition, and it usually handles shape and construction of animal and plant. Preprocessing of leaf image by Mathematical morphology can ensure leaf image behind Preprocess have the basic shape characteristic and the clear edge. Preprocess of leaf image often include three key step eliminate noise, remove background and verify edge. As a result of eroding by insect or other reason, some small internal hole in leaf sample after remove background in some plant leaf would exist. This will affect the handling of behind and can't accurate to extract the leaf feature.

From classify of plant, the most directly valid and the most simply method of identifying a plant is set about its leaves and is also to collect easily. The shape, the color and the skeleton of leaf are usually regard as basis of classify in botany. In this paper, we emphases the shape extracting feature as basis of identifying a plant. To use of moving center super-ball classifier which we have put forward classify the shape extracting feature, can realize to identify for parts of plant leaf quickly and successfully [1-4].

For a long time, the linear model occupies the main-current position which machine learning method. The traditional linear model supposes generally that sets of observing data have overall linear construction, this means that between each observing variable is independence and irrelevant, so Eulidean space which have overall linear construction may take for observation space. Many linear methods with this suppose for the bases such as principal component analysis (PCA) [5], independent component analysis (ICA) [6] have obtained many valid results and acquired extensive application. However, the overall linear supposes for many modes of actuality aren't always tenable. In fact, people usually discovers that the modes sampling in the realistic world had been influenced frequently by some key and implicit factor which are influence each other and then act on the mode, so various formation under the different circumstance take form. For example, the different picture in same facial person is decision of some key factors such as carriage, light, distance etc. each variety of them would cause variety of a great deal observing variable pixel, but variety of observing variables aren't linear pile up after each key factor changes respectively while several key factors variety together. This indicate that the sets of data which people handles usually has inherent construction of the lower dimension, there are highly nonlinear correlation between observing variables generally. From geometry point of view, we can think that the modes sampling in the realistic world locates a lower dimension manifold which inset high dimension space, and this moment the overall linear supposes aren't suit any more, linear method shouldn't usually have explored the nonlinear rule of the internal of data. Having admission of fact that nonlinear correlation in the modes between inherent construction of the lower dimension and observing variable exist, thus we must think the data which locates a lower dimension manifold which inset high dimension space as basic supposing (we call it as "manifold assumption"), establishing nonlinear learning model and developing method of nonlinear machine learning to discover inherent construction and inherent regulations in the sets of data. Manifold assumption are not only from geometrical conformation of the sets of data but also has closely relation between it and cognition model of human being. The most difficult of plant classification identifies consist in the very big variety of " kind of inherent " of leaf image, the image of the same of a leaf looks the very difference under differ condition such as the season, position and

illumination from the sun etc., and sometimes the leaf image even mistake for different plant. On a certain meaning, leaf image is a kind of typical manifold construction, the sets of data of leaf image is nonlinear manifold which is formed and control by some inherent variables. In order to accomplish the valid plant identify, "leaf slice manifold" is a quite good model. Since the variety of the season, position and illumination, exactly, it cause quite curvature distribution of leaf image in observing space, we can greatly lower the dimension of observing space as long as finding out the control variables such as the season, position and illumination, from "leaf image". In plant leaf classification identify, we can distinguish among differing leaf image by representative variables which are searched inherent regulation in the sets of training for the leaf image. LLE [7,8] is a representative local linear manifold learning method. Based on the assumption of the local linearity, LLE first constitutes local coordinates with the least constructed cost and then maps them to a global one. LLE can find a mapping to preserve local linear relationships between neighbors.

The rest of the paper is organized as follows. Section 2 and Section 3 introduce locally linear embedding and moving Center hypersphere classifier, respectively. Section 4 proposes a method of leaf recognition. Experiments are illustrated in Section 5. Conclusion is given in Section 6.

2 Locally Linear Embedding

LLE is based on the idea of visualizing a manifold *M* as a collection of overlapping coordinate patches. If the neighborhood sizes are small and the manifold is smooth the patches can be assumed roughly linear. Besides, the chart from the manifold *M* to the lower dimensionality space R^d is assumed to be approximatively linear on the patches. Therefore the idea underlying LLE consists in looking for local small patches, describing their geometry and finding a chart to R_d that preserves the manifold geometry and is roughly linear. Besides, the local patches are assumed overlapped so that the local manifold reconstructions can be combined into a global one. For visualization, the goal of dimensionality reduction methods is to map the original data set into a (2-D or 3-D) space that preserves the intrinsic structure as well as possible. But for classification, it aims to project the data into a feature space in which the members from different classes could be clearly separated. LLE is an effective dimensionality reduction approach to visualize the high dimensional data into a 2-D space. However, little classification ability can be displayed by implementing the original LLE. The steps of LLE are described as follows:

1) Find weight matrix *W* of linear coefficients,

$$\varepsilon(W) = \left\| \sum_i X_i^{'} - \sum_i W_{ij} X_i^{'} \right\|^2 \tag{1}$$

Enforce sum-to one constraint with the Lagrange Multiplier,

$$W_j = \sum_k C_{jk}^{-1} (X^{'} \cdot \eta_k + \lambda) \tag{2}$$

2) Find projected vectors *Y* to minimize reconstruction error,

$$\phi(W) = \left\| \sum_i Y_i^{'} - \sum_j W_{ij} Y_i^{'} \right\|^2 \tag{3}$$

Must solve for whole dataset simultaneously, we add constraints to prevent multiple, degenerate solutions, $\sum_j Y_j = O$, $\frac{1}{N}\sum_j Y_j \oplus Y_j = I$.

Based on the weighted matrix W, we can define a sparse, symmetric, and positive semi-definite matrix M as follows:

$$M = (I - W)^T (I - W) \tag{4}$$

Note that Eq.(3) can be expressed in a quadratic form $\varepsilon(Y) = \sum_{ij} M_{ij} Y_i Y_j^T$,where $M = \left[M_{ij} \right]_{n \times n}$. By the Rayleigh-Ritz theorem, minimizing Eqn. (3) can be done by finding the eigenvectors with the smallest (nonzero) eigenvalues of the sparse matrix M.

The optimal embedded coordinates are given by bottom m+1 eigenvectors of the matrix M.

3 Moving Center Hypersphere Classifier

Because the sample quantity of leaves and the number of classify characteristic by our choose are more relatively, so the number and dimension of eigenvector are very high in eigenvector space, hence it must chooses that a reasonable classifier which not only can assure the rate of identification is high fairly but also decrease the saving space and calculate time to the greatest extent. According to this, we put forward the moving center super-ball classification method which is a kind of compression to the consult samples. Having been compress and handle for the sample data have reduced availably the saving space with calculating time and have no influence to the rate of correct identification. It's the basic thought is substitute the super-ball for a tuft points. We know that a sample is a point in higher dimension space and a classification is a set of point in the space correspondingly. Therefore, we can utilize a series of super-ball to fit the higher dimension space of these points. The general idea of its algorithm is use some super-ball to approach each sample, and moving the super ball's center, extending the super-ball's radius to contain possibly its many samples points at the same time, thus the saving quantity of the super-ball will decrease. Ultimately, it will achieve the whole sample points including sample space with many super-balls. Following is training step of an example with a sample point for introducing moving center super-ball classifier [9]:

1) Initialize the super-ball and marking, k=1, put the whole sample points into a set and find out the nearest point which distance the equilibrium point of all points in the set and act it as the initialization center s of the super-ball of number *k;*
2) Find out the nearest point which distance the center point *s* in other set , and defining it as the nearest distance of the other set from the center point *s*, record for d_1, Find out the farthest point from the center point *s* in this set in the super-ball which the central point is *s* with the radius of d_1, Define the distance from it to the center point s is the farthest distance of this set, record for d_2;

3) Establish a radius for the super-ball of number k as $r=(d_1+d_2)/2$;
4) Seek the point in the nearer points of m apart from the center point s in reverse direction of the nearest point direction in the other set which leave the center point s, if finding it out , we regard it as the new central point and switch to step (3); otherwise switch to next step;
5) The points of all with surrounding by super-balls in the sets have been removed, if there have some points in the sets, then $k=k+1$, and switch to step (2); otherwise the redundancy super-balls for involving other super-balls have been removed from;
6) The training end.

4 Leaf Recognition Method

Plant classification and recognition is an important area of research in pattern recognition. It can be described as: given a static or video image, the use of the existing leaf image databases to identify one or more individuals. How to extract the characteristics of effective identification and reduce the differential vector of people's dimension are the focus of the leaf image analysis, that is, how effective dimension reduction. We proposed a leaf classification method based on locally linear embedding and moving center hypersphere classifier. The step is as follows:

Step 1: For each leaf image X_i, identify its k nearest neighbors by kNN algorithm;

Step 2: Compute the reconstruction weights that minimize the error of linearly reconstructing X_i by its k nearest neighbors;

Step 3: Compute the low-dimensional embedding Y for X that best preserves the local geometry represented by the reconstruction weights;

Step 4: Classify leaf images by the moving center hypersphere classifier.

5 Experiments

We have tested performance of moving center super-ball classifier by select 20 the plant leaves such as gingko, wide yulan magnolia, sweet-scented osmanthus, tobira etc. (figure 1), and each kind of leaves collects 20 samples. There are 15 samples by random selecting as training sample and the surplus are testing samples among them. There are 60 super-balls totally by subscript of abscissa. We set the neighbors k to be from 4 to 15, after LLE, the classification feature vectors of leaf images are obtained. We use the same batch of data to have tested for Most Close neighbor classifier, 4-close neighbors classifier and BP nerve network (input node count for 15, latent-layer node count for 12, output node count for 20). Table 3 list training time, recognition time, saving space, rate of average identification of four kinds of classifier. From the table 1, we can see that the trained of moving center super-ball classifier is shorter than the most close neighbors classifier, 4-close neighbors classifier in recognition time, and the former is very small than both of the later for the saving vector counts but is faintly decline than both of the later for the rate of recognition. Although Moving Center super-ball classifier demands trains but two kinds of the other do not. But

owing to recognition time and saving space are more superior to an engineering of having enormous quantity of sample, it is a better choice. Comparing with BP nerve network can see that the BP nerve network has basically needed no saving space, and shorter recognition time, too. But its training time is very long than Moving Center super-ball classifier. And along with increasing of the sample quantity, the convergence rate of the BP network would be very slow. And it will reach local minimization at the same time. Therefore, Moving Center super-ball classifier may be more suitable for the actual application.

In this paper, we put forward a method that is extract the leaf shape feature and combine it with a kind of new Moving Center super-ball classifier for identifying leaves. The method which introduces in this paper has successfully applied to software system PLRS1.0 of our developing for identifying plant leaves. That system is developed by Visual C++6.0, it can achieve preprocessing, extracting feature and automatic recognition for 20 and more plant leaves such as gingko, wide yulan magnolia, sweet-scented osmanthus, tobira, Chinese littleleaf box, Chinese photinia etc. and the average rate of recognition comes to 92%.

Next we will put focal point of the work how to identify plant leaf image under the complicated environment and increases further the rate of dentification of Moving Center super-ball classifier.

Table 3. The properties contrast of four kinds of classifier

Method	Training time/ms	Identifying time/ms	Rate of average identification
The Most Close neighbors classifier	／	2.9	90.6
4- Close neighbors classifier	／	9.4	90.1
The BP nerve network classifier	125	1.1	90.4
Moving Center super-ball classifier	11.8	1.2	91.6
LLE+ Moving Center super-ball classifier	12.0	1.25	92.4

6 Conclusion

Plant classification is one major application of leaf image processing. Due to the high nature complexity of leaf image data, data dimension reduction has drawn special attention for such type of data analysis. A leaf recognition method is presented based on locally linear embedding and moving center hypersphere classifier. The experiment results show that the method performs very well on leaf recognition.

Acknowledgment

This work was supported by the grant of the National Natural Science Foundation of China, No. 60805021, the grant from the National Basic Research Program of China (973 Program), No.2007CB311002.

References

1. Ye, Y., Chen, C., Li, C.T., Fu, H., Chi, Z.: A Computerized Plant Species Recognition System. In: Proceedings of 2004 International Symposium on Intelligent Multimedia, Video and Speech Processing, Hong Kong (2004)
2. Miao, Z., Gandelin, M.H., Yuan, B.: An Oopr-based Rose Variety Recognition System. Engineering Applications of Artificial Intelligence 19 (2006)
3. de Oliveira Plotze, R., Falvo, M., Pdua, J.G., Bernacci, L.C.M., Vieira, L.C.G., Oliveira, C.X., Bruno, O.M.: Leaf Shape Analysis Using the Multiscale Minkowski Fractal Dimension, a New Morphometric Method: a Study with Passifliora (passifloraceae). Canada Journal of Botany 83 (2005)
4. Ridder, D., Duin, R.P.W.: Locally Linear Embedding for Classification. Technical Report PH-2002-01, Pattern Recognition Group, Dept. of Imaging Science & Technology, Delft University of Technology, Delft, The Netherlands (2002)
5. Shlens, J.: A Tutorial on Principal Component Analysis (2005), `http://www.cs.cmu.edu/_elaw/papers/pca.pdf`
6. Connie, T., Teoh, A., Goh, M., Ngo, D.: Palmprint Recognition with PCA and ICA. In: Image and Vision Computing New Zealand 2003, Palmerston North, New Zealand, November, pp. 232–227 (2003)
7. Roweis, S.T., Saul, L.K.: Nonlinear Dimensionality Reduction by Locally Linear Embedding. Science 290(5500), 2323–2326 (2000)
8. Saul, L.K., Roweis, S.T.: Think Globally, Fit Locally: Unsupervised Learning of Low Dimensional Manifolds. J. Mach. Learn. Res. 4, 119–155 (2003)
9. Wang, X.F., Huang, D.S., Du, J.X.: Feature Extraction and Recognition for Leaf Images. Computer Engineering and Applicationss 03, 190–193 (2006)

Survey of Gait Recognition

Ling-Feng Liu[1,2], Wei Jia[1], and Yi-Hai Zhu[1,2]

[1] Hefei Institute of Intelligent Machines, CAS, Hefei, China
[2] Department of Automation, University of Science and Technology of China
fengling963@gmail.com

Abstract. Gait recognition, the process of identifying an individual by his /her walking style, is a relatively new research area. It has been receiving wide attention in the computer vision community. In this paper, a comprehensive survey of video based gait recognition approaches is presented. And the research challenges and future directions of the gait recognition are also discussed.

Keywords: Gait recognition; Biometrics; Survey.

1 Introduction

Recently, biometric is attracting more and more attentions. Generally, biometric is a field of technology that uses automated methods for identifying or verifying a person based on a physiological or behavioral trait. And the traits that are commonly measured in different systems are the face, fingerprints, palmprint, handwriting, iris, gait, and voice etc. Among them, gait recognition, as a relatively new biometric technique, aims to recognize individuals by the way they walk. The advantages of gait recognition are that it can be applied unobtrusively and it offers potential for recognition at a distance or at low resolution when the human subject occupies too few image pixels [1,21]. Fig.1 illustrates the terms involved in a gait cycle [1].

The early medical and psychological studies [2,29] indicate that the human gait has 24 different components, and if all the components are considered, gait is peculiar to individual. Johansson' experiments [1,3] showed that the light points, attached to a

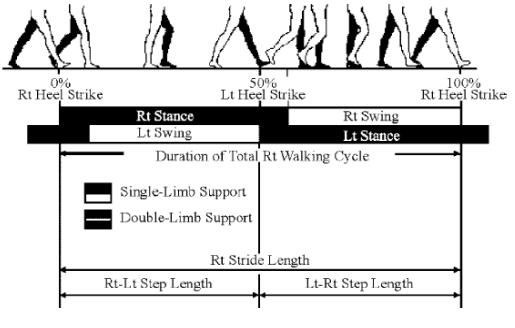

Fig. 1. The walking cycle

D.-S. Huang et al. (Eds.): ICIC 2009, LNAI 5755, pp. 652–659, 2009.

few joints of the moving person, were perceived as representing a human motion in motion when they were animated. Later, Binham' work [1,4] showed that point light displays were sufficient for the discrimination of different types of object motion and that discrete movements of parts of the body could be perceived. From the point of view of biomechanics, the muscular-skeletal structure varies from one another and it is believed to identify an individual according to her/his gait, though all humans follow the same basic walking pattern [2].

The first gait recognition approach was developed by Niyogi and Adelson on a small gait database in 1994 [6]. Subsequently, the HumanID program sponsored by Defense Advanced Research Projects Agency (DARPA) [5] assists greatly in advancing automatic gait recognition. Spurred by the HumanID program, many international famous universities and research institutes, such as the University of Southampton, the Massachusetts Institute of Technology (MIT), Carnegie Mellon University (CMU), Institute of Automation Chinese Academy of Sciences, etc, have made a lot of researches on gait recognition.

Generally, gait recognition approaches can be roughly divided into two categories, i.e., model-based approach and model-free approach [29]. Model-free approach aims to extract statistical features from the whole silhouette to identify individuals while model-based approach aims to model gait explicitly.

2 Model-Based Approach

Model-based approach aims to explicitly model human body or motion according to prior knowledge [7-14]. Usually, each frame of a walking sequence is fitted to the model and the parameters such as trajectories are measured on the model as gait features for recognition. These methods are easy to be understood, however, they tend to be complex and need high computational cost.

Lee and Grimson [7] divided the gait silhouettes into 7 regions, and ellipses were fitted to each region (see fig.2). Finally, the ellipses' parameters were computed as gait features for recognition.

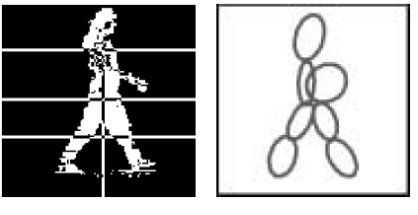

Fig. 2. The silhouette of a foreground walking person is divided into 7 regions, and ellipses are fitted

Cunado et al. [8] considered the legs' motion as a pendulum. The change in inclination of lines represented legs in sequences of video images followed simple harmonic motion and this motion was used for recognition. Yoo et al. [9] used a 2D stick

figure to represent the human body model and calculated trajectory-based kinematic features from gait sequences for analyzing the gait motion. Yam et al. [10] employed pendulum model to guide the motion extraction process (see fig.3).

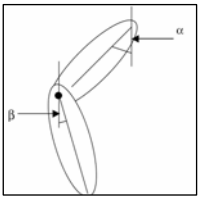

Fig. 3. Connected pendulums model

Urtasum and Fua [11] proposed the 3D temporal models to track and recover motion parameters that could be used to recognize people. Dockstader et al. [12] proposed a hierarchical model which used a set of thick lines joined at a single point to represent the legs and a periodic, pendulum motion model to described the gait pattern (see fig.4).

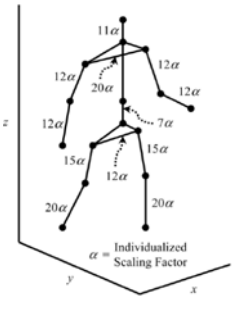

Fig. 4. The hierarchical model

Some approaches directly derive the structural parameters from the gait sequence [13,14]. BenAbdelkader et al. [13] used stride and cadence, which were functions of body height, weight, and gender, for identification and verification of people. Wang et al. [14] employed joint-angle trajectories of lower limbs together with the statistical characteristic for gait recognition.

3 Model-Free Approach

Model-free approach does not need the prior knowledge of the gait model. It compactly represents gait motion of the walking human based on the gait appearance without considering the underlying structure. There have been a lot of model-free approaches proposed in literatures [15-30].

Spatio-temporal approaches generally characterize the spatio-temporal distribution generated by gait motion in its continuum [6,15,16]. Spatio-temporal gait pattern ranges the gait sequence images such as grey-scale images, optical flow images, and binary silhouettes images to characterize the gait motion in 3D space (XYT).

Niyogi and Adelson [6] thought that the head and the legs contained distinctive signatures in XT dimensions (translation and time). In XT dimensions, snakes were used to process different patterns of the head and legs to determine the bounding contours and then a five stick model was fitted [1]. And then, the gait feature was obtained from the fitted model. Finally, their approach obtained a promising result, i.e., the correct classification rate was about 80%. Latter, this work was extended in [17]. They fitted the XYT pattern with a smooth spatio-temporal surface which was approximately periodic, reflecting the periodicity of the gait.

Little and Boyd [18] aimed more to describe features of an optical flow distribution. The shape of motion was the distribution of flow, characterized by several sets of measures of the flow: the moving points and their flow values. The features of the flow in [18] included the centroids and second moments of these distributions which was arranged to form a time series for each scalar. The authors thought that some phase features in the sequences of scalars were consistent for one person and showed significant statistical variation among persons, and the phase feature vectors were used to recognize individuals.

BenAbdelkader et al. [15] proposed an approach that used self-similarity plots (SSP), the same way that face images were used in eigenface-based face recognition techniques, and Principle Component Analysis (PCA) was applied to map the gait data to a lower dimensional space. Though the SSP preserved the dynamics of gait, but it was easily influenced by light and noise.

Hayfron-Acquah et al. [19] proposed a method based on analyzing the symmetry of human motion. The edge-map was obtained by using the Sobel operator on the gait silhouettes and the Generalized Symmetry Operator was then applied to give the symmetry map (see fig.5). The average of all the symmetry maps in a gait silhouette sequence was computed as a gait signature. Another gait signature deriving from the optical flow was proposed in [20]. Further analysis showed that the symmetrical approach was relatively insensitive to noise and it appeared to handle missing spatial data and missing image frames better.

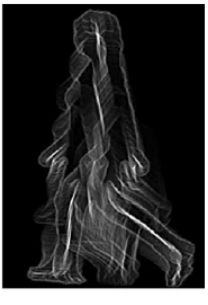

Fig. 5. A symmetry map of a gait silhouette

Han and Bhanu [22] proposed Gait Energy Image (GEI) for gait representation. The intensity of each pixel on GEI revealed the duration of foreground staying at that position. GEI captured both dynamic and static features which represented human motion sequence in a single image. Boulgouris and Chi [21] proposed a feature extraction process. A Radon template was constructed from a sequence of Radon transformed silhouettes and the set of all templates was subsequently subjected to Linear Discriminant Analysis (LDA). Liu and Zheng [23] proposed Gait History Image (GHI) for human gait representation. In [23], GHI was detailedly compared to other temporal templates—Motion Energy Image (MEI), Motion History Image (MHI), Gait Energy Image (GEI). In [24□25], GEI was segmented into several components for gender recognition, and the contributions of different components of the human body were analyzed.

Subspace approaches such as PCA, LDA, etc, have been effectively used for face recognition. They also widely utilized to reduce the dimensionality of the input data in gait recognition systems. Usually, subspace approaches consider gait motion as a static gait sequence [16].

Murase and Sakai [26] calculated eigenvectors from silhouette images with the eigenvalue decomposition. A gait silhouette image could be mapped to a point in the eigenspace spanned by the eigenvectors and a gait trajectory (see fig.6) in the low-dimensional eigenspace was obtained from one gait sequence which was parameterized by time. Then a temporal matching method based upon eigenspace representation was presented to distinguish different gaits. Huang et al. [27] extended the work in [26]. They combined Eigenspace transformation (EST) based on Principal Component Analysis with canonical space transformation (CST) based on Canonical Analysis to offer better separability of different gait sequences. The experimental results showed that the training gait sequences was transformed into widely separated clusters in the new space though the gait database used in the experiment was small.

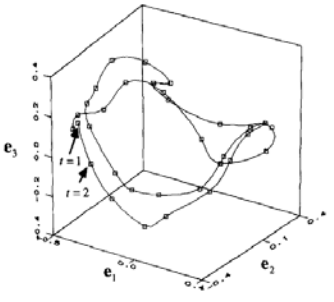

Fig. 6. A trajectory shown in a 3-dimensional eigenspace

Wang et al. developed an eigenspace transformation of an unwrapped human silhouette [28]. The silhouette's boundary was obtained by the border following algorithm and its outer-contour was unwrapped anticlockwise into a set of boundary pixel points (see fig.7). Temporal changes of the detected silhouettes were then represented as an associated sequence of complex vector configurations. The Procrustes shape analysis method was applied to obtain mean shape as gait signature.

The Hidden Markov Model (HMM) was used to capture the information in gait sequence and recognize individual in [29,30]. In [29], one way of gait representation was the width to the outer contour of a binaries silhouette. Frame to exemplar distance (FED) was used to captures a subject's shape and motion. HMM was trained for each person and then gait recognition was performed by evaluating the probability that a given observation sequence was generated by a particular HMM. In [30], Chen et al. employed the Factorial HMM as feature-level fusion scheme to fuse different gait features which was compared with the Parallel HMM decision-level fusion scheme.

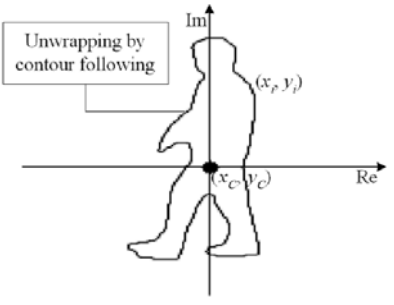

Fig. 7. Illustration of silhouette's unwrapped representation

4 Research Challenges and Future Directions

Compared with other widely used biometric features such as face and fingerprint recognition, gait recognition is still in its infancy [28]. There are several challenging problems for the research and application of gait biometric. 1) Moving object segmentation. Background subtraction technology is usually employed for gait silhouette segmentation. Under outdoor condition, gait silhouette is easily influenced by various sources of variations such as light, noise, shadow, and an adaptation background model is required. 2) Covering handle. Most of the current gait approaches were under the assumption that there was single moving object in a frame which was evidently unreasonable in real application environment. It is unavoidable that part of the human shape even the whole shape is covered in practical application environment. 3) Performance evaluation. Performance evaluation is restricted to the size of gait databases. Usually, not more than 200 persons were included in the existing gait database and the capturing background is simple.

Future directions for gait recognition are generalized based on the current research situation and the existing challenging problems. 1) 3-D modeling and multiple-camera employing. It is more accurate to analysis gait static and dynamic characteristics in 3-D space which is conducive for feature extraction and identification individuals. Multiple-camera capture system not only solves the limitation of the viewpoint, but also helpfully handles the covering challenge. 2) Data fusion. For optimal performance, the system must use as many cues as possible and combine them in meaningful ways. Gait static and dynamic features should be merged together for gait recognition such as [14] and gait biometric should be combined with other biometric. 3) Huge gait

database construction. The current experiments were carried out on a limited number of subjects, which makes the experiments fail in persuasiveness. In order to achieve practical purposes, a new gait database which includes a lager number of subjects and is captured under more complex background environment is needed to test the performance of gait recognition.

References

1. Nixon, M.S., Carter, J.N.: Advances in Automatic Gait Recognition. In: Sixth IEEE International Conference on Automatic Face and Gesture Recognition, Proceedings, pp. 139–144 (2004)
2. Murray, M.P.: Gait as a Total Pattern of Movement. American Journal of Physical Medicine 46(1), 290–332 (1967)
3. Johansso, G.: Visual Perception of Biological Motion and a Model for Its Analysis. Perception & Psychophysics 14(2), 201–211 (1973)
4. Bingham, G., Schmidt, R., Rosenblum, L.: Dynamics and the Orientation of Kinematic Forms in Visual Event Recognition. J. Experimental Psychology: Human Perception and Performance 21(6), 1473–1493 (1995)
5. Sarkar, S., Phillips, P.J., Liu, Z.Y., et al.: The HumanID Gait Challenge Problem: Data sets, Performance, and Analysis. IEEE Trans. Pattern Anal. Mach. Intell. 27(2), 162–177 (2005)
6. Niyogi, S., Adelson, E.: Analyzing and Recognizing Walking Figures in XYT. In: IEEE Computer Society Conference on Computer Vision and Pattern Recognition, Seattle, Wash, USA, pp. 469–474 (1994)
7. Lee, L., Grimson, W.E.L.: Gait Analysis for Recognition and Classification. In: Fifth IEEE International Conference on Automatic Face and Gesture Recognition, Proceedings, pp. 155–162 (2002)
8. Cunado, D., Nixon, M.S., Carter, J.N.: Using Gait as a Biometric, via Phase-Weighted Magnitude Spectra. In: Bigün, J., Borgefors, G., Chollet, G. (eds.) AVBPA 1997. LNCS, vol. 1206, pp. 95–102. Springer, Heidelberg (1997)
9. Yoo, J.H., Nixon, M.S.: Markerless Human Gait Analysis via Image Sequences. In: Proceedings of International Society of Biomechanics XIXth Congress, Dunedin, NZ (2003)
10. Yam, C.Y., Nixon, M.S., Carter, J.N.: Automated Person Recognition by Walking and Running via Model-based Approaches. Pattern Recognition 37(5), 1057–1072 (2004)
11. Urtasun, R., Fua, P.: 3D Tracking for Gait Characterization and Recognition. In: Sixth IEEE International Conference on Automatic Face and Gesture Recognition, Proceedings, pp. 17–22 (2004)
12. Dockstader, S.L., Berg, M.J., Tekalp, A.M.: Stochastic Kinematic Modeling and Feature Extraction for Gait Analysis. IEEE Transactions on Image Processing 12(8), 962–976 (2003)
13. BenAbdelkader, C., Cutler, R., Davis, L.: Stride and Cadence as a Biometric in Automatic Identification and Verification. In: Fifth IEEE International Conference on Automatic Face and Gesture Recognition, Proceedings, pp. 372–377 (2002)
14. Wang, L., Ning, H.Z., Tan, T.N., et al.: Fusion of Static and Dynamic Body Biometrics for Gait Recognition. IEEE Transactions on Circuits and Systems for Video Technology 14(2), 149–158 (2004)
15. BenAbdelkader, C., Cutler, R., Nanda, H., Davis, L.: EigenGait: Motion-based recognition of people using image self-similarity. In: Bigun, J., Smeraldi, F. (eds.) AVBPA 2001. LNCS, vol. 2091, pp. 284–294. Springer, Heidelberg (2001)

16. Wang, L., Tan, T.N., Ning, H.Z., et al.: Silhouette Analysis-based Gait Recognition for Human Identification. IEEE Transactions on Pattern Analysis and Machine Intelligence 25(12), 1505–1518 (2003)
17. Niyogi, S.A., Adelson, E.H.: Analyzing Gait with Spatiotemporal Surface. In: Proc. of IEEE Workshop on Motion of Non-rigid and Articulated Objects, pp. 64–69 (1994)
18. Little, J., Boyd, J.: Recognizing People by Their Gait: The shape of motion. Videre 1(2), 1–32 (1998)
19. Hayfron-Acquah, J.B., Nixon, M.S., Carter, J.N.: Human Identification by Spatio-Temporal Symmetry. In: 16th International Conference on Pattern Recognition, Proceedings, vol. I, pp. 632–635 (2002)
20. Hayfron-Acquah, J.B., Nixon, M.S., Carter, J.N.: Automatic Gait Recognition by Symmetry Analysis. Pattern Recognition Letters 24(13), 2175–2183 (2003)
21. Wagg, D.K., Nixon, M.S.: On Automated Model-Based Extraction and Analysis of Gait. In: Sixth IEEE International Conference on Automatic Face and Gesture Recognition, Proceedings, pp. 11–16 (2004)
22. Han, J., Bhanu, B.: Individual Recognition Using Gait Energy Image. IEEE Transactions on Pattern Analysis and Machine Intelligence 28(2), 316–322 (2006)
23. Liu, J.Y., Zheng, N.N.: Gait History Image: A Novel Temporal Template for Gait Recognition. In: 2007 IEEE International Conference on Multimedia and Expo, vol. 1-5, pp. 663–666 (2007)
24. Yu, S.Q., Tan, T.N., Huang, K.Q., et al.: A Study on Gait based Gender Classification. IEEE Transactions on Image Processing, 1–1 (2009) (accepted for future publication)
25. Li, X.L., Maybank, S.J., Yan, S.C., et al.: Gait Components and Their Application to Gender Recognition. IEEE Transactions on Systems, Man, and Cybernetics, Part C: Applications and Reviews 38(2), 145–155 (2008)
26. Murase, H., Sakai, R.: Moving Object Recognition in Eigenspace Representation: Gait Analysis and Lip Reading. Pattern Recognition Letters 17(2), 155–162 (1996)
27. Huang, P.S., Harris, C.J., Nixon, M.S.: Canonical Space Representation for Recognizing Humans by Gait and Face. In: 1998 IEEE Southwest Symposium on Image Analysis and Interpretation, pp. 180–185 (1998)
28. Wang, L., Tan, T.N., Hu, W.M., et al.: Automatic Gait Recognition Based on Statistical Shape Analysis. IEEE Transactions on Image Processing 12(9), 1120–1131 (2003)
29. Kale, A., Sundaresan, A., Rajagopalan, A.N., et al.: Identification of Humans Using Gait. IEEE Transactions on Image Processing 13(9), 1163–1173 (2004)
30. Chen, C.H., Liang, J.M., Zhao, H., et al.: Factorial HMM and Parallel HMM for Gait Recognition. IEEE Transactions on Systems Man and Cybernetics Part C-Applications and Reviews 39(1), 114–123 (2009)

Fingerprint Enhancement and Reconstruction

Rabia Malik and Asif Masood

Department of Computer Science, Military College of Signals,
National University of Science and Technology, Rawalpindi, Pakistan
rabiamalik.1@hotmail.com, amasood@mcs.edu.pk

Abstract. Generally, the minutiae sent to the final matching phase are extracted from the skeleton images. The accuracy of minutiae extraction depends on the quality of the skeleton image. This paper presents a novel approach of fully reconstructing the fingerprint images besides using the traditional procedures of fingerprint enhancement. The reconstruction would not only improve the quality of the skeleton image but also increase the accuracy of minutiae extraction and improve the recognition results. The proposed algorithm deals with the three quality degrading problems in skeleton images; ridges not being strictly continuous, parallel ridges not being well separated, and finally the ridges not being smooth.

Keywords: Enhancement, reconstruction, minutiae, ridge structure.

1 Introduction

Owing to their universality and uniqueness [1], fingerprints is still the most widely used biometric technology [2]. Having been acquired from various sources and conditions [3], the quality of these fingerprint vary accordingly. The degradation in quality has a direct influence on the minutiae extraction, which in turn has an influence on the recognition results. So a separate branch of fingerprint science has been allocated for improving quality of fingerprints that aims to suggest processes that make systems invariant to changing qualities. Systems that do not account this quality variation problem are restricted to a certain subset of good quality fingerprints, which are not available as a norm [4].

The paper is organized as follows: Section 2 gives an overview of the prevalent quality improvement techniques in literature. Section 3 gives general assumptions for the paper. Section 4 and 5 give an overview of the proposed algorithm while Section 6-9 discusses the proposed reconstruction algorithm in detail. Section 10 and 11 presents the results, contribution of the algorithm and concludes the work.

2 Related Work

The techniques proposed in fingerprint quality improvement are categorized as local or global, both aiming to bring out proper ridge structure. Global techniques aim to improve images using predefined parameters that are applied to area by area of the

D.-S. Huang et al. (Eds.): ICIC 2009, LNAI 5755, pp. 660–669, 2009.

entire image. These techniques mainly try to preserve the parallel structure of the ridges. They may also join some small gaps that happen to come inside the predefined areas, but, if parameters are explicitly adjusted for filling gaps, artifacts are generated that create spurious minutiae. Several works [5-8] have used variations of the traditional Gabor filters [4] that serve to preserve ridge structure. Short time Fourier transform [9] and enhancement in DCT domain [10] have also been successfully used as alternatives. The local techniques too like the global, keep in view the local flow of ridges. Changes are made to the ridges accordingly; missing portions are predicted [11], broken structures are reconnected [12, 13].

Both these categories improve quality till a certain number of minutiae are extracted. Alongside these methods, an additional post-processing phase [14, 15] is required to validate the extracted minutiae, as the quality not being the best possible, may have generated some false feature points. Incidentally only some Fingerprint Identification Systems (not all) have such additional phases. So till present no enhancement algorithm aims to improve fingerprint quality to the maximum possible extent so that minutiae extracted are as accurate as possible. This is what the proposed algorithm aims to do. It reconstructs the image locally alongside an initial global enhancement, ensuring proper extraction of minutiae. This would help not only compensating for absence of a post processing phase but also decreases complexity of the ones present.

3 Assumptions

In the paper, two conventional terms, ridge-ends and bifurcations, are used. These are not to be mixed with minutiae. Though similar in properties, here the terms are to be taken as the control points for the reconstruction process. The conventional terms are used merely for better understanding of the reader.

The reconstruction steps have been designed with the assumption that no previous global enhancement has been done. The algorithm formed keeps in view the poor quality image cases. An initial enhancement would not in any way contribute in degrading the performance of the reconstruction module.

A common assumption for all the processes (except Section 8) in the paper is that the bifurcations and endings found and processed do not include the ones at the boundary of the fingerprint region. A simple way to implement this is: For a binary image where '0' represents the ridge and '1' represents the background, extract all endings and bifurcations. For each end or bifurcation, trace four paths (upward, downward, left or right), till boundary of image is reached. If while tracing, a ridge is crossed i.e. '0' is encountered, then move to the next direction. For an end or bifurcation to satisfy boundary condition, at least one of the traced paths should be all '1' i.e. background.

4 Step 1: Global Enhancement

The ultimate goal of the entire process is to achieve an improved version of skeleton image (Fig 1 (f)). Instead of directly reconstructing a bad quality image, an initial pass from a contextual filter like Gabor filter [4], that preserve ridge structure, renders a

considerably better quality skeleton image to reconstruct. The reconstruction process shall remove the leftover problems of the already enhanced image.

Before the application of Gabor filter, the intensity values of the entire image is equalized to bring to the foreground the ridge structure that may be concealed a part of background. Histogram equalization is preferred over normalization [5] on basis of some results that showed during development of the algorithm. After the enhancement, the image is converted into its binary using an adaptive binarization method [16]. The binarized image is thinned using morphological operation that erodes the ridges till they are one pixel in thickness [17]. The fingerprint region mask is generated [18] which provides another condition besides the boundary condition for the ridge-ends and bifurcations' extraction.

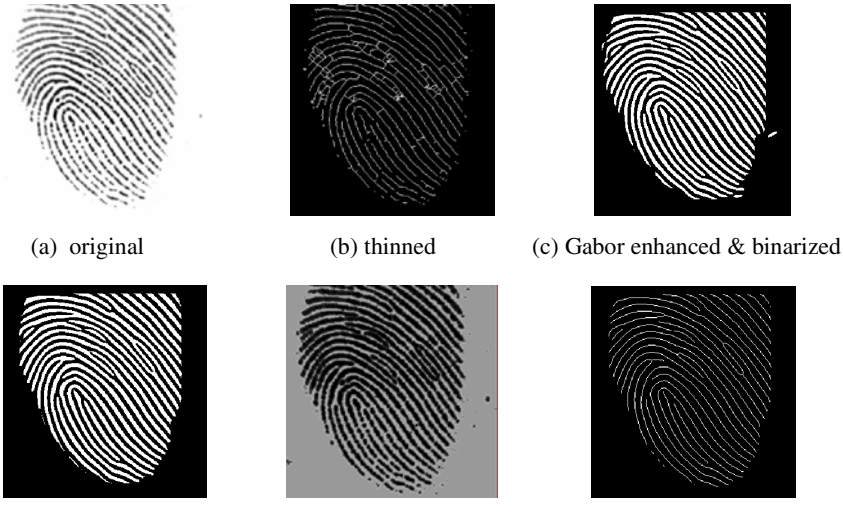

(a) original (b) thinned (c) Gabor enhanced & binarized

(d) segmented (e) histogram equalized (f) thinned after enhancement

Fig. 1. Improved skeleton image through initial enhancement

5 Step 2: Local Reconstruction

The global enhancement algorithm improves quality of a fingerprint image. The skeleton image formed is better than the one without initial enhancement (Fig 1(b),(f)). In spite of improvement in quality, the skeleton image may still have any of the three problems i.e. the ridges may not be parallel, discontinuity in ridges and quiver in the flow of ridges. A further pass of the enhanced image from the proposed local enhancement algorithm will improve the quality of skeleton images subsequently increasing performance of the minutiae extraction process.

5.1 Problems in Skeleton Images

Skeletonized fingerprint images generally face three kinds of problems as shown in Fig 2;

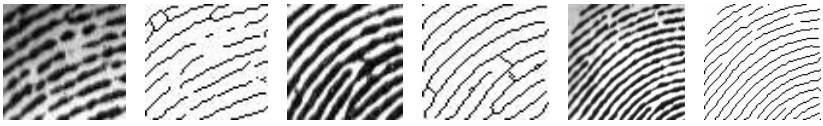

(a) original (b) skeleton (c) original (d) skeleton (e) original (f) skeleton

Fig. 2. Problems in skeleton images; (b) - Ridges may not be continuous, (d) - Ridges may not be parallel, (f) Ridges may not be smooth

The reconstruction process is designed to cater with these three problems. Like any quality improvement technique, the constraint for the reconstruction process is that it does not create any new problem.

5.2 Reconstruction Process

The reconstruction process consists of four steps;

1. Gap filling where the falsely broken ridges are joined
2. Breaking the wrongly connected ridges
3. Smoothing the ridges
4. Filtering the ridges

In the remaining paper, Section 6-9 explains in detail, each of these four reconstruction steps.

6 Gap Filling

The idea of ridge linking is used to join the broken ridges thus filling the gaps. Ridge-ends are extended to join with the nearest, 'most appropriate' ones, the criterion for which is defines by three parameters;

1. the distance between ends
2. the smoothness with which two ridges-ends are linked
3. intersection condition where linking two appropriate ends does not cross path of some third ridge

After finding all ridge-ends in the image, candidate ridge-ends for joining are found for each. This is done by finding a measure for each of the three above mentioned parameters. For each ridge-end find;

1. Its distance from all other ridge-ends. The distance between the points is based on the Euclidean Distance. Say to calculate the distance 'D' between two points P1(x1, y1) and P2(x2, y2), the computation would be:

$$D = \sqrt{(x2 - x1)^2 + (y2 - y1)^2} \quad (1)$$

2. Its smoothness with all other ridge-ends if joined. The smoothness with which two lines join is basically depicted by the angle differences between the existing line and the new line virtually constructed for joining. Two differences are

computed, one for each end, with the new line. Both these differences must lie within a common threshold. This threshold depicts allowable difference in angles, and classifies a join as smooth or not. If the difference is within the defined threshold, then the join is smooth and the joining line may have chances of being actually constructed in the image. If $angle_L$ is the angle of virtually joined line, $angle_{E1}$ and $angle_{E2}$ be the angles of the two existing ends, and T_{angle} be the allowable difference threshold;

$$angle diff_{LE1} = \min\left[abs(angle_L - angle_{E1}), 180 - abs(angle_L - angle_{E1})\right], \tag{2}$$

$$angle diff_{LE2} = \min\left[abs(angle_L - angle_{E2}), 180 - abs(angle_L - angle_{E2})\right], \tag{3}$$

$$angle diff = abs(angle diff_{LE1} - angle diff_{LE2}), \tag{4}$$

$$D = \begin{cases} angle diff & angle diff < T_{angle} \\ dmax & otherwise \end{cases}, \tag{5}$$

where dmax is some very large value. The angles, angle $_{E1}$ and angle $_{E2}$, are found tracing 5 to 6 pixels of the two ridge-ends E1(x1, y1) and E2(x2, y2). For the virtual line L, the angle is computed as;

$$angle_L = tan^{-1}\frac{(y2 - y1)}{(x2 - x1)}. \tag{6}$$

3. Its intersection with all other ridge-ends. For checking the intersection, a virtual line's path is traced between the two ends E1(x1, y1) and E2(x2, y2). If on the estimated path some other ridge part happens to be present, the condition accounts for an intersection. The line's path (x, y) is estimated as:

$$y = mx + c \quad where \quad m = \frac{(y2 - y1)}{(x2 - x1)}, \quad c = y1 - x1(m), \quad x = x1 \; to \; x2, \tag{7}$$

$$x = \frac{(y - c)}{m} \quad where \quad m = \frac{(y2 - y1)}{(x2 - x1)}, \quad c = y1 - x1(m), \quad y = y1 \; to \; y2. \tag{8}$$

These above three parameters are found for each ridge-end with respect to all other ridge-ends. The joining probability of the ridge-end to all others is found. The ridge-end is joined with candidate with the highest probability. Some simple rules for calculating this probability are:

1. A candidate which lies closest to the ridge under process, and when joined with gives the lowest change in angles i.e. line formed by joining is smooth, has a higher probability than the ones far away with the same smoothness.
2. Similarly, the joins at a smaller distance but abrupt change in angles have a lower probability than a join formed with an end further away but has a smoother join.

Keeping the above rules into consideration for calculating probability, weights have been assigned to the two parameter, distance and smoothness (angle difference). The calculated probability however comes into effect only when the joining ends do not intersect some ridge while being joined.

Suppose, 'P' is the joining probability of a candidate ridge-end, 'D' is the distance of a candidate from current ridge, 'A' is the angle difference, 'W_d' and 'W_a' are the weights assigned to distance and angle difference respectively. Then for calculating the probability, we take,

$$P_{i,j} = I_{i,j}(W_a A_{i,j} + W_d D_{i,j}) where \quad W_a + W_d = 1, \quad I_{i,j} = \{0,1\}, \tag{9}$$

In actual P, A, D and I are four symmetric matrices, where each row and column represents each ridge-end. Fig 3 shows the working of the joining methodology. The ridge-end A joins with B, as the distance of A from B is shortest, the join is smooth (angle differences with new line are nominal) and joining the two points does not cut any other ridge.

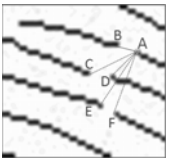

Fig. 3. Ridge end A joins with the most appropriate B

7 Breaking the Wrongly Connected Ridges

For the incorrectly joined ridge, three parameters are used for disconnecting as shown in Figure 9;

1. The distance
2. The connectedness
3. The orientation of bifurcations

For each bifurcation, the candidate bifurcations that may have chances of being wrongly joined to the current bifurcation are extracted. This is done by tracing each of the three or four arms that join to form a bifurcation. The tracing is done within a certain distance. This distance is taken to be the average inter-ridge distance of the fingerprint (explained at end of Section). If another bifurcation is met within this distance while traversing any of the arms, then the condition of being wrongly connected is checked for this pair of candidate bifurcations. For this, the angle 'A' (Fig 4) of the connecting line is found. Around the midpoint 'M' of this connecting line, a window (16x16 pixels) is constructed and a global orientation in the window is computed. If the difference between the local angle of the connecting line and the global angle of the window is nominal i.e. within an angle difference threshold (nearly parallel), then the connecting line remains as it is. However, for greater angle differences i.e. greater than the threshold (nearly perpendicular), the line connecting the two candidate bifurcations is removed.

For each window, the Least Square approximation of the window direction is achieved as,

$$tg2\beta = 2\frac{\Sigma\Sigma(g_x\, g_y)}{\Sigma\Sigma({g_x}^2 - {g_y}^2)}, \tag{10}$$

where g_x and g_y are the gradient values along x and y direction for each pixel in the window.

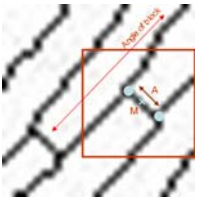

Fig. 4. Portion of skeleton image showing difference in angle of connecting line and angle of block

The inter-ridge distance is computed by taking a random window (16x16) on the fingerprint region where there are no ridge ends and bifurcations. An angle normal to the general orientation in the window is computed. And according to this angle, a line is traced across the region of fingerprint under the window. The points in the window where this line intersects with the ridges are extracted. An average distance between the adjacent intersecting points is computed. This distance is the inter-ridge distance for the fingerprint region under the window. The whole routine is carried out at two to three random regions in fingerprint and an average of all the distances give the inter-ridge distance of the fingerprint. The local and global angles computed lie in the range of 0 to 180. Equation (2) is used for estimating the angle differences.

8 Smoothing the Ridges

Generally the skeleton images formed depict a non smooth structure of ridges. This may create problems when doing some ridge pattern based analysis or when extracting minutiae, where the orientation is also saved along with the position of minutiae. Normally for smoothing of lines, an averaging method is used, wherein the new curved line formed deviates considerably from the path of the original curve. To overcome this, binomial smoothing is used where path traced by the original curve is lost to the minimum.

All ridges and bifurcations are found. Curves are extracted according to two rules and smoothened individually.

1. Curve that starts from a ridge-end and ends on a bifurcation or another ridge-end
2. Curves that start from a bifurcation and end on another bifurcation

The smoothing of ridges renders a visual improvement in quality of the fingerprint and is expected to render better line estimation towards the ridge ends and bifurcations. This may be helpful in the Minutiae Extraction step wherein orientation too is extracted.

9 Filtering the Ridges

In a binary skeleton image there may be several undesirable projections from the ridges (Fig 5) that occur due to low quality of images. This may result in generating spurious minutiae in the feature extraction phase. To remove these undesirable protrusions two parameters are used;

1. the property of connectedness
2. the distance

A tracing algorithm is devised that starts by extracting all ridge-ends and bifurcations in the image. From each ridge end, the length of the ridge is traced, till one-third of the inter-ridge distance. If within this distance another ridge-end or a bifurcation appears, then the traversed ridge is removed i.e. made part of the background.

(a) non-filtered image (b) filtered image

Fig. 5. Skeleton image after filtering

10 Results

The proposed quality improvement approach was tested on fingerprint images from FVC2002 [19]. Matching technique using hough transform [20] was used to generate the matching score. The recognition results were noted for enhanced images without the reconstruction process and then with the reconstruction process.

Table 1. Sample results; with and without reconstruction

Matched Image	Score (without)	No. of matches (without)	Score (with)	No. of matches (with)
101_2	23.9046	2	84.8668	11
101_4	66.8648	13	75.5929	12
101_8	27.3861	3	77.8981	14
102_2	44.5435	10	42.1464	9
102_8	44.0959	7	25.2861	5
103_6	54.4331	12	15.7135	2
103_8	73.0297	12	36.98	4
104_5	33.9683	3	27.2727	6

Table 1 shows a sample of the tests performed. In this sample, the enhanced version of 101_1.tif from the FVC2002 DB1_B is taken as reference image. Minutiae of fingerprints from database were matched with the minutiae extracted from this reference image. Table 1 shows some results (score towards 100 represents a better match).

It was observed that the reconstruction process not only increased the number of matched minutiae of same class but it also increased the matching score in some cases. In some cases, though the number of matched minutiae decreased, but an overall increase in matching score was noticed. No case was found where the reconstruction process degraded the recognition results. Table 2 gives the results for FVC2002 DB1_B. Total testing images taken were 80, making 6400 matches. The proposed reconstruction algorithm improved the recognition results. Fig 6 shows the visual results of the reconstruction process.

Table 2. Performance evaluation of proposed algorithm

Results with	Accuracy	FAR	FRR
Enhancement	505 (78.9%)	408 (7.1%)	135 (21%)
Enhancement + Reconstruction	540 (84%)	302 (5.2%)	100 (15.6%)

11 Conclusion and Future Work

The paper proposed a technique for improving quality of the skeleton image of a fingerprint. As ultimately for the phase of matching the minutiae are extracted from the skeleton image, so improving the quality of skeleton image improves accuracy of minutiae extraction, thereby generating less false points for the matching algorithm to match.

The technique is useful for those systems that do not have a mature post-processing phase. Owing to the reconstruction algorithm, the complexity of post-processing phase can be greatly reduced, maybe confined to only removing minutiae from the boundary. Performance evaluation of the algorithm against various matching algorithms is part of the future work.

(a) Original Skeleton (b) After joining (c) After disjoining (e) After smoothing (d) After filtering

Fig. 6. The steps of the reconstruction process (no initial enhancement)

References

1. Jain, A.K., Pankanti, S.: Beyond Fingerprinting: Is Biometrics the Best Bet for Fighting Identity Theft. Scientific American Magazine, 4 (September 2008)
2. International Biometric Group: Biometrics Market and Industry Report 2009-2014 (October 2008)
3. Maltoni, D., Maio, D., Jain, A.K., Prabhakar, S.: Handbook of Fingerprint Recognition. Springer, New York (2003)
4. Hong, L., Wang, Y., Jain, A.K.: Fingerprint Image Enhancement: Algorithm and Performance Evaluation. IEEE Trans. on Pattern Analysis and Machine Intelligence 20(8), 777–789 (1998)
5. Akram, M.U., Tariq, A., Khan, S.A., Nasir, S.: Fingerprint image: pre- and post-processing. International Journal of Biometrics 1(1), 63–80 (2008)
6. Wang, W., Li, J., Huang, F., Feng, H.: Design and implementation of Log-Gabor filter in fingerprint image enhancement. Pattern Recognition Letters 29(3), 301–308 (2008)
7. Porwik, P., Więcław, Ł.: A new efficient method of fingerprint image enhancement. International Journal of Biometrics 1(1), 36–46 (2008)
8. Areekul, V., Watchareeruetai, U., Tantaratana, S.: Fast separable gabor filter for fingerprint enhancement. In: Zhang, D., Jain, A.K. (eds.) ICBA 2004. LNCS, vol. 3072, pp. 403–409. Springer, Heidelberg (2004)
9. Chikkerur, S., Cartwright, A.N., Govindaraju, V.: Fingerprint Enhancement Using STFT Analysis. Pattern Recognition 40, 198–211 (2007)
10. Jirachawang, S., Areekul, V.: Fingerprint Enhancement Based on Discrete Cosine Transform. In: International Conference on Bioinformatics, pp. 96–105 (2007)
11. Rahmes, M., Allen, J.D., Elharti, A., Tenali, G.B.: Fingerprint Reconstruction Method Using Partial Differential Equation and Exemplar-Based Inpainting Methods. In: Biometrics Symposium, September 11-13, pp. 1–6 (2007)
12. Oliveira, M.A.D., Leite, N.J.: Reconnection of Fingerprint Ridges Based on Morphological Operators and Multiscale Directional Information. In: Proc. of XVII Brazilian Symposium on Computer Graphics and Image Processing, pp. 122–129 (2004)
13. Park, S., Smith, M.J.T., Lee, J.J.: Fingerprint enhancement based on directional filter bank. In: Proceedings of 2000 International Conference on Image Processing, vol. 10-13, pp. 793–796 (2000)
14. Feng, Z., Xiaoou, T.: Preprocessing and postprocessing for skeleton-based fingerprint minutiae extraction. Pattern Recognition 40(4), 1270–1281 (2007)
15. Xiao, Q., Raafat, H.: Fingerprint image postprocessing: a combined statistical and structural approach. Pattern Recognition 24(10), 985–992 (1991)
16. `http://homepages.inf.ed.ac.uk/rbf/HIPR2/adpthrsh.htm`
17. Lam, L., Lee, S.W., Suen, C.Y.: Thinning Methodologies-A Comprehensive Survey. IEEE Transactions on Pattern Analysis and Machine Intelligence 14(9), 879 (1992)
18. Chikkerur, S., et al.: Systematic approach for feature extraction in Fingerprint Images. In: International Conference on Biometric Authentication (2004)
19. Second International Fingerprint Verification Competition (2002), `http://bias.csr.unibo.it/fvc2002/`
20. Afsar, F.A.: Fingerprint based person identification and verification (2005), `http://fayyazafsar.googlepages.com/Afsar-Thesis-2ud.pdf`

A Level Set Based Segmentation Method for Images with Intensity Inhomogeneity

Xiao-Feng Wang[1,2,3] and Hai Min[1,3]

[1] Intelligent Computing Lab, Hefei Institute of Intelligent Machines, Chinese Academy of Sciences, P.O. Box 1130, Hefei Anhui 230031, China
[2] Key Lab of Network and Intelligent Information Processing, Department of Computer Science and Technology, Hefei University, Hefei Anhui 230022, China
[3] Department of Automation, University of Science and Technology of China, Hefei Anhui 230027, China
xfwang@iim.ac.cn

Abstract. In this paper, an efficient hybrid level set (HLS) model is proposed for segmenting the images with intensity inhomogeneity, which is a difficult problem for traditional region-based level set methods. The total energy functional for the proposed model consists of three terms, i.e., global term, local term and regularization term. By incorporating the local image information into the proposed model, the images with intensity inhomogeneity can be efficiently segmented. In addition, the time-consuming re-initialization step widely adopted in traditional level set methods can be avoided by introducing a penalizing energy. Finally, experiments on some synthetic and real images have demonstrated the efficiency and robustness of the proposed model.

Keywords: Image segmentation, Intensity inhomogeneity, Hybrid level set model.

1 Introduction

Image segmentation is an important step in image analysis since the segmentation result directly affects the performance of the subsequent processing steps. Up to now, a wide variety of algorithms have been proposed to solve the image segmentation problem. Researchers have also done great efforts to improve the performance of the image segmentation.

Active contour model, proposed by Kass et al. [1], has been proved to be an efficient framework for image segmentation. Level set method is based on active contour model and particularly designed to handle the segmentation of deformable structures. It uses a deformable curve front for approximating the boundary of an object. In the level set framework, the curve is represented by the zero level set of a smooth function, usually called the level set function. Moving the curves can be done by evolving the level set functions instead of directly moving the curves. Therefore, level set methods can efficiently handle the topological changes which is also a main advantage compared with classical active contour model.

D.-S. Huang et al. (Eds.): ICIC 2009, LNAI 5755, pp. 670–679, 2009.

It should be mentioned that the early edge-based level set methods [2-4] usually depend on the gradient of the given image to stop the evolution of the curve. Therefore, these methods can only detect objects with edges defined by the gradient. However, the corresponding discrete gradients are generally bounded and the energy functional will hardly approach zero on the boundaries in practice. So, the evolving curve may pass through the true boundaries, especially for the models in [2-4].

Recently, region-based level set methods [5-8] have been proposed and applied to image segmentation field by incorporating region-based information into the energy functional. Unlike edge-based level set methods using image gradient, region-based methods usually utilize the global region information to stabilize their responses to local variations (such as weak boundaries and noise). Thus, they can obtain a better performance of segmentation than edge-based level set methods, especially for images with weak object boundaries and noise. Among the region-based methods, Chan-Vese model [5] is a representative and popular one.

CV model has achieved good performance in image segmentation task due to its ability of obtaining a larger convergence range and handling topological changes naturally. However, it still has the intrinsic limitation, i.e., it generally works for images with intensity homogeneity. The reason is due to that the intensities in each region are assumed to maintain constant. Thus, it often leads to poor segmentation results for images with intensity inhomogeneity due to wrong movement of evolving curves guided by global image information.

In this paper, we proposed a hybrid level set (HLS) model which utilizes both global image information and local image information for image segmentation. The energy functional for the proposed model consists of three parts: global term, local term and regularization term. Moreover, the time-consuming re-initialization step widely adopted in traditional level set methods can be avoided by introducing a penalizing energy to the regularization term. The experimental results show that the proposed HLS model can successfully segment images with or without intensity inhomogeneity.

The rest of this paper is organized as follows: In Section 2, we briefly review the problem of intensity inhomogeneity. The proposed hybrid level set (HLS) model is presented in Section 3. In Section 4, the proposed model is validated by some experiments on synthetic and real images. Finally, some conclusive remarks are included in Section 5.

2 Intensity Inhomogeneity

Intensity inhomogeneity usually arises from the imperfect factors of acquisition process for ordinary images or medical images, such as non-uniform daylight and artificial illumination**,** static field inhomogeneity, radio-frequency excitation field nonuniformity and inhomogeneity of reception coil sensitivity, etc. These inhomogeneities are known to appear in images as systematic changes in the local statistical characteristics of target object. Although the presence of intensity inhomogeneity is usually hardly noticeable to a human observer, many image processing methods, including image segmentation methods, are highly sensitive to the spurious variations of image intensities since they are based on the assumptions that the intensities in each region are constant.

The generally accepted assumption on intensity inhomogeneity is that it manifests itself as a smooth spatial varying function over the image [9]. The most common model in describing the acquired images $X^{'}$ with intensity inhomogeneity effect is:

$$X^{'} = BX + N \,, \tag{1}$$

where X is the inhomogeneity-free image, B denotes the intensity inhomogeneity field and N is the noise. To simplify the computation, the noise is often ignored. Also, there have been theoretical modeling approaches to approximate the intensity inhomogeneity field. However, due to the complexity that causes the intensity inhomogeneity, it is difficult for ones to model the intensity inhomogeneity under a variety of image acquisition conditions [10].

Since the intensity inhomogeneity is slowly varying in the image domain, its spectrum in frequency domain will be concentrated in the low-frequency area. Thus, the intensity inhomogeneity effect mainly influences the non-contour pixels in the image, whereas for the pixels belonging to contour, this influence is less. Motivated by this observation, we proposed incorporating the local statistical information into the level set method for segmenting the images with intensity inhomogeneity effect. It should be noted that we do not try to eliminate the intensity inhomogeneity from the images which is still not a completely solved problem [10].

3 Hybrid Level Set Model

In this Section, we shall present and discuss the details of our proposed hybrid level set (HLS) model and its numerical implementation. The overall energy functional consists of three parts: global term E^G, local term E^L and regularization term E^R.

3.1 Global Term

The global term E^G is directly derived from the fitting term of the Chan-Vese model [5]. It can be seen that the global term is defined based on the global properties, i.e., the intensity averages c_1 and c_2 of u_0 inside and outside the boundary C.

$$E^G(c_1, c_2, C) = F_1(C) + F_2(C) = \int_{inside(C)} \left|u_0(x,y) - c_1\right|^2 dxdy + \int_{outside(C)} \left|u_0(x,y) - c_2\right|^2 dxdy \,, \tag{2}$$

Using the level set formulation, the boundary C is represented by the zero level set of a Lipschitz function $\phi : \Omega \to R$.

$$\phi(x,y)\begin{cases} > 0 & \text{if (x,y) is inside } C \\ = 0 & (x,y) \in C \\ < 0 & \text{if (x,y) is outside } C \end{cases} . \tag{3}$$

Accordingly, the global term in (2) can be rewritten so as to evaluate the level set function ϕ on the domain Ω:

$$E^G(c_1,c_2,\phi)=\int_\Omega |u_0(x,y)-c_1|^2 H(\phi(x,y))dxdy+\int_\Omega |u_0(x,y)-c_2|^2 (1-H(\phi(x,y)))dxdy \quad (4)$$

where $H(z)$ is the Heaviside function.

Usually, after (4) comes to a steady state, or approximately to be zero, the evolving curve C (zero level set of ϕ) will separate the object from the background. However, for the images with intensity inhomogeneity, the final obtained curve C can hardly divide the image into object region and background region even after a long iteration time. The reason is that the global term assumes that the image intensity is piecewise constant like the CV model. Thus, the averages c_1 and c_2 actually act as the global information and can not represent the inhomogeneous intensities of object region and background region in the images with intensity inhomogeneity. So, to achieve a good performance in segmenting the images with intensity inhomogeneity, the local image information needs to be included.

3.2 Local Term

Here, the local term is introduced in (5) which uses the local statistical information as the key to improve the segmentation capability of our model on the images with intensity inhomogeneity.

$$E^L(d_1,d_2,C)=\int_{inside(C)} |g_k * u_0(x,y)-u_0(x,y)-d_1|^2 dxdy+\int_{outside(C)} |g_k * u_0(x,y)-u_0(x,y)-d_2|^2 dxdy, \quad (5)$$

where g_k is a averaging convolution operator with $k\times k$ size window. d_1 and d_2 are the intensity averages of difference image $(g_k * u_0(x,y)-u_0(x,y))$ inside C and outside C, respectively.

The assumption behind the proposed local term is that smaller image regions are more likely to have approximately homogeneous intensity and the intensity of the object is statistically different from the background. It is significative to statistically analyze each pixel with respect to its local neighborhood. The most simple and fast statistical information function is the average of the local intensity distribution, the rationale being that if the object pixels are brighter than the background, they should also be brighter than the average. By subtracting the original image from the averaging convolution image, the contrast between foreground intensities and background intensities can be significantly increased. Note that the difference image $(g_k * u_0(x,y)-u_0(x,y))$ with higher image contrast is still not easily to be segmented due to the weak object boundaries and complicated topological structure. It needs under a level set evolution for obtaining better segmentation result. In the same manner as global term, the local term (5) can also be reformulated in terms of the level set function $\phi(x,y)$ as follows:

$$\begin{aligned} E^L(d_1,d_2,\phi)=&\int_\Omega |g_k * u_0(x,y)-u_0(x,y)-d_1|^2 H(\phi(x,y))dxdy \\ &+\int_\Omega |g_k * u_0(x,y)-u_0(x,y)-d_2|^2 (1-H(\phi(x,y)))dxdy. \end{aligned} \quad (6)$$

3.3 Regularization Term

In order to control the smoothness of the zero level set and further avoid the occurrence of small, isolated regions in the final segmentation, we add to the regularization term a length penalty term which is defined related to the length of the evolving curve C. Here, through replacing the curve C by the level set function $\phi(x, y)$, the length penalty term can be reformulated as:

$$L(\phi = 0) = \int_{\Omega} \left| \nabla H(\phi(x, y)) \right| dxdy = \int_{\Omega} \delta(\phi(x, y)) \left| \nabla \phi(x, y) \right| dxdy . \tag{7}$$

The use of length penalty term implies that the evolving curve C which minimizes the overall energy functional should be as short as possible. It imposes a penalty on the length of the curve that separates the two phases of image, i.e., foreground and background, on which the energy functional will make a transition from one of its values, $c1$ ($d1$), to the other, $c2$ ($d2$).

Re-initialization has been extensively used as a numerical remedy for maintaining stable curve evolution and ensuring desirable results in the level set methods. Unfortunately, it is obviously a disagreement between the theory of level set method and its implementation, since it has an undesirable side effect of moving the zero level set away from its original location. Moreover, it is quite complicated and time-consuming, and when and how to apply it is still a serious problem [11].

In this paper, we did not directly use the re-initialization step to keep the level set function as a signed distance function but add to the regularization term a penalty term [12] as follows:

$$P(\phi) = \int_{\Omega} \frac{1}{2} (\left| \nabla \phi(x, y) - 1 \right|)^2 . \tag{8}$$

which can force the level set function to be close to a signed distance function. Actually, this penalty term is more like a metric which characterizes how close a function ϕ is to a signed distance function. The metric plays a key role in the elimination of re-initialization in our method.

So, in the proposed model, the regularization term E^R should be composed of two terms:

$$\begin{aligned} E^R(\phi) &= \mu \cdot L(\phi = 0) + P(\phi) \\ &= \mu \cdot \int_{\Omega} \delta(\phi(x, y)) \left| \nabla \phi(x, y) \right| dxdy + \int_{\Omega} \frac{1}{2} (\left| \nabla \phi(x, y) - 1 \right|)^2 , \end{aligned} \tag{9}$$

where μ is the parameter which can control the penalization effect of length term: if μ is small, then smaller objects will be detected; if μ is larger, then larger objects are detected.

3.4 Level Set Formulation

In the level set formulation, the curve C is represented by the zero level set of a Lipschitz function ϕ. The overall energy functional can be described as follows:

$$
\begin{aligned}
E^{HLS}(c_1,c_2,d_1,d_2,\phi) &= \int_{\Omega}(\alpha\cdot|u_0(x,y)-c_1|^2+\beta\cdot|g_k*u_0(x,y)-u_0(x,y)-d_1|^2)H_\varepsilon(\phi(x,y))dxdy \\
&+\int_{\Omega}(\alpha\cdot|u_0(x,y)-c_2|^2+\beta\cdot|g_k*u_0(x,y)-u_0(x,y)-d_2|^2)(1-H_\varepsilon(\phi(x,y)))dxdy \\
&+(\mu\cdot\int_{\Omega}\delta_\varepsilon(\phi(x,y))|\nabla\phi(x,y)|dxdy+\int_{\Omega}\frac{1}{2}(|\nabla\phi(x,y)-1|)^2),
\end{aligned}
\tag{10}
$$

where α and β are two positive parameters which govern the tradeoff between the global term and the local term. g_k is the averaging convolution operator with $k\times k$ size window for local information detection. $H_\varepsilon(z)$ is the noncompactly supported, smooth and strictly monotone approximation of $H(z)$ and $\delta_\varepsilon(z)$ is the regularized approximation of $\delta(z)$ which are respectively computed by:

$$
H_\varepsilon(z)=\frac{1}{2}\left|1+\frac{2}{\pi}\arctan\left|\frac{z}{\varepsilon}\right|\right|,\quad \delta_\varepsilon(z)=\frac{1}{\pi}\cdot\frac{\varepsilon}{\varepsilon^2+z^2}. \tag{11}
$$

By calculus of variations, it can be shown that the constant functions $c1(\phi)$, $c2(\phi)$, $d1(\phi)$ and $d2(\phi)$ that minimize $E^{HLS}(c_1,c_2,d_1,d_2,\phi)$ for a fixed function ϕ are given by:

$$
c_1(\phi)=\frac{\int_{\Omega}u_0(x,y)H_\varepsilon(\phi(x,y))dxdy}{\int_{\Omega}H_\varepsilon(\phi(x,y))dxdy},\ c_2(\phi)=\frac{\int_{\Omega}u_0(x,y)(1-H_\varepsilon(\phi(x,y)))dxdy}{\int_{\Omega}(1-H_\varepsilon(\phi(x,y)))dxdy}. \tag{12}
$$

$$
d_1(\phi)=\frac{\int_{\Omega}(g_k*u_0(x,y)-u_0(x,y))H_\varepsilon(\phi(x,y))dxdy}{\int_{\Omega}H_\varepsilon(\phi(x,y))dxdy}. \tag{13}
$$

$$
d_2(\phi)=\frac{\int_{\Omega}(g_k*u_0(x,y)-u_0(x,y))(1-H_\varepsilon(\phi(x,y)))dxdy}{\int_{\Omega}(1-H_\varepsilon(\phi(x,y)))dxdy}. \tag{14}
$$

Keeping $c1$, $c2$, $d1$ and $d2$ fixed, and minimizing the overall energy function E^{HLS} in (10) with respect to ϕ, we can deduce the associated Euler–Lagrange equation for ϕ. The minimization of (10) can be done by introducing an artificial time variable $t\geq 0$, and moving ϕ in the steepest descent direction to a steady state with the initial condition defined in (16) and boundary condition defined in (17):

$$
\begin{aligned}
\frac{\partial\phi}{\partial t} &= \delta_\varepsilon(\phi)[-(\alpha\cdot(u_0-c_1)^2+\beta\cdot(g_k*u_0(x,y)-u_0(x,y)-d_1)^2) \\
&+(\alpha\cdot(u_0-c_2)^2+\beta\cdot(g_k*u_0(x,y)-u_0(x,y)-d_2)^2)] \\
&+[\mu\cdot\delta_\varepsilon(\phi)div(\frac{\nabla\phi}{|\nabla\phi|})+(\nabla^2\phi-div(\frac{\nabla\phi}{|\nabla\phi|}))],
\end{aligned}
\tag{15}
$$

$$\phi(0, x, y) = \phi_0(x, y) \; in \; \Omega \,, \tag{16}$$

$$\frac{\partial \phi}{\partial \vec{n}} = 0 \; on \; \partial\Omega \,, \tag{17}$$

where $\vec{n}$ denotes the exterior normal to the boundary $\partial\Omega$.

In fact, α and β should be set according to the intensity inhomogeneity presenting in the images. For images without intensity inhomogeneity, the value of α is suggested to be near or equal to that of β. If images present distinct intensity inhomogeneity, the value of α should be selected less than that of β so as to restrict the intensity inhomogeneity. It should be noticed that the case of $\alpha = 0$ may be acceptable in segmenting some images. However, it is not suggested since the global term can sometimes have a restriction effect on noise and maintain the boundary details. In our experiments, we usually fixed $\beta = 1$ and then dynamically adjusted the value of α according to the intensity property of images.

The partial differential equation in the continuous domain defined in (15) can be solved by a finite difference method in numerical scheme. All the spatial partial derivatives are approximated by the central difference and the temporal partial derivatives are approximated by the forward difference as follows:

$$\begin{aligned} \frac{\phi_{i,j}^{n+1} - \phi_{i,j}^{n}}{\Delta t} = \delta_\varepsilon(\phi_{i,j}^{n})\{&-(\alpha \cdot (u_{i,j} - c_1(\phi^n))^2 + \beta \cdot (g_k * u_{i,j} - u_{i,j} - d_1(\phi^n))^2) \\ &+ (\alpha \cdot (u_{i,j} - c_2(\phi^n))^2 + \beta \cdot (g_k * u_{i,j} - u_{i,j} - d_2(\phi^n))^2)\} \\ &+ [\mu \cdot \delta_\varepsilon(\phi_{i,j}^{n})\kappa + (\phi_{i+1,j}^{n} + \phi_{i-1,j}^{n} + \phi_{i,j+1}^{n} + \phi_{i,j-1}^{n} - 4\phi_{i,j}^{n} - \kappa)] \,, \end{aligned} \tag{18}$$

where Δt is the time-step and h is the grid spacing. Curvature κ can be discretized using a second-order central differencing scheme:

$$\kappa = div(\frac{\nabla \phi}{|\nabla \phi|} = \frac{\phi_{xx}\phi_y^2 - 2\phi_{xy}\phi_x\phi_y + \phi_{yy}\phi_x^2}{(\phi_x^2 + \phi_y^2)^{3/2}} \,. \tag{19}$$

4 Experimental Results

In this Section, we shall present the experimental results of our hybrid level set (HLS) model on some synthetic and real images. The proposed model was implemented by Matlab 7 on a computer with Intel Core 2 Duo 2.2GHz CPU, 2G RAM, and Windows XP operating system. The processing time referred later in this section starts after choosing the initial contour. We used the same parameters of the time-step $\Delta t = 0.1$, the grid spacing $h = 1$, $\varepsilon = 1$ (for $H_\varepsilon(z)$ and $\delta_\varepsilon(z)$), $\mu = 0.01 * 255^2$, the window size of averaging convolution operator $k = 15$ for all the experiments in this section. As described in Section 3.4, we fixed $\beta = 1$ and dynamically adjusted the value of

α. In our experiments, α has two corresponding values: 0.1 and 1 for images with/without intensity inhomogeneity.

We firstly considered the simplest case: segmentation of images with the intensity homogeneity. Fig.1 shows the segmentation of a noisy synthetic image using the proposed HLS model. The robustness property of our model is due to the usage of global term and length penalty term. To show the high efficiency of our model, the initial contour was placed at the bottom left corner (as shown in Fig.1 (b)) unlike other methods in which the initial contour was usually placed in the center of images or touches the target objects. It can be seen from Fig.1 (c), the evolving curve successfully reach the true boundary of flower shape after 25 iterations.

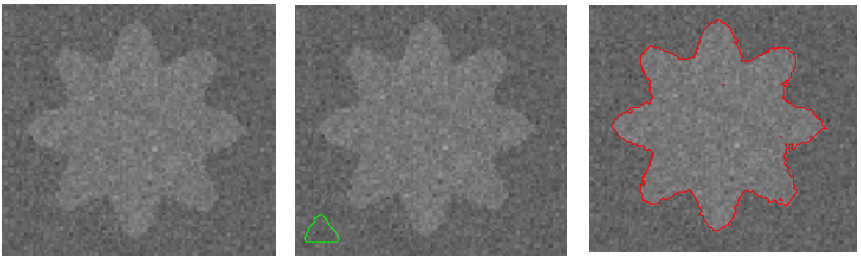

(a) (b) (c)

Fig. 1. Noisy synthetic image segmentation using the proposed HLS model. (a) Original noisy image. (b) Initial contour. (c) Final segmentation result at the 25^{th} iteration. Size= 98×90, $\alpha=\beta=1$. Processing time = 2.6s.

In the next two experiments (Fig.2 and Fig.3), we shall illustrate the ability of the proposed HLS model to segmenting images with the intensity inhomogeneity. Fig.2 shows the segmentation results for the well-known synthetic image using both the CV model and the proposed HLS model. It can be seen from Fig.2 (a) that the intensity decreases gradually from the left to the right. The initial contour was placed at the intersectional region of high intensity area and low intensity area, as shown in Fig.2 (b). The failing segmentation of this synthetic image using the CV model is illustrated in Fig.2(c), which shows that the evolving curve of the CV model can not pass through the intersectional region of high intensity area and low intensity area even after 100 iterations. Fig.2 (d) shows the segmentation result of the HLS model where the evolving curve of the HLS model can successfully reach the boundary of object after 15 iterations. Here, the value of the controlling parameter $\alpha=0.1$ is less than that of $\beta=1$ to maintain a restriction effect on the intensity inhomogeneity.

Fig.3 shows the segmentation results for two real blood vessel images with the intensity inhomogeneity using both the CV model and the proposed HLS model. It can be seen from the third column of Fig.3 that the CV model failed to segment both two images with the intensity inhomogeneity as we anticipated. The reason is due to the inherent disadvantage of not using the local information. The fourth column of Fig.3 shows that the proposed HLS model can successfully segment the images in the first column. It should be noticed that the iteration times will be efficiently decreased if the initial contours are placed on certain part of the objects.

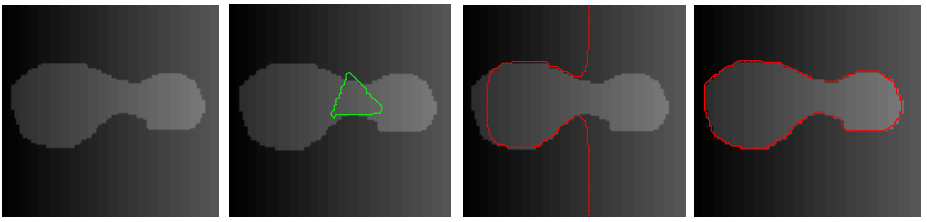

(a) (b) (c) (d)

Fig. 2. The comparisons of the CV model and the proposed HLS model on segmenting a synthetic image with the intensity inhomogeneity. (a) Original image. (b) Initial contour. (c) Final segmentation result using the CV model. (d) Final segmentation result using the proposed HLS model. Size= 88×85 , $\alpha=0.1$, $\beta=1$. Processing time=5.3s (CV), 0.9s (HLS).

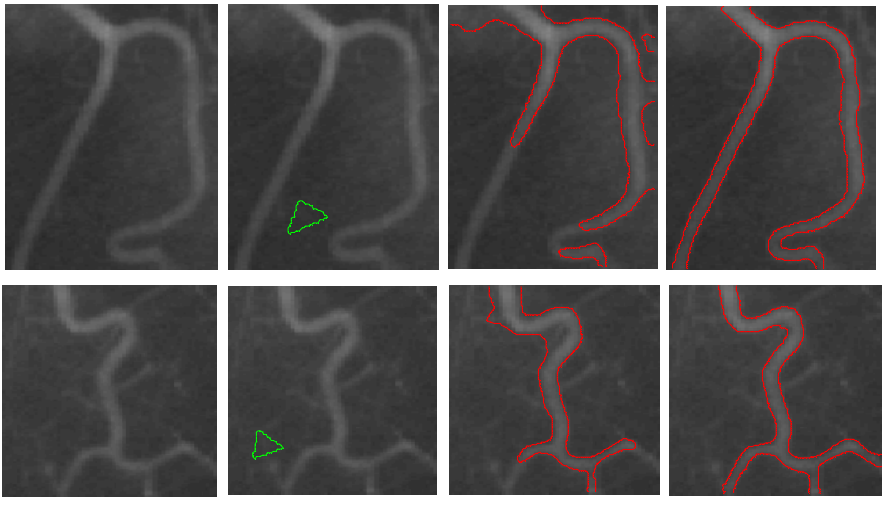

Fig. 3. The comparisons of the CV model and the proposed HLS model on segmenting two real blood vessel images with the intensity inhomogeneity. The first column: Original images. The second column: Initial contours. The third column: Final segmentation results using the CV model. The fourth column: Final segmentation results using the proposed HLS model. Size= 103×131 , 110×110 . $\alpha=0.1$, $\beta=1$.

5 Conclusions

In this paper, we propose a new hybrid level set (HLS) model for segmenting the images with intensity inhomogeneity. The total energy functional for the proposed model consists of global term, local term and regularization term. By incorporating the local image information into the proposed model, the images with intensity inhomogeneity can be efficiently segmented. To avoid the time-consuming re-initialization step, a penalizing energy is introduced into the regularization term. Finally, experiments on some synthetic and real images have demonstrated the desired segmentation performance of our proposed model for the images with or without intensity inhomogeneity.

Acknowledgments. This work was supported by the grants of the National Science Foundation of China, Nos. 60873012 & 60805021, the grant from the National Basic Research Program of China (973 Program), No.2007CB311002, the grant from the National High Technology Research and Development Program of China (863 Program), No. 2007AA01Z167, the grant of the Graduate Students' Scientific Innovative Project Foundation of CAS (X.F. Wang).

References

1. Kass, M., Witkin, A., Terzopoulos, D.: Snakes: Active contour models. Int. J. Comput. Vision 1(4), 321–331 (1987)
2. Caselles, V., Catte, F., Coll, T., Dibos, F.: A Geometric Model for Active Contours in Image Processing. Numer. Math. 66(1), 1–31 (1993)
3. Caselles, V., Kimmel, R., Sapiro, G.: Geodesic Active Contours. Int. J. Comput. Vision 22(1), 61–79 (1997)
4. Malladi, R., Sethian, J.A., Vemuri, B.C.: Shape Modeling with Front Propagation: A Level Set Approach. IEEE Trans. Patt. Anal. Mach. Intell. 17(2), 158–175 (1995)
5. Chan, T.F., Vese, L.A.: Active Contours without Edges. IEEE Trans. Image Processing 10(2), 266–277 (2001)
6. Tsai, A.Y., Willsky, A.S.: Curve Evolution Implementation of the Mumford-Shah Functional for Image Segmentation, Denoising, Interpolation, and Magnification. IEEE Trans. Image Processing 10(8), 1169–1186 (2001)
7. Paragios, N., Deriche, R.: Geodesic Active Regions and Level Set Methods for Supervised Texture Segmentation. Int. J. Comput. Vision 46(4), 223–247 (2002)
8. Gao, S., Bui, T.D.: Image Segmentation and Selective Smoothing by Using Mumford–Shah Model. IEEE Trans. Image Processing 14(10), 1537–1549 (2005)
9. Vovk, U., Pernuš, F., Likar, B.: A Review of Methods for Correction of Intensity Inhomogeneity in MRI. IEEE Trans. Med. Imag. 26(3), 405–421 (2007)
10. Hou, Z.J.: A Review on MR Image Intensity Inhomogeneity Correction. International Journal of Biomedical Imaging 2006, 1–11 (2006)
11. Gomes, J., Faugeras, O.: Reconciling Distance Functions and Level Sets. J. Visiual Communic. and Imag. Representation l(11), 209–222 (2000)
12. Li, C.M., Xu, C.Y., Gui, C.F., Fox, M.D.: Level set Formulation without Re-initialization: A New Variational Formulation. In: Proc. IEEE International Conference on Computer Vision and Pattern Recognition (CVPR 2005), vol. 1, pp. 430–436 (2005)

Analysis of Enterprise Workflow Solutions

Cui-e Chen[1], Shulin Wang[2], Ying Chen[1], Yang Meng[1], and Hua Ma[3]

[1] Changsha Social Work College, Changsha, Hunan, 410004, China
[2] School of Computer and Communication, Hunan University, Changsha, Hunan, 410082, China
[3] Hunan International Economics University, Changsha, Hunan, 410082, China
chins2000@163.com

Abstract. Since the 90's, workflow technology has been widely applied in various industries, such as office automation(OA), manufacturing, telecommunications services, banking, securities, insurance and other financial services, research institutes and education services, and so on, to improve business process automation and integration capabilities. In this paper, based on Workflow theory, the author proposed a set of policy-based workflow approach in order to support dynamic workflow patterns. Through the expansion of the functions of Shark, it implemented a Workflow engine component-OAShark which can support retrieval / rollback function. The related classes were programmed. The technology was applied to the OA system of an enterprise project. The realization of the enterprise workflow solutions greatly improved the efficiency of the office automation.

Keywords: Workflow, dynamic workflow, workflow pattern, office automation, Shark.

1 Introduction

Enterprise solutions, such as online shopping process (start -> browser -> options -> payment -> collection -> end), printing business processes (receiving and preparing documents -> proof -> make-up and ready to print -> RIP and printing -> post-processing -> archive -> printing business -> provide chain management), and issued business processes in office automation (OA) (in Fig.1) (draft -> review -> check -> sign -> issued -> reviewed circulation -> proof -> No maintenance -> archive -> form red head document), and so on, pursuit " shorter life cycle, less turn-around time, less cost, and higher cost-effective". "Better, faster and more inexpensive" hardware is of course important, but it is not the ultimate solution for enterprises. There is a growing concern about the operation of business processes, from the initial demand of the users to the service of the final product. The use of the same resource with more production, is to improve the efficiency of the entire process, and is the key to obtain more profit. To obtain such efficiency, the method is guaranteed a reasonable and logical business processes path, at the same time as much as possible to increase the degree of automation and process integration, and this is all the contents of the workflow.

D.-S. Huang et al. (Eds.): ICIC 2009, LNAI 5755, pp. 680–687, 2009.

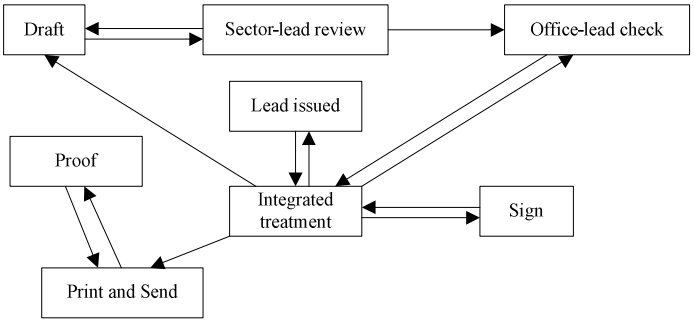

Fig. 1. Issued business processes in OA

2 Basic Concepts on Workflow

2.1 The Origin of Workflow

The concept of workflow was proposed in 1968 by Fritz Nordsieck. From the 70's to 80's, workflow technology was in research. In early workflow systems, only a few have been successful. After the 90's, as the technical conditions were mature, research and development of workflow systems came into a new craze. In August, 1993, the industry organization of standardization of workflow technology - Workflow Management Coalition (WfMC) was established. Workflow Management Coalition issued a workflow reference model which cooperates between workflow management systems and had formulated a series of industry standards, in 1994. Thus, workflow technology has been widely applied in various industries, such as office automation, manufacturing, telecommunications services, the consumer goods industry, banking, securities, insurance and other financial services, logistics services, property services, large and medium-sized import and export trade companies, government utilities, research institutes and education services, especially in large multinational enterprises, and so on.

2.2 The Definition of Workflow

Workflow Management Coalition references the definition of workflow [1]: Workflow is concerned with the automation of procedures where documents, information or tasks are passed between participants according to a defined set of rules to achieve, or contribute to, an overall business goal. Whilst workflow may be manually organised, in practice most workflow are normally organised within the context of an IT system to provide computerised support for the procedural automation and it is to this area that the work of the Coalition is directed. In short, the workflow is the series of operational activities or tasks which are interrelated and automatically carried out. We can consider the entire business as a river, the water which is flowing through the workflow.

The working efficiency of many companies is very low, using manual transmission mode with paper forms from a signature-level approval. It can not realize statistic report forms. By using workflow software, the user can simply fill out the relevant forms on his/her computer. The person at the next level of approval will receive the relevant information and may modify, track, manage, query, count, or print if necessary. They can obtain greater efficiency, realize the knowledge management, and enhance the company's core competitiveness.

2.3 Workflow Management System

The definition of the workflow management system given by the Workflow Management Coalition is [1]: A system that completely defines manages and executes workflows through the execution of software whose order of execution is driven by a computer representation of the workflow logic. A Workflow Management System is one which provides procedural automation of a business process by management of the sequence of work activities and the invocation of appropriate human and/or IT resources associated with the various activity steps.

Workflow management system is not a business system, but a software supporting environment provided for business systems. It can benefits the businesses as the following: improving and optimization of business processes to improve operational efficiency, achieving better control of business processes to improve customer service quality, improving flexibility of business processes, etc.

2.4 Workflow Engine

Workflow engine [2-3] is the core of workflow management system. It’s responsible for the execution of various process instances. It provides the core solutions to the transmission route of information and the content of level in accordance with different of role, division of labour and conditions which play a decisive role on application system. In recent years, a large number of workflow engines have emerged, such as Enhydra Shark, Gray Fox Willow, Osworkflow, Ofbiz, Xi'an synergy, etc.

3 Workflow Patterns

3.1 Basic Control Workflow Patterns

In the workflow modelling, workflow pattern [4] is usually considered as a prototype. A prototype pattern of the workflow can be used to test the performance of the workflow server capacity, that is, how the workflow meets the business needs. Professor Petri studied 21 kinds of workflow patterns [5-6] based on the principle of Petri nets for workflow modelling and analysis. There are five basic control workflow patterns mainly: Sequence workflow pattern, Parallel Split workflow pattern, Synchronization workflow pattern, Exclusive Choice workflow pattern, Simple Merge workflow pattern in Fig.2.

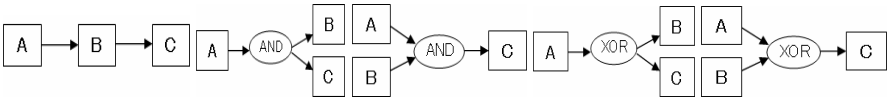

(1) Sequence (2) Parallel Split (3) Synchronization (4) Exclusive Choice (5) Simple Merge

Fig. 2. Basic control workflow pattern

3.2 Dynamic Workflow Patterns

Because of the uncertainty and variability of modern business process, workflow management system needs to have the flexibility and dynamic processing power, so the work has led to a dynamic flow study[7-8]. If a workflow management system supports to modify the running workflow process instance, we call this system a dynamic workflow system. Meanwhile, the workflow which has been modified is called dynamic workflow. In order to support the dynamic changes and flexible control in workflow, we need to increase operations (insert, delete, modify, Jump back, back, etc.) for the procedure of work process and organization model, and rules for related operating.

The dynamic characteristics of workflow are illustrated in Fig. 3, which is an "approval" process. The rollback list is ("draft") when the activities execute to the "trial". The rollback list is empty when the activities execute to "review 1". The rollback list is ("review 1") when the activities execute to "review 3". When the activities execute to "review 7" the rollback list is ("review 3", "review 4", "review 1"). The same token, when the activities execute to "review 8" the rollback list is ("review 5", "audit 6", "review 2"). When the activities execute to "general review" the rollback list is ("draft", "sent"). From this figure we know that the approval process include the five basic control workflow patterns and dynamic pattern for rollback.

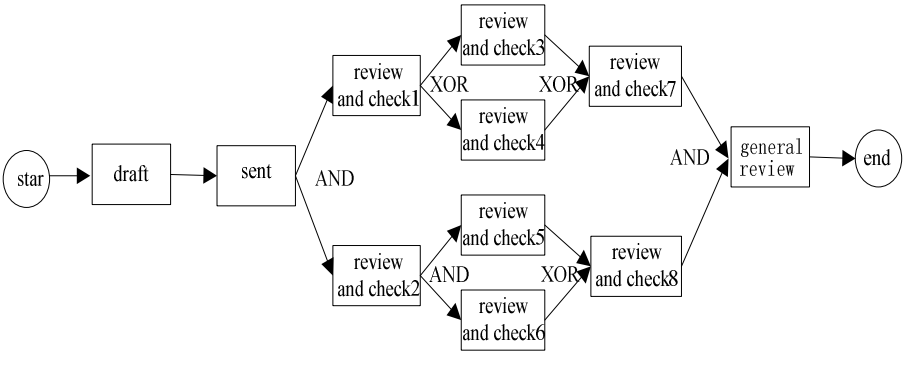

Fig. 3. "Approval" flowchart

4 Shark-Based Dynamic Workflow Strategy Set

4.1 Dynamic Workflow Based on Strategy Set

In order to achieve the support of dynamic workflow pattern, a workflow method is proposed based on static and dynamic strategy set, shown in Fig. 4.

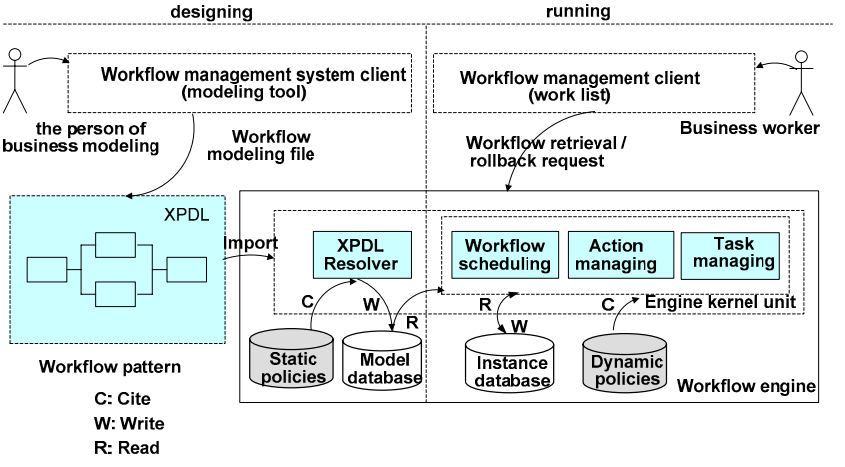

Fig. 4. The workflow method based on static and dynamic strategy set

4.2 Analysis of Instances

An instance based on static strategy set is shown in Fig. 5. An instance based on the dynamic strategy set is shown in Fig. 6.

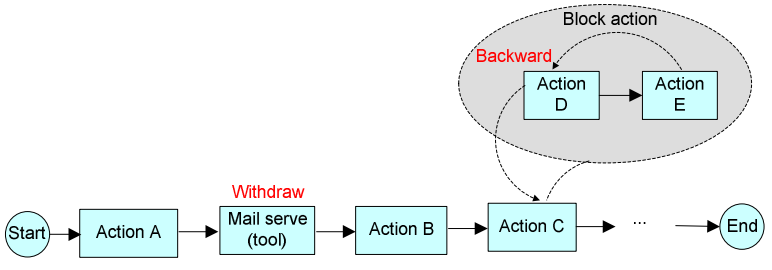

Fig. 5. An instance based on static strategy set

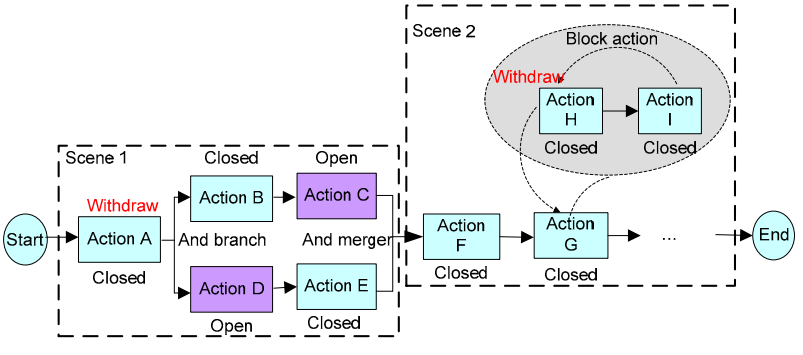

Fig. 6. An instance based on the dynamic strategy set

5 The Application Approach of Enterprise Workflow

5.1 System Architecture

The OA system is designed and developed to improve the office efficiency and accuracy. The system's main function includes: document processing, file management, personal secretary of subsystems, public information management, administrative office management, system management, etc. Since there are a large number of business flow relations between the modules, workflow applications is inevitable. The OA system was built with Shark-based workflow technology, thus it can obtain better system flexibility and dynamic characteristics. The architecture of the system is shown in Fig. 7.

As shown in Fig. 7, OA system modules (document flow, administrative logistics, personal information and information portal) are built on the "workflow engine" components. The workflow engine mainly realizes the core functions such as process control, resource scheduling, task distribution, and meets the practical needs of the system through developing open resource Shark workflow engine. The "workflow engine" unified and coordinated these five basic components that include a unified user management, system management, Web content management, e-mail system and the Domino / Notes, etc. These components were formed by a number of general-purpose modular of website and office automation system. We can quickly developed office automation systems and portal systems on the basis of these six components, according to different circumstances.

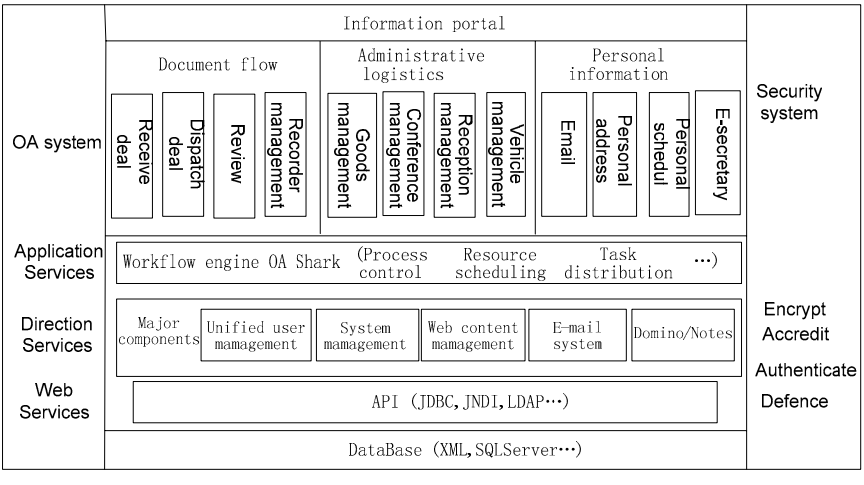

Fig. 7. OA system architecture

5.2 The Component Model of Shark Workflow Engine

A recovery / rollback process management was added on the workflow framework. It can manage recovery / rollback processes, which include accessing the rollback list, the implementation of rollback, workflow affair and data consistency. In the process of recovery / rollback, the affairs characteristics of business data should be guaranteed. So the operation of the business data and recovery / rollback operation of the processes are putted into the affairs in order to ensure the overall affairs characteristics of the

recovery / rollback. For this reason a recovery / rollback data manager was added. Through the extended functions of Shark, a Workflow engine component-OAShark which can support retrieval / rollback function has been implemented, the component model of which is shown in Fig. 8.

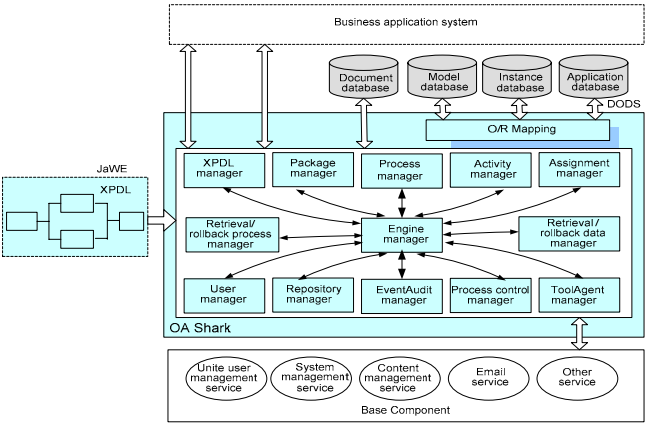

Fig. 8. Workflow engine component model supporting the retrieval / rollback

5.3 ActivityBackward Class

The workflow system only needs to provide a method of rollback activities, on the system of the business point of view, to implement the access control of recovery and rollback. A class of special deal with the activities of rollback has been created: ActivityBackward.java, which was called by the core class of engine to achieve recovery / rollback functions. Description of the class diagram is shown in Fig. 9.

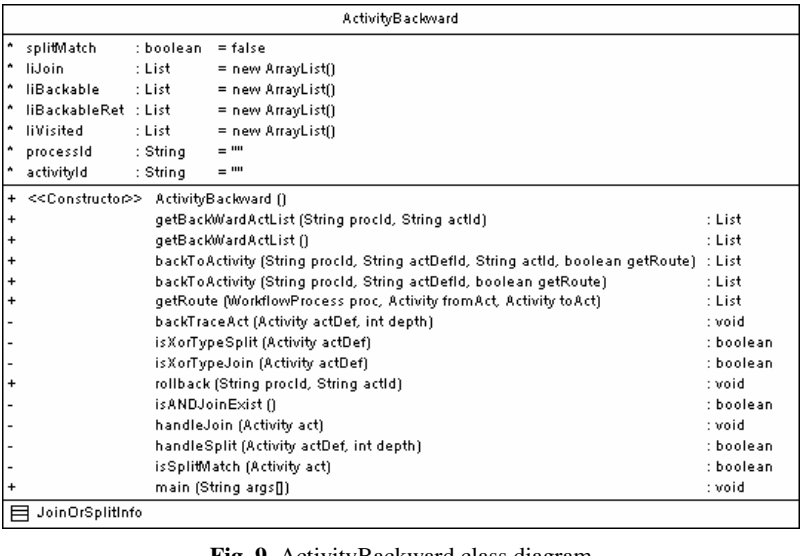

Fig. 9. ActivityBackward class diagram

6 Conclusions

In this paper, workflow pattern, dynamic workflow, Shark open source workflow engine based on the current workflow technology has been studied previously, in order to achieve the flexibility and dynamic characteristics of the workflow. A set of strategy-set-based workflow approaches have been achieved. Through the extended functions of Shark, solutions to the problems that how the recover / rollback needs dynamic support were found. The technology was applied to the OA system of an enterprise project. After the project has developed, it was put into operation to achieve the desired goal. The system is running stable.

References

[1] Fan, Y.H., Luo, H.B., Lin, H.P., et al.: Workflow management technology infrastructure, pp. 28–78. Tsinghua University Publisher, Springer Publisher, Beijing (2001)
[2] Wang, H.J., Fan, L.Q., Yang, L.F., Feng, Y.D., Cai, Y.: Research on Shark-based workflow process solution. Mechanical Engineering & Automation 2, 28–31 (2005)
[3] Wan, D.S., Yu, C.H.: Design and implementation of distributed workflow system based on shark system. Microelectronics and Computer 22(2), 96–99 (2005)
[4] Zhang, L., Yao, S.Z.: Research on workflow patterns based on Petrinets. Computer Integrated Manufacturing Systems (CIMS) 12(1), 54–58 (2006)
[5] Workflow Patterns, http://is.tm.tue.nl/research/patterns/patterns.htm
[6] Swaminathan, V.: Amazing Race analogy. The Architecture Journal 4(7), 8–15 (2006), http://msdn.microsoft.com/en-us/architecture/bb410935.aspx
[7] Mulle, J.A., Bohm, K., Roper, N., Sunder, T.: Building conference proceedings requires adaptable workflow and content management. In: Proceedings of the 32nd international conference on very large data bases, pp. 1129–1139 (2006)
[8] Chen, C.E.: Research and application of retrieval / rollback dynamic workflow pattern based on shark system. Application of Computer Systems 10, 85–87 (2007)

Cooperative Spectrum Sensing Using Enhanced Dempster-Shafer Theory of Evidence in Cognitive Radio

Nguyen-Thanh Nhan, Xuan Thuc Kieu, and Insoo Koo*

School of Electrical Engineering, University of Ulsan 680-749 San 29, Muger 2-dong, Ulsan, Republic of Korea
iskoo@ulsan.ac.kr
http://mcsl.ulsan.ac.kr

Abstract. Cooperative is an appropriate method for improving the performance of spectrum sensing when cognitive radio system is under the deep shadowing and fading environment. The Dempster-Shafer theory of evidence for fusion has similar reasoning logic with human. Thus an enhanced scheme for cooperative spectrum sensing based on an enhanced Dempster-Shafer Theory of Evidence is proposed in this paper. Our scheme utilizes the signal to noise ratios to evaluate the degree of reliability of each local spectrum sensing terminal on a distributed Cognitive Radio network to adjust the sensing data more accuratly before making fusion by Dempter-Shafer theory of evidence. Simulation results show that significant improvement of the cooperative spectrum sensing gain is achieved.

Keywords: Cognitive radio, Cooperative spectrum sensing, Data fusion, Dempter-Shafer theory of evidence.

1 Introduction

Recently, Cognitive Radio (CR) has been proposed as a promising technology to improve spectrum utilization. In order to exploit licensed bands, which are underutilized either temporally or spatially, Cognitive Radio users (CU), unlicensed users, must have capability of sensing the spectrum environment. CUs are allowed to use the licensed bands opportunistically when such bands are not occupied, and must abandon its contemporary band to seek for the new idle spectrum again when the frequency band is suddenly accessed by the licensed user (LU). Therefore the key role of Cognitive Radio is played by spectrum sensing. Generally, spectrum sensing can be achieved by a single CU. The detection techniques often used in local sensing are energy detection, matched filter and cyclostationary feature detection [1], [2]. In [1], it is showed that the receiver signal strength could be seriously weakened at a particular geographical location due to multi-path fading and shadow effect. On these circumstances, single sensing

* Corresponding author.

D.-S. Huang et al. (Eds.): ICIC 2009, LNAI 5755, pp. 688–697, 2009.

node is difficult to distinguish between an idle band and a deep fade one. In order to overcome this problem, cooperative spectrum sensing has been considered [5], [8], [10]. It uses a distributed detection model to solve the severe decadent of receiver signal strength at some location of the network. In distributed detection, a diversity of cooperative spectrum sensing scheme has been studied. Reference [8] proposes an optimal half-voting rule. However this rule only works well when all the threshold of CUs is identical, this is not regularly proper in practice. In [10], the optimal data fusion rule, which was first mention in [9] by Z. Chair and P. K. Varshney, combinning with a counting rule which is use for estimating the probability of detection and probability false alarm as [11], [12] has been proposed to obtain an adaptive cooperative spectrum sensing scheme. Although it gives a good performance, it needs a time to respond when the system is changed. In [5] a method to improve cooperative gain by combining both decisions and credibility of all the sensing nodes via Dempster-Shafer theory of evidence (D-S theory) is proposed. Nevertheless, under the practice condition of distributed cooperative spectrum sensing in CR context that there are a lot of conflict data, the D-S theory has showed a problem under such condition which has been mention in many studies [6], [7], [13].

In this paper, we proposed an enhanced cooperative spectrum sensing scheme based on D-S theory and reliability source evaluation. Compared with Bayesian theory the D-S theory feels closer to natural decision making logic of human. Its capability to assign uncertainty or ignorance to propositions is a powerful tool for dealing with a large range of problems that otherwise would seem intractable, especially in the case of the fast changing RF environment of CR network. The combination rule of evidence theory supplies a method to merge all of the mass function which has the similar meaning of credibility of each CUs sensing decision. Therefore, the mass function sent from sensing node has a very important role to the final decision. So we propose a new appropriate method to obtain it from source. Furthermore the credibility of each sensing node can be more accurate if they have been measured on the same scale. In other word, the credibility should have an adjustment based on the measurement relationship between nodes. From this aspect, we propose a *Reliability Source Evaluation* that utilizes all of available information to obtain an adjustment weight that quantifies the measurement correlation in order to enhance the performance of the fusion scheme.

The rest of this paper is organized as follows. In Section 2, we describe the system model briefly. Section 3 illustrates the evidence theory and its problem. In Section 4, we develop our proposal for an enhanced cooperative spectrum sensing scheme. In Section 5, the simulation results are shown and analyzed. Finally, we conclude this paper in the last section.

2 System Description

For LU detection, we consider the cooperative spectrum sensing scheme like figure 1.

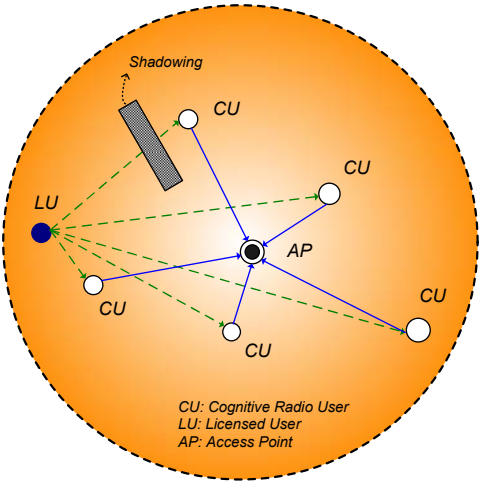

Fig. 1. Cooperative spectrum sensing scheme

Each CU conducts its local sensing process, calculates and estimates some necessary information that will be transmitted to AP. At AP, the final decision will be made. Generally, the whole process of the scheme includes two steps:

- Local spectrum sensing at CU
- Data fusion at AP

2.1 Local Spectrum Sensing

Each Cognitive Radio user (CU) conducts a spectrum sensing process, which is called local spectrum sensing in distributed scenario for detecting Licensed User's (LU) signal. Local spectrum sensing is essentially a binary hypotheses testing problem:

$$\begin{cases} H_0 : x(t) = n(t) \\ H_1 : x(t) = h(t)\, s(t) + n(t) \end{cases} \tag{1}$$

where H_0 and H_1 are respectively correspondent to hypotheses of absence and presence of LU's signal, $x(t)$ represents received data at CU, $h(t)$ denotes the amplitude gain of the channel, $s(t)$ is the signal transmitted from the primary user and $n(t)$ is the additive white Gaussian noise. Additionally, channels corresponding to different CUs are assumed to be independent, and further, all CUs and LUs share common spectrum allocation.

2.2 Energy Detection

Among various methods for spectrum sensing, energy detection has shown that it is quite simple, quick and possible to detect primary signal - even if the feature is unknown. Here we consider the energy detection for local spectrum sensing. Figure 2 shows the block diagram of energy detection scheme.

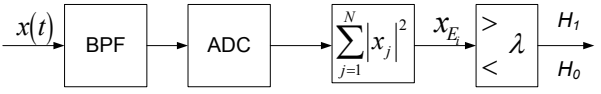

Fig. 2. Block diagram of energy detection scheme

To measure the signal power in particular frequency region in time domain, a band-pass filter is applied to the received signal and the power of signal samples is then measured at CU. The test statistic is equivalent to an estimation of received signal power which is given at each CU by:

$$x_E = \sum_{j=1}^{N} |x_j|^2 \tag{2}$$

where x_j is the j-th sample of received signal and $N = 2TW$ where T and W are correspondent to detection time and signal bandwidth in Hz, respectively. When N is relatively large (e.g. $N > 200$), x_E can be well approximated as a Gaussian random variable under both hypotheses H_1 and H_0 , with mean μ_1 , μ_0 and variance σ_1^2 ,σ_0^2 respectively [3] such that

$$\begin{cases} \mu_0 = N & \sigma_0^2 = 2N \\ \mu_1 = N(\gamma + 1) & \sigma_1^2 = 2N(2\gamma + 1) \end{cases} \tag{3}$$

where γ is the signal to noise ratio (SNR) of the primary signal at the CU.

3 The Dempster-Shafer Theory of Evidence

The D-S theory was first introduced by Dempster in 1960's, and was later extended by Shafer. In D-S theory, a representation of ignorance is provided by assigning a non-zero mass function to hypotheses m, also called the basic probability assignment, is defined for every hypothesis A, such that the mass value $m(A)$ belongs to the interval $[0, 1]$ and satisfies the following conditions:

$$m : \begin{cases} m(\emptyset) = 0 \\ \sum m(A) = 1 \quad A \subseteq \Theta \end{cases} \tag{4}$$

where, Θ is the framework of discernment, a fixed set of q mutually exclusive and exhaustive elements. Assigning a non-zero mass to a compound hypothesis $A \cup B$ means that we have an option not to make the decision between$A$ and B but leave it in the $A \cap B$ class. In D-S theory, two functions named belief (Bel) and plausibility (Pls) are defined to characterize the uncertainty and the support of certain hypotheses. Bel measures the minimum or necessary support whereas Pls reflects the maximum or potential support for that hypothesis. These two

measures, derived from mass values, are respectively defined as a map from set of hypotheses to interval[0, 1]:

$$Bel\,(A) = \sum_{B \subseteq A} m\,(B) \tag{5}$$

$$Pls\,(A) = \sum_{B \cap A \neq \emptyset} m\,(B) \tag{6}$$

Mass function from different information sources,$m_j\,(j = 1, ..., d)$ are combined with Dempsters rule, also called orthogonal sum. The result is a new mass function,$m\,(A_k) = (m_1 \oplus m_2 \oplus ... \oplus m_d)\,(A_k)$ which incorporates the joint information provided by the sources as follows:

$$m\,(A_k) = (1 - K)^{-1} \times \sum_{A_1 \cap A_2 ... A_d = A_k} \left(\prod_{1 \leqslant j \leqslant d} (m_j\,(A_j)) \right) \tag{7}$$

$$K = \sum_{A_1 \cap A_2 ... A_d = \emptyset} \left(\prod_{1 \leqslant j \leqslant d} (m_j\,(A_j)) \right) \tag{8}$$

where K is often interpreted as a measure of conflict between the different sources and is introduced as a normalization factor. The larger K is the more the sources are conflicting and the less sense has their combination. The factor K indicates the amount of evidential conflict. If $K = 0$, this shows complete compatibility, and if $0 < K < 1$, it shows partial compatibility. The orthogonal sum does not exist when $K = 1$. In this case the sources are totally contradictory, and it is no longer possible to combine them. In the cases of sources highly conflicting, the normalization used in the Dempster combination rule can be mistaking, since it artificially increases the masses of the compromise hypotheses. Such case is actually possible in our circumstance where there are a lot of difference environment conditions between sources. It is necessary to make some enhancement for combination rule as suggestion in [7],[13].

4 Cooperative Spectrum Sensing Ultilizing Enhanced D-S Theory of Evidence at AP

For LU detection, we consider an enhanced cooperative spectrum sensing scheme like figure 3. After local spectrum sensing process, each CU calculates and estimates some necessary information and transmits the data to data fusion center where the final decision is made.

4.1 Basic Probability Assignment Estimation

In order to apply D-S theory of evidence to make the final decision, the frame of discernment A is defined as $\{H_1, H_0, \Omega\}$, where Ω denotes either hypotheses is

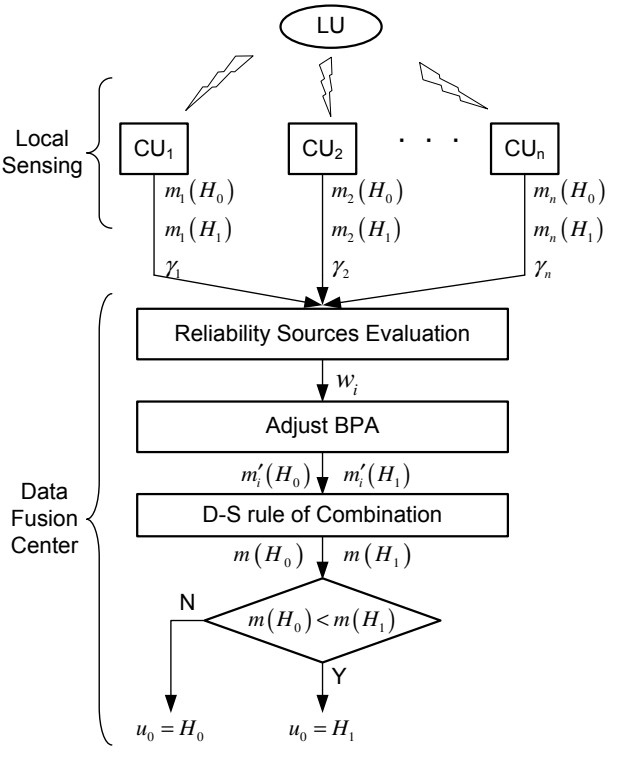

Fig. 3. Enhanced cooperative spectrum sensing scheme

true. After sensing time, each CU will estimate its self-assessed decision credibility which is equivalent to basic probability assignment (BPA) for two hypotheses. We propose a more appropriate BPA function as a form of the cumulative density function instead of probability density function [5] as follows:

$$m_i(H_0) = \int_{x_{E_i}}^{+\infty} \frac{1}{\sqrt{2\pi}\sigma_{0i}} e^{\left(-\frac{(x-\mu_{0i})^2}{\sigma_{0i}^2}\right)} dx \tag{9}$$

$$m_i(H_1) = \int_{-\infty}^{x_{E_i}} \frac{1}{\sqrt{2\pi}\sigma_{1i}} e^{\left(-\frac{(x-\mu_{1i})^2}{\sigma_{1i}^2}\right)} dx \tag{10}$$

where $m_i(H_0)$, $m_i(H_1)$ is respectively the BPA of hypotheses H_0 and H_1 of the i-th CU, respectively. Using these function, the BPA of hypotheses H_0 and H_1 are unique for each test statistics value x_{E_i} and vary in such a way that the larger x_{E_i} is the larger $m_i(H_1)$ and the smaller $m_i(H_0)$ are and vice versa.

4.2 Reliability Source Evaluation

Instead of combining all the CUs' self-assessed BPA which means treating all nodes equally, the BPA of each CU should be adjusted by relative relationship of reliability between nodes for more accuracy. The lower weight is allocated the less reliability to the CUs sensing data is, and vice verses. Subsequently, we propose an enhancing stage to the fusion center called *Reliability Source Evaluation*.

The reliability of CUs sensing information should be evaluated under considering of relative relationship with other CUs on the system. From this aspect, we consider again all of available information to obtain an adjustment weight with which we can quantify the measurement relationship between nodes.

From the fact that the BPA of both hypotheses of each CU depends on the value of test statistic, its mean, and variance and that the more distance between two means value of both hypotheses is, the more reliability the source should be assigned, we utilize the distance between two means value of both hypotheses, D_i

$$D_i = \mu_{1i} - \mu_{0i} \tag{11}$$

D_i is subsequently calculated by substituting (3) into (6)

$$D_i = N(\gamma_i + 1) - N = N\gamma_i \tag{12}$$

where γ_i is SNR of primary signal at the i-th CU. Finally, the weight w_i of the i-th CU is obtained by normalizing the distance:

$$w_i = \frac{D_i}{\max\limits_i (D_i)} = \frac{N\gamma_i}{\max\limits_i (N\gamma_i)} = \frac{\gamma_i}{\max\limits_i (\gamma_i)} \tag{13}$$

4.3 Data Fusion

The BPA of the i-th CU for both hypotheses $m_i(H_0)$ and $m_i(H_1)$ are adjusted with corresponding weight w_i as follows:

$$\begin{cases} m_i'(H_0) = w_i m_i(H_0) \\ m_i'(H_1) = w_i m_i(H_1) \\ m_i'(\Omega) = 1 - m_i'(H_1) - m_i'(H_0) \end{cases} \tag{14}$$

As mentioned in section 3, the combination of adjusted BPA can be obtained by D-S theory as follows:

$$m(H_0) = m_1' \oplus m_2' \oplus ... m_n'(H_0) = \frac{\sum\limits_{A_1 \cap A_2 \cap ... A_n = H_0} \prod\limits_{i=1}^{n} m_i'(A_i)}{1 - K} \tag{15}$$

$$m(H_1) = m_1' \oplus m_2' \oplus ... m_n'(H_1) = \frac{\sum\limits_{A_1 \cap A_2 \cap ... A_n = H_1} \prod\limits_{i=1}^{n} m_i'(A_i)}{1 - K} \tag{16}$$

where

$$K = \sum_{A_1 \cap A_2 \cap \ldots A_n = \emptyset} \prod_{i=1}^{n} m_i'(A_i).$$

In conclusion, the final decision is made upon a following simple strategy

$$m(H_0) \underset{H_0}{\overset{H_1}{\lessgtr}} m(H_1). \tag{17}$$

5 Simulation Results and Analysis

For our simulation, we assume the LU signal is DTV signal as in [4], and the probability of presence and absence LU signal are both 0.5. The bandwidth of LU signal is 6 MHz, and AWGN channel is considered. Five sensing nodes are spread in the network to perform local sensing. The local sensing time is 50 μs.

Our scheme of data fusion has been tested with many case of CUs' SNR. In figure 4, our algorithm have been experienced under condition that all the forth first CUs have same AWGN channel with SNR = -12dB, and the fifth CU's channel condition is changed from -22dB to -6dB, which is reasonable for spectrum sensing problem in CR context. Under such condition, probability of

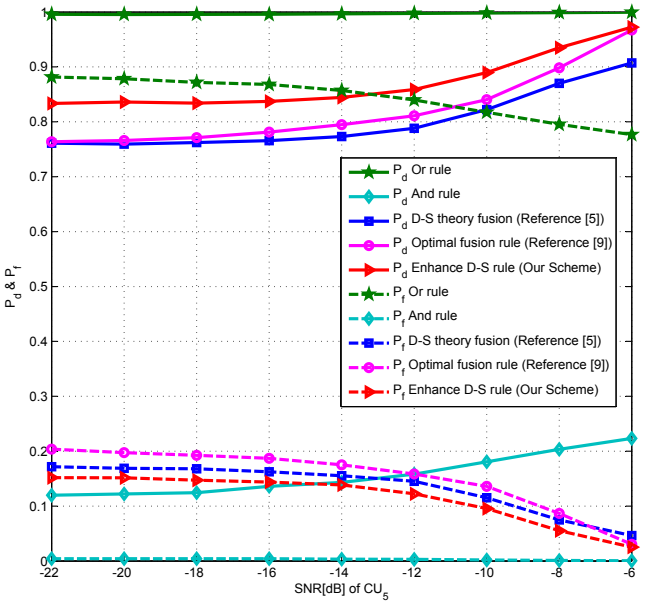

Fig. 4. Probability of detection and probability of false alarm comparison between proposed scheme and other combination rule under condition that SNR of CU_1 - CU_4 are -12dB, SNR of CU_5 is changed from -22dB to -6dB

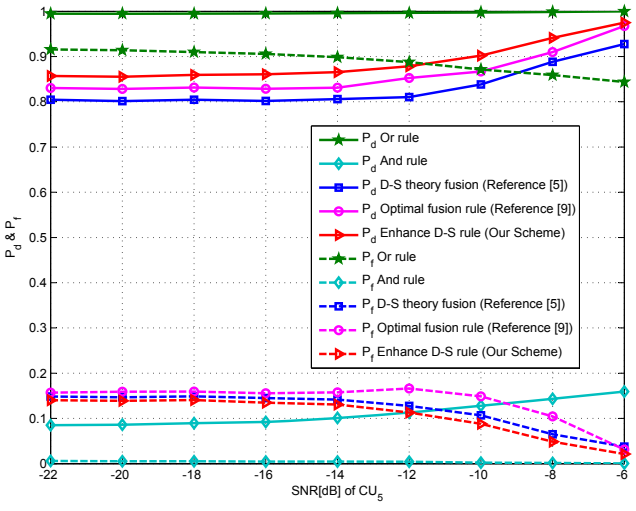

Fig. 5. Probability of detection and probability of false alarm comparison between proposed scheme and other combination rule under condition that SNR of CU_1 - CU_4 are -21dB, -17dB, -13dB, -9dB, respectively and SNR of CU_5 is changed from -22dB to -6dB

detection P_d of "And" rule is always largest but its probability of false alarm P_f also is similar, and vice versal for "Or" rule, i.e. both P_d and P_f are smallest, which means that both rules indicate bad performance. For our proposed scheme, both P_d and P_f always gives a remarkable improvement, compared to "D-S theory fusion" in [5] and even with "Optimal fusion rule" in [9].

In order to evaluate our proposed scheme with a more practical situation, where distributed CUs endure difference channel condition, we consider the condition that the received SNR of forth first CUs (CU_1 - CU_4) are -21dB, -17dB, -13dB, -9dB, respectively and SNR of CU_5 is changed from -22dB to -6dB. Under such condition, the figure 5 also shows that our proposed scheme is outperform the other rules. Numerous other situations have also been tested and our scheme have given similar best result.

6 Conclusions

In this paper, we have proposed an enhanced cooperative spectrum sensing scheme based on the combination between the D-S theory, using a more appropriate BPA function and a novel reliability source evaluation by utilizing SNR of LU signal. Simulation results have shown that this proposed scheme can achieve a better gain of combination for cooperative spectrum sensing than other rules like "And", "Or", and even better than "Optimal fusion rule".

Acknowledgement

This work was supported in part by the Ministry of Commerce, Industry, and Energy and in part by Ulsan Metropolitan City through the Network-based Automation Research Center at the University of Ulsan.

References

1. Cabric, D., Mishra, S.M., Brodersen, R.W.: Implementation Issues in Spectrum Sensing for Cognitive Radios. In: Conf. Record of the 38th Asilomar Conf. on Signals, Systems and Computers, vol. 1, pp. 772–776 (2004)
2. Akyildiz, I.F., Lee, W., Vuran, M.C., Mohanty, S.: NeXt Generation/Dynamic Spectrum Access/Cognitive Radio Wireless Networks: a survey. Computer Network 50, 2127–2159 (2006)
3. Urkowitz, H.: Energy Detection of Unknown Deterministic Signals. Proceedings of the IEEE 55, 523–531 (1967)
4. Shellhammer, S.J., Shankar, S., Tandra, R., Tomcik, J.: Performance of Power Detector Sensors of DTV Signals in IEEE 802.22 WRANs. In: Proc. of the 1st int. Workshop on Technology and Policy For Accessing Spectrum, vol. 222. ACM Press, New York (2006)
5. Peng, Q., Zeng, K., Wang, J., Li, S.: A Distributed Spectrum Sensing Scheme Based on Credibility and Evidence Theory in Cognitive Radio Context. In: IEEE 17th Int. Symposium on Personal, Indoor and Mobile Radio Communications, pp. 1–5 (2006)
6. Wentao, Z., Tao, F., Yan, J.: Data Fusion Using Improved Dempster-Shafer Evidence Theory for Vehicle Detection. In: 4th Int. Conf. on Fuzzy Systems and Knowledge Discovery, vol. 1, pp. 487–491 (2007)
7. Smets, P.: The Combination of Evidence in the Transferable Belief Model. Pattern Analysis and Machine Intelligence, IEEE Transactions, 12, 447–458 (1990)
8. Wei, Z., Mallik, R.K., Letaief, K.B.: Cooperative Spectrum Sensing Optimization in Cognitive Radio Networks. In: IEEE Int. Conf. on Communications, pp. 3411–3415 (2008)
9. Chair, Z., Varshney, P.K.: Optimal Data Fusion in Multiple Sensor Detection Systems. IEEE Trans. Aerospace and Electronic Systems AES-22, 98–101 (1986)
10. Chen, L., Wang, J., Li, S.: An Adaptive Cooperative Spectrum Sensing Scheme Based on the Optimal Data Fusion Rule. In: 4th Int. Symposium on Wireless Communication Systems, pp. 582–586 (2007)
11. Ansari, N., Chen, J.G., Zhang, Y.Z.: Adaptive Decision Fusion for Unequiprobable Sources. IEEE Proceedings on Radar, Sonar and Navigation 144, 105–111 (1997)
12. Mansouri, N., Fathi, M.: Simple counting rule for optimal data fusion. In: Proceedings of 2003 IEEE Conference on Control Applications, vol. 2, pp. 1186–1191 (2003)
13. Wang, P.: The Reliable Combination Rule of Evidence in Dempster-shafer Theory. In: Congress on Image and Signal Processing, CISP 2008, vol. 2, pp. 166–170 (2008)

A Secure Distributed Spectrum Sensing Scheme in Cognitive Radio

Nguyen-Thanh Nhan and Insoo Koo

School of Electrical Engineering, University of Ulsan 680-749 San 29, Muger 2-dong, Ulsan, Republic of Korea
iskoo@ulsan.ac.kr
http://mcsl.ulsan.ac.kr

Abstract. Distributed spectrum sensing provides an improvement for primary user detection but leads a new security threat into CR system. The spectrum sensing data falsification malicious users can decrease the cooperative sensing performance. In this paper, we propose a distributed scheme in which the presence and absence hypotheses distribution of primary signal is estimated based on past sensing received power data by robust statistics, and the data fusion are performed according to estimated parameters by Dempster-Shafer theory of evidence. Our scheme can achive a powerful capability of malicious user elimination due to the abnormality of the distribution of malicious users compared with that of other legitimate users. In addition, the performance of our data fusion scheme is enhanced by supplemented nodes' reliability weight.

Keywords: Cognitive radio, Spectrum sensing, Distributed, Malicious user, Robust statistics.

1 Introduction

Cognitive Radio (CR) has been proposed as a promising technology to improve spectrum utilization. CUs are allowed to use the licensed bands opportunistically when such bands are not occupied, and must abandon its contemporary band to seek for the new idle spectrum again when the frequency band is suddenly accessed by the licensed user (LU). Therefore the key role of CR is played by spectrum sensing. Generally, spectrum sensing can be achieved by a single CU. The detection techniques often used in local sensing are energy detection, matched filter and cylcostationary feature detection. In [1], it is showed that the receiver signal strength could be seriously weakened at a particular geographical location due to multi-path fading and shadow effect. On these circumstances, single sensing node is difficult to distinguish between an idle band and a deep fade one. In order to overcome this problem, distributed spectrum sensing has been considered [4], [5], [7].

In [7], a data fusion scheme which can give a significant improvement in detection probability as well as reduction false alarm rate based on Dempster-Shafer theory of evidence (D-S theory) was described. Numerous other fusion schemes

D.-S. Huang et al. (Eds.): ICIC 2009, LNAI 5755, pp. 698–707, 2009.

also have been proposed for such distributed model such as "And rule", "Or rule", "Optimal fusion rule", etc. However, few works have considered a novel security threat of distributed spectrum sensing which is called spectrum sensing data falsification [3] in which, an attacker or malicious user can send false local spectrum sensing results to a data fusion center and can cause data fusion center to make wrong spectrum sensing decision. This kind of security attack was firstly mentioned in [2] and further considered in [3], [4]. In [4] the spectrum sensing data falsification problem was solved by Weighted Sequential Probability Ratio Test which gives a good performance. However this method requires the knowledge of physical location of sensing terminals and position of LU for obtaining some required prior probabilities. This is inappropriate for applying to mobility CR system, and to such systems in which the information of primary user are completely not known.

In this paper, we propose a robust secure distributed spectrum sensing scheme that uses robust statistics to approximate the distributions for both hypotheses of all nodes, discriminatingly, based on their past data reports. Achieved parameters are used for testing of malicious users and calculating necessary information for data fusion by means of D-S theory. Our algorithm, taking the advantage of an appropriate method of data fusion and the benefit of robust statistics for outlier testing based on two estimated distribution separately, can operate without any requirement for knowledge of primary systems, even in a very bad circumstance where numerous of malicious users occur. Furthermore, a reliability evaluation stage from past performance of each node by a counting rule [11] is added to our scheme for improving cooperative gain of data fusion and capability of malicious user detection.

The rest of this paper is organized as follows. Section 2 describes the system model briefly. In section 3, we develop our proposal scheme based on evidence theory and robust statistics. In Section 4, the simulation results are shown and analyzed. Finally, we conclude this paper in the last section.

2 System Description

We consider a distributed spectrum sensing scheme in which CR users (CUs) endure different channel condition such as shadowing and multi-path fading as figure 1. Each CU conducts energy detection and transmits the received signal powers to Data Fusion Center (DFC). At DFC, the global decision will be made based on the combination of local data. Further, we assume that our distributed CR network is in an adversarial environment where presents of malicious users which send incorrect spectrum sensing data. Local spectrum sensing of each CU is essentially a binary hypotheses testing problem:

$$\begin{cases} H_0 : x(t) = n(t) \\ H_1 : x(t) = h(t)\, s(t) + n(t), \end{cases} \tag{1}$$

where H_0 and H_1 are respectively correspondent to hypotheses of absence and presence of LU's signal, $x(t)$ represents received data at CU, $h(t)$ denotes the

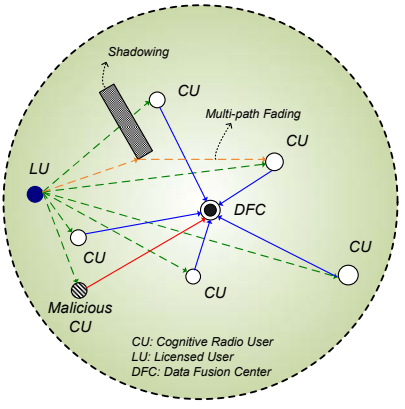

Fig. 1. Distributed spectrum sensing scheme

amplitude gain of the channel, $s(t)$ is the signal transmitted from the primary user and $n(t)$ is the additive white Gaussian noise. Additionally, channels corresponding to different CUs are assumed to be independent, and further, all CUs and LUs share common spectrum allocation.

In our system model, CU sensing technique is based on energy detection spectrum sensing. Each CU's test statistic is equivalent to an estimation of received signal power as following function:

$$x_E = \sum_{j=1}^{N} |x_j|^2, \tag{2}$$

where x_j is the j-th sample of received signal and $N = 2TW$ where T and W are correspondent to detection time and signal bandwidth, respectively. When N is relatively large (e.g. $N > 200$), x_E can be well approximated as a Gaussian random variable under both hypotheses H_1 and H_0 [10].

3 Secure Distributed Spectrum Sensing Scheme

After sensing, in our system, each CU sends its own received power data to a DFC where the global sensing decision is made. For purpose of improving security and cooperative sensing gain, we consider a robust secure distributed spectrum sensing scheme like figure 2.

3.1 Data Fusion at DFC

Basic Probability Assignment Estimation. In order to apply D-S theory of evidence to make the final decision, the frame of discernment A is defined as $\{H_1, H_0, \Omega\}$, where Ω denotes either hypotheses is true. At each sensing time k-th, each CU will send its received power signal to fusion center where each

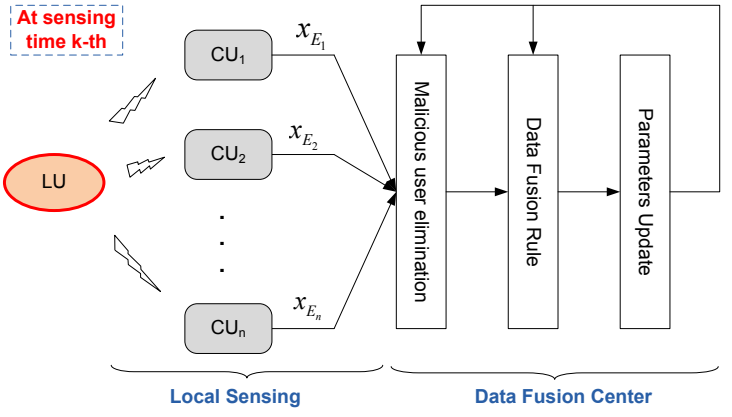

Fig. 2. Secure distributed spectrum sensing scheme

node's decision credibility corresponding to basic probability assignment (BPA) of two hypotheses are estimated. We propose a more appropriate BPA function as a form of the cumulative density function instead of probability density function [7] as follows:

$$m_i(H_0) = \int_{x_{E_i}}^{+\infty} \frac{1}{\sqrt{2\pi}\hat{\sigma}_{0i}} e^{\left(-\frac{(x-\hat{\mu}_{0i})^2}{\hat{\sigma}_{0i}^2}\right)} dx, \tag{3}$$

$$m_i(H_1) = \int_{-\infty}^{x_{E_i}} \frac{1}{\sqrt{2\pi}\hat{\sigma}_{1i}} e^{\left(-\frac{(x-\hat{\mu}_{1i})^2}{\hat{\sigma}_{1i}^2}\right)} dx, \tag{4}$$

where $m_i(H_0)$, $m_i(H_1)$ are the BPA of hypotheses H_0 and H_1 of the i-th CU, respectively, and $(\hat{\mu}_{0i}, \hat{\sigma}_{0i})$ and $(\hat{\mu}_{1i}, \hat{\sigma}_{1i})$ are the estimated means and estimated standard deviations, which will be described in subsection 3.2.

Using eqn. (3) and (4), the BPA of hypotheses H_0 and H_1 are unique for each test statistics value x_{E_i} and vary in the way that the larger x_{E_i} is the larger $m_i(H_1)$ and the smaller $m_i(H_0)$ are and vice versa.

BPA Adjustment. Instead of combining all the CUs' assigned BPA which means treating all nodes equally, the BPA of each CU should be adjusted by relative relationship of reliability among nodes rel_i which will be describe in subsection 3.2. The weight w_i of the i-th CU is obtained by normalizing the node's reliability $rel_i(n)$:

$$w_i(n) = \frac{rel_i(n)}{\max_i (rel_i(n))}. \tag{5}$$

The BPA of the i-th CU for both hypotheses $m_i(H_0)$ and $m_i(H_1)$ are adjusted with corresponding weight w_i as follows:

$$\begin{cases} m_i'(H_0) = w_i m_i(H_0) \\ m_i'(H_1) = w_i m_i(H_1) \\ m_i'(\Omega) = 1 - m_i'(H_1) - m_i'(H_0). \end{cases} \tag{6}$$

From eqn. (6), the effect of less reliable (lower performance) node is decreased and vice versa while the local spectrum sensing decision is being preserved.

D-S Theory Combination. According to D-S theory of evidence, the combination of adjusted BPA can be obtained by:

$$m(H_0) = m_1' \oplus m_2' \oplus ... m_n'(H_0) = \frac{\sum\limits_{A_1 \cap A_2 \cap ... A_n = H_0} \prod\limits_{i=1}^{n} m_i'(A_i)}{1 - K}, \tag{7}$$

$$m(H_1) = m_1' \oplus m_2' \oplus ... m_n'(H_1) = \frac{\sum\limits_{A_1 \cap A_2 \cap ... A_n = H_1} \prod\limits_{i=1}^{n} m_i'(A_i)}{1 - K}, \tag{8}$$

where $K = \sum\limits_{A_1 \cap A_2 \cap ... A_n = \emptyset} \prod\limits_{i=1}^{n} m_i'(A_i)$ and $m(H_0)$ and $m(H_1)$ are the final credibility of CR system for each hypothesis in form of BPA.

From these results, a simple decision strategy is chosen; the final decision is made upon as follows:

$$\begin{aligned} &H_0 : m(H_0) > m(H_1). \\ &H_1 : m(H_0) < m(H_1). \end{aligned} \tag{9}$$

3.2 Parameters Update

Without any other knowledge about primary system, our algorithm can utilize the advantage combination of D-S theory fusion rule and the benefit of outlier resistance of robust statistics. Therefore, the parameters updating stage will play a very important role for our scheme performance.

Reliability Source Evaluation. In distributed spectrum sensing, the global decision is usually more reliable than local decisions. Therefore, we can use it as a supervisor to estimate the nodes' reliability in the form of weight factor. That is, if the local decision is the same as the global decision, we think such local decision is correct; on the other hand, if the local decision contradicts the global decision, we think such local decision is incorrect. By counting the local decisions and global decisions, we can estimate the node's reliability exactly. For the ith sensing node at the kth time, $S_i(k)$ will denote for current state of decision, where occurs one over forth state as follows:

S_{11}: global decision is H_1 and local decision is H_1,
S_{00}: global decision is H_0 and local decision is H_0,
S_{10}: global decision is H_1 and local decision is H_0,
S_{01}: global decision is H_0 and local decision is H_1.

Then we get the cumulative state $J_i(n)$ of n dectection time slot

$$J_i(n) = \sum_{k=1}^{n} S_i(k) = n_{11_i}(n)S_{11} + n_{00_i}(n)S_{00} + n_{10_i}(n)S_{10} + n_{01_i}(n)S_{01}, \quad (10)$$

where $n_{11_i}(n)$, $n_{00_i}(n)$, $n_{10_i}(n)$ and $n_{01_i}(n)$ represent the times that S_{11}, S_{00}, S_{10} and S_{01} have occurred over n time slot, respectively. $J_i\,(n)$ can be rewritten as iterative format

$$J_i\,(n) = J_i\,(n-1) + S_i\,(n)\,. \quad (11)$$

For adapting to complicated RF environment, we use a window of fixed length over observed data.

$$J_i\,(n) = \sum_{k=n-L+1}^{n} S_i\,(k). \quad (12)$$

where L is the length of observation window. Intuitively, a good performance node which has both a low false alarm rate and a high detection rate simultaneously should have more reliability. Consequently, the reliability of each node is defined as follow

$$rel_i = \tilde{P}_d.(1 - \tilde{P}_f), \quad (13)$$

where $\tilde{P}_d$ and $\tilde{P}_f$ are detection rate and false alarm rate, respectively. From eqn.(13) and based on $J_i\,(n)$, we can estimate the reliability of node as

$$rel_i\,(n) = \frac{n_{11_i}\,(n)}{n_{11_i}\,(n) + n_{10_i}\,(n)}.\frac{n_{00_i}\,(n)}{n_{00_i}\,(n) + n_{01_i}\,(n)}. \quad (14)$$

With eqn.(14), the reliability of CUs can be achieved by a simple counting rule of their past performance.

Estimation Hypothesis Distribution Parameters. As mentioned in section 2, when time bandwidth product N is large enough, both hypotheses H_1 and H_0 can be approximated as a Gaussian distribution. Theoretically, according to reference [10] the mean and variance of these distributions can be estimated as follows

$$\begin{cases} \mu_0 = N & \sigma_0^2 = 2N \\ \mu_1 = N\,(\gamma+1) & \sigma_1^2 = 2N\,(2\gamma+1), \end{cases} \quad (15)$$

where γ is the signal to noise ratio (SNR) of the primary signal at the CU. However, in an adversarial environment, it is more secure to estimate the hypothesis distribution parameters based on the past sensing energy data. For our scheme, the mean and variance of hypotheses distribution H_1 and H_0 are estimated from available received power data by robust statistics.

In distributed spectrum sensing, the global decision is usually more reliable than local decisions. Therefore, after completing one fusion interval, the received signal power report of each node will be enforced to one of two data sets $\{x_{E_i}|H_0\}$ or $\{x_{E_i}|H_1\}$ corresponding to hypothesis of H_0 or hypothesis of H_1 of the global decision. After this step, the parameters of each hypothesis distribution (mean and variance) will be estimated by Hubber's method [8], [9] as follows:

- Step 1: sets initial value of mean and variance of observation data set Y

$$\begin{cases} \mu^{(0)} = MED\,(Y) \\ \sigma^{(0)} = 1.4826 MAD\,(Y), \end{cases} \tag{16}$$

  where $MED\,(Y)$ is the sample median of Y and $MAD\,(Y)$ is the sample median absolute deviation of Y.
- Step 2: tests and adjusts outlier data. Instead of removing the data as in [5], robust statistics is enable to use dubious data as follow.

$$\widetilde{Y}_i = \begin{cases} \mu^{(0)} - 1.5\sigma^{(0)} \; if \; Y_i < \mu^{(0)} - 1.5\sigma^{(0)} \\ \mu^{(0)} + 1.5\sigma^{(0)} \; if \; Y_i > \mu^{(0)} + 1.5\sigma^{(0)} \\ \quad Y_i \qquad\qquad\qquad elsewhere \end{cases}. \tag{17}$$

  where value 1.5 for the multiplier is chosen for our winsorisation process.
- Step 3: calculates an improved estimate of mean as $\mu^{(1)} = mean(\widetilde{Y}_i)$, and of the standard deviation as $\sigma^{(1)} = 1.134 stdev\left(\widetilde{Y}_i\right)$, where *mean* and *stdev* is the function of taking mean and standard deviation, and the factor 1.134 is derived from the normal distribution.
- Step 4: repeats step 2, and 3. Eventually, after j iteration times, the process converges to an acceptable degree of accuracy when no more value data have to be adjusted in step 2. The resulting values $\mu^{(j)}$ and $\sigma^{(j)}$ are the robust estimated mean and standard deviation, respectively.

As well as previous part, in order to well adapt to RF environment, we also consider a fixed length window L of observation data for estimating distribution parameters. Consequently, the parameters $(\hat{\mu}_{0i}, \hat{\sigma}_{0i})$ and $(\hat{\mu}_{1i}, \hat{\sigma}_{1i})$ are estimated from $\{x_{E_i}\,(Q-L+1)\,, ..., x_{E_i}\,(Q)\,|H_1\}$ and $\{x_{E_i}\,(S-L+1)\,, ..., x_{E_i}\,(S)\,|H_0\}$, respectively, where Q, S are corresponding to the length of data set $\{x_{E_i}|H_0\}$ and $\{x_{E_i}|H_1\}$.

If the data set belong to a malicious node its distribution will be differ from other normal node due to it abnormal data distribution.

3.3 Malicious User Detection

We consider two kinds of malicious nodes: "Always-yes" node and "Always-no" node. An "Always-no" user will always report the absence of primary signal whereas "Always-yes" node will always inform the presence of LU. "Always-yes" users increase the probability of false alarm P_f while "Always-no" users decrease the probability of detection P_d.

As already described in subsection 3.2, a malicious user will have abnormal estimated parameters. Based on this feature we can easily detect the consistent malicious users by the following test condition: $|\hat{\mu}_{1i} - \hat{\mu}_{0i}| < \varepsilon_1$ where N is mentioned in section 2, ε_1, is the detection thresholds which is predefined based on N so that the malicious can be removed exactly.

This test is used for detecting "consistent malicious" nodes which generate false sensing data from one hypothesis. An "always-yes" or "always-no" node will have very small difference between two hypotheses means and deviations since its data set $\{x_{E_i}|H_0\}$ and $\{x_{E_i}|H_1\}$ are derived from one hypothesis distribution or even from a constant value. If a node has the distance between two mean values of two hypotheses smaller than a minimum tolerable value, it will be considered as a consistent malicious user. For our scheme, the threshold ε_1 is defined as the theoretical lowest distance of two mean values and can be derived from eqn. (15) as

$$\varepsilon_1 = (\mu_1 - \mu_0)_{\min} = N\gamma_{\min}, \tag{18}$$

where $\gamma_{\min}$ is the minimum value of SNR for operating of energy detection.

4 Simulation Results and Analysis

For our simulation, we assume the LU signal is DTV signal as in [6]. The bandwidth of LU signal is 6 MHz, and AWGN channel is considered. The local sensing time is 50 μs and 10 sensing nodes are spread in the network to perform local sensing. The fixed length window size for both reliability source evaluation stage and hypothesis distribution parameters estimation stage is chosen to be 100 and the presence and absence probability of LU signal are both 0.5.

In fig. 3, we simultaneously observe the false alarm and detection probability according to the number of "Always yes" malicious user. Each "Always yes" malicious user randomly generates a large value derived from an only high SNR (0dB) distribution of hypothesis H_1. From the figure, we can see that both detection probability P_d and false alarm probability P_f of "Or rule" is approximately one which means that the "Or rule" is strongly affected by "Always yes" malicious user. For "And rule", the performance is better than that of "Or rule" but is not the best. With "D-S theory fusion rule" in which BPAs are obtained from both theoretical hypotheses distribution, the detection probability P_d always approximate one due to the effect of "Always yes" nodes. However, the false alarm probability P_f is increased very large when the number of "Always yes" node is increased. For our scheme, we use the detection probability P_d and the false alarm probability P_f of "D-S theory fusion rule" without malicious nodes as the comparison boundary of data fusion. The result indicates that our scheme can achieve approximately to the boundary of combination until the number of malicious user is up to eight nodes. Similar results, which is not presented in this paper, is obtained for case of "Always yes" user that generate large constant value.

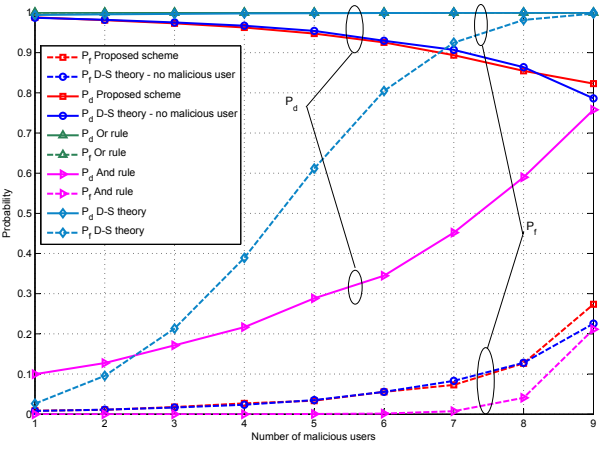

Fig. 3. Probabilitiy vs. number of "Always yes" user with various fusion rules

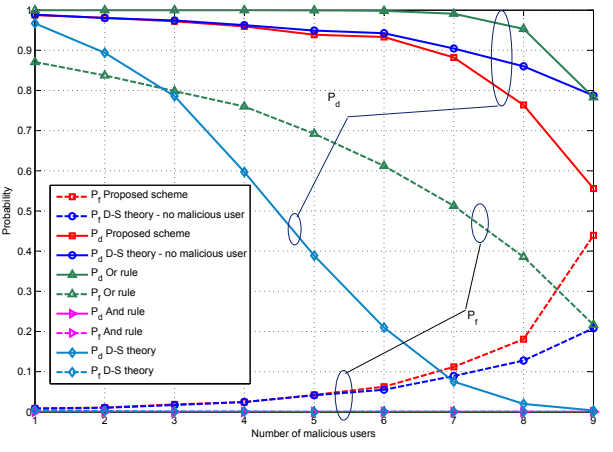

Fig. 4. Probabilitiy vs. number of "Always no" user with various fusion rules

In fig. 4, the effect of "Always no" malicious user is also considered. Similarly to previous cases, other data fusions that have not malicious node identification capability shows a degraded performance while our scheme with an effective malicious user detection can achieve the same performance of data fusion boundary of "D-S theory fusion rule" without malicious node.

5 Conclusions

In this paper, a secure distibuted spectrum sensing scheme has been proposed and analyzed. The scheme, which is only based on the past sensing nodes received

power data without any other knowledge of primary system, can utilize both the advantage of D-S theory fusion rule combined with an enhanced weighting stage and the powerful capability of robust statistics used for malicious user elimination. Numerical results indicate that our scheme can achive both a high gain datafusion and a powerful malicious users elimination.

Acknowledgement

"This work was supported by the Korea Research Foundation Grant funded by the Korean Government(MOEHRD)" (KRF-2009-0063958).

References

1. Cabric, D., Mishra, S.M., Brodersen, R.W.: Implementation Issues in Spectrum Sensing for Cognitive radios. In: Conf. Record of the 38th Asilomar Conf. on Signals, Systems and Computers, vol. 1, pp. 772–776 (2004)
2. Mishra, S.M., Sahai, A., Brodersen, R.W.: Cooperative Sensing among Cognitive Radios. In: IEEE International Conference on Communications, ICC 2006, pp. 1658–1663 (2006)
3. Ruiliang, C., Jung-Min, P., Hou, Y.T., Reed, J.H.: Toward Secure Distributed Spectrum Sensing in Cognitive Radio Networks. IEEE Communications Magazine 46, 50–55 (2008)
4. Ruiliang, C., Jung-Min, P., Kaigui, B.: Robust Distributed Spectrum Sensing in Cognitive Radio Networks. In: IEEE The 27th Conference on Computer Communications, INFOCOM 2008, pp. 1876–1884 (2008)
5. Kaligineedi, P., Khabbazian, M., Bhargava, V.K.: Secure Cooperative Sensing Techniques for Cognitive Radio Systems. In: IEEE International Conference on Communications, ICC 2008, pp. 3406–3410 (2008)
6. Stephen, J.S., Sai Shankar, N., Rahul, T., James, T.: Performance of Power Detector Sensors of DTV Signals in IEEE 802.22 WRANs. In: Proceedings of the first international workshop on Technology and policy for accessing spectrum. ACM, Boston (2006)
7. Peng, Q., Zeng, K., Wang, J., Li, S.: A Distributed Spectrum Sensing Scheme Based on Credibility and Evidence Theory in Cognitive Radio Context. In: IEEE 17th International Symposium on in Personal, Indoor and Mobile Radio Communications, pp. 1–5 (2006)
8. Rousseeuw, P.J.: Robust Regression and Outlier Detection. John Wiley & Sons, Inc., Chichester (1987)
9. Huber, P.J.: Robust Statistics. John Wiley & Sons, Inc., Chichester (1981)
10. Urkowitz, H.: Energy detection of unknown deterministic signals. Proceedings of the IEEE 55, 523–531 (1967)
11. Mansouri, N., Fathi, M.: Simple counting rule for optimal data fusion. In: Proceedings of 2003 IEEE Conference on in Control Applications, CCA 2003, vol. 2, pp. 1186–1191 (2003)

An Optimal Data Fusion Rule in Cluster-Based Cooperative Spectrum Sensing

Hiep-Vu Van and Insoo Koo*

School of Electrical Engineering, University of Ulsan
680-749 San 29, Muger 2-dong, Ulsan, Republic of Korea
iskoo@ulsan.ac.kr
http://mcsl.ulsan.ac.kr

Abstract. In this paper, we consider a cluster-based cooperative spectrum sensing approach to improve the sensing performance of cognitive radio (CR) network. In the cluster-based cooperative spectrum sensing, CR users with the similar location are grouped into a cluster. In each cluster, the most favorable user namely *cluster header*, will be chosen to collect data from all CR users and send the cluster decision to common receiver who makes a final decision on the presence of primary user. In the cluster-based cooperative spectrum sensing, data fusion rule in the cluster takes an important role to reduce the rate of reporting error. Subsequently we propose optimal fusion rule for each cluster header with which we can minimize the sum of probability of false alarm and probability of missed detection in each cluster header.

Keywords: Cognitive radio, Cooperative spectrum sensing, Optimal data fusion, Improvement sensing performance.

1 Introduction

Nowadays, wireless communication is applied in more and more applications of many fields in our modern life such as military, entertainment, communication and so on. Actually, in wireless network the licensed devices often occupy almost range of frequency, but they use those frequency bands with under 100% capability. Especially, in some cases this utilization is just few percentages [1]. Undoubtedly, frequency band is a limited resource. Thereby, all of frequency bands should be used more effectively by increasing their utilization proportion. Recently, CR technology is used as a useful tool for limited frequency bank [2], [3]. By using this technology, the available frequency from PU can be detected and used by CR users and otherwise CR users should vacate their occupied frequency when the presence of PU is detected. Therefore, sensing the status of PU is a prerequisite of CR technology. The best sensing performance will let every CR user know exactly whether PU is present or not and use free frequency band from PU without any harmful influence.

* Corresponding author.

D.-S. Huang et al. (Eds.): ICIC 2009, LNAI 5755, pp. 708–717, 2009.

In practice, the performance of individual sensing in CR network can be deteriorated by deep fading and shadowing. This problem can be solved by allowing some CR users to perform cooperative spectrum sensing [4]-[6]. In cooperative spectrum sensing, we rely on the variability of signal strength at various locations of CR users to obtain a better performance of detecting the PU's signal in a large CR network with sensing information integrated between neighbors compared to individual sensing [7]. Cooperative spectrum sensing process often has 3 steps: sensing, reporting and making a decision. In sensing step, all CR users perform spectrum sensing individually and later in reporting step, all local sensing observations are sent to common receiver. In final step, making a decision, common receiver uses a data fusion rule to fuse all local observations together as a global decision about presence of PU.

When some CR users coordinate to perform cooperative spectrum sensing, more accurate detection can be obtained. However, when the local observations are forwarded to a common receiver through fading channels, the sensing performance can be severely degraded. In order to overcome this problem, Sun et al. have proposed a cluster-based cooperative sensing method[8]. In this method, few CR users with similar location are collected into a cluster. In each cluster, a favorable user is selected to be cluster header. Cluster header will receive local sensing information from all CR users to make a cluster decision and later report to common receiver. This approach really improves the sensing performance in comparison with conventional method. However, in the reference paper [8] OR-rule is used in both cluster header and common receiver, which is not optimal.

In order to improve the performance of cluster-based cooperative sensing, in the paper we propose optimal data fusion rule for cluster header with which we can find optimal thresholds for both CR users in cluster and cluster header such that we can minimize the sum of probability of false alarm and probability of missed detection in each cluster header. We also consider three data fusion rules at common receiver: haft-voting rule, AND-rule and OR-rule to prove the efficiency of the proposed optimal fusion rule for cluster header.

2 System Model

This paper considers a CR network included K clusters with n_j $(j = 1, 2 \ldots K)$ CR users for each cluster and a common receiver. In a cluster, the position of all CR users is close together. Therefore, we assume that all CR users in the same cluster have the similar channel communicated with PU (same SNR, $\overline{\gamma_j}$) and common receiver (same SNR, $\overline{\rho_j}$) as shown in *Figure* 1. The common receiver functions as a base station (BS) which manages the cognitive radio network and all associated cognitive radio.

This network focuses to sense the presence of PU by performing cooperative spectrum sensing. In the network, each CR users should sense individually by using one of detection methods such as matched filter detection, energy detection, feature detection, and so on [9], [10]. In those detection methods, if the CR

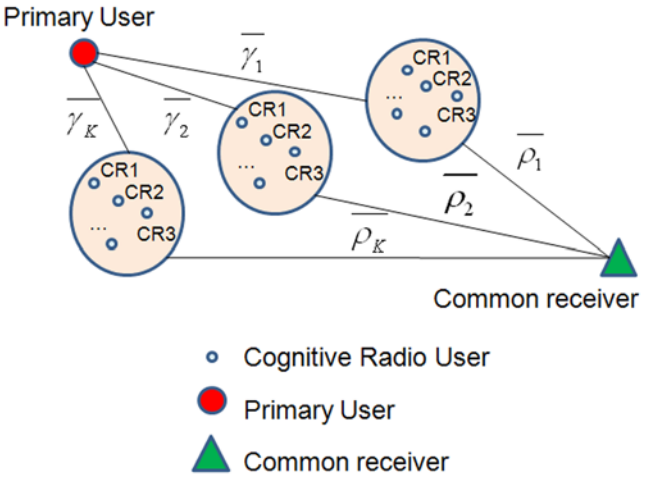

Fig. 1. System Model

user has limited information about signals of the PU, then the energy detection is optimal [10]. In the energy detection, the radio frequency energy in the sensing channel is collected in a fixed bandwidth W over an observation time window T to decide whether the channel is utilized or not. We assume that each CR user performs local spectrum sensing using energy detector independently and the sensing channel is time-invariant during the sensing process.

In the $i-th$ $(i = 1, 2 \ldots n_j)$ CR user, the local spectrum sensing is to decide between two following hypotheses.

$$\begin{cases} H_0 : x_i(t) = n_i(t) \\ H_1 : x_i(t) = h_i s(t) + n_i(t) \end{cases} \tag{1}$$

where $x_i(t)$ is the observation signal at the $i-th$ CR user, $s(t)$ is the signal of PU, $n_i(t)$ is the additive white Gaussian noise (AWGN), and h_i is the complex channel gain of the sensing channel between the PU and the $i-th$ CR user.

In energy detection, the collected energy in the frequency domain is denoted by E_i, which serves as a decision statistic and has the following distribution [11].

$$\begin{cases} H_0 : E_i = \chi^2_{2u} \\ H_1 : E_i = \chi^2_{2u}(2\gamma_i) \end{cases} \tag{2}$$

where χ^2_{2u} denotes a central chi-square distribution with $2u$ degrees of freedom and $\chi^2_{2u}(2\gamma_i)$denotes a noncentral chi-square distribution with $2u$ degrees of freedom and a non-centrality parameter $2\gamma_i$. The instantaneous SNR of the received signal at the i-th CR user is γ_i and $u = TW$ is the time-bandwidth product. In this paper, we use $u = 10$.

3 Cluster-Based Cooperative Spectrum Sensing

For the aim of enhancing the reliability ratio of sensing performance, we consider a cluster-based cooperative spectrum sensing method which is recognized through following steps [1].

- Step 1: All CR users in each cluster perform local spectrum sensing individually using energy detector and sends their local observations to the cluster header.
- Step 2: The cluster header receives those local observations and later makes a cluster decision.
- Step 3: The cluster decisions of each cluster are reported to the common receiver by their cluster header. After that a global decision will be made.

3.1 Local Spectrum Sensing with Energy Detection

For using the energy detector, the average probability of false alarm ($P_{f,i,j}$), the average probability of detection ($P_{d,i,j}$) and the average probability of missed detection ($P_{m,i,j}$) of local decision are given respectively, by [11].

$$P_{f,i,j} = \text{Prob}\{E_i > \lambda_j \,|H_0\} = \frac{\Gamma(u, \frac{\lambda_j}{2})}{\Gamma(u)} \tag{3}$$

$$P_{d,i,j} = \text{Prob}\{E_i > \lambda_j \,|H_1\} = Q_u(\sqrt{2\gamma_j}, \sqrt{\lambda_j}) \tag{4}$$

and

$$P_{m,i,j} = 1 - P_{d,i,j} \tag{5}$$

where λ_j and γ_j denote the energy threshold and the instantaneous SNR of CR users in the j-th cluster respectively, $\Gamma(a,x)$ is the incomplete gamma function which is given by $\Gamma(a,x) = \int_x^\infty t^{a-1}e^{-t}dt$, $\Gamma(a)$ is the gamma function, and $Q_u(a,b)$ is the generalized Marcum Q-function which is given by: $Q_u(a,x) = \frac{1}{a^{u-1}}\int_x^\infty t^u e^{-\frac{t^2+a^2}{2}} I_{u-1}(at)dt$, $I_{u-1}(.)$ is the modified Bessel functions of the first kind and order u-1.

3.2 Cluster Header Decision

All 1-bit decisions from CR users in a cluster are fused together according to following logic rule.

$$\begin{cases} B_j = 1, \sum_{i=1}^{n_j} G_{j,i} \geq th_j \\ B_j = 0, \sum_{i=1}^{n_j} G_{j,i} < th_j \end{cases} \quad where\ th_j \in [1, 2 \ldots n_j] \tag{6}$$

where th_j is a optimal threshold of the $j-th$ cluster header. $G_{j,i} = \{0,1\}$ is the local decision of the $i-th$ user in the $j-th$ cluster.

It can be easy seen that if $th_j = 1$ or $th_j = n_j$ the data fusion rule will be OR-rule or AND-rule respectively.

From the assumption that all CR users in the $j-th$ cluster has the same SNR, we have the same probability of false alarm ($P_{f,j}$), probability of detection ($P_{d,j}$) and also probability of missed detection $P_{m,j} = 1 - P_{d,j}$ in all CR users of the $j-th$ ($j = 1, 2 \ldots K$) cluster.

Therefore, the probability of false alarm in the $j-th$ cluster header ($Q_{f,j}$) is given by [12]

$$\begin{aligned} Q_{f,j} &= \text{Prob}\{H_1 | H_0\} \\ &= \sum_{l=th_j}^{n_j} C_{n_j}^{l} P_{f,j}^{l} (1 - P_{f,j})^{n_j - l} \end{aligned} \tag{7}$$

Similarly, the probability of missed detection in the $j-th$ cluster header ($Q_{m,j}$) is given by

$$\begin{aligned} Q_{m,j} &= \text{Prob}\{H_0 | H_1\} \\ &= 1 - \sum_{l=th_j}^{n_j} C_{n_j}^{l} P_{d,j}^{l} (1 - P_{d,j})^{n_j - l} \end{aligned} \tag{8}$$

In this paper, one of our objectives is to find the optimal energy threshold λ_j for all CR users in the $j-th$ cluster ($j = 1, 2 \ldots K$) as well as the optimal threshold th_j of the $j-th$ cluster header. Here, we define the optimal thresholds as λ_j^{opt} and th_j^{opt} that can minimize $(Q_{f,j} + Q_{m,j})$ of the $j-th$ cluster header, such that we have

$$[\lambda_j^{opt}, th_j^{opt}] = \underset{\lambda_j^{opt}, th_j^{opt}}{\arg} \min(Q_{f,j} + Q_{m,j}) \tag{9}$$

λ_j^{opt} and th_j^{opt} can be found by numerical method.

3.3 Global Decision

In common receiver, the global decision will be created by integrating all received cluster decisions according the below logic rule.

$$\begin{cases} H = H_1 : \sum_{j=1}^{K} B_j \geq th_g \\ H = H_0 : \text{otherwise} \end{cases} \tag{10}$$

where $B_j = \{0, 1\}$ is the decision of $j-th$ cluster and th_g is the threshold of common receiver.

For the sake to prove the efficiency of optimal rule in cluster, we consider three values of threshold th_g as follows.

No.	th_g	**Fusion Rule**
1	1	OR-rule
2	$\frac{K}{2}+1$	Half-Voting rule
3	K	AND-rule

Here, we let Q_{ej} be the error probability when cluster decision B_j is reported to the common receiver but the decision $\overline{B_j}$ is obtained.

For the case of BPSK and a given $\overline{\rho_j}$, the error probability of the $j-th$ cluster header over Rayleigh fading channels can be given by [8]

$$\begin{aligned} Q_{ej} &= \int_0^\infty Q_{ej|\rho_{\max,j}} f(\rho_{\max,j}) d\rho_{\max,j} \\ &= \sum_{m=0}^{n-1} C_{n-1}^m (-1)^{n-m-1} \frac{n}{2(n-m)} \left(1 - \sqrt{\frac{\overline{\rho_j}}{n-m+\overline{\rho_j}}}\right) \end{aligned} \tag{11}$$

where Q_{ej} is error probability of the channel between the $j-th$ cluster header and common receiver.

Commonly, the CR user with the highest SNR will be chosen to be the cluster header. However, as the assumption that all CR users in a cluster have the similar SNR of the channel with common receiver, the cluster header will be chosen randomly within all CR users in cluster.

In common receiver, the global decision will be made by integrating all cluster decisions with their channel errors according to respective data fusion rule. Those are assumed as below:

- **Data fusion rule is OR-rule** $(th_g = 1)$
  By using this rule, the global false alarm probability (Q_f) and global missed detection probability (Q_m) in common receiver are given by following, respectively.

$$Q_{f,or} = 1 - \prod_{j=1}^{K} ((1 - Q_{f,j}(1 - Q_{e,j}) + Q_{f,j}Q_{e,j}) \tag{12}$$

  and

$$Q_{m,or} = \prod_{j=1}^{K} (Q_{m,j}(1 - Q_{e,j}) + (1 - Q_{m,j})Q_{e,j}) \tag{13}$$

- **Data fusion rule is Half-Voting rule** $(th_g = \frac{\mathrm{K}}{2} + 1)$
  Actually, when we use half-voting rule to make global decision, we will confront with a difficult problem of calculation the global probabilities of false alarm $(Q_{f,half})$ and missed detection $(Q_{m,half})$ for the general case of K clusters. Therefore, we consider the case $K = 4$ and derive $(Q_{f,half})$ and $(Q_{m,half})$ for $K = 4$ as follows.

$$\begin{aligned} Q_{f,half} &= Q_{fe,1}.Q_{fe,2}.Q_{fe,3}.(1 - Q_{fe,4}) \\ &+ Q_{fe,1}.Q_{fe,2}.(1 - Q_{fe,3}).Q_{fe,4} \\ &+ Q_{fe,1}.(1 - Q_{fe,2}).Q_{fe,3}.Q_{fe,4} \\ &+ (1 - Q_{fe,1}).Q_{fe,2}.Q_{fe,3}.Q_{fe,4} \\ &+ Q_{fe,1}.Q_{fe,2}.Q_{fe,3}.Q_{fe,4} \end{aligned} \tag{14}$$

and

$$\begin{aligned}
Q_{m,half} &= Q_{me,1}.Q_{me,2}.(1-Q_{me,3}).(1-Q_{me,4}) \\
&+Q_{me,1}.(1-Q_{me,2}).Q_{me,3}.(1-Q_{me,4}) \\
&+Q_{me,1}.(1-Q_{me,2}).(1-Q_{me,3}).Q_{me,4} \\
&+(1-Q_{me,1}).Q_{me,2}.Q_{me,3}.(1-Q_{me,4}) \\
&+(1-Q_{me,1}).Q_{me,2}.(1-Q_{me,3}).Q_{me,4} \\
&+(1-Q_{me,1}).(1-Q_{me,2}).Q_{me,3}.Q_{me,4} \\
&+Q_{me,1}.Q_{me,2}.Q_{me,3}.(1-Q_{me,4}) \\
&+Q_{me,1}.Q_{me,2}.(1-Q_{me,3}).Q_{me,4} \\
&+Q_{me,1}.(1-Q_{me,2}).Q_{me,3}.Q_{me,4} \\
&+(1-Q_{me,1}).Q_{me,2}.Q_{me,3}.Q_{me,4} \\
&+Q_{me,1}.Q_{me,2}.Q_{me,3}.Q_{me,4}
\end{aligned} \tag{15}$$

where

$$\begin{aligned}
&Q_{fe,j} = (1-Q_{f,j})Q_{ej} + (1-Q_{ej})Q_{f,j} \\
&Q_{me,j} = (1-Q_{m,j})Q_{ej} + (1-Q_{ej})Q_{m,j} \\
&(j = 1, 2, 3, 4)
\end{aligned} \tag{16}$$

– **Data fusion rule is AND-rule** ($th_g = K$)
In this case, the global probabilities of false alarm ($Q_{f,or}$) and global probabilities of missed detection ($Q_{m,or}$) in common receiver are given by following.

$$Q_{f,and} = \prod_{j=1}^{K} (Q_{f,j}(1-Q_{e,j}) + (1-Q_{f,j})Q_{e,j}) \tag{17}$$

and

$$Q_{m,and} = 1 - \prod_{j=1}^{K} ((1-Q_{m,j})(1-Q_{e,j}) + Q_{m,j}Q_{e,j}) \tag{18}$$

4 Simulation Results

In this simulations, our concern is the efficiency of sensing performance in a cluster as well as in common receiver. Therefore, we consider the $j-th$ cluster with ten CR users ($n = 10$) and assume SNR uniformly within the range of $5dB$ to $10dB$ at each CR users. In the $j-th$ cluster header, optimal data fusion rule will be used to create cluster decision. For the sake of comparison, we also provide the sensing performance with the AND-rule and OR-rule.

Figure 2 shows the sensing performance of the cluster corresponding Optimal-rule, OR-rule and AND-rule. In which, we can see that the Optimal-rule can significantly reduce the error probability in cluster $Q_{f,j}+Q_{m,j}$ which is expressed by eqn. (7) and (8), when compared with OR-rule or AND-rule in each value of SNR. When the SNR is about $10dB$ the reporting error can achieve an acceptable value - less than 0.002 with Optimal-rule, but it achieves the value bigger than 0.015 with both AND-rule and OR-rule.

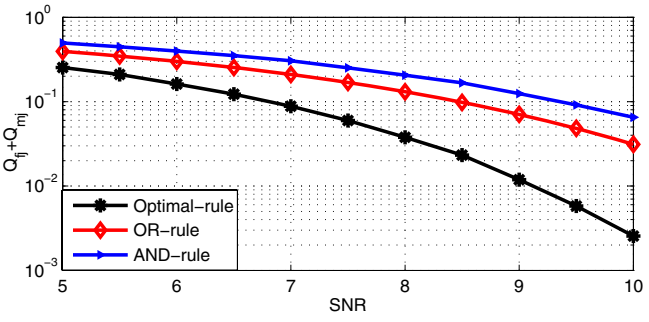

Fig. 2. Reporting error $Q_{f,j}+Q_{m,j}$ in the $j-th$ cluster corresponding different decision fusion rules and different values of SNR

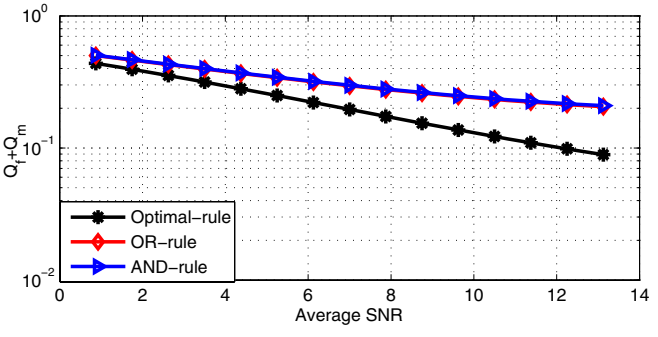

Fig. 3. Reporting error $Q_f + Q_m$ in common receiver versus different values of average SNR and different decision fusion rules in Cluster-Case 1

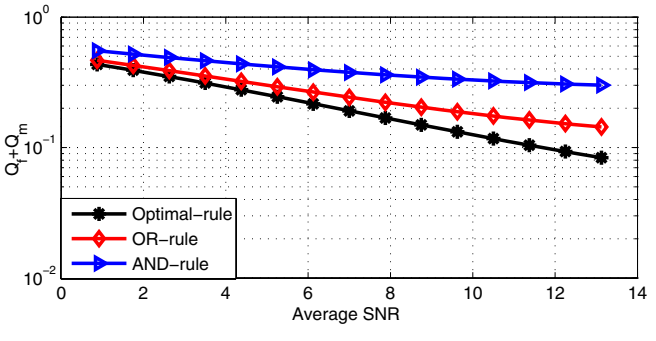

Fig. 4. Reporting error $Q_f + Q_m$ in common receiver versus different values of average SNR and different decision fusion rules in Cluster-Case 2

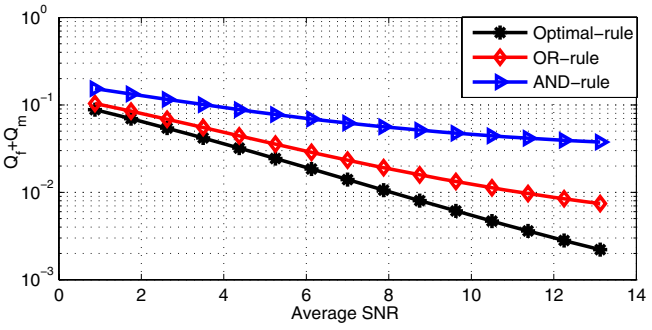

Fig. 5. Reporting error $Q_f + Q_m$ in common receiver versus different values of average SNR and different decision fusion rules in Cluster-Case 3

In the other hand, for our concern of sensing performance in common receiver, we consider network with four clusters which composed ten CR users for each cluster and the SNR of channels between PU and four clusters are $7.5dB$, $8.0dB$, $8.5dB$ and $9.0dB$ respectively. Moreover, SNR of channels between four clusters and common receiver will be changed by following table.

Channel	**1**	**2**	**3**	**4**
SNR (dB)	0.5*m	0.75*m	1*m	1.25*m

where m has value in frame within 1 and 15.

In this step, we consider three cases of applied data fusion rules in cluster as well as in common receiver, which can be determined as like below table.

Case	**In Cluster**	**In Common Receiver**
1	Optimal-Rule OR-Rule AND-Rule	OR-Rule
2	Optimal-Rule OR-Rule AND-Rule	AND-Rule
3	Optimal-Rule OR-Rule AND-Rule	Half-Voting Rule

In all cases of data fusion rule, cooperative spectrum sensing performance, which are shown in *Figure* $3-5$, can achieve better performance with optimal-rule in cluster. Specially, from *Figure* 5 we can get the best performance with optimal-rule and half-voting rule in cluster and common receiver respectively.

5 Conclusion

In this paper, we consider cluster-based cooperative spectrum sensing as well as data fusion rule to improve sensing performance. In cluster, we find an optimal-rule which is proved to be the best rule with the smallest value of reporting error. Moreover, the optimal-rule, which is utilized in cluster, and the half-voting rule, which is utilized in common receiver, are the best combination with the minimum ratio of reporting error.

Acknowledgement

This work was supported by the Korea Research Foundation Grant funded by the Korean Government(MOEHRD)" (KRF-2009-0063958).

References

1. Federal Communications Commission: Spectrum Policy Task Force. Rep. ET Docket, 02–135 (2002)
2. Mitola, J., Maguire, G.Q.: Cognitive Radio: Making Software Radios More Personal. IEEE Pers. Commun. 6, 138 (1999)
3. Haykin, S.: Cognitive Radio: Brain-empowered Wireless Communications. IEEE J. Select. Areas Commun. 23, 201–220 (2005)
4. Ganesan, G., Y. Li, G.: Cooperative Spectrum Sensing in Cognitive Radio Networks. In: Proc. IEEE Symp. New Frontiers in Dynamic Spectrum Access Networks (DySPAN5), Baltimore, USA (2005)
5. Ghasemi, A., Sousa, E.S.: Collaborative Spectrum Sensing for Opportunistic Access in Fading Environments. In: Proc. IEEE Symp. New Frontiers in Dynamic Spectrum Access Networks (DySPAN5), Baltimore, USA, vol. 81, pp. 131–136 (2005)
6. Mishra, S.M., Sahai, A., Brodersen, R.: Cooperative Sensing Among Cognitive Radios. In: Proc. IEEE Int. Conf. Commun., Turkey, vol. 4, pp. 1658–1663 (2006)
7. Cabric, D., Mishra, S.M., Brodersen, R.W.: Implementation Issues in Spectrum Sensing for Cognitive Radios. In: Proc. of Asilomar Conf. on Signals, Systems and Computers, Pacific Grove, CA, USA, pp. 772–776 (2004)
8. Sun, C., Zhang, W., Letaief, K.B.: Cluster-based Cooperative Spectrum Sensing for Cognitive Radio Systems. In: Proc. IEEE Int. Conf. Commun., Glasgow, Scotland, UK, pp. 2511–2515 (2007)
9. Hur, Y., Park, J., Woo, W., Lim, K., Lee, C.H., Kim, H.S., Laskar, J.: A Wideband Analog Multi-resolution Spectrum Sensing (MRSS) Technique for Cognitive Radio (CR) Systems. In: Proc. IEEE Int. Symp. Circuit and System, Greece, pp. 4090–4093 (2006)
10. Sahai, A., Hoven, N., Tandra, R.: Some Fundamental Limits on Cognitive Radio. In: Proc. Allerton Conf. on Communications, control, and computing, Monticello (2004)
11. Digham, F.F., Alouini, M.S., Simon, M.K.: In the Energy Detection of Unknown Signals Over Fading Channels. In: Proc. IEEE Int. Conf. Commun., Anchorage, AK, USA, pp. 3575–3579 (2003)
12. Zhang, W., Mallik, R.K., Letaief, K.B.: Cooperative Spectrum Sensing Optimization in Cognitive Radio Networks. In: Proc. IEEE Int. Conf. on Commun., Beijin, pp. 3411–3415 (2008)

Exact Bit Error Probability of Multi-hop Decode-and-Forward Relaying with Selection Combining

Bao Quoc Vo-Nguyen and Hyung Yun Kong

Department of Electrical Engineering, University of Ulsan,
San 29 of MuGeo Dong, Nam-Gu, Ulsan, 680-749 Korea
{baovnq,hkong}@mail.ulsan.ac.kr
http://wcomm.ulsan.ac.kr

Abstract. In this paper, an exact closed-form bit error rate expression for M-PSK is presented for multi-hop Decode-and-Forward Relaying (MDFR) scheme, in which selection combining technique is employed at each node. We have shown that the proposed protocol offers remarkable diversity advantage over direct transmission as well as the conventional decode-and-forward relaying (CDFR) scheme. Simulations are performed to confirm our theoretical analysis.

Keywords: Bit Error Rate (BER), Decode-and-Forward Relaying, Rayleigh fading, Selection Combining, M-PSK, cooperative communication.

1 Introduction

Recently, relaying dual-hop transmission has gained more attention under forms of cooperative communications and it is treated as one of the candidates to overcome the channel impairment like fading, shadowing and path loss [1]. The main idea is that in a multi-user network, two or more users share their information and transmit jointly as a virtual antenna array. This enables them to obtain higher diversity than they could have individually [1-9].

In the past, relatively few contributions concerning evaluating performance of the DF relaying protocol with multi relays and maximal ratio combining (MRC) or selection combining (SC) have been published [2-9]. In particular, in [2], Jeremiah Hu and Norman C. Beaulieu derived a closed-form expression for outage probability of the CDFR networks with SC when the statistics of the channels between the source, relays, and destination are assumed to be independent and identically distributed (i.i.d.) and independent but not identically distributed (i.n.d.). In [4, 5], the performance of CDFR with maximal ratio combining at the destination in terms of outage probability and bit error probability over independent but not identically distributed channels was also examined. In [3, 6-9], a class of multi-hop cooperative scheme employing decode-and-forward relaying with MRC, called multi-hop Decode-and-Forward Relaying (MDFR) scheme, was proposed, and various performance metrics were also provided.

D.-S. Huang et al. (Eds.): ICIC 2009, LNAI 5755, pp. 718–727, 2009.

However, to the best of the authors' knowledge, there is no publication concerning the exact expression for bit error rate of the MDFR with selection combining in both i.i.d. and i.n.d. Rayleigh fading channels.

In this paper, we focus on selective decode-and-forward relaying where the relay must make an independent decision on whether or not to decode and forward source information [1]. In addition, a concept of cooperative diversity protocols for multi-hop wireless networks, which allows relay nodes to exploit all information they overhear from their previous nodes along the route to the destination to increase the change of cooperation, is applied. To that effect, the receiver at each node can employ a variety of diversity combining techniques to obtain diversity from the multiple signal replicas available from its preceding relaying nodes and the source. Although optimum performance is highly desirable, practical systems often sacrifice some performance in order to reduce their complexity. Instead of using maximal ratio combining which requires exact knowledge of the channel state information, a system may use selection combining which is the simplest combining method. It only selects the best signal out of all replicas for further processing and neglects all the remaining ones. The benefit of using SC as opposed to MRC is reduced hardware complexity at each node in the network. In addition, it also reduces the computational costs and may even lead to a better performance than MRC, because in practice channels with very low SNR can not accurately estimated and contribute much noise.

The contributions of this paper are as follows. We derive an exact closed-form expression bit error rate for M-PSK of the MDFR scheme. In addition, the comparison between the performance of MDFR and that of CDFR [2] is performed and it confirms that the proposed protocol outperforms CDFR in all range of operating SNRs.

The rest of this paper is organized as follows. In Sect. 2, we introduce the model under study and describe the proposed protocol. Section 3 shows the formulas allowing for evaluation of average BER of the system. In Sect. 4, we contrast the simulations and the results yielded by theory. Finally, the paper is closed in Sect. 5.

2 System Model

We consider a wireless relay network consisting of one source, K relays and one destination operating over slow, flat, Rayleigh fading channels as illustrated in Fig. 1. The source terminal (T_0) communicates with the destination (T_{K+1}) via K relay nodes denoted as $T_1, \cdots, T_k, \cdots, T_K$. Due to Rayleigh fading, the channel powers, denoted by $\alpha_{T_i,T_j} = |h_{T_i,T_j}|^2$ are independent and exponential random variables where h_{T_i,T_j} is the fading coefficient from node T_i to node T_j with $i = 0, \cdots, K, j = 1, \cdots, K+1$ and $i < j$. We define λ_{T_i,T_j} as the expected value of α_{T_i,T_j}. The average transmit powers for the source and the relays are denoted by ρ_{T_i} with $i = 0, \cdots, K$, respectively. We further define $\gamma_{T_i,T_j} = \rho_{T_i}\alpha_{T_i,T_j}$ as the instantaneous SNR per bit for the link $T_i \to T_j$.

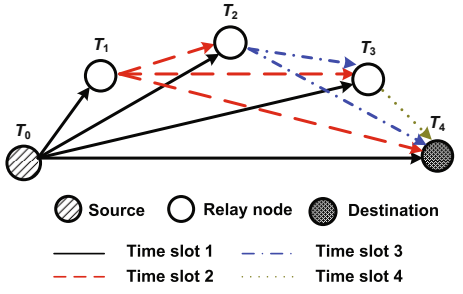

Fig. 1. A MDFR system with 3 relays ($K = 3$)

For medium access, a time-division channel allocation scheme with $K+1$ time slots is occupied in order to realize orthogonal channelization, thus no inter-relay interference is considered in the signal model.

According to the selective DF relaying protocol [1], the relay decides to cooperate or not with the source in its own time slot, based on the quality of its received signals. Since selection combining technique is used, the relay adaptively chooses the strongest signal (on the basic of instantaneous SNR) among available ones to demodulate and then check whether its received data are right or wrong. If they are right, that relay will cooperate with the source in its transmission time slot, otherwise, it will keep silent.

We define a decoding set $D(T_k)$ for node T_k, $k = 1, 2, \cdots, K+1$, whose members are its preceding relays which decode successfully. So it is obvious that $D(T_k)$ is a subset of $C = \{T_1, T_2, \cdots, T_K\}$. In real scenario, the decoding set is determined after receiving one frame by employing cyclic-redundancy-check (CRC). However, in this paper, we assumed that the decoding set can be decided by symbol-by-symbol for mathematical tractability of BER calculation [4]. We further assume that the receivers at the destination and relays have perfect channel state information (CSI) but no transmitter CSI is available at the source and relays.

3 BER Analysis

Similarly as in [2-7], namely applying the theorem of total probability, the bit error rate of the multi-hop decode-and-forward relaying can be derived as a weighted sum of the bit error rate for SC at the destination, $B_D[D(T_{K+1})]$, corresponding to each set of decoding relay $D(T_{K+1})$. Thus the end-to-end bit error rate for M-PSK of the system P_b can be written as

$$P_b = \sum_{D(T_{K+1}) \in 2^C} \Pr\left[D(T_{K+1})\right] B_D\left[D(T_{K+1})\right] \tag{1}$$

where 2^C denotes the power set of C that is the set of all subsets of C.

Since selection combining is exploited at each relay and the destination, the signal with largest SNR is always selected from the signals received from its decoding set as well as from the source. Let us define $\{\gamma_i\}_{i=1}^{n_k}$ as the instantaneous SNR per bit of each path received by the node T_k from the set $D^*(T_k)$ with their expected values $\{\bar{\gamma}_i\}_{i=1}^{n_k}$, respectively, where $D^*(T_k) = D(T_k) \cup \{T_0\}$ and n_k is the cardinality of the set $D^*(T_k)$, i.e., $n_k = |D^*(T_k)|$.

Under the assumption that all links are subject to independent fading, the cumulative distribution function (CDF) of $\beta_k = \max_{T_i \in D^*(T_k)} \rho_{T_i} \alpha_{T_i,T_k} = \max_{i=1,\ldots,n_k} \gamma_i$ can be determined by [10]

$$F_{\beta_k}(\gamma) = \Pr[\gamma_1 < \gamma, \ldots, \gamma_i < \gamma, \ldots, \gamma_{n_k} < \gamma] = \prod_{i=1}^{n_k} \left(1 - e^{-\gamma/\bar{\gamma}_i}\right) \tag{2}$$

Hence, the joint pdf of β_k is given by differentiating (2) with respect to γ [11].

$$f_{\beta_k}(\gamma) = \frac{\partial}{\partial \gamma} F_{\beta_k}(\gamma) = \sum_{i=1}^{n_k} \left[(-1)^{i-1} \sum_{\substack{m_1,\ldots,m_i=1 \\ m_1<\cdots<m_i}}^{n_k} \omega_i e^{-\omega_i \gamma} \right] \tag{3}$$

where $\omega_i = \sum_{l=1}^{i} \bar{\gamma}_{m_l}^{-1}$. It is noted that the joint pdf of β_k is expressed under a mathematic tractable form, which offers a convenient way to derive the average bit error probability of the system. Due to the fact that the decoding set is determined on symbol-by-symbol basics, the conditional probability that relay node T_k is involved in the cooperative transmission is obtained as follows:

$$\Pr[T_k \in D(T_{K+1}) | D^*(T_k)] = 1 - S_{T_k} \tag{4}$$

where S_{T_k} denotes the average symbol error rate (SER) of M-PSK modulated symbols transmitted from $D^*(T_k)$. For the case of coherently detected M-PSK, to evaluate S_{T_k}, the MGF-based approach is used [12], namely

$$S_{T_k} = \frac{1}{\pi} \int_0^{(M-1)\pi/M} M_{\beta_k} \left(-\frac{\log_2(M) g_{MPSK}}{\sin^2\theta} \right) d\theta \tag{5}$$

where $g_{MPSK} = \sin^2(\pi/M)$ and $M_{\beta_k}(s)$ is defined as follows [12, eq. (1.2)]:

$$M_{\beta_k}(s) = \int_0^{\infty} f_{\beta_k}(\gamma) e^{s\gamma} d\gamma = \sum_{i=1}^{n_k} \left[(-1)^{i-1} \sum_{\substack{m_1,\ldots,m_i=1 \\ m_1<\cdots<m_i}}^{n_k} \frac{1}{1 - s\omega_i^{-1}} \right] \tag{6}$$

Finally, substituting (6) into (5) and after some manipulations [12, eq. (5.79)] give us the desired result as eq. (7) as follows:

$$\begin{aligned} S_{T_k} &= \sum_{i=1}^{n_k} \left[(-1)^{i-1} \sum_{\substack{m_1,\ldots,m_i=1 \\ m_1<\cdots<m_i}}^{n_k} \frac{1}{\pi} \int_0^{(M-1)\pi/M} \frac{\sin^2\theta}{\sin^2\theta + g_{MPSK}\omega_i^{-1}\log_2 M} d\theta \right] \\ &= \sum_{i=1}^{n_k} \left\{ (-1)^{i-1} \sum_{\substack{m_1,\ldots,m_i=1 \\ m_1<\cdots<m_i}}^{n_k} \left[\left(\frac{M-1}{M}\right) \left[1 - \sqrt{\frac{g_{MPSK}\omega_i^{-1}\log_2 M}{1 + g_{MPSK}\omega_i^{-1}\log_2 M}} \left(\frac{M}{(M-1)\pi} \right) \times \right. \right. \right. \\ &\quad \left. \left. \left. \left[\frac{\pi}{2} + \tan^{-1} \left(\sqrt{\frac{g_{MPSK}\omega_i^{-1}\log_2 M}{1 + g_{MPSK}\omega_i^{-1}\log_2 M}} \cot \frac{\pi}{M} \right) \right] \right] \right] \right\} \end{aligned} \tag{7}$$

By using the relation of joint probability of mass function (pmf) and sequence of conditional pmf [13], the decoding set probability can be written as follows:

$$\Pr\left[D(T_{K+1})\right] = \left[\prod_{T_k \in D(T_{K+1})} \Pr\left[T_k \in D(T_{K+1}) | D^*(T_k)\right]\right] \times \left[\prod_{T_l \in C \setminus D(T_{K+1})} \left(1 - \Pr\left[T_l \notin D(T_{K+1}) | D^*(T_l)\right]\right)\right] \tag{8}$$

The closed-form expression for conditional bit error rate at the destination can be obtained by proceeding analogous to [14].

$$B_D\left[D(T_{K+1})\right] = \frac{1}{\log_2 M} \sum_{m=1}^{M} e_m \Pr\left\{\theta \in \Theta_m\right\} \tag{9}$$

where $\Theta_m = [\theta_L^m, \theta_U^m] = [(2m-3)\pi/M,\ (2m-1)\pi/M]$ for $m = 1, \cdots, M$ and e_m is the number of bit errors in the decision region Θ_m. Without loss of generality, it is assumed that $\phi = 0$, the probability $\Pr\{\theta \in \Theta_m\}$ is

$$\Pr\{\theta \in \Theta_m\} = \int_{\theta_L^m}^{\theta_U^m} \int_{0}^{\infty} f_\theta(\theta \,|\phi\,, \gamma) f_{\beta_{K+1}}(\gamma) d\gamma d\theta = \sum_{i=1}^{n_{K+1}} \left[(-1)^{i-1} \sum_{\substack{m_1,\ldots,m_i=1 \\ m_1<\cdots<m_i}}^{n_{K+1}} I\left(\theta_U^m, \theta_L^m; \omega_i^{-1}\right)\right] \tag{10}$$

where $f_\theta(\theta|\phi, \gamma)$ is defined by [14, eq. (9b)]. Furthermore, using the analysis in [14], $I(\theta_U^m, \theta_L^m; \omega_i^{-1})$ can be derived as follows:

$$I\left(\theta_U^m, \theta_L^m; \omega_i{}^{-1}\right) = \frac{\theta_U^m - \theta_L^m}{2\pi} + \frac{1}{2}\left[\psi_U^m\left(\frac{1}{2} + \frac{\tan^{-1}(\alpha_U^m)}{\pi}\right) - \psi_L^m\left(\frac{1}{2} + \frac{\tan^{-1}(\alpha_L^m)}{\pi}\right)\right] \tag{11}$$

with

$$\mu_U^m = \sqrt{\log_2(M)\omega_i^{-1}}\sin(\theta_U^m), \mu_L^m = \sqrt{\log_2(M)\omega_i^{-1}}\sin(\theta_L^m) \tag{12a}$$

$$\alpha_U^m = \frac{\sqrt{\log_2(M)\omega_i^{-1}}\cos(\theta_U^m)}{\sqrt{(\mu_U^m)^2 + 1}},\ \alpha_L^m = \frac{\sqrt{\log_2(M)\omega_i^{-1}}\cos(\theta_L^m)}{\sqrt{(\mu_L^m)^2 + 1}} \tag{12b}$$

$$\psi_U^m = \frac{\mu_U^m}{\sqrt{(\mu_U^m)^2 + 1}},\ \psi_L^m = \frac{\mu_L^m}{\sqrt{(\mu_L^m)^2 + 1}} \tag{12c}$$

Substituting (8)-(9) into (1), we can obtain the exact closed-form expression for bit error rate of the system.

4 Numerical Results

In this section, we provide some simulation results of the proposed protocol and verify these results with our derived formula. We consider a linear network

consisting of multiple nodes. The average channel power due to transmission between node T_i and node T_j is modeled as $\lambda_{T_i,T_j} = \kappa_0 d_{T_i,T_j}^{-\eta}$ where d_{T_i,T_j} is the distance from node T_i to node T_j, η is the path loss exponent and κ_0 captures the effects due to antenna gain, shadowing, etc [15]. However, for a fair of comparison to direct transmission, the overall distance of all hops is normalized to be one, i.e., $\sum_{k=0}^{K} d_{T_k,T_{k+1}} = 1$, and the uniform power allocation is employed in order to keep the total power constraint. Without loss of generality, we assume $\kappa_0 = 1$, $\eta = 3$ and each node is equidistant from each other, i.e., $d_{T_i,T_j} = (j-i)/(K+1)$ for all results except those in Fig. 4.

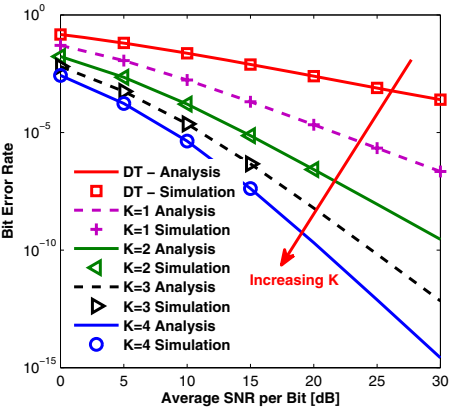

Fig. 2. Effect of increasing the number of relays on the average bit error rate of the multi-hop decode-and-forward cooperative networks with BPSK modulation ($M = 2$)

Fig. 2 shows the bit error rate of MDFR for BPSK with different numbers of cooperative nodes. As can clearly be seen in high SNR regime, the improvement of bit error rate is proportional to the number of relays.

In Fig. 3, we study the average BER performance for different levels of M-PSK. Note that with Gray code used for bit-symbol mapping, average BER for QPSK is same with that of BPSK. Furthermore, as expected, the results from theory and from simulation are in excellent agreement.

In Fig. 4, the performance of MDFR in both independent and identically distributed (i.i.d.) and independent but not identically distributed (i.n.d.) channels is examined. The results are based on the assumption that λ_{T_i,T_j} is set to be one and to be uniformly distributed between 0 and 1 for the i.i.d and i.n.d. case, respectively. It can be seen that the performance of MDFR under i.i.d. channels is better than that under i.n.d. channels.

In Fig. 5, the performance of CDFR and MDFR are compared and illustrated. As clearly shown, MDFR always outperforms direct transmission as well as CDFR with transmit power gain of about 2 dB and 4 dB for $K = 2$ and $K = 4$, respectively, for any value of operating SNRs.

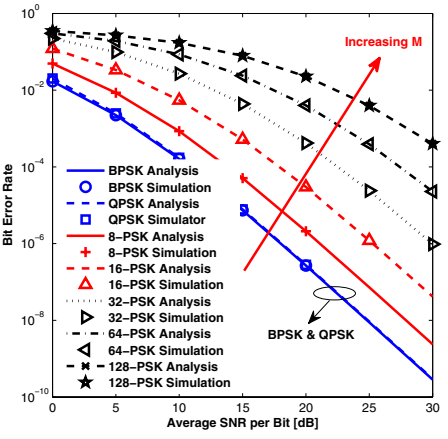

Fig. 3. Effect of modulation levels on the average bit error rate of the multi-hop decode-and-forward cooperative networks with $K = 2$

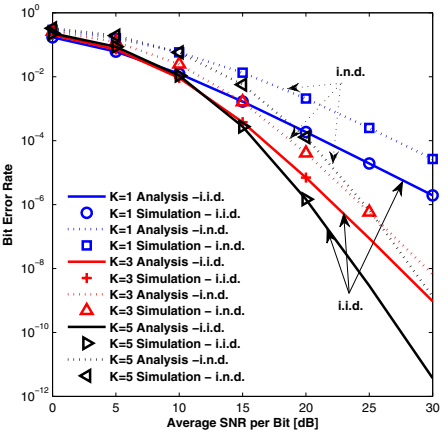

Fig. 4. BEP for 4-PSK ($M = 4$) of the multi-hop decode-and-forward cooperative networks under i.i.d. channels ($\lambda_{T_iT_j} = 1$) and i.n.d. channels ($\lambda_{T_iT_j}$ are uniformly distributed between 0 and 1) with $i = 0, \cdots, K, j = 1, \cdots, K+1$ and $i < j$

In Fig. 6, we investigate the bit error rate of the multi-hop decode-and-forward cooperative networks in different communication environments, η. More specifically, η typically varies between 2 (free-space path loss) and 5 to 6 (shadowed areas and obstructed in-building scenarios) [16]. It can be seen that under same conditions, the MDFR offers more benefit in poor communication environments.

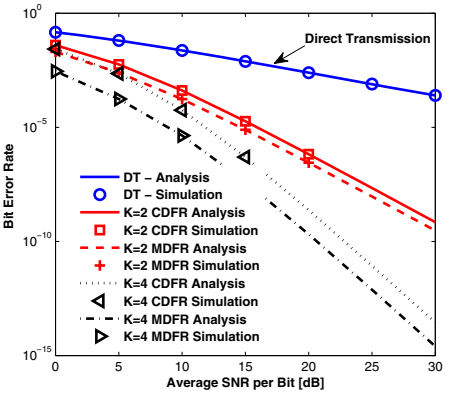

Fig. 5. Performance comparison between MDFR and CDFR with QPSK modulation ($M = 4$)

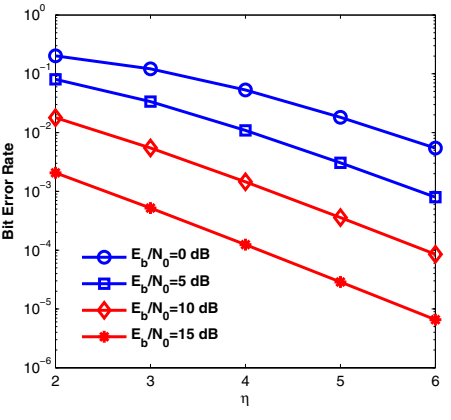

Fig. 6. Effect of pass loss exponents on the average bit error rate of the multi-hop decode-and-forward cooperative networks with 16-PSK modulation ($M = 16$)

Finally, in Fig. 7, we study the effect of diversity technique on the average BER of the multi-hop decode-and-forward cooperative networks. The BER curses confirm that, under same channel conditions, the performance of the system employing MRC receiver is always better as compared to an equivalent system using SC. Furthermore, the performance-loss gap between two systems tends to increase to be proportional to the number of relays. For example, the performance loss for the cases $K = 1, 2$ and 3 are 1,2 and 3 dB, respectively. However, it is reasonable because the advantage of MRC over SC comes at the price of complexity of the receiver at each node in the networks.

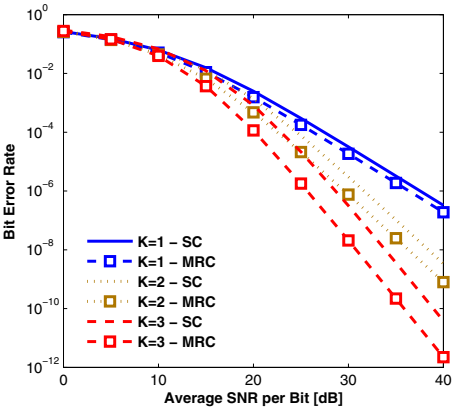

Fig. 7. Effect of combining technique on the average bit error rate of the multi-hop decode-and-forward cooperative networks with 8-PSK modulation ($M = 8$)

5 Conclusion

We have presented the exact closed-form expression for bit error rate of multi-hop DF relaying over Rayleigh fading channels. Its validity was demonstrated by a variety of Monte-Carlo simulations. The expression is general and offers a convenient way to evaluate MDFR system which exploits SC technique. In addition, the results were shown that employing the MDFR significantly enhances the system performance compared to that of CDFR.

Acknowledgment

This research was financially supported by the Ministry of Commerce, Industry and Energy (MOCIE) and Korea Industrial Technology Foundation (KOTEF) through the Human Resource Training Project for Regional Innovation.

References

1. Laneman, J.N., Tse, D.N.C., Wornell, G.W.: Cooperative Diversity in Wireless Networks: Efficient Protocols and Outage Behavior. IEEE Transactions on Information Theory 50(12), 3062–3080 (2004)
2. Hu, J., Beaulieu, N.C.: Performance Analysis of Decode-and-Forward Relaying with Selection Combining. IEEE Communications Letters 11(6), 489–491 (2007)
3. Jung, Y.S., Lee, J.H.: A New Participation Strategy for Cooperative Diversity with Multiple Partners. IEICE Trans. Commun. E89-B(11), 3152–3155 (2006)
4. Lee, I.H., Kim, D.: BER Analysis for Decode-and-Forward Relaying in Dissimilar Rayleigh Fading Channels. IEEE Communications Letters 11(1), 52–54 (2007)

5. Beaulieu, N.C., Hu, J.: A Closed-Form Expression for the Outage Probability of Decode-and-Forward Relaying in Dissimilar Rayleigh Fading Channels. IEEE Communications Letters 10(12), 813–815 (2006)
6. Sadek, A.K., Su, W., Liu, K.J.R.: A Class of Cooperative Communication Protocols for Multi-Node Wireless Networks. In: IEEE 6th Workshop on Signal Processing Advances in Wireless Communications (2005)
7. Sadek, A.K., Su, W., Liu, K.J.R.: Multinode Cooperative Communications in Wireless Networks. IEEE Transactions on Signal Processing 55(1), 341–355 (2007)
8. Boyer, J., Falconer, D.D., Yanikomeroglu, H.: Multihop Diversity in Wireless Relaying Channels. IEEE Transactions on Communications 52(10), 1820–1830 (2004)
9. Boyer, J., Falconer, D.D., Yanikomeroglu, H.: Cooperative Connectivity Models for Wireless Relay Networks. IEEE Transactions on Wireless Communications 6(5), 1–9 (2007)
10. Papoulis, A., Pillai, S.U.: Probability, Random Variables, and Stochastic Processes, 4th edn. McGraw-Hill, Boston (2002)
11. Bao, V.N.Q., Kong, H.Y., Hong, S.W.: Performance Analysis of M-PAM and M-QAM with Selection Combining in Independent but Non-Identically Distributed Rayleigh Fading Paths. In: IEEE 68th Vehicular Technology Conference, 2008. VTC 2008-Fall, Calgary, Canada, pp. 1–5 (2008)
12. Simon, M.K., Alouini, M.-S.: Digital Communication over Fading Channels, 2nd edn. John Wiley & Sons, Hoboken (2005)
13. Leon-Garcia, A.: Probability and Random Processes for Electrical Engineering, 2nd edn. Addison-Wesley, Reading (1994)
14. Chennakeshu, S., Anderson, J.B.: Error Rates for Rayleigh Fading Multichannel Reception of MPSK Signals. IEEE Transactions on Communications 43(234), 338–346 (1995)
15. Proakis, J.G.: Digital communications, 4th edn. McGraw-Hill, Boston (2001)
16. Karl, H., Willig, A.: Protocols and Architectures for Wireless Sensor Networks. Wiley, Hoboken (2005)

A Cooperative Transmission Scheme for Cluster Based Wireless Sensor Networks

Asaduzzaman and Hyung Yun Kong

Department of Electrical Engineering
University of Ulsan, Ulsan, Korea 680-749
asad78@mail.ulsan.ac.kr

Abstract. In this paper, a cross layer approach is used to obtain spatial diversity in physical layer. We develop a low complexity cooperative diversity protocol for Low Energy Adaptive Clustering Hierarchy (LEACH) based wireless sensor networks. A simple modification in clustering algorithm of LEACH protocol is proposed to exploit virtual MIMO based user cooperation. Instead of selecting a single cluster-head at network layer, we proposed M cluster-heads in each cluster to obtain a diversity order of M in long distance communication. Due to the broadcast nature of wireless transmission cluster-heads are able to receive the data from sensor nodes at the same time. This fact ensures the synchronization required to implement a virtual MIMO based space time block code (STBC) in cluster-head to sink node transmission. Analysis and simulation results show that our proposed cooperative LEACH protocol can save a huge amount of energy over LEACH protocol with same data rate, bit error rate, delay and bandwidth requirements.

Keywords: Cooperative Diversity, Fading Channel, Virtual MIMO, LEACH.

1 Introduction

Sensor nodes typically operate with small batteries for which replacement is very difficult and expensive. Thus, in many scenarios, the wireless nodes must operate without battery replacement for many years [1], [2], [3]. Consequently, minimizing the energy consumption is a very important design criterion which encourages us to implement energy-efficient transmission schemes in WSNs. Transmit diversity technique is a well known energy efficient transmission protocol. To provide transmit diversity when users cannot support multiple antennas a new method of transmit diversity for mobile users termed as cooperative diversity focused on the cooperation of active users [4]. Various cooperative transmission-protocols, implementation issues, performance and outage analysis have been studied in literature [4]-[6].

Unlike any other wireless networks, wireless sensor networks are structure less and highly energy limited. It has been shown in [7] that virtual MIMO systems are more energy efficient than SISO (Single-Input Single Output) systems

D.-S. Huang et al. (Eds.): ICIC 2009, LNAI 5755, pp. 728–737, 2009.

in Rayleigh fading channels when both transmission energy and circuit energy consumption are considered. Various cooperative MIMO protocols for clustering based WSNs have also been proposed in literature [7]-[11]. In [7]-[9], they proposed a virtual MIMO based cooperation where cooperative nodes form a cluster to exchange their information. A STBC encoded cooperative transmission for LEACH based protocols has been proposed in [10] and [11]. Cooperative diversity protocols can provide the powerful benefits of spatial diversity at the cost of spectral efficiency due to half-duplex operation of the protocols [4]. Therefore, the spectral efficiency of long haul transmission is half of LEACH protocol for the protocols proposed in [7]-[11].

In this paper, we introduce a cross layer approach to obtain higher order diversity without sacrificing any spectral efficiency. A simple modification in network layer of well known LEACH protocol [1] can obtain special diversity in physical layer. We termed our proposal as *cooperative LEACH* protocol. Instead of using only one cluster-head, we propose M cluster-heads within a single cluster. Due to the broadcast nature of wireless transmission, it is possible for all cluster-heads within a cluster to receive the same transmission. After receiving data from all nodes of a cluster, M cluster-heads cooperatively transmit toward the sink or higher layer cluster-heads. Our proposal can obtain a diversity of order M and ensures the same spectral efficiency as LEACH protocol. Interestingly, our proposal is suitable for Space Time Block Coded (STBC) transmission in terms of synchronization and delay which are the major hurdles to construct a virtual MIMO system. For the rest of this paper, we assumed only two cluster-heads (M=2) in a cluster and Alamouti diversity codes (2×1) [12] for simplicity.

2 System Model

We consider a wireless sensor network which is collecting information and sending them to a sink node as shown in Fig. 1. Consider that the nodes are randomly distributed over the area under investigation and they form clusters for the convenient of communication. Each cluster contains a cluster-head (CH), a cooperative cluster-head (CCH) and several sensor nodes (SNs). We define the inter cluster transmission (SNs to CH/CCH) as *local transmission* and the CH/CCH to sink node transmission as *long haul transmission*.

2.1 Local Communication

In this case the distance between the transmitter and receiver is relatively small compare to the long haul transmission. The local communication channels are considered as AWGN channel with free space propagation model; hence, the baseband equivalent received signal at node j due to the transmission of node i for symbol n is given by,

$$r_{ij(local)}(n) = \Gamma_{ij(local)} s(n) + \eta_j(n), \tag{1}$$

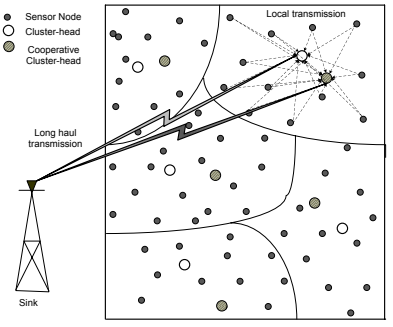

Fig. 1. System model of Cooperative LEACH protocol

where $\eta_j(n)$ is AWGN noise sample with variance $N_0/2$ per dimension at terminal j, $\Gamma_{ij(local)} = d_{ij}^{-2}$ with d_{ij} is the distance between node i and j, and $s(n)$ is the signal transmitted by node i with normalized unit transmit power.

2.2 Long Haul Communication

We consider the sink node is far away from the sensor field hence, for long haul communication channel the distance between the transmitter and receiver is quite long. We consider the channels between CH/CCH to sink node are subjected to flat Rayleigh fading with two ray ground propagation model plus AWGN. The baseband equivalent received signal at node j due to the transmission of node i for symbol n is given by,

$$r_{ij(long)}(n) = \Gamma_{ij(long)} h_{ij} s(n) + \eta_j(n), \tag{2}$$

where h_{ij} is fading coefficient between node i and j and $\Gamma_{ij(long)} = d_{ij}^{-4}$. We consider flat Rayleigh fading, hence, h_{ij} is modeled as independent samples of zero mean complex Gaussian random variable with variance $\sigma_{ij}^2/2$ per dimension. Assume, the fading coefficients are constant over the transmission period of a whole message.

3 Review of LEACH Protocol

LEACH protocol operates on round by round and each round has three phases: advertisement phase, cluster set-up phase and steady-state phase. The details of this protocol are explained in [1]. In this section we will give a brief introduction of each phase.

Advertisement phase: Each node decides whether or not to become a CH for current round. This decision is taken based on a prior percentage of CHs for the network and the number of times the node has been a CH so far. After making

this decision each node that has elected itself as a CH for the current round broadcasts an advertisement message to the rest of the nodes. At the end of this phase each non-CH node decides the cluster to which it belongs, for this round. This decision is taken based on the received signal strength of the advertisement message.

Cluster setup phase: Each node informs the selected CH node that it will be a member of the cluster. During this phase all CH nodes must keep their receivers on to receive all the messages from nodes that would like to be a member of the cluster. Depending on the number of nodes in the cluster, the CH creates a TDMA schedule and send this schedule to all other sensor nodes.

Steady-state phase: Sensor nodes start sending data to CH. Sensor nodes transmit their information towards CH in their own time slot allocated by the CH. The radio of each non-CH nodes can be turned off except node's allocated time slot. After receiving from all the sensor nodes CH performs some signal processing prior to transmit towards higher order CH or sink node.

4 Cooperative LEACH Protocol

4.1 Protocol Description

The proposed Cooperative LEACH protocol also operates in round by round fashion and each round has same three phases as LEACH protocol. The advertisement phase of our proposed protocol is same as LEACH protocol as explained in section III.

Modified cluster setup phase: Each non-CH node decides whether it will be a CCH or not. This decision is simply based on the number of times the node has been a CCH so far as the decision made for CHs in LEACH protocol. Each node informs the selected CH node that it will be a member of the cluster as well as the node is a candidate to become a CCH or not. The overhead of this procedure is just transmitting one extra bit along with the cluster joining packet. The CH node receives cluster joining packets from nodes that would like to be included in the cluster. It also selects a CCH from the interested candidates based on the minimum communication distance equivalently with maximum received signal strength of the acknowledgment. If there is no candidate for CCH within the cluster then the CH will select a CCH only on the basis of the received signal strength of acknowledgment. Therefore CH selects a cooperative CH which is located in minimum communication distance from the CH node. If the CH and CCH are in the same place or very close to each other (less than the half wave length) then the system will not get any diversity gain. Cluster-head can avoid this situation by setting a predefined threshold value of the receiver signal strength. Depending on the number of nodes in the cluster, the CH creates a TDMA schedule and sends this schedule to CCH and all other sensor nodes. At the same time Cluster-head informs the cooperative-cluster-head selection. As

soon as the CCH received the schedule from CH it will broadcast an acknowledgment signal toward the all sensor nodes. Therefore all the SNs can adjust their transmission power according to the broadcast signals from CH and CCH so that CH and CCH can receive the local transmission reliably. The overhead of this procedure is about transmitting few extra bits along with the TDMA schedule.

Modified steady-state phase: Sensor nodes start transmitting data and due to the broadcast nature of wireless transmission both cluster-head and cooperative-cluster-head will receive these transmissions. Similar to LEACH protocol we consider all the sensor nodes transmit their information in different time slot allocated by the CH. We also consider that neighboring clusters are using different orthogonal channel to avoid the inter-cluster interference. After receiving information from all sensor nodes, both CH and CCH perform data aggregation before transmitting them to the sink node using the proper signaling structure of cooperative communication. In this paper, we consider a full rate (Alamouti) space time block code as cooperative signaling structure. All kinds of signal processing at CH nodes like data fusion are beyond the scope of our analysis and it is straight forward that additional signal processing does not affect our protocol when both CH and CCH use the same signal processing techniques.

4.2 Transmission Scheme

In cooperative transmission protocols, relay terminals have to process their partner's received signals. However, current limitations in radio implementation preclude the terminals from full duplex operation, i.e., transmitting and receiving at the same time and frequency band [4]. Surprisingly, our modified LEACH structure overcomes this major limitation of cooperation technique. In this proposal, CH and CCH are gathering data independently from the sensor nodes at the same time. Therefore, cluster-heads (CH and CCH) do not require exchanging information among them for cooperation (like, [7]-[11]) which allows us to use a full rate transmission like direct transmission using LEACH.

We consider that both cluster-head and cooperative-cluster-head received the data packets from all sensor nodes inside the cluster. Total n modulated samples are divided in a k pair of samples to transmit in two time slot of Alamouti signaling structure. The k^{th} pair of symbols of Alamouti structure in CH and CCH can be represented as, $s_{CH,1}(k)$, $s_{CH,2}(k)$ and $s_{CCH,1}(k)$, $s_{CCH,2}(k)$ respectively. Here, $k = 1, 2, 3..n/2$, subscripts CH, CCH represents CH and CCH, and 1, 2 represents the first and second symbol of k^{th} pair. The received signals at the sink node for the transmission of k^{th} pair of symbols with Alamouti structure [12] is given by,

$$r_1 = \Gamma_{long} h_{CH} s_{CH,1} + \Gamma_{long} h_{CCH} s_{CCH,2} + \eta_1, \tag{3}$$

$$r_2 = -\Gamma_{long} h_{CH} s^*_{CH,2} + \Gamma_{long} h_{CCH} s^*_{CCH,1} + \eta_2, \tag{4}$$

where h_{CH} and h_{CCH} are the fading coefficients between CH to sink node and CCH to sink node. We assume flat Rayleigh fading; hence, fading coefficients are

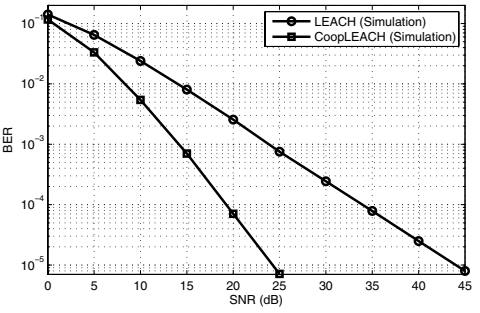

Fig. 2. BER performance comparison of LEACH and CoopLEACH protocol

constant over two symbol period. η_1 and η_2 are additive white Gaussian noise at sink node of symbol period 1 and 2 respectively. We omitted the time index k from all of our equations for simplicity.

We consider the sensor nodes adjust their power during the local transmission so that both the CH and CCH can decode the message correctly. So, the pair of symbols in k^{th} transmission $s_{CH,i}(k)$ and $s_{CCH,i}(k)$ are same symbols, where $i \in \{1, 2\}$. In this case, equation (3) and (4) become the same structure of Alamouti STBC received signals [12]. The decoding of k^{th} pair of symbols are straight forward as the decoding of 2×1 Alamouti codes and given by,

$$s_1 = h^*_{_{CH}} r_1 + h_{_{CCH}} r^*_2. \tag{5}$$

$$s_2 = h^*_{_{CCH}} r_1 - h_{_{CH}} r^*_2. \tag{6}$$

After decoding the transmission for all k, demodulation and maximum likelihood detection is done at sink node to find the information transmitted by all sensor nodes. It is clear from equation (5) and (6) that, we will achieve a diversity of order 2 [12] when local communication is perfect.

4.3 BER Performance

We perform a MATLAB simulation to evaluate the long haul bit error rate (BER) with respect to received SNR values at sink node. We consider the channel conditions explained in eqn. (2) and AWGN noise is modeled as zero mean complex random variable with variance 0.5 per dimension. The fading coefficients for long haul communication is generated by zero mean complex random variables with variance 0.5 per dimension. We also assume that perfect channel state information is available at the sink node so that a coherent detection is possible.

The BER performance against average received SNR of cooperative LEACH (CoopLEACH) and LEACH is shown in Fig. 2. Simulation and numerical results show that proposed Cooperative LEACH protocol outperforms the conventional LEACH. Cooperative LEACH can save about 10 dB (10 times) at BER of 10^{-3}, 15 dB (31.62 times) at BER of 10^{-4} and 20 dB (100 times) at BER of 10^{-5}, with perfect local communication.

5 Energy Efficiency

5.1 Energy Model

The total energy consumption of our proposed cooperative LEACH protocol can divide in three major parts: the energy consumption in cluster setup, local transmission and long haul transmission. For simplicity of analysis we include cluster setup energy in local communication energy. For our energy analysis we use the same approach of [1]. Each of the energy components can be divided into two parts: the energy consumed in transmit amplifier and the transmitter & receiver circuit energy dissipation. The total energy equation is given by,

$$E = E_{t\_local} + E_{c\_local} + E_{t\_long} + E_{c\_long}, \tag{7}$$

where the subscripts c represents circuit energy dissipation, t represents transmission energy, *long* represents long haul communication and *local* represents local communication. For local communication, we consider the same model proposed in LEACH protocol. In [1], the authors assume that, we require a SNR of 30 dB with a noise floor of -82 dBm for error free local communication hence, the threshold on received power is $P_{rx\_th} > (30-82)dB = -52dB \cong 6.3nW$. Following the Friis free space equation [13] and considering, $G_t = G_r = L = 1$, 2.4 G Hz carrier frequency and 1 Mbps bit rate we can get $\varepsilon_{amp\_local} \cong 10pJ/bit/m^2$. For fair comparison with LEACH we consider, CH and CCH of cooperative LEACH share the total energy in long haul transmission as,

$$P^L_{CH} = P^{CL}_{CH} + P^{CL}_{CCH}, \tag{8}$$

where P^L_{CH} is average transmitting power from CH of LEACH protocol and $P^C_{CH}L$ & $P^C_{CCH}L$ are average transmitting power from CH & CCH of cooperative LEACH protocol. We avoided the optimal power allocation technique and assume equal power allocation i.e., $P^{CL}_{CH} = P^{CL}_{CCH} = P^L_{CH}/2$ for simplicity.

In case of long haul transmission, we consider that the channels are subjected to the Rayleigh fading. Hence, the adjustment of the transmit power to achieve an error free communication requires channel state information (CSI) at the transmitting nodes (CH and CCH) which is very difficult to obtain in practical case. Therefore, we consider the CH and CCH transmits with an average power to achieve an arbitrary small BER at the sink node. We chose a moderate value of 10^{-4} as target BER for our energy analysis which is below than the standers. Fig. 2 shows that a BER of 10^{-4} is achieved by the LEACH and cooperative LEACH protocol approximately at 35 dB and 20 dB SNR respectively. The threshold value of the received power of LEACH and cooperative LEACH protocol can be given as, $P^L_{r\_th\_long} > 35 + (-82) = -47dBm \cong 20nW$ and $P^{CL}_{r\_th\_long} > 20 + (-82) = -62dBm = 0.63nW$. According to the two-ray ground propagation model [19] for path loss and considering the similar parameters of local communication along with $h_t = h_r = 1m$, we can get $\varepsilon^L_{amp\_long} \cong 0.02\text{pJ/bit/m}^4$ and $\varepsilon^{CL}_{amp\_long} \cong 0.00063\text{pJ/bit/m}^4$.

Table 1. Simulation Parameters

Nodes	100
Network size ($K \times K$)	$100m \times 100m$
Sink Node position ($K/2, Y$)	$(50, 100)$
ε_{amp_local}	$10pJ/bit/m^2$
$\varepsilon^{CL}_{amp\_long}$	$0.00063pJ/bit/m^2$
$\varepsilon^{L}_{amp\_long}$	$0.02pJ/bit/m^2$
Circuit Energy dissipation (TX or RX)	$50nJ/bit$
Data Aggregation energy	$5nJ/bit/message$
Data Aggregation ratio (r:1)	$10:1$
Percentage of Cluster-head	$10percent$

The circuit energy dissipation for local and long haul communication, and are modeled similarly as original LEACH proposal of [1]. We also consider data aggregation method at both CH and CCH that can compress the data with a ratio of $r:1$. In our energy model, we include the energy consumption for data aggregation in long haul circuit energy.

5.2 Energy Comparison

In this section, we perform a Monte Carlo simulation in MATLAB to evaluate the performance of both LEACH and Cooperative LEACH protocol. Assume, all sensor nodes have data of block size 2000 bits. We consider a 100 node network as shown in Fig. 1. Here the nodes are randomly distributed over the area $K \times K$ and sink node is located Y meter away from the nearest sensor node i.e., located at $(x = K/2, y = -Y)$. Table 1 summarizes the simulation parameters used for the comparison of protocols.

In previous section we analyze the energy saving of long haul transmission. Here, we will compare the energy required for local communication of Cooperative LEACH protocol (CoopLEACH) with LEACH protocol. Local communication also includes the cluster setup procedure and the proposed cooperative LEACH protocol introduces some overhead for selecting a cooperative clusterhead and synchronization among CH and CCH. To compensate this over head we consider Cooperative LEACH protocol transmits extra 100 bits along with the data packet of 2000 bits in local communication. Fig. 3 shows the amount of energy dissipated per round in local communication for both LEACH and cooperative LEACH. Simulation results indicate that the Cooperative LEACH protocol consume higher energy than the LEACH protocol in local communication. The sources of this extra energy consumption are the increase in local communication distance and an extra receiving operation at CCH. As the percentage of CH increases the local communication distance decreases. Therefore, for both protocols the local communication energy consumption decreases with

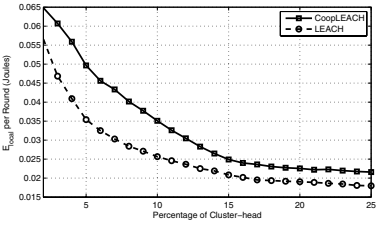

Fig. 3. Comparison of Local communication energy

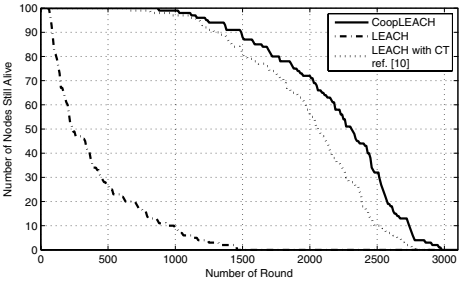

Fig. 4. Network life time of different protocols when each node is initially given 1 Joule

number CHs. This extra power consumption of Cooperative LEACH protocol in local communication is negligible compared with the diversity gain achieved in long haul communication shown in Fig. 2.

Fig. 4 shows a comparison of system lifetime of a network that using cooperative LEACH and LEACH protocol. We consider each node initially start with $1 Joule$ of energy and the simulation parameters of Table 1. Fig. 4 indicates that cooperative LEACH protocol can increase the system life time more than ten times compare with conventional LEACH in terms of both 50 percent nodes to die and first node to die. This huge improvement in network lifetime of cooperative LEACH protocol is achieved due to the diversity gain of long haul transmission.

The other clustering based virtual MIMO protocols like [10] also can achieve the same diversity order but they work on three hop transmission. The first hop is local transmission, second hop is information exchange between the cluster-head and cooperative node and the third phase is long haul transmission. In Fig. 4 we also compare our proposal with the proposal of [10]. With same network parameter and energy model our proposal performs better than the LEACH with Cooperative transmission (LEACH with CT) proposed in [10]. Our proposal reduces the transmission between cluster-head and cooperative node hence, reduces the power required for this transmission. This extra transmission also causes to increase the end to end delay when these LEACH based protocols use time division multiplexing as channel access method. The protocol proposed in [11] offers

a diversity of order 2 with one primary cluster-head and one secondary cluster-head, but sacrifices some performance due to synchronization error. Therefore, proposed cooperative LEACH protocol improves the energy efficiency over [10] and [11] with reduced complexity and delay.

6 Conclusion

In this paper we propose a novel virtual MIMO based LEACH protocol for wireless sensor network. Proposed cooperative LEACH protocol can reduces huge energy consumption with same bit error rate, spectral efficiency and delay requirements compared with LEACH under Rayleigh fading environment. Saving energy equivalently prolongs the network life time which is a prime performance criteria of WSN. We consider all the sources of power consumption in wireless nodes like transmit and receive electronic, transmit amplifier, cluster setup etc. Analysis and simulation result showed that our proposal outperforms conventional LEACH protocol with a minimum overhead.

References

1. Heinzelman, W.R., et al.: Energy-efficient communication protocol for wireless micro-sensor networks. In: Proceedings of the 33rd Annual Hawaii International Conference, vol. 2, pp. 102–114 (2000)
2. Niculescu, D.: Communication paradigms for sensor networks. IEEE Communications Magazine 43, 116–122 (2005)
3. Akyildiz, I.F., et al.: A survey on sensor networks. IEEE communication Magazine, 40(8), 68–73 (2002)
4. Laneman, J.N., et al.: Cooperative diversity in wireless networks: Efficient protocols and outage behavior. IEEE Trans on Inf. Theory 50(12), 3062–3080 (2004)
5. Hedayat, A., et al.: Cooperative Communication in Wireless Networks. IEEE communication Magazine 42(10), 68–73 (2004)
6. Liu, P., et al.: Cooperative Wireless Communications: A Cross-Layer Approach. IEEE Wireless Communications 13(4), 84–92 (2006)
7. Cui, S., et al.: Energy-efficiency of MIMO and cooperative MIMO techniques in sensor networks. IEEE Journ. on Select. Areas. Commun., 1089–1098 (2004)
8. Coso, A., et al.: Cooperative distributed MIMO channels in wireless sensor networks. IEEE Journ. on Select. Areas Commun. 25(2), 402–414 (2007)
9. Jayaweera, S.K.: Virtual MIMO based cooperative communication for energy constrained wireless sensor network. IEEE trans. 5(5), 948–989 (2006)
10. Cheng, W., et al.: An Energy-Efficient Cooperative MIMO Transmission Scheme for Wireless Sensor Networks. In: International Conference on WiCOM, pp. 1–4 (2006)
11. Li, X., et al.: Application of STBC-Encoded Cooperative Transmissions in Wireless Sensor Networks. IEEE signal processing letters 12(2), 134–137 (2005)
12. Alamouti, S.: A simple transmit diversity technique for wireless communications. IEEE J. Select. Areas Commun. 16, 1451–1458 (1998)
13. Rappaport, T.S.: Wireless Communications: Principles and Practice. Prentice Hall, Upper Saddle River (1996)

A Packet Scheduling Algorithm for IEEE 802.22 WRAN Systems and Calculation Reduction Method Thereof

Young-du Lee, Tae-joon Yun, and Insoo Koo*

School of Electrical Engineering, University of Ulsan 680-749 San 29, Muger 2-dong, Ulsan, Republic of Korea
iskoo@ulsan.ac.kr

Abstract. In the paper, a scheduling algorithm based on the estimation of packet loss amount is proposed for supporting real-time traffic in IEEE 802.22 WRAN systems. The proposed scheduling algorithm takes two steps for resource allocation. In the first step, it assigns resource to users having packets that are estimated to be dropped at next frame. In the second step, it assigns the remaining resource to the other users according to one of the existing scheduling algorithms. The simulation results show that the proposed scheduling algorithm provides much better performance than the PLFS and M-LWDF algorithm. In addition, a simple calculation method is proposed for the proposed scheme. With the simple method, we can reduce the number of checking packets in the queue as much as about a half time without any performance degradation in the case of video traffic.

Keywords: IEEE 802.22 WRAN, Scheduling algorithm, Packet loss amount, Calculation reduction method.

1 Introduction

Recently, cognitive radio (CR) has been a popular subject because it is a smart wireless communication system that utilizes a portion of the spectrum band that is allocated to licensed "primary" user but is not being used by primary user at a particular time or a specific geographic location [1]. The first attempt to make a standard based on CR technology is the IEEE 802.22 wireless regional area network (WRAN), which operates on a license-exempt and non-interference basis in the spectrum allocated to TV broadcast services (between 47–910 MHz). WRAN aims to provide alternative broadband wireless Internet access in rural areas without creating harmful interference to licensed TV broadcasting [2,3]. On the condition that customer premise equipments(CPEs) do not interrupt services of incumbent users (IUs) where CPE can be regarded a user and a CR machine, WRAN system can provide service to CPEs where IUs are denoted as "primary" users and CPEs are denoted as "secondary" users equipped with CR technology. Therefore, CPEs should vacate the spectrum band when IUs are activated because CPEs borrow spectrum from IUs. To release spectrum

* Corresponding author.

D.-S. Huang et al. (Eds.): ICIC 2009, LNAI 5755, pp. 738–747, 2009.

in real-time, WRAN system uses quiet period (QP) frame during which it does not access spectrum and focuses on detecting the appearance of IUs. Even though QP frame is essential to detect IUs, it will cause quality of service (QoS) degradation for CPEs especially when real-time traffic is serviced, which is due to the delay of whole packets for the length of the QP frame. The packet of real-time traffic can be discarded when a packet delay exceeds the maximum delay bound.

With regard to QoS of real-time traffic, it is more important to ensure a time delay bound than to maximize the data transmission rate or to ensure fairness among users. Hence, a packet scheduling algorithm that can fulfill the required delay bound is necessary. To date, various scheduling algorithms for supporting real-time traffic have been proposed [4,5,6,7]. Among them, the exponential rule (EXP) and modified largest weighted delay first (M-LWDF) are the scheduling algorithms that simultaneously utilize a channel state of the user and a delay of the packet in the head of line (HOL) of the buffer. More specifically, the EXP scheduling algorithm gives more weight to the delay of the packet in the HOL of the buffer, while the M-LWDF scheduling algorithm considers both the channel status of the user and the delay of packet in the HOL of the buffer. In the case of the packet loss fair scheduling (PLFS) algorithm, the average packet loss rates of users were considered along with the channel status of the user and the delay of the packet in the HOL of the buffer. However, the delay of the packet in the HOL of the buffer was considered only in the mentioned scheduling algorithms. In order to support real-time traffic more effectively in WRAN systems, in the paper we propose a scheduling algorithm by taking into the amount of expected packet loss account. The proposed scheduling algorithm utilizes the amount of packet loss expected in the next frame when radio resources will not be assigned in the current frame. Specifically, the proposed scheduling algorithm assigns radio resources in two steps; in the first step, the resources are assigned to users with packets that are expected to be dropped in the next frame if radio resources will not be assigned in the current frame and, in the second step, they are assigned to users according to the existing scheduling algorithms such as EXP, M-LWDF, PLFS or more simpler scheduling algorithms. In addition, a simple calculation method is proposed for the proposed scheme. With the simple method, we can reduce the number of checking packets in the queue as much as about a half time without any performance degradation in the case of video traffic.

The remaining parts of the paper are organized as follows. In Section 2 we introduce the WRAN briefly. In Section 3, we explain the proposed scheduling algorithm and simple calculation method thereof. In Section 4, we analyze the performances of M-PLFS, PLFS, and the proposed scheduling algorithm in terms of the average packet loss rate and the throughput. The performance of simple calculation method is also presented. In Section 5, some conclusions are given.

2 WRAN System

IEEE 802.22 WRAN selects OFDMA method to effectively provide multimedia service under limited radio resource environment and variable channel state. The OFDMA method has data transmission function, bandwidth assigning method and frame structure similar to 802.16. In addition, IEEE 802.22 WRAN utilizes the superframe

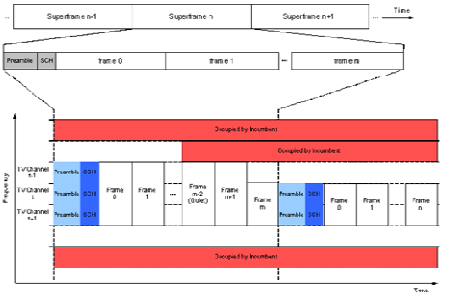

Fig. 1. The frame structure of the WRAN [2] [3]

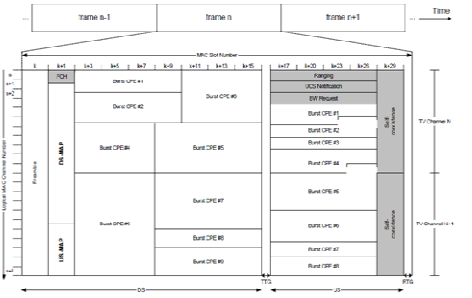

Fig. 2. The superframe structure of the WRAN [2] [3]

structure to facilitate channel combination function, partial bandwidth use and so on. As shown in Fig. 1, the frame structure of WRAN system is managed by superframe unit. The superframe is similar to 802.16 and it consists of n frames having length from 5ms to 10ms. Superframe Control Header(SCH) contains channel combination information, QP(Quiet Time: In-the band sensing, it's the time that stop transmission to scan channels that are using.) information, the number of frames, power information, location information and so on. Remarkable points are that the QP are assigned and managed per the superframe, and that the SCH and the preamble are repeated as the number of combined channels when channels are combined. If base station transmits data through combined three channels, even if CPE connects with one or more channel, in order to take the same information about the superframe, the SCH and the preamble are going to be repeated three times. The proposed frame structure in IEEE 802.22 WRAN uses Time Division Duplex (TDD) as Fig. 2 and it is divided into Downstream Subframe(DS) and Upstream Subframe(US). The frame structure of WRAN is basically similar to 802.16 but there is the main difference that it has Urgent Coexistence Solt(UCS) and coexistence slot in US. Fig. 2 shows a frame structure that two TV band channels are combined. Basically, when base station needs to detect to update the channel state information, it sends CPE message that has period and report information. And it beforehand points a location to transmit the response message on US-MAP. After CPE receives an order message for detecting channel through the DS from the base station, it sends the base station the report message through the US slot pointed. In receiver side of the WRAN, the preamble is designed to perform burst detection, synchronization and channel estimation per each frame. Transmit/Receive Transition Gap(TTG) represents a gap between the DS and the US. And Receive/Transmit Transition Gap(RTG) means frame interval.

In a frame, basic resource space shape is represented with 2-dimension array that has N subchannels in frequency domain and K slots in time domain(N x K). And the WRAN system assumes that the base station receives channel state feedback information about N subchannels from each user. When transmitting packet according to determined priority of users, the WRAN system confirms that there is an empty slot on feedback subchannel. And then if an empty slot exists, the packet is assigned there. Transmission ability of basic resource space is normalized with the number of packets and the standard is defined by SNR value of feedback subchannel. The WRAN

system utilizes a AMC(Adaptive Modulation and Coding) that applies different MCS (Modulation and Coding) according to the channel state.

3 The Proposed Scheduling Algorithm and the Simple Method

3.1 The Proposed Scheduling Algorithm

In case of real-time traffic, in order to provide multimedia service with high quality, it's very important to satisfy the required QoS than any different factors. To do that, the proposed scheduling algorithm has a purpose that should provide better QoS to real-time users by scheduling resource allocation sensitive to packet loss. The packet loss typically occurs when a packet exceeds the required maximum delay time, and the longest delay time that packets experience is the time to stay in queue. Therefore, in order to effectively provide real-time service, it's more effective to reflect queue state.

In this paper, in order to reflect the queue state we consider the packet loss amount(PLA). As follows, the PLA is simply calculated. After assigning resource in the current frame, the packet loss that is expected to occur at next-next frame is quantitatively estimated by comparing the maximum delay time with a time that subtracts the generated time of packet from the drop time of next-next frame. Here, the drop time means the time that the WRAN system discards the packets that exceed the maximum delay time. If the calculated time is over the maximum delay time, the PLA will be counted. In order to reduce the computation load of the WRAN system, the PLA is calculated after altogether finishing the resource allocation. In the step of transmitting, the computation load of the WRAN system is less than the resource assigning step. The reason that the resource assigning step has more the computation load is due to basically include the priority calculation process. The estimated PLA is applied when the scheduler calculates the priority value. The proposed scheduling algorithm has two steps for assigning resource. In the first step, it assigns resource to users who have the PLA. And in the second step, it assigns the remaining resource to the other users according to the existing scheduling algorithm after finishing the first step.

The equation (4) is a case of M-LWDF that the proposed scheduling algorithm is applied. User $\widehat{k_n}$ that n-th subchannel is assigned is determined by the following equation.

$$\widehat{k_n} = \arg\ \max_k \begin{cases} \Phi_{k,n}(t), & \text{if } N_{drop,k}(t+2FP)>0 \\ (\gamma_k \cdot W_k[t] \cdot r_k[t]), & \text{if } N_{drop,k}(t+2FP)=0 \end{cases}. \quad (1)$$

In this equation, t is current time, FP is Frame Period. $N_{drop,k}(t + 2FP)$ represents a PLA that is expected to occur when exceeding $D_{max,k}$ at starting point of next-next frame. $\Phi_{k,n}(t)$ represents a factor considering transmission characteristic and packet characteristic that is given per service class. It is defined as the following equation.

$$\Phi_{k,n}(t) = \min\left(A_{k,n}(t), N_{drop,k}(t + 2FP)\right) \cdot \beta, \quad (2)$$

β is the compensation factor. According to the traffic characteristic of the service, the amount of the generated PLA is different. Therefore, β provides the differentiated service and adjusts the unbalance between services. If $N_{drop,k}(t + 2FP) = 0$ for user

k, the proposed scheduling algorithm calculates the priority value with method of the existing M-LWDF. But if $N_{drop,k}(t + 2FP) > 0$, it calculates the priority value with the formula of upper part in equation (4). After $\Phi(t)$ selects a smaller value between an instant data transmission rate $A_{k,n}(t)$ and $N_{drop,k}(t + 2FP)$, it multiplies β. By selecting the smaller value, $\Phi_{k,n}(t)$ leads "scheduling" to the direction that the whole PLA is minimized.

In order to circumstantially explain difference of the operation characteristic between the existing M-LWDF and the proposed scheduling algorithm, we will explain a simple example. There are two users; user 1 and user 2. The number of the PLA is user 1 = 5, user 2 = 7. The packet delay value of queue HOL has user 1 > user 2, and the instant transmission rate of both users is 12 packets. The other factors for both users are the same. In such situation, when assigning resource, M-LWDF will select user 1 because the packet delay of user 1 is bigger than that of user 2, and as the result the whole PLA will be 7. But the proposed scheduling algorithm will select user 2 because the PLA of user 2 is bigger than that of user 1, as the result the whole PLA will be 5. Therefore, we know that the proposed scheduling algorithm effectively operates with the PLA. The detailed performance evaluation will show in the simulation part.

The equation (6) is a case of PLFS that the proposed scheduling algorithm is applied. User $\widehat{k_n}$ that n-th subchannel is assigned is determined by the following equation.

$$\widehat{k_n} = \arg\max_k \begin{cases} \Phi_{k,n}(t), & \text{if } N_{drop,k}(t+2FP)>0 \\ \left(\frac{A_{k,n}(t)}{\overline{A_k}}\right)\left(\frac{PLR_k(t)}{PLR_{req,k}\times D_{max,k}}\right)\cdot D_{HOL_k}(t), & \text{if } N_{drop,k}(t+2FP)=0 \end{cases}, \quad (3)$$

$D_{HOL_k}(t)$ factor is added to consider the packet delay. It is a delay time of packet of queue HOL of user k. It is calculated by subtracting A_{HOL_k} from current time ($D_{HOL_k}(t) = t - A_{HOL_k}$). A_{HOL_k} denotes the time that packet arrives in queue. The operation mode of the equation (5) and (6) is identical.

3.2 The Simple Method for Reducing the Complexity

Calculating the estimated PLA will occur a high complexity, especially in video traffic because it is generated a great deal of packet by each users. So in this subsection, the simple method is proposed to reduce the complexity.

Although the amounts of packet loss of users who belong to in case of $\Phi_{k,n}(t) > 0$ are a lot, the amount of transmittable packet is limited by the number of transmittable packets. And $\Phi_{k,n}(t)$ also compares which one is less between the number of packet transmittable just by subchannel and the amount of packet loss estimated. For all packets in queue, therefore, it has no need to check whether maximum delay time is exceeded or not, but it needs to check from the head of buffer to a value that it is added 1 with the number of packets transmittable of subchannel n of user k. If there are more than two subchannel information fedback by users, it selects the biggest number of packets transmittable of them since there exists just one amount of packet loss estimated even though user has some subchannel. The limited value of user k, $C_{k,bsc}(t)$ is defined as the following.

$$C_{k,bsc}(t) = A_{k,bsc}(t) + 1, \tag{4}$$

where $A_{k,bsc}(t)$ denotes the number of transmittable packets of the subchannel which has the best channel state, bsc means the subchannel which has the best channel state of subchannels of user k and is defined as the following.

$$bsc = arg_i(maxA_{k,i}). \tag{5}$$

4 Simulation Environments and Results

4.1 Voice Packet Model

The voice source generates the pattern of "active duration" and "non-active duration" independent to each other. The average of each duration is 1 and 1.35 seconds. The voice packet is generated only in active duration, it has the generation rate of 16 kbps bit, and it is made of 320 bits unit. If assume that there are 50 frames per 1 second, which means that it's possible to satisfy QoS of the voice service even if only one voice packet per a frame is transmitted.

Voice traffic assumes that the length of ON-OFF is determined by the exponential function. If t_1 is the average of "active duration", and if assume that active duration ends at time T, the probability γ is defined as the following equation.

$$\gamma = 1 - e^{-\frac{T}{t_1}}. \tag{6}$$

And, if t_2 is the average duration of "non-active duration", and if it ends at time T, the probability σ is defined as the following.

$$\sigma = 1 - e^{-\frac{T}{t_2}}. \tag{7}$$

4.2 Video Packet Model

Real-time video streaming traffic model is described with continuous generating of the frame that has constant duration. And a frame is divided in packet with fixed number. The size of each packet is determined by the Pareto distribution [11]. In a video session, the continuous video frames exist, 8 video packets that have variable length is generated per a frame. The length of each packet and the arrival time interval between packets is determined by the Pareto distribution. The Pareto distribution is defined by $Pareto(k, m, \alpha)$ where k is the minimum value, m is the maximum value, and α means the shape parameter. The average value and the peak value of the Pareto distribution are as follows.

$$\text{Average}: R_{avg} = \frac{64}{100}\left(\frac{\alpha k - m(k/m)^{\alpha}}{\alpha - 1}\right), \tag{8}$$

$$\text{Peak}: R_{peak} = \frac{64}{100}m. \tag{9}$$

Table 1. The system parameter

Parameter	Value
system	OFDMA / TDD
Downlink channel bandwidth	20 MHz
A number of slot per a frame	10
A number of subchannel to transmit data	12
A number of subcarrier per subchannel	128
Frame duration	10 ms
Slot duration	1 ms

4.3 Simulation Result Analysis

This simulation is based on the requirements of IEEE 802.22 WRAN, the simulator written by C-language is used. The superframe structure of the WRAN system consists of 16 frames. In order to analyze in the viewpoint of resource allocation, the control frame part is excepted. In each superframe, a QP frame exists. In order to support the voice and video user, we consider two service classes. The video users are fixed with 20, we observe while increasing by 10 of voice users from 50 to 100. We assume that all users feedback the best channel 3 in 12 channel states to base station. The required packet loss rate of voice and video, $\mathrm{PLR}_{\mathrm{req}}$, are given as 10^{-6} and 10^{-5} respectively[2] [3]. The maximum delay time for the voice and video , $\mathrm{D}_{\mathrm{max}}$, are 20 ms and 40ms. The other system parameter values are the same as Table 1. In order to analysis the performance of the proposed scheduling algorithm, we compare the existing M-LWDF with the proposed scheduling algorithm, and the existing PLFS with that. In the viewpoint of the packet loss rate and the whole throughput, the results are compared and analyzed.

Fig. 3 shows the PLR of the voice service. In the figure, "PLA is applied" represents the case that the proposed scheduling algorithm is applied. A part of all lines except the PLFS aren't drawn on the figure, because the PLR value is very low.

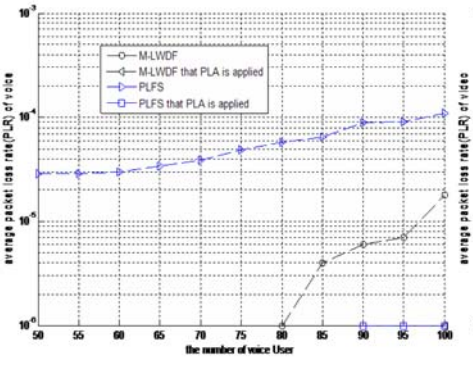

Fig. 3. Packet loss rate of the voice service

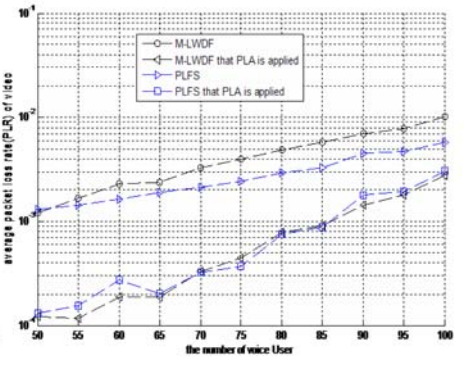

Fig. 4. Packet loss rate of the video service

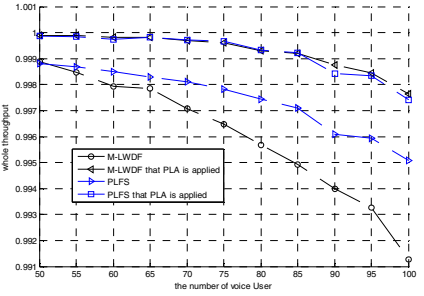

Fig. 5. The throughput of the whole users

The PLFS draws the fluent curve because of considering the PLR but it can't satisfy the required PLR. The reason that the PLR of the PLFS is much bigger than the other scheduling algorithms is because resource allocation of the PLFS is handled by the instant PLR between users. The M-LWDF satisfies the required PLR until 80 voice user, but it can't satisfy that from over that. In the case of the proposed scheduling algorithm completely satisfy it. Fig. 4 shows the PLR of the video service. Although the required PLR level is much lower than the voice service, the video service will show the low performance because it generates the packets much more than voice service per a frame. We can see that all scheduling algorithms can't satisfy the required PLR but the proposed scheduling algorithm is nearest to it. As comparing Fig. 3 and 4, we can find that the proposed scheduling algorithm has the similar PLR performance in both the voice and the video service. Through this, we easily can analogize that the influence determining PLR size of user will be bigger the PLA factor than the packet delay of queue HOL.

Fig. 5 shows the throughput of all users. This value is calculated as "(the number of packets that is successfully transmitted) / (the number of the packets that is generated)". As shown in the figure, the size of the enhanced gap of the M-LWDF is bigger than the PLFS. If the performance of the proposed scheduling algorithm is not almost affected by the scheduling algorithm for the second resource allocation, we could use the simpler scheduling algorithm for the second resource allocation. We, through Fig. 5, can find that the performance of the existing scheduling algorithms is enhanced when the proposed scheduling algorithm is applied.

Since now, in order to more easily notate the proposed packet scheduling algorithm we use EPLA(the Estimated PLA). Fig. 6 and 7 shows the number of checking packets in the queue which stores voice traffic and video traffic respectively. In voice traffic case, the number of checking has few differences between conventional EPLA and EPLA applied simple method. This is because it's enough to make a data transmission by using just a packet per a frame when considering the characteristic of voice traffic. In most of case, the amount of packet in the queue is less than the number of packet transmittable. In video traffic case, we can find that the number of checking packets in the queue for EPLA applied simple method is reduced as about a half when comparing to conventional EPLA. This is because the generated amount of video traffic is relatively much greater than that of voice traffic and in most of case it

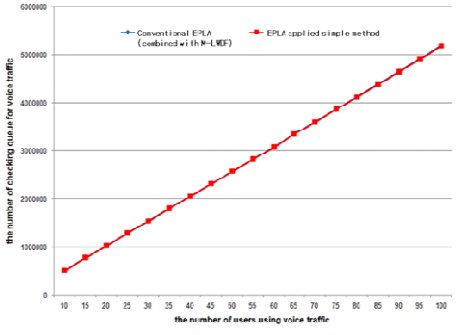

Fig.6. The comparison for the number of checking packet in the queue in voice traffic case

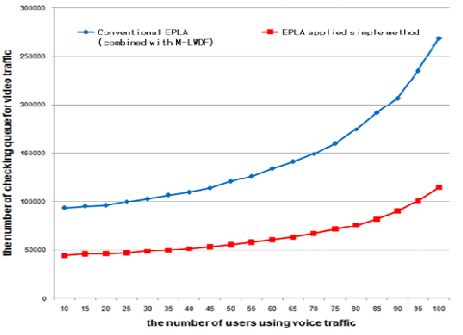

Fig.7. The comparison for the number of checking packet in the queue in video traffic case

is greater than the number of packets transmittable so that it will increase the number of packets remaining in the queue.

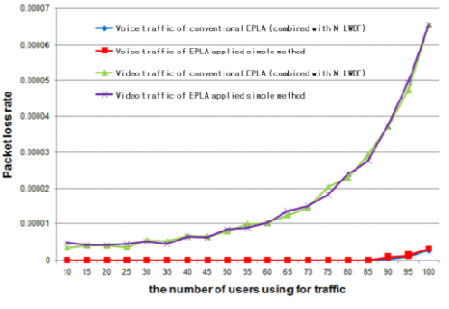

Fig. 8. The comparison for the performance through the packet loss rate

Fig. 8 shows that even though the number of checking packets in queue is reduced, the performance of packet loss rate is not reduced. Since the packet loss rate has direct relation to the throughput, we can think that the whole performance is not degraded.

5 Conclusion

WRAN system inevitably experiences a deep delay by the QP and the real-time traffic that has a short lifetime requires more urgent transmission. The situation will generate a lot of packet losses. Therefore, the WRAN system will need a scheduling algorithm sensitive to the packet loss. In this paper, we have proposed a scheduling algorithm based on the estimation of the PLA for supporting real-time traffic in IEEE 802.22 WRAN Systems. The proposed scheduling algorithm provides better PLR and throughput than the existing scheduling algorithms such as the M-LWDF and the PLFS. In order to reduce complexity for estimating PLA, the simple calculation

reduction method has also been proposed such that the number of checking packets in the queue is reduced as much as about a half time in the video traffic case without any performance degradation.

Acknowledgement

This work was supported in part by the Ministry of Commerce, Industry, and Energy and in part by Ulsan Metropolitan City through the Network-based Automation Research Center at the University of Ulsan.

References

1. Mitola, J.: Cognitive Radio for flexible mobile multimedia communications. In: Proc. of IEEE Workshop on Mobile Multimedia Comm., pp. 3–10 (1999)
2. IEEE 802.22.: IEEE 802.22 / D0.2 Draft Standard for Wireless Regional Area Networks Part22: Cognitive Wireless RAN Medium Access Control and Physical specifications: Policies and procedures for operation in the TV Bands (2006)
3. IEEE 802.22.: IEEE 802.22 / D0.3.7 Draft Standard for Wireless Regional Area Networks Part22: Cognitive Wireless RAN Medium Access Control and Physical specifications: Policies and procedures for operation in the TV Bands (2007)
4. Shakkottai, S., Stoylar, A.L.: Scheduling for Multiple Flows Sharing a Time-varying Channel: the Exponential Rule. Bell Laboratories Technical Report (2000)
5. Shakkottai, S., Stoylar, A.L.: Scheduling Algorithms for a Mixture of Real and Non-real-time Data in HDR. Bell Laboratories Technical Report (2000)
6. Shin, S.J., Ryu, B.H.: Packet Loss Fair Scheduling Schemefor Real-time Traffic in OFDMA System. ETRI Journal 26(5), 391–396 (2004)
7. Park, T.W., Shin, O.S., Lee, K.B.: Proportional Fair Scheduling for Wireless Communication with Multiple Transmit and Receive Antennas. In: Vehicular Technology Conference, vol. 3, pp. 1573–1577 (2003)
8. Shakkottai, S., Stoylar, A.L.: Scheduling Algorithm for a Mixture of Real-Time and Non-Real-Time Data in HDR. In: 17th International Teletraffic Congress (2001)
9. Andrews, M., Kumaran, K., Ramanan, K., Stolyar, A., Whiting, P., Vijayakumar, R.: Providing Quality of Service over a Shared Wireless Link. IEEE Comm. Mag., 150–154 (2001)
10. Andrews, M., Kumaran, K., Ramanan, K., Stolyar, A., Vijayakumar, R., Whiting, P.: CDMA Data QoS Scheduling on the Forward Link with Variable Channel Conditions. Bell Labs Tech. Memo (2000)

Study on Multi-Depots Vehicle Scheduling Problem and Its Two-Phase Particle Swarm Optimization*

Suxin Wang[1], Leizhen Wang[1], Huilin Yuan[1], Meng Ge[1], Ben Niu[2], Weihong Pang[1], and Yuchuan Liu[1]

[1] Northeastern University at Qinhuangdao, Qinhuangdao Hebei, 066004 China
[2] College of Management, Shenzhen University, Shenzhen, 518060 China
wsx96@126.com, wlz@mail.neuq.edu.cn,
drniuben@gmail.com

Abstract. To get global solution in multi-depots vehicle scheduling problem (MDVSP), MDVSP models are established. Two-phase particle swarm optimization (TPPSO) is established to solve MDVSP. The optimization course are as follow: first phase, set up goods number dimension particle position vector, vector's every column corresponds to goods, vector elements are random vehicle serial number, thus we can assign goods to vehicles. Second phase, particle position matrix is set up, matrix's column number equal to vehicle freight goods number, every column corresponds to a goods, and matrix has two row, the first row correspond to goods start depot, second row correspond to end depot, matrix elements are random number between 0 and 1, matrix elements are sort ascending according to sort rules, we can get single vehicle route. Then evaluate and filtrate particles by optimization aim, circulate until meet terminate qualification. TPPSO can assign all freights to all vehicles and easy to get optimized solution.

Keywords: Multi-depots vehicle scheduling problem (MDVSP), Particle swarm optimization (PSO), Two-phase method.

1 Introduction

Vehicle routing problem (VRP) was first proposed by Dantzig and Ramser in 1959. Multi-depots vehicle scheduling problem (MDVSP) is complex to single depot VRP, many algorithms are used to deal with MDVSP, such as one-stage approach[1], exact algorithm[2], variable neighborhood search (VNS) [3], genetic algorithm [4] and so on. These algorithms transform MDVSP into many single depots VRP, depot is visited only once, and easy get into local minima.

* This work is partially supported by National Scientific and Technical Supporting Programs Funded by Ministry of Science & Technology of China (NO.2006BAH02A09), National Natural Science Foundation of China (70431003), Hebei Procce Technical Research and Develop Instruct Programs (072135214), Shenzhen-Hong Kong Innovative Circle project (Grant no.SG200810220137A) and Project 801-000021 supported by SZU R/D Fund.

D.-S. Huang et al. (Eds.): ICIC 2009, LNAI 5755, pp. 748–756, 2009.

To deal with this issue, and get the global solution, two-phase particle swarm optimization (TPPSO) is proposed in this paper for MDVSP.

2 VSP Parameter Demarcate and Model

2.1 Multi-Depots Freight Modes

Multi-depots vehicle freight modes see (a) in Fig 1.

	depot 1	*depot 2*	*depot 3*	*depot 4*	…	*depot 1+n*	*depot 2+n*	*depot 3+n*	…
Mode 1:	(load	load	load	load	…)	(unload	unload	unload	…)
Mode 2:	(load	unload)	(load	unload)	…	(load	unload)	(load	…
Mode 3:	load	load	unload	load	…	unload	unload	load	…

(a) Freight Modes

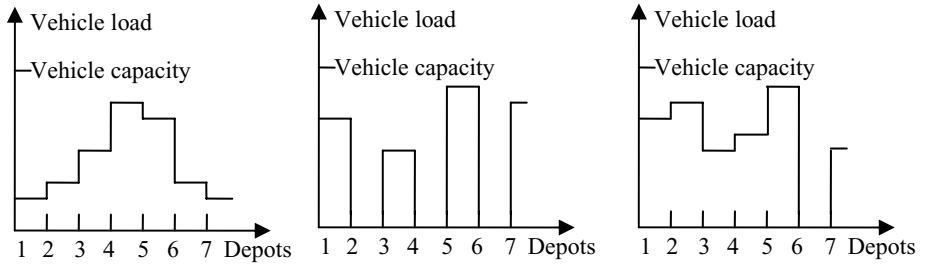

(b) Mode 1 vehicle load (c) Mode 2 vehicle load (d) Mode 1 vehicle load

Fig. 1. Multi-depots vehicle freight modes

In multi-depots vehicle freight modes, vehicle departs from depot, turn to start or another depot when vehicle accomplish goods conveyance. In mode 1, vehicle load continuous, then unload continuous, vehicle load first ascend, then descend, vehicle load changes we can see (b) in Fig 1. In mode 2, vehicle load goods, then unload goods and recurrence, vehicle load changes is rectangle wave, which we can see (c) in Fig 1. In mode 3, vehicle load and unload goods randomly, vehicle load is fluctuant, vehicle load changes we can see (d) in Fig 1. Mode 3 includes mode 1 and mode 2, vehicle position is random and it needn't go to its start point, which can make good use of goods and vehicle resource.

To MDVSP, goods start and end depot should be visited once, if goods beyond vehicle capacity, depot should be visited more than once.

2.2 Model Parameter Demarcate

Graph G= (V, A), where V is the depots set, depots i, j and $u \in$ V, A is the arc set. Q_v is vehicle capacity. N_v is vehicle numbers, n_v is vehicle serial number, $n_v \in N_v$; If vehicle n_v departs from depot i to j, $x_{ij}^{n_v}=1$, other wise $x_{ij}^{n_v}=0$. d_{ij} is the distance of depot i to j. $L_{v\max}$ is vehicle route length limit. O_{ij} is the goods which need to consign from depot i to j, O_{ij} start and end depots are linked by arrowhead. q_{ij} is O_{ij}'quality, $q_j^{n_v}$ is vehicle load when vehicle n_v departs from depot j, N_O is O_{ij} sum number ; If O_{ij} is on vehicle n_v, $o_{ij}^{n_v}=1$, otherwise $o_{ij}^{n_v}=0$; If O_{ju} is going to load on vehicle n_v, $y_{ju}^{n_v}=1$, otherwise $y_{ju}^{n_v}=0$.

2.3 MDVSP Model

Assumption:

(1) When O_{ij} load on vehicle n_v, it load until vehicle n_v reach O_{ij} end depot, which means no vehicle transfer.

(2) Vehicle types are multiplicity and there are enough vehicles, vehicle position is random.

(3) When vehicle finish all O_{ij} consignment, it needn't go to its start point.

Objective function:

$$\min \sum_{n_v \in N_v} \sum_{i \in \mathrm{V}} \sum_{j \in \mathrm{V}} (d_{ij} x_{ij}^{n_v}), \tag{1}$$

Subject to:

$$0 < q_{ij} \le Q_v, \tag{2}$$

$$0 \le q_j^{n_v} \le Q_v, \tag{3}$$

$$\sum_{i \in \mathrm{V}} \sum_{j \in \mathrm{V}} (d_{ij} x_{ij}^{n_v}) \le L_{v\max}, \tag{4}$$

$$\sum_{n_v \in N_v} o_{ij}^{n_v} = 1, \tag{5}$$

when $x_{ij}^{n_v}=1$,

$$q_j^{n_v} = q_i^{n_v} - \sum_{i \in \mathrm{V}} o_{ij}^{n_v} q_{ij} + \sum_{u \in \mathrm{V}} q_{ju} y_{ju}^{n_v}. \tag{6}$$

In the above proposed model, the objective function (1) is to minimize vehicle route length. The constraints for vehicle load and goods quantity are showed in (2) and (3). The constraint for vehicle route length is showed in (4). The same goods are ferried by one vehicle is showed in (5). Vehicle load and unload information are showed in (6).

3 MDVSP Model Strategy Based on TPPSO

3.1 Particle Swarm Optimization

Particle swarm optimization (PSO) [5-9] is a population based stochastic optimization technique developed by Dr. Eberhart and Dr. Kennedy in 1995, inspired by social behavior of bird flocking or fish schooling.

In PSO, every particle (individual) adjusts its "flying" according to its own flying experience and its companions' flying experience. Every particle is treated as a point in a D-dimensional space. Particle number is R, the r^{th} particle is represented as $X_r = (x_{r1}, x_{r2}, \ldots, x_{rd}, \ldots, x_{rD})$. The best previous position (the position giving the fitness value) of the r^{th} particle is recorded and represented as $P_r = (p_{r1}, p_{r2}, \ldots, p_{rd}, \ldots, p_{rD})$. The index of the best particle among all the particles in the population is represented by P_g. The position change rate (velocity) for particle r is represented as $V_r = (v_{r1}, v_{r2}, \ldots, v_{rd}, \ldots, v_{rD})$. The particles are manipulated according to the following equation:

$$v_{rd} = wv_{rd} + c_1b_1(p_{rd} - x_{rd}) + c_2b_2(p_{gd} - x_{rd}), \tag{7}$$

$$x_{rd} = x_{rd} + v_{rd,} \tag{8}$$

In (7), c_1 and c_2 are two positive constants, b_1 and b_2 are two random numbers between 0 and 1, and w is the inertia weight. Equation (7) is used to calculate the particle's new velocity according to its previous velocity and the distances of its current position from its own best experience (position) and the group's best experience. Then the particle flies toward a new position according to (8).

The d^{th} ($1 \le d \le D$) dimension bounds of X are $[x_{d\,\min}, x_{d\,\max}]$, V are $[v_{d\,\min}, v_{d\,\max}]$, if x_d or v_d exceed bound in iteration, take bound value.

Particle's position and velocity are produced randomly, and iterate according to (7) and (8) until meet terminate condition.

3.2 Two-phase Particle Swarm Optimization

MDVSP is optimized by TPPSO. First phase in TPPSO assign task (goods) to vehicle, second phase, optimize single vehicle route, the fix-and-optimize approach is shown in Fig 2.

1) First Phase Parameter Representation

At the first phase in TPPSO, to assign goods to vehicle, particle position vector expression is presented in Fig 3. Vector's every column corresponds to an O_{ij}, vector's element is random vehicle serial number, and by comparing vector's element, we can find the goods that vehicle to freight. For example, in Fig 3 we can see vehicle n_v ferry goods $O_{i\,(j+3)}$ and $O_{(j+2)\,u}$.

2) Second phase Parameter Representation

At the second phase in TPPSO, particle position matrix is set up. In particle position matrix, column number equal to vehicle freight goods number, every column corresponds to a O_{ij}, and matrix has two row, the first row corresponds to O_{ij} start depot,

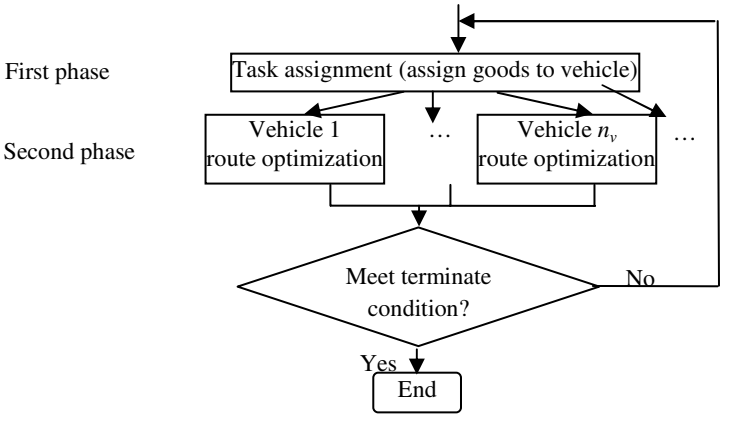

Fig. 2. Two-phase method for MDVSP

	O_{ij}	$O_{i(j+3)}$	…	$O_{(i-1)(j-1)}$	$O_{(j+2)u}$	O_{ju}
X=	n_v +2	n_v	…	n_v -2	n_v	n_v -3

Fig. 3. First phase particle position vector expression

second row correspond to O_{ij} end depot. Matrix elements are random number between 0 and 1. Particle position matrix expression is presented in Fig 4.

To get single vehicle route, matrix's elements are sort ascending, due to matrix elements corresponding to depots, we can get single vehicle route.

	(goods)	O_{ij}	$O_{i(j+3)}$	…	O_{ju}
	(O_{ij} start depot)	i	i	…	j
	(O_{ij} end depot)	j	j+3	…	u
X=	(O_{ij} start depot random number)	0.2	0.5	…	0.7
	(O_{ij} end depot random number)	0.1	0.7	…	0.9

Fig. 4. Second phase particle position matrix expression

To avoid consigning O_{ij} to reverse direction, sort rules are:

a) If random numbers are equal among some O_{ij}, random select a depot to get global solution.

b) O_{ij} end depot can't be visited until O_{ij} start depot is visited, so O_{ij} start depot random number should less to O_{ij} end depot, otherwise interchange random number. If random numbers are equal, then start depot first.

3.3 Optimization Process

The overall learning process can be described as follows:

Step 1——Initialize particles

1) Initialize PSO parameters

2) Get random integer numbers between 1 and N_v for particle position matrix

3) Get random numbers between $(1-N_v)$ and (N_v-1) for particle velocity matrix

4) Find the goods that vehicle to freight, get single vehicle route by PSO according to sort rules arrange matrix elements

5) Calculate particle fitness value by objective function

6) Make first particle position matrix as P_r and find P_g in particles

Step 2——Iterance hereinafter step until meet terminate condition

1) For every particle, calculate particle velocity according (7), update particle position according (8), take bound value if particle's velocity or position exceed boundary

2) Find the goods that vehicle to freight, get single vehicle route by PSO according to sort rules arrange matrix elements

3) Calculate particle fitness value by objective function

4) If the fitness value is better than the best fitness value in history (P_r), set current value as P_r, and save vehicle route

5) In particles, choose the particle with the best fitness value as P_g and save vehicle route, if there are multi-P_g, get a P_g randomly.

4 Computational Results

4.1 Example

In one area and certain time, goods consign information are showed in Fig 5, goods start and end depots are linked by arrowhead. Goods information is showed in Table1, set Q_v =10t, $L_{v\max}$ =100km, it is required to finish goods consignment with optimized vehicle route and without overload, if overload happened, objective function should be punished.

4.2 Optimized Solution

1) TPPSO for MDVSP

PSO parameters are set as $c_1 = c_2$=1.49445, w =0.729, particle septuple columns number, iterate 30 times. At the first phase in TPPSO for MDVSP, particle position matrix has 17 columns according to table 1, and every column corresponds to a O_{ij}. At the second phase, particle position matrix column are set by goods that the vehicle to freight.

Run TPPSO 20 times, vehicle optimized sum route length is 190.24km, and there are two vehicles, the detailed information can be seen in Tab 2. In Tab 2 we can see, depot 11, 13, 1, 8,9,0,5 and 14 are visited more than once due to vehicle load restriction, vehicle load or unload randomly, vehicle load is fluctuant. These phenomena relate to goods information and depots position.

2) ACO for MDVSP

Ant colony optimization (ACO) is used to MDVSP, ACO parameters set as: the relative influence of the pheromone trails α=1, the relative influence of the distances β=5, the number of ant equal to vehicle, trails retain coefficient ρ=0.7, constant

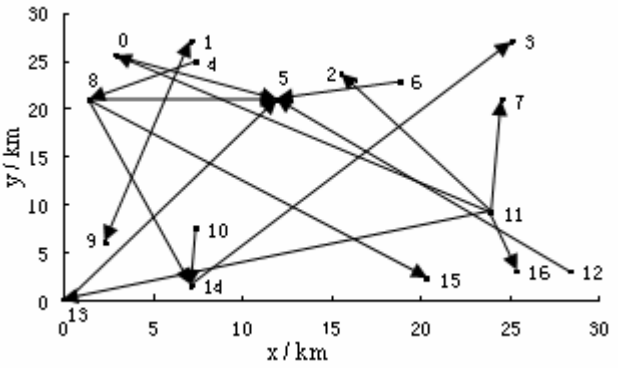

Fig. 5. Goods consign information

Table 1. Goods Information

O_{ij}	$q_{ij}(t)$	O_{ij}	$q_{ij}(t)$	O_{ij}	$q_{ij}(t)$	O_{ij}	$q_{ij}(t)$	O_{ij}	$q_{ij}(t)$
$O_{(0)(5)}$	2	$O_{(6)(5)}$	2	$O_{(11)(0)}$	3.8	$O_{(14)(3)}$	1.6	$O_{(4)(8)}$	3.3
$O_{(8)(5)}$	3	$O_{(11)(16)}$	4.2	$O_{(11)(13)}$	4.7	$O_{(10)(14)}$	2.1		
$O_{(13)(5)}$	2.6	$O_{(11)(7)}$	1.4	$O_{(1)(9)}$	1.4	$O_{(8)(14)}$	1.2		
$O_{(12)(5)}$	3.5	$O_{(11)(2)}$	0.6	$O_{(9)(1)}$	4.3	$O_{(8)(15)}$	2		

Q=100, iterate 30 times. Run ACO 20 times, vehicle optimized sum route length is 204.87/km and there are three vehicles.

3) Comparision between ACO and TPPSO for MDVSP

From the optimization result we can see, by TPPSO, vehicle optimized sum route length is 190.24km, and there are two vehicles take part in goods conveyance. By ACO, vehicle optimized sum route length is 204.87/km and there are three vehicle take part in goods conveyance.

So TPPSO is good to ACO in optimizing MDVSP.

Table 2. Load and unload information for vehicle

route	route length /km	vehicle route	load goods	unload goods	vehicle load /t
1	98.33	11→	$O_{(11)(16)}$ $O_{(11)(7)}$ $O_{(11)(2)}$ $O_{(11)(0)}$		10
		16→		$O_{(11)(16)}$	5.8
		12→	$O_{(12)(5)}$		9.3
		7→		$O_{(11)(7)}$	7.9
		6→	$O_{(6)(5)}$		9.9
		2→		$O_{(11)(2)}$	9.3
		5→		$O_{(6)(5)}$ $O_{(12)(5)}$	3.8

Table 2. (*continued*)

route	route length /km	vehicle route	load goods	unload goods	vehicle load /t
		4→	$O_{(4)\ (8)}$		7.1
		1→	$O_{(1)\ (9)}$		8.5
		0→		$O_{(11)\ (0)}$	4.7
		8→	$O_{(8)\ (15)}$ $O_{(8)\ (14)}$	$O_{(4)\ (8)}$	4.6
		9→		$O_{(1)\ (9}$	3.2
		10→	$O_{(10)\ (14)}$		5.3
		14→		$O_{(8)\ (14)}$ $O_{(10)\ (14)}$	2
		15		$O_{(8)\ (15)}$	0
2	91.91	11→	$O_{(11)\ (13)}$		4.7
		14→	$O_{(14)\ (3)}$		6.3
		13→	$O_{(13)\ (5)}$	$O_{(11)\ (13)}$	4.2
		9→	$O_{(9)\ (1)}$		8.5
		5→		$O_{(13)\ (5)}$	5.9
		1→		$O_{(9)\ (1)}$	1.6
		0→	$O_{(0)\ (5)}$		3.6
		8→	$O_{(8)\ (5)}$		6.6
		5→		$O_{(0)\ (5)}$ $O_{(8)\ (5)}$	1.6
		3		$O_{(14)\ (3)}$	0

5 Conclusions

There are two reasons to get the global solution. First, in MDVSP model, goods with start and end depots are denoted as O_{ij}, goods consignment relation is clear. Second, vehicle route to all goods is searched with optimized route by TPPSO, optimization processes are depended, and tend to get the global solution.

References

1. Lim, A., Wang, F.: Multi-depot vehicle routing problem: a one-stage approach. Automation Science and Engineering 397, 397–402 (2005)
2. Aristide, M.: The multi-depot periodic vehicle routing problem. In: Zucker, J.-D., Saitta, L. (eds.) SARA 2005. LNCS (LNAI), vol. 3607, pp. 347–350. Springer, Heidelberg (2005)
3. Michael, P., Richard, F.H., Karl, D., et al.: A variable neighborhood search for the multi depot vehicle routing problem with time windows. Springer Netherlands, Journal of Heuristics 10(6), 613–627 (2004)
4. Yang, Y.F., Cui, Z.M., Cheng, J.M.: An Improved Genetic Algorithm for Multiple-Depot Vehicle Routing Problem with Time Window. Journal of Soochow University (Engineering Science Edition) 26(2), 20–23 (2006)
5. Kennedy, J., Eberhart, R.C.: Particle swarm optimization. In: Proceedings of IEEE International Conference on Neural Networks, pp. 1942–1948 (1995)

6. Ben, N., Zhu, Y.L., He, X.X., Hai, S.: A Multi-swarm Optimizer Based Fuzzy Modeling Approach for Dynamic Systems Processing. Neurocomputing 71, 1436–1448 (2008)
7. Ben, N., Zhu, Y.L., He, X.X., Wu, H.: MCPSO: A Multi-Swarm Cooperative Particle Swarm Optimizer. Applied Mathematics and Computation 185(2), 1050–1062 (2007)
8. Niu, B., Li, L.: A novel PSO-DE-based hybrid algorithm for global optimization. In: Huang, D.-S., Wunsch II, D.C., Levine, D.S., Jo, K.-H. (eds.) ICIC 2008. LNCS (LNAI), vol. 5227, pp. 156–163. Springer, Heidelberg (2008)
9. Ben, N., Zhu, Y.L., He, X.X., Wu, H., Hai, S.: A Lifecycle Model for Simulating Bacterial Evolution. Neurocomputing 72, 142–148 (2008)

Image Segmentation to HSI Model Based on Improved Particle Swarm Optimization*

Bo Zhao[1], Yajun Chen[2], Wenhua Mao[1], and Xiaochao Zhang[1]

[1] The Institute of Electrical and Mechanical Technology, Chinese Academy of Agricultural Mechanization Sciences, Beijing 100083, China
[2] The Department of Information Science, Xi'an University of Technology, Xi'an 710048, China

Abstract. According to the characteristics of the particle swarm optimization, a method for the image segmentation to HSI model based on the improved particle swarm optimization was proposed in this paper. Firstly, the basic principle of the algorithm was introduced. Secondly, the characteristics on the image segmentation were analyzed. Finally, the image segmentation method based on the improved PSO was proposed, which can effectively overcome shortages which are the slow rate of the particle swarm optimization and the poor segmentation quality by using other algorithms. Experimental results proved that the improved algorithm was an effective method for the image segmentation in the practical application, which could segment the object accurately.

Keywords: Image segmentation, HIS model, PSO.

1 Introduction

Image segmentation is hot research issues on the image processing and a key process of the image analysis and the image comprehension. Traditional segmentation methods are effective to some images, but are limited to other images which are applied to the especial field and characteristics. Therefore, some intelligence algorithms were applied to the image segmentation, such as the neural network, genetic, swarm intelligence, and so on [1]. Swarm intelligence takes inspiration from the social behaviors of insects and of other animals. In particular, birds have inspired a number of methods and techniques among which the most studied and the most successful is the general purpose optimization technique known as particle swarm optimization (PSO).

The PSO which is a powerful stochastic evolutionary algorithm has some advantages which are the PSO can solve a variety of difficult optimization problems but has

* Project supported by The National High Technology Research and Development Program of China (863Program)(No. 2006AA10A305 and No. 2006AA10Z254), The National Natural Science Funds of China (No. 30771263) and The Key Technology R&D Program (No. 2007BAD89B04).

D.-S. Huang et al. (Eds.): ICIC 2009, LNAI 5755, pp. 757–765, 2009.

shown a faster convergence rate than other evolutionary algorithms on some problems, and the great advantage of the PSO is that it has very few parameters to adjust, which makes it particularly easy to implement. Therefore the algorithm takes on the excellent performance and the tremendous development potential, and it is successfully applied to the function minimization, the neural network training, the data mining, the control of the fuzzy system, and so on.

2 Particle Swarm Optimization

The PSO, first introduced by Kennedy and Eberhart [2] is a stochastic optimization technique which can be likened to the behavior of a flock of birds. A simple explanation of the PSO's operation is as follows. The population of the PSO is called a swarm and each individual in the population of the PSO is called a particle. Each particle represents a possible solution to the optimization task at hand. During each iteration, each particle accelerates in the direction of its own personal best solution found so far, as well as in the direction of the global best position discovered so far by any of the particles in the swarm. This means that if a particle discovers a promising new solution, all the other particles will move closer to it, exploring the region more thoroughly in the process [3],[4].

The swarm size of the PSO is denoted to s. Each particle has the following attributes which are a current position x_i in the search space, a current velocity v_i, and a personal best position p_i in the search space. During each iteration, each particle in the swarm is updated using (1) and (2).

$$v_{i+1} = \varpi v_i + c_1 r_1 (p_i - x_i) + c_2 r_2 (p_g - x_i) . \tag{1}$$

The new position of a particle is calculated using

$$x_{i+1} = x_i + v_{i+1} . \tag{2}$$

The variable ϖ is the inertia weight, this value is typically setup to vary linearly from 0 to 1 during the course of a training run.

The variable c_1 and c_2 are the acceleration coefficients, which can control how far a particle will move in a single iteration. Typically, these are both set to a value of 2.0, although assigning different values to c_1 and c_2 sometimes leads to improved performance.

The variable r_1 and r_2 are two random numbers in the range (0, 1).

The variable p_g is the global best position found by all particles.

The velocity v_i of each particle can be clamped to the range $[-v_{\max}, v_{\max}]$ to reduce the likelihood of particles leaving the search space. The value of $v_{\max}$ is usually chosen to be $k \times m_{\max}$, with $0.1 \le k \le 1.0$ [3]. Note that this does not restrict the values of x_i to the range $[-v_{\max}, v_{\max}]$, it only limits the maximum distance that a particle will move during one iteration.

3 Image Segmentation Based on the Improved PSO

The main purpose of the using PSO is to find an image segmentation method which could effectively process images of HSI model, which is applied to the traffic signs recognition, the license plate recognition, the vision navigation of the agricultural robot widely, as shown in Fig. 1, and the process effect of HIS model is superior to other model, such as RGB model, YUV model and so on. Fig. 2 shows the H component image after processing by using (3) to the original color image of Fig. 1.

$$\begin{aligned} I &= \tfrac{1}{3}(R+G+B)\,, \\ S &= 1-\tfrac{3}{(R+G+B)}\left[\min(R,G,B)\right], \\ H &= \arccos\left\{\frac{\left[(R-G)+(R-B)\right]/2}{\left[(R-G)^2+(R-B)(G-B)\right]^{1/2}}\right\}. \end{aligned} \tag{3}$$

(a)

(b)

Fig. 1. The original color image: (a) is an image of the traffic signs recognition, (b) is an image of the vision navigation of the agricultural robot

(a)

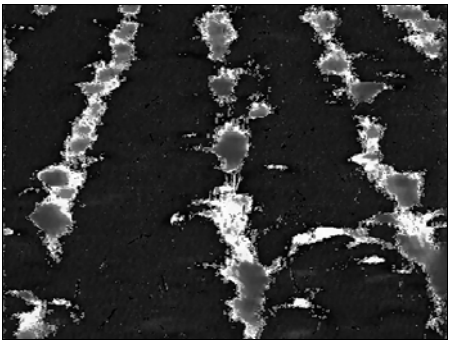

(b)

Fig. 2. The *H* component of HSI model: (a) is the *H* component of Fig.1 (a), (b) is the *H* component of Fig.1 (b)

3.1 Improved Algorithm

The results of the traditional PSO are exact, but its convergence rate is slow, therefore the algorithm has to be improved [6]. In order to the high convergence rate and exact image segmentation, we consider the maximum, the minimum and the average gray value as the starting position of three particles, the position of other particles are the random number in the range (0, 255), calculate the distance d_{ij} from each pixel to initializing position of all particles using (3), setup a personal best position of all particles and the global best position, compute by the PSO, and update the position of all particles. Through the heuristic guidance, the improved PSO could fast find the optimal value.

$$d_{ij} = \sqrt{(g_{ij} - x_k)^2} \ . \tag{4}$$

The variable g_{ij} is image gray value, The variable x_k is current position of each particle.

3.2 Algorithm Description

1) Initialize the parameters s, ω, c_1 and c_2, and setup the iterative times N.

2) Consider the maximum, the minimum and the average gray value as the position of three particles, setup the random position of other particles, and setup the random velocity of all particles.

3) Calculate the distance d_{ij} from each pixel to initializing position of all particles using (3), setup a personal best position of all particles and the global best position.

4) Start the circulation, update the position and the velocity of all particles using (1) and (2), clamp the velocity and the position of each particle, evaluate the new adaptive value using (4).

5) Compare the new adaptive value of each particle.

6) If the global best position is not change, end the circulation, otherwise, return to step 4, and continue the circulation.

7) Setup the global best position to segmentation threshold and segment the image.

4 Experimental Results and Discuss

4.1 Experimental Results

The improved PSO algorithm includes some tuning parameters which greatly influence the algorithm performance, often stated as the exploration–exploitation tradeoff. Exploration is the ability to test various regions in the problem space in order to locate a good optimum, hopefully the global one. Exploitation is the ability to concentrate the search around a promising candidate solution in order to locate the optimum precisely [5]. Therefore these parameters are adjusted as well.

The key parameters of the improved PSO are the swarm size s, the maximal velocity $v_{\max}$, the inertia weight ω and the iterative times N in this paper.

If the swarm size s was too many, the cost time will be increased, and the image segmentation results were inferiority. If the swarm size s was too few, the image segmentation results were also inferiority, although the cost time was short. Therefore the range of the swarm size s was from 25 to 40, the image segmentation results can meet requirement. With the increase of the iterative times N, the cost time of the image segmentation was also increased rapidly. When the inertia weight ω was from 0.5 to 0.9, the image segmentation results can meet requirement. When the range of the maximal velocity $v_{\max}$ was from 0.4 to 0.9, the image segmentation results can meet requirement. Typically the acceleration coefficient c_1 and c_2 were 2.

In order to meet the practical application, the criterion of the choosing optimization parameters is to decrease the convergence rate, and improve the image segmentation effect to the different images. By the above experiments, the optimization parameters of the improved algorithm were that the swarm size s was 30, the maximal velocity $v_{\max}$ was 0.5, the inertia weight ω was 0.9 and the iterative times N was 1 respectively. The twenty different images were tested by using these parameters. The average cost time was 495 *ms* and the segmentation results were excellent, as shown in Fig. 3(a) and Fig. 4 (a) (All images size is 640 × 480 in this paper.).

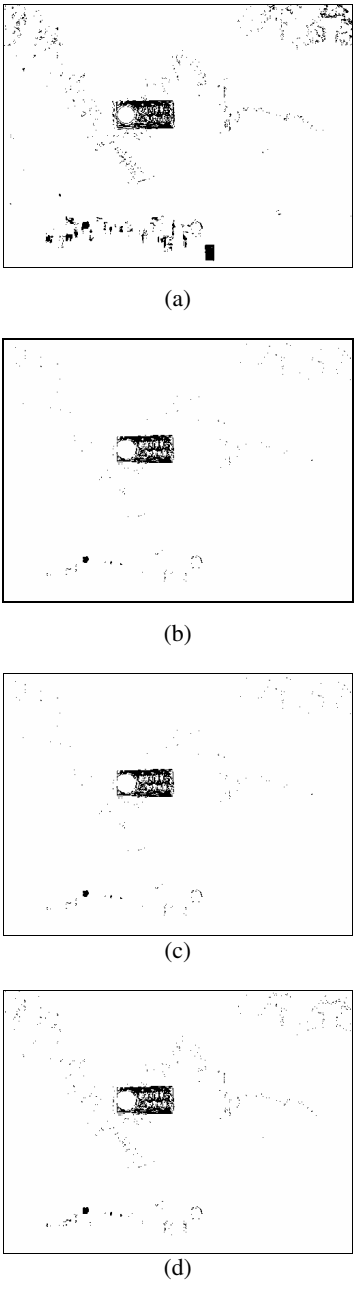

(a)

(b)

(c)

(d)

Fig. 3. The image segmentation: (a) is the image segmentation result of Fig. 2(a) by using the improved PSO, (b) is the image segmentation result of Fig. 2(a) by using the PSO, (c) is the image segmentation result of Fig. 2(a) by using the iteration threshold algorithm, (d) is the image segmentation result of Fig. 2(a) by using the *K*-means clustering

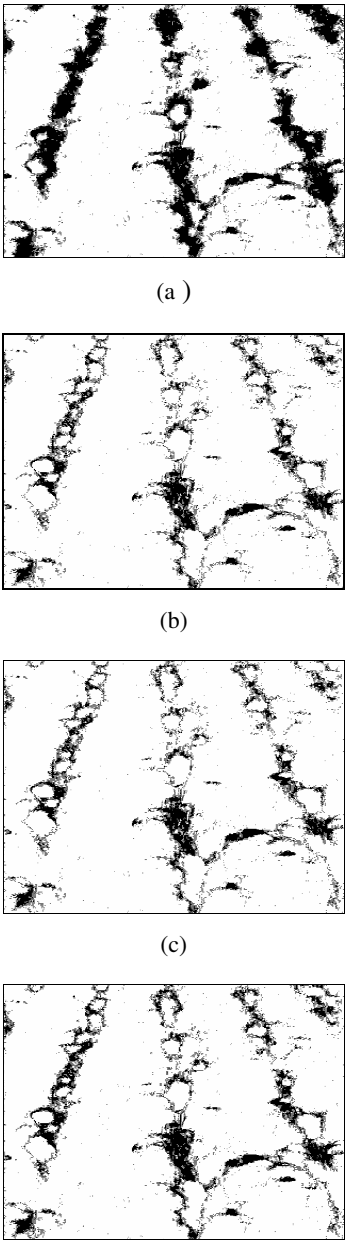

(a)

(b)

(c)

(d)

Fig. 4. The image segmentation: (a) is the image segmentation result of Fig. 2(b) by using the improved PSO, (b) is the image segmentation result of Fig. 2(a) by using the PSO, (c) is the image segmentation result of Fig. 2(b) by using the iteration threshold algorithm, (d) is the image segmentation result of Fig. 2(b) by using the *K*-means clustering

Table 1. The experiment results analysis of different algorithm

The algorithm	The segmentation quality	The average cost time(ms)
Improved PSO	excellent	495
PSO	good	19874
Iteration threshold algorithm	good	31
K-means clustering	good	83

In order to test image segmentation quality, the PSO, the *K*-means clustering algorithm and the iteration threshold algorithm were compared with the improved PSO. Fig. 3 and Fig. 4 show the image segmentation results of Fig. 2 respectively. Table 1 shows the experiment results analysis of different algorithm to the twenty different images including the segmentation quality and the average cost time. The segmentation quality of images was evaluated by the subjective observation and the subsequent process which could obtain object accurately.

4.2 Discuss

1) The improved PSO could apply to the HIS model image, and the segmentation result was excellent to the PSO, the iteration threshold algorithm and the *K*-means clustering obviously, due to exact calculating and the heuristic guidance of the improved PSO.

2) The improved PSO algorithm circulated one times only, the segmentation threshold could obtained, however the traditional PSO need circulate many times, the cost time is quite long.

3) Although the average cost time of the improved PSO was long to the iteration threshold algorithm and the *K*-means clustering, the average cost time was acceptable.

5 Conclusion

According to the characteristics of the PSO, a method for the image segmentation to HIS model based on the improved PSO was proposed in this paper. Experimental results proved that the improved PSO was an effective method for the image segmentation which could segment the object accurately.

References

1. Zheng, X.X., Yan, J.L.: A Survey of New Image Segmentation Methods. Computer and Digital Engineering 35(8), 103–106 (2007)
2. Eberhar, T.R.C., Kennedy, J.: A new optimizer using particle swarm theory. In: Proc. 6th Int. Symp. Micro Machine and Human Science, Nagoya, Japan, pp. 39–43 (1995)
3. Frans, V.D.B., Andries, P.: A cooperative approach to particle swarm optimization. IEEE Transaction on Evolutionary Computation 8(3), 225–229 (2004)

4. Tony, H., Ananda, S.M.: A Hybrid Boundary Condition for Robust Particle Swarm Optimization. IEEE Antennas and Wireless Propagation Letters 4, 112–117 (2005)
5. Shi, Y., Eberhart, R.C.: Parameter selection in particle swarm optimization. In: Porto, V.W., Saravanan, N., Waagen, D., Eiben, A.E. (eds.) Evolutionary Programming, vol. VII, pp. 591–600. Springer, Berlin (1998)
6. Han, S., Zhang, Q., Ni, B., et al.: A guidance directrix approach to vision-based vehicle guidance systems. Computers and Electronics in Agriculture 43, 179–195 (2004)
7. Shi, Y., Eberhart, R.C.: Empirical study of particle swarm optimization. In: Proc. Congr. Evolutionary Computation, Washington, DC, pp. 1945–1949 (1999)
8. Zhao, B., Qi, L.X., Mao, E.R., et al.: Image Segmentation Based on Swarm Intelligence and K-Means Clustering. The Journal of Information and Computational Science 4(3), 934–942 (2007)
9. Fang, C.Y., Chen, S.W., Fuh, C.S.: Road-Sign Detection and Tracking. IEEE Trans. on Vehicular Technology 52(5), 1329–1341 (2003)
10. Ng, H.F.: Automatic Thresholding for Defect Detection. In: IEEE Proc. Third Int. Conf. on Image and Graphics, pp. 532–535 (2004)
11. Niu, B., Zhu, Y.L., He, X.X., Shen, H., Wu, Q.H.: A Lifecycle Model for Simulating Bacterial Evolution. Neurocomputing 72, 142–148 (2008)
12. Niu, B., Li, L.: A novel PSO-DE-based hybrid algorithm for global optimization. In: Huang, D.-S., Wunsch II, D.C., Levine, D.S., Jo, K.-H. (eds.) ICIC 2008. LNCS (LNAI), vol. 5227, pp. 156–163. Springer, Heidelberg (2008)
13. Niu, B., Zhu, Y.L., He, X.X., Wu, Q.H.: MCPSO: A Multi-Swarm Cooperative Particle Swarm Optimizer. Applied Mathematics and Computation. 85(2), 1050–1062 (2007)

Emotional Particle Swarm Optimization

Wei Wang, Zhiliang Wang, Xuejing Gu, and Siyi Zheng

School of Information Engineering, University of Science and Technology Beijing, 100083 Beijing, China
wangwei8311@163.com

Abstract. It is known that there is only information sharing in most particle swarm optimization. But competition among particles which is a good feature for searching progress does not exist. For all these, based on the idea of multi-agent with emotion, bring in competition controlled by emotion to enhance performance of PSO after describing similarity between particles swarm and multi-agent system. And from the point of emotional view, problem that agents whether should compete or not is stated qualitatively. Furthermore, velocity threshold is deduced. Utilizing these, the method proposed could improve both local and global searching ability of particle swarm optimization. In addition, simulation results show that the improvement is effective. Algorithm with it has good efficiency.

Keywords: Optimization algorithm, Particle swarm optimization, Emotion, Multi-agent, Velocity.

1 Introduction

Without centralized controlling and global model, particle swarm optimization (PSO) provides a new method to find out the solution in complex distributed problem. There are two key issues in PSO algorithm. Firstly, achieve faster rate of convergence while searching at same accuracy. Raise the search precision while having comparable convergence speed. Secondly, based on this algorithm, effective method to solve practical problem should be studied.

Research on PSO has carried on for more than a decade. The main contributions are parameters setting [1, 2], swarms variety keeping [3, 4], population structure changing [5], multi-algorithm fusing [6, 7] and theory analyzing. The first improved method usually changes inertia weight ω and acceleration constant c_1, c_2. It is convenient. However, effect is limited. The second one uses various mechanisms to avoid prematurity in searching process. The third one changes topology structure of particles to influence on the type of information spreading. And the last improvements could utilize advantages of many other algorithms. But it increases algorithm complexity generally. Obviously, Improvement on algorithm could enhance its performance. Unlike the methods above, different thought is proposed from another point of view. It is known that there is only information sharing in PSO. But competition among particles which is a good feature for searching progress does not exist. To be

D.-S. Huang et al. (Eds.): ICIC 2009, LNAI 5755, pp. 766–775, 2009.

of this feature, explain PSO from aspect of multi-agent in artificial intelligent firstly. Then, emotion is brought in to reach the goal above. Therefore, emotional PSO (EPSO) is proposed. Through experiments, improvement effects are shown. The algorithm is also applied to a clustering problem.

This article is structured as follows: Sect. 2 describes similarity between particles swarm and multi-agent system from three aspects: particle description, single particle action and topology structure among multi particles. Furthermore, the reason why multi-agent idea is adopted is expatiated. In Sect. 3, emotion is brought in swarm, and analyzes its rationality. And upper threshold of particle speed is deduced. Sect. 4 tests effect of algorithm through experiments with Benchmark function. Moreover, apply the improved one to a clustering problem. Finally, this article is concluded in Sect. 5.

2 Similarity Explanations and Analysis

In this section, introduce standard PSO firstly. And then, based on this, similarity between particles in swarm and agents in multi-agent system is explained and analyzed.

2.1 Standard PSO

Assume that there are n particles in M-dimensional searching domain. $\mathbf{X}_i=(x_{i1},x_{i2},\cdots,x_{im}),i=1,2,\cdots,n$ is the location vector of particle i, and $\mathbf{V}_i=(v_{i1},v_{i2},\cdots,v_{im})$ is its speed vector. They all have *M* dimensions. $\mathbf{P}_i=(p_{i1},p_{i2},\cdots,p_{im})$ is the location vector with best fitness of particle i in the optimization process, which is called individual best location. Correspondingly, $\mathbf{P}_i=(p_{g1},p_{g2},\cdots,p_{gm})$ is named global best location representing the best solution so far. When the particle i in generation t evolves into next generation $t+1$, its speed and location of j^{th} dimension could be deduced with following equations:

$$v_{ij}(t+1)=\omega(t)v_{ij}(t)+c_1r_1(p_{ij}(t)-x_{ij}(t))+c_2r_2(p_{gj}(t)-x_{ij}(t)), \quad (1)$$

$$x_{ij}(t+1)=x_{ij}(t)+v_{ij}(t+1), \quad (2)$$

where, $i=1,2,\cdots,n,\ j=1,2,\cdots,M$, ω is inertia weight, c_1,c_2 is acceleration constant, and r_1,r_2 is uniform distributed random numbers in domain of $[0,1]$.

2.2 Explanation of Standard PSO Based on Multi-agent Idea

Agent is defined as a computing system which tries to reach a goal in complex dynamic surrounding by Maes. It could read environment by sensors, and interact with outside by actuators. And Wooldridge and Jennings gave the definition of agent.

According to the definition above, particles swarm could be considered as a generalized multi-agent system. And every particle is regarded as an agent. The reason to think so is that particles locate in solution space spontaneously. Moreover, they search global solution by themselves. Soon after, similarity between particles swarm and

multi-agent system will be introduced from three aspects: particle description, single particle action and topology structure among multi particles.

Particle Description

Definition 1: (Particle State). At a point of the discrete time, position of a particle in swarm is $\mathbf{S}_i : \mathbf{S}_i = \mathbf{X}_i = (x_{i1}, x_{i2}, \ldots, x_{im}), i = 1,2,\ldots,n$. Where m is the dimension of solution space, and the number of agent in multi-agent system is n.

Definition 2: (Particle Environment). At a point of the discrete time, collection of limited particle states in swarm is $\bigcup_{i=1}^{n} S_i$. $\mathbf{P}_g$ is the best state. And collection E constitutes all $\mathbf{P}_g$ at every point of the discrete time which is called particle environment $E = \{\mathbf{P}_g, \mathbf{P}_g', \ldots\}$.

Definition 3: (Particle Action). It could be deduced from evolution equation of particle swarm as follows:

$$v_{ij}(t+2) = \omega(t+1)v_{ij}(t+1) + c_1 r_1 (p_{ij}(t+1) - x_{ij}(t+1)) + c_2 r_2 (p_{gj}(t+1) - x_{ij}(t+1)), \tag{3}$$

$$x_{ij}(t+2) = x_{ij}(t+1) + v_{ij}(t+2), \tag{4}$$

$$\begin{aligned} x_{ij}(t+2) &= [1 + \omega(t+1) - c_1 r_1 - c_2 r_2] \cdot x(t+1) - \omega(t+1) \cdot x(t) \\ &\quad + c_1 r_1 \cdot p_i(t+1) + c_2 r_2 \cdot p_g(t+1) \\ &= \varphi[x(t+1), x(t), p_i(t+1), p_g(t+1)]. \end{aligned} \tag{5}$$

In Eq. (5) obtained above, $\varphi(\cdot)$ denotes particle action. $\varphi(\cdot) = \{\varphi(\cdot), \varphi'(\cdot), \cdots\}$. According to particle states of the first two steps, historical best state shored in particle and particle environment of multi-agent system, certain particle action is taken. Thus, a new particle state could be got.

Single Particle Action

Focusing on the agent with inner state, single particle action could be explained in Figure 1.

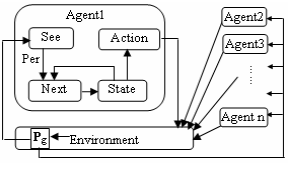

Fig. 1. This shows single particle activity. There exist *n* particles corresponding to *n* agents. Relation between agents and environment is demonstrated as well as the structure in agent.

As intelligent agent, there is inner data structure in it. For the i^{th} particle, states of the first two steps $S_i(t-1)$, $S_i(t-2)$ and its historical best state store in the data structure. Suppose that $S = \{S_i(t-1), S_i(t-2), P_i(t-1)\}$ is collection of all inner historical

state. Mapping relations of *See, Action* and *Next* is given in paper [8]. From environment to perception, $See: E \to Per$. From inner state to action, $Action: S \to \varphi(\cdot)$. And from inner state and perception to inner state, $Next: S \times Per \to S$ .To sum up, as an intelligent agent, particle action could be concluded as follows. Firstly, agent has an initial inner state $s_0 \in S$. Then, it observes particle environment $\mathbf{P}_g$ to produce perception $See(\mathbf{P}_g)$. Secondly, inner state of agent turns into $Next(S_0, See(\mathbf{P}_g))$ using Next function. Finally, agent goes into a new loop with $Action(Next(s_0, See(\mathbf{P}_g)))$.

Topology Structure among Multi Particles

A standard multi-agent system includes some agents which could interact with each other. They response to and influence on environment. Particles in swarm also have interactive topology structure Figure 2 shows five types defined by Mendes and Kennedy.

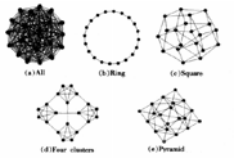

Fig. 2. This is topological structure of swarms. To simple optimization problem, particles connect to each other with All-Connection structure shown in Figure 2(a) usually. Particles are able to control particle environment P_g as agents could do. But situation is different on complex condition. Structures displayed in Figure 2(c)-(e) are adopted for agent could only control it partially.

2.3 Analysis

Through the description of similarity between particles swarm and multi-agent system from three aspects above, consider PSO from another point of view is possible.

According to the view of Nolfi and Floreano, evolution and study are two types with which organism could adapt to environmental change. They make agents in multi-agent system enhance the surviving possibility through competing with and studying from another agent. On the one hand, study is a strategy of agent itself to adapt to environment. Agents use some helpful information from outside to change its inner state. Sense changing, and adapt itself to it. This point exists in PSO already, such as sensing environment P_g . On the other hand, evolution is strategy of multi-agent system. It does not reflect in PSO. So competition among particles is brought in to enhance solving efficiency of algorithm in the article.

3 Emotional Reflections in Competition

In this section, emotional reflection is stated firstly. Based on this, how EPSO could capture competitive ability is proposed.

3.1 Emotion

PSO simulates scene that birds prey on food. Starvation exposes birds to death danger. To avoid this, they speed up to search food. But searching process reduces guard time which makes birds be preyed on. So when catching food, they slow down in order to get safe. Interpretation of contents above is given below in emotional view for emotion could influence actions [9]. According to Maslow's hierarchy theory of needs, needs could be divided into seven levels. In addition, the first two levels are called low demands. P. V. Siminov proposed the relation between information and emotion. Based on this theory, emotional model could be built from the point of information as follows:

$$E = -N(I_n - I_a), \tag{6}$$

where, E denotes emotion. N is need coefficient which influenced by physiological needs and security needs. $N=(N_p \oplus N_s)$. I_n is needs information. And I_a is received information [10]. When emotion is passive (E<0), relevant action is restrained. Moreover, when emotion is active (E>0), relevant action is promoted. To the agents that do not find the best solution, I_n of them is the best solution. I_a includes the solution they got. So E>0, prey action is promoted according to statement above. And to the agents that find the best solution, the situation is the opposite.

3.2 Competitive Action in EPSO

To bring in competitive action to improve PSO algorithm, an energy function should be proposed firstly.

$$Energy(k,i) = Starvation_{\max} - Starvation(k,i), \tag{7}$$

where, *Energy(k ,i)* is the i^{th} agent energy value at the time of *k*. $Starvation_{max}$ is maximum starvation value of agents. Correspondingly, *Starvation(k ,i)* is current one of the i^{th} agent. As an agent, every particle strives to increase its energy. In Eq. (7), energy increase denotes that *Starvation(k, i)* must decrease. Starvation value depends on whether agent finds the best solution, such as birds prey on food. If getting the best solution, *Starvation(k, i)* will reduce. Thus, competition among them happens.

Considering physiological needs and security needs at the same time, starvation value is given as $x(t)=x_0e^{-art}$ [11]. Where, x_0 is initial value, and t is diet time. a, r are constants. Because PSO uses difference equation for searching, some changes on the formula above should be done. New starvation value is expressed as:

$$\begin{aligned}&[Starvation(k,1)\ Starvation(k,2)\ \ldots\ Starvatio\ n(k,n)]^T\\ &=[Starvation(0,1)\ Starvation(0,2)\ \ldots\ Starvatio\ n(0,n)]\\ &\times\begin{bmatrix} e^{-ar(n_{1k}-n_{10})} & 0 & \cdots & 0\\ 0 & e^{-ar(n_{2k}-n_{20})} & \cdots & 0\\ \vdots & \vdots & \vdots & 0\\ 0 & \cdots & 0 & e^{-ar(n_{nk}-n_{n0})}\end{bmatrix},\end{aligned} \tag{8}$$

$$\mathbf{Starvation}(k)^T = \mathbf{Starvation}(\mathbf{0})^T \times e^{\mathbf{C}} \tag{9}$$

where, $\mathbf{C} = \begin{bmatrix} -ar(n_{1k} - n_{10}) & 0 & \cdots & 0 \\ 0 & -ar(n_{2k} - n_{20}) & \cdots & 0 \\ \vdots & \vdots & \vdots & 0 \\ 0 & 0 & 0 & -ar(n_{nk} - n_{n0}) \end{bmatrix}$,

n_{ik} is the number of getting the best solution for the i^{th} agent at the time of k. While the i^{th} agent gets the best value, n_{ik} adds one. Otherwise, it subtracts one. n_{i0} is an initial constant .For maximum speed of preying on food is proportional to starvation value, it could be deduced as follow. b is a constant.

$$\mathbf{V}_{\max}(k)^T = b \times \mathbf{Starvation}(k)^T . \tag{10}$$

4 Simulation and Results

4.1 Test with Benchmark Function

With improved method, three groups of comparing experiments with four Benchmark functions have been done. Emotion could be added to existed PSO algorithms, so experiments are comparison between standard PSO (SPSO) and SPSO with emotion, comparison between chaos PSO (CPSO) and CPSO with it, and comparison between niche PSO (NPSO) and NPSO with it. Four Benchmark functions are shown as:

1) Levy No.5 Function

$$\min F_1(x,y) = \sum_{i=1}^{5}[i\times\cos((i-1)\times x + i)] \times \sum_{j=1}^{5}[j\times\cos((j+1)\times y + j)] + (x+1.42513)^2 + (y+0.80032)^2. \tag{11}$$

2) Shaffer's F6 Function

$$\min \quad F_2(x,y) = \frac{\sin^2\sqrt{x^2+y^2} - 0.5}{(1+0.001(x^2+y^2))^2} - 0.5 . \tag{12}$$

3) Generalized Schwefel's Problem 2.26

$$\min \quad F_3(\mathbf{X}) = -\sum_{i=1}^{30}(x_i \cdot \sin(\sqrt{|x_i|})) . \tag{13}$$

4) Generalized Griewank Function

$$\min \quad F_4(\mathbf{X}) = \frac{1}{4000}\sum_{i=1}^{30} x_i^2 - \prod_{i=1}^{30}\cos(\frac{x_i}{\sqrt{i}}) + 1 . \tag{14}$$

Characters of every function are listed in Table 1.

Because F_3 and F_4 have 30 dimensions, population N_{pop} is set to 100. For F_1 and F_2, $N_{pop} = 50$. $k = 1, r = 0.2, x_0 = 80$, $V_{\max\_H} = 160$, $V_{\max\_L} = 40$, $c_1 = 1.8, c_2 = 1.8$, $\omega(t) = 1.0 - (0.5 * t)/\text{iter\_max}$. t is current generation. $iter\_\max$ is the maximum generation. Suppose that algorithm will stop when generation surpasses 1000. That is to say $iter\_\max = 1000$. Niche is stetted to 5. Minimum scale of sub-population is 15.

And the Maximum one is 40. Range of disturbance in chaos is $\delta = 0.5$. When accuracy is 0.00001, compare their iteration. Run every algorithm 20 times, and statistics are shown in Table 2.

From Table 2, it is known that variance of all particles value is smaller, which denotes that distributions of particles are centered in. And average value got closer to optimizing value. It shows that all particles in swarm are around optimizing value. Moreover, every algorithm with strategy stated in section 3 is a little better than corresponding one without the strategy in aspects of variance and average value. Improvement is effective. Because functions F_1、F_2 only have 2 dimensions, their Best value reached optimizing value when algorithm finished. But functions F_3、F_4 have 30 dimensions; searching process is a little difficult.

Table 1. Function characteristic

Function	Domain of definition	Best state	Best value	Features
F_1	$x \geq -10, y \leq 10$	(1.3068,-1.4248)	–176.1375	760 local extremums
F_2	$\|x\| \leq 100, \|y\| \leq 100$	(0,0)	-1.000	Infinitelocal extremums
F_3	$\|x_i\| \leq 500$	$\mathbf{X_i}$=420.9687	-12569.5	30Dim with many extremums
F_4	$\|x_i\| \leq 600$	$\mathbf{X_i}$=0	0	30Dim

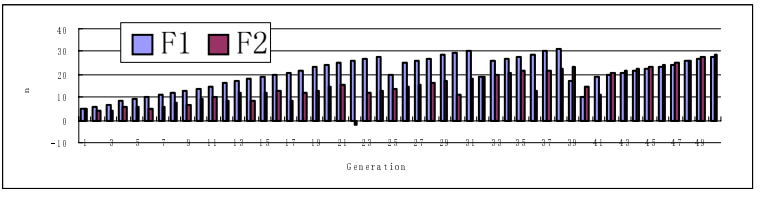

Fig. 3. Comparison of looking for food. Along with increasing of generation, the number grows. Correspondingly, the value of other agents who do not get the best solution should decrease.

Based on an overall consideration of Best value and Worst value, effects of algorithm with strategy are better than the one without it. On condition that every algorithm is running 20 times, average generation of algorithm with strategy is smaller than the corresponding one without it. Furthermore, generation variance is also smaller which shows that improvement make algorithm converge more rapidly and stably. Convergent generations are in a range of smaller fluctuations. Therefore improvement is effective. For agent who gets the best solution, upper threshold of its speed gets lower. It could make algorithm search around optimizing solution. And agents without the best solution increase their threshold to speed up in order to search the global solution. Table 2 demonstrates that upper threshold of speed could enhance performance of algorithm. Now if there is evidence that competition among agents could lead to changes of upper threshold, it can be said that adjusting strategy proposed in section 3 is effective. For function F_1、F_2, the number of getting the best

Table 2. Statistics of function value

		Average	Variance	Best	Worst	Average	Genera-	Best	Worst	Con-
F_1	SPSO	-148.909	1.89E+03	–176.13	0.00000	434.600	6.18E+02	369	1000	80%
	SPSO with	-143.576	1.57E+03	–176.13	0.00000	430.700	6.05E+02	386	1000	85%
	CPSO	-134.629	2.77E+03	–176.13	0.00000	381.500	1.70E+03	327	1000	90%
	CPSO	-136.935	2.29E+03	–176.13	-6.5019	431.750	1.48E+03	358	1000	90%
	NPSO	-165.895	6.05E+02	–176.13	-19.7140	348.900	1.73E+04	169	1000	85%
	NPSO	-167.036	1.01E+02	–176.13	-138.1500	297.100	5.88E+03	170	1000	90%
F_2	SPSO	-0.98937	1.31E-04	-1.00	-0.91917	507.0625	1.44E+04	353	1000	80%
	SPSO with	-0.98950	1.20E-04	-1.00	-0.92051	470.7500	6.16E+03	328	1000	80%
	CPSO	-0.98914	1.18E-04	-1.00	-0.92178	462.1333	5.67E+03	346	1000	75%
	CPSO	-0.99010	9.70E-05	-1.00	-0.92180	427.6471	4.50E+03	310	1000	85%
	NPSO	-0.97302	3.78E-03	-1.00	-0.50397	474.2222	1.02E+04	381	1000	60%
	NPSO	-0.98657	8.58E-04	-1.00	-0.63676	445.5000	5.55E+03	347	1000	60%
F_3	SPSO	-6393.880	7.90E-08	-7673.40	-5303.8	-	-	1000	1000	0%
	SPSO with	-8801.460	4.43E-08	-10713. 00	-6270.0	-	-	1000	1000	0%
	CPSO	-8114.680	1.65E-04	-11048. 00	-6370.2	679.0000	6.27E+03	623	1000	10%
	CPSO	-9224.160	5.97E-08	-12154. 00	-8008.3	644.0000	5.62E+03	591	1000	10%
	NPSO	-5937.690	4.82E+05	-7270.80	-676.52	-	-	1000	1000	0%
	NPSO	-7488.490	2.65E+05	-9618.10	-3032.1	-	-	1000	1000	0%
F_4	SPSO	1.00173	0	1.0015	1.00190	-	-	1000	1000	0%
	SPSO with	1.00103	0	1.0003	1.00150	-	-	1000	1000	0%
	CPSO	1.00193	0	1.0009	1.00280	-	-	1000	1000	0%
	CPSO	1.00083	0	1.0005	1.00150	-	-	1000	1000	0%
	NPSO	1.00237	0	1.0001	1.00019	-	-	1000	1000	0%
	NPSO	1.00097	0	1.0001	1.00015	-	-	1000	1000	0%

solution is shown in Figure 3. Along with increasing of generation, the number grows. Correspondingly, the value of other agents who do not get the best solution should decrease. According to Eq. (10), $\mathbf{V}_{\max}(k)^T$ is adjusting.

4.2 Clustering Problem Application

As we know, if there are two data $Object_i$ and $Object_j$, Euclid and Cosine distance is defined separately as follows:

$$d(Object_i, Object_j) = \left\| Object_i, Object_j \right\| = \sqrt{\sum_{k=1}^{m} (Object_{ik}, Object_{jk})^2}, \tag{15}$$

$$d(Object_i, Object_j) = 1 - sim(Object_i, Object_j) = 1 - \sum_{k=1}^{m} (Object_{ik}, Object_{jk}) \Big/ \sqrt{\sum_{k=1}^{m} (Object_{ik})^2 \cdot \sum_{k=1}^{m} (Object_{jk})^2}, \tag{16}$$

where, i, j=1,2,3,…,n is index, and $\|\bullet\|$ is Euclid distance, $Object_i, Object_j \in R^m$.

Apply SPSO and SPSO with emotion presented in section 3 to this clustering problem. Feature of data set Iris is listed in Table 3[12].

Table 3. Feature of data set

Data set	Instances Number	Attributes Number	Classes Number
Iris	150	4	3

According to the first two features of Iris, clustering result is shown in Figure 4.

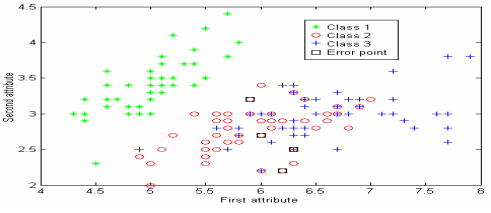

Fig. 4. Clustering result. In this figure, *, ○ and + denote three correct classes. There are some overlaps of ○ and +. It illustrates that the first two features could not classify the second and third type. □ is date classified falsely.

In this application, population is N_{pop}=100. And c_1=1.49, c_2=1.49, $iter\_max$=300. Clustering centers are selected randomly. In addition, date is not pretreated.

5 Conclusion

This article describes similarity between particles swarm and multi-agent system from three aspects: particle description, single particle action and topology structure among multi particles. Based on multi-agent idea, emotion brings competition in PSO. In addition, analyze emotion element in competition of preying on food. And upper threshold of speed is given with formula. Simulations show that improved PSO has good effect.

Acknowledgments

This work is supported by the National Natural Science Foundation of China (60573059), the High Technology Research and Development Program of China (2007AA01Z160).

References

1. Gallad, A.E., Hawary, M.E., Sallaam, A., et al.: Enhancing the Particle Swarm Optimizer via Proper Parameters Selection. In: Proceedings of IEEE Canadian Conference on Electrical and Computer Engineering, Winnipeg, Canada, pp. 792–797 (2002)
2. Shi, Y., Eberhart, R.: Fuzzy Adaptive Particle Swarm Optimization. In: Proceedings of Congress on Evolutionary Computation, Seoul, Korea, pp. 101–106 (2001)

3. Krink, T., Vesterstrom, J.S., Riget, J.: Particle Swarm Optimization with Spatial Particle Extension. In: Proceedings of the IEEE Congress on Evolutionary Computation, Honolulu, USA, pp. 1474–1479 (2002)
4. Lvbjerg, M., Rasmussen, T.K., Krink, T.: Hybrid Particle Swarm Optimizer with Breeding and Subpopulations. In: Proceedings of the Genetic and Evolutionary Computation Conference, San Francisco, USA, pp. 469–476 (2001)
5. Kennedy, J., Mendes, R.: Population Structure and Particle Swarm Performance. In: Proceedings of the IEEE Congress on Evolutionary Computation, Honolulu, USA, pp. 1671–1676 (2002)
6. Zhao, F.Q., Zhang, Q.Y., Yang, Y.H.: A Scheduling Holon Modeling Method with Petri-net and Its Optimization with a Novel PSO-GA Algorithm. In: Proceedings of 2006 10th International Conference on Computer Supported Cooperative Work in Design, Nanjing, China, pp. 1302–1307 (2006)
7. Peng, X.Y., Wu, H.X., Peng, Y.: Parameter Selection Method for SVM with PSO. Chinese Journal of Electronics 15(4), 638–642 (2006)
8. Shi, C.Y., Zhang, W., Xu, J.H.: An Introduction to MultiAgent System, Publishing House of Electronics Industry, Beijing (2003)
9. Wang, Z.L.: Artificial Psychology─A most Accessible Science Research to Human Brain. Journal of University of Science and Technology Beijing 22(5), 478–481 (2000)
10. Wang, Z.L.: Artificial Psychology. China Machine Press, Beijing (2007)
11. Lang, X.: Function Maximum Principles Used in Animal Behavior Modeling. Journal of Mathematics for Technology 16(3), 17–21 (2000)
12. Blake, C.L., Merz, C.J.: UCI Machine Learning repository of machine learning databases (1998), `http://www.ics.uci.edu/~mlearn/MLSummary.html`

Symbiotic Multi-swarm PSO for Portfolio Optimization

Ben Niu[1], Bing Xue[1], Li Li[1], and Yujuan Chai[2]

[1] College of Management, Shenzhen University,
Shenzhen, Guangdong 518060, China
[2] Faculty of Science, McMaster University,
Hamilton, Ontario L8S4L8, Canada
drniuben@gmail.com

Abstract. This paper presents a novel symbiotic multi-swarm particle swarm optimization (SMPSO) based on our previous proposed multi-swarm cooperative particle swarm optimization. In SMPSO, the population is divided into several identical sub-swarms and a center communication strategy is used to transfer the information among all the sub-swarms. The information sharing among all the sub-swarms can help the proposed algorithm avoid be trapped into local minima as well as improve its convergence rate. SMPSO is then applied to portfolio optimization problem. To demonstrate the efficiency of the proposed SMPSO algorithm, an improved Markowitz portfolio optimization model including two of the most important limitations are adopted. Experimental results show that SMPSO is promising for this class of problems.

Keywords: Symbiotic PSO, particle swarm, portfolio optimization**.**

1 Introduction

Portfolio Optimization (PO), also known as mean-variance optimization (MVO), is risk management tool which allows you to construct optimal portfolios considering the trade-off between market risk and expected returns.

PO problem is NP-hard and non-linear with many local optima. Mathematical programming methods have been applied to this problem for a long time [1, 2, 3]. Nowadays, a number of different heuristic algorithms have been proposed for solving this problem, including genetic algorithms (GA) [4, 5], simulated annealing [6], neural networks [7] and others [8, 9, 10].

However most of the PO models used in those pioneer works may often be considered too basic, as it ignores many of the constrains, such as the transaction fee and whether short sale is permitted, and the upper and the lower bounds of proportion of each asset in the portfolio. In this work, we use a modified PO model considering the transaction costs and no short sales. The main motivation of this study is to employ an improved multi-swarm cooperative PSO (MCPSO) for the modified PO model.

MCPSO was firstly proposed by B. Niu in 2005[11], which is inspired by the phenomenon of symbiosis in natural ecosystems, where many species have developed cooperative interactions with other species to improve their survival. MCPSO has been successfully applied in many problems, including function optimization [11],

D.-S. Huang et al. (Eds.): ICIC 2009, LNAI 5755, pp. 776–784, 2009.

neural networks training[12], fuzzy modeling designing[13] etc. In this paper we will apply an improved MCPSO, i.e. symbiotic multi-swarm particle swarm optimization (SMPSO) to find efficient portfolio by solving the PO model.

The rest of the paper is organized as follows. Section 2 gives a review of PSO and a description of the proposed algorithm SMPSO. Section 3 describes portfolio optimization model. Section 4 gives the detailed experimental studies. Finally, conclusions are drawn in Section 5.

2 PSO and SMPSO

2.1 Particle Swarm Optimization (PSO)

The basic PSO is a population based optimization tool, where the system is initialized with a population of random solutions and the algorithm searches for optima by updating generations. In PSO, the potential solutions, called particles, fly in a *D*-dimension search space with a velocity which is dynamically adjusted according to its own experience and that of its neighbors.

The position of the *i*th particle is represented as $\vec{x}_i = (x_{i1}, x_{i2}, ..., x_{iD})$, where $x_{id} \in [l_d, u_d]$, $d \in [1, D]$, l_d, u_d are the lower and upper bounds for the *d*th dimension, respectively. The rate of velocity for particle *i* is represented as $\vec{v}_i = (v_{i1}, v_{i2}, ..., v_{iD})$, is clamped to a maximum velocity vector $\vec{v}_{\max}$, which is specified by the user. The best previous position of the *i*th particle is recorded and represented as $P_i = (P_{i1}, P_{i2}, ..., P_{iD})$, which is also called *pbest*. The index of the best particle among all the particles in the population is represented by the symbol g, and p_g is called *gbest*. At each iteration step, the particles are manipulated according to the following equations:

$$v_{id} = wv_{id} + R_1 c_1 (P_{id} - x_{id}) + R_2 c_2 (p_{gd} - x_{id}), \tag{1}$$

$$x_{id} = x_{id} + v_{id}. \tag{2}$$

Where w is inertia weight; c_1 and c_2 are acceleration constants; and R_1, R_2 are random vectors with components uniformly distributed in [0, 1]. For Eq. (1), the portion of the adjustment to the velocity influenced by the individual's own *pbest* position is considered as the cognition component, and the portion influenced by *gbest* is the social component. After the velocity is updated, the new position of the *i*th particle in its *d*th dimension is recomputed. This process is repeated for each dimension of the *i*th particle and for all the particles in the swarm.

2.2 Symbiotic Multi-swarm Particle Swarm Optimizer (SMPSO)

In our previous proposed MCPSO algorithm, the population is divided into several sub-swarms, in which some sub-swarms are master swarms and the other sub-swarms are slave swarms. Both the master and slave swarms have different properties. The master swarms update particles information according to the slave swarms and their own. While the slave swarms update the particles information only based on their own

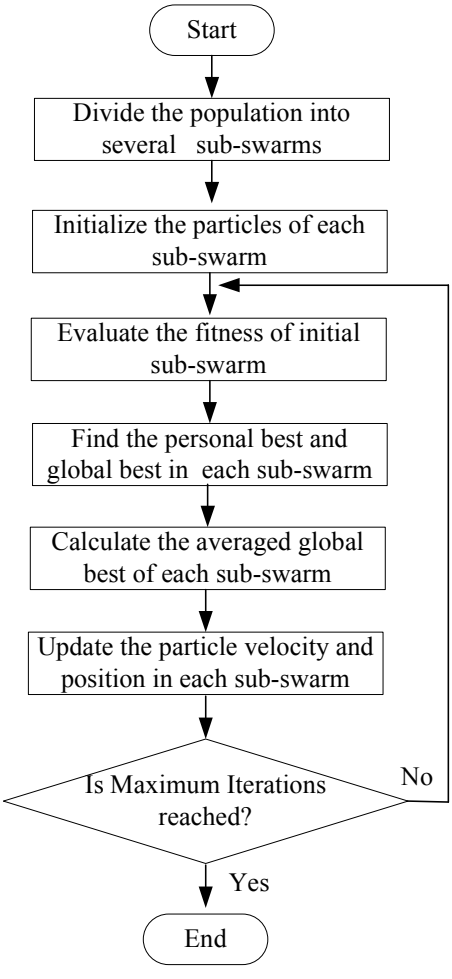

Fig. 1. Flow chart of SMPSO

information. It should be noted that there is no information exchange between slave swarms which will slow down the convergence rate. The detailed introduction of MCPSO can be referred to [11].

To deal with this issue, the population in SMPSO consists of several sub-swarms with the same properties, i.e. they are both identical sub-swarms. Each sub-swarm can supply many new promising particles to other sub-swarm as the evolution proceeds. Each sub-swarm updates the particle states based on the best position discovered so far by all the particles both in the other sub-swarms and its own. The interactions between the other sub-swarms and its own influence the balance between exploration and exploitation and maintain a suitable diversity in the population, even when it is approaching the global solution, thus reducing the risk of converging to local sub-optima.

Table 1. Pseudocode for SMPSO algorithm

Algorithm SMPSO
Begin
Randomize positions and velocities of $N \times P$ particles in search space. Divide whole population into N species with P particles randomly;
Evaluate the fitness value of each particle
Repeat
Do in parallel
Swarm n , $1 \le n \le N$
End Do in parallel
Barrier synchronization //wait for all processes to finish
Select the center particle and determinate its position according to Eq.(4)
Evolve each sub-swarm //Update the velocity and position using Eq. (3) and (2), respectively
Evaluate the fitness value of each particle
Until a terminate-condition is met
End

The search information can be transformed among sub-swarms by a center communication mechanism that uses a center particle whose position is averaged by the sub-swarms to guide the flight of particles in all the sub-swarms. During the flight each particle of the sub-swarm adjusts its trajectory according to its own experience, the experience of its neighbors, and the experience of the particles in other sub-swarms, making use of the best previous position encountered by itself, its neighbors and the center particle position. In this way, the search information can be transformed between sub-swarms which can accelerate the convergence rate.

In SMPSO, we use a population of $N \times P$ individuals, or in symbiosis terminology, an ecosystem of $N \times P$ organisms. The whole population is divided into N species to modeling symbiosis in the context of the evolving ecosystems (for convenience, each species has the same population size P). As in nature, the species are separated breeding populations and evolve parallel, while interact with one another within each generation and have a symbiotic relationship.

To realize this mechanism, we propose a modification to the original PSO velocity update equation. In each generation, particle i in species n will evolve according to the following equations:

$$v_i^n(t+1) = w v_i^n(t) + R_1 c_1 (p_i^n - x_i^n(t)) + R_2 c_2 (p_g^n - x_i^n(t)) + R_3 c_3 (p_c^n - x_i^n(t)), \quad (3)$$

where p_i^n and P_g^n are the best previous solution achieved so far by particle i and the species n, respectively. R_3 is a random value between 0 and 1. c_3 is acceleration constant; P_c^n represents the center position of the global best particle in all the sub-swarms. After N sub-swarms update their positions and best performed particle is found, a center particle is updated according to the following formula:

$$P_c^n(t+1) = \frac{1}{N}\sum_{i=1}^{N} p_g^n(t),$$
$$n = 1, 2, \cdots N, \tag{4}$$
$$i = 1, 2, \cdots P.$$

Unlike other particles, the center particle has no velocity, but it is involved in all operations the same as the ordinary particle, such as fitness evaluation, competition for the best particle, except for the velocity calculation. The flow chart SMPSO is shown in Fig.1. and pseudocode for the SMPSO is listed in Table 1.

3 Portfolio Optimization Problem

The portfolio optimization problem is one of the most important issues in asset management, which deals with how to form a satisfying portfolio. Modern portfolio analysis started from pioneering research work of Markowitz (1952) [14]. The original portfolio optimization model is usually called mean–variance model, firstly proposed by Markowitz. In this paper, we use an improved mean–variance model considering the transaction costs and no short sales. It assumes an investor allocates the wealth among *n* assets. Some notations are introduced as follows:

r_i : The yield of the i asset, $i = 1, \cdots \cdots, n$;

$R = (R_1 \cdots \cdots, R_n)$: $R_i = E(r_i)$ denoting the expected yield;

$\sigma_{ij} = \mathrm{cov}(r_i, r_j)$: the covariance of r_i and r_j ;

$X = (x_1 \cdots \cdots, x_n)$: x_i is proportionment of the i asset that investor want to invest;

$k = (k_1 \cdots \cdots, k_n)$: k_i is the transaction fee of the i asset;

λ : The risk factor distributing in [0, 1]. Larger λ represents investor love risk more.

Based on these defined variables, the function $f(x)$ and $g(x)$ denotes the revenue and risk in the portfolio optimization problem can be obtained as following:

$$f(x) = \sum_{i=1}^{n} R_i x_i - \sum_{i=1}^{n} k_i x_i, \tag{5}$$

$$g(x) = \sum_{i=1}^{n}\sum_{i=1}^{n} \sigma_{ij} x_i x_j. \tag{6}$$

The improved portfolio optimization model can be formulated as:

$$\min F(x) = \min\{\lambda g(x) - (1-\lambda) f(x)\}$$
$$\begin{cases} \sum_{i=1}^{n} x_i = 1; \\ 0 < x_i. \end{cases} \tag{7}$$

Where $0 < x_i$ means that the short sale is not permitted.

When we use SMPSO to solve the model, there is an n demension search space denoting n kinds of sassets, and the position of the particle $X = (x_1 \cdots \cdots , x_n)$ presents the proportionment of every assesst. The position of the particle with the minimum fitness value is the best selection of portfolio optimization.

4 Illustrative Examples

In order to test the effectiveness of SMPSO for portfolio optimization, we use the data of five assets as the sample that can be referred to [15]. k_i is set as 0.075%. Different risk preference is considering, where three value of risk factors λ (0.2, 0.5, 0.8) identifying the different kind of inverstors is used.

In applying PSO to the above model, $w_{\max}, w_{\min}, c_1, c_2$ are set to be 0.9, 0.4, 2.0, 2.0, respectively. For SMPSO, $c_1 = c_2 = 1.367$ and $c_3 = 2$ is used, $w_{\max}, w_{\min}$ is set the same as those defined in PSO. The max iterations of the two methods are set to be 200. A total of 50 runs are performed.

Numerical results with different λ obtained by the standard PSO and the SMPSO are showed in the Table 2-3. Figures 2-4 present the mean relative performance using different λ generated by PSO and SMPSO.

The max value, the min value, the standard deviation and the mean value are summarized in Table 2-3. It is clear that for almost of all the different risk preferences, SMPSO owns smaller standard deviation and mean value, which demonstrated it outperforms PSO in terms of result robustness and solution quality.

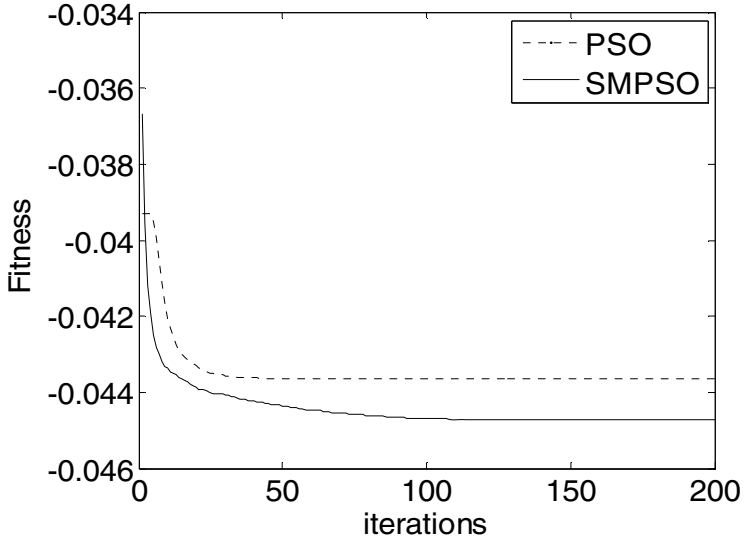

Fig. 2. Mean relative performance using $\lambda = 0.2$

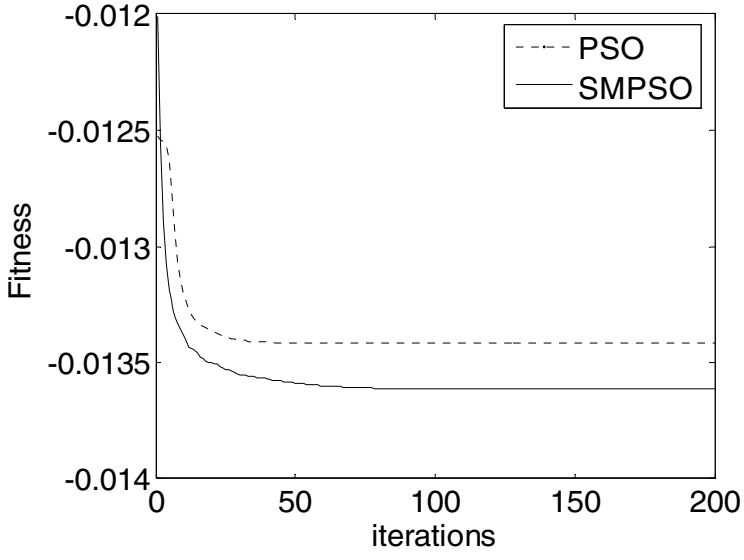

Fig. 3. Mean relative performance using $\lambda = 0.5$

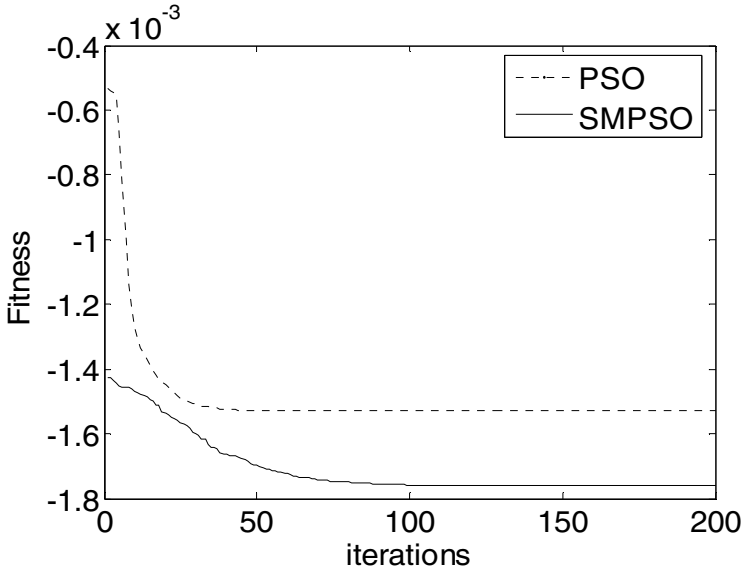

Fig. 4. Mean relative performance using $\lambda = 0.8$

From Figures 2-4, it is obviously found that SMPSO has quicker convergence rate in the different situations compared with PSO. Furthermore, its convergence process is much steadier than that of PSO.

Table 2. Numerical results with different λ

		Worst	Best	Mean	Std
$\lambda = 0.2$	PSO	-4.07894e-002	-4.46873e-002	-4.36409e-002	1.07146e-003
	SMPSO	-4.47326e-002	-4.47331e-002	-4.47331e-002	7.68445e-008
$\lambda = 0.5$	PSO	-1.29264e-002	-1.36157e-002	-1.34150e-002	1.617577e-004
	SMPSO	-1.36159e-002	-1.36159e-002	-1.36159e-002	4.32891e-012
$\lambda = 0.8$	PSO	-1.01019e-003	-1.76112e-003	-1.52787e-003	2.17589e-004
	SMPSO	-1.76128e-003	-1.76129e-003	-1.76128e-003	3.46453e-010

Table 3. Numerical results with different λ

		x_1	x_2	x_3	x_4	x_5
$\lambda = 0.2$	PSO	3.5878e-006	1.7489e-005	3.4526e-001	1.8246e-011	6.5472e-001
	SMPSO	2.2211e-008	1.2714e-007	2.9494e-001	6.1913e-008	7.0506e-001
$\lambda = 0.5$	PSO	5.4377e-013	1.3446e-001	7.9098e-001	4.4508e-002	3.0046e-002
	SMPSO	7.5996e-013	1.3851e-001	7.8621e-001	4.2837e-002	3.2448e-002
$\lambda = 0.8$	PSO	3.1966e-011	6.3375e-001	9.2079e-002	2.7417e-001	3.7942e-013
	SMPSO	1.3609e-010	6.3285e-001	9.1060e-002	2.7608e-001	1.5641e-009

All the results presented in the tables and figures can proved that the SMPSO could be a more effective way for the investors to solve the portfolio optimizations problems.

5 Conclusions

In this paper, we proposed a new variant of original PSO, i.e. symbiotic multi-swarm PSO that is inspired by the phenomenon of symbiosis in natural ecosystems. SMPSO is based on a multiple swarms scheme, in which the whole population is divided into several sub-swarms. The particles in each sub-swarm are enhanced by the experience of its own and the other sub-swarms. By introducing the center communication mechanism the search information can be transferred among sub-swarms, that help accelerate the convergence rate and avoid the particles be trapped into local minima.

We also use the improved Markowitz model considering two real-world constraints to test our proposed algorithm. The preliminary experimental results suggest that SMPSO have superior features, both in high quality of the solution and robustness of the results. Our proposed portfolio model and SMPSO are applicable and reliable in real markets with large number of stocks.

Acknowledgment

This work is supported by Shenzhen-Hong Kong Innovative Circle project (Grant no.SG200810220137A) and Project 801-000021 supported by SZU R/D Fund.

References

1. Young, M.R.: A Minimax Portfolio Selection Rule with Linear Programming Solution. Management Science 44, 673–683 (1998)
2. Arenas, M., Bilbao, A., Rodriguez Uria, M.V.: A Fuzzy Goal Programming Approach to Portfolio Selection. European Journal of Operational Research 133, 287–297 (2001)
3. Ballestero, E., Romero, C.: Portfolio Selection: A Compromise Programming Solution. Journal of the Operational Research Society 47, 1377–1386 (1996)
4. Oh, K.J., Kim, T.Y., Min, S.: Using Genetic Algorithm to Support Portfolio Optimization for Index Fund Management. Expert Systems with Applications 28, 371–379 (2005)
5. Yang, X.: Improving Portfolio Efficiency: A Genetic Algorithm Approach. Computational Economics 28, 1–14 (2006)
6. Crama, Y., Schyns, M.: Simulated Annealing for Complex Portfolio Selection Problems. European Journal of Operational Research 150, 546–571 (2003)
7. Fernandez, A., Gomez, S.: Portfolio Selection Using Neural Networks. Computers & Operations Research 34, 1177–1191 (2007)
8. Derigs, U., Nickel, N.H.: On a Local-search Heuristic for a Class of Tracking Error Minimization Problems in Portfolio Management. Annals of Operations Research 131, 45–77 (2004)
9. Derigs, U., Nickel, N.H.: Meta-heuristic Based Decision Support for Portfolio Optimization with a Case Study on Tracking Error Minimization in Passive Portfolio Management. OR Spectrum 25, 345–378 (2003)
10. Schlottmann, F., Seese, D.: A Hybrid Heuristic Approach to Discrete Multi-Objective Optimization of Credit Portfolios. Computational Statistics & Data Analysis 47, 373–399 (2004)
11. Niu, B., Zhu, Y.L., He, X.X., Wu, H.: MCPSO: A Multi-Swarm Cooperative Particle Swarm Optimizer. Applied Mathematics and Computation 185, 1050–1062 (2007)
12. Niu, B., Zhu, Y.-l., He, X.-X.: A Multi-Population Cooperative Particle Swarm Optimizer for Neural Network Training. In: Wang, J., Yi, Z., Żurada, J.M., Lu, B.-L., Yin, H. (eds.) ISNN 2006. LNCS, vol. 3971, pp. 570–576. Springer, Heidelberg (2006)
13. Niu, B., Zhu, Y.L., He, X.X., Shen, H.: A Multi-swarm Optimizer Based Fuzzy Modeling Approach for Dynamic Systems Processing. Neurocomputing 71, 1436–1448 (2008)
14. Markowitz, H.W.: Foundations of Portfolio Theory. Journal of Finance 46, 469–477 (1991)
15. Yang, K.Y., Wang, X.F.: Solving the Multi-solution Portfolio Selection Model Based on the GA (Chinese). Journal of ShanDong finance college 6, 60–63 (2003)

A Novel Particle Swarm Optimization with Non-linear Inertia Weight Based on Tangent Function

Li Li[1], Bing Xue[1], Ben Niu[1], Lijing Tan[2], and Jixian Wang[3]

[1] College of Management, Shenzhen University, Shenzhen 518060, China
[2] Measurement Specialties Inc, Shenzhen 518107, China
[3] School of Engineering, Anhui Agricultural University, Hefei 230036, China
drniuben@gmail.com

Abstract. Inertia weight is a most important parameter of particle swarm optimization (PSO), which can keep a right balance between the global search and local search. In this paper, a novel PSO with non-linear inertia weight based on the tangent function is provided. The paper also presents the method of determining a control parameter in our proposed method, saving the user from a tedious trial and error based approach to determine it for each specific problem. The performance of the proposed PSO model is amply demonstrated by applying it for four benchmark problems and comparing it with other three PSO algorithms. From experimental results, it can be concluded that using a non-linear dynamic inertia weight makes the rapidity of convergence rate with higher precision.

Keywords: Particle swarm optimization, inertia weight, tangent function.

1 Introduction

During the 1990's, the researchers paid their attentions on the group animals such as the birds, the ants, or the fishes, which is not very clever alone, but they can finished the high-performance cooperative work when they are together. Swarm intelligence algorithms were generated based on the investigations on these group animals. Particle swarm optimization (PSO) is one of the effective swarm intelligence algorithms firstly proposed by Eberhant and Kennedy [1, 2] in 1995.

As a relatively new swarm intelligence algorithm, PSO has shown some important advances, such as easy in implementation , few parameters to be adjusted, and has a faster convergence rate. It has been successfully applied in many areas [3, 4, 5, 6] However, in the original PSO, every particle searches the best solution based on the previous local best and the global best, and all the particles will be more and more familiar, which leads to the particles to be trapped in a local minima easily. To deal with these issues, many researchers provided different attempts, and adjusting the inertia weight is one of the most effective ways. The inertia weight can balance the global search and the local search to get better results: the global search is stronger when the inertia weight is larger, while the algorithm is good at the local search with a smaller inertia weight [7]. Therefore, the proper inertia weight can improve the performance with fewer generations. Many researchers have done lots of investigations

D.-S. Huang et al. (Eds.): ICIC 2009, LNAI 5755, pp. 785–793, 2009.

on it, such as Shi provided a linearly-decrease inertia weight [8] and the dynamic inertia weight based on fuzzy reasoning [9], Van offered the random inertia weight (RIW) [10], Han produced a novel PSO with an adapting inertia weight [11], Niu proposed a new hybrid global optimization algorithm PSODE combining particle swarm optimization (PSO) with differential evolution(DE) [12].

In the present paper, we proposed a novel non-linear inertia weight adjusting method based on tangent function. To illustrate the effectiveness and performance of the new strategy, a set of four representative benchmark functions was employed to evaluate it in comparison with other three different improved PSO with fixed inertia weight (FIW), a linearly-decrease inertia weight (LIW)[8], and Nonlinearly-decrease inertia weight (NIW)[13], respectively. The remaining contents of this paper are organized as follows: The next section introduces the standard PSO. A novel PSO with non-linear dynamic inertia weight is presented in Section 3. In Section 4, we describe the benchmark functions, experimental settings, and compare experimental results of the novel PSO with other three PSO with different inertia weight. Finally, Section 5 we end the paper with some conclusions and future work propositions.

2 Standard Particle Swarm Optimization Algorithm

PSO is a population-based searching algorithm and is initialized with a population of random solutions to search for the optima by updating generation. The particle i denoting one potential solution is flying in the *n*-dimensions; in the *t*th generation, it owns a position $x_i(t) = (x_{i1}, x_{i2} \cdots \cdots, x_{in})$, and velocity $v_i(t) = (v_{i1}, v_{i2} \cdots \cdots, v_{in})$. There is a fitness value evaluated with a predefined fitness function to appraise the particle's current position. At the same time, every particle can remember the best position they had ever been. Therefore, in every generation there are two "Best": The local best value is the best position that the particle has achieved in the current stage, which is called *Pbest;* the global best value is the overall best solution tracked by the particle swarm, which is called *Gbest*.

Based on the *Pbest* and *Gbest*, the PSO searches for the best solution by updating every particle's position and velocity until meeting the end conditions. And the following equations are used to update the generations:

$$V_{id}(t+1) = V_{id}(t) + c_1 \cdot rand() \cdot (p_{id} - x_{id}(t)) + c_2 \cdot rand() \cdot (p_{gd} - x_{id}(t)), \tag{1}$$

$$x_i(t+1) = x_i(t) + V_i(t+1). \tag{2}$$

Where the c_1、c_2 in the Eq(1) are the learning factors, they both are often taken as 2. $rand()$ is a random value, which is distributing during [0,1]. p_{id} presents the *Pbest* while p_{gd} presents the *Gbest*. In order to make sure the position $x_i(t)$ is in the feasible region, there is a maximum $v_i(t)$ denoted by $v_{\max}$ to confine the velocity:

$$V_{id}(t) = \begin{cases} V_{id}(t) \cdots\cdots\cdots\cdots \left|V_{id}(t)\right| < V_{\max} \\ V_{\max} \cdots\cdots\cdots\cdots \left|V_{id}(t)\right| \geq V_{\max} \end{cases}. \tag{3}$$

As when using the above equations to search the best solution, the convergence velocity in the earlier period is fast, but the local search is poor and the convergence velocity is slower along with generations, and the precise of the solution often can not meet the satisfactory level. For these problems, Shi [11] introduced the inertia weight w into the velocity equation:

$$V_{id}(t+1) = wV_{id}(t) + c_1 \cdot rand() \cdot (p_{id} - x_{id}(t)) + c_2 \cdot rand() \cdot (p_{gd} - x_{id}(t)) . \quad (4)$$

The Eq(4) also can be divided into three parts: the first part indicates the previous velocity of the particle, which can make sure the global search, the second and third part are the social reasons that lead to the change the velocity of the particle, and they can decide the local search of the algorithm. So the inertia weight w can control the influence of previous velocity on the new velocity, and it can make a balance between the global search and the local search: global search performance is fine with larger inertial weight while a smaller inertia weight facilitates a local search. The two searches with appropriate coordination can bring a better performance, so to find a proper w is one of the crucial ways to improve the capability of the algorithm.

3 Novel Non-linear Inertia Weight PSO Algorithms Based on Tangent Function

Based on lots of experiments, we found that the global search is strong when w is larger, and the algorithm owns faster convergence ability but it is hardly to get precise. On the other hand when w is smaller, the local search is stronger and the result is more precise, but the convergence ability is poorer, neither the ability to escape the local best. So the w should vary with the generations, and we try to find a proper variations to improve the performance of the PSO. During the initial experimental study, we tried to introduce a monotone increasing or decreasing strategy to update w. In our proposed method tangent function $y = \tan(x)$ is used to be the updating function, in which result y is increasing along with the independent variable x, and the speed of the increase also increases. When $x = 7/8$, $y = 1$. Based on this observation, we proposed a novel PSO with non-linear initial weight and the resulting inertia weight updating equation is as following:

$$w(t) = (w_{start} - w_{end}) * \tan(7/8 * (1 - (\frac{t}{t_{\max}})^k)) + w_{end} . \quad (5)$$

Where w_{start} is the initial value of the inertia weight, which is also the largest value and normally set w_{start}=0.9, w_{end} is the final value of the inertia weight, which also is the smallest one and normally set $w_{end} = 0.4$; $t_{\max}$ is the maximum number of iterations. According to the equation, w is nonlinearly-decrease along with the increase of the iterations. In the initial iteration, the PSO with the larger w is with stronger global search, so the particle can fly around the total search space quickly. The local research becomes stronger along with the w becoming smaller and smaller. The new strategy may enhance the capability of the algorithm to avoid premature convergence and

escapes the local optimal. There is a coefficient 7/8 in the Eq (5) to guarantee the w distributed in [0.4, 0.9]: When $t=1$, $w(t)=w_{start}=0.9$ and when $t=t_{\max}$, $w(t)=w_{end}=0.4$.

k is the control variable which can control the smoothness of the curve that reflects the relationship between the w and t. Figure 1-3 show the variation of inertia weight along with the generations when $k=0.2$、$k=1$、$k=3$, respectively. From these figures, it can be found that: when $k=0.2$, the functions between the w and t is convex function; when $k=1$, it is almost a linear one leaning to concave; and when $k=3$, it is a concave function.

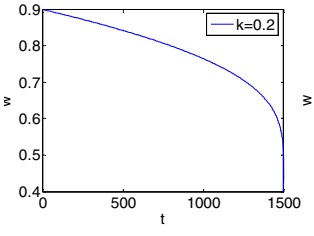

Fig. 1. $k=0.2$

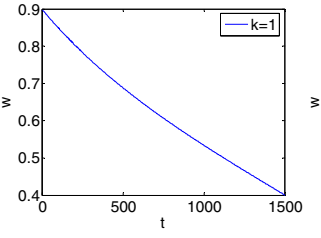

Fig. 2. $k=1$

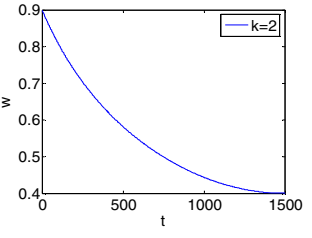

Fig. 3. $k=2$

In order to choose the best value of k, a multimode Griewank function is employed in the experiments. And k is confined in [0.1~2.0]. The experimental result (i.e., the mean and the standard deviations of the function values found in 20 runs) are listed in Table 1.

From Table 1, it shows that when k is within [0.4~0.6] and [1.4~1.7], the mean and the standard deviations of the function values are both stable. So we can choose the value which can take a faster convergence rate. Figure 4 and 5 show the variation of the logarithm (base 10) of the mean values along with the generations when $k=0.6$, $k=1.7$ respectively. It is easy to find it can get a faster convergence rate when $k=0.6$ than $k=1.7$. In the following experiments, we choose $k=0.6$.

Table 1. Experimental results on Griewank function using different k

k	mean value	standard deviation	k	mean value	standard deviation
0.1	0.0294	0.0276	1.1	0.0302	0.0230
0.2	0.0300	0.0223	1.2	0.0355	0.0194
0.3	0.0329	0.0248	1.3	0.0413	0.0291
0.4	0.0266	0.0191	1.4	0.0230	0.0212
0.5	0.0258	0.0278	1.5	0.0289	0.0273
0.6	0.0254	0.0207	1.6	0.0263	0.0200
0.7	0.0315	0.0307	1.7	0.0261	0.0198
0.8	0.0300	0.0343	1.8	0.0334	0.0219
0.9	0.0301	0.0235	1.9	0.0257	0.0253
1.0	0.0264	0.0267	2.0	0.0280	0.0256

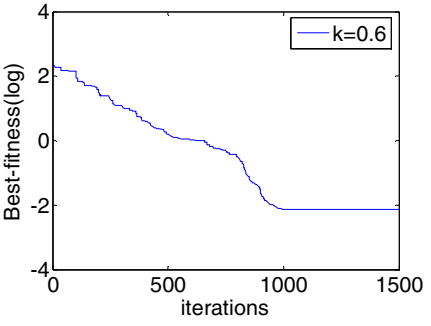

Fig. 4. $k = 0.6$

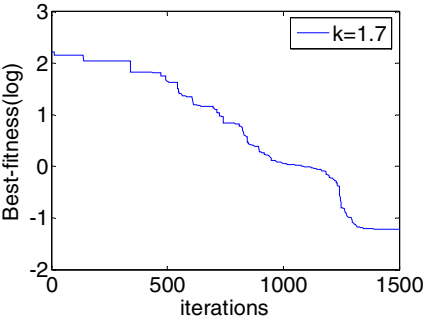

Fig. 5. $k = 1.7$

4 Experimental Studies

4.1 Test Functions and Parameters Settings

In order to test the effectiveness and performance of our proposed method four representative benchmark functions are used in comparison with other three different inertia weight strategies (FIW, LIW, and NIW). The parameter settings of these four functions are listed in Table 2.

Table 2. Test functions and parameters setting

Functions name	Function model	Dim	Search space	$V_{\max}$
Sphere	$f_1(x) = \sum_{i=1}^{n} x_i^2$	20	(-100,100)	100
Rosenbrock	$f_2(x) = \sum_{i=1}^{n} \left(100\left(x_{i+1} - x_i^2\right)^2 + \left(x_i - 1\right)^2\right)$	20	(-30, 30)	30
Rastrigin	$f_3(x) = \sum_{i=1}^{n} \left(x_i^2 - 10\cos\left(2\pi x_i\right) + 10\right)$	20	(-10, 10)	10
Griewank	$f_4(x) = \frac{1}{4000}\sum_{i=1}^{n} x_i^2 - \prod_{i=1}^{n} \cos\left(\frac{x_i}{\sqrt{i}}\right) + 1$	20	(-600, 600)	600

The four test functions can be classified as unimodal (Sphere function and Rosenbrock function) and multimodal functions (Rastrigin function and Griewank function). $w = 0.68$ is set in FIW. Eq (6) and Eq(7) are used to determine w in LIW and NIW , respectively.

$$w(t) = w_{start} - \frac{w_{start} - w_{end}}{t_{\max}} \times t \,, \tag{6}$$

$$w(t) = w_{start} - (w_{start} - w_{end}) \times \exp(-k * (\frac{t}{t_{\max}})^2) . \quad (7)$$

In our experimental studies, w used in w in the three methods (TANW□LIW and NIW) are all set within [0.9, 0.4], that is $w_{start} = 0.9$, $w_{end} = 0.4$. The other parameters $c_1 = c_2 = 2.0$, the swarm size is 40, and the allowable error $\sigma = 1e-80$, and $t_{\max} = 1500$. A total of 50 runs for each experimental setting are conducted.

4.2 Experimental Results

The results of the four functions are listed in Table 3, including the maximum value, the minimum value and the standard deviations. The graphs presented in Figs 6–9 illustrate the evolution of best fitness found by three algorithms, averaged for 50 funs for the four functions.

Table 3. Results for all algorithms on benchmark functions

Function	strategy	Max value	Min value	standard deviations	Mean value
Sphere	TANW	2.6552e-015	1.2535e-020	3.7727e-016	9.0940e-017
	NIW	6.3016e-012	1.1269e-015	1.3952e-012	7.4996e-013
	FIW	5.8000 e-002	1.000 e-003	1.4700e-002	1.0200e-002
	LIW	9.7600e-009	4.8377e-012	1.6531e-009	6.8240e-010
Rosenbrock	TANW	2.6385e+002	2.1250e-001	5.5068e+001	4.1048e+001
	NIW	4.4738e+002	1.1850e+001	7.7280e+001	5.0810e+001
	FIW	8.0398e+002	1.0502e+001	1.4272e+002	1.2477e+002
	LIW	5.6734e+002	4.4772e+000	1.0744e+002	7.0154e+001
Rastrigin	TANW	3.5819e+001	6.9647e+000	5.8282e+000	1.6916e+002
	NIW	3.1839e+001	5.9698e+000	5.3219e+000	1.8548e+001
	FIW	4.8523e+001	1.1067e+001	9.0932e+000	2.9706e+001
	LIW	3.3859e+001	6.9649e+000	5.3284e+000	1.8067e+001
Griewank	TANW	7.8700e-002	0.0000e+000	2.0800e-002	2.4000e-002
	NIW	1.3510e-001	2.6645e-015	2.6700e-002	2.6400e-002
	FIW	7.4520e-001	6.2000e-003	1.9350e-001	2.1550e-001
	LIW	1.0520e-002	9.9886e-011	2.5600e-002	3.2800e-002

The data in Table 3 show that new way of w (TANW) can obtain more precise results for all of the four functions than other three methods. As seen from the figures, TANW with the fastest convergence rate can get the best solution. Although for Rastrigin function, the standard deviations obtained by TANW is higher than the results obtained by LIW and NIW, while it still gets the faster convergence rate and more a promising end-results. FIW that owns fixed w cannot balance the global search and the local search. Therefore, it owns faster convergence rate in the earlier

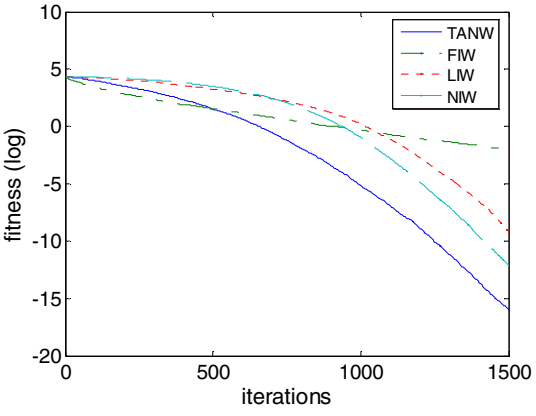

Fig. 6. Sphere function

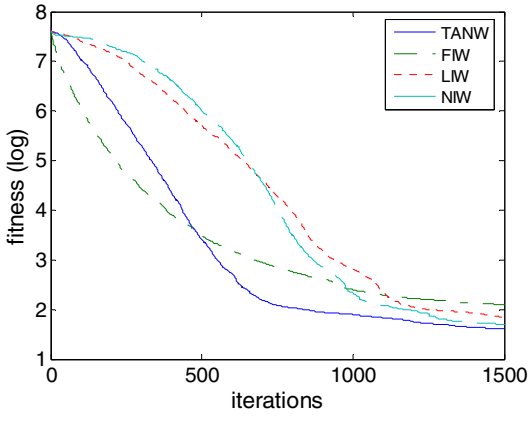

Fig. 7. Rosenbrock function

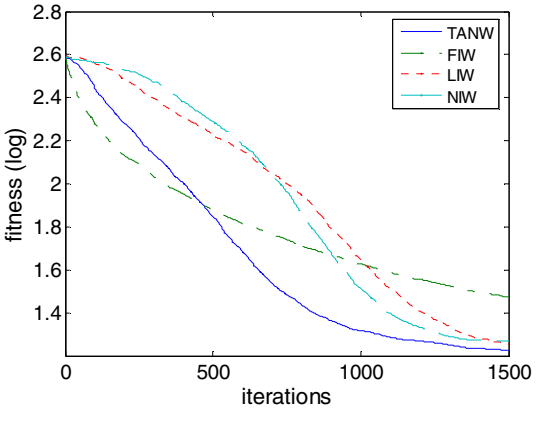

Fig. 8. Rastrigin function

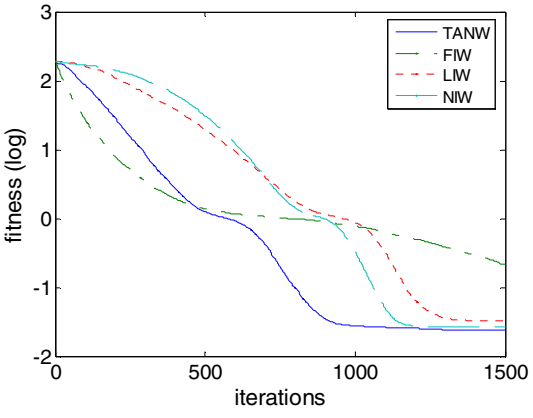

Fig. 9. Griewank function

period, but the final result is worst. NIW represented the weaker robustness (the larger standard deviations) in Griewank function and less precise (the larger mean of the function) in Rastrigin function than LIW, besides the two points, it produced better performance than LIW as a whole.

The results also indicated that in the most time, the fixed inertia weight （FIW） often cannot give the satisfactory result, and the non-liner inertia weight (NIW and TANW) performs better than linear one (LIW).

5 Conclusion and Future Work

Based on analyzing the effectiveness of the inertia weight and the features of the tangent function, a novel PSO with non-liner inertia weight is proposed in this paper. Its performance is evaluated by four benchmark functions compared with other three methods. The experimental results illustrated that our proposed TANW not only has a faster convergence rate but also yields high quality of the solution and robustness of the results.

Some further research to apply the proposed method to solve the actual problems should be carried out, such as the VRP and the portfolio optimization and other engineering problems.

Acknowledgment

This work is supported by Shenzhen-Hong Kong Innovative Circle project (Grant no.SG200810220137A) and Project 801-000021 supported by SZU R/D Fund.

References

1. Eberchart, R.C., Kennedy, J.: A New Optimizer Using Particle Swarm Theory. In: Proceedings of the 6th International Symposium on Micromachine and Human Science, Nagoya, Japan, pp. 39–43 (1995)

2. Eberchart, R.C., Kennedy, J.: Particle Swarm Optimization. In: Proceedings of the IEEE International Conference on Neural Networks, Perth, Australia, pp. 1942–1948 (1995)
3. Mendes, R., Cortez, P., Rocha, M., Neves, J.: Particle Swarms for Feedforward Neural Network Training. In: Proceedings of the International Joint Conference on Neural Networks (IJCNN 2002), pp. 1895–1899 (2002)
4. Venayagamoorthy, G.K., Doctor, S.: Navigation of Mobile Sensors Using PSO and Embedded PSO in a Fuzzy Logic Controller. In: Proceedings of the 39th IEEE IAS Annual Meeting on Industry Applications, Seattle, USA, pp. 1200–1206 (2004)
5. Parsopoulos, K.E., Papageorgiou, E.I., Groumpos, P.P.: A First Study of Fuzzy Cognitive Maps Learning Using Particle Swarm Optimization. In: Proceedings of IEEE Congress on Evolutionary Computation 2003 (CEC 2003), Canbella, Australia, pp. 1440–1447 (2003)
6. Abido, M.A.: Optimal Power Flow Using Particle Swarm Optimization. Int. J. Elect. Power Energy Syst. 24, 563–571 (2002)
7. Shi, Y., Eberhart, R.C.: Parameter Selection in Particle Swarm Optimizations. In: Porto, V.W., Waagen, D. (eds.) EP 1998. LNCS, vol. 1447, pp. 591–600. Springer, Heidelberg (1998)
8. Shi, Y., Eberhart, R.C.: A Modified Particle Swarm Optimizer. In: Proceedings of IEEE International Conference on Evolutionary Computation, Anchorage, AK, pp. 69–73 (1998)
9. Shi, Y., Eberhart, R.C.: Fuzzy Adaptive Particle Swarm Optimization. In: Proceedings of the Congress on Evolutionary Computation, Seoul, Korea, pp. 101–106 (2001)
10. Van den Bergh, F.: An Analysis of Particle Swarm Optimizer. Department of Computer Science. University of Pretoria, South Africa (2002)
11. Han, J.H., Li, Z.H.: An Adapting Particle Swarm Optimization and the Simulation Study. System simulation Journal (2006)
12. Niu, B., Li, L.: A novel PSO-DE-based hybrid algorithm for global optimization. In: Huang, D.-S., Wunsch II, D.C., Levine, D.S., Jo, K.-H. (eds.) ICIC 2008. LNCS (LNAI), vol. 5227, pp. 156–163. Springer, Heidelberg (2008)
13. Tan, L.J.: Particle Swarm Optimization and Its Application on the Control System of Continuous Conveyer of Disc-tube Assemble (Chinese). Master thesis, Liaoning Technical University (2007)

Particle Swarm Optimizer Based on Dynamic Neighborhood Topology

Yanmin Liu[1,2], Qingzhen Zhao[1], Zengzhen Shao[1], Zhaoxia Shang[1], and Changling Sui[2]

[1] College of Management and Economics, Shandong Normal University
[2] Department of math, Zunyi Normal College
yanmin7813@sohu.com

Abstract. In this paper, a novel dynamic neighborhood topology based on small world network (SWLPSO) is introduced. The strategy of the learning exemplar choice of the particle is based upon the clustering coefficient and the average shortest distance. This strategy enables the diversity of the swarm to be preserved to discourage premature convergence. Experiments were conducted on a set of classical benchmark functions. The results demonstrate good performance in solving multimodal problems used in this paper when compared with the other PSO variants.

Keywords: Particle swarm optimizer (PSO), dynamic neighborhood, topology, small world network.

1 Introduction

Optimization has been an active area of research for several decades. As many real-world optimization problems become increasingly complex, better optimization algorithms are always needed. The particle swarm optimization (PSO) algorithm is a new entrant to the family of evolutionary algorithms (EAs). It was first proposed by Kenney and Eberhart[1, 2] based on the metaphor of social behavior of birds flocking, fish schooling or the sociological behavior of a group of people. Each individual in the swarm called a particle (a point) with a fitness value and a velocity which is dynamically adjusted in the search space according to its own flying experiences and the best experiences of the swarm.

It is easy to implement PSO to solve the optimization problem. But when solving multimodal problems, it may be easily trapped in a local minimum. However, in real-world optimization problem, most of them are multimodal problems. Therefore, in order to overcome this defect and improve the PSO performance, some researches investigated neighborhood topology of the swarm [3-14]. In this paper, we propose a novel neighborhood topology based on small-world network [15] to improve the PSO performance when dealing with the multimodal problems.

Section 2 presents an overview of the PSO, as well as a discussion of previous attempts to improve its performance. In Sections 3, we will discuss the improved PSO based on the dynamic neighborhood topology. Section 4 presents the test functions,

D.-S. Huang et al. (Eds.): ICIC 2009, LNAI 5755, pp. 794–803, 2009.

the experimental settings for the comparative algorithms and the results. Finally, some conclusions and directions for future researches are discussed in section 5.

2 Particle Swarm Optimization (PSO)

2.1 Original Particle Swarm Optimization (OPSO)

Each individual as possible solution can be modeled as a particle that moves in *n*-dimensional search space. The velocity of each particle is determined by the vector $v_i \subset R^n$, and the velocity and position of the *i*th particle are updated as follows:

$$\vec{v}_i(t) = \vec{v}_i(t-1) + \varphi_1 \cdot rand_1(\vec{p}_i - \vec{x}_i(t-1)) + \varphi_2 \cdot rand_2(\vec{p}_g - \vec{x}_i(t-1)) \quad (1)$$

$$\vec{x}_i(t) = \vec{x}_i(t-1) + \vec{v}_i(t) \quad (2)$$

where $\vec{x}_i(t)=(x_i^1, x_i^2, \cdots, x_i^n)$ represents the position of the *i*th particle in current iteration *t*; *n* is the dimension of the search space. *t* is the number of current iteration; $\vec{v}_i(t) = (v_i^1, v_i^2, \cdots, v_i^n)$ denotes the *i*th particle velocity; φ_1 and φ_2 are two positive numbers known as the cognitive and social acceleration coefficients; $rand_1$ and $rand_2$ are two random numbers with the uniform distribution in the range of [0, 1]; $\vec{p}_i = (p_i^1, p_i^2, \cdots, p_i^n)$ is the best position of the current particle found so far by itself; $\vec{p}_g=(p_g^1, p_g^2, \cdots, p_g^n)$ is the best position of all particles found so far by the whole swarm. To make particle fly in the search space, each dimension velocity of a particle is limited to $v_{\max}$, which is constant value defined by the user.

2.2 Improved PSOs

Since the introduction of the PSO algorithm in 1995 by Kennedy and Eberhart, the PSO algorithm has attracted a great attention [17-20]. Many researchers have worked on improving its performance in various ways to derive several interesting variants. For example, the original PSO did not have an inertia weight, Shi and Eberhart [21] added it, as follows:

$$\vec{v}_i(t) = \omega \cdot \vec{v}_i(t-1) + \varphi_1 \cdot rand_1(\vec{p}_i - \vec{x}_i(t-1)) + \varphi_2 \cdot rand_2(\vec{p}_g - \vec{x}_i(t-1)) \quad (3)$$

where ω that is called the inertia weight, is used to balance the global and local search abilities. A large inertia weight is more appropriate for global search, and a small inertia weight facilitates local search. Inertia weight research also attracted a high level of interests [22-24]. These researchers proposed various value methods of inertia weight. In [25-27], Clerc *et al* indicated that a *constriction factor* (χ) may help to ensure the convergence. Application of the constriction factor results in Eq.(4).

$$\vec{v}_i(t) = \chi \cdot [\omega \cdot \vec{v}_i(t-1) + \varphi_1 \cdot rand_1(\vec{p}_i - \vec{x}_i(t-1)) + \varphi_2 \cdot rand_2(\vec{p}_g - \vec{x}_i(t-1))] \quad (4)$$

Kennedy [3, 4] claimed that PSO with a small neighborhood might perform better on complex problems, while PSO with a large neighborhood would perform better on simple problems. In [7], constructing a unified particle swarm optimizer (UPSO) by combining the global version and local version was proposed. Mendes and Kennedy [8] introduced a fully informed PSO to update the particle velocity instead of using the original PSO (OPSO) methods, all the neighbors of the particle are used to update the velocity. In [9], Peram *et al* proposed the fitness-distance-ratio-based PSO (FDR-PSO) with near neighbor interactions, when updating each dimension velocity dimension, the FDR-PSO algorithm selects one other particle, which has a higher fitness value and is nearer to the particle being updated. Liang *et al* [10, 11] proposed an improved PSO called CLPSO, which uses a novel learning strategy. Some researchers also combined the search techniques to improve particle swarm performance, for example, in [12-14], combining with evolutionary operators to improve PSO performance.

3 Particle Swarm Optimizer Based on Dynamic Neighborhood Topology

3.1 Small-World Network

Small-world network is one network which displays both the small diameter of the random graph, and the heavy clustering coefficient of the organized nearest-neighbor graphs. The small-world model [15] is an explicit construction of such graphs. Firstly, it starts with a regular network, such as a nearest-neighbor graph, and then rewires a probability p of the edges by changing one end to a uniformly random destination. Let p to vary from 0 to 1, one edge can be added (Fig.1. (c)). Small-world Network is one very similar to the random graphs of Erd¨os and Renyi [29]. Watts has suggested that information communication through social networks is affected by several aspects of the networks, as follows:

1) The degree of connectivity: The degree of connectivity among nodes in the network. Each particle in swarm identifies the best position found by its k neighbors; k is the variable that distinguishes local PSO from global PSO topologies, and is likely to affect performance.

2) The clustering coefficient (CC): If a node's neighbors are also neighbors to one another. The number of neighborhood in-common can be counted per node, and can be averaged over the graph.

3) The average shortest distance (L): The average shortest distance from one node to another was an important network characteristic for determining the spread of information through the network similar to choice of learning exemplar in the swarm.

Mendes and Kennedy[4] analyzed the effects of various population topologies on the particle swarm algorithm, and get a conclusion: the standard particle swarm topology learning from "*gbest*" facilitates the most immediate communication, and all particles are directly connected to the best position in the population (Fig.1.(a)). On the other hand, the ring lattice known as "*lbest*" is the slowest, most indirect communication pattern (Fig.1. (b)). Where i is opposite on the lattice, a good solution found by particle i

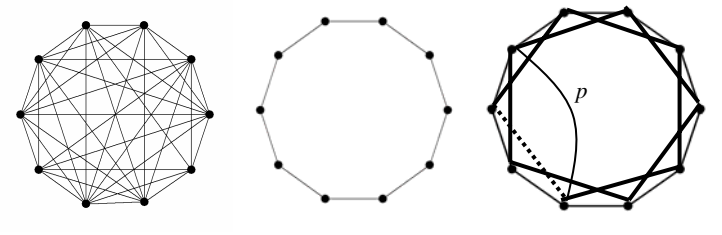

Fig. 1. The neighborhood topology[1]

has to pass through particle *i*'s immediate neighbor, that particle's immediate neighbor, and so on. Thus a solution found by particle *i*, moves very slowly around the ring.

3.2 Dynamic Neighborhood Topology Based on Small-world Network

In the PSO, each individual aims to produce the best solution by learning from other individuals, thereby the different neighborhood topology will effect each particle learning. The neighborhood topology is similar to small world network that affected the information communication in the swarm. In this paper, the proposed algorithm is constructed based on Eq.(3) and the small-world network. In this neighborhood topology, we use the following velocity updating equation:

$$\begin{aligned} &\vec{v}_i(t) = \omega \cdot \vec{v}_i(t-1) + \varphi_1 \cdot rand_1(\overrightarrow{p_{ibest}} - \vec{x}_i(t-1)) + \varphi_2 \cdot rand_2(\overrightarrow{p_g} - \vec{x}_i(t-1)) \\ &ibest = \{\, i \mid CC_i = \max(CC), L_i = \min(TP_1, TP_2)\} \quad , i \in TP_1 \ \ or \ \ i \in TP_2 \end{aligned} \tag{5}$$

where TP denotes total population. $CC_i = \frac{3(K-2)}{4(K-1)}$ is the biggest clustering coefficient for the *i*th particle in *TP*, *K* is the degree of the *i*th [30]. *ibest* is the best particle position which may equal to $\overrightarrow{p_g}$ or unequal to $\overrightarrow{p_g}$, this two different results don't affect our algorithm.

When updating the particle velocity in each iteration, which is shown in Fig.2, we firstly produce two small world networks as initial neighborhood topology (denoted as NT), and then choose the learning exemplar of the particle from other particle's pbest as the following criteria:

(1) *If* $CC(1) = CC(2) \,\&\, L_1 \neq L_2$, NT_1 wins. If $L_1 < L_2$, we choose particle *i* in NT_1 as the exemplar.

(2) *If* $CC(1) = CC(2) \,\&\, L_1 = L_2$, NT_1 or NT_2 is chose at will.

(3) *If* $CC(1) \neq CC(2) \,\&\, L_1 = L_2$, NT_1 wins. If $CC(1) > CC(2)$, we choose particle *i* in NT_1 as the exemplar.

(4) *If* $CC(1) \neq CC(2) \,\&\, L_1 < L_2$, NT_1 wins, and we choose particle *i* in NT_1 as the exemplar.

[1] (a) Global neighborhood. (b) Local neighborhood. (c) Small world network neighborhood.

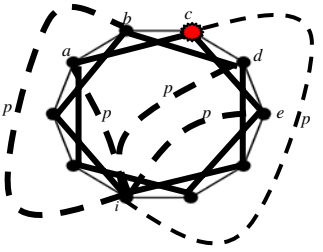

Fig. 2. Learning exemplar of particle *i* in the small world network[2]

(5) *If* $CC(1) > CC(2) \| L_1 < L_2$, NT_1 wins, then we choose particle *i* in NT_1 as the exemplar.

(6) *If* $CC(1) > CC(2) \| L_1 < L_2$, NT_1 wins, the particle *i* in NT_1 is chosen as the exemplar.

(7) *If* $CC(1) < CC(2) \| L_1 < L_2$ and the average degree $< K >$ in NT_2 is morn than the $< K >$ in NT_1, NT_2 wins, and we choose particle *i* in NT_2 as the exemplar. Otherwise, population NT_1 wins.

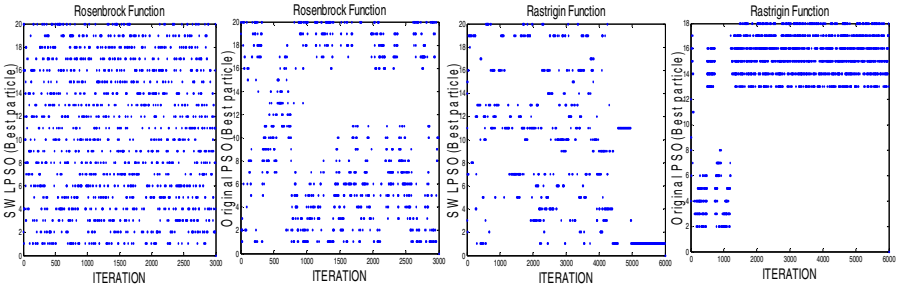

Fig. 3. The best particle index in the swarm

Complying with the above seven criteria, $\overline{p_{ibest}}$ can generate new positions in the process of the search using the information derived from the different particle historical best positions. Fig.3 shows that the SWLPSO has more diversities than the OPSO. We can observe the main differences between the SWLPSO and the original PSO: Instead of using particle's own $\overline{p_i}$ and $\overline{p_g}$ as the exemplars, all particles can learn from the most excellent neighbor by the *CC* and *L*. This strategy not only avoids the blind exemplar choice, but also saves a lot of computation time. The strategy of updating particle velocity increases the diversity of the swarm in contrast with the OPSO. The pseudocode of the SWLPSO is given in Fig.4.

[2] Particle *a, b, c, d* and *e* are connected with particle *i* by probability *p*. Particle *c* is choose as exemplar based on CC and L.

Begin
For each particle
1. Initialize small world network. Computer *CC* and *L*. (Predefined probability p)
2. Initialize the particles' position and velocity
3. Computer fitness value.
4. If pbestval(i)>pbestval(j) $i \neq j \in popsize$
Then pbest=pbest(i).
Gbestval=pbestval(i).
Endfor
While (stopping criteria)
For each particle
5. Updating particle velocity and position in terms of Eq.(5) and (2).
6. Choose learning exemplar in terms of *CC* and *L*.
7. Updating particle position
8. Updating global gbest and global fitness.
Endfor
Endfor

Fig. 4. The pseudocode of the SWLPSO algorithm

4 Experiment and Results

4.1 Test Function Description

To evaluate the performance of the proposed approach, we wish to test the SWLPSO on the diverse test functions and our main objective is to improve PSO's performance on multimodal problems, therefore we choose two unimodal functions and 4 multimodal benchmark functions, which can be considered "difficult" global optimization problems for an evolutionary algorithm. All test functions are tested on 30 dimensions. the parameters of these functions are presented in Table 1. More details about test function are collected in [11].

Table 1. The parameters of test function

Function name	n(Dimension)	Search space	Global optimum(x^*)	$f(x^*)$
Sphere	30	$[-100,100]^{30}$	[0,0,…,0]	0
Rosenbrock	30	$[-2.048,2.048]^{30}$	[1,1,…,1]	0
Ackley	30	$[-32.768,32.768]^{30}$	[0,0,…,0]	0
Griewanks	30	$[-600,600]^{30}$	[0,0,…,0]	0
Rastrigin	30	$[-5.12,5.12]^{30}$	[0,0,…,0]	0
Weierstrass	30	[-0.5,0.5]	[0,0,…,0]	0

4.2 Parameter Settings for SWLPSO Algorithms

The experiments were conducted to compare five PSO algorithms on the six test problems with 30 dimensions. The five PSO algorithms are the PSO with constriction factor (PSO-CF) [27], Fully informed particle swarm (FIPS)[8], FDR-PSO[9], CLPSO [11] ands the proposed algorithm(SWLPSO). In order to make these different

algorithms comparable, all parameters are set as follows: the population size is set at 30 and the maximum fitness evaluations (FEs) is set at 30000. All experiments were run 30 times. The mean values of the results are presented in Table 2.

Table 2. Result of Experiment Using Various PSO Variants

Function name	Optimal	The Means of Different PSO Algorithm				
		PSO-CF	FIPS	FDR-PSO	CLPSO	SWLPSO
Sphere	0	1.532e-080	2.574e-028	**2.237e-100**	6.432e-033	4.983e-018
Rosenbrock	0	2.256e+001	2.233e+000	**9.968e-002**	1.491e+000	1.512e-002
Ackley	0	1.155e+000	3.553e-015	2.254e-009	1.309e-014	**1.001e-016**
Griewank	0	2.675e-002	2.753e-002	6.132e-002	6.382e-002	**2.782e-009**
Rastrigin	0	8.955e+000	1.872e+000	1.992e+000	8.823e-014	**5.553e-015**
Weierstrass	0	1.573e+001	6.962e-001	1.112e+000	2.703e-002	**2.3381e-002**

Table 3. Result of t-tests for the PSO algorithms

a=0.05	PSO-CF SWLPSO	FIPS SWLPSO	FDR-PSO SWLPSO	CLPSO SWLPSO
p-value	0.0034	0.00026	0.0045	0.0059
result	1	1	1	1

4.3 Experiment Result

Table 2 presents the mean of the 30 runs of the five algorithms on six test functions with 30 dimensions. The best results among the five algorithms are shown in bold. Fig.5. presents the convergence characteristics in terms of the best fitness value of the median run of each algorithm for each test function. From the results, we observe that for the unimodal Sphere function, the SWLPSO could not converge as fast as other PSO algorithms. The reason is that when updating velocity in each iteration, a particle can learn from the best exemplar in all neighbors. The learning strategy may lead to a large search space and could not converge as fast as the other PSO algorithms. Note that on Rosenbrock function, the SWLPSO algorithm achieved the almost same best result as FDR-PSO. However, the SWLPSO algorithm performs well in all multimodal problems and outperforms all other PSO algorithms, especially on Griewanks, Ackley's and Rastrigin functions.

The PSO with constriction factor (PSO-CF) is the global versions where the whole population is neighborhood. It performs well on unimodal problems. The CLPSO algorithm performs better than the all other PSO variants on Rastrigin and Weierstrass functions except for the SWLPSO algorithm. Comparing the convergence characteristics graphs, we observed that SWLPSO has faster convergence speed than other PSO algorithms on Rosenbrock, Ackley's Griewank and Rastrigin functions.

The learning strategy of the SWLPSO is somewhat similar to elite learning strategy, but not the same. This learning strategy may avoid the blind learning from another particle. In order to determine whether the results obtained by the SWLPSO are statistically different from the results generated by other algorithms, we adopted the practice of performing t-tests on pairs of PSO variants with the SWLPSO.

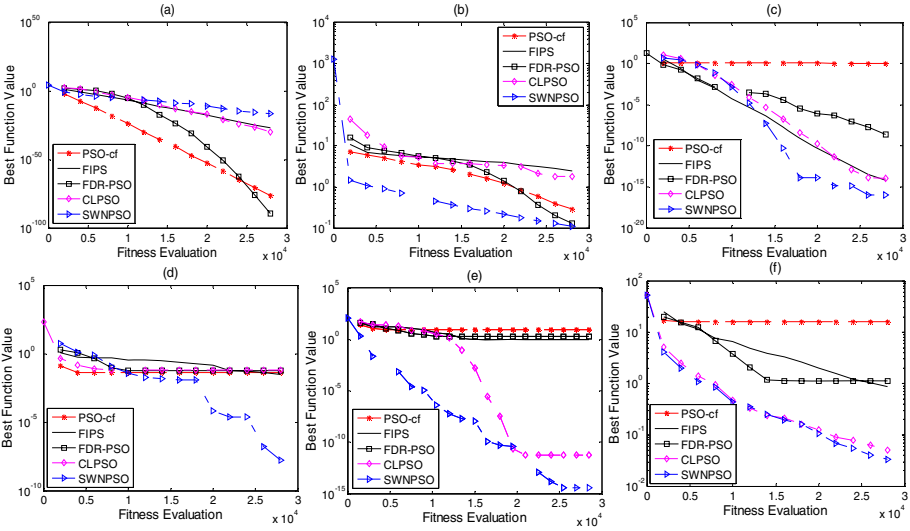

(a) Sphere (b) Rosenbrock (c) Acley (d) Griekwank (e) Rastrigin (f) Weierstrass

Fig. 5. The convergence characteristics

These tests give a *p-value* which is compared to a constant called a, to determine whether a difference is significant or not. This criterion is defined as follows:

$$result = \begin{cases} 1 & if \quad p < a \\ 0 & if \quad p \geq a \end{cases} \tag{6}$$

If p is less than a, the performance is statistically different, whereas, if p is equal or greater than a, it means that the performance is not statistically different. The comparison results are shown in Table 3.

5 Conclusions and Future Work

We have presented a novel neighborhood topology on based small world network. To assure a particle in the swarm to learn from the best exemplar in its neighbor, we apply some characteristics of small world network in the SWLPSO algorithm, such as the clustering coefficient which indicates the numbers of the neighbor around the current particle i and shows the particle i exploration and exploitation capability. According to the result of the experiments, the SWLPSO does not perform well for unimodal(Sphere function). But, in terms of "no free lunch" theorem [31], any elevated performance over one class of problems is offset by the performance over another class. It means that the SWLPSO does not perform well on the unimodal problems, but it will outperform on the modal test functions, or its performance does surpass other algorithms remarkably, but its convergence characteristics are better than others. Therefore, we may not expect the best performance on all test functions, as the purpose of the proposed algorithm is on improving the PSO's performance for

solving multimodal problems in the real world. The SWLPSO achieves the satisfied results. This implies that the SWLPSO is more effective in solving modal problems, which is experimented in this paper.

In the future, we will focus on: (i) experimenting to test our proposed algorithm effectiveness with more multimodal test problems and several composition functions that is more difficult to be optimized; (ii) applying the proposed algorithm to some applications to verify its effectiveness.

Acknowledgments. The first author acknowledges the support from Ministry of Education in Guizhou Province, Zunyi technology division Dean's Office and Department of Scientific Research Of Zunyi Normal College through the project number 070520, B07015, [2008]21 and 2007018, respectively.

References

1. Eberhart, R., Kennedy, J.: New Optimizer Using Particle Swarm Theory. In: Proc. 6th Int. Symp. Micro Machine Human Science, pp. 39–43 (1995)
2. Kennedy, J., Eberhart, R.: PSO Optimization. In: Proc. IEEE Int.Conf. Neural Networks, Perth, Australia, vol. 4, pp. 1941–1948 (1995)
3. Kennedy, J.: Small Worlds and Mega-minds: Effects of Neighborhood Topology on Particle Swarm Performance. In: Proc. Congr. Evol.Comput, pp. 1931–1938 (1999)
4. Kennedy, J., Mendes, R.: Population Structure and Particle Swarm Performance. In: Proc. IEEE Congr. Evol. Comput., Honolulu, HI, pp. 1671–1676 (2002)
5. Niu, B., Zhu, Y.L., He, X.X., Wu, H., Shen, H.: A Lifecycle Model for Simulating Bacterial Evolution. Neurocomputing 72, 142–148 (2008)
6. Niu, B., Li, L.: A novel PSO-DE-based hybrid algorithm for global optimization. In: Huang, D.-S., Wunsch II, D.C., Levine, D.S., Jo, K.-H. (eds.) ICIC 2008. LNCS (LNAI), vol. 5227, pp. 156–163. Springer, Heidelberg (2008)
7. Parsopoulos, K.E., Vrahatis, M.N.: UPSO-A Unified Particle Swarm Optimization Scheme. Lecture Series on Computational Sciences, pp. 868–873 (2004)
8. Mendes, R., Kennedy, J., Neves, J.: The Fully Informed Particle Swarm: Simpler, Maybe Better. IEEE Trans. Evol. Comput, 204–210 (2004)
9. Peram, T., Veeramachaneni, K., Mohan, C.K.: Fitness-distance-ratio Based Particle Swarm Optimization. In: Proc. Swarm Intelligence Symp., pp. 174–181 (2003)
10. Liang, J.J., Qin, A.K., Suganthan, P.N., Baskar, S.: Evaluation of comprehensive learning particle swarm optimizer. In: Pal, N.R., Kasabov, N., Mudi, R.K., Pal, S., Parui, S.K. (eds.) ICONIP 2004. LNCS, vol. 3316, pp. 230–235. Springer, Heidelberg (2004)
11. Liang, J.J., Qin, A.K., Suganthan, P.N., Baskar, S.: Comprehensive Learning Particle Swarm Optimizer for Global Optimization of Multimodal Functions. IEEE Transactions on Evolutionary Computation 10(3), 281–295 (2006)
12. Angeline, P.J.: Using Selection to Improve Particle Swarm Optimization. In: Proc. IEEE Congr. Evol. Comput., Anchorage, AK, pp. 84–89 (1998)
13. Lovbjerg, M., Rasmussen, T.K., Krink, T.: Hybrid Particle Swarm Optimizer with Breeding and Subpopulations. In: Proc. Genetic Evol.Comput. Conf., pp. 469–476 (2001)
14. Miranda, V., Fonseca, N.: New Evolutionary Particle Swarm Algorithm (EPSO) Applied to Voltage/VAR control. In: Proc. 14thPower Syst. Comput. Conf., Seville, Spain (2002)
15. Watts, D.J., Strogatz, S.H.: Collective Dynamics of Small-world Networks. Nature 393, 440–442 (1998)

16. Wilke, D.N.: Analysis of the Particle Swarm Optimization Algorithm. Master's thesis, Dept. Mechanical and Aeronautical Eng., Univ. of Pretoria, Pretoria, South Africa (2005)
17. Schutte, J.F., Groenwold, A.A.: Sizing Design of Truss Structures Using Particle Swarms. Struct. Multidisc. Optim. 25(4), 261–269 (2003)
18. Coello, C.A.C.G., Pulido, T., Lechuga, M.S.: Handling Multiple Objectives with Particle Swarm Optimization. IEEE Trans. Evol.Comput. 8, 256–279 (2004)
19. Messerschmidt, L., Engelbrecht, A.P.: Learning to Play Games Using a PSO-based Competitive Learning Approach. IEEE Trans. Evol.Comput. 8, 280–288 (2004)
20. Wachowiak, M.P.: An Approach to Multimodal Biomedical Image Registration Utilizing Particle Swarm Optimization. IEEE Trans. Evol. Comput. 8, 289–301 (2004)
21. Shi, Y., Eberhart, R.C.: A Modified Particle Swarm Optimizer. In: Proc. IEEE Congr. Evol. Comput., pp. 69–73 (1998)
22. Shi, Y., Eberhart, R.C.: Particle Swarm Optimization with Fuzzy Adaptive Inertia Weight. In: Proc.Workshop Particle Swarm Optimization, Indianapolis, pp. 101–106 (2001)
23. Ratnaweera, A., Halgamuge, S., Watson, H.: Self-organizing Hierarchical Particle Swarm Optimizer with Time Varying Accelerating Coefficients. IEEE Trans. Evol. Comput. 8, 240–255 (2004)
24. Fan, H.Y., Shi, Y.: Study on Vmax of Particle Swarm Optimization. In: Proc.Workshop Particle Swarm Optimization, Indianapolis, IN (2001)
25. Clerc, M.: The Swarm and the Queen: Toward a Deterministic and Adaptive Particle Swarm Optimization. In: Proc. ICEC 1999, Washington, DC, pp. 1951–1957 (1999)
26. Corne, D., Dorigo, M., Glover, F.: New Ideas in Optimizaton, pp. 379–387. McGraw-Hill, New York (1999)
27. Clerc, M., Kennedy, J.: The Particle Swarm: Explosion, Stability, and Convergence in a Multi-dimensional Complex Space. IEEE Trans. Evol.Comput. 6, 58–73 (2002)
28. Newmama, M.E.J., Watts, K.J.: Renormalization Group Analysis of the Small-world Network Model. Phys.Lett.A. 263, 341–346 (1999)
29. Erdös, P., Renyi, A.: On Random Graphs. Publicationes Mathematicae 6, 290–297 (1959)
30. Barrat, A., Weigt, M.: On the Properties of Small World Networks. Europe Physicals 13, 547–560 (2003)
31. Wolpert, D.H., Macready, W.G.: No Free Lunch Theorems for Optimization. IEEE Trans. Evol. Comput. 1, 67–82 (1997)

An Improved Two-Stage Camera Calibration Method Based on Particle Swarm Optimization

Hongwei Gao[1], Ben Niu[2], Yang Yu[1], and Liang Chen[1]

[1] School of Information Science & Engineering, Shenyang Ligong University, Shenyang, 110168 China
[2] College of Management, ShenzhenUniversity, Shenzhen, 518060 China
drniuben@gmail.com, ghw1978@sohu.com

Abstract. According to the calibration of binocular vision, an improved two-stage camera calibration method involved with multi-distortion coefficients is introduced in this paper. At the first stage, the 3D points' coordinate are calculated by the imitated direct linear transformation (DLT) triangulation based on distortion compensation. And at the second stage, particle swarm optimization (PSO) is selected to determine two cameras' parameters. In this way the parameters of the two cameras can be tuned simultaneously. In order to assist estimating the performance of the proposed method, a new cost function is designed. Simulation and experiment are made under the same calibration data sets. The performance of PSO used to tune the parameters is also compared to that of GA. The experiment results show that the strategy of taking the 3D reconstruction errors as object function is feasible and PSO is the best choice for camera parameters' optimization.

Keywords: Computer vision, Image analysis, 3D reconstruction, PSO.

1 Introduction

The accuracy of calibration will directly determine the performance of many vision tasks. Many classic camera calibration methods based on two-stage have been proposed until this time, among which Tsai's [1] method with radial lens distortion is famous and applied frequently for its high accuracy, However, it takes only one radial distortion coefficient into consideration which is efficient for long focal length and little distortion lens. J Weng [2] introduced a camera model considering radial decentering and thin prism distortions. The camera parameters can be calculated by matrix decomposition which is hard to achieve high accuracy. Some improved methods are put forward recently. Z Zhang [3] proposed a two-stage camera calibration method by viewing a planar pattern shown at a few different orientations which is easy to use and flexible. J Heikkilä [4] proposed a four-steps calibration method considering distortion compensation including tangent distortion. The cost functions in the above algorithms were defined as the distance between the measured image points and estimated image points, while the refined solution was only optimal to measured 2D image points, not to the real 3D points. Taking these factors into consideration, C Zhou [5]

D.-S. Huang et al. (Eds.): ICIC 2009, LNAI 5755, pp. 804–813, 2009.

used a new cost function which is based on the sum of distance in the world coordinate between ground truth 3D points and calculated 3D points. A Perspective 3-Point (P3P) algorithm is used to finish 3D point's reconstruction, but the optimization of two cameras is executes twice, that is to say two cameras' parameters are optimized respectively.

The traditional parameter optimal algorithms are gradient-based computation system. The drawbacks of them are sensitive to the initial value of variable and easy to get into local minimum, furthermore, the time consumption of these algorithms to run a good result are considerable. The advent of evolutionary algorithm (EA) has attracted considerable interest in the optimal calculation [6, 7], EA shows its excellent performance on global optimization. The most well known of which is genetic algorithm (GA). As compared to traditional gradient-based computation system, EA denotes all kinds of complicated data structure by simple coding technique, and then directs the direction of studying and searching by means of simple genetic operation and nature select of winner take all based on coding table. This strategy can solve the problems such as knowledge denotation and combination explosion. Recently, a new evolutionary computation technique, the particle swarm optimization (PSO) algorithm, is introduced by Kennedy and Eberhart [8], and has already come to be widely used in many areas [9, 10]. Compared to GA, PSO has some attractive advantages: (1) it has a fast convergence rate (2) it is easy to implement (3) it has few parameters to adjust. Consequently, we introduce PSO into the optimal procedure of new cost function and make some comparisons with other optimal algorithms.

Experiment and simulation results prove that the improved methods have much higher calibration precision than that of the traditional ones; the parameters obtained by PSO are more optimal than GA which shows that PSO can be applied into camera calibration.

2 Camera Model with Multi-distortion Coefficients

In the pin-hole model, the world coordinate and image coordinate of a point p is related by the formula as follows:

$$Z_c\begin{bmatrix} u \\ v \\ 1 \end{bmatrix} = \begin{bmatrix} fc(1) & alpha\_c * fc(1) & cc(1) \\ 0 & fc(2) & cc(2) \\ 0 & 0 & 1 \end{bmatrix} \begin{bmatrix} R & T \end{bmatrix} \begin{bmatrix} X_w \\ Y_w \\ Z_w \\ 1 \end{bmatrix} = K \begin{bmatrix} R & T \end{bmatrix} \begin{bmatrix} X_w \\ Y_w \\ Z_w \\ 1 \end{bmatrix} = M \begin{bmatrix} X_w \\ Y_w \\ Z_w \\ 1 \end{bmatrix}, \quad (1)$$

where M represents camera project matrix; K represents internal parameter matrix; $\begin{bmatrix} R & T \end{bmatrix}$ is defined by the pose of world coordinate system and called external parameter matrix; $fc(1)$ and $fc(2)$ represent variables of horizontal and vertical whose unit is pixel; alpha_c is the horizontal scale factor; $cc(1)$ and $cc(2)$ are coordinates of image center whose unit is also pixel. External parameter matrix can be represented by translate vector T and rotate vector R. Thus, the project matrix is equal to the product of internal and external parameter matrix.

There exist many kinds of distortion in camera lens, especially in short focal length lens. It is necessary to considerate the impaction of distortion in order to achieve high accurate calibration result. There are four main distortion: radial distortion, tangential distortion, decentering distortion and thin prism distortion. Generally speaking, radial distortion and tangential distortion are enough for describing the camera distortion model. Two kinds of distortion can be represented as follows:

$$k_c = (k_c(1), k_c(2), k_c(3), k_c(4), k_c(5))^T, \tag{2}$$

Set p as the 3D coordinate of vector $P = [X_c; Y_c; Z_c]^T$, imaging coordinate of this point on CCD plane has the relationship with inner parameters. Set x_n as the physical coordinate of imaging point under pinhole model:

$$x_n = \begin{bmatrix} Xc/Zc \\ Yc/Zc \end{bmatrix} = \begin{bmatrix} x \\ y \end{bmatrix}, \tag{3}$$

Set $r^2 = x^2 + y^2$, taking the lens distortion into consideration, the physical coordinate of imaging point x_d can be represented by:

$$x_d = \begin{bmatrix} x_d(1) \\ x_d(2) \end{bmatrix} = \left(1 + k_c(1)r^2 + k_c(2)r^4 + k_c(5)r^6\right)x_n + d_x, \tag{4}$$

where tangent distortion d_x can be represented as :

$$d_x = \begin{bmatrix} 2k_c(3)xy + k_c(4)(r^2 + 2x^2) \\ k_c(3)(r^2 + 2y^2) + 2k_c(4)xy \end{bmatrix}, \tag{5}$$

where k_c is the vector contains radial distortion and tangent distortion, and then the ideal imaging coordinate of point p is described by x in pixel. Where:

$$\begin{aligned} x_u &= fc(1)(x_d(1) + alpha\_c * x_d(2)) + cc(1) \\ y_u &= fc(2)x_d(2) + cc(2) \end{aligned}, \tag{6}$$

x in pixel can be written by:

$$\begin{bmatrix} x_u \\ y_u \\ 1 \end{bmatrix} = K \begin{bmatrix} x_d(1) \\ x_d(2) \\ 1 \end{bmatrix}. \tag{7}$$

Now we can know the calibration procedure from the above discussion. Firstly, the ideal image coordinates after distortion compensation is calculated. Secondly, the bi-projective matrixes of two cameras are acquired by directed linear transformation

(DLT) method with pinhole model. Finally, the stereo triangulation is made by two projective matrixes.

3 Calibration Method Based on 3D Reconstruction Error

3.1 Two-Stage Calibration Method

The traditional estimation for the camera parameters can be obtained by minimizing the residual between the model and N observations (U_i, V_i), where $i = 1, \cdots, N$. In the case of Gaussian noise, the objective function is defined as the sum of squared residuals:

$$F = \sum_{i=1}^{N} (U_i - u_i)^2 + \sum_{i=1}^{N} (V_i - v_i)^2 \ , \tag{8}$$

Where, (u_i, v_i) is the correct image points, (U_i, V_i) is the observed values. The least squares estimation technique can be used to minimize Eq. (7). Due to the nonlinear nature of the camera model, simultaneous estimation of the parameters involves applying an iterative algorithm. However, without proper initial parameter values the optimization may stick in a local minimum and thereby cause the calibration to fail. This problem can be avoided by using the parameters from the DLT method as the initial values for the optimization. A global minimum of Eq. (7) is then usually achieved after a few iterations.

The object function proposed here is as follows:

$$\sum_{i=1}^{n} \| P_i - P_{1i} \| = \sum_{i=1}^{n} \sqrt{(x_i - x_{1i})^2 + (y_i - y_{1i})^2 + (z_i - z_{1i})^2} \ , \tag{9}$$

Where, $P_i(x_i, y_i, z_i)$ is the ground truth 3D coordinate of space point, $P_{1i}(x_{1i}, y_{1i}, z_{1i})$ is the observed values, n represents the number of calibration points. Eq. (8) is based on 3D reconstruction error and different from Eq. (7) which is based on 2D reconstruction error. Two-stage calibration method based on 3D reconstruction error proposed here is described as follows:

First step: the inner parameters of two cameras are determined by Matlab Calibration Toolbox [4].

Second step: optimization of camera parameters. In this paper, we calculate the projective matrix directly, in this way the inner and outer parameters can be contained simultaneously. The traditional projective matrix composition method has 32 parameters need to be tuned at the same time including 10 inner parameters and 6 outer parameters for each camera, while in our proposed method only has 20 parameters to be optimized explicitly including only 10 inner parameters, the outer parameters are optimized non-obviously (implicitly), they are optimized embedded in the whole projective matrix. By this way the parameters to be tuned is reduced, the calibration speed is enhanced and the stability of the resolutions is also ensured which can be proved by the following experiments.

3.2 Optimal Algorithm Based on 3D Reconstruction Error

The triangulation is constructed by dual projective matrixes, meanwhile, the 3D reconstruction error is also constructed which realize the 20 parameters of two cameras to be optimized at the same time. The flow chart of this algorithm is as follows:

1) Calculate the initial value of $(fc(1), fc(2), cc(1), cc(2), alpha\_c, kc)$ by means of Matlab Calibration Toolbox, the initial value of $k_c = (k_c(1), k_c(2), k_c(3), k_c(4), k_c(5))^T$ is set to be 0.

2) Use character points' image coordinates (u_{1i}, v_{1i}), (u_{2i}, v_{2i}) and two cameras' $(fc(1), fc(2), cc(1), cc(2), alpha\_c, kc)$ to calculate the ideal image coordinates $(u_{1i}^{'}, v_{1i}^{'})$ and $(u_{2i}^{'}, v_{2i}^{'})$ according to Eq. (5).

3) Use ideal $(u_{1i}^{'}, v_{1i}^{'})$, $(u_{2i}^{'}, v_{2i}^{'})$ and world coordinate $P_i(x_i, y_i, z_i)$ to calculate two cameras' projective matrix M_1 and M_2 by means of DLT method.

4) Use ideal $(u_{1i}^{'}, v_{1i}^{'})$, $(u_{2i}^{'}, v_{2i}^{'})$ and M_1, M_2 to calculate $P_{1i}(x_{1i}, y_{1i}, z_{1i})$, meanwhile, set the following object function (8) to be minimized, and then the new value of $(fc(1), fc(2), cc(1), cc(2), alpha\_c, kc)$ can be achieved.

5) If the aforementioned iteration number is achieved, then get out the loop and return the optimal value of two cameras' $(fc(1), fc(2), cc(1), cc(2), alpha\_c, kc)$, or go back to step 2) to calculate again.

The goal of calibration is to achieve high triangulation accuracy. The optimized distortion coefficients and inner parameters acquired by our method possess physical meanings which can also ensure the triangulation error to be minimal.

4 Optimization Strategy Based on Particle Swarm Optimization

In order to test the performance of PSO, we also design the GA to optimize the same cost function. Comparisons are also made between PSO and GA in the following experiment results.

4.1 Optimization Scheme Based on PSO

Initialize population of PSO is a swarm of random particles, during every iteration, the particle updates itself by means of tracing two best values. One is the best solution found by itself which is named personal best point and represented by $pbest$. Another best point in global PSO is the best solution found by swarm named global best point which is represented by. After finding the two best solutions, the particles update its own velocity and position according to equation (9) and (10).

$$v_{id}^{k+1} = v_{id}^{k} + c_1 rand_1^k \left(pbest_{id}^k - x_{id}^k\right) + c_2 rand_2^k \left(gbest_d^k - x_{id}^k\right), \quad (10)$$

$$x_{id}^{k+1} = x_{id}^{k} + v_{id}^{k+1} , \tag{11}$$

Where, i is the particle index; v_{id}^{k} is the d th velocity of i th particle during the k th iteration; c_1, c_2 are accelerate coefficients (learning factors) which can adjust max flying pace length of global best particle and personal best particle respectively. $rand_{1,2}$ is the random numbers on the interval [0,1] applied to i th particle; x_{id}^{k} is the d th position of i th particle during the k th iteration; $pbest_{id}$ is the d th personal best point position of i th particle; $gbest_d$ is the d th global best point position of whole swarm.

According to the parameter optimization of calibration, the individual particle can be represented as follows:

$$b = \{\ fc1, fc2, cc1, cc2, alpha\_c1, kc1, fc21, fc22, cc21, cc22, alpha\_c2, kc2\ \}. \tag{12}$$

The initial values of two cameras' parameters can be determined by Matlab Calibration Toolbox. The calculation complication can be reduced by means of confirming the searching space before PSO is done. The individual of swarm is generated randomly between the initial value neighbor domain and the cost function adopted is formula (8), where the individual number $d = 20$.

The optimized procedure based on PSO is as follows:

1) Initialize the swarm randomly. The initialization of initial searching point position and its speed is finished randomly between the initial value's neighbor domain. The initial number of particle is selected as $d = 20$. Calculate $pbest_{id}$ correspondingly, then $gbest_d$ is the best value of $pbest_{id}$.
2) Evaluate every individual in the swarm. Calculate the particle's fitness value according to formula （8）, if the value is better than the current $pbest_{id}$, then update the $pbest_{id}$. If the $pbest_{id}$ in all particles is better than current $gbest_d$, then update $gbest_d$.
3) Update the swarm according to formula （9）and（10）.

If a terminate condition is met, then the searching procedure is terminated, except that return to step 2）.

4.2 Optimization Scheme Based on GA

The optimized procedure based on GA is as follows:

Initialization: generate M individuals randomly, where there is $M = 100$, suppose the evolution iteration number of swarm to be $t = 0$,

$$G^0 = \{b_1^0, \cdots, b_j^0, \cdots, b_M^0\}, \tag{13}$$

Where b is chromosome similar with the individual in PSO, superscript of it represents evolution iteration number, subscript of it represents the number of individuals.

1) Fitness value calculation: calculate the fitness value of every chromosome according to formula (8) and arrange them with sort ascending,

$$G^t = \{b_1^t, \cdots, b_j^t, \cdots, b_M^t\} \text{ and } \sum_{i=1}^{n} \left\| P_i - P_{1i}(b_j^t) \right\| \le \sum_{i=1}^{n} \left\| P_i - P_{1i}(b_{j+1}^t) \right\|, \tag{14}$$

2) Select operation: select k individuals according to the optimal and random principle,

$$G^{t+1} = \{b_1^{t+1}, \cdots, b_k^{t+1}\}, \tag{15}$$

3) Aberrance operation: select p individuals of new generated k individuals, apply aberrance operation to part of the individuals' genes,

$$G^{t+1} = \{b_1^{t+1}, \cdots, b_k^{t+1}, b_{k+1}^{t+1}, \cdots, b_{k+p}^{t+1}\}, \tag{16}$$

4) Crossover operation: select one gene to make crossover operation randomly, repeat the same step $M - k - p$ times,

$$G_i^{t+1} = \{b_1^{t+1}, \cdots, b_k^{t+1}, \cdots, b_{k+p}^{t+1}, \cdots, b_M^{t+1}\}, \tag{17}$$

5) Set evolution iteration number to increase onetime, that is $t = t + 1$, select the optimal individual as the current solution,

$$b_{best} = \{b_i^t \mid \sum_{i=1}^{n} \left\| P_i - P_{1i}(b_i^t) \right\| = \min_{j=1}^{M} (\sum_{i=1}^{n} \left\| P_i - P_{1i}(b_j^t) \right\|)\}. \tag{18}$$

If the ending condition is achieved, that is evolution iteration number is bigger than some value set beforehand or the fitness value is satisfied with $\sum_{i=1}^{n} \left\| P_i - P_{1i}(b) \right\| < \xi$, then the searching procedure is terminated, except that return to step 2) .

5 Simulation and Experiment Results

5.1 Experiment Conditions

Images of calibration and test objects were obtained with two black and white cameras, focal length of lens is 12.5mm. The calibration and test points are created by a sheet containing 49 black squares on the top surface of a foam block 20mm×20mm in size. The corners of the 169 squares are treated as control points, making a total of 169 points. The optical axis of two cameras is parallel with each other. There are 676

points for calibration extracted from the block 1~2 meters away in front of the camera at four different positions. Another 4732 points on other 28 images are used to test the triangulation accuracy. The software developing environment is based on MS VC++6.0 and foam block is moved on calibration table.

5.2 Experiment Results and Analysis

The experimental comparisons in terms of calculation speed and triangulation accuracy for these three methods are shown in Table 1. The calibration error represents the fitness between the calibration data and camera model. We can see that the average error of two methods is within 1mm along three directions (x , y and z) respectively which illustrates that these calibration data are fit for the camera model preferably. In order to test calibration result, the triangulation test is necessary. As seen from Table 1, the parameters got from PSO is more optimal than GA, the average triangulation errors obtained by PSO is lower. As we can see from Figs 1~2, the maximum value of absolute triangulation error is 2.3mm and 1.9mm respectively for GA and PSO. The convergence curves of cost function are achieved after 1000 iterations. The final value of formula (8) is constant which is 22.1 and 16.7 respectively in detail. The optimization procedure terminates after 660 times and 430 times respectively.

The conclusion can be draw from above results. On one hand, the same point of PSO and GA lies in the random initialization of swarm, evaluating the system with fitness value, and searching the solution randomly according to fitness value. On the other hand, there are some differences between PSO and GA. PSO search the optimal solution by tracing the optimal particle in the solution space without crossover and aberrance operation used in GA. By comparison with GA, the predominance of PSO lies in easy realization, fast speed and without lots of parameters to be adjusted.

Table 1. Error comparison for different optimal strategies

			GA		PSO	
left camera	k_1	f_{c11}	-0.057642	587.309864	-0.049015	597.787054
	k_2	f_{c12}	0.064481	565.162345	0.074469	570.937578
	k_3	alpha_c_1	0.001803	-0.000102	-0.027153	0.006843
	k_4	cc_{11}	0.000343	392.287535	-0.003405	395.434565
	k_5	cc_{12}	0.000016	291.160867	0.004772	296.664261
right camera	k_1	f_{c21}	-0.058743	579.123356	-0.073053	564.632476
	k_2	f_{c22}	0.092365	567.233876	0.079556	564.135606
	k_3	alpha_c_2	0.002133	0.000133	-0.019137	0.016851
	k_4	cc_{21}	-0.000653	411.345345	0.011664	406.753114
	k_5	cc_{22}	0.000026	286.271876	-0.018213	298.203234
Calibration error		AverageerrorX (mm)	0.114664		0.091065	
		AverageerrorY (mm)	0.096570		0.089456	
		AverageerrorZ (mm)	0.611689		0.539543	
Triangulation error		AverageerrorX (mm)	0.590186		0.602146	
		AverageerrorY (mm)	0.673654		0.657331	
		AverageerrorZ (mm)	1.996522		1.7833574	

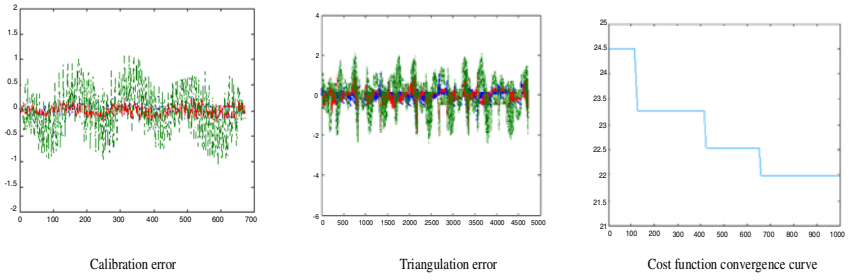

Fig. 1. Results of GA

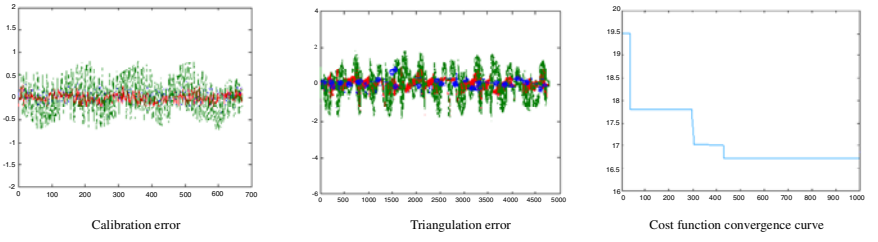

Fig. 2. Results of PSO

6 Conclusions

The goal of calibration is to do 3D measure and it is exciting to make the differences between practical results and true results to be as small as possible. With this hope, we take the sum of distance in the world coordinate between ground truth 3D points and calculated 3D points as cost function and calculate dual cameras' distortion coefficients and inner parameters at the same time. Furthermore, as the high accurate camera calibration is usually finished offline, the strategy proposed in this paper that optimizing parameters with PSO is feasible and can achieve more calibration accuracy than traditional optimal method. This attempt also extends the application field of PSO. Future work will focus on further improving the PSO by the proper selection of parameters and the design of different topologies. In addition, PSO applications in the image registration and image rectification will be investigated.

Acknowledgement

This work is supported by China Liaoning Province Educational Office fund (No.20080611), Shenzhen-Hong Kong Innovative Circle project (Grant No.SG200810220137A) and Project 801-000021 supported by SZU R/D Fund.

References

1. Tsai, R.Y.: A versatile camera calibration technique for high-accuracy 3D machine vision metrology using off-the-shelf TV cameras and lenses. IEEE Journal of Robotics and Automation, 323–344 (1987)

2. Weng, J., Cohen, P., Herniou, M.: Camera calibration with distortion models and accuracy evaluation. IEEE Transaction on Pattern Analysis and Machine Intelligence, 965–980 (1992)
3. Zhang, Z.: A flexible new technique for camera calibration. IEEE Transactions on Pattern Analysis and Machine Intelligence, 1330–1334 (2000)
4. Heikkilä, J., Silvén, O.: A Four-step Camera Calibration Procedure with Implicit Image Correction. In: Proceedings of IEEE Computer Vision and Pattern Recognition, pp. 1106–1112. IEEE Press, Puerto Rico (1997)
5. Zhou, C., Tan, D.L., Zhu, F.: A high-precision Calibration Method for Distorted Camera. In: Proceedings of IEEE International Conference on Intelligent Robots and Systems, pp. 2618–2623. IEEE Press, Sendai (2004)
6. Wang, C.H., Hong, T.P., Tseng, S.S.: Integrating Fuzzy Knowledge by Genetic Algorithms. IEEE Transactions on Evolutionary Computation, 138–149 (1998)
7. Ishibuchi, H., Nakashima, T., Murata, T.: Performance Evaluation of Fuzzy Classifier Systems for Multi Dimensional Pattern Classification Problems. IEEE Transactions on Systems, Man, and Cybernetics, 601–618 (1999)
8. Eberhart, R.C., Kennedy, J.: A New Optimizer Using Particle Swarm Theory. In: Proceedings of the Sixth International Symposium on Micro Machine and Human, pp. 39–43. IEEE Press, Nagoya (1995)
9. Niu, B., Li, L.: A novel PSO-DE-based hybrid algorithm for global optimization. In: Huang, D.-S., Wunsch II, D.C., Levine, D.S., Jo, K.-H. (eds.) ICIC 2008. LNCS (LNAI), vol. 5227, pp. 156–163. Springer, Heidelberg (2008)
10. Niu, B., Zhu, Y.L., He, X.X., Shen, H.: A Multi-swarm Optimizer Based Fuzzy Modeling Approach for Dynamic Systems Processing. Neurocomputing 71, 1436–1448 (2008)

EMD Based Power Spectral Pattern Analysis for Quasi-Brain-Death EEG

Qi-Wei Shi[1], Ju-Hong Yang[1], Jian-Ting Cao[1,3,4], Toshihisa Tanaka[2,3], Tomasz M. Rutkowski[3], Ru-Bin Wang[4], and Hui-Li Zhu[5]

[1] Saitama Institute of Technology
1690 Fusaiji, Fukaya-shi, Saitama 369-0293, Japan
[2] Tokyo University of Agriculture and Technology
2-24-16, Nakacho, Koganei-shi, Tokyo 184-8588, Japan
[3] Brain Science Institute, RIKEN
2-1 Hirosawa, Wako-shi, Saitama 351-0198, Japan
[4] East China University of Science and Technology
Meilong Road 130, Shanghai 200237, China
[5] Huadong Hospital Affiliated to Fudan University
221 Yanan West Rd, Shanghai 200040, China
cao@sit.ac.jp, zhuhuili@sh163b.sta.net.cn

Abstract. Evaluating the significance differences between the group of comatose patients and the group of brain death is important in the determination of brain death. This paper presents the power spectral pattern analysis for Quasi-Brain-Death EEG based on Empirical Mode Decomposition (EMD). We first decompose a single-channel recorded EEG data into a number of components with different frequencies. We then focus on the components which are related to the brain activities. Since the power of spontaneous activities in the brain is usually higher than that of non-activity components. Therefore, we can evaluate the power spectral patterns between comatose patients and quasi-brain-deaths. Our experimental results illustrate the effectiveness of proposed method.

Keywords: Electroencephalography (EEG), Quasi-Brain-Death, Empirical Mode Decomposition (EMD), Power Spectral Pattern.

1 Introduction

Brain death, briefly speaking, is defined as the absence and irreversibility of all brain and brain stem function [1]. Based on this definition, the medical criteria are established in the most countries [2]. For example, the Japanese criterion includes the following major items for brain death determination:

i. *Deep coma*: unresponsive to external visual, auditory and tactile stimuli and be incapable of communication.
ii. *Pupil test*: no pupils' response to light and pupils dilate to 4 mm.
iii. *Brain stem reflexes test*: e.g. gag reflex, cough reflex, corneal reflex, painful stimuli are absent.

D.-S. Huang et al. (Eds.): ICIC 2009, LNAI 5755, pp. 814–823, 2009.

iv. *Apnea test*: patient's loss of spontaneous respiration after disconnecting the ventilator.
v. *EEG confirmatory test*: persistence of brain dysfunction, six hours with a confirmatory EEG, flat EEG at level of 2 μV/mm.

The standard process of brain death diagnosis involves risky and time consuming items [3]. For example, in the apnea test, the respiratory machine is temporarily removed in order to determine the patient's spontaneous respiration. Moreover, in the EEG confirmatory test, the recordings should continue at least 30 minutes, and the test should be repeated again after 6 hours. To avoid the risks and develop a practical yet safe and reliable method in the diagnosis of brain death, the EEG-based preliminary examination has been proposed [4,5]. That is, after items i.–iii. have been verified, an EEG-based preliminary examination is to be applied at the bedside of patient.

Since EEG recordings might be corrupted by some artifacts or various sources of interfering noise, in the EEG preliminary examination system, it's critical to extract informative features from noisy EEG signals and evaluate their significance. To study statistical significance differences between the presence and absence of brain activities in our clinical EEG data, several complexity measures are developed for the quantitative EEG analysis [6]. To decompose brain activities with a specific frequency, the time-frequency EEG analysis technique based on empirical mode decomposition (EMD) has been proposed [7,8].

In this paper, we present an exploratory data analysis technique based on empirical mode decomposition method. The EMD method is used to decompose a single-channel recorded EEG data into a number of components with different frequency. Since the power of spontaneous activities in the brain is usually higher than that of non-activity components, we apply the power spectrum analysis technique to obtain the average maximum power of one thousand continuous samples of EEG data. The experimental results illustrate the proposed method is effective to extract the underlying data and show well performance on evaluating the differences between comatose patients and quasi-brain-deaths.

2 Empirical Mode Decomposition

The EMD is an analysis method that it adaptively decomposes any complicated data set into some oscillatory components called intrinsic mode function (IMF). The IMFs, usually expressed as the standard Hilbert transform, represent the oscillation modes embedded in the data. The local energy and the instantaneous frequency calculated from IMF components can be given a full energy-frequency-time distribution of the data. Thus, EMD can be seen as a unique spectral analysis technique.

For an observed time domain signal $x(t)$, we can always obtain its Hilbert transform $f(t)$, such as

$$f(t) = \frac{1}{\pi} P \int_{-\infty}^{\infty} \frac{x(\tau)}{t-\tau} d\tau. \tag{1}$$

It is impossible to calculate the Hilbert transform as an ordinary improper integral because of the pole at $\tau = t$. However, the P in front of the integral denotes the Cauchy principal value which expanding the class of functions for which the integral in Eq. (1) [9].

With this definition, $x(t)$ and $f(t)$ form the complex conjugate pair, so the complex signal $Z(t)$ can be formulated as

$$Z(t) = x(t) + jf(t) = a(t)e^{j\theta(t)}, \tag{2}$$

in which j is the imaginary unit ($j^2 = -1$), an instantaneous amplitude $a(t)$ and an instantaneous phase $\theta(t)$ are presented by

$$a(t) = \sqrt{x^2(t) + f^2(t)}, \tag{3}$$

$$\theta(t) = \tan^{-1}\left(\frac{f(t)}{x(t)}\right). \tag{4}$$

The instantaneous frequency $\omega(t)$ of the signal $x(t)$ can be defined as

$$\omega(t) = \frac{d\theta(t)}{dt}. \tag{5}$$

In principle, it is necessary that one limitation is a narrow band signal for the instantaneous frequency by Eq. (5).

An IMF component as a narrow band signal is a function that satisfies two conditions [9]:

a) In the whole data set, the number of extrema and the number of zero crossings must either equal or differ at most by one.
b) At any point, the mean value of the upper envelope with the lower envelope is zero. Here the upper envelope is defined by the local maxima, and the lower envelope is defined by the local minima.

The procedure to obtain the IMF components from an observed signal is called sifting and it consists of the following steps:

1. Identification of the extrema of an observed signal.
2. Generation of the waveform envelopes by connecting local maxima as the upper envelope, and connection of local minima as the lower envelope.
3. Computation of the local mean by averaging the upper and lower envelopes.
4. Subtraction of the mean from the data for a primitive value of IMF component.
5. Repetition above steps, until the first IMF component is obtained.
6. Designation the first IMF component from the data, so that the residue component is obtained.
7. Repetition above steps, the residue component contains information about longer periods which will be further resifted to find additional IMF components.

The sifting algorithm is applied to calculate the IMF components based on a criterion by limiting the size of the standard deviation (SD) computed from the two consecutive sifting results as

$$\mathrm{SD} = \sum_{t=0}^{T} \left[\frac{(h_{k-1}(t) - h_k(t))^2}{h_{k-1}^2(t)} \right]. \tag{6}$$

Based on the sifting procedure for one channel of the real-measured EEG data, we finally obtain

$$x(t) = \sum_{i=1}^{n} c_i(t) + r_n(t). \tag{7}$$

In Eq. (7), $c_i(t)(i = 1, \cdots, n)$ represents n IMF components, and r_n represents a residual component. The residual component can be either a mean trend or a constant.

3 EEG Preliminary Examination with EMD

3.1 EEG Signals and Brain Activity

The EEG preliminary examination was carried out in the Shanghai Huashan Hospital affiliated to Fudan University (China). A portable EEG system (NEUROSCAN ESI) was used to record the patient's brain activity. The EEG data was directly recorded at the bedside of the patients in the intensive care unit (ICU). In the examination, only nine electrodes are chosen to apply to patients. Among these electrodes, six exploring electrodes (F_{p1}, F_{p2}, F_3, F_4, F_7, F_8) as well as GND were placed on the forehead, and two electrodes (A_1, A_2) as the reference were placed on the earlobes (Fig. 1). The sampling rate of EEG was 1000 Hz and the resistances of the electrodes were set to less than 8 kΩ.

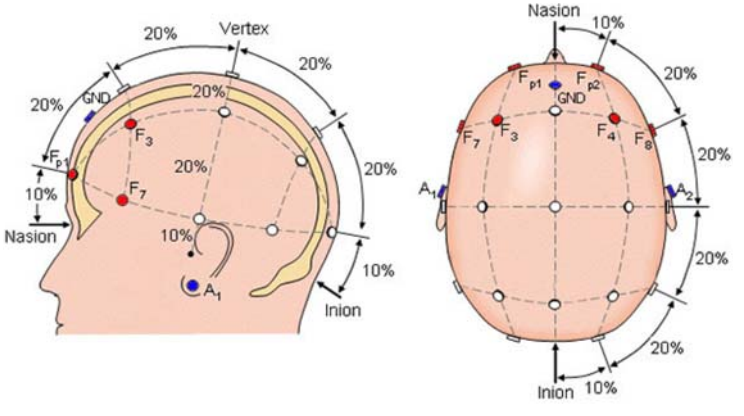

Fig. 1. The layout of six exploring electrodes, GND and two reference electrodes

A total of 35 coma and quasi-brain-death patients had been examined by using EEG from June 2004 to March 2006. The patients were classified into a deep-coma group (19 cases) and a quasi-brain-death group (17 cases) after medical diagnosis. One patient firstly showed being in the coma state and then behaved as quasi-brain-death. The total recording EEG data of these patients with an average signal length of 300 seconds were analyzed.

Expecting the brain activities of a comatose patient dominate in lower frequency bands, in our experimental analysis, we focus on the δ-wave (0.1–3 Hz), the θ-wave (4–7 Hz) and α-wave (8–13 Hz). Moreover, considering the power of activities in the brain is usually higher than that of non-activity components, we evaluate the power spectral when classifying coma and quasi-brain-death patient.

In the following, we will present two representative cases of coma and quasi-brain-death patients. Then, brain activities power distribution will be presented basing on the summary of all patients' EEG analysis results.

3.2 Patient A with Brain Activity

We first demonstrate our result by an example of a 17-year-old female patient (Patient A). The patient was suffered from encephalitis and was admitted to the hospital one month later. After two days' hospitalization, the clinical diagnosis showed that the patient was in a deep coma state since a very weak visual response appears in a few time. The EEG examination was taken in March, 2005 and lasted 314 seconds. As an example, a small time window of five seconds (78 $\sim$ 83 sec.) EGG signal is shown in Fig. 2(a).

From the EEG activity oscillates shown in Fig. 2(a), we paid attention to a randomly chosen channel. For instance, the sample of channel F4 from the beginning of 78 sec. is selected as an example. Applying the data analysis method described in Section 2 to the chosen data, we obtained the result shown in Fig. 2(b). In time domains, raw signal F4 was decomposed to five IMF components ($C_1 \sim C_5$) and a residual component (r). Then, in the right column, components are displayed in the frequency domain by applying the Fast Fourier Transform (FFT). Generally, component with such a high frequency like C_1 does not exist in brain and the residual component (r) is not related to brain activities.

As shown in Fig. 2(b), the right column gives the maximum value of each useful IMF component's power spectra in their frequency domain. Among the four components ($C_2 \sim C_5$), one with a frequency of 13 Hz and one with a frequency of 3 Hz can be seen clearly. Compared to others, their values of power separately go up to 2413.07 and 4199.57 that implied the high intensity of brain activities.

Then, we applied the same method to one thousand continuous samples of Channel F4 from 78 sec. (Fig. 3) and calculate each sample's maximum power among useful components. These 1000 samples' average power that the signal contained goes up to 3205.61. This data analysis result is identical to the clinical diagnosis that the patient was in coma state.

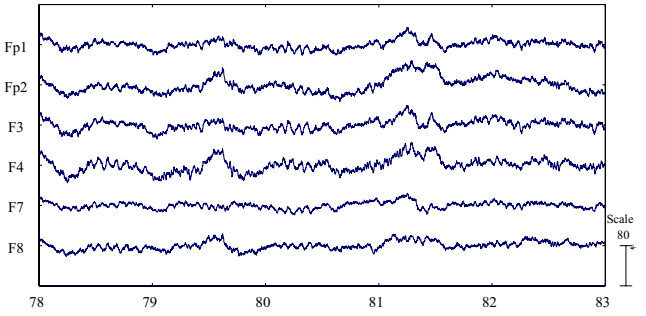

(a) A view of Patient A's recorded EEG data

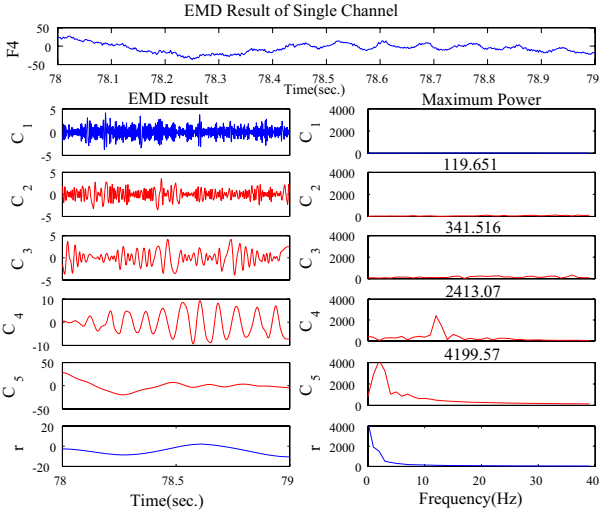

(b) EMD result for channel F4 in time and frequency domain

Fig. 2. EMD results for Patient A who has brain activity

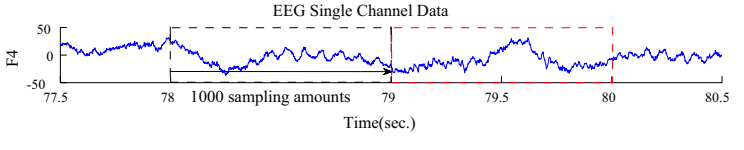

Fig. 3. 1000 sampling amounts of Channel F4 from 78 sec

3.3 Patient B without Brain Activity

In the second example, Patient B was a 56-year-old man who had a primary cerebral disease and was admitted to the hospital on October, 2005. One day

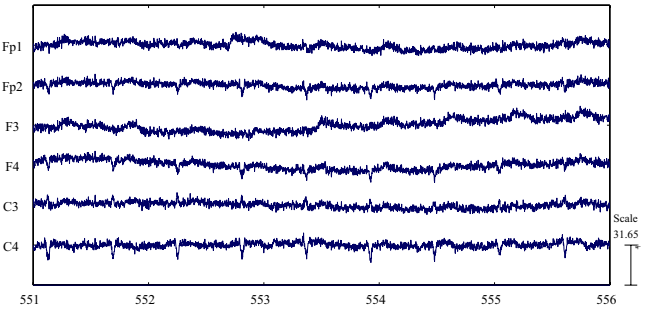

(a) A view of Patient B's recorded EEG data

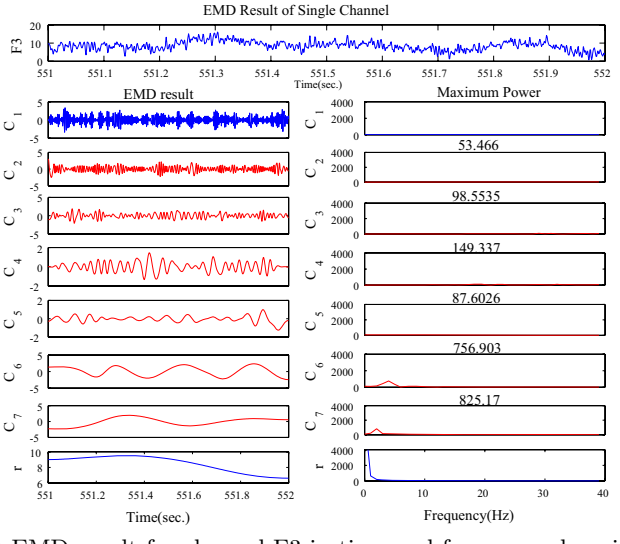

(b) EMD result for channel F3 in time and frequency domain

Fig. 4. EMD results for Patient B who has no brain activity

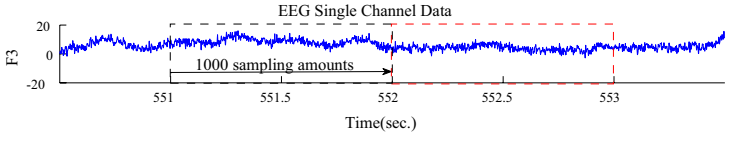

Fig. 5. 1000 sampling amounts of Channel F3 from 551 sec

later, the patient fell into a deep-coma state and his pupil dilated to 4 mm with no response to light. The EEG examination in the bedside of patient was taken for 1148 seconds. As an example, a window of five seconds (551 $\sim$ 556 sec.) EEG signals is plotted in Fig. 4(a). Applying the EMD method to the randomly

Table 1. The average value of power spectral patterns of comatose patients($C_1 \sim C_{19}$) and quasi-brain-deaths($D_{13} \sim D_{35}$)

Case No.	EEG Channel	Average Value of Power Spectrum	Case No.	Average Value of Power Spectrum
C_1	Fp2	3857.95	D_{13}	177.04
C_2	Fp2	2393.03	D_{20}	704.38
C_3	F3	3012.26	D_{21}	735.82
C_4	F4	1054.8	D_{22}	676.25
C_5	F4	3527.5	D_{23}	474.9
C_6	F4	7638.7	D_{24}	391.06
C_7	Fp2	2026.98	D_{25}	645.02
C_8	F4	3205.61	D_{26}	967.23
C_9	Fp2	6545.59	D_{27}	469.21
C_{10}	Fp1	2762.4	D_{28}	221.25
C_{11}	F8	2287.33	D_{29}	520.44
C_{12}	F8	4497.08	D_{30}	544.5
C_{13}	F3	3415.46	D_{31}	338.81
C_{14}	F3	3226.73	D_{32}	414.89
C_{15}	F8	3399.63	D_{33}	528.67
C_{16}	F3	3813.66	D_{34}	247.36
C_{17}	F3	5773.31	D_{35}	228.87
C_{18}	F8	4061.89		
C_{19}	F7	1885		

selected channel F3, for example, we obtained the EMD result of seven IMF components ($C_1 \sim C_7$) and one residual component (r) shown in Fig. 4(b).

Desirable components ($C_2 \sim C_7$) were transformed into frequency domain by Fourier Transform. The y-coordinate of the right column in Fig. 4(b) is in the same scope as the one of Fig. 3(b), however, the amplitudes of IMF components were all in a low range.

Same as Patient A mentioned before, EMD method was applied to one thousand continuous samples of Patient B's EEG signal (Fig. 5) and the average maximum value of IMFs' in the power spectra is only 544.5. Comparing to the result of Patient A, the average power implied the brain activity of Patient B can hardly be obtained. Without loss of generality, we applied the same process to other channels but only similar results were obtained. The standard clinical criteria also concluded the patient in brain-death.

3.4 Evaluation of All Patients' EEG Power Spectrum

The EMD method we proposed has been applied to the 35 quasi-brain-death patients. Distinct from the previous method which just focused on the maximum power of EEG data at one point [10], in this paper, we gave the average power of EEG signal in a period of time.

The evaluation of all cases are shown in Table 1. Obviously, the average value of brain activities in power spectral pattern of coma cases ($C_1 \sim C_{19}$) are rel-

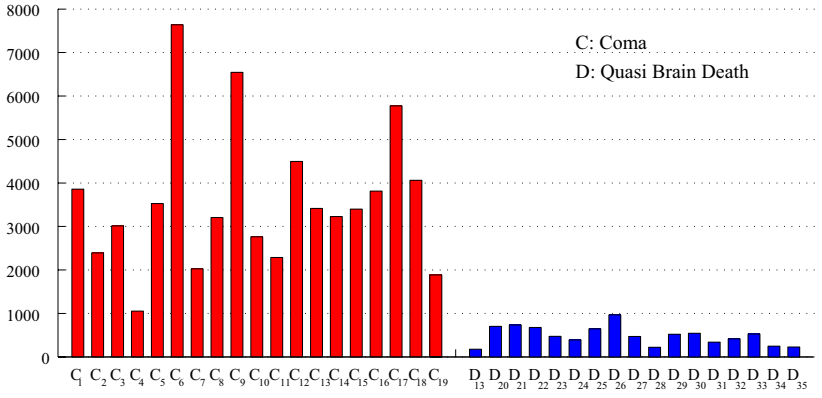

Fig. 6. The brain activities' power distribution of coma and brain death patients

atively higher than that of quasi-brain-death cases ($D_{13} \sim D_{35}$). As shown in Fig. 6, the experimental results provid the statistical evaluation of the average power of all patients' brain activities in a period of time. More specifically, in coma group, the lowest value of brain activities in spectral pattern (C_4: 1054.8) of coma cases is even larger than the highest value (D_{26}: 967.23) in the group of quasi brain death.

The results obtained in our paper have been compared to those by principal factor analysis (PFA) associated ICA [4] or complexity measures for the quantitative EEG analysis [6]. In classifying the group of come and quasi brain death cases, we could obtain the same results based on our proposed method.

4 Conclusion

In this paper, we proposed a practical EEG-based preliminary examination in the process of clinical diagnosis for brain death. The analysis method EMD was applied randomly on a channel of raw EEG signal. The amount of 1000 samples were analyzed and the average maximum value of power spectral pattern reflected the intensity of brain activities. The average power value demonstrated the high intensity of spontaneous brain activities among the 19 coma cases, as well as the absence of those among 17 quasi-brain-deaths excepted some noise. Moreover, we found the results of EMD method corresponding to the clinical diagnosis.

Since the EMD method showed its effectiveness and reliability, we expect to proposed more detail about statistical evidence in evaluating the power spectral patterns between comatose patients and quasi-brain-deaths. In the near future, we wish to apply this method to real-time measured data. Also, the diagnosis of brain death is expected to be more precise.

Acknowledgments

The authors would like to acknowledge Dr. GuoXian Zhu and Dr. Yue Zhang of Shanghai Huashan Hospital and Prof. Yang Cao and Prof. Fanji Gu of Fudan University for assistance in the EEG examinations and useful comments. This work was supported in part by KAKENHI (21360179).

References

1. Taylor, R.M.: Reexamining the Definition and Criteria of Death. Seminars in Neurology 17, 265–270 (1997)
2. Wijdicks, E.: Brain Death Worldwide: Accepted Fact but no Global Consensus in Diagnostic Criteria. Neurology 58, 20–25 (2002)
3. Marks, S., Zisfein, J.: Apneic Oxygenation in Apnea Tests for Brain Death: A Controlled Trial. Neurology 47, 300–303 (1990)
4. Cao, J.: Analysis of the quasi-brain-death EEG data based on a robust ICA approach. In: Gabrys, B., Howlett, R.J., Jain, L.C. (eds.) KES 2006. LNCS (LNAI), vol. 4253, pp. 1240–1247. Springer, Heidelberg (2006)
5. Cao, J., Chen, Z.: Advanced EEG Signal Processing in Brain Death Diagnosis. Signal Processing Techniques for Knowledge Extraction and Information Fusion, 275–298 (2008)
6. Chen, Z., Cao, J., Cao, Y., Zhang, Y., Gu, F., Zhu, G., Hong, Z., Wang, B., Cichocki, A.: An Empirical EEG Analysis in Brain Death Diagnosis for Adults. Cognitive Neurodynamics 2, 257–271 (2008)
7. Li, L., Saito, Y., Looney, D., Cao, J., Tanaka, T., Mandic, D.P.: Data Fusion via Fission for the Analysis of Brain Death. Evolving Intelligent Systems: Methodology and Applications, 279–320 (2008)
8. Saito, Y., Tanaka, T., Cao, J., Mandic, D.: Quasi-Brain-Death EEG Data Analysis by Empirical Mode Decomposition. Advances in Cognitive Neurodynamics, 837–842 (2007)
9. Huang, N.E., Shen, Z., Long, S.R., Wu, M.C., Shih, H.H., Zheng, Q., Yen, N.-C., Tung, C.C., Liu, H.H.: The Empirical Mode Decomposition and the Hilbert Spectrum for Nonlinear and Non-stationary Time Series Analysis. In: Proceedings of the Royal Society of London, vol. A 454, pp. 903–995 (1998)
10. Shi, Q., Yang, J., Cao, J., Tanaka, T., Wang, R., Zhu, H.: EEG Data Analysis Based on EMD for Coma and Quasi-Brain-Death Patients. Journal of Experimental & Theoretical Artificial Intelligence (in print, 2009)

Proposal of Ride Comfort Evaluation Method Using the EEG

Hironobu Fukai[1], Yohei Tomita[1], Yasue Mitsukura[1],
Hirokazu Watai[2], Katsumi Tashiro[2], and Kazutomo Murakami[2]

[1]Graduate School of Bio-Applications & Systems Engineering,
Tokyo University of Agriculture and Technology,
2-24-16, Naka-cho, Koganei, Tokyo, 184-8588, Japan
[2]Bridgestone Corporation,
3-1-1, Ogawahigashi, Kodaira, Tokyo, 187-8531, Japan
50007701291@st.tuat.ac.jp,
50008401213@st.tuat.ac.jp,
mitsu_e@cc.tuat.ac.jp,
muraka-k@bridgestone.co.jp

Abstract. In this study, we propose the ride comfort evaluation method by using the electroencephalography (EEG). Recently, the subjective evaluation method that is questionnaire survey etc. is used for introducing the human sensibility. However, it is not established because of the difficulty of obtaining the human sensibility. Moreover, the objective evaluation method is hoped because the subjective evaluation method has ambiguous criterion by individual, and difference of sensitivity. Therefore, we propose the evaluation method by using the EEG that objective evaluation is possible. In this study, we investigate a ride comfort of car driving. We use the general car and we investigate the ride comfort according to the difference of the tire. The EEG is measured in driving condition. Moreover, the ride comfort subjective evaluation is surveyed by semantic differential method (SD method). The feature of the EEG during the driving and feature of the subjective evaluation is extracted by the factor analysis (FA). From the result, the EEG feature and subjective evaluation feature has correlation. Thus, the effectiveness of the proposed method as an objective evaluation method was shown.

Keywords: electroencephalogram (EEG); factor analysis (FA); semantic differential method (SD method).

1 Introduction

Recently, many products and services for the people are supplied in the world. As a result, life consciousness of people is improved. Therefore, to give people the satisfaction, it is requested for innovative technology that to clarify a higher-order reaction of the sensibility and to take it to the product. Thus, the sensibility which people have originally is researched [1],[2]. Most of these researches are evaluated by questionnaire etc. that is subjective. However, the objective

D.-S. Huang et al. (Eds.): ICIC 2009, LNAI 5755, pp. 824–833, 2009.

evaluation method is hoped because the subjective evaluation method has ambiguous criterion and difference of sensitivity among each individual. Therefore, we propose the evaluation method by using the EEG that objective evaluation is possible. For the experiment, ride comfort is evaluated by using the car that is a familiar vehicle.

Ride comfort is a psychological reaction that the environment in the car gives, and the overall sense caused by the driving of the vehicle. When we consider the ride comfort, many factors including a temperature, besides sitting feelings of the vibration, the noise, the chair, humidity, feeling of quality, a smell, a lighting, an atmospheric pressure variation, and the indoor design, etc. influence the human sensibility. Therefore, present ride comfort evaluation is decided subjectively by the professional test driver. The test driver is an expert driver, and it is necessary and indispensable for the evaluation of the driving performance. However, general drivers has own preference. Thus, they have various evaluations of the preference. Therefore, for improvement of general driver's ride comfort that has various preference, not only professional driver but also general driver's evaluation is requested. However, it is difficult to evaluate a quantitative ride comfort. Then, the ride comfort research is researched physically.

In the ride comfort, inspection of evaluation including the characteristic of the human vibrational sensibility is widely researched [3]. General evaluation criterion by vibration is defined as the acceleration that is the vertical vibration etc. by specification of International Organization for Standardization (ISO). Human's vibration sensibility receiving characteristic is known to be sensitive to the bandwidth of the vertical vibration of 4-8Hz and the horizontal vibration of 1-2Hz well. Takei and Ishiguro proposed the ride comfort evaluation equation by doing the sensory evaluation and the vibration measurement that is a regular vibration and a transitional vibration in rough road driving [4]. Inagaki *et al.* proposed the ride comfort evaluation equation by doing the sensory evaluation and the vibration measurement that is a regular vibration and a transitional vibration in rough road driving [5]. Moreover, the evaluation to the load noise generated when driving in the car is done. Ishii *et al.* reported that the sample sound was evaluated by using the EEG including the load noise, and the regression to the sound that became comfortable was obtained [6]. Thus, the ride comfort is obtained from not only influence from a specific sensibility but also influence from several sensibilities though the research on the quantification of ride comfort is advanced. Therefore, the overall ride comfort is evaluated by actually measuring subject's EEG under driving.

In this study, we investigate the ride comfort according to the difference of the tire by using the EEG obtained from single channel EEG instrument.

2 The Procedure of the Proposed Method

The procedure of the proposed method is shown in followings.

1. The EEG signal measurement in moving car
2. Questionnaire survey

3. Feature extraction by factor analysis
4. Factor score plotting in two dimensions
5. Comparison of the EEG feature and the questionnaire result

First of all, when evaluating the ride comfort, we experiment with seven kinds of roads with three kinds of tires, and record the EEG that can be acquired in these cases. Secondly, we survey the psychological state by questionnaire. In this survey, we use the SD method.

In the acquired EEG, we use 4-22 Hz. Generally, it is said that sensibility will appear to 4-22 Hz in the conventional method[7]. Therefore, we used these frequency bandwidth.

Next, we construct the data matrix by using the obtained EEG and questionnaire result for factor analysis, respectively. In the EEG, we decide the frequency and the frequency spectrum average of each experiment as a variate and an individual.For the purpose of extracting of the psychological state, we decide the adjective and the adjective rate as a variate and an individual.

Then, we extract the features by the factor analysis. Where, principal factor method is used as factor loading, varimax rotation is adopted as factor rotation, and least-squares estimation is applied as the factor score estimation.

Furthermore, in order to make the EEG factor analysis result easy to see, factor score is plotted in two dimensions.

Finally, in order to show the effectiveness of proposed EEG feature extraction method, we compare the objective evaluation which EEG feature with subjective evaluation by the SD method feature. If these results are similarly, it is considered that the EEG extract the ride comfort is extracted by using the EEG.

2.1 The Simple Electroencephalograph

In this study, the simple electroencephalograph of the band type is used. This electroencephalograph is made by Brain Function Research & Development Center in Japan. Fig. 1 shows this electroencephalograph.

The conventional electroencephalograph is expensive, large, and impossible to measure under in a natural environment. Therefore, the subjects are strained.

Fig. 1. Simple electroencephalogram

Table 1. Pair of adjectives

Pair of adjectives	
Noiseless	Noisy
Pleasant	Unpleasant
Steady	Unsteady
Soft	Hard
Likable	Unlikable
Harsh	Gentle
Fast	Slow
Good	Bad

This electroencephalograph is compactly made as 120mm (W), 135mm (D), and 35mm (H) and can be measured under the practical environment. Therefore, it's less burdensome on subjects. The electrode is fixed to the headband. The measurement position is electrode arrangement Fp1 in international 10-20 system. We can obtain the discrete time data that the EEG of one second is analyzed frequency to 24Hz at 1Hz interval. The bandpass filter from 4Hz to 22Hz is used for this simple electroencephalograph. Therefore, we use the time series data of each frequency components between 4 and 22Hz.

2.2 SD Method

There is a multidimensional scale as a method of multiple evaluation. Moreover, the SD method is often used in a multidimensional scale. SD method is a type of a rating scale and measuring the connotative meaning of concepts. In sensory evaluation, it is important to measure the connotative meaning of concepts. SD method rates the impression by multiple rating scales constructed by the pair of various adjectives.

In this study, we use SD method as a psychological measurement. Subject evaluate by 5 stages of 8 pairs of adjectives. We use the pairs of adjectives in the Table1.

In these pair of adjectives, we select pair of adjectives based on questionnaire survey that consider as riding comfort from frequently-used pair of adjectives that is obtained by inoue [8]. In the proposed experiment, subjects write in the psychological state at the questionnaire paper during the car stopped between the road and road.

2.3 Factor Analysis

The factor analysis is used for the feature extraction of the EEG and the questionnaire survey. The factor analysis is a statistical method to explain the correlation between multivariate by small number of latent factors. The FA is modeled by equition (1).

$$X = AF + E \tag{1}$$

X is original signal. A indicates factor loading matrix. F means common factor. E is error. The feature data is extracted by the following methods.

- Step1 The data matrix is normalized.
- Step2 The correlation matrix (R) is calculated from the data matrix.
- Step3 Commonality (h^2) is substituted for diagonal component of the correlation matrix. Squared multiple correlation coefficient is used as an estimate of commonality, and calculated following equations.

$$R_{i,j} = \begin{bmatrix} h_{11}^2 & r_{12} & \cdots & r_{1n} \\ r_{21} & h_{22}^2 & \cdots & r_{2n} \\ \vdots & \vdots & \ddots & \vdots \\ r_{n1} & r_{n2} & \cdots & h_{nn}^2 \end{bmatrix} \tag{2}$$

  Inverse matrix of $R = (r_{ij})$ is defined as $R^{-1} = (r^{ij})$ Square of multiple correlation coefficient is utilized in the estimation of commonality. Hence, equation (3) is used for estimation of commonality.

$$h_{ij}^2 = 1 - \frac{1}{r^{ij}} \tag{3}$$

- Step4 The obtained correlation matrix is peculiarly resolved and the factor is extracted. The principal factor method is used for the factor extraction.

$$A = \begin{bmatrix} a_{11} & a_{12} & \cdots & a_{1m} \\ a_{21} & a_{22} & \cdots & a_{2m} \\ \vdots & \vdots & \ddots & \vdots \\ a_{m1} & a_{m2} & \cdots & a_{mm} \end{bmatrix} \tag{4}$$

  Factor loadings are calculated by computing eigenvalue or eigenvector that meet following equation:

$$RQ = Q\lambda \tag{5}$$

  Therefore, it is eigenvalue problem for correlation matrix. Then, factor loadings of principal factor analysis are calculated following equation:

$$A = Q\lambda^{1/2} \tag{6}$$

- Step5 Varimax rotation is done.
- Step6 The factor score is calculated by using least-squares estimation.

The factor score multiplies by itself.

3 Ride Comfort Evaluation Experiment

In order to show the effectiveness of the proposed method, we experiment and analyze the data. 3 times for 2 days experiments are performed in the Bridgestone

Proving Ground. The EEG is measured in a real car driver's seat and passenger's seat under driving. We use 2 professional drivers and five passengers as the subjects, and 3 kind of tires are used in this experiment. There are seven kinds of roads (smooth road, rough road, undulated road, bank1, bank2, track-groove road, uneven road), and it takes 12 minutes for driving around the Bridgestone Proving Ground.

Moreover, the same vehicle is used for all experiments. On the way, the psychological state is surveyed by SD method during the car stopped between the road and road.

4 Experimental Results and Discussions

We illustrate the effectiveness of the proposed method, we show the experimental results.

4.1 Analysis of the EEG

The EEG data which obtained from the all experiment are arranged as data matrix. Data is arranged according to the procedure mentioned above. We analyze the EEG to each subject because EEG include the characteristic of the individual. Fig.2 shows the result according to measured day. Where, x-axis indicates the 1st-order factor and y-axis means the 2nd-order factor.

Firstly, we verify the influence of difference by measurement day. In Fig. 2 (a), it is confirmed that data distribution of September 2nd is different from other day. It is considered that influence of physical condition appear in subject D compared with the subject P because subject D has task of driving. Thus, the data of September 2nd is considered as caused by the physical condition change. Moreover, in September 1st, we interrupted the measurement because raining. After that, we resumed the measurement because the rain stops. However, the road condition was different. The difference of the distribution of D2 is considered influence of weather. In Fig. 2 (b), it is difference in July data and September data. The measurement condition including weather, temperature, and so on is huge different between in July and September. Thus, this difference is considered to concern the EEG.

Next, when the schedule was different, it turned out that how to feel the person changed as a result. From these results, if the day changed, it turned out that the data was not effective though the tire was able to be distinguished by using EEG. It is considered that this is because how to feel person has changed by the physical condition etc. every day. Therefore, we compare the difference of the tire by using data of September 2nd. Fig. 3 shows the distribution of factor score of each tire on September 2nd. A,B, and C denote the kind of different tire, respectively. Furthermore, R0 means static state. Fig.3(a) shows the distribution difference on tire A and tire B, and Fig.3(b) indicates the distribution difference of tire B. The difference of these distribution is considered as the difference of ride comfort.

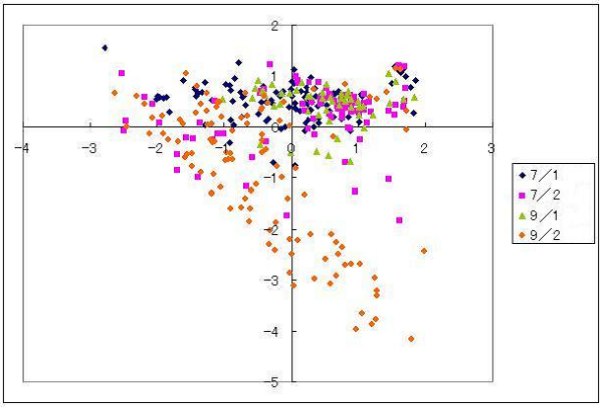

(a) D2

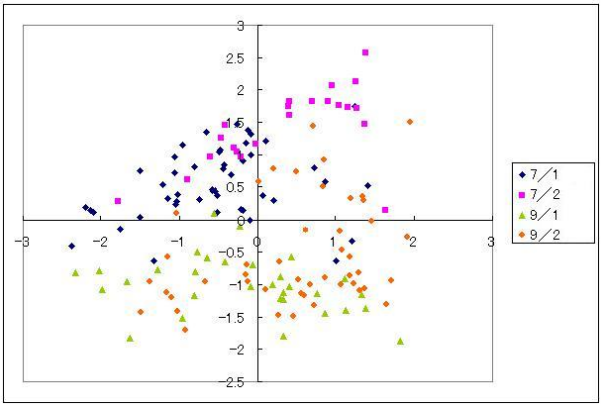

(b) P2

Fig. 2. Distribution of factor score (each measurement day)

4.2 Analysis of the Subjective Evaluation

We construe the factor of adjective pairs to subject D and P, respectively. We pay attention to the factor loadings that absolute value is over 0.4. Table 2 shows the factor loadings.

Showing the Table 2, 1st-order factor having maximum eigenvalue means emotional adjective, 2nd-order factor is construed as a physical value. Moreover, the sensitive factor is selected for subject D in 3rd-order factor. On the other hand, the sensory factor and the sensitive factor are selected for subject P. According to these results, the emotional factor is extracted firstly because content of the questionnaire is survey of the mental change of tire and road impression. In the secondly, the physical factor is extracted.

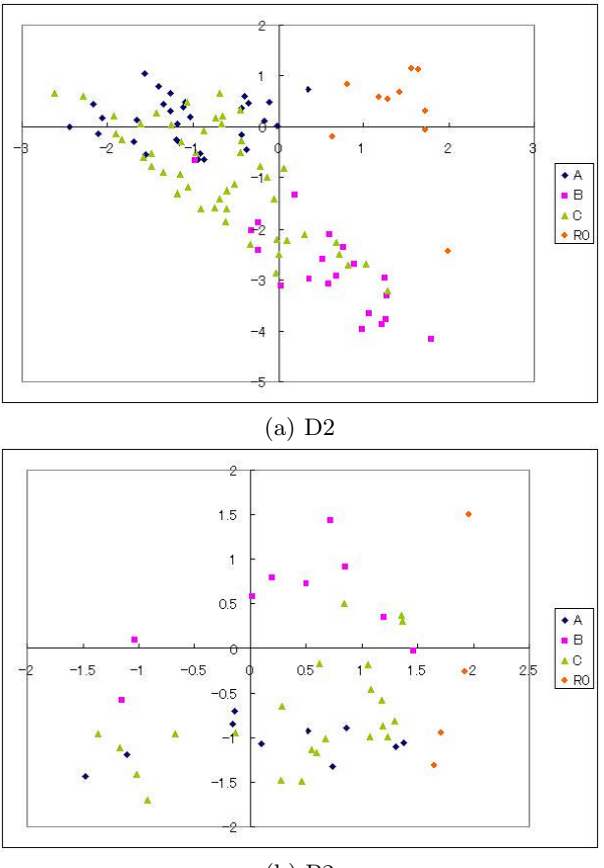

(a) D2

(b) P2

Fig. 3. Distribution of factor score (each tire [9/2])

4.3 Feature Comparison

In the EEG analysis, the features were different in each tire. Moreover, in subjective evaluation, the meaning of factor was construed. The subjective evaluation results of each tire indicate in Table 3.

The sensitive factor and emotional factor has the difference tire A and tire B is shown in subject D2. The tire A and B is shown in the separated area (Fig. 3 (a)). From this result, the relationship of the EEG feature and the subjective evaluation feature is indicated. The sensitive factor and emotional factor difference of tire B and tire C is shown in subject P2. From EEG analyze result, only tire B is shown in another area (Fig. 3 (b)). Relativity of the tire A was not able to be confirmed though the relativity of the EEG feature and the subjective evaluation feature was confirmed about tire B and tire C. Because it is considered that the subjectivity evaluation factor doesn't correspond to the EEG factor by the one to one but for multiple component to mix it.

Table 2. Factor loadings

	1st-order factor	2nd-order factor	3rd-order factor
Variate	Subject D		
	Subject D		
Variate	1st-order factor	2nd-order factor	3rd-order factor
Noiseless—Noisy	-0.111	-0.092	-0.517
Pleasant—Unpleasant	-0.559	-0.299	-0.467
Steady—Unsteady	-0.669	-0.292	-0.094
Soft—Hard	0.010	-0.533	-0.268
Likable—Unlikable	-0.724	-0.005	-0.194
Harsh—Gentle	0.216	0.598	0.003
Fast—Slow	-0.240	-0.016	-0.002
Good—Bad	-0.609	-0.201	-0.327
	Subject P		
Variate	1st-order factor	2nd-order factor	3rd-order factor
Noiseless—Noisy	0.317	0.606	-0.177
Pleasant—Unpleasant	0.608	0.369	-0.110
Steady—Unsteady	0.408	0.502	-0.438
Soft—Hard	0.020	0.499	-0.112
Likable—Unlikable	0.798	0.018	-0.125
Harsh—Gentle	-0.068	-0.430	0.610
Fast—Slow	-0.017	-0.068	0.523
Good—Bad	0.727	0.131	0.050

Table 3. Subjective evaluation result of each tire

	D2		
Tire	Emotion	Physical value	Sensibility
A	-0.555	-0.420	1.856
B	1.017	-1.010	-0.883
C	-1.228	0.670	0.832
	P2		
Tire	Emotion	Physical value	Sensibility
A	0.675	-0.244	-0.167
B	0.397	-0.207	0.077
C	0.896	-0.429	0.474

5 Conclusions

In this study, we proposed ride comfort evaluation method by using the EEG.

For the purpose of verifying the effectiveness of the proposed method, we analyze the real EEG of the subject in a real car driver's seat and passenger's seat under driving. The factor analysis was used as a method of extracting the feature of the EEG and SD method. In addition, to make analytical data easy to

see, it made it to visible. Moreover, the effectiveness of the EEG measurement was verified by the comparison with the subjectivity evaluation. The EEG feature and the psychological state feature indicated the correlation.

The future works are as following.

1. Rotation of factor score that considers tension level
2. EEG pattern classification
3. The trend review of the analysis result and the other biological information.
4. Semantic analysis of the EEG feature factor.

References

1. Kitajima, M., Utsugi, A.: On the Measurement of Kansei-Two Approaches to Model Sense, Feeling, Emotion, or Sensitivity. The Journal of the IEICE 76(3), 242–245 (1993)
2. Inokuchi, S.: Kansei Information Processing. The Journal of the IEICE 80(10), 1007–1012 (1997)
3. Shiiba, T., Suda, Y.: Ride Comfort Evaluation of Automobile with Driving Simulator:An Approach by Driving Simulator with Multibody Vehicle Model. The Journal of the JSME 68(670), 119–124 (2002)
4. Takei, K., Ishiguro, M.: Evaluation of Ride Comfort on the Basis of Subjective Judgement. R&D Review of Toyota CRDL 30(3), 47–56 (1995)
5. Inagaki, H., Taguchi, T., Yasuda, E., Doi, S.: Evaluation of Seat Kansei Quality. R&D Review of Toyota CRDL 35(4), 9–14 (2000)
6. Ishii, Y., Yamashita, T., Araga, Y.: Sensory Evaluation of Road Noise with Organic Reaction using Brain Waves. Honda R&D Technical Review 14(2), 181–188 (2002)
7. Ito, S., Mitsukura, Y., Fukumi, M., Akamatsu, N.: Proposal of the EEG Analysis Method using the Individual Characteristic of the EEG. T.IEE Japan 124-C(64), 1259–1266 (2004)
8. Inoue, M., Kobayashi, T.: The Research Domain and Scale Construction of Adjective-Pairs in a Semantic Differential Method in Japan. Jap. J. of Educ. Psychol. 33(3), 253–260 (1985)

Image Reconstruction Using NMF with Sparse Constraints Based on Kurtosis Measurement Criterion

Li Shang[1,2], Jinfeng Zhang[2], Wenjun Huai[2], Jie Chen[2], and Jixiang Du[3,4,5]

[1] JiangSu Province Support Software Engineering R&D Center for Modern Information Technology Application in Enterprise, Suzhou 215104, Jiangsu, China
[2] Department of Electronic Information Engineering, Suzhou Vocational University, Suzhou 215104, Jiangsu, China
[3] Department of Computer Science and Technology, Huaqiao University, Quanzhou 362021, Fujian, China
[4] Department of Automation, University of Science and Technology of China, Hefei 230026, Anhui, China
[5] Institute of Intelligent Machines, Chinese Academy of Sciences, Hefei 230031, Anhui, China
{sl0930,zjifeng,hwj,cj}@jssvc.edu.cn, jx_du@iim.ac.cn

Abstract. A novel image reconstruction method using non-negative matrix factorization (NMF) with sparse constraints based on the kurtosis measurement is proposed by us. This NMF algorithm with sparse constraints exploited the Kurtosis as the maximizing sparse measure criterion of feature coefficients. The experimental results show that the natural images' feature basis vectors can be successfully extracted by using our algorithm. Furthermore, compared with the standard NMF method, the simulation results show that our algorithm is indeed efficient and effective in performing image reconstruction task.

Keywords: NMF; Sparse constraints; Kurtosis; Image reconstruction.

1 Introduction

Non-negative matrix factorization (NMF) algorithm is a very efficient parameter-free method for decomposing multivariate data into strictly positive activations and basis vectors[1-4]. NMF usually produces a sparse linear representation of the data, but this representation does not always result in a parts-based one. Because sparse coding has also on theoretical grounds been shown to be a useful middle ground between completely distributed representations and unary representations, P. Hoyer[2] incorporated the notion of sparseness with NMF to improve the found decompositions. This sparse NMF method[2] can discover parts-based representations that are qualitatively better than those given by basis NMF[3-4] , and Hoyer has proved that his algorithm is successful in extracting face image features. However, in Hoyer's algorithm, the sparse measure is defined by the relationship between L_1 norm and L_2 norm[2], and the desired sparseness is set by the users rather than the data of feature basis vectors or features coefficients. Thus, the sparseness measure is not self-adaptive to natural

D.-S. Huang et al. (Eds.): ICIC 2009, LNAI 5755, pp. 834–840, 2009.

images. To remove or avoid the disadvantages mentioned above, in this paper, we propose a modified NMF with sparse constraints algorithm, which exploits the Kurtosis as the maximizing sparse measure criterion[5], so the natural image structure captured by the Kurtosis not only is surely sparse, but also is surely independent[6-8]. The experimental results also showed that utilizing our sparse NMF algorithm, the natural images' features can be extracted successfully. Further, applied these features, the original images can be reconstructed clearly.

2 The NMF with Kurtosis Based Sparse Constraints

2.1 The Cost Functions

Referring to the classical NMF algorithm[3], and combining the minimum image reconstruction error with Kurtosis measure of feature coefficients, we construct the following cost function of the minimization problem:

$$F(\mathrm{W},\mathrm{H}) = \frac{1}{2}\sum_{i}\left[\mathrm{V}_i(x,y) - \sum_{j=1}^{M}\mathrm{H}_{ij}(x,y)\mathrm{W}_j\right]^2 - \lambda\sum_{ij}\left|kurt\left(\mathrm{H}_{ij}\right)\right|, \tag{1}$$

where the matrices of V, W and H are all non-negative. Parameter λ is also positive constant. W is a $N\times M$ matrix containing the basis vectors W_j as its columns. V is a $N\times L$ matrix, which denotes the n-dimensional input image data. Thus, H is a $M\times L$ matrix. V_i and W_j are the columns of V and W, respectively, and H_{ij} is the activities used for the encoding of the data. Here, the index i in V_i accounts for the *ith* input, whereas the index j accounts for the *jth* basis vector W_j used for the image reconstruction. This means that ezch data vector V_i is approximated by the linear combination of the basis vectors W_j and their activities H_{ij}. In Eqn. (1), the first term is the image reconstruction error and it ensures a good representation for a given image, and the second term is the sparseness measure based on the absolute value of Kurtosis, also named sparsity penalty term, which is defined as:

$$\left|kurt\left(\mathrm{h}_i\right)\right| = \left|E\left\{\mathrm{h}_i^4\right\} - 3\left(E\left\{\mathrm{h}_i^2\right\}\right)^2\right|. \tag{2}$$

and maximizing $\left|kurt\left(\mathrm{h}_i\right)\right|$ (i.e., minimizing $-\left|kurt\left(\mathrm{h}_i\right)\right|$) is equivalent to maximizing the sparseness of coefficient vectors; The last term, a fixed variance term, can penalize the case in which the coefficient variance of the *ith* vector $\left\langle \mathrm{h}_i^2 \right\rangle$ deviates from its target value σ_t^2. Without this term, the variance becomes so small that the sparseness constraint can only be satisfied, and the image reconstruction error would become larger, which is not desirable either.

In Eqn. (1), to avoid the scaling misbehavior, usually a normalization step for the basis vectors is incorporated when minimizing Eqn. (1). Then, the Eqn.(1) can be rewritten as follows:

$$F(\mathrm{W},\mathrm{H}) = \frac{1}{2}\sum_i \left[\mathrm{V}_i(x,y) - \sum_{j=1}^{M} \mathrm{H}_{ij}(x,y) \frac{\mathrm{W}_j}{\left\|\mathrm{W}_j\right\|_2} \right]^2 - \lambda_1 \sum_{ij} \left| kurt\left(\mathrm{H}_{ij}\right) \right|. \tag{3}$$

Now we are looking at a cost function which effectively depends on variables $F\left(\left\{\bar{\mathrm{W}}_j\right\}_j, \mathrm{H}\right)$, with $\bar{\mathrm{W}}_j$ being the normalized basis vectors $\bar{\mathrm{W}}_j = \mathrm{W}_j / \left\|\mathrm{W}_j\right\|_2$.

2.2 Learning Rules

It should be noted that before updating the basis function and coefficient weights, the observed data X has been centered and whitened. Similarly to the quotients of standard NMF, we can reformulate the fixed point conditions or the cost function (1) into multiplicative update rules [2], the general steps are shown as follows:

Step 1. Calculate and store $\nabla \mathrm{W} \left\|\mathrm{W}_j\right\|_2$;

Step 2. Normalize the basis vectors W_j: $\mathrm{W}_j \leftarrow \mathrm{W}_j / \left\|\mathrm{W}_j\right\|_2$;

Step 3. Calculate the reconstruction according to the following equation:

$$\mathrm{R}_i = \sum_j \mathrm{H}_{ij} \bar{\mathrm{W}}_j. \tag{4}$$

Step 4. Update the activities according to

$$\mathrm{H}_{ij} \leftarrow \mathrm{H}_{ij} \odot \frac{\mathrm{V}_i^T \bar{\mathrm{W}}_j}{\mathrm{R}_i^T \bar{\mathrm{W}}_j + \lambda g'\left(\mathrm{H}_{ij}\right)}. \tag{5}$$

where $g'\left(\mathrm{H}_{ij}\right)$ is calculated as follows:

$$g'(\mathrm{H}_{ij}) = \frac{\partial \left| kurt(\mathrm{H}_{ij}) \right|}{\partial \mathrm{H}_{ij}} = \beta \left[\left\langle \mathrm{H}_{ij}^3 \right\rangle - 3 \left\langle \mathrm{H}_{ij}^2 \right\rangle \left\langle \mathrm{H}_{ij} \right\rangle \right], \tag{6}$$

where $\beta = sign\left(kurt\left(\mathrm{h}_i\right)\right)$, and for super-Gaussian signals, $\beta = 1$, and for sub-Gaussian signals, $\beta = -1$. Because of natural image data belonging to super-Gaussian, β is equal to 1.

Step 5. Calculate the reconstruction with new activities according to

$$\mathrm{R}_i = \sum_j \mathrm{H}_{ij} \bar{\mathrm{W}}_j. \tag{7}$$

Step 6. Update the non-normalized basis vectors according to

$$\mathrm{W}_j \leftarrow \mathrm{W}_j \odot \frac{\sum_i \mathrm{H}_i^j \left[\mathrm{V}_i + \left(\mathrm{R}_i^T \bar{\mathrm{W}}_j \right) \nabla \mathrm{W} \left\|\mathrm{W}_j\right\|_2 \right]}{\mathrm{H}_i^j \left[\mathrm{R}_i + \left(\mathrm{V}_i^T \bar{\mathrm{W}}_j \right) \nabla \mathrm{W} \left\|\mathrm{W}_j\right\|_2 \right]}. \tag{8}$$

Step 7. Return to step 1until convergence.

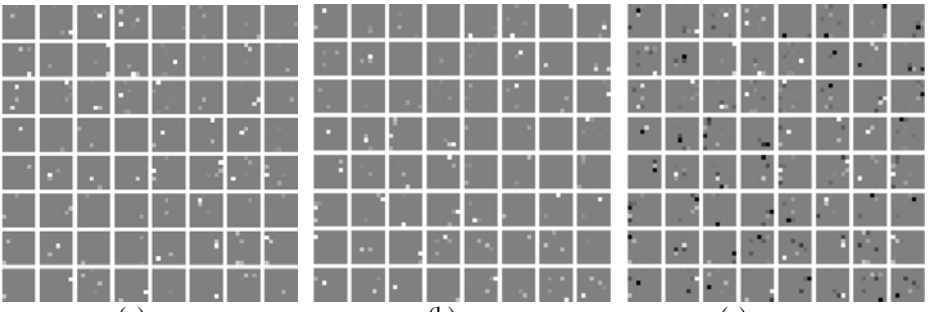

Fig. 1. Basis vectors obtained by our sparse NMF algorithm to natural scenes. (a) the positive basis for ON-channel; (b) the negative basis for OFF-channel; (c) the basis for ON-channel minus the basis for OFF-channel.

Figure 1 shows the feature basis vectors estimated for these ten natural images using the above-mentioned updating rules of the sparse NMF algorithm, where gray pixels denote zero weight, black pixels denote negative weight, and brighter pixels denote positive weights. From figure 1, it is clear to see that the feature basis are not only sparse, but also most of learned basis vectors behave the locality and orientation in spatial domain.

3 Experimental Results

3.1 Image Data Preprocessing

We select natural images as test images in our experiments. All test images used are available on the following Internet web: http:// www.cns.nyu.edu/lcv/denoise. Firstly, selecting randomly 10 noise-free natural images with 512×512 pixels. Then, we sampled patches of 8×8 pixels 5000 times from each original image, and converted every patch into one column. Thus, each image was converted a matrix with 64×5000, and the size of input data set X consist of 10 test images was 64×50000 pixels. Consequently, each image patch is represented by a 8×8 dimensional vector. Further, the data set X was centered and whiten by the method of principal component analysis (PCA), and the preprocessed data set was denoted by $\hat{X}$. Considering the non-negativity, we separate $\hat{X}$ into ON-channel and OFF-channel, denoted respectively by Y and Z. So, the non-negative matrix $V=(Y;Z)$ is obtained. And then, using the updating rules of W and H in turn, we minimized the objective function given in Eqn. (8). The extracted 64 feature basis vectors of natural scenes are shown in Fig. 1, as described in subsection 2.2.

3.2 Image Reconstruction

Using the feature bases extracted, we can implement the task of restoring the original images. The test image was selected as the classical image shown in Fig. 2 (a), used

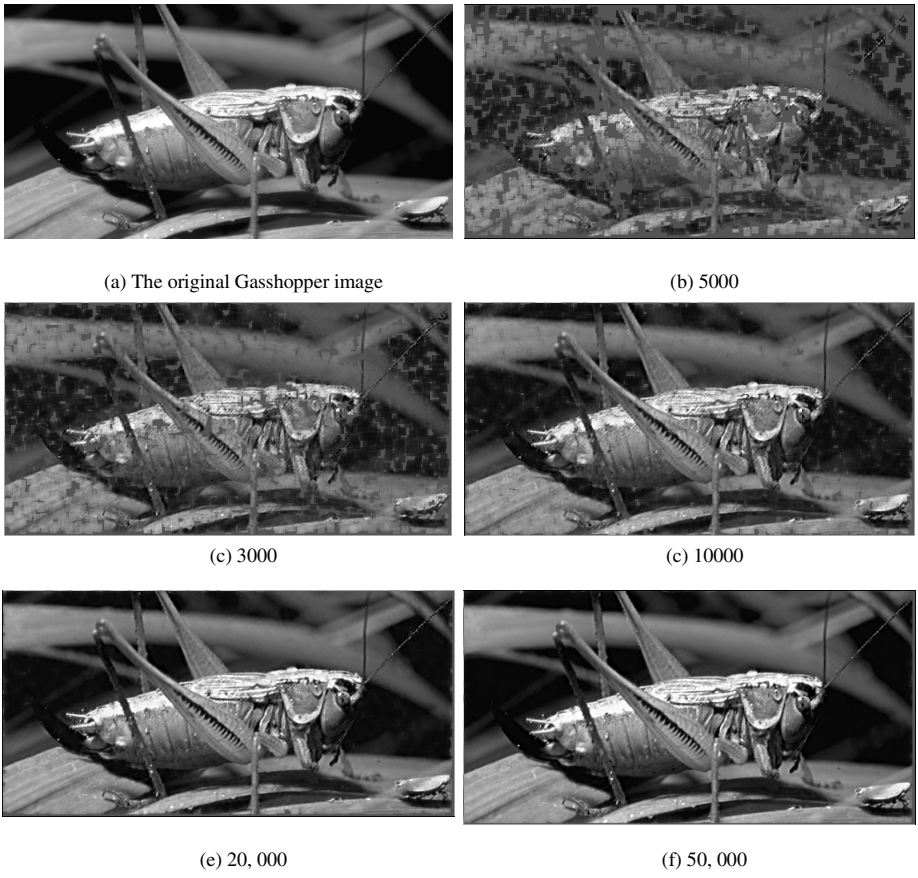

(a) The original Gasshopper image (b) 5000

(c) 3000 (c) 10000

(e) 20, 000 (f) 50, 000

Fig. 2. The original image and reconstructed results obtained by our SC algorithm. (a) The original Gasshopper image; (b) 5000 image patches; (c) 20000 image patches; (d) 50000 image patches.

widely in the image processing field, commonly known as Gasshopper with 256×512 pixels. Assume that the number of image patches with 8×8 pixels sampled randomly from the Gasshopper image was 3000, 5000, 10000, 20000 and 50000, respectively. Then, corresponding to different image patches, the image reconstruction results obtained by our sparse NMF algorithm were shown in Fig. 2 (b) to (f), in the same time, the reconstruction ones obtained by the standard NMF method were also given, which were shown in Fig. 3.

Note that to find the accurate position of any image patch, we need remember the positions of all image patches sampled randomly. Because of sampling randomly, the same pixel might be founded in different image patches. Therefore, for the sample pixel, we averaged the sum of the values of all reconstructed pixels, and used the averaged pixel value as the approximation of the original pixel. Distinctly, from Fig.2 and Fig.3, it can be seen that the larger the number of image patches is, the clearer the

Table 1. Values of *SNR* obtained by different algorithms corresponding to different image patches

Images patches	*SNR* of Image patches				
	3000	5000	10000	20000	50000
Standard NMF	8.91	11.18	15.31	18.27	20.96
Our sparse NMF	8.97	11.24	15.43	18.85	21.36

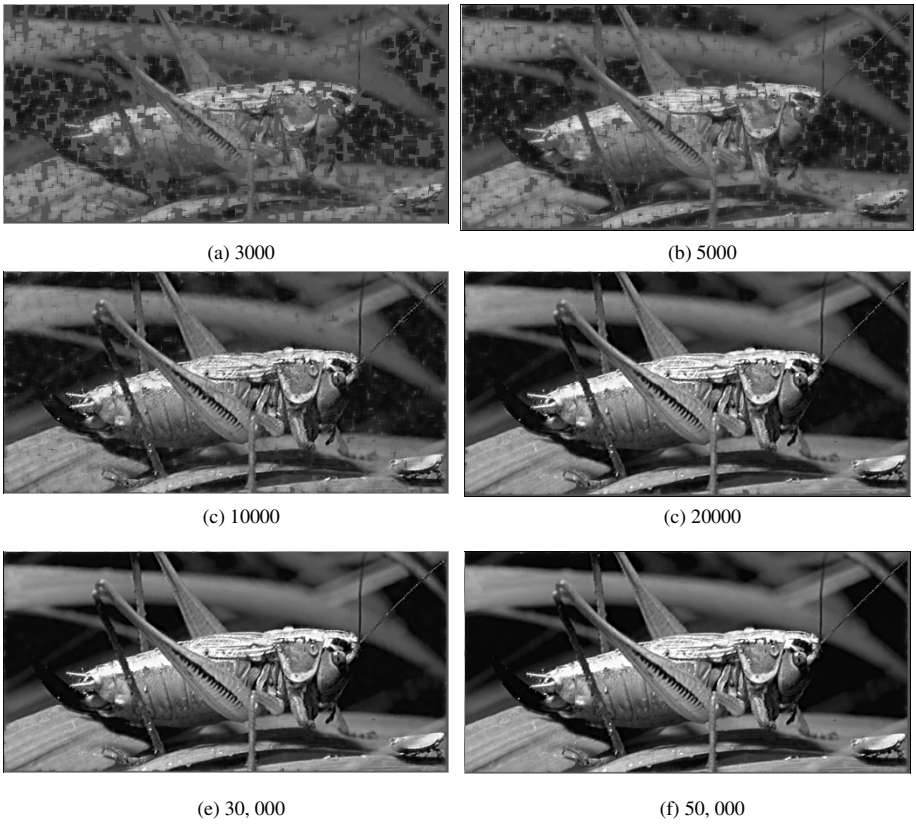

(a) 3000 (b) 5000

(c) 10000 (c) 20000

(e) 30, 000 (f) 50, 000

Fig. 3. The reconstructed results obtained by standard NMF algorithm. (a) 5000 image patches; (b) 20000 image patches; (c) 50000 image patches.

reconstructed image is. When the number of image patches equals to 50000, it is difficult to tell it from the original images only with naked eyes. Moreover, compared Fig. 2 with Fig. 3, correspond to each reconstruction image with the same patches, respectively obtained by algorithms of our sparse NMF and standard NMF, it is also not easy to tell them. Thus, to testify that our proposed NMF algorithm can be indeed successfully applied on image feature extraction, the signal to noise ratio (SNR) values of the output image were also calculated and listed in Table 1. According to

the experimental results, it is easy to see that our sparse NMF algorithm is surely better than standard NMF in feature extracting.

4 Conclusions

In this paper, a novel natural image feature extraction method using a modified sparse NMF algorithm developed by us is proposed. This sparse NMF algorithm exploits the Kurtosis as the maximizing sparse measure criterion, so the natural image structure captured by the Kurtosis not only is surely sparse, but also is surely independent. Using this algorithm, the features of nature images can be extracted successfully, and this features are not only sparse, but also most of learned basis vectors behave the locality and orientation in spatial domain, and utilizing these features, any nature image can be reconstructed. Compared with the standard NMF in performing image reconstruction, the experimental results show that our sparse NMF is indeed efficient in extracting features of natural images.

Acknowledgement

This research was supported by the Opening Project of JiangSu Province Support Software Engineering R&D Center for Modern Information Technology Application in Enterprise (No. eisecSX200806). And it was also sponsored by Qing Lan Project, Startup Foundations Research for Young Teachers of Suzhou Vocational University (SZDQ09L05), the grants of the National Science Foundation of China (No.60805021), the China Postdoctoral Science Foundation (No.20060390180 and 200801231), as well as the grants of Natural Science Foundation of Fujian Province of China (No.A0740001 and A0810010).

References

1. Julian, E., Edgar, K.: Sparse coding and NMF. In: proceedings of 2004 IEEE International Joint Conference on Neural Networks, vol. 4, pp. 2529–2533 (2004)
2. Hoyer, P.: Non-negative matrix factorization with sparseness constraints. Journal of Machine Learning Research 5, 1427–1469 (2004)
3. Lee, D.D., Seung, H.S.: Learning the parts of objects by non-negative matrix factorization. Nature 401(6755), 788–791 (1999)
4. Olshausen, B.A., Field, D.J.: Emergence of simple-cell receptive field properties by learning a sparse code for natural images. Nature 381, 607–609 (1996)
5. Li, S., Cao, F.W., Chen, J.: Denoising natural images using sparse coding algorithm based on the kurtosis measurement. In: Sun, F., Zhang, J., Tan, Y., Cao, J., Yu, W. (eds.) ISNN 2008, Part II. LNCS, vol. 5264, pp. 351–358. Springer, Heidelberg (2008)
6. Bell, A., Sejnowski, T.J.: The Independent Components' of Natural Scenes Are Edge Filters. Vision Research 37, 3327–3338 (1997)
7. Hyvärinen, A., Oja, E., Hoyer, P., Horri, J.: Image Feature Extraction by Sparse Coding and Independent Component Analysis. In: Proc. Int. Conf. on Pattern Recognition (ICPR 1998), Brisbane, Australia, pp. 1268–1273 (1998)
8. Hyvärinen, A.: Sparse coding shrinkage: denoising of nongaussian data by maximum likelihood estimation. Neural Computation 11, 1739–1768 (1997)

A Cyanobacteria Remote Monitoring System

Zhiqiang Zhao[1,2,3] and Yiming Wang[3]

[1] JiangSu Province Support Software Engineering R&D Center for Modern Information Technology Application in Enterprise
[2] Department of Electronics & Information Engineering, Suzhou Vocational University, Suzhou 215104,Jiangsu,China
[3] Suzhou University, Suzhou 215006,Jiangsu,China
zzq@jssvc.edu.cn

Abstract. This article analyzes the major factors and features of the Cyanophyta problem, and makes a research on some key attributes so as to build up a monitor system by analyzing all its steps, and utilizing the current theory and methodology. This article, in view of the traits of the Cyanophyta monitor techniques, fully focuses on the remote wireless monitoring of Cyanophyta in Tai Lake, and have realized software and hardware design of the end device, data excess point and remote monitoring platform. The application of WSNs has improved the Cyanophyta monitoring technique.

Keywords: Cyanophyta monitor; Sensor Networks; SimpliciTI.

1 Introduction

Safe drinking water has become a key concern of society [1]. With discharging a large number of water which polluted by industrial and domestic, it made cyanobacteria breakout easily which caused by eutrophication of water in the lake, and it polluted the drinking water seriously [2]. It has become a research hotspot to develop some real-time system which can monitoring the changes of cyanobacteria in the lake, and earlier warning to cyanobacteria breakout [3]. As the development of network technology, datebase technology, modern communication technology and sensor network technology, environmental monitoring system combine with computer and communication network has become an important direction of application. The change in cyanobacteria monitoring which from original artificial monitoring to remote automated monitoring network is an inevitable trend of development [4].

2 System Function and Overall Structure

2.1 System Function Introduce

As the requirements and characteristics of cyanobacteria monitoring in Tai Lake, the system needs such functions as follows: [4]

D.-S. Huang et al. (Eds.): ICIC 2009, LNAI 5755, pp. 841–848, 2009.

1) Monitoring the cyanobacteria situation of water bodies (especially near the water intake of the drinking water factory);

2) Monitoring the water temperature changes in Tai Lake;

3) Realizing the remote monitoring and early warning, long-range management and other functions.

2.2 Diagram of System Structure

This system consists of field data acquisition nodes(End Device, ED), data aggregation nodes(Access Point, AP) and remote monitoring platform. Field data acquisition nodes collects the information about consistency of Cyanobacteria chlorophyll and water temperature ,then transport the data to date aggregation nodes through sensor networks[5]. Data aggregation node is the aggregation points between sensor networks and GPRS transmission networks [6]. Data aggregation nodes collect all date from field data acquisition nodes in sensor networks. After treatmenting, data aggregation nodes upload the date to remote monitoring platform through the GPRS networks. Remote monitoring platform connect the data aggregation nodes via the Internet. Remote monitoring platform can real-time monitoring, query data, and make a early warning to the area in which the cyanobacteria concentrations in excess of the scope of permit, and the structure of Wireless Cyanobacteria remote monitoring system is shown in Figure 1.

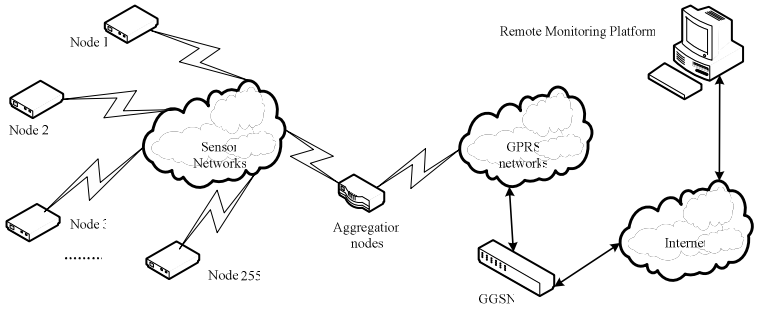

Fig. 1. The structure of Wireless Cyanobacteria remote monitoring system

3 Hardware Design

The main hardware of this system has two parts: field data acquisition nodes and data aggregation nodes. By constituted of the power supply module, temperature sensor, chlorophyll sensor, processor and RF modules, field data acquisition nodes be laid in the water where loop along the Tai Lake. By constituted of the processor, RF module, GPRS module and display module, data aggregation nodes be arranged in the shore of Tai Lake. Remote monitoring platform receiving data via the Internet, and it is responsible for data processing, display, store and provide user-friendly interface for researchers to monitoring the data convenient. System's hardware structure as shown in Figure 2.

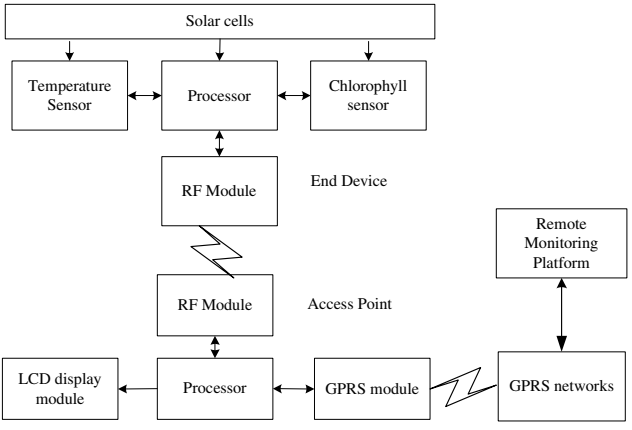

Fig. 2. System's hardware structure

3.1 ED Circuit

ED hardware structure is shown in Figure 3.ED is constituted by Processor, RF module, sensor.

The introduction and performance about this part as follows. CC1110[7][8] is a low-cost wireless SOC, for low-power wireless applications introduced by TI. The chip includes a standard enhanced 8051MCU, a wireless transceiver chip CC1110, both were packaged in a chip.8051 MCU own 32KB Flash and 4KB RAM. The main working frequency bands in the wireless communications for the ISM and ARD, in the ISM band can set up 300-348MHz,391-464MHz and 728-928MHz freely.

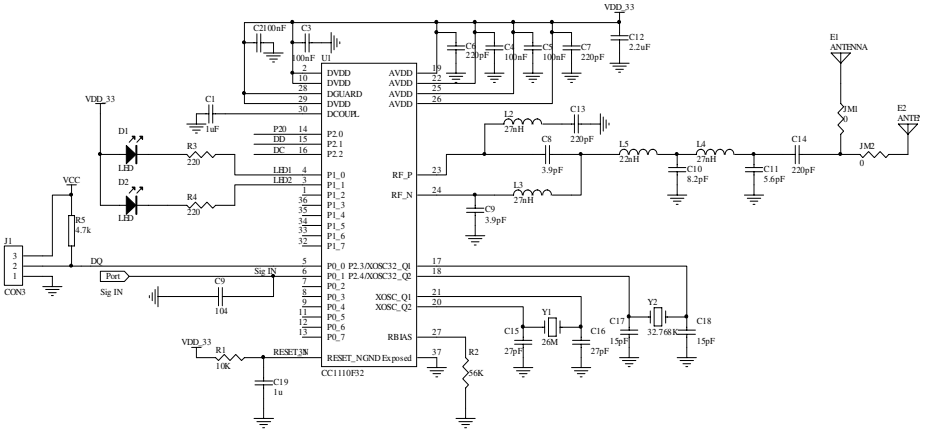

Fig. 3. ED hardware structure

RF transceiver of the CC1110 integrates a highly configurable modem. This modem supports different modulation format, the rate up to 500kbs.CC1110 offers a wide range of hardware support for packet processing, data buffering, burst data transmission, clear channel assessment, connection quality and electromagnetic wave excitation .In receive and transmit mode, the current is lower than 16.2mA or 16mA respectively, rate of 2.4 Kbaud. The ultra-short time of CC1110 from sleep mode to active mode conversion, especially fit for the applications which require very long battery life .CC1110 using QLP package in 6mm * 6mm, have 36 pins total. And there are many wireless module base on CC1110 in the marke. As the actual needs,choose the CC1110 wireless module designed by WXL corporation ChengDu China.

There are two types sensor: Chlorophyll sensor and Temperature sensor. System select Wetstar 1006P chlorophyll fluorescence sensor is designed by WETLABS. It is a multi-functional fluorescence with simple to use, high-precision, underwater and so on. Wetstar 1006P can measuring chlorophyll fluorescence of the water precise.Choose DS18B20[9] as the temperature sensor , and this sensor is widely used in application. This sensor with small size, simple connection, Single-bus, fit for romate monitoring system.

3.2 AP Circuit

AP use the same wireless processor as the ED, and use the GR64 GPRS module. The GR64 circuit is shown in Figure 4.

GR64 [10][11] is a GPRS module embedded TCP / IP protocol stack for GSM / GPRS designed by Sony / Ericssons,it can compatible GR47, and the embedded

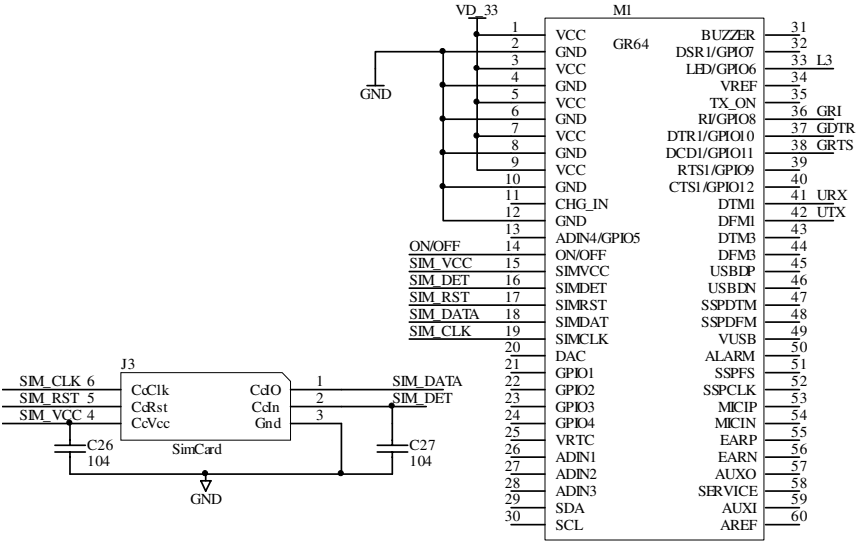

Fig. 4. GR64 circuit

ARM9 CPU can be opened to the user.GR64 has a wealth of storage resources: 256KB script space can accommodate two scripts that can remote upgrade script under CSD, at least 50KB of data NVM space and 100KB RAM.GR64 provides a wealth of interfaces: two serial ports can adaptive baud rate, USB2.0, SPI, antenna, audio interface, 12 I / O lines (8 Multiplexing), AD / DA, buzzer and so on.

4 Software Design

4.1 Sensor Network Architecture

System uses the SimpliciTI [12] network protocol :a small RF networks for low-power RF protocol.It can simplify the implementation of the microcontroller and minimize occupied resources. With a star network topology, contains a data center(AP) which is mainly responsible for network management. AP provide date process forward and equipment permissions, connect permissions and security about the network. AP also has a function which can expand the terminal equipment, and supporting the expansion of a network topology. Network structure is shown in Figure 5.

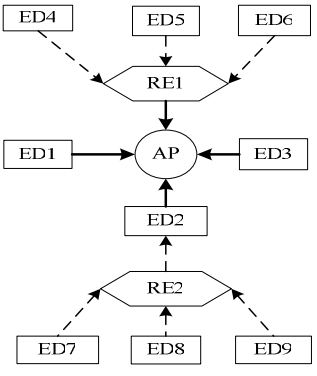

Fig. 5. Network structure

4.2 Software Flow Chart

ED is mainly responsible for collecting field data ,at the same time, in accordance with the network protocol to transmit data to AP. Its main features can be divided into the main program, data acquisition and network communication subroutine, and developed by C and assembler language. ED joined the network flow as shown in Figure 6.

Most of the ED nodes in network are in dormant state, wait for working until receive a activate order. At the same time, ED nodes can also be used as the RE node, when the address in receiving information does not same as the adress of the ED, this

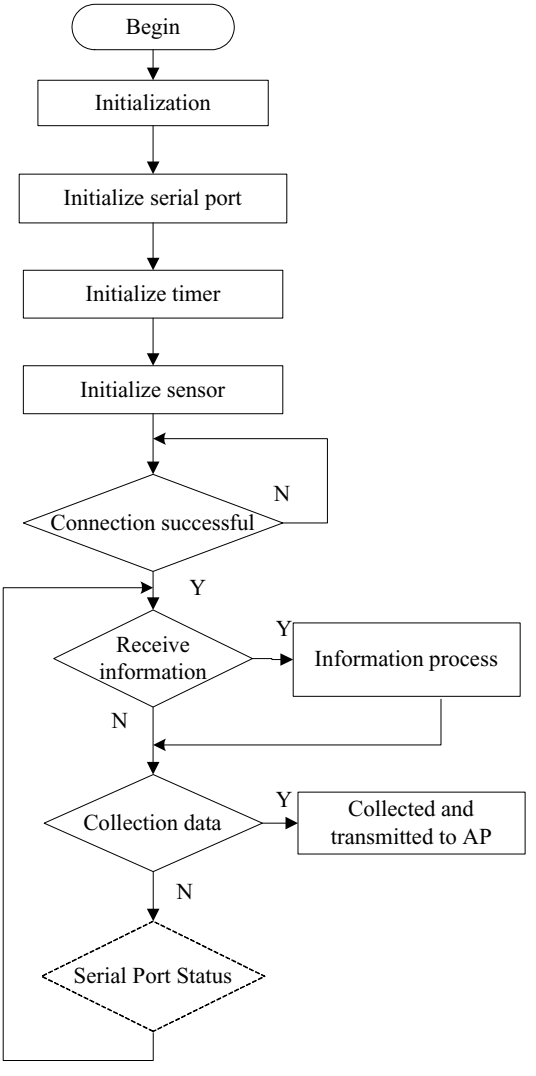

Fig. 6. Flow chart of ED add net

ED will forwarding the information.How to optimizing the route from ED to AP node, which is down the focus of further study.

In accordance with the network protocol, AP is mainly responsible for the management of network and data collection, data processing. At the same time, transferring data to the remote monitoring and control platform by the GPRS network. Constituing by the main program, network communications and GPRS communications Subroutine.AP set up the network as shown in Figure 7.

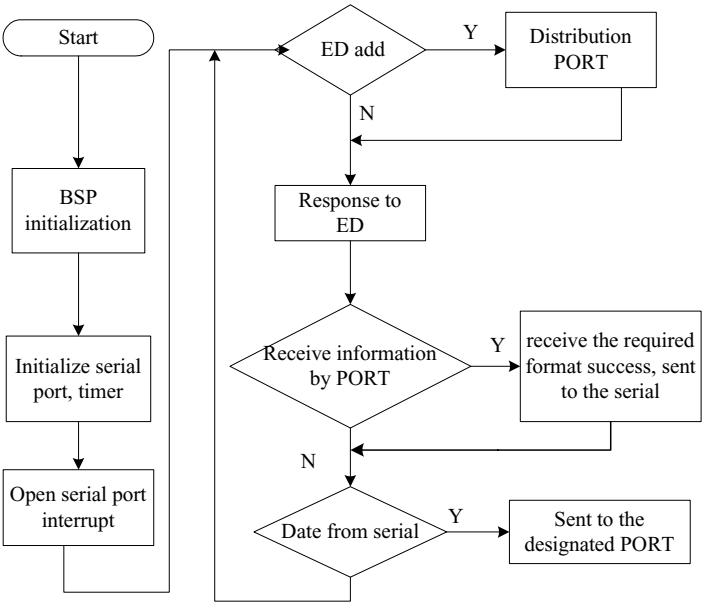

Fig. 7. Flow chart of AP set up the network

5 Conclusions

The cyanobacteria remote wireless monitoring system based on sensor networks is an unmanned automation, intelligent monitoring system for cyanobacteria. Research and application of this system will improve the study on prevent cyanobacteria break out ,it can monitoring implementation of the development of cyanobacteria, promoting the prevention capabilities of cyanobacteria outbreak. And the system's network structure and data transmission, information collection mode, data-processing methods provide a common, advanced, effective model for other data acquisition and monitoring system.

Acknowledgement

This research was supported by the Opening Project of JiangSu Province Support Software Engineering R&D Center for Modern Information Technology Application in Enterprise (No.eisecSX200806),and sponsored by Project and Startup Fundation Research for Young Teachers of Suzhou Vocational University (No.SZDQ09L03).

References

1. She, F.N.: Quantitative analysis On Chlorophyll Aconcentration In TaiHu Lake Using Thematic Mapper Date. Journal Of Lake Sciences 8(3), 201–207 (1996)
2. He, Y.L.: Cyanobacteria outbreak of incentives and governance approaches. Heilongjiang Science and Technology Information 114 (January 2008)

3. Kong, F.X.: Large-scale eutrophication of shallow lakes cyanobacterial algal consider the formation mechanism of: Acta Ecologica Sinica 25(3), 589–595 (2005)
4. Heng, Y.S.: Taihu cyanobacteria bloom early warning system of monitoring techniques. Chinese Environmental Monitoring 24(2), 63–65 (2008)
5. Sun, L.: Wireless Sensor Networks. Qing Hua University Press (2005)
6. Yan, L.H.: Remote data transmission system based on GPRS technology: Xi'an University of Science and Technology (2006)
7. CC1110 wireless single-chip microcomputer development system: Chengdu Wireless Communications Technology Co., Ltd (2007)
8. Chipcon Smart RF CC1100, Chipncon (2005)
9. DS18b20. Dallas Semicondoctor(2005)
10. GR64 Manual. Sony Ericsson(2006)
11. Ren, T.: TCP / IP protocol and network programming. Xi'an Electronic Technology University Press (2004)
12. Rudner, R.: Introduction to SimpliciT. Texas Insruments 28(2), 109–119 (2007)

Study on Fault Diagnosis of Rolling Mill Main Transmission System Based on EMD-AR Model and Correlation Dimension

Guiping Dai[1,2] and Manhua Wu[3]

[1] JiangSu Province Support Software Engineering R&D Center for Modern Information Technology Application in Enterprise
[2] Department of Electronic & Information Engineering , Suzhou Vocational University, Suzhou 215104, Jiangsu, China
luaiping_0127@163.com
[3] Department of Foreign Languages and International Exchange, Suzhou Vocational University, Suzhou 215104, Jiangsu, China
wmh@jssvc.edu.cn

Abstract. In order to improve the fault diagnosis accuracy of rolling mill main transmission system, a fault feature extraction method based on EMD (Empirical Mode Decomposition)-AR model and Correlation Dimension is proposed. In the proposed method, EMD is used to decompose the vibration signal of complex machine into several intrinsic mode functions (IMFs), then the AR models of some IMF components which contain main fault information are constructed respectively. Finally, the correlation dimensions of auto-regressive parameters in AR models are calculated. Analysis of the experimental results shows that this method not only can reflect the state changes of dynamic system profoundly and detailedly, but also can realize the separation of state features, thus it may judge the fault conditions of rolling mill main transmission system effectively.

Keywords: Empirical mode decomposition; AR model; Correlation dimension; Rolling mill main transmission system; Fault diagnosis.

1 Introduction

The rolling mill main transmission system is rolling mill's important component, which undertakes driven roll's rotation mechanical energy transportation work. In rolling mill's movement, the main transmission system represents torsional vibration phenomenon frequently, that may cause the main transmission system's spare part to have fatigue failure, even may occur sudden breaks when it is serious [1], but the vibration signal measured through sensor not only contains fault information, but also mixes with heavy background signal relating to the rolling mill running status and noise, which frequency band overlaps mutually, therefore the traditional time domain or frequency range method is very difficult to extract fault information [2].

D.-S. Huang et al. (Eds.): ICIC 2009, LNAI 5755, pp. 849–857, 2009.

Correlation dimension is an important parameter to reflect the nonlinear system behavior in state space, the use of fractal dimension may carry on quantification to nonlinear system's state [3], thus the rolling mill main transmission system's fault diagnosis can be realized effectively. However, strict fractal is only one kind of idealized model, the majority of vibration signal mixed with noise only has the fractal feature in some kind of criterion scope, actually random noise does not have strict fractal feature[4], therefore it is unreliable to use the primitive vibration signal to calculate correlation dimension directly in order to further distinguish transmission system's states; Moreover, when there is a great deal of primitive signal data, to calculate correlation dimension directly will be much work. Therefore before the calculation of correlation dimension, it is necessary to reduce the primitive vibration signal's dimensionality, then according to the processed signal or parameter, calculate the correlation dimension.

In view of the above questions, this paper firstly utilized the wavelet threshold denoising algorithm and empirical mode decomposes (EMD) to denoise, linearize and tranquilize the primitive vibration signal, in order to obtain some IMF components; Then, AR models of IMF components which contains main information were set up to carry on dimensionality reduction, then each AR model's autoregressive parameter can be calculated; Finally, the phase space of each AR model's autoregressive parameter was reconstructed through the time-delay phase diagram method, then correlation dimension can be calculated, thus the accurate judgment of the rolling mill main transmission system's faults was made.

2 The AR Model Based on EMD

AR model is a time series analysis method, which parameters contain essential information of system states and the accurate AR model can express objective characteristics of dynamic systems profoundly and concentratedly, while plenty of researches indicate that AR model's autoregressive parameters can reflect the state changes most sensitively. However, AR model can only apply to stationary signal analysis, while vibration signal of the rolling mill main transmission represents non-stationary features, the autoregressive parameters by setting up AR model directly from it will not reflect the original signal characteristics.

Therefore, the original vibration signal needs a stable pre-treatment before setting up AR model on it, which can be completed by EMD method, and the vibration signal is also mixed with random noise, which not only affects the quality of the EMD decomposition, but also makes the correlation dimension of the loss of physical meaning. Accordingly, before the EMD decomposition, this paper is talking about taking orthogonal wavelet transform denoising method to remove noise [5] and [6].

EMD is a adaptive signal decomposition method which is applicable to non-linear, non-stationary process, and its purpose is to decompose the signal into a set of intrinsic mode functions (IMFs), for each IMF component indicates an inherent characteristic vibrational form of signals, which must meet two conditions: ① the difference between the sum of local maximum、minimum points and the number of zero-crossing points does not exceed 1; ② at any point, the definition of mean envelope

given by the local maxima and local minimum must be zero [7]. The essence of this method is to obtain intrinsic vibration modes through characteristic time scales, and then by it to decompose the data sequence. Ideas are as follows:

(1) Initialization: $r_0(t) = x(t)$, i=1

(2) Obtains ith IMF ① Initialization: $h_0(t) = r_{i-1}(t)$, j=1; ② Find out $h_{j-1}(t)$ partial extreme point; ③ The maximum and minimum points of $h_{j-1}(t)$ were interpolated to form upper and lower envelope; ④ Calculate the average of upper and lower envelope $m_{j-1}(t)$; ⑤ $h_j(t) = h_{j-1}(t) - m_{j-1}(t)$; ⑥ If $SD = \sum_{t=0}^{T} \left[\left| h_j(t) - h_{j-1}(t) \right|^2 / h_j^2(t) \right] \le 0.3$, then $I_{imfi}(t) = h_j(t)$, otherwise j=j+1, switch to ②

(3) $r_i(t) = r_{i-1}(t) - I_{imfi}(t)$

(4) If extreme points of $r_i(t)$ were not less than 2, then i=i+1, switch to (2); Otherwise decomposition was completed, $r_i(t)$ was the remaining component.

Where, $x(t)$ is the decomposed signal; $m_j(t)$ is the average of upper and lower envelope of $h_j(t)$; $h_j(t)$ is the difference between $h_{j-1}(t)$ and $m_{j-1}(t)$; SD is the criterion of ending sifting process.

The algorithm may result in $x(t) = \sum_{i=1}^{n} I_{imfi}(t) + r_n(t)$ finally after the inferential reasoning:

$$x(t) = \sum_{i=1}^{n} I_{imfi}(t) + r_n(t). \tag{1}$$

At this point, the signal $x(t)$ is decomposed into a summation of n IMF components and a residual component. For each IMF component $I_{imft}(t)$, set up the following auto-regressive model AR (m)

$$I_{imft}(t) + \sum_{k=1}^{m} \phi_{ik} I_{imft}(t-k) = e_i(t) \tag{2}$$

Where, ϕ_{ik} 、 m are the model parameter and model order of autoregressive parameter model AR (m) of $I_{imft}(t)$, $e_i(t)$ is the model residual, which is white noise sequence of mean zero, variance σ_i^2. FPE criteria is used to determine the model order of m and least squares algorithm is used to estimate the autoregressive parameter ϕ_{ik}.

3 The Basic Principle of Correlation Dimension

The correlation dimension can be calculated directly by observing one-dimensional time series or dealing with data sequence using phase space reconstruction approach.

Mechanical system usually represents the highly complex characteristics and may has lots of free degrees mixed with noise, while in the normal circumstances, test results show a single time series, if let such a time series to reflect the characteristics of mechanical system, it will inevitably lose much information, so a single time-series should be re-constituted to higher-dimensional phase space. In order to obtain phase-space geometry of dynamical systems from one-dimensional time-series, in 1983, Grassberger and Procaccia put forward an algorithm of calculating correlation dimension directly from a given time-series data according to the embedding theory and the phase space reconstruction idea, that is GP algorithm [9].

Supposing that $\{x_k, k = 1,2,\cdots,N\}$ is time series obtained by observing a system, where x_k is the autoregressive parameter ϕ_{ik} and N is the model order m of AR model. The time series is reconstructed into phase space and embedded in m-dimensional Euclidean space R^m in order to get a point (or vector) set J (m) which elements were recorded as follows:

$$X_n(m,\tau) = (x_n, x_{n+\tau}, \cdots, x_{n+(m-1)\tau}),\ n = 1,2,\cdots,N_m\ . \tag{3}$$

In the upper formula, $\tau = k\Delta t$ is called time-delay and Δt is time interval of two adjacent sampling points, k is an integer.

$$N_m = N - (m-1)\tau\ . \tag{4}$$

Selecting a reference point X_i from these N_m points to calculate the distance from the remaining points N_m-1 to X_i

$$d_{ij} = d(X_i - X_j) = \left\| X_i - X_j \right\|\ . \tag{5}$$

For all X_i ($i = 1,2,\cdots,N_m$), repeat the process in order to obtain correlation integral function

$$C_m(r) = \frac{2}{N_m(N_m - 1)} \sum_{i=1}^{N_m} \sum_{j=1}^{N_m} H(r - d_{ij})\cdot \tag{6}$$

Where $r > 0$; H is Heaviside function which expression is:

$$H(x) = \begin{cases} 1, x > 0 \\ 0, x \le 0 \end{cases}\ . \tag{7}$$

Supposing $D_2(m, r_1) = \dfrac{d \ln C_m(r)}{d \ln r}$, that $D_2(m, r_2)$ is the slope of curve $\ln C_m(r) \sim \ln r$. When $r \to 0$, get $D_2(m) \approx \lim\limits_{r \to 0} D_2(m, r_1)$. Thus the value $D_2 \approx \lim\limits_{m \to \infty} D_2(m)$ of $D_2(m)$ which is not changed with the elevation of phase space dimension m is just the correlation dimension of time series.

4 The Algorithm Description Based on EMD-AR Model and Correlation Dimension

The EMD-AR model and correlation dimension were introduced into the fault vibration signal analysis of rolling mill main transmission, where EMD-AR model was used to linearize,tranquilize vibration signal and to reduce its dimension, and then correlation dimension was used to represent the fault characteristics of vibration signal accurately and quickly, the specific algorithm is as follows:

(1) Utilizing the denoising algorithm based on orthogonal wavelet transform to remove random noise from the vibration signal of rolling mill main transmission, and then combining with EMD decomposition algorithm, the signal is decomposed into a series of IMF components called as $I_{imft}(t)$.

(2) Reducing the dimension of IMF components which contain main information by setting up separately AR model, then obtaining the autoregressive parameter ϕ_{ik} of each AR model, where $k = 1,2,\cdots m$, m is the AR model order.

(3) Reconstructing the phase space of each autoregressive parameter ϕ_{ik} through time-delay phase diagram method, and then calculating its correlation dimension.

① Standardized treatment and removing the trend: Processing ϕ_{ik} with zero-mean and normalization, then utilizing the least square method to remove the trend for the zero-drift signal;

② Phase space reconstruction: Using mutual information method to determine the optimum time delay τ , Cao's method to determine the optimum embedding dimension m, and in accordance with time delay method to construct point set $J(m)$;

③ Calculation of correlation integral function $C_m(r) : C_m(r)$ displays spatial correlation of points, and its essence is the probability of distance less than r between two arbitrary points, which is the most critical and most time-consuming part in the calculation of correlation dimension. In this paper, referring to the K-Nearest Neighbor Search theory in computer search technology and utilizing the distance formula $d_{ij} = d_1(X_i - X_j) = \sum_{l=0}^{m-1} \left| x_{i+l\tau} - x_{j+l\tau} \right|$ in the rhombus field which topology is equivalent to the distance in spherical field , the speeding of the calculation is made;

④ Calculation of correlation dimension: Mapping $\ln C_m(r) - \ln r$ curve which is called the correlation integral curve, then select the section of good linearity for linear fitting to calculate the slope of fitting a straight line, that is a correlation dimension.

5 Experimental Results

This experiment makes vibration tests on the main transmission system of rolling mill, measures radial displacement vibration signal in normal, misalignment, collision and oil film whirling fault state. In the experiment, speed of the transmission shaft is 3000r/min, sampling frequency is 4096Hz and number of sampling points is 1024. The denoising algorithm based on orthogonal wavelet threshold is used to remove random noise.

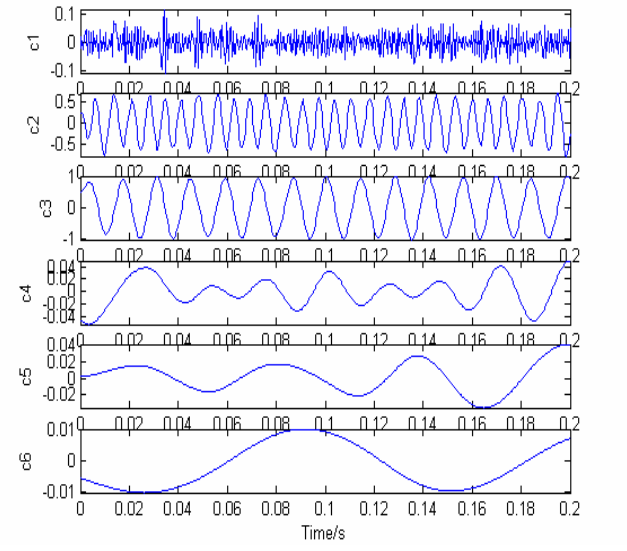

Fig. 1. EMD decomposition results of radial vibration signal in the state of misalignment fault. IMF components named $c1$, $c2$, $c3$, $c4$ each has relatively high frequency, while IMFcomponents named $c5$, $c6$ with lower frequency.

A series of IMF components are obtained by the EMD decomposition separately of the above fault vibration signals, and EMD decomposition results in the state of misalignment fault are shown in figure 1. From the Fig, we can see that each IMF component contains different characteristic time scales, and components named $c1$, $c2$, $c3$, $c4$ each has relatively high frequency, including main fault information, while components named $c5$, $c6$ with lower frequency, is the background signal and noise in relation to its speed. Thus, set up AR model on the former four IMF components $c1$, $c2$, $c3$, $c4$ respectively, then reconstruct the phase space of AR model's autoregressive parameters through time-delay phase diagram method and calculate its correlation dimension, thereby the fault characteristics can be extracted.

Figure2(a) displays correlation dimensions of AR mode's autoregressive parameters of IMF component $c1$ of vibration signals in different fault status, because different embedding dimension m can obtain different correlation dimension, so the figure gives correlation dimension corresponding to different embedding dimension, and it shows clearly that correlation dimension in the oil film whirling fault state is obviously smaller than the other three fault states; Figure2(b) displays correlation dimensions of AR model's autoregressive parameters of IMF component $c2$, and it indicates clearly the distinguish between the misalignment state and the other three states; Figure 2(c) displays correlation dimensions of AR model's autoregressive parameters of IMF component $c3$, from the graph not only the misalignment fault state can be distinguished, but also the difference between the normal state and the other three states ; Figure 2(d) displays correlation dimensions of AR model's autoregressive parameters of IMF component $c4$, from the graph, the collision fault is distinguished; Figure3(a) displays correlation dimensions corresponding to different embedding dimensions of

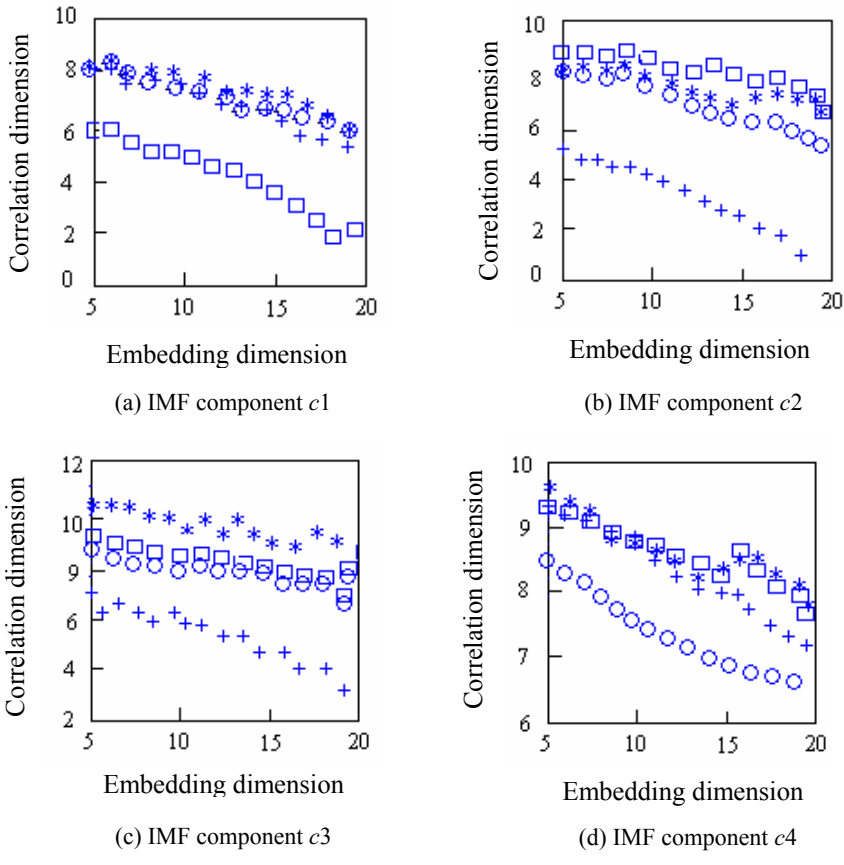

Fig. 2. Correlation dimensions of AR mode's autoregressive parameters of IMF components $c1$-$c4$ in different fault states. *: Normal state. □: Oil film whirling state. ○: Collision state. +: Misalignment state.

the original vibration signal, although the state of oil film whirling can be distinguished when embedding dimension is 10, but the other three states can not be distinguished; Figure3(b) displays correlation dimensions of AR model's autoregressive parameters of the original signal which is directly used to set up AR model, the figure can not state any clear distinction between the four.

From the above analysis we can see that the direct use of original vibration signal to calculate correlation dimension is difficult to extract the fault information comprehensively and accurately, because rotating machinery fault signals in general are more complex, which includes non-linear, non-stationary vibration characteristics, such as fundamental frequency, doubling of frequency, ultra-low frequency, while the AR model is only suitable for stationary signal analysis. Therefore, autoregressive parameters by setting up AR model directly on it can not adequately reflect information about the state of mechanical systems, however, EMD decomposition obtains intrinsic vibration modes through characteristic time scales, and then by intrinsic vibration

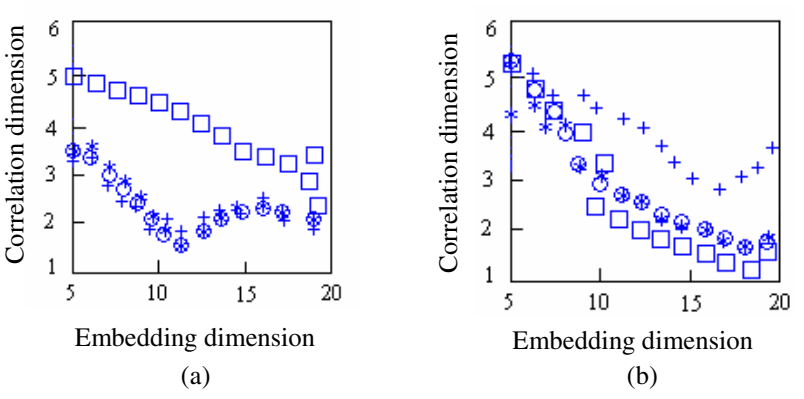

Fig. 3. Left (a): Correlation dimensions of the original vibration signal. *: Normal state. □: Oil film whirling state. ○: Collision state. +: Misalignment state. Right (b): Correlation dimensions of AR model's autoregressive parameters of the original signal. *: Normal state. □: Oil film whirling state. ○: Collision state. +: Misalignment state.

modes can decompose data sequence, which achieved the separation of system state features. So correlation dimensions of AR model's autoregressive parameters of different IMF components can distinguish between different fault types, which can provide a reliable basis for the fault diagnosis of rolling mill main transmission system.

6 Conclusion

Because of the influence of nonlinear stiffness, friction, unbalance and external load, the fault vibration signal of rolling mill main transmission system performs non-linear, non-stationary characteristics, it is difficult to extract fault information only by traditional time-frequency range analysis method. For this problem, the paper combined with EMD decomposition, AR model, fractal geometry theory and applied them to the fault diagnosis of rolling mill main transmission system. Theoretical and experimental study results indicated that this algorithm can not only profoundly and comprehensively express the objective law of dynamic system state change, but also realized the separation of system state characteristics. Therefore, correlation dimensions of AR model's autoregressive parameters of different IMF components can distinguish between different fault types and thus it improved the fault diagnosis accuracy of rolling mill main transmission system. The algorithm is feasible to combine pattern recognition techniques to develop more effective fault diagnosis system, with correlation dimensions of AR model's autoregressive parameters of each IMF component.

Acknowledgments

This paper was supported by the Opening Project of JiangSu Province Support Software Engineering R&D Center for Modern Information Technology Application in

Enterprise (No.eisecSX200806), and sponsored by Qing Lan Project and The Science & technology Foundation of Fujian province (No.2008F5046), and the Science Technology Foundation of Suzhou vocational university (No.SZD09L28).

References

1. Yu, W.K., Liu, B.: Processing's method of non-stationary transient impact torsional vibration signal for Rolling mill. Chinese Journal of Scientific Instrument 26(8), 504–505 (2005)
2. Zong, M., Dai, G.P.: Characteristics study on time-frequency analysis method based on empirical mode decomposition. Chinese Journal of Sensors and Actuators 19(4), 1029–1032 (2006)
3. Zhao, H.: Application research of correlation dimension in the machinery equipment fault diagnosis. China Safety Science Journal 16(3), 129–134 (2006)
4. Liu, T.X., Hua, H.X.: Application research of state monitoring method based on fractal geometry. Chinese Journal of Mechanical Engineering 37(5), 100–104 (2001)
5. Dai, G.P., Liu, B.: Instantaneous parameters extraction based on wavelet denoising and EMD. Acta Metrologica Sinica 28(2), 158–161 (2007)
6. Liu, B., Dai, G.P.: Adaptive wavelet thresholding denoising algorithm based on white noise detection and 3σ rule. Chinese Journal of Sensors and Actuators 18(3), 473–477 (2005)
7. Huang, N.E., et al.: The empirical mode decomposition and the Hilbert spectrum for nonlinear and non-stationary time series analysis. In: Proc.R Soc.Lond.A (1998)

Analysis of Mixed Inflammable Gases Based on Single Sensor and RBF Neural Network

Yu Zhang[1,2], Meixing Qi[3], and Caidong Gu[1,4]

[1] JiangSu Province Support Software Engineering R&D Center for Modern InformationTechnology Application in Enterprise, Suzhou, China, 215104
[2] Depart of Electronic information engineering, Suzhou Vocational University,Suzhou International Educational Park, Road 106, Zhineng Dadao, Suzhou 215104, Jiangsu, China
Zhixin331@163.com
[3] Department of Mechanical Engineering, Suzhou Industrial Park Institute of Vocational Technology, 68 Suqian Road, Suzhou Industrial Park, Suzhou 215021, Jiangsu, China
qimeixing@163.com
[4] Depart of computer engineering, Suzhou Vocational University, Suzhou International Educational Park, Road 106, Zhineng Dadao, Suzhou 215104, Jiangsu, China
gucaidong@163.com

Abstract. The sensitivity of a catalytic sensor changes according to different types of gases or different temperatures. To fully exploit this property, a sensor can be controlled to work under different temperatures to produce different output signals for a given mixture of inflammable gases. An Radial Basis Function(RBF) neural network can be used to analyze the mixture of gases by using a dynamic learning algorithm. The simulation experiment, with a sample mixture of firedamp, carbon monoxide and hydrogen, shows that the proposed method is indeed efficient in analyzing mixtures of inflammable gases.

Keywords: RBF neural network, Gas analysis, Catalytic sensor, Dynamic training algorithm.

1 Introduction

Gas analysis is very important in many areas such as industrial manufacturing, environmental protection, security monitoring and scientific research. Currently, multiple gas sensors are usually used to analyse mixed inflammable gases. However, the phenomenon of cross sensitivity in many gas sensors often undermines the result of the analysis. In recent years, sensor arrays and neural network units have also been used in gas analysis systems [1]. This method relies on the choice of special gases of the sensors. Since the sensors can be disturbed considerably by the environmental gases, this method is usually unable to provide reliable detection results. Thermo catalytic sensors are widely used in the detection of mine gases and other inflammable gases due to its unique selection of inflammable gases [2]. To fully exploit this nature, a single thermocatalytic sensor controlled to work under different temperatures for gases has different sensitivity, it make the analysis of mixed inflammable gases possible.

D.-S. Huang et al. (Eds.): ICIC 2009, LNAI 5755, pp. 858–864, 2009.

2 A Multiple Thermostatic Detection System of Catalytic Sensor

Since any change in the temperature of the catalytic sensor can damage the accuracy and sensitivity of the detection, the method of thermostatic detection is used in this paper. As shown in Fig. 1, the resistors R_1, R_2, R_3 and the catalytic r-sensor form a bridge, which is the closed loop control circuit along with the regulator A. The circuit works as follows: at the starting point, the current in the r-sensor is set to be its rated current I_0, the bridge is balanced ($R_1R_3 = R_2r$)and the output signal $U_O = I_0r$. When the inflammable gases are being detected, the gases undergo catalytic oxidized reaction at the surface of the catalytic circuit component. As a result, both the temperature at the component r and its resistance increases. Because of the control of the regulator A, the current at the catalytic sensor component is decreased to I_C , the temperature drops to the original level and the bridge returns to the balance point. At this point, the change in the output voltage is in reflection of the concentration of the gas being detected. With the addition of a programmable controlled potentiometer B, the operating current at the catalytic circuit component can be regulated. So, its operating temperature can be changed, and the multi-detection under constant temperature system is established.

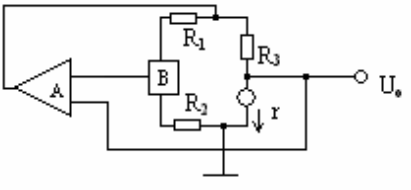

Fig. 1. Detection circuit with thermostatic sensor

3 Gas Analysis with a Single Catalytic Sensor Based on RBF Network

Assume that there is in the mixed mixture a combination of n different gases, whose concentration are $c_1, c_2 ... c_n$ respectively. Using multiple detection under the constant temperature system mentioned above, the operating temperature of the single catalytic sensor is changed n times through the regulation of operating current. The output voltage u_i under operating temperature T_i is written as follows :

$$u_i = f_i(c_1, c_2 ... c_n) \quad i = 1,2...n \ . \tag{1}$$

The equation (1) could be represented in the vector form of $U = F(C)$, in which $U = [u_1, u_2 ... u_n]^T$, $C = [c_1, c_2 ... c_n]$. In Eq.(1), the output voltages u_i is the input of the neural network. The output of this network would then be the desired concentration of the gases c_i' . The mappings between the inputs and the outputs of the neural network are:

$$c_i' = g_i(u_1, u_2 \ldots u_n) \quad i = 1,2 \ldots n \ . \tag{2}$$

Also the Eqn.(2) could be represented in the vector form of $C' = G(U)$, in which $C' = [c_1', c_2' \ldots c_n']^T$, $G = [g_1, g_2 \ldots g_n]^T$.

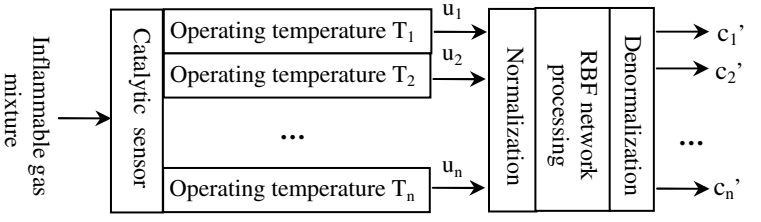

Fig. 2. Gas analysis model of RBF neural network

Obviously, utilizing the outstanding nonlinear mapping capability of the neural network, when the mappings satisfy $G = F^{-1}$, the outputs $C' = C$, it provides the accurate concentration of the different gases in the mixture. Since the RBF neural network can converge to any nonlinear function under any accuracy and is free of the problem of local minimums, the RBF neural network is used here[3]. The neural network is constructed according to a reasonable structure and is trained with a large amount of samples. The connection weights between the hidden and output layer are specified under given distortion constraints, which reflect the nonlinear mapping G of the neural network. Therefore, the concentration of the gases in the mixture can be accurately detected with a single catalytic sensor.

4 The Structure and the Learning Algorithm of RBF Network

The RBF neural network [4-7] is composed of three layers of neurons: the input layer, the hidden layer and the output layer. The number of neurons in the output and input are specified according to the number of the types of gases in the gas mixture, while the one in the hidden layer is computed dynamically using the online learning algorithm. The parameters of the RBF network are composed of three parts: the center α, the width σ and the weight w. The center and the width represent the spatial mode and the relative positions of the centers of the samples. And the RBF neural network is trained by using online training algorithm here.

4.1 Allocating Hidden Layer Units Online

Assume that the input dimension of the RBF network is N, the number of hidden units is P, and the dimension of the output is M. For the given sample pair $[U, C]$, assuming that the output of the neural network is C'. Let $E = C - C'$. If the following condition is satisfied, a new hidden unit is allocated:

$$\begin{cases} \|E\| > \varepsilon \\ \|U - C\_near\| > \delta(t) \end{cases} . \tag{3}$$

where $U = [U_1, U_2 ..... U_N]^T$ ($U_l = \{u_{1,} u_2 ..... u_n\} (l = 1,2 .... N)$) , and it represents the input sample space. $\|\bullet\|$ represents the norm, which is usually set as 2; C_near represents the center closest to X among all the centers in the current network; ε and $\delta(t)$ are the error threshold and the distance threshold, respectively.

4.2 The Learning Algorithm

The method stated above in subsection 3.1 is used to allocate the hidden layer units of the RBF neural network. The three parameters of the neural network, namely, the center α , the width σ and the weight w , are adjusted by using the gradient descent. The algorithm is described as follows:

The quality measure function is defined as:

$$J = \frac{1}{2}\sum_{j=1}^{M}(c_j - c_j')^2 . \tag{4}$$

where M is the dimension of the output of the network; c_j is the expectation of the output corresponding to the input sample; c_j' is the actual output of the network and $c_j' = \sum_{i=1}^{P} h_i w_{ij} = \sum_{i=1}^{P} \exp\{-\frac{\sum_{k=1}^{N}(u_k - c_i^{(k)})^2}{\sigma_i^2}\} w_{ij}$, $1 \le j \le M$,$1 \le i \le P$; $c_i^{(k)}$ is the output of the i -th center in response to the k –th input u_k .

Based on (4), the optimal searching direction for the weight w_{is} , the center $\alpha_i^{(r)}$ and the width σ_i in the gradient descent algorithm are respectively:

$$Sw_{is} = -\frac{\partial J}{\partial w_{is}} = e_s h_i . \tag{5}$$

$$S\alpha_i^{(r)} = -\frac{\partial J}{\partial \alpha_i^{(r)}} = \frac{2h_i(u_r - \alpha_i^{(r)})}{\sigma_i^2}\sum_{j=1}^{M} e_j w_{ij} . \tag{6}$$

$$S\sigma_i = -\frac{\partial J}{\partial \sigma_i} = \frac{2\|U - \alpha_i\|^2}{\sigma_i^3} h_i \sum_{j=1}^{M} e_j w_{ij} . \tag{7}$$

Therefore, the parameter adjustment algorithm for the RBF neural network is written as follows:

$$w_{is}(n+1) = w_{is}(n) + \lambda S w_{is} . \tag{8}$$

$$\alpha_i^{(r)}(n+1) = \alpha_i^{(r)}(n) + \lambda S \alpha_i^{(r)} \quad . \tag{9}$$

$$\sigma_i(n+1) = \sigma_i(n) + \lambda S \sigma_i \quad . \tag{10}$$

where Eqns.(8) to (10) constrain to $1 \le r \le N, 1 \le i \le P, 1 \le s \le M$. λ is the rate of learning. In order to have a better convergence, λ is adjusted online using the following iterative equation:

$$\lambda(k) = \begin{cases} a\lambda(k-1), J(k) \le J(k-1) \\ b\lambda(k-1), J(k) > J(k-1) \end{cases} . \tag{11}$$

where $a \ge 1.0, 0 < b < 1.0$

5 Experimental Results

Different samples of mixed gas with different concentrations of CH_4, CO, H_2 are formulated. In order to having considerable difference in analysis results, high concentrations are selected. For the mixed gas samples, the concentrations of CH_4, CO, H_2 are limited in the range of 0~1.0%、0~0.1% and 0~0.15% respectively. Altogether 115 groups of experiment samples are formulated, 110 groups are used for the training of the RBF neural network, while the other 5 groups are used for the testing of the neural network.

The SH-3 catalytic sensor is used[8], which has two parameters with the rated voltage at 2.8V and the rated current at 80mA. For each group of mixed gas sample, the operating current are respectively 40mA、65mA and 85mA, while the corresponding operating temperature are 150 °C 、350 °C and 560 °C. Totally 115 groups of output signals are detected. Some of the sample data are listed in Table 1.

Table 1. Some of the sample data in the experiment

Components in the gas mixture/%			Detected outputs under three operating temperatures/mv		
H_2	CO	CH_4	ΔU_{o1}	ΔU_{o2}	ΔU_{o3}
0.040	0.005	0.00	1.220	1.282	1.313
0.021	0.101	0.00	0.605	1.807	1.719
0.010	0.050	0.05	0.290	0.824	2.790
0.039	0.020	0.10	1.150	1.362	4.911
0.082	0.000	0.40	2.314	2.335	17.63
	…			…	
0.100	0.050	1.01	2.854	3.371	38.72

The RBF neural network has 3 input nodes and 3 output nodes. The maximum number of neurons in the hidden layer of the neural network is ranged in 10～45. After normalization, the sample data mentioned above is used to train the neural network. The tolerated error is assumed to be 0.001. After multiple simulations use the

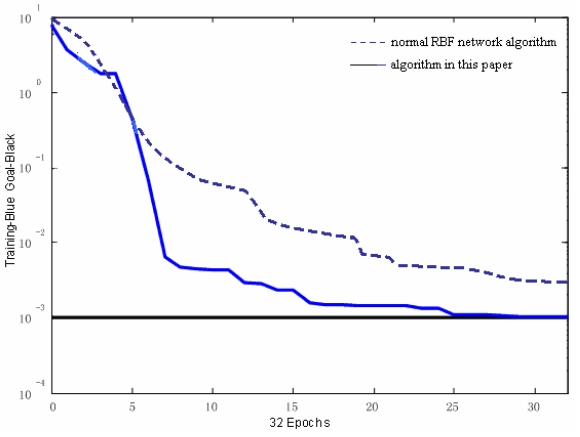

Fig. 3. Curve of neural network training error.The horizontal axis denotes the number of training steps,while the vertical axis denotes the training error.The dotted line denotes the normal RBF network algorithm ,while the continuous line denotes the training algorithm in this paper.

software of MATLAB, 32 hidden layer neurons are selected. The error curve of the network training is shown in Fig.3. It can be seen that the training algorithm for the RBF network proposed in this paper has a fast convergence rate and a high accuracy.

Finally, 5 groups of mixed inflammable gases are used to test the neural network. The training error values are shown in Table 2. It is clearly to see that most analysis error is less than 8%. According to the component fractions in the mixed gases to be detected, the single catalytic sensor can be used under different operating temperatures, the output signal of which can then be processed by the RBF neural network, which has been trained earlier. Experimental results show that the neural network can accurately calculate the actual volume fractions of the different gases in the inflammable gas mixture. And this provides a new method for the analysis of mixed inflammable gases.

Table 2. Result of mixed gas analysis

Components in the gas mixture /%			Detection results in the experiment /%		
CH_4	CO	H_2	CH_4	CO	H_2
0.20	0.015	0.022	0.18	0.019	0.025
0.35	0.036	0.028	0.40	0.034	0.031
0.50	0.020	0.083	0.51	0.026	0.084
0.61	0.052	0.055	0.58	0.052	0.057
0.86	0.085	0.100	0.89	0.083	0.098

Acknowledgments

This research was supported by the Opening Project of JiangSu Province Support Software Engineering R&D Center for Modern Information Technology Application in Enterprise (No.SX200901).

References

1. Tong, M.M., Zhang, Y., Dai, X.L.: Analysis of Mixed Inflammable Gases with Catalytic. Journal of China University Mining & Technology 35(1), 35–37 (2006)
2. Pang, O., Yang, C.R., Zhang, Y.Q.: Research on Gas Analysis of Artificial Neural Network. Chinese Journal of Scientific Instrument 20(2), 121–124 (1999)
3. Qu, J.L., Wang, L., Gao, F.: Quantitative Analysis of Gas Mixture Using an Artificial Neural Network. Journal of Northwestern Polytechnical University 21(4), 401–403 (2007)
4. Li, Y.H., Qiang, S., Zhuang, X.Y.: Robust and Adaptive Backstepping Control for Nonlinear Systems using RBF Neural Networks. IEEE Trans. on Neural Networks 15(3), 693–701 (2004)
5. Yanf, F., Paindavoine, M.: Implementation of an RBF Neural Network on Embedded Systems. IEEE Trans. of Neural Networks 14(5), 1162–1175 (2003)
6. Peng, J.X., Li, K., Huang, D.S.: A Hybrid Forward Algorithm for RBF Neural Network Construction. IEEE Trans. on Neural Networks 17(6), 1439–1451 (2006)
7. Huyberechts, G., Szecowka, P., Roggen, J.: Quantification of Carbon Monoxide and Methane in Humid Air Using a Sensor Array and an Artificial Neural Network. Sensors and Actuators 45(5), 123–130 (1997)
8. Tong, M.M.: Dynamic Analysis on Thermostatic Methane Detection with Catalytic Sensor. Journal of China University Mining & Technology 29(3), 275–278 (2003)

Image Segmentation of Level Set Based on Maximization of Between-Class Variance and Distance Constraint Function

Changxiong Zhou[1,2], Zhifeng Hu[1,2], Shufen Liu[1,2], Ming Cui[1,2], and Rongqing Xu[3]

[1] JiangSu Province Support Software Engineering R&D Center for Modern Information Technology Application in Enterprise, Suzhou, China
[2] Department of Electronic Information Engineering, Suzhou Vocational University, Suzhou, 215104, China
handzhou@sina.com
[3] College of Optoelectronic Engineering, Nanjing University of Posts and Telecommunications, Nanjing, China

Abstract. In most existing level set models for image segmentation, it is necessary to constantly re-initialize the level set function, or to acquire the gradient flow information of the image to restrict the evolution of the curve. A novel image segmentation model of level set is proposed in the paper, which is based on the maximization of the between-class variance and the distance-based constraint function. In this model, the distance-based constraint function is introduced as the internal energy to ensure that the level set function is always the signed distance function (SDF), so that the constant re-initialization of the level set function during the evolution process is avoided. Meanwhile, the external energy function (between-class variance function) is constructed based on the weighted sum of square of the difference between the average grey levels of the target region and the overall region, the background and the overall region respectively. This function is maximized to ensure that the curve represented by zero level set converges towards the target boundary stably. Experimental results show that the constant re-initialization in traditional models has been eliminated in the proposed model. Furthermore, since region information has been incorporated into the energy function, the model renders good performance in the segmentation of both weak edges images and those with Gaussian noise or impulse noise.

Keywords: Image segmentation, Between-class variance, Level set.

1 Introduction

Image segmentation is the process of separating objects of interest from background**.** It is an essential preliminary step in image processing. Over the past decades a great deal of image segmentation technique has emerged, including thresholding, active contour model and so on. One of the most commonly used methods for segmenting images is thresholding, such as mean shift, normalized cut methods [1], as well as the

D.-S. Huang et al. (Eds.): ICIC 2009, LNAI 5755, pp. 865–874, 2009.

threshold method proposed by Otsu et al. [2]. Active contour models based on the level set function are also effective methods of image segmentation. They can adapt to topological changes, break and merge automatically [3, 4, 5]. As a result, they have been extensively applied to image processing. In active contour methods, the contour energy functional is defined and then minimized so that the contour curve could move from the initial contour curve to the boundary of the desired object, following the descent flow in the energy functional [6,7,8]. These methods can often produce more robust results since relevant information such as region-based information [9], a prior information about the image [10, 11] and the distance functional constraint [12] could be incorporated into the energy functional.

Chan-Vese proposed a simplified method of MS model (C-V method) [8]. In their model, region-based information is incorporated into the energy functional as external energy, so that global segmentation is enabled, the requirements on the initial location of the curves represented by the zero level set are greatly reduced, and the robustness against noise is greatly enhanced. However, in their model, the internal energy functional only ensures that the curve represented by zero level set is smooth. As a result, it is necessary to re-initialize the level set functional to keep it close to the signed distance function in practical applications, which significantly increases the load of calculation. Although the re-initialization methods have been improved by many researchers, the results are still unsatisfactory. A level set image segmentation approach is proposed by Li et al. that does not involve re-initialization [10]. However, since the edge gradient information of the image is taken into consideration instead of the global information of the image, it is hard to obtain satisfactory results when the method is applied to the segmentation of images with weak edges. In this paper, the difference between the object and its background region is described by the external energy functional, which is constructed as a weighted sum of two terms. The first term is the square of the difference between the average gray values of the object and the whole image region. The second term is the square of the difference between the average gray values of the background region and the whole image region. An image segmentation method based on the maximization of the between-class differences under the distance function constraint is proposed in this paper, which effectively eliminates the need for re-initialization in traditional models. Also, since regional information is incorporated into the energy function, good segmentation results can be obtained when this method is applied to the segmentation of images with weak edges and those with noise.

2 Level Set with Li et al. Model

Given a closed contour curve C on a given plane, if $\phi(x, y)$ is the shortest distance from the point (x, y) to curve C , $\phi(x, y)$ is called the signed distance function, where $\phi(x, y) < 0$ if point (x, y) is inside the curve C , $\phi(x, y) > 0$ if point (x, y) is outside the curve C , and $\phi(x, y) = 0$ if point (x, y) is on the curve C . A level set is defined as a set of points with a fixed value of SDF. As a special case, the zero level set stands for the set of points that satisfy $\phi(x, y) = 0$, which describes a closed curve C on a plane. The level set function represents implicitly the contour curves of the active contour

model, while effectively eliminating the need of tracking the curve. The level set methods convert the problem of the movement of the contour curve into a problem involving the solution of a numerical partial differential equation represented as $\{(x, y), \phi(x, y, t) = 0\}$. In order to ensure the smoothness of the contour curve and the stable evolution of the curve toward the border of the object, it is necessary to constantly re-initialize the level set function during iteration to keep it close to the signed distance function. As a result, the load of computation is increased. The standard re-initialization method is to solve the following re-initialization equation:

$$\frac{\partial \phi}{\partial t} = \text{sgn}(\phi)(1 - |\nabla \phi|) \cdot \tag{1}$$

Where $\text{sgn}(\cdot)$ is the signed function, ∇ donates the gradient operator. In the actual iterative process, the level set will often deviate from the signed distance function, in which case the re-initialization of the level set function would become impossible to implement. Moreover, this phenomenon cannot be eliminated even if one round of re-initialization is carried out for every iteration. To completely eliminate this phenomenon, it is necessary to set the iteration time interval parameter Δt small enough. However, this would seriously affect the speed of evolution of the level set, thus unable to meet the requirements of practical applications. In the Image segmentation method based on the active contour model, the contour energy functional is defined and then minimized so that the contour curve could move from the initial contour curve to the boundary of the desired object, following the descent flow in the energy functional. The energy functional is defined by Li et al. as:

$$E(\phi) = \mu E_{\text{int}}(\phi) + E_{extr}(\phi) \cdot \tag{2}$$

Where $E_{\text{int}}(\phi)$ denotes the internal energy term, $E_{extr}(\phi)$ denotes the external energy term, and $\mu > 0$ is a parameter. Considering that the level set function needs to meet the requirement of the signed distance function, i.e., $|\phi| \equiv 1$, the internal energy function $E_{\text{int}}(\phi)$ can be defined as

$$E_{\text{int}}(\phi) = \iint_{\Omega} \frac{1}{2}\left(|\nabla \phi| - 1\right)^2 \cdot \tag{3}$$

Where Ω denotes image region. The expression (3) is formulated as a metric to characterize how close the function ϕ is to the signed distance function. By minimizing the expression in (3), $|\phi|$ can be made to converge to 1, so that the level set function is made close to the signed distance function. The greatest strength of this model lies in the fact that once an appropriate level set function is specified during initialization and made to converge to the signed distance function under the constraint of the internal energy (the distance constraint function), there is no need to re-initialize the level set. In Li et al. method, the external energy function is defined as

$$E_{extr}(\phi) = \lambda E_{extr\,1}(\phi) + \upsilon E_{extr\,2}(\phi) \cdot \tag{4}$$

$$E_{extr\,1}(\phi) = \iint_{\Omega} g\,\delta(\phi)\left|\nabla\phi\right| dxdy \cdot \tag{5}$$

$$E_{extr\,2}(\phi) = \iint_{\Omega} H(-\phi)\,dxdy \cdot \tag{6}$$

Where g stands for the edge indicator function of an image I defined as $g = \frac{1}{1+\left|\nabla G * I(x,y)\right|^2}$, G is the Gaussian operator, $*$ denotes the convolution integral, δ is the Dirac function, and H is the Heaviside step function. In Li et al. model, the edge gradient information of the image is taken into account instead of the global information of the image. As a result, good results can be obtained as long as the method is applied to the segmentation of images with distinct boundaries of the desired object.

3 Improving Energy Function and Represented by Level Set

Energy function plays a key role in the level set contour model. When there are only piecewise smooth areas of the object and its background in the image, let A denote the total area of the image $I(x,y)$ on the region Ω, which is divided by the curve C into two homogeneous regions, namely, Ω_1 of the object (inside C) and Ω_2 of the background (outside C). Let A_1, A_2 stand for the areas of the two regions respectively and let c_1, c_2 stand for the average gray values of the two regions respectively. Let C stand for the average gray value of the whole image. The energy functional can be defined as follows:

$$E(\phi) = \lambda_1 E(\phi) + \lambda_2 E(\phi) \cdot \tag{7}$$

$$E_1(\phi) = \iint_{\Omega} \frac{1}{2}(\left|\nabla\phi\right| - 1)^2\,dxdy \cdot \tag{8}$$

$$E_2(\phi) = -\frac{A_1}{A}(c_1 - c)^2 - \frac{A_2}{A}(c_2 - c)^2 \cdot \tag{9}$$

Where $c_1 = \frac{\iint_{\Omega} I(x,y)(1-H(\phi))\,dxdy}{A_1}$, $c_2 = \frac{\iint_{\Omega} I(x,y)H(\phi)\,dxdy}{A_2}$, $A = \iint_{\Omega} dxdy$, $A_1 = \iint_{\Omega} (1-H(\phi))\,dxdy$, $A_2 = \iint_{\Omega} H(\phi)\,dxdy$. The parameters λ_1 and λ_2 in Eqn. (7) are both greater than 0. The internal energy function in Eqn. (8) is the distance constraint function, which ensures that the level set function converges to the signed distance function, so that the need to re-initialize the level set function is eliminated, the load of computation is reduced and the speed of operation is increased. Moreover, since the level set function converges to the distance function, the curve represented by the zero level set becomes smooth. The external energy in Eqn. (9) is described by the variance between the object region and its background region, as represented by a weighted sum of the square of the difference between the average gray values of the

object and the whole image region and the square of the difference between the average gray values of the background region and the whole image region. As the curve evolves from the initial position to the actual object boundary, the between-class variance grows to its maximum. At this point, the curve C successfully completes the task of image segmentation, dividing the image into the object region that lies inside it and the background region that lies outside it. As the region information is incorporated into the external energy function in the model, image segmentation for images with weak boundaries is enabled and the robustness against noise is enhanced.

In this paper, we denote by $\frac{\partial E}{\partial \phi}$ the Gateaux derivative (or first variation) of the functional E. From (8) and (9), we have:

$$\partial E_1 / \partial \phi = -[\Delta \phi - div(\nabla \phi / |\nabla \phi|)] \cdot \tag{10}$$

$$\begin{aligned} \frac{\partial E_2}{\partial \phi} = & -\frac{1}{A}[(c_1 - c)^2 + A_1 2(c_1 - c)\frac{I - c_1}{A_1}](-\delta(\phi)) \cdot \\ & -\frac{1}{A}[(c_2 - c)^2 + A_2 2(c_2 - c)\frac{I - c_1}{A_2}]\delta(\phi) \end{aligned} \tag{11}$$

The formulation (11) can be simply written as

$$\partial E_2 / \partial \phi = (1/A)[(c_1 - c)(2I - c - c_1) - (c_2 - c)(2I - c - c_2)]\delta(\phi) \cdot \tag{12}$$

The following evolution equation is the gradient flow that minimizes the functional E:

$$\partial \phi / \partial t = -\partial E(\phi) / \partial \phi \cdot \tag{13}$$

The partial differential equation (PDE) for the level set corresponding to (7) is:

$$\begin{aligned} \frac{\partial \phi}{\partial t} = & \lambda_1[\Delta \phi - div(\frac{\nabla \phi}{|\nabla \phi|})] + \lambda_2 \frac{1}{A}[-(c_1 - c)(2I - c - c_1) \cdot \\ & + (c_2 - c)(2I - c - c_2)]\delta(\phi) \end{aligned} \tag{14}$$

The improved level set evolution model in (14) is called level set image segmentation method based on the maximization of the between-class variances and the distance constraint function. According to curve evolution theory, the movement equation of the curve with respect to time t is represented as follows:

$$\partial C / \partial t = F\boldsymbol{n} \cdot \tag{15}$$

Where F is the velocity, and $\boldsymbol{n}$ is the inner normal direction of the curve C. The contour C shrinks when $F > 0$ and expands when $F < 0$. The movement of the curve can be represented by either (14) or (15), with (14) utilizing the level set function for the representation of the movement of the curve.

Without loss of generality, assume that the average gray value of the object region c_1 is smaller than the average gray value of the background region c_2, so that $c_1 < c_2$ and $c_1 \le c \le c_2$. Let $F_1 = -(c_1 - c)(2I - c - c_1)$ and $F_2 = -(c_2 - c)(2I - c - c_2)$.

When $I < \frac{c+c_1}{2}$, F_1 and F_2 take negative values. When $I > \frac{c+c_2}{2}$, F_1 and F_2 take positive values. To understand the meaning of (14), let $I(x, y)$ denote the gray value of the point (x, y). When $I > \frac{c+c_2}{2}$, $F_1 + F_2 > 0$ and the contour curve C represented by the zero level set function shrinks. When $I < \frac{c+c_1}{2}$, $F_1 + F_2 < 0$ and the contour curve C represented by the zero level set function expands. When $\frac{c+c_1}{2} < I < \frac{c+c_2}{2}$, the contour curve C represented by the level set function converges stably to the object boundaries as controlled by the internal energy functional. As a result, the image is segmented by the contour curve C into the object region inside C and the background region outside C.

4 Experimental Results and Analysis

Medical image segmentation is an indispensable technique for extracting quantitative information of special tissues from medical images. However, the boundaries of the organs and lesions are inherently fuzzy and inhomogeneous in medical images. Moreover, noise is often introduced into medical images during the imaging process. As a result, there is considerable difficulty in the segmentation of such images with weak object boundaries. In the experiment, a computer with CPU Pentium(R) D 3.00GHz/ Memory 1GB/Matlab6.5 is used. The method proposed in this paper is applied on CT medical images of the Lateral Ventricle whose sizes are 385×393 pixels. Unless otherwise specified, the following parameters are used in this paper: $\mu = 0.04$, $\lambda = 5$, $\upsilon = 3$, $\lambda_1 = 0.04$, and $\lambda_2 = 1$.

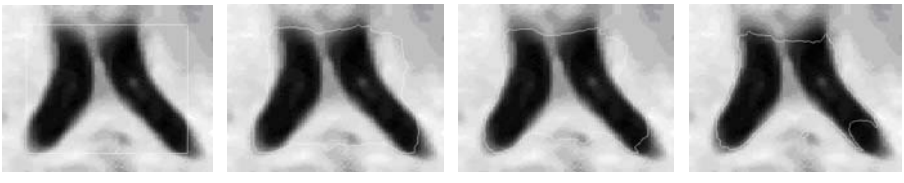

(a) (b) (c) (d)

Fig. 1. Image segmentation of Lateral Ventricle based on Li et al. model. (a) The initial contour. (b) 100 iterations. (c) 200 iterations. (d) 400 iterations.

Fig. 1 shows the image segmentation results on the Lateral Ventricle images using the Li et al. model, with the energy function taking the forms in Eqn.(2),(3)and(4). For these images, we used the parameters $\mu = 0.04$, $\lambda = 5$, and $\upsilon = 3$. The initial contour curve is the white rectangle in the Lateral Ventricle image shown in Fig. 1(a). The curve evolution takes respectively 100,200,400 iterations in Fig. 1(b), 1(c), 1(d). As the number of iterations increases, the contour curve crosses the boundaries and shrinks continuously. Since Li et al. model is a segmentation model based on edges in

the images, and the object boundaries are blurred in the Lateral Ventricle image, the contour curve can easily cross the weak boundaries under the control of the external energy in this case. As a result, the correct segmentation result can't be obtained using Li et al. model in this case.

The image segmentation result on the Lateral Ventricle image using the improved model that includes (7) as the energy functional and (14) as the level set is shown in Fig.2. For this image, we used the parameters $\lambda_1 = 0.04$, and $\lambda_2 = 1$. The 385×393 pixel image of the Lateral Ventricle is shown in Fig. 2(a), where the initial contour curve is provided by the white rectangle. The curve evolution takes respectively 100,200 and 400 iterations in Fig. 2(b), 2(c) and 2(d). Let $I(x, y)$ denote gray value of point (x, y). When the contour curve is in the background region, $I > \frac{c + c_2}{2}$ and the contour curve represented by the zero level set shrinks. Since the region information, which includes the average gray values of the object region and the background region, is incorporated into the improved model, the correct image segmentation result of the Lateral Ventricle image with weak boundaries is obtained when the evolution exceeds 400 iterations. As the number of iterations continues to grow, the contour curve stops evolution and stabilizes at the segmentation result.

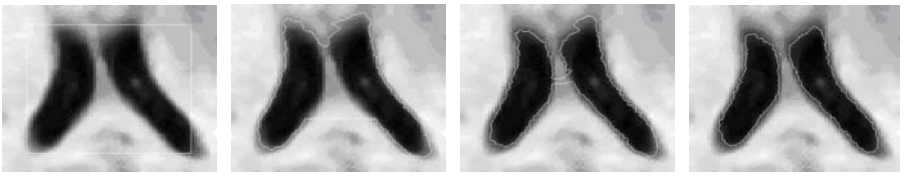

(a) (b) (c) (d)

Fig. 2. Image segmentation of Lateral Ventricle based on the proposed model. (a) The initial contour. (b) 100 iterations. (c) 200 iterations. (d) 400 iterations.

The image segmentation result on the Lateral Ventricle image with Gaussian noise using the improved model that includes (7) as the energy functional and (14) as the level set is shown in Fig.3. For this image in Fig.3, we used the parameters $\lambda_1 = 0.04$, and $\lambda_2 = 1$. The 385×393 pixel image of the Lateral Ventricle with Gaussian noise is shown in Fig. 3(a), where the initial contour curve is provided by the white rectangle. The Gaussian noise has a mean value of 0 and a standard deviation of 0.0001. The curve evolution takes respectively 100,300,600 iterations in Fig. 3(b), 3(c), 3(d). Compared with the case shown in Fig.2, due to the addition of the Gaussian noise in the case shown in Fig.3, the difference between the average gray values of the region inside the contour curve C and the region outside C decreases, i.e., the speed corresponding to the external energy function becomes smaller. Therefore, the evolution of the contour curve becomes slower. Using the improved model, the correct image segmentation result of the Lateral Ventricle image with weak boundaries is obtained when the number of iterations reaches 600. Compared with the case shown in Fig.2, 200 more iterations are needed to obtain the correct result.

(a) (b) (c) (d)

Fig. 3. Gaussian noise image segmentation of Lateral Ventricle based on the proposed model. (a) The initial contour. (b) 100 iterations. (c) 300 iterations. (d) 600 iterations.

The image segmentation result on the Lateral Ventricle image with impulse noise using the improved model that includes (7) as the energy functional and (14) as the level set is shown in Fig.4.

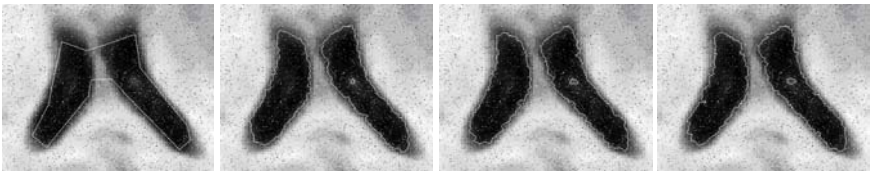

(a) (b) (c) (d)

Fig. 4. Impulse noise image segmentation of Lateral Ventricle based on the proposed model. (a) The initial contour. (b) 100 iterations. (c) 300 iterations. (d) 400 iterations.

For this image, we used the parameters $\lambda_1 = 0.04$, and $\lambda_2 = 1$. The 385×393 pixel image of the Lateral Ventricle with impulse noise is shown in Fig. 4(a). The impulse noise has a density of 0.04. The initial contour curve is provided by the white curve, most of which is located inside the object region and is close to the object boundary. Let $I(x, y)$ denote gray value of point (x, y) . When the contour curve is in the object region, $I < \frac{c + c_1}{2}$ and the contour curve represented by the zero level set expands. When the contour curve is in the background region, $I > \frac{c + c_2}{2}$ and the contour curve represented by the zero level set shrinks. As the number of iterations grows, the contour curve converges to the object boundary. Since the initial curve is close to the object boundary, the contour curve successfully converges to the object boundary when the number of iterations reaches 400. It can be seen from Fig.4 that the addition of the strong impulse noise into the left Lateral Ventricle area in the middle has increased the average gray value of this region to a high value. As a result, the region is isolated when image segmentation based on the proposed improved model is applied to the image.

In Fig.5, we segment respectively Lateral Ventricle images with Gaussian noise and with impulse noise, applying the model proposed by Li et al. in which the parameters are set as $\mu = 0.04$, $\lambda = 5$ and $\upsilon = 3$. The image segmentation results on the Lateral Ventricle image with Gaussian noise are shown in Fig. 5(a) and (b), where

300 and 600 iterations have been carried out on the initial contour curve as shown in Fig.3(a). The image segmentation results on the Lateral Ventricle image with impulse noise are shown in Fig. 5(c) and (d), where 100 and 300 iterations have been carried out on the initial contour curve as shown in Fig.4(a).

It can be seen from Fig.5 that since the model proposed by Li et al. is an edge-based information model, the correct segmentation of the Lateral Ventricle image with Gaussian noise and impulse noise cannot be obtained based on it, whether the initial contour is located inside the object region or in the background region.

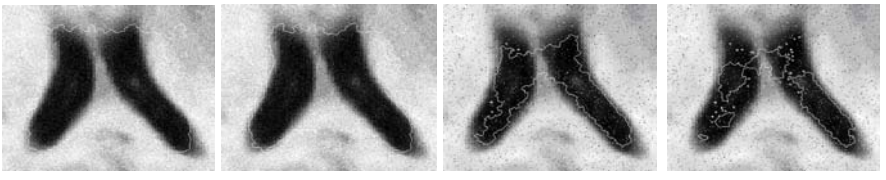

(a) (b) (c) (d)

Fig. 5. Iimage segmentation based on Li et al. model for Lateral Ventricle with Gaussian noise and impulse noise. (a) 300 iterations with Gaussian noise. (b) 600 iterations with Gaussian noise. (c) 100 iterations with impulse noise. (d) 300 iterations with impulse noise.

5 Conclusions

In this paper, a novel image segmentation model of level set function is proposed based on the maximization of the between-class variance and the distance-based constraint function. The energy function in this model consists of the external energy function and the distance constraint function. The distance constraint function is introduced as the internal energy to penalize the deviation of the level set function from a signed distance function, so that the constant re-initialization of the level set function during the evolution process is avoided. In addition, since the level set function is kept close to a signed distance function, the contour curve represented by the zero level set function converges smoothly. The external energy is represented by the between-class variance, which leads the contour curve to evolve from its initial position towards the object boundaries. Whether the initial contour curve is placed inside or outside the object, and no matter the image has Gaussian noise or impulse noise, the contour curve can converge to the object boundary correctly so that the image can be segmented correctly, since region information has been incorporated into the energy function in the model. In addition to the edge information incorporated into the Li et al. model, region information has been incorporated into the improved model, so that good performance can be achieved when it is applied to the segmentation of images with weak edges and those with Gaussian noise or impulse noise.

Acknowledgements

This research was supported by the Opening Project of JiangSu Province Support Software Engineering R&D Centerfor Modern Information Technology Application in Enterprise. (No. SX200906).

References

1. Tao, W., Jin, H., Zhang, Y.: Color Image Segmentation Based on Mean Shift and Normalized Cuts. IEEE Trans. Syst., Man, Cybern. B, Cybern. 37(5), 1382–1389 (2007)
2. Sahoo, P.K., Soltani, S., Wong, A.: A Survey of Thresholding Techniques. Computer Vision, Graphics and Image 41, 233–260 (1988)
3. Osher, S., Fedkiw, R.: Level Set Methods and Dynamic Implicit Surfaces. Cambridge University Press, New York (2003)
4. Sethian, J.: Level Set Methods and Marching Methods, 2nd edn. Springer, New York (1999)
5. Han, X., Xu, C., Prince, J.L.: A Topology Preserving Level Set Method for Geometric Deformable Models. IEEE Trans. PAMI 25(6), 755–768 (2003)
6. Kichenassamy, S., Kumar, S., Olver, P., Tannenbaum, A., Yezzi, A.: Conformal Curvature Flow: From Phase Transitions to Active Vision. Archives for Rational Mechanics and Analysis 134(3), 275–301 (1996)
7. Caselles, V., Kimmel, R., Sapiro, G.: Geodesic Active Contours. Int. J. Comput. Vis. 22(1), 61–79 (1997)
8. Vese, L., Chan, T.: A Multiphase Level Set Framework for Image Segmentation Using the Mumford and Shah Model. International Journal of Computer Vision 50(3), 271–293 (2002)
9. Chan, T., Vese, L.: Active Contours without Edges. IEEE Trans. on Image Processing 10(2), 266–277 (2001)
10. Zhu, S., Yuille, A.: Region Competition: Unifying Snakes, Region Growing, and Bayes/MDL for Multiband Image Segmentation. IEEE Trans. PAMI 18(9), 884–900 (1996)
11. Chen, Y., Tagare, H., Thiruvenkadam, M.S.R., Huang, F., Wilson, D., Geiser, A., Gopinath, K., Briggs, R.: Using Prior Shapes in Geometric Active Contours in A Variational Framework. International Journal of Computer Vision 150(3), 315–328 (2002)
12. Li, C., Xu, C., Gui, C., Martin, D.F.: Level Set Evolution without Re-initialization: A New Variational Formulation. In: IEEE International Conference on Computer Vision and Pattern Recognition (CVPR), San Diego, 20-25 June, vol. 1, pp. 430–436 (2005)

Active MMW Focal Plane Imaging System

Pingang Su[1,2], Zongxin Wang[2], and Zhengyu Xu[2]

[1] Department of Electronic Information Engineering, Suzhou Vocational University, Suzhou215104, Jiangsu, China
[2] State Key Lab of Millimeter Wave, Southeast University, Nanjing 210096, Jiangsu, China
supg@jssvc.edu.cn

Abstract. Millimeter wave imaging technology has received a lot of attention in recent years. It has been widely applied in aircraft landing guidance system, dangerous substance inspection, plasma tests and human carry on safety inspection. It can be applied in many areas in the future. This paper studies an active millimeter wave focal plane imaging system. Among the theory and key techniques of millimeter wave imaging, the optical imaging system is designed and automatic scanning, automatic data collection and image processing are implemented. In the experiment system, the automatic focal plane scanning of the receiver antenna array, data collection around the imaging spots of the 94GHz millimeter wave, automatic imaging and image optimization are carried out at the computer. The experiment verifies the practicability of the design of the diffractive lens and the detection of hidden objects.

Keywords: MMW, Focal plane, Imaging, Diffractive lens, Test system.

1 Introduction

Millimeter wave imaging technology derives from the electric magnetic theory and optical imaging theory. This technology can be widely applied in the aircraft landing guidance system, dangerous substance inspection, plasma tests, buries detection and safety inspection of human carrying covered arms. Millimeter technology appeared in the end of the 30s of the 20th century [1-2]. However, due to the limitation of the millimeter equipments, it developed slowly during the past 50 years. In the nineties of the 20th century, because the millimeter equipments developed quickly and the demand for safety arises, it became a hot research area. This paper studies the application of millimeter technology in human carry on safety inspection [2-3, 7-8].

There are many types of millimeter technology and each has its own characteristics. According to the radiation source, the millimeter wave imaging technology is sorted to be passive [5, 9] and active [7]. According to the imaging process, it can be classified into focal plane imaging [4] and holographic imaging [6]. In term of the pixel scanning scheme, it can be classified into mechanical scanning and electronic scanning [10].

D.-S. Huang et al. (Eds.): ICIC 2009, LNAI 5755, pp. 875–881, 2009.

Millimeter wave imaging has many advantages. Compared with X-ray imaging, it is safe for the human body. Compared with optical and infrared optical imaging, it has a deeper inspection distance and a smaller influence from the clothing material. However, millimeter wave imaging has some apparent disadvantages too. The equipments have a relatively larger volume. It also has a relatively low resolution. The mechanical scanning scheme renders a poor real time performance. However, the technological development during the recent decades has improved hardly the performance of the mechanical scanning model.

Considering the fact that millimeter wave focal plane imaging has a good real time performance and the main application situation in the future will be indoors, the prototype machine used in this research is based on millimeter wave focal plane imaging [12-13]. The system provides a good diffractive lens focal plane imaging quality. It is capable of automatic mechanical scanning, data collection and image processing. After a few months' testing, it shows a good stability and adaptability. It can be used as a platform for practical imaging systems in the future.

2 The Imaging Process of the Prototype Machine

The prototype machine designed in this paper is based on active focal plane imaging. In passive millimeter wave imaging, the radiation source is from outer space. Because the atmosphere has different absorption rates for different electromagnetic waves, several millimeter wave frequency bands are formed in the atmosphere, respectively around 35GHz, 94GHz and 120GHz. In general, passive millimeter wave imaging system can selects the 94 GHz frequency band. The above-mentioned does not need additional radiation source. However, when the imaging environment has to be outdoors it has a poor frequency band selection quality. Compared with passive millimeter wave imaging technique, active one needs additional radiation source. As a result, the imaging process is not limited by the application environment. If it were necessary, broad spectrum scanning could be used to improve the imaging quality.

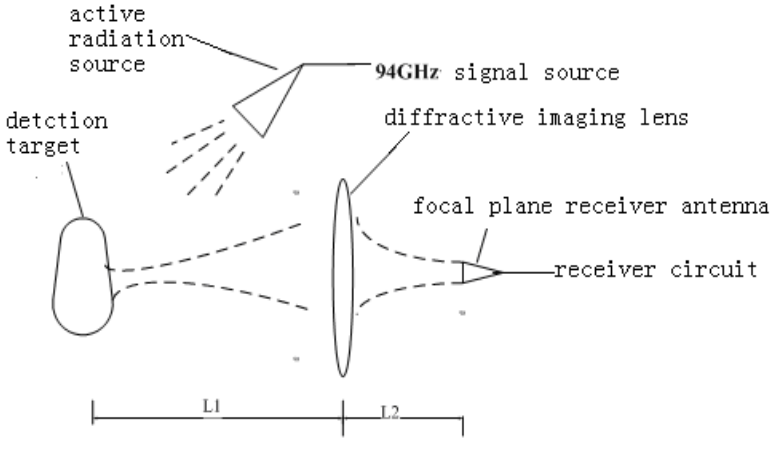

Fig. 1. The active millimeter wave imaging system

The active millimeter wave imaging system applies optical imaging principles in millimeter wave imaging. The whole system is similar to optical imaging system, as shown in Figure 1. The radiation source emits 94GHz continuous millimeter wave through an angular antenna onto the target. After reflected by the target, the millimeter wave runs through a finer diffractive lens and focuses into diffraction spots with different intensities on the image plane. The intensity of the diffraction spots at different positions corresponds to the reflection quality on the millimeter wave of the target. The diffraction spots are detected and received by antenna arrays on the focal plane, forwarded to the receiver and transformed into low frequency band. Finally, the computer analyzes the wave and applies image processing techniques to render the image.

In the imaging system designed in this paper, the receiver antenna array is run by the computer to carry out two dimensional scanning. The computer then processes the intensity data and carries out image processing techniques to render the image.

3 The Design and Analysis of the Imaging Diffractive Lens

Imaging diffractive lens is one of the key techniques used in millimeter wave focal plane imaging. The idea of diffractive lens comes from the diffraction theory in optics. It was first proposed by physicists such as Fresnel and Rayleigh during their research in optics [16]. This idea was first applied in millimeter wave frequency band in America in 1936[15]. Compared with traditional defective lens, diffractive lens is thin, light and has a lower consumption rate. Our research uses diffraction imaging lens, and studies in depth its imaging characteristic. Figure 2 show the structural plane and focal characteristic of the diffractive lens with a diameter of 250mm used in the experiment system [12-13].

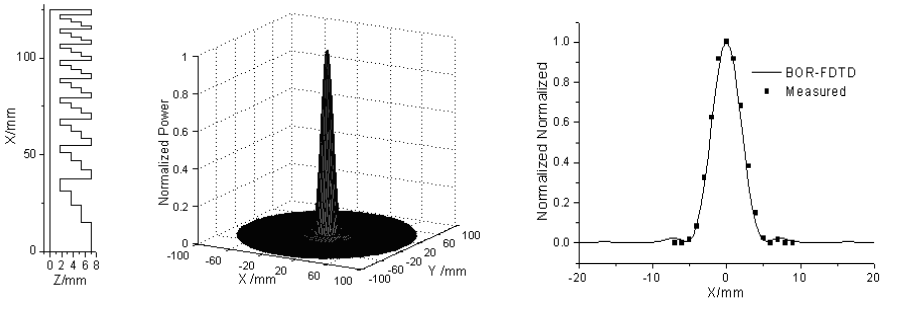

(a) (b)

Fig. 2. (a) Power distribution on the cross-section and focal plane of the diffractive lens; (b) Power distribution on the central optical axis

The lens in the experiment system has a focal length of f=250mm, whereas the number of f equals 1, the diameter of the lens is D=250mm, and the working wave length is λ=3.19mm. As a result, the imaging resolution on the focal plane is:

$$\eta=1.22*f*\lambda/D=3.89. \quad (1)$$

4 The Software and Hardware Implementation of the Receiver Antenna Scanning and Data Collection

This system uses a receiver antenna to carry out two dimensional mechanical scanning on the imaging focal plane in order to measure the distribution of the diffraction spots on the focal plane. The two dimensional mechanical scanning is implemented with the computer controlling two stepper motors in two directions. The millimeter wave intensity is measured by the spectrum analyzer. The computer collects real time data through the network port.

The hardware of the system showed in Figure 3 includes the two dimensional mechanical scanning structure run by the stepper motors, the single-chip circuit for the stepper motor controllers, the computer and the spectrum analyzer.

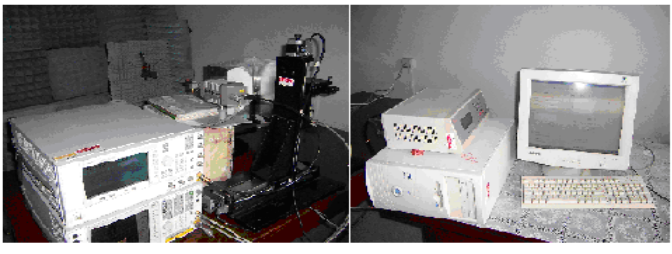

Fig. 3. The millimeter wave focal plane imaging system

In the design of the software, the computer is programmed to control the stepper motors through serialized port. The communication of the spectrum analyzer (controlling and data transfer) is realized through the network port. The controlling and data collection are programmed to be synchronized. The software process is shown in Figure 4.

5 The Performance Quality of the System and the Imaging Result

The system uses mechanical scanning, for which the scanning step can be adjusted. The current resolution of the system is 3.89mm, and the scanning step is set as 2.5mm. This system scans an image made of 41*41 pixels during a time length of 12min. Since March, 2007, a dozen of imaging experiments have been carried out on this system. Figure 5 shows an optical image, for which the millimeter wave imaging result is shown in Figure 6. A comparison is made between the two situations where a handgun is covered and uncovered by some clothing.

Figure 7 shows the image processing results using Origin, which can be compared with the direct imaging results.

As shown in these figures, the covering of the clothing on the handgun does not deteriorate the imaging results on the focal plane. This system can be used to detect metal objects such as handguns which are hidden under clothing.

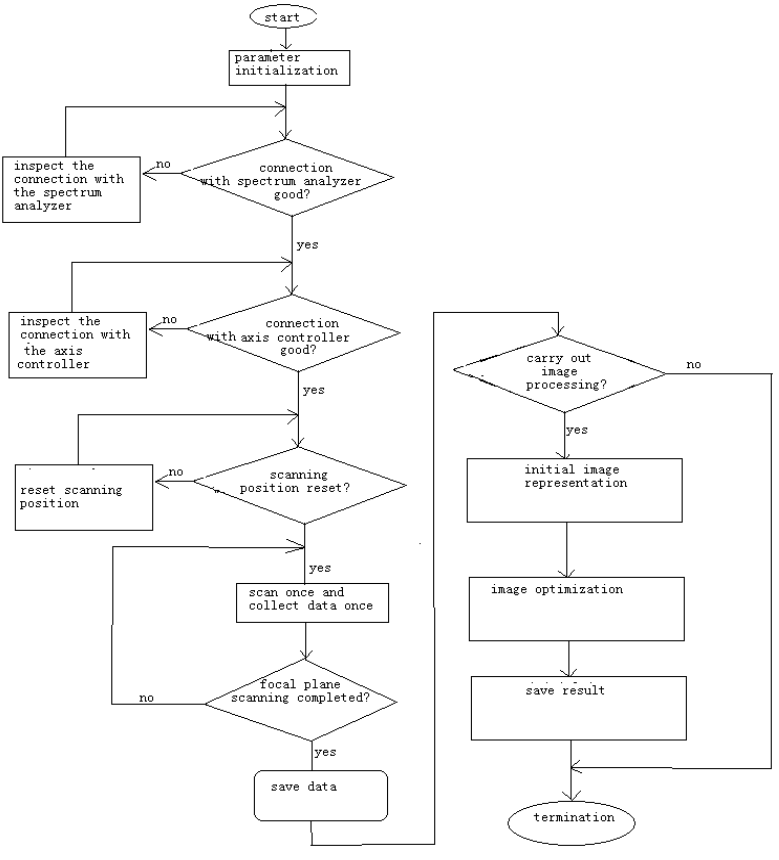

Fig. 4. Program flow chart

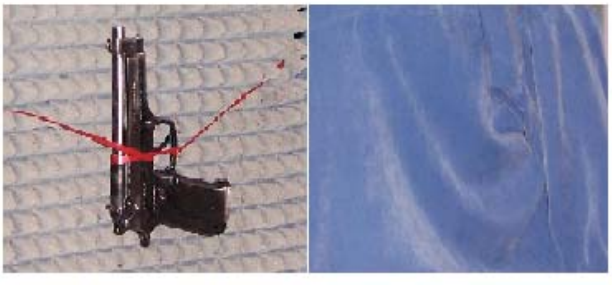

Fig. 5. The optical photo of the handgun (left) and the optical photo of the handgun covered by clothing (right)

This paper studies millimeter imaging theory and its key techniques. The imaging optical system is designed and automatic scanning, automatic data collection and

image processing are implemented. The practicability of the design of the diffractive lens and the detection of hidden objects are verified.

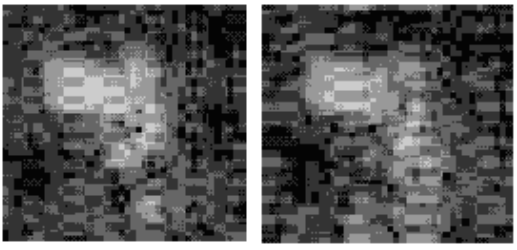

Fig. 6. The millimeter wave focal plane imaging of the handgun (left) and the millimeter wave focal plane imaging of the handgun covered by clothing (right)

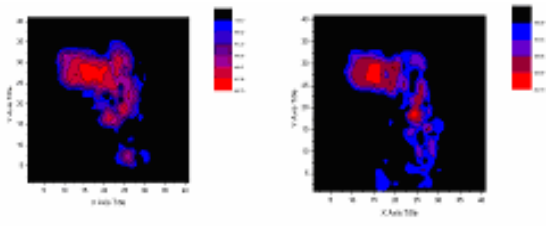

Fig. 7. The millimeter wave focal plane imaging of the handgun (left) and the millimeter wave focal plane imaging of the handgun covered by clothing (right) after processing using Origin

6 On-Going Improvements of the System

Improvements on the system are currently underway, which include: Using a diffractive lens with a larger diameter in order to increase the angular resolution; The further optimization of the receiver antenna array and its peripheral signal processing circuit; A better simulation of diffusion of the radiation source and the further optimization of the image processing techniques. Upon the completion of such improvements, the resolution, imaging quality and real time performance of the system will be greatly improved.

References

1. Wiltse, J.C.: History of millimeter and submillimeter waves. IEEE Trans. Microwave Theory and Techniques 32, 1118–1127 (1984)
2. Appleby, R., Gleed, D.G., Anderton, R.N.: Advances in passive millimetre wave imaging. In: Proc. SPIE, vol. 2211, pp. 312–317 (1994)
3. Lettington, A., Qi, H.H., Dean, A.: An Overview of Recent Advances in Passive Millimetre Wave Imaging in the UK. In: Proc. SPIE, vol. 2744, pp. 146–153 (1996)

4. Goldsmith, P.F., Hsieh, C.T., Huguenin, G.R.: Focal Plane Imaging Systems for Millimeter Wavelengths. IEEE Transaction on Microwave Theory and Techniques 41(T10) (1993)
5. Gleed, D.G., Appleby, R., Salmon, N.A.: Operational issues for passive millimetre wave imaging systems. In: Proc. SPIE, vol. 3064, pp. 22–33 (1997)
6. McMakin, D.L., Sheen, D.M., Collins, H.D.: Millimeter wave, high reso1ution, holographic surveillance system. In: Proc. SPIE, vol. 2092, pp. 525–535 (1993)
7. Grossman, N., Miller, A.J.: Active Millimeter-wave Imaging for Concealed Weapons Detection. In: Proc. SPIE, vol. 5077, pp. 62–70 (2003)
8. Chen, H.M., Lee, S., Rao, R.M.: Imaging for Concealed Weapon Detection. IEEE Signal Processing Magazine, 52–61 (2005)
9. Sinclair, G.N., Anderton, R.N., Appleby, R.: Passive millimetre-wave concealed weapon detection: Enabling Technologies for Law Enforcement and Security. In: Proc. SPIE, vol. 4232, pp. 142–151 (2001)
10. Appleby, R., Anderton, R.N., Price, S., Salmon, N.A.: Mechanically scanned real time passive millimetre wave imaging at 94GHz: Passive Millimeter-Wave Imaging Technology VI and Radar Sensor Technology VII. In: Proc. SPIE, vol. 5077, pp. 1–6 (2003)
11. Haworth, C.D., Petillot, Y.R., Trucco, E.: Image processing techniques for metallic object detection with millimetre-wave images. Pattern Recognition Letters 27, 1843–1851 (2006)
12. Wang, Z.X.: Study on the application of defective and diffractive instruments in millimeter wave single pulse antenna and focal plane imaging. Doctoral thesis. Southeastern University, China (2006)
13. Mei, Z.L.: Analysis of defective and diffractive lens focal field in small f number millimeter wave imaging. Doctoral thesis. Southeastern University, China (2004)
14. Agilent Technologies: Agilent PSA and ESA Series Spectrum Analyzers Measurement Guide and Programming Examples (April 2004)
15. Bruce, E.: Directive Radio System. U. S. Patent 2,169,553, August 15 (1939)
16. Jenkins, F.A., White, H.E.: Fundamental of Optics, 4th edn., pp. 380–381. McGraw-Hill Book Company, New York (1976)

Application of RBF Network Based on Immune Algorithm in Human Speaker Recognition

Yan Zhou[1,2] and Xinming Yu[1,2]

[1] Jiangsu Research & Development Centre for Modern Enterprise Information Software Engineering, Suzhou 215104, Jiangsu, China
[2] Department of Electronics & Information Engineering, Suzhou Vocational University, Suzhou, 215104, Jiangsu, China
zhyan@jssvc.edu.cn

Abstract. When using traditional clustering algorithms based on Radial Basis Function(RBF)network to recognize human speakers, it is hard to decide the numbers and locations of the cluster centers. To overcome these shortcomings, this paper proposes an RBF network based on artificial immune mechanism for human speaker recognition. The artificial immune mechanism can adaptively compute the number and initial locations of the centers in the hidden layer of the RBF network based on the audio sample data set. Experimental tests show that the system has a fast learning speed for network weights. The system is very good at searching for global optimum. It has a high recognition rate and is a new practical method for human speaker recognition.

Keywords: Human Speaker Recognition, RBF Network, Immune Algorithm.

1 Introduction

Human Speaker Recognition is used to extract the voice features from the speech samples and analyze them , so that human speakers can be differentiated and recognized [1,2]. Generally, Human Speaker Recognition is mainly comprised of three parts [3], It can be seen from fig 1, collecting speech samples and extracting the speech features; obtaining the speaker's voice codebook through computation based on immune algorithm, which is also called training; comparing the features from the speech samples in application with those in the codebook to make decisions, which is also called recognition.

In Human Speaker Recognition, the Vector Quantization (VQ)technique is used to carry out clustering analysis on the speech features of the Human Speaker, so that a model of the Human Speaker can be constructed based on a codebook of the cluster centers. Currently, the k-means method and LBG algorithm have been mainly used for the clustering process. In [4], the k-means method is used for the clustering of the speech sample data. This algorithm is simple, fast and capable of processing large databases. However, it could result in different clustering results when initiated with different initial values. Moreover,

D.-S. Huang et al. (Eds.): ICIC 2009, LNAI 5755, pp. 882–889, 2009.

the algorithm may result in local minimums since it is a clustering algorithm based on target functions. To overcome the shortcomings stated above, genetic algorithm (GA)is used in [5] to optimize the target function. However, experiments show that as the number of samples, clusters and dimension grow, the clustering methods based on genetic algorithm may often become premature. Artificial immune system [6] is starting to be widely used in recent years. It has become a research hotspot following fuzzy logic, neural network and genetic algorithm in the field of intelligent systems. Many artificial immune models and algorithm have been proposed in recent years. As the field continues to grow, it is providing many new solutions to the problems stated above [7-9].

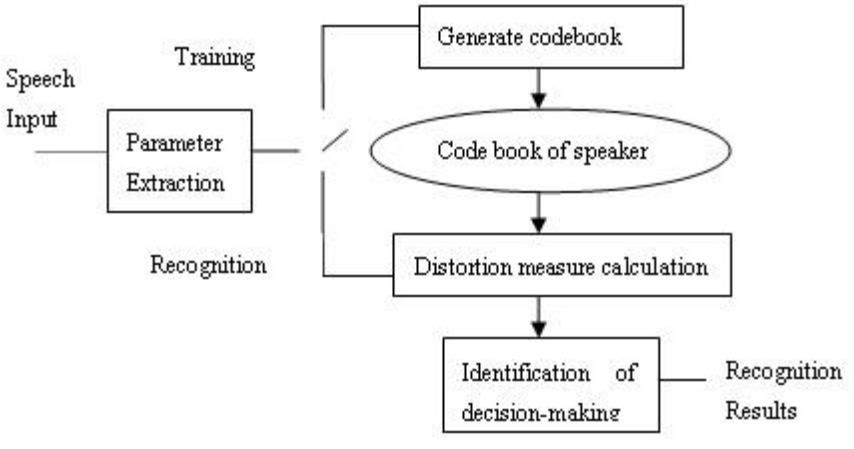

Fig. 1. system diagram of the human speaker recognition system

The Human Speaker Recognition system proposed in this paper is comprised mainly of two stages. During the first stage, Artificial Immune Clustering Algorithm is used to specify the positions and number of cluster centers in the hidden layer of the RBF network. During the second stage, analysis and training is carried out on the RBF network using input samples to compute the output weights of the network.

2 System Description

2.1 Feature Extraction

Feature extraction is a key part of pattern recognition. Currently, the most widely used parameters are the LPCC based on the audio channel model and the MFCC based on the human ear characteristics. Researches have shown that the MFCC can achieve better results than the LPCC and is less sensitive to noise than LPCC. As a result, it has been more widely used. Therefore, MFCC is adopted in this

paper. Real frequency measures can be converted to the Mel frequency measure based on the following relationship between the MFCC parameters and the linear frequency:

$$Mel(f) = 2595 \lg(1 + f/700). \tag{1}$$

The Calculating process of the MFCC parameters is shown following.

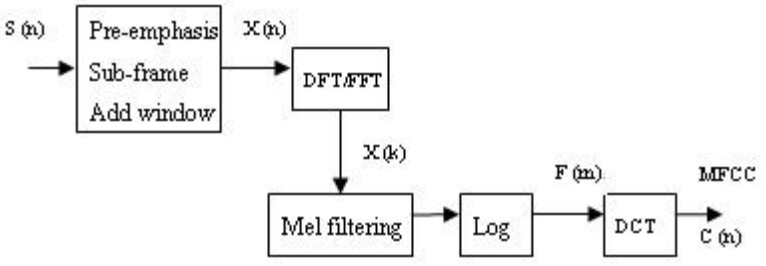

Fig. 2. system diagram of the human speaker recognition system

Through the fig upon,we can summarize like this:

(1) The number of sample points in each speech sample array is specified as first. For each sample array *s(n)*, preprocessing is carried out followed by discrete FFT conversion. The discrete power spectrum *X(k)* is obtained after the orders are squared.
(2) Compute the power value after *X(k)* is processed with a group of $H_m(n)$ numbered by *M*. In other words, compute the product of *X(k)* and $H_m(n)$ at the discrete frequency points. As a result, parameters are obtained, which are denoted as $P_m, m = 0, 1, 2, ..., M$.
(3) Compute the natural logarithm of P_m, which are denoted as $L_m, m = 0, 1, 2, ..., M$.
(4) Compute the discrete cosine transform of L_0, L_1,... which are denoted as $L_m, m = 0, 1, 2, ..., M$, among which the direct current part, $D_0$is discarded. Adopt the parameters as the MFCC parameters D_1,D_2,..., D_k. The value of k in the MFCC parameters is usually set as low as *12-16*. In this paper, it is set as *k=12*.

2.2 RBF Network Architecture

Since the RBF network has simple architecture, fast learning speed and good function approximation capability, it has been widely used in speech recognition and system recognition. An RBF network is composed of three layers of forward feed neurons.

The first layer is the input layer. As with the input layers of other neural network, this layer is responsible for the input of outside information into the

neural network and is not capable of information processing. The second layer is the hidden layer, which is the main functional layer of the RBF neural network. The radial base function is used as the transfer function in this layer, which often takes the form of the Gaussian function. The conversion from the input layer to the hidden layer is nonlinear while the conversion from the hidden layer to the output layer is linear. Assume the input sample is x, the output from the i-th unit in the hidden layer is:

$$R_i(x) = \exp\{- \mid X - {Z_i}^2 \mid /2\sigma_i^2\}, \quad i = 1, 2, ...k. \tag{2}$$

In Eq.2, k is the number of units in the hidden layer, Z_i is the center of the base function, σ_i is the width of the Gaussian function of the i-th unit in the hidden layer. The corresponding output of the output node is:

$$Y_j(x) = \sum_{i=1}^{k} W_{ij} R_i(x), \quad j = 1, 2, ...k. \tag{3}$$

In Eq.3, W_{ij} is weight from the i-th node in the hidden layer to the j -th output node, N is the number of output nodes and Y_j is the output of the j -th output ndoe. The training process for the RBF network architecture and its parameters is arranged as follows in this paper: the center of the base function Z_i, the width of the Gaussian function of the i-th unit in the hidden layer σ_i are obtained with the use of the AICA, and the weight from the hidden layer to the output layer W_{ij} is obtained through GA. The emphasis of this paper is to use immune algorithm to specify the cluster centers Z_i. The number of cluster centers is the number of nodes in the hidden layer of the RBF network.

3 Algorithm Specify RBF Network Cluster Centers

A clustering method based on immune principles is used in this paper. The speech data is treated as antigen, and the clustering centers are treated as antibody in the immune system. The clustering process for the speech data is equivalently the process in which the immune system continuously generates antibody to recognize the antigen and finally generates the optimal antibody that could capture the antigen. The clustering algorithm based on immune mechanism[10] introduced in this paper effectively overcomes the hardship traditional RBF network training algorithm encounters in the specification of the number and positions of the cluster centers. Moreover, the encoding, crossover and mutation operators of the algorithm are designed based on the real situation in the clustering problem. As a result, the algorithm operates faster and can effectively converge to the global optimal solution.

The basic steps of the algorithm are as follows:

Step 1: Input n antigens. Altogether C initial antibodies are randomly chosen to form the antibody set.

Step 2: Each antibody recognizes the antigen in its adjacent space. Euclidean distance is chosen as the intimacy indicator between the antibody and the antigen, which are then grouped according to their intimacy level. The decision function for the grouping could be defined as:

$$J(\mu, c) = \sum_{i=1}^{C} J_i$$
$$= (\sum_{i=1}^{c} \sum_{j=1}^{n} (\mu_{ij} \parallel X_j - C_i \parallel^2). \tag{4}$$

In Eq.4 , μ_{ij} is the extent the vector X_i belong to the group C_i,$i = 1, 2, 3, ..., c$, whose value ranges between 0 and 1. During each time grouping,the n data objects are assigned to different C_i,$i = 1, 2, 3, ..., c$ according to the intimacy level, and

$$u_{ij} = \begin{cases} 1 & if\ k \neq i \quad and \quad \|x_j - c_i\| \neq \|x_j - c_k\| \\ 0 & otherwise \end{cases}. \tag{5}$$

Step 3: The optimization of antibody is carried out with the directed search method for optimal antibody in the *aiNet* immune network. The following equation is used: $C = C - \alpha(C - X)$, where C stands for the antibody in the shape space, X stands for the antigen and α stands for the learning rate. For each $C_i, i = 1, 2, 3, ..., c$, cloning inside the group is used to generate$C_{is}(s = 1, 2, 3...n, 1 \leq s \leq n)$through evolution. Then the intimacy level between the newly generated s antibody and the s antigen is computed, and the one with the highest intimacy level among the new antibody is chosen as the optimal one(clustering center).

Step 4: Using the antibody suppression principle, delete all the antibody except the optimal ones in the C groups.

Step 5: Repeat steps 2,3,4 until the following condition is satisfied:

$$min(J(\mu, c) = \sum_{i=1}^{C} J_i$$
$$= (\sum_{i=1}^{c} \sum_{j=1}^{n} (\mu_{ij} \parallel X_j - C_i \parallel^2). \tag{6}$$

At this point, the algorithm terminates and the results are the cluster centers. The number of clustering centers is the number of nodes in the hidden layer of the RBF network.

The Gauss width σ_i of every hidden node, can be calculated by the distance, which is the node to the clustering center, specific calculating process is:

$$\sigma_i = \mid X - Z_i \mid / \sqrt{-2 \ln R_i(x)}, \quad i = 1, 2, ..., k. \tag{7}$$

In Eq.7, x is input samples, Z_i is clustering centers

4 System Implementation

4.1 Human Speaker Recognition Process

In the Human Speaker Recognition experiments using the RBF network based on Artificial Immune Clustering Algorithm (AICA), all the speech sample data comes from the recording voice of human speakers. To ensure the audio sample is irrelevant to the text, continuous voice recording based on different texts are used to train the network for different human speakers. The training speech length is 20s. Altogether 32 people participated in the experiment, each of whom recorded 15 different paragraphs of voice. The speech samples are divided into two groups, among which 6 paragraphs are used to train the network, and the other 9 are used for speaker recognition. The 12 dimensional MFCC speech parameters are extracted from the two groups of speech recording and then stored.

Point detection, pre-weighting, framing and applying the hamming windows are carried out on the input speech sample orderly. For each frame, the 12 dimensional MFCC speech parameters are computed. The frame length for the data is N=256, and the frame shift is 128. The (1-0.95Z^{-1}) high-pass filter is used for pre-weighting. Finally, noise is discarded to form the speech feature vector array.

The parameters in the artificial immune algorithm are set as follows:the scale of the sample set is set as $N = 32 \times 6 = 192$. The 120 samples are then divided into 48 groups to generate 48 clustering centers, i.e., 48 nodes in the hidden layer. The crossover probability is set as P_c =0.8, and the mutation probability is set as P_m=0.001. α is set as 5.0×10^{-8}. Since the experiment result requires 32 recognized human speakers, there are 32 output nodes in the neural network. In conclusion, the node numbers of the RBF network is as follows: 12-48-32.

VisualC++ is used as the development platform for the system. The criteria for the network used by the program are as follows: select the maximum from the outputs from the 32 output nodes and set it 1. Set the rest of the outputs 0. The error is E=$1/2\sum_{k=1}^{N} e_k^2$,is the number of samples. The training process and the whole program terminate when E$\leq 10^{-5}$ is satisfied or the number of training iterations exceeds 1000.

During the recognition stage, the 12 dimensional speech feature vectors of the human speakers to be recognized are feed into the network. The previously stored network weights W_{ij} of each speaker are called to compute a 32 dimensional matrix, in which the 1 entries correspond to the recognized speakers.

4.2 Analysis of the Experiment Result

(1)comparison of clustering code book adaptability

In Fig 4, the adaptability distribution curve generated by the clustering centers when there are 15 speakers and 48 clustering centers is shown. It can be seen from the figure that a higher adaptability can be achieved when the immune

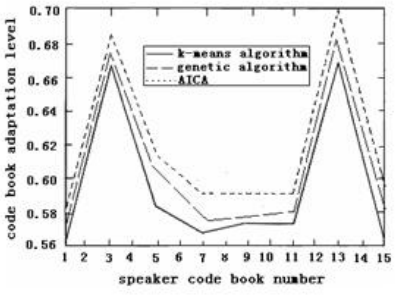

Fig. 3. comparison of clustering code book adaptability

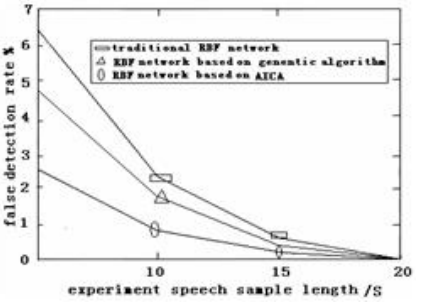

Fig. 4. comparison of clustering code book adaptability

algorithm is used. This shows that the clustering centers generated by the immune algorithm are more optimized than those generated by the k-means algorithm and GA algorithm.

(2)comparison of recognition rate

The false detection rate curves for different lengths of voice samples with the use of different algorithms are shown in Fig 5, where the number of clustering centers equals 48. the recognition rate of the speaker recognition system based on immune algorithm proposed in this paper is higher than that of normal RBF network.

5 Conclusion

In this paper, an RBF network based on artificial immune mechanism is proposed for human speaker recognition. The artificial immune clustering algorithm is used in the system to specify the number and positions of the initial centers of the RBF network. As a result, the network has enhanced local search ability and a higher convergence speed. Also, the phenomenon of degeneration is eliminated. Experimental tests show that the RBF network based on immune algorithm can yield a high recognition rate for human speakers.

Acknowledgments

This research was supported by the Opening Project of JiangSu Province Support Software Engineering R&D Center for Modern Information Technology Application in Enterprise (No. eisecSX200806), and sponsored by Qing Lan Project, the Shanghai Education Committee Innovate Foundation (No.08YZ189), and the Science and technology Foundation of suzhou vocational university (No.SZD09L26), and The Science & technology Foundation of Fujian province (No. 2008F5046).

References

1. Benzeghiba, M., Mori, R.D.: Automatic speech recognition and speech variability:A review. speech communication 49, 763–786 (2007)
2. Cerisara, C., Fohr, D.: Multi-band automatic speech recognition. Computer Speech and Language 15, 151–174 (2001)
3. Marchewka, J., Geottee, T.: Implications of speech recognition technology. Business Forum 17(2), 26–29 (1992)
4. Ding, Y.S., Ren, L.H.: Aritificial immune system:theory and application. Pattern recognition and artificial intelligence 13(1) (2000)
5. Kim, S., Eriksson, T.: A pitch synchronous feature extraction method for speaker recognition. IEEE,Acoustics Speech and Speech and Signal Proceedings 1, 405–408 (2004)
6. de Castro, L.N., Timmis, J.I.: Artificial immune systems as a novel soft computing paradigm. Soft Computing 7(8), 526–544 (2003)
7. Wang, H.P., Yang, H.C.: A Research of Feature Extraction Method for Sound Print Recognition. Journal of Chinese People's Public Security University (Nature Science Edition) 1, 28–30 (2008)
8. Mezghani, A., O'Shaughnessy, D.: Speaker verification using a new representation based on a CMFCC and fomants. IEEE Electrical and Computer Engineering 22, 1469–1472 (2005)
9. Shao, Y., Liu, B.Z.: Speaker Recognition based on MFCC and Weighting Vector Quantification. Computer Engineering and Applications 38(5), 127–128 (2002)
10. Liu, T., Wang, Y.C., Wang, Z.J.: A Cluster Algorithm based on Artificial Immune System. Computer Project and Design 25(11), 2051–2053 (2004)

Adaptive Immune Response Network Model

Tao Liu[1,2], Li Zhang[2], and Binbin Shi[2]

[1] JiangSu Province Support Software Engineering R&D Center for Modern Information Technology Application in Enterprise, Suzhou 215104, Jiangsu, China
[2] Department of Electronics & Information Engineering, Suzhou Vocational University, Suzhou 215104, Jiangsu, China
bankl t@163.com

Abstract. Artificial immune system (AIS) and its applications have become a search hotspot in recent years. According to the theory of immune response and immune network, the Adaptive Immune Response Network (AIRN) is presented in this paper. In AIRN, the expression and procedure are given. The AIRN is applied to the clustering analysis, and this cluster method can receive data modes more quickly. The testing results show that the AIRN has better performance in data partition and pattern recognition than the clustering algorithm based on GA and the others.

Keywords: self-adaptation, immune response, network, model.

1 Introduction

In recent years, Artificial Immune Systems(AIS) has received a lot of research attention and is becoming a research hotspot in artificial intelligence as well as fuzzy logic, neural networks and genetic algorithms[1][2]. Many artificial immune models and algorithms have been proposed based on biological immune principles and have been applied in areas such as automatic control[3], fault diagnosis[4][5], optimized computation[6], pattern recognition[7], machine learning[8] and data analysis[9][10]. Based on natural immune mechanism, Adaptive Immune Response Network (AIRN) is proposed in this paper. It is applied in clustering analysis and is shown to be capable of data clustering and pattern recognition.

2 Artificial Immune System

In the idiotypic immune network proposed by Jerne, each kind of antigen is characterized by the epitope that is located on its surface. A certain antibody recognizes the antigen through integrating its own variable area with the epitope. The area of the antibody that integrates with the epitope of the antigen is called the paratope, whose integration with the epitope leads to the specialization of the immune response. The epitope on the antibody that can be recognized by other antibodies are generally idiotypical antigen decision clusters, or idiotopes. After the

D.-S. Huang et al. (Eds.): ICIC 2009, LNAI 5755, pp. 890–898, 2009.

paratope of a certain antibody integrates with an eptitope or an idiotope, the B cells that secrete this type of antigen would be stimulated, and when the stimulation has exceeded a certain threshold, the cloning expansion would start and the immune response would be carried out. Meanwhile, the antibody or antigen that is integrated would be suppressed, and the number of B cells corresponding to the antigen would be reduced. A network is thus formed with the interaction among the antigens and antibodies. Starting from the simplified assumption of the immune network as stated above, we try to pin down the data analysis target of the network, specifying the form of the antigen and antibody of the Adaptive Immune Response Network (AIRN) based on the specific problem, and the structure of the system. The basic design of the network is as follows: the antigen corresponds to the original data array; the antibody corresponds to the feature value, and is represented as a data item; the antibodies form the network through interaction; the application aim is to use the network to reveal the patterns in the original data set. Therefore, the principles of the network setup are as follows: the network comprises of data items, each of which includes a data value and a stimulation value; there are connections among the data items in the network, and whether two data items are connected is determined by their similarity and a certain threshold: the connection exists if and only if the similarity is greater than the threshold; each pattern class is a sub network comprised of a group of data items that are interconnected; the network converges to a stable state through training, which is the final result of the pattern class analysis.

3 Proposed Algorithm

3.1 The Initialization of AIRN

To deal with the recognition between antigen and antibody, AIRN introduces the concept of shape-space from Perelson: if there are m characteristics influencing the mutual function among molecules and P_i is $no.i(i = 1, 2, ..., m)$ characteristic, thus every molecule can be expressed as space S with m dimensions $(S = P_1 \times P_2 \times ... \times P_m)$. Define the data waiting to be processed as the antigen set $AG = \{ag_1, ag_2, ..., ag_I\}$ and I is the scale of antigen space. Through the immune response recognition process, the acquired set $M$of memory cells is the mode. Suppose that scale of M is I', then $I > I'$ meaning that the antibody space if compressed. The process of immune response is:

$$AG = \begin{bmatrix} ag_1 \\ ag_2 \\ \cdots \\ ag_i \\ \cdots \\ ag_I \end{bmatrix} \Longrightarrow M = \begin{bmatrix} m_1 \\ m_2 \\ \cdots \\ m_i \\ \cdots \\ m_I \end{bmatrix} \quad (I < I').$$

Antigen of the system is:

$$AG = (ag_1), ..., ag_I)^T = \begin{bmatrix} ag_{11} \cdots ag_{1m} \\ \vdots \quad \ddots \quad \vdots \\ ag_{I1} \cdots ag_{Im} \end{bmatrix}. \tag{1}$$

In Eq.(1), $ag_{ij} \in [0,1]^m$, $i = 1, ..., I, j = 1, ..., m$,$ag_i$ is *No.i* antigen and ag_{ij} is *No.j* vector of the *No.i* antigen.

Randomly, new antibody would be generated by Eq.(2) .

$$AB = (ab_1), ..., ab_k)^T = \begin{bmatrix} ab_{11} \cdots ab_{1m} \\ \vdots \quad \ddots \quad \vdots \\ ab_{k1} \cdots ag_{km} \end{bmatrix}. \tag{2}$$

In Eq.(2), $ab_{ij} \in [0,1]^m$,$i = 1, ..., k, j = 1, ..., m$,$ab_i$ is *No.i* antibody and ab_{ij} is *No.j* vector of the *No.i* antibody.

3.2 Antigen Presentation

AIRN takes Euclidean-distance between antigen and antibody as an indicator for the matching degree. For any antigen ag_i and antibody ab_j, distance $d(i,j)$ can be calculated through the following equation:

$$d(i,j) = (\sum_{t=1}^{m}(ag_{it} - ab_{jt}))^{\frac{1}{2}}. \tag{3}$$

For any antibody ab_i and ab_j, distance $sl(i,j)$ can be calculated through the following equation:

$$sl(i,j) = (\sum_{t=1}^{m}(ab_{it} - ab_{jt}))^{\frac{1}{2}}. \tag{4}$$

For any $ab_j(ab_i \in AB, i = 1, ..., K)$, stimulation $sl(i,j)$ from antigen $(ag_j \in AB, j = 1, ..., I)$ is:

$$sl(ij) = \begin{cases} 1/\sqrt{d(i,j)} & d(i,j) < T_{sl} \\ 0 & other \end{cases}. \tag{5}$$

In Eq.(5), $i = 1, 2, ..., I, j = 1, 2, ..., k$, and T_{sl} is the threshold value of stimulation from antigen to antibody:

$$T_{sl} = k_{sl} \frac{\sum_{i=1}^{I}\sum_{j=1}^{k} d(i,j)}{\frac{I \times k}{2}}. \tag{6}$$

Here, $k_{sl} \in [0,1]$ and is a constant.

3.3 Clone and Mutation

When the stimulation to antibody from antigen arrives certain degree, the immune system is activated and begins to clone antibody. The number of cloned antibody ab_j stimulated by antigen ag_i is:

$$c_1(ij) = \begin{cases} \lfloor sl(i,j) \rfloor & d(i,j) < T_{sl} \\ 0 & other \end{cases}. \tag{7}$$

In Eq.(7), $\lfloor \rfloor$ represents the closest integer to $sl(i,j)$. If the clone set from antibody ab_j stimulated by ag_i is Ab_{ji}, then the clone set C_j of ab_j stimulated by antigen group is:

$$C_j = Ab_{j1} \cup Ab_{j2} \cup ... \cup Ab_{jc_1}(i,j) = \bigcup_{i=1}^{c_1(i,j)} Ab_{jt}. \tag{8}$$

The new antibody set C after clone corresponding antibody set AB is formed:

$$C = C_1 \cup C_2 \cup ... \cup C_i = \bigcup_{i=1}^{k} C_i. \tag{9}$$

The clone cell needs mutation process to bestow the newly born cell higher affinity with the selected antigen. Suppose

$$Mut(i,j) = d(i,j). \tag{10}$$

It is the new antibody mutation rate from antibody ab_j stimulated by antigen ag_i. Suppose the mutation set of antibody ab_j stimulated by antigen group is $C_j^{'}$, then:

$$C_j^{'} = C_j + Mut(i,j) \times (C_j - ag_i). \tag{11}$$

Suppose the mutation set of antibody ab_j stimulated by antigen group is $C_j^{'}$, then the antibody set from mutation is:

$$C^{'} = C_1^{'} \cup C_2^{'} \cup ... \cup C_i^{'} = \bigcup_{i=1}^{k} C_i^{'}. \tag{12}$$

Mutation grantees the diversity of new born antibody, which is the internal characteristic of learning reinforcement of immune system. The system enhances its proficiency of recognizing antigen through repeating the above process.

3.4 Clone Suppression and Clone Selection

Clone suppression will be taken after clone mutation. After clone mutation. for set C', calculate again the affinities between antigen and antibody and among

antibodies after clone mutation. Calculate suppression threshold value T_d of antigen-antibody and suppression threshold value T_s of antibody-antibody.

$$T_d = k_d \frac{1}{p} \sum_{j=1}^{p} \min_{i=1,..,I} d(i,j). \tag{13}$$

$$T_s = k_s \frac{\sum_{i=1}^{p} \sum_{j=1}^{p} s(i,j)}{\frac{p \times p-1}{2}}. \tag{14}$$

In Eq.(13) and Eq.(14),$k_d, k_s \in [0,1]$,and they are the constant. In the clone suppression phrase, delete the antibody cells which have bigger affinity value with antigen than threshold value T_d first and then delete the memory cell which has smaller affinity value than threshold value T_s considering the affinity value among antibody cells. After this phrase, the formed antibody set is $C^{''}$ and its elements satisfy the followings:

$$ab_j = \begin{cases} ab_j & \exists ag_i,\ d(i,j) < T_d \\ 0 & other \end{cases}. \tag{15}$$

$$ab_j = \begin{cases} ab_j & \exists ab_j,\ s(i,j) > T_s \\ 0 & other \end{cases}. \tag{16}$$

After the phrase of clone suppression, the formed antibody set $C^{''}$ has a reduced scale than $C^{'}$. Then with the consideration of affinity scale with antigen, select $\xi\%$ cells having clone mutation as memory cells of antibody of set $C^{''}$ and put them in the memory cell set M.

3.5 Affinity Maturation

Suppose the number of elements in memory cell set $M(M = \{m_1, m_2, ..., m_z, M \in \Re^z)\}$ is $p1$ and define the threshold value of memory cell affinity maturation is:

$$T_s^{'} = k_s^{'} \frac{\sum_{i=1}^{p_1} \sum_{j=1}^{p_1} s(i,j)}{\frac{p_1 \times p_1 - 1}{2}}. \tag{17}$$

In Eq.(17), $k_s^{'} \in [0,1]$, and is the constant. After the stated process, elements in M should satisfy the followings:

$$ab_j = \begin{cases} ab_j & \exists ab_j,\ s(i,j) > T_s^{'} \\ 0 & other \end{cases}. \tag{18}$$

In Eq.(18), $i = 1, 2, ..., p_1; j = 1, 2, ..., p_1$

3.6 Termination of Network Training

Network training can set certain iteration as termination or set stimulation degree value of antigen and memory cell after the iteration. That is to say, for any ag_i, there can be found an antibody ab_j and $d(i,j) \leq T_s^{''}$. Through the cycling of above process, immune system studied the processed data until satisfied the study termination. The final antibody memory set M is the required study pattern. Thus the study and accumulation of knowledge is completed. Summarily, AIRN has the following characteristics: through the first immune response to establish antibody memory set to illustrate characteristics of antigen data for recognizing the pattern of antigen; through second immune response to complete the recognition of newly input data. In the real calculation, these characteristics can be used to realize data compression, data clustering and grouping.

4 Experimentations and Results

4.1 Experiment Result on Artificial Data Set

To clearly illustrate the result of the experiment, two artificial data sets with Gaussian distribution around the cluster center are used for the experiment. The first data set has 380 samples, with 5 clusters of two dimensional data sets. The second data set has 550 samples, with 7 clusters of three dimensional data sets. The following parameters are used as the network threshold: k_{sl}=1,k_d=1,k_s=1,$k_s{'}$=1. Fifty experiments are carried out for each data set, and the proposed algorithm is shown to converge to the correct number of clusters with probability 100%.The result of one experiment is shown in Fig. 1 and Fig. 2. For the first data set, the average scale of the model solution is 56, and the network can converge to the optimal solution within 30 rounds of iteration. For the second data set, the average scale of the model solution is 82, and the network can converge to the optimal solution within 45 rounds of iteration.

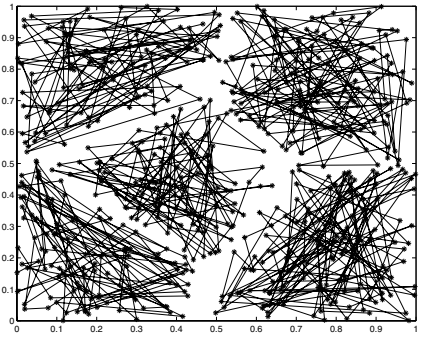

Fig. 1. Experiment result on data set No. two

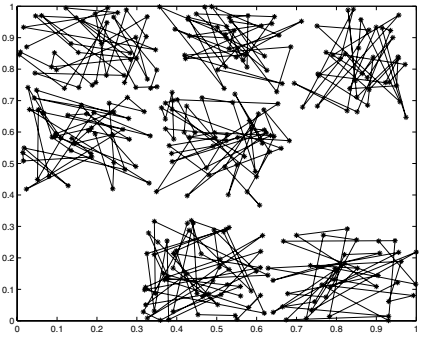

Fig. 2. Experiment result on data set No. one

4.2 The Experiment Result on the Iris Data Set

To further verify the effectiveness of the proposed algorithm, the Iris data set in the machine learning library UCI [12] is used for the experiment. Since the data set has 4 characteristic dimensions, the cluster result can not be viewed directly. Because the data set is classified into 3 groups physically and the second and third groups are overlapped due to the data characteristic, there have always been different views on the optimal number of clusters. According to paper [13], the optimal number of clusters in the Iris data set is 2 when the evaluation function $v_{DB,22}$ is used. Set the network threshold parameters as follows: k_{sl}=1,k_d=1,k_s=1,$k_s{}'$=1. The average scale of the model solution is 16. The AIRN usually achieves the same result as that in paper [14] within 25 rounds of iteration, i.e., the number of clusters equals 2 and the evaluation value $v_{DB,22}$= 0.46. In some cases in the experiment, the algorithm converges to a solution with the evaluation value equal to 0.44. Since the goal of the clustering algorithm is to find out the number and positions of the clusters hidden in the data set, the performance of the algorithm can be measured through these parameters. In this paper, GA [14], aiNet [15] and the algorithm proposed in this paper are carried out on the Iris data set for 50 times. The genetic algorithm iterates for 40 generations. The value in paper [13] is used for the result of the BHCM algorithm. The clustering result of the algorithm proposed in this paper is shown in Fig. 3. A comparison of the performance of the algorithms is made in Table 1.

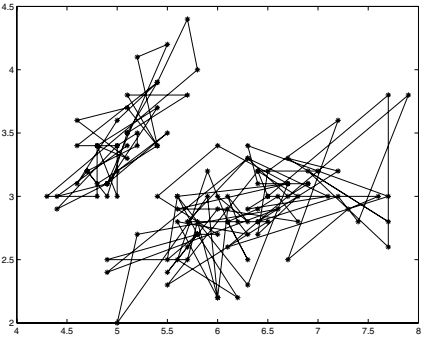

Fig. 3. Lifetime of WSNs

The experiment result in Table 2 shows that even though the optimal estimation can be achieved through GA, the probability of converging to the optimal point is very small since it has a large search space. The BHCM algorithm discovers the optimal number of clusters through trying out all the possible values. However, the optimal estimation value is not discovered as a result of the direct utilization of the K-means method. The aiNet method has a small probability of converging to the optimal estimation value, i.e., it diverges from the optimal cluster center set[16].

Table 1. Performance comparison on the Iris data set

algorithm	Number of iterations	Optimal estimation estimation	the correct number of clusters	the optimal estimation number of clusters
AIRN	50	0.44	50	49
GA	50	0.44	22	17
aiNet	50	0.44	50	20
BHCM	50	0.46	23	34

5 Conclusions

This paper proposes an adaptive immune response network (AIRN). Before analyzing data, this network needs the user to input parameters, which include: the randomly generated initial antibodies, the stimulation level of the antibody sl and its weight k_{sl}, the suppression threshold of the antibody to the antigen T_d and its weight k_d, the suppression threshold of the antibody between each other T_s and its weight k_s, the intimacy maturity threshold $T_s^{'}$ and its weight $k_s^{'}$. However, the values of these parameters have specific physical interpretations, and can be used to control the scale and structure of the network, the granularity and the connection status of the network. Among them, the intimacy maturity threshold $T_s^{'}$ is the most important parameter. It can be used to control the ultimate network structure and scale. High threshold values can generate highly concentrated antibody (cluster). When the AIRN is applied in data analysis, good results can be obtained in data classification and pattern recognition. However, the spatial distribution of the data generated by the network needs to be further analyzed.

Acknowledgments

This research was supported by the Opening Project of JiangSu Province Support Software Engineering R&D Center for Modern Information Technology Application in Enterprise (No. eisecSX200806), and sponsored by Qing Lan Project, the Science & Technology Foundation of Fujian Province (No. 2008F5046), and the 2009 Senior Talent Culture Project of Suzhou Municipal Government.

References

1. Dasgupta, D.: Advances in artificial immune systems. Computational Intelligence Magazine, IEEE 1, 40–49 (2006)
2. Timmis, J., Hone, A., Stibor, T., Clark, E.: Theoretical advances in artificial immune systems. Theoretical Computer Science 403, 11–32 (2008)
3. Jin, X., Zhao, J., Wang, H.F.: On-line stability control of power systems integrated with distributed generation systems. In: 41st International Universities Power Engineering Conference, UPEC, Conference Proceedings, vol. 2, pp. 472–476 (2006)

4. Ding, Y.S., Ren, L.H.: Artificial immune system: Theory and applications. Pattern recognition and artificial intelligence 13(1), 31–35 (2000)
5. Dasgupta, D., Yu, S., Majumdar, N.S.: MILA - Multilevel Immune Learning Algorithm. In: The proceedings of the Genetic and Evolutionary Computation Conference (GECCO), Chicago, pp. 578–585 (2003)
6. Chun, J.S., Lim, J.P., Jung, H.K.: Optimal design of synchronous motor with parameter correction using immune algorithm. IEEE Trans Energy Conversion 14(3), 610–615 (1999)
7. Carter, J.H.: The immune system as a model for pattern recognition and classification. Journal of the American Medical Informatics Association, 7(3), 28–41 (2000)
8. Bentley, P.J., Gordon, T.G., Kim, J., et al.: New trends in evolutionary computation. In: Proc IEEE International Congress on Evolutionary Computation, Seoul, Korea, pp. 162–169 (2001)
9. Timmis, J., Neal, M.A.: Resource limited artificial immune system for data analysis. Knowledge Based Systems 14(3-4), 121–130 (2001)
10. Timmis, J., Knight, T.: Artificial immunes system: Using the immune system as inspiration for data mining. In: Abbass, H.A., Sarker, R.A., Newton, C.S. (eds.) Data Mining: A Heuristic Approach, pp. 209–230. Idea Publishing Group, Hershey (2001)
11. Jerne, N.K.: The immune system. Scientific American 229(1), 51–60 (1973)
12. Blake, C.L., Merz, C.J.: UCI Repository of Machine Learning Databases [DB/OL] (2007), http://www.ics.uci.edu/mlearn/MLRepository.html
13. Bezdek, J., Pal, N.: Some New Indexes of Cluster Validity. IEEE Transactions on Systems, Man and Cybernetics—Part B: Cybernetics 28, 301–315 (1998)
14. Wang, H.H., Zhao, W.J.: Data clustering based on approach of genetic algorithm. In: Proceedings of Chinese Control and Decision Conference, pp. 2753–2757 (2008)
15. Castro, L.N., Von Zuben, F.J.: An Evolutionary Immune Network for Data Clustering. In: Proceedings of the IEEE SBRN 2000 (Brazilian Symposium on Artificial Neural Networks), pp. 84–89 (2000)
16. Zhang, W.X.: Mathematical basis of genetic algorithms, pp. 146–170. Xi'an Jiaotong University publishing house, Xi'an (2000)

Researches on Robust Fault-Tolerant Control for Actuator Failures in Time-Varying Delay System

Dong Li

Suzhou Institute of Trade and Ecommerce, Suzhou, Jiangsu, China, 221009
tsonglee@126.com

Abstract. Based on Lyapunov stability theory and linear matrix inequality, a kind of state feedback and time-delay state feedback control law is presented. The sufficient conditions for the closed-loop system robust fault-tolerant capability against actuator failures are given. The results of fault-tolerant controller can involved through solving several linear matrix inequalities. A simulation example shows the effectiveness and feasibility of the proposed approach.

Keywords: Robustness, Time-varying delay, Linear matrix inequality, Actuator failures.

1 Introduction

During running of the control system, once system actuator malfunction or lose effectiveness, the control system based on the design of traditional approach can not guarantee close-loop system performance, even destroys the stability of system. Fault-tolerant control system (FTCS) is a kind of system, which can still maintain stability of the closed-loop system and has the property of acceptability under the malfunction of the components (sensors, actuator). So it provides a important way to guarantee the reliability and safety of control system. The integrity control in passive fault-tolerant control which is an important branch of fault tolerant control system is valued broadly [1-3], because it neither needs fault detection and diagnosis, nor increases investment in hardware; in addition, it has a good real-time performance. Time-delaying is a class of complex property which exits broadly in engineering practice, and due to the factors such as modeling errors, environmental change, etc in system, the system inevitably exists uncertainty, so the system model with time-delay uncertainty is more close to the actual system. In recent years, the research which aims for the robust fault-tolerant control of time-delay uncertain system is highly valued by control academia, and it also obtains some achievements [1-7].

At present, the design of linear time-delay system controller mainly applies to the solving of Riccati equations (inequality) [1-4] or Linear Matrix Inequality (LMI) [5-9] to design the corresponding controller. Reference [2] studies robust fault-tolerant control problem in uncertain linear time-varying delay continuous systems, when bounded parameters which exists in system are not sure, one proposes a design method which guarantee the robust stability of system for the invalidation and malfunction of actuator. Reference [3] considers the robust fault-tolerant control problem of uncertain systems with states and control-delay performance. Based on Riccati

D.-S. Huang et al. (Eds.): ICIC 2009, LNAI 5755, pp. 899–911, 2009.

equation and Lyapunov stability theory, one present robust fault-tolerant controller design method with integrity for the problem of the invalidation of sensors or actuator. The literatures above, when designing controller, need to adjust some parameters in advance, which not only brings inconvenience to practical application, but also causes the design of controller to have more conservative. Reference [5] studies robust fault-tolerant control problem of delay-time uncertain systems, employs LMI method to produce sufficient condition in which the closed-loop system is asymptotically stable under the failures of actuator and to present a controller design method. Reference [6,7] studies fault-tolerant control problem of delay-time system under the invalidation of actuator. But the system only considers state-delay, ignores the case of control input delay. Compared to delay-time which exits in actual system , it has a certain limitation.

This paper, based on Lyapunov stability theory, develops robust fault-tolerant controller when actuator failure-for uncertainty. Linear continuous systems with state and control delay by solving LMIs. The system not only maintains integrity for actuator failure, but also has robust stability for parameter uncertainty and state and control delay. The method can easily obtain corresponding controller through solving corresponding linear matrix inequality (LMI) by the LMI toolbox of Matlab; in addition, it doesn't need to adjust any parameters, so it brings great convenience to the design of system. The proof of the theorem also reveals that it has the equivalence of mathematical sense and adaptability in control application for the robust fault-tolerant sufficient conditions of the actuator failure.

2 System Description

Considering linear continuous time-varying delay uncertain systems below:

$$\begin{cases} \dot{x}(t) = (A_1 + \Delta A_1(t))x(t) + (A_2 + \Delta A_2(t))x(t - h_1(t)) \\ \qquad +(B_1 + \Delta B_1(t))u(t) + \left(B_2 + \Delta B_2(t)\right)u\left(t - h_2(t)\right), \\ x(t) = \phi(t), \qquad t \in [-h, 0], \qquad h = \max\{h_1, h_2\}, \end{cases} \tag{1}$$

Where $x(t) \in R^n$ is the state vector, and $u(t) \in R^m$ is the control input vector.A_1,A_2,B_1 and B_2 are real constant matrices with appropriate dimensions. $\Delta A_1(t)$, $\Delta A_2(t)$, $\Delta B_1(t)$ and $\Delta B_2(t)$ are time-varying uncertain terms of system model, and satisfies condition below:

$$\begin{bmatrix} \Delta A_1 & \Delta A_2 & \Delta B_1 & \Delta B_2 \end{bmatrix} = DH \begin{bmatrix} E_1 & E_2 & E_3 & E_4 \end{bmatrix}, \tag{2}$$

Where D, E_1, E_2, E_3 and E_4 are known real constant matrices of appropriate dimensions, and $H(t)$ is an unknown and time-varying real value matrix function with Lebesgue measurable elements satisfying.

$$H^T(t)H(t) \le I, \tag{3}$$

$h_1(t)$,$h_2(t)$are unknown time-varying delay, and are assumed to satisfy.

$$\begin{aligned} &0 \le h_1(t) \le h_1, \qquad \dot{h}_1(t) \le d_1 < 1, \\ &0 \le h_2(t) \le h_2, \qquad \dot{h}_2(t) \le d_2 < 1, \qquad h = \max\{h_1, h_2\}. \end{aligned} \tag{4}$$

For the time-varying uncertain time-delay system satisfying condition(2)-(4) formula(1),suppose the system$(A_1,B_1),(A_2,B_2)$ are controllable, and the states are measurable, if memoryless state feedback control is employed.

$$u(t) = Kx(t) \ . \tag{5}$$

Then the closed-loop system is:.

$$\begin{aligned} \dot{x}(t) &= [(A_1 + \Delta A_1(t)) + (B_1 + \Delta B_1(t))K]x(t) + (A_2 + \Delta A_2(t))x(t - h_1(t)) \\ &\quad + (B_2 + \Delta B_2(t))Kx(t - h_2(t)) \\ &= [(A_1 + DHE_1) + (B_1 + DHE_3)K]x(t) + (A_2 + DHE_2)x(t - h_1(t)) \\ &\quad + (B_2 + DHE_4)Kx(t - h_2(t)). \end{aligned} \tag{6}$$

Below we will discuss robust fault-tolerant control problem for actuator failure.

3 Major Results

Considering the likely failures of actuator, we introduce a switching matrix $L = diag(l_1, l_2, ..., l_n)$, which is nominal between the matrix of time-delay uncertain systems (6) matrix B and feedback matrix K, where

$$l_i = \begin{cases} 1 & \text{When the } i\text{th actuator is nomal} \\ 0 & \text{When the } i\text{th actuator is invalidate} \end{cases} \qquad i=1, 2,\ldots n$$

Then the closed-loop fault systems under actuator failures is

$$\begin{aligned} \dot{x}(t) &= [(A_1 + DHE_1) + (B_1 + DHE_3)LK]x(t) + (A_2 + DHE_2)x(t - h_1(t)) \\ &\quad + (B_2 + DHE_4)LKx(t - h_2(t)). \end{aligned} \tag{7}$$

For actuator failure, the design goal of robust fault-tolerant controller is to determine the state feedback gain matrix K, such that for any possible actuator failure $L \in \Psi$, system (7) is asymptotically stable, then the condition above illustrates that system has robust integrity(Ψ is a set which contains all possible failures in actuator fault switching matrix).

Theorem 1. For any possible actuator fault matrix $L \in \Psi$ and scalar $\varepsilon_i > 0$ $(i=1,2\ldots 20)$, if there exits matrix K and positive definite symmetric matrix $P>0$, satisfying linear matrix inequality

$$\begin{bmatrix} W & M_1 & M_2 & M_3 & M_4 & M_5 & M_6 & M_7 \\ M_1^T & -J_1 & 0 & 0 & 0 & 0 & 0 & 0 \\ M_2^T & 0 & -J_2 & 0 & 0 & 0 & 0 & 0 \\ M_3^T & 0 & 0 & -J_3 & 0 & 0 & 0 & 0 \\ M_4^T & 0 & 0 & 0 & -J_4 & 0 & 0 & 0 \\ M_5^T & 0 & 0 & 0 & 0 & -J_5 & 0 & 0 \\ M_6^T & 0 & 0 & 0 & 0 & 0 & -J_6 & 0 \\ M_7^T & 0 & 0 & 0 & 0 & 0 & 0 & -J_7 \end{bmatrix} < 0 \tag{8}$$

Then, the closed-loop system is still asymptotically stable under actuator fault, and the system has robust integrity. Where

$$
\begin{aligned}
&P^{-1} = X, Y = KX,\\
&W = A_1X + (A_1X)^T + B_1LY + (B_1LY)^T + 2A_2X + 2B_2X,\\
&M_1 = \begin{bmatrix} D & X^TE_1^T & (E_3LY)^T & X^TE_2^T & (E_4LY)^T \end{bmatrix},\\
&M_2 = \begin{bmatrix} A_2 & A_2 & A_2 & A_2 \end{bmatrix},\\
&M_3 = \begin{bmatrix} B_2L & B_2L & B_2L & B_2L \end{bmatrix},\\
&M_4 = \begin{bmatrix} A_2P_1E_2^T & A_2P_2E_2^T & A_2P_3E_2^T & A_2P_4E_2^T \end{bmatrix},\\
&M_5 = \begin{bmatrix} B_2LLE_4^T & B_2LLE_4^T & B_2LLE_4^T & B_2LLE_4^T \end{bmatrix},\\
&M_6 = \begin{bmatrix} X^TA_1^T & (B_1LY)^T & X^TA_2^T & (B_2LY)^T \end{bmatrix},\\
&M_7 = \begin{bmatrix} X^TA_1^T & (B_1LY)^T & X^TA_2^T & (B_2LY)^T \end{bmatrix},
\end{aligned}
$$

$$
\begin{aligned}
&J_1 = diag([(\varepsilon_1+\varepsilon_2+\varepsilon_3+\varepsilon_4)+h_1(\varepsilon_5+\varepsilon_6+\varepsilon_7+\varepsilon_8)+kh_2(\varepsilon_9+\varepsilon_{10}+\varepsilon_{11}+\varepsilon_{12})]^{-1}I,\\
&\quad (\varepsilon_1^{-1}+h_1\varepsilon_{13}^{-1})^{-1}I,\quad (\varepsilon_2^{-1}+h_1\varepsilon_{14}^{-1})^{-1}I,\quad (\varepsilon_3^{-1}+h_1\varepsilon_{15}^{-1})^{-1}I,\quad (\varepsilon_4^{-1}+h_1\varepsilon_{16}^{-1})^{-1}I),\\
&J_2 = diag(h_1^{-1}P_1^{-1}I, h_1^{-1}P_2^{-1}I, h_1^{-1}P_3^{-1}I, h_1^{-1}P_4^{-1}I),\\
&J_3 = diag((kh_2)^{-1}I, (kh_2)^{-1}I, (kh_2)^{-1}I, (kh_2)^{-1}I),\\
&J_4 = diag(h_1^{-1}(\varepsilon_5I - E_2P_1E_2^T), h_1^{-1}(\varepsilon_6I - E_2P_2E_2^T), h_1^{-1}(\varepsilon_7I - E_2P_3E_2^T), h_1^{-1}(\varepsilon_8I - E_2P_4E_2^T)),
\end{aligned}
$$

$$
\begin{aligned}
&J_5 = diag((kh_2)^{-1}(\varepsilon_9I - E_4LLE_4^T), (kh_2)^{-1}(\varepsilon_{10}I - E_4LLE_4^T),\\
&\quad (kh_2)^{-1}(\varepsilon_{11}I - E_4LLE_4^T), (kh_2)^{-1}(\varepsilon_{12}I - E_4LLE_4^T),\\
&J_6 = diag(h_1^{-1}(P_1 - \varepsilon_{13}DD^T), h_1^{-1}(P_2 - \varepsilon_{14}DD^T), h_1^{-1}(P_3 - \varepsilon_{15}DD^T), h_1^{-1}(P_4 - \varepsilon_{16}DD^T)),\\
&J_7 = diag(h_2^{-1}(I - \varepsilon_{17}DD^T), h_2^{-1}(I - \varepsilon_{18}DD^T), h_2^{-1}(I - \varepsilon_{19}DD^T), h_2^{-1}(I - \varepsilon_{20}DD^T)).
\end{aligned}
$$

Proof. By Newton- Leibniz formula

$$x(t-h_1(t)) = x(t) - \int_{-h_1(t)}^{0} \dot{x}(t+s)ds\,, \tag{9}$$

$$x(t-h_2(t)) = x(t) - \int_{-h_2(t)}^{0} \dot{x}(t+s)ds\,. \tag{10}$$

For the closed-loop system (7), we construct proper Lyapunov functional as follows:

$$V(x,t) = V_1(x,t) + V_2(x,t)\,, \tag{11}$$

Where $V_1(x,t) = x^T(t)Px(t)$ .Then along the trajectory of any solution of the closed-loop system (7), the derivative of $V_1(x,t)$ on time *t* is:

$$
\begin{aligned}
\dot{V}_1(x,t) &= 2\dot{x}^T(t)Px(t)\\
&= x^T(t)[PA_1 + A_1^TP + PB_1LK + K^TLB_1^TP]x(t) + 2x^T(t)PDH(E_1 + E_3LK)x(t)\\
&+2x^T(t)P(A_2 + DHE_2)x(t-h_1(t)) + 2x^T(t)P(B_2 + DHE_4)LKx(t-h_2(t)),
\end{aligned} \tag{12}
$$

By (9, 10)

$$
\begin{aligned}
&2x^T(t)P(A_2+DHE_2)x(t-h_1(t))\\
&=2x^T(t)P(A_2+DHE_2)x(t)-2x^T(t)P(A_2+DHE_2)\int_{-h_1(t)}^{0}\dot{x}(t+s)ds\\
&=2x^T(t)P(A_2+DHE_2)x(t)-2x^T(t)P(A_2+DHE_2)\int_{-h_1(t)}^{0}\{[A_1+B_1LK+DH(E_1+E_3LK)]x(t+s)\\
&+(A_2+DHE_2)x(t+s-h_1(t))+(B_2+DHE_4)LKx(t+s-h_2(t))\}ds,
\end{aligned}
\tag{13}
$$

$$
\begin{aligned}
&2x^T(t)P(B_2+DHE_4)LKx(t-h_2(t))\\
&=2x^T(t)P(B_2+DHE_4)LKx(t)-2x^T(t)P(B_2+DHE_4)LK\int_{-h_2(t)}^{0}\dot{x}(t+s)ds\\
&=2x^T(t)P(B_2+DHE_4)LKx(t)-2x^T(t)P(B_2+DHE_4)\int_{-h_2(t)}^{0}\{[A_1+B_1LK+DH(E_1+E_3LK)]x(t+s)\\
&+(A_2+DHE_2)x(t+s-h_1(t))+(B_2+DHE_4)LKx(t+s-h_2(t))\}ds,
\end{aligned}
\tag{14}
$$

By the lemma 2.6, we can get inequality below

$$
\begin{aligned}
&-2x^T(t)P(A_2+DHE_2)\int_{-h_1(t)}^{0}(A_1+DHE_1)x(t+s)ds\le h_1x^T(t)P(A_2+DHE_2)\\
&\times P_1(A_2+DHE_2)^TPx(t)+\int_{-h_1(t)}^{0}x^T(t+s)(A_1+DHE_1)^TP_1^{-1}(A_1+DHE_1)x(t+s)ds,
\end{aligned}
\tag{15}
$$

$$
\begin{aligned}
&-2x^T(t)P(A_2+DHE_2)\int_{-h_1(t)}^{0}(B_1LK+DHE_3LK)x(t+s)ds\le h_1x^T(t)P(A_2+DHE_2)P_2(A_2+\\
&DHE_2)^TPx(t)+\int_{-h_1(t)}^{0}x^T(t+s)(B_1LK+DHE_3LK)^TP_2^{-1}(B_1LK+DHE_3LK)x(t+s)ds,
\end{aligned}
\tag{16}
$$

$$
\begin{aligned}
&-2x^T(t)P(A_2+DHE_2)\int_{-h_1(t)}^{0}(A_2+DHE_2)x(t+s-h_1(t))ds\le h_1x^T(t)P(A_2+DHE_2)P_3(A_2+\\
&DHE_2)^TPx(t)+\int_{-h_1(t)}^{0}x^T(t+s-h_1(t))(A_2+DHE_2)^TP_3^{-1}(A_2+DHE_2)x(t+s-h_1(t))ds,
\end{aligned}
\tag{17}
$$

$$
\begin{aligned}
&-2x^T(t)P(A_2+DHE_2)\int_{-h_1(t)}^{0}(B_2LK+DHE_4LK)x(t+s-h_2(t))ds\le h_1x^T(t)P(A_2+DHE_2)P_4(A_2+\\
&DHE_2)^TPx(t)+\int_{-h_1(t)}^{0}x^T(t+s-h_2(t))(B_2LK+DHE_4LK)^TP_4^{-1}(B_2LK+DHE_4LK)x(t+s-h_2(t))ds,
\end{aligned}
\tag{18}
$$

$$
\begin{aligned}
&-2x^T(t)P(B_2+DHE_4)LK\int_{-h_2(t)}^{0}(A_1+DHE_1)x(t+s)ds\le h_2x^T(t)P(B_2+DHE_4)LKP_5K^T\\
&\times L(B_2+DHE_4)^TPx(t)+\int_{-h_2(t)}^{0}x^T(t+s)(A_1+DHE_1)^TP_5^{-1}(A_1+DHE_1)x(t+s)ds,
\end{aligned}
\tag{19}
$$

$$
\begin{aligned}
&-2x^T(t)P(B_2+DHE_4)LK\int_{-h_2(t)}^{0}(B_1LK+DHE_3LK)x(t+s)ds\\
&\le h_2x^T(t)P(B_2+DHE_4)LKP_6K^TL(B_2+DHE_4)^TPx(t)\\
&+\int_{-h_2(t)}^{0}x^T(t+s)(B_1LK+DHE_3LK)^TP_6^{-1}(B_1LK+DHE_3LK)x(t+s)ds,
\end{aligned}
\tag{20}
$$

$$
\begin{aligned}
&-2x^T(t)P(B_2+DHE_4)LK\int_{-h_2(t)}^{0}(A_2+DHE_2)x(t+s-h_1(t))ds\\
&\le h_2x^T(t)P(B_2+DHE_4)LKP_7K^TL(B_2+DHE_4)^TPx(t)\\
&+\int_{-h_2(t)}^{0}x^T(t+s-h_1(t))(A_2+DHE_2)^TP_7^{-1}(A_2+DHE_2)x(t+s-h_1(t))ds,
\end{aligned}
\tag{21}
$$

$$
\begin{aligned}
&-2x^T(t)P(B_2+DHE_4)LK\int_{-h_2(t)}^{0}(B_2LK+DHE_4LK)x(t+s-h_2(t))ds\\
&\le h_2x^T(t)P(B_2+DHE_4)LKP_8K^TL(B_2+DHE_4)^TPx(t)\\
&+\int_{-h_2(t)}^{0}x^T(t+s-h_2(t))(B_2LK+DHE_4LK)^TP_8^{-1}(B_2LK+DHE_4LK)x(t+s-h_2(t))ds,
\end{aligned}
\tag{22}
$$

According to (15)-(22), in order to eliminate integral term in above formula, then set

$$
\begin{aligned}
V_2(x,t)=&\int_{-h_1(t)}^{0}\int_{t+s}^{t}x^T(u)(A_1+DHE_1)^TP_1^{-1}(A_1+DHE_1)x(u)duds\\
&+\int_{-h_1(t)}^{0}\int_{t+s}^{t}x^T(u)(B_1LK+DHE_3LK)^TP_2^{-1}(B_1LK+DHE_3LK)x(u)duds\\
&+\int_{-h_1(t)}^{0}\int_{t+s-h_1(t)}^{t}x^T(u)(A_2+DHE_2)^TP_3^{-1}(A_2+DHE_2)x(u)duds\\
&+\int_{-h_1(t)}^{0}\int_{t+s-h_2(t)}^{t}x^T(u)(B_2LK+DHE_4LK)^TP_4^{-1}(B_2LK+DHE_4LK)x(u)duds\\
&+\int_{-h_2(t)}^{0}\int_{t+s}^{t}x^T(u)(A_1+DHE_1)^TP_5^{-1}(A_1+DHE_1)x(u)duds\\
&+\int_{-h_2(t)}^{0}\int_{t+s}^{t}x^T(u)(B_1LK+DHE_3LK)^TP_6^{-1}(B_1LK+DHE_3LK)x(u)duds\\
&+\int_{-h_2(t)}^{0}\int_{t+s-h_1(t)}^{t}x^T(u)(A_2+DHE_2)^TP_7^{-1}(A_2+DHE_2)x(u)duds\\
&+\int_{-h_2(t)}^{0}\int_{t+s-h_2(t)}^{t}x^T(u)(B_2LK+DHE_4LK)^TP_8^{-1}(B_2LK+DHE_4LK)x(u)duds,
\end{aligned}
\tag{23}
$$

Obviously $V_2(x,t)$ is positive definite, then along the trajectory of any solution of the closed-loop system (7), the derivative of $V_2(x,t)$ on time t is

$$
\begin{aligned}
\dot{V}_2(x,t)\le\ & h_1x^T(t)(A_1+DHE_1)^TP_1^{-1}(A_1+DHE_1)x(t)\\
&-\int_{-h_1(t)}^{0}x^T(t+s)(A_1+DHE_1)^TP_1^{-1}(A_1+DHE_1)x(t+s)ds\\
&+h_1x^T(t)(B_1LK+DHE_3LK)^TP_2^{-1}(B_1LK+DHE_3LK)x(t)\\
&-\int_{-h_1(t)}^{0}x^T(t+s)(B_1LK+DHE_3LK)^TP_2^{-1}(B_1LK+DHE_3LK)x(t+s)ds\\
&+h_1x^T(t)(A_2+DHE_2)^TP_3^{-1}(A_2+DHE_2)x(t)\\
&-\int_{-h_1(t)}^{0}x^T(t+s-h_1(t))(A_2+DHE_2)^TP_3^{-1}(A_2+DHE_2)x(t+s-h_1(t))ds\\
&+h_1x^T(t)(B_2LK+DHE_4LK)^TP_4^{-1}(B_2LK+DHE_4LK)x(t)\\
&-\int_{-h_1(t)}^{0}x^T(t+s-h_2(t))(B_2LK+DHE_4LK)^TP_4^{-1}(B_2LK+DHE_4LK)x(t+s-h_2(t))ds\\
&+h_2x^T(t)(A_1+DHE_1)^TP_5^{-1}(A_1+DHE_1)x(t)\\
&-\int_{-h_2(t)}^{0}x^T(t+s)(A_1+DHE_1)^TP_5^{-1}(A_1+DHE_1)x(t+s)ds\\
&+h_2x^T(t)(B_1LK+DHE_3LK)^TP_6^{-1}(B_1LK+DHE_3LK)x(t)\\
&-\int_{-h_2(t)}^{0}x^T(t+s)(B_1LK+DHE_3LK)^TP_6^{-1}(B_1LK+DHE_3LK)x(t+s)ds\\
&+h_2x^T(t)(A_2+DHE_2)^TP_7^{-1}(A_2+DHE_2)x(t)\\
&-\int_{-h_2(t)}^{0}x^T(t+s-h_1(t))(A_2+DHE_2)^TP_7^{-1}(A_2+DHE_2)x(t+s-h_1(t))ds\\
&+h_2x^T(t)(B_2LK+DHE_4LK)^TP_8^{-1}(B_2LK+DHE_4LK)x(t)\\
&-\int_{-h_2(t)}^{0}x^T(t+s-h_2(t))(B_2LK+DHE_4LK)^TP_8^{-1}(B_2LK+DHE_4LK)x(t+s-h_2(t))ds,
\end{aligned}
\tag{24}
$$

By (15)-(22), along the trajectory of any solution of the closed-loop system (7), the derivative of $V(x,t)$ on time t is

$$\begin{aligned}
\dot{V}(x,t) \le\ & x^T(t)[PA_1 + A_1^T P + PB_1 LK + K^T LB_1^T P]x(t) + 2x^T(t)PDH(E_1 + E_3 LK)x(t) \\
& + 2x^T(t)P(A_2 + DHE_2)x(t) + 2x^T(t)P(B_2 + DHE_4)LKx(t) \\
& + h_1 x^T(t)P(A_2 + DHE_2)P_1(A_2 + DHE_2)^T Px(t) \\
& + h_1 x^T(t)P(A_2 + DHE_2)P_2(A_2 + DHE_2)^T Px(t) \\
& + h_1 x^T(t)P(A_2 + DHE_2)P_3(A_2 + DHE_2)^T Px(t) \\
& + h_1 x^T(t)P(A_2 + DHE_2)P_4(A_2 + DHE_2)^T Px(t) \\
& + h_2 x^T(t)P(B_2 + DHE_4)LKP_5K^T L(B_2 + DHE_4)^T Px(t) \\
& + h_2 x^T(t)P(B_2 + DHE_4)LKP_6K^T L(B_2 + DHE_4)^T Px(t) \\
& + h_2 x^T(t)P(B_2 + DHE_4)LKP_7K^T L(B_2 + DHE_4)^T Px(t) \\
& + h_2 x^T(t)P(B_2 + DHE_4)LKP_8K^T L(B_2 + DHE_4)^T Px(t) \\
& + h_1 x^T(t)(A_1 + DHE_1)^T P_1^{-1}(A_1 + DHE_1)x(t) \\
& + h_1 x^T(t)(B_1 LK + DHE_3 LK)^T P_2^{-1}(B_1 LK + DHE_3 LK)x(t) \\
& + h_1 x^T(t)(A_2 + DHE_2)^T P_3^{-1}(A_2 + DHE_2)x(t) \\
& + h_1 x^T(t)(B_2 LK + DHE_4 LK)^T P_4^{-1}(B_2 LK + DHE_4 LK)x(t) \\
& + h_2 x^T(t)(A_1 + DHE_1)^T P_5^{-1}(A_1 + DHE_1)x(t) \\
& + h_2 x^T(t)(B_1 LK + DHE_3 LK)^T P_6^{-1}(B_1 LK + DHE_3 LK)x(t) \\
& + h_2 x^T(t)(A_2 + DHE_2)^T P_7^{-1}(A_2 + DHE_2)x(t) \\
& + h_2 x^T(t)(B_2 LK + DHE_4 LK)^T P_8^{-1}(B_2 LK + DHE_4 LK)x(t),
\end{aligned} \tag{25}$$

By lemma 2.6 and 2.7, we can get inequality below

$$2PDHE_1 \le \varepsilon_1 PDD^T P + \varepsilon_1^{-1} E_1^T E_1, \tag{26}$$

$$2PDHE_3 LK \le \varepsilon_2 PDD^T P + \varepsilon_2^{-1} K^T LE_3^T E_3 LK, \tag{27}$$

$$2PDHE_2 \le \varepsilon_3 PDD^T P + \varepsilon_3^{-1} E_2^T E_2, \tag{28}$$

$$2PDHE_4 LK \le \varepsilon_4 PDD^T P + \varepsilon_4^{-1} K^T LE_4^T E_4 LK, \tag{29}$$

$$\begin{aligned}
& h_1 x^T(t)P(A_2 + DHE_2)P_1(A_2 + DHE_2)^T Px(t) \\
& \quad \le h_1 x^T(t)P[A_2 P_1 A_2^T + A_2 P_1 E_2^T(\varepsilon_5 I - E_2 P_1 E_2^T)^{-1} E_2 P_1 A_2^T + \varepsilon_5 DD^T]Px(t),
\end{aligned} \tag{30}$$

$$\begin{aligned}
& h_1 x^T(t)P(A_2 + DHE_2)P_2(A_2 + DHE_2)^T Px(t) \\
& \quad \le h_1 x^T(t)P[A_2 P_2 A_2^T + A_2 P_2 E_2^T(\varepsilon_6 I - E_2 P_2 E_2^T)^{-1} E_2 P_2 A_2^T + \varepsilon_6 DD^T]Px(t),
\end{aligned} \tag{31}$$

$$\begin{aligned} &h_1 x^T(t)P(A_2+DHE_2)P_3(A_2+DHE_2)^T Px(t) \\ &\quad \le h_1 x^T(t)P[A_2P_3A_2^T + A_2P_3E_2^T(\varepsilon_7 I - E_2P_3E_2^T)^{-1}E_2P_3A_2^T + \varepsilon_7 DD^T]Px(t), \end{aligned} \tag{32}$$

$$\begin{aligned} &h_1 x^T(t)P(A_2+DHE_2)P_4(A_2+DHE_2)^T Px(t) \\ &\quad \le h_1 x^T(t)P[A_2P_4A_2^T + A_2P_4E_2^T(\varepsilon_8 I - E_2P_4E_2^T)^{-1}E_2P_4A_2^T + \varepsilon_8 DD^T]Px(t), \end{aligned} \tag{33}$$

$$(A_1+DHE_1)^T P_1^{-1}(A_1+DHE_1) \le A_1^T(P_1 - \varepsilon_{13}DD^T)^{-1}A_1 + \varepsilon_{13}^{-1}E_1E_1^T, \tag{34}$$

$$\begin{aligned} &(B_1LK+DHE_3LK)^T P_2^{-1}(B_1LK+DHE_3LK) \\ &\quad \le (B_1LK)^T(P_2 - \varepsilon_{14}DD^T)^{-1}(B_1LK) + \varepsilon_{14}^{-1}(E_3LK)^T(E_3LK), \end{aligned} \tag{35}$$

$$(A_2+DHE_2)^T P_3^{-1}(A_2+DHE_2) \le A_2^T(P_3 - \varepsilon_{15}DD^T)^{-1}A_2 + \varepsilon_{15}^{-1}E_2E_2^T, \tag{36}$$

Let P_5=P_6=P_7=P_8=I, if $KK^T \le kI$, then by lemma 2.7, we obtain inequality below

$$\begin{aligned} &(B_2LK+DHE_4LK)^T P_4^{-1}(B_2LK+DHE_4LK) \\ &\quad \le (B_2LK)^T(P_4 - \varepsilon_{16}DD^T)^{-1}(B_2LK) + \varepsilon_{16}^{-1}(E_4LK)^T(E_4LK), \end{aligned} \tag{37}$$

$$\begin{aligned} &h_2 x^T(t)P(B_2+DHE_4)LKP_5K^TL(B_2+DHE_4)^T Px(t) \\ &\le kh_2 x^T(t)P[(B_2L)(B_2L)^T + (B_2L)(E_4L)^T(\varepsilon_9 I - E_4L(E_4L)^T)^{-1}(E_4L)(B_2L)^T + \varepsilon_9 DD^T]Px(t), \end{aligned} \tag{38}$$

$$\begin{aligned} &h_2 x^T(t)P(B_2+DHE_4)LKP_6K^TL(B_2+DHE_4)^T Px(t) \\ &\le kh_2 x^T(t)P[(B_2L)(B_2L)^T + (B_2L)(E_4L)^T(\varepsilon_{10} I - E_4L(E_4L)^T)^{-1}(E_4L)(B_2L)^T + \varepsilon_{10} DD^T]Px(t), \end{aligned} \tag{39}$$

$$\begin{aligned} &h_2 x^T(t)P(B_2+DHE_4)LKP_7K^TL(B_2+DHE_4)^T Px(t) \\ &\le kh_2 x^T(t)P[(B_2L)(B_2L)^T + (B_2L)(E_4L)^T(\varepsilon_{11} I - E_4L(E_4L)^T)^{-1}(E_4L)(B_2L)^T + \varepsilon_{11} DD^T]Px(t), \end{aligned} \tag{40}$$

$$\begin{aligned} &h_2 x^T(t)P(B_2+DHE_4)LKP_8K^TL(B_2+DHE_4)^T Px(t) \\ &\le kh_2 x^T(t)P[(B_2L)(B_2L)^T + (B_2L)(E_4L)^T(\varepsilon_{12} I - E_4L(E_4L)^T)^{-1}(E_4L)(B_2L)^T + \varepsilon_{12} DD^T]Px(t), \end{aligned} \tag{41}$$

$$(A_1+DHE_1)^T P_5^{-1}(A_1+DHE_1) \le A_1^T(I - \varepsilon_{17}DD^T)^{-1}A_1 + \varepsilon_{17}^{-1}E_1E_1^T, \tag{42}$$

$$\begin{aligned} &(B_1LK+DHE_3LK)^T P_6^{-1}(B_1LK+DHE_3LK) \\ &\quad \le (B_1LK)^T(I - \varepsilon_{18}DD^T)^{-1}(B_1LK) + \varepsilon_{18}^{-1}(E_3LK)^T(E_3LK), \end{aligned} \tag{43}$$

$$(A_2+DHE_2)^T P_7^{-1}(A_2+DHE_2) \le A_2^T(I - \varepsilon_{19}DD^T)^{-1}A_2 + \varepsilon_{19}^{-1}E_2E_2^T, \tag{44}$$

$$\begin{aligned}&(B_2LK+DHE_4LK)^T P_8^{-1}(B_2LK+DHE_4LK)\\&\quad\le (B_2LK)^T(I-\varepsilon_{20}DD^T)^{-1}(B_2LK)+\varepsilon_{20}^{-1}(E_4LK)^T(E_4LK),\end{aligned}\tag{45}$$

We substitute some terms of (25) with (26)-(45), obtain

$$\begin{aligned}\dot V(x,t)\le x^T(t)\{&PA_1+A_1^TP+PB_1LK+K^TLB_1^TP+2PA_2+2PB_2\\&+\varepsilon_1PDD^TP+\varepsilon_1^{-1}E_1^TE_1+\varepsilon_2PDD^TP+\varepsilon_2^{-1}(E_3LK)^T(E_3LK)\\&+\varepsilon_3PDD^TP+\varepsilon_3^{-1}E_2^TE_2+\varepsilon_4PDD^TP+\varepsilon_4^{-1}(E_4LK)^T(E_4LK)\\&+h_1P[A_2P_1A_2^T+A_2P_1E_2^T(\varepsilon_5I-E_2P_1E_2^T)^{-1}E_2P_1A_2^T+\varepsilon_5DD^T]P\\&+h_1P[A_2P_2A_2^T+A_2P_2E_2^T(\varepsilon_6I-E_2P_2E_2^T)^{-1}E_2P_2A_2^T+\varepsilon_6DD^T]P\\&+h_1P[A_2P_3A_2^T+A_2P_3E_2^T(\varepsilon_7I-E_2P_3E_2^T)^{-1}E_2P_3A_2^T+\varepsilon_7DD^T]P\\&+h_1P[A_2P_4A_2^T+A_2P_4E_2^T(\varepsilon_8I-E_2P_4E_2^T)^{-1}E_2P_4A_2^T+\varepsilon_8DD^T]P\\&+kh_2P[(B_2L)(B_2L)^T+(B_2L)(E_4L)^T(\varepsilon_9I-E_4L(E_4L)^T)^{-1}(E_4L)(B_2L)^T+\varepsilon_9DD^T]P\\&+kh_2P[(B_2L)(B_2L)^T+(B_2L)(E_4L)^T(\varepsilon_{10}I-E_4L(E_4L)^T)^{-1}(E_4L)(B_2L)^T+\varepsilon_{10}DD^T]P\\&+kh_2P[(B_2L)(B_2L)^T+(B_2L)(E_4L)^T(\varepsilon_{11}I-E_4L(E_4L)^T)^{-1}(E_4L)(B_2L)^T+\varepsilon_{11}DD^T]P\\&+kh_2P[(B_2L)(B_2L)^T+(B_2L)(E_4L)^T(\varepsilon_{12}I-E_4L(E_4L)^T)^{-1}(E_4L)(B_2L)^T+\varepsilon_{12}DD^T]P\\&+h_1A_1^T(P_1-\varepsilon_{13}DD^T)^{-1}A_1+\varepsilon_{13}^{-1}h_1E_1^TE_1\\&+h_1(B_1LK)^T(P_2-\varepsilon_{14}DD^T)^{-1}(B_1LK)+\varepsilon_{14}^{-1}h_1(E_3LK)^T(E_3LK)\\&+h_1A_2^T(P_3-\varepsilon_{15}DD^T)^{-1}A_2+\varepsilon_{15}^{-1}h_1E_2^TE_2\\&+h_1(B_2LK)^T(P_4-\varepsilon_{16}DD^T)^{-1}(B_2LK)+\varepsilon_{16}^{-1}h_1(E_4LK)^T(E_4LK)\\&+h_2A_1^T(I-\varepsilon_{17}DD^T)^{-1}A_1+\varepsilon_{17}^{-1}h_2E_1^TE_1\\&+h_2(B_1LK)^T(I-\varepsilon_{18}DD^T)^{-1}(B_1LK)+\varepsilon_{18}^{-1}h_2(E_3LK)^T(E_3LK)\\&+h_2A_2^T(I-\varepsilon_{19}DD^T)^{-1}A_2+\varepsilon_{19}^{-1}h_2E_2^TE_2\\&+h_2(B_2LK)^T(I-\varepsilon_{20}DD^T)^{-1}(B_2LK)+\varepsilon_{20}^{-1}h_2(E_4LK)^T(E_4LK)\}x(t)\\&=x^T(t)\Delta x(t),\end{aligned}\tag{46}$$

If $\Delta<0$, (47)

Then $\dot V(x,t)<0$. By the Lyapunov stability theory, the closed-loop system (7) is asymptotically stable, which explain that the system has robust integrity. Multiplying P^{-1} on both sides of formula (47) at the same time, and let $P^{-1}=X$, $Y=KX$, then

$$\begin{aligned}\Delta^*=&A_1X+X^TA_1^T+B_1LY+Y^TLB_1^T+2A_2X+2B_2X\\&+\varepsilon_1DD^T+\varepsilon_1^{-1}X^TE_1^TE_1X+\varepsilon_2DD^T+\varepsilon_2^{-1}(E_3LY)^T(E_3LY)\\&+\varepsilon_3DD^T+\varepsilon_3^{-1}X^TE_2^TE_2X+\varepsilon_4DD^T+\varepsilon_4^{-1}(E_4LY)^T(E_4LY)\\&+h_1[A_2P_1A_2^T+A_2P_1E_2^T(\varepsilon_5I-E_2P_1E_2^T)^{-1}E_2P_1A_2^T+\varepsilon_5DD^T]\\&+h_1[A_2P_2A_2^T+A_2P_2E_2^T(\varepsilon_6I-E_2P_2E_2^T)^{-1}E_2P_2A_2^T+\varepsilon_6DD^T]\\&+h_1[A_2P_3A_2^T+A_2P_3E_2^T(\varepsilon_7I-E_2P_3E_2^T)^{-1}E_2P_3A_2^T+\varepsilon_7DD^T]\\&+h_1[A_2P_4A_2^T+A_2P_4E_2^T(\varepsilon_8I-E_2P_4E_2^T)^{-1}E_2P_4A_2^T+\varepsilon_8DD^T]\\&+kh_2[(B_2L)(B_2L)^T+(B_2L)(E_4L)^T(\varepsilon_9I-E_4L(E_4L)^T)^{-1}(E_4L)(B_2L)^T+\varepsilon_9DD^T]\end{aligned}\tag{48}$$

$$
\begin{aligned}
&+kh_2[(B_2L)(B_2L)^T+(B_2L)(E_4L)^T(\varepsilon_{10}I-E_4L(E_4L)^T)^{-1}(E_4L)(B_2L)^T+\varepsilon_{10}DD^T]\\
&+kh_2[(B_2L)(B_2L)^T+(B_2L)(E_4L)^T(\varepsilon_{11}I-E_4L(E_4L)^T)^{-1}(E_4L)(B_2L)^T+\varepsilon_{11}DD^T]\\
&+kh_2[(B_2L)(B_2L)^T+(B_2L)(E_4L)^T(\varepsilon_{12}I-E_4L(E_4L)^T)^{-1}(E_4L)(B_2L)^T+\varepsilon_{12}DD^T]\\
&+h_1X^TA_1^T(P_1-\varepsilon_{13}DD^T)^{-1}A_1X+\varepsilon_{13}^{-1}h_1X^TE_1^TE_1X\\
&+h_1(B_1LY)^T(P_2-\varepsilon_{14}DD^T)^{-1}(B_1LY)+\varepsilon_{14}^{-1}h_1(E_3LY)^T(E_3LY)\\
&+h_1(A_2X)^T(P_3-\varepsilon_{15}DD^T)^{-1}A_2X+\varepsilon_{15}^{-1}h_1X^TE_2^TE_2X\\
&+h_1(B_2LY)^T(P_4-\varepsilon_{16}DD^T)^{-1}(B_2LY)+\varepsilon_{16}^{-1}h_1(E_4LY)^T(E_4LY)\\
&+h_2X^TA_1^T(I-\varepsilon_{17}DD^T)^{-1}A_1X+\varepsilon_{17}^{-1}h_2X^TE_1^TE_1X\\
&+h_2(B_1LY)^T(I-\varepsilon_{18}DD^T)^{-1}(B_1LY)+\varepsilon_{18}^{-1}h_2(E_3LY)^T(E_3LY)\\
&+h_2X^TA_2^T(I-\varepsilon_{19}DD^T)^{-1}A_2X+\varepsilon_{19}^{-1}h_2X^TE_2^TE_2X\\
&+h_2(B_2LY)^T(I-\varepsilon_{20}DD^T)^{-1}(B_2LY)+\varepsilon_{20}^{-1}h_2(E_4LY)^T(E_4LY)<0.
\end{aligned}
$$

By lemma 2.5, formula (48) is equivalent to formula (8), which implies the desired conclusion.

4 Example

Considering the linear time-varying delay uncertain systems (1), which

$$
A_1=\begin{bmatrix}0.3 & 0.5\\ 0.6 & -0.8\end{bmatrix},\quad A_2=\begin{bmatrix}0.1 & -0.2\\ 0.2 & -0.1\end{bmatrix},\quad B_1=\begin{bmatrix}-0.8 & 0.3\\ 0.5 & 0.6\end{bmatrix},\quad B_2=\begin{bmatrix}0.1 & 0.2\\ 0.3 & 0.2\end{bmatrix},\quad D=\begin{bmatrix}0.1 & 0\\ 0 & 0.1\end{bmatrix},
$$

$$
E_1=\begin{bmatrix}0.1 & 0\\ 0 & 0.1\end{bmatrix},\quad E_2=\begin{bmatrix}0.2 & 0\\ 0 & 0.2\end{bmatrix},\quad E_3=\begin{bmatrix}0.1 & 0.2\\ 0.2 & 0.1\end{bmatrix},\quad E_4=\begin{bmatrix}0.1 & 0.2\\ 0.2 & 0.1\end{bmatrix}
$$

$$
H(t)=\begin{bmatrix}\sin(0.01t) & 0\\ 0 & \cos(0.01t)\end{bmatrix}.
$$

For actuator failures, let matrix $L_0=diag(1,1)$ denotes the normal situation of actuator, let $L_1=diag(0,1)$ and $L_2=diag(1,0)$ respectively represent totally failure of actuator 1, 2. Introducing memoryless state feedback control law (5), according to theorem 1 in this paper, by solving linear matrix inequality LMIs which is constituted by matrix L_0,L_1,L_2, setting $\varepsilon_i=0.1$ $(i=1,2...20)$, h_1=0.6s, h_2=0.2s, k=0.8, we obtain

$$
X=\begin{bmatrix}-0.6560 & -0.6133\\ -0.6133 & 0.3980\end{bmatrix},\ Y=\begin{bmatrix}0.3906 & 0.0832\\ -0.2276 & -0.4398\end{bmatrix},\ \texttt{then}
$$

$$
K=YX^{-1}=\begin{bmatrix}-0.3241 & -0.2903\\ 0.5655 & -0.2337\end{bmatrix}.
$$

Respectively set $h_1(t)=0.3t+0.5$, $h_2(t)=0.3t+0.5$, the initial condition of system is $x(0)=[1,1]^T$, for actuator in the L_0,L_1,L_2, the zero input response curve of state x_1,x_2 is shown in figure 1.

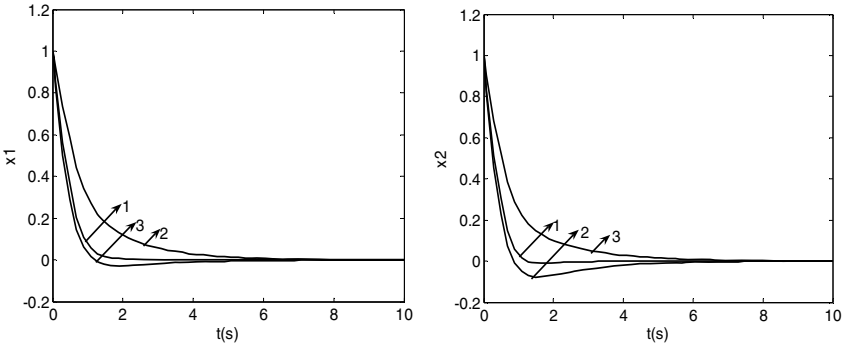

(a) The zero input response of state x_1 (b) The zero input response of state x_2

Fig. 1. The zero input response of system under actuator failures condition

In figure 1, curve 1 is the state response for the normal state of actuator, curve 2 and 3 respectively represent zero input response of state x_1, x_2 for L_1 and L_2 failure of actuator. The simulation results show that the system is asymptotically stable under actuator failure, which implies this method has robust integrity for uncertain linear system with state and control time-delay.

5 Conclusions

This paper, based on Lyapunov stability theory, proposes a state feedback controller design method which can ensure the closed-loop system is still asymptotically stable under the malfunction of actuator, for uncertain linear system with state and control time-delay. Designing examples and simulation results show that this method is effective. By the proof of the theorem and the simulation, also show that for the same system with the same number of sensors and actuator, the feedback control law solved by this method has the equivalence of mathematical sense and adaptability in practical applications.

References

1. Liu, P., Zhou, H.D.: Study on Robust Fault Tolerant Control of Uncertain Linear Time-delay Systems. Control Theory & Applications 20(1), 78–80 (2003)
2. Zheng, Y., Li, L., Fang, J.H.: Controlling Tolerable Fault of Robust in Continuous Systems with Time Variant & Time-delay. Journal of Huazhong University of Science and Technology 29(9), 40–45 (2001)
3. Li, Z.H., Tong, D.S., Shao, H.H.: Robust Fault-Tolerant Control of Uncertain Systems with State and Control Time-delay. Journal of Hunan University (Natural Science) 27(5), 60–64 (2000)

4. Yang, J.J., Wu, F.X., Shi, Z.K.: Robust H_∞ Fault-Tolerant Controller Design for Linear Delay Systems with Uncertainty. Control Theory & Applications 17(3), 442–444 (2000)
5. Yang, H., Sun, J.S., Wang, Z.Q., et al.: Robust Fault-tolerant Control of Uncertain System. Journal of Nanjing University of Science and Technology 29(2), 132–143 (2005)
6. Zhao, Q., Cheng, C.W.: State Feedback Control for Time-Delayed Systems with Actuator Failures. In: Proceedings of the American Control Conference, Denver, Colorado, June 4-6, pp. 827–832 (2003)
7. Zhao, Q., Cheng, C.W.: Robust State Feedback for Actuator Failure Accommodation. In: Proceedings of the American Control Conference, Denver, Colorado, June 4-6, pp. 4225–4230 (2003)
8. Lien, C.H.: Delay-dependent Stability Criteria for Uncertain Neutral Systems with Multiple Time-varying Delays via LMI Approach. IEEE Proc.-Control Theory Appl. 152(6), 707–714 (2005)
9. Xu, S., Lam, J., Zou, Y.: Simplified Descriptor System Approach to Delay-dependent Stability and Performance Analyses for Time-delay Systems. IEEE Proc.-Control Theory Appl. 152(2), 147–151 (2005)
10. Cheng, N.C., Zhao, Q.: Reliable Control of Uncertain Delayed Systems with Integral Quadratic Constraints. IEEE Proc. Control Theory Appl. 151(6), 790–796 (2004)
11. Jing, X.J., Tan, D.L., Wang, U.C.: An LMI Approach to Stability of Systems with Severe Time-Delay. IEEE Trans. Automat. Contr. 49(7), 192–1195 (2004)
12. Mahmoud, M.S.: New Results on Robust Control Design of Discrete-time Uncertain Systems. IEEE processing Control Theory Apply 152(4), 453–459 (2005)
13. Yue, D., Han, Q.L.: Delay-dependent Robust H8 Controller Design for Uncertain Descriptor Systems with Time-varying Discrete and distributed Delays. IEEE Processing Control Theory Apply 152(6), 628–638 (2005)
14. Chen, W., Jiang, J.: Fault-tolerant Control Against Stuck Actuator Faults. IEEE Processing Control Theory Apply 152(2), 138–146 (2005)
15. Mondie, S., Kharitonov, V.L.: Exponential Estimates for Retarded Time-Delay Systems: An LMI Approach. IEEE Transactions on Automatic Control 50(2), 268–273 (2005)

Appendix

Lemma 2.5 (Schur complement properties). Given constant matrices S_{11}, S_{12} and S_{22}, where $S_{12} = S_{12}^T$ and S_{11} is the set of all the $r \times r$ real matrices and

$$S = \begin{bmatrix} S_{11} & S_{12} \\ S_{12}^T & S_{22} \end{bmatrix}$$

The following three conditions are equivalent

$$i)\ S < 0 \qquad ii)\ S_{11} < 0, S_{22} - S_{12}^T S_{11}^{-1} S_{12} < 0 \qquad iii)\ S_{22} < 0, S_{11} - S_{12} S_{22}^{-1} S_{12}^T < 0$$

Lemma 2.6. For any real vectors or matrices X, Y and Z with appropriate dimensions and a positive constant α, and matrix H with appropriate dimensions satisfying $H^T H \le I$, the following inequalities hold:

$$2Y^T HZ \le Y^T Y + Z^T Z \qquad \pm 2X^T Y \le \alpha^{-1} X^T X + \alpha Y^T Y$$

Lemma 2.7. Let A, D, E, F be real matrices of appropriate dimensions with F satisfying $F^T F \le I$. Then, we have

(i) For any real number $\varepsilon > 0$,

$DFE + E^T F^T D^T \le \varepsilon DD^T + \varepsilon^{-1} E^T E$

(ii) For any matrix $P > 0$ and any real number $\varepsilon > 0$ satisfying $\varepsilon I - EPE^T > 0$,

$(A + DFE)P(A + DFE)^T \le APA^T + APE^T(\varepsilon I - EPE^T)^{-1}EPA^T + \varepsilon DD^T$

(iii) For any matrix $P > 0$ and any real number $\varepsilon > 0$ satisfying $P - \varepsilon DD^T > 0$,

$(A+DFE)^T P^{-1}(A+DFE) \le A^T(P-\varepsilon DD^T)^{-1}A+\varepsilon^{-1}E^T E$.

Design of a Single-Phase Grid-Connected Photovoltaic Systems Based on Fuzzy-PID Controller

Fengwen Cao and Yiwang Wang

Department of Electronic & Information Engineering, Suzhou Vocational University, Suzhou 215104, Jiangsu, China
cfw@jssvc.edu.cn

Abstract. The output power of photovoltaic (PV) module varies with module temperature, solar isolation and 1oads changes etc. In order to control the output power of single-phase grid-connected PV system according to the output power PV arrays. In this paper a Fuzzy-PID controller is designed for single-phase grid connected PV system, which includes a DC/DC converter and a single-phase DC/AC inverter that connected to utility grid. Fuzzy-PID control technique is used to realize the system control. The matlab simulation experimental results show that, the proposed method has the good performance.

Keywords: photovoltaic system, Fuzzy-PID control, DC/AC inverter, grid-connected.

1 Introduction

To protect the environment from the industrial pollution and the greenhouse effect, several research and development projects have been realized on renewable energy. The conventional energy sources for electrical power include hydroelectric, fossil fuels, nuclear energy and so on. The wide use of fossil fuels has resulted in the problem of greenhouse emissions worldwide, which also seriously damages the earth's environment and fossil fuels will be exhausted in the future, and their cost has obviously increased. However, photovoltaic is one of the important renewable energy sources. The cost of the photovoltaic is on a falling trend and is expected to fall further as demand and production increases [1-3].

The PV energy is increasing interest in electrical power applications, which is crucial to operate PV energy conversion systems near maximum power point (MPP) to increase the output efficiency of PV arrays. Now, there are many different control methods, such as the inverter control method can be divided into output voltage feedback control and output current feedback control. However, the single phase grid-connected PV system is commonly used inverter output current control method. So far in the current control methods, PID control method has the characteristics of external interference in response to the process of control without overshoot, but the use of conventional PID controller, due to the need for the establishment of precise mathematical model, which can't satisfy the requirements of flexibility of the system. As a result, this paper give a design based on the Fuzzy PID controller to realize the single

D.-S. Huang et al. (Eds.): ICIC 2009, LNAI 5755, pp. 912–919, 2009.

phase PV grid-connected control method, using Fuzzy logic control to overcome the shortcomings of conventional PID control, which application to the single-phase grid-connected PV system to control the inverter, the inverter in order to enhance anti-jamming capability. In this paper, a complete simulation model of the grid-connected PV system based on Fuzzy-PID controller is obtained by MATLAB7.01/SIMULINK software. The results of the simulation experiment are presented and showed the eliminates the concussion at maximum power point and improves system stability.

The grid-connected PV system designed in this paper can feed energy into the existing AC grid system, where the cost of batteries for energy storage can be reduced. In this paper, the grid-connected PV system is given first. Then, the Fuzzy PID controller is described. The controller for grid-connected PV system is designed also. Finally, the simulation experimental results of grid-connected PV system by the Fuzzy PID controller are gotten and discussed.

2 Single-Phase Grid Connected Photovoltaic System

2.1 System Block Diagram

Figure.1 shows the block diagram of the grid-connected PV power system, which includes PV arrays, DC/DC converter, DC/AC inverter and Fuzzy-PID control system. Wher the DC/DC converter is a boost type power converte is applied to trace the maximum power point of the PV arrays' output. The output voltage of DC/DC power converter is regulated by the grid-connected DC/AC full-bridge inverter.

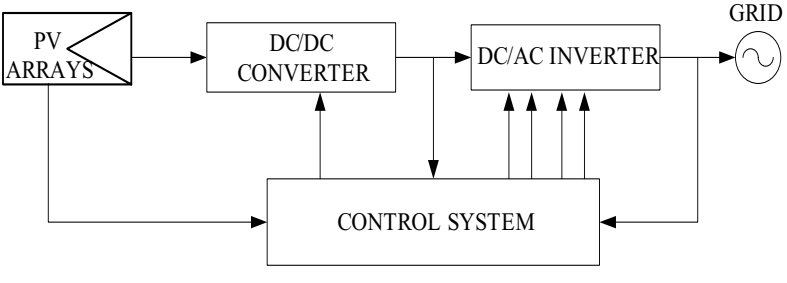

Fig. 1. The block diagram of proposed PV system

The schematic diagram is shown in Figure.2. The boost DC/DC converter with MOSFET switch is used between the PV arrays and the DC/AC inverter. The boost converter duty cycle (D) is adjusted such that maximum PV arrays' output power is extracted under all operating conditions.

2.2 The PV Cell Model

The equivalent circuit of PV solar cell in photovoltaic systems is shown in Figure.3[4]. A photovoltaic cell is based on the physical phenomenon called "photovoltaic effect". The principle consists to transform the photons emitted by the sun in electrical energy.

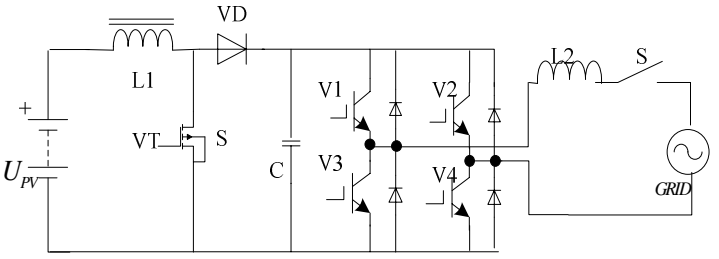

Fig. 2. Grid-connected PV system schematic diagram

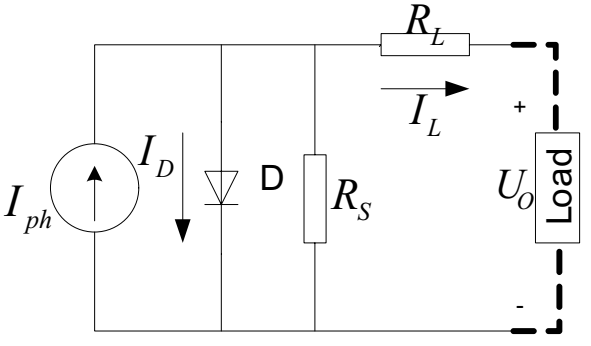

Fig. 3. The equivalent circuit of PV cell model

The output current of a cell is function of the insulation and the temperature, given by the equation below:

$$I_L = I_{ph} - I_D \left[\exp\left(\frac{U_{oc} + I_L R_L}{AkT} \right) - 1 \right] - \frac{U_D}{R_s} \ , \quad i = 1, 2 \ldots n \ . \tag{1}$$

Where, I_D is the saturation current of D, K is the Boltzmann's constant, T is the cell temperature formulated in Kelvin, e the electron charge, k the idealistic factor for a p-n junction. I_L and U_o are the output current and voltage of the PV cell model respectively, I_{ph} is the PV cell model short-circuit current depending on the insulation and the temperature, R_s the shunt resistance which characterized the leakage current of the junction and R_S is the series resistance which represented the different contact and connection resistances. The constants in the above equations will be described by PV cells manufacturers.

According to Eqn.1, the electrical characteristics I (U) of the PV cell model is non linear. The typical I-U curves can be showed in Fig.4.

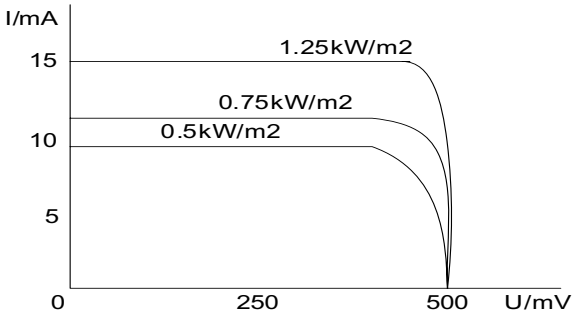

Fig. 4. Typical I-U curve for a PV cell under variable irradiance

2.3 The Control System

Because the change operating voltage of the PV cell array will produce different output power, the ripple voltage of solar cell array will decrease the efficiency of the photovoltaic system. The Fuzzy-PID controller is used to produce a pulse-width modulation (PWM) control signal to turn on or off the power electronic switch of the DC/DC boost converter. The average output voltage across power electronic switch can be derived as:

$$U_{DC} = U_{PV} /(1 - t_{on} / T) = U_{PV} /(1 - D) \quad . \tag{2}$$

Where U_{PV} is input voltage (output voltage of PV arrays), U_{DC} is output voltage and D is the duty ratio of power electronic switch. The DC/AC full-bridge inverter circuit converts to alternate current by closed-loop current control, which can generate a sine wave connected the existence utility grid-connected.

The control block diagram of the PV system is shown in Figure 5. The function of the DC/DC boost converter is to output a stable DC voltage to the grid-connected DC/AC inverter, the feedback control of output voltage and current is designed. As seen in Figure5, the output voltage of the DC/DC boost converter is sensed by a voltage sensor and compared with a setting voltage, and then, the compared result is sent to a Fuzzy-PID controller. The output of Fuzzy PID controller is sent to a PWM control circuit. The output of the PWM circuit is sent to a driver circuit to generate the driver signal for the power electronic device of the DC/DC boost converter. The DC/AC inverter control use SPWM control, which can output a sine alternate current to connected the grid. In this paper, MPPT is done by a Fuzzy-PID controller as shown in Figure 5. to reach the output panel characteristics around the optimal voltage for the maximum energy.

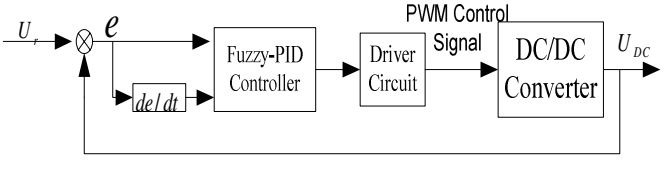

Fig. 5. Control system of the DC/DC converter based on Fuzzy-PID controller

The inputs to the Fuzzy PID controller are error of the DC/DC boost converter output voltage and the preset voltage. The two inputs are processed by the fuzzy logic controller. Thus during transient conditions the fuzzy logic controller outputs a larger incremental reference current to speed up the transient response but outputs almost zero incremental reference current near the peak power region to reduce oscillations about the MPP.

3 The Fuzzy PID Control for Single Phase Grid-Connected PV Generation System

In order to reach stable efficient high-precision control method in the PV generation system. But PV system is a complex multi-variable, non-linear, strong-coupling system, difficult to establish accurate mathematical model, based on fuzzy control is a knowledge and experience of control methods, so Fuzzy PID control for grid-connected those system can get better control results. A typical block diagram of a Fuzzy PID controller is shown in Figure 6. In generally, Fuzzy-PID control method not only has the advantage of fuzzy control without precise mathematical model, good robustness, good dynamic response curve, short response time etc, but also owns the advantage of dynamic tracking characteristic and steady state precision. The fuzzy rule base is used to realize the online modulation of the three revised parameters of PID ΔK_p, ΔK_i and ΔK_d.

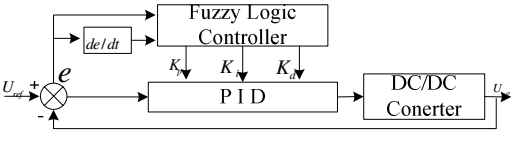

Fig. 6. Block diagram of the Fuzzy PID controller

3.1 Fuzzification and Variables

The inputs to the Fuzzy PID controller are the error signal e, the change of the error Δe and the three outputs ΔK_p, ΔK_i and ΔK_d, which are used to modify PID parameters.

Both input variables e and Δe are divided into seven fuzzy levels or subsets in this design, which are PB (Positive Big), PM (Positive Medium), PS (Positive Small), ZZ (Zero), NS(Negative Small), NM (Negative Medium) and NB (Negative Big). The Fuzzy set PS assumes a membership value greater than zero beginning at the origin, in the present model, the Fuzzy set PS is offset from the origin in order to speed up the start-up process and at the same time prevent variation of the reference current at the MPP. Additional Fuzzy sets PM and NM have also been added to improve the control surface and allow a smooth transition from the transient to the steady-state.

In the same way, the output variables ΔK_p, ΔK_i and ΔK_d are also divided into seven fuzzy sets as the input variables, which are PB (Positive Big), PM (Positive Medium), PS (Positive Small), ZZ (Zero), NS (Negative Small), NM (Negative Medium) and NB (Negative Big).

3.2 Fuzzy Rules for Control

A rule base is a set of (IF-Then) rules, which contains a fuzzy logic quantification of the expert linguistic description of how to achieve good control [7]. The basic rule base of these controllers types is given by:

$$\text{IF } e \text{ is A and } \Delta e \text{ is B THEN } \begin{matrix} u \\ \Delta K_i \end{matrix} \text{ is C.}$$

Where u represents the fuzzy output variable. For input and output membership function table 1 show the control rule that used for fuzzy Kp, Ki and Kd respectively.

Table 1. Rule base for fuzzy PID controller

ΔK / Δe \ e	NB	NM	NS	ZZ	PS	PM	PB
NB	PB	PB	PM	NM	NS	ZZ	ZZ
NM	PB	PB	PM	PS	PS	ZZ	NS
NS	PM	PM	PM	PS	PS	ZZ	NS
ZZ	PM	PM	PS	ZZ	NS	NM	NM
PS	PS	PS	ZZ	NS	NS	NM	NM
PM	PS	ZZ	NS	NM	NM	NM	NB
PB	ZZ	ZZ	NM	NM	NM	NS	NB

ΔK / Δe \ e	NB	NM	NS	ZZ	PS	PM	PB
NB	NB	NB	NM	NM	NS	ZZ	ZZ
NM	NB	NB	NM	NS	NS	ZZ	ZZ
NS	NB	NM	NS	NS	ZZ	PS	PS
ZZ	NM	NM	NS	ZZ	PS	PM	PM
PS	NM	NS	ZZ	PS	PS	PM	PB
PM	ZZ	ZZ	PS	PS	PM	PB	PB
PB	ZZ	ZZ	PS	NM	PM	PB	PB

ΔK / Δe \ e	NB	NM	NS	ZZ	PS	PM	PB
NB	PS	NS	NB	NB	NB	NM	PS
NM	PS	NS	NB	NM	NM	NS	ZZ
NS	ZZ	NS	NM	NM	NS	NS	ZZ
ZZ	ZZ	NS	NS	NS	NS	NS	ZZ
PS	ZZ	ZZ	ZZ	ZZ	ZZ	ZZ	ZZ
PM	PB	PS	PS	PS	PM	PB	PB
PB	PB	PM	PM	PM	PS	PS	PB

3.4 Defuzzification Method

The output of the Fuzzy PID controller is Fuzzy sets. However a crisp output value is required. Hence the output of the Fuzzy controller should be defuzzified. The most popular method, center of gravity or center. This method has good averaging properties and simulation results showed that it provided the best results.

4 System Simulations

The establishment of PV generation system model in the MATLAB7.01/ SIMLINK is designed. The maximum power point tracking was controlled by using a fuzzy logic control and inverter current control using predicted current control to control current of inverter to be sinusoidal wave shape.

The simulation results of system following parameters are listed as follows: PV arrays: 100W; AC = 220V, 50Hz.

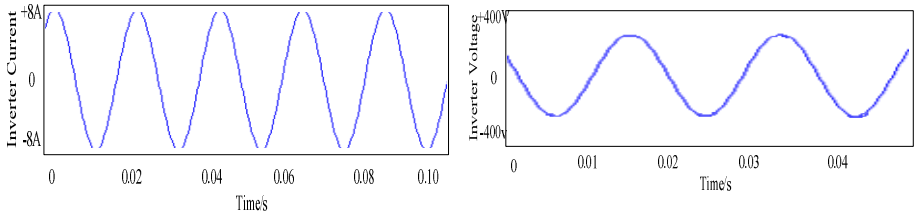

Fig. 7. The waveform of inverter current and voltage

This grid-connected PV system is simulated by use MATLAB/SIMULINK. Fig.7. shows the output voltage of inverter, which demonstrate this system can provide energy to utility with low harmonics and high power factor.

5 Conclusion

In this paper, a single-phase grid connected PV based on Fuzzy-PID controller has been built by applying the proposed control strategy. The Fuzzy-PID controller has been designed in details. The designed system has simulated. The matlab simulation experimental results show that, the proposed method has the expected good performance.

Acknowledgment

This work was supported by the 2009 Senior Talent Culture Project of Suzhou Municipal Government and the Innovative Team's Scientific Research Program of Suzhou Vocational University(200802).

References

1. Jou, H.L., Chiang, W.J., Wu, J.C.: Novel Maximum Power Point Tracking Method for the Photovoltaic System. In: 7th International Conference on Power Electronics and Drive Systems, pp. 620–623 (2007)
2. Kroposki, B., DeBlasio, R.: Technologies for the New Millennium: Photovoltaics as a Distributed Resource. In: Proc. IEEE Power Engineering Society Summer Meeting, vol. 3, pp. 1798–1801 (2000)
3. Wu, T.F., Nien, H.S., Shen, C.L., Chen, T.M.: A Single-Phase Inverter System for PV Power Injection and Active Power Filtering with Nonlinear Inductor Consideration. IEEE Trans. on Industry Applications 41(4), 1075–1083 (2005)
4. Veerachary, M., Senjyu, T., Uezato, K.: Voltage-Based Maximum Power Point Tracking Control of PV System. IEEE Trans. on Aerospace Electronic System 38(1), 262–270 (2002)
5. Mol, J.H., He, S.J., Zoul, Y.P.: Fuzzy PID Controller Design for PWM-Buck EBW Stabilized High-Voltage Source Using Saber-Matlab Co-simulation. In: 2007 IEEE International Conference on Control and Automation, Guangzhou, China, pp. 2003–2007 (2007)

6. Zhang: Fuzzy Modeling and Fuzzy Control, 3rd edn., pp. 116–229. Birkhauser Press, Basel (2006)
7. Passino, K.M., Yurkovich, S.: Fuzzy Control. Addison Wesley longnan, Inc, Reading (1998)
8. Reznik, L., Ghanayem, O., Bourmistrov, A.: PID Plus Fuzzy Controller Structures as A Design Base for Industrial Applications. Engineering appliaction of artificial Intelligence 13(4), 419–430 (2000)
9. Khaehintung, N., Pramotung, K., Tuvirat, B., Sirisuk, P.: RISC-Microcontroller Built-in Fuzzy Logic Controller of Maximum Power Point Tracking for Solar-Powered Light-Flasher Applications. IEEE IECON 3, 2673–2678 (2004)

Ontology-Based Decision Support for Security Management in Heterogeneous Networks

Michał Choraś[1,2], Rafał Kozik[2], Adam Flizikowski[1,2], Rafał Renk[1,3], and Witold Hołubowicz[1,3]

ITTI Ltd., Poznań
Institute of Telecommunications, UT&LS Bydgoszcz
Adam Mickiewicz University, Poznań
michal.choras@itti.com.pl, chorasm@utp.edu.pl, holubowicz@amu.edu.pl

Abstract. In this paper our original methodology of applying ontology-based logic into decision support system for security management in heterogeneous networks is presented. Such decision support approach is used by the off-network layer of security and resiliency mechanisms developed in the INTERSECTION Project. Decision support application uses knowledge about networks vulnerabilities to support off-network operator to manage and control in-networks components such as probes, intrusion detection systems, Complex Event Processor, Reaction and Remediation. Hereby, both *IVO* (Intersection Vulnerability Ontology) as well as *PIVOT* - decision support system based on the vulnerability ontology are presented.

1 Introduction

INTERSECTION (INfrastructure for heTErogeneous, Resilient, SEcure, Complex, Tightly Inter-Operating Networks) is a European co-funded project in the area of secure, dependable and trusted infrastructures. The main objective of INTERSECTION is to design and implement an innovative network security framework which comprises different tools and techniques for intrusion detection and tolerance.

The INTERSECTION framework as well as the developed system called IDTS (Intrusion Detection and Tolerance System) consists of two layers: in-network layer and off-network layer. Our decision support system is placed in the off-network layer of the INTERSECTION security-resiliency framework. The role of the off-network decision support system is to support network operators in controlling complex heterogeneous and interconnected networks and real-time security processes such as network monitoring, intrusion detection, reaction and remediation.

The knowledge about vulnerabilities is needed to more effectively cope with threats and attacks, and to understand interdependencies and cascade effects within the networks. Therefore network vulnerabilities should be identified, described, classified, stored and analyzed. The framework operator should be able to control in-network processes and trigger/stop their reactions on the basis of

D.-S. Huang et al. (Eds.): ICIC 2009, LNAI 5755, pp. 920–927, 2009.

the vulnerability knowledge which is incorporated in our decision support system intelligence by means of the vulnerability ontology.

In this paper we show, how the previously described concept of INTERSECTION Vulnerability Ontology in [1] [2] [3] is now used for decision support. The paper is structured as follows: ontology-based approach is introduced and motivated in Section 2. Our vulnerability ontology is presented in Section 3. Decision support application based on ontology is described in Section 4.

2 Vulnerability Knowledge for Decision Support-Ontology-Based Approach

In both computer science and information science, an ontology is a form of representing data model of a specific domain and it can be used to e.g.: reason about the objects in that domain and the relations between them. Since nowadays, we can observe the increasing complexity and heterogeneity of the communication networks and systems, there is a need to use high-level meta description of relations in such heterogeneous networks.

This need and requirement is particularly apparent in the context of Future Internet and Next Generation Networks development. From operators point of view, two important issues concerning communications networks are: security and Quality of Service.

In the past years critical infrastructures were physically and logically separate systems with little interdependence. As digital information gained more and more importance for the operation of such infrastructures especially on the communication part. Communication part of critical infrastructures are the one of the most important part that represents the information infrastructure on which critical infrastructures rely and depend.

The communication part is typically related to telecom operators or separate department inside company that manages the network. The last decade has seen major change in telecommunication market in most of European countries.

The are two main factors that cause those changes:

- Market deregulation that enables new telecom providers to enter the market
- New technologies and solutions that cause lower costs of services, introduction of the new services and increased telecom traffic.

Unfortunately, the increasing complexity and heterogeneity of the communication networks and systems increase their level of vulnerability.

Furthermore, the progressive disuse of dedicated communication infrastructures and proprietary networked components, together with the growing adoption of IP-based solutions, exposes critical information infrastructures to cyber attacks coming from the Internet and other IP based networks.

To deal with those problems there is a need to create good information security management system that will allow the administrators to deal with a great amount of security information and make the decision process effective and efficient.

To support those tasks we propose to develop the security framework consisting of several modules as well as of the decision support system based on the applied ontology.

3 Ontology Design

One of the goals of the INTERSECTION project is to identify and classify heterogeneous network vulnerabilities. To match this goal we have proposed a vulnerability ontology. The major aim of our ontology is to describe vulnerabilities beyond single domain networks and to extend relations/restrictions onto heterogeneous networks. Our ontology is now called *IVO* - INTERSECTION Vulnerability Ontology.

Networks vulnerabilities tend to be often mistaken with threats and attacks. Therefore we decided to clearly define vulnerability as asset-related network weakness. Obviously, then such weaknesses are exploited by threats and attacks. Such vulnerability definition is based on ISO/IEC 13335 standard and is shown in Figure 1 [4].

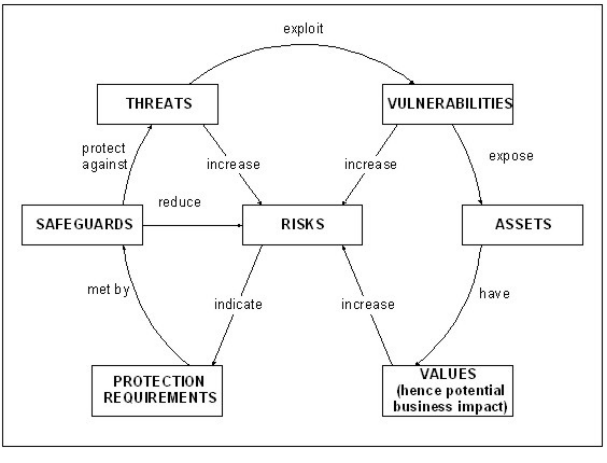

Fig. 1. Vulnerabilities identification and definition on the basis of networks assets

Networks assets should also be defined and described. We decided to use Shared Information/Data (SID) Model in which networks assets and relations between them are defined. SID Model provides Physical Resource Business Entity Definitions [5]. SID assets description is specified in UML and visualized using UML diagrams.

In our ontology approach, we found Resources and Vulnerabilities classes as a the most important components. Class Resources is based on division proposed in SID (Shared Information/Data Model).

It includes following subclasses:

- Physical Resources,
- Logical Resources,
- Software
- Service.

Class Vulnerabilities is connected with Resources (exposed by them). That is why subclasses of Vulnerability class are:

- Physical Resources Vulnerabilities,
- Logical Resources Vulnerabilities,
- Software Vulnerabilities.

Every subclass inherited properties and restrictions from its superclass that is why we decided to classified our ontology in this way. For example classes Wired and Wireless inherited Resources, Topology, Vulnerabilities, Network Structure, Risk and Safeguards from superclass Network.

Our vulnerability ontology is focused on network design vulnerabilities (e.g. protocols weakness etc.). In contrast there are some implementation vulnerabilities, however these are already stored in National Vulnerability Database (NVD) [6].

4 Ontology Applied to Decision Support

The created ontology is applied in our decision support system intelligence providing knowledge about vulnerabilities and how they influence specific interconnected scenarios.

Decision support system applied to security management in heterogeneous networks has the following functionalities:

1. Provides information about influence of heterogeneity onto networks security and resiliency issues
2. Provides information to Intrusion Detection and Anomaly Detection Systems decision support tool provides information about security risks and threats in particular scenarios (what networks are interconnected, what technologies are used etc.). Intrusion detection systems receive information on how to act in such scenarios (e.g. how often the packets should be sniffed, what features should be extracted etc.)
3. Supports decisions of Intrusion Tolerance Systems decision support system provides information about tolerance, expected False Positives etc.
4. Provides useful information for security architecture visualization module additional information for end-users (network management operators)
5. Supports Complex Event Processor Module (a part of IDS system) - decision support drives the decision engine while performing the correlation activity
6. Decision support system cooperates with the relational vulnerabilities database (IVD) created in FP7 INTERSECTION Project.

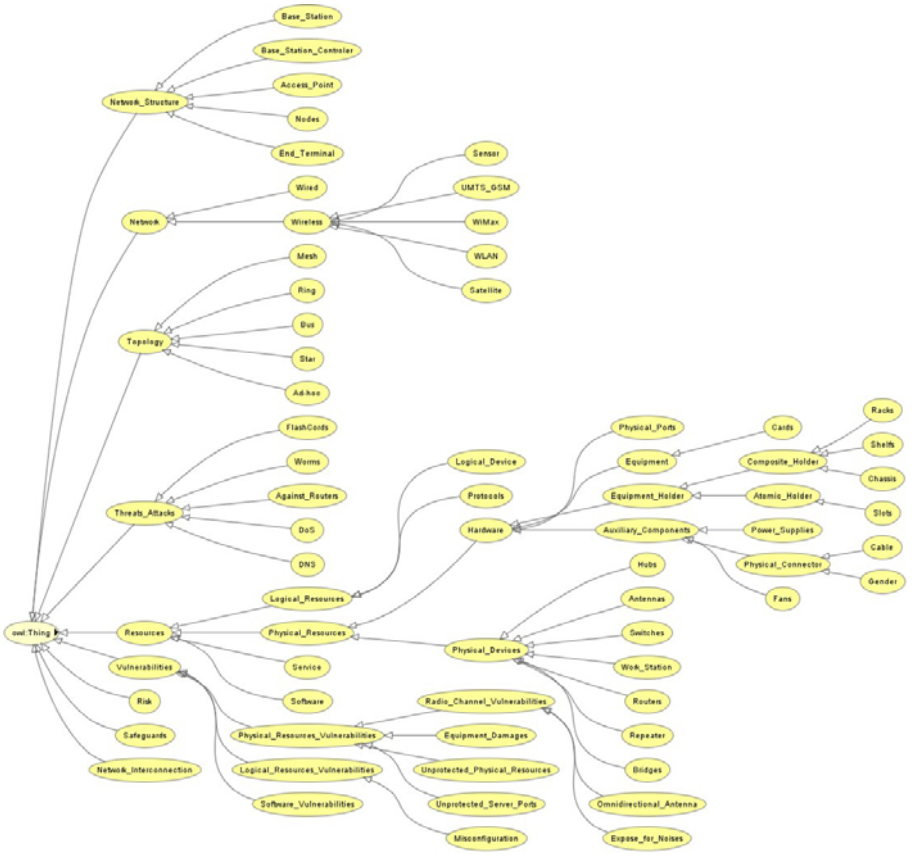

Fig. 2. IVO Visualized in Protege

PIVOT (Project INTERSECTION Vulnerability Ontology Tool) is the ontology-logic based decision support tool. Our goal was to apply ontology in a real-life decision-support application.

It is end-user oriented application, which allows to modify and browse the vulnerability ontology. One of the biggest advantages is tool has client-server architecture, what allows to share one ontology by multiple users (e.g. by network operators).

The ontology interface built in PIVOT is user-friendly and intuitive.

The application consists of MySQL storage database, Protege OWL API, Tomcat WWW server and OpenLaszlo framework. The backbone of the tool is Protege API. It is an open-source Java library for the Web Ontology Language and RDF(S).

The API provides classes and methods to load and save OWL files, to query and manipulate OWL data models, and to perform reasoning. Furthermore, the API is optimized for the implementation of graphical user interfaces. The

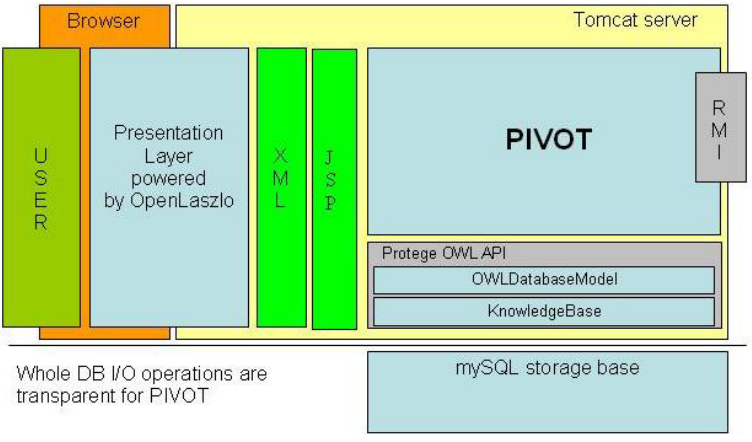

Fig. 3. PIVOT architecture

greatest part of API is that Protege allows to work with OWL model having MySQL database in backend, what makes dramatic performance improvements.

Client-server architecture allows to share one ontology model with multiple users. Each connection to PIVOT is transactional, what provide better ontology database integrity. All database operation (the way the model is stored in db) are transparent for PIVOT, what means that user do not have to worry about establishing connection, committing changes (made on model) or bothering where and how the particular instance is stored.

Actual version of PIVOT allows to establish two types of connection - the RMI and the HTTP. RMI (Java Remote Method Invocation API) is a Java application programming interface for performing the remote procedure calls. This type of PIVOT interface was developed to be use with other components in local network. This gives opportunity to share ontology among other processes running on remotes machines.

The HTTP interface is developed to perform easy OWL model maintenance and management through the web browser. This functionality is provided by Apache Tomcat server. This server is developed by the Apache Software Foundation (ASF). Tomcat implements the Java Servlet and JavaServer Pages (JSP) specifications form Sun Microsystems, and provides a pure Java HTTP web server environment for Java. It is used as a PIVOTs module which is started on PIVOT boot up.

Java Server Pages (JSP) is Java technology that allows software developers to dynamically generate HTML, XML or other types of documents in response to web client request. The technology allows Java code and certain predefined actions to be embedded into static content. PIVOT benefits from easy XML document generation. This format allows to define own elements and to help share structured information via network, what makes PIVOT more universal.

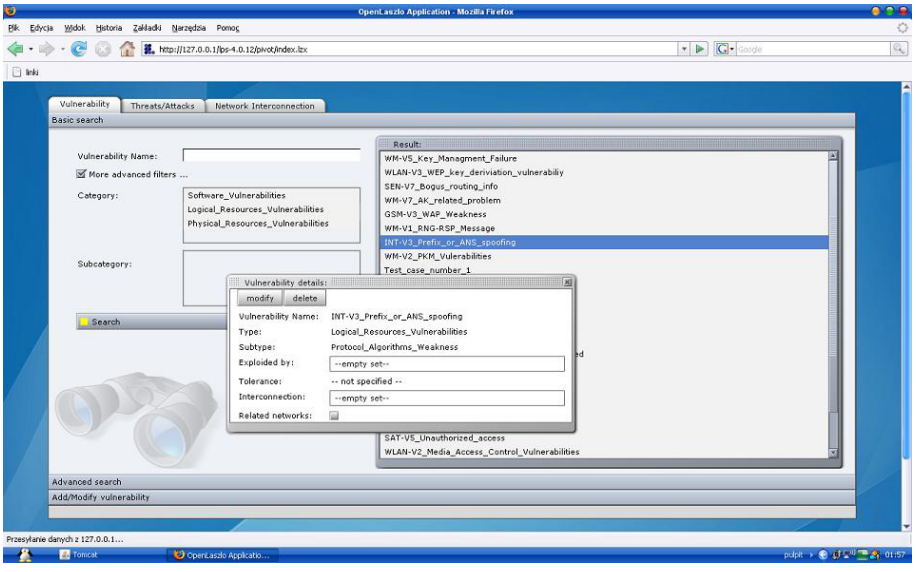

Fig. 4. PIVOT in operation (screenshot)

To boost the presentation layer OpenLaszlo is used. It is an open source platform for the development and delivery of rich Internet applications.

PIVOT architecture is presented in Figure 3.

PIVOT is now available at: http://193.142.112.119:8081/lps-4.1.1/pivot/. PIVOT interface in operation is shown in Figure 4.

5 Conclusions

The major contribution of this paper is a new approach to vulnerability description and handling based on the ontology logic. INTERSECTION Vulnerability Ontology has been motivated and presented in detail. We also showed how to apply *IVO* in an innovative decision support system used in INTERSECTION security-resiliency framework. Moreover, PIVOT - ontology-logic based decision support application has been developed and presented.

Our decision support system can be used by end-users such as networks operators and telecoms to manage heterogeneous and interconnected networks.

Acknowledgement

The research leading to these results has received funding from the European Community's Seventh Framework Programme (FP7/2007-2013) under grant agreement no. 216585 (INTERSECTION Project).

References

1. FP7 INTERSECTION Deliverable D.2.2: Identification and classification of vulnerabilities of network infrastructures (2008)
2. Flizikowski, A., et al.: On Applying Ontologies to Security and QoS Management in Heterogeneous Networks. In: Information Systems Architecture and Technology - Information Systems and Computer Communications Network, 189-200, ISBN 978-83-7493-416-9 (2008)
3. Michal, C., et al.: Ontology-based description of networks vulnerabilities. Polish Journal of Environmental Studies 5c (2008)
4. ISO/IEC 13335-1:2004, Information Technology Security Techniques Management of information and communications technology security Part 1: Concepts and models for information and communications technology security management
5. Shared Information/Data Model TeleManagement Forum (2002)
6. http://nvd.nist.gov/
7. FP7 INTERSECTION (INfrastructure for heTErogeneous, Reislient, Secure, Complex, Tightly Inter-Operating Networks) Project Description of Work.
8. Ekelhart, A., et al.: Security Ontologies: Improving Quantative Risk Analy-sis. In: Proc. of the 40th Hawaii International Conference on System Sciences (2007)
9. http://protege.stanford.edu/
10. OWL Web Ontology Language Semantics and Abstract Syntax (2006), http://www.w3.org/TR/owl-features/
11. SWRL: A Semantic Web Rule Language Combning OWL and RuleML, W3C Member Submission, http://www.w3.org/Submission/SWRL/
12. Spector, A.Z.: Achieving application requirements. Distributed Systems, 0-201-41660-3, 19-33 (1990)
13. Gomez, A., Corcho, O.: Ontology languages for the Semantic Web. IEEE Intelligent Systems 1904, 54–60 (2002)

A Constrained Approximation Algorithm by Encoding Second-Order Derivative Information into Feedforward Neural Networks

Qing-Hua Ling[1] and Fei Han[2]

[1] School of Computer Science and Engineering, Jiangsu University of Science and Technology, Zhenjiang, Jiangsu, 212003, China
[2] School of Computer Science and Telecommunication Engineering, Jiangsu University, Zhenjiang, Jiangsu, 212013, China
lingee_2000@163.com, hanfei1976@163.com

Abstract. In this paper, a constrained learning algorithm is proposed for function approximation. The algorithm incorporates constraints into single hidden layered feedforward neural networks from the *a priori* information of the approximated function. The activation functions of the hidden neurons are specific polynomial functions based on Taylor series expansions, and the connection weight constraints are obtained from the second-order derivative information of the approximated function. The new algorithm has been shown by experimental results to have better generalization performance than other traditional learning ones.

1 Introduction

The popular method for training a feedforward neural network (FNN) is the back-propagation (BP) algorithm [1] which applies the gradient descent method to derive the updated formulae of the weights. However, first, these learning algorithms are apt to be trapped in local minima but global minima. Second, they have not considered the network structure features as well as the involved problem properties, thus their generalization capabilities are limited [2-6]. A proper matching between the underlying problem complexity and the network structure complexity is crucial for improving the network generalization capability [4].

In the literature [5-6], a class of constrained learning algorithm (CLA) was proposed by coupling the *a priori* information from problems into the cost functions defined at the network output layer. As a result, the solutions for the involved problems finding the roots of polynomials can be very easily obtained. In the literatures [7-8], two learning algorithms were proposed that are referred to as Hybrid-I and Hybrid-II methods. In the Hybrid-I algorithm, the cost terms for the additional functionality based on the first-order derivatives of neural activation at hidden layers were designed to penalize the input-to-output mapping sensitivity in the course of training the weights. By forcing the hidden layer neurons to work in saturating mode, this algorithm can increase the problem complexity and improve the generalization

D.-S. Huang et al. (Eds.): ICIC 2009, LNAI 5755, pp. 928–934, 2009.

capability for the involved network. As for the Hybrid-II algorithm, it incorporates the second-order derivatives of the neural activations at hidden layers and output layer into the sum-of-square error cost function to penalize the high frequency components in training data. In the literature [9], a modified hybrid algorithm (MHLA) is proposed according to the Hybrid-I and Hybrid-II algorithms to improve the generalization performance. Nevertheless, these learning algorithms do not consider the information of the approximated function when they are used to solve the function approximation problem.

In the literature [10], a new learning algorithm referred as FDCLA was proposed for function approximation. The first-order derivative information of the approximated function was incorporated in the FDCLA. Similar to FDCLA, the new algorithm in this paper incorporates both architectural constraints and connection weight constraints. The former are realized by selecting the activation functions of the hidden neurons as a class of specific polynomial functions which are extracted from Taylor series expansion. The latter are extracted from the second-order derivative of the approximated function. Finally, simulated results are given to verify the better convergence performance of the proposed algorithm.

2 The Proposed Approximation Algorithm

Assume that the sample points of the function are selected at identically spaced intervals. In addition, these points, i.e., (x_i, y_i), $i = 1,2,\ldots,N.$, are very close in space.

According to Mean-Value Theorem, the corresponding approximate estimated values of the functional first-order derivative can be obtained as follows [10]:

$$f'(x_i) \approx {(y_{i+1} - y_{i-1})}\Big/{(x_{i+1} - x_{i-1})}, i = 2,\cdots,N-1. \tag{1}$$

$$f'(x_1) \approx {(y_2 - y_1)}\Big/{(x_2 - x_1)}, f'(x_N) \approx {(y_N - y_{N-1})}\Big/{(x_N - x_{N-1})} \tag{2}$$

As for the second-order derivative of the approximated function, its approximation value can be obtained as follows:

$$f'(x_{i+\frac{1}{2}}) \approx {(y_{i+1} - y_i)}\Big/{(x_{i+1} - x_i)}, i = 1,2,\ldots,N-1. \tag{3}$$

$$f''(x_i) = {(f'(x_{i+\frac{1}{2}}) - f'(x_{i-\frac{1}{2}}))}\Big/{(x_{i+\frac{1}{2}} - x_{i-\frac{1}{2}})}, \ i = 2,\ldots,N-1. \tag{4}$$

$$f''(x_1) = f''(x_2), \ f''(x_N) = f''(x_{N-1}) \tag{5}$$

When the function is approximated by the FNN, $\phi(x)$, the following constraints can be easily obtained:

$$\phi''(x_i) - f''(x_i) = 0, i = 1,2,\cdots,N. \tag{6}$$

This constraint can be simplified as:

$$\Phi 2 \equiv \phi''(x) - f''(x) = 0 \tag{7}$$

where $f''(x)$ is a constant, but it varies with different value of the variable x.

First, according to the literature [10], a single hidden layered FNN is adopted for approximating the function and the transfer function of the k th hidden neuron is selected as the function of $x^k/k!$, $k = 1,2,\ldots,n.$. The activation function of the $(n+1)$ th hidden neuron is fixed as $-1.$. The weights from the input layer to the hidden layer are all fixed to one, i.e., $w_{k,1}^{(1)} = 1, k = 1,2,\cdots,n.$ Second, the constraints containing derivative information of the approximated function can be obtained, as shown in Eqn. (7). Finally, from literatures [5-6,10], a constraint for updated synaptic weights is imposed to avoid missing the global minimum as follows:

$$\sum_{i=1}^{n} (d\, w_{1,i}^{(2)})^2 = (\delta P)^2 \tag{8}$$

where $d\, w_{1,i}^{(2)}$ denotes the change of synaptic weight $w_{1,i}^{(2)}$, and δP is a predetermined positive value.

A sum-of-square error cost function is defined at the output of the FNN:

$$E = \frac{1}{2N} \sum_{i=1}^{N} (t_i - y_i)^2 \tag{9}$$

where t_i denotes the target signal, y_i is the actual output of the network, and N is the number of training samples.

Suppose that $d\Phi = (d\Phi 2)^T$ is equal to a predetermined positive value δQ, designed to bring $d\Phi$ closer to its target (zero).

As for k th training pattern, by introducing the function ε_k, $d\varepsilon_k$ is expanded as follows [5-6,10]:

$$d\varepsilon_k = \sum_{i=1}^{n} J_i d\, w_{1,i}^{(2)} + (\delta Q - \sum_{i=1}^{n} d\, w_{1,i}^{(2)} F_i) v + ((\delta P)^2 - \sum_{i=1}^{n} (d\, w_{1,i}^{(2)})^2) u \tag{10}$$

$$J_i = \frac{\partial E^k}{\partial w_{1,i}^{(2)}}, \ (E^k = \tfrac{1}{2}(t_k - y_k)^2), \quad F_i = \frac{\partial \Phi 2}{\partial w_{1,i}^{(2)}}, \ (i = 1,2,\cdots,n+1.) \tag{11}$$

According the above FNN, the following results can be obtained:

$$J_i = -(t_k - y_k)\frac{x_k^i}{i!}, \ i = 1,2,\ldots,n. \quad J_{n+1} = (t_i - y_i) \tag{12}$$

$$F_i = \frac{\partial \Phi 2}{\partial w_{1,i}^{(2)}} = \frac{x_k^{i-2}}{(i-2)!}, \quad (i = 2,\cdots,n.) \quad F_1 = F_{n+1} = 0 \tag{13}$$

In order to maximize $|d\varepsilon|$ at each epoch, the following equations are obtained:

$$d^2\varepsilon_k = \sum_{i=1}^{n}(J_i - F_i v - 2ud\, w_{1,i}^{(2)})\, d^2 w_{1,i}^{(2)} = 0 \tag{14}$$

$$d^3\varepsilon_k = -2u\sum_{i=1}^{n}(d^2 w_{1,i}^{(2)})^2 < 0 \tag{15}$$

According to the Eqns.(14)-(15), the synaptic weights updated formula is obtained:

$$d\, w_{1,i}^{(2)} = \frac{J_i}{2u} - \frac{F_i v}{2u} \tag{16}$$

$$u = -\frac{1}{2}\left(\frac{I_{JJ} - I_{JF}^T I_{FF}^{-1} I_{JF}}{(\delta P)^2 - \delta Q I_{FF}^{-1}\delta Q}\right)^{1/2},\ v = -2u\, I_{FF}^{-1}\delta Q + I_{FF}^{-1} I_{JF} \tag{17}$$

where $I_{JJ} = \sum_{i=1}^{n} J_i^2$, $I_{JF} = \sum_{i=1}^{n} J_i F_i$, and $I_{FF} = \sum_{i=1}^{n} F_i^2$. According to literatures [5-6,10], δP and δQ can be selected as:

$$\delta P(t) = \delta P_0(1 - e^{-\theta/t}),\ \delta Q = -\zeta\Phi 2 = -\eta\delta P\Phi 2 \Big/ (|\Phi 2|\sqrt{I_{FF}^{-1}}) \tag{18}$$

where δP_0 is the initial value for δP; t is the time index for training, θ is the scale coefficient of time t; ζ and η are free parameters , which η is a positive value which is less than one.Since this new algorithm encodes the constraints from the second-order derivative of the approximated function, we call it as the second-order derivative CLA (SDCLA).

3 Experiment Results

In this section we shall conduct the experiments with a unimodal function, $y = \frac{\sin(x) + (\frac{x}{3} + \frac{x^2}{9})e^{-0.5x^2}}{2}$, and a bimodal function, $y = \frac{\frac{\sin(2x)}{2} + (\frac{x}{2} + \frac{x^2}{6} + \frac{x^3}{10})e^{-0.5x^2}}{2}$. This new algorithm is compared with the Hybrid-I, Hybrid-II, MHLA, FDCLA and traditional BP algorithms. The transfer functions of the neurons in all layers for all algorithms except for FDCLA and SDCLA are tangent sigmoid function. In the experiments for approximating the unimodal function, the number of the hidden neurons for the above five learning algorithms is eight. As for approximating the bimodal function, ten hidden neurons are selected in FNN for all learning algorithms.

In the experiments, assume that the number of the total training data is 126, which are selected from [0,π] at identical spaced interval. Likely, 125 testing samples are also selected from [0.0125, π-0.0125] at identical spaced interval.

For approximating the unimodal function, the free parameters of SDCLA are initiated as ($\delta P_0 = 1, \theta = 10.0, \eta = 0.1$). As approximating the bimodal function, the ones are initiated as ($\delta P_0 = 2, \theta = 6.0, \eta = 0.12$).As a result, the approximation error of the testing samples for two functions with the SDCLA is shown in Fig. 1.

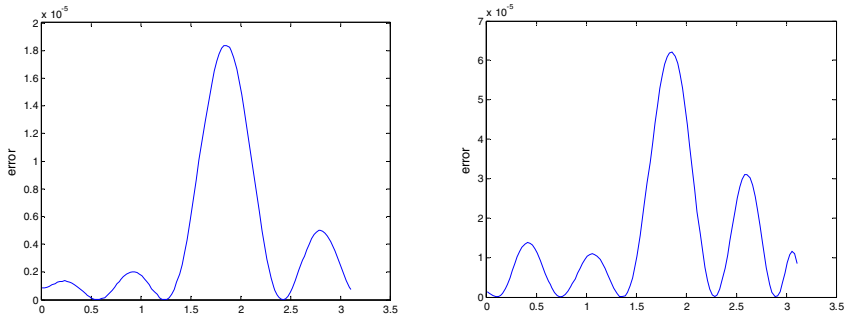

(a) (b)

Fig. 1. The approximation error of the testing samples with the new CLA. (a) the unimodal function; (b) the bimodal function.

In order to statistically compare the approximation accuracies of the above six algorithms for the two functions, the experiments are conducted fifty times for each algorithm, and the corresponding results are summarized in Table 1-2.

Table 1. The approximation accuracies for the unimodal function with six algorithms

Learning algorithm	Training error	Testing error
Traditional BP	1.0606e-5	1.0105e-5
Hybrid-I	8.6619e-6	8.5290e-6
Hybrid-II	9.2100e-6	8.5750e-6
MHLA	7.0775e-6	7.0586e-6
FDCLA	2.7178e-6	2.6696e-6
SDCLA	2.1497e-6	2.1642e-6

Table 2. The approximation accuracies for the bimodal function with six algorithms

Learning algorithm	Training error	Testing error
Traditional BP	1.4979e-5	1.4734e-5
Hybrid-I	1.0302e-5	1.0319e-5
Hybrid-II	1.9193e-5	1.8527e-5
MHLA	1.0023e-5	1.0030e-5
FDCLA	5.1417e-6	5.1460e-6
SDCLA	7.4606e-6	7.5060e-6

From the above experiments, it can be found that the SDCLA has the smaller training and testing errors than other algorithms but FDCLA. Therefore, the FDCLA and SDCLA have the better generalization capability than the other four learning algorithms This phenomenon is mainly caused by the fact that the new CLA encodes the *a priori* information from the involved problem while the traditional BP learning one, Hybrid-I algorithm, Hybrid-II algorithm and MHLA can not do so. Obviously, from Eqns.(1)-(7), the errors between the estimated and actual first-order derivative values

is smaller ones between the estimated and actual second-order derivative values. Hence, the approximation accuracy of the SDCLA is slightly worse than that of the FDCLA.

In the following, we discuss the effects of the three parameters, δP_0, θ and η, with the proposed CLA on approximating the unimodal function. Three cases are considered. Case I: $\delta P_0 = 1.0$ and $\theta = 10.0$ are kept unchanged, η is selected as 0.1, 0.12, 0.14 and 0.16, respectively. From the simulation results, it can be seen that the bigger the η is, the more the test error is. Case II: $\delta P_0 = 1.0$ and $\eta = 0.1$ are kept unchanged, θ is selected as 10, 12, 14 and 16, respectively. From the simulation results, it can seen that the bigger the η is, the more the test error is. Case III: $\theta = 10.0$ and $\eta = 0.1$ are kept unchanged, δP_0 is selected as 1, 2, 3 and 4, respectively. From the simulation results, it can seen that the bigger the η is, the more the test error is. All the results are shown in Table 3.

Table 3. The effects of the parameters with the SDCLA on approximating the unimodal function

Indices	Mean Squared Errors of test samples			
$\delta P_0 = 1.0$	$\eta = 0.10$	$\eta = 0.12$	$\eta = 0.14$	$\eta = 0.16$
$\theta = 10.0$	2.1502e-6	3.9832e-6	7.3364e-6	1.0675e-5
$\delta P_0 = 1.0$	$\theta = 10$	$\theta = 12$	$\theta = 14$	$\theta = 16$
$\eta = 0.10$	2.1502e-6	4.0056e-6	7.1213e-6	1.1502e-5
$\theta = 10.0$	$\delta P_0 = 1.0$	$\delta P_0 = 2.0$	$\delta P_0 = 3.0$	$\delta P_0 = 4.0$
$\eta = 0.10$	2.1502e-6	3.6737e-6	6.0953e-6	8.4236e-6

4 Conclusions

In this paper, a new CLA encoding the *a priori* information of function approximation problem into FNN was proposed. The CLA considered the network structure features as well as the involved problem properties. The activation functions of the hidden neurons were selected as specific polynomial functions. The connection weight constraints were extracted from the second-order derivative of the approximated function. Therefore, the new CLA had better generalization capability than the traditional BP algorithm, Hybrid-I algorithm, Hybrid-II algorithm and MHLA. Finally, simulated results were given to verify the efficiency and effectiveness of the proposed CLA. Future research works will include how to apply this new learning algorithm to resolve more real problems.

Acknowledgements

This work was supported by the National Science Foundation of China (No.60702056) and the Initial Funding of Science Research of Jiangsu University (No.07JDG033).

References

1. Nasr, M.B., Chtourou, M.: A Fuzzy Neighborhood-Based Training Algorithm for Feedforward Neural Networks. Neural Computing and Applications 18(2), 127–133 (2009)
2. Ng, S.C., Cheung, C.C., Leung, S.H.: Magnified Gradient Function with Deterministic Weight Modification in Adaptive Learning. IEEE Transactions on Neural Networks 15(6), 1411–1423 (2004)
3. Karras, D.A.: An Efficient Constrained Training Algorithm for Feedforward Networks. IEEE Trans. Neural Networks 6, 1420–1434 (1995)
4. Baum, E., Haussler, D.: What Size Net Gives Valid Generalization? Neural Computation 1, 151–160 (1989)
5. Huang, D.S., Chi, Z.R.: Finding Roots of Arbitrary High Order Polynomials Based on Neural Network Recursive Partitioning Method. Science in China Series F Information Sciences 47, 232–245 (2004)
6. Huang, D.S., Ip, H.H.S., Chi, Z.R.: A Neural Root Finder of Polynomials Based on Root Momnets. Neural Computation 16, 1721–1762 (2004)
7. Jeong, S.Y., Lee, S.Y.: Adaptive Learning Algorithms to Incorporate Additional Functional Constraints into Neural Networks. Neurocomputing 35, 73–90 (2000)
8. Jeong, D.G., Lee, S.Y.: Merging Back-propagation and Hebbian Learning Rules for Robust Classifications. Neural Networks 9, 1213–1222 (1996)
9. Han, F., Huang, D.-S., Cheung, Y.-m., Huang, G.-B.: A new modified hybrid learning algorithm for feedforward neural networks. In: Wang, J., Liao, X.-F., Yi, Z. (eds.) ISNN 2005. LNCS, vol. 3496, pp. 572–577. Springer, Heidelberg (2005)
10. Han, F., Huang, D.S.: A New Constrained Learning Algorithm for Function Approximation by Encoding a Priori Information into Feedforward Neural Networks. Neural Computing and Applications 17(5-6), 433–439 (2008)

Weighted Small World Complex Networks: Smart Sliding Mode Control

Yuequan Yang[1] and Xinghuo Yu[2]

[1] Department of Automation, College of Information Engineering
Yangzhou University, Yangzhou 225009, China
[2] School of Electrical and Computer Engineering
RMIT University, Melbourne VIC 3001, Australia
yangyq@yzu.edu.cn

Abstract. In this paper, we establish a novel weighted small world complex network which is generated by assigning special weight to rewired links according to concrete scenarios. The smart sliding mode control for weighted small world complex networks is developed based on the ergordicity characteristic of chaos dynamical systems. The most distinctive of this scheme is without involvement of linearization and other ideal assumptions, which forces system state of the modified small-world complex network to approach to the desired manifolds and eventually realize the asymptotical synchronization behavior of weighted small world complex networks.

Keywords: Complex network, Sliding mode, Smart control, Synchronization.

1 Introduction

In recent years, complex networks have attracted much attention among researchers. Nowadays, main complex networks models include regular networks model, random network model, small-world network model, and scale free network model[1-8]. In 1998, Watts and Strogatz introduced the concept of small-world network. It is notable that the small world phenomenon is indeed very common. Collective motions of complex networks have been the subject of considerable interest within the science and technology communities. Especially, one of the interesting and significant phenomena in complex networks is the synchronization. Synchronization research of complex networks has been recently reported in the literatures [9-12]. The study of the synchronization in a scale-free dynamical network has been made, and a positive threshold of coupling strength of scale-free network has been obtained which can guarantee the synchronization of the network systems in [9]. For the characteristics of small world dynamical networks, some important concepts such as synchronization matrix, associated feedback system, sensitive and robust edge, have been initially given, and robustness analysis of networks synchronization has been made in [10]. Several criteria for both robust local and robust global impulsive synchronization for uncertain dynamical networks have been established using the impulsive control systems theory [14]. In [17], the master stability function has been established to decide

D.-S. Huang et al. (Eds.): ICIC 2009, LNAI 5755, pp. 935–944, 2009.

whether or not any linear coupling arrangement produce stable synchronization dynamics, while variations of desynchronization bifurcation mode have been revealed with change of coupling scheme and coupling strength. Based on master stability function rationale, synchronizablity and synchronization enhancement of some complex networks has been discussed using eigenratio λ_N / λ_2 of out-coupling matrix by rewiring links or by assigning proper weights for existing links [18-21].

Though, the main methodology of synchronization of complex networks is by means of linearization around the desired equilibrium in these literatures. Sliding mode control is a kind of control strategy that exhibits discontinuity on certain predefined manifolds. Yu has initialed the idea of the smart variable structure control in [23-24]. The main advantages of such control mechanism are robustness and easy realization. One of contributions in this paper is that a modified small world network model called weighted small world network is provided. Based on this model of complex network, a novel smart sliding mode control channeled into the corresponding chaos nodes for the synchronization of complex network is initially developed by employing pinning control approach. For a general chaos node subsystem of complex networks, multiple sliding mode manifolds are to be established to generate a multiple dimension attraction region. Considering the sensitive characteristics of chaos systems, a new smart sliding mode control with limited small control magnitude is established.

2 Construction of Weighted Small World Complex Network

Originally, Watts and Strogatz [1] introduced a small world network model(WS) that is capable of interpolating between a regular network and a random network using a single parameter. The WS small world model can be described as follows. To begin with, take a one-dimensional lattice on a ring with N nodes in which every node is connected to its nearest neighbors up to the range. In the second step, rewire each connection with some probability p, which means that one end of the link is shifted to a new node selected at random in the whole lattice. During the rewiring process, there must remain at most one link between two nodes, and there is no node with the connection to itself.

Because WS small world network might lead to the formation of isolation clusters in the complex network, a famous variant model(NW) was introduce by Newman and Watts[23], referred to as the NW small-world complex network model. In the NW network model, the distinctive is no break among any initial nearest links. With $p = 0$, the NW network model reduces to the original nearest neighbor coupled network while it becomes a globally coupled network if $p = 1$. For sufficiently small p and sufficiently large N, the NW network model is essentially equivalent to the WS network model.

Considering special roles played by the new shifted links, we establish a novel weighted small world complex network model. The special distinctive lies in the different weight value assigned to new shifted links. As far as weight value is concerned, it may be assigned a large weight when one added link has a positive effect to small world. However, when negative effect may be happened, a small weight is

generated to suppress disadvantage overspread, such as swine flu in 2009. For simplicity, here we assume the weighted valued are all same and known here.
Generation algorithm 1:

```
Program Generation-of-weighted-small-world {G}
{Assuming the size of the network is N and the probability of rewiring is p }
begin
     Construct a regular ring graph G with N vertexes,
     with each vertex connected to the nearest and
     next-nearest neighbors;
     k=1;
     while k<= N
          begin
              Rewiring for each edge of vertex k with
              the probability p , observing the rule that
              duplications of edges are forbidden;
              For the new rewiring link, it is assigned
              to the weight value ω;
              k=k+1
         end
end.
```

3 Model Description and Preliminaries

In general, complex network system consisted of identical linearly and diffusively coupled nodes is considered, whose an individual node dynamics is

$$\dot{x}_i(t) = f(x_i(t)) + c\sum_{j=1}^{N} a_{ij}\Gamma(t)x_j(t), \tag{1}$$

where $x_i(t) = \left(x_{i1}(t), x_{i2}(t), \cdots, x_{in}(t)\right)^T \in R^n$ is the state of the ith node, $f(\cdot): R^n \to R^n$ is a chaos dynamic system, c is the coupling strength, $\Gamma(t) = (\Gamma_{ij}(t)) \in R^{n\times n}$ is a constant 0-1 inner-coupling matrix which represents links between coupled variables, $A = (a_{ij})_{N\times N}$ is the out-coupling configuration matrix. As far as out-coupling matrix is concerned, there is $a_{ij} = a_{ji} = 1$ with a connection between node i and node j, and $a_{ij} = a_{ji} = 0$ otherwise.

According to the above generation algorithm 1, it is easy to know that out-coupling matrix A is irreducible, which means the complex network is connected without isolated clusters. Moreover, the diagonal elements of matrix A are defined by $\sum_{j=1, j\neq i}^{N} a_{ij} = \sum_{j=1, j\neq i}^{N} a_{ji} = -a_{ii}$ for $i = 1, 2, \cdots, N$. It is notable to point out a_{ij} is the weight value if there is a new generated connection between node i and node j. For simplicity, without loss of generality, suppose $a_{ij} = a_{ji} = \omega$, $\omega > 0$ for new generated link, and other links remain original value. According to the above section, a novel weighted small world complex network with an individual dynamic is

$$\dot{x}_i(t) = f(x_i(t)) + c\sum_{j=1}^{N} a_{ij}\Gamma x_j(t) \quad . \tag{2}$$

Further, (2) can be represented in a compact form

$$\dot{x}(t) = F(x) + cA(t) \otimes \Gamma x(t) \quad , \tag{3}$$

where $x(t) = \left(x_1^T(t), x_2^T(t), \cdots, x_N^T(t)\right)$, $F(x) = \left(f^T(x_1), f^T(x_2), \cdots, f^T(x_N)\right)^T$, $\otimes$ denotes the matrix Kronecker product operator.

Definition 1. The weighted small world network (3) is called global asymptotical synchronization, if there exist control laws $u(t)$ which activates the system (3)

$$\dot{x}(t) = F(x, u(t)) + c(A(t) \otimes \Gamma)x(t) \quad , \tag{4}$$

such that $x_1(t) = x_2(t) = \cdots = x_N(t) = s$ as $t \to \infty$, where s is an equilibrium which may be unstable one for chaos dynamics.

Remark 1. The controller $u(t)$ in (4) may be designed using pinning approach [8-9]. Here we will discuss a novel smart sliding mode control scheme for weighted small world network to observe the asymptotical synchronization performance by employing the pinning approach.

Remark 2. The most synchronization analysis of complex networks is based on linearization method and other ideal assumptions in [7-21], while it is not involved with linearization in our scheme.

4 Smart Sliding Mode Control

Employing the smart control idea, we propose the smart sliding mode control strategy for a weighted small world complex network. For the sensitive characteristic of chaos systems, the gain of controller can not be a very large magnitude. For complex

network of dynamical chaos systems, the difficulty is the determination of sliding manifolds. In this paper, a multiple sliding mode manifolds scheme is developed to realize the synchronization of complex networks under consideration. Consider a general chaotic dynamic in (2)

$$\dot{x}_i(t) = f(x_i(t)). \tag{5}$$

The equilibrium set of (5) is

$$M_s = \left\{ x_i(t) \in R^n \mid f(x_i(t)) = 0 \right\}. \tag{6}$$

By employing the channel control approach in [23-24], p controller terms $u_{ik}^s(t)$ are channeled into the nonlinear terms denoted as $\zeta_k(\cdot)$, that is,

$$\begin{cases} \dot{x}_{i1}(t) = l_1(x_i(t)) + \zeta_1(x_i(t), u_{i1}^s(t)) \\ \qquad \vdots \\ \dot{x}_{i,p}(t) = l_p(x_i(t)) + \zeta_p(x_i(t), u_{ip}^s(t)) \\ \dot{x}_{i,p+1}(t) = l_{p+1}(x_i(t)) \\ \qquad \vdots \\ \dot{x}_{in}(t) = l_n(x_i(t)) \end{cases}, \tag{7}$$

where $l_k(\cdot)$ is the linear part of the controlled chaos systems, $\zeta_k(\cdot)$ is nonlinear one, $k = 1, 2, \cdots, n$. Assume there exist nonlinear dynamic terms in the p right parts of the system (2). Without loss of generality, suppose they lie in the p front subsystems. To stabilize chaos node, define the set of the p switching manifolds as follows

$$S_i = \left\{ (x_{i1}, x_{i2}, \cdots, x_{in}) \in R^n \,\middle|\, s_{ik} = x_{ik}(t) - x_{ik}^{eq} = 0, k = 1, 2, \cdots, p \right\}. \tag{8}$$

From (8), it is apparent that the chaotic attractor lies in the intersect part of the p multiple manifolds, that is, $x^{eq} \in S_i$. For the manifold $s_{ik} = 0$, considering the influence of the coupling nodes of complex network, then (2) is represented as

$$\dot{x}_i(t) = \psi_{ik}(\cdot) + g_{ik}(\cdot, u_p^s(t)) + \Xi_i, \tag{9}$$

where

$$\psi_{ik}(\cdot) = \sum_{j=1}^{k-1} \left(l_j(\cdot) + \zeta_j(\cdot) \right) b_j + \sum_{j=k+1}^{p} \left(l_j(\cdot) + \zeta_j(\cdot) \right) b_j + \sum_{j=p+1}^{n} l_j(\cdot) b_j,$$

$$g_{ik}(\cdot, u_{ik}^s) = \left[l_k(x_i(t)) + \zeta_k(x_i(t), u_{ik}^s(t)) \right] b_k, \quad \Xi_i = c \sum_{j=1}^{N} a_{ij} \Gamma(t) e_j(t).$$

Fortunately, Ξ_i is known for the complex networks during the control process. The sliding mode is reached if and only if

$$s_{ik} = x_{ik}(t) - x_{ik}^{eq} = 0 \quad , \quad \dot{s}_{ik} = 0 \quad , \tag{10}$$

According to variable structure control principle, the equivalent control is calculated by solving the equation

$$\dot{s}_{ik} = \frac{\partial s_{ik}}{\partial x_i}\dot{x}_i = \left\langle \nabla s, \psi_{ik}(x_i(t)) + g_{ik}(x_i(t), u_p^s(t)) + \Xi_i \right\rangle = 0 \quad , \tag{11}$$

Consequently we can obtain the equivalent control

$$u_i^{eq}(t) \triangleq \arg_{u_{ik}^s} \left\{ \dot{s}_{ik} = l_k(x_i(t)) + \zeta_k(x_i(t), u_k^s(t)) + \Xi_{ik} = 0 \right\} \quad , \tag{12}$$

where Ξ_{ik} is the kth row entry of the known term Ξ_i , that is, $\Xi_{ik} = c\sum_{j=1}^{N} a_{ij}\Gamma_k e_j(t)$, $\Gamma_k(t)$ is the k row vector.

The sliding mode controller is designed as follows

$$u_{ik}^s = \begin{cases} u^+, & s_{ik} > 0 \\ u^-, & s_{ik} < 0 \end{cases} . \tag{13}$$

Here, we restrict the difference and magnitudes of upper control force u^+ and the down control force u^- for the sensitive property of chaos dynamic system. According to existence necessary and sufficient condition of sliding mode in [22], it require the following conditions

$$\lim_{s\to 0^+} \left\langle \rho_{ik}, \psi_{ik}(\cdot) + g_{ik}(\cdot, u^+) + \Xi_i \right\rangle < 0 \ , \tag{14}$$

and

$$\lim_{s\to 0^-} \left\langle \rho_{ik}, \psi_{ik}(\cdot) + g_{ik}(\cdot, u^+) + \Xi_i \right\rangle > 0 \quad , \tag{15}$$

where ρ_{ik} is a norm vector of manifold $s_{ik} = 0$, $\langle \cdot, \cdot \rangle$ is inner product operator. From (9) and (11), the attraction region towards the sliding region can be defined as

$$\Omega_{ik} = \Omega_{ik}^+ \bigcup \Omega_{ik}^- \quad , \tag{16}$$

where $\Omega_{ik}^+ = \left\{ x_i(t) \in R^n \middle| l_k(x_i(t)) + \zeta_k(x_i(t), u^+(t)) + \Xi_{ik} < 0, x_{ik}(t) - x_{ik}^{eq} > 0 \right\}$, and $\Omega_{ik}^- = \left\{ x_i(t) \in R^n \middle| l_k(x_i(t)) + \zeta_k(x_i(t), u^+(t)) + \Xi_{ik} > 0, x_{ik}(t) - x_{ik}^{eq} < 0 \right\}$. Then the global attraction region is obtained as

$$\Omega_i = \bigcup \Omega_{ik} \ . \tag{17}$$

With multiple sliding mode manifolds, it can easily ensures the system state will enters the intersection (8) while the system state falls into the global attraction region (17). Moreover, while the system partial state reach their corresponding parts of the unstable equilibrium. The rest partial state will fast reach to their corresponding parts of the equilibrium state under suitable conditions [23]. Based on the above analysis, therefore, we have the following result.

Theorem 1. Under the smart sliding mode controller (12) and (13), the system (2) is globally asymptotical synchronization via weighted small world complex network generated by *Generation algorithm 1*, when the system state enters the attraction region (17), if the following autonomous linear subsystem

$$\begin{cases} \dot{x}_{i,p+1}(t) = l_{p+1}(x_i(t)) \\ \qquad\qquad \vdots \\ \dot{x}_{in}(t) = l_n(x_i(t)) \end{cases}, \tag{18}$$

is asymptotical stable to the manifolds S_i, $i = 1, 2, \cdots, N$.

Remark 3. Employing the smart sliding mode control with a small magnitude, the attraction region (15) is restricted in a very narrow gorge for each ideal tracking to the corresponding sliding mode manifold. Fortunately, these kinds of narrow attraction regions always exist due to the ergordicity of chaotic dynamics. The trajectory will be eventually attracted to the intersection of manifolds when the region Ω is entered.

5 Simulation Tests

In this section, a weighted small world network *G* with 50 nodes is firstly constructed. After that, the Liu chaos and Lorenz chaos systems are investigated, respectively. The ith Liu chaos system is given as

$$\begin{cases} \dot{x}_{i1} = a(x_{i2} - x_{i1}) \\ \dot{x}_{i2} = bx_{i1} - hx_{i1}x_{i3} \\ \dot{x}_{i3} = -cx_{i3} + kx_{i1}^2 \end{cases}, \tag{19}$$

when $a = 10, b = 40, c = 2.5, h = 1, k = 4$, (19) shows chaos property.

The Lorenz chaos system of the ith node is

$$\begin{cases} \dot{x}_{i1} = \sigma(x_{i2} - x_{i1}) \\ \dot{x}_{i2} = rx_{i1} - x_{i2} - x_{i1}x_{i3} \\ \dot{x}_{i3} = x_{i1}x_{i2} - bx_{i3} \end{cases}, \tag{20}$$

where σ is called Prandtl number. Let $\sigma = 10$, $r = 28$, and $b = 8/3$.

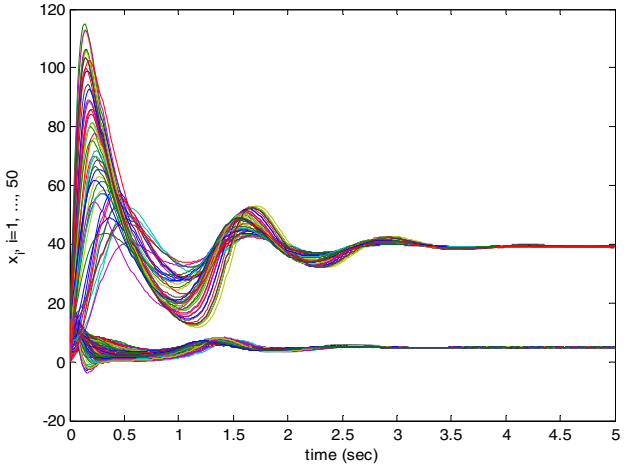

Fig. 1. Synchronization behavior of Liu systems on weighted small world network

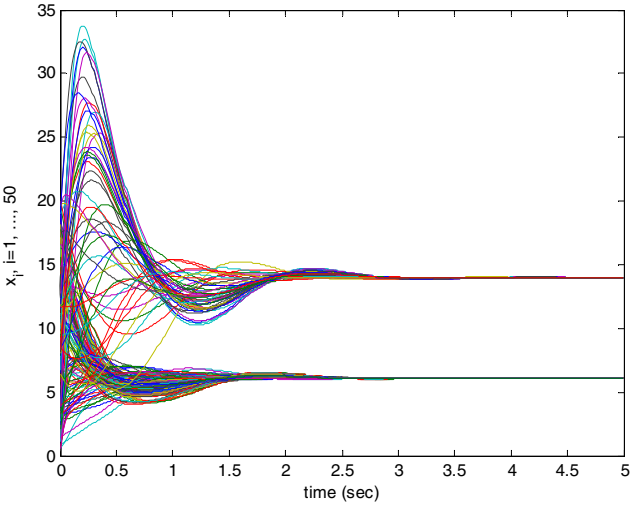

Fig. 2. Synchronization behavior of Lorenz systems on weighted small world network

The objective is to control the synchronization behavior approaches to the desired state x_d. Let $c = 2$, and channel a pinning controller for the corresponding system $\dot{x}_{i2} = bx_{i1} - hx_{i1}x_{i3}u_i^s$ for (19) and $\dot{x}_{i2} = rx_{i1} - x_{i2} - x_{i1}x_{i3}u_i^s$ for (20), respectively.

Design the smart sliding mode controller is designed

$$u_i^s = \begin{cases} 1.5, & \text{for } s_i > 0 \\ 0.5, & \text{for } s_i < 0 \end{cases}, \tag{21}$$

and the sliding manifolds are designed as $s_i = \{(x(1), x(2), x(3)) \mid x(2) - x_d(2) = 0\}$. The inner-coupling matrix of weighted small world network is supposed that only the second variable for coupled node dynamics is inner-coupled. $\omega = 10$.

As shown in the simulations, Fig. 1 exhibits coupled Liu system states fast approach the desired state, while Fig. 2 shows that the coupled Lorenz system states exhibit good synchronization behavior.

6 Conclusion

In this paper, a novel weighted small world complex network model was established. Furthermore, a smart sliding mode control strategy was proposed for synchronization realization. Compared with other synchronization analysis and control method, our smart control scheme exhibited good performance without local linearization and other idea assumptions.

Acknowledgement

This work is partially supported by the China National Natural Science Foundation Project (60774017 and 60874045) and the Open Projects of Key Laboratory of Complex Systems and Intelligence Science of Chinese Academy of Sciences (20060101).

References

1. Watts, D.J., Strogatz, S.H.: Collective Dynamics of Small-world Networks. Nature 393, 440–442 (1998)
2. Strogatz, S.H.: Exploring Complex Networks. Nature 410, 268–276 (2001)
3. Barabasi, A.L., Albert, R.: Emergence of Scaling in Random Networks. Science 286, 509–512 (1999)
4. Barabasi, A.L., Albert, R., Jeong, H.: Mean-field Theory for Scale-free Random Networks. Physcia A 272, 173–187 (1999)
5. Holmgren, A.J.: Using Graph Models to Analyze the Vulnerability of Electric Power Networks. Risk Analysis 26(4), 955–969 (2006)
6. Wang, X.F., Chen, G.: Complex Networks: Small-world, Scale-free, and Beyond. IEEE Circuits Syst. Mag. 3(1), 6–20 (2003)
7. Abdallah, C.T., Tanner, H.R.: Complex Networked Control Systems: Introduction to the Special Section. IEEE Control Systems Magazine, 30–32 (2007)
8. Wang, X.F., Chen, G.: Pinning Control of Scale-free Dynamical Networks. Physica A 310, 521–531 (2002)
9. Chen, T., Liu, X., Lu, W.: Pinning Complex Network by a Single Controller. IEEE Trans Circuits and Systems-I: Regular Papers 54(6), 1317–1326 (2006)
10. Wang, X.F., Chen, G.: Synchronization in Scale-free Dynamical Networks: Robustness and Fragility. IEEE Trans Circuits and Systems-I: Fundamental Theory and Applications 49(1), 54–62 (2002)
11. Lü, J., Yu, X., Chen, G., et al.: Characterizing the Synchronizability of Small-world Dynamical Networks. IEEE Trans Circuits and Systems-I: Regular Papers 51(4), 787–796

12. Li, C., Chen, G.: Synchronization in General Complex Dynamical Networks with Coupling Delays. Physica A 343, 263–278 (2004)
13. Lü, J., Chen, G.: A Time-varying Complex Dynamical Network Model and Its Controlled Synchronization Criteria. IEEE Trans Automatic Control 50(6), 841–846 (2005)
14. Liu, B., Liu, X., Chen, G., et al.: Robust Impulsive Synchronization of Uncertain Dynamical Networks. IEEE Trans Circuits and Systems-I: Regular Papers 52(7), 1431–1441 (2005)
15. Yang, M., Wang, Y., Wang, H.O., et al.: Delay Independent Synchronization of Complex Network via Hybrid Control. In: Proceedings of 2008 American Control Conference, Seattle, Washington, USA, pp. 2206–2271 (2008)
16. Chen, M.: Chaos Synchronization in Complex Network. IEEE Trans Circuits and Systems-I: Regular Papers 55(5), 1335–1346 (2008)
17. Pecora, L.M., Carroll, T.L.: Master Stability Functions for Synchronized Coupled Systems. Physical Review Letters 80, 2109–2112 (1998)
18. Chavez, M., Hwang, D., Amann, A., et al.: Synchronizing is Enhanced in Weighted Complex Networks. Physical Review Letters 94(21), 8701 (2005)
19. Wu, C.W.: Synchronization and Convergence of Linear Dynamics in Random Directed Networks. IEEE Trans Automatic Control 51(7), 1207–1210 (2006)ss
20. Jalili, M., Ajdari, R.A., Hasler, M.: Enhancing Synchronizability of Dynamical Networks Using the Connection Graph Stability Method. Int. J. Ciurcuit Theory Appl. 35, 611–622 (2007)
21. Jalili, M., Ajdari, R.A., Hasler, M.: Enhancing Synchronizability of Weighted Dynamical Networks Using Betweenness Centrality. Physical Review E 78, 16105 (2008)
22. Utkin, V.I.: Sliding Modes in Control Optimization. Springer, Berlin (1992)
23. Yu, X.: Controlling Lorenz Chaos. International Journal of Systems Science 27(4), 355–359 (1996)
24. Tian, Y.P., Yu, X.: Adaptive Control of Chaotic Dynamical Systems Using Invariant Manifold Approach. IEEE Trans Circuits and Systems-I: Fundamental Theory and Applications 47(10), 1537–1542 (2000)

A Novel Method to Robust Tumor Classification Based on MACE Filter

Shulin Wang[1,2,*] and Yihai Zhu[1,3,*]

[1] Intelligent Computing Lab, Hefei Institute of Intelligent Machines, Chinese Academy of Science, Heifei, 230031, China
[2] School of Computer and Communication, Hunan University, Changsha, Hunan, 410082, China
[3] Department of Automation, University of Science and Technology of China, Hefei, Anhui, 230026, China
jt_slwang@hotmail.com

Abstract. Gene expression profiles consisting of thousands of genes can describe the characteristics of specific cancer subtype. By efficiently using the overall scheme of gene expression, accurate tumor diagnosis can be performed well in clinical medicine. However, faced many problems such as too much noise and the curse of dimensionality that the number of genes far exceeds the size of samples in tumor dataset, tumor classification by selecting a small set of gene subset from the thousands of genes becomes a challenging task. This paper proposed a novel high accuracy method, which utilized the global scheme of differentially expressed genes corresponding to each tumor subtype which is determined by tumor-related genes, to classify tumor samples by using Minimum Average Correlation Energy (MACE) filter method to computing the similarity degree between a test sample with unknown label in test set and the template constructed with training set. The experimental results obtained on two actual tumor datasets indicate that the proposed method is very effective and robust in classification performance.

Keywords: Gene expression profiles, MACE filter, tumor classification, similarity degree, DNA microarray.

1 Introduction

Gene expression profiles (GEP), which can provide systematic quantitative information on the simultaneous expression of thousands of genes within cells in any given state, is emerging as a powerful and cost-effective tool for the analysis of cell state, and thus provides the understanding and insights into biological processes and disease etiology. The advance of DNA microarray technology has made its clinical applications to tumor diagnosis possible, and further makes personal medicine realizable. However, due to many problems such as too much noise and the curse of dimensionality that the number of genes far exceeds the size of samples in tumor dataset,

[*] These authors contributed equally to this work.

D.-S. Huang et al. (Eds.): ICIC 2009, LNAI 5755, pp. 945–954, 2009.

dimensionality reduction by selecting a small set of gene subset or by extracting a small set of feature subset from thousands of genes in GEP becomes a challenging task.

As stated by Dabney [1], the constructed classification model may be evaluated from three aspects: accuracy, interpretability, and practicality. It is possible that a complicated classification model may be rejected for a simpler alternative even if the simpler alternative does not perform as well because of the poorer interpretability of the complicated classification model. Therefore, many existing methods focused on constructing simpler classification model by finding the smallest gene subset. For example, Wang *et al.* [2] proposed a very effective method involving two steps: (1) choosing some important genes using a feature importance ranking scheme, (2) evaluating the classification capability of all simple combinations of those important genes by using a good classification model. Huang *et al.* [3] proposed an efficient evolutionary approach to gene selection from GEP, which can simultaneously optimize gene selection and tissue classification for microarray data analyses.

However, although these methods classifying tumor subtypes by identifying the smallest gene subsets have many merits such as the selected genes can be used as the biomarker of tumor subtype and the constructed classification model is very simple, their computational costs are also very big and the optimal gene subset selected is not unique. The method to overcome these problems is that we just utilize the overall scheme of those differentially expressed genes to construct classification model. Common methods to select differentially expressed genes are t-test [4] and rank sum test [5], etc. If all differentially expressed genes are used as the input of classifier such as k-nearest neighbor (k-NN) [6] or support vector machines (SVM) [7], the classification model with good generalization performance is not always obtained. As we know, the tumor subtypes are determined by all differentially expressed genes in cell. Therefore, different tumor subtypes are determined by different gene expression patterns. In this paper, we proposed a novel high accuracy method to tumor classification by computing the similarity degree of the expression pattern of differentially expressed genes between a test sample with unknown label in test set and the template constructed with training set by using Minimum Average Correlation Energy (MACE) filter method [12].

2 Methods

2.1 Flowchart of Analysis

Our method involves two key steps: the selection of differentially expressed genes (gene selection) and the computing of similarity degree between a test sample and known template constructed by training set (correlation filter). The normalization step will make the dataset have zero mean and one variance. The decision that a test sample belongs to a certain subtypes is very sample only according to the peak value obtained by correlation filter. The analysis flowchart of our method is shown in Fig. 1. More details on how to select differentially expressed genes and to compute similarity degree between a sample and a template are described in subsection 2.3 and 2.4, respectively.

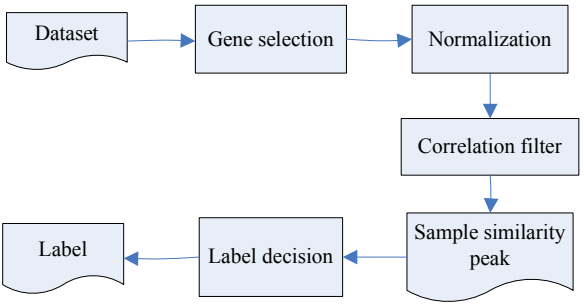

Fig. 1. The analysis flowchart of our method

2.2 Representation of GEP

DNA microarray is composed of thousands of individual DNA sequences printed in a high density array on a glass microscope slide. Samples are generated under multiple conditions which may be a time series during a biological process or a collection of different tissue samples. Let $G=\{g_1,\cdots g_n\}$ be a set of genes and $S=\{s_1,\cdots s_m\}$ be a set of samples. The corresponding gene expression matrix can be represented as $X=\{x_{i,j}|1\le i\le m,1\le j\le n\}$. The matrix X is composed of m row vectors. $s_i\in R^n;i=1,2,\cdots,m$, m denotes the number of samples, and n denotes the number of genes measured.

2.3 Selection of Differentially Expressed Genes

We focused on obtaining the overall scheme of differentially expressed genes, so one of important tasks is to identify differentially expressed genes from tumor dataset before computing similarity degree by using MACE filter method because too many genes will lead to the increase of similarity between every two samples in different subtypes. Troyanskaya *et al*. [8] systematically assessed the performance of three methods including nonparametric t-test, Wilcoxon rank sum test, and a heuristic method. Their experiments on simulated and real-life dataset under varying noise levels and *p*-value cutoffs suggest that the rank sum test appears most conservative. Usually, there are two kinds of rank sum test methods: Wilcoxcon rank sum test (WRST) [9,10] which is only suitable for binary sample set, and Kruskal-Wallis rank sum test (KWRST) [11] which is suitable for multi-class sample set. And KWRST is also a non-parameter method for test equality of population medians among classes.

2.4 Minimum Average Correlation Energy Filter

Composite correlation filters, also called the advanced correlation filters or synthetic discriminant functions, were developed in the mid 1980s and early 1990s for classification and track [13]. Recently, correlation filters have been extraordinarily notable and applied to biometric recognition, such as faces, irises, and palmprint, which is successful [14]. The block diagram of correlation process is shown in Fig. 2.

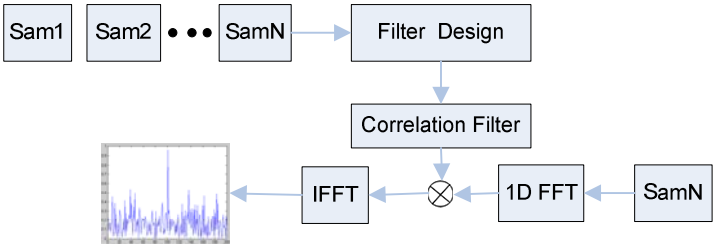

Fig. 2. Block diagram of correlation process

One of the famous composite correlation filters is the Minimum Average Correlation filter (MACE), proposed by the Abhijit Mahalanobis et al. in 1987 [12]. In 1980, Hester and Casasent suggested the synthetic discriminant function approach (SDF). After their introduction, SDF's have been the focus of much research and a lot of new techniques were added to this method, which formed minimum variance synthetic discriminant function (MVSDF) [15] and minimum average correlation energy (MACE). Because, the original SDF's did not consider any input noise, they were not optimized for noise tolerance. Vijaya Kumar introduced the MVSDF in 1986, which maximized the noise tolerance of the SDF's. The original SDF method controlled only the cross-correlation value at the origin, and thus could not guarantee that the correlation output plane had its peak (i.e., maximum value) at the origin, which might produce large peak-to-sidelobe rate (PSR). To solve this problem, Mahalanobis *et al.* introduced, MACE filter capable of producing sharp correlation peaks at the origin.

MACE filters: If we have N training samples of a class, the *i-th* sample is described as a 1-D discrete sequence denoted by $x_i(n)$. Its discrete Fourier transform (DFT) is denoted by $X_i(k)$. In this section, we describe the discrete sample sequence as a column vector x_i of dimensionality d equal to the length of the sample $x_i(n)$, i.e.,

$$x_i = [x_i(1), x_i(2), \cdots, x_i(d)]^T \tag{1}$$

where the superscript 'T' denotes transpose. All DFTs are also of the length of d. We define a matrix

$$X = [X_1, X_2, \cdots, X_N] \tag{2}$$

with column vectors X_i, where X_i denotes the discrete Fourier transform of $x_i(n)$. Upper case symbols refer to the frequency plane terms, while the lower case symbols represent quantities in the space domain. A correlation filter is a class-specific template synthesized from a set of training samples with the purpose of recognizing their class, while the template is often called as a filter. So we use some training samples to synthesized the class-dependent filter. The vector h represents the filter $h(n)$ in the space domain and the vector H its Fourier transform $H(k)$ in the frequency domain. We denote the correlation function of the *i-th* sample sequence $x_i(n)$ with the filter sequence $h(n)$ by $g_i(n)$, i.e.,

$$g_i(n) = x_i(n) \otimes h(n) \tag{3}$$

We denote the DFT of the correlation function by $G_i(k)$. The energy of the *i-th* correlation plane is

$$E_i = \sum_{n=1}^{d} \left| g_i(n) \right|^2 = (1/d) \sum_{k=1}^{d} G_i(k) = (1/d) \sum_{k=1}^{d} \left| H(k) \right|^2 \left| X_i(k) \right|^2 \tag{4}$$

Equation (4) is a direct realization of Parseval's theorem. Using the vector form of the sample sequence, we can also write Eq.(4) as

$$E_i = H^+ D_i H \tag{5}$$

where the superscript + denotes the conjugate transpose of a complex vector, and D_i is a diagonal matrix of size $d \times d$ whose diagonal elements are the magnitude square of the relative element of X_i, i.e.,

$$D_i(k,k) = \left| X_i(k) \right|^2 \tag{6}$$

Note that the diagonal elements of D_i describe the power spectrum of $x_i(n)$.

We wish to design a correlation filter that ensures sharp correlation peaks while allowing constraints on the correlation peak values. To achieve good detection, it is necessary to reduce correlation function levels at all points except at the origin of the correlation plane, where the imposed constraints on the peak value must be met. Specifically, the value of the correlation function must be at a user specified value at the origin but is free to vary elsewhere. This is equivalent to minimize the energy of the correlation function while satisfying intensity constraints at the origin. In the vector notation, the correlation peak amplitude constraint is

$$g_i(0) = X_i^+ H = u_i \quad i = 1, 2, \cdots, N \tag{7}$$

where $g_i(0)$ is the value of the output correlation at the origin (peak), u_i is the user specified value of the *i-th* correlation function at the origin. The filter must also minimize the correlation plane energy $E_i (i=1,2,\cdots,N)$. Thus in matrix-vector notation, the problem is to find the frequency domain vector *H* that minimizes the $H^+ D_i H$ for all i, while satisfying the peak constraints in Eq.(7), which can also be written for all samples as

$$X^+ H = u \tag{8}$$

where $u=[u_1, u_2, \cdots, u_N]$. The solution of this problem does not exist because the simultaneous constrained minimization of all $E_i (i=1,2,\cdots,N)$ is not possible. We, therefore, attempt to minimize the average value of E_i in Eq.(5), while meeting the linear constraints in Eq.(8).

The average correlation plane energy is

$$E_{av} = (1/N)\sum_{i=1}^{N} E_i = (1/N)\sum_{i=1}^{N} H^+ D_i H = (1/N) H^+ (\sum_{i=1}^{N} D_i) H \tag{9}$$

where we define D as

$$D = (1/N)\sum_{i=1}^{N} \alpha_i D_i \tag{10}$$

where α_i are constants. If all α_i=1 , we may rewrite Eq.(9) as

$$E_{av} = (1/N)\sum_{i=1}^{N} H^+ DH \quad \alpha_i = 1, i = 1, 2, \cdots, N \tag{11}$$

The solution to this problem may be found using the method of Lagrange multipliers. This solution method is possible since we solve for the filter in the frequency domain. The vector H is given by

$$H = D^{-1} X (X^+ D^{-1} X)^{-1} u \tag{12}$$

3 Experiments

3.1 Descriptions of Two Tumor Datasets

In our experiments we applied our approach to two publicly available tumor datasets: Small Round Blue Cell Tumor (SRBCT) [17] and Acute Lymphoblastic Leukemia (ALL) [16] datasets, which are described in Tables 1 and 2. The SRBCT dataset contains 88 samples with 2,308 genes in every sample. According to the original literature, there are 63 training samples and 25 test samples containing five non tumor-related samples. The 63 training samples contain 23 Ewing family of tumors (EWS), 20 rhabdomyosarcoma (RMS), 12 neuroblastoma (NB), and eight Burkitt lymphomas (BL) samples. The test samples contain six EWSs, five RMSs, six NBs, three BLs, and five non tumor-related samples that were removed in our experiments. ALL dataset totally contains 248 samples, in which 148 samples were used as training set and 100 samples were used as test set. For example, for subclass BCR-ABL, there are 15 samples. According to the rank of samples in original dataset, the first nine samples were used as training set, and the last six samples were used as test set. The others were deduced similarly.

Table 1. Descriptions of SRBCT dataset

Subclass	#Original dataset	#Training set	#Test set
EWS	29	23	6
NB	18	12	6
RMS	25	20	5
BL	11	8	3
Non-SRBCT	5	0	5
Total	88	63	25

Table 2. The partition of training set and test set for ALL dataset

NO.	Subclass	#Training set	#Test set
1	BCR-ABL	9	6
2	E2A-PBX1	16	11
3	Hyperdip>50	39	25
4	MLL	12	8
5	T-ALL	25	18
6	TEL-AML1	47	32
Total		148	100

3.2 Experimental Method

The correlation filters trained for each class are MACE filters without using any false-class samples, which means that each class has its own filter. In the verification process, a test sample has correlation with all filter templates, yielding correlation output planes (COP). Then, we check each COP to search the maximum values of each COP. According to those values, we can get the maximal value and its class label. For each filter, if the test sample is a true sample, there will be theoretically sharp value in the COP. On the contrary, a false sample will not yield a sharp value. Fig. 4 shows the illustrative diagram of this process.

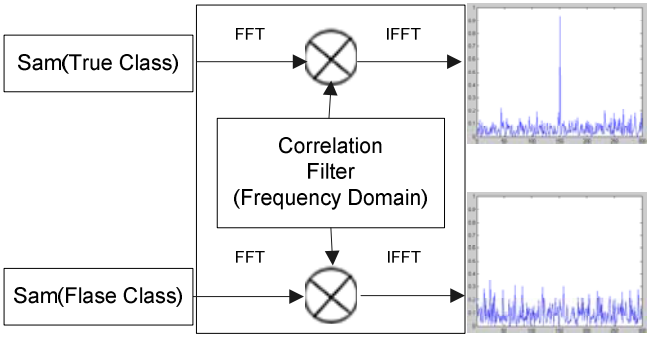

Fig. 3. The demonstration of correlation filter on actual tumor samples

For one test sample there will be N similarity peak values, because there are N correlation filters for N classes. According to the N similarity peak values, we can obtain the maximum peak value and its filter-dependent class label, which is the calculated label. After we have already known the test sample's label, we can compare the two labels, the calculated label and the known label of a test sample, to validate whether they are consistent with each other or not. Obviously, if the calculated label accords with the known one, we think that the test sample is classified correctly; on the contrary, we deem that the test sample is classified wrongly. According to the above process, we can gain the correctness of classification of every test sample, and achieve corresponding prediction accuracy.

3.3 Experimental Results

On the SRBCT dataset, the average accuracy is 87.12%±3.75 which is computed with the selected number of top-ranked genes from 300 to 600. Meanwhile, we got an excellent result on the ALL dataset, with the average accuracy of 97.19%±0.66 which is also computed with the selected number of top-ranked genes from 300 to 600. The classification accuracy on the two datasets with different numbers of top-ranked genes is shown in Fig. 4.

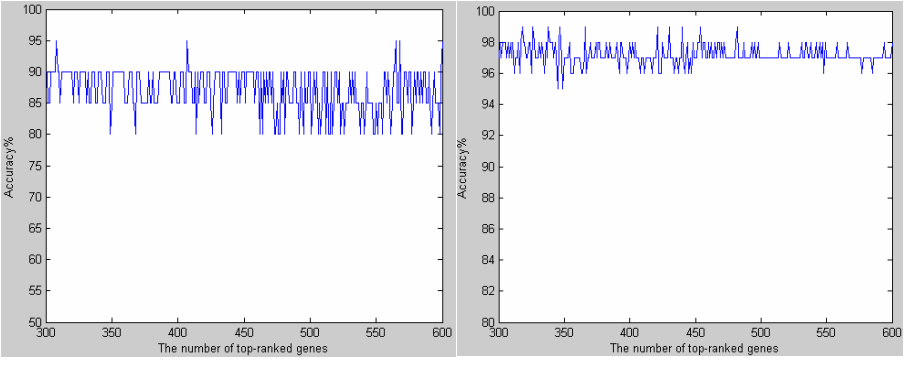

Fig. 4. The classification accuracy on SRBCT and ALL datasets with different numbers of top-ranked genes

4 Comparisons with Other Methods

Tumor classification based on GEP has been extensively studied. For example, the nearest shrunken centroid method proposed by Tibshirani *et al*. can identify discriminant genes by a shrinkage parameter [19]. Dabney [1] proposed a classification to nearest centroids (ClaNC) method which performs class-specific gene selection.

Table 3. Comparisons with other related methods

No.	Methods	Classifier	Datasets	Accuracy %	Ref.
1	KWRST + MACE	--	SRBCT	95.0 (unbiased)	Ours
			ALL	99.0 (unbiased)	
2	The significance for classification	Artificial Neural Network	SRBCT	100.0 (biased)	[17]
3	Genetic Evolution of Subsets of Expressed Sequences (GESSES)	k-Nearest Neighbor	SRBCT	100.0 (biased)	[18]
4	Class Separability	Fuzzy Neural Network	SRBCT	95.0 (unbiased)	[2]
5	Nearest Shrunken Centroid	--	SRBCT	95.0 (unbiased)	[19]
			ALL	86.0 (unbiased)	
6	ClaNC	--	SRBCT	95.0 (unbiased)	[1,20]
			ALL	99.0 (unbiased)	

Usually, ClaNC method outperforms the nearest shrunken centroid method in classification performance. In fact, some methods are biased due to the gene selection on whole dataset, such as the methods in [17] and [18]. Comparing the best results obtained by our unbiased method with the best ones obtained by other related methods are shown in Table 3, from which we can see that our method is equivalent to the best one in classification accuracy.

5 Conclusions

Most of the traditional methods to tumor classification focused on the gene selection and feature extraction of GEP, and the selected genes or extracted features are commonly used as the input of a classifier. The merit of gene selection is that the important tumor-related genes may be selected out, but its drawbacks are that finding a small set of gene subset from GEP will cost more CPU time and the classifier constructed by the selected gene subset possibly lacks generalization performance. Although the methods of feature extraction are time-saving, there exists information loss in the extracted features.

To avoid these problems, we proposed a novel high accuracy method which combines Kruskal-Wallis rank sum test with MACE filter to compute the similarity degree of the expression pattern of differentially expressed genes between a test sample and the template constructed with training sample for tumor classification. The merits of our method are that it not only is time-saving but also can obtain very high accuracy by sufficiently utilizing the overall scheme of differentially expressed genes. 95% of the best prediction accuracy on SRBCT dataset and 99% on ALL dataset indicate that compared with other methods the proposed method is more effective and robust, which is appropriate for the classification of large numbers of tumor samples in future.

Acknowledgments

This work was supported by the grants of the National Science Foundation of China, No. 30700161, the grant of the Guide Project of Innovative Base of Chinese Academy of Sciences (CAS), No.KSCX1-YW-R-30, and the grant of Oversea Outstanding Scholars Fund of CAS, No.2005-1-18.

References

1. Dabney, A.R.: Classification of microarrays to nearest centroids. Bioinformatics 21(22), 4148–4154 (2005)
2. Wang, L.P., Chu, F., Xie, W.: Accurate cancer classification using expressions of very few genes. IEEE/ACM Transactions on computational biology and bioinformatics 4(1), 40–53 (2007)
3. Huang, H.L., Lee, C.C., Ho, S.Y.: Selecting a minimal number of relevant genes from microarray data to design accurate tissue classifiers. BioSystems 90(1), 78–86 (2007)

4. Sreekumar, J., Jose, K.K.: Statistical tests for identification of differentially expressed genes in cDNA microarray experiments. Indian Journal of Biotechnology 7(4), 423–436 (2008)
5. Deng, L., Ma, J.W., Pei, J.: Rank sum method for related gene selection and its application to tumor diagnosis. Chinese Science Bulletin 49(15), 1652–1657 (2004)
6. Li, L.P., Darden, T.A., Weinberg, C.R., Levine, A.J., Pedersen, L.G.: Gene assessment and sample classification for gene expression data using a genetic algorithm/k-nearest neighbor method. Combinatorial Chemistry & High Throughput Screening 4(8), 727–739 (2001)
7. Zhou, X., Tuck, D.P.: MSVM-RFE: extensions of SVM-RFE for multiclass gene selection on DNA microarray data. Bioinformatics 23(9), 1106–1114 (2007)
8. Troyanskaya, O.G., Garber, M.E., Brown, P.O., Botstein, D., Altman, R.B.: Nonparametric methods for identifying differentially expressed genes in microarray data. Bioinformatics 18(11), 1454–1461 (2002)
9. Lehmann, E.L.: Non-parametrics: Statistical methods based on ranks, Holden-Day, San Francisco (1975)
10. Wilcoxon, F.: Individual comparisons by ranking methods. Biometrics 1, 80–83 (1945)
11. Kruskal, W.H., Wallis, W.A.: Use of ranks in one-criterion variance analysis. Journal of the American Statistical Association 47(260), 583–621 (1952)
12. Mahalanobis, A., Kumar, B.V.K., Casasent, D.: Minimum average correlation energy filters. Appl. Opt. 26, 3633–3640 (1987)
13. Kumar, B.V.: Tutorial survey of composite filter designs for optical correlators. Appl. Opt. 31, 4773–4801 (1992)
14. Kumar, B.V., Savvides, V.M.K., Xie, C., Thornton, J., Mahalanobis, A.: Biometric verification using advanced correlation filters. Appl. Opt. 43, 391–402 (1992)
15. Kumar, B.V.: Minimum variance synthetic discriminant functions. Opt. Soc. Am. A 3, 1579–1584 (1986)
16. Yeoh, E.J., Ross, M.E., Shurtleff, S.A., Williams, W.K., Patel, D., Mahfouz, R., Behm, F.G., Raimondi, S.C., Relling, M.V., Patel, A., Cheng, C., Campana, D., Wilkins, D., Zhou, X., Li, J., Liu, H., Pui, C.H., Evans, W.E., Naeve, C., Wong, L., Downing, J.R.: Classification, subtype discovery, and prediction of outcome in pediatric acute lymphoblastic leukemia by gene expression profiling. Cancer Cell 1(2), 133–143 (2002)
17. Khan, J., Wei, J.S., Ringner, M., Saal, L.H., Ladanyi, M., Westermann, F., Berthold, F., Schwab, M., Antonescu, C.R., Peterson, C., Meltzer, P.S.: Classification and diagnostic prediction of cancers using gene expression profiling and artificial neural networks. Nature Medicine 7(6), 673–679 (2001)
18. Deutsch, J.M.: Evolutionary algorithms for finding optimal gene sets in microarray prediction. Bioinformatics 19(1), 45–52 (2003)
19. Tibshirani, R., Hastie, T., Narasimhan, B., Chu, G.: Diagnosis of multiple cancer types by shrunken centroids of gene expression. Proceedings of the National Academy of Sciences of the United States of America 99(10), 6567–6572 (2002)
20. Dabney, A.R., Storey, J.D.: Optimality driven nearest centroid classification from genomic data. PLoS ONE, 2(10), e1002. doi:10.1371/journal.pone.0001002 (2007)

Ensemble Classifiers Based on Kernel PCA for Cancer Data Classification

Jin Zhou[1], Yuqi Pan[1], Yuehui Chen[1], and Yang Liu[2]

[1] School of Information Science and Engineering,
University of Jinan, Jinan 250022, P.R. China
ise_zhouj@ujn.edu.cn
[2] Department of Mathematics,
Hong Kong Baptist University, Kowloon Tong, Hong Kong

Abstract. Now the classification of different tumor types is of great importance in cancer diagnosis and drug discovery. It is more desirable to create an optimal ensemble for data analysis that deals with few samples and large features. In this paper, a new ensemble method for cancer data classification is proposed. The gene expression data is firstly preprocessed for normalization. Kernel Principal Component Analysis (KPCA) is then applied to extract features. Secondly, an intelligent approach is brought forward, which uses Support Vector Machine (SVM) as the base classifier and applied with Binary Particle Swarm Optimization (BPSO) for constructing ensemble classifiers. The leukemia and colon datasets are used for conducting all the experiments. Results show that the proposed method produces a good recognition rate comparing with some other advanced artificial techniques.

Keywords: Cancer data classification, Kernel principal component analysis, Support vector machine, Ensemble classifier, Binary particle swarm optimization.

1 Introduction

The recent advent of DNA microarray technique has made simultaneous monitoring of thousands of gene expressions possible [1]. With this abundance of gene expression data, researchers have started to explore the possibilities of cancer data classification. Quite a number of methods have been proposed in recent years with promising results.

Usually, the classification of gene expression data requires two steps: feature selection and data classification. As the microarray data consists of a few hundreds of samples and thousands or even ten thousands of genes, it is extremely difficult to work in such a high dimension space using traditional classification methods directly. So feature selection methods, which include principal components analysis (PCA), Fisher ratio, t-test, correlation analysis etc, have been proposed and developed to reduce the dimensionality [2]. Along with the feature selection methods, intelligent methods have been applied for microarray data classification, such as artificial neural network (ANN) [3], K nearest neighbor (KNN) [4], decision tree [5] and flexible

D.-S. Huang et al. (Eds.): ICIC 2009, LNAI 5755, pp. 955–964, 2009.

neural tree (FNT) [6]. Recent years, ensemble approaches [7] have been put forward. It combines multiple classifiers together as a committee to make more appropriate decisions for classifying microarray data instances. Much research has showed that it can offer improved accuracy and reliability.

In this paper, the gene expression data is firstly preprocessed for normalization in which four steps are taken. Kernel principal component analysis (KPCA) is then applied to extract features. Secondly, an intelligent approach is brought forward, which uses Support Vector Machine (SVM) as the base classifier and applied with Binary Particle Swarm Optimization (BPSO) for constructing ensemble classifiers. The leukemia and colon datasets, which were obtained from the Internet, are used for conducting all the experiments.

The paper is organized as follows: Section 2 introduces the normalization of gene expression data. The feature selection method based on KPCA is described in section 3. The optimal design method for constructing ensemble classifiers is discussed in section 4 and 5. Section 6 gives the experiment results. And in section 7, we present our conclusions.

2 Gene Expression Data Normalization

Due to the noisy nature of dataset provided by microarray experiment, preprocessing is an important step in the analysis of microarray data. The raw intensities have a wide dynamic range. Both datasets have to be normalized to decrease the variation before submitting them to the evolutionary algorithm. In this paper, four steps are taken:

1) If a value is greater than the ceiling 16000 and smaller than the floor 100, this value is replaced by the ceiling/floor.

2) Leaving out the genes with (max - min) $\leq$ 500, here max and min refer to the maximum and minimum of the expression values of a gene, respectively.

3) Carrying out logarithmic transformation with 2 as the base to all the expression values.

4) For each gene i, subtract the mean measurement of the gene μ_i and divide by the standard deviation σ_i. After this transformation, the mean of each gene will be zero, and the standard deviation will be one.

3 Feature Selection Based on Kernel PCA

The traditional Principal Component Analysis (PCA) [8] is based exclusively on the second-order statistics with smooth Gaussian distribution. It is difficult to describe the data with non-Gaussian distribution, so the Kernel-based algorithm (KPCA algorithm[9,10]) is proposed for nonlinear PCA. KPCA uses kernel function to obtain the arbitrary high-order correlation between input variants, and find the principal components needed through the inner production between input data.

First of all, a nonlinear mapping Φ is used to map the input data space R^n into the feature space F:

$$\begin{aligned} &\Phi:\ \mathrm{R}^{\mathrm{N}} \rightarrow \mathrm{F}, \\ &\mathrm{x} \rightarrow \Phi(\mathrm{x}). \end{aligned} \tag{1}$$

Correspondingly, a pattern in the original input space R^{n} is mapped into a potentially much higher dimensional feature vector in the feature space F.

An initial motivation of KPCA is to perform PCA in the feature space F. Let us construct the covariance matrix in the feature space F:

$$C = \frac{1}{M}\sum_{j=1}^{M} (\Phi(x_j) - \overline{\Phi})(\Phi(x_j) - \overline{\Phi})^{\mathrm{T}}, \tag{2}$$

where

$$\overline{\Phi} = \frac{1}{M}\sum_{j=1}^{M} \Phi(x_j). \tag{3}$$

However, it is not easy to centralize data directly in the feature space F. To avoid this difficulty, we make the assumption again that

$$\sum_{j=1}^{M} \Phi(x_j) = 0. \tag{4}$$

So let us consider the following noncentralized covariance matrix:

$$\tilde{C} = \frac{1}{M}\sum_{j=1}^{M} \Phi(x_j)\Phi(x_j)^{\mathrm{T}}. \tag{5}$$

Now we have to solve the Eigenvalue equation:

$$\lambda V = \tilde{\mathrm{C}} V, \tag{6}$$

for Eigenvalues $\lambda \geq 0$ and Eigenvectors $V \in \mathrm{F} \setminus \{0\}$.

It is very computationally intensive or even impossible to calculate $\tilde{C}$'s eigenvectors in a high-dimensional (even infinite-dimensional) feature space. KPCA can be viewed as utilizing two key techniques to solve this problem artfully. One is the SVD technique[11] adopted in Eigenfaces, and the other is the so-called kernel-tricks[9]. SVD technique can be used to transform the eigenvector calculation problem of a large-size matrix to the eigenvector calculation problem of a small-size matrix and, kernel-tricks can be used to avoid the computation of dot products in the feature space by virtue of the following formula:

$$K(x_i, x_j) = (\Phi(x_i) \cdot \Phi(x_j)). \tag{7}$$

Specifically, let $\mathrm{Q} = [\Phi(x_1),...,\Phi(x_M)]$; then $\tilde{\mathrm{C}}$ can also be expressed by

$$\tilde{\mathrm{C}} = \frac{1}{M}\mathrm{Q}\mathrm{Q}^{\mathrm{T}}. \tag{8}$$

Let us form the matrix $\tilde{\mathrm{R}} = \mathrm{Q}^{\mathrm{T}}\mathrm{Q}$: By virtue of kernel-tricks, we can determine the elements of the $M \times M$ matrix $\tilde{\mathrm{R}}$ by

$$\tilde{\mathrm{R}}_{\mathrm{ij}} = \Phi(x_i)^T \cdot \Phi(x_j) = (\Phi(x_i) \cdot \Phi(x_j)) = K(x_i, x_j). \tag{9}$$

Let us calculate the orthonormal eigenvectors u_1, u_2, …, u_m of $\tilde{R}$ corresponding to m largest eigenvalues $\lambda_1 \geq \lambda_2 \geq \ldots \geq \lambda_m$. Then, by SVD technique, the orthonormal eigenvectors w_1, w_2, …, w_m of $\tilde{C}$ corresponding to m largest eigenvalues λ_1, λ_2, …, λ_m are

$$w_j = \frac{1}{\sqrt{\lambda_j}} Q u_j, \quad j = 1, \ldots, m. \tag{10}$$

After the projection of the mapped sample Φ (x) onto the eigenvector w_j, we can obtain the *j*-th feature

$$y_j = w_j^{\mathrm{T}} \Phi(x) = \frac{1}{\sqrt{\lambda_j}} u_j^{\mathrm{T}} Q^{\mathrm{T}} \Phi(x). \tag{11}$$

The resulting features y_1, y_2, …, y_m form a KPCA-transformed feature vector $Y=(y_1, y_2, \ldots, y_m)^{\mathrm{T}}$ for sample x.

4 Data Classification Using Support Vector Machine

There are many kinds of methods for microarray data classification. Since Support Vector Machine (SVM) is suitable for data analysis that deals with few samples and large features, in recent years, most researchers applied Support Vector Machine (SVM) as the base classifier to learn microarray datasets and obtained very good results.

4.1 Support Vector Machine

Support Vector Machine (SVM), which was originally introduced by Vapnik and coworkers [12], is now used in many classification problems. SVM builds up a hyperplane as the decision surface in such a way to maximize the margin of separation between positive and negative examples. SVM achieves this by the structural risk minimization principle. The error rate of a learning machine on the test data is bounded by the sum of the training-error rate and the capacity of this machine depends on the Vapnik Chervonenkis (VC) dimension. Given a labeled set of training samples (X_i, Y_i), $i=1, \ldots, M$, where $X_i \in R^N$ and $Y_i \in \{-1, 1\}$, the discriminant hyperplane is defined by:

$$f(X) = \sum_{i=1}^{M} Y_i \alpha_i K(X, X_i) + b, \tag{12}$$

where $K(X, X_i)$ is a kernel function and the sign of $f(X)$ determines the membership of X.

The selection of an appropriate kernel function is very important for SVM. At present, the selection of kernel function in microarray data classification is mostly artificial and unitary. An improvement scheme can combine several kinds of kernel functions to gain a higher performance.

The polynomial kernel function has good global quality and strong extrapolation ability. As a result of a low polynomial exponent, a higher computation speed can be obtained. To the opposite, the Gauss radial basic function is the locally strong kernel

function. Its interpolation ability will be weakened along with the parameter σ 's growth. Therefore, to get a kernel function that has high learning capability, strong generalization, both good extrapolation and interpolation abilities, we need to design a mixed kernel function that combine several kinds of kernel functions together.

In this paper, K_{mix} is adopted as the kernel function in SVM.

$$K_{mix} = \lambda K_{poly} + (1-\lambda) K_{rbf}, \quad \lambda \in (0,1) . \tag{13}$$

4.2 Parameter Optimization with PSO

Particle Swarm Optimization (PSO) [13] is one of the evolutionary optimization methods inspired by nature. Since PSO was first introduced by Kennedy and Eberhart(1995), it has been successfully applied to optimize various continuous nonlinear functions. In this paper, PSO is used to optimize parameters of the SVM.

A population of particles is randomly generated initially. Each particle represents a potential solution and has a position represented by a position vector x_i. A swarm of particles moves through the problem space with the moving velocity of each particle represented by a velocity vector v_i. At each iteration step t, each particle keeps track of the best position among all the particles $p_g(t)$ and its own best position $p_i(t)$, a new velocity for particle i is updated by

$$v_i(t+1) = w * v_i(t) + c_1 * rand_1 * (p_i(t) - x_i(t)) + c_2 * rand_2 * (p_g(t) - x_i(t)), \tag{14}$$

where c_1 and c_2 are positive constant and $rand_1$ and $rand_2$ are uniformly distributed random number in [0, 1]. The term v_i is limited to the range of $\pm v_{\max}$. If the velocity violates this limit, it is set to its proper limit. Changing velocity in this way can enable the particle i to search around its individual best position, p_i, and global best position, p_g. Based on the updated velocities, each particle changes its position according to the following equation

$$x_i(t+1) = x_i(t) + v_i(t+1). \tag{15}$$

5 An Ensemble Classifiers Design with Binary PSO

Selecting several classifiers to construct the committee is better than any one [14]. So we should select appropriate classifiers to form the classification committee. In this paper, we introduce the selection method classifiers ensemble using Binary of Particle Swarm Optimization (BPSO) [15].

5.1 Particle Representation

Suppose N base classifiers are generated after trained by the feature subsets. They are expressed as C_1, C_2, C_3, ..., C_N. In this new ensemble approach for Cancer Data Classification, X_i^k is the *i-th* particle in swarm at iteration k. It is represented by a N-dimensional vector which is introduced to denote the N base classifiers and can be defined as $X_i^k = \left[x_{i1}^k, x_{i2}^k, ..., x_{in}^k\right]$, where x_{ij}^k is the position of the *i-th* particle with

respect to *j-th* dimension. A binary value of 1 for the *j-th* dimension implies that C_j is selected in the solution and 0 otherwise.

5.2 Initial Population

pop^k is the set of *Popsize* particles in the swarm at iteration *k*, i.e. $pop^k = [X_1^k, X_2^k, \ldots, X_{Popsize}^k]$. For each dimension of a particle, a binary value of 0 or 1 is assigned according to a probability of *e*. In particular,

$$x_{ij}^0 = \begin{cases} 1, & \bigcup(0,1) > e, \\ 0, & otherwise \end{cases}, \tag{16}$$

where V_i^k is the velocity of particle *i* at iteration *k*. It can be described as $V_i^k = \left[v_{i1}^k, v_{i2}^k, \ldots, v_{in}^k\right]$, v_{ij}^k is the velocity of particle *i* with respect to *j-th* dimension.

Velocity values are restricted to some minimum and maximum values, namely $V_i^k = [V_{\min}, V_{\max}]$ where $V_{\min} = -V_{\max}$. The velocity of particle *i* in the *j-th* dimension is established by

$$v_{ij}^0 = V_{\min} + \bigcup(0,1) * (V_{\max} - V_{\min}). \tag{17}$$

This limit enhances the local search exploration of the problem space.

5.3 Fitness Function

In order to measure individuals, the fitness function should be created. We first generate the validation set V and then calculate the error E_{vi}^k of each individual on *V* at iteration *k*. $f(X_i^k)$ is the fitness of the *i-th* particle at iteration *k* depicted as follows:

$$f(X_i^k) = 1 \Big/ E_{vi}^k, \tag{18}$$

$$E_{vi}^k = \sum_{j=1}^{N} x_{ij}^k \times classifier_j, \tag{19}$$

where *N* is the total number of base classifiers, x_{ij}^k is the position of the *i-th* particle with respect to *j-th* dimension at iteration *k*, $classifier_j$ is the error of the *j-th* base classifier on *V*.

5.4 Finding New Solutions

Since the BPSO algorithm is employed in this study, we need to use two useful functions for generating new solutions, namely a limitative function *H* to force the real values between 0 and 1, and a piecewise linear function *G* to force velocity values to be inside the maximum and minimum allowable values.

$$G(v_{ij}^k) = \begin{cases} V_{\max}, & if \quad v_{ij}^k > V_{\max}, \\ v_{ij}^k, & if \quad \left|v_{ij}^k\right| \le V_{\max}, \\ V_{\min}, & if \quad v_{ij}^k < V_{\min}. \end{cases} \tag{20}$$

After applying the piecewise linear function, the following limitative function is used to scale the velocities between 0 and 1, which is then used for converting them to the binary values. That is

$$H(v_{ij}^k) = \frac{1}{1+\left|\frac{V_{\max} - v_{ij}^k}{v_{ij}^k - V_{\min}}\right|^2}. \tag{21}$$

So, new solutions are found by updating the velocity and dimension respectively.

First, we compute the change in the velocity v_{ij}^k such that

$$v_{ij}^{k-1} = w * v_{ij}^{k-1} + c_1 * rand_1 * (pb_{ij}^{k-1} - x_{ij}^{k-1}) + c_2 * rand_2 * (gb_j^{k-1} - x_{ij}^{k-1}), \tag{22}$$

where PB_i^k is the best value of the particle i obtained until iteration k. The best position associated with the best fitness value of the particle i obtained so far is called particle best and defined as $PB_i^k = \left[pb_{i1}^k, pb_{i2}^k, ..., pb_{in}^k\right]$. GB^k is the best position among all particles in the swarm, which is achieved so far and can be expressed as $GB^k = \left[gb_1^k, gb_2^k, ..., gb_n^k\right]$. c_1 and c_2 are social and cognitive parameters and $Rand_1$ and $Rand_2$ are uniform random numbers between 0 and 1.

Then we update the velocity v_{ij}^k by using the piecewise linear function such that

$$v_{ij}^k = G(v_{ij}^{k-1} + \Delta v_{ij}^{k-1}). \tag{23}$$

Finally we update the dimension j of the particle i such that

$$x_{ij}^k = \begin{cases} 1, & if \quad \cup(0,1) < H(v_{ij}^k) \\ 0, & otherwise \end{cases}. \tag{24}$$

6 Experiments

We performed extensive experiments on two benchmark cancer datasets, which were obtained from the Internet, namely the Leukemia and Colon database. The Leukemia dataset consists of 72 samples taken from leukemia patients: 25 samples of AML and 47 samples of ALL [16]. A total of 38 out of 72 samples were used as training data and the remaining samples were used as test data. Each sample contained 7129 gene expression levels. The Colon dataset consists of 62 samples of colon epithelial cells taken from colon-cancer patients [16]. Each sample contains 2000 gene expression levels. A total of 31 out of 62 samples were used as training data and the remaining samples were used as test data.

For this experiment, the normalization procedure is firstly used for preprocessing the raw data. Four steps were taken. Then the KPCA is employed, 60 informative features of each sample are extracted and 9 training datasets are chosen for training the 9 base classifiers. SVM is employed to be the base classifier and PSO is used to

Table 1. Parameters used in this paper

Parameters for KPCA	
$K(x_i, x_j)$: kernel function	RBF
Parameters for SVM	
λ : kernel function proportion coefficient	0.95
$K(X, X_i)$: kernel function	K_{mix}
Parameters for PSO	
L: population size	30
w: weight	1.0
c_1, c_2: learning factor	2.0
X_{up}: the upper boundary of x	3.0
X_{down}: the lower boundary of x	-3.0
V_{max}: the max velocity	1.8
$rand_1$, $rand_2$: uniform random number	(0, 1)
Parameters for BPSO	
L: population size	30
w: weight	1.0
c_1, c_2: learning factor	2.0
V_{max}: the max velocity	1
$rand_1$, $rand_2$: uniform random number	(0, 1)

Table 2. Comparison of different approaches on Leukemia dataset

Author	Classification Rate (%)
This paper	97.1~100
Furey et al. [17]	94.1
Li et al. [18]	84.6
Ben-Dor et al. [19]	91.6~95.8
Nguyen et al. [20]	94.2~96.4
Zhao et al. [21]	95.8~97.2

Table 3. Comparison of different approaches on Colon dataset

Author	Classification Rate (%)
This paper	93.7~99.7
Furey et al. [17]	90.3
Li et al. [18]	94.1
Ben-Dor et al. [19]	72.6~80.6
Nguyen et al. [20]	87.1~93.5
Zhao et al. [21]	85.5~93.3

optimize the parameters for each SVM. Then BPSO is applied for selecting appropriate base classifiers to construct the classification committee.

In our experiment, the parameters that used are shown in Table 1. A comparison of different feature extraction methods and different classification methods for leukemia dataset is shown in Table 2, for colon dataset is shown in Table 3.

7 Conclusions

In this paper, a new ensemble of classifiers is proposed for cancer data classification. The leukemia and colon datasets are used for conducting all the experiments. The raw data is first preprocessed for normalization. Gene features are then extracted based on the KPCA, which greatly reduces dimensionality, as well as maintains the informative features. At last the SVM is employed to construct the classifier committee based on BPSO for classification. The experimental results show that the proposed framework is efficient in recognition rate comparing with some other advanced artificial techniques.

Acknowledgments

This research was partially supported by the Natural Science Foundation of China under contract number 60573065, the Key Subject Research Foundation of Shandong Province and the Natural Science Foundation of Shandong Province under contract number Y2007G33.

References

1. Sarkar, I., Planet, P., Bael, T., Stanley, S., Siddall, M., DeSalle, R.: Characteristic Attributes in Cancer Microarrays. Computers and Biomedical Research 35(2), 111–122 (2002)
2. Koller, D., Sahami, M.: Towards optimal feature selection. In: Machine Learning, Proceeding of 13th Int. Conf. (1996)
3. Azuaje, F.: A Computational Neural approach to Support the Discovery of Gene Function and Classes of Cancer. IEEE Transactions on Biomedical Engineering 48(3), 332–339 (2001)
4. Li, L., Weinberg, C., Darden, T., Pedersen, L.: Gene Selection for Sample Classification Based on Gene Expression Data: Study of Sensitivity to Choice of Parameters of the GA/KNN Method. Bioinformatics 17(12), 1131–1142 (2001)
5. Camp, N., Slattery, M.: Classification Tree Analysis: A Statistical Tool to Investigate Risk Factor Interactions with an Example for Colon Cancer. Cancer Causes Contr. 13(9), 813–823 (2002)
6. Chen, Y., Peng, L., Abraham, A.: Gene expression profiling using flexible neural trees. In: Corchado, E., Yin, H., Botti, V., Fyfe, C. (eds.) IDEAL 2006. LNCS, vol. 4224, pp. 1121–1128. Springer, Heidelberg (2006)
7. Tan, A., Gilbert, D.: Ensemble Machine Learning on Gene Expression Data for Cancer Classification. Applied Bioinformatics 2(3), 75–83 (2003)
8. Sergios, T., Konstantinos, K.: Pattern Recognition. China Machine Press (2002)

9. Scholkopf, B., Smola, A., Muller, K.R.: Nonlinear component analysis as a kernel eigenvalue problem. Neural Comput. 10(5), 1299–1319 (1998)
10. Yang, J., Yang, J.Y., Frangi, A.F.: Combined Fisherfaces framework. Image and Vision Computing 21, 1037–1044 (2003)
11. Golub, G.H., Van Loan, C.F.: Matrix Computations. The Johns Hopkins University Press, Baltimore (1996)
12. Vapnik, V.N.: The Nature of Statistical Learning Theory. Springer, Heidelberg (1999)
13. Kennedy, J., Eberhard, R.C.: Particle Swarm Optimization. In: Proceeding of IEEE International Conf. on Neural Networks, Piscataway, NJ, USA, pp. 1942–1948 (1995)
14. Zhou, Z.H., Wu, J., Tang, W.: Ensembling Neural Networks: Many Could Be Better Than All. Artificial Intelligence 137(1-2), 239–263 (2002)
15. Kennedy, J., Eberhart, R.C.: A Discrete Binary Version of the Particle Swarm Optimization. In: Proceeding Of the conference on Systems, Man, and Cybernetics SMC 1997, pp. 4104–4109 (1997)
16. Ben-Dor, A., Bruhn, L., Friedman, N., Nachman, I., Schummer, M., Yakhini, N.: Tissue classification with gene expression profiles. Computational Biology 7, 559–584 (2000)
17. Golub, T.R., Slonim, D.K., Tamayo, P., Huard, C., GaasenBeek, M., Mesirov, J.P., Coller, H., Loh, M.L., Downing, J.R., Caligiuri, M.A., Blomfield, C.D., Lander, E.S.: Molecular Classification of Cancer: Class Discovery and Class Prediction by Gene Expression Monitoring. Science 286(12), 531–537 (1999)
18. Eisen, M.B., Brown, B.O.: DNA Arrays for Analysis of Gene Expression. Methods in Enzymology 303, 179–205 (1999)
19. Cho, S.B.: Exploring Features and Classifiers to Classify Gene Expression Profiles Of acute Leukemia. Artifical Intellegence 16(7), 1–13 (2002)
20. Harrington, C.A., Rosenow, C., Retief, J.: Monitoring Gene Expression Using DNA Microarrays. Curr. Opin. Microbiol. 3, 285–291 (2000)
21. Zhao, Y., Chen, Y., Zhang, X.: A novel ensemble approach for cancer data classification. In: Liu, D., Fei, S., Hou, Z., Zhang, H., Sun, C. (eds.) ISNN 2007. LNCS, vol. 4492, pp. 1211–1220. Springer, Heidelberg (2007)

A Method for Multiple Sequence Alignment Based on Particle Swarm Optimization

Fasheng Xu[1] and Yuehui Chen[2]

[1] School of Science,
University of Jinan, Jinan, 250022, P.R. China
[2] School of Information Science and Engineering,
University of Jinan, Jinan, 250022, P.R. China

Abstract. Sequence Alignment is a basic information disposal method in Bioinformatics. However, it is difficult to deal with multiple sequence alignment problem(MSA). In this paper, an improved particle swarm optimization is designed to solve MSA. In the algorithm, each particle represents an alignment and flies to the particle which has the best solution by some rules. Moreover, in order to expand the diversity of the algorithm and enhance the possibility of finding the optimal solution, three operators are designed, that is, gaps deletion, gaps insertion, and local search operator. Simulation results show that for MSA proposed algorithm is superior to Clustal X.

Keywords: Multiple Sequence Alignment; Bioinformatics; Particle Swarm Optimization.

1 Introduction

Multiple alignments of protein sequences are important in many applications, including phylogenetic tree estimation, secondary structure prediction and critical residue identification. Sequence alignment is by far the most common task in bioinformatics. Procedures relying on sequence comparison are diverse and range from database searches to secondary structure prediction . Sequences can be compared two by two to scour databases for homologues, or they can be multiply aligned to visualize the effect of evolution across a whole protein family. However, it is difficult to align multiple sequence. A common heuristic is to seek a multiple alignment that maximizes the SP score (the summed alignment score of each sequence pair), which is NP complete[1]. Therefore the design of algorithms for multiple sequence alignment has been a very active research area.

Many efforts have been made on the problems concerning the optimization of sequence alignment. Needleman and Wunsch [2] presented an algorithm for sequence comparison based on dynamic programming (DP), by which the optimal alignment between two sequences is obtained. The generalization of this algorithm to multiple sequence alignment is not applicable to a practical alignment that consists of dozens or hundreds of sequences, since it requires huge CPU time proportional to N^K, where K is the number of sequences each with

D.-S. Huang et al. (Eds.): ICIC 2009, LNAI 5755, pp. 965–973, 2009.

length N. Stochastic methods such as Gibbs sampling can be used to search for a maximum objective score [3], but have not been widely adopted. A more popular strategy is the progressive method [4] [5], which first estimates a phylogenetic tree. A profile (a multiple alignment treated as a sequence by regarding each column as a symbol) is then constructed for each node in the binary tree. If the node is a leaf, the profile is the corresponding sequence; otherwise its profile is produced by a pair-wise alignment of the profiles of its child nodes . Current progressive algorithms are typically practical for up to a few hundred sequences on desktop computers, the best-known of which is CLUSTALW [6]. A variant of the progressive approach is used by T-Coffee [7], which builds a library of both local and global alignments of every pair of sequences and uses a library-based score for aligning two profiles. On the BAliBASE benchmark [8] [9], T-Coffee achieves the best results, but has a high time and space complexity that limits the number of sequences it can align to typically around one hundred. There are also some non-deterministic approaches using genetic algorithms, such as SAGA [10], which was reported to find optimal alignments even in search spaces of a considerable size (more that 10 sequences). The approach is to use a progressive alignment as the initial state of a stochastic search for a maximum objective score (stochastic refine refinement). Alternatively, pairs of profiles can be extracted from the progressive alignment and re-aligned, keeping the results only when an objective score is improved (horizontal refinement)[11].

In this paper, we developed a method for multiple sequence alignment based on the particle swarm optimization(PSO). The organization of this paper is as follows. In Section 2, the sequence alignment problem is introduced. Then, the outline procedure of the improved particle swarm optimization for multiple sequence alignment problem is designed in Section 3. To verify the feasibility and efficiency of the proposed approach, an empirical example is presented in Section 4. Some concluding remarks are given in Section 6.

2 The Sequence Alignment Problem

In bioinformatics, the most important data sets are biological sequences, including DNA sequences and protein sequences. A DNA sequence can be seen as symbols of the ACGT four strings, a protein sequence can be seen as 20 kinds of proteins string symbols. In the process of evolution there can insert, delete or mutate elements of the sequences. Thus, in order to highlight the similarities of the sequences it is often convenient to insert gaps in them, leading to a higher number of symbol matches. The similarity of aligned sequences is measured using a scoring function, which is based on a matrix that assigns a score to every pair of symbols (based on a mutation probability). For proteins, the most commonly used matrices are PAM(Percent Accepted Mutation) and BLOSUM (Blocks Substitution Matrix)[12]. Additionally, a penalization to the insertion of gaps is required in order to avoid the insertion of an excessive number of them. The process of finding an optimum (or at least good) match between the sequences is called sequence alignment.

3 Improved Particle Swarm Optimization for MSA

3.1 Particle Swarm Optimization

Particle Swarm Optimization (PSO) was first introduced by Kennedy and Eberhart [13] [14] in 1995 and partly inspired by the behavior of large animal swarms such as schooling fish or flocking birds. PSO conducts search using a population of a random solutions, corresponding to individual. In addition, each potential solution called particles is also assigned a randomized velocity. Each particle in PSO flies in the hyperspace with a velocity which is dynamically adjusted according to the flying experiences of its own and its colleagues. Each particle adjusts its position according to their own and their neighboring-particles experience, moving toward two points: the best position so far by itself called Pbest and by its neighbor called Gbest at every iteration. The particle swarm optimization concept consists of, at each time step, changing the velocity each particle toward its Pbest and Gbest.

Suppose that the search space is D dimensional, then the ith particle of the swarm can be represented by a D dimensional vector $X_i = (x_{i1}, x_{i2}, \ldots, x_{iD})'$. The particle velocity can be represented by another D dimensional vector $V_i = (v_{i1}, v_{i2}, \ldots, v_{iD})'$. The best previously visited position of the ith particle is denoted as $P_i = (p_{i1}, p_{i2}, \ldots, p_{iD})'$. Defining g as the index of the best particle in the swarm, and let the superscripts denote the iteration number, then the position of a particle and its velocity are updated by the following equations :

$$v_{id}^{k+1} = wv_{id}^{k} + c_1 r_1^k (p_{id}^k - x_{id}^k) + c_2 r_2^k (p_{gd}^k - x_{id}^k) \tag{1}$$

$$x_{id}^{k+1} = x_{id}^{k} + v_{id}^{k+1} \tag{2}$$

where $d = 1, 2, \ldots, D$, $i = 1, 2, \ldots, N$, and N is the size of swarm; w is called inertia weight: c_1, c_2 are two positive constants, called cognitive and social parameter respectively; r_1, r_2 are random numbers, uniformly distributed in $[0, 1]$; and $k = 1, 2, \ldots$ determines the iteration number.

3.2 Improved Particle Swarm Optimization

The sequence alignment problem can be considered as an optimization problem in which the objective is to maximize a scoring function. Thus, the PSO algorithm was adapted to be used with biological sequences. In the adapted PSO algorithm, a particle represents a sequence alignment. Thereby, as the main mechanism of the PSO algorithm is the movements of the particles towards the leader, suitable operators to implement this mechanism are proposed. The general algorithm is shown as follows[15]:

```
PSOMSA ( )
1. Generate a set of initial particles
2. Determine the leader particle gbest
3. Repeat until the termination criterion is met
```

```
a. Measure distance between gbest and every particle
b. Move every particle towards gbest
c. Determine the leader partic
```

The termination criteria can be a maximum number of iterations, or a number of iterations after which the best score do not improve. The implicit idea of the PSO algorithm is that a set of particles that are randomly sparse over a search space will progressively move to regions which will provide better solutions to the problem, until the swarm finds a solution that it cannot improve anymore.

Next, some implementation details will be discussed, such as the particle representation, scoring function and the implementation of the particle movement mechanism.

Data Representation. In general, a swarm is made up by a set of particles, and a particle of the swarm is designated as the leader (gbest).Additionally, each particle preserves a memory with its best historical location (pbest). As mentioned above, in the adapted PSO algorithm, a particle will correspond to a sequence alignment. An alignment is then represented as a set of vectors, where each vector specifies the positions of the gaps for one of the sequences to be aligned. Thus, a coordinate of the particle corresponds to a sequence to be aligned, and is represented with a vector of size s, where s is the maximum allowed number of gaps, which may be different for each sequence. Therefore, a set of n sequences to be aligned correspond to an n-dimensional search space.

Initialization. The size of the swarm (i.e., the number of particles) is determined by the user. Additionally, the length of the alignment has a minimum value given by the length of the largest sequence, and a maximum length given, for instance, as twice the length of the largest sequence. The initial set of particles is generated by adding gaps into the sequences at random position, thus all the sequences have the same length L (the typical value of L is 1.4 times of the longest sequences).

Scoring Function. The global alignment score is based on the score of the alignment of each pair of sequences. Thus each sequence should be aligned with the every other sequence. In general, the score assigned to each particle (alignment) is the sum of the scores(SP) of the alignment of each pair of sequences. The score of each pair of sequences is the sum of the score assigned to the match of each pair of symbols, which is given by the substitution matrix. This matrix includes all the possible symbols, including the gap and the related penalization. The score of a multiple alignment is then:

$$SP - Score(A) = \sum_{i=1}^{k-1} \sum_{j=i+1}^{k} s(A_i, A_j) \tag{3}$$

where the $s(A_i, A_j)$is the alignment score between two aligned sequencesA_i and A_j.

Speed Update. In the PSO algorithm each particle moves towards the leader at a speed proportional to the distance between the particle and the leader. In this paper, the speed is defined:

$$v_{id}^{k+1} = c_1 r_1^k (p_{id}^k - x_{id}^k) + c_2 r_2^k (p_{gd}^k - x_{id}^k) \tag{4}$$

where c_1 and c_2 are the weights. If the value of v_{id}^{k+1} is not an integer, rounded it.

Position Update. After the update of speed, each particle updates its coordinate(x) according to:

$$x_{id}^{k+1} = x_{id}^k + v_{id}^{k+1} \tag{5}$$

When the position updated, the sequence may become illegal(Figure 1 shows an example).

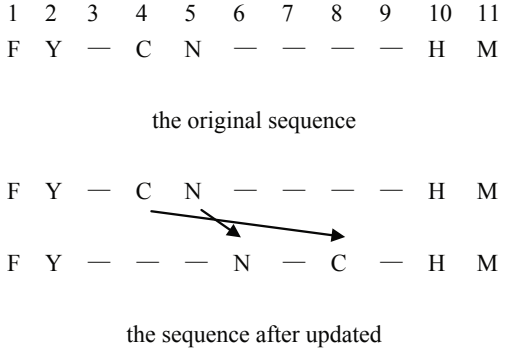

Fig. 1. An example of illegal update. The location of residue C and N is changed after update and the sequence is illegal.

An adjustment must be done in order to eliminate such illegal sequence. The adjustment is using

$$if \quad x_{id} \leq x_{i(d-1)}, \quad then \quad x_{id} = x_{i(d-1)} + 1 \tag{6}$$

An example is depicted in Figure 2.

Operators. According to the traditional PSO, three types of operators are represented in PSOMSA: the insertion, deletion and local search.

1)Gaps Deletion

After a number of iterations, some columns may only have gaps. They not only useless, but also extended the length of alignment. Therefore, we remove them from the alignment.It is shown in Figure 3.

2) Gaps Insertion

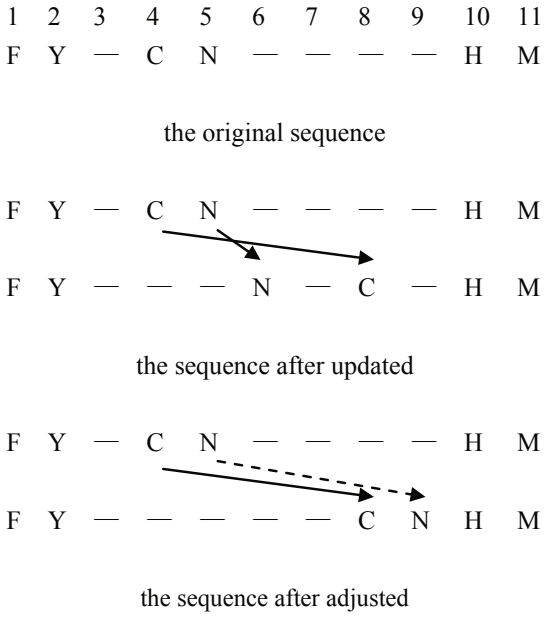

Fig. 2. An example of the adjustment of illegal sequence. The location of residue C is updated according to 5 and the residue of N is adjusted according to 6.

F	P	E	Y	V	N	K	-	-	D	F	H	I	A	G	E	S	Y
H	P	E	F	A	K	N	-	-	D	F	F	I	T	G	E	S	Y
F	P	E	Y	K	N	N	-	-	K	L	F	L	T	G	E	S	Y
F	P	E	D	L	T	R	-	-	K	I	I	L	S	G	E	S	Y

Fig. 3. An alignment with gap columns

The gaps insertion operators are added in order to avoid the PSO converge into a local optimal solution. We insert some gap columns into the current best alignment by a probability m. For example, we insert L columns into the alignment. The location to insert is defined in two ways as follows:

```
Insert L gap columns into a random location in the alignment
  or
Insert one gap column into the alignment at L random locations.
```

One of the operators is randomly selected by the program when it is running. Because the gap columns do not change the score of alignment, the gaps insertion operators do not help to improve the result of alignment. But the operators will affect the other particles, all particles' gaps will to be increased; thereby

increasing the diversity of the algorithm and avoiding the algorithm converge into a local optimal solution.

3) Local Search Operator

In this paper, we use a local search to enhance the search performance. Assuming the count of gaps in the sequence which has the least gaps is L, we remove some gaps ranged from 0 to L from all the sequences. After that, we compute the score of the alignment. If the score is higher than before, the alignment is reserved; otherwise, we resume the alignment.

4 Simulation Experiments and Discussion

The proposed algorithm, called PSOMSA, was implemented in order to test its performance. The number of particles is determined taking into account the length of the sequences and the number of sequences to align. In order to test the algorithm, eight protein families of different length and different percentages of sequence identity were selected from the alignments database BALiBASE, available in [16]. One protein family was selected from each length category (short, medium and large), and one from each range of identity percentage (less that 25%, between 25% and 40% and greater that 35%). Table 1 presents the protein families used in the experiments. These protein families were previously

Table 1. Protein families used in the experiments

Reference	Name	Length	Identity%
1r69	repressor	Short	< 25
1tgxA	cardiotoxin	Short	20-40
1fmb	hiv-1 protease	Short	> 35
1mrj	alpha tricosanthin	Medium	20-40
1ezm	elastase	Medium	> 35
1cpt	cytochrome p450	Large	< 25
1ac5	b-galactoxidase	Large	20-40
1ad3	aldehyde dehydrogenase	Large	> 35

aligned using the well known algorithm Clustal X 2.0. The alignment obtained using Clustal was evaluated using a PAM250 matrix. The alignment was obtained using a penalty of 10 for each open gap and a penalty of 0.3 for each expend gap. The algorithm stopped after 10 gaps insertion operators without improving the quality of the solution. Table 2 shows the results of the experiments.

It can be found from the results that the PSOMSA algorithms has superior performance when compared to Clustal X, especially when the data has smaller sequences and shorter length. However, when the data has a longer length, the results is similar. There are still many enhancements that must be done to PSOMSA in order to achieve satisfying results. Also, new fitness functions based on different scoring methods are possible straightforward developments.

Table 2. Experimental results

Reference	Number of Sequences	Length	Clustal X Score	PSOMSA Score
1r69	4	63-78	2.7	287.9
1tgxA	4	57-64	447.9	890.7
1fmb	4	98-104	1513.4	1578
1mrj	5	247-266	2361.1	2367.9
1ezm	4	297-380	8223.8	8628.8
1cpt	5	378-434	1267.2	1795
1ac5	4	421-485	2814.5	3105.6
1ad3	4	424-447	5710.6	5726.8

5 Conclusions

In this work an algorithm based on the PSO algorithm, was proposed to address the multiple sequence alignment problem with SP score. The proposed approach was tested using some protein families and compared with the alignments generated by the Clustal X 2.0 algorithm. From simulation results, it is shown that the proposed PSOMSA algorithms has superior performance when compared to Clustal X .

In future work, additional experimentation should be performed, including experimentation with sequences of nucleic acids, the use of other algorithms to find initial sequence alignments , the use of other scoring schemes based on PAM or BLOSUM matrices and improving the speed of PSOMSA.

Acknowledgments

This research was supported by the NSFC (60573065), the Natural Science Foundation of Shandong Province (Y2007G33), and the Key Subject Research Foundation of Shandong Province.

References

1. Wang, L., Jiang, T.: On the Complexity of Multiple Sequence Alignment. J. Comput. Biol. 1(4), 337–348 (1994)
2. Needleman, S.B., Wunsch, C.D.: A General Method Applicable to the Search for Similarities in the Amino Acid Sequence of Two Proteins. J. Mol. Biol. 48, 443–453 (1970)
3. Lawrence, C.E., Altschul, S., Boguski, M., Liu, J., Neuwald, A., Wootton, J.: Detecting Subtle Sequence Signals: a Gibbs Sampling Strategy for Multiple Alignment. Science 262, 208–214 (1993)
4. Hogeweg, P., Hesper, B.: The Alignment of Sets of Sequences and the Construction of Phyletic Trees: an Integrated Method. J. Mol. E 20, 175–186 (1984)
5. Feng, D.F., Doolittle, R.F.: Progressive Sequence Alignment as a Prerequisite to Correct Phylogenetic Trees. J. Mol. E 25(4), 351–360 (1987)

6. Thompson, J.D., Higgins, D.G., Gibson, T.J.: Clustal W: Improving the Sensitivity of Progressive Multiple Sequence Alignment through Sequence Weighting, Position-specific Gap Penalties and Weight Matrix Choice. Nucleic Acids Res. 22(22), 4673–4680 (1994)
7. Notredame, C., Higgins, D.G., Heringa, J.: T-Coffee: A Novel Method for Fast and Accurate Multiple Sequence Alignment. J. Mol. Biol. 302(1), 205–217 (2000)
8. Bahr, A., Thompson, J.D., Thierry, J.C., Poch, O.: Balibase (Benchmark Alignment Database): Enhancements for Repeats, Transmembrane Sequences and Circular Permutations. Nucl. Acids Res. 29(1), 323–326 (2001)
9. Thompson, J.D., Plewniak, F., Poch, O.: Balibase: A Benchmark Alignment Database for the Evaluation of Multiple Alignment Programs. Bioinformatics 15(1), 87–88 (1999)
10. Notredame, C., Higgins, D.G.: Saga: Sequence Alignment by Genetic Algorithm. Nucleic Acids Res. 24(8), 1515–1524 (1996)
11. Hirosawa, M., Totoki, Y., Hoshida, M., Ishikawa, M.: Comprehensive Study on Iterative Algorithms of Multiple Sequence Alignment. Comput. Appl. Biosci. 11(1), 13–18 (1995)
12. Henikoff, S., Henikoff, J.G.: Amino Acid Substitution Matrices from Protein Blocks. Proc. Natl. Acad. Sci. USA 89(22), 10915–10919 (1992)
13. Kennedy, J., Eberhart, R.C.: Particle Swarm Optimization. In: Proceedings of IEEE International Conference on Neural Networks, pp. 1942–1948. IEEE Press, Piscataway (1995)
14. Eberhart, R., Kennedy, J.: A New Optimizer Using Particle Swarm Theory. In: Proc. 6th Int Sympossum on Micro Machine and Human Science, pp. 39–43. IEEE Press, Piscataway (1995)
15. Rodriguez, P.F., Nino, L.F., Alonso, O.M.: Multiple Sequence Alignment using Swarm Intelligence. International Journal of Computational Intelligence Research 3(2), 123–130 (2007)
16. National Center for Biotechnology Information, http://www.ncbi.nlm.nih.gov
17. Clustal W Download Page, http://www.clustal.org/download/current/

Inference of Differential Equation Models by Multi Expression Programming for Gene Regulatory Networks

Bin Yang, Yuehui Chen, and Qingfang Meng

Computational Intelligence Lab.
School of Information Science and Engineering
University of Jinan, Jinan 250022, P.R. China
yhchen@ujn.edu.cn

Abstract. This paper presents an evolutionary method for identifying the gene regulatory network from the observed time series data of gene expression using a system of ordinary differential equations (ODEs) as a model of network. The structure of ODE is inferred by the Multi Expression Programming (MEP) and the ODE's parameters are optimized by using particle swarm optimization (PSO). The proposed method can acquire the best structure of the ODE only by a small population, and also by partitioning the search space of system of ODEs can be reduced significantly. The effectiveness and accuracy of the proposed method are demonstrated by using synthesis data from the artificial genetic networks.

Keywords: Evolutionary method, multi expression programming, ordinary differential equations, particle swarm optimization, artificial genetic networks.

1 Introduction

Gene expression programs which produce the living cells involving regulated transcription of thousands of genes depend on recognition of specific promoter sequences by transcriptional regulatory proteins. The problem is how a collection of regulatory proteins associates with genes can be described as a transcriptional regulatory network. The most important step is to identify the interactions among genes by the modeling of gene regulatory networks.

Many models have been proposed to describe the network including the Boolean network [2] [18], Dynamic Bayesian network [3], the system of differential equations [4] and so on. A recent review for inferring genetic regulatory networks based on data integration and dynamical models can be seen in ref. [19]. The system of differential equations is powerful and flexible model to describe complex relations among components [6], so many methods are proposed for inferring a system of differential equations for the gene regulatory network during the last few years. But it is hard to determine the suitable form of equations which describe the network. In the previous studies, the form of the differential equation was being fixed. The

D.-S. Huang et al. (Eds.): ICIC 2009, LNAI 5755, pp. 974–983, 2009.

only one goal was to optimize parameters and coefficients. For example, Tominaga D. used the Genetic Algorithms (GA) to optimize the parameters of the fixed form of system of differential equations [5]. In recent years some researchers studied the learning of gene regulatory network by inferring the structures and parameters of a system of ODEs. Erina Sakamoto proposed an ODEs identification method by using the least mean square (LMS) along with the ordinary genetic programming (GP) to identifying the gene regulatory network [6]. Dong Yeon Cho proposed a new representation named S-tree based GP to identify the structure of a gene regulatory network and to estimate the corresponding parameter values at the same time [7]. Li jun Qian proposed GP was applied to identify the structure of model and kalman filtering was used to estimate the parameters in each iteration. Both standard and robust kalman filtering were considered [1]. But their inference algorithms can only be applied to the small-scale networks.

In this paper, we propose a new method, in which the Muti Expression Programming(MEP) and particle swarm optimization(PSO) are employed to overcome structure form and parameters identification problems in discovering of a system of differential equations. We infer the structure of the right-hand sides of ODEs by MEP and optimize the parameters of ODEs by PSO. Compared with GP which was applied in the previous studies, a MEP chromosome encodes several genes and each gene can present a ODE, so we can acquire the best structure of the ODE only by a small population. To reduce the complexity of the genetic network inference problem, the partitioning [8] is used in the process of identification of structure of system. Each ODE of the ODEs can be inferred separately and the research space reduces rapidly. Thus for the the large-scale networks, our method performs better.

2 Method

2.1 Structure Optimization of Models Using MEP

Encoding MEP [9] is a new technique in evolutionary algorithms that is first introduced in 2002 by Oltean. A traditional GP [10] encodes a single expression. By contrast, a MEP chromosome contains several genes. Each gene encodes a tree which contains the terminal or function symbols selected from a terminal set T or a function set F. The two sets for a given problem are pre-defined. A gene that encodes a function includes some pointers towards the function arguments. The best of the encoded solution is chosen to represent the chromosome [11]. We use MEP to identify the form of the system of differential equations. For this purpose, we encode right-hand side of each ODE into a MEP chromosome. For example a ODEs model with the form of

$$\begin{cases} \dot{X}_1 = aX_1 + bX_2 \\ \dot{X}_2 = cX_1 \\ \dot{X}_3 = dX_2 + e \end{cases} \tag{1}$$

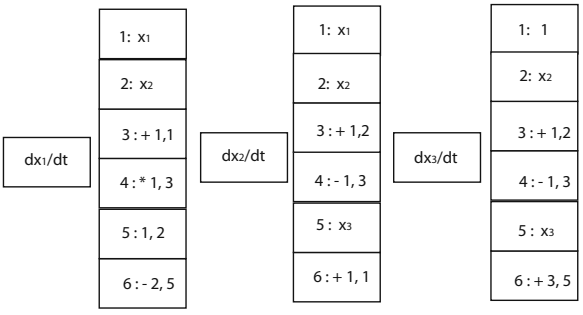

Fig. 1. Example of a ODEs

can be represented as three MEP chromosomes$\{E_3, E_6, E_3\}$ illustrated in Fig. 1, where the coefficients a, b, c, d, e are derived by PSO (as described later in this paper).

We infer the system of ODEs with partitioning. Partitioning, in which equations describing each variable of the system can be inferred separately, significantly reducing the research space. When using partitioning, a candidate equation for a signal variable is integrated by substituting references to other variables with data from the observed time series. This allows us to infer the structure of systems comprising more variables and higher degree of coupling than were inferred by other methods [8].

Genetic Operate. The genetic operators used within MEP algorithm are crossover and mutation.

(1) Crossover. In this paper, we choose the one-point crossover. Firstly, two parents are selected according to the predefined crossover probability P_c. One crossover point is randomly chosen and the parents exchange the sequences at this point.
(2) Mutation. One parent is selected according to the predefined mutation probability P_m. One mutation point is randomly chosen. If the mutation point encodes a function symbol, it may be changed into a terminal symbol or another function with arguments and parameters. And we can mutate the function arguments and parameters into another arguments and parameters produced randomly.

2.2 Parameter Optimization of Models using PSO

At the beginning of this process, we check all the constants contained in each equation , namely count their number n_i and report their places. Distribution of parameters in each chromosome is illustrated in Fig. 2.

According to n_i, the particles are randomly generated initially. Each particle x_i represents a potential solution. A swarm of particles moves through space,

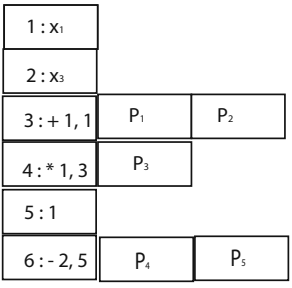

Fig. 2. Distribution of parameters in each chromosome

with the moving velocity of each particle represented by a velocity vector v_i. At each step, each particle is evaluated and keep track of its own best position, which is associated with the best fitness it has achieved so far in a vector $Pbest_i$. And the best position among all the particles is kept as Gbest [12]. A new velocity for particle i is updated by

$$v_i(t+1) = v_i(t) + c_1 r_1 (Pbest_i - x_i(t)) + c_2 r_2 (Gbest(t) - x_i(t)) \tag{2}$$

where c_1 and c_2 are positive constant and r_1 and r_2 are uniformly distributed random number in [0,1]. Based on the updated velocities, each particle changes its position according to the following equation:

$$x_i(t+1) = x_i(t) + v_i(t+1) \tag{3}$$

2.3 Fitness Definition

For inferring a system of ODEs, the fitness of each variable is defined as the sum of squared error and the penalty for the degree of the equations:

$$fitness(i) = \sum_{k=0}^{T-1} \left(x_i'(t_0 + k\Delta t) - x_i(t_0 + k\Delta t)\right)^2. \tag{4}$$

Where t_0 is the starting time, $\triangle t$ is the stepsize, T is the number of the data point, $x_i(t_0 + k\triangle t)$ is the actual outputs of i-th sample, and $x_i'(t_0 + k\triangle t)$ is ODEs outputs. All outputs are calculated by using the approximate forth-order Runge-Kutta method. And a is the penalty for the degree of the equations.

2.4 Summary of Algorithm

The proposed method for the optimal design of the system of ODEs can be described as follows.

(1) Create a initial population randomly (structures and their corresponding parameters);

(2) Structure optimization is achieved by MEP as described in subsection 2.1;
(3) At some interval of generations, select the better structures to optimize parameters. Parameter optimization is achieved by PSO as described in subsection 2.2. In this process, the structure is fixed.
(4) If satisfactory solution is found, then stop; otherwise go to step (2).

3 Experimental Results

We have prepared two tasks to test the effectiveness of our method. Experimental parameters are summarized in Table 1. Function and terminal sets F and T are described as follows,

$$F = \{+, -, *, x^a\}$$
$$T = \{X_1, ..., X_n, 1\}. \tag{5}$$

3.1 Example 1: The Small Artificial Gene Regulatory Network

Fig.3 shows an example of gene regulatory network. This type of network can be modeled as a so-called S-system model [14]. This model is based on approximating kinetic laws with multivariate power-law functions. A model consists of n non-linear ODEs and the generic form of equation i is given as follows:

$$X_i^{'}(t) = \alpha_i \prod_{j=1}^{n} X_j^{g_{ij}}(t) - \beta_i \prod_{j=1}^{n} X_j^{h_{ij}}(t) \tag{6}$$

where X is a vector of dependent variable, α and β are vectors of non-negative rate constants and g and h are matric of kinetic orders.

The parameter of the genetic network are given in Table 2. And the initial conditions is $\{0.7, 0.12, 0.14, 0.16, 0.18\}$ for X_1, X_2, X_3, X_4, X_5 [13]. Experimental parameter for this task are shown in Table 1. The search region of the parameters was [0.0, 15.0]. Five runs are carried out. In each run, the proposed method produces one candidate solution . Select 10 better structures to optimize parameters by PSO at every 30 generations and end when the generation is achieved

Table 1. Parameters for experiments

	Exp1	Exp2
Population size	1000	1000
Generation	500	2000
Crossover rate	0.7	0.7
Mutation rate	0.3	0.3
Time series	1	1
Stepsize	0.01	0.01
Data point	15	20
gene size	5	15

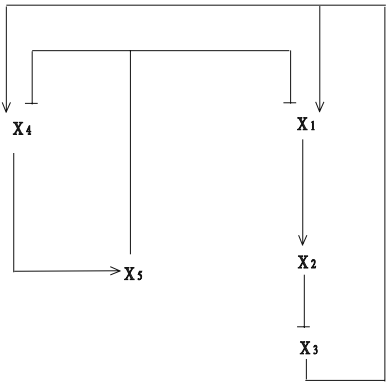

Fig. 3. The targeted gene regulator network

Table 2. Parameters of the genetic network system

i	α_i	g_{i1}	g_{i2}	g_{i3}	g_{i4}	g_{i5}	β_i	h_{i1}	h_{i2}	h_{i3}	h_{i4}	h_{i5}
1	5.0			1.0		-1.0	10.0	2.0				
2	10.0	2.0					10.0		2.0			
3	10.0		-1.0				10.0		-1.0	2.0		
4	8.0			2.0		-1.0	10.0				2.0	
5	10.0				2.0		10.0					2.0

or the best model is gained. To handle the powers of the component variable, we used the following terminal set:

$$T = \{X_1, X_1^{-1}, X_2, X_2^{-1}, X_3, X_3^{-1}, X_4, X_4^{-1}, X_5, X_5^{-1}\} \tag{7}$$

The experiments were performed in the Windows XP system with Intel Pentinum Dual 2.00GHz processor and 1GB memory. We created the following ODEs by our method and throughout simulation, we further confirm that the identified system is quite close to the original system (Fig. 4).

$$\begin{cases} \dot{X_1} = 4.999994X_3X_5^{-1} - 9.999994X_1^2 \\ \dot{X_2} = 10.000023X_1^2 - 10.000014X_2^2 \\ \dot{X_3} = 10.000016X_2^{-1} - 10.000015X_3^2X_2^{-1} \\ \dot{X_4} = 8.000003X_3^2X_5^{-1} - 10.000001X_4^2 \\ \dot{X_5} = 9.999994X_4^2 - 10.000019X_5^2 \end{cases} \tag{8}$$

In [7], Dong Yeon Cho proposed a new representation named S-tree based genetic programming(GP) to identify the structure of a gene regulatory network and the size of population was assumed as 10 000 and the proposed scheme was terminated after 5×10^5 iterations. Compared with it our size of population and

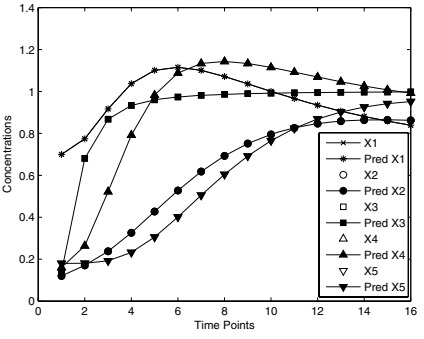

Fig. 4. Time series of the acquired model

Table 3. Obtained Parameters of the ODEs by our proposed method and S-tree(GP), α_i', β_i': parameters by our proposed method, α_i'', β_i'': parameters by S-tree(GP), α_i, β_i: true parameters

i	$\alpha_i'/\alpha_i''/\alpha_i$	$\beta_i'/\beta_i''/\beta_i$
1	8.5854/4.9999/5.0	13.7959/9.9999/10.0
2	9.7709/10.0000/10.0	10.0117/10.0000/10.0
3	13.7629/10.0000/10.0	13.9742/10.0000/10.0
4	8.3954/8.0000/5.0	13.7959/10.0000/10.0
5	9.4643/9.9999/5.0	13.7959/10.0000/10.0

number of iteration are far smaller (Table 1). And The execution time for each experiment was $\sim$ 400s. We obtain the true structure during the every experiment. Table 3 shows the best parameters obtained among all the experiments. Obviously the parameters are very closed to the targeted model in our method.

3.2 Experiment 2: The Large-Scale Artificial Gene Regulatory Network with Noisy Environment

This test system which is the same with Experiment 1 is a reduced version of test system ss30 genes that was introduced by [15]. Fig.5 shows the example of gene regulatory network. The system represents a genetic network with 15 variables. Table 4 shows the parameters of S-system formalism.

As we have to estimate a relatively large number of parameters and structure of the system of ODEs with an a small data set, there can be a lot of different possible network structures all of which bring about only small differences in estimating the given data set. These false candidates can be decreased by reducing the structural search space based on the available constraint. The constant is that all the diagonal elements in the matrix h are not zero (h_{ii} for $i = 1, ..., n$) [7]. Namely the i-th equation must contain X_i. This is because as the concentration X_i is higher, X_i can participate in the reaction more actively (i.e. it disappears fast) [7].

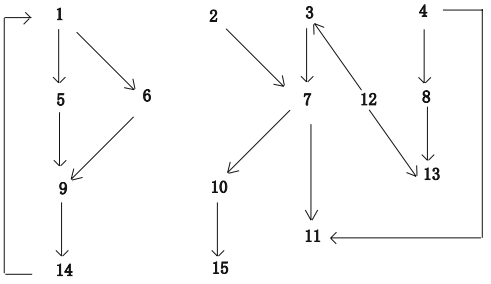

Fig. 5. The large-scale Artificial Gene Regulatory Network

Table 4. S-system parameters of the large-scale target model of the large Artificial Gene Regulatory Network

α_i	1.0
β_i	1.0
$g_{i,j}$	$g_{1,14} = -0.1, g_{3,12} = -0.2, g_{5,1} = 1.0, g_{6,1} = 1.0, g_{7,2} = 0.5, g_{7,3} = 0.4, g_{8,4} = 0.2,$ $g_{9,5} = 1.0, g_{9,6} = -0.1, g_{10,7} = 0.3, g_{11,4} = 0.4, g_{11,7} = -0.2, g_{12,13} = 0.5, g_{13,8} = 0.6, g_{14,9} = 1.0,$ $g_{14,15} = -0.2, g_{15,10} = 0.2, otherg_{i,j} = 0.0, h_{i,j}1.0, ifi = j, 0.0otherwise$

The set of time-series data began from randomly generated initial values and was obtained by solving the set of differential equations on the targeted model. In the previous studies, for the large-scale Artificial Gene Regulatory Network, the form of the differential equation was being fixed, and the only one goal was to optimize parameters and coefficients [16]. In this paper we apply the Multi Expression Programming to evolve the righthand side of the equation. Experimental parameter for this task are shown in Table 1. Ten runs were carried out. The search region of the parameters was [-1.0, 1.0]. And The execution time for each experiment was $\sim$ 1.8 h. During the experiments, we could obtain the best structure and parameters which were the same with the targeted model(Fig.5 and Table 4) except the 11-th gene. We only obtained the 11-th differential equation: $\dot{X_{11}} = X_7^{-0.199999} X_{11}^{0.018851} - X_{11}$. So the only interaction $X_4 \rightarrow X_{11}$ could not be identified.

To test the performance of our method in a real-world setting, we added 1, 2, 5, 10 and 15% Gaussian noise to the time-series data in order to simulate the measurement noise that often corrupts the observed data obtained from actual measurements of gene expression patterns. Except that the size of population is fixed at 10000, other settings are same as in the previous experiment. In the same execution time for each run, we can obtain the same structure by the time-series data which is added 1, 2, 5 and 10% Gaussian noise as the data without noise. When the noise ratio is similar up to the 15%, the $X_3 \rightarrow X_7$ and $X_4 \rightarrow X_{11}$ are not identified. Hence, we can conclude that the proposed algorithm is robust within 10% random noise. And we further confirm that our method will perform well in the real-world network.

4 Conclusion

In this paper, a new approach for evolving ODEs is proposed from the observed time series by using MEP along with the PSO algorithm. By applying the proposed method to the identification of the artificial genetic networks based on generated time-course data, we have succeeded in creating the systems of ODEs which are very close to the targeted systems. Simulation results shown that the method performs well for generating the correct genetic networks even adding Gaussian noise to the time-series data. The key problem for inferring a genetic network is how to reduce computational complexity for a real genetic network. This problem can be easily solved by the proposed method, and then enhancing the applicability of the proposed algorithm for large-scale genetic regulator networks. The method has following two advantages: (1) a MEP chromosome encodes several expressions, so we can acquire the best structure of the ODE only by a small population; (2) with partitioning, we can acquire the best system very fast, and each node of the genetic regulator network can be inferred separately and the research space is reduced significantly. Thus the proposed method is suitable for inferring the large-scale genetic regulator networks.

Finally, like for any system identification method, the possibility to generate several time-series data sets displaying a variety of dynamical behaviors of the system, will be critical for the application of the method to larger systems. In the future, we will apply our approach to solve some of the real biochemical network problems, especially to the real large-scale biochemical networks.

Acknowledgment

This research was supported by the NSFC (60573065), the the Natural Science Foundation of Shandong Province (Y2007G33), and the Key Subject Research Foundation of Shandong Province.

References

1. Qian, L.: Inference of Noisy Nonlinear Differential Equation Models for Gene Regulatory Networks using Genetic Programming and Kalman Filtering. IEEE Transactions on Signal Processing 56(7), 3327–3339 (2008)
2. Akutsu, T., Miyano, S., Kuhara, S.: Identification of Genetic Networks from a Small Number of Gene Expression Patterns under the Boolean Network Model. In: Proc. of Pacific Symposium on Biocomputing, pp. 17–28 (1999)
3. Murphy, K., Mian, S.: Modeling Gene Expression Data using Dynamic Bayesian Network. Computer Science Division, University of California Berkeley (1999)
4. Chen, T., He, H.L., Church, G.M.: Modeling Gene Expression with Differential Equations. In: Proc. of Pacific Symposium on Biocomputing, pp. 29–40 (1999)
5. Tominaga, D., Koga, N., Okamoto, M.: Efficient Numerical Optimization Algorithm Based on Genetic Algorithm for Inverse Problem. In: Proc. of Genetic and Evolutionary Computation Conference, pp. 251–258 (2000)

6. Sakamoto., E., Iba, H.: Inferring a System of Differential Equations for a Gene Regulatory Network by using Genetic Programming. In: Proc. Congress on Evolutionary Computation, pp. 720–726 (2001)
7. Cho, D.Y., Cho, K.H., Zhang, B.T.: Identification of Biochemical Networks by S-tree Based Genetic Programming. Bioinformatics 22, 1631–1640 (2006)
8. Bongard, J., Lipson, H.: Automated Reverse Engineering of Nonlinear Dynamical Systems. Proceedings of the National Academy of Science 104, 9943–9948 (2007)
9. Groşan, C., Abraham, A., Han, S.-Y.: MEPIDS: Multi-expression programming for intrusion detection system. In: Mira, J., Álvarez, J.R. (eds.) IWINAC 2005. LNCS, vol. 3562, pp. 163–172. Springer, Heidelberg (2005)
10. Andrew, H.W., et al.: System Identification using Genetic Programming. In: Proc. of 2nd Int. Conference on Adaptive Computing in Engineering Design and Control (1996)
11. Oltean, M., Grosan, C.: Evolving Digital Circuits using Multi Expression Programming. In: Zebulum, R., et al. (eds.) NASA/DoD Conference on Evolvable Hardware, Washington, pp. 24–26 (2004)
12. Chen, Y.H., Yang, B., Abraham, A.: Ajith Abraham. Flexible Neural Trees Ensemble for Stock Index Modeling. Neurocomputing. 70, 697–703 (2007)
13. Gennemark, P., Wedelin, D.: Efficient Algorithms for Ordinary Differential Equation Model Identification of Biological Systems. IET Syst Biol 1, 120–129 (2007)
14. Savageau, M.A.: Biochemical Systems Analysis: a Study of Function and Design in Molecular Biology. Addison-Wesley Pub. Co., Advanced Book Program, Reading (1976)
15. Maki, Y., Tominaga, D., Okamoto, M., Watanabe, S., Eguchi, Y.: Development of a System for the Inference of Large Scale Genetic Networks. In: Pac. Symp. Biocomput.., pp. 446–458 (2001)
16. Kimura, S., Ide, K., Kashihara, A.: Inference of S-system Models of Genetic Networks using a Cooperative Coevolutionary Algorithm. Bioinformatics 21, 1154–1163 (2005)
17. Kikuchi, S., et al.: Dynamic Modeling of Genetic Networks using Genetic Algorithm and S-system. Bioinformatics 19, 643–650 (2003)
18. Bornholdt, S.: Boolean Network Models of Cellular Regulation: Prospects and Limitations. J. R. Soc. Interf. 5, 85–94 (2008)
19. Hecker, M., Lambeck, S., Toepfer, S., van Someren, E., Guthke, R.: Gene Regulatory Network Inference: Data Integration in Dynamic Models A Review. Biosystems 96, 86–103 (2009)

Function Sequence Genetic Programming

Shixian Wang, Yuehui Chen, and Peng Wu

Computational Intelligence Lab.
School of Information Science and Engineering
University of Jinan
Jiwei road 106, Jinan 250022, Shandong, P.R. China
{ise_wangsx,yhchen,ise_wup}@ujn.edu.cn

Abstract. Genetic Programming(GP) can obtain a program structure to solve complex problem. This paper presents a new form of Genetic Programming, Function Sequence Genetic Programming (FSGP). We adopt function set like Genetic Programming, and define data set corresponding to its terminal set. Besides of input data and constants, data set include medium variables which are used not only as arguments of functions, but also as temporary variables to store function return value. The program individual is given as a function sequence instead of tree and graph. All functions run orderly. The result of executed program is the return value of the last function in the function sequences. This presentation is closer to real handwriting program. Moreover it has an advantage that the genetic operations are easy implemented since the function sequence is linear. We apply FSGP to factorial problem and stock index prediction. The initial simulation results indicate that the FSGP is more powerful than the conventional genetic programming both in implementation time and solution accuracy.

Keywords: Genetic Programming, Function Sequence Genetic Programming, factorial problem, stock index prediction.

1 Introduction

Genetic Programming (GP) [4] [7] can evolve a program structure to solve complex problems. It uses parse tree to present program. The tree depicts an expression. The internal nodes of the tree are functions, and the external leaves of the tree are terminals that can be input data or constants, as arguments of functions. Evolving program tree was popularized by the work of Koza [4] [7].

To mimic true program structure, many variants of Genetic programming have been presented so far. Each of them has different presentation of program structure. Linear Genetic Programming (LGP) [9] uses directly binary machine code string to present program. This presentation is a real program which can be directly executed during fitness calculation. But it has a poor portability because machine code depends on specific machine. Markus introduced an interpreting variant of linear genetic programming [1]. In his LGP approach, an individual program is represented as a variable length string composed of simple C instructions. Each C instruction is encoded in 4 bytes holding the operation identifier,

D.-S. Huang et al. (Eds.): ICIC 2009, LNAI 5755, pp. 984–992, 2009.

indexes of the participating variables and constant value. Adopting this presentation, programs of an imperative language(like C) were evolved, instead of the tree-based GP expression of a functional programming language (like LISP). Line-Tree Genetic Programming [2] is a combination of Markus's approach [1] with Genetic Programming based on tree [4] [7]. In this approach, the program tree has two kinds of nodes, the node of linear C instruction string and branch node. According to conditions, branch node selects a linear string node to execute. Whole program runs from the root of tree to the leaf. Line-Graph Genetic Programming [3] is a natural expansion since several branch nodes may select the same following nodes.

Graph is more general than tree. In order to evolve more complex program to deal with difficult or specific problems, other program evolutions based on graph was also presented. Parallel Algorithm Discovery and Orchestration(PADO) [8] is one of the graph based GP. PADO with action and branch-decision nodes uses stack memory and index memory. The execution of PADO is carried out from the start node to the end node in the network. Poli proposed an approach by using graph with functions and terminals nodes located over a grid in literature [10]. In Graph structured Programming Evolution(GRAPE) [11], program is depicted as an arbitrary directed graph of nodes and data set. The genotype of GRAPE adopts the form of a linear string of integers.

This paper proposes a novel method, Function Sequence Genetic Programming (FSGP), to evolve program. The details of FSGP are described in section 2. In section 3, we apply this approach to two problems, factorial problem and stock index prediction. In section 4, conclusions are finally drawn.

2 FSGP

2.1 Representation

FSGP was inspired by the real procedure of programming. We make an assumption that operators of program language had been implemented by functions. When we write a program, we may define some variables and may use several constants. One part of variables denoted as data variable are used to store input data and the other part of variables denoted as medium variable here, often changed, are used to store the value of functions temporarily. All defined variables and constants can serve as arguments of the implemented functions. Of course, there often exist some variables not to be used or whose usage might have no effect on the result of whole program. After defining variables and constants, we continue to give a specific sequence of functions aiming to specific problem, and the argument variables of the functions in the sequence are explicitly told, so as to the medium variables which store the function return value. All functions run orderly according to their position in the sequence.

The individual program in our approach is given as a fixed length function sequence instead of tree and graph, and data set D differentiated from the other evolving paradigm are adopted. Each function in sequence comes from function set $F = \{f_1, f_2, f_3, \ldots, f_m\}$, which has the same definition as those in Genetic

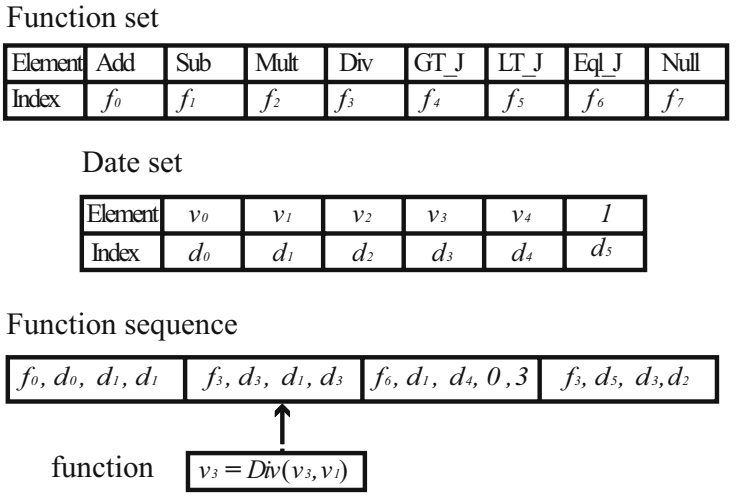

Fig. 1. An individual programm in FSGP for factorial problem(see section 3.1). The function sequence holds the message of 4 functions. All functions in the sequence are executed orderly after inputting an integer to data variable(v_4) and initializing media variables(v_0, v_1, v_2, v_3) with 1. The second position in the sequence represents the function $Eql\_J(v_1, v_4, 0, 3)$. If v_1 is equal with v_4, the function will return 0, otherwise 3, the individual program will jump there and continue to run. The output of the last function stored to v_2 is the result of this individual.

Programming [4]. The data set D, as the counterpart of terminal set T in Genetic Programming, is extended in this presentation. It includes data variables storing input data, constant(s), and medium variables. All members in data set D can serve as the arguments of functions. Beyond the usage of arguments all medium variables can store the function return value. The sequence of function holds the necessary message for the execution of function. Generally indexes of function, arguments, and media variable(s) are included. For some functions there are special message, such as GT_J, LT_J and Eql_J (as defined in section 3.1) with 4 arguments need a function index, two argument indexes, and two addition integers directing the positions in function sequence. Figure 1 illustrates a FSGP model. The sequence of functions is generated randomly. Then it is optimized by evolutionary algorithm. The number of the functions is the length of individual program. All functions in the sequence run orderly. The final result of an executed program is the return value of the last function.

The function sequence in FSGP is linear like Markus's approach [1]. But the differences are also obvious: (1) Beside of implementing the instruction of program language, domain-specific functions in FSGP can take more than 2 arguments usually; (2) Modules or motifs can also be initialized as function sequences in FSGP.

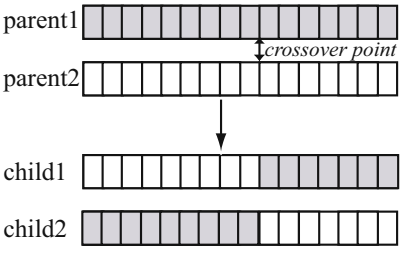

Fig. 2. Crossover operator of FSGP

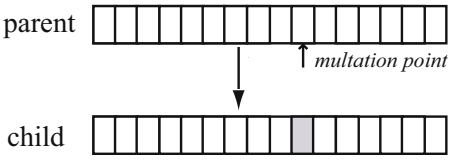

Fig. 3. Mutation operator of FSGP

2.2 Evolutionary Process

In genetic programming, evolutionary algorithms are used to search the optimal program structure according to an objective function. Various evolutionary algorithms have been developed so far, such as Genetic Algorithms (GA), Evolution Strategies (ES), Evolutionary Programming (EP), and their variants. For finding an optimal function sequence in FSGP, the operators used in Genetic Algorithms are employed due to its simpleness and effectiveness. The key steps of evolutionary process are described as following.

Crossover. Crossover used here was one-cut point method. We selected randomly two parental program individuals and a position in their functions sequence according to crossover probability P_c. The right parts of two parent functions sequence were exchanged. The information of exchanged functions was kept in this course. Figure 2 illustrates the recombination operation.

Mutation. A position in the sequence was randomly selected according to mutation probability P_m. Then new function message was generated randomly and placed into the selected position. Figure 3 illustrates the procedure of mutation.

Reproduction. The reproduction simply chooses an individual in the current population and copies it without changing into the new population. In this phase, we adopted roulette selection along with the elitist strategy. Using the strategy, an best individual in the current population was chosen and copied into the new population.

It is clear that evolutionary process is simpler than other GP based on tree and graph structure.

3 Experimental Results

In order to verify the efficiency of the FSGP, we applied this approach to two problems, factorial problem and stock index prediction. With the first one we aimed to testify the capacity of FSGP constructing complex program, and with the second to the capacity of constructing prediction model. The parameters of FSGP for both experiments are given in Table 1.

Table 1. The parameters of FSGP algorithm

Parameter	value
Generations for Factorial	200000
Generations for Stock index prediction	2000
Population size	100
Crossover rate P_c	0.9
Mutation rate P_m	0.5

3.1 Factorial Problem

The objective is to evolve a program into one which can calculate the factorial of input integer. We used the same data as those in the GRAPE [11]. Training data are input/output pairs $(a, b) : (0, 1), (1, 1), (2, 2), (3, 6), (4, 24), (5, 120)$. The integers from 6 to 12 were used as the test set.

We defined function set F={Add,Sub,$Mult$,Div, GT_J,LT_J, Eql_J, $Null$}. The former 4 functions implement the operator +, -, *, and /, respectively. Function $GT\_J, LT\_J, andEql\_J$ have four arguments, x_0, x_1, x_2, x_3, implementing relation operator $>$, $<$ and $==$, respectively. The operator operates on x_0 and x_1, and x_2, x_3 are two positions in the function sequence. If comparison result is true, the function will return x_2, otherwise x_3. The individual program will jump to the position and continue to run when they returns. The $Null$ function used to reduce the size of program does nothing. We constructed a function sequence containing 15 functions and data set $D = \{v_0, v_1, v_2, v_3, v_4, 1\}$. The former 4 variables are used as medium variables, and v_4 as data variable. We used "number of hit" as fitness value. The fitness function used in this experiment is

$$fitness = \frac{r}{n} \tag{1}$$

Where r is the number of training data computed correctly, n is the total number of training data. In order not to trap into infinite execution, program will exit and its fitness value will be set to 0 if a program passes 200 functions. The higher the fitness value indicates the better performance. We think the program individual whose fitness equals 1 is competent, then it is verified by test data.

We obtained fifteen appropriate program structures with twenty independent runs. This result shows that FSGP is more efficient than GRAPE [11] for factorial problem, which had the best success rate of 59% for test set with 2500000 evaluations. One of the structures evolved by FSGP is similar to the following pseudo code.

1. double v_0, v_1, v_2, v_3, v_4;
2. const double $v_5 = 1$;
3. initialize v_0, v_1, v_2, v_3 with 1;
4. input an integer to v_4;
5. v_1 = Add(v_0, v_1);
6. v_3 = Div(v_3, v_1);
7. if(!(v_1 == v_4))
   go to 5;
8. v_2 = Div(v_5,v_3);
9. v_2 is the result of the program.

This program implements a novel idea for factorial problem. When computing the factorial of integer n, using division it lets $v_3 = \frac{1}{2*3...*n}$ through n iterations, then makes $v_2 = \frac{1}{v_3}$ as the result of the program. It is right for the integer n.

3.2 Stock Index Prediction

The other problem is the stock market prediction. In this work, we analyzed the Nasdaq-100 index valued from 11 January 1995 to 11 January 2002 [12] and the NIFTY index from 01 January 1998 to 03 December 2001 [13]. For both the indices, we divided the entire data into almost two equal parts. No special rules were used to select the training set other than ensuring a reasonable representation of the parameter space of the problem domain [14]. Our target was to evolve a program that could predict the index value of the following trade day based on the opening, closing and maximum values of the same on a given day. The assessment of the prediction performance was quantifying the prediction obtained on an independent data set. The root mean squared error(RMSE) was used to study the performance of the evolved program for the test data. The RMSE is defined as follows:

$$RMSE = \sqrt{\frac{1}{n}\sum_{i=1}^{N}(y_i - y_i^{'})^2} \tag{2}$$

Where y_i is the actual index value on day i, $y_i^{'}$ is the forecast value of the index on that day, N is the number of train sample.

For Nasdaq-100 index variables from v_0 to v_{11} belonged to the data set $D = \{v_0, v_1, v_2, \ldots, v_{14}, 1\}$ were used as medium variables, variable v_{12}, v_{13} and v_{14} were employed as data variables. In addition, the length of individual program was set to 60. For NIFTY index, data set was $D = \{v_0, v_1, \ldots, v_{18}, 1\}$. The former 14 variables were used as medium variables, variables from v_{14} to v_{18} were

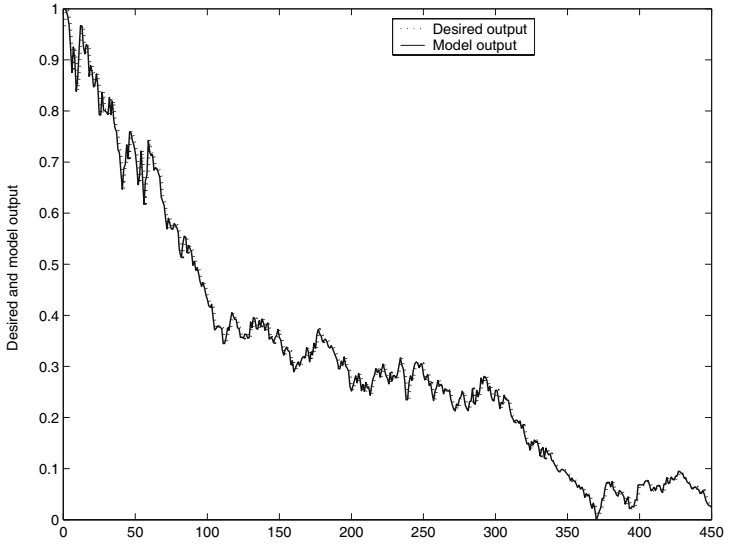

Fig. 4. The result of prediction for Nasdap-100 index

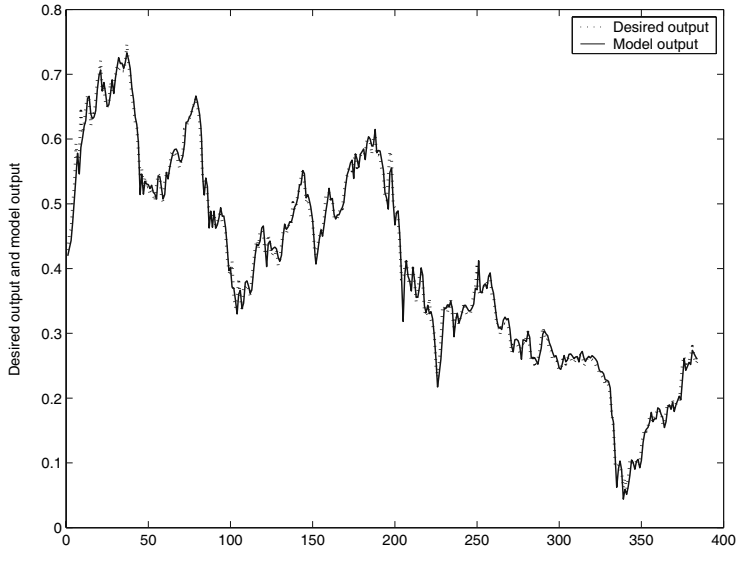

Fig. 5. The result of prediction for NIFTY index

corresponding to input data, and the length of program was set to 80. The test results of RMSE obtained using this approach and other different diagram [5] for the two stock indices are showed in Table 2.

Table 2. Experimental results for the two indices

	ANN[5]	NF[5]	MEP[5]	LGP[5]	SFGP
Nas-100	0.0284	0.0183	0.021	0.021	0.0160
NIFTY	0.0122	0.0127	0.0163	0.0124	0.0131

From Table 2, it is obvious that FSGP are better than other models for Nas-100 stock index, and for both indices, FSGP has better prediction than that in GEP. The result of prediction for Nasdaq-100 index is shown in Figure 4 and that for NIFTY is shown in Figure 5.

4 Conclusion

This paper propose a novel method for program evolution, Function Sequence Genetic Programming (FSGP). This approach adopts a fixed-length functions sequence to present the program individual. This presentation is closer to hand-writing program. We applied FSGP to factorial problem and stock index prediction. As the result we illustrate this approach was an applicable and effective model.

Acknowledgment

This research was supported by the NSFC (60573065), the the Natural Science Foundation of Shandong Province (Y2007G33), and the Key Subject Research Foundation of Shandong Province.

References

1. Brameier, M., Banzhaf, W.S.: A Comparison of Linear Genetic Programming and Neural Networks in Medical Data Mining. IEEE Transactions on Evolutionary Computation 5(1), 7–26 (2001)
2. Kantschik, W., Banzhaf, W.: Linear-tree GP and its comparison with other GP structures. In: Miller, J., Tomassini, M., Lanzi, P.L., Ryan, C., Tetamanzi, A.G.B., Langdon, W.B. (eds.) EuroGP 2001. LNCS, vol. 2038, pp. 302–312. Springer, Heidelberg (2001)
3. Kantschik, W., Banzhaf, W.: Linear-graph GP - A new GP structure. In: Foster, J.A., Lutton, E., Miller, J., Ryan, C., Tettamanzi, A.G.B. (eds.) EuroGP 2002. LNCS, vol. 2278, pp. 83–92. Springer, Heidelberg (2002)
4. Koza, J.R.: Genetic Programming: On the Programming of Computers by Means of Natural Selection. MIT Press, Cambridge (1992)
5. Grosan, C., Abraham: Stock Market Modeling Using Genetic Programming Ensembles. In: Genetic Systems Programming: Theory and Experiences, vol. 13, pp. 131–146. Springer, Heidelberg (2006)

6. Miller, J.F., Thomson, P.: Cartesian Genetic Programming. In: Proceedings of the European Conference on Genetic Programming, pp. 121–132. Springer, London (2000)
7. Koza, J.R.: Genetic Programming II: Automatic Discovery of Reusable Programs. MIT Press, Cambridge (1994)
8. Teller, A., Veloso, M.: Program Evolution for Data Mining. J. The International Journal of Expert Systems 8(1), 216–236 (1995)
9. Nordin, P.: A Compiling Genetic Programming System that Directly Manipulates the Machine-Code. In: Advances in Genetic Programming. MIT Press, Cambridge (1994)
10. Poli, R.: Evolution of Graph-like Programs with Parallel Distributed Genetic Programming. In: Genetic Algorithms: Proceedings of the Seventh International Conference, pp. 346–353. Morgan Kaufmann, MI USA (1997)
11. Shirakawa, S., Ogino, S., Nagao, T.: Graph Structured Program Evolution. In: Genetic And Evolutionary Computation Conference Proceedings of the 9th annual conference on Genetic and evolutionary computation, pp. 1686–1693. ACM, New York (2007)
12. Nasdaq Stock MarketSM, http://www.nasdaq.com
13. National Stock Exchange of India Limited, http://www.nseindia.com
14. Abraham, A., Philip, N.S., Saratchandran, P.: Modeling Chaotic Behavior of Stock Indices using Intelligent Paradigms. J. Neural, Parallel & Scientific Computations 11(1&2), 143–160 (2003)

Speech Emotion Recognition Research Based on Wavelet Neural Network for Robot Pet

Yongming Huang, Guobao Zhang, and Xiaoli Xu

School of Automation, Southeast University, Nanjing Jiangsu 210096, China
huang_ym@163.com

Abstract. In this paper, we present an emotion recognition system using wavelet neural network and BP neural network for special human affective state in the speech signal. 750 short emotional sentences with different contents from 5 speakers were collected as experiment materials. The features relevant with energy, speech rate, pitch and formant are extracted from speech signals. Neural network are used as the classifier for 5 emotions including anger, calmness, happiness, sadness and boredom. Compared with the traditional BP network, the results of experiments show that the wavelet neural network has faster convergence speed and higher recognition rate.

Keywords: Wavelet neural network; BP neural network; Emotional speech; Recognition of emotion.

1 Introduction

Emotion recognition by computer is a topic which has been researched in recent years, and becomes more and more important with the development of the artificial intelligence. An effective human emotion recognition system will help to make the interaction between human and computer more natural and friendly. It has many potential applications in areas such as education [1], entertainment, custom service etc.

Considering this and its potential uses, we design a context independence system in speech-based emotion recognition in this paper. For the robot pet becoming smarter and more humanoid, it's important for the machine to possess the emotional recognition ability. The ultimate goal of this research is to make a Personal Robot Pet which can recognize its host's emotion.

The remainder of this paper is organized as follows. Section 2 describes the design and implementation of our system. Section 3 presents the results of the two different neural networks. Conclusions and discussions are given in section 4.

2 System Design

2.1 Processing Flow

Fig.1 illustrates the processing flow of our system which is divided into two main parts: speech processing and emotion recognition. First, some pre-processing should

D.-S. Huang et al. (Eds.): ICIC 2009, LNAI 5755, pp. 993–1000, 2009.

be done to get the effective speech period by using the Cool Edit Pro 1.2a, including filtering and intercepting the speech period (determining the beginning and end points in Fig 4). Second, the features for each speech are extracted and compiled into a feature vector. Last, PCA (Principle Component Analysis) is used to reduce the dimensions of the feature vector, forming the final input vectors [2].

In the training stage, the input vector is used to train the neural network; in the recognition stage it is applied to the completely trained network and the output is a recognized emotion; also the system can study based on the output.

These steps are explained further in the following sections.

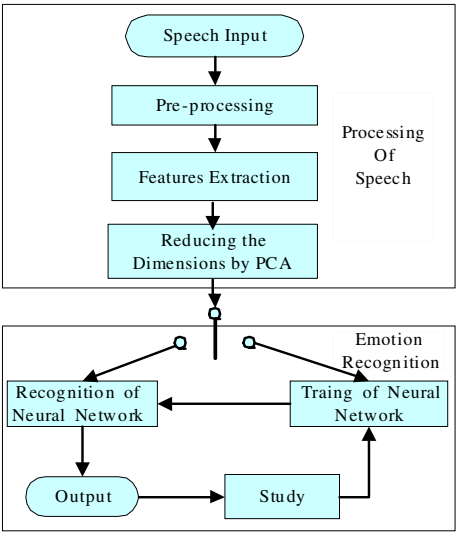

Fig. 1. Processing flow of Emotion Recognition System

2.2 Emotions and Features

Emotions. How to classify emotions is an interesting and difficult issue. A wide investigation on dimensions has been performed in the past, but researchers still haven't established a standard so far. Different researchers on emotion recognition differ on the number of categories and the kinds of categories [3, 4].

Our motivation to do this study is to make a Personal Robot Pet which can recognize its host's emotion, so it is enough to select common basic emotions in life: angry, calm, happy, sad and bore.

Features. Speech signal is short-term stable, so we choose short-term acoustic features in this emotion recognition system. Some features have been proved to be useful for emotion recognition in many papers [5].

Pre-processing should be done to the effective speech period by the Cool Edit Pro 1.2a, including filtering and intercepting the speech period (determining the beginning and end points in Fig 4).

speech power, pitch,12 LPC[1] parameters, Delta LPC parameters [6].

energy, median of F1[2],variance of duration of energy plateaus, minimum of F1, median of F0[3], mean F0, maximum/mean duration of energy plateaus, variance of F0 [7].

signal energy, sub-band energy, spectral flux, zero- crossing rate, fundamental frequency, MFCC, FFBE [8].

pitch average, pitch variance, intensity average, intensity variance, jitter pitch tremor, shimmer intensity tremor, speech rate [9].

After examining these examples, we select the following features in this study:

speech rate, max-Energy, mean-Energy, number of pole, max-Pitch, mean-Pitch (fundamental frequency), max-formant.

2.3 Neural Network Architecture

The network is composed of five sub-neural networks in this paper, with one network for each of the five emotions that are examined. As to each sentence, the recognition processing flow is diagrammed in Fig2. The features vector is input to each of the five sub-networks, then each sub-network will give an output ($v_1, v_2, \cdots v_5$) that represents the likelihood to the sub-network's emotion. At last, the Logic Decision selects the "best" emotion based on these outputs.

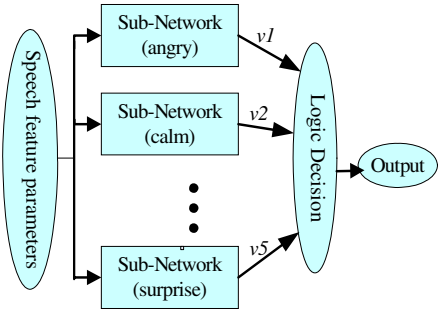

Fig. 2. The steps of recognition

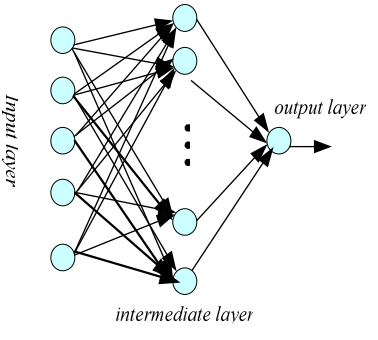

Fig. 3. Sub-network configuration

Wavelet Neural Network is a feed forward neural network whose activation functions are wavelets [10]. WNN is not essentially different from BP neural network in the structure or the form. As to the connection of the wavelets and the neural network, we adopt the compact metric structure. To draw close to the engineering application, a three-layer feed forward neural network which has only one intermediate layer is selected. We take the Wavelet network as the sub-network. Fig.3 illustrates the configuration of each of the five sub-networks. Each network contains three layers. One input layer with six nodes, one intermediate layer with twelve nodes and

[1] LPC means the linear predication coefficients.
[2] F1 means the first formant frequency.
[3] F0 means the fundamental frequency.

one output layer with one node, which is an analogical value 0.99 or 0.01 for training utterance. If the emotion of input utterance is the same as the sub-network, the value is 0.99, else 0.01.

Adopting separate sub-network for the five emotions allows each network to be adjusted separately, and we are able to easily change each network separately without redesigning the entire system which is good for network's study and can be updated in the feature.

To demonstrate the advantage of wavelet neural network on the speech emotion recognition, we also take the BP network as the sub-network. Section 3 will presents the results of the two different neural networks.

2.4 Learning Algorithm and Wavelet Function

In this paper, the WNN's structure is three-layer feed forward, Supposed that the input layer has *L* neuron, the layer has *M* neuron, the output layer has *S* neuron, *Vij* is the connection weight between the input layer cell *i* and the hidden layer cell *j*, *wjk* is the connection weight between the hidden layer cell *j* and the output layer cell *k*, the total number of samples is N, the input of the nth sample is $x_i^n(i=1,2,\cdots,L;n=1,2\cdots,N)$, the output of the network is $o_k^n(k=1,2,\cdots,S;n=1,2\cdots,N)$, the corresponding goal output is D_k^n. The excitation of the input layer is linear transform (output = input), the excitation of the hidden layer is wavelet function, and the excitation of the output layer is Sigmoid function.

Depending on the above network parameters, the output of the network is as following:

$$o_k^n = f\left(\sum_{j=1}^{M} \psi\left(\frac{\sum_{i=1}^{L} v_{ij} x_i^n - b_j}{a_i}\right) w_{jk}\right) \tag{1}$$

Where: $k = 1, 2, \ldots, S$; $n = 1, 2, \ldots, N$.

Using the learning algorithm of increasing the momentum gradient descent, there have:

$$\Delta w_{jk}(t) = -\eta \frac{\partial E}{\partial w_{jk}} + \alpha \Delta w_{jk}(t-1) \tag{2}$$

$$\Delta v_{ij}(t) = -\eta \frac{\partial E}{\partial v_{ij}} + \alpha \Delta v_{ij}(t-1) \tag{3}$$

$$\Delta a_j(t) = -\eta \frac{\partial E}{\partial a_j} + \alpha \Delta a_j(t-1) \tag{4}$$

$$\Delta b_j(t) = -\eta \frac{\partial E}{\partial b_j} + \alpha \Delta b_j(t-1) \tag{5}$$

Where α is the momentum parameter, $\alpha \in (0,1)$ as usual. The momentum item reflects the empirical value accumulated before, and it plays damping action on the adjustment at the moment *t*.

So far there has no unified theory for selecting the wavelet functions. The Morl-et wavelet $\cos(1.75x)e^{-0.5x^2}$, which is limit supportive, symmetric, cosine modulat-ed Gaussian Wave, has been widely employed in various fields. Based on this, the M-orlet wavelet is selected to be the excitation of the hidden layer in this study.

3 Experiments and Results

3.1 Database

A record of emotional speech data collections is undoubtedly useful for researchers interested in emotional speech analysis. In this study, emotional speech recordings were made in a recording studio, using a professional-quality microphone and digital audio record software-Cool Edit Pro1.2a (*Fig 4*), at a sampling rate of 11025, using a single channel 16-bit digitization.

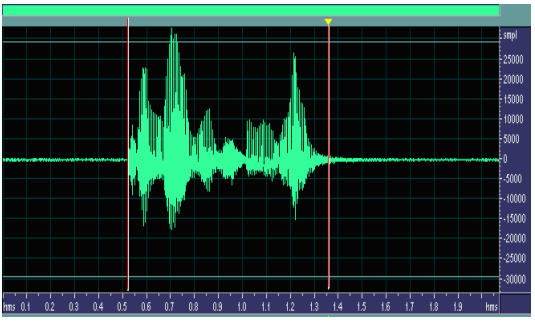

Fig. 4. Cool Edit Pro1.2a

We invited five classmates-three male, two female, who are good at acting, to be served as subjects. Each subject uttered a list of 30 Chinese sentences for five times, one time for each of the five emotions. When finished, the speech database must be e-amined by a listening test. If disqualified, the sentence will be deleted and recorded again.

At last, some pre-processing should be done to get the effective speech period in the Cool Edit Pro, including filtering and determining the beginning and end points in Fig 4.

3.3 Results

3.3.1 Training Speed

The data in Table 1 stand for the training epochs, which are acquired by the speech features of the same person, training the wavelet neural network and the

Table 1. Training speed of WNN and BPNN

Samples / Network/step	training separately			training by increasing samples on the previous training net		
	50	100	150	50	100	150
BPNN	82	165	263	82	166	39
WNN	1200	1600	1650	1200	400	150

BP neural network separately until the networks are both convergent and the error accuracies are the same.

In the table, training separately means that the first 50 samples need train a network and the second 100 samples need train another network as before; while training by increasing samples on the previous training net means that the first 50 samples need train a network, but the second 100 samples needn't, for adding the later 50 samples to train the known network. From the table, under the same training conditions, when trained at the first time, the training speed of BPNN is faster than the WNN's. However, the WNN only converges slowly at first. Once converged and "remembered" the nonlinear functions, its training speed will enhances obviously; as a result, the convergent speed of WNN is faster than the BPNN's when increasing the train samples. So the WNN has more engineering significance.

3.3.2 Generalization Ability

The central problem of that neural network can be employed in the robot pet effectively is its generalization ability, that is to say, the trained network have the ability of precise reaction to the test samples or the work samples.

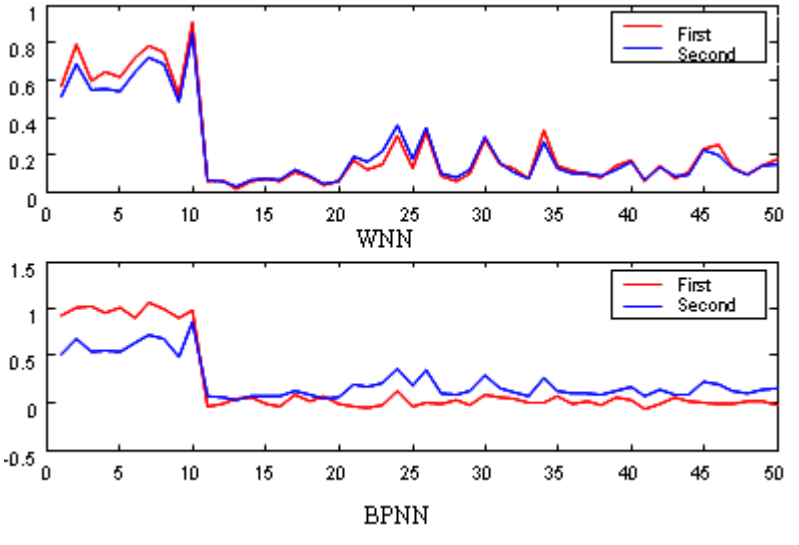

Fig. 5. Generalization Ability between WNN and BPNN

The results of the experiments(Fig. 5)show that BPNN has well stability, in which the outputs of each sample in different experiment are similar, but simulation results after entry are lager derivate of that before entry. As for WNN, though there is some volatility, it is only volatile around a small area of original value under statistics. As a result, WNN has more generalization ability.

3.3.3 Recognition Comparison

For all the cases, the mean recognition rates of the five emotions from five speakers (F1, F2, M1, M2, M3), who are three male and two female, are acquired from the WNN and BPNN.

Table 2. Mean Recognition Rate between WNN and BPNN

Speaker	F1	F2	M1	M2	M3
WNN	94%	84%	86%	90%	86%
BPNN	84%	78%	82%	78%	82%

From the table, under the same training conditions, the recognition rate of WNN is higher than that of BPNN. The results prove that WNN is effective to employ to the speech emotion recognition system oriented the Personal Robot Pet.

4 Conclusions and Discussions

Aim at the personal intelligent robot pet, we studied the speech emotion recognition and artificial neural network deeply, and researched the results of speech emotion recognition rate classified by wavelet neural network. Compared to BPNN, the effective neural network established by the wavelet algorithm has faster convergent speed, more generalization ability and better recognition rates. From the results, the wavelet neural network has more engineering signification. In order to improve the learning ability of the intelligent robot pet, the feedback idea of the control engineering was taken into the learning algorithm to make the emotional communication more easily, so the pet can be more understanding.

There is still more work to be done in the field of emotion recognition in speech. The speech features used in this study need to be reduced because of the large number of them. And if we want to design a speaker independent system, we should increase other features, such as the first formant, the variance of the first formants. But in the aspect of the engineering, extracting more features from the recordings of the host by the robot pet means more computing time, and the real-time character will be drastically reduced, as a result, the robot pet will not be propitious for marketing promotion. In addition, feature trials with different topologies of neural networks may also help improve performances. The combination of audio and visual data will convey more information about the human emotional state than speech alone. Therefore, the robot pet who can both hear and see can obtain more recognition rate when communicating with its host, and the communication can be more smoothly.

References

1. Fragopanagos, N., Taylor, G.: Emotion Recognition in Human-Computer Interaction. Neural Networks 18, 389–405 (2005)
2. Cheriyadat, A.: Limitations of principal component analysis for dimensionality-reduction for classification of hyperspectral data, pp. 31–56. Mississippi State University, America (2003)
3. Bhatti, M.W., Wang, Y., Guan, L.: A Neural Network Approach for Human Emotion Recognition in Speech. In: ISCAS 2004, pp. 181–184 (2004)
4. Murry, I.R., Arnott, J.L.: Applying an analysis of acted vocal emotions to improve the simulation of synthetic speech. Computer Speech and Lauguage 22, 107–129 (2008)
5. Ververidis, D., Kotrropoulos, K.: Emotional speech recognition: Resource, features, and methods. Speech Communication 48, 1162–1181 (2006)
6. Nicholson, J., Takahashi, K., Nakatsu, R.: Emotion Recognition in Speech Using Neural Networks. Neural Computing & Applications 9, 290–296 (2000)
7. Zhongzhe, X., Dellandrea, E., Weibei Deal, E.: Features Extraction and Selection for Emotional Speech Classification. IEEE, 411–416 (2005)
8. Temko, A., Nadeu, C.: Classification of acoustic events using SVM-based clustering schemes. Patttern Recognition 39, 682–694 (2006)
9. Amir, N.: Classifying emotions in speech: a comparison of methods. In: EUROSPEECH 2001 Sandinavia 7th European Conference on Speech Communication and Technology 2th INTERSPEECH Even, pp. 127–130 (2001)
10. Bhatti, M.W., Wang, Y., Guan, L.: A Neural Network Approach for Human Emotion Recognition in Speech. In: ISCAS 2004, pp. 181–184 (2004)

Device Integration Approach to OPC UA-Based Process Automation Systems with FDT/DTM and EDDL

Vu Van Tan, Dae-Seung Yoo, and Myeong-Jae Yi*

School of Computer Engineering and Information Technology
University of Ulsan, San-29, Moogu-2 dong, Namgu, Ulsan 680-749, Korea
{vvtan,ooseyds,ymj}@mail.ulsan.ac.kr,
ymj@mail.ulsan.ac.kr

Abstract. Manufacturers and distributors alike are seeking better ways to more efficiently manage the assets of their operators. Advances in communication technologies and standards are now making them easier and more cost justifiable to deliver information from measurement instrumentation as well as manage these instrumentation assets more efficiently. Today's technologies such as Electronic Device Description Language (EDDL) and Field Device Tool (FDT) are available for device integration. This paper introduces a flexible device integration approach to achieving the advantages of both such technologies for the device management to new OPC Unified Architecture (UA)-based process automation systems. This approach is suitable not only for the process automation industry, but also for the factory automation industry. Visibility of and access to field device information through the OPC standards, FDT, and EDDL contribute to efforts to improve the life cycle management of process plants and associated distribution operations.

Keywords: Automation system, Device integration, EDDL, FDT/DTM, OPC, Process automation, Unified architecture.

1 Introduction

Many field devices from different vendors are now being connected to process automation systems through fieldbus communication. These field devices have intelligence, and so many settings and adjustments can be made through fieldbus communication [9,11,13,14]. Process automation systems, i.e., Distributed Control Systems (DCSs) or Programmable Logic Controllers (PLCs), are the traditional way to acquire information from measurement devices and effect control of motors and valves. Many plant environments have more than one control system platform installed. Even those with control systems from one vendor may have a variety of field device interface implementations to communicate with field devices. The challenge can only be faced with open standard and standardized device integration. In addition, another challenge is to employ a permanent

* Corresponding author.

D.-S. Huang et al. (Eds.): ICIC 2009, LNAI 5755, pp. 1001–1012, 2009.

cost effective information bridge from selected devices to the maintenance people without interfering with the existing control systems.

Two technologies available today for device integration such as Electronic Device Description Language (EDDL) [5] and Field Device Tool (FDT) [6] come from process automation society [7]. The EDDL technology defines own language that device manufacturers use to write textual descriptions, i.e., Electronic Device Description (EDD), for their devices. EDDs are processed by an EDD interpreter within a device independent engineering system. Unlike, the FDT technology uses programmed software components, i.e., Device Type Managers (DTMs), for device integration. These DTMs run inside the FDT frame application which manages and coordinates the DTMs.

More recently, the OPC Foundation has been proposed new specifications to design and develop automation control softwares running on independent platforms based on XML, Service Oriented Architecture (SOA), and web services, i.e., OPC Unified Architecture (UA) specifications [16]. The solution is to share information in more complex data structure formats with enterprise level Manufacturing Execution System (MES) and Enterprise Resource Planning (ERP) systems. The most important feature of the OPC UA standard is the possibility to define powerful information models. These models can define the organization of data in the address space of an OPC UA server in terms of structure and semantic [16]. However, this standard is making a challenge to propose a new device integration concept to researchers and hardware and software vendors [8].

The study presented in this paper aims at proposing a flexible device integration approach to OPC UA-based process automation systems. This approach is proposed based on the OPC UA client-server model with using FDT/DTM and EDDL technologies. It achieves the advantages of both technologies to field device integration in unified architecture for OPC UA-based systems.

This paper is organized as follows: The next section presents some background on the FDT/DTM, EDDL, and the OPC UA specifications and reviews several related approaches. The approach to device integration for OPC UA-based process automation systems complying with the client-server model is introduced in Section 3. The system analysis according to the proposed approach in enabling efficient collaboration between device-level SOA on the one hand and on the other hand services and applications is presented in Section 4. Finally, some conclusions are marked in Section 5.

2 Background and Related Work

2.1 FDT/DTM

Field devices have gained intelligence along with the spread of digital communication. As the number of field devices increases, the more complicated settings and adjustments need using the advanced functions in such devices have become challenges [10,11,3,1,9]. As a consequence, some field device vendors now provide dedicated softwares on PCs to completely supplement the functional limitations on dedicated terminal.

The FDT technology [6,15] uses programmed software components, called Device Type Manager (DTM), for field device integration. The DTMs runs on the FDT Frame Application that manages and coordinates the DTMs. Since a DTM complies with the interface specification, the device manufacturer is not restricted in the design of functionality, the implementation of the DTM components, and the programming languages. The DTM is composed of two types of DTM: (i) device DTM for field devices and (ii) communication DTM for field communication control. Furthermore, a gateway DTM is also available to connect HART devices via the HART[1] multiplexer or PROFIBUS and supports communication between devices.

Device DTMs can be classified into two types: (i) the first one is a dedicated device DTM to support a specific field device, and (ii) the other one is a universal device DTM in order to apply to many kinds of field devices.

2.2 Electronic Device Description Language

The open and standardized EDDL technology defines own language that the device manufacturers use to write textual descriptions, i.e., Electronic Device Description (EDD), for their devices [5]. EDDs are processed by an EDD interpreter within a device independent engineering system. The amount of language elements is limited and specific for device description. It allows for easy and efficient development of the EDD as common functionality for device integration.

An EDD is independent of operating systems and hardware platforms, and provides a uniform mechanism for device operations, the interpretation to yield high robustness. All software tools equipped with an interpreter to accept the EDDL grammar can extract the device data out of the EDDL file.

There are several differences in the working mode between FDT/DTM and EDDL [12], such as (i) passive storage of data in case of EDDL and active storage of data in case of FDT/DTM; (ii) EDDLs do not communicate with their devices, but DTMs do; (iii) applications relying on EDDL concept need an EDDL interpreter, FDTs do not need further plug-ins or software; (iv) applications relying on EDDL concept communicate with device through appropriate interfaces e.g., fieldbus, while a DTM is the interface to the device; (v) EDDL programming needs less effort to learn and handle than the development of DTMs does; (vi) the set of EDDL describable devices is a subset of DTM manageable devices.

2.3 OPC Unified Architecture

The OPC UA standard (a twelve-part specification has been released now) [16] is the next generation technology for secure, reliable, and inter-operable transport of raw data and preprocessed information from the plant floor (or shop floors) to production planning or the ERP system. It is based on XML, web services, and SOA to share information in more complex data structure formats with enterprise level MES and ERP systems in a way that they can understand. It

[1] http://www.hartcomm2.org/

embodies all functionalities of the existing OPC standards and expands on top of them. It enables all three types of data – current data, historical data, and alarms and events – to be accessed by a single OPC server because three different data with different semantics now have been required, for example, to capture the current value of a temperature sensor, an event resulting from a temperature threshold violation, and the historic mean temperature. The role of the OPC technology and the OPC UA standard can be illustrated in Fig. 1.

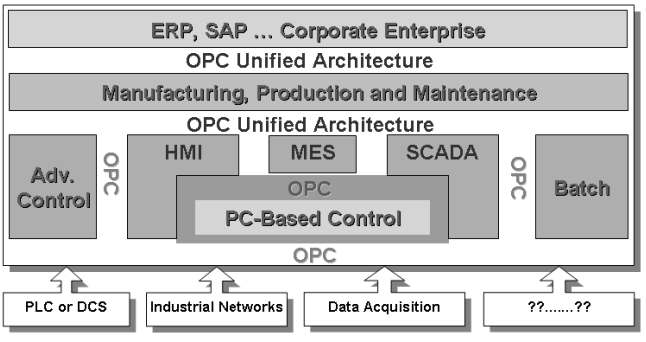

Fig. 1. The role of the OPC technology and the OPC UA standard in process and factory automation

The OPC UA standard defines a vendor and protocol independent sever-client model with utilization of standard web technologies. However, it is making new challenges to researchers such as (i) new device integration concept, (ii) new scenarios like Asset Management and Manufacturing Execution System (MES), and (iii) the design and implementation of this new standard for automation system applications.

2.4 Problem Statements

Today most of the human-machine interface (HMI), supervisory control and data acquisition (SCADA), and distributed control system (DCS) manufacturers offer interfaces that conform the OPC specifications. The OPC UA standard now is defined with the utilization of XML, web services, and SOA [16]. This makes a significant asset to business network applications. However, it seems that the OPC UA standard is geared for the future, but not for now [16,17]. This standard is making a challenge to develop field device integration concept to researchers and software and manufacturer vendors.

The field device configuration software packages offering a graphical interface and easy operation by adopting FDT/DTM are developed as an open framework for field device tools [13,18,12,14]. As a result, the FDT/DTM technology can be used not only to build an open system independent of a specific vendor, but also to implement various communication protocols and functions based on

advanced technologies. It is highly popular with factory automation vendors as well as process automation vendors. However, the device integration for OPC-based automation systems has not covered by these tools. Grossmann et al. [7] presented an approach to field device integration by integrating both the FDT and EDDL technologies into a unified architecture. The architecture of this approach consists of clients and server complying with the OPC UA client-server model. The server loads the device description containing Device Information Model (DIM) and Device Operation Model (DOM). The DIM is directly processed within the server to establish the information model while the DOMs are only handled in terms of server storage. The server information model allows OPC UA clients to access the device data and functions which are part of the DIM.

The key issues in establishing FDT as an open core technology are the technical cooperation between the OPC Foundation and the Field Device Tool-Joint Interest Group (FDT-JIG). They provide the end-users both within process and factory automation a totally seamless, truly open and easy enterprise wide communication. The reasons for the cooperation are (i) OPC is not suitable for cases where devices need to be addressed through several different protocols because of designing purely for communication, and (ii) the FDT technology adds a *nested communication* or *stacked communication* interface to the OPC technology for supporting communication to devices with several different protocols.

This research presents a unified and flexible approach to field device integration for OPC UA-based process automation systems with the utilization of both FDT/DTM and EDDL technologies. This approach has modified the device integration concept developed by Grossmann et al. [7]. It ensures the flexibility and powerful information models of OPC UA systems when deploying to industrial environments in terms of Internet of Things (IoT) [3], aiming at developing an ultimate solution for both process and factory automation today.

3 Device Integration Concept for OPC UA-Based Process Automation Systems

3.1 The OPC UA-Based Process Automation System Architecture

Internet-based manufacturing, leveraging the latest technologies to achieve distributed information systems, provides new possibilities not only for static, data centric integration of the plant floor into an overall enterprise architecture, but also for full process control integration of control and field devices by means of SOA, XML, and web services. The OPC UA standard was proposed to create a standardized data exchange model for automation systems. It defines a vendor and protocol independent of client-server architecture based on web technologies to ensure interoperability. Another potential feature is the ability to define powerful information models. These information models can define the organization of data within the UA server's address space in terms of structure and semantic. The OPC UA architecture is perfectly suited as the central interface

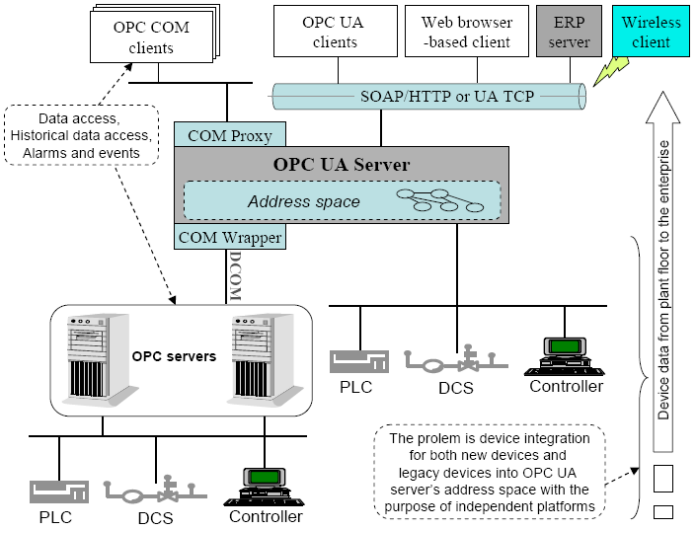

Fig. 2. The architecture of an OPC UA-based process automation system

for the vertical integration of automation systems. The challenge now is to make a flexible mechanism for device integration.

The architecture of an OPC UA-based process automation system is proposed as shown in Fig. 2. It indicates that all the functionalities of the existing OPC standards such as *data access*, *historical data access*, and *alarms and events*. In addition, the SOA is on the move and is foreseeable that this architectural paradigm will be dominant in the future. The integration of devices into the business IT-landscape through SOA is a promising approach to digitalize physical objects and to make them available to IT-systems [3]. This can be achieved by running instances of web services on these devices, creating an Internet of Services to collaborate and empower the future service-based factory. Considering these issues, the device integration concept developed by Grossmann et al. [7] has not completely solved the requirements of integration of devices for the architecture of OPC UA-based process automation systems as aforementioned.

3.2 Device Integration Approach

The address space of an OPC UA server is created by adding device type definitions. These definitions are generated using the device information provided by the FDT/DTM and EDDL. The device type definitions are composed of the parameters and their default values as well as the communication channels, the parameters, and default values. The end-users can create derivative definitions from the device types for defining the operation mode-specific device types. For example, the information from FDT/DTM can be used to create the device type information for a pressure transmitter. The relations between the OPC UA

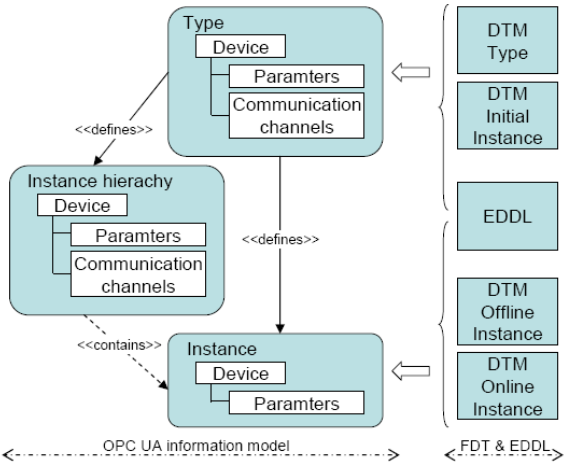

Fig. 3. The relations between OPC UA information model and both FDT/DTM and EDDL technologies

information model and both FDT/DTM and EDDL are shown in Fig. 3. The type definitions in the server's address space are then used to generate device instances. These instances can be created either directly from the default type definitions by the FDT/DTM information or from the derived definitions.

In order to realize the architecture of an OPC UA-based process automation system and to enable efficient collaboration between device-level SOA on the one hand and on the other hand services and applications, the approach developed by Grossmann et al. can be modified as shown in Fig. 4. The device-specific DIM is established as a *well-defined* information model on the server side. It concentrates on the representation of the device regarding structure and behavior. EDDL is developed to describe device specific properties and is perfectly suited for describing the DIM running by an interpreter.

The Server: The device specific DIM described in EDDL is the base for information model in the OPC UA server. The EDDL-interpreter of the server will process the EDD of a device and then establishes the appropriate information model to the server's address space.

As Fig. 4 shows, each device is represented by a `Device` object. The device object includes variables that hold the data items of the data model. This covers meta information such as unit, range, values, parameters, etc. When an OPC UA client accesses data from the server side, the server will read the corresponding device data from the plant floor. To offer the DIM access to the device data, the server will communicate with the devices over the fieldbus protocols such as FOUNDATION fieldbus, PROFIBUS, CANopen, DeviceNet, and HART through HART gateway. Having the services on devices will not be much of use if they cannot be dynamically discovered by the server. As a result automatic

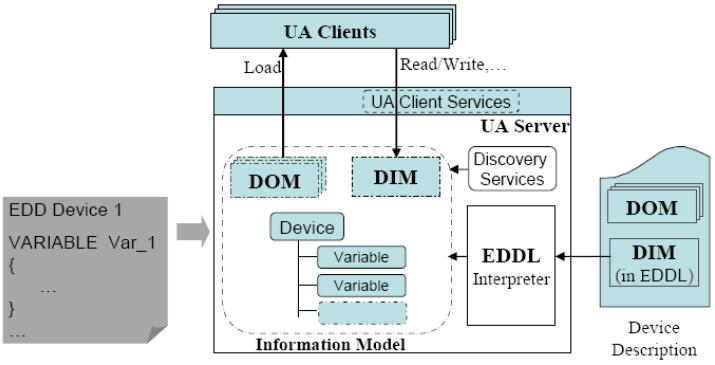

Fig. 4. The device integration approach based on both FDT/DTM and EDDL

service discovery will allow us to access them in a dynamic way without having explicit task knowledge and the need of a binding. The discovered services will be used by the clients in terms of web services enabled devices [3,19]. Therefore, the discovery services should be implemented to find devices.

The Client: In the standard case there are three different types of clients: (i) The universal Device Engineering Framework (DEF), (ii) application specific clients, and (iii) web browser-based clients. The application specific clients directly access device data via the DIM in the OPC UA server and process those in a specific mechanism. The universal DEF concentrates on the device operation via the device specific user interface. This offers a dynamic plug-in mechanism for DOMs, which are composed of the device specific user interface. The elements provided by EDDL are sufficient for simple graphical user interfaces (GUIs) and the DOM is completely described in EDDL. The DEF has to include the OPC UA client's services that provide functions for the DOMs to access device data and functions via the DIM in the server. To support web browser-based clients, the client components embedded in the server side should render the GUIs that are compatible with a web browser showing an HTML document as webpage.

3.3 General Prototype

The OPC UA standard tends to offer the possibility of powerful information model, a critically important feature. It suits perfectly the role of central interface for vertical integration of automation systems. How field level sensors and devices are set up and how they communicate with the higher control levels over the network are the potentially ideal application for XML-based web services. In addition, the XML-based unified device integration is a promising approach to both existing field device management solution and new device integration concept. Due to the high number of different field device types and fieldbus types within a single control system, it is still making a challenge to software and

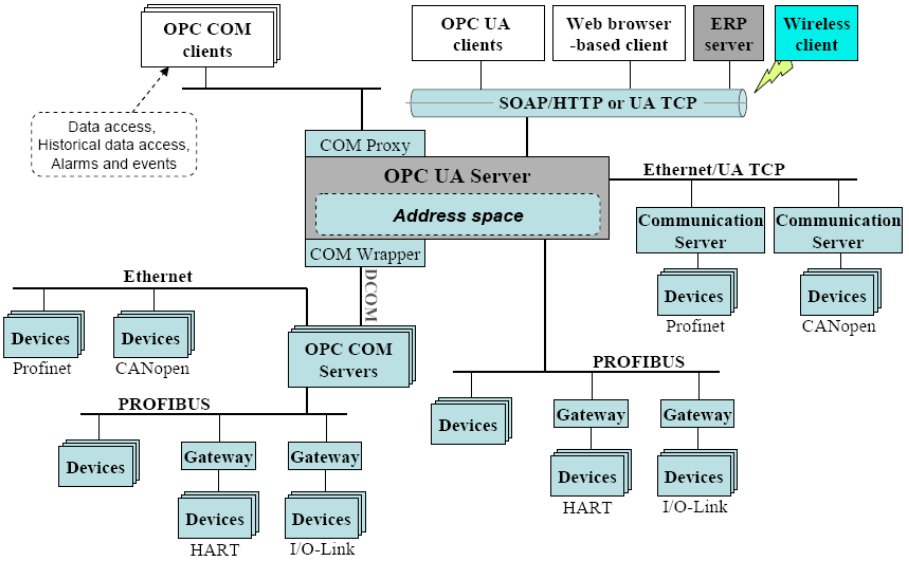

Fig. 5. A general prototype for the OPC UA-based process automation systems using the proposed device integration approach

hardware vendors since the new OPC UA standard has been proposed. A general prototype for the OPC UA-based process automation systems with different fieldbus protocols is illustrated in Fig. 5.

Networks of automation systems are normally heterogenous and use different protocols with a hierarchical structure. The transitions between networks are managed by gateway devices. The general prototype has addressed a *nested communication* through heterogenous networks with integrating PROFIBUS-HART gateway as well as PROFIBUS-I/O Link gateway, etc. The services of the OPC UA client should be embedded in the server side in order to support web browser-based clients. In the case using an ERP system like SAP is guaranteed, it acts as an OPC UA client communicating to the DIMs of the devices. As Fig. 5 shows, the usage of Profinet, CANopen, and I/O-Link devices within the prototype indicates that the device integration approach introduced in this research is suited not only for process automation devices, but also for factory automation devices as well. This prototype will be investigated carefully for the further deployment of OPC UA-based systems.

4 System Analysis

To evaluate a system for satisfying the requirements of industrial system applications, some issues such as *fault*, *configuration*, *administration*, *performance*, and *security* should be addressed and ensured. Such issues will be given as the first attempt in order to evaluate the field device integration approach for the OPC UA-based process automation systems:

- **Fault issue:** When the OPC UA-based process automation systems are part of the IT industry system, both faults of particular parts of manufacturing processes and faults need to be managed. By complying with the advantages of both FDT/DTM and EDDL technologies, the approach of device integration will enable the end-users to identify faults in their production process not only in high system level but in lower system level.
- **Configuration issue:** Mapping the field devices into the OPC UA server's address space is a major challenge because of needing a new device integration concept for the new OPC UA standard. With the utilization of the FTD/DTM and EDDL technologies, this issue will be guaranteed well.
- **Administration issue:** By integrating both the FDT/DTM and EDDL technologies for device integration, it is possible to integrate devices to the OPC UA server's address space in an efficient way to achieving the advantage of both such technologies. However, the field of research on device integration needs to be developed and supported by both hardware and software vendors.
- **Performance issue:** It is still an open question for the cases of integration of more devices due to the originality of the new OPC UA standard. The proposed system based on the new OPC UA specifications is implementing. This issue will be investigated carefully in the future work because only several preliminary results from experiment have been achieved.
- **Security issue:** This issue is part of the OPC UA-based process automation systems and fieldbus protocols. In the point of view of system, it can meet the security objective requirements in each level by the security supports of each automation system level [4]. Both devices as well as middleware services have to be authorized when they want to communicate. In the point of view of the enterprise, it can be ensured by using the `WS`-security and web technologies for the integrity and confidentiality of all messages exchanged between the client and server. Security of remote invocations including the authentication of clients, encryption of messages, and access control can be guaranteed by both XML signature and XML encryption. The XML signature can meet the security objectives such as *integrity*, *non-repudiation*, *authentication*, *accountability*, and *confidentiality*. Besides, the XML encryption complies with the security objective *confidentiality* [2]. The XML security is consequently suitable for process and factory automation in terms of IoT.

5 Concluding Remarks

This paper has introduced an approach to field device integration for the OPC UA-based process automation systems, i.e., distributed control systems or programmable logic control systems. The architecture of an OPC UA-based process automation system was also presented to make readers easy to understand the field device integration concept. A general prototype related to the device integration issue and the automation system was fully illustrated and analyzed. This indicates the future process automation systems with the new OPC UA

standard. In addition, the system analysis demonstrated the ability of the proposed device integration solution to identify the faults, to maintain the system, to configure the system, etc.

Platform independence and robustness via the interpreter allow a long-term independence that is an important issue in industry today. Since the migration strategy assures that all existing DTMs and EDDs can be used for the future without changes, the protection of investments is achieved. The potential of the new OPC UA standard is making new scenarios like Asset Management or Manufacturing Execution System (MES) and leads to a robust and platform independent solution. By introducing a flexible field device integration issue, it is important to note that the use of both FDT/DTM and EDDL technologies can be reused throughout the life cycle. Both such technologies now are being expected to play an important role in both process and factory automation.

Although client-server architectures are playing an important role in the field of business software systems, the SOA is on the move and is foreseeable that it will be dominant in the future. The integration of field devices into the business IT system through SOA is a promising approach to digitalize physical objects and to make them available to IT-systems. This can be achieved by running instance of web services on these devices. It is a challenge to researchers and developers for the case of field devices on the plant floor.

Acknowledgements. The authors would like to thank the Korean Ministry of Knowledge Economy and Ulsan Metropolitan City which partly supported this research through the Network-based Automation Research Center (NARC) at the University of Ulsan. The authors also would like to thank three anonymous referees for their carefully reading and commenting this paper.

References

1. Bohn, H., Bobek, A., Golatowski, F.: SIRENA – Service Infrastructure for Real-time Embedded Networked Devices: A Service Oriented Framework for Different Domains. In: Proceedings of the Int. Conf. on Systems and Int. Conf. on Mobile Communications and Learning Technologies, p. 43. IEEE CS Press, Los Alamitos (2006)
2. Braune, A., Hennig, S., Hegler, S.: Evaluation of OPC UA Secure Communication in Web browser Applications. In: Proceedings of the IEEE Int. Conf. on Industrial Informatics, pp. 1660–1665 (2008)
3. de Souza, L.M.S., Spiess, P., Guinard, D., Köhler, M., Karnouskos, S., Savio, D.: SOCRADES: A web service based shop floor integration infrastructure. In: Floerkemeier, C., Langheinrich, M., Fleisch, E., Mattern, F., Sarma, S.E. (eds.) IOT 2008. LNCS, vol. 4952, pp. 50–67. Springer, Heidelberg (2008)
4. Dzung, D., Naedele, M., Hoff, T.P.V., Crevatin, M.: Security for Industrial Communication Systems. Proceedings of IEEE 93(6), 1152–1177 (2005)
5. EDDL - Electronic Device Description Language, http://www.eddl.org/
6. FDT-JIG Working Group: FDT Interface Specification, version 1.2.1. FDT Joint Interest Group (2005), http://www.fdtgroup.org/

7. Grossmann, D., Bender, K., Danzer, B.: OPC UA based Field Device Integration. In: Proceedings of the SICE Annual Conference, pp. 933–938 (2008)
8. Hadlich, T.: Providing Device Integration with OPC UA. In: Proceedings of the 2006 IEEE Int. Conf. on Industrial Informatics, pp. 263–268. IEEE Press, Los Alamitos (2006)
9. Ivantysynova, L., Ziekow, H.: RFID in Manufacturing – From Shop Floor to Top Floor. In: Günther, O.P., Kletti, W., Kubach, U. (eds.) RFID in Manufacturing, pp. 1–24. Springer, Heidelberg (2008)
10. Jammes, F., Mensch, A., Smit, H.: Service-Oriented Device Communications using the Devices Profile for Web Services. In: Proceedings of the 3rd Int. Workshop on Middleware for Pervasive and Ad-Hoc Computing, pp. 1–8. ACM Press, New York (2005)
11. Karnouskos, S., Baecker, O., de Souza, L.M.S., Spiess, P.: Integration of SOA-ready Networked Embedded Devices in Enterprise Systems via a Cross-Layered Web Service Infrastructure. In: Proceedings of the 12th IEEE Int. Conf. on Emerging Technologies and Factory Automation, pp. 1–8. IEEE Press, Los Alamitos (2007)
12. Kastner, W., Kastner-Masilko, F.: EDDL inside FDT/DTM. In: Proceedings of the 2004 IEEE Int. Workshop on Factory Communication Systems, pp. 365–368. IEEE Press, Los Alamitos (2004)
13. Neumann, P., Simon, R., Diedrich, C., Riedl, M.: Field Device Integration. In: Proceedings of the 8th IEEE Int. Conf. on Emerging Technologies and Factory Automation, vol. 2, pp. 63–68. IEEE Press, Los Alamitos (2001)
14. Simon, R., Riedl, M., Diedrich, C.: Integration of Field Devices using Field Device Tool (FDT) on the basis of Electronic Device Descriptions (EDD). In: Proceedings of the 2003 IEEE Int. Symp. on Industrial Electronics, vol. 1, pp. 189–194. IEEE Press, Los Alamitos (2003)
15. Tetsuo, T.: FDT/DTM Framework for new Field Device Tools. Yokogawa Technical Report, no. 44, pp. 13–16 (2007), http://www.yokogawa.com/rd/pdf/TR/rd-tr-r00044-004.pdf
16. The OPC Foundation (2008) The OPC Unified Architecture Specification: Parts 1-11. Version 1.xx (2008), http://www.opcfoundation.org/Downloads.aspx
17. Tom, H., Mikko, S., Seppo, K.: Roadmap to Adopting OPC UA. In: Proceedings of the IEEE Int. Conf. on Industrial Informatics, pp. 756–761 (2008)
18. Yamamoto, M., Sakamoto, H.: FDT/DTM Framework for Field Device Integration. In: Proceedings of the SICE Annual Conference, pp. 925–928 (2008)
19. Zeeb, E., Bobek, A., Bohn, H., Golatowski, F.: Service-Oriented Architectures for Embedded Systems Using Devices Profile for Web Services. In: Proceedings of the 21st Int. Conf. on Advanced Information Networking and Applications Workshops, pp. 956–963. IEEE Press, Los Alamitos (2007)

A SOA-Based Framework for Building Monitoring and Control Software Systems

Vu Van Tan, Dae-Seung Yoo, and Myeong-Jae Yi*

School of Computer Engineering and Information Technology
University of Ulsan, San-29, Moogu-2 dong, Namgu, Ulsan 680-749, Korea
{vvtan,ooseyds,ymj}@mail.ulsan.ac.kr,
ymj@mail.ulsan.ac.kr

Abstract. This paper proposes a SOA-based framework for building complex monitoring and control software systems used in modern process and factory automation today where production processes will span over all types of systems. This framework is developed with utilization of the OPC Unified Architecture (UA) specifications and Object-Oriented Design (OOD). It provides generic components upon which sophisticated production processes can be modeled. Solutions to security of remote invocations are implemented to make this framework capable and reliable. The preliminary experiment results are provided, and the comparison with existing approaches and the discussion are also presented. They demonstrate that the proposed framework is feasible for applying to web service-based monitoring and control system applications.

Keywords: Framework, Monitoring and control, OPC, Object-oriented design, SOA, Software system, Unified architecture, XML, Web service.

1 Introduction

Web services enable distributed applications to be independent of any operating system, so that users can deploy one application on Windows Platforms and another application on UNIX or Linux, and have two systems communicating with each other seamlessly. Web services and XML technology were proposed to use into industrial system applications [19]. Programmers have several choices to consider the design and implementation of their applications such as Microsoft's .NET technology and C# programming language or Java.

More recently, the OPC Foundation has defined new specifications as the next generation for process control and monitoring running on various platforms, i.e., the OPC Unified Architecture (UA) specifications [23]. The OPC UA standard is based on XML, web services, and Service-Oriented Architecture (SOA). This standard makes a significant asset to business network applications and has the potential to open the business world to industrial connectivity. However, the OPC UA standard now is making a great challenge to propose a new device

* Corresponding author.

D.-S. Huang et al. (Eds.): ICIC 2009, LNAI 5755, pp. 1013–1027, 2009.

integration concept to researchers [24]. It also makes new challenging scenarios like Asset Management and Manufacturing Execution System (MES).

A monitoring and control system can be characterized as a distributed and integrated monitoring, control, and coordination system with partially cyclic and event-based operations. Its control functions can be divided into continuous, sequential, and batch control. The role of continuous control makes process control system different from others like discrete manufacturing systems. In addition to control functions, this system has other functions including performance monitoring, condition monitoring, abnormal situation handling and reporting.

In the last few years, a small number of approaches based on the OPC XML-DA specification [20] have been proposed and developed in order for applying OPC-based web services to monitoring and control systems. However, the performance of these approaches is limited because of using pure XML textual data representation. Furthermore, the design solutions implemented within existing approaches are still difficult to identify, evaluate, and reuse in terms of framework components and software engineering.

Despite recent software engineering, e.g., object-oriented programming, design patterns, components, etc., it is still difficult to build industrial software systems [9]. An object-oriented framework was defined as a prefabricated extensible set of classes or components with predefined collaboration between them and extension interfaces. A framework therefore forms a predefined architecture that models the interaction between its components and potential extensions.

The study of this paper aims at proposing a scientific framework to develop monitoring and control software systems applying for process and factory automation. The binary data representation is supported to guarantee high performance issue. To ensure security of remote invocations in the heterogeneous environments, the security solutions are implemented into the proposed framework for application developers and programmers. The proposed framework is designed and developed according to the suggested design criteria and Object-Oriented Design (OOD). They make the framework relatively easy to reuse, maintain, and upgrade. This framework also complies with the requirements of control and monitoring applications used in industry today.

2 Background and Related Work

2.1 Related Work

In recent decades there have been significant developments in both hardware and software such as high-speed networks, web services, and grid computing [6]. It is important to recognize the benefits of these new developments and to design software to make use of them. Web services are the latest tools from major computer hardware and software vendors such as Microsoft, IBM, Sun Microsystems, and other. Based on the OPC XML-DA specification, several approaches focused on XML web services have been proposed and developed for industrial systems recently.

Chilingaryan and Eppler [4] developed a data exchange protocol using the OPC XML-DA specification. Its development was motivated by achieving consistency with high level standards, multi-platform compatibility, and high performance systems. However, the design solutions implemented within the protocol are not clearly provided. The system performance related to high performance requirements has not evaluated because only some parts were developed.

Jia and Li [14] presented a design of embedded web server used for process control system based on the OPC XML-DA specification. A layer of XML-DA services was added between web service interface and embedded operation system in embedded web server by applying OPC, Java, and XML in order to link to the Internet through TCP/IP. Unfortunately, no experimental results according to their design were provided to readers.

Usami et al. [25] developed a prototype embedded XML-DA server on the controller that can either send or receive the information instead of the field devices. The client can communicate with the controllers. The performance was provided to illustrate the system has an acceptable performance. However, the design solution in this prototype is not easy to identify and evaluate for reusing in terms of framework components and software engineering.

Khalgui et al. [16] proposed two refinement mechanisms with the four policies for selecting data according to the expectation of clients for improving the network traffic between the OPC XML-DA server and its clients. The first refinement allows us to reduce the size of a message by applying a selection method for the returned value. The second one is to allow reducing the amount of communications by increasing the acquisition period.

Eppler et al. [8] suggested some control system aspects to build control applications for transferring data in an efficient way. These aspects are based on the SOAP protocol with attachment of the binary data representation. By this way the size of a SOAP message size can be reduced about more than six times or more. As a result XML parsing and application performance can be improved upon through binary encodings.

On the other hand, commercially available systems based on the XML-DA specification are successfully developed by some software companies such as Advosol, Softing AG, Technosoftware, etc., applying them to the control systems of relatively slow processes that used in process and factory automation in terms of enterprise application level. Unfortunately, the technical documents related to the design solutions of these systems have not provided because of secret.

2.2 State-of-the-Art OPC Unified Architecture Standard

The OPC UA standard shares information in more complex data structure formats with enterprise level MES and ERP systems in a way that they can understand. It embodies all functionalities of the existing OPC servers and expands on top of them. One of the key problems with the new standard is that implementing them can be quite challenging. The OPC Foundation has taken many steps to guarantee that the implementation of the standard would be relatively straightforward and easy process.

To facilitate the adoption of the new standard and to reduce the barrier to entry, an OPC-UA Software Development Kit (SDK) is being developed. The SDK is the entry point to jump-start the existing applications and makes them OPC-UA-enabled. The SDK consists of a series of application programming interfaces and sample code implementations. To that end, the UA specifications are written to be platform-agnostic and, for that reason, the SDK comes in different flavors to facilitate the adoptions on different platforms. The .NET, ANSI C, and Java implementation samples will be provided.

The OPC UA standard intends to enable enterprise interoperability and expects to solve enterprise integration challenges. This is a very ambitious undertaking and has been difficult to determine what elements of enterprise interoperability can actually be standardized. It is clear that this standard does not provide everything needed for interoperability from the enterprise-IT perspective, but the impact is expected to be considerable.

2.3 Research Contribution

Frameworks for developing monitoring and control system applications are widely accepted and provide support for easy and fast development to application developers. However, most of existing approaches are generic with a focus on infrastructure issues and only rarely dedicated to a specific domain. This research describes a scientific application framework for building monitoring and control software systems in application domains of process and factory automation, including all relevant software development issues: (i) infrastructure issues and technical details, (ii) framework architecture, (iii) components, (iv) device integration concept, and (v) security solutions. This framework provides generic components upon which production processes can be modeled. It enables real-world devices to seamlessly participate in business processes that span over several systems from back-end down to the field devices on the plant floor.

3 Framework Design Criteria

As an object-oriented framework is defined as a prefabricated extensible set of classes or components with predefined collaboration between them and extension interfaces [9], a framework therefore forms a predefined architecture that models the interactions between its components and potential extensions. Moreover, a software framework has to meet the requirements that rise from the software engineering point of view and the changes in technology.

A two-step requirement analysis should be performed to construct the framework design criteria including *domain analysis* and *domain design* [17]. Thereby, the objective of the domain analysis is the development of a domain model that contains the knowledge of a domain in a systematic way. The key of the domain design is the transformation of the results of the domain analysis into reusable form, implementation-oriented objects and the design relations between the objects. The six design criteria are suggested as follows:

1. **Generic requirements.** The fucus of suggested framework is the application development of the monitoring and control system domain. Therefore, a universal architecture is necessary with treating different organizational types of monitoring and control systems.
2. **Methodology.** The framework concept introduces a new level of abstraction that provides an easier conceptualization of the problem domain. This enables the implementation of more complex control and monitoring strategies where process control is distributed and large amounts of distributed data are collected.
3. **Flexibility.** This feature indicates that a system should be able to adapt to various circumstances. Flexibility in the proposed framework is incorporated in the context of control and monitoring of process and factory automation.
4. **Reusability.** Software reusability is one of the important goals of developing frameworks. The suggested framework is ensured by designing and developing a generic structure, architecture, and modules.
5. **Openness.** By complying with the OPC technology, the proposed framework makes it flexible and open for the development of a specific application.
6. **Compatibility with existing standards.** Because of using the OPC UA specifications, the suggested framework embodies all functionalities of existing OPC specifications [19,20,21,22]. It is that backward compatibility with previous standards will ensure quick adoption on the development. However, this criterion is quite challenging to researchers and developers.

4 The Framework Architecture

4.1 The Infrastructure Issues and Technical Details

Despite the role of client-server architectures in the field of business software systems, the Service-Oriented Architecture (SOA) is on the move and is foreseeable that this architectural paradigm will be dominant in the future. Enabling efficient collaboration between device-level SOA on the one hand and on the other hand services and applications that constitute the enterprise back-end is a challenging task. By integrating web services on the plant floor, devices have the possibility of interacting seamlessly with the back-end systems [12,13]. However, to provide mechanisms for discovering other service-enabled devices or methods for maintaining a catalogue of discovered devices, it is difficult task for current products [6,1]. There are still big differences between device-level SOA and the one that is used in back-end systems. These differences can be overcome by using a middleware between the back-end applications and the services which are offered by devices, service mediators, and gateways.

The fundamental architecture of system integration to integrate device-level services with enterprise software systems running on the application level using web service technology can be shown in Fig. 1. It shows that there are at leat two different ways to couple networked embedded devices with enterprise services.

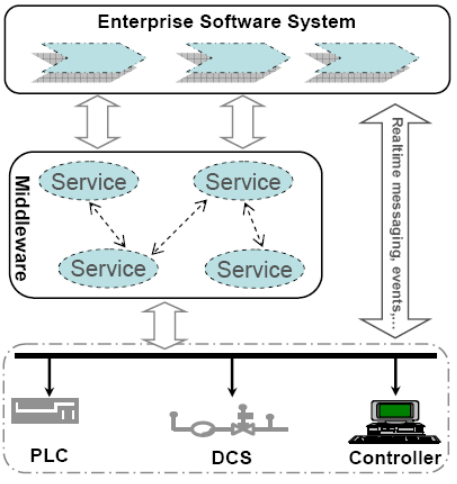

Fig. 1. The fundamental architecture of a system integration

One way is that a direct integration of device-level services in business processes should be built, while another way exposes device functionality to the application layer via a middleware layer.

Today most of human-machine interface, supervisory control and data acquisition (SCADA), distributed control system (DCS), and software programmable logic controller (PLC) manufacturers offer interfaces that conform to the OPC specifications because of supporting industry-standard interoperability, enhanced productivity, and better collaboration across systems.

4.2 Architectural Overview

The integration of devices into the business IT-landscape through SOA is a promising approach to digitalize physical objects and to make them available to IT systems. It can be tackled by running instances of web services on these devices, which move the integration of back-end applications such as Enterprise Resource Planning (ERP) systems, creating an Internet of Services to collaborate and empower the future service-based factory. One key advantage of using services is that functionality provided by different devices can be composed to allow for more sophisticated application behavior. The use of services is also desirable because business software today is built more and more in a service-oriented way based on web services [12,13].

Since 1996, the OPC Foundation has been provided specifications for communication among devices used in process automation, published protocols that quickly became the standard for connecting to software and hardware. Such devices include sensors, instruments, programmable logic controllers, human-machine interfaces, and alarm subsystems used in manufacturing, oil, and gas. Based on the OPC UA specifications [23], the architecture to integrate the

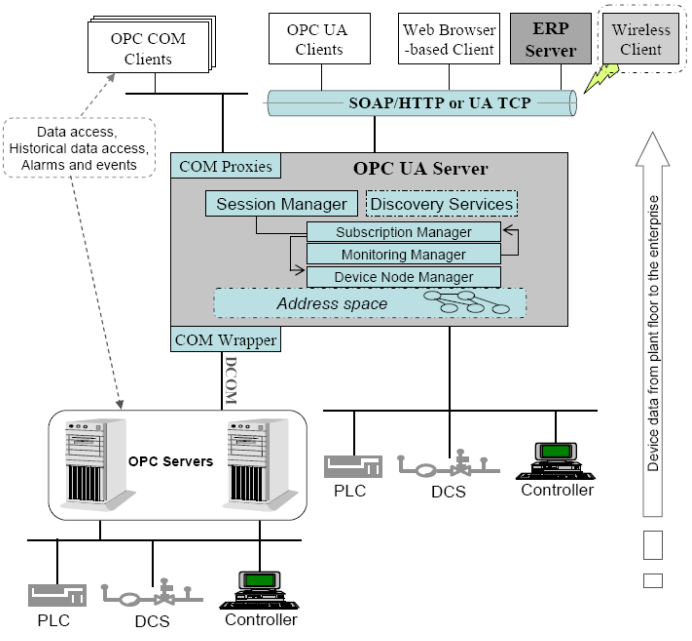

Fig. 2. The proposed architecture for monitoring and controlling field devices

devices from the plant floor to enterprise applications can be proposed as shown in Fig. 2. It shows that there are two methods for mapping devices to the address space at the enterprise applications. One method is to directly integrate embedded devices and their functionality to the OPC UA server and other one is to map the embedded devices through existing OPC DA servers. This framework architecture is based on the OPC client-server model. It provides a means for aggregating one or more OPC servers into its address space. Although the client does not need accesses to multiple servers in the normal case, this feature is provided to make a flexible architecture in order to satisfy multiple servers for different clients in some special cases.

The UML (Unified Modeling Language) sequence diagram to establish the connection between the client and the server is shown in Fig. 3. To do this, the *Discovery* services will find *endpoints* which provide security requirements and services for clients. Since the system has developed, the implementation is based on the assumption that the clients have known that endpoint to address. If the endpoint is known, a secure channel to the client is established by the *Secure Channel* services and the *Session* services allows to be created a session between the client and server [23]. When a client has completed its task for the connection, it will add a new node to the appropriate object in the address space. Once the client has been connected to the server, the objects to be monitored are registered.

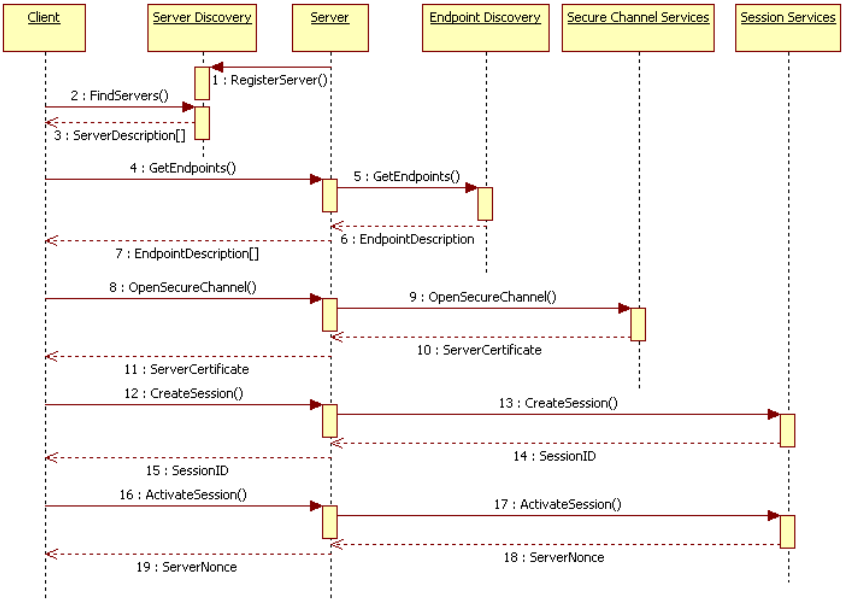

Fig. 3. Interactions for a connection between the client and server

4.3 Components

The proposed architecture is the bridging technology which enables the use of existing software systems and OPC servers enabled devices. Although direct access from an ERP system to devices is possible, the proposed architecture simplifies the management of field devices and acquires data from these devices. The components of the proposed architecture are briefly described as follows:

(1) **Discovery Component.** This component defines services used to discover the endpoints implemented by a server and to read the security configuration for these endpoints. The Endpoint Discovery that is part of this component is provided by server for client to access without establishing a session. In general, the endpoint may or may not have the some session that clients use to establish a Secure Channel. Once a client retrieves the endpoints, this client can save this information and use it to connect to server again.
Servers may register themselves with a well-known Server Discovery using the `RegisterServer` service. The Server Discovery which is part of the Discovery Component is used for clients to discover any registered servers by calling `FindServers` service. In a case the server's configuration has changed, the client needs to go through the discovery process again.

(2) **Session Manager.** This component consists of services that manage session for clients. It is responsible for validating incoming requests and cleaning up when a session expires. Before calling these services, the client must create a secure channel to ensure integrity of all messages exchanged during a session.

The secure channel is created together with a session by means of security solutions. A communication channel opened with a secure channel ensures the confidentiality and integrity of all messages exchanged between the client and server.

(3) **Subscription Manager.** After creating a connection with the establishment of secure channel between the client and server, the users in the client side can read or subscribe to data or events from field devices on the plant floor. The Subscription Manager component provides services to manage the subscription.

(4) **Device Node Manager.** This component is composed of services that manage the server's address space. It is an abstraction that collects data and events from different sources, i.e., field devices on the plant floor, and exposes them via a standard interface. The services provided by this component are used to add and delete *address space* nodes and *reference* between them.

(5) **Monitoring Manager.** Clients define `monitored items` to subscribe to data and events. Each monitored item identifies the item to be monitored and the subscription to use to send notifications. This is also assigned a sampling interval that is either inherited from the publishing interval of the subscription or that is defined specifically to override that rate. The attributes and variables for value or status changes of a node, including the caching of values and the monitoring of nodes for events are focused.

(6) **COM Wrapper.** This component is used to map the OPC server's address space onto the UA information model. It consists of a Device Node Manager, which encapsulates all accesses to the OPC server (or simply COM server). The Session Manager is responsible for mapping the user identity associated with a session. This component also allows different sessions to use the same COM server instance for the clients to access.

(7) **COM Proxies.** This component was implemented for supporting the COM clients to access the OPC UA server. These Proxies map the UA server's address space onto the COM address space. All of the mappings hide any part of the UA server's address space that cannot be represented with the COM address space.

4.4 Data Representation

The fundamental approach to solve the bandwidth problems today is using binary data representation, which is integrated into XML such as BXML [3], BXSA [5], etc. Recently, some solutions are available to satisfy these conditions like SOAP with attachment or HTTP message using XLink [8].

To provide a fast and reliable solution to process monitoring and control applications based on XML and web services, the binary data are incorporated into SOAP message, i.e., the SOAP header is still XML in order to pass the firewall and the body of the SOAP message is encoded as binary data to reduce the size of a message.

4.5 Field Device Integration

As the number of field devices increases, the more complicated settings and adjustments need to use advanced functions in such devices have become challenges [1,6,13]. Today's technologies such as Electronic Device Description Language (EDDL) [7] and Field Device Tool (FDT) [10] are available for device integration [26,11,15,18]. The FDT technology uses programmed software components, called Device Type Manager (DTM). Distributed control system (DCS) or automation system vendors would like to achieve robustness while assuring a high level of technology and platform independence. Device manufacturers want to support only one technology instead of two in order to reduce effort. The presented device integration strategy integrates (i) the advantages of EDDL – platform independence, ease of use and robustness and (ii) the advantages of FDT – unlimited functionality, extensibility, and market differentiation.

To realize the ability of Internet-based monitoring and control, and to enable efficient collaboration between device-level SOA on the one hand and on the other hand services and applications, the solution developed by Grossmann et al. [11] was modified to apply the proposed framework, including Device Information Model (DIM) and Device Operation Model (DOM). The DIM presents the device data and function exposed by device firmware and is unique for each device. It encapsulates the communication with a device and ensures that applications can access data and functions independently from connection-specific properties. All DOMs access the device's DIM to request device data and functions.

The server loads the device description containing DIM and DOMs. While the DIM is directly processed within the server to establish the information model to the address space, the DOMs are only handled in terms of sever storage. The server information allows OPC UA clients to access the device data and functions that are part of the DIM. The architecture model of device integration using DIM and DOM is shown in Fig. 4. Each device is represented by a *Device* object. The device object includes sub-objects which hold the data items

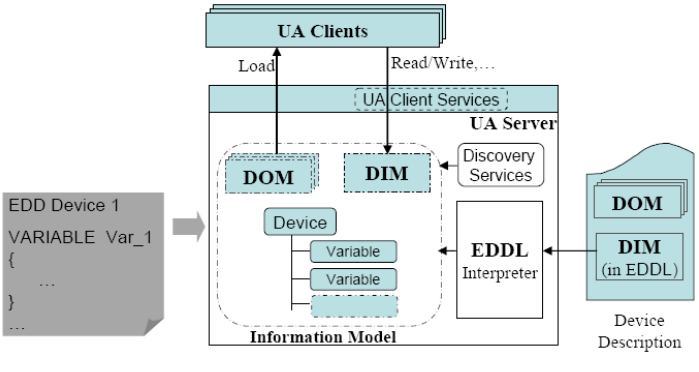

Fig. 4. The device integration concept based on both FDT/DTM and EDDL

of the data model. To offer the DIM access to the device data, the server will communicate with the devices over the fieldbus protocols such as FOUNDATION fieldbus, PROFIBUS, CANopen, DeviceNet, and HART through HART gateway. But having the services on devices will not be much of use if they can not be dynamically discovered by the server. Thus, discovery services should be implemented in order to find installed devices on the plant floor.

5 The Framework Security Solutions

Security of remote invocations in the heterogenous environments is very important for Internet-based monitoring and control including the authentication of clients, encryption of messages, and the access control. The security objectives for these systems are integrity, confidentiality, availability, authentication, non-repudiation, accountability, and reliability [2,23].

The XML security consisting of XML signature and XML encryption is the key concept to meet the required security objectives. The XML encryption complies with the generic security objective *confidentiality*. The XML signature meets the requirements of the security objectives like *integrity*, *non-repudiation*, and *authentication*. The XML signature also implicitly meets the security objectives *accountability* and *confidentiality* due to the *authentication*. Thus, digital signatures are suitable for OPC UA-based monitoring and control applications.

The XML signature is a system to encode digital signatures in an XML document. It uses the same standards and technologies of cryptography as usual digital signatures. The basic of digital signatures is asymmetric cryptography. In contrast to symmetric cryptography, an entity in asymmetric cryptography creates a key pair in which one of them is the public key that can safely be published. By this way data can be encrypted for only the private key to decipher. The private key can be also used to generate digital signatures that are used to verify the public key. The steps to sign a message and to verify the signed message by communication partner using digital signatures are presented as follows:

(1) Calculating the hash code for data to be signed.
(2) Encrypting the hash code using private key. It ensures the security objective non-repudiation.
(3) Attaching the hash code and the encrypted hash code into the message before transmitting this message.
(4) The receiver of the singed message will decrypt the encrypted hash code with the public key of the communication partner. If the decrypted hash code and the plain hash code of the message are identical then the communication partner is the expected one. Otherwise the message has to be discarded or rejected because of a potential attack.
(5) The receiver calculates the hash code of the same data and compares the two has codes. If the hash codes are identical the integrity of the message has been guaranteed. Otherwise the data were modified that must be discarded.

6 Experiment Results and Performance Evaluation

6.1 Experiment Setup

A number of performance tests were performed by verifying the various number of OPC items in the client side. The setup was composed of the OPC UA server and client running on Windows XP Service Pack 2 as follows:

(1) Intel Pentium IV CPU with the clock frequency of 2.66 Ghz.
(2) Capacity of PC 3200 DDRAM is 1 Gb.
(3) Hard disk at least 5 Gb of free space.
(4) The OPC UA client and server running on the same computer.
(5) Microsoft .NET Framework 3.0 Service Pack 1.

6.2 Preliminary Results and Performance Evaluation

The time taken for operation `Read` to fetch a various number of items under various conditions is set out to measure. The comparison of the time taken for operation `Read` under the fixed conditions (binary encoding, signature and encryption, 256-bit Basic) with either using HTTP or TCP is shown in Fig. 5(a). It indicates that using binary encoding will improve performance much.

The comparison of the time taken for operation `Read` under the fixed conditions (binary encoding, HTTP, and 256-bit Basic) with using signature and encryption, signature, and none, respectively, can be shown in Fig. 5(b). It indicates that the overall performance of the proposed system when using both signature and encryption is approximately about two times slower than the case of not using both ones. It also indicates that the overall performance of the proposed system when using only signature is about three second times faster than the case of using both encryption and signature. The preliminary results show that the proposed system has a sufficient good performance and can be acceptable to many real monitoring and control system applications.

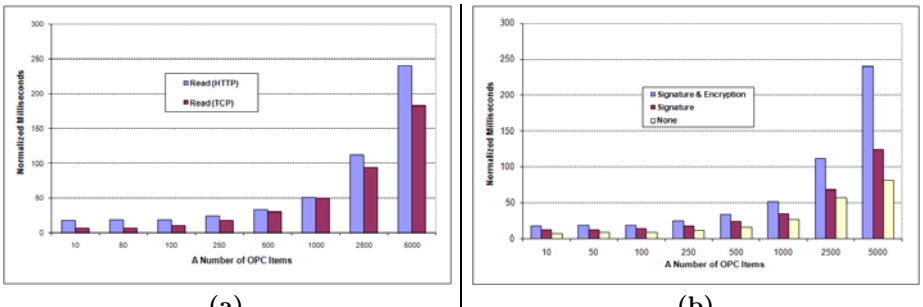

(a) (b)

Fig. 5. (a) The time taken for operation `Read` using either HTTP or TCP protocol. (b) The time taken for operation `Read` with different security modes: *Signature and Encryption*, *Signature*, and *None*.

7 Comparison and Discussion

7.1 Comparison with Existing Approaches

The comparison of the proposed architecture with existing approaches [4,14,25, 16,8] is difficult due to their conceptual nature, architecture, and wide range of production environments. A qualitative comparison of the proposed framework with others could be made. The proposed system has the following advantages:

1. The proposed framework provides a single and interoperable way to access process data from the plant floor to the enterprise applications such as Computer Maintenance Management System (CMMS), Enterprise Resource Planning (ERP) system, Enterprise Asset Management (EAM) system, and Manufacturing Execution System (MES) in easy mechanism.
2. This framework fully addresses the issues of sharing information in complex data structure formats with the enterprise systems in a way that they can understand. It can do them by providing the means to handle complex data structures and to transport them in a securable, reliable, and SOA approach.
3. All data such as current data, historical data, and alarms and events are provided in a unified address space to make them relative with each other while existing approaches only collect each type of data into theirs address space without relations.
4. The proposed framework will open a flexible gate to enterprise applications to communicate with plant floor via OPC DA or others. This means that existing products still play as they are by using wrappers.
5. By complying with six framework design criteria, the structure of the proposed framework is designed and developed in a systematic way. The framework provides generic components upon which sophisticated processes can be modeled.

7.2 Discussion

Since the work presented in this paper is part of ongoing research on the area of automation systems with OPC technologies, it seems to have such a framework in particular to access future work. The potential areas of the proposed framework include the followings:

- The applications of process monitoring and control systems used in process and factory automation where control is distributed and large amounts of distributed data are collected.
- Business applications such as CMMS, ERP, and EAM systems. These applications require data updates that the frequency is in second(s) or minute(s) and usually update every shift or more typical.
- Process Analysis applications such as Enterprise Process Historian, Analysis Reporting, Trending, and others. The frequency of data capture of these applications is not nearly as important as the fact that data donot get loss.
- Remote Monitoring applications such as web-based process visualization.

8 Concluding Remarks and Future Works

A SOA-based framework was introduced for designing and developing monitoring and control system applications. The proposed framework fulfills the six suggested design criteria to make it flexible, open and compatible with existing OPC functionality. The security solutions were incorporated into the proposed framework for developers and programmers to develop their applications in a systematic way. The proposed framework has a good performance and is expected to deploy for modern process and factory automation systems.

Industrial systems now need to be independent of any operating systems and platforms. Therefore, the OPC UA standard is a good choice for the development of web-enabled industrial automation and manufacturing software systems. Technology in turn will mature in time and the OPC UA standard will surely rise as the eventual winner. It will be included in the future products made by many leading companies in area of industry. The SOA will be dominant in the future. Therefore, the integration of field devices into the business-IT systems through SOA is a promising approach to researchers.

Trying to use the proposed framework for the implementation of a control and monitoring approach for flexible systems is the major task. The application case studies will be also investigated and deployed in the future work.

Acknowledgements. This work was supported in part by the Korean Ministry of Knowledge Economy and Ulsan Metropolitan City through the Network-based Automation Research Center (NARC) at the University of Ulsan and by the Korea Research Foundation Grant funded by the Korean Government (KRF-2009-0076248).

References

1. Bohn, H., Bobek, A., Golatowski, F.: SIRENA – Service Infrastructure for Real-time Embedded Networked Devices: A Service Oriented Framework for Different Domains. In: Proceedings of the Int. Conf. on Systems and Int. Conf. on Mobile Communications and Learning Technologies, p. 43 (2006)
2. Braune, A., Hennig, S., Hegler, S.: Evaluation of OPC UA Secure Communication in Web browser Applications. In: Proceedings of the IEEE Int. Conf. on Industrial Informatics, pp. 1660–1665 (2008)
3. Bruce, C.S.: Cubewerx Position Paper for Binary XML Encoding, http://www.cubewerx.com/main/HTML/Binary_XML_Encoding.html
4. Chilingargyan, S., Eppler, W.: High Speed Data Exchange Protocol for Modern Distributed Data Acquisition Systems based on OPC XML-DA. In: Proceedings of the 14th IEEE-NPSS Real-time Conference, pp. 352–356 (2005)
5. Chiu, K., Devadithya, T., Lu, W., Slominski, A.: A Binary XML for Scientific. In: Proceedings of the 1st Int. Conf. on e-Science and Grid Computing (2005)
6. de Souza, L.M.S., Spiess, P., Guinard, D., Köhler, M., Karnouskos, S., Savio, D.: SOCRADES: A web service based shop floor integration infrastructure. In: Floerkemeier, C., Langheinrich, M., Fleisch, E., Mattern, F., Sarma, S.E. (eds.) IOT 2008. LNCS, vol. 4952, pp. 50–67. Springer, Heidelberg (2008)

7. EDDL - Electronic Device Description Language, http://www.eddl.org/
8. Eppler, W., Beglarian, A., Chilingarian, S., Kelly, S., Hartmann, V., Gemmeke, H.: New Control System Aspects for Physical Experiments. IEEE Transactions on Nuclear Science 51(3), 482–488 (2004)
9. Fayad, M.E., Schmidt, D.C., Johnson, R.E.: Building Application Frameworks: Object-Oriented Foundation of Framework Design. Wiley, Chichester (1999)
10. FDT-JIG Working Group: FDT Interface Specification, Version 1.2.1. FDT Joint Interest Group (2005), http://www.fdtgroup.org/
11. Grossmann, D., Bender, K., Danzer, B.: OPC UA based Field Device Integration. In: Proceedings of the SICE Annual Conference, pp. 933–938 (2008)
12. Jammes, F., Smit, H.: Service-Oriented Paradigms in Industrial Automation. IEEE Transactions on Industrial Informatics 1(1), 62–70 (2005)
13. Jammes, F., Mensch, A., Smit, H.: Service-Oriented Device Communications using the Devices Profile for Web Services. In: Proceedings of the 3rd Int. Workshop on Middleware for Pervasive and Ad-Hoc Computing, pp. 1–8 (2005)
14. Jia, Z., Li, X.: OPC-based architecture of embedded web server. In: Wu, Z., Chen, C., Guo, M., Bu, J. (eds.) ICESS 2004. LNCS, vol. 3605, pp. 362–367. Springer, Heidelberg (2005)
15. Kastner, W., Kastner-Masilko, F.: EDDL inside FDT/DTM. In: Proceedings of the 2004 IEEE Int. Workshop on Factory Comm. Systems, pp. 365–368 (2004)
16. Khalgui, M., Rebeuf, X., Zampognaro, F.: Adaptable OPC-XML Contracts Taking into Account Network Traffic. In: Proceedings of the 10th IEEE Conf. on Emerging Technologies and Factory Automation, pp. 31–38 (2005)
17. Mönch, L., Stehli, M.: Manufag: A Multi-agent-System Framework for Production Control of Complex Manufacturing Systems. Information Systems and e-Business Management 4(2), 159–185 (2006)
18. Simon, R., Riedl, M., Diedrich, C.: Integration of Field Devices using Field Device Tool (FDT) on the basis of Electronic Device Descriptions (EDD). In: Proceedings of the 2003 IEEE Int. Symp. on Indus. Electronics, pp. 189–194 (2003)
19. The OPC Foundation (2004a): The OPC Data Access Specification. Version 3.0 (2004), http://www.opcfoundation.org/Downloads.aspx
20. The OPC Foundation (2004b): The OPC XML-Data Access Specification. Version 1.01 (2004), http://www.opcfoundation.org/Downloads.aspx
21. The OPC Foundation (2003): The OPC Historical Data Access Specification. Version 1.0 (2003), http://www.opcfoundation.org/Downloads.aspx
22. The OPC Foundation (2002): The OPC Alarms and Events Specification. Version 1.0 (2002), http://www.opcfoundation.org/Downloads.aspx
23. The OPC Foundation (2008): The OPC Unified Architecture Specifications: Parts 1-11. Version 1.xx (2008), http://www.opcfoundation.org/Downloads.aspx
24. Tom, H., Mikko, S., Seppo, K.: Roadmap to Adopting OPC UA. In: Proceedings of the IEEE Int. Conf. on Industrial Informatics, pp. 756–761 (2008)
25. Usami, K., Sunaga, S.-I., Wada, H.: A Prototype Embedded XML-DA Server and its Evaluations. In: Proceedings of the SICE-ICASE Int. Joint Conference, pp. 4331–4336 (2006)
26. Yamamoto, M., Sakamoto, H.: FDT/DTM Framework for Field Device Integration. In: Proceedings of the SICE Annual Conf., pp. 925–928 (2008)

Data Fusion Algorithm Based on Event-Driven and Minimum Delay Aggregation Path in Wireless Sensor Network*

Tianwei Xu[1], Lingyun Yuan[1], and Ben Niu[2]

[1] College of Computer Science and Information Technology, Yunnan Normal University, Yunnan, China
[2] College of Management Shenzhen University, Shenzhen, China
xutianwei@ynnu.edu.cn, yuan_ling_yun@yahoo.com.cn, drniuben@gmail.com

Abstract. Emergent event detection is one of the most important applications in event-driven wireless sensor network. In order to save energy, a dynamic clustering routing algorithm based on event severity degree is presented rather than period monitoring in the paper. The lifetime and the scale of clusters lie on the emergent event severity degree. On the other hand, the data must be collected, fused and transmitted in real time for the emergencies. Most existing data aggregation methods in wireless sensor networks just have longer network delay. The minimal delay aggregation path mechanism is put forward to reduce the network delay. The hop-count from itself to its cluster head and the degree determine the waiting time for a fusing node. With every waiting time for the fusing nodes in the path, the minimal delay aggregation path can be obtained. The simulation results show that our algorithm can save energy efficiently, and reduce the network delay remarkably. It achieved a better tradeoff between the energy and delay. Moreover, it provides a good method for wireless sensor network applied to monitoring emergencies.

Keywords: Wireless Sensor Network, Data Fusion, Event Driven, Minimum Delay Aggregation Path.

1 Introduction

The emergent event detection is a crucial application in wireless sensor network, such as fire, earthquake and et al. For the emergent event detection, event-driven wireless sensor network which has some characteristics such as emergency, abundant data and high redundancy is the most appropriate model. The sensor nodes have limited

* The work is supported by the general project of social development in Yunnan Province (Grant no. 2008CD113), the foundation project of education office in Yunnan province (Grant no. 08Y0136), and Shenzhen-Hong Kong Innovative Circle project (Grant no. SG200810220137A).

D.-S. Huang et al. (Eds.): ICIC 2009, LNAI 5755, pp. 1028–1038, 2009.

energy, and can not replace expediently. To extend the network lifetime in emergent event detection is one of the most important goals. On the other hand, emergent events always need to be reported in time. If some event occurs, the data will increase abruptly in a short time. The event message must be transmit to the sink node accurately and in real-time. So the network delay is another factor which must be considered. How to fusing the event data with low network delay and long lifetime is a very important problem for the event-driven wireless sensor network.

At present, data fusion methods in wireless sensor network are mostly based on routing algorithm, such as LEACH [1], TEEN [2], Steiner tree [3]. In SRDA [4], the nodes only need to transmit the variation rather than original data, in which the variation is made by comparing the original data to reference data. In SIA [5], the nodes only transmit the fused data to base station, in which a lot of fusing functions such as max, min, average, sum are involved. A new data aggregating model Q-Digest [6] is presented, in which wireless sensor network can respond to multi-request. The member nodes and cluster heads are executed independently in distributing KMDBA [7], and the network is divided into multi-clusters to avoid that the redundancy data is directly transmitted to the cluster head from the member nodes. These protocols in [1-3] mainly focus on constructing the shortest path tree to achieve data fusion. The methods in [4-7] aim to study the data fusing algorithm based on periodicity and center-based query. The authors [8] presented the detection standard while event occurs, and the data fusion method is based on the data correlativity in space-time. Tang and et al. [9] put forward an event correlativity method based on finite state machine. But it's just a theory model. The characteristics of emergent event are not considered, such as the severity degree, the location and the data comparability from the nodes in the event areas in all above algorithms. In the paper, a dynamic clustering method based on the properties of emergent event is presented as the first phase of data fusion algorithm with which energy consumption of network nodes is reduced.

On the other hand, to decrease network delay is another important goal. In LEACH[1], SCT[10], all fusing nodes have the same waiting time before the fusing operations are performed, in which the waiting time is enough long so that the fusing nodes can receive all fusing data before timeout. The method would increase the network delay, while saving the network nodes' energy. In [11, 12], the authors propose a fusing time mechanism. A diverse fusing tree would be built between the source node and sink node by transmitting the data. The fusing nodes set up their waiting time according to the distance from themselves to sink node. Yuan and et al [13] put forward a controllable multi-level fusing time scheme. The fusing nodes set up their waiting time according to the distance from themselves to sink node, and the sink node tunes up the maximum delay. In the timing control protocol [14], the waiting time can be tuned up according to the fusing quality. Wang [15] has presented a group aware real-time data aggregation tree algorithm, in which the path can be selected with satisfying the latency constraint and lower energy consumption. An aggregate contribution based delay-time allocation algorithm [16] is proposed, in which the impact on aggregation efficacy of different positions in the route tree is quantified, and the aggregation time of every node at sink is allocated.

Through all above fusing timing methods are trying to reduce network delay, the real-time of data is very important for the event-driven network. Taking the factor into consideration, the minimum delay aggregation path is put forward in this paper,

in which the waiting time is determined by the hop-count from the member node to its cluster head and the degree of the member node. With the waiting time of all nodes in the paths, the minimum delay aggregation path can be achieved. So a data fusion algorithm based on event-driven and minimum delay aggregation path (EDMDP) is presented for emergent event detection in the paper.

This paper is organized as follows. Network model and radio model are introduced in section 2. In section 3, data fusion algorithm based on event-driven and minimum delay aggregation path is described in detail. And the experimental results and analysis are given in section 4. Finally, the conclusions are drawn in section 5.

2 Network Model

2.1 Network Model

This research is based on event-driven wireless sensor network. We assume that there are *N* nodes deployed in the monitoring area *A* randomly. And some characteristics are described as following:

(a) The sensor nodes are static, and they will never move when deployed.

(b) There is only one base station. The base station can be deployed in the center of network or somewhere out of *A*. The experimental results indicate it's more efficient when the base station is deployed in an immobile location out of *A*. The base station has unlimited energy, and can send information to all nodes.

(c) All nodes have the same initial energy which can't be replaced. And all nodes have similar processing and communicating capabilities.

(d) The energy consumption of these sensor nodes is different in each round. The base station can calculate the residual energy after each round ends up.

(e) The sensor nodes can obtain their location information by the base station.

2.2 Radio Energy Model

Low-power and wireless communication are studied in recent years widely. We use the same radio model as used in LEACH, PEGAIS, which is the first order radio model. In this model, a radio dissipates $E_{elec} = 50nJ/bit$ to run the transmitter or receiver circuitry and $\varepsilon_{amp} = 100pJ/bit/m^2$ for the transmitter amplifier. The radios have power control and can expend the minimum required energy to reach the intended recipients. The radios can be turned off to avoid receiving unintended transmissions. This radio model defines a distance threshold d_0 which is a constant and its value depends on applications. When the distance between transmitting node and receiving node is below on d_0, the energy consumption of the transmitting nodes is in inverse proportion to d^2, otherwise it' s in inverse proportion to d^4, namely free space model and multi-path fading model. According to the distance between the transmitting nodes and the receiving nodes, the transmitting nodes can use different energy consumption model to calculate the needful energy which is used to transmit data.

The equations are used to calculate transmitting costs and receiving costs for a *k-bit* message and a distance *d* are shown below:

Transmitting:

$$E_{Tx}(k,d) = E_{Tx-elec}(k) + \varepsilon_{Tx-amp}(k,d), \tag{1}$$

$$E_{Tx}(k,d) = E_{elec} * k + \varepsilon_{amp} * k * d^2, \tag{2}$$

$$E_{Tx}(k,d) = E_{elec} * k + \varepsilon_{amp} * k * d^4. \tag{3}$$

Receiving:

$$E_{Tx}(k,d) = E_{Tx-elec}(k), \tag{4}$$

$$E_{Rx}(k) = E_{elec} * k. \tag{5}$$

On the other hand, the energy consumption on data fusion also can not be ignored. 5nJ/bit/message is use to calculate the energy cost for data fusion. In this paper, it is assumed that the radio channel is symmetric so that the energy required to transmit a message from node *i* to node *j* is the same as the energy required to transmit a message from node *j* to node *i* for a given signal-to-noise ratio. For the comparative evaluation purposes, we assume that there are no packet losses in the network. It is not difficult to model errors and losses in terms of increased energy cost per transmission. With known channel error characteristics and error coding, this cost can be modeled by suitably adjusting the constants in the above equations.

3 Data Fusion Algorithm Based on Event-Driven and Minimum Delay Aggregation Path

3.1 Dynamic Clustering

In order to save energy, after the nodes are deployed in the monitoring environment, all nodes will be set to "restraining" state rather than clustered. And they're activated just when some emergent event occurs. Then the nodes will be clustered. The scale and lifetime of the clusters lie on the event severity degree, in which several thresholds are set to label.

3.1.1 Threshold Definition

Def.1 Basic Hard Threshold (BHT), is used to estimate the emergent event severity degree. Its value will not vary with *Mdata*, in which *Mdata* is the measurement data from restraining nodes.

Def.2 Standard Hard Threshold (NHT). The restraining nodes use this NHT to compete to be a cluster. If Mdata >BHT &&| Mdata-NHT|>=ST , the restraining nodes will change to the "working" state from "restraining" state. And the NHT value will be replaced with Mdata. Moreover, if Mdata >BHT &&| Mdata-NHT|>=ST , then NHT=Mdata , and the number nodes will transmit the data Mdata to their upper layer nodes.

Def.3 Soft Threshold (ST) is used to denote the minimal change of measurement data that make the nodes exciting or transmitting Mdata.

Def.4 Relative Exciting Threshold (RETT) is used to confirm the live time of the cluster head. The value of RETT varies with the event severity degree, $RETT = \alpha |Mdata - BHT|$, where α is the live time factor.

Def.5 Absolute Exciting Threshold (AETT). The cluster head broadcasts the CH message with AETT, with which the member nodes can estimate the live time of their cluster. AETT=t+RETT , here t is the current time. If t > AETT , the node will change "working" state to "restraining" state.

3.1.2 Dynamic Clustering Based on Event Severity Degree

The cluster-tree structure is used to save energy in the paper, with multi-hop rather than single hop from the member nodes to the cluster head. The scale and lifetime of the clusters lie on the severity degree of emergent event as defined in the section 3.1.1. The dynamic clustering steps are described as following:

Step 1: The nodes are initialized after deployed. The base station first sends its location information to all nodes. The nodes get their location information, neighbors' location and the distance between itself and base station.

Step 2: After they are initialized, all nodes will not be clustered beforehand, just be in "restraining" state.

Step 3: Cluster head node. When some emergent event occurs in some area, for the measurement data from some restraining node i $(i \in N)$, if $Mdata_i > BHT \,\&\&\, |Mdata_i - NHT| >= ST$, then node i will change to the "working" state from "restraining" state, and become a cluster head. The severity degree |Mdata-BHT| determines the lifetime time and the scale of the cluster. After the node becomes a cluster head, they will calculate the hop count of CH message broadcast K, K=u |Mdata-BHT|. And the value of RETT and AERR will also be calculated.

$RETT = \alpha |Mdata - BHT|$, AETT=t+RETT .

To update the value of NHT that is replaced with new *Mdata*. The cluster head broadcasts the CH message, the broadcast packet consists of the sign of CH, cluster head ID, transmitting hop-count K, new NHT, AETT and the residual energy.

Step 4: number nodes. The restraining nodes join into the cluster and change to the "working" state when they received the CH broadcast message. If $K-1>0$, (the value of K comes from the CH broadcast packet), the nodes will modify the hop-count K and forward this message. If the value of ID and AETT is same to the former, the message will be dropped. If the nodes what already change to the working state receive the different CH broadcast message, they will decided to join some cluster according to the severity degree, hop count and the residual energy of cluster head.

Step 5: When some emergent event occurs, the first cluster will be formed in event area regarding the first node activated as its cluster head at once. In order to avoid the redundant cluster, the nodes which have been cluster head can't be into exciting state again, and the member node in the first cluster can't be the other cluster head, when they are activated by the same event.

Step 6: If t > AETT, which means that the exciting time of the cluster head is over, the cluster will be released. And the cluster head and the member nodes will get back

to the restraining state. If some new emergent event occurs, the nodes will compete to be a cluster head over again. An example of dynamic clustering based on event severity degree in some time is shown in fig.1. The sink node is denoted with green, the cluster head is denoted with blue, and others are member nodes.

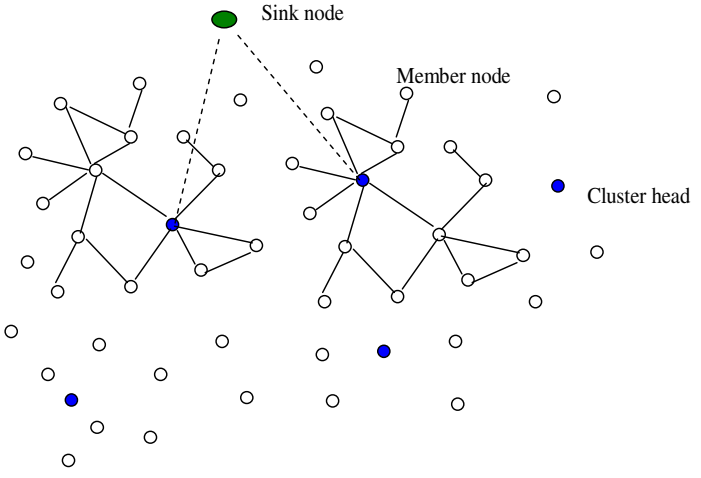

Fig. 1. An example for dynamic clustering based on event severity degree

3.2 Minimum Delay Aggregation Path

After the clusters are formed in wireless sensor networks, the member nodes can collect data, and transmit to the upper layer nodes if Mdata>BHT && | Mdata-NHT|>=ST with some communicating path. For a multi-hop cluster, the member nodes can not only collect data, also can fuse and forward the data. There are multiple paths from the source nodes to cluster head. In the paper, we present the minimum delay aggregation path to minimize the network delay. The most important factor is the fusion timing mechanism in data fusion algorithm. Here, we regard all member nodes as the fusing nodes. The waiting time is used to determine when data fusion begins and ends in the node. The waiting time of one fusing node *i* can be defined in the following (6):

$$wt(i) = \alpha \frac{d_i}{k_i} \qquad (i \in M), \tag{6}$$

Where k_i is the hop-count from node *i* to its cluster head, d_i is the degree of node *i,* α is regarded as the waiting timing coefficient, which will be set to some constant according to the actual demand. M is the number of member nodes in this cluster. The equation (6) show that the waiting time increases with the degree of the nodes. Larger d_i indicate more amount data from node *i*. To ensure the integrality of data, long

waiting time should be given. At the same time, larger k_i show that node *i* is far from the cluster head, the waiting time will be set shorter so that the data can be transmit more quickly. It just has a tradeoff between the integrality of data and delay.

The total waiting time of the fusing path equals to the sum of the waiting time (wt(i)) of all nodes in this path. With the following equation (7), we can calculate the delay of all paths, and get the minimal delay path.

$$D = \min \sum_{l} \sum_{i=1}^{k} wt(i) . \tag{7}$$

4 Simulation and Analysis

4.1 Simulation Setup

To evaluate the performances of the proposed algorithm, we simulated it in NS-2.27, and compared to LEACH and TEEN. The simulation parameters are set up in Table 1.

Table 1. Experiment parameters

Parameters	*Scenes*
Monitoring areas	100m×100m
the numbers of nodes	100
The initial energy	2J
The number of cluster head	%5
The location of base station	(50, 250)
The length of data	512bytes
The number of emergent	20
$E_{threshold}$	0.01J
E_{elec}	50nJ
E_{amp}	100pJ/bit/m^2

4.2 Energy Consumption

One of the most important goals of data fusion in-network is to save energy by reducing the amount of transmitting data packets. The average energy consumption of all nodes in LEACH, TEEN, and EDMDP is shown in fig.2. When the same emergent event occurs, the average energy consumption in EDMDP is less than that in LEACH and TEEN remarkably. For LEACH and TEEN, the clustering is not correlative to the emergent event, especially, the cluster head is selected with random probability. The data can not be fused in the event area in a good time. Moreover the periodic clustering also consumes more energy. The clusters are formed only when some emergent event occurs in EDMDP. And the nodes joining into clustering are just those in event area. The scale and lifetime is not periodic, just determined by the event severity degree. The clusters are released after the event ends.

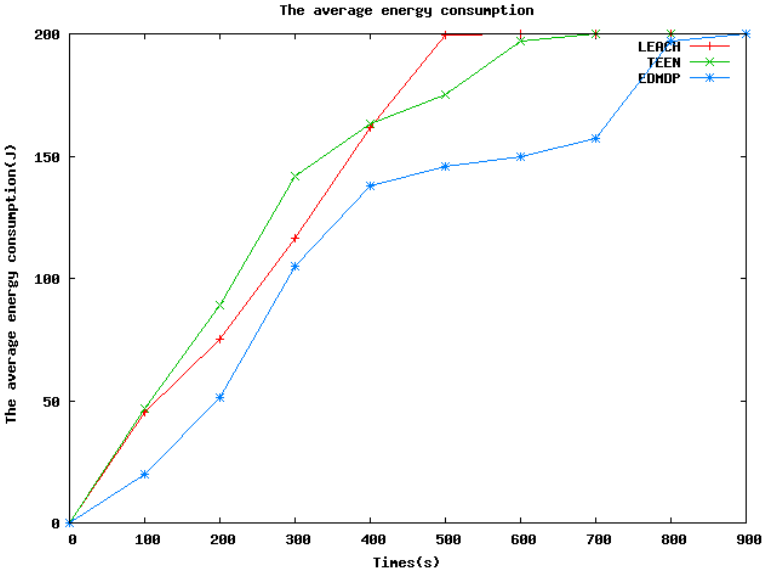

Fig. 2. The average energy consumption in LEACH, TEEN and EDMDP

The number of live nodes is shown in fig.3. From the figure, we find that the TEEN and EDMDP have the similar death rate of nodes before 300 seconds. With more emergent event, EDMDP gives a good live rate of nodes, because event-driven dynamic clustering is just triggered by the emergent event. The nodes don't need to monitor the area and transmit the data periodically, which will decrease the energy consumption. So after 350 seconds, EDMDP is better than TEEN in death rate of nodes. LEACH is better than EDMDP before 550 seconds, but there's a sharp drop after 550 seconds. EDMDP has a longer lifetime, in which the final nodes die until 900 seconds.

4.3 Network Delay

When some node wants to fuse data, it need wait to receive the data from other nodes. If more nodes regard it as the route node, it will wait more long time. So the minimum delay fusing delay path is obtained to fuse and transmit with the minimum delay. Comparing to the other data fusion method based on reducing network delay, EDMDP can choose the path dynamically, just with the acutal minimum delay. At the same time, the cluster structure of network is not destroyed. The network delay varying with the simulation time is shown in Fig.4. In LEACH, all member nodes send their sensing data to the cluster head with single-hop in which the delay mainly comes from the cluster head. The cluster fuses data with some period. In our proposed algorithm, all member nodes can fuse the data with a waiting time. The total delay is much more than LEACH. Comparing to GART[15], EDMDP has a lower delay which will not vary obviously with the increasing of number in emergent event area, because the minimum delay path is always selected according to the total waiting time.

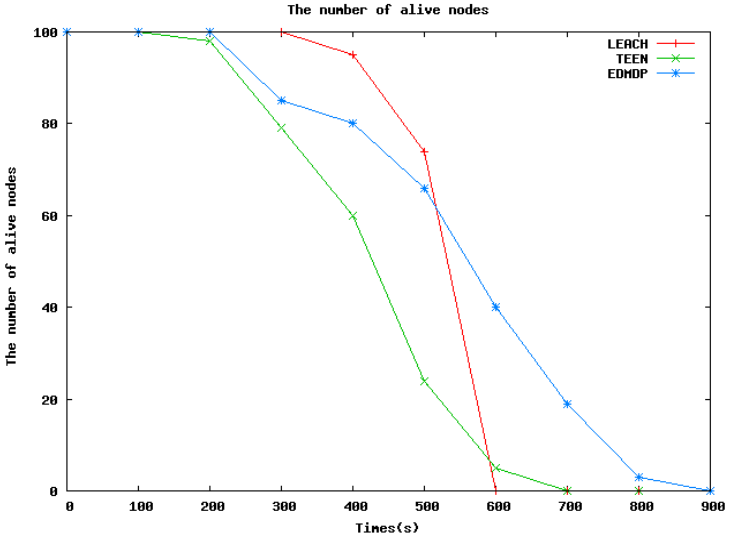

Fig. 3. The number of live nodes in LEACH, TEEN and EDMDP

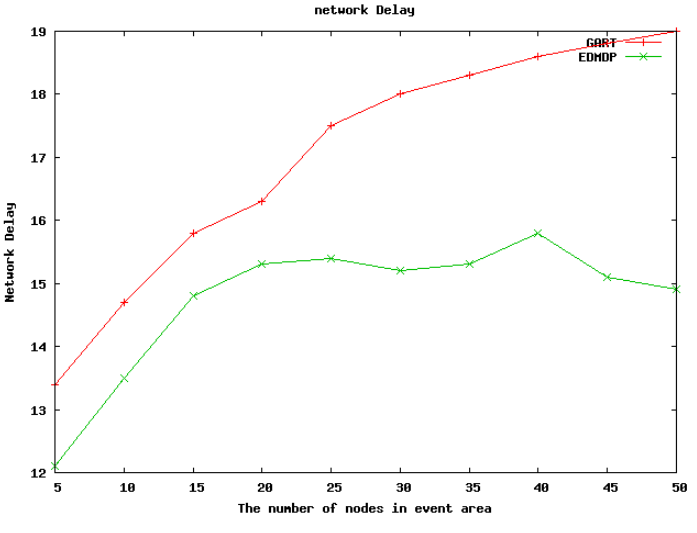

Fig. 4. The network delay in EDMDP

5 Conclusions

Event-driven wireless sensor network is an appropriate application in emergent event detection. Taking energy consumption and network delay into consideration, we present a new data fusion algorithm based on event-driven and minimum delay aggregation path

for monitoring emergencies, in which dynamic clustering method based on emergent event severity degree are proposed, and the minimum delay aggregation path is achieved by calculating the total waiting time of all node in the paths, under the consideration of the hop-count and the degree of member nodes. The experimental results show that our algorithm has a better performance, comparing to the other data fusion method. The more residual energy indicates that dynamic clustering method can reduce energy consumption remarkably, to prolong the network lifetime. What's more, there is a lower network delay in our algorithm. In the future, we will do more work on optimizing the waiting time, taking more factors into consideration, such as data veracity and time synchronization precision.

References

1. Heinzelman, W.R., Chandrakasan, A., Balakrishnan, H.: Energy-efficient Communication Protocol for Wireless Micro-sensor Network. In: Proc. of the 33rd Intl Conf on System Science, pp. 1–10 (2000)
2. Manjeshwar, A., Agrawal, D.P.: TEEN: A Routing Protocol for Enhanced Efficiency in Wireless Sensor Network. In Proc of the first Intl Workshop on Parallel and Distributed Computing Issues in Wireless Networks and Mobile Computing (2001)
3. Krishnamachari, B., Estrin, D., Wicker, S.: Modeling Data-Centric Routing in Wireless Sensor Networks. In: Proc. of IEEE Infocom (2002)
4. Sanli, H.O., Suat, O., Hasan, C., et al.: SRDA: Secure Reference-Based Data Aggregation Protocol for Wireless Sensor Networks. In: Proc. of IEEE VTC Fall 2004 Conference, pp. 4650–4654. IEEE Society Press, New York (2004)
5. Haowen, C., Adrian, P., Bartosz, P., et al.: SIA: Secure Information Aggregation in Sensor Networks. In: Proc. of the first ACM Conference on Embedded Networked System, pp. 255–265. ACM Press, New York (2003)
6. Nisheeth, S., Chiranjeeb, B., Divyakant, A.: Medians and Beyond: New Aggregation Techniques for Sensor Networks. In: Proc. of the second ACM Conf on Embedded Networked Sensor Systems, Baltimore, pp. 239–249 (2004)
7. Shipa, D.: Energy Aware Topology Control Protocols for Wireless Sensor Networks. University of Calcutta, India (2005)
8. Melmet, C.V., Ozgur, B.A., Ian, F.A.: Spatiotemporal Correlation: Theory and Applications for Wireless Snsor Networks. Computer Networks 45, 245–259 (2004)
9. Tang, Y., Zhou, T.M.: Study on the Event Correlativity in Large Scale Wireless Sensor Network. Computer Science 34(9), 356–359 (2007)
10. Zhu, Y.J., Vedantham, R., Park, S.J.: A Scalable Correlation Aware Aggregation Strategy for Wireless Sensor Networks. In: Proc. of IEEE International Conference on Wireless Internet (WICON), Budapest (2005)
11. Ignacio, S., Katia, O.: The Impact of Timing in Data Aggregation for Sensor Networks. Proc. of IEEE International Conference on Communications, 3640–3645 (2004)
12. Ignacio, S., Katia, O.: In-network Aggregation Trade-offs for Data Collection in Wireless Sensor Networks. International Journal of Sensor Networks 1(3/4), 200–212 (2006)
13. Yuan, W., Srikanth, V.K., Satish, K.T.: Synchronization of Multiple Levels of Data Fusion in Wireless Sensor Networks. In: Proc. of Global Telecommunications conference, pp. 223–225 (2003)

14. Hu, F., Cao, X.J., May, C.: Optimized Scheduling for Data Aggregation in Wireless Sensor Networks. In: Proc. of the 9th International Symposium on Computers and Communications, pp. 200–225 (2004)
15. Wang, J.T., Xu, J.D., Yu, H.X.: Group aware real-time data aggregation tree algorithm in wireless sensor networks. Chinese Journal of Sensors and Actuators 21(10), 1760–1764 (2008)
16. Duan, B., Ke, X., Huang, F.W.: An Aggregate Contribution Based Delay-Time Allocation Algorithm for Wireless Sensor Networks. Journal of Computer Research and Development 45(1), 34–40 (2008)

Handling Multi-channel Hidden Terminals Using a Single Interface in Cognitive Radio Networks

Liang Shan and Myung Kyun Kim*

Computer Network Lab, University of Ulsan,
Mugoo-Dong, Nam-Ku, Ulsan, Republic of Korea
shangliang718@yahoo.com.cn, mkkim@ulsan.ac.kr

Abstract. Cognitive networks enable efficient sharing of the radio spectrum. Multi-hop cognitive network is a cooperative network in which cognitive users take help of their neighbors to forward data to the destination. Control signals exchanged through a common control channel (CCC) to enable cooperation communication. But, using a common control channel introduces a new issue like channel saturation which degrades the overall performance of the network. Moreover, the multi-channel hidden terminal problem will be another important challenge in cognitive radio networks, in which the multi-channel hidden terminals can decrease the throughput, cause much overhead, and sometimes even make the whole network invalidated. In this paper, a novel MAC protocol to resolve the multi-channel hidden terminal problem using a single interface which avoid using the CCC.

Keywords: Cognitive Radio Networks, Multichannel Hidden Terminal Problem, Single Interface, Synchronization.

1 Introduction

A cognitive network is an opportunistic network. *Spectrum opportunity* deals with the usage of an available (free) channel that is a part of the spectrum which is not currently used by primary users [1]. The licensed owner of a frequency band is called a *primary user* and the one who utilizes spectrum opportunities for communication is called a *secondary user*. When the receiver is not in the transmission range of the sender, data is forwarded through several hops forming a Multi-Hop Cognitive Radio Network (MHCRN). But unlike in a normal multi-hop network in which all users operate in the same channel, users in a MHCRN use different frequencies depending on spectrum availability. As a result, all users are connected depending on whether they have a common frequency band for operation.

A MHCRN is, in many ways, similar to a multi-channel network. In both networks, each user has a set of channels available for communication. When two users want to communicate, they negotiate via a common control channel (CCC)

* Corresponding author.

D.-S. Huang et al. (Eds.): ICIC 2009, LNAI 5755, pp. 1039–1048, 2009.

to select a communicating channel. Two major differences in these two network environments are:

a) the number of channels available at each node is fixed in a multi-channel network whereas it is a variable in a MHCRN. It is possible that a user has no available channel at all due to the complete occupancy of the spectrum by primary users.
b) in general, the channels in a multi-channel environment have equal transmission ranges and bandwidths unlike in a MHCRN in which the environment is heterogeneous.

Thus, a MHCRN is a combination of a multi-hop and a multi-channel network. The protocols used in multi-channel networks cannot be applied to a MHCRN due to the above mentioned differences in the two networks. However, the issues and challenges related to these networks apply to a MHCRN as well. For example, CCC and multi-channel hidden terminal problems [2], [5], [6] which are related to a multi-channel network are common to a MHCRN.

In this paper, a novel MAC protocol for MHCRNs is proposed, which avoids the need of a dedicated CCC and solves the multi-channel hidden terminal problem, only using a single interface. The main techniques are using a novel channel structure to fully exploit the multiple channels available in a scalable manner for communication, channel switching and periodic resynchronization.

Firstly, we use the default channel for nodes which randomly choosed by themselves and each node can know its two hops neighbors' information by gathering the control signal (i.e. ATIM message which is employed in IEEE 802.11 PSM,) from its neighbors. Each superframe is comprised of two consecutive parts: the Control signal Transfer Period (CTP) and the Data Transfer Period (DTP). At the beginning of each Control signal Transfer Period (CTP), all nodes in the corresponding channel listen to the channel, represents for exchanging control signals. Thus, all nodes in the network are synchronized. It can switch to another channel for transmitting out of the CTP for some requirements such as avoid multi-channel hidden terminals, QoS and load balancing of the network. After transmitting, the interface should be switched back to the default channel, periodic resynchronization and update the channel information. To my best knowledge it is the first paper which focus on solving the multi-channel hidden terminal problem using a single radio in cognitive radio networks.

The rest of the paper is organized as follows: Section 2 identifies some of the major issues such as CCC saturation and multi channel hidden terminal problem in a MHCRN. Section 3 reviews existing protocols and discusses the drawbacks. Section 4 describes the proposed MAC layer protocol. Section 5 analyses the protocol and shows the simulation result. Section 6 concludes the paper.

2 Issues in Multi-Hop CR Network

In this section, we describe the common control channel (CCC) problem and briefly explain the multi-channel hidden terminal problem [2], [7], [8] in the context of a MHCRN.

2.1 Common Control Channel Problem

As discussed earlier, all users in a MHCRN are connected if they have a common channel for communication. It is possible that each user has a choice of more than one channel. In that case, the sender and the receiver need to agree upon a common communicating channel which is available to both. The initial handshake signals to negotiate the choice of a common channel are called control signals. But such negotiations require communication over a common signaling channel and in Cognitive Radio (CR) Networks, it is difficult to find an available common channel for all nodes. This is called the common control channel problem.

2.2 Multi-channel Hidden Terminal Problem in MHCRNs

The multi-channel hidden terminal problem was identified in [2], [9] for multi-channel networks. The same problem is extended to a cognitive network environment in [4]. To avoid the references mentioned disadvantages, a MAC protocol which does not need a pre-allotted control channel and which solves the multi-channel hidden terminal problem, is proposed in this paper.

3 Related Work

In [3], a synchronized MAC protocol for multi-hop cognitive radio networks is proposed, which avoids the need of a dedicated CCC and solves the multi-channel hidden terminal problem. In this paper, every node is equipped two radios, one is used for listening and the other is used for transmitting. According to this, the multi-channel hidden terminal problem can be solved ideally, but it also has some disadvantages, the most evidently one is the cost. The benefits brought by multi-channel operation in CR networks, such as higher aggregate throughput and better robustness, should not come at the expense of other factors such as increased cost and complexity.

In [2], the MAC protocol for Ad Hoc Networks requires only a single transceiver per node, but solves the multi-channel hidden terminal problem using temporal synchronization. The simulation result shows that it can not only solve the multi-channel hidden terminal problem but also improve network throughput significantly, but Ad Hoc network is different from CR network. So the scheme used in this paper is not suit for CR network for the requirement of the dynamic character.

4 The Proposed Protocol

4.1 Assumption

In this section, the proposed scheme is presented. Firstly, the assumption is summarized below:

Each node is equipped only a single half-duplex radio. In other words, at any given time a node is capable of either transmitting or receiving, but not both. In addition, a terminal can only send or receive in one channel at a time, in such a way that when the terminal is receiving in one channel, it cannot perform carrier sense in another.

4.2 Default Channel (DC) and Backup Channel (BC)

In the Network initialization state each node randomly choose one of all available channels as the default channel (DC). The DC is used to manage the entire network as follows:

Through DC The following features can be accomplished:

(1) Synchronization:

Nodes that do not send beacons within the DC periodically visit the DC to get resynchronized. This is used to adjust the CTP Start Time of all channels as to make them non-overlapping.

(2) Neighborhood discovery:

It is used to get information about network connectivity by exchanging ATIM or ATIM-ACK messages among its neighbors.

(3) Communication Detection:

Every node can detect as far as two hop neighbors' communication in the network by receiving the ATIM messages from its one hop neighbors. In this way the multi-channel hidden terminals can be addressed.

The conception of BC is employed to make the network connectivity extremely robust. BC's function is that when the DC invalidation it will be instead of DC or help the DC for the out-band-measurement.

There are some substantial control signals a node have to receive in each ATIM Message, (NDC) Name of the Default Channel of the neighbor, if NDC is marked i, it means the neighbor's default channel is channel i, (CPB) Channel Name of Primary user comes Back, if the primary user comes back in channel j, the value of CPB will be j, (NAC) Name of the Available Channel in its neighbor, which contains all available channels name. (NPN) Name of Previous Node i.e. two hop neighbor, (NTC) Name of Transmitting channel on the two hop neighbor at the previous superframe, (NFN) Name of two hop neighbors Forward Nodes in current superframe, it is so called transmission schedule, (NPC) Name of Possible channel a two hop neighbor with its downstream node. The usage of the control signals introduced above will be proposed in the example in section 4.

It should be clear that the function of DC and BC are absolute the same, when the radio locates in their owns.

Moreover, even after nodes are already associated with one DC, they periodically scan other available channels. This is so called out-of-band measurements, which are used to detect the presence of primary users, identify other overlapping DCs, determine a suitable BC.

4.3 Multi-channel Structure

While there is plenty of research in channel structure for single channel MAC, to the best of our knowledge no existing work has addressed this issue from a multi-channel perspective.

Algorithm for determining DC & BC

1) Add a node N_i to the graph G for each user in MHCRN.
2) Set NDC, NPN, NTC, NFN, NPC to NULL
3) Choose an available channel C_i randomly for Ni as the default channel and set the NDC to i then Ni sends a ATIM message in CTP and also listens to the ATIM and ATIM-ACK from nodes N_a, N_b… ,which N_a, N_b… are the neighbors of node N_i on channel C_i.
4) If there is not any data should be transmitted in the default channel then the node continue scan C_q, C_k. C_q and C_k are the other available channels. It can quickly figure out information about the network connectivity.
5) If there is no ATIM and ATIM-ACK it receives on default channel in the first CTP, then the node will choose an available channel randomly again and set NDC from i to j if i is not equal to j, then send the ATIM on C_j (here j can be equal to i) in the CTP on channel C_j, using this way until it receives a ATIM or ATIM-ACK, then C_j is a BC, in this case, it can instead of DC for communication then go to step 4.

To fully exploit the multiple channels available in a scalable manner, the channel structure illustrated in Figure 1. Each channel has its own superframe structure, and out of all the channels in use one is uniquely identified as the DC (channel 2, in Figure 1 – see also Section 4.2). This is in contrast to the channel structure where a superframe is only used in the common channel, hence requiring all network nodes to switch back to the common channel upon the start of every new superframe (which limits scalability). Another added benefit of the channel structured is that it also overcomes the bandwidth wastage for using a common control channel, as beacons can be trans- mitted on any channel and not only on the common channel. Hence, this leads to a better load balancing and allows more time for actual data transfer.

Each superframe is comprised of two consecutive parts: the Control signal Transfer Period (CTP) and the Data Transfer Period (DTP). A distinctive feature of this multi-channel structure is that the CTPs across channels are non-overlapping (see Figure 1). It allows a node to quickly gather information from other channels in an optimized fashion by simply switching channels in repeating order of CTP start time and listening for ATIM message during the CTP. All a node needs is information about which node is located on which channel, this can be efficiently obtained from ATIM message received on the DC channel itself. Notice that, we use the ATIM message only as the control message in the Control signal Transfer Period other than the ATIM window which is employed in IEEE 802.11 PSM, also node will never go to the doze zone for it should continuously sensing on other channel when there was no data for transmission in the default channel.

4.4 Exchange of Control Signals and Data

When any of information events which are shown below occurs, a node should exchange the control signals. To exchange the control signals it chooses DC for communication between itself and its neighbor. If there is not any data required to transfer or receive on the default channel during current super frame, it will choose a BC and

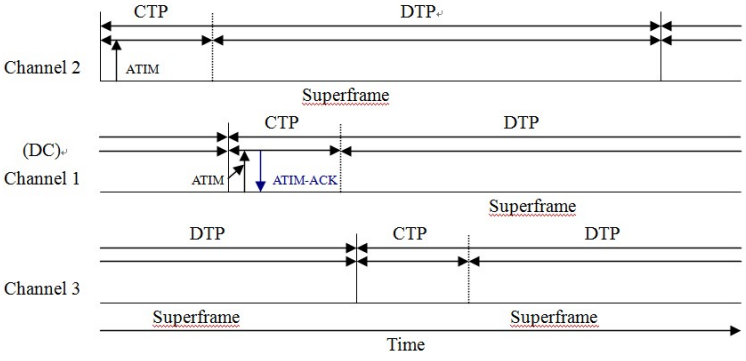

Fig. 1. Multi-channel structure for node A whose available channel are 1,2 and 3

continue try to send the control signal to its neighbors who is on the same channel. The 5 kinds of information events which are:

1) When a new node enters the network, it should notify its arrival to its neighboring nodes.
2) When the available channel list at a node changes due to the primary user traffic.
3) When a node changes its channel for communication
4) When a node wants to communicate with its neighbor
5) When a node receives a ATIM from its previous neighbor it should forward to the other neighbor in the next ATIM window.

4.5 Channel Selection

Contrary to a number of existing multi-channel MAC protocols that include complex channel selection and negotiation schemes, this is not needed in this protocol. Once on a channel, all data communication of a node happens on that channel. If a node wants to communicate in some other channel which is not the DC, it has to first visit the DC. To do it so, nodes have to first announce their impending channel change via ATIM message transmission over the DC. For the receiver who will switch to another channel for communication, it also has to announce its communication channel to all its neighbors. Once the communication pair of nodes switch to the specified channel they should start to transmit data until DTP coming on this channel other than immediately.

4.6 Two-Hop Neighbors Information

In our protocol, nodes are required to transmit a ATIM message during the CTP of a superframe when any of 5 kinds of information events occurred. The node rebroadcasts information that it received from its neighbors in the previous superframe. Thus, nodes have the information about their neighbor's neighbors, such as occupied channel and communication schedules. With this mechanism, it is possible to overcome the multi-channel hidden terminal problem.

The complete process of communication is illustrated with an example. Consider a network of 15 nodes as shown in Fig.2. There are a total of 4 possible channels among them. The array of blocks above each node represents the available channels at that node.

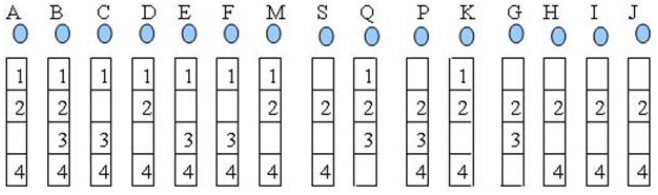

Fig. 2. Fifteen cognitive nodes with a set of free channels at each node

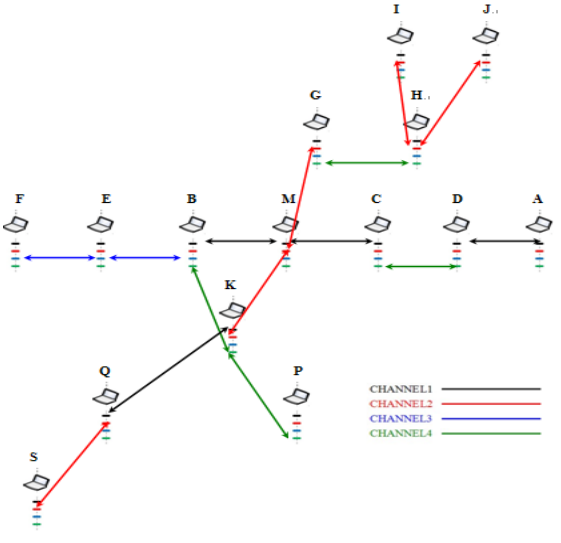

Fig. 3. The default channel between each pair of cognitive nodes

Now, suppose that, node M enters the network. Then it will randomly chooses an available channel according to the available channel list in the block of itself, i.e. 1, 2 and 4. we assume the default channel is channel 4, if it can not receive any ATIM or ATIM-ACK during the CTP, then it will choose an available randomly again out of the CTP in channel 4, and continuously search for its neighbors, using this way, after some time, it will find all its neighbors. In like manner, all nodes in the network find their neighbors and a possible graph of the network connectivity is represented in Fig.3.

In the CTF of the i^{th} superframe, node C sends a ATIM message in which there are some communication information received by node C in the previous superframe i.e. the $i\text{-}1^{th}$ superframe, then it transmits its information to node M (Information Event 5),

the information in ATIM message from node C to M is shown in Fig 4. It reminds node M there is no current primary users come back. In the previous superframe i.e. the i-1th superframe. node D had a communication on the previous superframe, i.e. the i-1th superframe. Node D had a communication on channel 1 and it would communicate with node C in the channel 4, in the ith superframe, which is so called communication schedule. According to this message, node M should avoid to use the channel 4 for communication with its neighbors. Multi-channel hidden terminal problems can be ideally resolved in this manner.

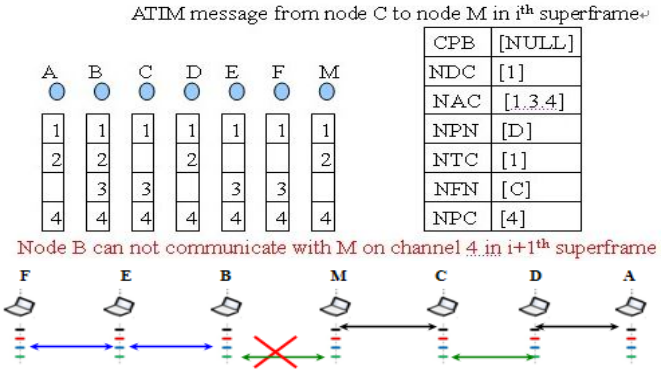

Fig. 4. Addressing the hidden nodes

5 Performance Evaluation

For simulations, we used Qualnet 4.0 simulator. Firstly, to understand the maximum throughput the novel protocol can provide, we consider a single transmitter-receiver pair per channel and assume that the transmitter has infinite frames to send to the receiver till the end of the simulation. We assume the Control signal Transfer Period length to be fixed at 20ms and the superframe size is 100ms. Similar figures as in 802.11a are adopted for this analysis, and so we further assume that the physical data rate per channel is 54 Mbps (as in 802.11a) Figure 5 depicts the maximum MAC throughput achievable for different frame sizes when 1, 2, 3, 4 and 5 channels are available. As expected, larger frame sizes better throughputs because of small overheads. More importantly, we can see that the maximum throughput increases significantly as more channels are added to the network.

Secondly, to do the simulation which our protocol comparing with the 802.11 and the CCC-MAC, 100 nodes are randomly placed in a 500m×500m area. 40 nodes are chosen to be sources and 40 nodes are chosen be destinations. Because of the 802.11 maximum physical data rate is 2Mbps, the physical data rate per channel is also 2Mbps. The transmission range of each node is 250*m* and the length of the superframe is set to 100*ms*. The length of the Control signal Transfer Period is 20 *ms*. We also assume that the packet size is fixed to 1024 bytes. A set of 5 channels is chosen, each

of which is available at each node with a probability of p = 70 %.Each source node generates and transmits constant-bit rate (CBR) traffic. Each data point in the result graphs is an average of 10 runs.

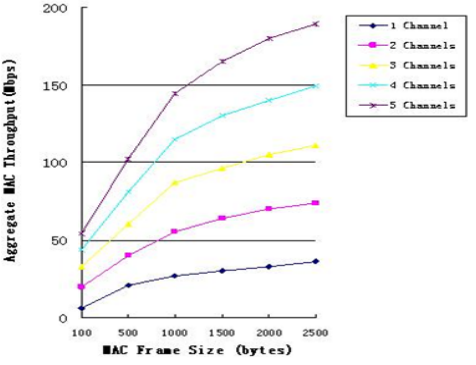

Fig. 5. Maximum MAC throughput VS different frame size

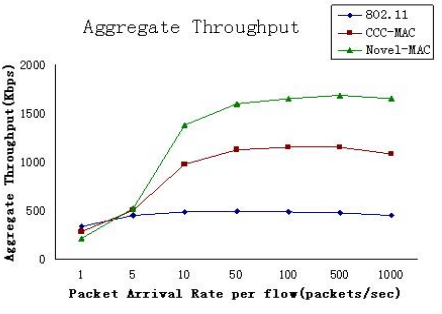

Fig. 6. Aggregate throughput for different protocols

Now we look at results in our multi-hop CRNetwork simulations, a node can be a source for multiple destinations, or it can be a destination for multiple sources. Figure 6 shows the aggregate throughput of different protocols as the network load increases. Five channels are used in Figure 6. In Fig.6, our protocol performs better than CCC-MAC protocol, because in CCC-MAC protocol, if a node has flows to two different destinations, each destination may choose a different channel and one flow may have to wait for an entire beacon interval to negotiate the channel again. Also, if a node is a destination for two flows from other sources, these two flows must be transmitted on the same channel, reducing the benefit of having multiple channels.

As the network load becomes very high, throughput of CCC-MAC protocol drops faster than our protocol. This is because a single control channel is shared by every node in CCC-MAC protocol. When the network load is very high, the collision rate of control packets increases, degrading the throughput. We call this *control channel*

saturation, also in the Cognitive Radio Network, all nodes having the same channels as a control channel is difficult to achieve.

6 Conclusion

In this paper we have presented a MAC protocol for MHCRNs which avoids the need for a common control channel for the entire network. The multi-channel hidden terminal problem is solved only use one transceiver by introducing synchronization and two-hop neighbors' information into the protocol.

Reference

1. Zhao, Q., Sadler, B.M.: A Survey of Dynamic Spectrum Access: Signal Processing, Networking, and Regulatory Policy. IEEE Signal Processing Magazine (2007)
2. So, J., Vaidya, N.: Multi-Channel MAC for Ad Hoc Networks: Handling Multi-Channel Hidden Terminals Using A Single Transceiver. In: Proc. ACM MobiHoc (2004)
3. Kondareddy, Y.R., Agrawal, P.: Synchronized MAC Protocol For Multi-Hop Cognitive Radio Networks Communications, 2008. In: ICC 2008. IEEE International Conference (2008)
4. Nan, H., Yoo, S., Hyon, T.: Distributed Coordinated Spectrum Sharing MAC Protocol for Cognitive Radio. In: IEEE International Symposium on New Frontiers in Dynamic Spectrum Access Networks, pp. 240–249 (2007)
5. Adya, A., Bahl, P., Padhye, J., Wolman, A., Zhou, L.: A multiradio unification protocol for IEEE 802.11 wireless networks. In: Proc. of Broadnets (2004)
6. Alichery, M., Bhatia, R., Li. L.: Joint Channel Assignment and Routing for throughput optimization in Multi-Radio wireless mesh networks. In: ACM MobiCom (2005)
7. Vaidya, N., Kyasanur, P.: Routing and Interface Assignment in Multi-channel Multi-interface Wireless Networks. In: WCNC (2005)
8. Raniwala, A., Chiueh, T.: Architechture and Algorithms for an IEEE 802.11-based Multi-channel Wireless Mesh Network. In: IEEE Infocom (2005)
9. Raniwala, A., Gopalan, K., Chiueh. T.: Centralized Channel Assignment and Routing Algorithms for Multi-Channel Wireless Mesh Networks. ACM SIGMOBILE Mobile Computing and Communications Review 8(2), 50–65 (2004)

Network Construction Using IEC 61400-25 Protocol in Wind Power Plants

Tae O Kim, Jung Woo Kim, and Hong Hee Lee*

School of Electrical Engineering,
University of Ulsan, Nam-Gu, 680749 Ulsan, South Korea
{gskim94,jwkim,hhlee}@mail.ulsan.ac.kr

Abstract. In recent years, the wind power plants are widely developing as an alternative energy source. In order to provide a uniform communications basis for the monitoring and control of wind power plants, IEC 61400-25 has been developed. This paper describes a Web service based network construction using communication protocol stack which is included in IEC 61400-25-4. This system is necessary to implement remote control systems for wind power plants.

Keywords: IEC 6140-25, Wind Power Plants, Web Service, MMS.

1 Introduction

The Wind Power Plants (WPPs) technology has been proved one of the promising generation technologies among the renewable energy sources and globally increases due to its profitability. The wind generator supplies electric power to many part of the power demand. The wind generation technology had been developed consistently in Europe, and the related products are introduced in large numbers by many makers.

Generally, the control center is far away from the WPPs in the wind farm. Furthermore, each wind power generators is installed separately with long distance within the same wind farm. The communication infrastructure is very important to control the system and to monitor the condition of WPPs. In order to keep compatibility with the different maker's devices, the single standard for communication is needed so that the products of the various makers are able to make the mutual communication. In 2006, the communication standard IEC 61400-25 for the supervisory control of the WPPs was announced based on the international standard IEC 61850 of the substation automation system by the IEC technical committee TC 88. Currently, it is published that the IEC 61400-25 standard with the part 1, 2, 3, 4, and 5. The part 6 is under consideration finally and it will be published soon[1].

The new technologies such as the communication structure, the Web browser, the communication protocol have been developed in order to implement the new information model in the automation or the network system in the power system. Moreover, the important researches for construction the information infrastructures for the power systems are progressed actively.

* Corresponding author.

D.-S. Huang et al. (Eds.): ICIC 2009, LNAI 5755, pp. 1049–1058, 2009.

After analysis of the power system disturbances, the work of Xie et al. emphasized on the importance of information systems under the regulated and the competitive environment, for which an information architecture for power systems was proposed[2]. But the work in [2] focuses only on constructing the physical communication architecture without addressing the appropriate information integration required for the proposed information architecture. Qiu et al. discussed the communication issues for the SPID system[3], where An XML-based Client/Server architecture for information exchange was proposed. A new communication architecture called GridStat was proposed in [4]. But this study is limited only to control-related applications in the power systems. Khatib et al. proposed a new internet based Power System Information Network architecture (PSIN) where information in power system was posted in Web pages[5].

In this paper, we survey the various study and efforts to process the information infrastructure and propose the implementation of the supervisory control information system using Web service technologies which are suitable to the wind power generation system. The new information integrating requirement for operation and maintenance of the wind power generation systems are considered. And we also propose the prototype about the framework and Web service-based system to integrate information for the Web service infrastructure in the wind power generation system. The proposed Web service system is an open, flexible, and scalable framework with higher cooperation and integration capability. We perform information exchange between host node and the wind tower to construct the network system of wind power generation facility using MMS communication service and construct the environment to monitor the important information through the Web browser in the remote control center.

2 Network Modeling for Control and Monitoring in WPPs

2.1 Information Model in WPPs

In the basic device of the WPPs, each component member of the system devices (wind turbine, control center, meteorological system, etc.) has been modeled in a data structure which is the logical node. The logical node is a data holder that can hold different types of information related to the respective component. In part 2, the logical device class, the logical node class, data class and theoretical common data class are defined abstractedly based on the logical node defined in IEC 61850-7-2. But it does not provide that compatibility between devices in IEC 61400-25.

Wind farm has several wind towers and each wind tower has brake system, gear box, generator, controller and protection unit inside it. Figure 1 shows logical node of the wind tower. This is modeled as a information model that control and monitoring can be possible about functions and resources combined with the real device of the wind power facility to the communication system of wind farm which is defined in part 2[6].

The logical nodes which are defined in logical device in figure 1 are well known functions and are modeled by virtual model related to real device. In figure 1, LN WROT with rotator of wind tower inside, WGEN with generator, WCNV with converter and WAPC are modeled with a controller.

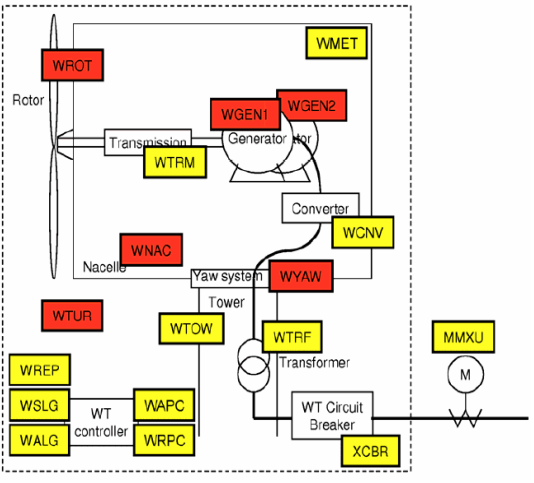

Fig. 1. Wind Tower Logical Nodes

Table 1 shows logical nodes of WPPs. The number of logical node which is defined in IEC 61400-25 is 16. Logical node related to overall WPPs is 5, 12 in wind turbine.

Table 1. Logical Node List for WPPs

LN classes	Description	M/O
WTUR	Wind turbine general information	M
WROT	Wind turbine rotor information	M
WTRM	Wind turbine transmission information	O
WGEN	Wind turbine generator information	M
WCNV	Wind turbine converter information	O
WTRF	Wind turbine transform information	
WNAC	Wind turbine nacelle information	O
WYAW	Wind turbine yawing information	M
WTOW	Wind turbine tower information	O
WMET	Wind power plant meteorological information	M
WALM	Wind power plant alarm information	M
WSLG	Wind turbine state log information	O
WALG	Wind turbine analogue log information	O
WREP	Wind turbine report information	
WAPC	Wind power plant active power control information	
WRPC	Wind power plant reactive power control information	

Service subset of ACSI (Abstract Communication Service Interface) which needs to carry out all exchange of the information within the WPPs is defined in part 3. It describes client certification, transmission of control command, protocol and mechanism of data exchange.

2.2 Mapping of Communication Profile in WPPs

Mapping of communication profile is described in part 4. According to figure 2 the SCSM (Specific Communication Service Mapping) maps the abstract communication

services, objects and parameters to the specific application layers. The wind power plant information models and the information exchange models need to be mapped to appropriate protocols. The protocol TCP/IP is the basic lower layer protocols provided by all mappings. Specific data link and physical layers are beyond the scope of this standard. Depending on the technology of the communication network, these mappings may have different complexities, and some ACSI services may not be supported directly in all mappings but the equivalent services are provided[7].

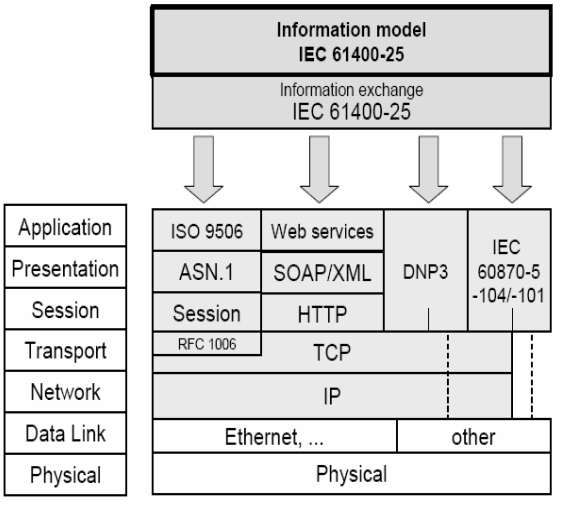

Fig. 2. Mapping and communication profiles

In order to decide the solution which is suitable for monitoring and control application, the mapping which can satisfy supplier and client firstly has to be selected. Moreover, the selected mapping should have conformance fitted for the international standard be selected at least. Recently, the IEC 61400-25-4 standard has been published with the new proposal, which includes the following 5 mapping methods:

- SOAP based Web Services
- OPC/XML-DA
- IEC 61850-8-1 MMS
- IEC 60870-5-104
- DNP 3(Distributed Network Protocol 3)

3 Web Service Based Wind Power System

3.1 Network Based Modeling of WPPs

Wind farm has several wind towers, and brake system, gear box, generator, controller and protection unit are located inside of each wind tower. The method to construct network system which is composed of server and client can be classified into three types such as centralized topology, distributed topology and mixed topology. In this

work, we propose Ethernet method based on centralized topology to construct network system between wind tower and local system. Each wind tower is structurally working as an independent server. Control center collects the information from each wind tower and operates as a server for the remote control center.

3.2 Mapping of Information Model in WPPs

Information model of WPPs is defined from logical node class, data class, data attribute type, DA-Component type. Figure 3 shows information model of WPP using XML schema. The converter as logical node (LN) included in WPP is described and its attribute data which is instant value of 'Generator Frequency' is given 50.1 as 'mag'. This schema (ex. converter) can be used in all services through instance values of WPPs information model.

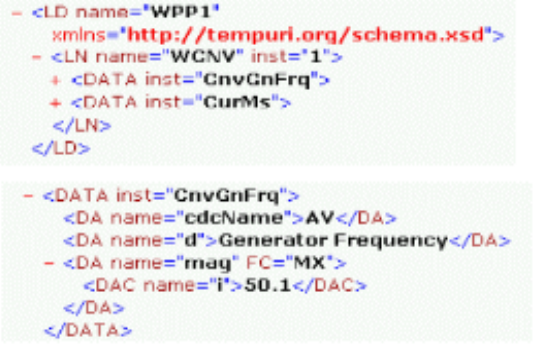

Fig. 3. XML Schema-Information Model of WPP

3.3 Implementation of MMS Service

Figure 4 shows a flow chart to implement MMS service. In the select mode, it is determined if MMs service is working MMS server or MMS client before declaring variables. After initializing memory of each section, the logging parameters of WPP are defined. We set lower 4 layers from OSI 7 layer for MMS service of WPP and MMS object is added. MMS server remains in ready-state response until request of MMS client.

MMS service is implemented using SISCO's MMS-EASE Lite tool. It is used to develop communication services in IEC 61850 based Substation Automation System. But MMS service used in IEC 61400-25 is the same as in IEC 61850 about basic communication method and protocol. Therefore, this work develops MMS service using modified information model and functions with SISCO's tool to apply IEC 61400-25 service. Abstraction model which is defined in IEC 61850-7 should be mapped into application layer. ACSI object of IEC 61850-7-2 should be mapped into IEC 61400-25 MMS object. The VMD, Domain, Named Variable, Named Variable List, Journal, and File management included in information model and the various control blocks are also mapped into the corresponding MMS services.

Figure 5 shows operation window of MMS communication service in IEC 61400-25. This work describes transmission service of various information (frequency,

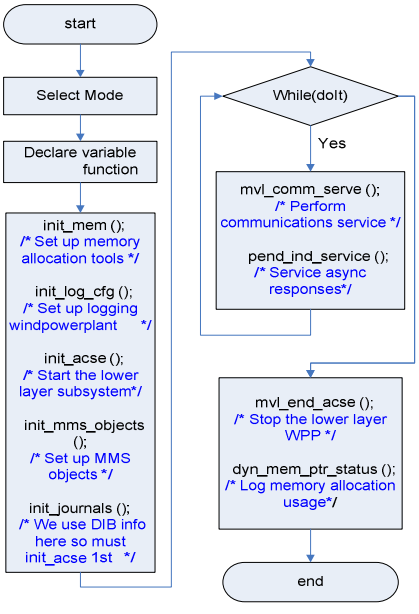

Fig. 4. MMS Service Flow Chart

speed, temperature, etc) between MMS server and client using logical node about rotator, generator and converter which are defined in wind tower.

3.4 Implementation of Web Service

Web service is accessed through SOAP interface and the interface of Web service describes in WSDL. SOAP which is extended technology of XML message protocol is based on Web service. In this work, SOAP server is implemented by using JAVA and Apache Tomcat is used for Web service system. JAVA's SOAP is implemented through AXIS (Apache eXtensible Interactive System). This work develops Web service using AXIS under Tomcat environment. The important thing to implement Web service is as follows:

- Web Service: the software offered on an internet operates to be identical in the different devices.
- XML: XML which is the standard of data exchange makes competition technology communicate and cooperate.
- SOAP: SOAP describes how to communicate between Web services through Internet.
- WSDL: WSDL describes what Web service is and how to access to that.

After JAVA makes SOAP server and creates WSDL using AXIS. Web service server is composed with WSDL. The function which is offered in Web service is described in this WSDL.

Figure 6 shows Web service user interface which performs control and monitoring service to connect local control center through Web browser to client of remote

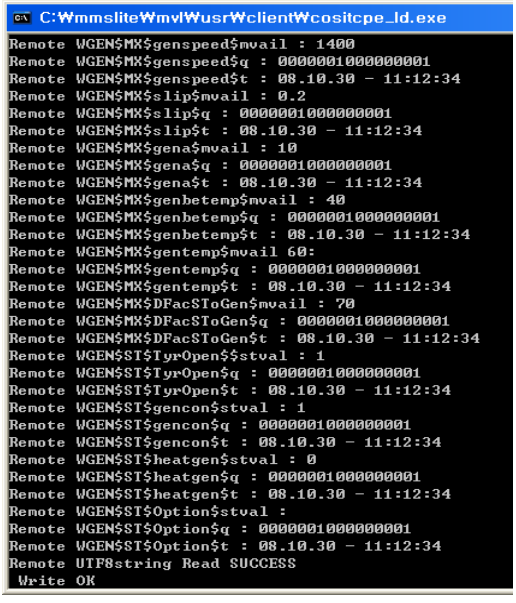

Fig. 5. MMS Communication between Server and Client

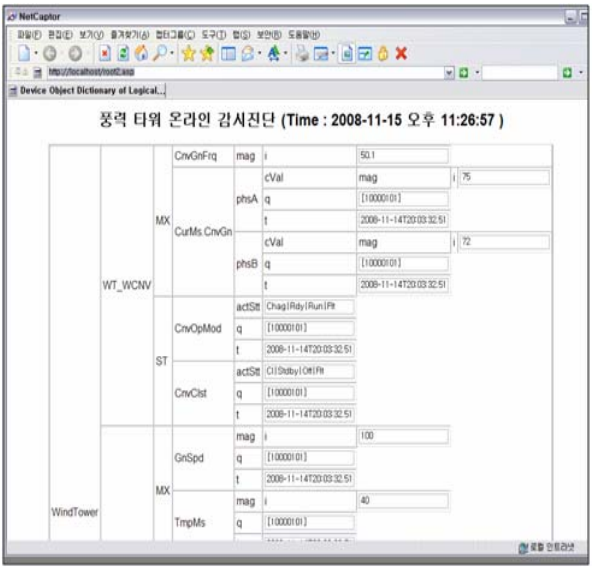

Fig. 6. Web Service using Web Browser

control center. The data of WPP transmitted through MMS communication service are mapped into XML variables of Web server system. The real-time data are transmitted from remote control center to local control center and the data can be confirmed on Web browser through Internet.

4 Experiments and Discussion

Figure 8 shows network construction of control and monitoring system in WPPs. Each wind tower operates as a server, local control center as a client in WPPs. Local

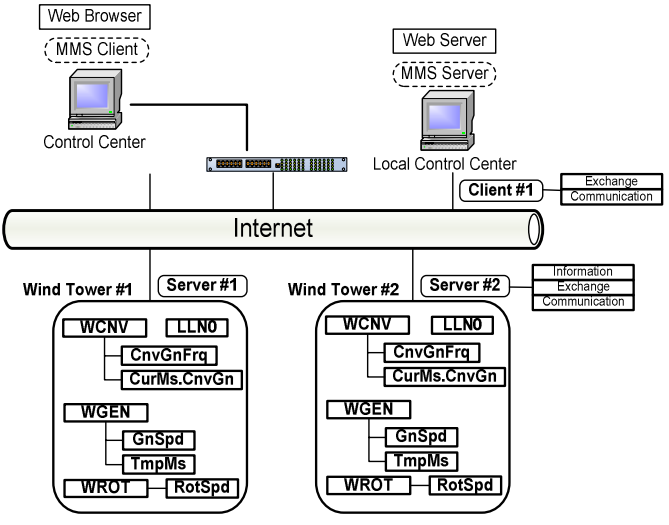

Fig. 7. Network based WPPs System

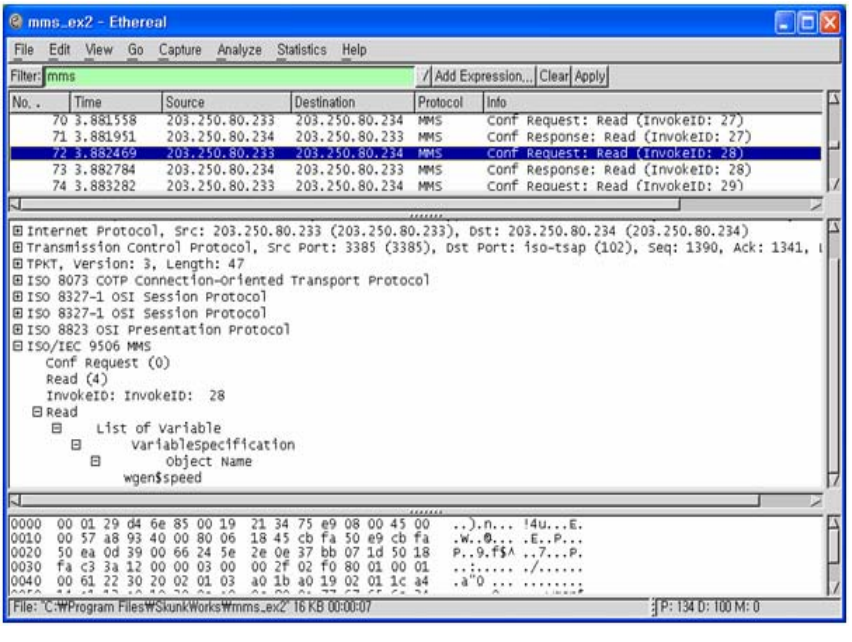

Fig. 8. Analysis of MMS using MMS-Ethereal Tool

control center receives information from wind tower server and operates as a MMS server and Web server for remote control center. Remote control center operates as a MMS client and can monitor information of WPP by connecting Web server of local control center through Web browser. Therefore, the data exchange is required between MMS service and Web service in local control center.

In order to confirm performance of MMS service and data transmission, MMS messages using MMS-Ethereal network analyzer are analyzed and data exchanges between MMS server and client are investigated. Data are exchanged according to the message request and response signal while MMS message are being monitored in Figure 8. It is verified that the variable list and variable values of transmission data are suitable to MMS service request. As shown in Fig. 8, the time from data request to response is lower than 1[ms], and it is enough to control and monitoring in control center. The result of MMS message analysis using MMS network analyzer shows that the proposed Web service works well in PC based IEC 61400-25 communication system.

5 Conclusions

This work develops test bed system using IEC 61400-25 communication protocol which comes from the extended type of IEC 61850 for control and monitoring system of WPPs. MMS communication and XML based Web service are implemented and the Web service to monitor the data of wind tower on the Web browser is realized. To verify the proposed system, we have analyzed MMS message through MMS-Ethereal network analyzer and Web browser, and then the stable operation of network system which is constructed using PC is proved.

Acknowledgment

The authors would like to thank Ministry of Knowledge Economy and Ulsan Metropolitan City which partly supported this research through the Network-based Automation Research Center (NARC) at University of Ulsan.

References

1. International Standard IEC 61400-25, Wind Turbine Generator Systems part 25: Communications for Monitoring and Control of Wind Power Plants, WD edn. (2001)
2. Xie, Z., Manimaran, G., Vittal, V.: An Information Architecture for Funiture Power Systems and Its Reliability Analysis. IEEE Trans. on Power Systems, 857–863 (2002)
3. Qiu, B., Liu, Y., Phadke, A.G.: Communication Infrastructure Design for Strategic Power Infrastructure Defence (SPID) System. In: IEEE Power Engineering Society Winter Meeting, pp. 672–677 (2002)
4. Tomsovic, K., Bakken, D.E., Bose, A.: B.: Designing the Next Generation of Real-Time Control, Communication, and Computations for Large Power Systems. Proceeding of the IEEE 93(5), 965–979 (2005)

5. Khatib, A., Dong, X., Qiu, B., Liu, Y.: Thoughts on Future Internet Based Power System Information Network Architecture. In: Power Engineering Society Summer Meeting, 2000 IEEE, vol. 1, pp. 155–160 (2000)
6. International standard.: WD IEC 61400-25 Wind Turbine Generator Systems Part 25: Communications for Monitoring and Control of Wind Power Plants, First edn. (2003-05)
7. International standard. IEC 61850-7-1: Basic Communication Structure for Substation and Feeder Equipment – Principles and Models, First edn. (2003-05)

Stability and Stabilization of Nonuniform Sampling Systems Using a Matrix Bound of a Matrix Exponential

Young Soo Suh

Dept. of Electrical Eng., University of Ulsan,
Mugeo, Nam-gu, Ulsan, 680-749, Korea
yssuh@ulsan.ac.kr

Abstract. This paper is concerned with stability and stabilization of networked control systems, where sampling intervals are time-varying. A nonuniform sampling system is modeled as a time-varying discrete time system. With the assumption that the sampling time variation bounds are known, the stability condition is derived in the form of linear matrix inequalities. Compared with previous results, a less conservative stability condition is derived using a matrix bound of a matrix exponential.

Keywords: matrix exponential, sampled-data control, networked control systems, linear matrix inequalities.

1 Introduction

In networked control systems, control elements (sensors and actuators) are connected through a network. Since only one node can transmit data over a network, a node must wait until a network is available (*i.e.*, no higher priority data are being transfered). From the viewpoint of a control system, the system can be modeled as a time delay system. The time delay systems have been extensively studied in [1].

On the other hands, some networked control systems can be modeled as a nonuniform sampling system. For example, suppose a node tries to transmit sensor data $y(t)$ at time t_1 and a network is not available until time t_2 ($t_2 > t_1$). At time t_2, instead of transmitting $y(t_1)$ (old data), the current sensor data $y(t_2)$ (new data) can be transmitted. This method was called "try-once-and-discard" in [2]. If the sensor node tries to transmit sensor data periodically with this method, this system can be modeled as a nonuniform sampling system, where sampling intervals are time-varying. One more example is an event-based sampling system [3,4]. Instead of using the periodic sampling, if the sampling is based on the value of output $y(t)$, the sampling interval is time-varying. Thus the system can also be modeled as a nonuniform sampling system.

There are many results about stability and stabilization of a nonuniform sampling systems. The results can be classified into three approaches. The first approach is to model a system as a continuous system with a time-varying input

D.-S. Huang et al. (Eds.): ICIC 2009, LNAI 5755, pp. 1059–1066, 2009.

delay. This input delay methods are proposed in [5,6]. The second approach is to model a system as a hybrid system. The third approach [7], which is most relevant to this paper, is to model a time-varying sampling interval as a parameter variation in a discrete time system. The key technical idea in this approach is to bound a matrix exponential function integral by a scalar function as follows:

$$\| \int_0^\tau \exp Ar \, dr \| \leq s(\tau) \tag{1}$$

where $s(\tau) \in R$.

However, a scalar bound does not exploit the structure of A matrix and a stability condition based on (1) could be conservative. In this paper, a stability condition is derived using the following matrix bound:

$$(\int_0^\tau \exp Ar \, dr)'(\int_0^\tau \exp Ar \, dr) \leq M(\tau) \tag{2}$$

where $M(\tau)$ is a matrix with the compatible dimension.

2 Problem Formulation

Consider the following continuous time linear system

$$\dot{x}(t) = Ax(t) + Bu(t) \tag{3}$$

where $x \in R^n$ is the state and $u \in R^m$ is the control input.

We assume that the state $x(t)$ is sampled at the discrete time instances

$$0 = t_0 < t_1 < \cdots < t_k < \cdots$$

and the control input $u(t)$ is piecewise constant between the discrete time instances:

$$u(t) = Kx(t_k), \ \forall t \in [t_k, t_{k+1}). \tag{4}$$

The sampling interval T_k is defined as

$$T_k \triangleq t_{k+1} - t_k.$$

It is assumed that T_k is time-varying and its lower bound and upper bound are known:

$$0 < T_{min} \leq T_k \leq T_{max}, \quad \forall k. \tag{5}$$

The system (3) and (4) can be written as a time-varying discrete time system:

$$x(t_{k+1}) = G(T_k)x(t_k) \tag{6}$$

where

$$G(T_k) \triangleq \exp(AT_k) + \int_0^{T_k} \exp(Ar)Bdr \, K.$$

Let a nominal point T_{nom} be chosen so that

$$T_{min} \le T_{nom} \le T_{max}. \tag{7}$$

Note that $G(T)$ can be written as

$$G(T) = G(T_{nom}) + \Delta(\tau)Q(T_{nom}) \tag{8}$$

where

$$\begin{aligned} \tau(T, T_{nom}) &\triangleq T - T_{nom} \\ \Delta(\tau) &\triangleq \textstyle\int_0^\tau \exp(Ar)\, dr \\ Q(T_{nom}) &\triangleq A\exp(AT_{nom}) + A\textstyle\int_0^{T_{nom}} \exp(Ar)\, drK + BK. \end{aligned}$$

From the assumption (5), note that τ satisfies

$$T_{min} - T_{nom} \le \tau(T, T_{nom}) \le T_{max} - T_{nom}. \tag{9}$$

We will treat Δ as a uncertainty matrix whose matrix bound is given. In Lemma 1, a matrix bound of $\Delta(\tau)'\Delta(\tau)$ is derived for $\tau_1 \le \tau \le \tau_2$, where τ_1 and τ_2 are the same sign. In Lemma 2, a matrix bound of $\Delta(\tau)'\Delta(\tau)$ is derived for $-\tau_l \le \tau \le \tau_u$, where $\tau_l > 0$ and $\tau_u > 0$.

Lemma 1. *Let $\bar{\beta}$ be a constant satisfying*

$$\|\int_0^\tau \exp(At)\, dt\|_2 \le \bar{\beta}, \quad -\frac{\tau_2 - \tau_1}{2} \le \tau \le \frac{\tau_2 - \tau_1}{2}. \tag{10}$$

Let $R_1(\tau_1, \tau_2)$ and $R_3(\tau_1, \tau_2)$ be defined by

$$R_1(\tau_1, \tau_2) \triangleq \int_0^{\frac{\tau_2+\tau_1}{2}} \exp(Ar)\, dr, \quad R_3(\tau_1, \tau_2) \triangleq \exp(A\frac{\tau_2 + \tau_1}{2}).$$

If there exist $M = M' \in R^{n\times n} > 0$ and $\epsilon \in R > 0$ such that

$$L(M, \tau_1, \tau_2, \bar{\beta}, \epsilon) \triangleq \begin{bmatrix} -M + (1+\epsilon)R_1'R_1 + \bar{\beta}^2 R_3'R_3 & R_3' \\ R_3 & -\frac{\epsilon}{\bar{\beta}^2}I \end{bmatrix} < 0, \tag{11}$$

then

$$\left(\int_0^\tau \exp(Ar)\, dr\right)' \left(\int_0^\tau \exp(Ar)\, dr\right) \le M, \quad \tau_1 \le \tau \le \tau_2 \tag{12}$$

where $\tau_1\tau_2 \ge 0$ (i.e., τ_1 and τ_2 do not have different signs.)

Proof. Note that

$$\begin{aligned} \textstyle\int_0^\tau \exp(Ar)\, dr &= \textstyle\int_0^{\frac{\tau_2+\tau_1}{2}} \exp(Ar)\, dr + \int_{\frac{\tau_2+\tau_1}{2}}^\tau \exp(Ar)\, dr \\ &= R_1 + R_2R_3 \end{aligned} \tag{13}$$

where $R_2(\tau_1, \tau_2, \tau)$ is defined by

$$R_2(\tau_1, \tau_2, \tau) = \int_0^{\tau - \frac{\tau_1+\tau_2}{2}} \exp(Ar)\, dr.$$

Using R_1, R_2, and R_3, we have the following:

$$\begin{aligned} &\left(\int_0^\tau \exp(Ar)\, dr\right)' \left(\int_0^\tau \exp(Ar)\, dr\right) \\ &= (R_1 + R_2 R_3)'(R_1 + R_2 R_3) \\ &= R_1' R_1 + R_3' R_2' R_2 R_3 + R_3' R_2' R_1 + R_1' R_2 R_3. \end{aligned} \tag{14}$$

If $\tau_1 \le \tau \le \tau_2$, we have

$$-\frac{\tau_2 - \tau_1}{2} \le \tau - \frac{\tau_1 + \tau_2}{2} \le \frac{\tau_2 - \tau_1}{2}$$

and from (10), we have

$$R_2' R_2 \le \bar{\beta}^2 I. \tag{15}$$

Inserting (15) into (14), we obtain

$$\left(\int_0^\tau \exp(Ar)\, dr\right)' \left(\int_0^\tau \exp(Ar)\, dr\right) \le R_1' R_1 + \bar{\beta}^2 R_3' R_3 + R_3' R_2' R_1 + R_1' R_2 R_3. \tag{16}$$

Using the following inequality

$$R_3' R_2' R_1 + R_1' R_2 R_3 \le \epsilon R_3' R_3 + \frac{\bar{\beta}^2}{\epsilon} R_1' R_1$$

for any $\epsilon > 0$, we have

$$\left(\int_0^\tau \exp(Ar)\, dr\right)' \left(\int_0^\tau \exp(Ar)\, dr\right) \le R_1' R_1 + \bar{\beta}^2 R_3' R_3 + \epsilon R_3' R_3 + \frac{\bar{\beta}^2}{\epsilon} R_1' R_1 < M \tag{17}$$

for any $\epsilon > 0$. Applying the Schur complement, we obtain (11). □

To derive a less conservative matrix bound, the interval $[-\tau_l, \tau_u]$ is divided into several partitions (see Fig. 1):

$$\begin{aligned} \tau_{l,i} &\triangleq -\tau_l + i\tfrac{\tau_l}{N_1} \\ \tau_{u,i} &\triangleq i\tfrac{\tau_u}{N_u} \end{aligned}$$

Based on this partition, a less conservative matrix bound is derived in Lemma 2.

Lemma 2. *Assume that $\tau_l > 0$ and $\tau_u > 0$. Let β_l and β_u be constants satisfying*

$$\begin{aligned} &\left\|\int_0^\tau \exp(Ar)\, dr\right\|_2 \le \beta_l, \ \ |\tau| \le \tfrac{\tau_l}{2N_l} \\ &\left\|\int_0^\tau \exp(Ar)\, dr\right\|_2 \le \beta_u, \ \ |\tau| \le \tfrac{\tau_u}{2N_u}. \end{aligned} \tag{18}$$

If there exist $M = M' \in R^{n\times n} > 0$, $\epsilon_{l,i} \in R > 0$ $(i = 1, \cdots, N_l)$, and $\epsilon_{u,i} \in R > 0$ $(i = 1, \cdots, N_u)$

$$\begin{aligned} &L(M, \tau_{l,i-1}, \tau_{l,i}, \beta_l, \epsilon_{l,i}) < 0, \quad i = 1, \cdots, N_1 \\ &L(M, \tau_{u,i-1}, \tau_{u,i}, \beta_u, \epsilon_{u,i}) < 0, \quad i = 1, \cdots, N_u \end{aligned} \tag{19}$$

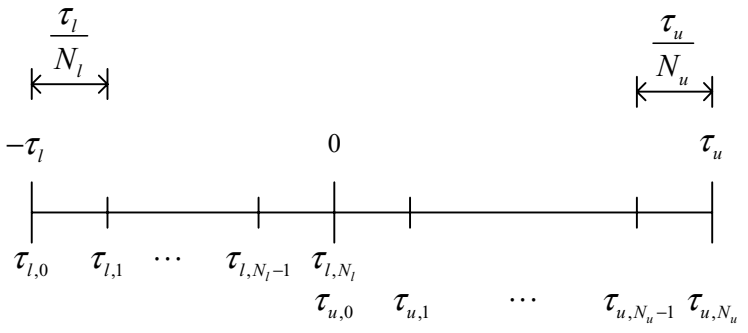

Fig. 1. Partitioning of the interval

then

$$\left(\int_0^\tau \exp(Ar)\,dr\right)' \left(\int_0^\tau \exp(Ar)\,dr\right) \le M, \quad -\tau_l \le \tau \le \tau_u. \tag{20}$$

Proof. From Lemma 1,

$$L(M, \tau_{l,i-1}, \tau_{l,i}, \beta_l, \epsilon_{l,i}) < 0$$

implies that

$$\left(\int_0^\tau \exp(Ar)\,dr\right)' \left(\int_0^\tau \exp(Ar)\,dr\right) \le M, \quad -\tau_{l,i-1} \le \tau \le \tau_{l,i}.$$

Thus N_l inequalities in the first row of (19) imply

$$\left(\int_0^\tau \exp(Ar)\,dr\right)' \left(\int_0^\tau \exp(Ar)\,dr\right) \le M, \quad -\tau_l \le \tau \le 0. \tag{21}$$

Similarly N_u inequalities in the second row of (19) imply

$$\left(\int_0^\tau \exp(Ar)\,dr\right)' \left(\int_0^\tau \exp(Ar)\,dr\right) \le M, \quad 0 \le \tau \le \tau_u. \tag{22}$$

Combining (21) and (22), we obtain (20). □

3 Stability and Stabilization

In the next theorem, the stability condition of (3) is derived.

Theorem 1. *Let M be derived from (19) with*

$$\tau_l = T_{nom} - T_{min}, \quad \tau_u = T_{max} - T_{nom}.$$

If there exist $P = P' \in R^{n\times n} > 0$ *and* $\epsilon \in R > 0$ *satisfying the following*

$$\begin{bmatrix} -P & \star & \star \\ G(T_{nom})P & -P+\epsilon I & \star \\ QP & 0 & -\epsilon M^{-1} \end{bmatrix} < 0, \tag{23}$$

then the system (3) with the feedback control (4) is stable for any sampling intervals satisfying (5). In (23), $\star$ *denotes symmetric elements of the matrix.*

Proof. The system is stable if there exists $P = P' > 0$ satisfying the following inequality:

$$\begin{bmatrix} -P & \star \\ G(T_{nom})P + \Delta(\tau)QP & -P \end{bmatrix} < 0 \tag{24}$$

for all τ satisfying (9). Note that (24) can be rewritten as follows:

$$\begin{bmatrix} -P & PG(T_{nom})' \\ G(T_{nom}) & -P \end{bmatrix} + R\Delta(\tau)S + S'\Delta(\tau)'R' < 0 \tag{25}$$

where

$$R \triangleq \begin{bmatrix} 0 \\ I \end{bmatrix} \quad S \triangleq \begin{bmatrix} QP\, 0 \end{bmatrix}.$$

We use the following inequality: if $\Delta'\Delta \le M$, then

$$R\Delta S + S'\Delta' R' \le \epsilon RR' + \frac{1}{\epsilon}S'MS \tag{26}$$

for any $\epsilon > 0$. Invoking (26) in (25), we have for any $\epsilon > 0$

$$\begin{bmatrix} -P & \star \\ G(T_{nom})P + \Delta(\tau)QP & -P \end{bmatrix} \le \begin{bmatrix} -P & PG(T_{nom})' \\ G(T_{nom}) & -P \end{bmatrix} + \epsilon RR' + \frac{1}{\epsilon}S'MS < 0. \tag{27}$$

Applying the Schur complement, we obtain (23). Thus (23) guarantee the stability for any τ satisfying (9). □

Now a stabilization problem (*i.e.*, finding K) is given in the next theorem.

Theorem 2. *If there exist* $P = P' > 0 \in R^{n\times n}$, $\epsilon \in R > 0$, *and* $Z \in R^{m\times n}$ *satisfying*

$$\begin{bmatrix} -P & \star & \star \\ \Gamma & -P+\epsilon I & \star \\ A\Gamma + BZ & 0 & -\epsilon M^{-1} \end{bmatrix} < 0 \tag{28}$$

with

$$\Gamma = \exp(AT_{nom}) + \int_0^{T_{nom}} \exp(Ar)Bdr\, Z,$$

then the feedback controller $K = ZP^{-1}$ *stabilizes the system (3) for any sampling intervals satisfying (5).*

Proof. The proof is immediate by letting $Z = KP$ in (23).

4 Simulation

To verify the proposed stability condition, we consider the following system

$$A = \begin{bmatrix} 0 & 1 \\ 0 & -0.1 \end{bmatrix}, \; B = \begin{bmatrix} 0 \\ 0.1 \end{bmatrix}, \; K = \begin{bmatrix} -3.75 \\ -11.5 \end{bmatrix}.$$

This system was considered in [8] and also considered in [7,9].

Comparison with existing stability conditions are given in Table 1. The result of the proposed stability condition is "Result 7", where we can see the stability condition is less conservative than the existing ones. We note that the stability condition can be further improved by partitioning the interval as in [10].

Table 1. Largest stable T_{max} comparison

	largest stable T_{max}
Result 1 [5]	0.869
Result 2 [7]	1.113
Result 3 [11] ($T_{min} = 0.3$)	1.283
Result 4 (constant sampling interval assumption) [7]	1.327
Result 5 [10] ($N = 1$)	1.335
Result 6 [9]	1.365
Result 7 (proposed result with $N_u = N_l = 4$ and $T_{min} = 0.3$)	1.583
Result 8 (analytic result with constant sampling interval assumption)	1.729

5 Conclusion

By using a matrix bound (instead of a scalar bound) of a matrix exponential, we have derived a new stability condition for a nonuniform sampling system. Through the numerical simulation, it is shown that the proposed stability condition is less conservative than the existing results.

Acknowledgment

This work was supported by the Korea Research Foundation(KRF) grant funded by the Korea government (MEST) (No. 2009-0067447).

References

1. Niculescu, S.I.: Delay Effects on Stability. Springer, Heidelberg (2001)
2. Walsh, G.C., Ye, H.: Scheduling of Networked Control Systems. IEEE Control Systems Magazine 21, 57–65 (2001)
3. Miskowicz, M.: Send-on-delta Concept: An Event-based Data Reporting Strategy. Sensors 65, 49–63 (2006)

4. Suh, Y.S., Nguyen, V.H., Ro, Y.S.: Modified Kalman Filter for Networked Monitoring Systems Employing a Send-on-delta Method. Automatica 43, 332–338 (2007)
5. Fridman, E., Seuret, A., Richard, J.P.: Robust Sampled-data Stabilization of Linear Systems: an Input Delay Approach. Automatica 40, 1441–1446 (2004)
6. Hu, L.S., Bai, T., Shi, P., Wu, Z.: Sampled-data Control of Networked Linear Control Systems. Automatica 43, 903–911 (2007)
7. Naghshtabrizi, P., Hespanha, J.P., Teel, A.R.: On the Robust Stability and Stabilization of Sampled-data Systems: A Hybrid System Approach. In: Proc. of the 45th IEEE Conference on Decision and Control, pp. 4873–4878. IEEE Press, New York (2006)
8. Zhang, W., Branicky, M.S., Phillips, S.M.: Stability of Networked Control Systems. IEEE Control Systems Magazine 21, 84–99 (2001)
9. Mirkin, L.: Some Remarks on the Use of Time-varying Delay to Model Sample-and-hold Circuits. IEEE Trans. Automat. Contr. 52, 1109–1112 (2007)
10. Suh, Y.S.: Stability and Stabilization of Nonuniform Sampling Systems. Automatica 12, 3222–3226 (2008)
11. Fujioka, H.: Stability Analysis for a Class of Networked/Embedded Control Systems: A discrete-time Approach. In: Proceedings of American Control Conference, pp. 4997–5002. IEEE Press, New York (2008)

Implementation of Induction Motor Control System Using Matrix Converter Based on CAN Network and Dual-Port RAM

Hong-Hee Lee* and Hoang M. Nguyen

School of Electrical Engineering, University of Ulsan, Ulsan, Republic of Korea
hhlee@ulsan.ac.kr,nmhoang@ulsan.ac.kr

Abstract. This paper presents induction motor control system operation using matrix converter based on the controller area network (CAN). The hardware control system is designed with dual microcontrollers which communicate to each other by a dual-port RAM. The advantages of matrix converter are utilized with the CAN network on the field oriented control method of induction motor. The performances of the motor control fully guarantee the system stability and the successful data communication by network. The experimental results are given on 5Hp induction motor to verify the effectiveness and feasibility of the control system using network.

Keywords: Matrix converter, CAN network, dual-port RAM.

1 Introduction

As the importance of quality and efficiency in power supply and usage has increased over the past two decades, the three-phase matrix converter (MC) has become a modern energy converter and has emerged as one of the best energy conversion substitutions [1], [2]. It fulfils all requirements of the conventionally used rectifier/dc link/inverter structures. As shown in Fig. 1, the MC has a simple topology and a compact design due to its lack of a dc-link capacitor for energy storage.

The MC has the following advantages:

- Sinusoidal input and output current waveforms.
- A unity input power factor.
- Operation in all four quadrants of the torque- speed plane due to regenerative capabilities.
- High reliability and long life due to the absence of bulky electrolytic capacitors.
- Smaller and lighter than other regeneration inverters with equivalent power ratings.

This paper describes the MC control system using dual microcontrollers based on the dual-port RAM communication. The field oriented control method for induction

* Corresponding author.

D.-S. Huang et al. (Eds.): ICIC 2009, LNAI 5755, pp. 1067 – 1074, 2009.

motor fed by a MC is implemented based on an industrial network (Controller Area Network – CAN). The communication protocol of the dual port RAM with microcontrollers is explained in details. The operation of the motor control system using CAN network is given to verify the high dynamic performances of the induction motor control using industrial network.

2 Matrix Converter Theory

2.1 Space Vectors of Matrix Converter

A three-phase MC module includes nine bidirectional switches and the structure of a three-phase ac-ac MC is shown in Fig. 1. The voltage and current at the input side of the MC are denoted by a, b and c while those at the output side are denoted by A, B and C. There are 27 possible switching configurations (SCs), which can be split into three groups:

- Group I: Two output lines are connected to a common input line. The remaining output line is connected to one of the other input lines (±1, ±2,…, ±9)
- Group II: All output lines are connected to a common input line.
- Group III: Each output line is connected to a different input line which is rarely used in the MC control.

2.2 Field Oriented Control of Induction Motor Using Matrix Converter

Due to the advantages of the field oriented control (FOC) method with the fast response and easy implementation, the advantages of MC and the FOC method are combined to control the induction motor in Fig. 3.

The motor speed and currents are used as inputs of the FOC method. The reference output voltage vector is synthesized by the direct space vector modulation (DSVM) technique to obtain the control command and also keep the main input power factor to be unity. The FOC control algorithm is explained in [3].

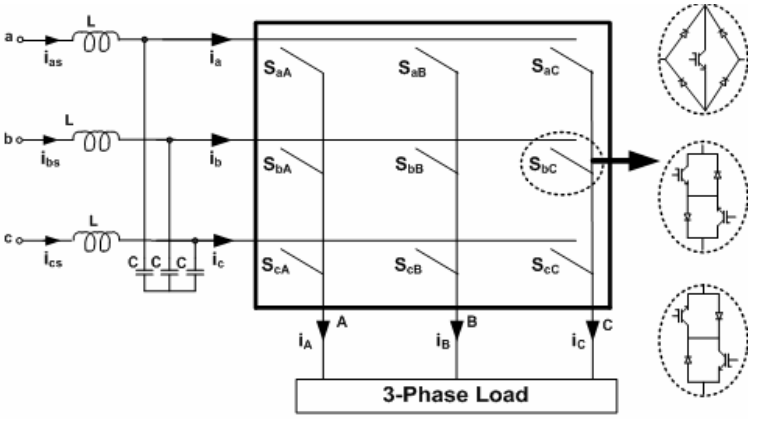

Fig. 1. Structure of a three-phase ac-ac matrix converter

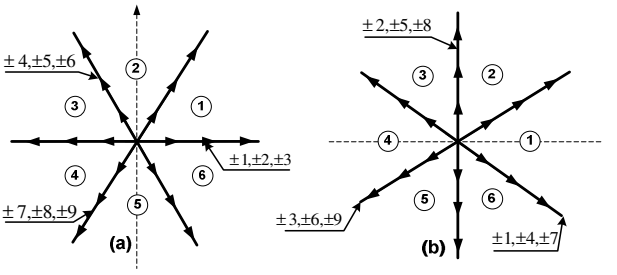

Fig. 2. (a) Output line-to-neutral voltage vector (b) Input line current vector

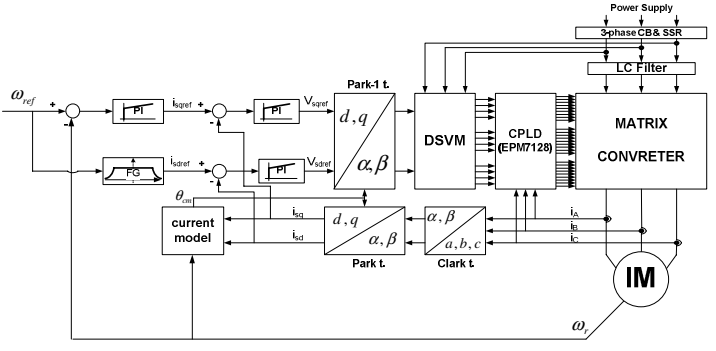

Fig. 3. Block diagram of the FOC method for induction motor fed by a MC

3 Hardware Design Using Dual Microcontrollers Based on Dual-Port RAM

Figure 4 shows the block diagram of hardware design consisting of two 32-bit DSPs (TMS320F2812) operating at clock frequency 150MHz, which communicates with each other through a dual-port RAM (CY7C028):

- The first DSP is the main controller which dedicates to the main control algorithm: measure input/output currents and input voltage through a 12-bit AD converter (AD7864). Motor speed is updated and monitored by a graphic user interface (GUI) in PC through SCI standard. The entire control data can be viewed by either PC through CAN network or Oscilloscope through SPI standard.
- The second DSP is the PWM signal generation which updates the new selected switching configurations for the DSVM method, and also in corporation with a CPLD (EPM 7128) to handle the 4-step commutations which is very important fact for the matrix converter control.
- The CY7C028 is a low-power CMOS 32Kx16 dual-port static RAM made by Cypress. Various arbitration schemes are included on the devices to handle situations when multiple processors access the same piece of data. As shown in Fig. 5, two ports are provided to permit independent and asynchronous access for reads and to write to any location in memory.

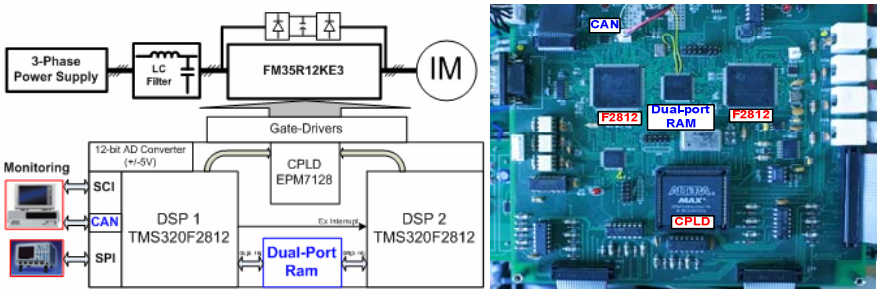

Fig. 4. Block diagram and hardware prototype of matrix converter control system based on dual DSP TMS32F2812s and dual-port RAM

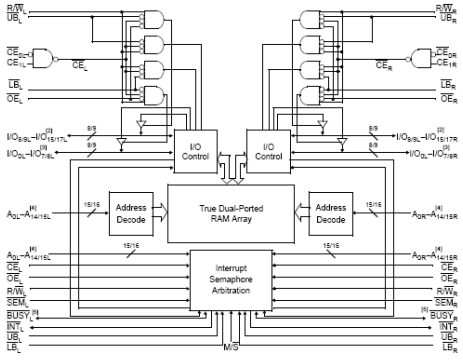

Fig. 5. Logic block diagram of the dual-port RAM CY7C028

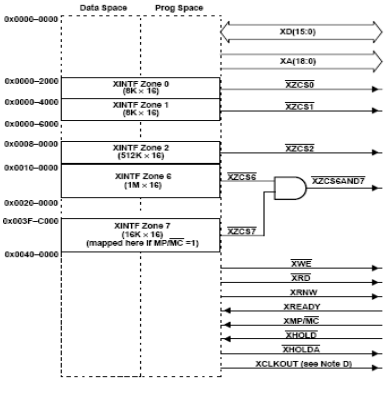

Fig. 6. External interface block diagram of TMS320F2812

The communication of two DSPs with the dual-port RAM is operated at the external memory interface of TI DSP, TMS320F2812, which has the total external memory up to 1.5MB. The asynchronous interface consists of 19 address lines, 16 data lines, and four chip-select lines as shown in Fig. 6. The chip-select lines are mapped

to five external zones, Zone 0,1,2,6 and 7. Zone 6 and 7 share a single chip-select. Each of the five zones can be programmed with different number of wait states, strobe signal setup and hold timing and each zone can be programmed for extending wait states externally or not.

4 Induction Motor Control Using Matrix Converter Based on CAN Network

4.1 CAN Network

Controller Area Network (CAN) was initially created by German automotive system supplier Robert Bosch in the mid-1980s for automotive applications as a method for enabling robust serial communication. The goal was to make automobiles more reliable, safe and fuel-efficient while decreasing wiring harness weight and complexity. Since its inception, the CAN protocol has gained widespread popularity in industrial

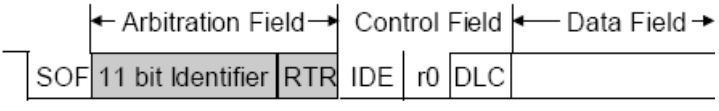

Fig. 7. Standard fame format of CAN network

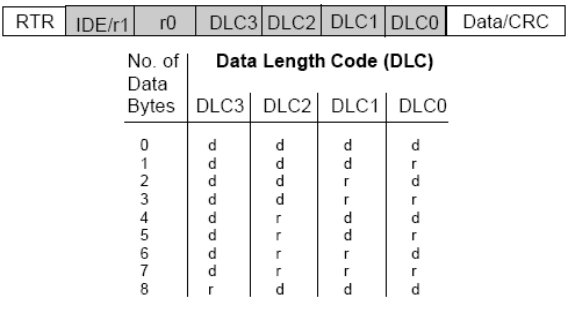

Fig. 8. The format of the Control Field

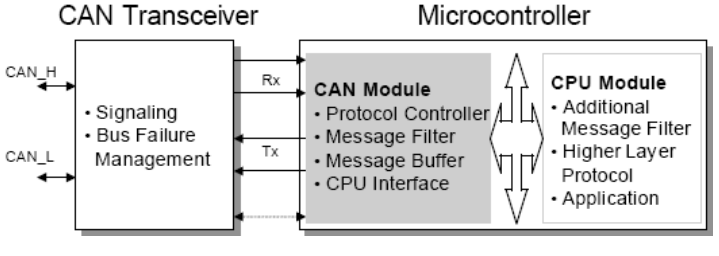

Fig. 9. Integrated CAN controller of TMS320F2812 and TMS320F2407

automation and automotive/truck applications. Other markets, where networked solutions can bring attractive benefits like medical equipment, test equipment and mobile machines, are also starting to utilize the benefits of CAN network. Fig. 7 shows the standard frame format of CAN network which has 11-bit ID and the maximum bytes can be transferred in the CAN network is 8.

4.2 Induction Motor Control System Based on CAN Network

Fig. 10 shows the block diagram of the induction motor control system based on CAN network. In the figure, the rotor speed is measured by a DSP TMS320F2407, and then the measured speed is transferred to the main controller of matrix converter though CAN network. In certain applications, the converters are equipped far from motors, and the encoder pulse data are less accurate due to the long distance transmission, it is necessary to use the industrial network to collect real control data and also to monitor data of the control system.

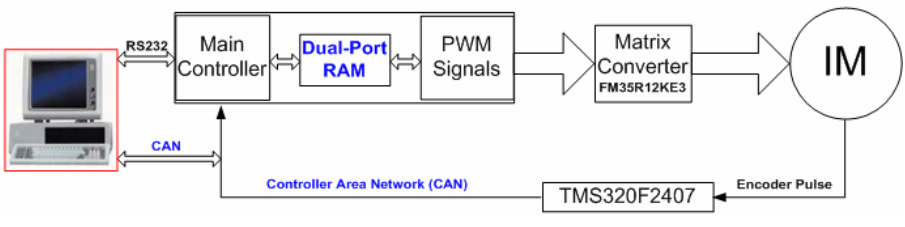

Fig. 10. Induction motor control using matrix converter based on CAN network

Fig. 11 shows the hardware prototype of the 5HP induction motor control fed by Eupec MC module (FM35R12KE3) based on CAN network. The MC's input filter is designed with the cut-off frequency 900Hz. Induction motor is coupled with a changeable mechanical load.

Fig. 11. Hardware prototype of the induction motor control based on CAN network

5 Experimental Verification

The experiment is carried out at the control sampling frequency 10kHz. And the rotor speed is updated through CAN network each 10ms. Controlled data and monitored data are entirely viewed by CANalyser using CANcardX.

Fig. 12 shows the induction motor operation as the rotor speed change between +500rpm and -500rpm, and it is shown the rotor speed is fully follows the speed references.

Fig. 13 shows the input/output currents and voltages of MC at the rotor speed 500rpm and load torque 2Nm. At the input side, the input current is controlled entirely in phase with the input line-to-neutral voltage and the near unity power factor is achieved. The input and output currents are almost sinusoidal waveforms.

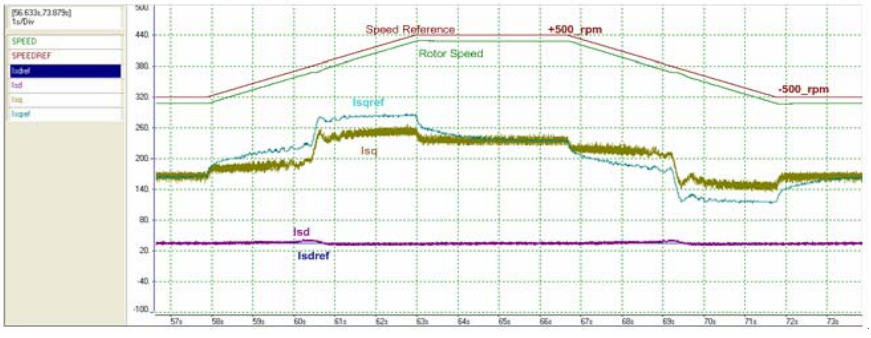

Fig. 12. Operation of induction motor control based on CAN network under the rotor speed command between +500rpm and -500_rpm, monitored by CANalyser

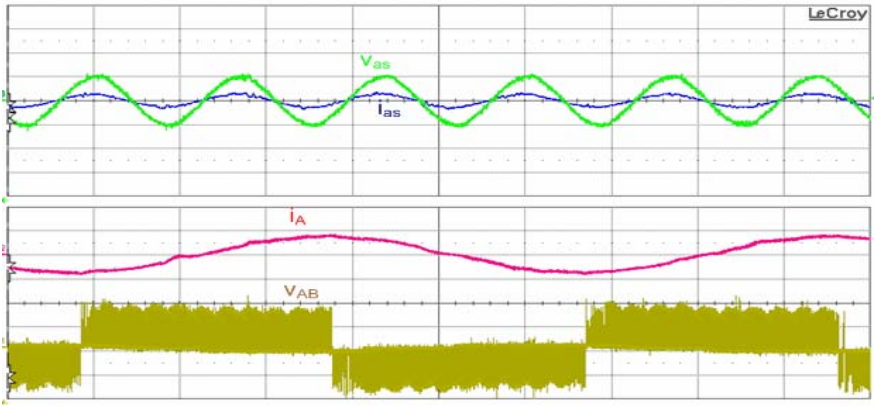

Fig. 13. Input/output waveforms of matrix converter at rotor speed 500rpm, load torque 2Nm

6 Conclusions

This paper describes the matrix converter controller design using dual microcontrollers based on a dual-port RAM, which enables the control information perfectly communicated between two micro-controllers. The industrial network (CAN) is successfully applied to the MC controller to control the induction motor by the FOC method. The motor control performance fully takes the advantages of the matrix converter with the near unity power factor at the main power supply and input current waveform is almost sinusoidal.

Acknowledgment

The authors would like to thank Ministry of Knowledge Economy and Ulsan Metropolitan City which partly supported this research through the Network-based Automation Research Center (NARC) at University of Ulsan.

References

1. Watanabe, E., Ishii, S., Yamamoto, E., Hara, H., Kang, J.K., Hava, A.M.: High performance motor drive using matrix converter. In: Proc. the IEE Seminar: Advances in induction motor control (Ref. No. 2000/072) (2000)
2. Matsuo, T., Bernet, S., Colby, R.S., Lipo, T.A.: Application of the matrix converter to induction motor drives. In: Proc. the Thirty-First IAS Annual Meeting Conference Record, October 1996, vol. 1, pp. 60–67 (1996)
3. Lee, H.H., Nguyen, H.M., Chun, T.W.: A study on rotor FOC method using matrix converter fed induction motor with common-mode voltage reduction. In: Proc. the 7th International Conference on Power Electronics, ICPE 2007, October 22-26, pp. 159–163 (2007)

Fuzzy Data Fusion for Updating Information in Modeling Drivers' Choice Behavior

Mauro Dell'Orco and Mario Marinelli

Dept. of Highways and Transportation, Technical University of Bari, Italy
dellorco@poliba.it

Abstract. In this paper, a method for fusing fuzzy data relevant both to drivers' experience and provided information is presented. Expected travel time is then updated according to the results of fusion. The method takes into account the "compatibility" of data originating from different sources, and provides information about acceptability of results. Influence of uncertainty on drivers' compliance with provided information is examined in detail, according to uncertainty-based Information Theory.

Keywords: Fuzzy Fusion; Uncertainty Theory; ATI Systems; driver behaviour; route choice model.

1 Introduction

Several researchers have dealt with conceptual models of drivers' behavior under information provision. Basic idea in these models is that each driver updates his/her knowledge of costs of alternatives using provided information. Then, he/she compares the updated costs of alternatives and chooses, among them, the best one from his point of view. However, since both knowledge of alternatives and information are rarely perfect, uncertainty affects single person's decision. Handling uncertainty is therefore an important issue for these models. Approaches followed by different scientists to face this issue can be arranged into two main groups, according to how uncertainty has been modeled. In the first group, the approach followed in general uses randomness to represent uncertainty. For this kind of models, unavailability of full numerical data could limit the model reliability; in fact, these models are generally unable to handle non-numerical values of parameters. On the contrary, models included in the second group can easily model uncertainty through verbal, incomplete or imprecise data using the concepts of Fuzzy Logic. In fact, the fundamental concepts of Fuzzy Sets Theory, linguistic variables, approximate reasoning, and computing with words introduced by Zadeh have more understanding for uncertainty, imprecision, and linguistically articulated observations. These concepts support "the brain's crucial ability to manipulate perceptions-perceptions of distance, size, weight, colour, speed, time, direction, force, number, truth, likelihood, and other characteristics of physical and mental objects. A basic difference between perceptions and measurements is that, in general, measurements are crisp whereas perceptions are "fuzzy" [1]. Fuzzy Set Theory based route

D.-S. Huang et al. (Eds.): ICIC 2009, LNAI 5755, pp. 1075–1084, 2009.

choice model was proposed for the first time by Teodorović and Kikuchi [2]. In this work, drivers' compliance with information is examined, according to uncertainty-based Information Theory. In particular, we made the hypothesis that drivers' compliance with information services is a function of uncertainty. Therefore, we have developed a relation between uncertainty and compliance level. Finally, the effects of information are illustrated through a numerical example.

2 Provision and Updating of Information

An informative system, like the Advanced Traveler Information Systems (ATIS), may provide information to users before they begin the trip (pre-trip information) or while they are moving (en-route information). In the first case, static choice models are involved; in the second case, dynamic ones. In both cases, travellers combine information with their previous experience to obtain a prediction about the cost of each path and to choose the best one.

To incorporate information on system conditions in the choice process, we assume that drivers:

- have some experience about the attributes of the transportation system;
- use information to update his experience;
- choose an alternative according to his updated experience.

Since the drivers' knowledge about the transportation system could be imprecise or approximate, it can be expressed in the same way we used for perceived information. So both drivers' knowledge and information can be expressed in terms of Possibility, like in Figure 1.

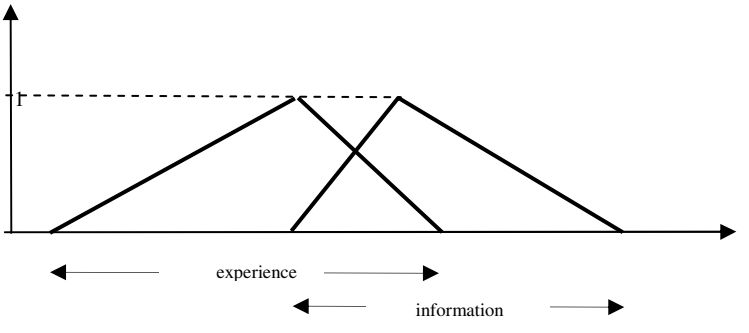

Fig. 1. Possibility distributions of experience and information

To update knowledge of the system, drivers aggregate data coming both from their experience and from current information. However, aggregation could be not always meaningful, since data coming from different sources can be far from each other, and thus not compatible. Therefore, a suitable aggregation function should include also a measure of compatibility.

To measure compatibility, Yager and Kelman [3] proposed the relationship $R:X^2 \rightarrow I = [0,1]$ such that:

- $\forall x \in X, R(x,x) = 1$
- $\forall (x,y) \in X^2, R(x,y) = R(y,x)$
- For a given x, R(x,y) is a convex fuzzy set.

A suitable expression for a compatibility function R defined in X^2 is :

$$R(x_1, x_2) = \begin{cases} 0 & \text{if } |x_1 - x_2| > k \\ 1 - \frac{1}{k}|x_1 - x_2| & \text{if } |x_1 - x_2| \leq k \end{cases} \quad (1)$$

where k must be carefully selected case by case, to obtain a proper compatibility measure. Also extension to X^n of R is possible, through the relation:

$$\mathbf{R}(x_1,\ldots x_n) = \min_{i,j=1,\ldots n} R(x_i, x_j) \quad (2)$$

In this paper, we have used for data fusion the *Ordered Weighted Average* (OWA) operator and the compatibility function R, defined in equation (1).

Given a set $A= \{a_1, a_2,\ldots a_n\}$ and a fusion function F, an OWA operator is a weighting vector $W= [w_1, \ldots w_n]$ such that:

- $w_i \in [0,1]$;
- $\Sigma_i w_i = 1$;
- $F(a_1, a_2,\ldots a_n) = \Sigma_i b_j w_j$

in which b_j is the j-th largest element of A. By adjusting the weighting vector, we can represent different drivers' attitudes: when W favours the smaller valued arguments in the aggregation process it reflects an *aggressive* driver, otherwise it reflects a *cautious* driver.

O'Hagan [4] suggested a method to calculate the weights w_i (i = 1,…n) through the following simple mathematical programming problem:

$$\text{Maximize} \quad -\sum_{i=1}^{n} w_i \ln w_i$$

$$\text{subject to} \quad \begin{cases} \sum_{i=1}^{n} w_i \; h_n(i) = \beta \\ \sum_i w_i = 1 \\ w_i \geq 0 \quad \forall i \end{cases} \quad (3)$$

where $h_n(i) = \frac{n-i}{n-1}$, and $\beta \in [0,1]$ is a coefficient representing, in our case, drivers' cautiousness. Note that, if fusion involves only two sets, then $h_2(1) = 1$, $h_2(2) = 0$. Thus, from the constraints of previous program (Eq. 3):

$$w_1 = \beta, \tag{4}$$

$$w_2 = 1-\beta. \tag{5}$$

The basic hypothesis we have made in this work to set up a value of β, is that drivers' cautiousness is a function of uncertainty related to perceived information. Let us explain this last concept through an example. Assume that the shorter one of two alternative paths is temporarily closed by barriers. In this case, information that path is closed is not uncertain, that is U(I) = 0, and drivers must choose the longer path. This means that the OWA operator should favour the largest value, that is $w_1 = 1$, and consequently $\beta = 1$ from equation (4). Conversely, if instead of barriers there is an informative system giving very vague information about the condition of the path, uncertainty U(I) is very large, and drivers should prefer to rely on their own experience. In this case, the OWA operator favours the smallest value, that is w_2 approaches 1 and thus, from equation (5), β approaches 0. From this example it appears that the parameter β can be interpreted also as drivers' compliance with information. In fact, $\beta = 1$ means that the driver is totally compliant with information, $\beta = 0$ means the opposite.

Experimental studies have been carried out in last years by some researchers to find out a value of drivers' compliance. Different values, ranging from 0.2 to 0.7, have been found, mainly due to the fact that β is affected by the level of uncertainty imbedded in information. In this study we have assumed that:

- drivers' compliance with information decreases with increasing of uncertainty. This means that the relative elasticity of compliance with respect to uncertainty is negative. In analytical terms: $\frac{d\beta/\beta}{dU(I)/U(I)} < 0$;
- the increase of compliance with additional information is greater in case of ignorance than in case of complete knowledge. That is, the relative elasticity is a function of uncertainty itself.

On the basis of these hypotheses, the following linear relationship between relative elasticity uncertainty level has been carried out:

$$\frac{d\beta/\beta}{dU(I)/U(I)} = -\gamma \cdot U(I) \tag{6}$$

and hence:

$$\beta = \frac{1}{e^{\gamma U(I)}} \tag{7}$$

where γ is a parameter to be calibrated, which takes into account individuals' attributes like age and gender. When n different sources provide information I_i (i=1,…n) with uncertainty $U(I_i)$, compliance rate is calculated as

$$\beta = \min_{i=1,\ldots n} \frac{1}{e^{\gamma U(I_i)}} \tag{8}$$

Now, to incorporate the compatibility concept in the fusion function, we follow the method suggested by Yager and Kelman [3]. Therefore, let

- A_i (i= 1,…n) be a collection of fuzzy sets. Recall that fuzzy sets and Possibility distributions can be represented in the same way;
- $B = F(A_i)$ be the result of aggregation;
- $A_{i\alpha}=[\, l_{i\alpha}, r_{i\alpha}]$ be the α-cut associated with A_i;
- $l^*_\alpha = \max_i[l_{i\alpha}]$ be the largest lower bound of any α-cut;
- $r^*_\alpha = \min_i[r_{i\alpha}]$ be the smallest upper bound of any α-cut;
- $U^*_\alpha = \inf\{x \mid R(l^*_\alpha,x) \geq \alpha\}$ be the smallest value compatible with l^*_α at level α;
- $V^*_\alpha = \sup\{x \mid R(r^*_\alpha,x) \geq \alpha\}$ be the largest value compatible with r^*_α, at level α.

Provided that $U^*_\alpha \leq r^*_\alpha$ and $V^*_\alpha \geq l^*_\alpha$, the α-cut of B can be calculated as:

$$B_\alpha = [F(d_{1\alpha},\ldots d_{n\alpha}), F(e_{1\alpha},\ldots e_{n\alpha})] \tag{9}$$

where:

$$d_{i\alpha} = \begin{cases} l_{i\alpha} & \text{if } l_{i\alpha} \geqslant U^*_\alpha \\ U^*_\alpha & \text{otherwise} \end{cases} \qquad e_{i\alpha} = \begin{cases} r_{i\alpha} & \text{if } r_{i\alpha} \geqslant V^*_\alpha \\ V^*_\alpha & \text{otherwise} \end{cases} \tag{10}$$

The information fusion model incorporates important aspects such as:

- dynamic nature of information integration. The perceived cost of an alternative is influenced by the user's previous experience and memory;
- accuracy of the informative system. The more accurate information is, the more important is the effect on the drivers' perception;
- non-linear relationship between information and perception. The parameter β itself is function of information, so that the updated cost is a non-linear function of information.

3 Numerical Application

The Figure 2 represents a path between the Origin-Destination pair i-j; at the origin i there is a Variable Message Signal (VMS), displaying real-time traffic information. Assume that users have the historical knowledge that the travel time for this OD pair lies in the range 12 to 22 minutes; or, in other words, they have experience that travel time related to the path i-j is "approximately 17 minutes".

Assume additionally that an ATIS service can provide the drivers, via VMS, with some real-time en-route information about the traffic conditions on the path like, for example, "congestion ahead", "3 km queue", "minor accident". In case of the message "congestion ahead", drivers perceive this information in terms of increased travel time, say 18 to 30 minutes. In Figure 3, the fuzzy sets corresponding to approximate values of historical travel time and perceived information are depicted.

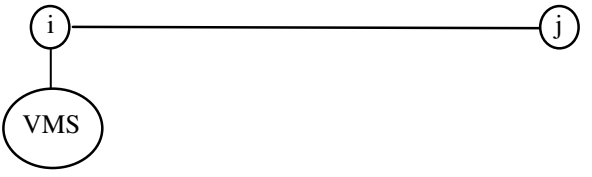

Fig. 2. Test path

Calculating uncertainty, we obtain: $U_{information} = \log_2(30\text{-}18) = 3.58$. Consequently, setting $\gamma = 0.15$ in equation (8), $\beta = \left(\frac{1}{1.71}\right) = 0.58$. Since only two sets are involved in the fusion, according to equations (4) and (5) the weights of these two sets result: $w_1 = 0.58$, $w_2 = 0.42$.

The set B_α, resulting from the fusion, is reported in Figure 3 in bold line. Note that the maximum value of Possibility for the fusion is less than 1, due to not complete compatibility of experience and information.

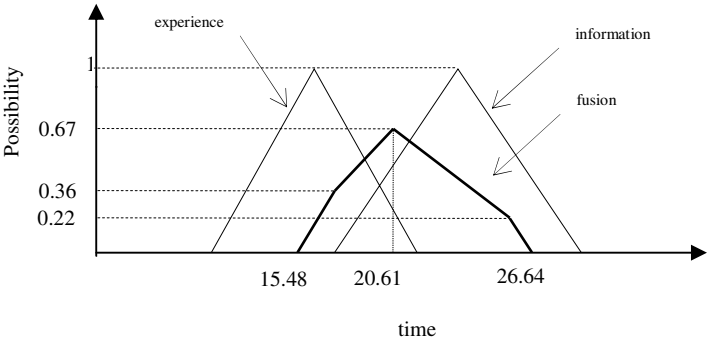

Fig. 3. Fusion of experience and perceived information

Applications of this methodology can be useful in management of transportation networks: path choice models assume that users make choices comparing the costs of different alternatives. Thus, providing additional fortuitous costs through different VMS messages, en-route changes of pre-trip choices are possible.

For example, assume that, in addition to the link in Figure 2, another path connects the O-D pair i-j (Figure 4).

Drivers have the imprecise knowledge that the travel time on this additional path is "approximately 25 minutes", ranging from 20 to 30 minutes.

When VMS does not release any information, drivers compare, on the basis of their knowledge, the travel times on path a (t_a), and on path b (t_b).

The comparison is carried out on the basis of the relations:

Possibility that $t_a < t_b = \prod(t_a < t_b) = \max(\min(\prod(t_a), \prod(<t_b))$;
Possibility that $t_b < t_a = \prod(t_b < t_a) = \max(\min(\prod(t_b), \prod(<t_a))$,

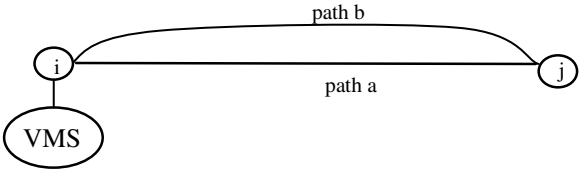

Fig. 4. Alternative paths from i to j

where $\prod(t_i)$ and $\prod(<t_i)$, i={a,b}, are the Possibilities that travel time is t_i or smaller than t_i, respectively.

Results of comparison are:

- $\prod(t_a < t_b) = 1$
- $\prod(t_b < t_a) = 0.2$

Possibility is a useful concept in representing decision-maker's uncertainty about the attributes of individual alternatives, but cannot be used directly by analysts; for this reason, a conversion to Probability values on the basis of a justifiable principle is needed.

To pass from Possibility to Probability we use the probabilistic normalization ($\sum_i p_i = 1$), along with the *Principle of Uncertainty Invariance*, systematized by Klir and Wang [5]. This principle specifies that uncertainty in a given situation should be the same, whatever is the mathematical framework used to describe that situation.

Under the requirement of normalization and uncertainty equivalence, we should use a transformation having two free coefficients. Thus, according to Geer and Klir [6], we use the log-interval scale transformations having the form:

$$\Pi_i = \beta \cdot (p_i)^{\alpha} \tag{11}$$

where Π_i is Possibility and p_i Probability of the i-th alternative; α and β are positive constants.

From equation (11) we obtain: $p_i = (\Pi_i/\beta)^{1/\alpha}$ and, applying the probabilistic normalization,

$\beta = \left(\sum_i \Pi_i^{1/\alpha} \right)^{\alpha}$ whence, setting $\varepsilon = 1/\alpha$:

$$p_i = \Pi_i^{\varepsilon} \Big/ \left(\sum_i \Pi_i^{\varepsilon} \right) \tag{12}$$

To calculate ε, we use the Principle of Uncertainty Invariance. Given an ordered Possibility distribution $\{\Pi_1, \Pi_2, \ldots \Pi_i, \Pi_{i+1}, \ldots \Pi_n\}$ for which is always the case that $\Pi_i \geq \Pi_{i+1}$, the possibilistic counterpart of the probabilistic uncertainty, called U-Uncertainty, is given by the following function:

$$U = \sum_{i=1}^{n} (\Pi_i - \Pi_{i+1}) \log_2 i \tag{13}$$

According to the Principle of Uncertainty Invariance, information I and uncertainty U must have the same value:

$$-\sum_{i=1}^{n} p_i \log_2 p_i = -\sum_{i=1}^{n} \frac{\Pi_i^{\varepsilon}}{\sum_{j=1}^{n} \Pi_j^{\varepsilon}} \log_2 \frac{\Pi_i^{\varepsilon}}{\sum_{j=1}^{n} \Pi_j^{\varepsilon}} = \sum_{i=1}^{n} (\Pi_i - \Pi_{i+1}) \log_2 i \tag{14}$$

where $\Pi_{n+1} = 0$ by definition. Numerical solution of equation (13) is always possible, except when $\Pi_i = K \ \forall i$, $K \in [0, 1]$. However, in this case, from equation (12) we can easily obtain:

$$p_i = 1/n \ \forall i. \tag{15}$$

Excluded this case, we can calculate the value of ε that makes equal the two Uncertainties through equation (13) and then, through equation (12), the value of p_i. In our case, we have obtained: $\varepsilon = 1.72$, $p_a = 0.94$, $p_b = 0.06$. Thus, in ordinary conditions, 94% of drivers choose the path a.

Now, assume that, at a certain time, the VMS releases the information message "congestion ahead" for the path a. The result of information fusion has been calculated before, and reported in Figure 3 as the bold line t_f, which is a *subnormal* fuzzy set because its height h_f is less than 1 (0.67).

In order to interpret the information given by this fuzzy set, t_f must be redefined as follows:

$$r_f = t_f + 1 - h_f \tag{16}$$

The values of t_f are increased by the same amount of $1-h_f = 0.33$. The result of this redefinition is reported in Figure 5. The interpretation of information contained in a subnormal fuzzy set is explained by Klir [7].

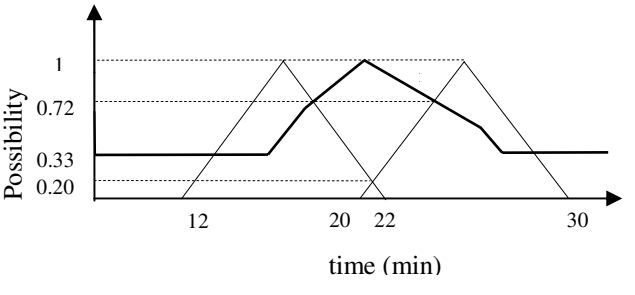

Fig. 5. Comparison of alternatives after redefinition

Thus, the comparison is now carried out between r_f and t_b, and gives:

- $\prod(r_f < t_b) = 1$,
- $\prod(t_b < r_f) = 0.72$.

Using again the Principle of Uncertainty Invariance, we can calculate now: $\varepsilon = 2.35$, $p_f = 0.64$, $p_b = 0.32$. This means that, in presence of information "congestion ahead", about 32% of the total number of drivers shift from path a to path b.

Additionally, assume that another source, for example radio traffic information, provides at the same time the information "minor accident" for the path a. Drivers perceive this information as an increased travel time, ranging from 25 to 35 minutes.

In this case, $U_{information} = \log_2(35\text{-}25) = 3.32$ and, from equation (8), $\beta = \min\left(\frac{1}{1.71}, \frac{1}{1.64}\right) = 0.58$. Thus, from the program (3), we obtain: $w_1 = 0.42$, $w_2 = 0.33$, $w_3 = 0.25$.

Applying the same procedure previously used, the result of data fusion is reported in Figure 6.

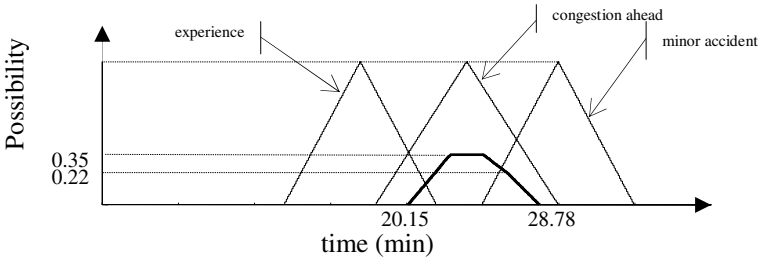

Fig. 6. Fusion of experience and information from two different sources

Due to their scarce compatibility, different information can result somehow confusing, so the new set t_f resulting from fusion has a quite low maximum value of Possibility (0.35). Anyway, the effect of additional information is to displace the result of the fusion toward greater values of time, with respect to those relevant to the first fusion. This is the case in which $\prod(r_f < t_b) = \prod(t_b < r_f) = 1$; therefore, from equation (14) we obtain $p_f = p_b = 0.5$. So, when two simultaneous messages are received, such as "congestion ahead" and "minor accident", about 50% of the total number of drivers shift from path a to path b. In terms of Possibility Theory, this result corresponds to the maximum of uncertainty, and is in accordance with the fact that scarce compatibility of different information can result confusing. In table 1, results of all numerical examples examined are summarized.

Table 1. Distribution of travelers (percent) for different and multiple information

	no information	"congestion ahead"	"congestion ahead" and "minor accident"
path a	94	68	50
path b	6	32	50

From these results it emerges that an appropriate tailoring of released information makes it possible to use the informative system as a road pricing tool. We can also

realize the advantage of the proposed model: the use of fuzzy logic combined to data fusion allows to approach the real human behaviour which is characterized by fuzziness and uncertainty.

4 Conclusions

In this paper, the emphasis was on capturing the reasoning process of drivers making en-route choices in presence of traffic information. The influence of uncertainty in updating the knowledge of attributes of a transportation system, like expected travel time on a path, has been modeled using the concept of *compatibility* between previous knowledge and current information. The presented model points out the relevant role of the Possibility Theory in calculating uncertainty and thus drivers' compliance level with released information. Through the Possibility Theory a modeling framework, which represents the uncertainties imbedded in the perception of travel attributes, has been developed. The model allows the quantitative calculation of users' compliance with information, and thus a realistic updating of expected travel time. In a wider framework, the outcomes of this paper can be used to carry out a road pricing system based on information provision. For example, from results of the numerical application can be noticed that, releasing the message "congestion ahead", about 32% of travelers shift from path a to path b. In other words, the impact of information can be considered an additional cost perceived by users. Therefore, a VMS system can be used as a tool for traffic management. Future works are intended to test the proposed model which much more real data in order to take a comparison with probabilistic models such as Bayesian method.

References

1. Zadeh, L.: Fuzzy sets as a basis for a theory of possibility. Fuzzy Sets and Systems 1, 3–28 (1978)
2. Teodorović, D., Kikuchi, S.: Transportation route choice model using fuzzy inference technique. In: Proceedings of the First international symposium on uncertainty modeling and analysis, College Park, USA, pp. 140–145. IEEE Computer Society Press, Los Alamitos (1990)
3. Yager, R.R., Kelman, A.: Fusion of Fuzzy Information With Consideration for Compatibility. Partial Aggregation, and Reinforcement, International Journal of Intelligent Systems 15, 93–122 (1996)
4. O'Hagan, M.: Using maximum entropy-ordered weighted averaging to construct a fuzzy neuron. In: Proceedings 24th Annual IEEE Asilomar Conference on Signals, Systems and Computers, Pacific Grove, CA, pp. 618–623 (1990)
5. Klir, G.J., Wang, Z.: Fuzzy Measure Theory. Plenum Press, New York (1992)
6. Geer, J.F., Klir, G.J.: A mathematical analysis of information-preserving transformations between probabilistic and possibilistic formulations of Uncertainty. Intern. J. of General Systems 20, 143–176 (1992)
7. Klir, G.J.: On fuzzy-set interpretation of possibility theory. Fuzzy Sets and Systems 108, 263–273 (1999)

Multi-view Ear Recognition Based on Moving Least Square Pose Interpolation

Heng Liu[1,2], David Zhang[3], and Zhiyuan Zhang[4]

[1] School of Information Engineering, Southwest University of Science and Technology, Mianyang, 621010, P.R. China
[2] Institute of Image Processing and Pattern Recognition, Shanghai Jiao Tong University, Shanghai, 200240, P.R. China
hengliusky@gmail.com
[3] Department of Computing, The Hong Kong Polytechnic University, Hong Kong, P.R. China
csdzhang@comp.polyu.edu.hk
[4] Bio-computing Research center, Harbin Institute of Technology, Shenzhen Graduate School
zzy380@163.com

Abstract. Based on moving least square, a multi-view ear pose interpolation and corresponding recognition approach is proposed. This work firstly analyzes the shape characteristics of actual trace caused by ear pose varying in feature space. Then according to training samples pose projection, we manage to recover the complete multi-view ear pose manifold by using moving least square pose interpolation. The constructed multi-view ear pose manifolds can be easily utilized to recognize ear images captured under different views based on finding the minimal projection distance to the manifolds. The experimental results and some comparisons show the new method is superior to manifold learning method and B-Spline based recognition method.

1 Introduction

Since human ear holds many similar characteristics as human face - in the head, a stable structure of appearance, ease of data acquisition, it is natural to consider applying ear recognition under occasions where face recognition has been to shown to work. So far, some works have shown ear owns some desirable properties for biometrics such as universality, uniqueness, and permanence [1]. Ear biometrics is expected to be a creditable technique for human identification, and it actually attracts much attention in recently. Compared with some popular biometrics such as face, fingerprint and iris, ear biometrics holds many excellences. Firstly, ear biometrics is not affected by facial expressions and cosmetics. And the appearance of the auricle (external ear) is nearly unaffected by aging (from 7 to 70). Secondly, ear data can be easily collected by a non-invasive way. In addition, on the ear itself, ear owns abundant and unique shape structure features and special pose information which make itself play a primary role in human profile image recognition. Therefore, in the field

D.-S. Huang et al. (Eds.): ICIC 2009, LNAI 5755, pp. 1085–1095, 2009.

of human appearance-oriented biometrics, ear recognition may work as a useful and necessary biometrics means.

Recent years there have appeared some biometrics techniques [2-5] which utilize 2D intensity images for ear recognition. D.J. Hurley et al. [2] apply force field energy function to acquire 2D ear features. Michał Choraś [3] has tried to extract abundant ear geometrical features from ear edge images. M. Burge and W. Burger [4] constructs Voronoi neighborhood graph model for ear curves matching. Bustard et al. [5] utilize SIFT feature points detection and matching for 2D ear registration and recognition. Moreno et al. [6] apply three kinds of neural networks to do 2D ear recognition experiments. K. Chang et al. [7] combine and compare ear and face images in appearance based biometrics.

Actually, all above mentioned works only use front view images for ear recognition and do not address ear multiple views recognition problems. As we know, the imaging of ear shape is always affected by the rotation of human head. When subject's ear is captured in different views between training samples and test samples, these front view based methods will result in matching failure. On the other hand, Ping Yan et al. [8] and Hui Chen et al. [9] propose 3D ear recognition techniques respectively. Although they both report good 3D recognition performance respectively, the cost of 3D ear data capturing and the time consuming for the whole recognition procedure are very high, which hints that the 3D approach will be inefficient in practice. That is also to say, the current 3D ear recognition approach has limited capability of solving the problem of ear pose variation.

However, among these existing 2D front view and 3D range image recognition methods, there is a margin way: multi-view ear recognition, which not only extends 2D ear front view method but also has partly similar traits of 3D range technique. Multiple views of ear carry abundant shape features in different sides which can boost up recognition performance. Naturally, we turn to explore the alternative way multi-view recognition against ear pose variation. In very recently, Zhao-xia Xie et al. [10] try to apply the LLE manifold learning method for multi-view ear recognition. Due to the requirement of large learning samples and noise sensitivity, the practical recognition performance of the method is not good. In addition, Zhiyuan Zhang et al. [11] propose a B-Spline based pose interpolation strategy for multi-view ear recognition. They report good performance using pose interpolation techniques.

As moving least square (MLS) has better numerical approximation traits and with weight function MLS is more flexible not only for global fit but also local approximation than B-Spline does, thus in this work, we consider to take moving least square technique to interpolate multiple ear poses in discriminative feature projection space formed by null space kernel discriminate analysis (NKDA), and then propose the corresponding multi-view ear recognition approach.

The rest of this paper is organized as follows. Section 2 illustrates the basic motivation and consideration of our multi-view ear pose interpolation based recognition strategy. And the multi-view ear dataset used in the work is introduced in the Section also. In Section 3, the concrete processing of NKDA multi-view ear feature extraction and moving least square pose interpolation, and the corresponding recognition approach are presented. Section 4 provides our recognition experiments, and some comparisons with B-Spline based interpolation and manifold learning recognition methods. Finally, we make short conclusions in Section 5.

2 The Framework of MLS Pose Interpolation Based Recognition

2.1 Recognition Framework

According to human vision system (HVS), human vision can capture the differences of different ears and even can take advantage of the trace continuity when ear pose varies. In addition, recent works [12-14] on face recognition across large pose changing have shown that face varieties of subjects, with lighting fixed, can be regarded as a 2D manifold which contain and represent face pose variation and facial expression transformation. Stimulated by these thinking, since ear do not hold expression changing, we may get the hints: ear pose varying will form a one dimension manifold - curve in certain feature space; and different ears with pose changing lie on different manifolds. The illustration of these suggestions is shown in Fig.1.

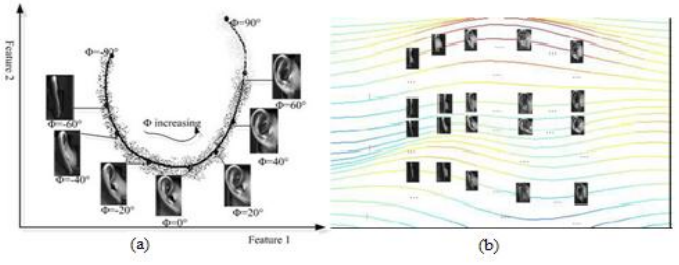

Fig. 1. Ear pose manifold characteristics illustration. (a) Ear pose trajectory in feature space. (b) Different ears lying on different pose manifolds.

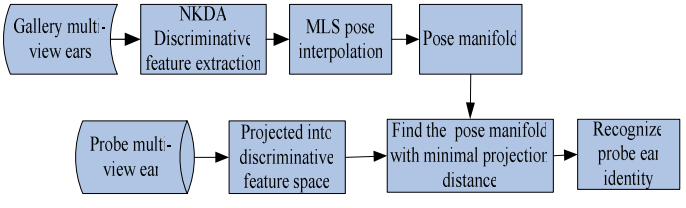

Fig. 2. Block diagram of the proposed MLS pose interpolation based multi-view ear recognition approach

From these hints and the figure, we can deduct that if we can use pose interpolation technique to construct the complete pose manifold, multi-view ear recognition can be solved. Based on this, our multi-view ear recognition approach can be formed with two main parts: NKDA feature extraction and moving least square pose interpolation. Fig.2 shows the framework of our MLS pose interpolation based recognition approach.

Considering if multiple pose interpolation can be built upon certain discriminative feature space, the good multi-view ear recognition performance could be expected. Thus following such thingking , we take NKDA method to extract discriminative features from gallery multi-view ears and thus construct the discriminative feature

space for pose interpolation. Obviously, every ear training sample can be projected onto this feature space at different locations. Then we can adopt MLS interpolation method to produce new multiple poses of certain projected training ear. In this way, since the good virtue of MLS, new poses of each subject ear can be accurately and smoothly obtained which are denoted by new projected points in the discriminative feature space. Once pose interpolation for all subject ears is completed, the pose manifold of every subject ear is constructed. In test stage, one probe ear is projected onto the discriminative feature space firstly. Then, we calculate the project distance of probe point to all existing MLS pose manifolds. And the subject of certain pose manifold which has the minimal distance to the probe point in this space is recognized as its identity.

2.2 Multi-view Ear Dataset

Our multi-view ear dataset are obtained by using high-resolution camera capturing with moving on a half-circle orbit with angle indication. In our case, we capture ear eight views ($-60°,-50°,-40°,-20°,0°,+20°,+40°,+60°$) in two sessions (one month interval) for multi-view ear recognition. Totally, we sampled 60 individuals' right ear and led to acquire 480 sampled images (eight views per individual). The pixel size of every sampled image is 1280×1024. The original sampled images were segmented in semi-supervised way and saved as multi-view ear data set. Thus, there are 60 ear individuals, and every ear individual has eight multiple views ($-60°,-50°,-40°,-20°,0°,+20°,+40°,+60°$) in our data set. The size of each final image is 134×255. For example, Fig. 3 shows ten ear individual different views and the views of each individual turn from -60^o into 60^o gradually from left to right. From Fig. 3, we see, multi-views ear preserve abundant shape features in different pose.

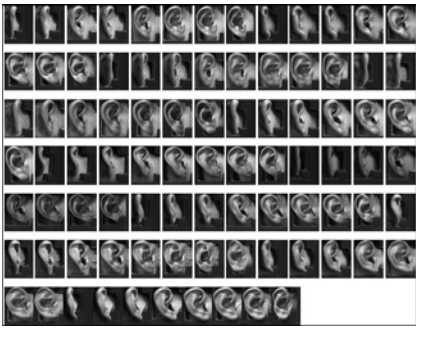

Fig. 3. Ten ears' multiple pose samples

3 Methodology

Multi-view ear location regression is analyzed firstly. Then null space kernel discriminate analysis (NKDA) is used to extract multiple pose non-linear features.

Finally, MLS is utilized to interpolate pose for constructing pose manifold explicitly in NKDA discriminative feature space for multi-view ear recognition.

3.1 Multi-view Ear Pose Location Regression Analysis

As far as ear is concerned, without expression (different from the face), the variability is simpler – only pose variation can take place. In our case, ear multiple pose images are acquired by rotating camera horizontally, which means there is only one freedom degree in motion, i.e., our pose variation is one dimension intrinsic manifold.

Suppose multi-view ear samples have been projected to certain feature space of which the dimension is d , x_i is one arbitrary projected pose sample in this space, e.g., $x_i \in IR^d$, and y_i is the true pose location of this sample in the feature space. From a statistical learning point of view, ear pose variation and the corresponding formed manifold (one dimension curve) can be regarded as one dimension pose location regression problem, i.e., finding one pose location regression function with constrains on smoothness and low variance to minimize the penalized residual sum of squares (RSS) via least squares method:

$$\arg\min_f RSS(f,\lambda) = \sum_{i=1}^{N} \left(y_i - f(x_i)\right)^2 + \lambda \int \left(f''(t)\right)^2 dt \tag{1}$$

where $f(x)$ denotes pose location regression function, N is the number of samples. The penalty term $\int \left(f''(t)\right)^2 dt$, weighted by smoothing parameter λ , forces smoothness on the function whereas the data fidelity measure term $\sum_{i=1}^{N} \left(y_i - f(x_i)\right)^2$ would make it rough so as to mimic the data. Remarkably, it has been shown that (1) has an explicit unique solution which is a natural cubic spline with knots at each $x_i, i = 1...N$ [15]. This approach is also called "spline smoothing" procedure.

With certain basis expansion, the regression pose location function $f(x)$ can be denoted by

$$f(x_i) = \sum_{m=1}^{M} \alpha_m p_m(x_i) = p^T(x_i)\alpha(x_i) \tag{2}$$

where $f(x_i)$ is a pose location approximation function for pose x_i . $p(x) = [p_1(x), p_2(x), \cdots, p_M(x)]^T$ is the k order complete monomial basis function, $\alpha(x) = [\alpha_1(x), \alpha_2(x), \cdots, \alpha_M(x)]^T$ is the coefficient of the basis function or parameter of the regression model, and M is the number of basis functions. For example, for two variables linear and quadratic monomial basis functions are, respectively,

$$\begin{aligned} p(x) &= [1, x, y]^T, M = 3 \\ p(x) &= [1, x, y, x^2, xy, y^2]^T, M = 6 \end{aligned} \tag{3}$$

Obviously, the work [11] takes the cubic spline, i.e. B-Spline, as pose location approximation basis function. However, for B-Spline, the number of support knots of the basis function and the calculation form of coefficient $\alpha(x)$ are fixed, this may lead pose approximation or interpolation not to be good. Thus, considering the coefficient $\alpha(x)$ are determined by a weighted least squares method minimizing the error $J(\alpha)$ between the experimental and approximated values of the objective function

$$J(\alpha) = \sum_{i=1}^{N} w(\|x_i - x\|)(p^T(x_i - x)\alpha - f(x_i))^2 \tag{4}$$

where N is the number of performed experiments and x_i is the experimental designs. The weights w_i insure the continuity and the locality of the approximation and are defined $w_i > 0$, decreasing within a fixed region around the point i called domain of support of x_i and vanish outside.

Min (J) gives

$$\alpha(x) = A^{-1}Bf(x) \tag{5}$$

where

$$A(x) = \sum_{i=1}^{N} w(x - x_i)p(x_i)p(x_i)^T, B(x) = [w(x - x_1)p(x_1), \cdots, w(x - x_N)p(x_N)],$$

finally, the approximate pose location function can be gotten as

$$f^h(x) = p^T(x)A^{-1}(x)B(x) \cdot f(x) \tag{6}$$

The more detail about MLS approximation procedure can be found in [16]. The weight function $w(x)$ plays a crucial role by influencing the way that the coefficients α depend on the location of the design point x. The precision of MLS approximation or interpolation in a large extent depends on weight function chosen.

Thus, in this way, we choose proper weight function and basis function to do MLS multi-view ear pose interpolation.

3.2 NKDA Multi-view Ear Discriminative Feature Extraction

Since multi-view ears are severely non-linear, in this work, null space kernel discriminate analysis (NKDA) is adopted to extract the non-linear ear discriminative features across multiple views. The details of NKDA can be found in [17]. We make a short introduction on the basic rules to derivate NKDA. Suppose we have a set of

n $d-$ dimension samples $x_1, x_2, ...x_n$ belonging to c classes of ear. The optimal projection direction W will be obtained from the following:

$$W = \arg\max_{W} \frac{W^T S_B W}{W^T S_W W} \tag{7}$$

where S_W is within-class scatter matrix and S_B is between-class scatter matrix. This is the basic rule of LDA. It will be easily proved that if S_W is a non-singular matrix then the optimal projection vectors W are the eigenvectors of $S_W^{-1} S_B$. Unfortunately, in small sample size problem in which the numbers of samples is much smaller than the dimension of samples space which makes S_W is always singular. Seeing that, one substitute- null space based LDA (NLDA) [18] was proposed. In this kind of method, the optimal projection W should satisfy:

$$W^T S_W W = 0, W^T S_B W = I \tag{8}$$

This equation means that the optimal discriminatory vectors must exist in the null space of S_W. Based on kernel function, NLDA can be extended to NKDA which will hold stronger potential both on non-linear feature extraction and class discriminating. Assuming the number of samples is N, the number of total classes is c, the dimension of input space is , the kernel function is $K(x, y)$, and the output non-linear dimension reduction mapping is Γ, the main step of NKDA can be summarized as:

Step1. Computing Kennel mapping matrix on every training sample: $K(x_i, x_j), i = 1...N, j = 1...N$.

Step2. Calculating every class mean and within-class scatter matrix: $m_j = \sum_{i \in C_j} K(x_i) / N_j$, $K_w = \sum_{j=1}^{c} \sum_{i \in C_j} (K(x_i) - m_j)(K(x_i) - m_j)^T$.

Step3. Extract the null space P of K_w such that $P^T K_w P = 0$. P is usually in $(N-1) \times (c-1)$.

Step4. The output mapping on the sample set is: $\Gamma(x) = (P^T K) \cdot (x) = P^T \cdot K(x)$.

We apply NKDA to extract non-linear features of multi-view ears. There are three popular kernel functions, and the RBF (Gauss) kernel is adopted in our experiments as:

$$K(x, y) = (\phi(x) \cdot \phi(y)) = \exp\left(\frac{-\| x - y \|^2}{\sigma^2} \right) \tag{9}$$

where σ is set to1000 in our experiments.

3.3 MLS Pose Interpolation Based Multi-view Ear Recognition

In most cases, existent ear pose are not consecutive and they need to be interpolated to form a continuous and smooth pose curve (see the illustration in Fig.1). Among all forms of numerical interpolation, thanks to MLS good characteristics, we use MLS method for pose interpolation to construct pose manifold. As we have discussed, in MLS approximation, if we take one order basis function with cubic spline weight function, MLS pose interpolation equals B-Spline based pose interpolation. In our approach, we take two order monomial basis function and gauss weight function for MLS pose interpolation. The gauss weight function is taken as:

$$w_i(x)=\begin{cases}\dfrac{e^{-r^2\beta^2}-e^{-\beta^2}}{1-e^{-\beta^2}} & 0\le r\le 1\\ 0 & r>1\end{cases} \tag{10}$$

where $r=d_I/d_{mI}$, $d_I=\|x-x_I\|$ is the distance from the point x_I to its' neighbor point x, $d_{mI}=\kappa\times c_I$ is the radius of influencing region at the knot point x_I, κ is the influencing region radius factor, greater than one), β is called weight factors. c_I represents the density feature of points distribution around the knot point x_I, β reflects the contribution degree for the neighbor points around the knot point x_I to get the weights. In our case, we find, as for ears' pose variation in $\lfloor -40^\circ,+40^\circ \rfloor$, if c_I is set to be the distance from x_I to its' closest neighbor with $\beta=2$, and for other ear poses, if c_I is set to be the distance from x_I to the second closest neighbor distance with $\beta=4$, the multi-view recognition performance is better

Then after pose interpolation, the category of unknown ear can be determined by ransacking all constructed ears pose manifolds. Suppose the pose manifold C_p for each individual ear p is known, then the recognition of ear multiple pose can be formally defined as: for a probe ear view I, the identity p^* can be determined by ransacking all pose manifolds to find the manifold C_p with minimal "distance" to I, i.e.,

$$p^*=\arg\min_p d_f(I,C_p) \tag{11}$$

where d_f represents L^2-Hausdorff distance between image I and C_p in feature space. Let $x\in C_p$ denotes a point on a manifold C_p and x^* is the point on C_p which is closest to I (i.e. at minimal L^2 distance), then $d_f(I,C_p)=d(I,x^*)$ where $d(\cdot,\cdot)$ denotes the corresponding L^2 distance. This procedure can be illustrated in Fig. 4.

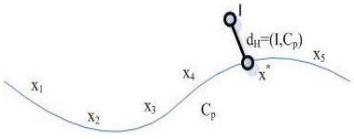

Fig. 4. Constructed pose manifold for multi-view ear recognition

4 Experiments and Comparisons

Our experiments are done based on our multi-view ear data set and ear samples are chosen randomly. In this data set, every ear has 8 multi-view samples. Firstly, we apply MLS pose interpolation technique in NKDA feature extraction space to construct pose manifold for multi-view ear identification. In order to make compare the performance with the work [11], we adopt the same training and test strategy, i.e., five views (-60^o,-50^o,-20^o,$+20^o$,$+60^o$) are treated as training samples and the left views (-40^o,$+0^o$,$+40^o$) are taken as probe samples. Since using Gauss weighted function for MLS pose interpolation, we show our method recognition performance with different parameters in Tabel.1.

Table 1. MLS pose interpolation based multi-view ear recognition with different parameters. (Adaptive c_1 and β mean in pose range [-40°, $+40^\circ$] c_1 takes the 1st closest point distance with $\beta = 4$, elsewhere c_1 takes the 2rd closest point distance with $\beta = 2$)

Parameters	Object numbers	Recognition rate
c_1 takes 1st, β=4	30, 60	91.7%, 96.7%
c_1 takes 2rd, β=2	30, 60	90.0%, 95.0%
Adaptive c_1 and β	30, 60	93.3%, 98.3%

For performance comparisons, we adopt different methods including manifold learning method [19-20], B-Spline based method, and our MLS pose interpolation based method for 60 subjects multi-view ears recognition. All experimental conditions are consistent to the previous experiments. The contrast results are shown in Table.2.

Table 2. Recognition contrast with manifold learning and B-Spline based methods

Methods	Dimension embedded	Neighbors	Recognition rate
LLE	22	35	65.0%
LPP	59	18	81.7%
B-Spline	59	3	96.7%
MLS pose interpolation based	59	Adaptive	98.3%

In addition, MLS pose interpolation based method does not need at least four training pose samples or knots, which is very different from B-Spline based recognition method. If we adjust d_{mI} and β of Gauss weight function to proper values for MLS interpolation, we can need the less available training views for multi-view ear recognition. Table.3 shows such experimental results with 60 subjects' ears. In the experiments, the left views excluding training views are taken as test views.

Table 3. Recogniton performance when taking different available training views

Available training views	Methods	Recognition rate
$(-50^\circ, -40^\circ, 0^\circ, +40^\circ)$	MLS interpolation based	85%
	B-Spline based	70.0%
$(-40^\circ, 0^\circ, +40^\circ)$	MLS interpolation based	73.3%
	B-Spline based	Unable to work

5 Conclusions

In this work, we investigate multi-view ear recognition methods beyond existing work in 2D ear biometrics. We take NKDA to extract multi-view ear non-linear features and do MLS pose interpolation in discriminative feature space to construct pose manifold. Adopting gauss weight function for MLS, we can get a 98.3% rank-one recognition rate against large pose variations in our multi-view ear data set. Experiments and comparisons have shown our MLS pose interpolation based method is very efficient for solving multi-view ear recognition problem. In the future, we will pay more attention on applying our MLS pose interpolation based method for multi-view face recognition.

Acknowledgement

This work is partially support by the Key Research Foundation of the Education Bureau of Sichuan Province (Grant no. 08ZA013), the CERG fund from the HKSAR Government, the central fund from Hong Kong Polytechnic University, and the Scientific Research Starting Foundation for Doctoral Scientist of Southwest University of Science and Technology.

References

1. Iannarelli, A.: Ear Identification. Paramont Publishing Company (1989)
2. Hurley, D., Nixon, M., Carter, J.: Force Field Feature Extraction for Ear Biometrics. Computer Vision and Image Understanding 98, 491–512 (2005)
3. Choras, M.: Ear Biometrics Based on Geometric Feature Extraction. Electronic Letters on Computer Vision and Image Analysis 5(3), 84–95 (2005)

4. Burge, M., Burger, W.: Ear Biometrics in Computer Vision. In: Proceedings of 15th International Conf. of Pattern Recognition, vol. 2, pp. 822–826 (2000)
5. Bustard, J.D., Nixon, M.: Robust 2D Ear Registration and Recognition Based on SIFT Point Matching. In: Proceedings of 2nd IEEE International Conference on Biometrics: Theory, Applications and Systems, pp. 1–6 (2008)
6. Moreno, B., Sanchez, A., Velez, J.: On the Use of Outer Ear Images for Personal Identification in Security Applications. In: Proceedings of IEEE Int'l Carnaham Conf. Security Technology, pp. 469–476 (1999)
7. Chang, K., Bowyer, K., Sarkar, S., Victor, B.: Comparison and Combination of Ear and Face Images in Appearance-based Biometrics. IEEE Trans. Pattern Analysis and Machine Intelligence 25, 1160–1165 (2003)
8. Yan, P., Bowyer, K.W.: Biometric Recognition Using 3D Ear Shape. IEEE Trans. Pattern Analysis and Machine Intelligence 29, 1297–1308 (2007)
9. Chen, H., Bhanu, B.: Human Ear Recognition in 3D. IEEE Trans. Pattern Analysis and Machine Intelligence 29, 718–737 (2007)
10. Xie, Z.X., Mu, Z.C.: Improved Locally Linear Embedding and Its Application on Multi-Pose Ear Recognition. In: Proceedings of 2007 International Conference on Wavelet Analysis and Pattern Recognition, pp. 1367–1371 (2007)
11. Zhang, Z.Y., Liu, H.: Multi-view Ear Recognition Based On B-Spline Pose Manifold Construction. In: Proceedings of the 7th World Congress on Intelligent Control and Automation, Chongqing, China, pp. 2416–2421 (2008)
12. Prince, S.J.S., Elder, J.H.: Tied Factor Analysis for Face Recognition Across Large Pose Changes. In: Proc. British Machine Vision Conference, vol. 3, pp. 889–898 (2006)
13. Li, Y.M., Gong, S.G., Liddell, H.: Constructing Facial Identity Surfaces for Recognition. International Journal of Computer Vision 53, 71–92 (2003)
14. Lee, K.C., Ho, J., Yang, M.H., Kriegman, D.: Video-Based Face Recognition Using Probabilistic Appearance Manifolds. In: Proc. of the IEEE Computer Society Conference on Computer Vision and Pattern Recognition, vol. I, pp. 313–320 (2003)
15. Green, P., Silverman, B.: Nonparametric Regression and Generalized Linear Models. Chapman and Hall, Glasgow (1994)
16. Lancaster, P., Salkauskas, K.: Surfaces Generated by Moving Least Squares Methods. Mathematics of Computation 37, 141–158 (1981)
17. Liu, W., Wang, Y.H., Li, S.Z., Tan, T.N.: Null Space-based Kernel Fisher Discriminate Analysis for Face Recognition. In: Proc. Sixth IEEE International Conference on Automatic Face and Gesture Recognition, pp. 369–374 (2004)
18. Chen, L.F., Liao, H.Y.M., Lin, J.C., Ko, M.T., Yu, G.J.: A New Debased Face Recognition System Which Can Solve the Small Sample Size Problem. Pattern Recognition 33, 1713–1726 (2000)
19. Roweis, S.T., Saul, L.K.: Nonlinear Dimensionality Reduction by Locally Linear Embedding. Science 290 (2000)
20. He, X.F., Yan, S.C., Hu, Y.X., Niyogi, P., Zhang, H.J.: Face Recognition Using Laplacianfaces. IEEE Trans. Pattern Analysis and Machine Intelligence 27, 328–340 (2005)

Experimental Comparison among 3D Innovative Face Recognition Frameworks

Vitoantonio Bevilacqua[1,2], Giuseppe Mastronardi[1,2], Raffaele Piarulli[1], Vito Santarcangelo[1,2], Rocco Scaramuzzi[1], and Pasquale Zaccaglino[1]

[1] Department of Electrical and Electronics, Polytechnic of Bari, Via Orabona, 4 – 70125 Bari, Italy
[2] E.B.I.S. s.r.l. (electronic Business In Security), Spin-Off of Polytechnic of Bari, Via Pavoncelli, 139 – 70125 Bari, Italy
bevilacqua@poliba.it

Abstract. In this paper, starting to the previous work on 3D face recognition, is presented an optimization of the search of the points ALS and ALD of the nose and a new graph approach for the recognition base on several new points. Experiments are performed on a dataset (44 3D faces) acquired by a 3D laser camera at eBIS lab with pose and expression variations. The face recognition performance on the 44 faces considered reach the 100% percentage.

Keywords: Head 3D model face recognition pose estimation symmetry self organizing map, Graph matching.

1 Introduction

Always more and more researchers work on 3D face processing including modelling and recognition [1]. Usually, a 3D face is a group of high dimensional vectors of the x, y and z positions of the vertexes of a face surface. Face recognition based on 3D has the potential to overcome the challenging problems caused by the expression, illumination variations [8]. However, many 3D face recognition approaches, especially the feature based ones require a robust and accurate facial feature localization. To the best of our knowledge, most of the methods do not use benchmark datasets to evaluate their results. Romero et al.[4] presented the first work on benchmark datasets based on FRGC database. They manually marked landmarks of eleven facial features including nose tip and eye corners. With those marked feature locations, the results of automatic feature identification can be measured and evaluated. This paper focuses on a different task and proposes two different steps where the former concerns the automatic identification and localization of a 3D Nose facial features, and the latter is the validation of the correct data obtained by means two independent 3D face recognition tasks. Experiments was performed by using an ASE format dataset of 23 images acquired in by a 3D laser scanner based on structured light with a resolution of 640 by 480. The applied 3D reconstruction method is based on analysis of two images, obtained illuminating sequentially the target surface, with two sinusoidal fringe patterns shifted in phase by 180° and the obtained data are a 3D clouds of point in ASE

D.-S. Huang et al. (Eds.): ICIC 2009, LNAI 5755, pp. 1096–1105, 2009.

format. Due to the short integration time, images may be acquired without room darkening (normal ambient illumination). Optical methods used for measurement of 3D geometry are based on two general principles, one related to the almost direct measurement/analysis of the light flight time (lidars, interferometers and holography) and the second related to geometrical triangulation. In the last group the viewing angles of a point of the object can be calculated from its position in the registered image/images or from the applied system settings (scanning devices). Single image acquisition with a projected fringe pattern of high spatial frequency is another kind of compromise towards one-shot entire scene 3D photography. This type of acquisition is usually related to the Fourier analysis of the image. As the main drawback of this approach is its sensitivity to the quality of the registered image (fringe pattern), which directly influences the precision of the phase unwrapping procedures as well as the final accuracy. Another weak point of this method is its intrinsic low resolution and artefacts caused by the extensive filtering applied in the spatial frequency domain, and in particular, in zones close to the analyzed lobe borders. As nose tip is the most prominent feature of the face, most of the previous work perform nose tip detection and uses the nose tip as the foundation to detect other features. However, many previous facial feature identification algorithms use an assumption that the nose is the closest point to the camera or device which acquires the 3D data [7][8].Although this supposition is true in most cases, there is no 100% guarantee due to the noise. Various pose rotations and the complex situation of hair and clothes could make some places closer than the nose. Some algorithms make use of the corresponding 2D texture information to detect the face area first then localize the nose tip within the selected 3D face crop[8]. This technique requires 2D texture and 3D shape to correspond correctly. However, for example, in some face datasets such as the Spring2003 subset of FRGC, the 2D texture channel is not always perfectly matched with the 3D shape channel. In [5] the authors addressed automatic nose tip localisation adapting Khoshelham GHT and describe an automatic repere point detection system with the purpose of obtaining a biometric system for AFR (Automatic Face Recognition) using 3DFace templates. That research was lead on a database of 3D-faces in ASE format, the GavaDB, given by the GAVAB research group of computer science department at the University of King Juan Carlos in Madrid and the authors show their results and claim successful localization rate of nose tip by means several correspondences in terms of very close results obtained by different algorithms but using a limited dataset without benchmark evaluation. Then starting from the 3D nose tip co-ordinates, obtained running the same previous code developed to automatically localize nose tip in ASE format cloud of points, in this paper the authors, propose firstly a new algorithm to localize other four 3D nose features, and two other different approaches to perform a 3D face recognition by using all the five nose points. In [4] a novel 2D face recognition method is proposed, in which face images are represented by a set of local labelled graphs, each containing information about the appearance and geometry of a 3-tuple of face feature points, extracted using Local Feature Analysis (LFA) technique. That method automatically learns a model set and builds a graph space for each individual, then proposes a two-stage method for optimal matching between the graphs extracted from a probe image and the trained model graphs is proposed and achieves perfect result on the ORL face set and an accuracy rate of 98.4% on the FERET face set. This paper is organized as follows. In section 2, are described the necessary steps performing a new

algorithm to localize ten typical nose repere points after the nose tip point detection obtained by using the 3D Hough method in [3]. The algorithm is presented in terms of geometrical 3D properties relevant in 3D cloud of points and is based on a graph approach that considers nine distances from nose tip point (approach explained in the section 3). Section 4 describes in details several techniques for Graph Matching considering the information of profile and angles. Section 5 shows the experimental results comparing the results obtained with PRN Graph Matching with our K5 Graph Matching previous approach [5].

2 Algorithms

Differently from previous publication we have implemented other algorithms for the search of points of repere, considering also the points of the eyebrow arched. An unstructured organization of points as that obtained from ASE file is complicated to manage, because it is impossible to move easily in the cloud. In this context has been useful to have the points organized in a YY matrix where each position has the relative Y value. This matrix has been obtained through the creation of a polygonal mesh that interpolates the terns of the point cloud. This approach permits a more easier scansion of the surface of the face using the easy management of the data in the matrix structure. The search of points of repere has been done by the scansion of the face made by the use of a "sliding vector" on the polygonal mesh, in order to determine the geometric-statistic features typical of the face. The "sliding vector" is an observation window that contains some elements of the YY matrix that at every step "scrolls" along the particular direction of movement.

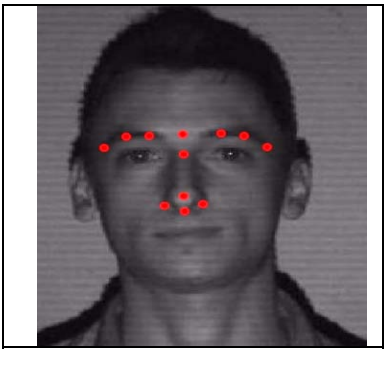

Fig. 1. Map of points of repere detected

This methodology allows the individuation of the following points:

-SN'
-ALS'
-ALD'
-G
-OTSx
-OTDx-SCLS2
-SCLS1
-SCLD1
-SCLD2

2.1 SN' Detection

The SN' point correspond to the nasal septum. Its search starts with the PRN point on the mesh and uses an horizontal sliding vector with vertical displacement. The algorithm consists of two phases:

-The first phase deals with the identification of the region where SN is expected and the individuation is done through a control on the variance of the sliding vectors. The phase ends when the difference between the variance of the current vector and the previous one is less than a set value of the threshold.

The procedure is based on the idea that, assuming a horizontal vector that encompass the entire width of the nostrils, the variance of its Y value is quite high in the vicinity of PRN point and quite low near the SN point where nose meets a flat surface.

-The second phase performs a detailed analysis of the region of interest determined to establish the horizontal coordinate more observant of the SN point.

This is achieved by exploiting the information on the orientations of the normals of the mesh considered in order to select as the final horizontal coordinate of the polygon whose normal forms the smallest angle with the Y axes.

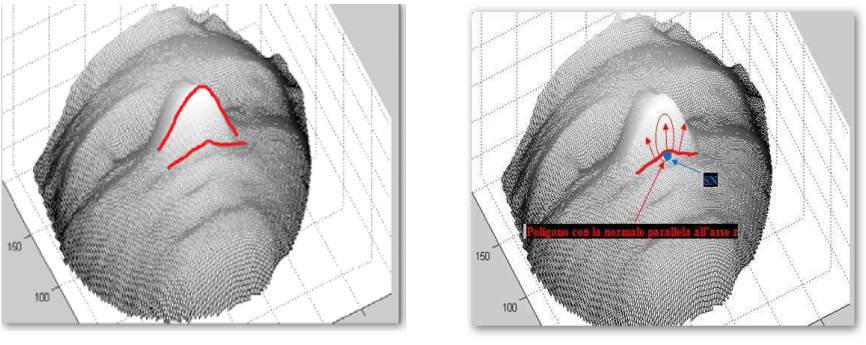

Fig. 2. Sliding vectors on the face for the individuation of the point

2.2 ALS' e ALD' Detection

Identified the SN point, is possible to search the two points ALS' and ALD '. The ALS-ALD points are located just outside the nasal cavities, specifically at the ends of wing cartilage. The algorithm starts by the coordinates of the SN point previously determined : the surface at the left of that point is scanned scrolling a sliding vertical vector (1st phase). The stop condition of the first phase is given by a control on the standard deviation of sliding Vectors: when the deviation is sufficiently low, the sliding vector crosses the nasal cavity because the Y are almost constant. After the 1st phase the x coordinate of ALS point is detected, and from this point found starts a horizontal sliding vector in the direction of increasing z coordinate: the goal is to identify the corresponding point outside the nasal cavity. The mission is to determine,

which among all the sliding vectors, is the one in which there is a greater standard deviation of Y: this equates to select the vector corresponding to the outermost point of the nostril. The algorithm of the identification of ALD point is opposite.

2.3 G Detection

G point is located just above the N point (whose algorithm has been mentioned in the previous publication), and corresponds to the start of frontal sinus, and also it can be noted that has planar characteristics in its area. The algorithm designed for its identification is based precisely on this observation: starting by the PRN point the upper surface is scanned through horizontal sliding vectors until reaching the front. The stop condition of the algorithm is given by a control on the standard deviation of sliding vectors: when the deviation is low, it can be assumed that the surface is planar.

2.4 OTSx-OTDx Detection

Points OTsx - Otdx are located outside the ends of the eyebrow arches : at such points the eyebrow arch closes, and there it's possible to detect a steep slope that leads to the lateral surface of the face. Starting from the found G point, the surface immediately to its left is analyzed to found the eyebrow arch, then continue along the arch until terminates.

The stop condition of the algorithm is reached when the difference between the average number of Y of the current vector and the next vector exceeds a certain threshold value. The overcoming of this threshold indicates the transition in an area where the slope is very pronounced, distinctive feature of the region where there is the point OTsx.

2.5 SCLs Detection

The SCLs points are located in an intermediate position between point G and points OTsx and OTDx. They are descriptive of the profile of the eyebrow arch, so it is possible to calculate it quite simply, using the information of these profiles, obtained in the algorithms of the points OTSx and OTDx. The individuation of these points can be considered as a sort of sampling of the profile of the eyebrow arch, in fact, they are determined dividing the distance (in terms of horizontal coordinate) between point G and point OTSx into three equal parts; then the point SCLs1 is the point of the arch corresponding to one third of that distance, while the SCLs2 point corresponds to the point of two thirds of that distance. The specular procedure is for the SCLd points.

3 Prn Graph Matching

PRN Graph Matching is based on the matching of the distances calculated regarding a point of reference (PRN point). In this technique are considered 9 points of reference and PRN for a total of 9 distances to match.

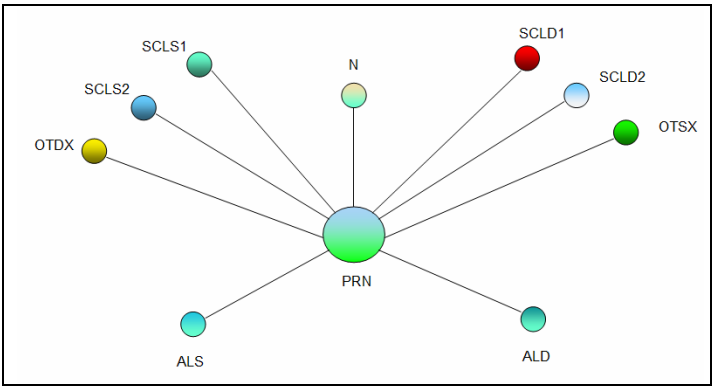

Fig. 3. PRN Graph

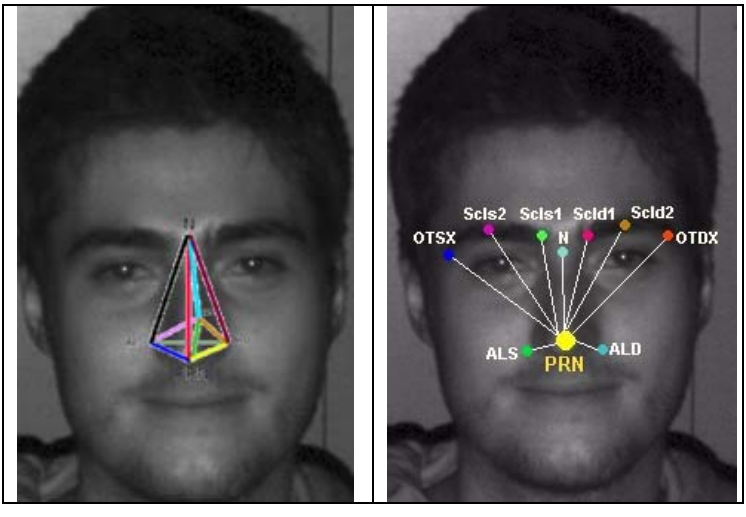

Fig. 4. K5 Graph Matching and PRN Graph Matching

The technique as that of K5 Graph Matching [5] is based on the use of the dissimilarity coefficient :

$$Z(Gi,Gj)=\frac{1}{n}\sum_{k=1}^{n}\frac{(e_{ik}-e_{jk})^2}{(e_{jk})^2}, \tag{1}$$

where $G_i=\{(e_{i1},e_{i2},....,e_{in})\}$ is the MODEL GRAPH and $G_j=\{(e_{j1},e_{j2},....,e_{jn})\}$ is the TEST GRAPH, where e_{ij} are the edges .

Besides to consider only the distances between points and PRN, an other difference regarding K5 Graph Matching [5] is not considering the SN point because , being the SN-PRN distance little important, the performance get worse considering it.

4 Support Tecniques for Graph Matching (Profile Matching, Triple Graph Matching)

The recognition system based on PRN Graph Matching can be optimized considering two methods of support, one based on a profile analysis and the other on the study of the angles between each point of repere and the point PRN (reference point).

4.1 Profile Matching

The information about the profile can be a key parameter to set a good algorithm for recognition, because:

1) working with 3D models involves a high computational cost, so the use of the information of the profile can be used to define a kind of indexing of the faces of the reference database. In this case, identified the profile of the face to search, we considers only the faces compatible with this profile.

2) it is possible to improve the accuracy of the recognition, excluding the faces corresponding to the "incompatible" profiles with that to search.

The algorithm "Profile Matching" is designed to make a first check on profiles, testing the compatibility of the profile of the face to identify with all the profiles of the faces in the database.

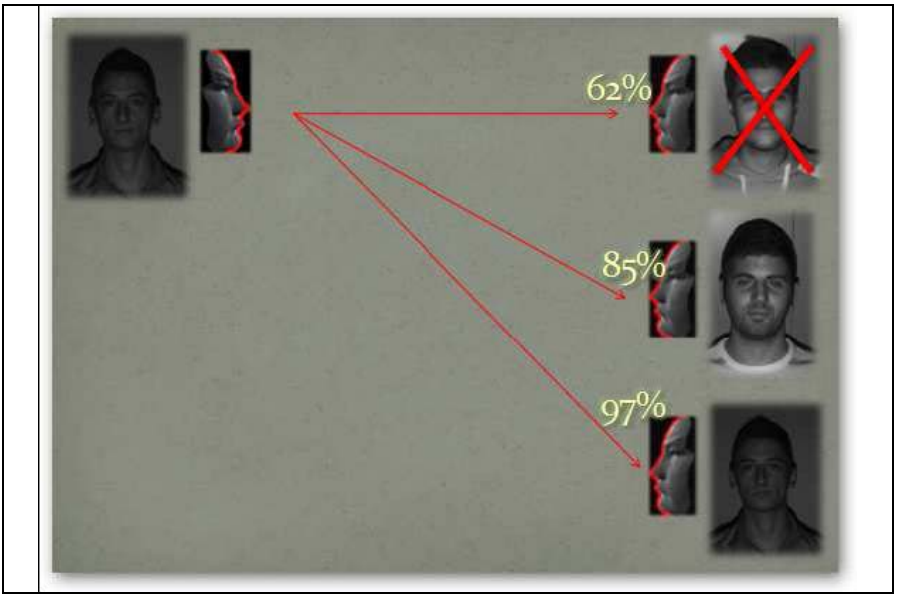

Fig. 5. Profile Matching

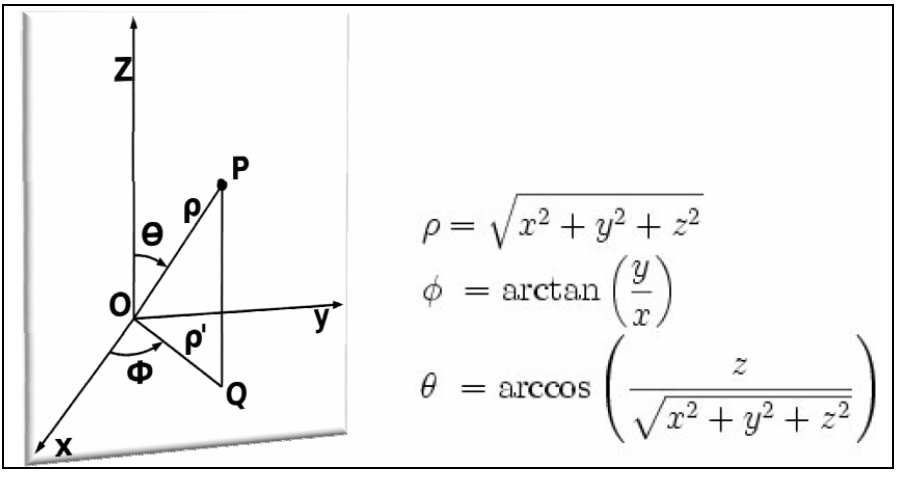

Fig. 6. Spherical Reference System

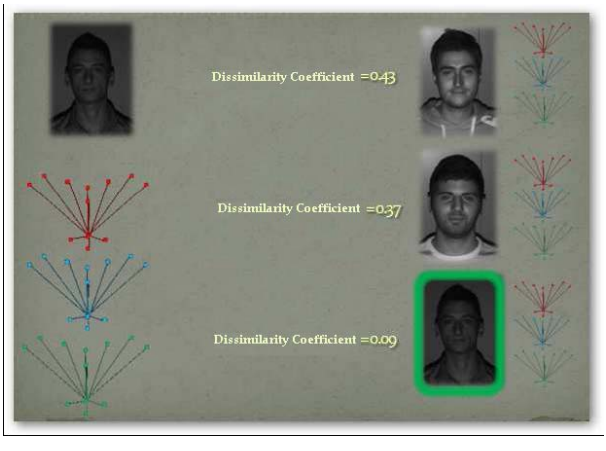

Fig. 7. Triple Graph Matching

4.2 Triple Graph Matching

In order to implement this technique is necessary to switch to a spherical reference system considering the point PRN as source. Thus for each point of repere we have two further information (θ and Φ angles).

It's so possible to exploit the tern of the information available for each point:

1)The matching of similar graphs (distances, tetha, phi) is used to obtain a tern of dissimilarity coefficients;

2)The information of the three coefficients is used "merged" by adding them into a single dissimilarity index ,possibly weighted by appropriate coefficients;

3)By comparing these indexes is possible to establish which tern of graph is globally more similar to the considered tern.

5 Results

In this paper we have considered a dataset of 5 people A,B,C,D,E , and precisely:

-11 acquisitions of A,
-6 acquisitions of B,
-10 acquisitions of C,
-9 acquisitions of D,
-8 acquisitions of E

for a total of 44 acquisitions.

Using K5 Graph Matching [5] the performances are of 77,2% , while considering PRN Graph Matching the performances of correct recognition are of 100%

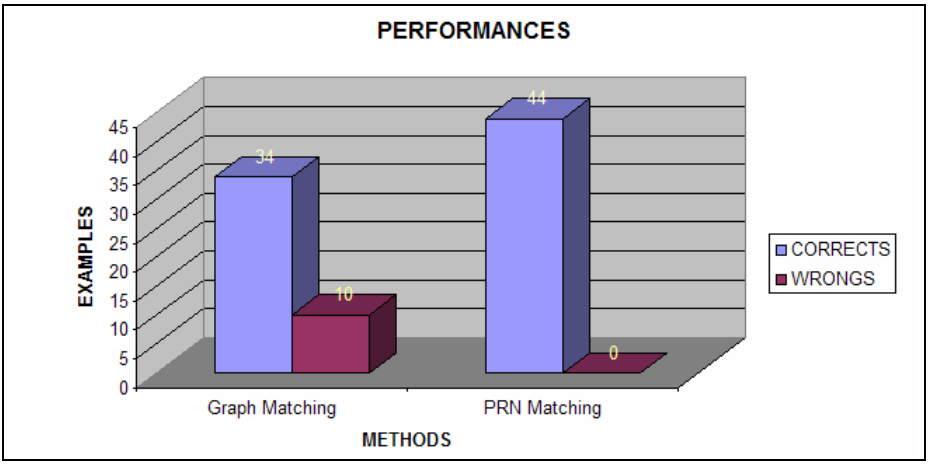

Fig. 8. Performances

Acknowledgements

V. Bevilacqua and G. Mastronardi were supported in part by PELAGOS Project, Interreg III A Grecia-Italia 2000-2006, Asse I - Misura 2 - Azione D1, (http://www.pelagosproject.org/).

References

1. Akarun, L., Gökberk, B., Salah, A.A.: 3D Face Recognition for Biometrical Applications
2. John, S.Z., Tsotsos, J.K.: Robust Face Recognition Through Local Graph Matching
3. Bevilacqua, V., Casorio, P., Mastronardi, G.: Extending hough transform to a points' cloud for 3D-face nose-tip detection. In: Huang, D.-S., Wunsch II, D.C., Levine, D.S., Jo, K.-H. (eds.) ICIC 2008. LNCS (LNAI), vol. 5227, pp. 1200–1209. Springer, Heidelberg (2008)

4. Romero, M., Pears, N.: 3D Facial Landmark Localisation by Matching Simple Descriptors. In: 2nd IEEE Int. Conf. Biometrics: Theory, Applications and Systems, Arlington VI (2008)
5. Bevilacqua, V., Mastronardi, G., Santarcangelo, V., Scaramuzzi, R.: 3D NOSE Feature Identification and Localisation Tthrough Self Organizing Map and Graph matching. Journal of Circuits, Systems and Computers (2009)
6. Hesher, C., Srivastava, A., Erlebacher, G.: A Novel Technique for Face Recognition Using Range Imaging. In: Internat. Multiconference Comput. Sci.
7. Lee, Y., Park, K., Shim, J., Yi, T.: 3D Face Recognition using Statistical Multiple Features for the Local Depth Information. In: Proc. 16th Internat. Conf. Vision Interf
8. Bowyer, K., Chang, K., Flynn, P.: A Survey of Approaches and Challenges in 3D and Multi-Model 3D+2D Face Recognition. In: CVIU vlo 101, pp. 1—15 (2006)

Retinal Vessel Extraction by a Combined Neural Network–Wavelet Enhancement Method

Leonarda Carnimeo[1], Vitoantonio Bevilacqua[1,2], Lucia Cariello[1,2], and Giuseppe Mastronardi[1,2]

[1] Department of Electrical and Electronics, Polytechnic of Bari, Via Orabona, 4 – 70125 Bari, Italy
{bevilacqua,mastrona,carnimeo}@poliba.it, cariello@deemail.poliba.it
[2] e.B.I.S. s.r.l. (Electronic Business In Security), Spin-Off of Polytechnic of Bari, Via Pavoncelli, 139 – 70125 Bari, Italy

Abstract. This paper presents a combined approach to automatic extraction of blood vessels in retinal images. The proposed procedure is composed of two phases: a wavelet transform-based preprocessing phase and a NN-based one. Several neural net topologies and training algorithms are considered with the aim of selecting an effective combined method. Human retinal fundus images, derived from the publicly available ophthalmic database DRIVE, are processed to detect retinal vessels. The approach is tested by considering performances in terms of sensitivity and specificity values obtained from vessel classification. The quality of vessel identifications is evaluated on obtained image by computing both sensitivity values and specificity ones and by relating them in ROC curves. A comparison of performances by ROC curve areas for various methods is reported.

Keywords: Retinal vessel extraction, Wavelet filter, Vessel evidencing, Vessel confidence measurement, Artificial neural network.

1 Introduction

It is well known that retinal images can provide information about human fundus blood supply systems to be used in a variety of ophthalmic disorders [1, 2]. In fact, retinal vessel detection techniques can effectively help to assess the severity of retinal diseases by analyzing abnormal retinal images [3]. Over the past 15 years exciting developments in image processing relevant to ophthalmologists were achieved, including, for example, improvements towards automated diagnostic systems in cases of diabetic retinopathies [4]. It should be précised that diagnostic systems reveal very important for supporting eye doctors in large-scale screening programs, due to their significant resource savings, being manual measurements throw visual inspection quite time-consuming or even impossible [5]. In particular, the development of retinal vessel detection techniques is an important area in a variety of medical applications. However, the accuracy with which blood vessels are extracted from images is crucial.

D.-S. Huang et al. (Eds.): ICIC 2009, LNAI 5755, pp. 1106–1116, 2009.

Approaches to blood vessel detection in digital retinal images can be roughly divided into two main classes: synchronous network segmentation and single vessel tracking [5-10]. In synchronous segmentation each pixel is classified on the basis of identical local features, including local adaptive thresholding [6], wavelet transform [7-9] and morphological filtering [10], whereas in tracking methods a continuous vessel segment search starting from a given point is provided [5]. Beyond this one, in [8] the feature vectors from ridge extraction and a kNN-classifier for vessel detection are employed. Taking into account that blood vessels of different caliber should be all properly detected [11, 12]. in this paper a contribution for segmenting blood vessels in retinal images by a combined neural network - wavelet enhancement method is presented. The proposed approach is composed of two steps: a wavelet transform-based preprocessing phase and a Neural Network-based one followed by the necessary postprocessing code operation. The method is applied to human retinal fundus images provided by ophthalmologists in the publicly available database DRIVE [13]. The quality of vessel identifications in each obtained image is locally evaluated by computing sensitivity values and specificity ones and by relating them in ROC curves. Performances are evaluated on the same images by means of a comparison of ROC curve areas developed by other methods.

2 Retinal Vessel Extraction

The objective of this experiment is to elaborate a system that enables retinal blood vessel structure extraction from fundus oculi images. For this purpose, retinal images are firstly processed through some subsequent filtering operations, and then a neural net classifies every pixel as belonging to a retinal image either as “Vessel” or “Not Vessel”. As shown in Fig. 1, the fundus oculi image is input to a preprocessing phase in which two filtering methods are applied. The successively transform-wavelet phase has the most important task of extracting the main characteristics from input images, evidencing vessels through a Hessian Matrix and by measuring vessel confidence. The objective of the preprocessing stage is to provide specific features to the Neural Net-based block. Neural net outcomes will be properly codified by a postprocessing block to obtain output images.

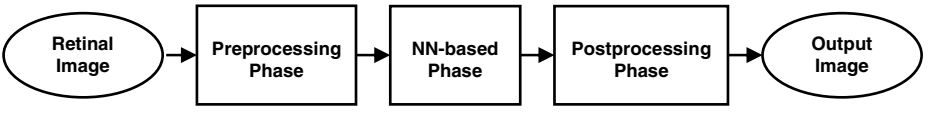

Fig. 1. Block diagram of retinal vessel extraction method

2.1 Preprocessing Phase

Throughout the preprocessing phase, RGB fundus images undergo various filtering that highlight vessel structures and play down on other anatomic parts (considered as disturbances in this context). All images come from the publicly available database DRIVE [13] made up of (768×576)-size retinal fundus images (8bit per channel).

Every image IRGB, is firstly separated into its RGB components: IR, IG, and IB. As vessels in the green component are more evident, image IG is used as an input for successive filters. A mask is extracted from the red component IB, which is the round area that limits the section of interest, by excluding corner black bands. This mask is used in different filtering steps to avoid considering black band areas. The used filters, i.e., wavelet transform, vessel evidencing and vessel confidence measurement, will be herein described.

Wavelet Transform. An image can be a square signal, f, obtained as the integral defined on $\Re^2$, $f \in \mathbf{L}^2(\Re^2, d^2\mathbf{x})$ which can be expressed as [7]:

$$\|f\|^2 = \int_{\mathbb{R}^2} |f(\mathbf{x})|^2 \, d^2\mathbf{x} < \infty, \tag{1}$$

where $\mathbf{x} \in \Re^2$ is a vector. As a consequence, the transformed continuous wavelet of $f(\mathbf{x})$ is given by:

$$W(\mathbf{b}, \vartheta, a) = \frac{(C_\psi)^{-1/2}}{a} \int f(\mathbf{x}) \psi^*(a^{-1} r_{-\vartheta}(\mathbf{x} - \mathbf{b})) d^2\mathbf{x}, \tag{2}$$

where C_ψ is a normalization constant. Thus, the complete form of 2D CWT is a function with four variables: the pair (b_x, b_y), that defines the position on the image plane, and the pair (a^{-1}, ϑ), that is responsible for spatial frequency, expressed in polar coordinates (note that the term a^{-1} is equivalent to frequency) [7].

Calculating and visualizing the whole CWT 2D and its variables is very difficult to obtain, and for this reason, some variables are held as fixed. Specifically, in order to identify border, shape or position of the objects, a spatial representation is used in image analysis, where pairs (a, ϑ) are fixed and the CWT is the function of (b_x, b_y). As in [8], in order to calculate the transformed wavelet, a fixed scale a is adopted and relation (2) is calculated, by varying ϑ in such a way as to take the different vessel orientations into account. Specifically, the angle ϑ it is varied by a ten degree rate on the [0°, 170°] range. From this transform set, the maximum value is calculated on the module:

$$W_a(\mathbf{b}) = \max_{\vartheta} |W(\mathbf{b}, a, \vartheta)|. \tag{3}$$

The wavelet filter is applied to the I_G image with the scale values a=2, 3, 4, 5. In Fig. 2 an example of application of this filter for a = 2 is shown.

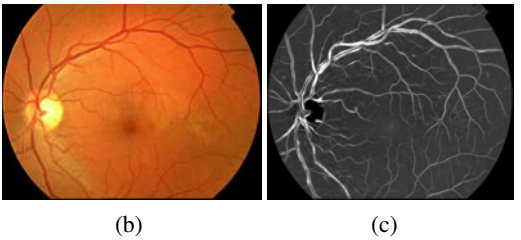

(b) (c)

Fig. 2. Wavelet filtering phase: (a) I_{RGB} selected retinal image; (b) output image after applying filtering to image I_G with a =2

Vessel Evidencing. The second filter in the pre-processing phase aims at evidencing of vessels, particularly of smaller vessels, as in [11]. In order to achieve this target, parameters of image I_G are calculated, based on the Hessian matrix auto-values.

Then an estimation of probability is derived from these measures. The analysis of the Hessian matrix auto-values targets extraction of the main directions which can be decomposed, in a local structure of the second stage image [11]. The auto-values of the Hessian matrix H are:

$$\lambda_1 = \frac{1}{2}\left[\left(I_{xx} + I_{yy}\right) - \sqrt{\left(I_{xx} - I_{yy}\right)^2 + 4\left(I_{xy}\right)^2}\right]$$

where $|\lambda_1| \le |\lambda_2|$.

$$\lambda_2 = \frac{1}{2}\left[\left(I_{xx} + I_{yy}\right) + \sqrt{\left(I_{xx} - I_{yy}\right)^2 + 4\left(I_{xy}\right)^2}\right] \tag{4}$$

Through the analysis of relations amongst auto-values, it is possible to individuate various structures within the image. Due to the fact that retinal vessels are herein to be individuated, it is necessary to search for "tubular" structures which satisfy:

$$|\lambda| \approx 0, \qquad |\lambda| \le |\lambda_2| \tag{5}$$

Taking into account (4), the following relation can be computed:

$$R = \frac{\lambda_1}{\lambda_2}. \tag{6}$$

which provides a measure of the "circularity" (distinguishing the form of an anatomical structure from a circular one); for tubular structures, $R = 0$.

Besides information deriving from the anatomy, it is necessary to consider also the fact that vessels present lighter in shade than background in image I_G. In order to transform this information in a quantifiable measure, the Frobenius norm is applied to the Hessian matrix. As the Hessian matrix is true and symmetrical, its Frobenius norm can be expressed as a function of auto-values:

$$S = \|H\|_F = \sqrt{\lambda_1^2 + \lambda_2^2}. \tag{7}$$

This measure is negligible in the areas where anatomical features are not present (background areas) and vice-versa, it assumes a high value where there are anatomical structures (i.e. a stronger contrast compared to background areas).

Conditions (5) and (6) merge in the following function [11]:

$$v(s) = \begin{cases} 0 & \text{se } \lambda_2 > 0 \\ e^{-\frac{R^2}{2\beta^2}}\left(1 - e^{-\frac{S^2}{2c^2}}\right), \end{cases} \tag{8}$$

where the factor $\beta = 0.5$ and $c = \max(S)/2$.

This expression involves the various measures calculated in (5) and (6) in a probability estimation. Therefore, relation (7) indicates the probability of each pixel belonging to a vessel or not on the s scale. For a group of pixels, probability will be maximum in correspondence to the scale proximate to the thickness of the vessel to which it belongs. The final outcome of the filter integral on all scales of measure (7):

$$E = \max_{s_{\min} \le s \le s_{\max}} \nu(s), \tag{9}$$

where $s_{\min}$ and $s_{\max}$ are minimum/maximum scales with which vessels are analyzed, respectively.

Conforming to results given in [12], range scale pixels are used at a $0.5 \le s \le 3$ pixel rate.

In order to implement (8), all $v(s)$ calculated on a $\boldsymbol{V}$ matrix are memorized and then used to calculate the maximum value. Besides the maximum E, the s scale (s_m) is also computed and to which maximum value this is presented, as well as the corresponding matrix $\boldsymbol{V}$ index i.

Finally, the orthogonal direction of the autovector $\mathbf{u}_2$ corresponding to the maximum auto-value λ_2 is calculated:

$$\phi(s) = \tan^{-1}(\mathbf{u}_2) + 90° = \tan^{-1}\left(\frac{I_{xy}}{\lambda_2 - I_{xx}}\right) + 90°. \tag{10}$$

All values of $\phi(s)$ of the variant s, are memorized in the **D** matrix. The matrix $t=\boldsymbol{D}(i)$ is extracted from this and corresponds to the perpendicular direction of the autovector $\mathbf{u}_2$, with its maximum scale calculated at each point. The block diagram of the vessel evidencing filter and the output image are highlighted in Fig. 3. Moreover, the values of s_m and t will be the filter inputs for the measurement of vessel confidence.

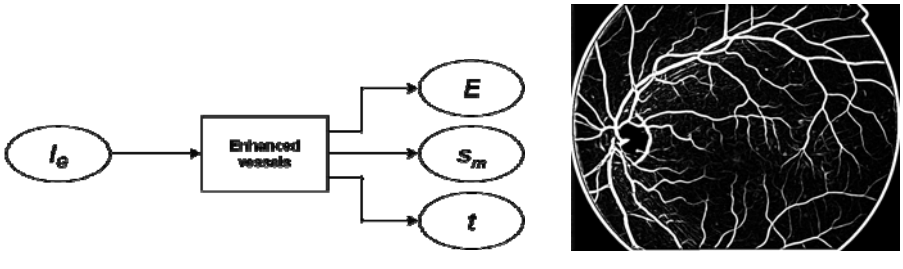

(a) (b)

Fig. 3. Vessel evidencing filter: (a) block diagram; (b) outcome filtered image

Vessel Confidence Measurement. A proper multi-scale filtering, which computes how much each pixel adapts to the retinal blood vessel model, is here realized. It is represented by a Gaussian profile along the vessel orientation and from the derivative according to the Gaussian function along the transversal direction of the same vessel [12]. By considering **M** as the filter matrix and the **F** matrix as corresponding pixels

of the image and by reordering their columns in vectors **m** and **f** respectively, the convolution at the *(x,y)*-coordinate can be defined as:

$$P(x, y) = \mathbf{f}^T \cdot \mathbf{m}. \tag{11}$$

The filter is defined as:

$$M(x_1', y_1') = \frac{\sqrt{s}}{2\pi s^2}\left(\frac{x_1'^2}{s^2} - 1\right) e^{-\frac{x_1'^2}{2s^2}} e^{-\frac{y_1'^2}{2b}}. \tag{12}$$

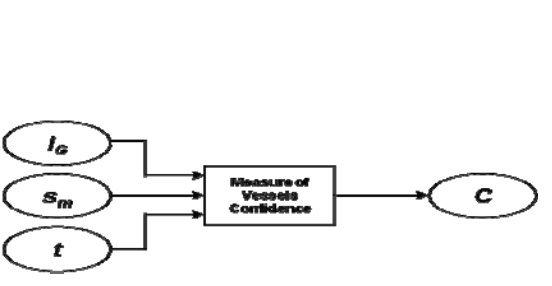

(a)

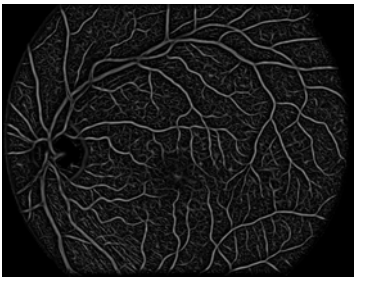

(b)

Fig. 4. Vessel confidence measurement: (a) block diagram; (b) outcome filtered image

2.2 Artificial Neural Network

The outputs of previous filters result to be inputs to the subsequent neural network. All pre-processing filters, however, have matrices as outcomes, whereas the neural net usually accepts vectors (as f(.) in Fig.5). These vectors are normalized in such a way as to obtain a null media and a unit standard deviation. More in detail, 9 vectors constitute the neural network entry vector: v=[vR, vG, vB, va=2, 3, 4, 5, vE, vC]T. (see Fig. 5). The first element of every vector corresponds to the exit of a filter for each pixel which has the task of classifying pixels as "Vessel" or "Not Vessel" ones.

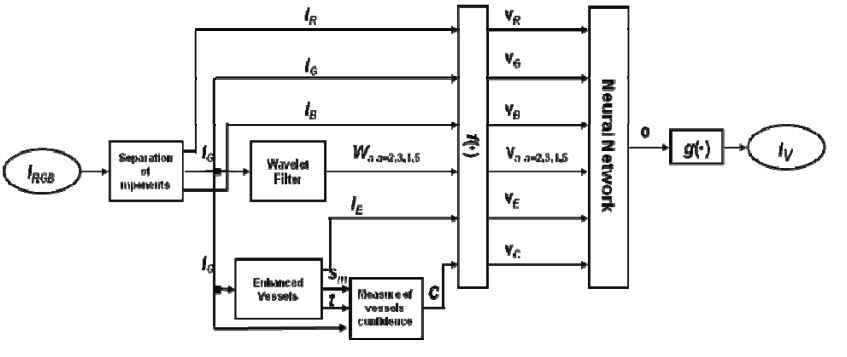

Fig. 5. Detailed block diagram of the proposed retinal vessel extraction method

A supervised Multilayer Perceptron net topology was preferred for this operation. It is widely used in literature for classification tasks. From Fig.5, it can be noted how the nine subvectors vi are obtained at the end of the pre-processing phase and are used as entry to the neural net. This implies that the MLP net has nine input neurons. Then, only one output neuron will be necessary to make the net classify pixels as "Vessel" or "Not Vessel". Finally, a single hidden layer topology was adopted. Concerning with hidden neurons, the testing of several nets with a variable number of neurons (between 5,10 and 15) was deemed best practice. Tested topologies were: 9-5-1, 9-10-1 and 9-15-1. The behavior of each of these topologies, was analyzed by considering different training algorithms: GDX (Gradient Descendent adaptive learning rate with momentum), SCG (Scaled Conjugate Gradient) and LM (Levenberg-Marquardt) ones. All neurons present a non-linear hyperbolic tangent activation function. In Fig.5 the neural net output values were progressively stored in vector form and re-coded to obtain the output image Iv.

3 Experimental Results

In order to train different net topologies, the human retinal images shown in Fig.6 were considered.

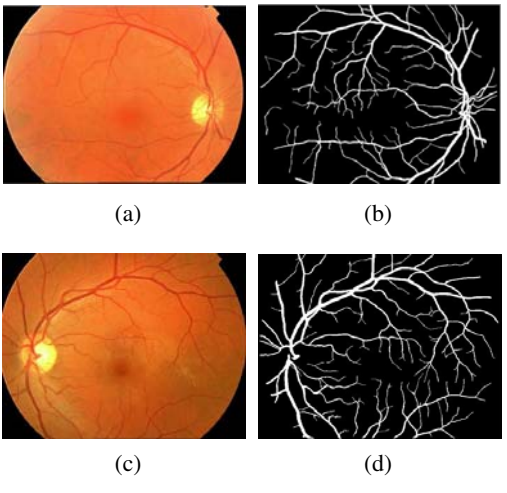

Fig. 6. Selected human retinal images and their gold standard: (a), (b) right eye; (c), (d) left eye

After the pre-processing phase, the vector **v** of (9×768×576) elements was obtained. An amount of 100,000 randomly chosen elements of the two images was considered for training purposes. These samples were collected in such a way as to maintain the same proportion of Vessels and Not Vessels existing in the two training images (11.7% Vessel, 88.3% Not Vessel). The total of samples were then divided into a *training set* and a *validation set.* The training set was composed of over 70,000 samples and the validation set was made up of 30,000 samples. In order to carry out

the net test, a further image was selected. After validating the synthesized net, the obtained outcome image in Fig.7 (a) was compared with the gold standard image in Fig.7 (b). In order to evaluate the best neural net topology, a ROC (*Receiver Operating Characteristic*) graph has been considered. The ROC analysis is a technique used to visualize and select classifiers on the basis of their performance [8, 9, 12-15, 17]. Each net outcome sample is compared with a threshold value: TP=True Positive, TN=True Negative, FN=False Negative and FP=False Positive where pixels classified as Vessel are TP or TN, if vessel is present or absent, respectively; moreover pixels classified as Not Vessel are FN or FP, if vessel is present or absent respectively.

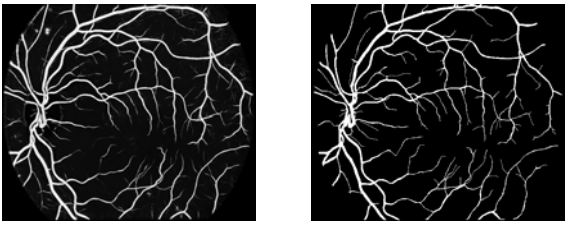

(a) (b)

Fig. 7. (a) Obtained outcome of retinal test image; (b) corresponding gold standard image

Being Sensitivity and Specificity defined as:

$$sensitivity = \frac{TP}{TP + FN}, \qquad specificity = \frac{TN}{FP + FN} \tag{13}$$

then, the ROC curve is a representation of Sensitivity versus 1-Specificity in case of different number of hidden neurons and for the same training algorithm. This curve represents the equilibrium between benefits (TP) and costs (FP) [18]. The net performance can be evaluated by means of the areas of ROC curves. A neural net performs better if its ROC curve supports those of the other considered nets. In all cases for the GDX, SCG and LM training algorithms, good performances have been obtained. Moreover, differences among ROC curves when varying the number of hidden neurons, reveal negligible except for the LM training algorithm, for which the (9-5-1) net topology performs much better than those with 10 or 15 hidden neurons, as its curve significantly subtends the others.

As predicted, the LM algorithm converges faster than the other algorithms, despite the drawback of an increased computational burden and memory requirements. The GDX algorithm, though demanding less resources, converges much slower (employing more training epochs) than the LM and SCG algorithms. The SCG algorithm represents a good compromise as it requires less resources than the LM algorithm, but converges quicker than the GDX algorithm.

In Table 1, the ROC curve areas are listed for all training algorithms for the adopted (9-5-1) topology, even if the difference in performance between SCG and LM is reduced.

Table 1. Comparative results of the various training algorithms

Training algorithm	Net topology	Area ROC	Training steps	Error (MSE)
GDX	9-5-1	0.9664	177	0.0725
SCG	**9-5-1**	**0.9841**	**126**	**0.0669**
LM	9-5-1	0.9804	27	0.0664

In order to compare obtained performances by the proposed method with other architectures developed in literature, the DRIVE database [13] is considered.

The DRIVE (*Digital Retinal Images for Vessel Extraction*) database is constituted of a series of color images (565x584 pixels) of human fundus oculi collected during a screening program carried out in Holland [13]. This database is formed by a total of 40 images divided into a training set and a test one, both containing 20 images. Manual segmentations are available on each set of the database. The first two images of the training set, from which 100,000 samples were taken (70,000 for training set and 30,000 for the validation set), were used to train the MLP neural net. Testing was carried out on all test sets provided by the database and by the image in Fig.7(a). The ROC curve area was used to compare segmentation methods from literature [16]. The corresponding results are shown in Table 2 together with performances obtained from the synthesized MLP net.

Table 2. Comparison with other methods cited in literature

Method	**ROC Curve Area**
Staal [13]	0.9520
Niemeijer [16]	0.9294
Zana [10]	0.8984
Soares [8]	0.9614
Net SCG 9-5-1	0.9623

It can be noted that result is very similar to the one obtained by Soares et al. in [8] using the 2D Gabor wavelet.

4 Conclusions

This paper presents a combined method for supporting automatic extraction of blood vessels in retinal images for diagnosis of eye disorders. The proposed approach is based on two phases: a wavelet transform-based preprocessing phase and a neural network-based one, with an image post-processing code. The method is applied to human retinal fundus images derived from the publicly available database DRIVE. The algorithm is tested by considering performances in terms of sensitivity and

specificity values obtained from vessel identification and by relating them in ROC curves. A comparison of performances by ROC curve areas for various methods has been reported and the proposed approach reveals comparable and thus satisfactory..

References

1. Pattona, N., Aslamc, T.M., Mac, G.T., Dearye, I.J., Dhillonb, B., Eikelboomf, R.H., Yogesana, G.K., Constablea, I.J.: Retinal image analysis: Concepts, applications and potentials. Progress in Retinal and Eye Research 25, 99–127 (2006)
2. Kanski, J.J.: Clinical Opthalmology, 3rd edn. Butterworth Heinemann, Butterworths (1997)
3. Kirbas, C., Quek, F.K.H.: Vessel extraction techniques and algorithms: a survey. In: Third IEEE Sym. on Bioinformatics & Bioengineering, Bethesda, Maryland, March 10-12, pp. 238–245 (2003)
4. Carnimeo, L.: Diabetic Damage Detection in Retinal Images via a Sparsely-Connected Neurofuzzy Network. In: Huang, D.-S., Wunsch II, D.C., Levine, D.S., Jo, K.-H. (eds.) ICIC 2008. LNCS (LNAI), vol. 5227, pp. 1175–1182. Springer, Heidelberg (2008)
5. Li, H., Hsu, W., Lee, M.L., Wang, H.: Automatic grading of retinal vessel calibre. IEEE Trans on Biomedical Engineering 52(7), 1352–1355 (2005)
6. Jiang, X., Mojon, D.: Adaptive local thresholding by verification-based multithreshold probing with application to vessel detection in retinal images. IEEE Trans. on Pattern Analysis & Machine Intelligence 25(1), 131–137 (2003)
7. Antoine, J., Carette, P., Murenzi, R., Piette, B.: Image analysis with two-dimensional continuous wavelet transform. Signal Processing 31(3), 241–272 (1993)
8. Soares, J.V.B., Leandro, J.J.G., Cesar-Jr, R.M., Jelinek, H.F., Cree, M.J.: Retinal vessel segmentation using the 2-d gabor wavelet and supervised classification. IEEE Trans. on Medical Imaging 25(9), 1214–1222 (2006)
9. Cornforth, D.J., Jelinek, H.J., Leandro, J.J.G., Soares, J.V.B., Cesar-Jr, R.M., Cree, M.J., Mitchell, P., Bossomaier, T.: Development of retinal blood vessel segmentation methodology using wavelet transforms assesment of diabetic retinopathy. In: Proc. of 8th Asia Pacific Sym. on Intelligent & Evolutionary Systems, Cairns, Australia, December 6-7, pp. 50–60 (2004)
10. Zana, F., Klein, J.C.: Segmentation of vessel-like patterns using mathematical morphology and curvature evaluation. IEEE Trans. on Image Processing 10(7), 1010–1019 (2001)
11. Frangi, A.F., Niessen, W.J., Vincken, K.L., Viergever, M.: Multiscale vessel enhancement filtering. In: Proc. of the 1st Int. Conf. on Medical Image Computing & Computer-Assisted Intervention, Cambrige MA, USA, October 11-13, pp. 130–137 (1998)
12. Sofka, M., Stewart, C.V.: Retinal vessel extraction using multiscale matched filters, confidence and edge measures. IEEE Trans. on Medical Imaging 25(12), 1531–1546 (2006)
13. Staal, J., Abramoff, M.D., Niemeijer, M., Viergever, M.A., van Ginneken, B.: Ridge based vessel segmentation in colour images of the retina. IEEE Trans. on Medical Imaging 23, 501–509 (2004)
14. Staal, J., Kalitzin, S.N., Viergever, M.A.: A trained spin-glass model for grouping of image primitives. IEEE Trans. on Pattern Analysis and Machine Intelligence 27(7), 1172–1182 (2005)
15. Vermeer, V., Lemij, V.: A model based method for retinal blood vessel detection. Computers in Biology and Medicine 34(3), 209–219 (2004)

16. Niemeijer, M., Staal, J., van, G.B., Loog, M., Abramoff, M.D.: Comparative study of retinal vessel segmentation methods on a new publicly available database. In: SPIE Medical Imaging, San Diego, CA, USA, February 14, pp. 648–656 (2004)
17. Heneghan, F., O'Keefe, C.: Characterization of changes in blood vessel width and tortuosity in retinopathy of prematurity using image analysis. Medical Image Analysis 6(4), 407–429 (2002)
18. Fawcett, T.: An introduction to ROC analysis. Pattern Recognition Letters 27(8), 861–874 (2006)

Erratum to: Using Bayesian Network and AIS to Perform Feature Subset Selection

Boyun Zhang[1,2]

[1] School of Information Science and Engineering, Central South University, Changsha, 410083, P.R. China
[2] Department of computer Science, Hunan Public Security College, Changsha, 410138, P.R. China
hnjxzby@hotmail.com

D.-S. Huang et al. (Eds.): ICIC 2009, LNAI 5755, pp.573--580, 2009.

DOI 10.1007/978-3-642-04020-7_119

The paper starting on page 573 of this publication has been retracted, because it was copied, to a large extent, from "Learning Bayesian Networks to Perform Feature Selection'' by Pablo A.D. Castro and Fernando J. Von Zuben, 978-1-4244-3553-1/09 /$25.00©2009IEEE.

The original online version for this chapter can be found at
http://dx.doi.org/10.1007/978-3-642-04020-7_61

Author Index